Vernadsky Institute of Geochemistry and Analytical Chemistry
of Russian Academy Of Sciences

Institute of Mineralogy
of the Ural Branch of the Russian Academy of Science

South Ural State University (national research university)

Magmatism of the Earth and related strategic metal deposits

Proceedings of XXXIV International conference

Miass, 4-9 August 2017

VERNADSKY INSTITUTE OF GEOCHEMISTRY AND ANALYTICAL CHEMISTRY OF RUSSIAN ACADEMY OF SCIENCES (GEOKHI RAS)

INSTITUTE OF MINERALOGY OF THE URAL BRANCH OF RUSSIAN ACADEMY OF SCIENCE (INSTITUTE OF MINERALOGY UB RAS)

SOUTH URAL STATE UNIVERSITY (NATIONAL RESEARCH UNIVERSITY)

Magmatism of the Earth and related strategic metal deposits

Proceedings of XXXIV International Conference

4-9 August 2017, Miass

УДК 552.3:[553.49+553.81]

Editors:

Ph.D. **V.A. Zaitsev**
Ph.D. **V.N. Ermolaeva**

"Magmatism of the Earth and related strategic metal deposits". Proceedings of XXXIV International Conference. Miass, 4-9 August 2017/Editors V.A. Zaitsev & V.N. Ermolaeva.-M: GEOKHI RAS, 2017. 345 p. - ISBN 978-5-905049-21-7.

The mineral deposits of strategic metals are vulnerable to political and economic changes, and their availability is essential for high-technology, green energy, and other applications. The most of them are related to the deep-seated alkaline magmas.

This book offers a collection of papers presented at the 34th International Conference on Magmatism of the Earth and Related Strategic Metal Deposits held from August 4th to 9th 2017 in Miass, Russia. The conference articles are focused on understanding of the geological processes that produce high concentrations of critical metals in geological systems such as the transport of metals in the mantle and crust and enrichment processes, hydrothermal and metasomatic processes leading to the formation of such significant deposits. Papers in this book give a representative overview including mineralogy, geochemistry and origin of strategic metals deposits.

The cover pictures are geological map of the Urals and «Ridges of Ural» of E.V. Nikolsky

Evgeny Vasilyevich Nikolsky (1917-1978) was a famous Russian artist who lived in Miass. The main theme of his artworks was Ural landscape. He had been making his paintings in different styles and techniques, but most of all he liked to paint with watercolours. In 1969 with this type of paint he had made an artwork "Ridges of Ural" which was painted in the mountains of Southern Ural. Nowadays, this artwork is being kept in local museum of Miass. This year we celebrate the centenary of the birth of this artist.

REVIEW OF PETROGENESIS AND TECTONIC IMPLICATIONS OF A-TYPE GRANITES IN QINLING-DABIE OROGENIC BELT, CENTRAL CHINA

Ahmed Hafizullah Abba[1,2], Habib Mukhtar[1], Zaheen Ullah[1], Amjad Hussain[1]
[1]China University of Geosciences, Wuhan, China, hifzullahahmed@yahoo.com
[2]Modibbo Adama University of Technology, Yola Adamawa State, Nigeria

A-type granites are group of distinctive felsic rocks that are usually occurring within an extensional setting. These rock units were scarce before the Middle Paleoproterozoic but now become abundant since the Late Paleoproterozoic, a situation described by many workers as probable indication of a causal change of tectonics and geodynamic mechanism in the continental evolution of the earth. Occurrence of A-type granites in parts of Qinling-Dabie Orogenic belt has been reviewed in this study to determine their compositional and petrogenetic variability and their relationship to tectonic events within the study area. Representative granitoid units range in age from Paleoproterozoic to Mesozoic across the belt. Geochemical characteristic of the granitoids are typical of the A-type granites with enrichments in silicon and total alkali, depletion of MgO, CaO and P_2O_2, with negative Eu, Sr and Ti anomalies, as well as high $FeOt/MgO$, TiO_2/MgO and Ga/Al ratios and high HFSEs (i.e., Zr, Nb, Ce, Y) concentrations. While majority of the A-type granites in the areas reviewed range from metaluminous to peraluminous, only Huangyangshan pluton in the southern margin of the Tongbai-Dabieshan in south qinling has shown peralkaline affinity, indicating rarity of peralkalinity in anorogenic A-type granites. Partial melting of crustal materials is responsible for the bulk of the granitoids investigated. Considering the widespread in time and space of these granitoids, previous researches have linked the A- type granites of the study area to the opening of the Eastern Paleotethyan Ocean, assemblage of Rodinia supercontinent in South China and the breakup of Columbia supercontinent.
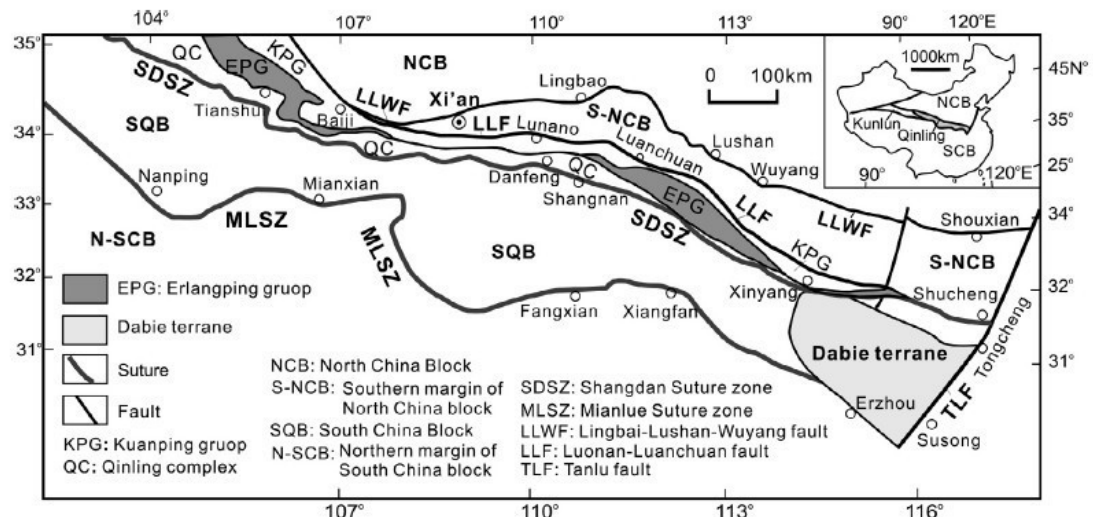
Fig. 1. Tectonic Sketch Map of Qinling Orogen (From Wang et al, 2013).
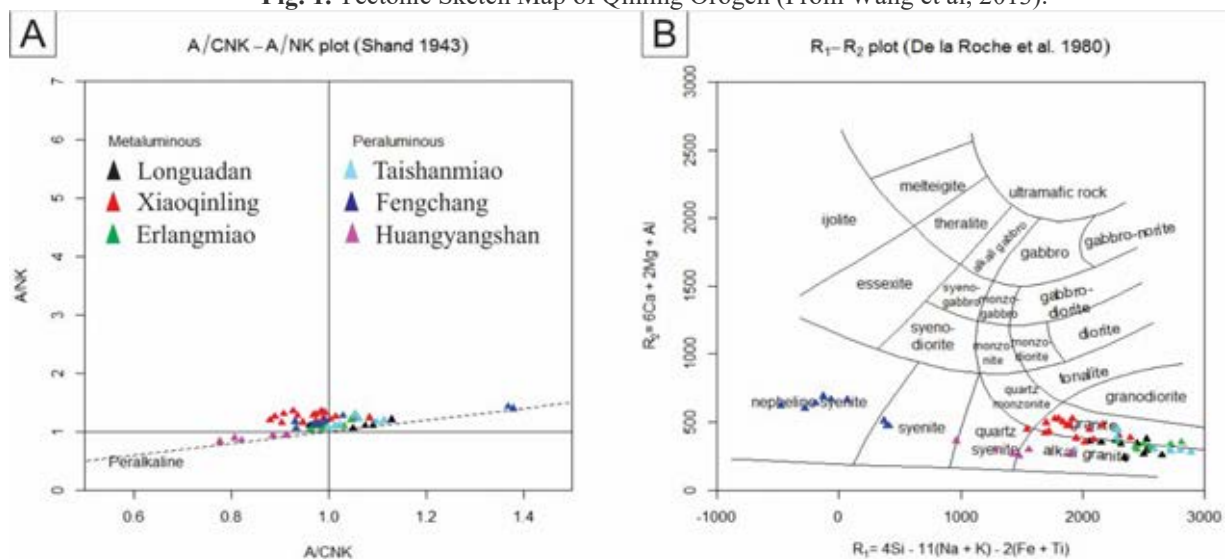

Fig. 2. a=A/CNK-A/NK Plot (after Shand 1943) b= TAS Diagram after Roche et al. Data from Deng et al, (2016), Wang et al, (2016), Bao et al (2008, 2011), Chen et al, (2009) and Ma et al, (2005).
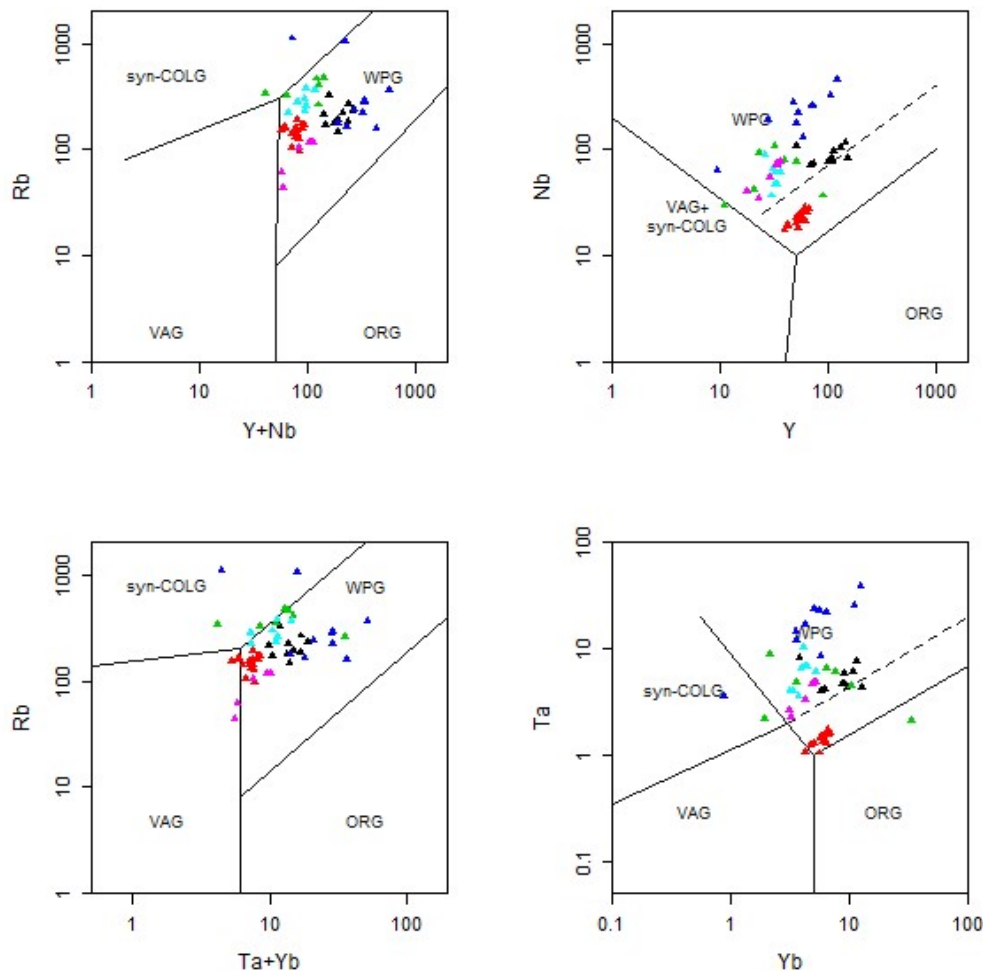
Fig. 3. Granite Tectonic descrimination after Pearce eta, 1984.

References

Bao ZhiWei, Wang Qiang, Bai GuoDian, Zhao ZhenHua, Song YaoWu & Liu XiaoMing (2008). Geochronology and geochemistry of the Fangcheng Neoproterozoic alkali-syenites in East Qinling orogen and its geodynamic implications. Chinese Science Bulletin 53(13) 2050-2061

Bao Zhiwei, Wang Qiang, and Du Fengjun (2011). Geochemistry and geodynamic significance of the rare-earth mineralized Paleoproterozoic Longwangzhuang granite on the southern margin of the North China Craton. Chin.J.Geochem. Springer 30:270–279

Chen Ling, Ma Changqian, Zhen-Bing, Mason Roger, Yang Jin-Zhang and Zhang Chao. (2009). Petrogenesis and tectonic implications of A-type gr anites in the Dabie-Orogenic belt, China: Geochronological and geochemical constraints. Geol. Mag. Cambridge University Press 146 (5), 638-651.

De La Roche, H., Leterrier, J., Grandclaude, P. & Marchal, M. (1980). A classification of volcanic and plutonic rocks using R1R2-diagram and major element analyses – its relationships with current nomenclature. *Chemical Geology* **29,** 183–210.

Deng Xiaoqin, Peng Touping, Zhao Taiping (2016). Geochronology and geochemistry of the late Paleoproterozoic aluminous A-type granite in the Xiaoqinling area along the southern margin of the North China Craton: Petrogenesis and tectonic implications. Precambrian Research 285 127–146.

Ma Changqian, She Zhenbing, Xu Pin & Wang Lingyan (2005). Silurian A-type granitoids in the southern margin of the Tongbai-Dabieshan: Evidence from SHRIMP zircon geochronology and geochemistry. *Science in China* Ser. D Earth Sciences 48 (8) 1134—1145

Pearce, J. A., Harris, N. W. & Tindle, A. G. (1984). Trace element discrimination diagrams for the tectonic interpretation of granitic rocks. *Journal of Petrology* **25,** 956–983.

Shand, S. J. (1943). *Eruptive Rocks. Their Genesis, Composition, Classification, and Their Relation to Ore-Deposits with a Chapter on Meteorite.* New York: John Wiley & Sons.

Wang Xiaoxia, Wang Tao, Zhang Chengli 2013. Neoproterozoic, Paleozoic, and Mesozoic granitoid magmatism in the Qinling Orogen, China: Constraints on orogenic process Journal of Asian Earth Sciences 72 (2013) 129–151

Wang Changming, Chen Liang, Bagas Leon, Lu Yongjun and He Xinyu (2016). Characterization and origin of the Taishanmiao aluminous A‑type granites: implications for Early Cretaceous lithospheric thinning at the southern margin of the North China Craton. Int J Earth Sci (Geol Rundsch) 105:1563–1589

STRATEGIC METALS IN COMPLEXES OF SUBALKALINE RARE-METAL GRANITES AND METASOMATITES FROM THE RUSSIAN SECTOR OF ASIA-PACIFIC GEODYNAMIC ZONE

Alekseev V.I., Alekseev I.V.

Saint-Petersburg Mining University, Saint-Petersburg, Russia, wia59@mail.ru

Deposits of strategic metals, coupled with subalkaline lithium-fluoric granites, are common to vast areas in the Russian Far East. They shape an extended rare-metal belt – Large igneous province – LIP) – spreading from Primorye to Chukotka, which is a part of Russian sector of the Pacific ore belt. Main metallogenic speciality of the rare-metal belt was noted by Smirnov S.S. in 1946, who isolated so called "East-Asian tin-tungsten zone". In the meantime he pointed out, that in a large part of the territory exploration survey was focused on gold and tin deposits, whereas lean ore clusters were studied deficiently. Composition and scale of the rare-metal ore body as well as prospects of strategic metals in the Russian East require today serious clarification.

Dealing with issue of derivation and distribution of strategic rare-metals deposits within the Pacific ore belt should include analyzing mineral forms of their concentration in rocks with different genesis. We attacked the problem of rare-metals composition and distribution in the Far East from mineralogical positions by examining accessory minerals and mineral assemblages in rare-metal granites and associated with them hydrothermal-metasomatic formations. The investigation is based on a concept of positional and possibly genetic connection of rare-metal deposits in the region with subalkaline rare-metal lithium-fluoric granites, which compose a gigantic belt extending from South-East China to Chukotka. Considering a display role of rare-metal granite magmatism for geodynamic environment of endo-plate extension, we distinguish the Far East belt of lithium-fluoric granites – a linear set of "hot spots", tracing the zone of post-accretion mantle diapirism (fig. 1).
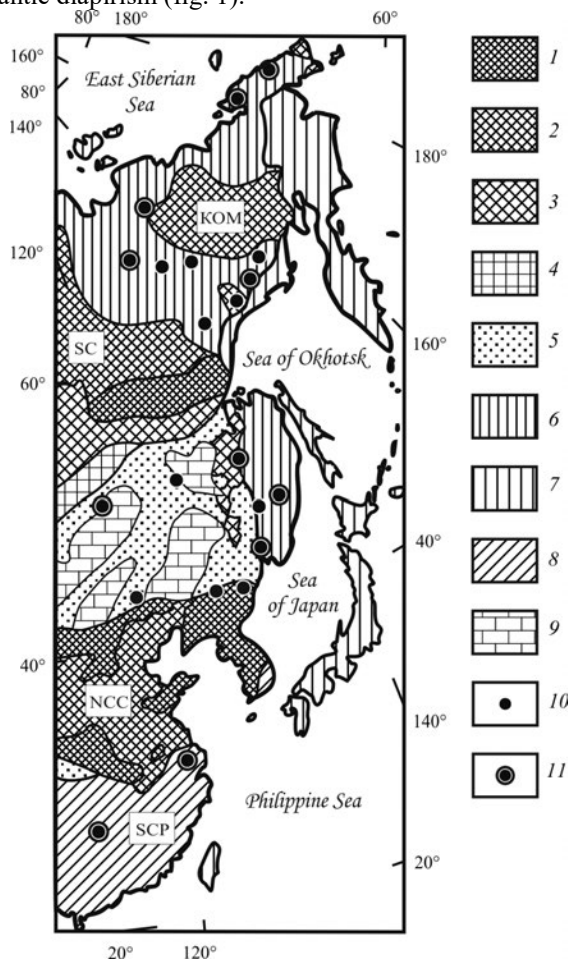

Fig. 1. Schematic plan of rare-metal granites areas and deposits within Asia-Pacific geodynamic zone.
1 – shields; *2* – cratons (SC – Siberian, NCC – North Chinese) and microcontinents with Pre-Cambrian basement (KOM – Kolyma and Omolon); *3* – Riphean folded basement; *4-7* – orogenic belts: Caledonian (*4*), Hercynian (*5*), Mesozoic (*6*), Alpine (*7*); *8* – South-Chinese platform (SCP) with Yanshan diastrophisms; *9* – Mesozoic and Cenozoic platform cover; *10* – areas of rare-metal granite magmatism; *11* – ore-magmatic systems with rare-metal lithium-fluoric granites.

Formation of the Far East subalkaline granite super-province is related to the Pacific plate subducting under the Eastern margin of Asian continent, whereas hot spots appearance beacons apparently windows in immersing slab during its transform movements (Gonevchuk, 2002; Geodinamics…, 2006; Mitrofanov, 2013; Alekseev, 2014). Main features of subalkaline granitoids distribution are: 1) focal nature of magmatism; 2) variety of localizing tectonic conditions; 3) positional connection with rigid framing structures of folded areas; 4) integration with magmatic formations of previous stages of territory development.

Through the example of stanniferous districts – Kujviveem-Pyrkakayskiy (Novosibirsk- Chukchi rare-metal province), Central-Polousnyy (Jano-Kolyma province), Badzhal'skiy and Arminskiy (Sikhote-Alin province) – were isolated Late Cretaceous rare-metal granite series, including near-contemporaneous complexes of lithium-fluoric granites.

Each series was placed in correspondence with a complex of post-magmatic rare-metal hydrothermalites – zwitters, tourmalinites, chloritites – assembled in a zwitter-tourmalinite metasomatic formation.

Table 1. Strategic metals in mineral associations of the Russian Far East deposits, that are associated with lithium-fluoric granites.

Metal	Li-F-granites	Zwitters	Tourmalinites	Chloritites
Sn	Cassiterite, ixiolite, wodginite, (ishikawaite, wolframoixiolite, rutile)	Cassiterite, stannite, ixiolite, sakuraiite, (wolframoixiolite)	Cassiterite, stannoidite, stannite, mawsonite, (rutile)	Cassiterite
W	Wolframoixiolite, ferberite, scheelite, russellite, (samarskite, aeschynite, rutile, ilmenite, liandratite, bismutopyrochlore, ishikawaite)	Ferberite, scheelite, russellite, (rutile, polycrase, cassiterite)	Tungstite, uranotungstite, (rutile)	Scheelite
Nb, Ta	Wolframoixiolite, samarskite, ishikawaite, aeschynite, fergusonite, liandratite, columbite, ilmenorutile, ixiolite, bismutopyrochlore, microlite, struverite, ishikawaite, wodginite, betafite, euxenite, (ilmenite)	Wolframoixiolite, columbite, fergusonite, polycrase, uranopolycrase, bismutopyrochlore, ishikawaite, tapiolite, petscheckite, (ferberite, rutile, uranopolycrase)	Uranopolycrase, polycrase, bismutopyrochlore, (rutile)	
Y, REE	Monazite, xenotime, samarskite, fluocerite, ishikawaite, allanite, fergusonite, aeschynite, chernovite, britholite, gadolinite, euxenite, tveitite, cerianite, yttrialite, (fluorite, cyrtolite)	Monazite, xenotime, chernovite, fergusonite, polycrase, euxenite, uranopolycrase, ishikawaite, gasparite, (fluorite, cyrtolite)	Monazite, allanite, xenotime, fluocerite, polycrase, uranopolycrase, chernovite, agardite, britholite, (fluorite)	Fluocerite, allanite, monazite, parisite, bastnasite, britholite, synchysite
U	Ishikawaite, samarskite, thorite, uraninite, liandratite, euxenite, thorianite, betafite, uranosphaerite, (cyrtolite, bismutopyrochlore)	Uranopolycrase, ishikawaite, euxenite, petscheckite, thorite, asselbornite, zeunerite, uranosphaerite, thorutite, (bismutopyrochlore)	Uranopolycrase, thorite, zeunerite, polycrase, uranotungstite, (bismutopyrochlore)	Uranophane, kasolite, autunite, torbernite

Underlined are main accessory and ore minerals – concentrators of strategic metals. In parenthesis – minerals containing metal in form of impurities.

Ore-magmatic systems of the Far East largest tungsten-tin deposits (Pyrkakayskoye, Odinokoye, Kesterskoye, Olonoyskoye, Pravourmiyskoye, Tigrinoye et al.) include Late Cretaceous plutonic series with late lithium-fluoric granites. The ore-magmatic systems are components of sedimentary and volcanogenic series in passive continental margin and accretion zones generated and processed in a course of the Yanshanian, Verkhoyanian and Laramide orogeny. Granitoid magmatism develops in the crust chamber structures and culminates with a formation of multistage granite domes topped with complexes of rare-metal granites and greisens (Romanovsky, 1999; Gonevchuk, 2002; Geodinamics..., 2006; Mitrofanov, 2013). The major metallogenic feature of ore-magmatic systems with lithium-fluoric granites of the Pacific ore belt is a weak denudation and poor exposure on the modern daylight surface of top layers, which include various nonindustrial accessory mineralization of additional and veined phases of plumasite granites, ongonites and the richest industrial mineralization of zwitters and tourmalinites (Gonevchuk, 2002; Alekseev, 2014).

In the rare-metal granites and complementary metasomatites were found accessory and ore minerals, containing constitutional and trace components of strategic metals such as Sn, W, Nb, Ta, Y, REE, U, that are playing role of industrial minerals on specific deposits (table 1). In the table 1 were not included multiple minerals of Th, As, Cu, Ag, In, Zn, Pb, accompanying main accessories. Particularly variegated are mineral groups of W, Sn, Nb, Bi, Cu. Wide spread of tungsten and tungsten-containing accessory minerals: ferberite, tungsten ixiolite and tungsten-containing accessories (rutile, ilmenite, fergusonite-(Y), ishikawaite, bismutopyrochlore, samarskite-(Yb), aeschynite-(Y), struverite, liandratite, russellite) is a newly established regional feature of rare-metal granites in the Far East (Alekseev, Marin, 2014).

Accessory magmatic and multistage hydrothermal mineral complexes have similar geochemical features. They are formed due to the presence of mentioned metals and characterized by natural alternation in time. Mineralogical and

geochemical evolution of rocks is expressed in transforming mineral concentration of strategic metals, in changing chemically related mineral species and in controlled content alteration. Distinguishing characteristic of mineralogical and geochemical evolution of zwitter-tourmalinite rare-metal deposits is an inheritance by post-magmatic minerals of chemical and species composition of accessories encountered in rare-metal lithium-fluoric granites, which implicates a transfer of ore-forming role from main lithophylic components (W, Nb, Y, REE) to minor chalcophylic metals (Bi, As, Pb), which are present in magmatic minerals in a form of isomorphic and micromineral impurities.

On a postmagmatic stage we observe an inheritance by hydrothermalites of mineralogical and geochemical features of rocks from a previous stage. Moreover, a great number of minerals forming during two or three stages was established along with end-to-end magmatogene-hydrothermal minerals: cassiterite, monazite, allanite, scheelite, W-Pb-rutile, bismutopyrochlore, thorite and others. Thus, hydrothermalite ore mineralization of zwitter-tourmalinite formation on the largest tungsten-tin deposits of the Far East is close and geochemically related to accessory mineralization of complementary lithium-fluoric granites.

The complex of associated metals has a mixed lithophylic-chalcophilic composition. Besides, an evolution of ore mineralization can be observed: Sn, W, Nb, As, Bi, Y, HREE in zwitters is alternating by mineral association of Sn, Cu, In, Ag, LREE in tourmalinites, and later by mineral association of Pb, Zn, LREE in chloritites. Mineralogical and geochemical resemblance of rare-metal granites with accompanying ore-bearing metasomatites of zwitter-tourmalinite formation, together with similarity in mineral complexes evolution indicate the connection between strategic metals deposits and subalkaline rare-metal lithium-fluoric granites.

References:

Alekseev V.I. Lithium-fluoric granites of the Far East. National university of mineral resources «Mining». St Petersburg, 2014. 244 p. (in Russia).

Alekseev V.I., Marin Yu.B. Composition and Evolution of Accessory Mineralization of Li–F granites in the Far East As Indicators of Their Ore Potential // Geology of Ore Deposits. 2015. Vol. 57. No. 8. P. 635-644.

Geodinamics, magmatism and metallogeny of the Russian East: in 2 books / ed. by A.I. Khanchuk. Vladivostok: Dalnauka, 2006. Book 1. P. 1-572. (in Russia).

Gonevchuk V.G. Tin-bearing magmatic systems of the Far East: magmatism and ore genesis. Vladivostok: Dalnauka, 2002. 298 p. (in Russia).

Mitrofanov N.P. Geodynamic conditions of stanniferous deposits formation in the North-Western sector of the Pacific ore belt // Mineral raw material. No. 29. M.: VIMS, 2013. P. 17-25. (in Russia).

Romanovsky N.P. The Earth's Pacific segment: deepstructure, granitoid ore-magmatic systems. Khabarovsk- ITG, Far East Branch RAS, 1999. 167 p. (in Russia).

P-T CONDITIONS OF GOLD MINERALIZATION FORMATION IN ORES FROM KYZYL-TASHTYG VMS-POLYMETALLIC DEPOSIT, EASTERN TUVA, SIBERIA

Ankusheva N.N.[1,2], Kuzhuget R.V.[3]
[1]Institute of Mineralogy, Ural Branch of the Russian Akademy of Sciences, Miass, Russia, ankusheva@mail.ru
[2]South-Urals State University, Miass, Russia
[3]Tuvinian Institute for Exploration of Natural Resources of Siberian Branch of the Russian Akademy of Sciences, Kyzyl, Russia

The Kyzyl-Tashtyg massive sulfide polymetallic deposit is situated 120 km north-east of Kyzyl (the capital of Tuva Republic, Russia). It is located in the Ulug-O volcanic zone which is interpreted as the northern segment of the Kaa-Khem rift in Sayano-Tuva marginal sea, one of the Paleoasian Ocean margin (Zaykov, 2006). The Kyzyl-Tashtyg deposit is located in rhyolite-basaltic complex of the Lower Cambrian Tumat-Tayga formation on the northern side of a volcano-tectonic depression (Kuzebny et al., 2001; Zaykov, 2006). This depression is the most important ore-bearing structure in the region known as Kyzyl-Tashtyg ore area including Kyzyl-Tashtyg, Dalneye deposits, and Yuzhnoye, Perevalnoye, Rudonosnoye, etc. ore mineralizations. Kyzyl-Tashtyg depression is 4×12 km size, and bounded of the Kyzyl-Tashtyg fault at the north and Kaadyr fault – at the south (fig. 1).

The host rocks at the ore area are metamorphosed in greenschist facies, and metasomatites are altered with quartz and sericite formation. Volcanic rocks are transformed to argillites and secondary quartzites. Ores are confined to dacite-rhyolite intrusions. Ore bodies are located in a narrow belt zone of 1200 m length and 130–250 m width.

The average contents of metals in ores are Pb – 2.8 %, Zn – 10.3 %, Cu – 0.65 %, Au up to 2.5 ppm, Ag up to 121 ppm. The reserves of deposit of $B+C_1+C_2$ categories are Zn – 1295 000 t; Pb – 202 000 t; Cu – 166 600 t; Cd – 2 200 t, Se – 670 t. The Au reserves of C_2 category are 15.4 t, with an average content of 1.027 ppm; Ag – 730.6 t, with an average content of 48.71 ppm (Lebedev, 2012; Voytov, 2012).

This study is aimed to establish the conditions of formation of the gold mineralization in ores of the Kyzyl-Tashtyg deposit based on the fluid inclusion data. Previous studies (Kuzebny et al., 2001) and our data (Kuzhuget, Ankusheva, 2016) distinguished six stages (mineral associations) of VMS mineralization at Kyzyl-Tashtyg deposit. Gold mineralization is confined to two of them: *polymetallic ores* with galena, chalcopyrite, sphalerite, pyrite, dolomite, quartz, barite, calcite, chlorite, magnesite, Zn-tennantite-tetrahedrite (Ag up to 1.35 мас. %), electrum ± acanthite ±

pearceite ± kervelliite; and *polymetallic-barite ores* with barite, quartz, chlorite, pyrite, galena, chalcopyrite, sphalerite, tennantite-tetrahedrite, dolomite, ankerite, calcite, enargite, native gold, electrum ± acanthite (fig. 2). Ore mineral associations at the deposit are separated in time by tectonic schifts with ore crushing and breccia structures formation.
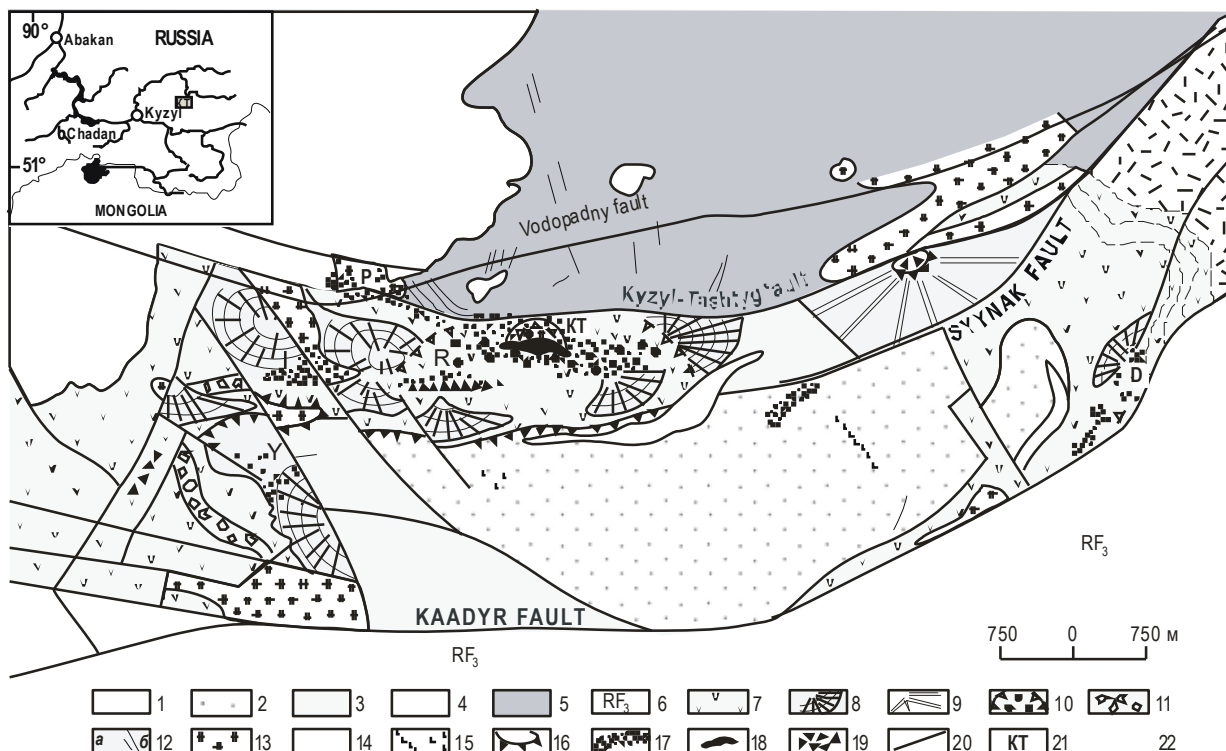

Fig. 1. The geological structure of Kyzyl-Tashtyg ore field, simplified after (Zaykov, 2006):
1 – sandstones and aleurolites of the Tashtyg-Chem suit ($Є_3$ $t/ь$); 2 – tuffs, sandstones, aleurolites and limestones of the Syynak suit ($Є_1sn$); 3 – volcanogenic-sedimentary rocks of the Tumat-Tayga upper subsuit ($Є_1tm_2$); 4–5 – volcanic uplifts: 4 – rhyolites and dacites of the Tumat-Tayga upper subsuit ($Є_1tm_2$); 5 – basalts of the Tumat-Tayga lower subsuit ($Є_1tm_1$); 6 – schistosed sandstones and aleurolites, calcic schists of the Okhem suit (RF_3oh): 7 – basalt, andesite-basalt sheets; 8 – rhyolite-dacite domes; 9 – andesite-dacite-rhyolite edifices; 10 – caldera depression with volcanogenic-terrigenic rocks; 11 – block breccia; 12–14 – latter subvolcanic and hypabyssal intrusions and dykes; 12 – diabase dykes and sills (a), rhyolites and dacites (b); 13 – large subvolcanic and hypabyssal rhyolite intrusions and volcanic breccia; 14 – gabbro-diabase and gabbro-diorites; 15 – dolerites; 16 – thrusts; 17 – sericite-quartz metasomatites; 18 – VMS-polymetallic ore bodies; 19 – ore clasts; 20 – faults; 21 – deposits (KT – Kyzyl-Tashtyg, D – Dalneye) and ore mineralizations (Y – Yuznoe, P – Perevalnoye, R – Rudonosnoye); 22 – Kyzyl-Tashtyg ore field boundaries.
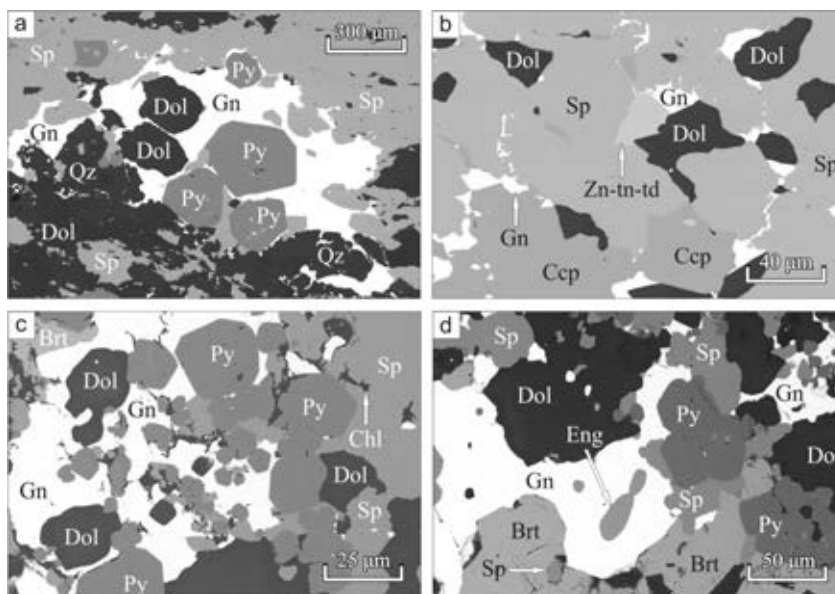

Fig. 2. Mineral composition of polymetallic (a, b) and polymetallic-barite (c, d) ores.
a – Idiomorphic pyrite grains (Py) with galena (Gn), sphalerite (Sp), dolomite (Dol) and quartz (Qz);
b – Zn-tennantite-tetrahedrite (Zn-tn-td) associated with sphalerite (Sp), chalcopyrite (Ccp), galena (Gn) and dolomite (Dol);
c – Idiomorphic pyrite grains (Py) with galena (Gn), sphalerite (Sp), dolomite (Dol) and barite (Brt);
d – Enargite (Eng) in galena (Gn) associated with sphalerite (Sp), pyrite (Py), barite (Brt) and dolomite (Dol).
BSE-photos, MIRA LM scanning electronic microscope (Institute of Geology and Mineralogy SB RAS, Novosibirsk, operator N.S. Karmanov).

Polymetallic ores have sublatitudinal strike (260–300°), and incline to the south from 15–20° up to 65–85° angularly. They confined to the interstratal and cutting schist-forming zones. The thickness of the ore bodies ranges between 1.4 and 74.8 m. The vertical extent ranges between 300 and 520 m, and horizontal extent is 280–710 m. Polymetallic ores are subdivided into essentially polymetallic, barite-polymetallic, and barite-dolomite-polymetallic ore types. The latter types contain from 30 up to 70 % of transparent minerals, however, in massive polymetallic ores they are from 15 up to 50 %. Gold in polymetallic ores is viewed as the electrum grains of 15–135 □m size confined to tennantite-tetrahedrite or contact zone with sphalerite. According to published data [Kovalev et al., 2004], the composition of electrum is following (mass %): Au 67.71–39.52; Ag 60.42–32.18; Hg 0.00–0.07; Cu 0.00–0.26.

The latest polymetallic-barite ores are lower spread, and viewed as the veinlets with thickness ranged between 0.5 and 3 cm, and veins up to 3 m which are cutting ore bodies of polymetallic and barite-polymetallic ore bodies, and host rocks. Their contacts with host rocks are strong. Barite contents range between 80 and 95 %. The ores have streaky, disseminated, nest-disseminated textures, and xenomorphic-granular, fine- and medium-grained structures. Gold is viewed as low-grade native graines and electrum. The compositions (mass %) of native gold is Au 70.43; Ag 30.01; and electrum – Au 61.12–33.52; Ag 66.42–36.25; Hg 0.00–0.01; Cu 0.00–0.01.

Fluid inclusions were studied in double-polished sections using TMS-600 (Linkam) thermo- cryostage at the laboratory of thermobarogeochemistry of the South-Urals State University (Miass). The temperatures between –20 and +80°C were measured with a precision of ±0.1 °C and ±1 °C – out of this range. Salt composition and salinity of the aqueous phase of inclusions were determined using methodologies described by Borisenko [1977]. Salinities were calculated using the temperatures of final ice melting of fluid inclusions [Bodnar, Vityk, 1994]. Microthermometric measurements were obtained from over 100 individual inclusions.

Fluid inclusions are two-phase (V+L$_{H_2O}$) and occurred as either isolated individual inclusions, as groups unrelated to healed fractures. Inclusions are irregular or subrounded, locally as negative crystal shapes; and their sizes are 10–20 µm.

The eutectic temperatures measured in fluid inclusions from quartz of barite-polymetallic ores range between –21.6 and –23.8 °C. These temperatures are close to the eutectic temperatures in the systems NaCl-H$_2$O and NaCl-KCl-H$_2$O (Borisenko, 1977). For most inclusions the final melting temperatures of ice range between –3 and –5.7 °C. This corresponds to the salinities of 4 to 8.8 mass % (NaCl equiv). The homogenization temperatures range between 150 and 250 °C, with multimode frequency (fig. 3a, b).
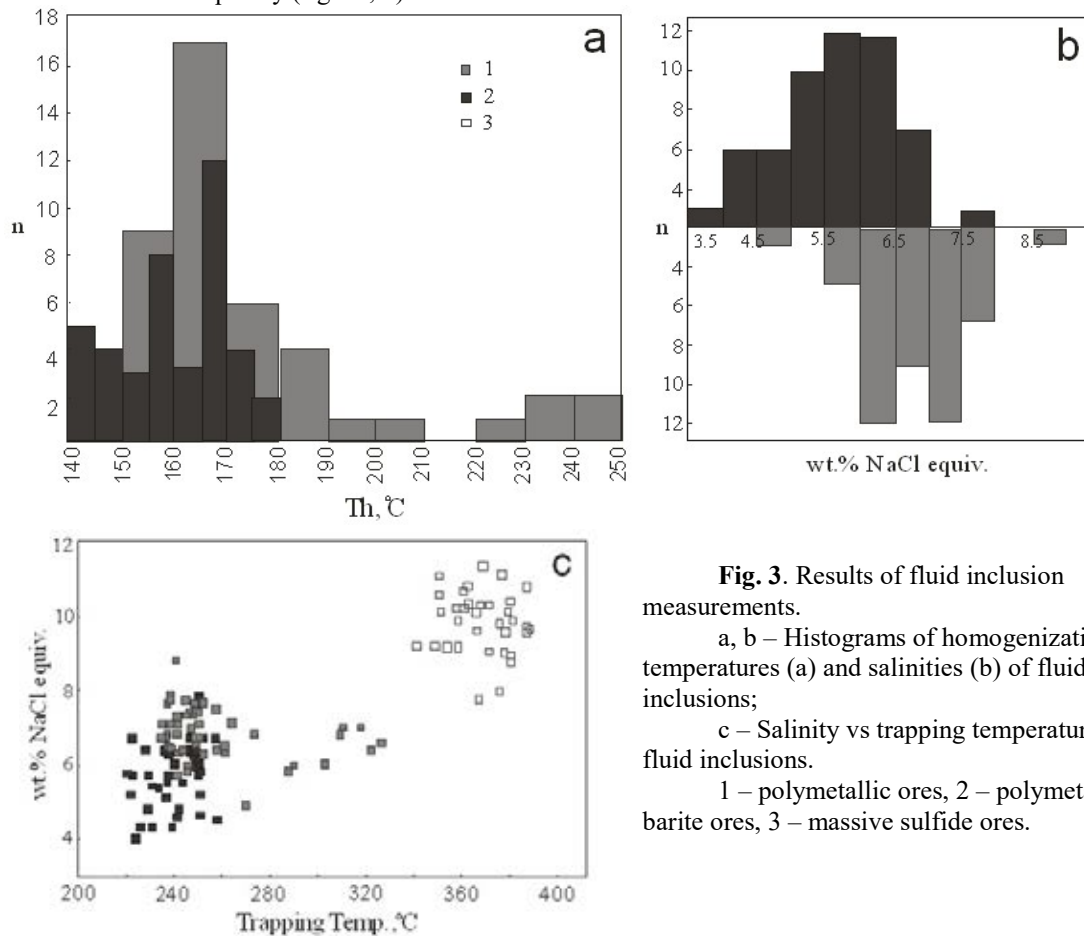

Fig. 3. Results of fluid inclusion measurements.

a, b – Histograms of homogenization temperatures (a) and salinities (b) of fluid inclusions;

c – Salinity vs trapping temperatures of fluid inclusions.

1 – polymetallic ores, 2 – polymetallic-barite ores, 3 – massive sulfide ores.

The latest polymetallic-barite ores were formed due to NaCl-H$_2$O and NaCl-KCl-H$_2$O fluids with a similar salinity of 4–7.8 mass % NaCl-equiv, and temperatures of fluid inclusion homogenization 140–170°C, with multimode frequency (see fig. 3a, b). These data are close to the published data of fluid inclusions in barite (Simonov and Kotlyarov, 2013).

The pressure of mineral formation calculated for Cu-Zn ores is 0.91 kbar (Kuzebny et al., 2001), and ΔT for the homogenization temperatures is 80ºC (Potter, 1977). If approve that the depths of Cu-Zn and polymetallic and polymetallic-barite ores are similar, therefore their trapping temperatures are 230–330 and 220–250°C, respectively (fig. 3c).

According to (Melekestseva et al., 2007) and our data, fluid inclusions trapped in quartz from the primary pyrite-sphalerite ores are $MgCl_2$-$NaCl$-H_2O with a salinity of 8–11 mass % NaCl-equiv, and temperatures of homogenization 300–400°C.

Thus, the fluid inclusion study of ore mineral associations in Kyzyl-Tashtyg deposit clarified the reduction of the trapping temperatures and fluid salinities from the primary pyrite-sphalerite ores to the Au-bearing polymetallic and polymetallic-barite ores: from 400 up to 220°C and from 11 up to 4 mass %, respectively. The similar fluid characteristics indicate the common fluid source for different ore types of Kyzyl-Tashtyg deposit. The presence of Mg and K chlorides and higher fluid salinity up to 9 mass % may be related to a magmatic contribution.

References:

Bodnar R., Vityk M. Interpretation of microthermometric data for H_2O-NaCl fluid inclusions // In: Fluid inclusions in minerals: methods and applications. 1994. P. 117–130.

Borisenko, A.S. The study of the salt composition of fluid inclusion in minerals using a criometry method // Geol. Geofiz. 1977. № 8. P. 16–28.

Kuzebny V.S., Makarov V.A., Kaleyev E.A. Kyzyl-Tashtyg VMS-polymetallic ore cluster of the Eastern Tuva. 2001. 292 p.

Kuzhuget R.V., Ankusheva N.N. Mineralogy and PT-conditions of Cu-Zn and Cu ores formation from Kyzyl-Tashtyg VMS-polymetallic deposit, Eastern Tuva // Uspekhi covremennogo estestvoznania. 2016. №12-2. P. 414–422.

Lebedev N.I. Mineral resources of Tuva: a review of ore minerals. Kyzyl: TuvIENR SB RAN. 2012. 284 p.

Melekestseva I.Yu., Ankusheva N.N., Tret'yakov G.A., Zaykov V.V., Simonov V.A. Massive sulfides from ancient and modern margins of the Asian paleoocean and Pacific: Textures, mineralogy and fluid inclusion data // Marine minerals of the Pacific: Science, Economics, and the Environment: 37th Underwater Mining Institute. Tokyo. 2007. P. 177–187.

Potter R.V. Pressure correction for fluid-inclusion homogenization temperatures, based on the volumetric properties of the system NaCl-H_2O // U.S. Geological Survey J. Research. 1977. Vol. 5. P. 603–607.

Simonov V.A., Kotlyarov A.V. Physic-chemical parameters of the paleohydrothermal systems of Kyzyl-Tashtig VMS-polymetallic deposit, Eastern Tuva // In: Metallogeny of Ancient and Modern Oceans. 2013. P. 152–155.

Voytov M.D., and Veti A.A. A review of the resources of Kyzyl-Tashtyg polymetallic deposit for the reasoning of the mine project // Vestnik KyzSTU. Kemerovo, 2012. № 6. P. 45–48.

Zaykov V.V. Volcanism and sulphide mounds of the paleoceanic structures by the example of the Urals and Siberia. M.: Nauka, 2006. 429 p.

SULPHIDE CONTROLLED FRACTIONATION OF PGE AT POST-CUMULUS CRYSTALLIZATION OF PRIMITIVE OLIVINE CUMULATE PILES FROM THE YOKO-DOVYREN LAYERED INTRUSION

Ariskin A.A.[1,2], Spiridonov E.M.[1], Nikolaev G.S.[2], Danyushevsky L.V.[3], Fiorentini M.L.[4], Kislov E.V.[5], Pshenitsyn I.V.[1]

[1]Lomonosov Moscow State University, Moscow, Russia, ariskin@rambler.ru
[2]Vernadsky Institute of Geochemistry and Analytical Chemistry of the Russian Academy of Sciences, Moscow, Russia
[3]University of Tasmania, Hobart, Australia
[4]The University of Western Australia, Perth, Australia
[5]Geological Institute, Siberian Branch of the Russian Academy of Sciences, Ulan-Ude, Russia

The Dovyren Intrusive Complex (Northern Baikal region, 728 Ma) includes the layered dunite-troctolite-gabbronorite Yoko-Dovyren massif (YDM), associated mafic-ultramafic sills, and dykes of olivine-rich to olivine-free gabbronorite. Major rock types of the YDM include a diversity of olivine orthocumulates to olivine-plagioclase and gabbroic adcumulates, as well as Cu-Ni-PGE mineralisation (Konnikov, 1986; Kislov, 1998). We focus on the mineralogy and geochemistry of poorly mineralised plagioperidotite and plagiodunite in the lower part of the intrusion. Assuming these rocks contain key information on the timing of sulphide immiscibility in the original cumulate pile, we deciphered this record, using a novel approach, which combines estimates of the average sulphide compositions in each particular rock with thermodynamic modeling of the geochemistry of the original sulphide liquid.

To approach the goal, an updated sulphide version of the COMAGMAT-5 model is used (Ariskin et al., 2013). Combining petrochemical reconstructions for the most primitive rocks and calculations using the COMAGMAT-5 model,

it is shown that the central and peripheral parts of the intrusion formed by olivine-laden parental magmas ranged in their temperatures by 100ºC, approximately from 1290ºC (~11 wt% MgO, olivine Fo88) to 1190ºC (~8 wt% MgO, olivine Fo86). Thermodynamic modelling suggests that the most primitive high-Mg magma was S-undersaturated, whereas its derivatives became S-saturated at T<1240-1200°C (Ariskin et al., 2016, 2017). These estimates are consistent with geological observations that mostly sulphide-poor mineralisation occurs in the centre of the intrusion, whereas in its NE and SW parts, as well as in the underlying plagioperidotite sills, Cu-Ni sulphide ores (locally net-textured) are present.
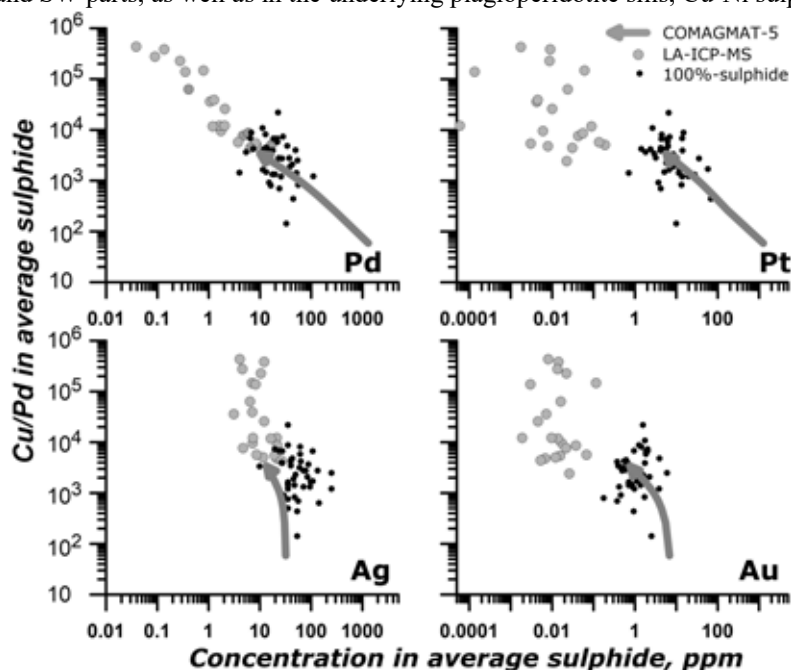

Fig. 1. Weighted average sulphide (LA-ICP-MS) and 100%-sulphide compositions from the lower poorly mineralised zone of the Yoko-Dovyren massif, and modeled compositions of immiscible sulfide melt originated in the olivine cumulate pile. Modelling was performed at 1 atm anhydrous conditions using COMAGMAT-5 (Ariskin et al., 2013). The calculations represent the closed system crystallization of a primitive olivine cumulate, with modeled onset of sulfide immiscibility at 30-40ºC below the initial magma temperature (Ariskin et al., 2016). Immiscible sulfide compositions are calculated using a novel approach proposed in (Ariskin et al., 2017).

The primitive S-undersaturated olivine cumulates became sulphide-saturated at a post-cumulus stage. As a result, Ni-rich immiscible sulphides formed within and migrated through the early olivine-rich cumulate piles to generate poorly mineralised plagiodunite. Results of simulations of sulphide immiscibility in initially S-undersaturated olivine cumulates demonstrate a strong effect of the decreasing fraction of the silicate melt, due to crystallization of silicate minerals, on the composition of the intercumulus Ni-rich sulphide liquid. Comparison of the observed and modeled sulphide compositions indicates that the proposed modeling reproduces well the highest average concentrations of Pd and Ag, and the lowest Cu concentration in the natural sulphides (Fig. 1). This evidences that sulphide is the main control on the distribution of these elements in the rocks.

Conversely, calculations for Pt and Au resulted in much higher concentrations, thus suggesting that a significant portion of the chalcophile elements is present in another mineral form, affecting their budget in coexisting sulphides (Ariskin et al., 2016). To test this possibility, we performed mass-balance calculations producing the composition of a 100% sulphide for each particular rock. As a result, the virtual concentrations of all noble metals (Pd, Ag, Pt, and Au) in the 100% sulphides are consistent with those calculated using the COMAGMAT-5 model (Table 1, Fig. 1).

This supports for the above conclusion that despite the original sulphide liquid control, a part of palladium and silver, as well as almost all platinum and gold may present in the rocks as rare PGE minerals and native alloys. This is supported by single findings of sub-micron grains of sperrylite, native Pt and gold, as well as Pt-Pd alloys in cracks of serpentization of the primitive poorly mineralised plagioperidotite. Overall, these observations evidence an efficient phase separation of platinum elements minerals from the original sulphide liquid, proceeded during post-cumulus recrystallization of sulphide minerals and followed later by low temperature pneumatolytic processes.

Table 1. Concentrations of Cu and precious metals in a primitive olivine cumulate*

Modeled elements	Cu, ppm	Ag, ppb	Pd, ppb	Pt, ppb	Au, ppb
Whole rock composition	47.8	19	12.8	7.3	1.3
Sulfide-melt partition coefficients	951	1005	67000	125000	4100

* Updated table, after (Ariskin et al., 2016, 2017).

References:

Ariskin A.A., Bychkov K.A., Nikolaev G.S. (2017) Modeling of trace-element composition of sulphide liquid in a crystallizing basalt magma: development of the R-factor concept. Geochem. Intern. 55: 465-473.

Ariskin A.A., Danyushevsky L.V., Bychkov K.A., McNeill A.W., Barmina G.S., Nikolaev G.S. (2013) Modeling solubility of Fe-Ni sulphides in basaltic magmas: The effect of Ni in the melt. Econ. Geol. 108: 1983-2003.

Ariskin A.A., Danyushevsky L.V., Kislov E.V., Nikolaev G.S., Fiorentini M., Gilbert S., Goemann K., Malyshev A. (2016) Cu-Ni-PGE fertility of the Yoko-Dovyren layered massif (Northern Transbaikalia, Russia): thermodynamic modeling of sulphide compositions in low mineralized dunites based on quantitative sulphide mineralogy. Miner. Depos. 51: 993-1011.

Kislov E.V. (1998) The Yoko-Dovyren layered massif. BNTsRAN, Ulan-Ude (in Russian).

Konnikov E.G. (1986) Differentiated ultrabasic-basic complexes in the Precambrian rocks of Transbaikalia. Nauka, Novosibirsk (in Russian).

THE FORMATION OF MAGMATIC ORE DEPOSITS
Arndt N.T.
University Grenoble Alpes, Grenoble, France

The formation of magmatic Ni-Cu sulfide deposits is directly linked to interaction between mafic-ultramafic magma and rocks of the continental crust. This interaction decreases the solubility of sulfide in the magma and/or adds sulfur to generate an immiscible sulfide liquid. Strongly chalcophile Ni, Cu and PGE become concentrated in the sulfide and if this phase accumulates in sufficient quantity and with sufficient tenor, an ore deposit is formed.

Most models propose that sulfide droplets segregate and accumulate from magma that flows rapidly through conduits. These 'high-flux' models are at odds, however, with the following observations. Many ores appear to have been emplaced as magmatic breccias (Norilsk-Talnakh, Russia; Aguablanca, Spain) or crystal mushes (Jinchuan, China) that contain a high proportion of sulfide. Such mixtures are very dense and could not have migrated upwards through the crust from a deeper staging chamber. In the Uitkomst and Platreef deposits (South Africa), screens of sedimentary rock maintaining the same orientation as adjacent sedimentary strata separate layers of ultramafic cumulates, some containing abundant sulfide ore. This geometry suggests that ultramafic mush and ore sulfides oozed into the sedimentary sequence, replacing less resistant strata.

These features can be explained if sulfide-rich masses of magma accumulated higher in the magmatic plumbing system then slumped downwards. Most mafic-ultramafic intrusions do not differentiate in place but grow through the injection of magmas of differing compositions and crystallinities. Highly mafic magmas, particularly those charged with ferromagnesian crystals and sulfide, have high densities and they are injected into the lower parts of growing intrusions while less-dense, more evolved and/or plagioclase-rich magmas are injected at higher levels. Many ore-bearing intrusions are hosted in conduits with sloping margins. As magma flows up along these margins, the denser sulfide/inclusion/crystal-rich mush accumulates near the lower border while a sulfide-crystal-poor silicate liquid ascends along the upper part. This process differentiates the magma, producing evolved decanted liquids that flow upwards and erupt, and a sulfide-rich slurry that periodically becomes unstable and slumps down the conduit. The magma interacts with the slumping sulfide in the lower part of the conduit, enriching the sulfide in chalcophile metals. This interpretation, if correct, requires re-evaluation of the geological criteria used to locate ore deposits in magmatic systems. High fluxes are associated with decanted magma flowing upwards through the system but ore formation results from intermittent downward flow of sulfide mushes. To understand these processes requires detailed 3D mapping of magma conduits.

Density also plays an important role, but at a larger scale, during the formation of the Cr and platinum-group-element deposits (PGE) in the Bushveld Complex in South Africa. This is the world's biggest mafic-ultramafic intrusion and one of the richest repositories of magmatic ores. Despite decades of study, many aspects of the emplacement of the intrusion continue to pose problems. Foremost are mismatches between the volume of magma required to account for the major deposits of Cr and PGE and the volume of mafic rock preserved in the complex. A large volume of magma is missing, but the most obvious explanation - that the missing magma erupted - is contradicted by the small volumes of mafic lava at the surface. The recent discovery of highly magnesian rocks at the periphery of the complex exacerbates the situation because these would have produced large volumes of ultramafic cumulates. Geophysical data are also problematic. The centre of the complex, where a large mass of dense rock should be present if the intrusion had the funnel shape that is normal for large mafic-ultramafic intrusions, displays negative gravity anomalies.

A solution is offered by recent analogue and numerical modelling of the emplacement of mafic magma into crustal magma chambers. This modelling shows that the dense lower mafic-ultramafic cumulates of an intrusion with the form, size and geological context of the Bushveld Complex would founder and descend deeper in the crust. It is proposed that the complex, as currently exposed at the surface, represents only a small portion of an initially much larger intrusion.

DENSITY STRUCTURE OF THE CRATONIC MANTLE IN SIBERIA, CORRELATIONS WITH MANTLE PETROLOGY AND KIMBERLITE DISTRIBUTION
Artemieva I.M.[1] Cherepanova Yu.
University of Copenhagen, Denmark, irina@ign.ku.dk.

We present a new regional model for the density structure of the cratonic lithospheric mantle in the Archean–Proterozoic Siberian Craton (Cherepanova and Artemieva, 2015) and discuss it in relation to regional tectonic evolution, geochemical data on kimberlite-hosted mantle xenoliths, and data on kimberlite ages and distribution. The nearly isostatic balance of the Siberian Craton allows us for applying the free-board modeling to calculate the density structure of the lithospheric mantle beneath the Craton. Availability of the reliable regional crustal model (Cherepanova et al., 2013) and

the thermal model of the lithospheric mantle secures high reliability of free-board modeling, with the overall uncertainty of mantle density better than 0.02 g/cc or better than ca. 0.6% with respect to primitive mantle.

The free-board modeling provides a vertically-averaged mantle density in the layer from the Moho down to base of the chemical boundary layer (CBL). The depth extent of the CBL is debated, and while geophysical studies suggest that it may extend down to the LAB, xenolith-based studies from different cratons worldwide suggest that the correlation between CBL and LAB may be complex. We perform the analysis of the density structure of the cratonic lithospheric mantle for two models of the CBL thickness. Model 1 assumes that the base of the CBL coincides with the LAB and is laterally variable within the Siberian craton, whereas in Model 2 the base of the CBL is fixed at a 180 km depth, and the layer below 180 km depth down to the LAB is ascribed fixed, nearly fertile, density value.

The results, calculated at in situ and at room temperature (SPT) conditions, indicate a heterogeneous density structure of the Siberian lithospheric mantle with a strong correlation between mantle density variations and the tectonic setting. For Model 1, the lithospheric mantle is significantly less depleted than in Model 2, in particular in regions with deep lithospheric keels, whereas there is little difference between the two models for intracratonic sedimentary basins where the lithosphere thickness is less than 180 km. Three types of cratonic mantle are recognized from mantle density anomalies, and we report here the values calculated for two-layer Model 2, which is supported by petrologic data.

1) 'Pristine' cratonic regions not sampled by kimberlites have the strongest depletion with density deficit of 1.8–3.0% (and SPT density of 3.29–3.33 g/cc as compared to 3.39 g/cc of primitive mantle).

2) Cratonic mantle affected by magmatism (including the kimberlite provinces) has a typical density deficit of 1.0–1.5%, indicative of a metasomatic melt-enrichment.

3) Intracratonic sedimentary basins have a high density mantle (3.38–3.40 g/cc at SPT conditions) which suggests, at least partial, eclogitization. Moderate density anomalies beneath the Tunguska Basin imply that the source of the Siberian LIP lies outside of the Craton.

In situ mantle density is used to test the isopycnic condition of the Siberian Craton. Both CBL thickness models indicate significant lateral variations in the isopycnic state, correlated with mantle depletion and best achieved for the Anabar Shield region and other intracratonic domains with a strongly depleted mantle. A comparison of synthetic Mg# for the bulk lithospheric mantle calculated from density with Mg# from petrological studies of peridotite xenoliths from the Siberian kimberlites suggests that melt migration may produce local patches of metasomatic material in the overall depleted mantle.

References:

Cherepanova Y. and Artemieva I.M. (2015). Density heterogeneity of the cratonic lithosphere: A case study of the Siberian Craton. Gondwana Research, 28, 1344-1360, http://dx.doi.org/10.1016/j.gr.2014.10.002

Cherepanova Y., Artemieva I.M., Thybo H., Chemia Z. (2013). Crustal structure of the Siberian craton and the West Siberian basin: An appraisal of existing seismic data. Tectonophysics, 609, 154-183, http://dx.doi.org/10.1016/j.tecto.2013.05.004

IS THE PROTEROZOIC LADOGA RIFT (SE BALTIC SHIELD) A RIFT?

Artemieva I.M.[1], Shulgin A.[2]

[1]University of Copenhagen, Copenhagen, Denmark, irina@ign.ku.dk, iartemieva@gmail.com
[2]University of Oslo, Oslo, Norway, Alexey.shulgin@geo.uio.no

The southern part of the Baltic Shield hosts a series of mafic dykes and sills of Mesoproterozoic ages, including a ca. 1.53–1.46 Ga sheet-like gabbro-dolerite sills and the Salmi plateau-basalts from the Lake Ladoga region. Based on chiefly geochemical data, the region is conventionally interpreted as an intracratonic Ladoga rift (graben). We question the validity of this geodynamic interpretation by analyzing regional geophysical data (crustal structure, heat flow, Bouguer gravity anomalies, magnetic anomalies, and mantle Vs velocities).

We provide a complete list of tectonic, magmatic, and geophysical characteristics typical of continental rifts in general and demonstrate that, except for magmatic and, perhaps, some gravity signature, the Lake Ladoga region lacks any other rift features. We also compare the geophysical data from the Lake Ladoga region with similar in age Midcontinent and Valday rifts, and provide alternative explanations for Mesoproterozoic geodynamic evolution of the southern Baltic Shield.

We propose that Mesoproterozoic mafic intrusions in southern Fennoscandia may be associated with a complex deformation pattern during reconfiguration of (a part of) Nuna (Columbia) supercontinent, which led to magma intrusions as a series of mafic dykes along lithosphere weakness zones and ponding of small magma pockets within the cratonic lithosphere. Consequent magma cooling and its partial transition to eclogite facies could have led to the formation of a series of basement depressions, similar to intracratonic basins of North America, while spatially heterogeneous thermo-chemical subsidence, with phase transitions locally speeded by the presence of (subduction-related) fluids, could have produced a series of faults bounding graben-like structures.

References:

Artemieva I.M., A. Shulgin (2015). Is the Proterozoic Ladoga Rift (SE Baltic Shield) a rift? Precambrian Research, 259, 34–42, http://dx.doi.org/10.1016/j.precamres.2014.08.011

GEOPHYSICAL CONSTRAINTS ON GEODYNAMIC PROCESSES AT CONVERGENT MARGINS: A GLOBAL PERSPECTIVE

Artemieva I.M.[1], Thybo H.[2,3], Shulgin A.[2]
[1]University of Copenhagen, Copenhagen, Denmark, irina@ign.ku.dk, iartemieva@gmail.com
[2]University of Oslo, Oslo, Norway, Alexey.shulgin@geo.uio.no; thybo@geo.uio.no
[3]Istanbul Technical University, Istanbul, Turkey; h.thybo@gmail.com

We review global geophysical data on the convergent margins worldwide in order to illustrate the effects of the plate tectonic processes on the crustal and upper mantle structure, seismicity, and geometry of subducting slab. Our analysis includes all three types of convergent margins, formed by ocean–ocean, ocean–continent, and continent–continent collisions, for which we show 20 profiles across different margins types. A global analysis of data on gravity anomalies, heat flow and seismicity for allows us to recognize the following patterns:

(1) Plate convergence rate depends on the type of convergent margins and, generally, it is significantly larger when, at least, one of the plates is oceanic. However, the oldest oceanic plate in the Pacific ocean has the smallest convergence rate.

(2) The presence of an oceanic plate is, in general, required for generation of high-magnitude (M N 8.0) earthquakes and for generating intermediate and deep seismicity along the convergent margins.

(3) Subduction of oceanic slabs beneath a continent is characterized by a gap in the seismogenic zone at depths between ca. 250 km and 500 km. In case of continent–continent collision the seismogenic zone terminates at ca. 200 km depth, and we use this observation to propose oceanic origin of subducting slabs beneath the Zagros, the Pamir, and the Vrancea zone.

(4) Dip angle of the subducting slab in continent–ocean collision does not correlate neither with the age of subducting oceanic slab, nor with the convergence rate. However, we recognize clear trends for ocean–ocean subduction: steeply dipping slabs are characteristic of young subducting plates and of oceanic plates with high convergence rate, with slab rotation towards a near-vertical dip angle at depths below ca. 500 km at very high convergence rate.

(5) Local isostasy is not satisfied at the convergent margins as evidenced by strong free air gravity anomalies of positive and negative signs. However, near-isostatic equilibrium may exist in broad zones of distributed deformation such as Tibet.

Reference:

Artemieva I.M., H. Thybo, A. Shulgin (2016). Geophysical constraints on geodynamic processes at convergent margins: A global perspective. Gondwana Research, 33, 4–23; http://dx.doi.org/10.1016/j.gr.2015.06.010

DENSITY STRUCTURE OF THE CRATONIC MANTLE IN SOUTHERN AFRICA, KIMBERLITE DISTRIBUTION, MANTLE VELOCITIES, MOHO SHARPNESS, AND DYNAMIC TOPOGRAPHY

Artemieva I.M.[1], Vinnik L.P.[2]
[1]University of Copenhagen, Denmark, irina@ign.ku.dk.
[2]Institute of the Earth Physics of the Russian Academy of Sciences, Moscow, Russia, vinnik@ifz.ru

We present a new regional model for the density structure of the cratonic lithospheric mantle in southern Africa and discuss it in relation to regional seismic models for the crust and upper mantle, geochemical data on kimberlite-hosted mantle xenoliths, and data on kimberlite ages and distribution. Our calculations of mantle density are based on free-board constraints, account for mantle contribution to surface topography of ca. 0.5-1.0 km, and have uncertainty ranging from ca. 0.01 g/cc for the Archean terrains to ca. 0.03 g/cc for the adjacent fold belts (Artemieva and Vinnik, 2016a).

We demonstrate that in southern Africa the lithospheric mantle has a general trend in mantle density increase from Archean to younger lithospheric terranes. SPT density of the Kaapvaal mantle is typical cratonic, with a subtle difference between the eastern, more depleted, (3.31-3.33 g/cc) and the western (3.32-3.34 g/cc) blocks. The Witwatersrand basin and the Bushveld Intrusion Complex appear as distinct blocks with an increased mantle density (3.34-3.35 g/cc) with values typical of Proterozoic rather than Archean mantle. We attribute a significantly increased mantle density in these tectonic units and beneath the Archean Limpopo belt (3.34-3.37 g/cc) to melt-metasomatism. The Proterozoic Kheis, Okwa and Namaqua-Natal belts and the Western Cape Fold Belt with the late Proterozoic basement have an overall fertile mantle (ca. 3.37 g/cc) with local (100-300 km across) low-density (down to 3.34 g/cc) and high-density (up to 3.41 g/cc) anomalies. High (3.40-3.42 g/cc) mantle densities beneath the Eastern Cape Fold belt require the presence of a significant amount of eclogite in the mantle, such as associated with subducted oceanic slabs.

We find a strong correlation between the calculated density of the lithospheric mantle, the crustal structure, the spatial pattern of kimberlites and their emplacement ages (Artemieva and Vinnik, 2016b).

(1) Blocks with the lowest values of mantle density (ca. 3.30 g/cc) are not sampled by kimberlites and may represent the "pristine" Archean mantle.

(2) Young (<90 Ma) Group I kimberlites sample mantle with higher present-day density (3.35±0.03 g/cc) than the older Group II kimberlites (3.33±0.01 g/cc), but the results may be biased by incomplete information on kimberlite ages.

(3) Diamondiferous kimberlites are more typical of a low-density cratonic mantle (3.32-3.35 g/cc), while non-diamondiferous kimberlites sample mantle with a broad range of density values. Diamondiferous kimberlites that sample a dense mantle (3.35-3.37 g/cc) are all older than 200 Ma.

(4) Kimberlite-rich regions have a strong seismic velocity contrast at the Moho, thin crust (35-40 km) and low-density (3.32-3.33 g/cc) mantle, while kimberlite-poor regions have a transitional Moho, thick crust (40-50 km), and denser mantle (3.34-3.36 g/cc). We explain this pattern by a lithosphere-scale (presumably, pre-kimberlite) magmatic event in kimberlite-poor regions, which affected the Moho sharpness and the crustal thickness through magmatic underplating and modified the composition and rheology of the lithospheric mantle to make it unfavourable for consequent kimberlite eruptions.

(5) Density anomalies in the lithospheric mantle show weak inverse correlations with seismic Vp, Vs velocities at 100-150 km depth, but only when averaged over large tectonic blocks, suggesting that density-velocity relationship in the cratonic mantle is strongly non-unique.

References:

Artemieva I.M. and Vinnik L.P. (2016a). Density structure of the cratonic mantle in southern Africa: 1. Implications for dynamic topography. Gondwana Research 39, 204-216, http://dx.doi.org/10.1016/j.gr.2016.03.002

Artemieva I.M. and Vinnik L.P. (2016b). Density structure of the cratonic mantle in southern Africa: 2.Correlations with kimberlite distribution, seismic velocities, and Moho sharpness. Gondwana Research 36, 14-27, http://dx.doi.org/10.1016/j.gr.2016.05.002

DEVONIAN ALKALINE MAGMATISM OF THE NORTHEASTERN FENNOSCANDIAN SHIELD: PRECURSORY AND SUBSEQUENT EVENTS

Arzamastsev A.A.[1,2], Veselovskiy R.V.[3,4]

[1]Institute of Precambrian Geology and Geochronology of the Russian Akademy of Science, Saint-Petersburg, Russia
[2]Saint-Petersburg State University, Saint-Petersburg, Russia, arzamas@ipgg.ru
[3]Lomonosov Moscow State University, Moscow, Russia
[4]Shmidt Institute of Physics of the Earth, Russian Academy of Sciences, Moscow, Russia, roman.veselovskiy@ya.ru

The Kola magmatic province in the northeastern Fennoscandian Shield is made up of giant plutons of agpaitic syenite, carbonatite intrusions, dykes and volcanics, which were formed at 380—360 Ma. The province shows some typical characteristics of plume magmatism occurrences, however, tholeiitic magmatism, which is characteristic of the areas of extensive plume—lithosphere interaction, has not been found yet. Since 1.85 Ga a long amagmatic period preceded intrusion of the Devonian alkaline magmas and no manifestations of precursory or subsequent magmatic events have been detected in this part of the shield. Investigation of numerous Early Proterozoic dyke swarms showed that some of them appear to be of Paleozoic age.

Precursory magmatism is represented by volcanics preserved in the Paleozoic calderas of Lovozero, Kontozero, and Khibiny and dolerite dykes grouped in three swarms: Pechenga, Barents Sea, and Eastern Kola (Fig. 1). The Pechenga swarm includes a series of large vertical dykes trending approximately N—S (SE 10°), some of which were traced over a distance of more than 80 km. Dykes with petrographic and geochemical characteristics similar to those of the Pechenga swarm dolerites were documented in northern Norway and the island of Mageroy. The Eastern Kola swarm includes several near-meridional dykes 15—30 m thick and up to 100 km long. The Barents Sea swarm comprises dykes at the coastline between the settlements of Teriberka and Ostrovnoi. Most of 2—10-m thick subvertical dykes have a northeastern strike and were traced inside the peninsula over several kilometers. The mouths of the Drozdovka and Ivanovka rivers are the area of co-occurrence of Paleozoic tholeiitic and alkaline magmatism. In the Lovozero caldera, volcanic rocks occur mainly in the northeastern part of the massif; lujavrite—foyaite—urtite complexes host large (up to 200 m thick) blocks of volcanic rocks, which are spatially associated with sediments of the Lovozero Formation. Almost all volcanics underwent strong metasomatic alteration caused by the agpaitic melts that formed the intrusive series of the Lovozero massif.

Plateaus ages from 393 to 368 Ma were obtained for biotite and feldspars from five samples of rocks of the Barents Sea dyke swarm. The weighted mean of five datings for dykes from the Barents Sea swarm (380 ± 2 Ma) is consistent with the age of biotite from a dyke of the Pechenga swarm. Reliable plateau ages were obtained for plagioclase and feldspars from three dyke samples of the Eastern Kola swarm. The weighted mean age of these samples (380.5 ± 3.3 Ma) is in agreement with the results of dating of the Pechenga and Barents Sea dyke swarms. Rb—Sr isotope ages were obtained for samples of volcanic rocks from the Lovozero and an alkaline ultrabasic rock from the Ivanovka volcano-plutonic complex and major mineral phases separated from these samples. A Rb—Sr age of 373 ± 25 Ma was obtained from the four-point isochron of ankaramite from a large remnant of the volcanic sequence of Lovozero. The obtained age value corresponds to the formation of volcanics of the Lovozero caldera concurrently with the formation of comagmatic plutonic rocks in the Kurga massif. Isotopic compositions of major minerals from the olivine melteigite porphyry of the Ivanovka massif yields an age of 371 ± 3 Ma, which is identical to the age of formation of the most alkaline ultrabasic intrusions of the province. The initial isotope ratio ($^{87}Sr/^{86}Sr)_{T=380}$ of the samples from all the regions of dolerite occurrence ranges from 0.7029 to 0.7071 and is correlated with the neodymium isotope ratios recalculated to the same age.
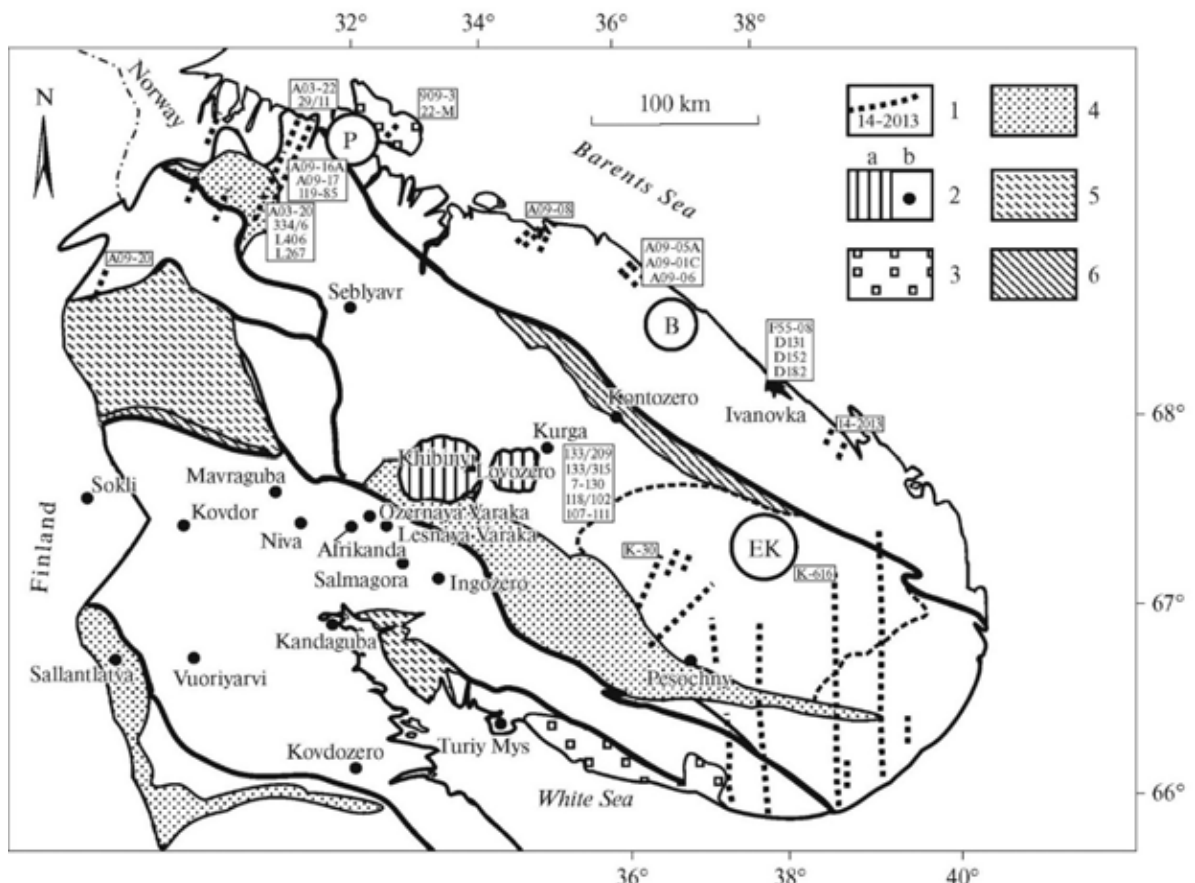
Fig. 1. Occurrences of Paleozoic magmatism in the northeastern Fennoscandian shield. (1) Paleozoic dolerite dykes of the Pechenga (P), Barents Sea (B), and Eastern Kola (EK) swarms; (2) massifs of (a) nepheline syenite and (b) alkaline ultrabasic rocks and carbonatite. Basement rocks: (3) Riphean terrigenous complex, (4) Karelian volcanosedimentary complex, (5) Lapland granulite complex, and (6) Archean granite gneiss. Numbers of samples studied by us are given in rectangles.

Taken into account the accuracy of age estimates for dolerites from different regions of the Kola Peninsula, it can be concluded that the tholeiitic magmatism either preceded or coincided with the appearance of the first portions of alkaline melts. The relatively early emplacement of tholeiitic magmas is supported by the intersection of dolerite bodies by melanephelinite dykes in the Ivanovka Fiord, where the occurrences of alkaline and tholeiitic magmatism overlap spatially. Our isotope geochronological data for the dolerite dykes and bodies of olivine melteigite porphyry of this region suggest that, taking into account the accuracy of age reconstruction, they are separated by a considerable time interval (393 ± 5 and 371 ± 2.5 Ma, respectively). Thus, the whole body of geochronological data leads to the conclusion that the duration of formation of the Kola magmatic province was no less than 25 Myr.

The finding that Devonian tholeiites raises the problem of their place in the general model of the evolution of Paleozoic magmatism and, first of all, their relation to alkaline melts. The spatial association of tholeiites and alkaline rocks, their formation within a relatively short time interval, and similarity of isotopic characteristics indicate unequivocally that these two melt types were produced by a common mantle process. Taking into account the geochronological results and petrologic models described above, it can be concluded that the dolerites correspond to the initial phase of Paleozoic plume-lithosphere interaction, which resulted in the formation of tholeiitic melts through the partial melting of an unenriched and unmetasomatized material under spinel lherzolite facies conditions. The subsequent development of the plume-lithosphere process triggered the melting of deeper mantle zones showing clear evidence for fertilization under the conditions of the garnet lherzolite facies. The first products of melting of the metasomatized material were the subalkaline volcanics of the Lovozero caldera and their plutonic analogues in the Kurga polyphase intrusion. The melting of mantle domains affected by metasomatism resulting in significant enrichment of the mantle material in HFSE, REE, and LILE produced the melanephelinite melts that gave rise to the alkaline magmas. Based on the obtained geochronological evidence and isotope systematics of the rocks, it can be suggested that the process of mantle enrichment was relatively short, which is consistent with the inference of Kramm and Kogarko (1994).

According to petrological data, tholeiitic melts are generated at higher degrees of mantle melting compared with melanephelinite melts, which are derived by a few percent melting. This is consistent with the large volumes of tholeiitic magmas forming giant lava fields in large igneous provinces and the much smaller volumes of alkaline melts. In contrast to these provinces, only minor occurrences of Paleozoic tholeiitic magmatism were observed in the northeastern Fennoscandian Shield, where agpaitic syenite massifs and intrusions of alkaline ultrabasic rocks and carbonatites occur. The suggestion that large volcanic fields of basic rocks (traps) existed in the Kola part of the shield, but were eroded is

unwarranted, because magmatic bodies that could have been interpreted as conduits on an appropriate scale were not found in the region. Moreover, the available geophysical data do not indicate the existence of lower crustal domains that could be interpreted as complementary derivatives of tholeiitic magmas (Kukkonen and Peltonen, 1999). Thus the volume proportions of tholeiitic and alkaline magmatism, duration of plume-lithosphere processes, and the sequence of melt emplacement are characteristic features of the Paleozoic magmatism of northeastern Fennoscandia different from the respective characteristics of the large igneous provinces of Siberia (Meimecha-Kotui), and others, in which enormous volumes of tholeiitic flood basalts were intermittently formed both before and after the appearance of alkaline intrusions (Kogarko and Zartman, 2007; Kogarko et al., 2010; Ernst and Bell, 2010).

The existence of derivatives of tholeiitic magmas in the Kola magmatic province provides a new insight into the problem of the extent of influence of tectonic processes at the periphery of the Fennoscandian Shield on the character of Paleozoic plume-lithosphere interaction responsible for numerous occurrences of intraplate magmatism. Our investigations allowed us to localize the zone of dolerite dyke occurrence in a coast of the Barents Sea over a distance of more than 650 km from Mageroy Island to the Svyatoi Nos Peninsula, i.e., the junction zone between the Murmansk block and geologic structures of the Barents Sea basin. In terms of tectonics, this oceanic region is an extended wedge-shaped structure cutting the continental margin platform from north to south and adjoining the system of pericratonic depressions of the East European platform at the level of the Fennoscandian shield. Geophysical data indicate a considerable thickness (>20 km) of the Paleozoic— Mesozoic sedimentary cover (Shipilov, 2015); hence, it can be supposed that the geometry of the lithosphere changes significantly in a zone bounding in the north the region of the mantle keel, the central and thickest parts of which are situated in the Belomorian zone (Kukkonen and Peltonen, 1999; Glaznev, 2003). The variable thickness of the asthenospheric layer in the transition zone between the mantle keel and oceanic crust can be considered as a reason for the asymmetry of the Paleozoic plume, which gave rise to all the occurrences of Paleozoic magmatism. According to the numerical model of Burov et al. (2007), the asymmetry of the plume had developed over several million years owing to its ascent into the region of the mantle keel and displacement of the plume head to the periphery of the keel. This process could be accompanied by the activation of different magma generation levels, which resulted in mantle melting at different depth facies. As to the Paleozoic processes in northeastern Fennoscandia, this model is supported by the different mantle sources of tholeiitic and alkaline melts, which were derived at the spinel and garnet depth facies, respectively. The regular spatial distribution of the dolerite dykes and alkaline intrusions relative to the area of the thickest mantle keel also supports the lateral zoning of Paleozoic magmatism.

Subsequent events. Analysis of the information shows an absence of any geological or geochronological evidence for post-Devonian geological events that took place within the Kola Peninsula and the adjacent region of the Fennoscandian Shield. In order to obtain new data corresponding the modern criteria of reliability, we carried out paleomagnetic studies of dolerite and alkaline lamprophyric dykes, whose ages fall within the interval of 390–370 Ma according to the geochronological methods (Rb–Sr, Sm–Nd, $^{40}Ar/^{39}Ar$). Principal component analysis has shown that natural remanent magnetization apart from the Paleozoic component, contains another magnetization component, whose direction close to the known Mesozoic (Middle Jurassic) one, which was found in nearly all the studied dolerite dykes of the Barents Sea shore, in the northern framing of the Pechenga structure and alkali lamprophyres of the southern part of the region (Veselovskiy et al., 2013, 2016); the geochronological age of all these objects was also estimated to be as old as the Devonian (Veselovskiy et al., 2013; Arzamastsev et al., 2017). In a series of samples, this magnetization component is found jointly with the components of Devonian age (the Pz group), occupies the middle part of the spectrum of blocking temperatures, and has steep positive inclinations. The samples from Archean gneisses that host Devonian dykes, taken at distances up to several hundred meters from dykes to implement the baked contact test, usually carry only the Mz magnetization component. The paleomagnetic pole, calculated at the site level and corresponding to the average direction of the Mz component, tends to the Mesozoic part of the apparent polar wander path for the East European Craton that can be considered as a direct sign about the time of formation of this magnetization component.

In order to find manifestations of post-Devonian thermal event which was responsible for remagnetization of dolerite dykes and alkaline complexes, apatite fission track (AFT) dating of samples was performed. Samples were selected from the main rock types of the Paleozoic Khibina (Veselovskiy et al., 2015), Kovdor and other Pz alkaline intrusions, and from Archean alkaline granites of the eastern part of the Kola. Mean track lengths (MTL) value lie between 12.5 and 14.4 μm. Inverse time–temperature modeling was conducted on the age and track length data from seven samples of the Khibina massif. Thermal histories that best predict the measured data from three samples with the most reliable data show three stages: (1) 290–250 Ma—rapid cooling from 110 °C to 70 °C/50 °C for lower/upper sample correspondingly; (2) 250–50 Ma—a stable temperature stage; (3) 50–0 Ma—slightly increased cooling rates down to modern temperatures. We propose that the first cooling stage is related to late-Hercynian orogenesis; the second cooling stage may be associated with tectonics accompanying with opening of Arctic oceanic basin. The obtained data show that geothermal gradient at the center of Kola Peninsula has remained close to the modern value of 20 °C/km for at least the last 250 Myr. AFT data show that the Khibina and the other Paleozoic massifs have been exhumed not more then 5–6 km in the last 290 Myr.

References:

Arzamastsev AA, Veselovskiy RV, Travin AV, Yudin DS, Belyatsky BV. (2017) Paleozoic tholeiitic magmatism of the Kola Province: areal distribution, ages, and relation to alkaline magmatism. Petrology 25 (1): 42-65. DOI: 10.1134/S0869591116060023

Arzamastsev AA Wu Fu-Yan (2014) U–Pb Geochronology and Sr–Nd Isotopic Systematics of Minerals from the Ultrabasic Alkaline Massifs of the Kola Province. *Petrology* 22 (5): 462-479. DOI: 10.1134/S0869591114050026.

Burov E, Guillou-Frottier L, d'Acremont E. Le Pourhiet L. Cloetingh S. (2007) Plume head lithosphere interactions near intra-continental plate boundaries. *Tectonophysics* 434: 15-38. doi.org/10.1016/j.tecto.2007.01.002

Ernst R, Bell K. (2010) Large igneous provinces (LIPs) and carbonatites. *Mineral. Petrol.* 98: 55-76. DOI 10.1007/s00710-009-0074-1

Kogarko LN, Zartman RE. (2007) A Pb isotope investigation of the Guli massif, Maymecha-Kotuy alkaline-ultramafic complex, Siberian flood basalt province, Polar Siberia. *Mineral Petrol* 89: 113-132. DOI 10.1007/s00710-006-0139-3.

Kogarko LN, Lahaye Y, Brey GP. (2010) Plume-related mantle source of super-large rare metal deposits from the Lovozero and Khibina massifs on the Kola Peninsula, Eastern part of Baltic Shield: Sr, Nd and Hf isotope systematics Miner Petrol 98:197–208. DOI 10.1007/s00710-009-0066-1

Koptev AI, Calais E, Burov EB, Leroy S (2015) Dual continental rift systems generated by plume-lithosphere interaction. *Nature Geosci* 8: 388-392. DOI: 10.1038/NGEO2401

Kramm U, Kogarko LN (1994) Nd and Sr isotope signatures of the Khibina and Lovozero agpaitic centres, Kola Alkaline Province, Russia. *Lithos* 32: 225-242.

Kukkonen IT, Peltonen P (1999) Xenolith-controlled geotherm for the central Fennoscandian Shield: implications for lithosphere–asthenosphere relations. *Tectonophysics* 304: 301-315.

Shipilov EV (2015) Late Mesozoic magmatism and Cenozoic tectonic deformation of the Barents Sea continental margin: implication to Hydrocarbon Potential Distribution, *Geotectonics* 49(1): 53-74. DOI: 10.7868/S0016853X1501004X

Veselovskiy RV, Bazhenov ML, Arzamastsev AA (2016) Paleomagnetism of Devonian dykes in the northern Kola Peninsula and its bearing on the apparent polar wander path of Baltica in the Precambrian. Tectonophysics 675: 91–102. http://dx.doi.org/10.1016/j.tecto.2016.03.014

Veselovskiy RV, Thomson SN, Arzamastsev AA, Zakharov VS (2015) Apatite Fission Track Thermochronology of Khibina Massif (Kola Peninsula, Russia): Implications for post-Devonian Tectonics of the NE Fennoscandia. Tectonophysics 665: 157-163. http://dx.doi.org/10.1016/j.tecto.2015.10.003

Veselovskiy RV, Arzamastsev AA, Demina LI, Travin AV, Botsyun SV (2013) Paleomagnetism, Geochronology, and Magnetic Mineralogy of Devonian Dikes from the Kola Alkaline Province (NE Fennoscandian Shield). Izvestiya Physics of the Solid Earth 49(4): 526–547. DOI: 10.1134/S106935131303018X.

PARADOX OF THE CONSTANCY OF THE DISTRIBUTION COEFFICIENTS OF RARE ELEMENTS IN THE FRACTIONATION OF RARE ELEMENTS IN ALKALINE-BASALT SERIES

Asavin A.M.[1]

[1]Vernadsky Institute of Geochemistry and Analytical Chemistry of the Russian Academy of Sciences, Moscow, Russia, aalex06@inbox.ru

The distribution coefficient of the trace element between mineral and liquid (Kp) is defined as the ratio of the concentration of this element in the mineral to the concentration in the equilibrium melt. In fact, this value is a constant of the reaction of the redistribution of components between the melt and the crystals from which they crystallize, and naturally determines, ultimately, the behavior of rare elements in differentiation. This position has long been widely used by geochemists and based on known Kp values set, a number of successful calculation models for the fractionation of rare elements in volcanic series and intrusive complexes have been published. Especially many such models are built on alkaline-basalt series of oceanic islands. Many old works, and a number of recent calculations, use the permanently chosen values of Kp. And then there is a certain paradox. As the value of the reaction constant Kp depends essentially on the temperature, and consequently in the course of differentiation with a drop in temperature, Kp generally increases strongly in most cases. Such growth in the final acid differentiates can reach several orders of magnitude. It turns out that the success of calculations with a constant value of Kp contradicts our idea of a change in Kp under the influence of temperature.

The equilibrium temperatures were estimated by geothermometers [Toplis 2005; Putirka, 2008]. The performed geothermometry shows that in the course of evolution the equilibrium temperature decreased by 100-150 degrees. It was possible to obtain data on the variations in Kp as during differentiation, and within individual groups of rocks (Table 1). Here, due to the limited volume, we give data only for the characteristic elements - Ni and Co. An interesting fact was that very often within the same type of volcanics the equilibrium temperatures also have a very wide interval reaching hundreds of degrees. It is also interesting to note that, since in the main series in these series the crystallization takes place in the cotectic conditions of simultaneous crystallization of olivine and pyroxene their calculated temperatures are quite close. This incidentally proves the equilibrium of the analyzed mineral-groundmass pairs.

Table 1. Distribution Kp variation and thermometric Ol Cpx minerals.

Sample	oRock	T C by geotermometrs		Kp			
		Ol-Liq	Cpx-Liq	Ol		Cpx	
				Ni	Co	Ni	Co
CE9	A	1220	1250			2.273	1.133
CE1	A	1200	1150	9.97	4.12	1.6	1.047
CE7	A	1150	1060	9.98	5.33	1.76	1.25
12885	A	1230		3.8	4.12	1.95	0.921
12875	A	1280	1090	5.62	3.32		
12873	A	1220	1097	8.61	3.17	2.235	1.383
12896	A	1020		9.37	3.09		
TK46	A	970	970	11.5	5.82	1.515	1.026
TK34	A	900	1050	12.06	5.36	1.32	0.897
TK3	Ab	1040	990	7.05	4.88	1.24	0.8
TK41	Ab		1056			1.32	0.929
TK11	Ob	940		5.61	1.11	1	0.689
TK4	Ob		1100			1.6	0.943
TK7	Ob		1140			1.111	1.026
TK7	Ob	1140		13.8	5.67		
TK40	Ob	1250	980	15.1	5.97	1.27	0.907
TK43	Ob		1048			1.538	1.071
TK35	Ob		1100			1.282	0.971
TK8	Ob	1200	1200			1.458	1.032
TK13	Ob	1080		9.78	5.32	1.268	1.053
12894	Ob	950		4.27	1.64		
CE13	Ob		1071			0.926	0.744
CE2	Ob		967			0.889	0.833
CE17	Ob		900			0.4	0.745
TK42	Tb	900	900			1.136	
TK20	Tb	1000		6.63	4.86		
TK49	Ta		680			1.32	0.929

*A – ankaramite, Ab – ankaramitobasalt, Ob – alkaline olivine basalt, ; Tb – trachibasalt; Ta – trachiandesite

Either there is some factor that, along with a decrease in temperature, affects the value of Kp. A study was conducted to evaluate the variations of Kp olivine and pyroxene in volcanics of differentiated oceanic series: ankaramite – ankaramitobasalt - alkaline olivine basalt - trachibasalt-trachyandesite.

In this connection, we analyzed the data separately for each of the groups of rocks - ankaramites, ankaramitobasalt and alkaline olivine basalts and trachybasalts-trachyandesites. Data on the latter group is small and therefore these points could only help in assessing general patterns. On the chart, conditional trends, therefore, are drawn with two different lines for ankaramites (solid line) and for the rest of the rocks (dotted line). As it turned out, the trends in the change in Kp values for more fractioned differences are significantly different from earlier ankaramites. For olivine, for example, in the first case, the trends correspond to an increase in Kp with decreasing temperature, and for the second trend, the opposite picture is noted. For clinopyroxene, Kp for both groups decreases with decreasing temperature. In general, we can conclude that in the course of differentiation, Kp remain either almost unchanged or decrease. Our data on the Cr-lithophile elements, TR, Sr, Ba, Rb, Pb in two groups of rocks of ankaramites and trachybasalts also show this. These spectra are extremely similar in form and the level of Kr is also close (Fig. 2). Thus, for many elements of Cr of the main dark-colored minerals, the values of Kp change in evolution only slightly, and a decrease in the Kp values is noted for a number of elements.
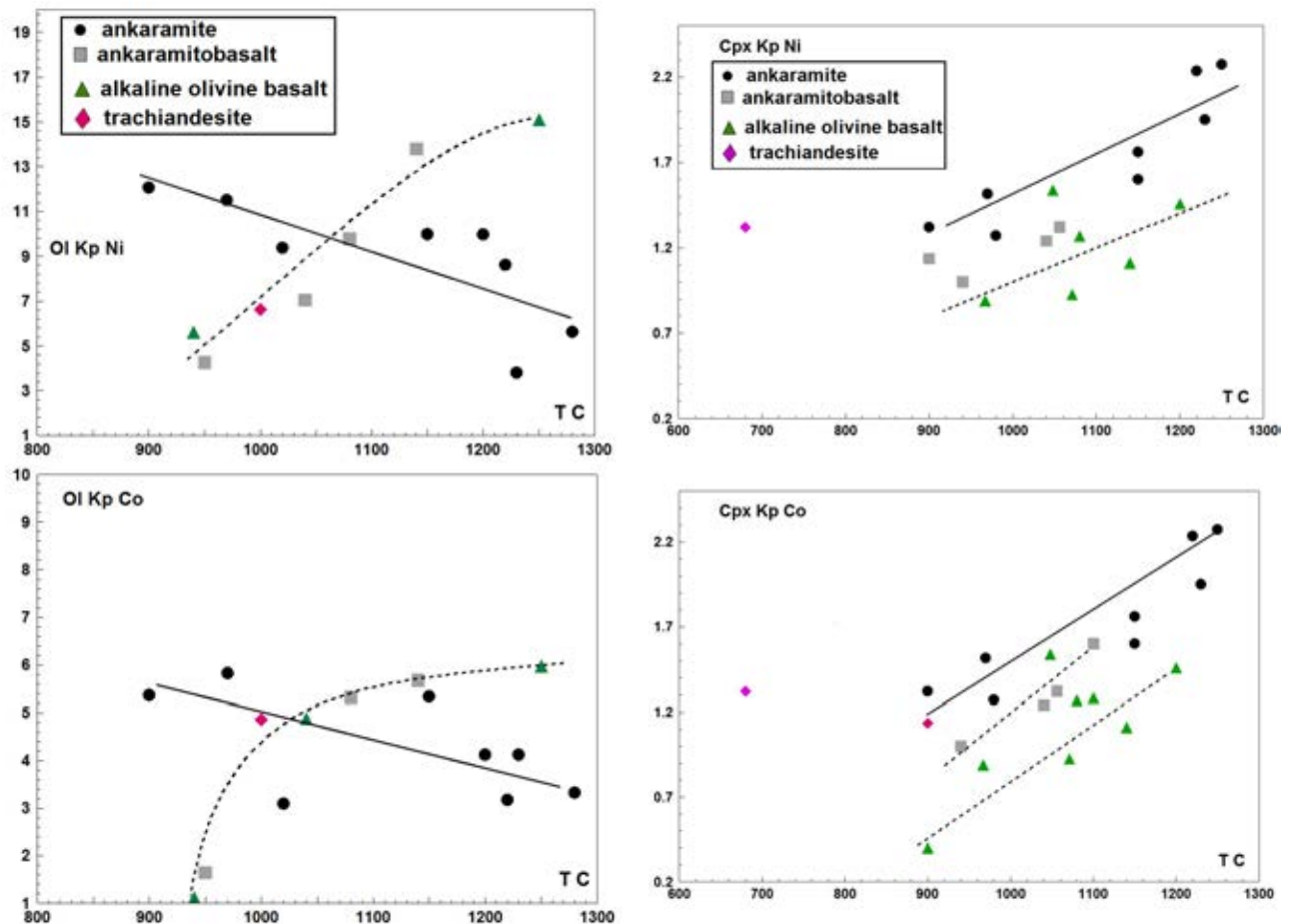
Fig. 1. Kp Ni, Co, variation and trends. In alkaline basalt systems.

An important controlling factor for the value of Kp is the melt alkalinity. Normally, NBO/T is used to estimate it numerically. Figure 3 shows the dependencies for these rock groups on the temperature of the NBO/T value. As can be seen from the figure, the inverse dependence of alkalinity on temperature is typical for ankaramites. In general, the alkalinity varies little and its decrease in the group reaches 1.5 times. In the second group, the picture is the opposite. With the drop in temperature, the alkalinity increases sharply (almost 2.5 times).

Increasing alkalinity leads to a decrease in the value of Kp. Apparently, therefore, this factor blocks the effect of temperature, leading to an increase in Kp and as a result the value decreases or remains at the same level. It should be noted that the natural phase system of the alkaline-basaltic series appears to have a fairly common relationship between the temperature and alkalinity of the melt during evolution. On the contrary, the differentiation of ankaramitic smelters apparently has an unusual evolutionary trend. Actually, in this variety of trends, the cause of the revealed paradox of Kp constancy lies.
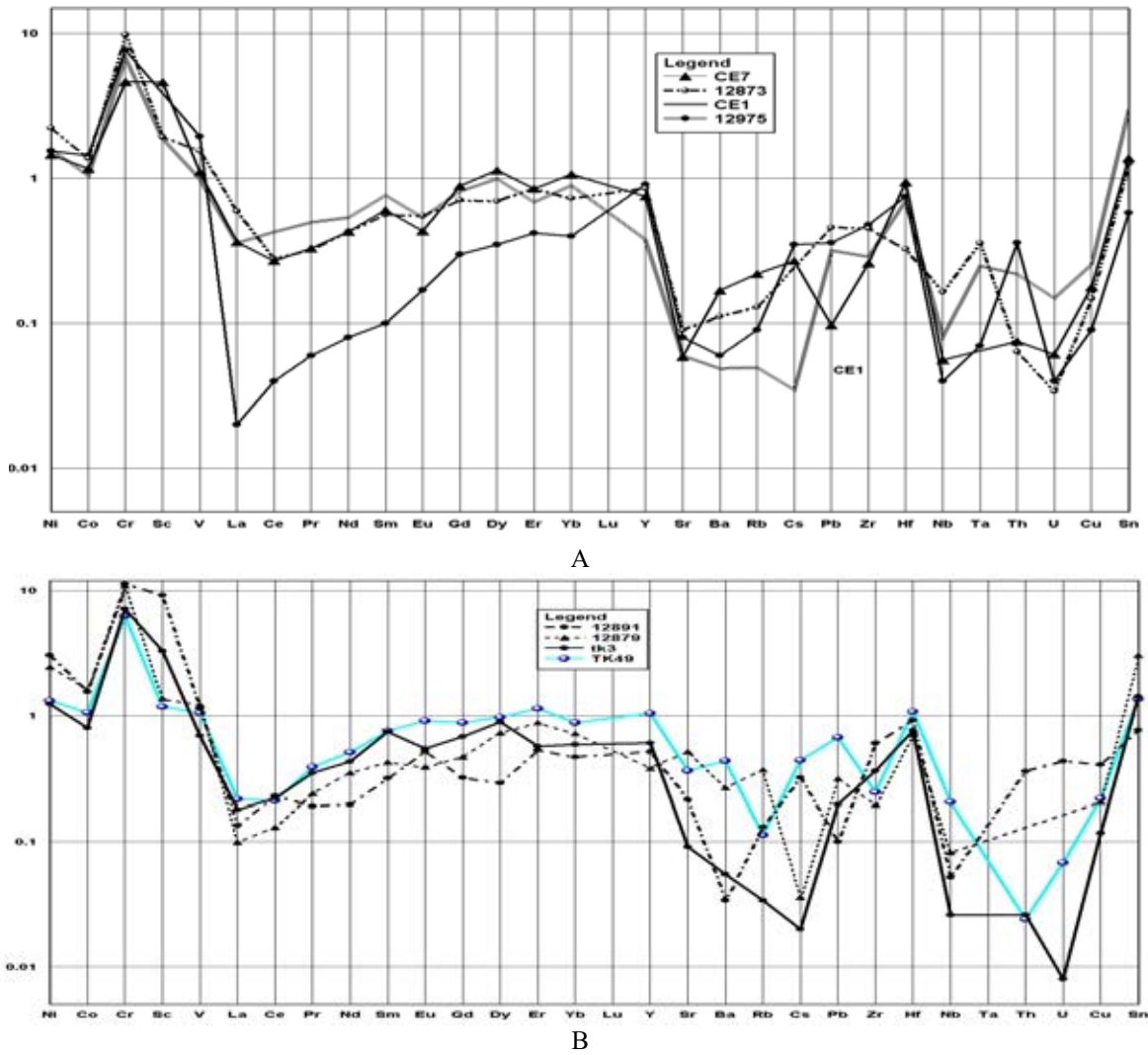
Fig. 2. Kp trace elements for pyroxene in ankaramite (A) and in alkaline basalt and trachibasalt (B).
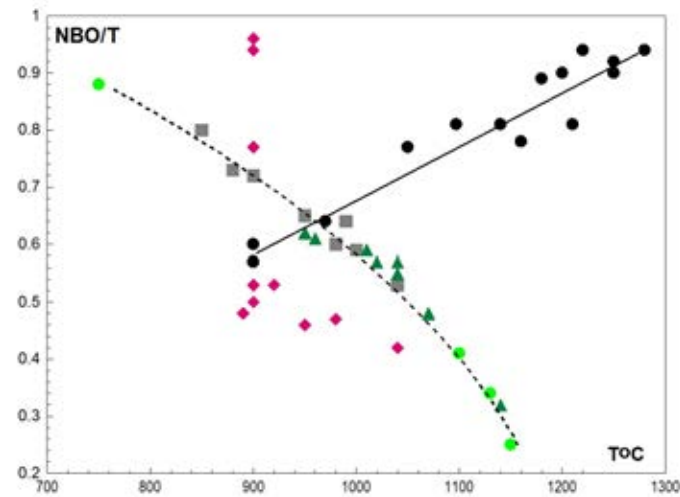

Fig. 3. Dependence between temperature and alkalinity of the melts.

References:

Elkins-Tanton Linda T. , David S, Draper, Carl B. Agee, Jessica Jewell, Andrew Thorpe, Hess P. C. (2007) The last lavas erupted during the main phase of the Siberian food Volcanic province: results from experimental petrology *Contributoin to Mineralogy and Petrology,* 153,pp. 191–209

Toplis M. J. (2005) The thermodynamics of iron and magnesium partitioning between olivine and liquid: criteria for assessing and predicting equilibrium in natural and experimental systems *Contrib Mineral Petrol* , 149: 22–39

VARIETIES OF ECLOGITES AND THEIR LOCATION IN THE CRATONIC MANTLE LITHOSPHESRE REVEALED BY JD-DI AND GARNET TERMOBAROMETRY AND GEOCHEMISTRY

Ashchepkov I.V.[1], Logvinova A.M.[1], Spetsius Z.V.[2], Ntaflos T.[3], Downes H.[4], Vladykin N.V.[5], Kostrovitsky S.I.[5], Ravi S.[6], Stegnitsky Yu.B.[2], Babushkina S.A.[7], Ovchinnikov Y.I.[1]

[1]Institute of Geology and Mineralogy, Siberian Branch of the Russian Academy of Sciences, Novosibirsk, Russia
[2]Alrosa Stock Company, Mirny, Russia [3]Vienna University, Vienna, Austria [4]University of London, UK
[5]Geological Survey of India, Bangalore, India
[6] Vinogradov Institute of Geochemistry, Siberian Branch of the Russian Academy of Sciences, Irkutsk, Russia
[7]Diamond and Precious Metal Geology Institute of Siberian Branch Russian Academy of Sciences, Yakutsk, Russia

Monomineral thermobarometry for clinopyroxenes (based on Jd-Di exchange) and garnets (based om majorite) (Ashchepkov et al. 2017) allow to estimate the position of different groups of eclogites in the cratonic lithospheric mantle of Yakutia and worldwide. The division to three groups (Dawson, 1977) was completed by the Ca- rich group.
We used division eclogites into four large groups (Spetsius et al., 2008; Viljoen et al., 2010) instead of common three groups based on MgO-Na2O variations in clinopyroxene (Dawson, 1980; Neal et al., 1992). Several subgroups can be identified according to previous studies described in literature trace element signatures and by their positions on the PTX diagrams.
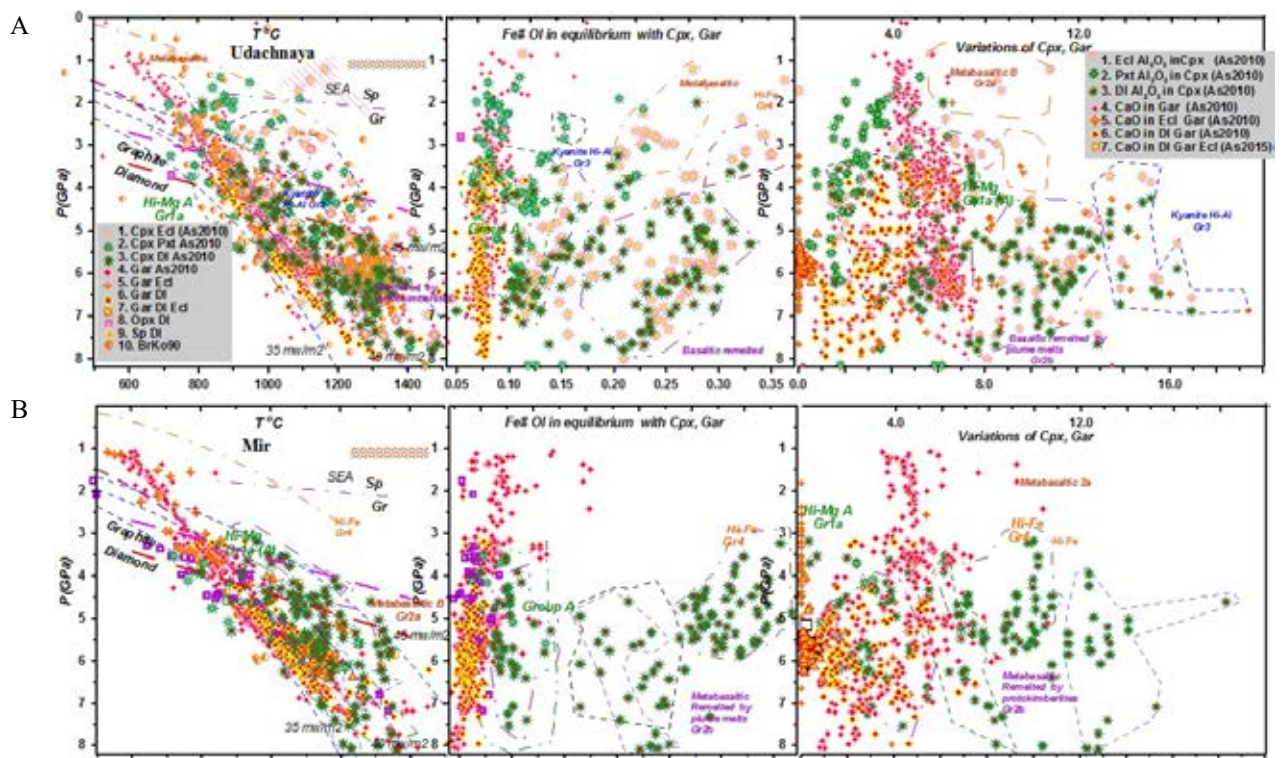

Fig.1. PTX diagram for xenoliths and minerals concentrates from: A) Udachnaya pipe; B) Mir pipe. Symbols: 1. Cpx: ToC Nimis &Taylor, 2000 - P (GPa) Ashchepkov et al., 2010) for common eclogites; 2. The same for pyroxenites; 3. The same for diamond inclusions; 4 Garnet (monomineral): ToC (O'Neill &Wood, 1979) - P (GPa) Ashchepkov et al., 2010); 5. The same for eclogitic diamond inclusions. 6. The same for peridotitic diamond inclusions; 7. The same for eclogitic garnets. 8. Opx for diamond inclusions: ToC (Brey & Kohler, 1990) - P (GPa) (McGregor, 1974); 9. Chromite for diamond inclusions: ToC (O'Neill & Wall, 1987) - P (GPa) (Ashchepkov et al., 2010); 10. Opx- Gar: ToC – P (GPa) (Brey & Kohler, 1990). Position of conductive geotherms are after Pollack & Chapman (1977) and the graphite – diamond transition after Kennedy and Kennedy (1976); the line above after Day (2012).

1. The high-Mg eclogites (Fe=0.07-0.15) (Group A) consist of several Groups: 1a) a Cr-bearing group formed after crystallization of partial melts produced by volatile fluxes or heating (Heaman et al., 2006; Smart et al., 2009); 1b) a group formed by hybridization of subduction-related melts and fluids with mantle peridotites (Aulbach et al., 2011); 1c) a group derived by crystallization of differentiated protokimberlite melts (Haggerty et al., 1979; Kamenetsky et al., 2009); 1d) a low-Cr group which could be restites (Wyman & Kerrich, 2009) or deep cumulates from tonalite- trondhjemite magmas or Mg-rich arc magmas (Horodytskyi et al., 2007; Barth et al., 2002).
2. The largest group (Group B) with Fe# (~ 0.20-0.30, moderate Al2O3 and Na2O values, commonly reveal Eu anomalies. The most abundant rocks form Group 2a interpreted as subducted basalts and their modifications as well as eclogitized metagrabbro (with relics of ophitic structures), close to MORB basalts (Jagoutz et al., 1974; Beard et al., 1996;

Pearson, 1995; Snyder et al., 1997) reacted with oceanic water (Neal et al., 1990). Enriched "gabbroic" type. Group 2b eclogites are thought to be products of fluid melting of ancient oceanic crust and interaction with peridotites during subduction (Aulbach et al., 2007). Group 2c eclogites are considered as shallow mantle basaltic cumulates derived from plume or ancient arc magmas in cratonic margins (Wyman & Kerrich, 2009); those near Moho may be eclogitized lower crustal cumulates (Shu et al., 2014). Group 2d eclogites are "metabasaltic of remelting or hybridization with protokimberlite and other plume melts (Shatsky et al., 2008).

3. The high-Fe -Na Group 4 (Group C) eclogites (Fe# > 0.27) may be subducted Fe- basalts (Group 3a); Ca-enriched varieties may be meta-tonalites or trondhjemites (Group 3b) (Barth et al., 2002) and those which are very rich in Al could be metasediments (Group 3c) (Mazzone & Haggerty, 1989).

4. High –Ca- Al Group eclogites were divided to: Group 4a rocks are high-Ca and low-Fe varieties, commonly Al-rich and kyanite-bearing (sometimes with coesite) (grosspydites) which may be originally carbonate metasomatites (Smyth, 1977) or metapelites (Liou et al., 2014); Group 4b eclogites are high-Ca and moderate-Fe and may be ancient Mg-granites (Barth et al., 2002; Jacob et al., 2003) .

High-Mg eclogites (produced by partial melts or arc cumulates) are related to low-temperature geotherms and commonly refer to the lower part of the mantle sections.

Beneath Siberia and most localities worldwide the Na- Al -Fe- rich eclogites were found within the 3.5-4.0 GPa pressure interval were formed in Early Archean time when the mantle lithosphere was 130 km in thickness. In the Middle and Late Archean, eclogites and their restites divided subducted peridotite layers.

During the subduction partial melts of eclogites group B created ascending channels and reacted with peridotites producing hybrid Cr- bearing high alumina pyroxenites sometimes. But most eclogites crystallized in Cr- less system but most of them demonstrate magmatic signs.

Melt-metasomatized eclogites commonly trace high temperature geotherms and are often close to the middle part of the mantle lithosphere. Abundant eclogitic diamond inclusions from Siberia also mostly belong to the middle part of the lithosphere. Ca-rich eclogites (group D) from Precambrian kimberlites of India are located in the middle lithospheric mantle whereas those entrained in Phanerozoic magmas are derived from the lithosphere base. In the Wyoming craton, kimberlites carry eclogite xenoliths captured from the 4.0-2.5 GPa interval. In mantle lithosphere sampled by Proterozoic kimberlites, Ca-rich eclogites and grospydites occur in the 4.0-5.0 GPa interval.

Most eclogites in the mantle sections beneath Udachnaya and Mir pipes refer to the group B and show the showing an increase in Fe# with the decreasing pressures. They show very wide thermal conditions tracing from 33 to 45 mv/m geotherms.
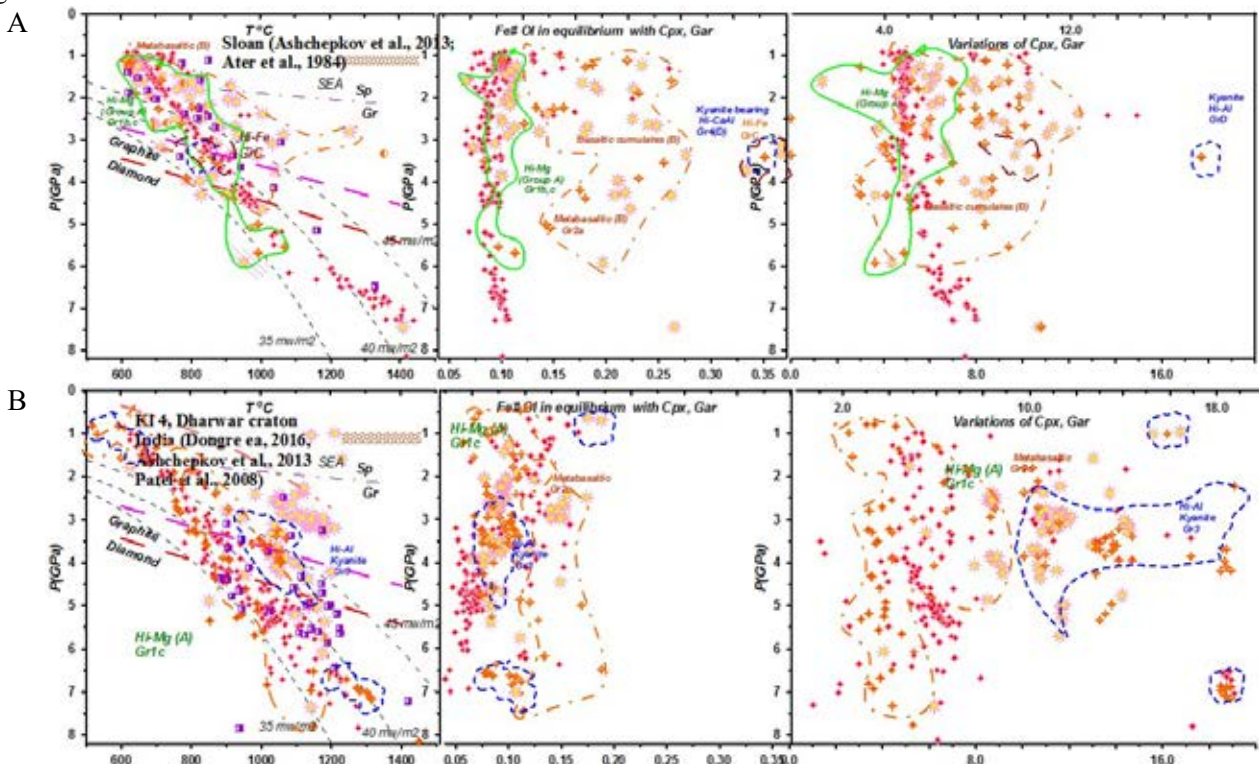

Fig. 2. PTX diagram for xenoliths and mineral concentrates from: A) Sloan pipe, Front range field, Wyoming craton; B) Kl-4 pipe, Wajrakarur field; Dharwar craton. Symbols are the same as for Fig. 1.

The eclogitic diamond inclusions in Nyurbinskaya pipe Ca-Al rich type and found in the lower part of SCLM. Th Ebelyakh diamond inclusions (Shatsky et al., 2016) show wide range of PT conditions. In Precambrian kimberlites South

Africa HT eclogites and diamond eclogitic inclusions like in Premier kimberlites are derived from the deeper part of the mantle lithosphere and trace a high-T geotherm at depths of 7.0-4.0 GPa and as well in Kl4 pipe in Dharwar craton.
 Similar trends are common beneath the Catoca cluster kimberlites in Angola where there many hybrid eclogites and Lace kimberlites (Aulbach, Viljoen,2015). Very often remelting tend to the transition eclogites to pyroxenites.
Mantle eclogites have clinopyroxenes and garnet trace element patterns with opposite inclinations determined by melt KDs. Flatter and bell-like REE patterns with HFSE troughs and U, Pb peaks are common for MORB-type eclogites. High-Mg eclogites show less fractionated incompatible element patterns. LILE-enrichments and HFSE troughs are typical for kyanite-bearing eclogites. Clinopyroxenes from diamond-bearing eclogites show lower REE and troughs in Nb and Zr, peaks in Pb and U concentrations compared to barren eclogites with round smooth trace element patterns and small depressions in Pb and Ba.Supported by RFBR grant 16-05-00860a.
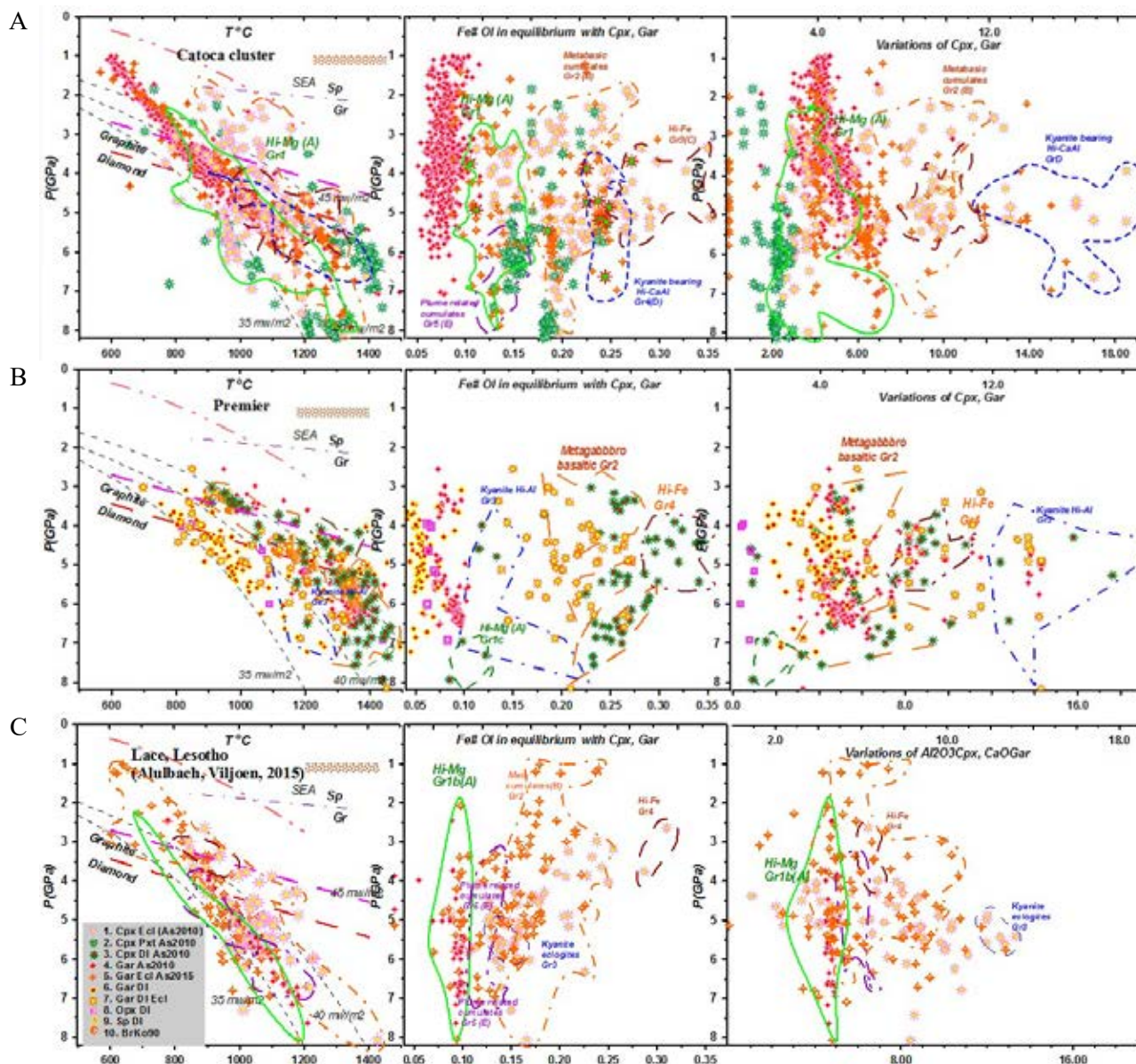
Fig. 3. PTX diagram for xenoliths and mineral concentrates from: A) Catoca cluster, Kasai craton. B) Premier pipe, Kaapvaal craton. C) Lace pipe, Kaapvaal craton. Symbols the same as for Fig.1

References:

Ashchepkov, I.V., Vladykin, N.V., Ntaflos, T., Downes, H., Mitchell, R., Smelov, A.P., Alymova, N.V., Kostrovitsky, S.I., Rotman, A.Ya, Smarov, G.P., Makovchuk, I.V., Stegnitsky Yu.B., Nigmatulina E.N., Khmelnikova O.S. . Regularities and mechanism of formation of the mantle lithosphere structure beneath the Siberian Craton in comparison with other cratons// Gondwana Research. 2013. v.23, № 1.. pp. 4-24.

2. Ashchepkov I.V., Kuligin S.S., Vladykin N.V., Downes H., Vavilov M.A., Nigmatulina E.N., Babushkina S.A., Tychkov N.S., Khmelnikova O.S. Comparison of mantle lithosphere beneath early Triassic kimberlite fields in Siberian craton reconstructed from deep-seated xenocrysts.// Geoscience Frontiers -2016- V. 7, № 4.- pp. 639–662.

3. Ashchepkov I.V., Logvinova A.M., Ntaflos T., Vladykin N.V., Kostrovitsky S.I., Spetsius Z., Mityukhin S.I., Prokopyev S.A., Medvedev N.S., Downes H. Alakit and Daldyn kimberlite fields, Siberia, Russia: Two types of mantle sub-terranes beneath central Yakutia?// Geoscience Frontiers -2017- (в печати)

4. Ashchepkov, I.V., Vladykin, N.N., Ntaflos, T., Kostrovitsky, S.I., Prokopiev, S.A., Downes, H., Smelov, A.P., Agashev, A.M., Logvinova, A.M., Kuligin, S.S., Tychkov, N.S., Salikhov, R.F., Stegnitsky, Yu.B., Alymova, N.V., Vavilova, M.A., Minin, V.A., Babushkina, S.A., Ovchinnikov, Yu.I., Karpenko, M.A., Tolstov, A.V., Shmarov, G.P., Layering of the lithospheric mantle beneath the Siberian Craton: Modeling using thermobarometry of mantle xenolith and xenocrysts.// Tectonophysics -2014. № 5.- 634,- pp.55–75.

VERTICAL MASS TRANSPORT IN CONTINENTAL LITHOSPHERE AND MAGMATIC METALLOGENY

Bagdassarov N.S.

Goethe Universität Frankfurt am Main, Frankfurt am Main, Deutschland, nickbagd@geophysik.uni-frankfurt.de

Ore deposits are non-uniformly distributed in the continental crust in time and in space, which is attributed to an uneven and impulsive character of the vertical mass transfer in the continental crust. The periods of metallic mineralization may be explained by a stepwise character of continental block collisions, and lithospheric compression - extension stages. The crustal mass transport mechanisms include flow of melts, crystallizing magmas, dense fluids and volatiles. These types of flows are accompanied by fluid/melt phase separation, flow differentiation, and particle/gas barbotage due to secondary boiling. Several principle geodynamic environments are playing a key role in the ore-deposit formation: 1. Hydro-thermal activity and fluid circulation above zones with an anomaly heat flux (Heinrich et al., 2004). A high temperature-pressure solubility of some elements drops under cooling in the upper part of the crust favoring precipitation of some metals from fluids in rock fractures. The examples is sedimentary-exhalative (SEDEX) mineralization (Olson et al., 1994) or a stratabound sediment hosted mineralization of sulphides, associated with elevated concentrations of some metals. The SEDEX mineralization might have formed by accumulation of sulphides from vent-distal metalliferous brine pools (generally <250°C) in an anoxic environment on the seafloor or just below the sediment surface due to hydrothermal activity controlled by active extensional faults within the rift basin. 2. Porphyry deposits which origin is correlated with an escape of magmatic fluids from crustal magma chambers. In magmatic systems many types of ore deposits, including world-class deposits of Cu and Au, melts are commonly an important source of metals and ore-forming fluids (porphyry style ore formation due to the cooling of hydrous magma chambers). In many magmatic-hydrothermal systems, low-density and high-mobile aqueous fluids, or vapors, are significant metal carriers by itself. 3. A magmatic fluid may also separate into two phases at the depth or during a vertical transport to the surface. Light and less viscous component of this physical separation may be transported effectively in fractured porphyry rocks reaching fast the upper epithermal environment (Heinrich et al., 2004). 4. The change of local redox conditions in upper crustal rocks may cause a secondary precipitation and mineralization. Fluxing of CO_2-rich vapor exsolved from deeper magma leads to a sharp drop in metal solubility, up to a factor of several orders of magnitude and thereby provides a highly efficient mechanism for metal deposition (van Hinsberg et al., 2016). 5. Particle segregation, suspension and transport during uprising flow of crystallizing magmas. For iron oxide–apatite (IOA) deposits there are three radically different processes suggested for their formation. a. Direct crystallization of immiscible Fe-rich melt that separated from a parent silicate magma. b. Deposition of Fe-oxides from hydrothermal fluids of either magmatic or crustal origin. c. Enhanced concentration of magnetite takes place by the preferred wetting of magnetite, followed by buoyant segregation of the early formed magmatic magnetite-bubble pairs, which become a rising magnetite suspension that deposits massive magnetite in regional faults (Knipping et al., 2015). The presence of low water activity fluids such as high-density CO_2 and/or concentrated saline solutions (granulate fluids) cause seismic activity which may continue till the free fluids leave the granulite-facies environment during repeated retrograde events ending in formation of quartz veins commonly associated with the vein-type Au deposits.

References:

Heinrich, C. A., Driesner, T., Stefánsson, A., Seward T. M. (2004) An overview of hydrodynamic studies of mineralization. Geology 32(9), 761–764

van Hinsberg, V. J., Berlo, K., Migdisov, A.A., Williams-Jones, A. E. (2016) CO2-fluxing collapses metal mobility in magmatic vapour Geochem. Persp. Let. 2, 169-177

Knipping, J.L., Bilenker, L.D., Simon, A. C., Reich, M., Barra, F., Deditius, A.P., Lundstrom, C., Bindeman, I., Munizaga, R. (2015) An overview of hydrodynamic studies of mineralization. Geology 43(7), 591-594

Olson, R.A., Dufresne, M.B., Eccles, D.R., Freeman, M.E. and Richardson, R.J.H. (1994) Regional metallogenic evaluation of Alberta; Alberta Research Council, Alberta Geological Survey, URL http://www.ags.gov.ab.ca/publications/abstracts/OFR_1994_08.html.

THE ROLE OF THE PALEOZOIC SUPERPLUME IN THE FORMATION OF THE GEOLOGICAL STRUCTURES OF KAZAKHSTAN WITH LARGE METAL DEPOSITS

Baibatsha A.B.

Kazakh National Research Technical University named after K.I. Satpaev, Almaty, Republic of Kazakhstan, baibatsha48@mail.ru

According to various estimations, between half and three quarters of the modern continental crust of Kazakhstan was formed in the Early Precambrian to the beginning of the late Proterozoic as continent «Qazaqia» (Koronovskij N.V. *et. al.,* 2008). As a result of atrophy and the closure of the Early Proterozoic deep basin, this crust in the Early Riphean was shrunk into a single supercontinent called *Pangaea* I or *Megageya*, unlike Late Paleozoic-Early меsozoic *Pangaea II* (firstly isolated by A. Wegener). On the supercontinent, the paleomagnetic data indicated that the similarity of the curves of apparent migration of the magnetic poles that define different continents. With the beginning of Proto-Tethys mobile belt, Pangaea I was split into two parts, original part (Rodinia) in the north and Gondwana in the south. Already in the Neoproterozoic Kazakhstan began to exist independently (Heraskova T.N. *et. al.,* 2010).

Assigned by modern geophysical data (Daukeev S.Zh. *et. al.*, 2004; Uzhkenov B.S. *et. al.,* 2004) that the introduction of the plume and the picked materials from the mantle and the asthenosphere into the lithosphere led to local rising and the formation of a fixed nuclei in the form of ring structure (the prototype of the Qazaqia continent). The nuclei-ring structure diameters were approximately 2.5-3.0 km.

The action of mantle plumes is known in Archean, Proterozoic and Paleozoic (Joachim R.R. *et al.,* 2007; Pirajno. F., 2007; David A. Yuen *et al.,* 2007*;* Baibatsha A.B.; 2008, 2016; Zhirov D.; 2016)

The role of mantle superplume in the formation of Kazakhstan subsurface geodynamics

New data on the deep structure of the crust and upper mantle of continents form complex studies of the international system geo-traverses were collected. Some of them have been laid through the territory of Kazakhstan. On their basis, the models of the lithosphere to a depth of 100-200 km in the Republic were established, which revealed non-uniform-block structure of the upper mantle. At a depth of about 200 km, the mantle electrical resistance is dramatically reduced, which presumably is linked with the rise of the roof of the asthenospheric layer. The structures of the crust in some cases are continuing in the upper mantle. Asthenosphere in the geo-suture areas rise to the level of 80-100 km, and asthenolith penetrate above the Moho in the crust (Figure 1).

Fig. 1 Tectonic map of Kazakhstan with ring structures.

The vertical oscillatory motion covered both the individual rings and geosuture zones between the ring structures. During the non-uniform oscillatory motion, when one margin of a continent or a single ring structure sank, while the other rose, on them were formed, marine or continental conditions, respectively. Sea in form of narrow channel was often infiltrated in geosuture zones. The general intensive thermodynamic conditions had led to a fairly dense network of fractures in consolidated rigid ring structures (Dobretsov N.L. *et. al.,* 2001; Glubinnoe stroenie, 2002, Koshkin V.Ya., 2008).

Starting from Ediacaran, Qazaqia continent was actively influenced by the surrounding continents. In the Paleozoic era, continental margin washed the ancient oceans between the approaching neighboring continents – Paleo-Asian (between Siberia), Paleo-Urals (between Eastern Europe) and Paleo-Tethys (between Cat-Asia, Tarim). Also strata of sedimentary rocks with relevant mineral resources were accumulated. Geosuture shifting (concentric faults under the pressure of intra-drifting

nearby continents) was intensified and individual strained blocks were subjected to further autonomous shifts (Golonka J. *et. al.,* 2006; Baibatsha A.B., 2008, 2016).

The external part of nuclei with a width of 500-600 km, which is located in western Kazakhstan (the Kara Kum Ustyurt-Precaspian-Ural tectonic system) has presented its own plate as a flank of the Mediterranean region (Koshkin V.Ya., 2008).

The most active parts of the continent Qazaqia are geosuture zones and faults which have a direct connection with the mantle. On the active zone ,the introduction of magma in the crust was a primary mantle intrusion. These intrusions in the upper crust were assimilated with its components. During the geosuture subsidence was formed sea channels and basins where volcanic eruptions were occurred and oceanic crust with typical ophiolite rockcomplexs were formed. The deep faults and zones of crushing served as ore-bearing fluids channels in the upper crust. The flooded areas of the sea created typical marine conditions, i.e. «Oceanic» environment. Ring structures were Orogey zone with active volcanoes, magma intrusions- mostly ultramafic, sedimentary basins and denudation islands arcs.

The proposed geodynamic model of the Kazakhstan development explains the features of the localization of active zones of sedimentation, intrusions and effusive magmatism and metamorphism of the geological formations, ophiolitic zones and olistostromes availability and promising metallogenic zones and areas with large and unique mineral deposits (Figure 2).
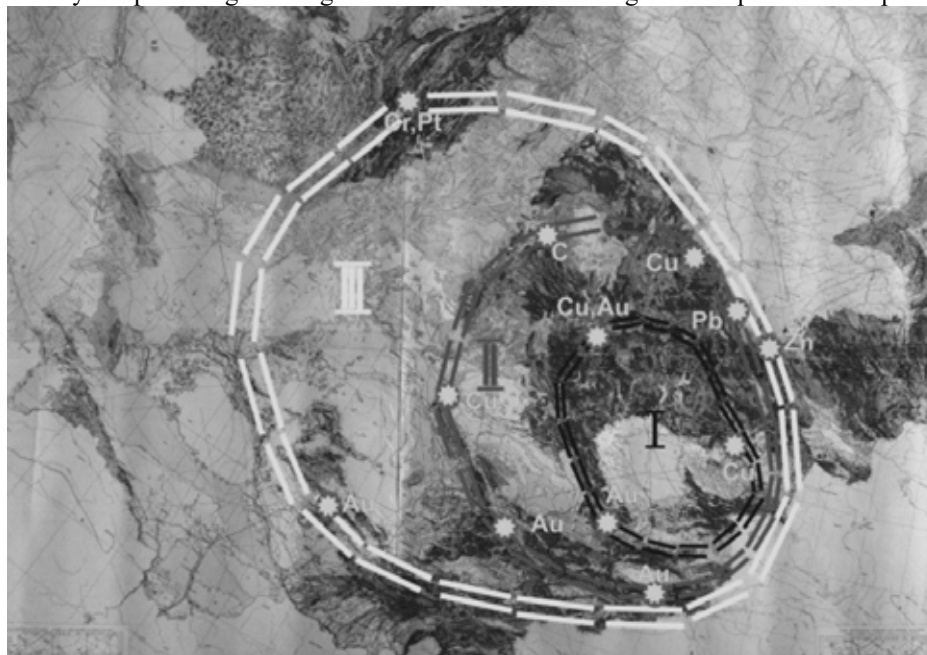
Fig. 2 Location of metallogenic zones with the largest metal deposits.

References:

Baibatsha A.B. O novom vzglyade na geologicheskoe stroenie i geodinamicheskoe razvitie territorii Kazahstana//Izv. NAN RK, seriya geol., 2008, № 2. S. 66–74.

Baibatsha A.B. Plume-tectonic nature of geological structures and geodynamics of the territory of Kazakhstan // GeoBaikal 2016 - Irkutsk, Russia, August 22-26, 2016

Daukeev S.Zh., Uzhkenov B.S., Lyubeckij V.N. Evolyuciya Zemli i processy formirovaniya mestorozhdenij//Geologiya Kazahstana. Almaty, 2004.

David A. Yuen, Shigerenori Maruyama, Shun-Ichiro Karato, Brian F. Windley. Superplumes: Beyond Plate Tectonics. 2007. XIV, 569 p. ISBN: 978-1-4020-5749-6.

Dobretsov N.L., Kirdyashkin A.G., Kirdyashkin A.A. Glubinnaya geodinamika. – Novosibirsk, SO RAN, 2001. 409 s.

Glubinnoe stroenie i mineral'nye resursy Kazahstana. T. 1. Glubinnoe stroenie i geodinamika. Almaty, 2002. 224 s.

Golonka J., Krobicki M., Pajak N., Zuchiewicz W. Global plate tectonics and paleogeography of southeast Asia. Krakow. 2006. 128 p.

Heraskova T.N., Bush V.A., Didenko A.N., Samygin S.G. Raspad Rodinii i rannie stadii razvitiya Paleoaziatskogo okeana // Geotektonika, 2010, № 1. S. 5–28.

Joachim R.R., Ritter, Ulrich R. Christensen. Mantle Plums. 2007. VIII, ISBN: 978-3-540-68045-1. 502 p.

Koronovskij N.V., Hain V.E., Yasamanov N.A. Istoricheskaya geologiya: uchebnik dlya studentov vuzov. M., Izdatel'skij centr «Akademiya». 2008. 464 s.

Koshkin V.Ya. Paleozoidy zapadnoj chasti Uralo-Mongol'skogo skladchatogo poyasa // Geologiya i ohrana nedr. – 2008, № 3(28). S. 2–10.

Pirajno. F. Ore Deposits and Mantle Plumes. 2000. 576 p. ISBN: 978-0-412-81140-1.

Tektonicheskaya karta Kazahstana. Ob"yasnitelmnaya zapiska/V.YA. Koshkin i dr. Almaty, 2007. 130 s.

Uzhkenov B.S., Mazurov A.K., Bykadorov V.A. i dr. Paleogeografiya i geodinamika Kazahstana i sopredel'nyh territorij. V kn: Geonauki v Kazahstane. Almaty, 2004. S 39–54.

Zhirov D. Controlling sntructures of the Paleozoic Plume in the Kola alkaline large igneous Province//16th International Multidisciplinary Scientific Geoconference SGEM2016, 30 June - 6 July, 2016, Albena, Bulgaria. 2016. ISBN 978-619-7105-55-1. PP. 133-140.

SULFIDE MINERALIZATION OF SILICATE MANTLE BY REDUCED S-BEARING METASOMATIC FLUIDS AND MELTS

Bataleva Y.V.[1,2], *Palyanov Y.N.*[1,2], *Borzdov Y.M.*[1,2]

[1]Institute of Geology and Mineralogy, Siberian Branch of the Russian Academy of Sciences, Novosibirsk, Russia
[2]Novosibirsk State University, Novosibirsk, Russia, bataleva@igm.nsc.ru

According to modern concepts, the subduction processes play one of the main roles in the global geochemical sulfur cycle that describes the behavior of sulfur in deep zones of the Earth (Evans, 2012). Data on composition of inclusions in diamonds and minerals of mantle xenoliths as well as the results of experimental studies indicate that sulfur in the lithospheric mantle, depending on P-T-fO_2,
can occur as sulfides/sulfide melts, sulfates, C-O-H-S fluid, or can present in dissolved form in silicate melts. In recent years, the behavior of sulfur in mantle metasomatic processes with implications for sulfide genesis in eclogites and peridotites of the subcontinental mantle have been extensively studied (Alard et al., 2011; Bataleva et al., 2016). In particular, a number of studies have suggested that sulfide formation can occur during interaction between reduced S-bearing fluids and silicate minerals, i.e. via the sulfidation reactions (Lehner et al., 2013). These reactions are very probable upon subduction of S-bearing rocks into a silicate mantle that is accompanied by the generation of melts and fluids, which are metasomatic agents enabling sulfur mobilization. However, experimental studies in this direction are still rare. The main sulfidation reactions are supposed to be as follows: $Fe_2SiO_4 + S_2 \rightarrow 2FeS + O_2 + SiO_2$, and $2Fe_2SiO_4 + S_2 = 2FeS + Fe_2Si_2O_6 + O_2$.

To understand the mechanism of sulfide formation upon interaction between S-bearing melts/fluids and mantle silicates in the lithospheric mantle, experimental studies were performed in olivine-sulfur and olivine-pyrite systems at pressure of 6.3 GPa, in the temperature range of 1050−1550 ºC, and with the duration from 40 to 60 h, on a multi-anvil high-pressure apparatus. The methodical features of experiments, high-pressure cell schemes, and also information on calibration details were published previously (Palyanov et al., 2010; Sokol et al., 2015). The starting materials were natural specimens of Fe,Ni-bearing olivine, with the FeO and NiO concentrations of 9.3 wt% and 0.45 wt%, respectively (garnet lherzolite xenolith from kimberlite of Udachnaya pipe, Yakutia), pyrite (Chelyabinsk region, Russia) with an impurity content of < 0.5 wt%, and powders of chemically pure sulfur (99.99 %). Weight proportions were 7:1 for starting olivine and sulfur and 6:1 for olivine and pyrite. The traditional procedure for the ampoule assembly, in which starting reagents are finely crushed and homogenized, was used to provide optimal conditions for the formation of equilibrium associations of silicate and sulfide phases. Graphite was used as capsule material. After termination of the experiments, samples were studied using a microprobe analysis (Cameca Camebax-Micro), as well as optical and scanning electron microscopy (TESCAN MIRA 3 LMU scanning electron microscope). All analytical studies were conducted at the Center for Collective Use of Multi-element and Isotopic Analyses of the Siberian Branch of the Russian Academy of Sciences.
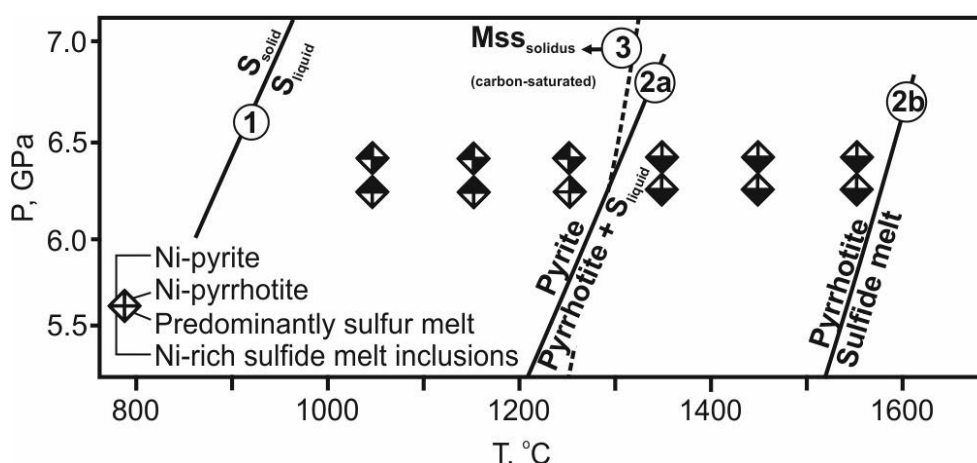

Fig. 1. Experimental results of the olivine-sulfur (circles) and olivine-pyrite (rhombs) interaction, with experimentally determined curves: 1 - melting of sulfur; 2a - decomposition of pyrite; 2b – melting of pyrrhotite; 3 - Mss solidus.

The experimental results and compositions of final phases are provided in Figures 1 and 2. In the course of olivine-sulfur interaction at T ≤ 1250 ºC, the formation of olivine and orthopyroxene polycrystalline aggregate, containing pools of quenched sulfur melt with sulfide microdendrites and pyrite crystals (Fig. 3a,b), occurred via the reaction:

$(Mg,Fe,Ni)_2SiO_4 + S_{melt} \rightarrow MgSiO_3 + Mg_2SiO_4 + [S\text{-}Fe\text{-}Ni\text{-}O\text{-}Si_{trace}\text{-}Mg_{trace}]_{melt/fluid}$. Implementation of this reaction led to the recrystallization of olivine in a sulfur melt/fluid, as evidenced by an increase in the size of olivine crystals up to 50−300 μm (relative to starting grains ~ 20 μm) and by the formation of zoned crystals with the relicts of starting olivine in the core and contrast decrease in Fe and Ni and an increase in Mg towards the rims, which are considered to be the main feature of olivine sulfidation. The recrystallization was found to be accompanied by extraction of Fe and Ni from olivine into a sulfur melt/fluid to form sulfide and by enrichment of this melt in Si, Mg, and O (traces of these elements were found in a quenched melt using energy-dispersive X-ray spectroscopy). An excess of Si led to the crystallization of orthopyroxene, as it was supposed in previous studies. It is important to note that no partial melting of silicates occurred in the entire temperature range that was previously thought to be a prerequisite for implementation of the sulfidation reactions.

The main compositional features of silicates, shown in Figure 2, were a decrease in the FeO and NiO concentrations in recrystallized olivine relative to the baseline concentrations and regular decrease of FeO and NiO contents in both silicates as temperature was increased. This was accompanied by increase in concentrations of iron and nickel, dissolved in the sulfur melt (Fig. 2c,d) and corresponding increase in quantity of dissolved pyrite. The formation of pyrite from the sulfur melt with dissolved components occurred according to the schematic reaction: $(Mg,Fe,Ni)_2SiO_4 + [S\text{-}Fe\text{-}Ni\text{-}O]_{melt/fluid} \rightarrow MgSiO_3 + Mg_2SiO_4 + (Fe,Ni)S_2 + S_{melt/fluid}$. This sulfur melt/fluid, being constantly enriched in new portions of the sulfide component due to extraction of Ni and Fe from olivine, reached saturation that led to crystallization of pyrite as a separate phase. The resulting pyrite was characterized by elevated nickel content (Fig. 2d). Similar pyrite mineralization of ultramafic rocks is commonly interpreted as an effect of metasomatic alteration by S-bearing fluids or melts.
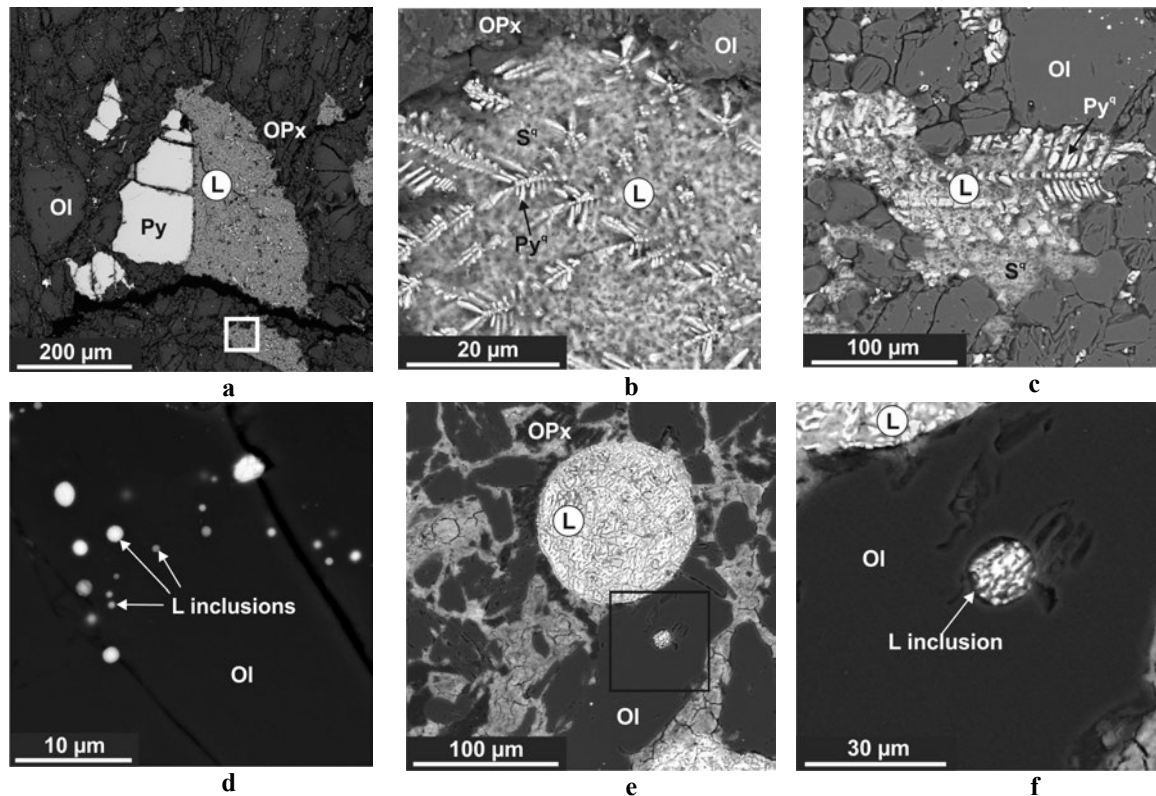

Fig. 2. SEM micrographs (BSE images) of polished samples after experiments on the olivine-sulfur (A-D) and the olivine-pyrite (E-F) interaction. Ol – olivine, OPx – orthopyroxene, L – predominantly sulfur melt/fluid, Py – pyrite, q – quenched phase;

At T ≥ 1350 °C, interaction in the olivine-sulfur system was accompanied by the generation of sulfide-sulfur melt (Fig. 2c) and formation of almost Fe-free forsterite-enstatite assemblage. The main feature of melt composition is an increase in the Fe/S and Ni/S ratios at an elevated temperature insomuch that the melt can be considered a sulfide-sulfur one. According to the experimental studies carried out in the Ol_{10-24}-Fe-S system at similar P and T, the oxygen concentration in Fe-S-O melts varies from 2.85 to 6.12 at%, and these data may be regarded as a rough estimate of oxygen content in our melts. During the recrystallization of olivine in the sulfide-sulfur melt, spherical inclusions of sulfide liquid (Fig. 2d) with extremely-high Ni concentrations up to 30 wt% (1550 °C), were formed in olivine crystals. A most probable mechanism of formation of these inclusions is the capture of sulfide droplets formed during liquation, according to the scheme: $xFeO_{ol} + yNiO_{ol} + S_{melt} \rightarrow Fe_{x-z}O_{x+y}S_{melt} + Ni_yFe_zS_{melt}$.

The study of the olivine-pyrite interaction, which supplemented the main direction of research and went logically through with it, was aimed at assessing the impact of evolution of the metasomatic agent composition in a series: sulfur

melt/fluid → sulfur-sulfide melt → sulfide melt, in the course of the olivine sulfidation reactions. Results of olivine-pyrite interaction are presented in Fig. 1. It was found that at T ≤ 1250 °C in the olivine-pyrite system recrystallization of olivine and formation of olivine + orthopyroxene + pyrite + pyrrhotite assemblage occurred according to the schematic reaction: $(Mg,Fe,Ni)_2SiO_4 + FeS_2 \rightarrow Mg_2SiO_4 + MgSiO_3 + (Fe,Ni)S_2 + (Fe,Ni)S + O_2$. At higher temperatures generation of [Fe-Ni-S-O]$_{melt}$ took place (Fig. 2e). The (Fe+Ni)/S proportions in this melt corresponded to pyrrhotite. Recrystallized olivine (200−400 µm crystals) contained large sulfide melt inclusions (Fig. 2f), with composition close to Ni-pyrrhotite. On the basis of these data and the results of research in the olivine-sulfur system, we suppose that these inclusions of high-Ni pyrrhotite are the main feature of the processing of olivine by reduced S-bearing metasomatic agents. Therefore, based on the main regularities of silicate sulfidation/recrystallization in the olivine-sulfur and olivine-pyrite systems, it was found that the compositions of recrystallized olivine and newly formed orthopyroxene do not actually depend on the composition of a reduced metasomatic agent (sulfur fluid/melt, sulfide-sulfur melt, or sulfide melt) and the appropriate fugacity of sulfur; however, the FeO and NiO concentrations in silicates vary regularly with temperature.

The studied olivine-sulfur and olivine-pyrite interactions can be considered as the basis for modeling of metasomatic processes under subduction conditions with involvement of reduced S-bearing melts/fluids. S transfer in the form of slab-derived fluids from the oceanic crust to the mantle wedge was experimentally found to be fO_2 independent and to occur over a range of fO_2 conditions that confirms possible interactions of mantle rocks and melts/fluids, bearing S in the reduced form. Our data indicate that the recrystallization of olivine and its sulfidation can occur in the presence of a small amount of a S-bearing melt/fluid (± sulfide melt) at the boundary of the cold subducted slab and the mantle wedge at relatively low temperatures. Therefore, one of the most important results demonstrated in this work is identification of the P-T-fO_2 conditions necessary for implementation of the olivine sulfidation reactions in the natural environments of subduction zones. Partial melting of olivine was demonstrated not to be a mandatory aspect for its exposure and extraction of Fe and Ni to form sulfides, and, in addition, this mechanism of sulfide formation can be realized under moderately oxidizing conditions, not only under highly reducing conditions, as it was previously assumed. Based on the obtained data, we developed a model for the sulfidation of ultramafic rocks during their interaction with S-bearing metasomatic melts/fluids. In this model, at the first relatively low-temperature stage of metasomatism, which develops on the boundary between the cold slab and mantle wedge, alteration of silicate rocks by slab-derived mobile sulfur-rich fluids occurs, that results in the partial sulfidation of FeO, NiO-silicates. This metasomatic alteration leads to recrystallization of silicates, extraction of metals from a solid-phase silicate matrix into S-bearing fluids, and ultimately pyrite mineralization of ultramafic rocks. The further, more intensive (higher temperature) metasomatic interaction of these rocks with a S-bearing metasomatic agent enriched with sulfide and oxide components results in the formation of harzburgite assemblage of forsterite + enstatite + Ni-pyrrhotite (as inclusions), i.e. to the complete sulfidation of FeO, NiO-silicates. Significant enrichment of S-bearing fluids/melts with sulfide leads to a decrease in their mobility and the formation of sulfide cumulates. An experimentally validated mechanism of the formation of mantle sulfides and sulfide melts via olivine sulfidation can be regarded as one of the causes for the formation of Ni-pyrrhotite inclusions (primary sulfide) in forsterite crystals and the lack of S^0 or fluid enriched in the reduced form of sulfur in inclusions in mantle minerals.

References:

Alard O, Lorand JP, Reisberg L, Bodinier JL, Dautria JM, O'Reilly S (2011) Volatile-rich metasomatism in Montferrier xenoliths (Southern France): Implications for the abundances of chalcophile and highly siderophile elements in the subcontinental mantle. J. Petrol. 52(10):2009-2045.

Bataleva YV, Palyanov YN, Borzdov YM, Sobolev NV (2016) Sulfidation of silicate mantle by reduced S-bearing metasomatic fluids and melts. Geology 44(4): 271–274.

Evans KA (2012) The redox budget of subduction zones. Earth Sci. Rev. 113:11–32.

Lehner SW, Petaev MI, Zolotov MY, Buseck PR (2013) Formation of niningerite by silicate sulfidation in EH3 enstatite chondrites. Geochim. Cosmochim. Acta 101:34–56.

Palyanov YN, Borzdov YM, Khokhryakov AF, Kupriyanov IN, Sokol AG (2010) Effect of nitrogen impurity on diamond crystal growth processes. Cryst. Growth Des. 10:3169—3175.

Sokol AG, Borzdov YM, Palyanov YN, Khokhryakov AF (2015) High-temperature calibration of a multi-anvil high pressure apparatus. High Pressure Res. 35(2):139-147.

ASSESSMENT OF A TRAPPED MELT COMPOSITION IN DUNITE BY ROCK GEOCHEMISTRY: A METHODIC AND EXAMPLES

Bazylev B.A.[1], Ledneva G.V.[2], Bychkova Ya.V.[3]
[1]Vernadsky Institute of Geochemistry and Analytical Chemistry of the Russian Academy of Sciences, Moscow, Russia, bazylev@geokhi.ru
[2]Geological Institute RAS, Moscow, Russia, ledneva@ilran.ru
[3]Lomonosov Moscow State University, Moscow, Russia, yanab66@yandex.ru

At a final stage of formation, dunites of various (cumulative or replacive) origin are expected to be in equilibrium with an intergranular melt, which cannot be completely expelled out of them (Bédard, 1994; Sundberg et al., 2010). So

at this stage dunite incorporates a certain amount of a trapped melt probably crystallized during its cooling into fine-grained mainly intergranular grains or/and aggregates of clinopyroxene, plagioclase and amphibole. Small size and intergranular position of these grains and aggregates make easy their replacement by hydrous silicates at the earliest stages of dunite hydrous metamorphism or serpentinization, so primary mineral relics of these grains are rare in dunites. Composition of trapped melt in dunite provides information on P-T parameters and a geodynamic setting of rock formation. However its direct measurements in molten inclusions in dunite Cr-spinels are rather rare (Simonov et al., 2015). Compositions of trapped melts evaluated from geochemistry of accessory clinopyroxene strongly depend on used clinopyroxene-melt partition coefficients of trace elements and analytical accuracy of trace-element measurements in clinopyroxene (e.g. Tian et al., 2011), so estimated contents of the most informative highly incompatible trace elements in trapped melts in some cases vary by two-three orders of magnitude (e.g. Tian et al., 2011).

A composition of trapped melt can be in fact calculated by mass balance if bulk chemistry of dunite, compositions of olivine and Cr-spinel and a set of mineral-melt partition coefficients are known (Bédard, 1994) and an amount of trapped melt (*tm*) is determined or given. An element/oxide content in a rock can be expressed as a sum of contents of elements in phases composing this rock, including trapped melt. In particular the equation for dunites with a mineral assemblage of olivine (Ol) - Cr-spinel (Spl) is

$$C_i^{\text{rock}} = (\varphi^{\text{Ol}} C_i^{\text{Ol}}) + (\varphi^{\text{Spl}} C_i^{\text{Spl}}) + (\varphi^{\text{tm}} C_i^{\text{liq}}),$$

where i is element, φ is mineral mode, and C is a content of element i in a rock and in an individual phase. If a trace element content in a mineral is unknown, its content can be estimated using values of mineral/melt partition coefficients (Bédard, 1994)

$$C_i^{\text{Min}} = C_i^{\text{liq}} D_i^{\text{Min-liq}},$$

and element contents in trapped melt can be estimated using data on values of mineral/melt partition coefficient D_i, modal mineral composition of rock and calculated or given amount of trapped melt

$$C_i^{\text{liq}} = C_i^{\text{rock}} / (\varphi^{\text{Ol}} D_i^{\text{Ol-liq}} + \varphi^{\text{Spl}} D_i^{\text{Spl-liq}} + \varphi^{\text{tm}}).$$

Olivine/melt and Cr-spinel/melt partition coefficients of incompatible elements (excluding Ti and HREE for olivine and Nb and Ti for Cr-spinel) are very small and insignificantly influence calculated contents of elements in trapped melt. According to experiments (Wijbrans et al., 2015, Horn et al., 1994, Nielsen, Beard, 2000),

$$D_{Nb}^{\text{Spl-liq}} = -1.802 - 3.15[Al],$$

where [Al] is an aluminum content in structural formula of Cr-spinel normalized to Σcat=3.

Thus the main problem is an assessment of an amount of trapped melt in dunite. To solve this problem Sundberg et al. (2010) proposed to use bulk rock contents of CaO, Al_2O_3, and TiO_2. Contents of these oxides incorporated into olivine and spinel can be estimated using mineral modes, which were calculated employing a non-negative least-squares fit of the measured mineral compositions to the whole-rock XRF results. The difference ("residual" contents) between measured and calculated contents of these oxides was assigned to be incorporated into trapped melt. An amount of trapped melt is calculated as ratio of these "residual" contents to their inferred contents in trapped melt.

However aluminum and titanium contents in silicate melt equilibrated with olivine and Cr-spinel can be calculated using experimental data. The difference between aluminum contents evaluated using different calibrations (Bazylev, 1996; Rollinson, Adetunji, 2015) is less than 10 rel. % for the most data ranging in the interval of Al_2O_3 contents of 8-19 wt. %. To assess aluminum contents we use equation (Bazylev, 1996)

$$C_{Al2O3}^{\text{liq}} = (1000(1-\text{Cr\#Spl}))^{(0.444-0.0021P)},$$

where Al_2O_3 contents are in weight %, Cr#=Cr/(Cr+Al), and P is in kbar.

According to experiments (Horn et al., 1994; Kamenetsky et al., 2001; Mallmann, O'Neill, 2009; Wijbrans et al., 2015) titanium content in a melt equilibrated with Cr-spinel can be calculated using the equation of

$$D_{Ti}^{\text{Spl-liq}} = 0.300 - 0.116[Al] + 1.871[Fe^{3+}],$$

where [Al] and [Fe^{3+}] are contents of aluminum and ferric iron in structural formula of Cr-spinel normalized to Σcat=3. This equation can be applied to Cr-spinel with [Fe^{3+}] less than 0.55 and it isn't dependent on temperature in the interval of 1200-1430°C. For calculations considered above core compositions of coarse Cr-spinel grains of dunites are preferable.

From our experience, assessments of a trapped melt amount based on aluminum are preferable. Precision of XRF measurements of Al_2O_3 contents in bulk dunites which was evaluated from repeated analyses in GEOKHI RAS and calibration using internal standards is about 0.04 wt. %. This means that an amount of trapped melt in dunites evaluated using residual aluminum contents can be evaluated with an uncertainty of 0.3 wt. % (1σ, for average melt composition of 12.7 wt. % of Al_2O_3) and with an uncertainty of 0.5 % for the lowest aluminum melt compositions.

Cooling of dunites is accompanied by significant lowering of Cr and Al contents in olivine and by crystallization of some subsolidus spinel, so φ^{Spl} value calculated using measured compositions of minerals in dunites differs from that at the temperature of melt trapping, which appears in equations above. The difference between these values is small and significant only for Al, Cr and Ti balance, but for its calculation temperature of melt trapping and closure temperature of Ol-Spl exchange reactions of these elements in dunite should be known. As the rule these data are absent.

This difficulty can be overcome taken into account the regularity presented by De Hoog et al. (2010). According to it, Cr#Spl and Cr#Ol at Cr#Spl>0.2 are nearly the same in peridotites at a wide range of temperatures. This observation is consistent with experimental data (e.g., Mallmann, O'Neill, 2009) and allows the suggestion that Cr# of primary and subsolidus Cr-spinels in dunites are nearly the same. This is proved by no regular variations of Cr# between core and rim spinel compositions in dunites. In this case, an amount of trapped melt can be calculated using a simplified equation of

$$\varphi^{tm} C_{Al2O3}{}^{liq} = C_{Al2O3}{}^{rock} - C_{Cr2O3}{}^{rock}(C_{Al2O3}{}^{Spl}/C_{Cr2O3}{}^{Spl}).$$

Thus a calculation of modal mineral composition of dunites (using contents of SiO_2, FeO, MnO, MgO and Cr_2O_3) is required only for evaluation of influence of Cr-spinel on Nb content in trapped melt.

The method described above was applied to calculate compositions of trapped melts in dunites of various types isochemically serpentinized in respect of SiO_2, MgO and FeO. Compositions of minerals were determined using a Cameca SX-100 microprobe at GEOKHI RAS, contents of major elements in dunites were measured by XRF at GEOKHI RAS, concentrations of trace elements were analyzed using ICP-MS at MSU, IGEM RAS and GEOKHI RAS as well as using LA-ICP-MS at the Max Planck Institute for Chemistry (Mainz, Germany). Some rocks were analyzed in different laboratories; precision of analyses is better than 25 rel.% for REE (except Eu), Y, Zr and Nb, and 30-50 rel.% for Eu, Rb, Sr, Ba, U and Pb. Analytical accuracy was evaluated from measurements of international standards (DTS-1, UB-N) and does not exceed the analytical precision.

Pekul'ney massif (Central Chukotka, NE Russia) (Bazylev et al., 2013). Cumulative dunite intercalates with peridotite and clinopyroxenite. Mg# of olivines varies in a wide range of 92.0-83.6. Cr# of spinels decreases from 0.7 to 0.45 as Mg# of olivines decreases. Some dunites include trace clinopyroxenes in interstices. The contents of elements in trapped melt calculated at an assumed pressure of 12 kbar are 9.9-12.0 wt.% for Al_2O_3 and 0.20-0.61 wt.% for TiO_2. The amount of trapped melt in dunites is estimated at 0.7-2.3 wt.%. The calculated contents of trace and rare earth elements in the trapped melt are shown in Figure 1.

Brezovica massif (Dinarides, Serbia) (Bazylev et al., 2003). Dunites composing veins and bodies in residual harzburgite are of replacive or reaction type typical of ophiolites. Primary minerals exhibit only slight compositional variations (Cr#Spl 0.69-0.80, Mg#Ol 90.1-91.7). Some dunites contain trace interstice clinopyroxene and hornblende presumably crystallized from trapped melt. The compositions of the trapped melt calculated at an assumed pressure of 5 kbar are 10,9-14,9 wt.% for Al_2O_3 and 0.35-0.60 wt.% for TiO_2. The amount of trapped melt is estimated at 0.1-1.6 wt.%. The calculated contents of trace and rare earth elements in the trapped melt are presented in Figure 2.
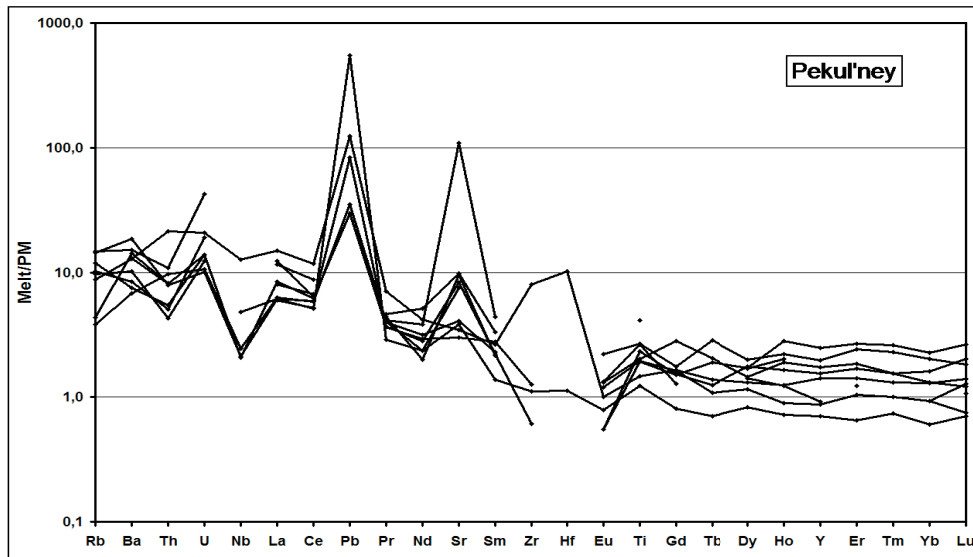

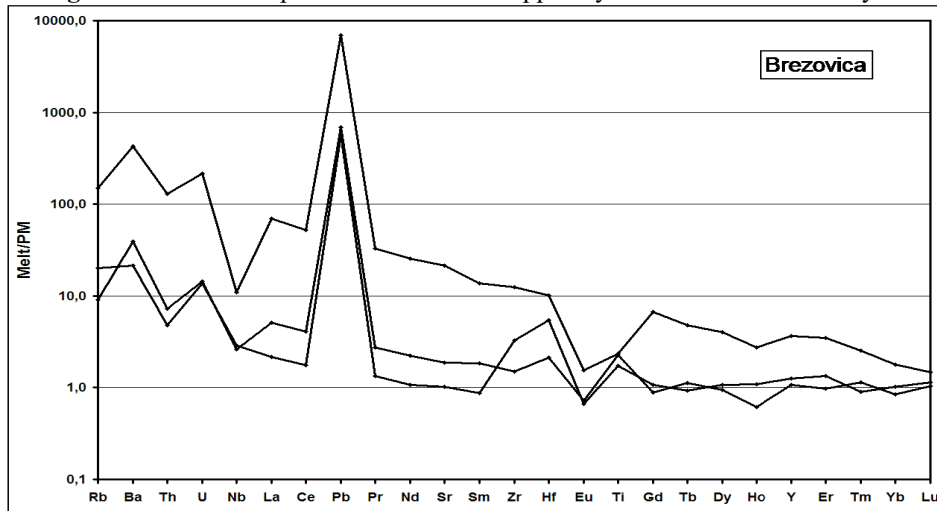**Fig.1**. Calculated composition of the melt trapped by dunites of the Pekul'ney massif.

Fig.2. Calculated composition of the melt trapped by dunites of the Brezovica massif.

Despite of wide variations of the calculated absolute contents of incompatible elements in the trapped melts, which are resulted from uncertainties of calculation of the low trapped melt amount, assessments obtained for both individual samples and averaged trapped melt compositions for both investigated objects exhibit features typical of subduction-related magmas such as IAT, BABT and boninites (enriched REE spectra, positive anomalies of Pb, Sr, U and Ba, and negative anomaly of Nb). This is consistent with high Cr# of Cr-spinels in dunites and with the calculated contents of TiO_2 and Al_2O_3 in trapped melts. The observed consistency between the calculated and natural compositions of melts indicates that the method proposed is applicable to isochemically metamorphosed dunites of various types.
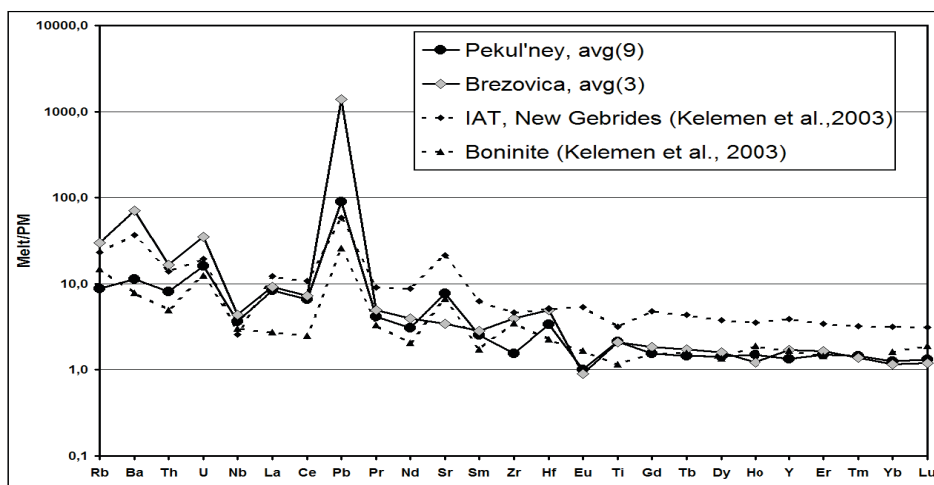
Fig.3. Comparison of the averaged calculated compositions of the melts trapped by the dunites investigated with compositions of typical subduction-derived magmas (Kelemen et al., 2003).

References

Bazylev B.A. Compositions of Clinopyroxene and Spinel in Restite Hyperbasites as Indicators of the Generation Conditions and Compositions of Coupled Primary Mantle Magmas. Geochemistry International, 1996, Vol.33, No.3, pp.115-124.

Bazylev B.A., Karamata S., Zakariadze G.S. Petrology and evolution of the Brezovica ultramafic massif, Serbia. In: Dilek, Y. & Robinson P.T. (eds). Ophiolites in Earth History. Geol. Soc. London Spec. Publ., 218, 2003, 91-108.

Bazylev B.A., Ledneva G.V., Ishiwatari A. High pressure ultramafics in the lower crustal rocks of the Pekul'ney complex, Central Chukchi Peninsula. 2. Internal structure of blocks and ultramafics bodies, geology and geodynamic setting of rock formation // Petrology. 2013. V. 21. No.4. P. 336-350.

Bédard J.H. A procedure for calculating the equilibrium distribution of trace elements among the minerals of cumulate rocks, and the concentration of trace elements in the coexisting liquids // Chem. Geol. 1994. V. 118. P. 143-153.

De Hoog J.C.M., Gall L., Cornell D.H. Trace-element geochemistry of mantle olivine and application to mantle petrogenesis and geothermobarometry // Chem. Geol. 2010. V. 270. P. 196-215.

Horn I., Foley S.F., Jackson S.E., Jenner G.A. Experimentally determined partitioning of high field strength- and selected transition elements between spinel and basaltic melt // Chem. Geol. 1994. V. 117. P. 193-218.

Kamenetsky V.S., Crawford A.J., Meffre S. Factors controlling chemistry of magmatic spinel: an empirical study of associated olivine, Cr-spinel and melt inclusions from primitive rocks // J. Petrol. 2001. V. 42. P.655-671.

Kelemen P.B., Hanghøj K., Greene A.R. One View of the Geochemistry of Subduction-Related Magmatic Arcs, with an Emphasis on Primitive Andesite and Lower Crust // Treatise on Geochemistry. V. 3. Editor: Roberta L. Rudnick. Executive Editors: Heinrich D. Holland and Karl K. Turekian. Elsevier, 2003. P. 593-659.

Nielsen R.L., Beard J.B. Magnetite–melt HFSE partitioning. Chemical Geology 164 (2000) 21-34.

Rollinson H., Adetunji J. The geochemistry and oxidation state of podiform chromites from the mantle section of the Oman ophiolite: A review. Gondwana Research 27 (2015) 543-554.

Sundberg M., Hirth G., Kelemen P.B. Trapped Melt in the Josephine Peridotite: Implications for Permeability and Melt Extraction in the Upper Mantle. J.Petrol. 2010. V.51 No 1&2. 185-200.

Simonov V.A., Vasiliev Yu.R., Stupakov S.I., Kotlyarov A.V., Karmanov N.S. (2015) Physicochemical parameters of crystallization of dunite from the Guli ultrabasic massif (Maimecha Kotui province). Doklady Earth Sciences vol.464, part1, pp.979-982.

Tian W., Chen B., Ireland T.R., Green D.H., Suzuki K., Chu Z. Petrology and geochemistry of dunites, chromitites and mineral inclusions from the Gaositai Alaskan-type complex, North China Craton: Implications for mantle source characteristics. Lithos 127 (2011) 165-175.

Wijbrans C.H., Klemme S., Berndt J., Vollmer C. Experimental determination of trace element partition coefficients between spinel and silicate melt: the influence of chemical composition and oxygen fugacity // Contrib. Mineral. Petrol. 2015. V. 169. P. 45.

GEOLOGICAL PRECONDITIONS, MANIFESTATIONS AND SIGNS OF PARTICIPATION OF NATURAL SALTS IN ALKALINE MAGMATISM

Belenitskaya G.A.
Federal State Budgetary Enterprise 'A. P. Karpinsky Russian Geological Research Institute', Saint Petersburg, Russia,
gab_2212@mail.ru

The issue of the source of alkaline metals and volatiles is of great importance in the problem of genesis of alkaline magmatic rocks. Most often, various types of deep and super-deep inputs are discussed: through-magmatic solutions (D.S. Korzhinsky), alkaline melt fluids (L.N. Kogarko, et al.), fluid-salt systems (L.S. Borodin, et al.), derivatives of mantle recycling of the material of oceanic crust, which is drawn into the mantle in subduction zone (A.W. Hofmann), fluid plumes generated on the boundary with the liquid core (N.L. Dobretsov, F.A. Letnikov, et al.). The solution to the issue so far remains largely controversial. Meanwhile, in the earth's crust, a large source of both alkaline metals and volatiles is quite widespread along paths of the ascending movement of magmas. These are salt-bearing (often salt-carbonate) complexes and accompanying brines, which form large concentrated accumulations of sodium, potassium, chlorine, and a wide range of macro- and microcomponents, including volatile ones, in the earth's crust.

Preconditions. There are a number of preconditions to attract salts as a participant in alkaline magmatism. The main of them are: 1) similarity of sets of specific and typomorphic components and microcomponents of the composition of salt (halophilic – salt-loving) and alkaline (foidophilic, according to (Lazarenkov, 1988)) complexes; 2) their fairly frequent space proximity including affinity of potassium salts and potassium varieties of alkaline rocks; 3) similarity of a number of important patterns in the location of both of them (geotectonic position, stratigraphic distribution, inherited-cyclical character of location, etc.).

Salt-alkaline associations, distribution, examples. A purposeful comparative analysis of the regional and global material, characterizing the location of saline and alkaline complexes, showed their frequent spatial proximity and allowed to consider such complexes as salt-alkaline association, and their distribution areas as salt-alkaline provinces. The associations composition is as follows: alkaline magmatic complexes and older salts buried in their substrate (main dominant pair); sub-synchronous to magmatism "younger" salt strata, often associated with the destruction of older salts and their recycling (tectonic, salt-tectonic or injection-sedimentation) (Belenitskaya, 2016, 2017); frequently also older alkaline and salt layers.

Issues of old buried salts spread in zones of magmatism shows have been specially discussed in (Belenitskaya, 2017). Main difficulty of their detection in the substrate of alkaline complexes consists in poor preservation, while sharply decrease with time, and their poor accessibility for observation. In such environments deformation, displacement and partial removal of salts took place both during the time preceding alkaline magmatism and synchronously with its manifestations during tectonic-magmatic activation, and then in postmagmatic time under the influence of deep or near-surface factors. As a result, salt distribution in the substrate has often been relatively reduced already at the time of the development of magmatism, and at present, in most cases, it is not clearly expressed and can be reconstructed only by their relict fragments, injections, tectonic wedges, but more by a set of various indirect indicators, as well as by the presence of brines and young salts regenerative nature. The reconstruction of pre-magmatic salts almost always requires special research.

Depending on thesituation, three main tectonic types of salt-alkaline provinces are distinguished: 1) cover-folded, 2) riftogenic, and 3) activated passive margins. In the cover-folded type, the most widespread, conditionally involved folded areas (together with zones of tectonic overlaps by napped-thrust packages of platform margins and median massifs), of various age, including those developed in the basements of young and ancient platforms.

Co-occurrences with older salt-bearing complexes are reconstructed most confidently and often for Neogene-Quaternary alkaline complexes, less often for older Phanerozoic and especially for Precambrian complexes (Belenitskaya, 2015). Typical representatives of neogeodynamic salt-alkaline provinces of each type – Italian, Upper Rhine, and Northwest African – are accepted as standard ones. The nature of their salinity of these regions is discussed in detail in (Belenitskaya, 2016, 2017), where a survey of studies on this problem was also presented. For each of the provinces traced the pattern of lateral and vertical relationships between alkaline and salt objects have been restored. In all the provinces, there are two main members of the association: Triassic salts (older ones) buried in the substrate (Busson, 1982; **Yunov, 1980; Ziegler et al., 1996; et al.**), and alkaline Neogene-Quaternary complexes (Alkaline..., 1974**; Borodin, 1974; Peccerillo, Martinotti, 2006; Kogarko, Asavin, 2009; Mazarovich A.O. et al., 1990; et al.**). Triassic salt (potassium-bearing) bodies in all the provinces are distributed at depths from 2-4 to 5-8 km and more. In the Italian province of cover-folded type, sub- and intrathrust salt bodies of residual and injective-tectonic nature is dominated. The Upper Rhine riftogenic province is characterized by buried in deep parts of rift structures residual and saline-tectonic deposits. In the Northwest African passive margin province injective salt masses (salt-tectonic and partially orthotectonic), deeply buried and laterally displaced up to the adjacent parts of abyssal areas (zones of frequent distribution of alkaline magmatism), prevail. Magmatism in all situations is due to tectonic-magmatic activation. In addition to the two dominant members, in the Italian and Upper Rhine provinces there are young salt bodies sub-synchronous to magmatism, whose formation, according to the author, is largely due to the high-intensity processes of tectonic (in the Italian province) or salt-tectonic (in the Upper Rhine) transportation of Triassic salts and their participation in the accumulation of salt masses of new levels. Potassium specialization is typical for salts of both levels and for alkaline magmatic complexes. Lateral and vertical relationships between alkaline and salt objects in each province form

characteristic types of regional spatial zonality. In all the provinces, on the paths of ascending deep magmas the tomography data record the presence of intermediate magmatic chambers at about salinity levels.

There are preconditions for the detection of older (pre-Neogen) Phanerozoic alkaline-salt associations, for example, in the following regions: Yuzhnoytamyrsko-Khatangsko-Pranabarskiy, Baikal-Nepsky, Varanger-Timan-Mezensky, Cordillera, Tien Shan, Ural-Predural, North Appalachian, Yeniseisko-Chadobetsky, Fitzroy-Kimberly, etc. The issue with Precambrian is more complicated, primarily because of the insignificant preservation of Precambrian salts. But nevertheless, special studies of their relics and indirect features allow the reconstruction of Precambrian alkaline-salt associations.

Geological model, role of salt components in magmatism. The results of analysis of many salt-alkaline provinces show that the occurrence of salt-bearing rocks on the paths of ascending movement of deep magmas related to tectomagmatic activation is a rather widespread and geologically regular phenomenon. Physico-chemical parameters of such rocks distribution levels are favorable for the formation of intermediate crust foci, centers of interactions of hot aluminosilicate magmas with the assimilated components of saline (or salt-carbonate) complexes, and of formation of various nonequilibrium melt mixtures, which are highly enriched (oversaturated) with alkali and volatile components.

Localized reserves of halophilic components in saline complexes can serve as their concentrated sources in processes of interaction with the aluminosilicate melts. On the character of the influence of saline complexes components on petrogenesis processes, two main groups can be conventionally distinguished: 1) material ones ("donors") – Na, K, partially Cl (main salt components), a number of smaller and microcomponents; 2) volatile components – CO_2, SO_3, H_2O, Cl, F, etc., enriching salts and paragenous anhydrite (gypsum) and carbonate. The role of those and others in alkaline magmatism (outside the connection with natural salts) was discussed in many works (**Aiuppa et al., 2009; Kogarko, 1977; Kogarko, Ryabchikov, 1978; Purtov et al., 2002;** et al.).

The contents of Na, K and Cl in salts (in 1 m^3 of sodium salts about 0.8 t Na and about 1.0 t Cl, and in 1 m3 potassium salts about 0.1-0.2 t K) can easily provide them necessary "additives" to the alkaline rocks. Inclusion of salt-bearing masses in the hot magmatic process explains quite simply the nature of the source of sodium and potassium, replenishing their reserve necessary for processes of alkaline magmatism. The source is powerful, concentrated and located in the areal of intermediate magmatic chambers. The excess of alkaline metals and their high activity, creating the preconditions for the formation of "oversaturated" minerals, including nepheline and leucite, can also promote their early crystallization, preceded by the formation of dark minerals, disrupting the usual sequence of mineral formation that determines the "agpaitic" features of emerging rocks. Participation in the interaction of salts of sodium (halite) or potassium types can determine the mainly sodium or potassium specialization of the forming alkaline complexes. In addition, the inclusion in the processes of potassium salts characterized by their "own" set of accompanying microcomponents (Rb, Cs, Br, etc.) can influence the spectrum of microimpurities that enrich alkaline rocks. Chlorine, not being an important rock-forming agent in magmatic aluminosilicate systems, in alkaline petrogenesis affects many specific features of chemical and mineral composition and, to a large extent, the character of conjugate mineralization (Ryabchikov, Hamilton, 1971**; Marakushev et al., 1997; et al.**). On the one hand, it contributes to wide distribution of many Cl-enriched petrogenic and accessory minerals, which in alkaline complexes often reach rock-forming values, on the other hand, to the differentiation of fluid-magmatic systems with the separation of chloride fluids, which dissolve and accumulate the complex of ore ("chlorophilic", according to A.A. Marakushev) components. Volatile components, enclosed in the composition of salt-bearing complexes, to a greater extent initiate and regulate the course of interactions, manifested in the specificity of the material, structural, morphological and spatial parameters of the rocks.

Thus, high contents of alkaline and volatile components in salt-bearing complexes together influence both the composition (rock, mineral, chemical, isotopic) of the alkaline magmatic bodies and the accompanying metasomatic formations, and on their structural and textural features, morphology and spatial relationships. The ability of these components to contribute to the emergence of all these specific features of alkaline rocks can serve as an important argument in favour of the reality of their participation.

Signs of salt participation. The presented views is confirmed by many material and structural-morphological signs typical of alkaline magmatic rocks (**Aiuppa et al., 2009;** Alkaline..., 1974**; Borodin, 1974; Kogarko, 1977; Lazarenkov, 1988; Pokrovsky, 2000; et al.**), which can be the result of processes of magma contamination with salts and at the same time their important evidence. They are as follows: (1) frequent significant enrichment of many varieties of magmatic rocks with chlorine (up to 1.2-1.3%), sulfate ion (up to 3.0%), and carbonate ion (up to 5.4%); widespread occurrence of minerals containing these ions (sodalite, hauyn, cancrinite, etc.), up to sodalite, hauyn and cancrinite rocks; (2) diversity and contrast character of changes in chemical and mineral composition; (3) coincidence of potassium orientation of alkaline magmas with that of spatially conjugated salts, often enrichment of both with Br, Rb, Cs; the presence of Cl, sometimes Br in solid and liquid inclusions in alkaline rocks, as well as in volcanic gases ("halogen degassing", according to (**Aiuppa et al., 2009**); the presence of salts in ejecta of active volcanoes; crystallization in craters and incrustation of their walls with salts and with native sulfur (due to the presence in the section of its main source - anhydrite); variations in the C, O, Sr isotope indexes (Alkaline..., 1974**; Faure, 1986; Pokrovsky, 2000;** et al.), which often correspond to those typical of salt-carbonate complexes and, on the whole, do not contradict the possibility of the participation of salt-bearing sequences in alkaline magmatism.

Many papers are devoted to experimental studies on the interaction of high-temperature alumosilicate melts with NaCl and KCl salt systems (for example, **Aiuppa et al., 2009;** Alkaline..., 1974**;** Carbonatites, 1969**; Kogarko, Ryabchikov, 1978; Marakushev et al., 1997; Purtov et al., 2002; Safonov et al., 2007;** and many others) and their

results are very indicative. Unfortunately, as long as mainly low-concentration salt solutions are being studied, the information on the interactions of aluminosilicate melts with natural salts is limited. But the available experimental data do not contradict the given geological model, and in many respects confirm it.

All of the above allows author to give a positive assessment to the geological probability of salt participation in alkaline magmatism and to accept the presented ideas as a working version of the geological model of alkaline magma formation.

Comparative analysis of geological-genetic models. The large reserve of alkaline and volatile components contained in saline complexes makes up the advantage of salts as their source in aluminosilicate magmas before any mantle supplies, for which their quantity is constrained not only by possible concentrations in the incoming fluids, but also by possible total mass of the fluids themselves. The proposed model is most close to widely known concepts of assimilation of carbonate rocks by magma developed by R.A. Daly and S.J. Shand and supported to various extent by many researchers (Alkaline..., 1974**; Borodin, 1974; Rittmann , 1962; et al.**). These views, which have been corrected in accordance with data on litho-tectonic features of sedimentary sections crossed by the magma (first of all about their salt content) indicate a high probability of salt assimilation together with its almost constant satellites – carbonates, particularly dolomite. There are good reasons to believe that participation in the assimilation of both members of the persistent natural salt-carbonate paragenesis determines to a great extent the character of interaction processes, so their joint analysis is one of promising directions for further studies. In the course of such studies, theoretical and experimental developments in studying processes of carbonate assimilation by magma can be used.

As compared to the A.W. Hofmann's model (Hofmann, 1997), which allows the enrichment of super-deep reservoirs in alkaline and volatile components as a result of mantle recycling of oceanic crust material, the proposed model is focused on specialized crustal (cover-crustal) recycling – involvement in magmatism of salt-bearing (often salt-carbonate) components located at less significant depths, mainly within the continental crust, and possibly tectonically "dragged" in even deeper parts of the lithosphere.

The model discussed is not offered as an alternative to existing concepts; it does not deny the probability of emergence of high-alkalinity magmas in the mantle as well as the participation of other mechanisms of its growth in the process of their evolution. Manifestation of different processes and existence (and even combination) of alkaline rocks of different genesis due to different geological factors is quite possible. However, the author would like the proposed model with crustal alkaline metals and volatile sources could occupy a place as an appropriate link in the system of the discussed views on alkaline magma formation.

The model explains many specific, including some "unclear", features of the composition and structure of alkaline rocks repeatedly emphasized by many researchers. It can be used for forecasting in the studies of both alkaline and salt-bearing complexes, as well as attracting more serious attention to salts in studying alkaline-metasomatic and other endogenous processes, including ore-generating ones. Some of the geological concepts of the discussed model are presented by the author for the first time and undoubtedly require further studies with the participation of specialists dealing with the problems of alkaline petrogenesis.

References

Aiuppa A., Baker D.R., Webster J. (2009) Halogenes in Volcanic Systems and Their Environmental Impacts. Special Issue. Chemical Geology. 263 (1-4). 163 p.

Alkaline rocks (1974) Ed. H. Serensen. John Wiley and Son. New York. 400 p.

Belenitskaya G.A. (2015) Participation of natural salts in alkaline magmatism. Tectonic-sedimentary preconditions. Probabilistic lithological and petrological models of alkaline magmatism with salt participation. Petrography of igneous and metamorphic rocks. Petrozavodsk: KSC RAS, pp. 96-101. (In Russian).

Belenitskaya G.A. (2016) Salt Tectonics at the Margins of Young Oceans. Geotectonics. 50 (3), pp. 244–256.

Belenitskaya G.A. (2017) Salt in the Earth's crust: distribution and kinematic history.Lithosphere (in press). (In Russian).

Borodin L.S. (Ed.) (1974) Major provinces and formations of alkaline rocks. Moscow: Science. 376 p. (In Russian).

Busson G. (1982) Le Trias comme periode salifere Geologische Rundschau. 71 (3). Stuttgart, pp. 857-880.

Carbonatites (1969) Ed. O. Tuttle and J. Gittins. Trans. from English. Moscow: Mir. 487 p. (In Russian).

Faure G. (1986) Principles of isotope geology. 2nd ed.New York: Wiley. 589 p.

Hofmann A.W. (1997) Mantle geochemistry: the message from oceanic volcanism. Nature. 385, pp. 219-229.

Kogarko L.N. (1977) Problems of agpaitic magma genesis. Moscow: Science. 294 p. (In Russian).

Kogarko L.N., Asavin A.M. (2009) Potassium magmatism of the World's ocean (case study of the Atlantic). Geochemistry international (9), pp. 899-909.

Kogarko L.N., Ryabchikov I.D. (1978) Volatiles in magmatic processes. Geochemistry. (9), pp. 1293-1321. (In Russian).

Lazarenkov V.G. (1988) Formation analysis of alkaline rocks of continents and oceans. Leningrad: Nedra. 236 p. (In Russian).

Marakushev A.A., Suk N.I., Novikov M.P. (1997) Chloride extraction of metals and problem of their migration from magmatic chambers. DAN RAS. 352 (1), pp. 83-86. (In Russian).

Mazarovich A.O., Frikh-Khar D.I., Kogarko L.N. (1990) Tectonics and magmatism of Cape Verde Islands. Trudy GIN. (451). Moscow: Science. 246 p. (In Russian).

Peccerillo A., Martinotti G. (2006) TheWestern Mediterranean lamproitic magmatism: origin and geodynamic significance. Terra Nova, 18, pp. 109–117.

Pokrovsky B.G. (2000) Crustal contamination of mantle magmas on evidence of isotope geochemistry. Moscow: Science: MAIK "Science: Interperiodica". 225 p. (In Russian).

Purtov V.K., Anfilogov V.N., Egorova L.G. (2002) Interaction of basalt with chloride solutions and mechanism of acid melt formation. Geochemistry international, (10), pp. 1084-1097.

Rittmann A. (1962) Volcanoes and Their Activity. New York: Interscience (Wiley). 305 p.

Ryabchikov I.D., Hamilton D.L. (1971) Possibility of separation of concentrated chloride solutions in the course of acid magma crystallization. DAS SSSR. 197 (4), pp. 933-936. (In Russian).

Safonov O.G., Perchuk L.L., Litvin Yu.A. (2007) Interaction of Diopside and Jadeite with Potassium Chloride at 5 Gpa. Doklady Earth Sciences. 415 (5), pp. 789–793.

Yunov A.Yu. (1980) Structure, evolution, and oil-and-gas potential of continental margins of West Africa and East Asia. Tectonics of Siberia. IX, pp. 127-139. (In Russian).

Ziegler P.A., Horvath F. (Eds). (1996) Peri-Tethys Memoir 2: Structure and Prospects of Alpine Basins and Forelands. Mem. Mus. Natn. Hist. nat. Paris. 170. 511 p.

PHASE RELATIONS AND FORMATION OF CR-RICH PHASES UPON MELTING OF MODEL PYROLITE AT 2.5–7.0 GPA AND 1400–1900°C

Bendeliani A.A.[1,2], *Sirotkina E.A.*[1,2,3], *Bobrov A.V.*[1,2,3]

[1]Lomonosov Moscow State University, Moscow, Russia, garmr9@gmai.com
[2]Vernadsky Institute of Geochemistry and Analytical Chemistry of the Russian Academy of Sciences, Moscow, Russia,
[3]Institute of Experimental Mineralogy, Chernogolovka, Russia

Chromium is one of typical minor elements, which, despite the low concentrations in the Earth's mantle (0.42 wt % Cr_2O_3) (Ringwood, 1966), may be accumulated in deep minerals. In our experiments, we studied the distribution of Cr between crystal phases and melt upon partial melting of pyrolite within the garnet (at a fixed pressure of 7.0 GPa and temperatures 1600, 1700, 1800, and 1900°C) and spinel (2.5 and 3.0 GPa) depth facies. Experiments were performed on a toroidal anvil-with-hole apparatus at the Vernadsky Institute of Geochemistry and Analytical Chemistry, Russian Academy of Sciences. The starting composition was represented by the model pyrolite (46.18 SiO_2, 3.58 Al_2O_3, 0.50 Cr_2O_3, 38.32 MgO, 8.17 FeO, 3.17 CaO, 0.58 Na_2O); in some runs, the content of Cr_2O_3 in pyrolite was 3.0 wt %.

The phase associations obtained at 7 GPa include low-Cr garnet and olivine (the zone of restite), as well as orthopyroxene in the fine-granular garnet-pyroxene aggregate (the zone of quenched melt). An estimated bulk composition of restite contains ≤0.4 wt % Cr_2O_3, which indicates redistribution of Cr into melt upon partial melting in the garnet depth facies. The concentration of Cr_2O_3 in garnet from the zone of restite reaches 4.5 wt %, whereas garnets from the quenched aggregate (melt) contain up to 8.0 wt % Cr_2O_3. All garnets synthesized in melting experiments of pyrolite within the garnet depth facies belong to the dunite-harzburgite assemblage. However, the concentrations of chromium in these garnets are much lower than those in natural garnets of the ultrabasic assemblage (up to 15 wt % Cr_2O_3) (Meyer et al., 1987).

In the spinel-depth facies (2.5 and 3.0 GPa), Cr is predominantly accumulated in chrome spinel (up to 35 wt % Cr_2O_3) from the zone of olivine-rich restite; garnet (at 3.0 GPa) and olivine also contain chromium, up to 3.6 and 0.12 wt % Cr_2O_3, respectively. The estimated bulk content of Cr_2O_3 in olivine-spinel (±garnet) restite at 3.0 GPa reaches 1.4 wt %. Thus, partial melting of model pyrolite in the spinel depth facies is accompanied with significant Cr redistribution into restite. Such Cr-rich restite formed as a residue from partial melting in the spinel depth facies may provide a protolith, which further transport into the garnet depth facies will result in the formation of Cr-rich garnets (Bulatov et al., 1991; Stachel et al., 1998).

Thus, our data provide quantitative support for the idea that high-Cr garnets were formed in the protolith subjected to partial melting within the spinel-depth facies (with the high Cr/Al ratio) with further subduction into the garnet-depth facies (Bulatov et al., 1991; Stachel et al., 1998). To model partial melting of protolith with the high Cr/Al ratio, we carried out several runs with addition of 3 wt % Cr_2O_3 to the starting composition. Garnets produced in these runs contain up to 12 and 16 wt % Cr_2O_3 in the zones of restite and melting, respectively.

References:

Bulatov V, Brey GP., Foley SF (1991) Origin of low-Ca, high-Cr garnets by recrystallization of low-pressure harzburgites. 5th Inter-national kimberlite conference, extended abstracts, CPRM, special publication 2/91:29–31

Meyer HOA (1987) Inclusions in diamond. In: Mantle xenoliths (ed. P.H. Nixon). Chichester: John Wiley Sons, pp. 501–522

Ringwood AE (1966) Advances in Earth science. Hurley, P.M. (Editors), M.I.T. Press, Cambridge, pp. 287–356

Stachel T, Viljoen KS, Brey G, Harris JW (1998) Metasomatic processes in lherzolitic ang harzburgitic domains of diamondiferous lithospheric mantle: REE in garnets from xenoliths and inclusions in diamonds. Earth Planet Sci Lett 159:1-12

MINERALS OF SODIUM IN THE EARTH'S TRANSITION ZONE AND LOWER MANTLE: EVIDENCE FROM EXPERIMENTS AND NATURAL DATA

Bobrov A.V.[1,2,3], Tamarova A.P.[1], Sirotkina E.A.[1,2,3], Bindi L.[4], Pushcharovsky D.Yu.[1], Irifune T.[5]

[1]Lomonosov Moscow State University, Moscow, Russia, archi@geol.msu.ru
[2]Vernadsky Institute of Geochemistry and Analytical Chemistry of the Russian Academy of Science, Moscow, Russia
[3]Institute of Experimental Mineralogy, Chernogolovka, Russia
[4]Università di Firenze, Firenze, Italy
[5]Ehime University, Matsuyama, Japan

Mg-silicates, such as majorite, wadsleyite, ringwoodite, akimotoite and bridgmanite are considered very important mineralogical constituents of the transition zone and the uppermost lower mantle. Some of these phases may incorporate Na, although the number of probable mineral hosts for sodium is limited to majorite ($Na_2MgSi_5O_{12}$ end-member; Dymshits et al. 2010; Bindi et al. 2011), ringwoodite and bridgmanite (Bindi et al. 2016), hexagonal new aluminous (NAL) and Ca-ferrite-type (CF) phases with the composition of $NaAlSiO_4$–$MgAl_2O_4$ (Dai et al. 2013). Several synthetic Na-rich Mg-silicates have been also reported as mineralogically possible phases in the deep geospheres. Among them are: $Na_{1.78}(Mg_{1.89}Al_{0.13})Si_{2.02}O_7$, $Na_{1.16}K_{0.01}(Mg_{1.89}Al_{0.14})Si_{2.02}O_7H_{0.65}$ (anhydrous and hydrous sodic phase X, known as NMS phase; Yang et al. 2001), $Na_2Mg_{4+x}Fe^{3+}_{2-2x}Si_{6+x}O_{20}$, $(K,Na)_{0.9}(Mg,Fe)_2(Mg,Fe,Al,Si)_6O_{12}$, $Na_2Mg_2Si_6O_{15}$ and solid solutions of $Na(Mg_xSi_xAl_{1-2x})Si_2O_6$ ($0 \leq x \leq 0.5$) composition (see Litvin et al. 1998 and a complete review in Yang et al. 2009).

Although the concentration of alkalis in the Earth's transition zone and lower mantle is low and Na remains incompatible in most of the high-pressure solid phases, it is expected that some mantle phases could act as important hosts for Na, and perhaps K, in the deep transition zone and lower mantle. As it was shown before, Na-bearing majoritic garnet (up to 1.5 wt % Na_2O; Bobrov et al. 2008), Na-rich ringwoodite (up to 4.4 wt % Na_2O; Bindi et al. 2016) and bridgmanite (up to 1.5 wt % Na_2O; Bindi et al. 2016) could crystallize from Na-rich carbonated melts produced by partial melting upon the crust–mantle interaction. In the model of Walter et al. (2008), melting occurs as slabs descend and stagnate in the transition zone, and heat up to the carbonated eclogite solidus where they release a low-degree melt. Such low-degree carbonatitic melts from eclogite are expected to be mobile and rich in alkali, and so may act as effective metasomatizing agents. The presence of such melts in the deep mantle is supported by inclusions of Na-carbonates [nyerereite $(Na,K)_2Ca(CO_3)_2$ and eitelite $Na_2Mg(CO_3)_2$] in lower mantle diamonds (Kaminsky et al. 2016) and incorporation of sodium in major mantle silicates, such as majoritic garnet and bridgmanite. In contrast, proper Na–Mg silicates have not been registered as inclusions in diamonds or in mantle rocks, although they were obtained as products of experiments in many Na-rich model systems. This is explained by the fact that all natural lithologies are characterized by an excess of Al with respect to Na. However, the finding of an inclusion in diamond with the composition $(Na_{0.16}Mg_{0.84})(Mg_{0.92}Si_{0.08})Si_2O_6$ in a Chinese kimberlite (Wang and Sueno, 1996) suggests that some local areas of the Earth's deep mantle previously involved in the mantle–crust interaction may be significantly enriched in Na. In this relation, study of Na-rich Mg-silicates will increase our knowledge on the composition and properties of the deep mantle. Thus, the successful high-pressure synthesis and structural refinement of Na_2MgSiO_4 allow us to consider this phase as a probable host for sodium in some locally metasomatized mantle areas.

References:

Bindi L, Dymshits AM, Bobrov AV, Litasov KD, Shatskyi AF, Ohtani E, Litvin YuA (2011) Crystal chemistry of sodium in the Earth's interior: the structure of $Na_2MgSi_5O_{12}$ synthesized at 17.5 GPa and 1700°C. Am Miner 96:447−450

Bindi L, Tamarova A, Bobrov AV, Sirotkina EA, Tschauner O, Walter MJ, Irifune T (2016) Incorporation of high amounts of Na in ringwoodite: possible implications for transport of alkali into lower mantle. Am Miner 101:483–486

Bobrov AV, Litvin YuA, Bindi L, Dymshits AM (2008) Phase relations and formation of sodium-rich majoritic garnet in the system $Mg_3Al_2Si_3O_{12}$–$Na_2MgSi_5O_{12}$ at 7.0 and 8.5 GPa. Contrib Mineral Petrol 156:243–257

Dai L, Kudo Y, Hirose K, Murakami M, Asahara Y, Ozawa H, Ohishi Y, Hirao N (2013) Sound velocities of $Na_{0.4}Mg_{0.6}Al_{1.6}Si_{0.4}O_4$ NAL and CF phases to 73 GPa determined by Brillouin scattering method. Phys Chem Minerals 40:195–201

Dymshits AM, Bobrov AV, Litasov KD, Shatskyi AF, Ohtani E, Litvin YuA (2010) Experimental study of the pyroxene–garnet phase transition in the $Na_2MgSi_5O_{12}$ system at pressures of 13–20 GPa: first synthesis of sodium majorite. Doklady Earth Sciences 434:1263–1266

Kaminsky FV, Ryabchikov ID, Wirth R (2016) A primary natrocarbonatitic association in the Deep Earth. Miner Petrol 110: 387–398

Litvin YuA, Gasparik T, Tikhomirova VI, Chichagov AV (1998) Na–Mg silicates as possible minerals in the Earth's mantle: Melting and structural stability at 1 atm and high pressures. Doklady Earth Sciences 361A:883–887

Walter MJ, Bulanova GP, Armstrong LS, Keshav S, Blundy JD, Gudfinnsson G, Gobbo L (2008) Primary carbonatite melt from deeply subducted oceanic crust. Nature 454:622-625

Wang W, Sueno S (1996) Discovery of a NaPx-En inclusion in diamond: Possible transition zone origin. Min Journal 18:9–16

Yang H, Konzett J, Frost DJ, Downs RT (2009) X-ray diffraction and Raman spectroscopic study of clinopyroxenes with six-coordinated Si in the $Na(Mg_{0.5}Si_{0.5})Si_2O_6-NaAlSi_2O_6$ system. Am. Mineral. 94:942–949

Yang H, Konzett J, Prewitt CT (2001) Crystal structure of phase-X, a high pressure alkali-rich hydrous silicate and its anhydrous equivalent. Am. Mineral. 86:1483–1488

REEF SOPCHA ORE LAYER IN THE MONCHEGORSK PLUTON (KOLA PENINSULA): GEOLOGICAL, MINERALOGICAL, GEOCHEMICAL, AND ISOTOPE-GEOCHEMICAL DATA

Bogina M.M.[1], Sharkov E.V.[1], Chistyakov A.V.[1], Khvostikov, V.A.[2], Zlobin V.L.[3]

[1]Institute of Geology of Ore Deposits, Petrography, Mineralogy and Geochemistry of the Russian Academy of Sciences, Moscow, Russia, lekhta@mail.mail
[2]Institute of Microelectronics Technology and High Purity Materials of the Russian Academy of Sciences, Chernogolovka, Russia
[3]Geological Institute RAS, Moscow, Russia, vzlobin@bk.ru

Layered mafic-ultramafic intrusions frequently host PGE-Cu-Ni bearing ores. Several types of deposits are usually distinguished in them, but most economically important PGE sources are contained in so-called "reefs" representing stratified layers or horizons containing disseminated sulfides with elevated PGE abundance. These reefs are observed in many intrusions, for instance, the Merensky Reef in the Bushveld complex and the J-M Reef in the Stillwater complex. The PGE reefs are typically confined to a lithological change in the layered intrusions, which may be controlled both by the appearance of a new cumulus mineral in the course of normal magma evolution or in relation with a change in the crystallization order of minerals. Several hypotheses have been proposed to explain the origin of the "reefs": (1) a magmatic hydrothermal fluid generated in the already formed upward moving crystal pile scavenges and concentrates the PGEs until the deposition in the reef horizon (Boudreau and McCallum, 1992); (2) multiple injections of a new portion of melt already enriched in ore components (Sharkov et al., 2014); (3) assimilation of host rocks resulting in the decrease of the sulfur saturation level and sharp segregation of immiscible sulfide melt enriched in PGE, Cu, and Ni (cf. Naldrett, 2011; Ripley et al., 2003). In any case, the main question is whether the parental melts of the reefs were initially enriched in PGE, or were formed through the accumulation of ore components either from wall rocks or due to sudden exsolution of a sulfide liquid in relation with sulfur saturation of silicate magmas. We attempted to answer this question by detailed geological, mineralogical, geochemical, and isotope-geochemical studying of the Cu-Ni-PGE-bearing Sopcha ore layer and host ultramafic portion of the Monchegorsk layered intrusion.

The Monchegorsk pluton is located in the central part of the Kola Peninsula, being restricted to the northwestern termination of the Paleoproterozoic Imandra-Varzuga structure. It was formed in the Paleoproterozoic (2504 ± 2 Ma) (Amelin et al., 1995) and consists of two branches: sublongitudinal Nittis-Kumuzh'ya-Travyanaya (NKT) and sublatitudinal Sopcha-Nyud-Poaz ones. The NKT branch and Mt. Sopcha consist mainly of ultramafic rocks subdivided in two zones (from bottom upward): (1) Peridotite Zone; (2) Pyroxenite or Bronzitite Zone. The upper part of the Bronzitite zone at Mount Sopcha hosts the 2-3 m thick reef-like Sopcha Ore Layer (SOL), or 330 Layer (300-330 m altitude) with PGE-bearing Cu-Ni disseminated sulfide ores (Smolkin et al., 2004; Sharkov et al., 2012). Slump structures and "pseudobreccias" of olivine orthopyroxenites are developed at the contacts of the layer with massive orthopyroxenites, thus indicating the emplacement in a semiliquid state (Smolkin et al., 2004; Sharkov et al., 2012). This is a persistent horizon of thin layered dunites, harzburgites and bronzitites, while its upper part is made up of coarse-grained bronzitites (Sharkov et al., 2014). Dunites and harzburgites usually contain low-sulfur assemblage whereas otrhopyroxenites host high-sulfur assemblage (Neradovsky et al., 2002).

Microprobe study of rock-forming minerals revealed no any core-rim zoning relationships. All minerals are compositionally homogenous, while rare variations may be related to the incorporation of mineral inclusions or exsolution lamellae.

Olivine from the SOL peridotite has the lower Fo composition 83.99-85.05 as compared to the olivine in peridotite from the Peridotite Zone 86.05-86.65. The remarkable feature of the olivines from the SOL is the clearly higher contents of ore components as compared to those of the Peridotite Zone: Cu (from 1.0 to 78.5 ppm relative to 0.03-6.76), Co (187-368 relative to 172-188), Zn (65-111 relative to 27-94), and Pb (0.092-1.95 relative to 0.035-0.45 ppm). At the same time, Ni shows nonsystemic variations (from 2589 to 3363 ppm in the SOL and from 3095 to 3253 ppm in the Peridotite Zone), because its content is simultaneously controlled by two processes: magmatic evolution of melt and exsolution of sulfide liquid. The absence of correlation between ore components and S in olivine suggests their accumulation either in host silicate minerals or as intermetallides. The Mn content in olivine can be considered as controlled by only fractional crystallization, increasing with its degree (Yudovskaya et al., 2013). Olivine from the Peridotite Zone is characterized by the uniform MnO content of 0.16-0.18 wt %, whereas MnO content in olivine from the SOL have the higher contents of 0.18-0.21, which is generally consistent with crystallization differentiation upward the sequence. In the diagram Ni-Mn/Fe, the olivines define trends of gentle decreasing Ni at steady Mn/Fe ratio. This trend would be explained by the exsolution of sulfide melt, however, the absence of a drastic change in Ni content as a marker of segregation of sulfide melt is not observed. Hence, its behavior was rather controlled by magma evolution. The olivine composition can be also used to determine the nature of its mantle source. In particular, olivines have excess Ni as compared to those in equilibrium with mantle peridotites. This suggests the contribution of olivine-free pyroxenites formed through the interaction between

recycled crust and peridotite (Sobolev et al., 2007). The position of data points of olivine in the diagram 100Mn/Fe-Ni(Mg/Fe)100 (Sobolev et al., 2007) indicates that the rocks were derived from a peridotite source with some pyroxenite contribution.

Orthopyroxene in the studied rocks shows sufficiently narrow variations in Mg#. Orthopyroxene in peridotites from the SOL has Mg# from 85.8 to 87, while orthopyroxene in peridotites from the Peridotite Zone has slightly higher Mg# from 87.4 to 87.9. Close values are noted in the orthopyroxenites from Mt. Nittis, whereas orthopyroxene from orthopyroxenites beneath the Ore layer have similar Mg# from 85.8 to 86.2. Cr in pyroxenes is strongly compatible element and can be used for deciphering the magma replenishment events. Variations of the Cr content in Opx in layered intrusions is typically attributed to fresh magma pulses (Tanner et al., 2014). However, the studied rocks show no any positive excursions in the Cr_2O_3 contents, which vary from 0.56 to 0.71 wt. % in the SOL, from 0.56 to 0.72 in the orthopyroxenite beneath it, and slightly increases (up to 0.74) in the Peridotite Zone.

Major and trace element variations in the peridotites and pyroxenites are determined by the proportions of cumulus minerals. At the same time, like mineral composition, they are different in peridotites from the Peridotites Zone and SOL, and in orthopyroxenites from the Peridotite and Pyroxenite zones. Thus, peridotites from the Peridotite Zone (samples M20/366, M20/535,8, M20/589,5, M20/725,7) have SiO_2 content between 36,54 and 39.57 at Mg# 89-90 and up to 4.42 Al2O3 (up to), while peridotites from the SOL have higher SiO_2 (42.35), higher FeO at lower Mg# 86-87, which is consistent with magmatic differentiation. The latters also have much higher contents of Ni (up to 6004 ppm), Cu, Zn, and Co. The high Cu content in combination with higher Ni contents (4188-5814 ppm) relative to Ni content in the Peridotite Zone (2376-2821 ppm) are indicative of mineralized interval of the SOL.

Significant differences are also seen in the REE distribution patterns (figure): peridotites from SOL have U-shaped pattern with MREE depletion (($La/Yb)_N$ = 0,40-1.9, ($La/Sm)_N$ = 1.57-2.59; ($Gd/Yb)_N$ = 0.29-0.76)), extremely low REE abundance (below 1 times chondrites), and locally with the negative Eu anomaly. Their spider diagrams show the negative Nb and Eu anomaly, and positive Zr anomaly. Peridotites from the Peridotite Zone are characterized by the higher REE abundances, absence of Eu anomaly, and, in general, slightly LREE enriched pattern (($La/Yb)_N$ = 1,6-2.94 ($La/Sm)_N$ = 1.52-2.59; ($Gd/Yb)_N$ = 0, 89-0.96)). They also display negative Nb anomaly and variations in LILE contents. Some orthopyroxenites immediately above and below the SOL also reveal U-shaped pattern with MREE depletion (($La/Yb)_N$ = 1,01-2.60, ($La/Sm)_N$ = 1.81-2,53; ($Gd/Yb)_N$ = 0,46-0,94)) and abundances from 1 to 5 chondrites. The rocks also have negative Nb anomaly, enrichment in Th, and positive Ti anomaly. Orthopyroxenites from the Peridotite Zone have LREE-enriched pattern (($La/Yb)_N$ = 2,69-4.99, ($La/Sm)_N$ = 1.71-1,98; ($Gd/Yb)_N$ = 1,15-2,24)) at slightly higher REE abundance (6-20 times chondrites). Throughout the section, the Peridotite Zone shows no any increase in the content of the incompatible elements and Mg #, which is expected in the case of the presence of interstitial liquid.

Nd isotope studies were performed to determine the role of crustal contamination in the formation of the Monchegorsk pluton and, in particular, in the generation of the SOL. The peridotites from the Peridotite Zone have εNd = -0.3. Gabbroids from the lower marginal zone have a close εNd = -0.2. Close values were also determined in the peridotites from the SOL: from -0.8 to -0.6. At the same time, orthopyroxenites beneath and above the SOL have the much lower values of -2.4 and -2.5, indicating crustal contamination of these rocks.

The study of the PGE distribution in the rocks revealed that the peridotites from the Peridotite Zone contain 0.021 ppm PGE, with Pt/Pd = 3.33. The PGE contents increases in the bronzitites containing the SOL, being slightly higher in orthopyroxenites beneath the ore layer (PGE = 0.073; Pt/Pd = 0.51) as compared to those in the upper part of the Bronzitite Zone (PGE = 0.068, Pt/Pd = 0.38). Peridotites from the SOL have the highest PGE content (0.903 ppm) with decrease of Pt/Pd to 0.16. Note that the Au content is below detection limit, being detectable in the Orthopyroxenite and Peridotite zones (0.024-0.057 and 0.036, respectively). Such a trend of Pt/Pd decrease is indicative of differentiation processes (Wilson, Chunnett, 2006).

SOL was not a result of sequential crystallization differentiation during solidification of the massif but formed as an additional injection of an ultramafic melt in the Orthopyroxenite Zone. Based on the mineralogy, major, and trace and PGE geochemistry of its peridotites, this melt was more fractionated than the melts that formed the Peridotite Zone. The study of the Nd isotope composition revealed that the rocks of the SOL either did not experience significant crustal contamination or were contaminated by rocks with close Nd isotope composition. The high contents of ore components in the olivine from the SOL in combination with an upward increase of PGE content suggest initially high content of ore components in the melt. Assimilation of rocks enriched in PGE, Cu, and Ni, for instance, komatiites, may be proposed as one of the possible explanations. With allowance for the absence of serpentinization and significant crustal contribution, slightly U-shaped REE profiles can be explained by the interaction of a depleted (peridotite) melt with an LREE-enriched residual fluid/melt phase. If this is the case, it is possible that ore components were initially accumulated in this fluid. The U-shaped pattern is also typical of orthopyroxenite in the immediate contact with the ore horizon. This indicates that the melt emplaced as a sill in the Orthopyroxenite Zone was enriched in a fluid, which percolated in these "outer-contact" rocks. However, additional studies are required to determine its composition. While injecting, the fluid-bearing melt heated and partially melted host pyroxenites along SOL contacts and involved them in ductile flow with formation of eruptive breccias.
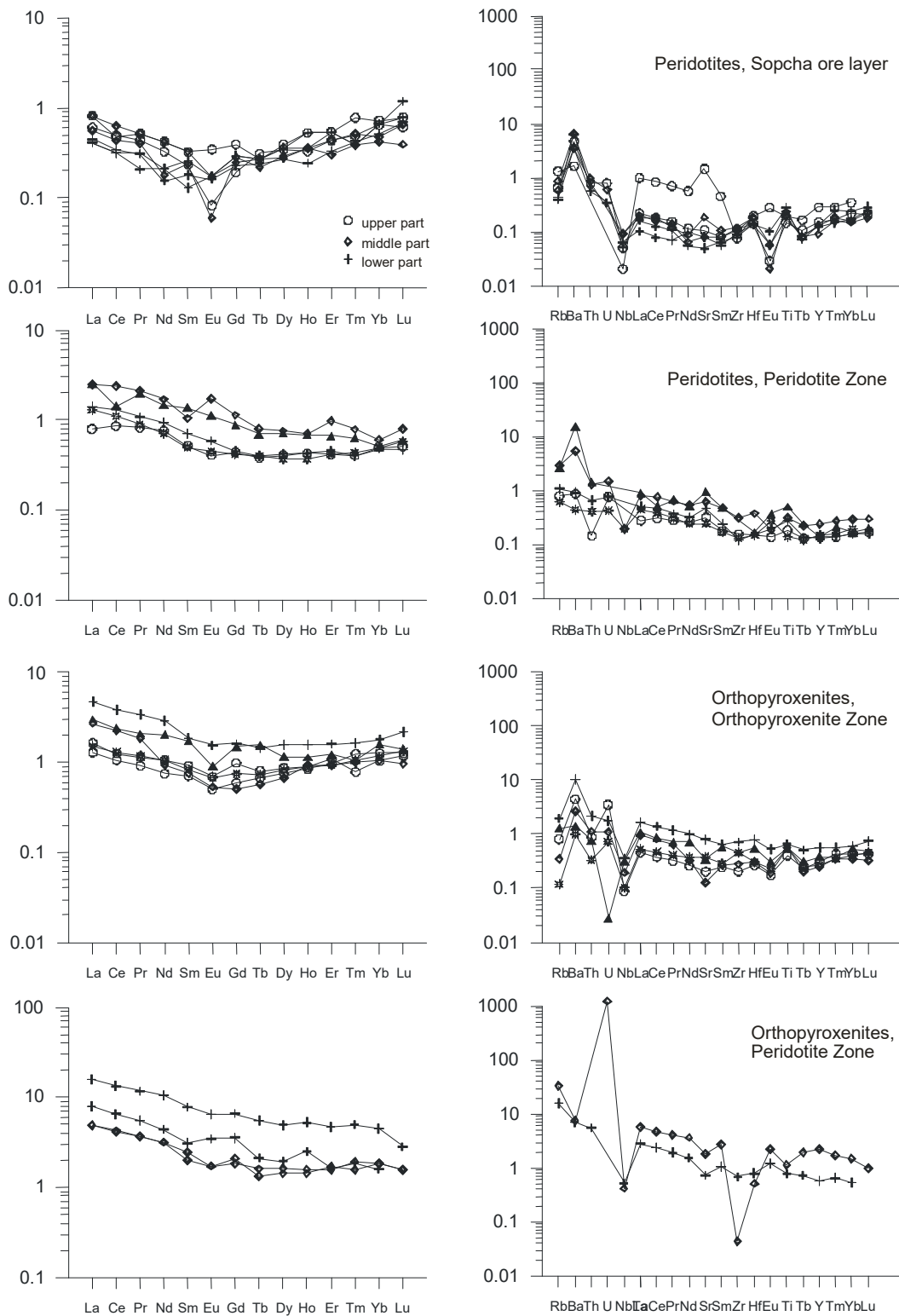
Fig. 1. REE and trace-element distribution patterns in ultramafic rocks from different zones of the Monchegorsk Pluton.

References:

Amelin Yu.V. Jeaman L.M., Semenov V.S. (1996). U-Pb geochronology of layered mafic intrusions in the eastern Baltic Shield: implications for the timing and duration of Paleoproterozoic continental rifting. Precambrian Res. 75: 31-46.

Boudreau A.E. McCallum I.S. (1992). Concentration of platinum group elements by magmatic fluids in layered intrusions. Econ. Geol. 87: 1830-1848.

Naldrett A.J. (2011). Fundamentals of magmatic sulfide deposits. Rev Econ. Geol. 17: 1-50.

Neradovsky Yu.N., Rundkvist T.V., Galkin A.S., Kliment'ev V.N. (2002).On the problem of the platinum contet of "layer-330" of Mt. Sopcha and its economic application (Monchegorsk pluton). Vestn. Murmansk. Gos. Tekhn. Univ. 5: 1-14.

Ripley, E.M., Li, C. (2003). Sulfur isotope exchange and metal enrichment in the formation of magmatic Ni-Cu-(PGE) deposits. Econ. Geol. 98: 635-641.

Sharkov E.V., Chistyakov, A.V. (2012).The Early Paleoproterozoic Monchegorsk layered mafic-ultramafite massif in the Kola Peninsula: geology, petrology and ore potential. Petrology 20: 607-639.

Sharkov E.V., Chistyakov, A.V. (2014). Geological and Petrological Aspects of Ni–Cu–PGE Mineralization in the Early Paleoproterozoic Monchegorsk Layered Mafic–Ultramafic Complex, Kola Peninsula. Geol. Ore Deposits 56: 147-168.

Smolkin, V.F., Fedotov, Zh. A., Neradovsky, Yu N., et al. (2004). Layered Intrusions of Monchegorsk Ore Region: Petrology, Minerlization, Isotopy, Deep Structure. Kola Science. Centre, Apatity.

Sobolev, A.V., Hofmann, A.W., Kuzmin, D.V., et al. (2007). The amount of recycled crust in sources of mantle-derived melts. Science 316: 412-417.

Tanner, D., Mavrogenes, J.A., Arculus, R.J., Jenner, F.E. (2014). Trace element stratigraphy of ythe Bellevue Core, Northern Bushveld: multiple magma injections obscured by diffusive processes. J. Petrol. 55: 859-882.

Wilson, A., Chunnett, G. (2006).Trace element and platinum group element distribiutions and the genesis of the Merensky Reef. Western Bushveld Complex, South Africa. J. Petrol. 47: 2369-2403.

Yudovskaya, M.A., Kinnaird, J.A., Sobolev, A.V., et al., (2013). Petrogenesis of the Lower Zone Olivine-rich cumulates beneath the Platreef and their correlation with recognized occurrences in the Bushveld Complex. Econ Geol. 108: 1923-1952.

FERRIC/FERROUS RATIO IN SILICATE MELTS: WHAT WE KNOW AND WHAT WE DON'T KNOW ABOUT IT

Borisov A.A.

Institute of Geology of Ore Deposits, Petrography, Mineralogy and Geochemistry of the Russian Academy of Sciences, Moscow, Russia, aborisov@igem.ru

The ferric/ferrous equilibrium in melts is typically described by the reaction:

$$FeO + \tfrac{1}{4} O_2 = FeO_{1.5} \tag{1}$$
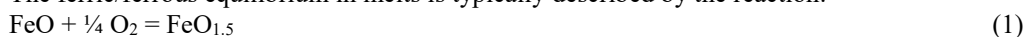
which leads to the following relation:

$$\log (X_{FeO1.5}/X_{FeO}) = \tfrac{1}{4} \log fO_2 + \log K - \log (\gamma_{FeO1.5}/\gamma_{FeO}) \tag{2}$$

where X_i and γ_i are mole fraction and activity coefficients of iron oxides in silicate melts, respectively, fO_2 is the oxygen fugacity and K is the constant of the reaction (1). For practical purposes Eq. (2) can be replaced by an empirical equation in the form:

$$\log(X_{FeO1.5}/X_{FeO}) = k \cdot \log fO_2 + h/T + \Sigma d_i X_i + c \tag{3}$$

where T is the temperature in K, and k, h, d_i and c are constants and X_i are mole fractions of the main oxide components in silicate melts, such as SiO_2, Al_2O_3, MgO, CaO, Na_2O and K_2O (e.g., Sack et al. 1980; Kilinc et al. 1983).

Tree main issues with Eq. (3) are the subject of discussion: (1) the deviation of the coefficient k from an ideal value of 0.25 down to about 0.20-0.22 (e.g., Kress and Carmichael 1988, 1989; Jayasuriya et al. 2004; Borisov 2010); (2) possible variations of coefficient h (at 1/T) as a function of melt composition (e.g., Mysen et al. 1985; Borisov 1988; Borisov and Shapkin 1990; Borisov and McCammon 2010); (3) sufficiency of $\Sigma d_i X_i$ to correctly describe the effect of melt composition on ferric/ferrous ratio (Borisov et al., 2015).

Based on our experimental and theoretical results we concluded:

(1) Complex models ($Fe^{2+} \cdot nFe^{3+}$ clusters, ferric-ferrous interaction, etc) are not better than "simple" empirical ones. We should assume k (at log fO_2) to be the same for all melt compositions and just accept that $k < 0.25$.

(2) We also should assume h (at 1/T) to be the same for all melt compositions.

(3) Although silicate melts are more complex than symmetric regular solutions, addition of only two term, $d_{SiAl} \cdot X_{SiO2} \cdot X_{Al2O3}$ and $d_{SiMg} \cdot X_{SiO2} \cdot X_{MgO}$ in empirical equation (3) allows precisely describe all our experimental compositions.

Based on literature data (e.g., Zhang et al., 2017; Waters and Lange, 2016) effects of pressure and water contents in silicate melts on ferric/ferrous ratio are also briefly discussed.

References:

Borisov A, Behrens H, Holtz F (2013) The effect of titanium and phosphorus on ferric/ferrous ratio in silicate melts: an experimental study. Contribution to Mineralogy and Petrology 166: 1577-1591

Borisov A, Behrens H, Holtz F (2015) Effects of melt composition on Fe^{3+}/Fe^{2+} in silicate melts: a step to model ferric/ferrous ratio in multicomponent systems. Contributions to Mineralogy and Petrology 169: Article 24

Borisov A, Behrens H, Holtz F (2017) Effects of strong network modifiers on Fe^{3+}/Fe^{2+} in silicate melts: An experimental study. Contributions to Mineralogy and Petrology, in press.

Borisov A, McCammon C (2010) The effect of silica on ferric/ferrous ratio in silicate melts: An experimental investigation using Mössbauer spectroscopy. American Mineralogist 95: 545-555

Borisov AA (1988) Temperature dependence of redox reactions involving variable-valency elements in model and natural melts. Geochemistry International 25: 85-93

Borisov AA (2010) Ferric-ferrous ratio in liquid iron oxides: Analysis and applications to natural basaltic melts. Petrology 18: 471-481

Borisov AA, Shapkin AI (1990) A new empirical equation relating Fe^{3+}/Fe^{2+} in magmas to their composition, oxygen fugacity, and temperature. Geochemistry International 27: 111-116

Jayasuriya KD, O'Neil HStC, Berry A, Campbell SJ (2004) A Mössbauer study of the oxidation state of Fe in silicate melts. American Mineralogist 89: 1597-1609

Kilinc A, Carmichael ISE, Rivers ML, Sack RO (1983): The ferric-ferrous ratio of natural silicate liquids equilibrated in air. Contributions to Mineralogy and Petrology 83: 136-140

Kress VC, Carmichael ISE (1988) Stoichiometry of the iron oxidation reaction in silicate melts. American Mineralogist 73: 1267-1274

Kress VC, Carmichael ISE (1989) The lime-iron-silicate melt system: Redox and volume systematics. Geochimica et Cosmochimica Acta 53: 2883–2892

Mysen BO, Virgo D, Neumann E-R, Seifert FA (1985) Redox equilibria and the structural states of ferric and ferrous iron in melts in the system $CaO-MgO-Al_2O_3-SiO_2-Fe-O$: relationships between redox equilibria, melt structure and liquidus phase equilibria. American Mineralogist 70: 317-331

Sack RO, Carmichael ISE, Rivers ML, Ghiorso MS (1980): Ferric-ferrous equilibria in natural silicate liquids at 1 bar. Contribution to Mineralogy and Petrology 75: 369-376

Waters LE, Lange RA (2016) No effect of H_2O degassing on the oxidation state of magmatic liquids. Earth and Planetary Science Letters 447: 48–59

Zhang HL, Hirschmann MM, Cottrell E, Withers AC (2017) Effect of pressure on $Fe^{3+}/\Sigma Fe$ ratio in a mafic magma and consequences for magma ocean redox gradients. Geochimica et Cosmochimica Acta 204: 83–103

HIGH-PRESSURE RAMAN STUDY OF SHORTITE CA2NA2(CO3)3

Borodina U.O., Goryainov S.V., Rashchenko S.V., Likhacheva A.Yu., Korsacov A.V., Golovin A.V.,

Institute of Geology and Mineralogy, Siberian Branch of the Russian Academy of Sciences, Novosibirsk, Russia,

uli-aniya@mail.ru

Pressure-induced changes of Raman bands parameters (position and width) of crystalline shortite, $Na_2Ca_2(CO_3)_3$, have been studied under hydrostatic compression up to 8 GPa at room temperature in diamond anvil cell. Shortite is a rare carbonate mineral with orthorhombic structure (space group *Amm*2, *a*=4.947, *b*=11.032, *c*=7.108 Å) (Dickens et al., 1971). It was first found in Green River Basin, Wyoming (Fahey, 1939), in a matrix of montmorillonite clay, but is of our interest due to its presence in kimberlitic diamonds as inclusions (Kamenetsky et al., 2006; Meyer et al., 1986).

The spectrum of shortite at atmospheric pressure contains two strong bands related to symmetric C−O stretching vibrations (ν_1), four in-plane bending (ν_4) modes, and several low-wavenumber modes of lattice vibrations. Upon the pressure increase, almost all the bands exhibit linear up-shift, and the bands of C−O stretching modes demonstrate linear broadening. The shift rates vary from 0.5 to 9.5 cm^{-1}/GPa for lattice modes and are 3.56 and 4.96 cm^{-1}/GPa for CO_3^{2-} ν_1 modes.

There are currently no Raman data on natural kimberlite diamond inclusions, but our study can be useful regarding the possibility of reconstruction of diamond formation conditions as soon as these measurements will be made. By means of comparison of such inclusions high-pressure Raman data with natural kimberlite samples spectra one can get important information about the value of residual pressures around the inclusions. In this way the depth of diamond formation can be estimated (Kagi et al., 2009; Nasdala et al., 2005).

Experimental and analytical conditions

The sample of crystalline shortite was selected from alkaline-carbonate nodules in ultra-fresh Udachnaya east kimberlites (Kamenetsky et al., 2006). A polycrystalline shortite aggregate was placed into the gasket hole of a diamond anvil cell (DAC) and compressed up to 8 GPa. KBr powder was used as an anhydrous pressure medium. The DAC is based on a modified Mao-Bell design (Fursenko et al., 1984) and employs two diamonds with 1 mm diameter culets. A Horiba Jobin Yvon LabRam HR800 spectrometer equipped with a 1024-channel liquid nitrogen/charge-coupled device detector was used. Raman spectra were excited with a 40-mW power neodymium laser (532-nm line) and collected in the spectral region of 70 to 3800 cm^{-1}. Spectral resolution was 2.5 cm^{-1}. The pressure values were measured before and after Raman measurements from a shift of the $^5D_0-^7F_0$ fluorescence band of Sm^{2+} ion (Rashchenko et al., 2015) with an accuracy of ±0.05 GPa.

Results and discussion

The Raman spectrum of shortite at ambient pressure is presented in Fig. 1a. The most intense bands at 1071 and 1090 cm^{-1}, named $\nu_{1L}(CO_3)$ and $\nu_{1H}(CO_3)$, belong to the two components of the $(CO_3)^{2-}$ symmetric stretching vibration (ν_1), in agreement with the literature data (RRUFF Database ID R040184 and ID R050248). The bands at 695-731 cm^{-1}, namely at 695, 710, 718, 731 cm^{-1}, are related to ν_4 bending region. In the region of lattice vibrations, 100-300 cm^{-1}, a number of bands are observed, mainly at 100, 172, 197 and 261 cm^{-1}.
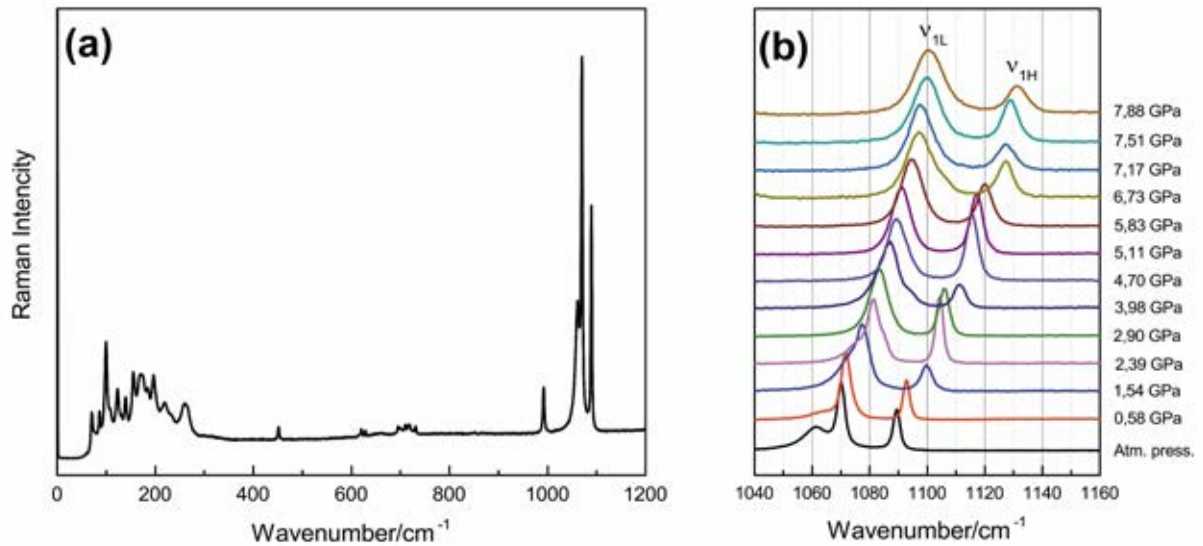
Fig. 1. Raman spectra of shortite: a – at ambient pressure; b – at high pressures in the range of $(CO_3)^{2-}$ ν_1 vibrations.

The Raman spectra of regions $(CO_3)^{2-}$ ν_1 collected at high pressure up to 7.88 GPa are presented in Fig. 1b. The modes display a linear change in wavenumber with the pressure increase (Fig. 2a). Pressure-dependent shifts, $\partial\nu_i/\partial P$, for each mode are presented in Table 1. It should be noted, that the shoulder of the $\nu_{1L}(CO_3)$ mode at 1061 cm^{-1} is well-distinguished at atmosphere pressure, but disappears at about 3 GPa when merged with the main mode (1071 cm^{-1}). At 4 GPa it appears again at higher energies side of the $\nu_{1L}(CO_3)$ mode, that is probably related to a phase transition. In the $(CO_3)^{2-}$ ν_4 region similar effect is observed. The mode at 718 cm^{-1} is well-distinguished at atmosphere pressure, but at pressures more than 1.5 GPa it presents as a shoulder of the mode at 710 cm^{-1}, and merged with the latter at about 5 GPa.
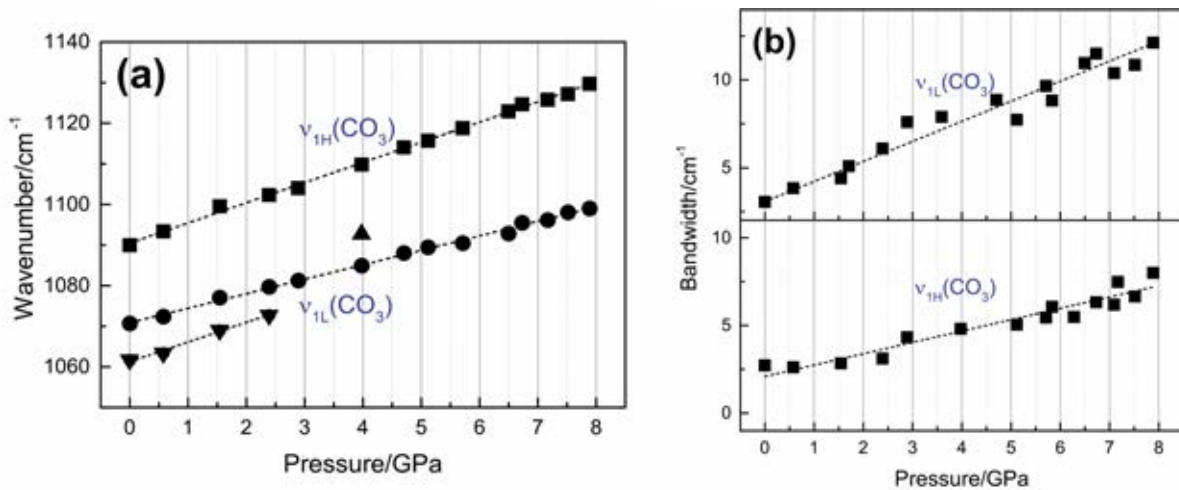
Fig. 2. The pressure dependences of the wavenumber (a) and FWHM (b) of shortite symmetric stretching modes.

Besides the increase in wavenumber, the pressure-induced broadening of stretching modes is observed. The pressure dependences of the width (FWHM) of $(CO_3)^{2-}$ ν_1 modes are shown in Fig. 2b. Both the lattice and bending ν_4 modes shift linearly with pressure, whereas their widths do not demonstrate definite pressure dependence. Rates of change for the modes are also presented in table 1. The lowest pressure-induced shifts in shortite spectra are observed for the lattice modes in the range of 100-172 cm^{-1} and the shifts of the lattice bands at 183-261 cm^{-1} are larger than those of internal (ν_1, ν_4) vibrations.

The slope of the $\nu(P)$ dependence for the symmetric stretching $\nu_{1L}(CO_3)$ and $\nu_{1H}(CO_3)$ modes is determined to be of 3.56 and 4.96 cm^{-1}/GPa, respectively, that is close to the data from (Williams et al., 2015). The shortite pressure scale based on our measurements is the following:

$$P \text{ (GPa)} = 0.28 * \nu_{1L} \text{ (cm}^{-1}) - 299.82, \tag{1}$$

$$P \text{ (GPa)} = 0.20 * \nu_{1H} \text{ (cm}^{-1}) - 218.00. \tag{2}$$

Table 1. Pressure-dependent shifts of shortite Raman modes and the pressure range the linearity of $\partial v_i/\partial P$ is fulfilled for.

v_i, cm^{-1} (at atm. pressure)	Lattice vibrations								$v_4(CO_3)$				$v_1(CO_3)$	
	100	124	149	172	183	197	213	261	695	710	718	731	1071	1090
$\partial v_i/\partial P$, cm^{-1}/GPa	1.2	0.5	2.4	2.2	4.4; 9.4	5.0	4.9	7.4	3.2	2.5	1.5	4.1	3.6	5.0
Range, GPa	0.6–4.0	2.4–6.5	5.7–7.9	0–2.9	1.7–4.0; 4.5–7.0	0–6.5	1.5–6.5	0.6–4.0	0.6–6.7	0.6–7.9	2.4–4.7	0.6–6.7	0–7.9	0–7.9

References:

Dickens B, Hyman A, Brown W (1971) Crystal Structure of Ca$_2$Na$_2$(CO$_3$)$_3$ (Shortite). J. Res. Natl. Bur. Stand. Sec. A-Phys. Chem., A 75: 129-135.

Fahey J (1939) Am. Mineral. 24: 514.

Fursenko B A, Kholdeyev O V, Litvin Y A, Kropachev V D (1984) Apparatus with transparent anvils-windows for optical and X-ray analysis under high pressure. In: Prib. Tekh. Eksp. (Moscow, USSR) 5: 174-178.

Kagi H, Odake S, Fukura S, Zedgenizov D A (2009) Raman spectroscopic estimation of depth of diamond origin: technical developments and the application. Russian Geology and Geophysics 50 (12): 1183-1187. doi: 10.1016/j.rgg.2009.11.016.

Kamenetsky V S, Sharygin V V, Kamenetsky M B, Golovin A V (2006) Chloride–Carbonate Nodules in Kimberlites from the Udachnaya Pipe: Alternative Approach to the Evolution of Kimberlite Magmas. Geochem. Int. 44 (9): 935-940. doi: 10.1134/S0016702906090084.

Meyer H O, McCallum M E (1986) Mineral inclusions in diamonds from the Sloan kimberlites, Colorado. The Journal of Geology 94 (4): 600-612.

Nasdala L, Hofmeister W, Harris J W, Glinnemann J (2005) Growth zoning and strain patterns inside diamond crystals as revealed by Raman maps. Am. Mineral. 90 (4): 745-748. doi: 10.2138/am.2005.1690.

Rashchenko S V, Kurnosov A, Dubrovinsky L, Litasov K D (2015) Revised calibration of the Sm:SrB$_4$O$_7$ pressure sensor using the Sm-doped yttrium-aluminum garnet primary pressure scale. J. Appl. Phys. (Melville, NY, U. S.) 117 (14): 145902. doi: 10.1063/1.4918304.

Williams Q C, Vennari C, O'Bannon III E F (2015) High pressure Raman and single crystal X-ray diffraction of the alkali/calcium carbonate, shortite. In: AGU Fall Meeting Abstracts. MR13B-2703.

EVOLUTION AND FORMATION CONDITIONS FOR PYROCHLORE-SUPERGROUP MINERALS OF CHUKTUKON CARBONATITE MASSIF, CHADOBETS UPLAND (KRASNOYARSK TERRITORY, RUSSIA)

Chebotarev D.A.[1], Doroshkevich A.G.[1,2], Sharygin V.V.[1,3]
[1]Institute of Geology and Mineralogy, Siberian Branch of the Russian Academy of Sciences, Novosibirsk, Russia, chebotarev@igm.nsc.ru
[2]Geological Institute, Siberian Branch of the Russian Academy of Sciences, Ulan-Ude, Russia, doroshkevich@igm.nsc.ru
[3]Novosibirsk State University, Novosibirsk, Russia, sharygin@igm.nsc.ru

Niobium is a relatively rare lithophile transition metal. It is a critical metal, which is very useful in the industry. The bulk of global production of niobium comes from pyrochlore-supergroup minerals and, to a lesser degree, from columbite group minerals and loparite. Minerals of the pyrochlore supergroup are common accessory phases of carbonatites and related alkaline rocks (Lumpkin and Ewing, 1995, 1996). The pyrochlore-supergroup mineral concentrates are produced mainly from carbonatites.

Although current nomenclature for the pyrochlore supergroup, approved by CNMNC-IMA (Atencio et al., 2010) allows the presence of Si at B-site and pyrochlore-supergroup minerals with high Si contents are fairly common in geochemically evolved parageneses, thus far the role of Si in the structure of the mineral still remains controversial. It is belived, that the Si presented as a dispersed crystalline or amorphous phase (Hogarth 1977, Hogarth & Horne 1989, Voloshin et al. 1989) or as an essential part of the structure. The authors of the current nomenclature recommend to attribute no more than 50% of Si to B-site and assuming that low Si contents can be included to B-site.

Here we present a new information about the pyrochlore-group minerals from carbonatites of the Chuktukon carbonatite massif. Our work describes zoning and chemistry and possible conditions of crystallization and alteration of the pyrochlore-group minerals during the evolution of the massif.

The Chuktukon carbonatite massif one of intrusion complexes of the Chadobets upland (SW of Siberian platform, Russia). Intrusive rocks of the Chadobets upland are presented by ultramafic alkaline rocks (melilitite-nepheline and pyroxene peridotites, picrite, melteigite), carbonatite and kimberlite (Slukin, 1994; Lapin, 1997, 2001; Lapin and Lisitsyn, 2004; Kirichenko et al., 2012). Carbonatites compose stockwork of veins and streaks and stock-like bodies of 1.2x0.7 km. Among the carbonatites composing stock-like bodies and large veins, the fine- and medium-grained varieties are predominant. The main primary mineral is calcite; the minor and accessory primary minerals are dolomite, strontianite, pyrochlore-supergroup minerals, Nb-rutile, rippite, fluorapatite, pyrite, tainiolite, ancylite-(Ce) and potassic feldspar (Chebotarev, 2016; Chebotarev et al., 2016, 2017 (in press); Doroshkevich et al., 2016a,b; Sharygin et al, 2016a,b). The carbonatites underwent hydrothermal alteration from weak to very intensive, which led to the formation of quartz, barite, goethite, romanechite, parisite-(Ce), synchysite-(Ce), monazite-(Ce), carbonate-rich fluorapatite, aegirine. In the weathering crust upon carbonatites goethite, florencite-(Ce), romanechite, kaolinite and monazite-(Ce) are the main minerals and churchite-(Y), zircon and rutile are accessory minerals.

Table 1. Composition of the pyrochlore-group minerals from the Chuktukon carbonatite

wt.%	Fluorcalcipyrochlore Average, n=10	Strontiopyrochlore Average, n=5	Sr-rich calcipyrochlore	Calcipyrochlore	
Na_2O,	6.9 (3)	0.8 (9)	1.1	2	1.6
CaO	16.7 (6)	4 (1)	6.8	15.5	10.6
SrO	0.82 (14)	11.2 (5)	9.7	2	6.3
BaO	-	-	2.39	0.02	1.3
PbO	-	-	-	-	-
La_2O_3	0.05 (3)	0.4 (1)	0.25	0.17	0.18
Ce_2O_3	0.13 (8)	0.5 (7)	0.12	0.07	0.13
Nd_2O_3	0.04 (2)	0.03 (1)	-	0.04	0.03
Pr_2O_3	0.03 (1)	0.07 (3)	0.08	0.01	0.02
ThO_2	0.1 (1)	0.09 (8)	0.03	-	0.02
UO_2	0.06 (5)	0.4 (4)	0.14	0.3	0.16
SiO_2	1.4 (14)	2.7 (9)	3.1	0.12	3.3
TiO_2	3.3 (7)	3.3 (3)	3.2	2.9	3.2
ZrO_2	1.1 (9)	1.3 (11)	2.0	0.1	1.9
Fe_2O_3	0.7 (5)	2 (1)	1.2	0.8	1.3
Nb_2O_5	64 (2)	59.4 (12)	61.4	69.9	60.9
Ta_2O_5	0.07 (3)	0.2 (1)	0.06	0.1	0.09
F	4.9 (2)	1.9 (8)	1.8	1.8	2
K_2O	0.08 (6)	0.2 (1)	0.11	0.04	0.16
Total	99.98 (13)	91.26 (19)	93.47	95.96	93.13

Standart deviation is presented in parentheses.

Pyrochlore-supergroup minerals form octahedral light brown, brown to black crystals 0.2-1 mm in size. The minerals contain primary inclusions of calcite, strontianite, fluorapatite and secondary inclusions of barite and carbonate-rich fluorapatite (Chebotarev et al., 2016). It has two types of zonation: oscillatory and spotty-mosaic. The spotty-mosaic zonation might combine within one crystal with oscillatory one and confined to the outer crystal parts and crystal defect borders: cracks and weakened areas along inclusions. The spotty-mosaic crystals are abundant in the hydrothermally altered carbonatites.

The B-site of all the Chuktukon pyrochlore-supergroup minerals are generally occupied by Nb, matching the pyrochlore group composition (Atencio et al., 2010), and occupancy of the A- and Y-sites highly varies (table 1, fig. 1). The crystals with oscillatory zaonation can be classified as fluorcalciopyrochlore. Composition of altered pyrochlores generally falls to calico-, strontio- and kenopyrochlore subgroups (Atencio et al., 2010).

The constancy of fluctuations of Nb, Ti and Si and other elements in the oscillation-zoned pyrochlore crystals can be related to the rhythmical chemistry variations of the mineral-forming environment during pyrochlore formation. It may have relatively high activity of Si, which allowed incorporating Si in the structure of the mineral. It is also confirmed by presence of rippite (potassium-niobium silicate) in the primary Chuktukon carbonatite. Rippite also contains inclusions of pyrochlore with a composition close to the oscillation-zoned pyrochlore crystals.

Some researchers (Nasraoui, Bilal, 2000; Nasraoui, 1996) believe that fluids with relatively low pH, a_{Na^+}, and $a_{Ca^{2+}}$ and relatively high a_{LREE} allow the redistribution of pyrochlore substance with the origin of areas enriched with LREE.

Li and Zhou (2015) hypothesized that fluids rich in F, Cl, CO_2, but undersaturated in Na, Ca and REE interact with REE-rich fluorapatite, leaching out REE from the mineral, especially LREE. It led to formation of spotty-mosaic fluorapatite with REE-inclusions. LREE, leached out from fluorapatite and saturated in fluid, at a small distance transform into REE minerals, forming bastnaesite-(Ce) and monazite-(Ce) grains. Such metasomatic alteration events are described in numerous natural objects: the Yinachang Fe-Cu-REE deposit, Southwest China; the Pogranichnoe and Seligdar carbonatites, Russia; Gloserhia Granite Pegmatite, Norway; the Se-Chahun deposit, Iran and others.
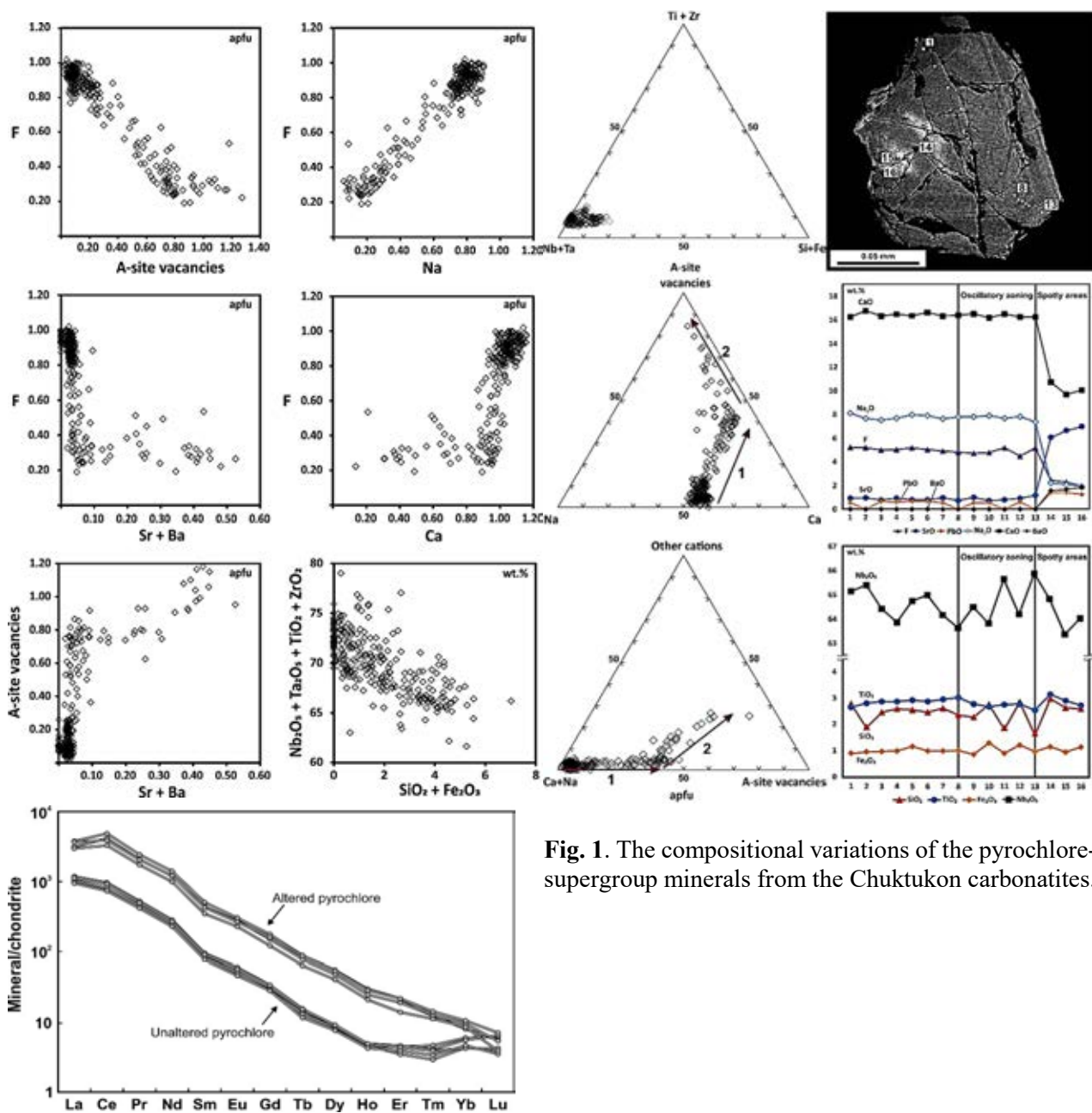
Fig. 1. The compositional variations of the pyrochlore-supergroup minerals from the Chuktukon carbonatites.

These natural observations are confirmed by experimental data with removal of REE from primary apatites and formation of monazite induced by the rich in F and Cl fluids (Harlov et al., 2002; Harlov and Forster, 2003; Harlov et al., 2005).

We believe that a similar model can be applied to describe the evolution of pyrochlore from the Chuktukon carbonatites. Strong differences in the content of REE between unaltered and altered pyrochlore indicates that the enrichment of REE was the result of the interaction with the fluid. Hydrothermal alteration process led to redistribution of components in the primary pyrochlore crystals, leaching out Na, Ca, F and enrichment of its certain domains by Sr, Ba, Pb, Nb and REE. Considering fibre aggregates of Ca-REE-fluorcarbonates in quartz and according to experimental data (Soisson et al., 1961; Timofeev et al., 2015), alteration fluid likely have relatively high activity of HF.

Pyrochlore enrichment in Sr, Ba, Pb, and REE and depletion in F, Na, Ca and Nb may occur according to the following substitution reactions (fig. 1):

$Na + F^- \rightarrow VA + VY$ (trend 1)

$Ca + O \rightarrow VA + VY$; $VA + VY \rightarrow A^{2+}$, REE + O, H_2O, OH^- (trend 2)
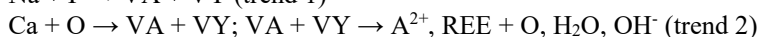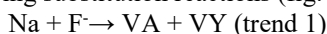
where A^{2+} - A-site cation (Sr, Ba, etc), VA and VY are A- and Y-site vacancies, respectively.

The pyrochlore transformation is summarized by follow equation (Nasraoui, Bilal, 2000):

$3H^+_{(aq)} + H_2O_{(aq)} + [NaCaNb_2O_6F]_{(s)} = [\square_2Nb_2O_5\square 2H_2O]_{(s)} + Na^+_{(aq)} + Ca^{2+}_{(aq)} + HF_{(aq)}$
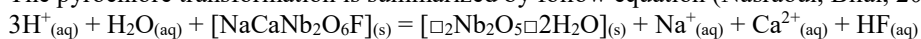
The described alteration trends is common to most carbonatitic pyrochlores worldwide (Lumpkin and Ewing, 1995).

Conclusions

The oscillatory-zoned pyrochlore-group minerals from the Chuktukon carbonatite is seemed to crystallized at relatively high a_{Si} in the melt. Hydrothermal changes in carbonatites led to an alteration of the pyrochlore-supergroup minerals and to the formation of spotty-mosaic zonation.

References:

Atencio D., Andrade M.B., Christy A.G., Giere R., Kartashov P.M. (2010) The pyrochlore-supergroup of minerals: nomenclature. The Canadian Mineralogist, v. 48, pp. 673-698.

Chebotarev D.A. (2016) Compositional and internal structure features of pyrochlores from carbonatites of the Chuktukon carbonatite complex // Moscow International School of Earth Sciences – 2016. Abstracts of International conference. 23-28 May of 2016/ Editor-in-chief L.N. Kogarko. – M.: GEOKHI RAS, p. 41-42.

Chebotarev D.A., Doroshkevich A.G., Sharygin V.V. (2016) The niobium mineralization in the carbonatites of the Chuktukon massif, the Chadobets upland (the Krasnoyarsk region, Russia). 33rd International conference «Alkaline Magmatism of the Earth and related strategic metal deposits», Moscow, Russia. Abstracts. 27 may, 2016. Editor-in-chief L.N. Kogarko – M.: GEOKHI RAS, p. 36. (In Russian).

Doroshkevich A.G., Sharygin V.V., Seryotkin Y.V., Karmanov N.S., Belogub E.V., Moroz T.N., Nigmatulina E.N., Eliseev A.P., Vedenyapin V.N. and Kupriyanov I.N. (2016a) Rippite, IMA 2016-025. CNMNC Newsletter No. 32, August 2016, page 919; Mineralogical Magazine, vol 80, p 915–922.

Doroshkevich, A.G., Chebotarev, D.A., Sharygin, V.V. (2016b) Alkaline ultrabasic carbonatitic magmatism of the Chadobets upland. // In: Kogarko, L.N. (Ed.): Moscow International School of Earth Sciences - 2016, Moscow (23-28 May 2016), Abstracts, 48-49.

Doroshkevich A.G., Wall F., Ripp G.S. (2007) Magmatic graphite in dolomite carbonatite at Pogranichnoe, North Transbaikalia, Russia. Contributions to Mineralogy and Petrology, v. 153, p. 339-353.

Harlov D.E., Forster H.J. and Nijland T.G. (2002) Fluid-induced nucleation of REE-phosphate minerals in apatite: nature and experiment. Part I. Chlorapatite. American Mineralogist, v. 87, p. 245–261.

Harlov D. E. and Forster H. J. (2003) Fluid-induced nucleation of REE phosphate minerals in apatite: nature and experiment. Part II. Fluorapatite. American Mineralogist, v. 88, p. 1209–1229.

Harlov D.E., Wirth R. and Forster H.J. (2005) An experimental study of dissolution–reprecipitation in fluorapatite: fluid infiltration and the formation of monazite. Contributions to Mineralogy and Petrology, v. 150, p. 268–286

Harlov D.E. (2011) Formation of monazite and xenotime inclusions in fluorapatite megacrysts, Gloserheia Granite Pegmatite, Froland, Bamble Sector, southern Norway. Mineralogy and Petrology, v. 102, p. 77–86.

Hogarth, D.D. & Horne, J.E.T. (1989): Non-metamict uranoan pyrochlore and uranpyrochlore from tuff near Ndale, Fort Portal area, Uganda. Mineralogical Magazine, v. 53, p. 257-262.

Li X.C. and Zhou M.F. (2015) Multiple stages of hydrothermal REE remobilization recorded in fluorapatite in the Paleoproterozoic Yinachang Fe-Cu-(REE) deposit, Southwest China. Geochimica et Cosmochimica Acta, v. 166, p. 53–73.

Lumpkin, G.R., Ewing, R.C. (1995) Geochemical alteration of pyrochlore group minerals: pyrochlore subgroup. American Mineralogist 80, 732–743.

Lumpkin, G.R., Ewing, R.C. (1996) Geochemical alteration of pyrochlore group minerals: betafite subgroup. American Mineralogist 81, 1237–1248.

Nasraoui M., Bilal E. (2000) Pyrochlores from the Lueshe carbonatite complex (Democratic Republic of Congo): a geochemical record of different alteration stages. Journal of Asian Earth Sciences, v. 18, p. 237-251.

Nasraoui, M. (1996) Le gisement de Nobium de Lueshe (Nord Est du Zaire): evolution geochimique et mineralogique d'un complexe carbonatitique en contextes hydrothermale et supergene. // Ph.D. thesis, Ecole des Mines de Paris/Ecole des Mines de Saint Etienne.

Prokopyev I.R., Doroshkevich A.G., Ponomarchuk A.V., Sergeev S.A. (2017) Mineralogy, age and genesis of apatite-dolomite ores at the Seligdar apatite deposit (Central Aldan, Russia), Ore Geology Reviews, v. 81, №1, p. 296-308.

Sharygin V.V., Doroshkevich A.G., Seryotkin Y.V., Karmanov N.S., Belogub E.V., Moroz T.N. (2016a) A new K-Nb-cyclosilicate $K_2(Nb,Ti)_2(Si_4O_{12})O(O,F)$ from Chuktukon carbonatite massif, Chadobets upland, Russia // 2nd European Mineralogical Conference. Rimini, Italy. P.421-421.

Sharygin V.V., Doroshkevich A.G, Chebotarev D.A. (2016b) Na-Sr-Ba-REE-carbonates and phosphates in minerals of Chuktukon massif carbonatites, Chadobets upland, Krasnoyarsk territory // Conference: XVII Russian Fluid Inclusion conference, September 2016, At Ulan-Ude, Russia, p. 180-182

Soisson D.J., McLafferty J.J., Pierret J.A. (1961) Staff-Industry Collaborative Report: Tantalum and Niobium. Industrial and Engineering Chemistry, v. 53, №11, p. 861–868. doi:10.1021/ie50623a016

Timofeev A., Migdisov Art.A., Williams-Jones A.E. (2015) An experimental study of the solubility and speciation of niobium in fluoride-bearing aqueous solutions at elevated temperature. Geochimica et Cosmochimica Acta, v. 158, p. 103-111.

Voloshin, A.V., Pakhomovskiy, Ya.A., Pushcharovskiy, L.Yu., Nadezhina, T.N., Bakhchisaraytsev, A.Y. & Kobyashev, Yu.S. (1989): Strontium pyrochlore: composition and structure. Novye Dannye o Mineralakh SSSR, v. 36, p. 12-24 (in Russian).

EXTERNALLY HEATED DIAMOND ANVIL CELL TECHNIQUE FOR HIGH-PRESSURE STUDIES OF MANTLE FLUIDS

Chertkova N.V., Ohfuji H., Nomura R., Irifune T.
Ehime University, Matsuyama, Japan, chertkova.nadezda.sj@ehime-u.ac.jp

A diamond anvil cell is a remarkable tool for the investigation of various properties of fluids, melts and minerals *in situ* directly at experimental conditions. Heating methods in the diamond anvil cell experiments include internal laser heating, external and internal resistive heating and inductive heating (Ming and Bassett, 1974; Shen et al., 1996; Dubrovinsky et al., 2009; Bassett et al., 1993; Balzaretti et al., 1999; Zha and Bassett, 2003; Shinoda and Noguchi, 2008). Among these methods, internal laser heating and external resistive heating are the most commonly used techniques. One of the main disadvantages of laser-heating method is a steep temperature gradient across the sample (e.g., Rainey and Kavner, 2014), which makes it difficult to reach thermal and chemical equilibrium during experiment (e.g., Ozawa et al., 2009; Sinmyo and Hirose, 2010).

In this work, we describe an external heating system, which is compatible with a lever type diamond anvil cell (Whale cell) and suitable for experiments at simultaneous high temperatures and high pressures. An external heater was placed in the central part of the diamond anvil cell, in which heat was transferred to the sample through radiation mechanism. This configuration provided effective heating of the metal gasket, containing sample, while the temperature of the backside of diamond anvils was maintained at low enough, thus protecting the diamond anvils from graphitization at high temperatures. A number of wire heaters with variable lengths, diameters and metal compositions were tested in the pure argon or argon + hydrogen atmosphere. Temperatures above 900 °C were achieved with this heating system at pressures of ~6 GPa without any substantial damages to the anvils. These experimental conditions exceed those reported in the previous optical studies by hydrothermal diamond anvil cells with resistive heaters (e.g., Bureau and Keppler, 1999; Audétat and Keppler, 2004; Mysen, 2015). The main advantages of our developed system are homogeneous heating of the sample, visual and spectroscopic access to the sample for *in situ*, direct observation at high-pressure conditions (at least, up to ~6 GPa).

This developed heating system was applied for the investigation of behavior of C-O-H fluid under upper mantle conditions. Visual observations and *in situ* Raman spectroscopy were carried out during experiments. Some of the observed phases were not quenchable and were only detected during heating, which underlines the importance of the obtained *in situ* data. Experimental results of this study give insights on the mobility and transporting properties of C-O-H fluid in the Earth's interior.

References:

Audétat A., Keppler H. (2004) Viscosity of fluids in subduction zones. Science, 303: 513-516.

Balzaretti NM, Gonzalez EJ, Piermarini GJ, Russell TP (1999) Resistance heating of the gasket in a gem-anvil high pressure cell. Review of scientific instruments, 70: 4316-4323.

Bureau H., Keppler H. (1999) Complete miscibility between silicate melts and hydrous fluids in the upper mantle: experimental evidence and geochemical implications. Earth and Planetary Science Letters 165: 187-196.

Dubrovinsky L, Glazyrin K, McCammon C, Narygina O, Greenberg E, Übelhack S, Chumakov AI, Pascarelli S, Prakapenka V, Bock J, Dubrovinskaia N (2009) Portable laser-heating system for diamond anvil cells. Journal of synchrotron radiation 16: 737-741.

Ming LC, Bassett WA (1974) Laser heating in the diamond anvil press up to 2000 C sustained and 3000 C pulsed at pressures up to 260 kilobars. Review of Scientific Instruments 45: 1115-1118.

Mysen, B. (2015) Carbon speciation in silicate-COH melt and fluid as a function of redox conditions: An experimental study, in situ to 1.7 GPa and 900 C. American Mineralogist, 100: 872-882.

Ozawa H, Hirose K, Mitome M, Bando Y, Sata N, Ohishi Y (2009) Experimental study of reaction between perovskite and molten iron to 146 GPa and implications for chemically distinct buoyant layer at the top of the core. Physics and Chemistry of Minerals 36: 355-363.

Rainey ESG, Kavner A (2014) Peak scaling method to measure temperatures in the laser-heated diamond anvil cell and application to the thermal conductivity of MgO. Journal of Geophysical Research: Solid Earth 119: 8154-8170.

Shen G, Mao HK, Hemley RJ (1996) Laser-heated diamond anvil cell technique: double-sided heating with multimode Nd: YAG laser. Computer 1: L2.

Shinoda K, Noguchi N (2008) An induction heating diamond anvil cell for high pressure and temperature micro-Raman spectroscopic measurements. Review of Scientific Instruments 79: 015101.

Sinmyo R, Hirose K (2010) The Soret diffusion in laser-heated diamond-anvil cell. Physics of the Earth and Planetary Interiors 180: 172-178.

Zha CS, Bassett WA (2003) Internal resistive heating in diamond anvil cell for in situ X-ray diffraction and Raman scattering. Review of scientific instruments 74: 1255-1262.

SERBO-MACEDONIAN MAGMATIC AND METALLOGENETIC BELT REVISITED: FOUR EXAMPLES OF THE LINK BETWEEN MAGMA MIXING AND MINERALIZATION PROCESSES

Cvetković V., Šarić K., Prelević D.

University of Belgrade, Belgrade, Serbia, vladica.cvetkovic@rgf.bg.ac.rs, kristina.saric@rgf.bg.ac.rs; dejan.prelevic@rgf.bg.ac.rs

The Balkan sector of the Alpine – Carpathian – Balkan orogen chain hosts two important magmatic and metallogenic provinces (Fig. 1). The eastern one is the Carpatho-Balkan Province that is represented by the well-known Late Cretaceous Banatite-Timok-Srednjegorje Belt with Cu-Au±Pb-Zn porphyry and high sulphidation epithermal deposits (Von Quadt et al., 2001, 2005, among others). In the west occurs the Cenozoic Serbo-Macedonian Metallogenic and Magmatic Province (hereafter SMMP; Janković, 1984), which is characterized by the Pb-Zn-Ag±Sb±W metallogeny. It is generally accepted that the SMMP resulted from a complex geodynamic history that post-dates the closure of the Mesozoic Tethys (e.g, Schmid et al., 2008; Cvetković et al., 2016a), however, at the local scale, the details of the relationship between tectonomagmatic processes and the formation of various epithermal vein, skarn, carbonate replacement, and detachment fault-hosted ore deposits is much less understood.
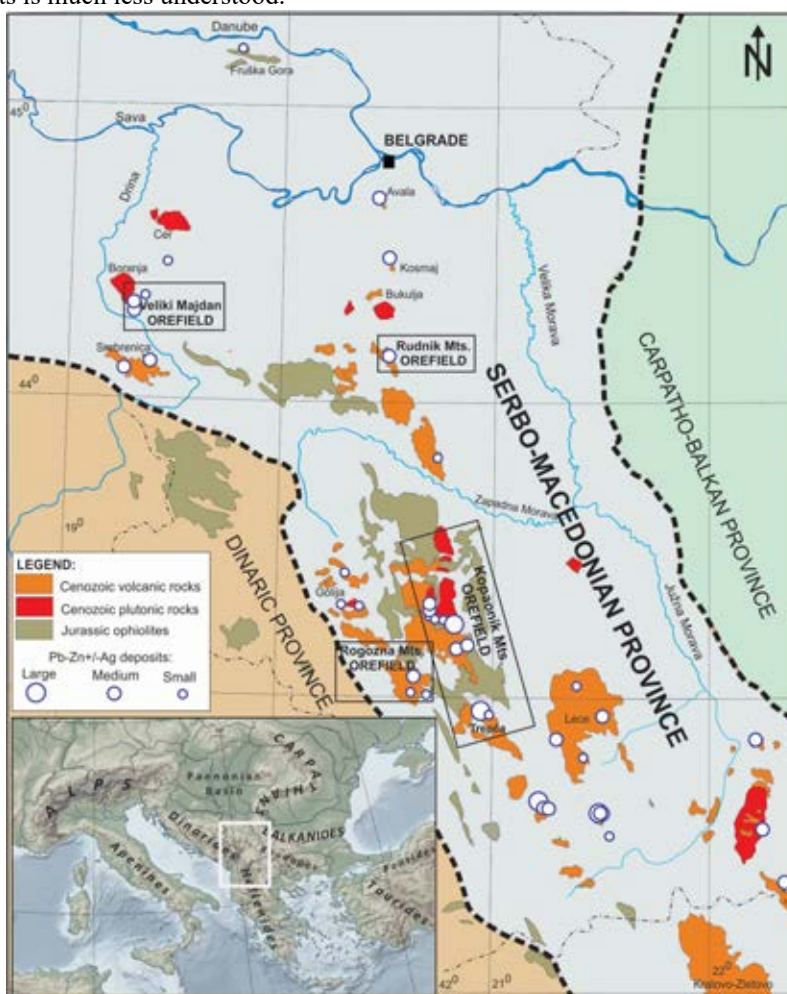
Fig. 1. The distribution of Cenozoic magmatic complexes and Pb-Zn±Ag ore deposits (Geological Atlas of Serbia - Dimitrijević, 1992, in combination with data from Monthel et al., 2002); the orefields addressed in this study are squared.

In this short review we revisit the Serbian sector of the SMMP in order to shed more light on the link between magmatism and mineralization. This approach is principally enabled by a recent progress in the current knowledge about Cenozoic post-collisional magmatism in this area. Recent interpretations of new geochemical and petrological data provide additional constraints on the genetic relationship between multi-episodic igneous activity responsible for given mineralization events. Here we briefly present the geology of four different areas (orefields) where similar magmatic-metallogenic patterns have been recorded (see squares in Fig. 1). On the basis of this information we suggest that magma-mixing events were likely of large importance for hydrothermal processes in the SMMP.

The four case examples

The **Veliki Majdan orefield** situated in NW Serbia, in the vicinity of the Early Oligocene (K/Ar age ≥30 Ma) granodiorite pluton of Boranja and subordinate and presumably younger (?) Late Oligocene/Early Miocene (27-31 Ma) dacite-quartz latite volcanics (Karamata et al., 1992), which both intrude a pre-Cenozoic basement composed of shists and limestones. The Pb-Zn±Ag orebodies are irregular to tabular in shape and are located mostly along the contacts

between dacite to quartz latite dykes and dolomitic limestones. The origin of mineralization, which is predominantly represented by pyrrhotite, pyrite, galena, sphalerite and Ag-bearing tetrahedrite, is attributed to the effects of contact metamorphism caused by the Boranja pluton, similarly to all other deposits in the wider area (Radosavljevic et al., 2013). However, it is clear that the Veliki Majdan orebodies are spatialy very closely associated to variably hidrothermally altered shallow intrusive dykes which were considered composite igneous bodies (dacite-quartzlatite-leucominette) originated by magma mixing processes (Prelević et al., 2004).

The **Rudnik Mts. orefield** is located in central Serbia, where a basement of various Cretaceous flysch sediments with abundant limestone olistoliths is overlain and cut by acid to intermediate calc-alkaline volcanic and shallow intrusive rocks, respectively. Cvetković et al. (2016b) recognized two clearly different volcanic events; the first occurred ≥35 Ma (K/Ar and U/Pb zircon ages) when only extrusive to intrusive dacite-andesite facies originated, whereas the second occurred ≤23 Ma and gave rise to widespread volcanic, pyroclastic and shallow intrusive facies of mostly quartz latite compositions. The orebodies are spatially related to the younger dyke facies and appear as mostly platy to vein- and lens-like bodies composed of pyrrhotite, Ni-bearing pyrrhotite, sphalerite, galenite, chalcopyrite and subordinate arsenopyrite (Stojanović et al., 2006). Cvetković et al. (2016b) reported an U/Pb concordia age for zircons from a hydrotermally altered quartz latite, thereby constraining the maximum age of the formation of ore deposit. The same authors suggest that the younger volcanic event was associated to large (Plinian?) explosive events that were likely triggered by injection of hot ultrapotassic lamproite-like melts into an already stratified chamber with a fractionating calc-alkaline dacite-like melt. The role of magma mixing events in this area in the formation of a composite semilamprophyre volcanic dome was earlierly invoked by Prelević et al. (2001).

The **Rogozna Mts. orefield** is located in south Serbia. It is petrogenetically associated with the Mts. Rogozna Oligocene-Early Miocene volcanic complex that was developed over a basement composed of Jurassic serpentinite (±amphibiolite) overlain by Upper Cretaceous flysch deposits. The available superposition and K/Ar and Ar/Ar ages (Memović, 1990; Borojević-Šoštarić et al., 2012) suggest that magmatism developed roughly in two phases: the first was dacite-andesite in compostion, whereas the second one was related to the formation of high-K calc-alkaline to ultrapotassic quartz latite. Pb–Zn±Ag occurrences and deposits represented by vein-type deposits hosted in amphibolites, gneisses and Triassic schists and listwanite deposits are mainly hosted in serpentinites. Borojević-Šoštarić et al. (2012) reported an age of hydrothermal alteration of 28.6±0.5 Ma and confirmed that the main Pb-Zn-Ag mineralization event was associated to the younger volcanic phase. The same authors reported numerous examples of disequilibrium reactions, such as phlogopitized biotites and Mg-rich rims of hornblende phenocrysts, and suggested that the quartz latites associated to the ore formation originated via mixing processes between dacite-like melts and lamproite-like magmas.

The **Kopaonik Mts. orefield** is part of a much larger magmatic and metallogenic district situated in south Serbia and further on in Kosovo and Metohija. The basement consists of various members of ophiolite melange rocks that are overlain by Upper Cretaceous flysch sediments. There are various plutonic and volcanic rocks that widely range in age (from >30 Ma to ~10 Ma) and composition (from acid/intermediate to basaltic and from calc-alkaline to high-K alkaline and ultrapotassic). These plutonic-volcanic rocks host several very large Pb-Zn-Ag hydrothermal and vein deposits, the largest of which is Trepča (Monthel et al., 2002). Tectonomagmatic reconstructions in this area (e.g., Schefer et al., 2011; Mladenović et al., 2015) allow for recognizing at least two stages of acid to intermediate calc-alkaline magmatism - an Early Oligocene magmatic stage (>30 Ma), when granodiorite to dacite-andesite magmas emplaced and a Late Oligocene/Early Miocene stage (<30 Ma) when quartzmonzonite to quartzlatite rocks originated. Mladenović et al. (2015) argued that the younger stage was associated to magma mixing events that likely triggered intensive explosive eruptions and formation of widespread pyroclastic products.

Discussion and conclusions

The above presented key examples on four different orefields in the CMMP suggest that apart of the generally known temporal link between Cenozoic magmatism and metallogeny in this region, there are likely other specific aspects of this relationship that may be underlined. First, in all areas occurred at least two stages of calk-alkaline magmatism, second, the younger stage shows evidence that magma mixing has played important petrogenetic role and third, it is this younger stage that most likely has controlled Pb-Zn±Ag mineralization events.

A simplified time frame sketch of magmatic and mineralization events in the studied orefields is given in Fig. 2. The temporal succession of events seems to be best resolved in the Rudnik Mts. and the Rogozna Mts. orefields, because in these areas both fresh and hydrothermally altered magmatic rocks are dated radiometrically and with sufficient precision. The largest repose periods between the two magmatic events (cca 10 my) was revealed in the Rudnik Mts, whereas in the Rogozna Mts. there likely occurred continuous magmatism with the younger phase of <30 Ma. In addition, in both Rudnik Mts. and Rogozna Mts. there is convincing evidence that during the younger phase occurred mixing between a dacite magma and lamproite-like melts, which most likely was responsible for explosive volcanic activity and the formation of various pyroclastic rocks. The role of similar hybridization processes is unequivocally explained in case of the composite leucominette dykes of the Veliki Majdan orefield, which is taken as a classical example of how lamprophyre ropcks can be formed by mixing between dacite and lamproite melts (Prelević et al., 2004). Unfortunately, the available radiometric data do not exhibit difference in age between the emplacement of the Boranja granodiorite pluton and the formation of the leucominette of Veliki Majdan, although some dykes are found to cut the pluton thereby suggesting that they emplaced later (Kubat et al., 1968). The situation in the area of the Kopaonik Mts. is very similar in that there occurred also two stages of magmatism with the younger one associated to mixing between a calc-alkaline dacite-like magma and a high-K melt. The true link between the younger magmatic stage and mineralization has not been

unequivocally established, but it should be noted that the largest deposit of Trepča is spatially associated to presumably hybridized quartz latite rocks and their abundant pyroclastic products.
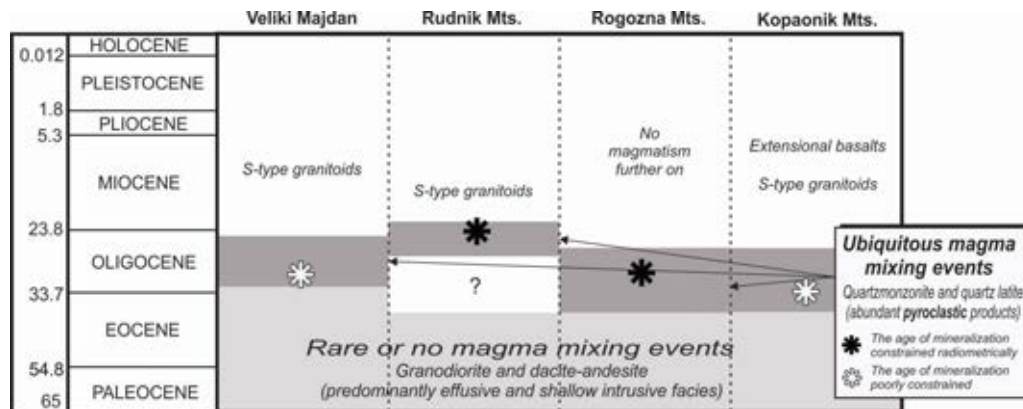

Fig. 2. The time frame of magmatic and metallogenic events in the studied orefields.

We suggest that these four examples inevitably indicate that there is a strong link between magma mixing processes and the formation of Pb-Zn deposits. It further means that future studies should focus on recognizing other areas where a similar petrology-ore deposit pattern exists and also try to perform more detailed geochronological and geochemical investigations in order to provide answers such as, for instance, how important magma mixing events were for introducing more water in the late magmatic systems and how much newly injected lamproite-like magmas acted as Pb-source for hydrothermal fluids and formation of ore deposits.

References:

Borojević Šoštarić S, Cvetković V, Neubauer F, Palinkaš LA, Bernroider M, Genser J (2012) Oligocene shoshonitic rocks of the Rogozna Mts. (Central Balkan Peninsula): evidence of petrogenetic links to the formation of Pb-Zn-Ag ore deposits. Lithos 148, 176-195

Campbell IH, Turner JS (1986) The influence of viscosity on fountains in magma chambers. J Petrol 27, 1, 1–30

Cvetković V, Prelević D, Schmid S (2016a) Geology of South-Eastern Europe. In: Papić P (ed) Mineral and Thermal Waters of Southeastern Europe. Springer, pp 1-30

Cvetković V, Šarić K, Pécskay Z, Gerdes A (2016b) The Rudnik Mts. volcano-intrusive complex (central Serbia): An example of how magmatism controls metallogeny. Geol Croatica 69, 1, 89-99

Dimitrijević MD (1992) Geological atlas of Serbia 1.200.000, no14: Metallogenic map and map of ore formations Ministry for Mining and Energetics Republics of Serbia

Foley SF, Wheller GE (1990) Parallels in the origin of the geochemical signatures of island arc volcanics and continental potassic igneous rocks: the role of residual titanites. Chem Geol 85, 1–18

Janković S (1984) Major metallogenic units and ore deposits in Yugoslavia. Exp. Memoir of the metallogenic map of Europe, 1:2500000, UNESCO, Paris, 385-395

Karamata S, Delaloye M, Lovrić A, Knežević V (1992) Two genetic groups of Tertiary granitic rocks of central and western Serbia. Ann Geol Penin Balk 56, 1, 263–283

Kubat I, Mojsilović S, Veljković D, Reljić D, Strajin V, Begić F, Dimitrov P (1968) Geological Map 1:100000 of the Sheet Ljubovija. Geoinženjering, Institut za regionalnu geologiju, rudna ležišta i ekonomsku geologiju, Sarajevo

Memović E (1990) Petrology of trachybasaltic rocks of Rogozna Mts. Unpublished Ms. Theses, Faculty of Mining and Geology, University of Belgrade, (in Serbian with English summary)

Mićić I (1980) Alterations pyrometasomatiques, pneumatolytiques et hydrothermales, comme phenomenes accompagnant le jeune plutonisme aux versants occidentaux du Kopaonik et du Ţeljin. Rasprave Zav geol geofiz istr Belgrade. (in Serbian with French summary). XIX, 261–287

Mladenović A, Trivić B, Cvetković V (2015) How tectonics controlled post-collisional magmatism within the Dinarides: Inferences based on study of tectono-magmatic events in the Kopaonik Mts. (Southern Serbia). Tectonophysics. 646, 36-49

Monthel J, Vadala P, Leisten JM, Cottard F, Ilić M, Strumberger A, Tosović R, Stepanović A (2002) Mineral deposits and mining districts of Serbia; compilation map and GIS databases. Ministry of Mining and Energy of Serbia, Geoinstitut. (BRGM Repost EC-51448-FR, of free public access on the website http://giseurope.brgm.fr)

Poli G, Tommasini S, Halliday AN (1996) Trace elements and isotopic exchange during acid–basic magma interaction processes. Transactions of the Royal Society of Edinburgh: Earth and Environmental Science. 87, 225–232

Prelević D, Cvetković V, Foley SF (2001) Composite igneous intrusions from Serbia: two case studies of interaction between lamprophyric and granitoid magmas. In: Downes H. & Vaselli O (eds) Tertiary magmatism in the Dinarides Balkan Peninsula. Acta Vulcan 3, 145-157

Prelević D, Foley SF, Cvetković V, Romer RL (2004) Origin of minette by mixing of lamproite and dacite magmas in Veliki Majdan, Serbia. J Petrol 45, 4, 759-792.

Radosavljevic SA, Stojanovic JN, Radosavljevic-Mihajlovic AS, Kasic VD (2013) Polymetallic mineralization of the Boranja orefield, Podrinje Metallogenic District, Serbia: zonality, mineral associations and genetic features. Period Mineral 82, 1, 61-87.

Righter K, Carmichael ISE (1996) Phase equilibria of phlogopite lamprophyres from western Mexico: biotite–liquid equilibria and P–T estimate for biotite-bearing igneous rocks. Contrib Mineral Petrol 123, 1–21.

Schefer S, Cvetković V, Fugenschuh B, Kounov A, Ovtcharova M, Schaltegger U, Schmid MS (2011) Cenozoic granitoids in the Dinarides of southern Serbia: age of intrusion, isotope geochemistry, exhumation history and significance for the geodynamic evolution of the Balkan Peninsula. Int J Earth Sci (Geol. Rundsch.) 100, 5, 1181-1206.

Schmid SM, Bernoulli D, Fugenschuh B, Matenco L, Schefer S, Schuster R, Tischler M, Ustaszewski K (2008) The Alpine–Carpathian–Dinaridic orogenic system: correlation and evolution of tectonic units. Swiss J Geosci 101, 139–183.

Stojanović JN, Radosavljević SA, Karanović LjC, Cvetković Lj (2006) Mineralogy of W-Pb-Bi ores from Rudnik Mt., Serbia. Neues Jahr Mineral – Abhand 182, 299-306.

Von Quadt A, Ivanov Z, Peytcheva I (2001) The Central Srednogorie (Bulgaria) part of the Cu (Au-Mo) belt of Europe: A review of the geochronological data and the geodynamical models in the light of the new structural and isotopic studies. In: Piestrzynski A (ed) Mineral Deposits at the Beginning of the 21st Century. Proceedings of the Joint Sixth Biennial SGA-SEG Meeting, Krakow. Tokyo: A.A. Balkema Publishers 555-558.

Von Quadt A, Moritz R, Peytcheva I, Heinrich C (2005) Geochronology and geodynamics of Late Cretaceous magmatism and Cu-Au mineralization in the Panagyurishte region of the Apuseni-Banat-Timok-Srednogorie belt, Bulgaria. Ore Geol Rev 27, 95-126.

MECHANISM OF COPPER ENRICHMENT OF MAFIC ENCLAVES AT ARC SETTING: INSIGHT FROM SULFIDE MINERALOGY OF BEZYMIANNY VOLCANO (KAMCHATKA)

Davydova V.O.[1], Shcherbakov V.D.[1], Plechov P.Yu.[1], Perepelov A.B.[2]
[1]Lomonosov Moscow State University, Moscow, Russia, vestadav@gmail.com
[2]Vinogradov Institute of Geochemistry, Siberian Branch of the Russian Academy of Sciences, Irkutsk, Russia

Copper ore typically associated with intrusions of magma in the crust above subduction zones, but mechanism of their formation is the subject under discussion (Loucks, 2014; Blundy et al., 2015 and other). We present petrological data on the behavior of sulfides at different levels of the magma pluming system of typical arc volcano (at the case of Bezymianny volcano, Kamchatka).

The 2006-2012 eruption products of the Bezymianny volcano (Kamchatka) are represented by two-pyroxene andesites with 56.5 to 57.5 wt. % SiO_2. Andesites contain various enclaves, which exhibitsigns of molten state at time of intrusion with host andesite.

All enclaves have non-equilibrium phenocryst assemblages, which correspond to crystallization at different levels of magma plumbing system. We subdivide three major mineral paragenesis:

- "shallow reservoir paragenesis" – Pl-Opx-Cpx-Ti-Mt (T: 940-980ºC, P ~ 1 kbar)
- "deep reservoir paragenesis" – Hbl-Pl±Px (T: 960-1040ºC, P: 5-9 kbar)
- "mantle paragenesis" – xenocrysts of Ol with Cr-Spl or detritus of spinel harzburgites

Mixed mineral assemblage meet two-chamber magma plumbing system, which was proposed by result of geophysical (Fedotov et al., 2010; Thelen et al., 2010; Koulakov et al., 2013) and petrological (Shcherbakov et al., 2011; Turner et al., 2013) studies, and allow to specify the P-T conditions of magma interaction (fig. 1).

In spite of the very similar bulk composition, mafic enclaves notably differ from host andesites in specific chalcophile and siderophile elements concentration. The most significant difference is observed for copper: Cu concentration is 70-310 ppm for mafic enclaves and 46-53 ppm for host andesites. Some of enclaves are also enriched with Ni (up 45-65 ppm) in relation to most abundant enclaves and andesites (15-20 ppm). Bulk sulfur content ranging from <200 ppm in andesites to 200-900 ppm in mafic enclaves.

The most S-rich phases are sulfides. We distinguish several distinct morphological types:

1.	Sulfides in matrix glass (fig. 2a).

a.Globular sulfides (1-50 mkm) with homogeneous core (cubanite-chalcopyrite, 20-33 wt.% Cu) and thin high-Cu rim. Part of it contains high-Cu area or area with exsolution textures (40-70 wt.% Cu). Several sulfides are crosscut by Cu-Fe-sulfate veins.

b.	Globular sulfides with frothy texture, that contain different inclusion (melt inclusions, Ti-magnetite, pyroxene). Their compositions range from cubanite to chalcopyrite, heterogeneity represents by pentlandite.

2.	Aggregates in contact of matrix glass and bubbles (fig. 2d). Globules, located in the glass, have closely chalcopyrite composition. In contact with bubbles they overgrown thin (0.1-2 mkm) high-Cu film, on which Fe-oxide are formed.

3.	Sulfides included in minerals.

a. In hornblende and plagioclase core. Sulfides are homogeneous and have a globular to irregular shape (5-200 mkm). Their compositions are pyrrhotite. In some phenocrysts occurred MSS-globules (monosulfide solid solution), which segregate into pirrhotite and cubanite (fig. 2c).
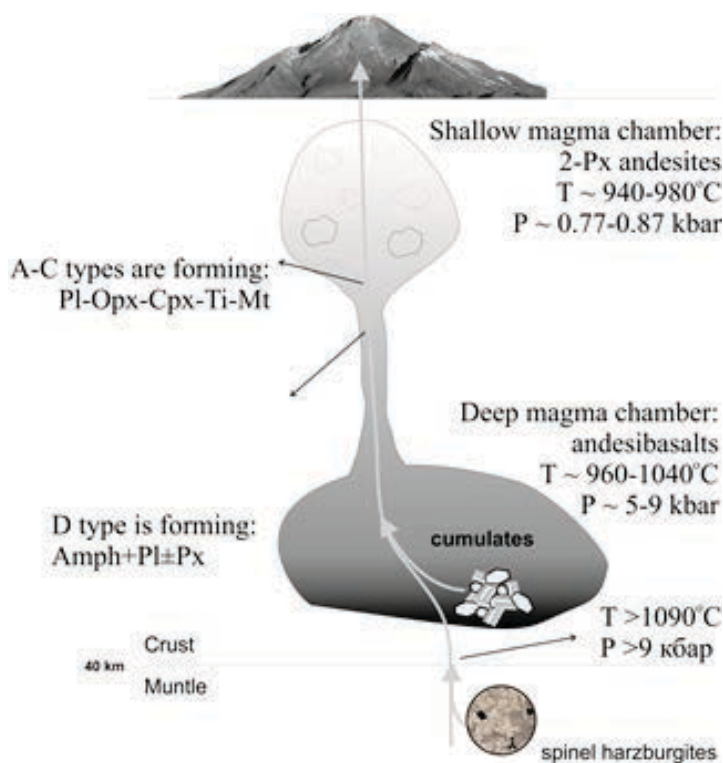

Fig. 1. The magma plumbing system of Bezymianny volcano (by Davydova et al., 2017)

b. In normal-zoning plagioclase rim, pyroxene, Ti-magnetite. They are represented by cubanite-chalcopyrite and have patchy structure. Patchy structure is specified by oxidized patch or thin line.

c. In contact of phenocryst with the matrix glass. Phenocrysts rim contain pyrrotite which has cubanite zone in contact with matrix glass or which is partially desulfidized in contact with the matrix glass (fig. 2b).
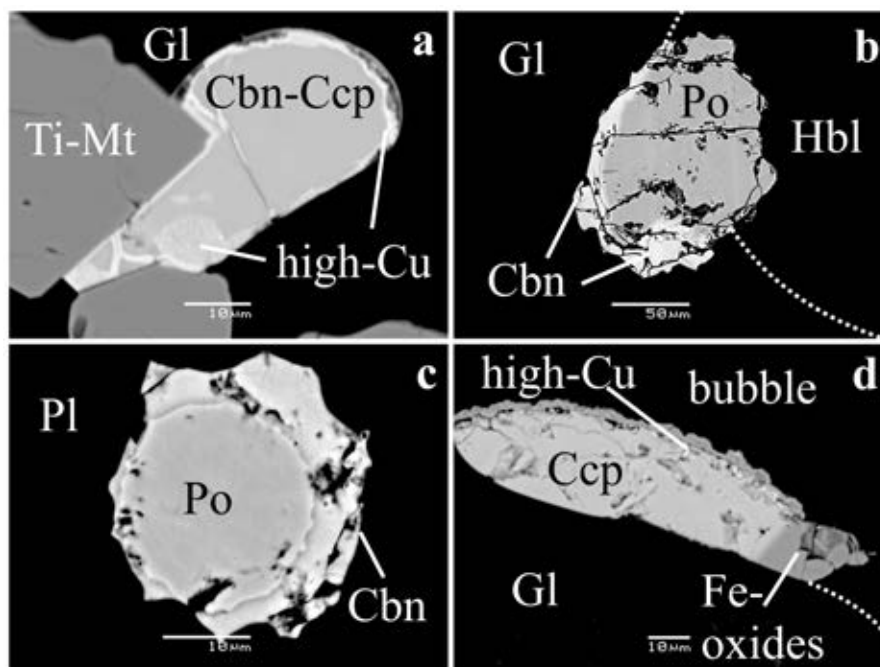
Fig. 2. Different type of sulfides. a) Globular sulfide in matrix glass with homogeneous core, thin high-Cu rim and area with exsolution of solid solutions. b) Sulfide in contact of hornblende with matrix glass. c) Sulfide included in plagioclases core: MSS which disaggregated into pyrrotite and some cubanite. d) Aggregates in contact of matrix glass and bubbles

Hornblende and sieve-textured core of plagioclase related to "deep paragenesis". Consequently, sulfides, which are included in them, were captured during crystallization in the deep magma chamber or during upward transport. Such sulfides are Cu-poor (pyrrotite or rare MSS which disaggregated into pyrrotite and some cubanite).

The abundance of sulfides suggests that the dominant oxidation state of sulfur in deep magma chamber is S^{2-}. As sulfur present as S^{2-}, Cu is strongly partitioned into sulfide minerals (D $_{sulfide\ liquid/silicate\ melt}$ ~ 600-1200) (Lynton et al., 1993;

Gaetani, Grove, 1997; Ripley et al., 2002). Therefore, Cu content in sulfides is a tracer of Cu content in parental magmas. Segregation of Cu-poor sulfides indicates that initially magmas from deep chamber contain a sufficient amount of sulfur to sulfide phase separation, but are Cu-poor.

Ti-magnetite, rim of plagioclase and pyroxene crystals related to "shallow chamber paragenesis". Consequently, sulfides, which are included in this minerals and matrix glass, formed after ascent magma from deem magma chamber into shallow magma chamber. Such sulfides are Cu-bearing (cubanite-chalcopyrite), so after injection into shallow magma chamber mafic enclaves enriched by Cu, which is reflected in the changes in the composition of sulfides inclusions in phenocrysts. Thin high-Cu rim on matrix glass-sulfides and high-Cu area in contact of minerals and glass formed after mixing, during the interaction of enclaves and host andesites. So, during mingling the degree of enrichment increases. The most Cu-rich phases occur on the melt-bubbles boundary.

Why does enrichment occur and where from does copper come? The most possible source of copper is host andesites. Previously, it was proposed that magmas in arc shallow magma chamber are concentrated ore metals during magmatic differentiation (Borisova et al., 2006). Sulfides segregate in limited amounts under the hydrous, oxidizing conditions resulting in incompatible behavior for Cu and other chalcoplile elements in silicic magmas. Transfer of this elements is carried due to fluid phase (Borisova et al., 2006). (Blundy et al., 2015) suggested, interaction of the accumulated copper with sulphur-rich gases, liberated in short-lived bursts from the underlying mafic magmas is initialized sulfides precipitation.

Consequently, incompatible behavior of copper leads to its accumulation in Bezymianny's shallow chamber. Injection of S-rich, Cu-poor magma from deep magma chamber reduced to redistribution of mobile element by fluids percolating in the shallow chamber. Interaction of S-rich enclave's magma and Cu-rich fluids lead to forming of Cu-bearing sulfides in mafic enclaves and transforming of early Cu-poor sulfides to Cu-bearing sulfides. Further crystallization in the oxidizing conditions of shallow chamber leads to the formation of sulphate crusts and veins at the sulfides.

References:

Blundy J. J., Mavrogenes J., Tattitch B., Sparks S., Gilmer A. Generation of porphyry copper deposits by gas-brine reaction in volcanic arcs // Nature Geoscience. 2015. V. 8. №. 3. P. 235-240.

Borisova A. Y., Pichavant M., Polvé M., Wiedenbeck M., Freydier R., Candauda, F. Trace element geochemistry of the 1991 Mt. Pinatubo silicic melts, Philippines: Implications for ore-forming potential of adakitic magmatism // Geochimica et Cosmochimica Acta. 2006. V. 70. №. 14. P. 3702-3716.

Davydova V.O., Shcherbakov V.D., Plechov P.Y., Perepelov A.B. Characterization of mafic enclaves in the erupted products of Bezymianny volcano, 2006-2012 // Petrology. 2017. In print.

Fedotov S. A., Zharinov N. A., Gontovaya L. I. The magmatic system of the Klyuchevskaya group of volcanoes inferred from data on its eruptions, earthquakes, deformation, and deep structure // Journal of Volcanology and Seismology. 2010. V. 4. №. 1. P. 1-33.

Gaetani G.A., Grove T.L. Partitioning of moderately siderophile elements among olivine, silicate melt, and sulfide melt: constraints on core formation in the Earth and Mars // Geochimica et Cosmochimica Acta. 1997. V. 61. №. 9. P. 1829-1846.

Koulakov I., Gordeev E.I., Dobretsov N.L., Vernikovsky V.A., Senyukov S., Jakovlev A., Jaxybulatov K. Rapid changes in magma storage beneath the Klyuchevskoy group of volcanoes inferred from time-dependent seismic tomography // Journal of Volcanology and Geothermal Research. 2013. V. 263. P 75-91.

Loucks R. R. Distinctive composition of copper-ore-forming arcmagmas // Australian Journal of Earth Sciences. 2014. V. 61. №. 1. P. 5-16.

Lynton S.J., Candela P.A., Piccoli P.M. An experimental study of the partitioning of copper between pyrrhotite and a high silica rhyolitic melt // Economic Geology. 1993. V. 88. №. 4. P. 901-915.

Ripley E.M., Brophy J.G., Li C. Copper solubility in a basaltic melt and sulfide liquid/silicate melt partition coefficients of Cu and Fe // Geochimica et Cosmochimica Acta. 2002. V. 66. №. 15. P. 2791-2800.

Shcherbakov V.D., Plechov P.Y., Izbekov P.E., Shipman J.S. Plagioclase zoning as an indicator of magma processes at Bezymianny Volcano, Kamchatka // Contributions to Mineralogy and Petrology. 2011. V. 162. P. 83-99

Thelen W., West M., Senyukov S. Seismic characterization of the fall 2007 eruptive sequence at Bezymianny Volcano, Russia // Journal of Volcanology and Geothermal Research. 2010. V. 194 P. 201-213.

Turner S.J., Izbekov P.E., Langmuir C. The magma plumbing system of Bezymianny Volcano: Insights from a 54 year time series of trace element whole-rock geochemistry and amphibole compositions // Journal of Volcanology and Geothermal Research. 2013. V. 263. P. 108-121.

NEW FINDING ALKALINE LAMPROPHYRE DYKES CLUSTER IN THE WESTERN MARGIN OF THE PROTEROZOIC PAKHAL BASIN IN AND AROUND KHAMMAM, TELANGANA, INDIA: EVIDENCE OF ALKALINE MAGMATISM

Debapriya Adhikary[1], Rajesh Kumar Sahoo[2], K.K.Behara[2]
[1]Geological Survey of India, Kolkata, India, debapriya.adhikary@gmail.com
[2]Geological Survey of India, Hyderabad, India

The various parts of Cudappah Igneous Province (CIP)/Prakasham Alkaline Province (PAP) of the Eastern Dharwar Craton (EDC), southern India is known for the occurrence of lamprophyre (Chalapati Rao,N.V 2008). Present paper reports new six lamprophyre dykes in and around Khammam area, Telangana, India (Fig.a).
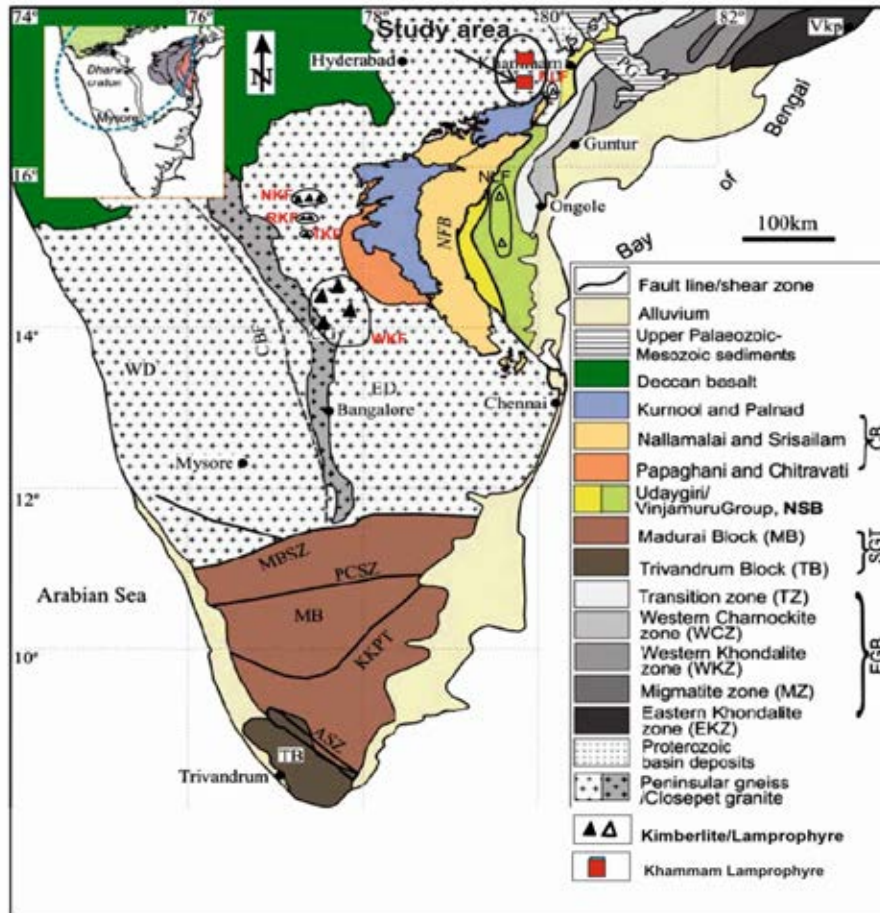
Fig.a: Generalised geological map of southern India modified from Drury et al. (1984) and Geological Survey of India (1998) showing kimberlite, lamproite and lamprophyre fields in the Dharwar craton. BC = Bastar Craton; EDC = Eastern Dharwar Craton; KLF = Krishna lamproite field; NKF = Narayanpet kimberlite field; NLF = Nallamalai lamproite field; TKF = Tungabhadra kimberlite field; WDC = Western Dharwar Craton; WKF = Wajrakarur kimberlite field, (Map source – www.researchget.net)

All the lamprophyre dykes are present in the contact zone between northeastern margin of the EDC and western margin of the proterozoic Pakhal Basin. In the south of the present study area in the contact zone between EDC and proterozoic Cuddapah basin lamprophyre and lamproits are reported earlier. First reported lamprophyre in the bayyaram area in the present lamprophyre cluster done by T.Meshram et al 2015.The lamprophyre of the study area has been intruded within granitoids of the EDC but not intruded in the Proterozoic Pakhal Basin (Fig.b). This field evidence indicate that alkaline magmatism was occur before the Proterozoic sedimentation started. These NE-SW trending lamprophyre dykes show petrographic and geochemical similarity with other lamprophyre dykes of the EDC.

These dykes are ~0.5 to 1 mt wide having ~50 mt exposed in the study area. Petrographically clinopyroxene and olivine are present as a phenocryst in the rock showing the panidiomorphic texture; carbonate-rich ocelli also present in the rock. In some of the part carbonate replace the clinopyroxene and olivine (Fig.c,d and e). Mineralogy it is dominated by volatile content i.e. amphibole, carbonate, chlorite, epidote, phlogopite mica and serpentine (Fig.f). Zoining of mica is also present in the lamprophyres (Fig.g). All these petrography constitute important evidence for its identification as the lamprophyre. As this rock contains clinopyroxene and olivine as the phenocrysts and mainly plagioclase feldspar in the groundmass, this lamprophyre belongs to alkaline type. In geochemistry, all the lamprophyre are characterized by

low SiO2, generally high MgO, medium Al2O3 and high K2O, also having high FeO + MgO and MgO/FeO. These lamprophyre shows low SiO2 content varying from 42.00 to ~45.00 wt.%; Na2O + K2O from 4.60 to ~ 4.65 wt.% and K2O/Na2O from 7 to 8 wt.%. The chondrite-normalized REE patterns of the studied rocks confirm crystallization from a LREE-enriched magma. The multi-element spider diagrams involving HFSE indicate their source region characteristic as subduction-zone related. Samples plot in overlapping field between subduction zone and within plate field with more affinity towards subduction- related source. Based on combined petrography and geochemistry study, this lamprophyre is considered to belong to the alkaline lamprophyre category in general. These newly finding alkali lamprophyre, indicate a phase of alkali magmatism in the margin of the EDC before the Proterozoic sedimentation

Fig.b: Field photograph of lamprophyre near Khammam.

Fig c: Photomicrograph of lamprophyre showing altered carbonates and CPX phenocrysts (PPL).
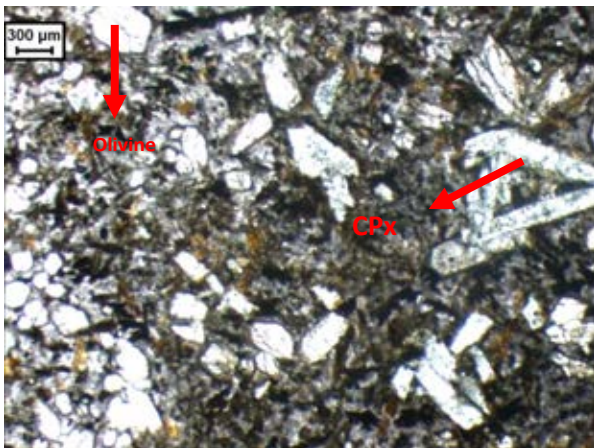
Fig.d: Photomicrograph of lamprophyre showing Olivine and CPX phenocrysts (PPL).
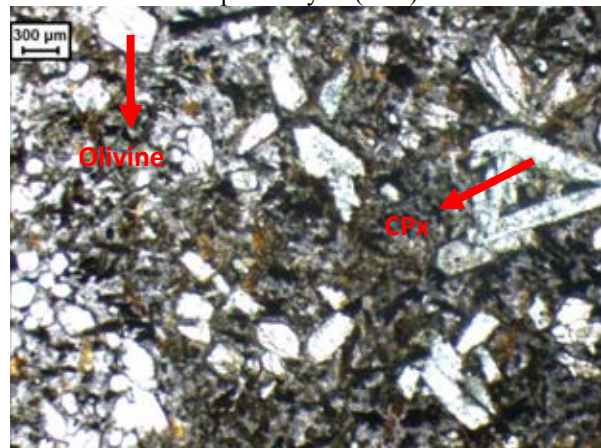
Fig.e: Photomicrograph of lamprophyre showing Olivine and CPX phenocrysts (XPL).
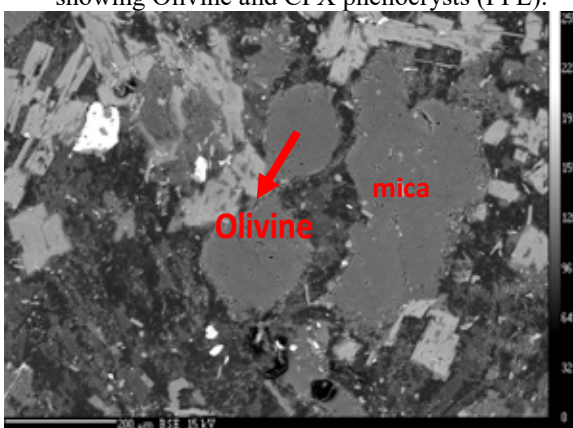
Fig.f: BSE image of Olivine and Mica in lamprophyre.
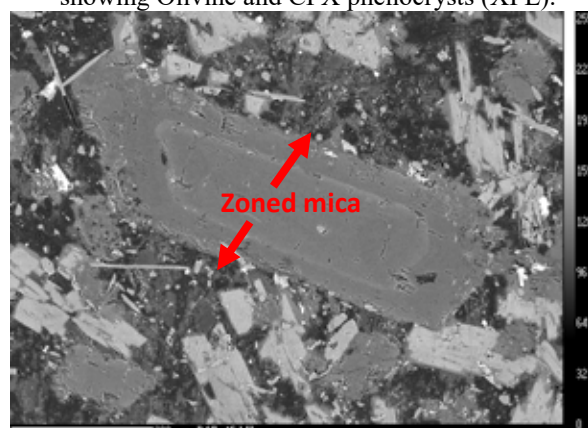
Fig.g: BSE image of zoned Mica in lamprophyre.

valuable guidance and suggestions. Thanks are also due to the Directors of Petrology Division, GSI, SR, Hyderabad, for providing necessary laboratory support during the work. The authors are indebted to Shri. S.N. Mahapatro, Dr. S. Ravi for their valuable suggestions and discussion during petrographic study.

References:

Chalapathi Rao, N.V. (2008). Precambrian alkaline potassicultrapotassic, mafic ultramafic magmatism in Peninsular India. Jour. Geol. Soc. India, v.72, pp.57-82.

T.Meshram, D.Shukla, K.K..Behera (2015): Alkaline lamprophyre (Camptonite) from Bayyaram area, NE margin of the Eastern Dharwad Craton,South India. Current Science,VOL,109,No 11,10 December,2015

SKARN-HOSTED MOLYBDENITE±SCHEELITE MINERALIZATION IN NW BULGARIA
Dimitrova D.A.[1], Mladenova V.G.[2], Gorolomova, V.D.[2]

[1]Geological Institute, Bulgarian Academy of Sciences, Sofia, Bulgaria
[2]Sofia University "St. Kliment Ohridski", Sofia, Bulgaria

The Mo skarns are one of the main sources for molybdenum mining and extraction. They are mostly associated with leucocratic granites, having relatively high Mo grade, but small resources, unlike porphyry Cu±Mo deposits. Most molybdenum skarns contain also a wide variety of metals including W, Cu, Zn, Pb, Bi, Sn and U. The molybdenite±scheelite mineralization in the skarns of the Perchinki and Prekop mine sections of the Martinovo mine was experimentally mined in 1981-1984. During this short period were extracted 91 t of molybdenum from 79000 t ore at 0.12% Mo (Milev et al., 1996). It is not known if tungsten was also extracted together with molybdenum.

Materials and analytical procedures

Polished and thin sections were made from representative samples, collected from the skarns found in the Perchinki and Prekop mine sections (levels 1170 and 1200). The mineral relationships were examined by transmitted and reflected light microscopy, as well as SEM. Electron microprobe analyses were performed on JEOL Superprobe at the Geological Institute. Trace element concentrations in molybdenite were done using the PerkinElmer ELAN DRC-e ICP-MS equipped with a New Wave UP193-FX excimer laser ablation system at the Geological Institute, BAS. NIST SRM 610 glass and MASS1 sulfide standards were used for external standardization. The laser system was operated at constant 4-6 Hz pulse rate; laser energy was 4.90-5.60 J/cml on the sample for 20-35 μm spot size. The following 40 isotopes were monitored: ^{42}Ca, ^{49}Ti, ^{51}V, ^{53}Cr, ^{55}Mn, ^{57}Fe, ^{59}Co, ^{62}Ni, ^{65}Cu, ^{66}Zn, ^{69}Ga, ^{73}Ge, ^{75}As, ^{77}Se, ^{88}Sr, ^{89}Y, ^{90}Zr, ^{93}Nb, ^{95}Mo, ^{105}Pd, ^{107}Ag, ^{111}Cd, ^{115}In, ^{118}Sn, ^{121}Sb, ^{125}Te, ^{139}La, ^{140}Ce, ^{141}Pr, ^{146}Nd, ^{147}Sm, ^{182}W, ^{185}Re, ^{197}Au, ^{202}Hg, ^{205}Tl, ^{208}Pb, ^{209}Bi, ^{232}Th, ^{238}U. Acquisition dwell time for all masses was set to 0.01 s. Data reduction was done, using SILLS ver. 1.1.0 software (Guillong et al., 2008) and theoretical Mo content in molybdenite as internal standard.

Geological setting

The Martinovo iron ore deposit is located NW of the village of Martinovo, in the western part of the Balkan Mountains. It is hosted in the rocks of the Diabase-Phyllitoid Complex (DFC) (Haydoutov, 1991). Its formation is related to the intrusion of the Sveti Nikola granite (313.8 ± 3.5 Ma, Late Carboniferous age, Carrigan et al., 2005) into the DFC rocks. The exoskarn zone, developed in the siderite and calcite marbles, is divided into 3 subzones (Tarassova, Tarassov, 1988): pyroxene, garnet-pyroxene and garnet, showing subsequent transition in chemical composition of garnets - from predominant grossular to andradite in the garnet zone. The economically important magnetite ore is related to the outer garnet zone. The origin of magnetite is considered as a result mainly of the thermometamorphic alteration of siderite (Dragov, 1992). The skarns can be classified as Mo±W according to the abundant molybdenite±scheelite mineralization associated with the garnet (grossular-andradite) – pyroxene skarns (Einaudi, Burt, 1982, Meinert, 1992). Rare accessory minerals observed and typical for this type of skarns are uraninite and apatite.

Results and discussion

The molybdenite±scheelite mineralization is spatially related to garnet or garnet-clinopyroxene skarns (outer retrograde skarn zone), where it partially replace garnet. The garnet zone contains mainly garnet - grossular-andradite and lesser amounts of pyroxene – diopside-hedenbergite. Titanite, chlorite and apatite are also found. Molybdenite, scheelite, pyrite, hematite, magnetite and uraninite are formed during the retrograde metasomatic alteration. Molybdenite occurs as coarse lamellar rosettes, or thin folded lamellae within the garnet, frequently intergrown with pyrite and/or magnetite (Fig. 1). Pyrite also appears as well formed cubic crystals (up to 2-3 mm), sometimes including uraninite. Chalcopyrite is rarely observed accompanying pyrite crystals. Uraninite occurs as small (5-20 μm) cube-octahedral, octahedral and rounded crystals embraced by molybdenite or within garnet (Fig. 1a). Scheelite is found as anhedral grains (Fig. 1c). Magnetite also appeared as much larger in size (up to 170 μm) cube-octahedral crystals often accompanied by hematite (Fig. 1d) or as anhedral grains together with molybdenite. The electron microprobe analysis of uraninite determined small amounts of PbO ranging between 1.25 and 4.54 wt.%, resulting of the U radioactive decay, while scheelite contains up to 1.91 wt.%MoO_3. LA-ICP-MS analyses of molybdenite show presence of elements that are: 1) lattice-bound; 2) isostructural in molybdenite substituting for S; 3) part of mineral inclusions.

As lattice-bound elements in molybdenite are considered Re and W (Newberry, 1979, others), in some cases also Nb, as their extent of incorporation depend also on the polytypism of molybdenite and fluids involved in deposition. The measured contents of Re in molybdenites vary between 7.6 and 311.8 ppm, usually <70 ppm, suggesting mixed crustal/mantle source (Pašava et al. 2016 and references therein). Wolfram concentrations vary significantly from 19.1 to

802.8 ppm, as W always shows flat intensity in time resolved spectra. Both Re and W have positive correlation to Mo, but negative between each other. Niobium contents are around 7.4-9.2 ppm and Nb intensities do not imply presence of inclusions. Niobium correlates positively with Re.
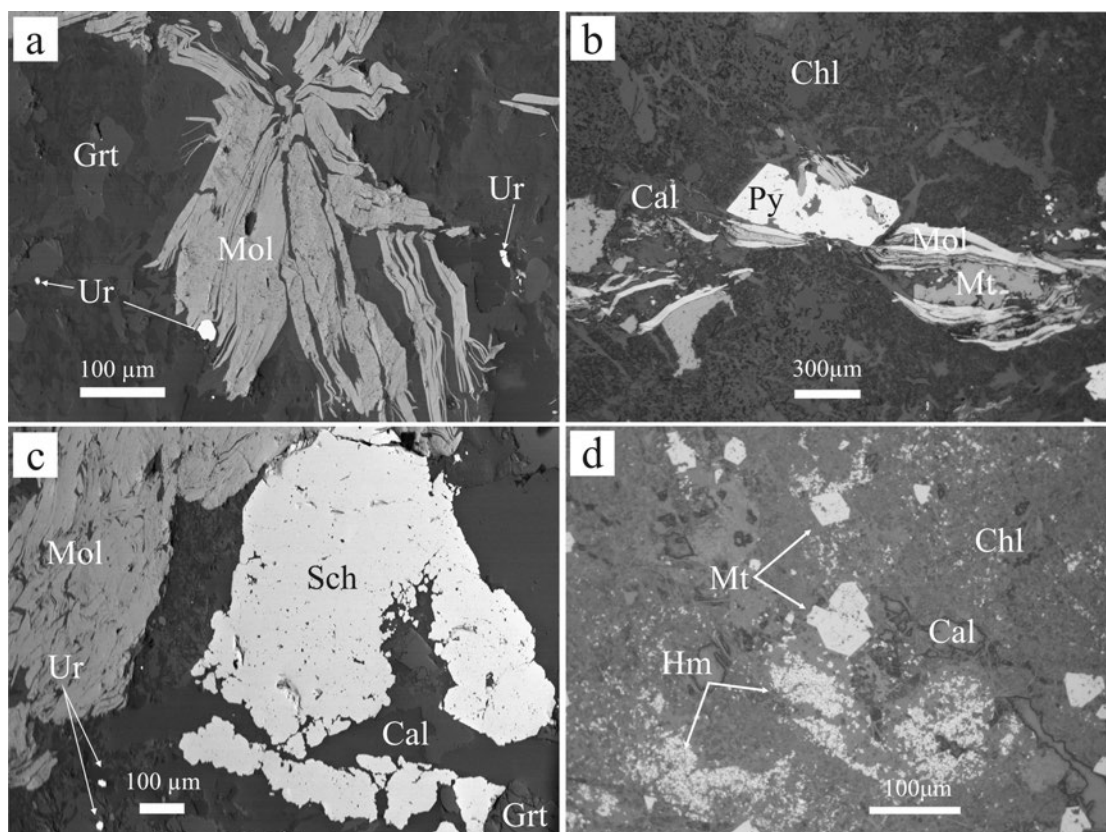

Fig. 1. BSE images of the Mo-bearing assemblage: A) slightly folded platy molybdenite embracing uraninite within garnet; B) deformed molybdenite plates embracing pyrite and magnetite in calcite-chlorite matrix; C) molybdenite and scheelite in garnet, tiny uraninite crystals in garnet; D) magnetite and hematite in chlorite-calcite matrix. Abbreviations: Cal – calcite, Chl – chlorite, Grt – garnet, Hm – hematite, Mol – molybdenite, Mt – magnetite, Py – pyrite, Sch – scheelite, Ur – uraninite.

Selenium and tellurium present in molybdenite as isostructural substitution for S as it could be suggested by the flat depth profiles. Their concentrations vary between 57 and 324 ppm for Se and <MDL (minimum detection limit) to 48.3 ppm for Te. These contents are much smaller than those reported for these elements from Ciobanu et al. (2013).

Typical elements that are related to interlamellae inclusions are Pb, Bi and Ag. Sometimes it could be presumed that they are from galena inclusion (all three showing same intensity pattern in time resolved spectra) or both galena and native bismuth (Se and Te intensities do not match Bi and Ag intensities) inclusions, as sometimes Ag is paired with Pb in other times with Bi. Although galena and native bismuth were not observed together with molybdenite in reflected light microscopy and SEM, they were found in the post-skarn arsenide-sulfide mineralization deposited later. Thus it is possible for them to present as micrometer-sized interlamellae depositions in molybdenite aggregates. The specific "zig-zag" pattern of the intensities in time resolved spectra suggests "areas" of enrichment and depletion throughout the ablated volume in depth. During data reduction such enriched "areas" were avoided where it was possible to exclude these high concentrations. Nevertheless they were unavoidable in most cases, thus Pb contents usually vary from 97 to 1033 ppm, in few analyses they are from 1.7 to 69.5 ppm. Same applies for Bi and Ag with respective concentrations from 2.1 to 343.6 and from 1.0 to 53.6 ppm. In one analysis Ag and Sb show same intensity pattern in the time resolved spectrum suggesting presence of Ag-Sb(+S) mineral. Several times individual micro- or even nano-scale inclusions of gold were detected in the spectra yielding Au concentrations 0.17-0.49 ppm. Inclusions of uraninite and apatite, as well as mixed signal of ablating in depth molybdenite with magnetite, carbonate or garnet were also determined. This was the reason why Ca and Sr were also monitored in order to distinguish flat intensities of Mn and Fe from garnet, carbonate matrix or magnetite. Garnet intercalations in the signal could be discerned over carbonate on the intensities of REE present, since garnets are enriched in them compared to carbonates. Uranium, Y and REE peaks in the spectra suggest the presence of uraninite, apatite and possibly other phosphate minerals, but not rutile (flat Ti spectrum). Titanium always shows in the spectra; however it is unlikely that it is lattice-bound in molybdenite. The most probable explanation is a polyatomic interference of S with O or N (May, Wiedmeyer, 1998) on ^{49}Ti. It can be presumed that actual concentrations of Ti could be expected only in case a magnetite/garnet signal appears in depth. Some of the measured isotopes (Ce, Pr, Nd, Sm) also show flat intensities in the time resolved spectra, however so far microchemical studies of molybdenite have not reported such presence, so we assume that these intensities are likely to be a result of some polyatomic interference. Partly or

entirely a polyatomic interference should be also considered the intensities of ^{111}Cd, as $^{95}MoO^+$ may occur (May, Wiedmeyer, 1998). Cadmium also showed flat intensities in the spectra that yielded concentrations between167 and 484 ppm. LA-ICP-MS analyses detected also (in ppm): V (<MDL – 56 ppm), Co (0.95-25.14), Ni (<MDL – 8.9), Cu (<MDL – 38.7), Zn (<MDL – 161.9), Ga (<MDL – 22.3), As (<MDL – 79.1), In (<MDL – 0.2), Sb (<MDL – 22.3), Hg (1.2-14.7) and Tl (0.2-3.9). The presence of these elements cannot be explained synonymously. While in some case they clearly appeared as peaks in the time resolved spectra, e.g. inclusions, in other cases they show flat intensities (usually V, Co, Hg and Tl). So far it cannot be concluded if these elements could be impurities in molybdenite or occupying defects in the lattice. Currently microchemical data about scheelite, pyrite and magnetite is absent.

Conclusions

Molybdenite is known important carrier of Re, however the concentrations of Re determined in molybdenite from Martinovo skarn deposits are low (<300 ppm, usually several tens of ppm), which is normal for crustal derived granite-related molybdenite mineralizations (Pašava et al. 2016, references therein), as such is the Sveti Nikola collisional Variscan granite. Low Re concentration would decrease the interest for future molybdenite extraction from the deposit. Although molybdenite polytypes were not studied yet, low contents of Re suggest that the hexagonal (2H) is more likely to occur since rhombohedral 3R is commonly richer in Re (McCandless et al., 1993). All major impurities are related to micro-scale inclusions of galena and native bismuth. The formation of uraninite and apatite during retrograde metasomatic alteration and consecutive deposition of pyrite and molybdenite suggests that uranium probably occurred in the solution as $UO_2(HPO_4)_2^{2-}$ or $UO_2SO_4^0$ and the values of logfO_2 were reduced. Geochemical features of the mineralization represent association characteristic for Mo±W skarns.

References:

Carrigan CW, Mukasa SB, Haydoutov I, Kolcheva K (2005) Age of Variscan magmatism from the Balkan sector of the orogen, Central Bulgaria. Lithos 82:125-147

Ciobanu CL, Cook NJ, Kelson CR, Guerin R, Kalleske N, Danyushevsky L (2013) Trace element heterogeneity in molybdenite fingerprints stages of mineralization. Chem Geol 347:175-189.

Dragov P (1992) Ore-Forming Processes in the Chiprovtsi Ore Zone. DSc Thesis, Geological Institute, BAS, Sofia 179p (in Bulgarian)

Einaudi MT, Burt DM (1982) Introduction - terminology, classification, and composition of skarn deposits. Econ Geol 77:745-754

Guillong M, Meier DL, Allan MM, Heinrich CA, Yardley BWD (2008) Appendix A6: SILLS: A MATLAB-based program for the reduction of laser ablation ICP-MS data of homogeneous materials and inclusions, In: Sylvester P (ed.), Laser Ablation ICP–MS in the Earth Sciences: Current Practices and Outstanding Issues. Mineralogical Association of Canada Short Course 40: pp328–333

Haydoutov I (1991) Origin and Evolution of the Precambrian Balkan-Carpathian Ophiolite Segment. Sofia, BAS Press, 179p (in Bulgarian)

May TW, Wiedmeyer RH (1998) A table of polyatomic interferences. At Spectrosc, 19:150-155

Meinert LD (1992) Skarns and skarn deposits. Geosci Canada 19:145-162

Milev V, Stanev V, Ivanov V (1996) The Extracted Ores in Bulgaria during 1878-1995 - Statistical Reference Book. Sofia, Zemya 93, 196p (in Bulgarian)

McCandless TE, Ruiz J, Campbell AR (1993) Rhenium behaviour in molybdenite in hypogene and near surface environments: implications for Re-Os geochronology. Geochim Cosmochim Acta 57:889-905.

Newberry RJJ (1979) Polytypism in molybdenite (I): a non-equilibrium impurity induced phenomenon. Am Mineral, 64:758-767

Pašava J, Svojtka M, Veselovský F, Ďurišová J, Ackerman L, Pour O, Drábek M, Halodová P, Haluzová E (2016) Laser ablation ICPMS study of trace element chemistry in molybdenite coupled with scanning electron microscopy (SEM) – An important tool for identification of different types of mineralization. Ore Geol Rev 72:874-895.

Tarassova E, Tarassov M (1988) Horizontal zonality and mineral composition of skarns in the Martinovo deposit. Geochem Mineral Petrol 24:68-76 (in Bulgarian).

PARAGENESES OF OXYGEN-BEARING MINERALS WITH CHALCOPHILE ELEMENTS IN METASOMATITES OF THE PELAGONIAN MASSIF, MACEDONIA

Ermolaeva V.N.[1,2], Chukanov N.V.[3], Jančev S.[4], Van K.V.[1]

[1]Institute of Experimental Mineralogy, Russian Academy of Sciences, Chernogolovka, Russia, cvera@mail.ru
[2]Vernadsky Institute of Geochemistry and Analytical Chemistry of the Russian Academy of Sciences, Moscow, Russia
[3]Institute of Problem of Chemical Physics of the Russian Academy of Sciences, Chernogolovka, Russia
[4]Faculty of Technology and Metallurgy, Saints Cyril and Methodius University, Skopje, Macedonia

Metamorphic rocks of Precambrian age (gneisses, mica schists and amphibolites) are wide spread in the Pelagonian massif, Republic of Macedonia (Majer, 1983; Mircovski, 2002). Metasomatic rocks forming exo-contact aureoles around the Early Paleozoic meta-rhyolite formation embedded in this metamorphic complex are characterized by high concentrations of chalcophile elements (S, As, Sb, Zn, Pb) concentrated both in the main rock-forming minerals (baryte,

gahnite, franklinite, Zn-bearing phlogopite, aegirine-augite, alkaline amphiboles, spessartine, *etc*.) and in diverse accessories (nežilovite, rinmanite, Zn-bearing braunite, tilasite, members of the högbomite, epidote, roméite and apatite groups, *etc*.). Among accessory minerals of the orogenetic zone related to the "Mixed Series" metamorphic complex of the Pelagonian massif, there are numerous extremely rare, as well as new and potentially new species, including almeidaite, piemontite-(Pb), nežilovite, ferricoronadite, plumbobetafite, Sb-rich variety (or analogue) of zincohögbomite *etc*. (Stojanov, 1967-1968; Ivanov and Jančev, 1976; Chukanov et al., 2015). These parageneses, which are notable for their diversity, evidently reflect unusual conditions of mineral formation. Post-magmatic fluids related to meta-rhyolites are considered as a possible source of a number of specific, ore and rare elements (Pb, Zn, Sb, As, Cu, Ba, *REE etc*.) in the contact-metasomatic rocks (Jančev, 1998). A specific Zn-spinellide mineralization represented by fine-grained aggregates of gahnite, franklinite and hetaerolite, is typically confined to dolomitic marbles or baryte schists.

Endogenic ore deposits of chalcophile elements concentrated predominantly in oxygen-bearing minerals are relatively rare. Along with the orogenetic zone related to the "Mixed series" of the Pelagonian massif, the well-known examples of such objects are Franklin and Sterling Hill Fe-Zn deposits in New Jersey, USA (Tarr, 1929; Palache, 1929a; Palache, 1929b; Wilkerson, 1962), as well as Långban, Nordmark (including Jakobsberg) and Pajsberg (including Harstigen) Fe-Mn deposits in the Bergslagen ore province, Värmland, Sweden (Palache, 1929b).

In this work we studied a predominantly oxide (almost without silicates) mineral association characterized by extremely high concentrations of Zn and Pb, as well as a substantial (but subordinate) role of Sb and As, discovered about 15 km NW of the village of Nežilovo and about 40 km SW of the city of Veles, Republic of Macedonia (41°34′ N, 21°34′ E). The material described in this work was collected in the valley of the Babuna river, in talus at the bottom of the Kalugeri Hill.

The major minerals of the rock are gahnite, franklinite and hetaerolite. The rock is crossed by hydrothermal veinlets that are up to 8 mm thick and are composed of a complex of oxide minerals with predominant ferricoronadite. Two zones can be distinguished in the Zn-oxide rock. One of them (spinellide zone that corresponds to the upper part of Fig. 1) is mainly composed of the fine-grained aggregate of gahnite, with subordinate franklinite and hetaerolite. Another one (spinellide-zincohögbomite zone – lower part of Fig. 1) is enriched in a högbomite-group mineral that forms epitaxial intergrowths with Zn-spinellides.
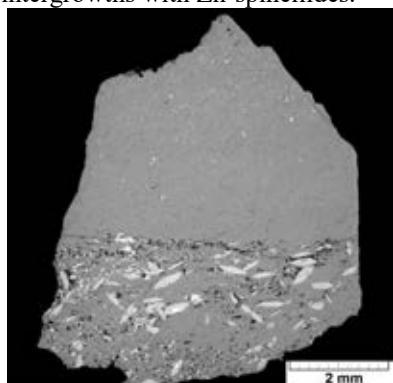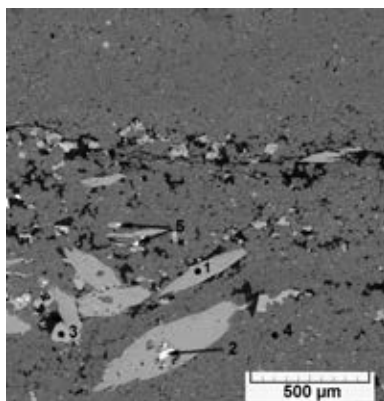
Fig. 1. Zn-oxide rock near the border between spinellide and spinellide-zincohögbomite zones: (*a*) general view and (*b*) an enlarged fragment. 1 - Fe-analogue of zincohögbomite, 2 – ferricoronadite, 3 – hetaerolite, 4 – gahnite, 5 – roméite. BSE image.
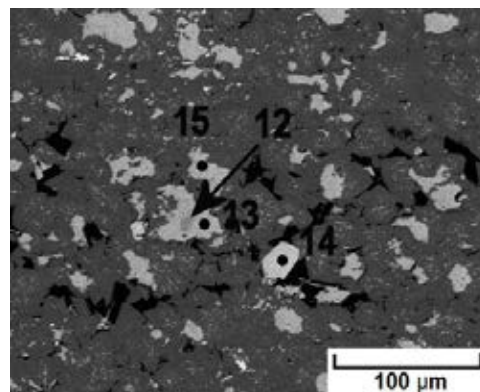
Fig. 2. Franklinite (13, 15) with zincochromite inclusion (12) and zircon (14) in granular gahnite (the main phase). BSE image.

Gahnite with the typical composition $(Zn_{1.01}Mg_{0.01})_{\Sigma1.02}(Al_{1.75}Mn_{0.12}Fe_{0.11})_{\Sigma1.98}O_{3.99}$ is the major component of the spinellide zone. The subordinate minerals of this zone are franklinite $(Zn_{1.08}Mg_{0.02})_{\Sigma1.10}(Fe_{1.10}Mn_{0.55}Al_{0.24}Ti_{0.01})_{\Sigma1.90}O_{3.96}$ and hetaerolite $(Zn_{0.99}Mn_{0.01})_{\Sigma1.00}(Mn_{1.73}Fe_{0.22}Al_{0.05})_{\Sigma2.00}O_4$. As-rich fluorapatite $(Ca_{4.93}Sr_{0.05}Na_{0.03}Pb_{0.01})_{5.02}(P_{2.12}As_{0.86}Si_{0.02})_{3.00}O_{12.06}F_{0.87}$, roméite $(Ca_{1.30}Ce_{0.49}Na_{0.05}Pb_{0.03}Sr_{0.02}Ba_{0.01}La_{0.01}U_{0.01})_{\Sigma1.92}(Sb_{0.97}Ti_{0.91}Mn_{0.07}Fe_{0.04}Al_{0.01})_{\Sigma2.00}O_6[(OH)_{0.84}O_{0.16}]_{1.00}$, Zn-bearing talc $Sr_{0.02}K_{0.01}(Mg_{2.51}Zn_{0.39}Mn_{0.01}Al_{0.01})_{\Sigma2.92}(Si_{4.00}O_{10})(OH)_2$, almeidaite $(Pb_{0.98}Ce_{0.15})_{\Sigma1.13}(Zn_{1.92}Mg_{0.08})_{\Sigma2.00}(Mn^{2+}_{0.54}Zn_{0.38}Y_{0.08})_{\Sigma1.00}[Ti_{12.07}Fe^{3+}_{3.66}(Mn^{3+},Mn^{4+})_{1.69}Zr_{0.20}Al_{0.13}Sb_{0.09}Nb_{0.03}]_{\Sigma17.87}(O,OH)_{38}$, Mn-analogue of plumboferrite $Pb_{1.79}[(Mn^{3+},Mn^{4+})_{3.66}Fe_{2.61}Ti_{2.53}Zn_{1.99}Al_{0.18}Sb_{0.03}]_{\Sigma11.00}O_{19-x}$, zincochromite $Zn_{1.00}(Cr_{1.45}Al_{0.47}Fe_{0.05}Mn_{0.03})_{\Sigma2.00}O_4$, zircon $(Zr_{1.01}Ti_{0.01})_{\Sigma1.02}Si_{1.00}O_{4.04}$, ferricoronadite $(Pb_{1.06}Ba_{0.35})_{\Sigma1.41}[(Mn^{4+},Mn^{3+})_{5.94}Fe^{3+}_{1.36}Ti_{0.44}Zn_{0.17}Al_{0.08}Mg_{0.01}]_{\Sigma8.00}O_{15}(OH,O)$, quartz and baryte are present as accessory components. Gahnite crystallized after franklinite. The relationships between these minerals are especially obvious in relics of spinellides at salbands of ferricoronadite veinlets (Fig. 7): gahnite partly or completely substitutes franklinite.

The earliest minerals of the spinellide zone are zincochromite (cores of some franklinite grains) and zircon that forms idiomorphic crystals (Fig. 2). Talc and hetaerolite also belong to the early paragenesis. Fig. 3 illustrates the relationship between these minerals: hetaerolite crystallized after Zn-bearing talc.

The spinellide-zincohögbomite zone is marked by abundant inclusions of högbomite-group minerals. Their specific features are habit (platy individuals forming clusters) and high contents of Sb and Ti (Chukanov et al., 2015).

The typical formula $(Zn_{6.55}Al_{0.45})_{\Sigma 7.00}(Fe^{3+}_{6.84}(Mn^{3+},Mn^{2+})_{\Sigma 4.95}Al_{2.37}Ti_{1.23}Sb_{0.32}Mg_{0.28}Zr_{0.01})_{\Sigma 16.00}(O,OH)_{32}$ corresponds to the Fe-dominant analogue of zincohögbomite. Inclusions of gahnite, Mn-analogue of plumboferrite and even ferricoronadite are observed inside aggregates of the högbomite-group mineral (Figs. 4, 5). Consequently, Sb-bearing Fe-analogue of zincohögbomite is one of the latest minerals in this association
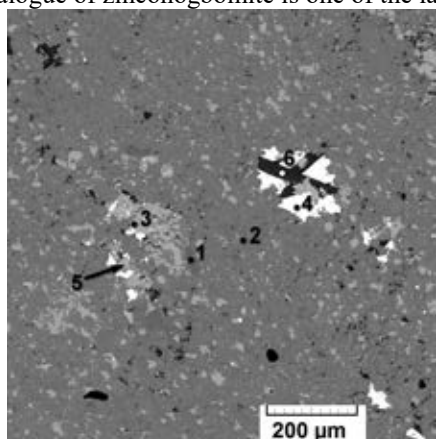

Fig. 3. As-rich fluorapatite (1), gahnite (2), franklinite (3), baryte (4), hetaerolite (5), Zn-bearing talc (6). BSE image.
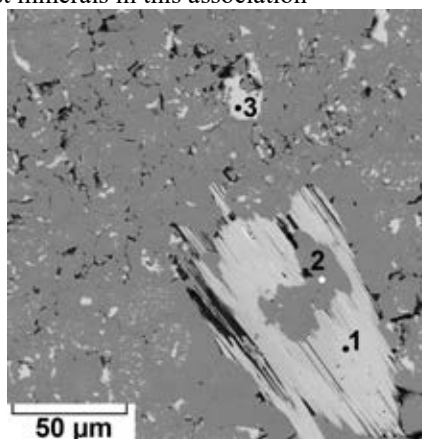
Fig. 4. Fe-analogue of zincohögbomite (1), gahnite (2), franklinite (3). BSE image.
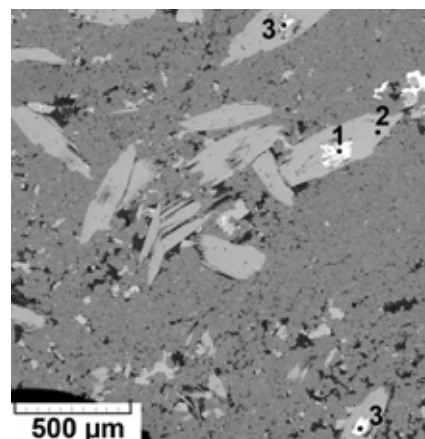
Fig. 5. Mn-analogue of plumboferrite (1), Fe-analogue of zincohögbomite (2), ferricoronadite (3). BSE image.

The mail concentrator of As in this association is As-rich fluorapatite, which form zoned grains (Fig. 6). Ferricoronadite is the major mineral of the latest hydrothermal veinlets. Inner zones of these veinlets are almost monomineral, whereas outer zones (Fig. 7) contain relics of earlier minerals (franklinite and hetaerolite, partly or completely substituted by gahnite, baryte, talc), as well as quartz. Chemical data for the studied minerals are given in Table 1.
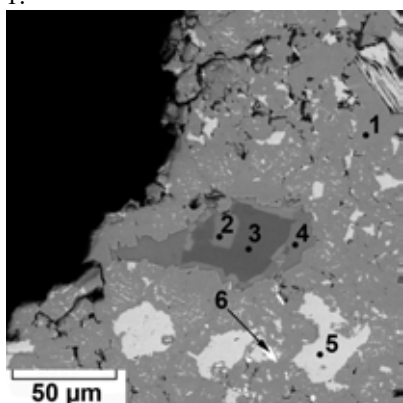
Fig. 6. Gahnite (1), As-rich fluorapatite (2-4), franklinite (5), baryte (6). BSE image.
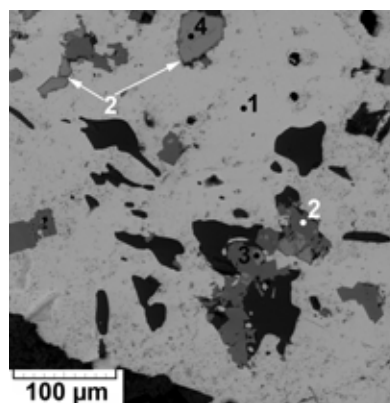
Fig. 7. Outer zone of the ferricoronadite veinlet containing ferricoronadite (the main phase, 1, gahnite (2) franklinite (3), hetaerolite (4). The darkest areas correspond to quartz. BSE image.

Based on the spatial relationships of different phases, the earliest minerals of the rock are zincochromite (relic isolated grain inside franklinite grain, see Fig. 2), zircon (idiomorphic crystals: Fig. 2) and talc (idiomorphic plate crystals in baryte, Fig. 3).

In the second stage crystallization of franklinite and hetaerolite took place. Grains of these minerals are included in granular gahnite aggregates (Figs. 2-4, 6, 7).

In the third stage, grains of franklinite and hetaerolite were partly (in peripheral parts) or completely substituted with gahnite, which is the main component of the rock (Fig. 6). Roméite and almeidaite forms xenomorphic inclsions in gahnite.

The association formed in the fourth (hydrothermal) stage is presented by ferricoronadite veins crossing aggregates of earlier minerals. Granular aggregates of ferricoronadite, as well as accessory Fe-analogue of zincohögbomite, contain inclusions of earlier minerals: franklinite, hetaerolite, gahnite, quartz *etc.* (Fig. 6). Our microscopic investigations of thin sections of the Zn-oxide rock show that similar rounded grains of quartz are present as inclusions in baryte and, consequently, belong to the earliest paragenesis.

Fe-analogue of zincohögbomite is most abundant in the spinellide-zincohögbomite zone where it is one of the latest minerals. It forms epitaxial structures on Zn-spinellides (Figs. 1, 4, 5). Some grains of Sb-bearing Fe-analogue of zincohögbomite contain inclusions of ferricoronadite and Mn-analogue of plumboferrite (Fig. 5). This fact indicates that the supply of Sb occurred after the supply of Pb. Some grains of As-rich fluorapatite consist from 3 zones. Inner and outer zones are enriched by As (0.8-0.9 apfu), whereas As content in intermediate zone are relatively low (0.2 apfu). This fact show, that at crystallization of As-rich fluorapatite was at least two maximum of As activity.

Table 1. Representative compositional data for rock-forming and some accessory minerals from the Zn-oxide rock.

Mineral	Gahnite	Frank-linite	Fe-rich zinco-högbomite	Heta-erolite	Ferri-coronadite[1]	Zinco-chromite[2]	Roméite[3]	Almei-daite[4]	Mn-analogue of plumbo-ferrite[5]
					Wt.%				
	1	2	3	4	5	6	7	8	9
CaO	bdl	bdl	bdl	bdl	bdl	bdl	18.46	bdl	bdl
PbO	bdl	bdl	bdl	bdl	23.75	bdl	1.56	11.76	32.29
SrO	bdl	bdl	bdl	bdl	bdl	bdl	0.79	bdl	bdl
BaO	bdl	bdl	bdl	bdl	5.70	bdl	0.39	bdl	bdl
MgO	0.13	0.40	0.44	0.07	bdl	bdl	bdl	0.26	bdl
ZnO	42.09	35.54	32.76	36.25	3.05	36.94	bdl	10.00	13.11
Ce_2O_3	bdl	bdl	bdl	bdl	bdl	bdl	18.61	1.41	bdl
Al_2O_3	50.18	5.87	7.42	8.52	0.33	10.79	0.12	0.47	0.71
Mn_2O_3	3.86	24.08	22.20	33.65	bdl	1.22	bdl	8.11	23.20
Fe_2O_3	3.67	32.78	31.10	20.21	11.66	1.62	0.37	15.95	16.84
SiO_2	bdl	bdl	bdl	bdl	bdl	bdl	bdl	bdl	bdl
TiO_2	bdl	0.50	4.04	0.40	6.50	bdl	16.94	51.37	16.30
ZrO_2	bdl	bdl	bdl	0.31	0.28	bdl	bdl	1.39	bdl
UO_2	bdl	bdl	bdl	bdl	bdl	bdl	1.11	bdl	bdl
Sb_2O_5	bdl	bdl	1.29	bdl	bdl	bdl	38.86	0.83	0.42
Total	99.93	99.17	99.25	99.41	100.72	100.21	98.80[6]	101.86	103.55[7]
					Formula coefficients				
Ca	–	–	–	–	–	–	1.40	–	–
Pb	–	–	–	–	1.01	–	0.03	0.98	1.78
Sr	–	–	–	–	–	–	0.03	–	–
Ba	–	–	–	–	0.35	–	0.01	–	–
Mg	–	0.02	0.20	0.02	–	–	–	0.12	–
Zn	0.97	1.03	7.18	1.02	0.36	1.00	–	2.30	1.98
Ce	–	–	–	–	–	–	0.48	0.16	–
Al	1.85	0.27	2.60	0.38	0.06	0.47	0.01	0.17	0.17
Mn^{3+}	0.09	0.71	5.02	0.98	–	0.03	–	2.14	3.63
Fe^{3+}	0.09	0.96	6.96	0.58	1.39	0.05	0.02	3.74	2.60
Si	–	–	–	–	–	–	–	–	–
Ti	–	0.01	0.90	0.01	0.77	–	0.90	12.04	2.51
Zr	–	–	–	0.01	0.02	–	–	0.21	0.02
U	–	–	–	–	–	–	0.02	–	–
Sb^{5+}	–	–	0.14	–	–	–	1.03	0.09	0.03
Basis of calculation	3 cations	3 cations	23 cations	3 cations	8 cations, excluding Pb and Ba	3 cations	(Sb+Ti+Al+Mn+Fe) = 2	22 cations	11 cations, excluding Pb

Note:

[1] Additionally contains 49.45 wt.% MnO_2 corresponding to 5.40 apfu Mn^{4+}

[2] Additionally contains 49.64 wt.% Cr_2O_3 corresponding to 1.45 apfu Cr

[3] Additionally contains 0.70 wt.% Na_2O and 0.89 wt% MnO_2 corresponding to 0.09 apfu Na and 0.04 apfu Mn

[4] Additionally contains 0.30 wt.% Y_2O_3 corresponding to 0.05 apfu Y

[5] Additionally contains 0.67 wt.% Nb_2O_5, corresponding to 0.06 apfu Nb

[6] Possibly, deficiency of the sum is due to the absence of analytical data for *REE* other than Ce.

[7] The high total value may be explained by the presence of Mn predominantly in the bivalent state.

References:

Majer V. High-pressure metamorphism between the Pelagonian Massif and Vardar Ophiolite Belt, Yugoslavia // Mineral. Mag. 1983. Vol. 47. P. 139–141.

Mircovski V. Amphibolitic rocks of the lower precambrian matamorphic complex of the Pelagonian massif // Proc. of the XVII Congress of Carpatian-Balkan Geological Association. Skopje: Saints Cyril and Methodius University. 2002. P. 53–57.

Stojanov R. Phengites of the Pelagonian massif // Trudovi na Geoloskiot Zavod na Socijalisticka Republika Makedonija. 1967–1968. Vol. 13. P. 59–73.

Ivanov T., Jančev S. "Nežilovo" – a complex polimetallic deposit of "Franklin Furnace" type in Macedonia // Proc. of the Jogoslavian Geological Congress 5. Ljubljana. 1976. pp. 69–78.

Chukanov N.V., Jančev S., Pekov I.V. The association of oxygen-bearing minerals of chalcophile elements in the orogenetic zone related to the "Mixed Series" complex near Nežilovo, Republic of Macedonia // Macedonian Journal of Chemistry and Chemical Engineering. 2015. Vol. 34. № 1. P. 115–124.

Jančev S. Zn-rich pyroxenes from the occurrences in the mixed series in the upper part of the Babuna River, Macedonia // Geologija (Ljubljana). 1998. Vol. 40. P. 283–289.

Tarr W.A. The origin of the zink deposits at Franklin and Sterling Hill, New Jersey // The American Mineralogist. 1929. Vol. 14. P. 207–221.

Palache Ch. Paragenetic classification of the minerals of Franklin, New Jersey // Amer. Miner. 1929a. Vol. 14. № 1. P. 1–18.

Palache Ch. A comparison of the ore deposits of Longban, Sweden, with those of Franklin, New Jersey // Amer. Miner. 1929б. Vol. 14. № 2. P. 43–47.

Wilkerson A.S. The minerals of Franklin and Sterling Hill, New Jersey // Bull. 65. New Jersey Geological Survey. Department of Conservation and Economic Development. Trenton, New Jersey. 1962. 80 pp.

LOCAL ELEMENTAL ANALYSIS METHODS IN GEOCHEMISTRY

Fedik I.V.[1], Moret M.P.[2], Peres P.[2], Saliot P.[2], Horréard F.[2], Clifton P.[3], Shilobreeva S.N.[4]

[1]AMETEK, Moscow, Russia, igor.fedik@ametek.com
[2]CAMECA SAS, Paris, France
[3]CAMECA Instruments, Madison, USA
[4]Vernadsky Institute of Geochemistry and Analytical Chemistry of the Russian Academy of Sciences, Moscow, Russia

Geological samples generally are highly heterogeneous, with complex phase and chemical composition. Analysing objects of micron and nanometer scale for example dust particles, impurities, thin layers in intergrain space in minerals becomes increasingly important in modern geochemistry. Therefore recently the methods of local analysis become more widely spread and developed.

At the same time, requirements to detection limits of analytical methods increase. Particularly, in precious metals and rare-earth elements deposits exploration finding trace elements in the range of 1 to 10 ppm can bear a lot of valuable information.

Due to physical limitations a combination of high spatial resolution (or lateral resolution if only the sample's surface is investigated) and high detection limit (sensitivity) is a general challenge in development of analytical instruments. The chart on Fig.1 demonstrates that often selection of an analytical technique comes down to a compromise between lateral resolution and detection limit.
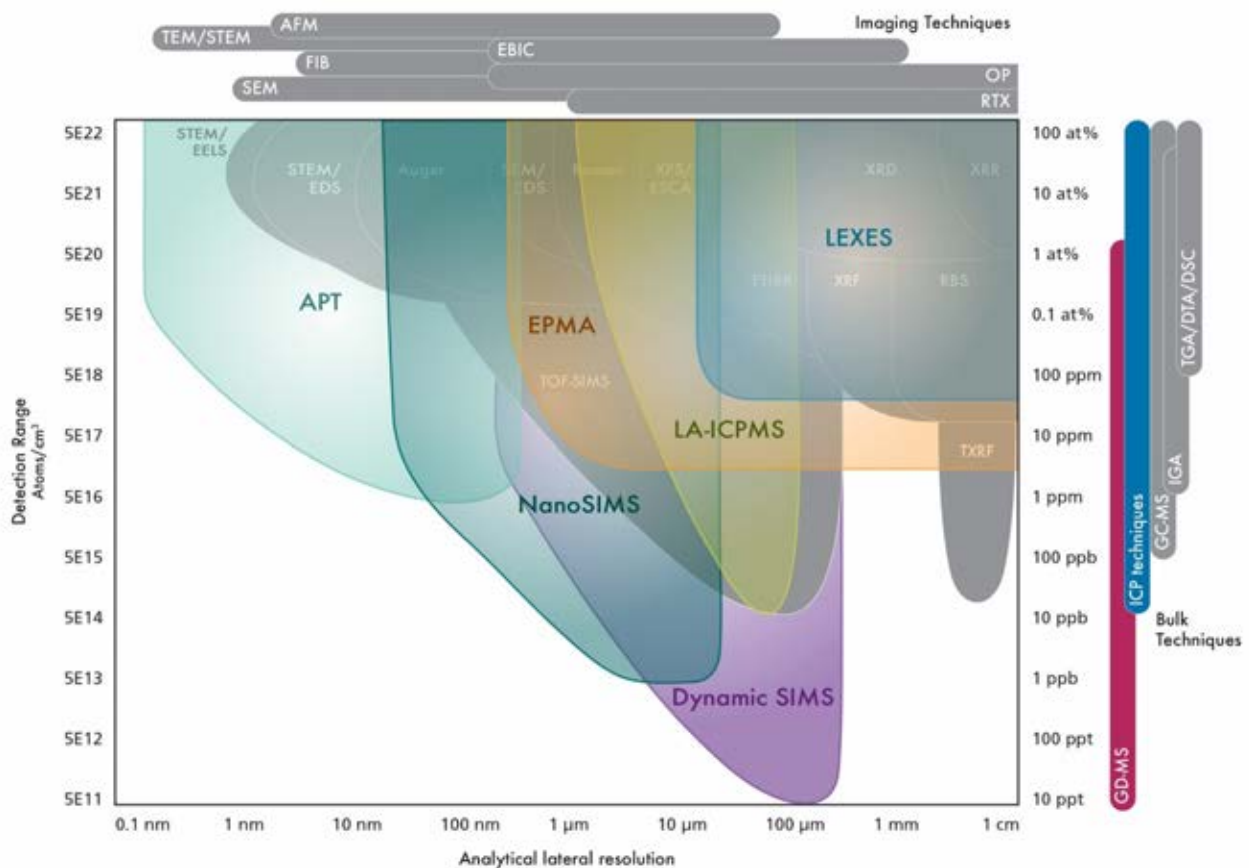
Fig.1. Lateral resolution vs detection range landscape for different analytical techniques.

The current discussion is to raise a problem of selection of appropriate local elemental analysis technique for various applications in geochemistry and petrology.

Electron probe microanalysis (EPMA) is an analytical technique that has stood the test of time. Not only is EPMA able to trace its origins back to the discovery of X-rays at the end of the nineteenth century, but the first commercial instrument appeared over 50 years ago. Nevertheless, EPMA remains a widely used technique for determining the

elemental composition of solid specimens, able to produce maps showing the distribution of elements over the surface of a specimen while also accurately measuring their concentrations.

EPMA involves bombarding a specimen with a focused electron beam and analyzing the emitted X-rays. It generally combines two related analytical techniques - wavelength-dispersive spectroscopy and energy-dispersive spectroscopy (which is also the subject of a separate Essential Knowledge Briefing) - in a single instrument known as a microprobe. Both techniques work by collecting characteristic X-rays and continuum released when the surface of a specimen is bombarded with electrons. As their names suggest, wavelength-dispersive spectroscopy separates emitted X-rays according to their wavelengths while energy-dispersive spectroscopy separates them according to their energies.

Wavelength-dispersive spectroscopy exhibits far better spectral resolution than energy-dispersive spectroscopy, but data collection is not as fast. When combined together in EPMA, energy-dispersive spectroscopy and wavelength-dispersive spectroscopy complement each other to produce a powerful analytical instrument. Energy-dispersive spectroscopy can conduct a quick initial analysis to identify the major elements, while wavelength- dispersive spectroscopy can perform a more detailed analysis to identify trace elements and measure the concentrations accurately.

EPMA has proved particularly adept at analyzing geological materials and metal alloys, able to reveal both the concentration and the distribution of elements at the sub-micrometer scale (Heath, et al., 2015).

The basic output of EPMA is a spectrum showing peaks that represent X-rays with specific energies (EDS) or wavelengths (WDS), with each peak corresponding to a specific element. The lateral distribution of each element is obtained, by either beam or stage scanning, after acquiring X-ray maps at peak and off-peak (background) positions. The sizes and proportions of phases identified in the analyzed material can be determined by combining several X-ray maps (Fig. 2).

EPMA can also determine the concentration of the elements based on the intensities of the emitted X-rays, allowing it to conduct absolute quantitative analyses. This usually involves first collecting a spectrum with WDS and/or EDS to identify which elements are present in a specimen. Quantitative analysis is then performed using just the WDSs, by comparing the X-ray intensities measured for all the elements identified in the initial spectral analysis against standards of known composition. After matrix correction for fluorescence, absorption and atomic number effect, the concentrations of all the elements identified in the specimen are accurately determined. The results of quantitative EPMA analyses are commonly displayed as weight percentages of elements and/or oxides This ability to conduct quantitative analyses is a major strength of WDS EPMA, which is recognized as the only nondestructive analytical technique able to provide absolute and accurate quantification for a specimen of interest. Using well- defined standards, it is possible to achieve quantitative analysis with an accuracy better than $\pm1\%$ (Heath, et al., 2015).

Recently Secondary Ion Mass Spectrometry (SIMS) became a technique of ever-growing use in geochemistry.

SIMS is the most sensitive method of the local elemental and isotopic analysis. In this method sample surface is bombarded with a focused beam of primary ions which leads to local ionization of the sample and to sputtering of the secondary ions which are analyzed with a mass-spectrometer. Generally in geochemistry O^-, O_2^+, Cs^+ are used as primary ions (Werner, et al., 2003).
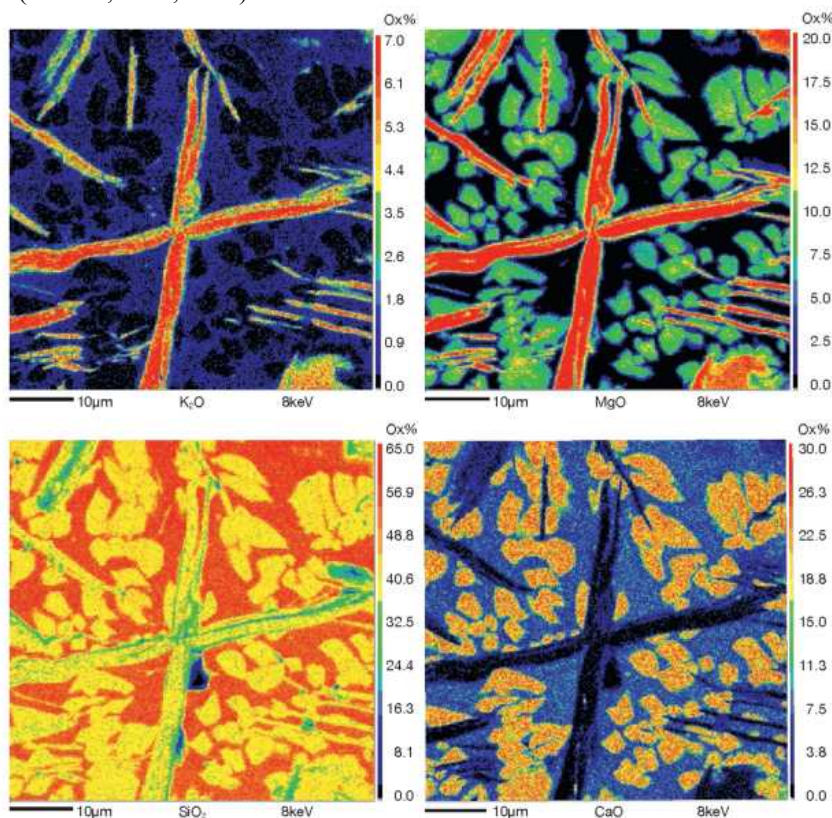

Fig. 2. X-ray maps acquired at high magnification on synthetic volcanic rock clearly reveal three phases: clinopyroxene (no K_2O), glass (with 2% of K_2O) and phlogopite (with 5% of K_2O). Data courtesy of Ida di Carlo, Institut des Sciences de la Terre d'Orleans, France.

SIMS method provides an unique combination of high sensitivity for all elements from hydrogen to uranium and further (with detection limits for the majority of elements down to ppb levels), high spatial resolution (down to 50 nm) and extremely wide dynamic range (more than 5 orders). It is the only method which allows to examine surface and volume distribution of elements in both organic, and inorganic solid bodies. In fact the SIMS method is destructive, however this feature allows to perform in-depth analysis and 3D-mapping.

CAMECA had developed a range of SIMS instruments which are particularly useful in geological applications:

The IMS 1300-HR[3] which is the high sensitivity/ high precision SIMS required for precise trace elements (U/Pb dating, REE, …) or ultra-fast stable isotope measurements in FC multicollection mode. Typical analytical performance:

- down to or below 1E-4 range (0.1 permil) reproducibility for stable isotope measurements in automated, FC multicollection mode (Schuhmacher, et al., 2004) ,

- high throughput - high precision U/Pb geochronology on zircons from smaller spots (5-15μm) in automated, EM monocollection mode.

The NanoSIMS 50L which is the SIMS instrument allowing to reach spatial resolution down to 50 nm without loss of sensitivity for light elements thanks to unique design of coaxial ion optics.

Studying of some geological and cosmochemical samples require ultimately high spatial resolution. For example this instrument has been used for studying distribution of H, D, ^{12}C, ^{13}S-, ^{18}O, ^{28}Si, ^{29}Si, ^{30}Si isotopes and ^{26}CN, ^{12}C^{14}N-, ^{12}C^{15}N compounds in chondrites and presolar grains (Remusat, et.al, 2008, Bose, et al, 2014, Piani, et al, 2015).

Other distinctive features of NanoSIMS 50L are:

- Multicollector allowing the parallel detection of seven masses. Each multicollection trolley can receive one EM and one FC. Mass dispersion for parallel detection Mmax/Mmin is 21 and the minimum mass interval is Mmax/58.

- High reproducibility of isotopic measurements thanks to the development of software routines for automated secondary ion beam alignment in the optics and addition of field compensating coils before the entrance slits.

- All moveable slits and apertures of the optics as well as the hexapole and the Z-axis of the sample stage have are automated.

Operating the NanoSIMS 50L in multiple FC mode allows to envision earth science applications requiring permil isotopic ratio reproducibility at sub-μm scale.

Atom probe tomography (APT) can determine chemical identity (mass/charge ratio) and 3D position of individual atoms in conductive and non-conductive samples with sub-nanometer resolution. Recently, this unique capability has been applied to geological applications and the 3D chemical and spatial information has provided new insights into the age and thermal history of minerals.

APT method can be used in synergy with EPMA and SIMS and, especially in these geological applications, to identify regions of scientific interest and then use the nano-scale 3D information to help date and detail giga-year geological events.

For example SIMS analysis was used to identify and age a 2.4Ga Albion-Raft R-Grouse Ck core complex, Utah. Higher spatial resolution analysis with APT was used to demonstrate that incompatible elements, including Pb and Y, were concentrated in ~5-10nm diameter domains, spaced ~50 nm apart, while U is homogeneously distributed (John, et al., 2012).

In a compositional interface in a natural zircon crystal [(Zr,Hf)SiO4], a region of the specimen with an unusual concentration of rare earth elements was mapped for Th by CAMECA SX Five FE EPMA (7kV, 100nA) to reveal the surface position of this otherwise cryptic feature of interest. Superposition of the mapping data on a BSE image of the specimen guided the specific site selection for FIB-based specimen preparation for APT analysis. The feature of interest was successfully captured within a 100nm long APT analysis, and the Th Mα signal observed by EPMA was found to emerge from a 25nm thick band containing 0.2at% Th. The other rare earths included an inhomogeneous distribution of U, Y along with P, and Al and subnanometer compositional analysis revealed this interface to be a core/overgrowth fossil resorption front (Snoeyenbos, et al., 2012).

References:

Bose M., Zega T.J., Williams P. (2014) Earth and Planetary Science Letters. Vol. 399, P. 128–138.

Heath J., Taylor N. (2015) Electron probe microanalysis

John W. Valley, T. Ushikubo, A. Strickland, D. Reinhard, D. Snoeyenbos, D. Lawrence, I. Martin, T.F. Kelly, A. Cavosie, (2012) AGU Abstracts

Piani L., Robert F., Remusat L. (2015) Earth and Planetary Science Letters. Vol. 415, P. 154–164.

Remusat L., Guan Y., Eiler J.M.(2008) 39th Lunar and Planetary Science Conference. Texas (USA),. P. 2477.

Schuhmacher M., Fernandes F., De Chambost E.. (2004) Applied Surface Science 231–232.

Snoeyenbos D., Jercinovic M.J., Reinhard D.A., Hombourger C., (2012) American Geophysical Union Abstracts V23C.

Werner H.W. (2003) Surf. Interface Anal.. Vol. 35, P. 859–879.

CAMECA IMS 1300-HR3: THE NEW GENERATION ION MICROPROBE

Fedik I.[1], Peres P.[2], Choi S.-Y.[2], Fernandes F.[2], Renaud L.[2]

[1]AMETEK, Moscow, Russia, igor.fedik@ametek.com
[2]CAMECA SAS, Paris, France

The success of secondary ion mass spectrometry (SIMS) in Geo- and Cosmo-chemistry relies on its performance in terms of: 1) very high sensitivity (mandatory for high precision measurements or to achieve low detection limits); 2) a broad mass range of elemental and isotopic species, from low mass (H) to high mass (U and above); 3) in-situ analysis of any solid flat polished surface; and 4) high spatial resolution from tens of microns down to sub-micron scale.

The IMS 1300-HR[3] (High Reproducibility, High spatial Resolution, High mass Resolution) is the latest generation of CAMECA's large geometry magnetic sector SIMS (or ion microprobe), successor to the internationally recognized IMS 1280-HR. The 1300-HR[3] (Fig. 1) delivers unmatched analytical performance for a wide range of applications (stable isotopes, geochronology, trace elements, and environmental studies...).

Fig.1. IMS 1300-HR[3] large geometry SIMS instrument

The CAMECA ion microprobe has been extensively used for trace element analysis in minerals as it provides µm-scale elemental information over a large mass range. When analyzing trace elements, one must deal with several molecular interferences of extremely close masses which must be eliminated using high mass resolution and/or energy filtering methods. A high-brightness O^-/O_2^- ion source combined with ion imaging capabilities is also mandatory for performing analysis in small areas while keeping high sensitivity. The IMS 1300-HR[3] has been designed to meet all these requirements.

Several results have been published recently in the scientific literature with pioneering results on mineralogy applications. A selection of these data will be presented, including:

- Correlated microanalysis of zircon. Complex chemistry of zircons requires in-situ microanalysis for trace element and oxygen isotope analysis. The CAMECA ion microprobe can perform rapidly U-Pb dating, stable isotope measurements, as well as REE elemental analysis (with the flexibility to switch from O to Cs source in a very short time), all with the required precision (Cavosie et al., 2007).
- Ti ion imaging in zircon. Ti concentration in Hadean zircons is an indicator of the crystallization temperature. Quantitative ion imaging of titanium in zircon permits detailed insights of Ti concentration distributions. Ti ion images obtained on Jack Hills zircon show that Ti contents greater than 20ppm are associated with cracks or other imperfections (Harrison, et al., 2007).
- Trace elements to study magmatic processes. Crystals in volcanic rocks provide records of magma reservoir processes and timescales before eruptions. Trace element analyses (Ti, Sr, Mg) have been performed on chemically zoned crystals from the Minoan caldera, formed after eruption of Santorini volcano (late 1600 BC) (Druitt, et al. 2012).
- Volatile contents in melt inclusions. Mid-ocean ridge (MOR) magmas undergo cooling and crystallization to form the oceanic crust. However, there is no consensus on where crystallization occurs (within the crust or upper mantle). Volatile concentrations (H_2O, CO_2, F, S, Cl) were measured in melt inclusions (melt entrapped in crystallizing mineral phases) from two MORs in Pacific Ocean. Volatile contents allow calculation of crystallization depth by deriving vapour-saturation pressures (Druitt, et al. 2012).
- Ore Deposits & Sulfur isotopes. Sulfur is often localized in mineralized systems associated with ore deposits, where it acts as an important complexing ligand for metal transport and precipitation. As such, sulfide-hosted ore deposits are an important source of Ni, Cu, and platinum group elements (PGE). Constraining the sulfur isotopic signature is useful in delineating the sources of sulfur in magmatic-hydrothermal ore deposits, and is an important parameter to better understand the geodynamic environment in which the mineralization process occurred (Jeon, et al. 2015).

References:

Cavosie A.J., Valley J.W., Wilde S.A. (2007) The Oldest Terrestrial Mineral Record: A Review of 4400 to 4000 Ma Detrital Zircons from Jack Hills, Developments in Precambrian Geology 15, 91–111.

Druitt T. H., Costa F., Deloule E., M. Dungan & Scaillet B. (2012) Decadal to monthly timescales of magma transfer and reservoir growth at a caldera volcano, Nature 482, 77–80.

Harrison T.M. and Schmitt A.K. (2007) High sensitivity mapping of Ti distributions in Hadean zircons, Earth Planet. Sci. Lett. 261 (1-2), 9-19.

Data courtesy of Jeon H., Kilburn M., LaFlamme C., Martin L., (2015) Univ. of Western Australia.

Wanless, D, and Shaw, A.M. (2012) Lower crustal crystallization and melt evolution at mid-ocean ridges, Nature Geoscience, 5, 651–655.

COMPOSITIONAL EVOLUTION IN AMPHIBOLE OF THE NIVA INTRUSION AND DYKE PERALKALINE NEPHELINE SYENITE (KOLA PENINSULA, RUSSIA)

Filina M.I., Kogarko L.N., Kononkova N.N.

Vernadsky Institute of Geochemistry and Analytical Chemistry of the Russian Academy of Sciences, Moscow, Russia,
makimm@mail.ru

In this paper presented new data on the chemical composition and characteristics of the distribution of trace elements in amphibole from Niva intrusions and dyke peralkaline nepheline syenite (Kola Peninsula).

Amphiboles from peralkaline nepheline syenite from the Niva intrusion and dyke (Akimenko et al., 2014; Arzamastsev et al., 2000) have been investigated. It is situated in the northwestern part of the Belomorian mobile belt (Kola Peninsula, Russia). Among the major minerals of the syenite are nepheline (10–15 vol %), orthoclase (15–20 vol %), lamprophyllite group minerals (15–20 vol %), titanian aegirine–augite (10–15 vol %), aenigmatite (10–15 vol %), alkaline amphibole (5–10 vol %), natrolite (5-10 vol %), and astrophyllite (up to 5 vol %).

Amphibole forms elongated coarse grains (1-1.5 mm in size), brown colored, with a faint bluish tint, the cross sections often have a hexagonal shape. Amphibole is most often associated with aegirine-augite, the fine needle-like grains of which are located both on the edges and inside the crystals.

The chemical composition of amphiboles was measured on a microprobe Cameca SX-100, representative analyzes are shown in Table. 1. The studied amphiboles are sodium-calcium and sodium group, typical for peralkaline rocks. The amphibole is zonal, the cores correspond to K-Ti-cathophorite or K-Ti-enkermanite, the rims of K-Ti-arfvedsonite. The presence of fluorine is characteristic.

The compositions of the amphibole correspond to the general trend in the evolution of pyroxene compositions in the studied syenite (Filina and Kogarko, 2017) - increase in the contents of sodium, potassium, and iron from the core to the rim, and a decrease in the magnesium and calcium contents (Fig. 1), while the content of potassium, titanium and fluorine remains high - up to 4.81 wt. %, up to 4.71 wt. %, up to 3.54 wt. %. The content of fluorine correlates with the content of titanium - with a decreasing content of titanium the content of fluorine decreases.
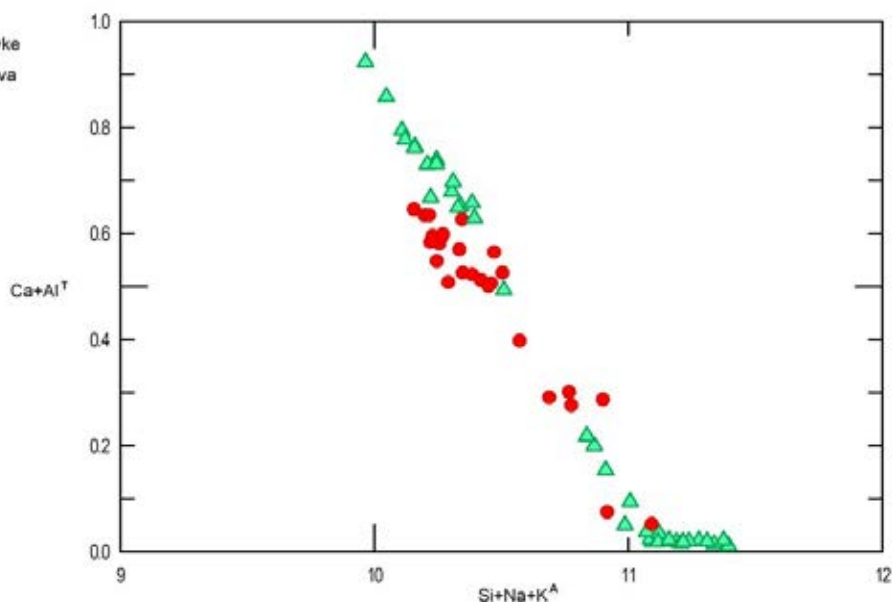
Fig. 1 Compositional variation in amphiboles (as a.p.f.u.) $Ca+Al^T$ vs $Si+Na+K^A$.

Contents of rare and trace elements in the amphiboles were determined by secondary ion mass spectrometry on the Cameca 5f. The distribution of rare-earth elements in amphiboles is similar of amphiboles from other alkaline complexes (Fig. 2).

In earlier experimental studies of the stability fields of amphiboles, depending on the oxygen fugacity and temperature, it was shown that the trend of a change in the amphibole composition from Ca through Na-Ca to Na amphiboles reflects a decrease in temperature and oxygen fugacity at or below the QFM buffer (Mitchell, 1990).
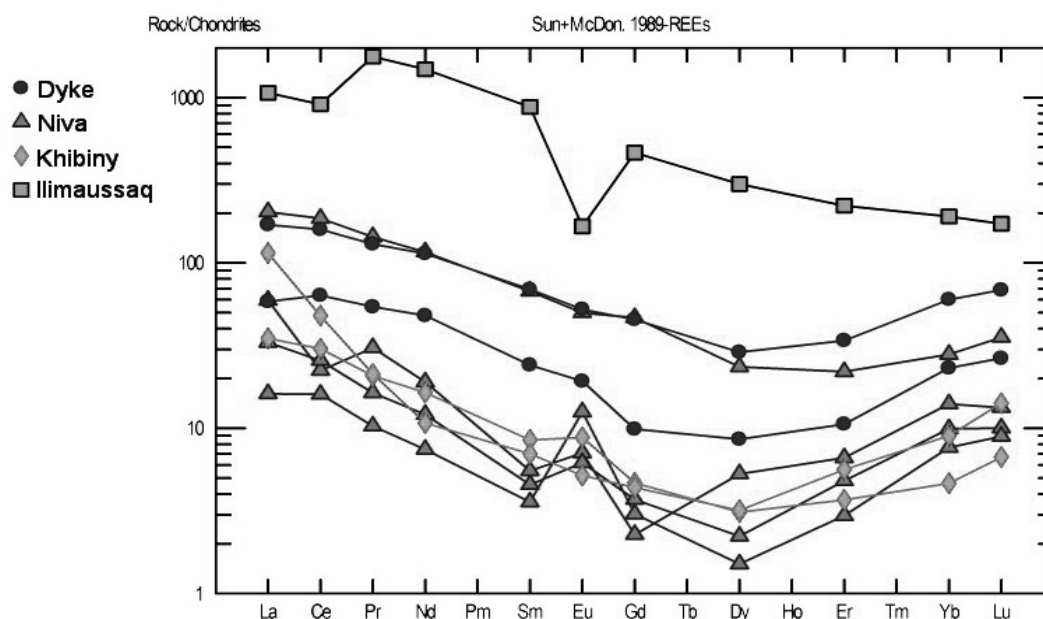
Fig. 2 Chondrite-normalized distribution of rare-earth elements in amphiboles from the Niva intrusion, agpaitic dyke and the alkaline complexes of the Baltic Shield (Marks et al, 2004; Arzamastsev et al, 2005).

Table. 1. Representative analyses (wt.%) of zonal amphibole crystals from the dyke and Niva intrusions.

Component	1 C	2 R	3 C	4 R	5 C	6 R	7 C	8 R
SiO_2	52.62	50.08	49.86	48.65	50.91	49.57	50.81	50.28
TiO_2	3.16	2.74	3.02	2.11	4.36	2.83	4.71	0.60
Al_2O_3	0.76	0.83	0.75	0.88	1.57	0.18	1.83	0.81
MnO	0.52	0.33	0.53	0.27	0.46	0.72	0.53	0.46
FeO	14.16	25.90	14.19	24.20	13.92	29.32	14.15	29.25
MgO	12.53	5.69	12.40	6.49	11.64	1.13	11.73	2.56
CaO	3.11	0.79	3.05	0.75	2.86	0.06	3.35	0.13
Na_2O	6.43	7.06	6.36	7.15	6.72	7.21	6.44	7.00
K_2O	3.76	4.55	3.60	4.19	3.25	4.81	3.11	4.58
ZrO_2	0.79	0.00	0.85	0.06	0.48	BDL	0.12	BDL
BaO	0.11	0.05	0.07	0.05	0.29	0.22	BDL	BDL
SrO	0.49	0.03	0.57	0.17	0.33	0.05	0.60	0.04
$Cr2O3$	ND	ND	ND	ND	0.03	0.01	0.06	0.04
Nb_2O_5	0.02	0.01	0.05	0.10	ND	ND	ND	ND
UO_2	0.64	0.73	0.73	0.88	ND	ND	ND	ND
F	3.34	0.83	3.54	1.44	3.04	0.02	2.97	0.38
Total	102.44	99.62	99.57	97.39	99.86	96.13	100.41	96.13
O=F	1.41	0.35	1.49	0.61	1.28	0.01	1.25	0.16
Total	101.03	99.27	98.08	96.78	98.58	96.12	99.16	95.97

Note. 1-4 - amphiboles from the dyke (samples № 11-UK-8, 11-UK-32), 5-8 - amphiboles from the Niva intrusion (samples № H-8-1, H-8-3). Zones of crystals: C – core, R-rim. BDL - below the detection limit, ND - not determined.

References:

Akimenko M. I., Kogarko L. N., Sorokhtina N. V., Kononkova N. N., Mamontov V. P. (2014): A New Occurrence of Alkaline Magmatism on the Kola Peninsula: An Agpaitic Dyke in the Kandalaksha Region. Doklady Earth Sciences., 458, 1125–1128.

Arzamastsev A. A., Bea F, Arzamastseva L.V., Montero P (2005) Rare elements in minerals of the Khibiny massif as indicators of the evolution of mineral formation processes: results of the LA-ICP-MC study. Geochemistry 1:80-95.

Arzamastsev A. A., Belyatsky B.V., Arzamastseva L.V. (2000) Agpaitic magmatism in the northeastern Baltic Shield: a study of the Niva intrusion, Kola Peninsula, Russia. Lithos 51:27–46.

Hawthorne F.C., Oberti R., Harlow G.E., Maresch W.V., Martin R.F., Schumacher J.C., Welch M.D. (2012) IMA Report. Nomenclature of the amphibole supergroup Amer Min 2031-2048.

Marks M., Halama R., Wenzel T., Markl G. (2004) Trace element variations in clinopyroxene and amphibole from alkaline to peralkaline syenitas and granites: implications for mineral-melt trace element partitioning. Chemical geology 211: 185-215.

Mitchell R.H., (1990) A review of the compositional variation of amphiboles in alkaline plutonic complexes. Lithos 26:135-156.

Filina M. I., Kogarko L. N., Kononkova N. N. (2017) Evolution of pyroxene from peralkaline magmatic systems: Dyke complex of agpaitic syenite and Niva Intrusion (Kola Peninsula). Geochem Int 7:1-7.

BRATSIGOVO-DOSPAT VOLCANIC AREA (CENTRAL RHODOPES, BULGARIA) – THE LINK BETWEEN EAST AND WEST RHODOPE MAGMATISM IN LATE PALEOGENE: CONSTRAINTS FROM SR-ND-HF ISOTOPIC STUDIES

Filipov P.[1], Marchev P.[1], Peytcheva I.[1,2], von Quadt A.[2], Georgiev S.[1]

[1]Geological Institute, Bulgarian Academy of Sciences, Sofia, Bulgaria, p_philipov@geology.bas.bg

[2]IGP-ETH Zürich, Zürich, Switzerland

Late Eocene-Early Oligocene magmatism in the Rhodope Massif is a remarkable example about relationship between crustal thickness and composition of magmatic products. From east to west, these products exhibit progressive volume increase of the felsic varieties along with crustal input (Marchev et al., 1994). East Rhodope volcanic rocks are related to relatively thin crust, reaching to up to 35 km (Shanov & Kostadinov, 1992), and characterized by prevailing intermediate to mafic compositions over the felsic. In contrast, the West Rhodope Mesta volcanic complex, located on tectonically thickened crust (42-50 km), exposes exclusively felsic rocks and the lack of mafic-intermediate compositions. Mesta rhyolites and dacites were interpreted to have originated from extreme crustal contamination of a mantle-derived end member (Filipov et al. 2014). Bratsigovo-Dospat volcanic area (BDVA) in Central Rhodopes is situated between these two regions with contrasting crustal thickness and comprises uniform rhyolitic tuffs, seldom monzogranodiorite dykes and a subvolcanic monzonite intrusion. Here we provide new data on U-Pb zircon ages and Sr-Nd-Hf isotopic compositions of the Bratsigovo-Dospat (BD) ignimbrites and dykes in order to study the compositional modification of the magmas related to thickened crust and constrain the link with the neighboring Late Paleogene volcanic regions.
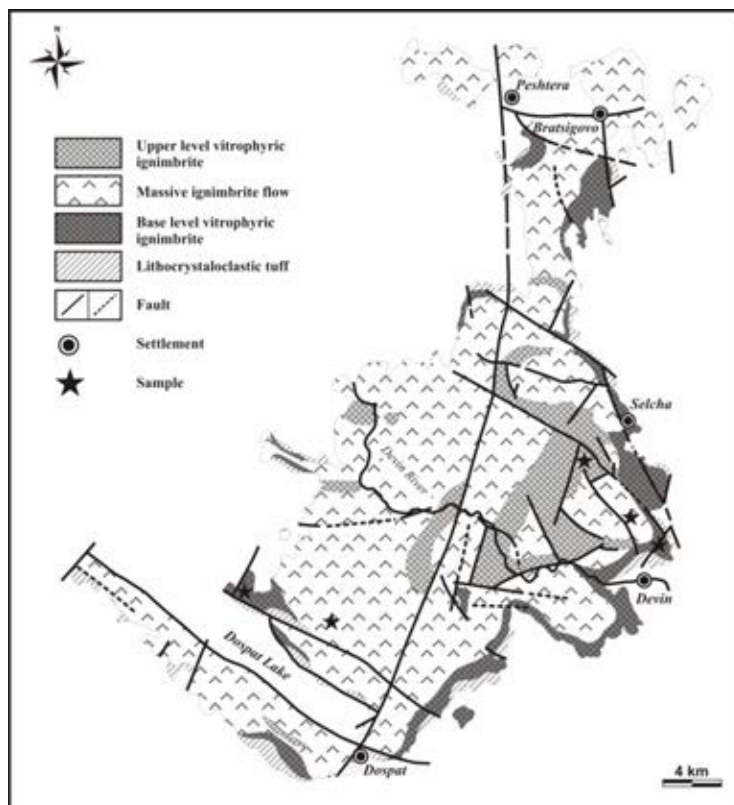
Fig. 1. Geological map of Bratsigovo-Dospat volcanic area after Kackov (1987)

Geological Background

Bratsigovo-Dospat volcanic products spread over an area of some 650 km^2 (Fig. 1) that overlay either conglomerates and breccia-conglomerates of gneiss, schist, amphibolite, granite, marble clasts or directly local basement rocks (Katskov, 1980). Following the tectonostratigraphic division of Rhodope metamorphic complex of Jahn-Awe et al. (2012 and references therein), BDVA borders the basement rocks of several allochthonous units. Arda metamorphic dome locates to the east of BDVA, considered a part of the Lower and Middle Allochthon and built up of Late Paleozoic orthogneisses. To the west and north-east BDVA neighbors the Asenitsa Unit of the Middle Allochthon, which ortogneiss

protolith is of Jurassic age. Parvenets Unit, referred to as a constituent of the Early Paleozoic Upper Allochthon, is situated to the north of BDVA, and Early Eocene Barutin-Buynovo-Elatia granitic pluton limits BDVA from the south.

Bratsigovo-Dospat ignimbrites (SiO_2=70.1-72.8 % wt) expose deposits of up to 800 m at their maximum thickness, north of Devin Town (Fig. 1). Stratigraphically their section has been divided into several levels (Kackov, 1987): (1) vitrophyric ignimbrite, that is densely welded with typical parallel alignment of shards, stands at the base of the section; (2) massive ignimbrite flow builds the thickest part of the section, reaching to up to 500 m in thickness. Massive ignimbrite shows structures of welding, but is characterized by a low degree of compaction in comparison to the other ignimbrite levels; (3) the uppermost part of BD section is occupied by vitrophyric ignimbrite, exhibiting extreme degree of compaction, as its glass shards have been welded in coherent mass. Thus, the upper vitrophyre level might be considered the base of another flow unit. All types of ignimbrite have similar mineralogy, composed of phenocrysts of quartz, plagioclase, K-feldspar, biotite, amphibole and accessories of magnetite, apatite, zircon and sphene. The ignimbrites are intruded by a monzonitic subvolcanic intrusion, enveloped in extensive advance argillic alteration (Marchev & Jelev, 2010).

Several monzogranodioritic dykes (SiO_2=63.4-67.5 % wt) were observed to intrude the basement of the Middle Allochthon near the borders with BDVA. They are porphyritic with mineral composition similar to the ignimbrites of BDVA.

Materials and Methods

Seven representative rock samples have been selected for this study (Fig. 1): 1) two samples from the ignimbrite base level near the dam of Dospat Lake and in the vicinity of the Town of Devin; 2) two samples of the massive ignimbrite flow from Dospat Lake and 4 km north of Devin; 3) one vitrophyre sample of the upper ignimbrite level, 9 km north of Devin; and 4) two samples of monzogranodioritic dykes, collected south of the villages of Varvara and Patalenitsa. U-Pb zircon dating of five samples was performed at the Geological Institute – BAS using New Wave UP193FX LA coupled to ELAN DRC-e quadrupole ICP-MS. Six whole rock samples (four ignimbrites and two monzogranodiorites) were analyzed for Sr-Nd isotope composition at ETH Zurich using a Thermo Scientific Triton TIMS and Nu Instruments Nu Plasma II MC-ICP-MS. $^{176}Hf/^{177}Hf$ isotopic composition in zircon from two ignimbrites is determined on *GEOLAS* Ar-F excimer laser coupled to the same Nu Plasma II MC-ICP-MS at ETH Zurich. Cathode-luminescence (CL) imaging of the zircon samples were obtained at Belgrade University using JEOL JSM-6610 LV SEM-EDS.

Analytical Results

Dating of the rocks was made by using the autocryst zircons (in the sense of Miller et al., 2007), which comprise most of the extracted crystals. Both zircon of the base vitrophyric and massive ignimbrites show identical ages, determined by a Concordia age at 30.93±0.28 Ma and 30.92±0.36 Ma respectively. The sample of upper vitrophyre ignimbrite yielded a slightly younger U/Pb age of 30.55±0.25 Ma, but indistinguishable within the error. Dating of antecrysts yielded ages between 36-32 Ma. Scarce xenocrysts and inherited cores, represented mostly in the base vitrophyre ignimbrite, are dated between 448-55 Ma, giving constraints on contamination by the rocks of the Lower and Upper Allochthons and Barutin-Buynovo-Elatia pluton.

Unlike zircon samples of ignimbrites, xenocrysts in monzogranodioritic dykes are abundant. Most xenocrysts match the protolith age of the Lower (327-271 Ma) and Upper (469-452 Ma) Allochthons and one grain (173 Ma) fits the age of the Middle Allochthon. Few xenocryst ages fall into the range of Late Cretaceous (94-84 Ma) and Early Eocene (61-53 Ma). Very frequently CL images of xenocrysts reveal thin (5-10 µm) oscillatory terminations. The most like timing of intrusion is given by a single grain from every dyke, aged at 35.8±1.5 Ma and 32.1±0.8 Ma.
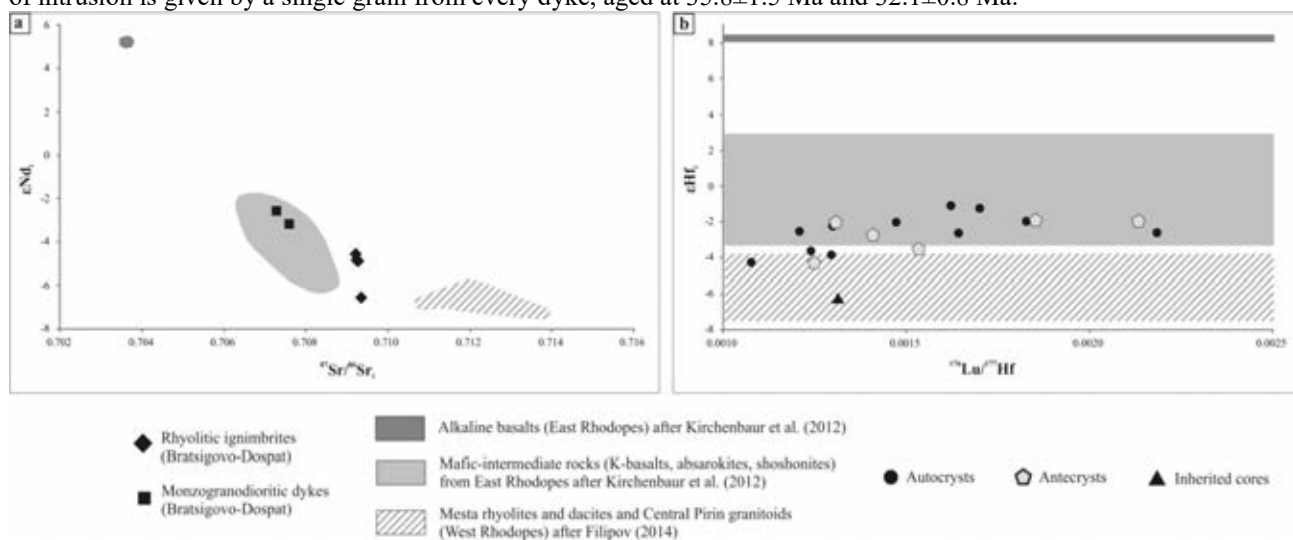

Fig. 2. (a) Comparison between Sr-Nd isotopic compositions of Bratsigovo-Dospat, East and West Rhodope magmatic rocks; (b) Comparison of εHf in zircon samples from Bratsigovo-Dospat ignimbrites and whole rock samples from East and West Rhodope lithologies.

The ignimbrites are characterized by very radiogenic $^{87}Sr/^{86}Sr_i$ composition (0.7092-0.7094) and unradiogenic $^{143}Nd/^{144}Nd_i$ (εNd_i=-6.6 – -4.6). Monzogranodioritic dykes have less radiogenic $^{87}Sr/^{86}Sr_i$ (0.7073-0.7076) and more radiogenic $^{143}Nd/^{144}Nd_i$ (εNd_i=-3.2 – -2.6) compared to the ignimbrites. Fig. 2 a compares Sr-Nd isotopic composition of BD lithologies with contemporaneous Late Eocene-Early Oligocene magmatic rocks from East and West Rhodopes. It shows a well-defined tendency of $^{87}Sr/^{86}Sr_i$ increase and εNd_i decrease from East to West Rhodope magmatic rocks (Fig. 2 a). In the diagram, both monzogranodiorites and ignimbrites define continuous variation trends with monzogranodiorites showing similarity to East Rhodope mafic-intermediate rocks and ignimbrites positioned between East and West Rhodope fields. The main difference between ignimbrites and East Rhodope compositions generally comes from higher $^{87}Sr/^{86}Sr_i$ of the ignimbrites, whereas εNd_i is more or less similar.

Fig. 2 b demonstrates correlation between Hf isotope compositions of zircon and whole rock samples from the East and West Rhodope rocks, giving further insights into genesis of BD ignimbrites. εHf_i of the autocrysts (-4.3 – -1.1) and antecrysts (-4.3 – -1.9) from BD ignimbrites overlap isotope composition of both East Rhodope mafic-intermediate and West Rhodope felsic rocks with most zircons falling into the field of the East Rhodope compositions.

Discussion and Conclusion

The ages obtained within our study show, that the oldest magmatic event in BDVA has been preserved in the monzogranodioritic dykes. Monzogranodioritic dykes host mostly inherited zircon populations and very few magmatic zircons compared to the later ignimbrites. This is consistent with a relatively limited storage of dyke parental melts in the magma chamber and picking up material from local basement during their ascent to the surface. Nevertheless, dykes are still characterized by lower $^{87}Sr/^{86}Sr_i$ ratio, suggesting lesser degree of modification through assimilation and/or isotope diffusion in comparison to the younger ignimbrites. Monzogranodioritic dykes exhibit a close $^{87}Sr/^{86}Sr_i$ to the East Rhodope mafic-intermediate rocks, implying an origin of similar magmatic sources and comparable extent of crustal contamination. Thus, chemical composition of BD monzogranodiorites can be explained by combined fractionation and crustal contamination (AFC) of a more mafic magma, similarly to the East Rhodope mafic-intermediate rocks.

Bratsigovo-Dospat ignimbrites have preserved only small amount of inherited xenocrysts and most of their zircons are autocrysts. This favors an interpretation of the complete resorption of crustal component, that must have influenced the final composition of the ignimbrite magma composition, regarding their less radiogenic zircon Hf isotopes. Isotope signature of magma at the time of zircon crystallization, based on the similarity of the εHf_i isotopes, was less contaminated and strongly resembles the East Rhodope mafic-intermediate rocks. This, coupled with their higher $^{87}Sr/^{86}Sr_i$, serves as an indication, that BD ignimbrites have evolved to exclusively felsic compositions through an AFC process.

This study demonstrated, that BDVA represents a compositional transition from the less evolved and less contaminated East Rhodope magmas to the exclusively felsic and extremely contaminated West Rhodope magmatic products. Therefore we conclude, that Bratsigovo-Dospat monzogranodiorites and rhyolitic ignimbrites seem to have originated from sources similar to the East Rhodope mafic and intermediate rocks.

References:

Filipov P. (2014) Petrology, geochemistry, geochronology of Mesta Volcanic Complex and Central Pirin Batholith. PhD Thesis, Geological Institute-BAS

Filipov P., Marchev P., Peytcheva I., Münker C., Kirchenbaur M. (2014) Comparison between $^{176}Hf/^{177}Hf$ of zircon and whole rock samples from Mesta Volcanic Complex, West Rhodopes: Evidence for crustal contamination. In: Proc XX CBGA Congress 1:433-436.

Jahn-Awe S., Pleuger J., Frei D., Georgiev N., Froitzheim N., Nagel T.J. (2012) Time constraints for low-angle shear zones in the Central Rhodopes (Bulgaria) and their significance for exhumation of high-pressure rocks. Int J Earth Sci 101:1971-2004.

Kackov N. (1987) Reconstruction des Paleovulkanismus im Bracigovo-Dospater Vulkanitmassiv (Bulgarien). Z Angew Geol 33:175-179.

Katskov N. (1980) Structure of the Bratsigovo-Dospat effusion. Geotect Tectonophy Geodyn 11: 3-23.

Kirchenbaur M., Münker C., Schuth S., Garbe-Schönberg D., Marchev P. (2012) Tectonomagmatic constraints on the sources of Eastern Mediterranean K-rich lavas. J Pet 1:27-65.

Marchev P., Jelev D. (2010) Monzonites in the Stomanovo prospect: first finding of Paleogene intrusive rocks in the Bratsigovo-Dospat area. Proc GEOSCIENCES 2010, Sofia, Bulgaria 41-42.

Marchev P., Larson P., Rogers G., Vaselli O., Raicheva R. (1994) Crustal thickness control on the Sr, Nd, and O isotopic variation in the Macedonean-Rhodope-North Aegean Magmatic Belt (MRNAMB). Proc IAVCEI 1994, Ankara, Turkey Unpaginated.

Miller J.S., Matzel J., Miller C.F., Burgess S.D., Miller R.B. (2007) . Zircon growth and recycling during the assembly of large, composite arc plutons. J Vol Geotherm Res 167:282-299.

Shanov S., Kostadinov I. (1992) Configuration of the deep geophysical discontinuities beneath the territory of Bulgaria. Geol Balc 22:71-79.

PETROLOGY, GEOCHEMISTRY AND GEOCHRONOLOGY OF CARBONATE-DYKES AND RELATED ALKALINE ROCKS FROM THE IVREA-VERBANO ZONE (ITALY)

Galli A., Grassi D.N., Gobbi P., Fux M., Sartori G., Frei D., Schulthess C.
ETH Zurich, Zurich, Switzerland, andrea.galli@erdw.ethz.ch

In the Ivrea-Verbano Zone (Italy/Switzerland) a complete transect through the lower crust is exposed. Its geological evolution has been controlled by large underplating of mantle-derived mafic magmas (the "Mafic complex", MC) into the high-grade basement of the Southern Alps. The MC is composed of both enriched gabbro-norites of Permian age and MORB-like tholeiitic gabbros of Triassic age. The host basement comprises migmatitic paragneisses and intercalated mafic rocks both metamorphosed at amphibolite to granulite facies conditions in Permian time. Several peridotite bodies with different petrology, degree of depletion, metasomatic overprint as well as pipe-like bodies of alkaline clinopyroxenite and gabbro occur widespread within the mafic complex, often related to oligoclasite veins as well as syenite and carbonate-dykes. The geological significance of such carbonate-dykes is still a matter of debate and their formation has been imputed to tectonic extrusion, melting of crustal carbonate or immiscibility from alkali-rich melts.

In this study, we present preliminary results of petrological, geochemical and geochronological investigations on different carbonate-dykes and associated alkaline rocks. Carbonate-dykes occur: i) within the Mafic complex as up to 40 meter thick isolated dykes which bear meter-sized clinopyroxenite enclaves different from the host mafic rocks or ii) as dykes associated to alkaline UM-mafic bodies. The architecture of such bodies define a concentric-zoned structure and is characterized by metasomatised peridotite cores surrounded by phlogopite-amphibole-bearing clinopyroxenite, (garnet) hornblendite and garnet-clinopyroxene gabbro or clinopyroxene leucogabbro. Core peridotites display different metasomatic features such as amphibole, apatite or chromitite-rich layers, phlogopite veins or pockets and diffuse carbonate-bearing wehrlite zones, suggesting that they were infiltrated by alkaline, CO_2-rich melts. Carbonate-dykes, together with oligoclasite veins and (nepheline) syenite-dykes, cut across UM-mafic rocks and contain leucocratic, feldspar-rich enclaves.

Carbonate-dykes show an enrichment of LREE over HREE ((La/Yb)N = 12-14), with Σ REE = 85-200 ppm and Y/Ho = 25-33. On the chondrite-normalized REE abundances diagram, no or only weak negative Eu anomaly is observed. Mantle-normalized pattern shows strong negative anomalies at Cs, Rb, K, Nb, Ta, P, Zr, Hf and Ti and positive Ba, Th, U, Pb, Sr, Nd anomalies, similarly to the "world average carbonatite" composition. Absolute trace element concentrations are lower than average carbonatites but higher than in limestone and similar to typical cumulate carbonatites. Pyroxenite (X_{Mg} = 0.70-0.86) and hornblendite (X_{Mg} = 0.48-0.63) from the UM-mafic bodies are nepheline-normative. Grt-cpx gabbro (X_{Mg} = 0.56) are enriched in LREE over HREE and display positive anomalies at Rb, Ba, K, Pb, Sr, whereas the cpx leucogabbro (X_{Mg} = 0.51) is richer in Na_2O and display a trace element pattern similar to carbonate-dykes, with positive Ba, Th, U and negative Rb, Hf, Zr, Ti anomalies, suggesting a genetic link between these two rock types.

Zircons separated from one carbonate-dyke are faint-zoned, present low REE and U concentrations and display a Th/U ranging between 0.35 and 1.37. On the chondrite-normalized REE diagram, no Eu and Ce anomalies are observable. Zircon U-Pb dating by laser ablation yielded an age of 186.7 ± 2 Ma, which is interpreted as the intrusion age of the dyke.

Field observations including cross cutting relationships, metasomatic contacts, fluidal texture, chilled margins and occurrence of enclaves often different from the host rocks indicate that the carbonate-dykes experienced a magmatic stage, excluding tectonic extrusion as forming mechanism. The Jurassic magmatic age, the spatial association of carbonate-dykes with alkaline UM-mafic rocks and oligoclasite and syenite, together with geochemical features explained above, all suggest that carbonate-dykes from the Ivrea-Verbano Zone may be Jurassic carbonatites genetically associated to alkaline UM-mafic intrusive complexes. Further geochronological and geochemical investigations on other carbonate-dykes and related alkaline rocks as well as trace element composition of the most important minerals such as olivine, clinopyroxene, amphibole and phlogopite will give clues on the validity of this working hypothesis.

CENOZOIC MAGMATIC ACTIVITY OF DISTINCT MAGMATIC AREAS OF SW BULGARIA, FYR OF MACEDONIA AND NORHTERN GREEGE AND ITS RELATION TO THE MINERALISATION

Georgiev S.[1], Peytcheva I.[1,2], von Quadt A.[2], Grozdev V.[1], Marchev P.[1], Serafimovski T.[3]
[1]Geological Institute, Bulgarian Academy of Sciences, Sofia, Bulgaria, kantega@abv.bg
[2]ETH Zürich, Zürich, Switzerland
[3]University of Štip, Macedonia

The Late Alpine magmatism (from Late Cretaceous to present) in the Balkanides and Aegean area is represented by several generally east-west trending magmatic episodes, which partially overlap. It is caused by steepening/retreat and southward migration of the subduction slab during a long-lived north-directed subduction (Jolivet et al., 2013 and references therein), complicated by episodes of slab roll-back, back arc extension, delamination and asthenosphere uplift. The present study is focused on 7 distinct areas, situated in SW Bulgaria, FYR of Macedonia (FYROM, hereafter) and Northern Greece along a transect through the rejuvenating Cenozoic magmatic/metallogenic belt. A key for understanding the magma generation and its metal-fertility are the timescale, geochemical evolution and the geodynamic frame in a more regional context. The aim is to compare the zircon geochronology, geochemistry and geodynamic position of the

individual magmatic centers in the area studied and to constrain plausible time periods and factors that favored ore mineralisation.

Analytical methods

A combination of geochronology, geochemistry and petrology study is applied to rocks from the distinct magmatic areas studied. The obtained data is compared and correlated with the published one and the geodynamic evolution of the region. Major and trace elements of bulk samples are determined on fused pellets using a Philips PW2400 XRF spectrometer (at ETH–Zurich) and LA–ICPMS (at GI–BAS, Sofia). In-situ U-Pb age dating of the zircons is made applying the LA-ICP-MS method (GI–BAS) and precise dating of selected samples by ID–TIMS (TritonPlus) at ETH–Zurich. The whole-rock $^{87}Sr/^{86}Sr$ and $^{143}Nd/^{144}Nd$ ratios are obtained after a chromatographic cleaning procedure and ID–TIMS at ETH–Zurich.
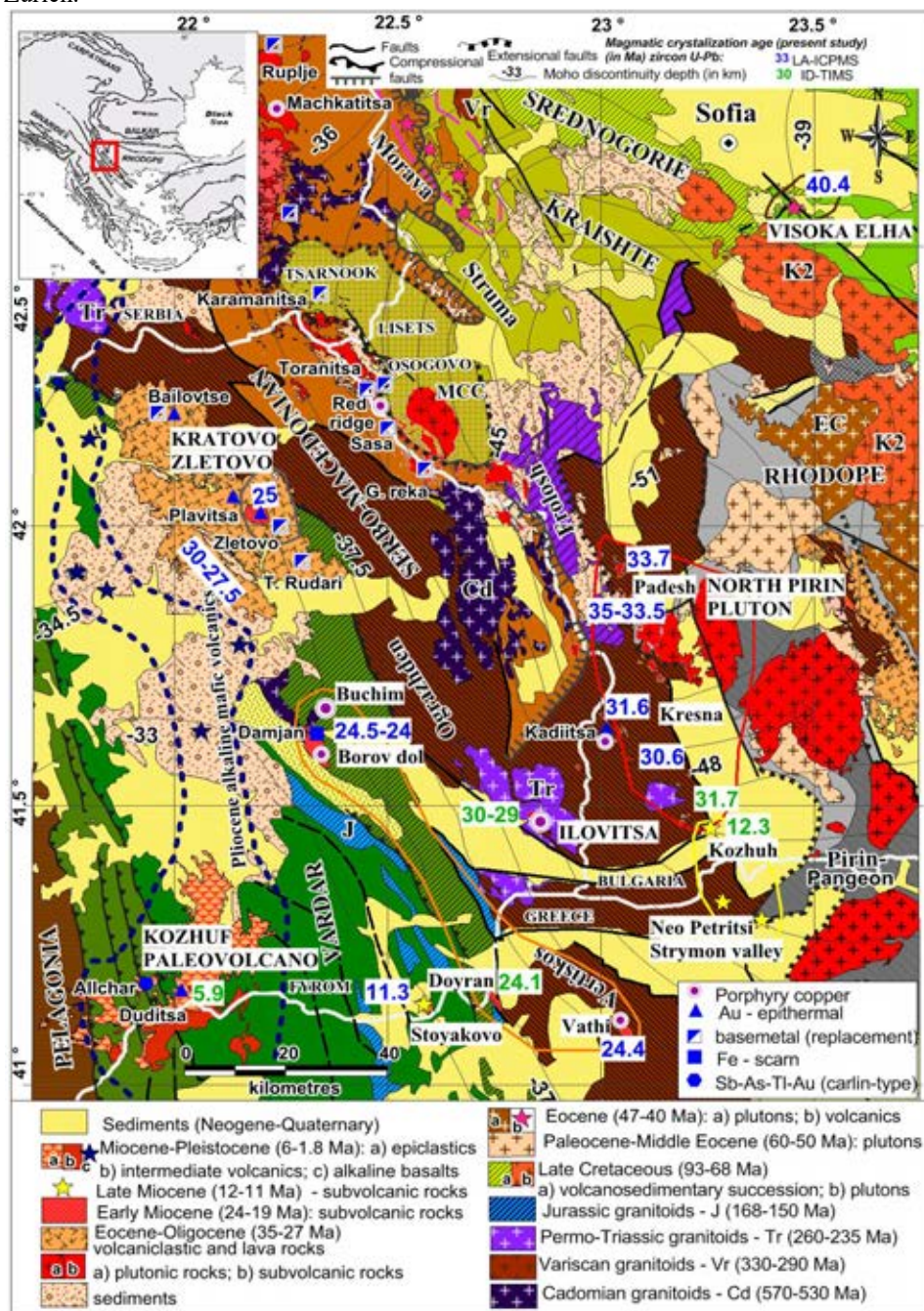
Fig.1. Geological map of the studied area with U-Pb zircon geochronology and ore deposits/occurrences.

Magmatism and mineralisations of the studied areas in the geodynamic frame

The present research is focused on the Cenozoic magmatic-metalogenic activity along a NNE–SSW transect and covers rejuvenating magmatic episodes (40–6 Ma) in 7 distinct areas of SW Bulgaria, FYROM and Northern Greece (Fig. 1). Although it postdates the main Late Cretaceous subduction event, the magmatism preserves subduction-related features as sourced in the subcontinental mantle lithosphere and lower crust that were enriched during the previous subduction. The rocks from the distinct magmatic areas show specific geochemistry and petrological characteristics and can be assigned to several evolving geodynamic episodes:

1. Paleocene to Early – Middle Eocene. The Late Cretaceous subduction-related magmatism (93–68 Ma) is followed by a magmatic gap of ≈ 10–14 Ma, related to compressional regime and crustal thickening. Afterwards the magmatic activity was rejuvenated forming a Late Paleocene to Early – Middle Eocene magmatic belt (56–40 Ma; Marchev et al., 2013 and references therein). It is represented by scattered felsic plutons in the Rhodope Massif, dyke swarms in the Kraishte Zone and asthenosphere alkaline basalts in NE Serbia. The ***Visoka Elha paleovolcano*** is part of that magmatic activity. It is deeply eroded acid volcano with epiclastic aprons − a product of debris flows and alluvial fans. The rocks are intruded in the basement of the Srednogorie Zone. They are medium-K calk-alkaline. The rocks exhibit geochemical adakite-like features with high Sr (550–795 ppm), high Sr/Y (86–100), low Y (6.4–8) and low HREE, negligible negative Eu anomaly (0.85–0.92) and high fractionation of HREE with La/Yb$_{(N)}$ in the range of 71–102. These features imply that most probably the garnet was residue in their source during the partial melting. The $^{87}Sr/^{86}Sr_{(i)}$ ratio of 0.70565–0.70579 and εNd$_{(i)}$ (-2.16/-2.44) show intermediate values between mantle and continental crust. The Concordia U-Pb zircon age of the rhyolite is determined at 40.38±0.48 Ma. Age data for the xenocrystic zircons define two clusters with Campanian (72.4±0.52 Ma) and Maastrichtian (68.16±0.34 Ma) age and are most probably assimilated from a not-outcropping plutonic body. The origin of the magma probably include episode of melting of juvenile (cumulates and underplated magmas formed during the Late Cretaceous subduction) mafic lower crust which is caused by slab steepening/tear followed by initial asthenosphere uplift and delamination. It also includes fractionation and assimilation in middle-upper crustal chamber(s). No mineralization is found.

2. Eocene-Oligocene. The later magmatic activity was followed by 5–7 Ma regional uplift, exhumation of the Late Cretaceous and Paleocene to Early-Mid-Eocene granitoids, migmatisation (at ≈ 38 Ma) and core-complex formation in the Rhodopes, caused by the delamination and asthenosphere uplift (e.g., Burg 2012 and references therein). These processes were accompanied by a major episode of extension, block faulting and formation of E-W to NNW-SSE sedimentary basins. The magmatic activity resumed over the entire Rhodope Massif at 35 to 28 Ma forming a Late Eocene–Early Oligocene magmatic belt. This extensional magmatism is represented by intermediate-felsic to mafic volcanic and plutonic rocks and dykes of shoshonitic to calc-alkaline affinity whose composition correlates with the present-day crustal thickness. The magmatic activity ended at around 28 Ma, with intraplate-plate (WP) alkaline basalts and lamprophyres in the Eastern Rhodopes. Studied areas: North Pirin pluton, Ilovitsa, Kratovo-Zletovo:

The ***North Pirin pluton and related subvolcanic rocks in Padesh, Kresna and Karnalovo area*** are predominantly intermediate to acid in composition, high-K calc-alkaline, metaluminous to peraluminous. They are intruded in the Rhodope and Serbo-Macedonian Massifs. The $^{87}Sr/^{86}Sr_{(i)}$ (0.71010–0.71448) and εNd$_{(i)}$ (-6.47/-8.34) ratios of the magmatic rocks correspond to that of the upper continental crust. A clear tendency of decreasing $^{87}Sr/^{86}Sr_{(i)}$ and encreasing εNd$_{(i)}$ with crustal depth (Moho discontinuity) is found. The U-Pb zircon geochronological data suggest Late Alpine plutonic and volcanic-subvolcanic activity at 35 to 31 Ma. The analyses of the zircon populations and distribution of the xenocrysts and inherited cores point out high crustal input to the parental magma and the xenocrystic ages correspond to the direct basement. Limited Pb-Zn occurrences are observed.

Subvolcanic bodies (stocks), numerous dikes and related ***Ilovitsa*** Cu-Au deposit are formed during the Oligocene in the area of Ilovitsa village, SE FYROM. They are intruded in the Permo-Triassic Ograzhden pluton and metamorphic rocks of the Serbo-Macedonian Massif. The Cenozoic rocks are presented predominantly by granodiorite-porphyries, while in some dykes the groundmass has more volcanic-like appearance and they can be considered as dacites. In the granodiorite-porphyry complex stock, mingling between texturally different but compositionally similar varieties is observed. The rocks are high-K calc-alkaline. The granodiorite-porphyry stock that hosts the Cu-Au mineralisation is formed in two magmatic phases dated by ID–TIMS at 30.31±0.054 Ma and 30.13±0.032 Ma, respectively. The ages of the post-mineralisation dykes are in the interval of 29.6–28.8 Ma. The xenocrystic zircons and inherited cores are poorly presented. The $^{87}Sr/^{86}Sr_{(i)}$ ratio of 0.70791–0.70883 and εNd$_{(i)}$ (-5.25/-7.14) is in accordance to the thinner crust (compared with N Pirin) and is most probably due to mantle derived magma affected by crustal assimilation, fractionation and mixing.

Kratovo – Zletovo is a large volcanic area located at the border of Serbo-Macedonian Massif and Vardar Zone. It is presented by several main volcanic phases with mainly intermediate to dacitic – trachydacitic rocks, rarely more mafic in composition, high K calc-alkaline to shoshonitic. Several paleovolcanoes with lava flows, subvolcanic bodies and domes and associated pyroclastic and epiclastic deposits can be observed. A large elliptical caldera (13x7 km) filled with latite to trachydacite in composition, moderately to densely welded ignimbrites is located in the SW part of the area. At least two outflow ignimbrite sheets, representing large explosive activity cover the whole territory and can be observed in concrete (marking) levels of the succession. The $^{87}Sr/^{86}Sr_{(i)}$ ratio is in the range of 0.705859–0.708647 and εNd$_{(i)}$ (-1.57/-6.7). The volcanic activity, based on the zircon U-Pb geochronology is dated at 32.5 to 27 Ma, nevertheless a few subvolcanic bodies with ages around 25 Ma are observed. The xenocrystic zircons and inherited cores are rare, but antecrysts are common. Au-epithermal, basemetal and porphyry copper mineralisations are related to that magmatic activity.

3. Early Miocene. Since ca. 24–18 Ma, the Aegean region has been the site of pronounced late orogenic crustal extension, which is considered to be a result of the rollback of the Hellenic slab and formation of the Aegean Sea basin (e.g. Jolivet et al., 2013 and references therein). This time coincides with the onset of the formation of the metamorphic core complexes in the Mediterranean region such as Southern Rhodopes, Cyclades and Menderes Massif, followed by magmatic activity compositionally similar to the Eocene-Oligocene in the Rhodopes. Studied area: **Buchim – Borov dol – Doyran – Vathi** magmatic area is presented by several subvolcanic bodies and epiclastics and pyroclastics (in Borov

dol), predominantly with latite-trachydacitic, rarely rhyolitic composition and high-K calc-alkline to shoshonitic seriality. They are intruded in the Vardar Zone and Serbo-Macedonian Massif. Some of the rocks exhibit adakite-like characteristics due to amphibole fractionation. Mingling and mixing is often observed. The $^{87}Sr/^{86}Sr_{(i)}$ ratio is in the range of 0.70634–0.70739 and $\varepsilon Nd_{(i)}$ (-2.30/-3.80). The U-Pb zircon ages are very close 24.5–24.0 Ma with just a few rare xenocrystyc zircons found. The Buchim porphyry copper deposit and the Vathi porphyry copper occurance are related to this magmatic activity. Several epithermal and Fe-scarn (Damjan) mineralisations are also observed and related to the porphyry copper systems.

4. Middle to Early Miocene. During the Middle to Late Miocene the region was a site of variable magmatism. In western Anatolia, this was alkaline to super-alkaline OIB-like magmatism, which spans 12–6.5 Ma. The rocks are spatially associated with major extensional faults that acted as conduits for the transport of uncontaminated alkaline magmas. In the Cyclades, magmatic activity is represented by I-type granites aged at 15–11 Ma, representing a magmatic arc stage. Rare occurrences of mafic rocks (12–10 Ma) are found in Serbia. The formation of those magmatic rocks can be directly linked to the Miocene extensional tectonic regime and formation of the curvature of the Hellenide orogeny. Studied area: Limited occurrences of small and scattered subvolcanic bodies crop out along ***Strimon River valley (Kozhuh and Neo Petritsi) and Doyran region*** (Stoyakovo) in the area between the Rhodopes, Serbo-Macedonian Massif and Vardar Zone. The rocks are fractionated high-K trachyte to trachydacites, which exhibit adakite-like signatures most probably due to amphibole fractionation in a crustal chamber. The relatively high $^{87}Sr/^{86}Sr_i$ ratios (0.70616–0.70648) and negative $\varepsilon Nd_{(i)}$ (-3.29/-3.46) are observed. The rocks are dated by ID–TIMS at 12.24±0.03 Ma (Kozhuh cryptodome) and LA–ICPMS at 11.32±0.10 Ma (subvolcanic body near Stoyakovo village) respectively. Findings of abundant xenocrystic zircons confirm the essential participation of crustal material in the formation of the rocks. Only metasomatic alternations are observed, with no mineralisation found.**5. Late Miocene to Pleistocene.** The last magmatic episode in the region is represented by Late Miocene to Pleistocene extensional magmatism (6–1.8 Ma) in the Vardar zone in FYROM, and in southern Serbia (e.g., Yanev et al., 2008 and references therein). Potassic to ultrapotasic, basic to intermediate, rarely acid volcanic and subvolcanic rocks of this episode are interpreted to originate in the metasomatised lithospheric mantle. Studied rocks are trachytes and represent one of the most widespread phases of **Kozhuf paleovolcano**. They exhibit geochemical adakite-like features with weak Eu (0.79–0.93) anomaly, high La/Yb$_{(N)}$ ratio (28–40), high Sr (1200–1800 ppm) and low Y (12–13.5 ppm) content. One of the most probable mechanisms for generation of strongly fractionated REE patterns and high Sr/Y ratios is fractional crystallization of minerals that preferentially partition Y and HREE during water-suppressed plagioclase fractionation. Hornblendes and clinopyroxenes partition the HREE over LREE (with preferation partitioning of MREE) and their fractionation is referred to formation of the so-called listric-shaped REE pattern and adakite-like signatures. The trachytes are dated by ID–TIMS at 5.988±0.026 Ma. The $^{87}Sr/^{86}Sr_{(i)}$ (0.709048–0.709145) and $\varepsilon Nd_{(i)}$ (-6.77/-6.96) is probably due to melting of a substrate modified by previous metasomatic event. In the Kozhuf area, the Sb-As-Tl-Au Allchar deposit and Au Duditsa mineralisation are well known and are related to this magmatic activity (Boev, Jelenkovic, 2012).

References:

Boev B. and Jelenković R. (2012) Allchar deposit in Republic of Macedonia – petrology and age determination. in: Ali Ismail Al-Jaboury (Eds.). Petrology – New Perspectives and Applications. In Tech. pp 224. chapter 6: 131–168.

Burg, J.-P. Rhodope: (2012) From Mesozoic convergence to Cenozoic extension. Review of petro-structural data in the geochronological frame. J. Virtual Explorer. 39: 1–44

Jolivet L., Faccenna C., Huet B., Labrousse L., Le Pourhiet L., Lacombe O., Lacomte E., Burov E., Denele Y., Brun J., Philippon M., Paul A., Salaun B., Karabulut H., Piromallo C., Monie P., Gueydan F., Okay A., Oberhänsli R., Pourteau A., Augier R., Gadenne L. and Driussi O. (2013) Aegean tectonics: strain localization, slab tearing and trench retreat. Tectonophysics. 597–598: 1–33.

Marchev P., Georgiev St., Raicheva R., Peytcheva I., von Quadt A., Ovcharova M. and Bonev N. (2013) Adakitic magmatism in post-collisional setting: An example from the Early-Middle Eocene Magmatic Belt in Southern Bulgaria and Northern Greece. Lithos. 180-181: 159–180.

Yanev Y., Boev B., Doglioni C., Innocenti F., Manetti P., Pecskay Z., Tonarini S. and D'Orazio M. (2008) Late Miocene to Pleistocene potassic volcanism in the Republic of Macedonia. Contrib. Mineral. Petrol. 94: 45–60.

THE ROLE OF FRACTIONATION AND CONTAMINATION PROCESSES IN THE FORMATION OF COEXISTING QUARTZ AND NEPHELINE SYENITES AT ABU KHRUQ RING COMPLEX, SOUTHEASTERN DESERT, EGYPT

Hegazy H.A.

Assiut University, Assiut, Egypt, hhegazy4451@yahoo.com

Abu Khruq is one of the youngest Egyptian ring complexes, i.e. 89± 2 Ma and is related to the structural lineament trending N30°W parallel to the Red Sea. It crops out over a roughly circular area of approximately 50 km^2 and intruded into the late – Proterozoic gneisses and schists at about 85 km from the Red Sea and 130 km NW of Aswan.

Field investigation revealed that the Abu Khruq ring complex (ARC) present as slightly elliptical epizonal polyphases of alkaline rocks, rising up to 874 m.a.s.l. It composes of early volcanics (mainly trachyte, phonolite and

rhyolite as well as their pyroclastic equivalents) successively intruded by uralitized alkaline essixitic gabbro and both silica over and more common undersaturated nepheline syenites.

The field relationships as well as the petrographic and chemical characteristics of the ARC reflect the cogenetic nature of the entire suite. The chemical data support a model in which a mantel derived alkaline mafic magma was emplaced at a lower crustal block and then extensively fractionated to give an evolved syenitic liquid. The incompatible trace elements (e.g. Nb, Zr, Ce) show enrichment trends with silica increasing, consistent with fractional crystallization. Moreover the low Cr- content in gabbros is consistent with the derivation from an evolved mafic magma.

The large range of major and trace element concentrations and identification of cumulates in some of the studied rocks indicate extensive fractional crystallization in the petrogenesis of coeval silica-saturated and silica-undersaturated alkaline rocks. However isotopic results indicate that quartz syenite bear the signature of substantial amount of crystal contamination. This provides important insight into the processes that occur in subvolcanic complexes in continental settings.

A PRELIMINARY RESULT OF PROSPECTING ON PODIFORM CHROMITITE IN BOPHIVUM AREA, MYANMAR

Heo Chul-Ho

Korea Institute of Geoscience and Mineral Resources, Daejeon, Korea

In order to grasp the geological characteristics, the occurrence mode of ore body and development potential of Bophi Vum chromite mineralized zone in northwestern Myanmar, Korea Institute of Geoscience and Mineral Resources(*KIGAM*) and Department of Geological Survey and Mineral Exploration(*DGSE*) of Myanmar carried out joint exploration targeting on $12km^2$ area. In this area, chromitites occur as a major Cr-ore body, and are enveloped by dunite. As a result of geological survey, the geological map was drawn in the scale of 1:1,000, and both parties discovered that chromitites ores are mainly distributed at the elevation range between 200 and 400m. The area is geologically composed of harzburgite, dunite and serpentinite. To identify the extension of the chromite ore bodies, both parties carried out trench surveys. Chromite ore bodies have 0.3 to 1.5m wide and several meters of extension, and deformed strongly as a sigmoid and a boudin shapes with dunite and harzburgite by ductile deformation. Ductile deformation have a top-to-the-west shear sense, indicating the existence of a westward thrusting. NW-SE trending distribution of ore bodies is related to the dextral ductile shearing and/or to the block rotation as a book-shelf structure by dextral strike-slip movement. Soil geochemical exploration was conducted by collecting soil samples in the interval of 50m after pitting ground surface under 0.7 to 1.0m. Geochemical anomaly maps of Cr, Ni, Fe, and Mn were prepared by PXRF and ICP-AES. For analyzing the distribution of chromite, magnetic survey was carried out on the chromium mineralized belt. As a result, the magnetic susceptibility of chromite is lower than those of dunite and harzburgite, which are background rocks of chromite. Also, the locations of low magnetic anomaly zone and low magnetic susceptibility models of 3D magnetic inversion results are spatially well matched with those of chromite occurrences confirmed by the surface geological and trench survey. Some of low magnetic effects are expanded to the periphery area of chromite occurrences. Considering the magnetic susceptibility characteristics of various rocks in this area, the expanded low magnetic anomaly zones are estimated as the high potential areas bearing chromite.

Generally, chromitites occurred as two types: Type 1, podiform chromite ore; Type 2, massive chromite ore in the periphery of shear zone. Type 1 is covered with dunite bearing silicate vein. The size of each pod ranges from a few mm to cm. Some pods tend to increase the size of pod if they are closer to dunite. Lithological facies change in chromitite from dunite through harzburgite enriched in olivine to harzburgite is well developed in this type. In some place, chromite have the shape to intrude as vein into dunite. Considering the occurrence mode of chromite, type 1 ore is thought to preserve the original texture of chromitite at the lower part of boundary between crust and mantle. Type 2 is mainly near to the shear zone or are distributed in the periphery of shear zone. In type 2 ore, dunite cover is very shallow or is not observed. Alternating texture between chromite and olivine observed in typical podiform chromitite is not shown and most of the ore are composed of massive chromite. Type 2 ore is thought to be formed as the secondary product related to the shear zone after the formation of type 1 ore.

Based on the occurrence mode of chromitite and mantle rock, it is thought that this chromitite formed at the lower part of boundary between crust and mantle. And, it is thought that dunite and chromitite formed as the intrusion of the different kinds of silicate melts into the harzburgite mantle. The presence of highly depleted harzburgite indicate that the mantle exposed in this area may coincide with the subduction related mantle rather than MORB mantle. Based on the rock occurrence mode and mineral assemblage, it is thought that this chromitite have the similar characteristic feature with Type I suggested by Gonzalea-Jimenez et al.(2014).

References:

Chhibber, H.L. (1934) The geology of Burma. MacMillan, London. 320p.

Gonzalez-Jimenez, J.M., Griffin, W.L., Proenza, J.A., Gervilla, F., O`Reilly, S.Y., Akbulut, M., Pearson, N.J., Arai, S. (2014). Chromitites in ophiolites: How, where, when, why? Part II. The crystallization of chromitites, Lithos 189, p. 140-158.

Heo, C.H., Chi, S.J., Kang, I.M. and Kin, K.M. (2014) Occurrence characteristics of Bophi Vum chromite mineralized zone in the northwestern Myanmar. Econ. Environ. Geol., v. 47, p. 351-362

Park, G. and Heo, C.H. (2014) Magnetic data analysis of the chromium mineralized belt in Bophi Vum area, northwestern Myanmar. Geophysics and Geophysical Exploration. V. 17, p. 147-154.

Ryoo, C.R., Heo, C.H. and Zaw Linn Aung. (2015) Geological structure and mineralization in Bophi Vum Cr mineralized zone. Jour. Petrol. Soc. Korea. v. 24, p. 307-321.

Hutchison, C.S. (1975) Ophiolite in Southeast Asia. Geol. Soc. Amer. Bull., V. 86, p. 797-806

Soe Win and Marlar Myo Myint. (1998) Mineral potential of Myanmar. Resource Geology, V. 48, p. 209-218.

Wagner, C. (1983) Chromite exploration at the southern Mwetaung and the Tagaung Taung. ECAMS Interim rept., Rangoon (unpubl.)

Park, J.W. (2016) Some thoughts on the genetic model of Bophivum chromitites in Myanmar(unpubl.). Technical report.

THE ORIGIN OF NELSONITE AND KIRUNA-TYPE APATITE-MAGNETITE DEPOSITS

Hou T.[1], Wang M.[1], Veksler I.V.[2,3]
[1]China University of Geosciences, Beijing, China, t.hou@mineralogie.uni-hannover.de
[2]GFZ Potsdam, Potsdam, Germany, veksler@gfz-potsdam.de
[3]Perm State University, Perm, Russia

The origin of layers and irregular discordant bodies composed of iron oxide minerals (ilmenite, magnetite, or hematite) and apatite in mafic layered intrusions, massif anorthosites and other types of igneous rocks has been controversial. The enigmatic rocks, essentially devoid of silicates and strongly enriched in Fe and P_2O_5, up to the levels suitable for mining, have been traditionally classified to Ti-rich nelsonites and Ti-poor Kiruna-type mineral deposits. The distinction based of the difference in Ti content may be important for mining and economic geology but hardly helpful for understanding the processes, capable of concentrating apatite along with iron oxide minerals and effectively separating them from ubiquitous silicates. Conventional models of crystallization differentiation offer no obvious reason for accumulation of apatite and Fe(Ti) oxide minerals in large quantities in the same place. Therefore, attention of many researches has been drawn to liquid immiscibility and the idea of a separate Fe-P-rich immiscible magma. A broad range of magmatic silicates melts has been known to unmix to Fe-rich and silica-rich liquid phases. Notably, P_2O_5 strongly concentrates in the Fe-rich liquid and even small amounts of the phosphate component significantly broaden the miscibility gap. However, the magmatic Fe-rich immiscible liquids, which have been well documented in numerous experiments and natural lavas so far, contain around 40 wt.% SiO_2 and just a few weight percent P_2O_5. Silicates are still predominant minerals in crystallization products of such liquids and the formation of essentially silicate-free nelsonite and Kiruna-type rock would have required some additional mechanism of apatite and iron oxide enrichment. A single early experimental demonstration of apatite and magnetite immiscible liquids (Philpotts, 1967) has not been supported by later experimental studies. Crystallization temperatures of those liquids have been shown to be forbiddingly high (Wang et al., 2016).

Our recent experiments revealed a new type of immiscible magmatic liquid containing only a few weight percent of silica and dominated by iron phosphate. We have found that the presence of dissolved H_2O component is crucial for the formation of such liquid. The products of our experiments (Fig. 1) also showed that the iron phosphate immiscible melt acts as a "glue" preferentially wetting and binding together apatite and magnetite crystals. Such wetting properties should enhance spatial separation of apatite and Fe-Ti oxide minerals from silicates and formation of large nelsonite and Kiruna-type deposits in natural magmatic systems.

The experiments were performed at 0.1 GPa in large volume internally heated pressure vessels (IHPV) at the Leibniz University of Hannover (Germany). Argon was used as the pressure medium. Some of the experiments were performed under controlled reduced oxygen fugacity conditions by adding H_2 to the Ar pressure medium.
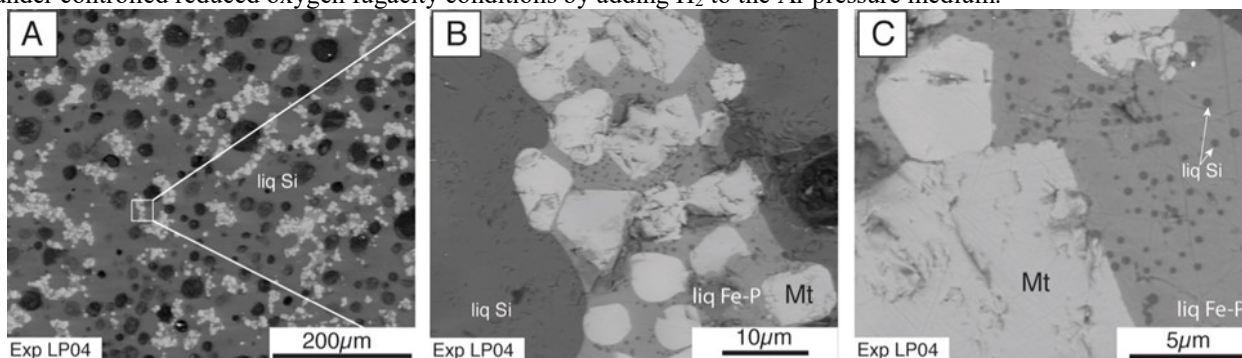

Fig. 1. Back-scattered electron (BSE) images of run products showing immiscibility texture in sample LP04. (A) Run products containing magnetite crystals and Fe phosphate liquids (liq Fe-P) separated from the rhyolitic liquids (liq Si). (B) Magnetite crystals are predominantly wetted by the Fe phosphate liquid. (C) The Fe phosphate liquids exsolved nano-scale rhyolitic globules.

The immiscible Fe phosphate melt in our experimental products (Fig. 1) contains 32.6-33.4 wt.% FeOt, 39-39.4 wt.% P_2O_5, and minor amounts of other components: 3.1-4.5 SiO_2, 1.0-1.5 TiO_2, 2.2-3.9 Al_2O_3, 4.9-5.2 MgO and 5.13-5.7 CaO (all in weight percent). The conjugate Si-rich liquid contains (in weight percent) 71-74 $SiO2$, 9.2-9.7 Al_2O_3, 2.5-3.2 FeOt and 4.2-4.8 K_2O. Solid phases comprise magnetite, fayalite and, in some cases, apatite.

Our experimental results support previously published observations in the K_2O-FeO-Fe_2O_3-Al_2O_3-SiO_2 ($\pm H_2O$) model system (Lester et al., 2013) that the addition of H_2O to reactant mixtures broadens the miscibility gap and makes the compositions of immiscible Fe-rich and silica-rich immiscible liquids more contrasting. However, our study is the first to examine the effects of $H2O$ on multicomponents compositions relevant to natural magmas and the first demonstration of the Fe phosphate immiscible melt.

Independent evidence for the important role of H_2O and liquid immiscibility in the formation of nelsonite bodies has been provided by studies of crystallized inclusion in apatite from the Upper Zone of the Bushveld Complex in South Africa (Fischer et al., 2016) and Damiao anorthosite massif in China (Wang et al., 2017). Hydrated silicates are abundant in daughter mineral assemblages of the inclusions (Fig. 2) and the FeO(t) in the inclusions tends to be very high, at about 30-35 wt. %.
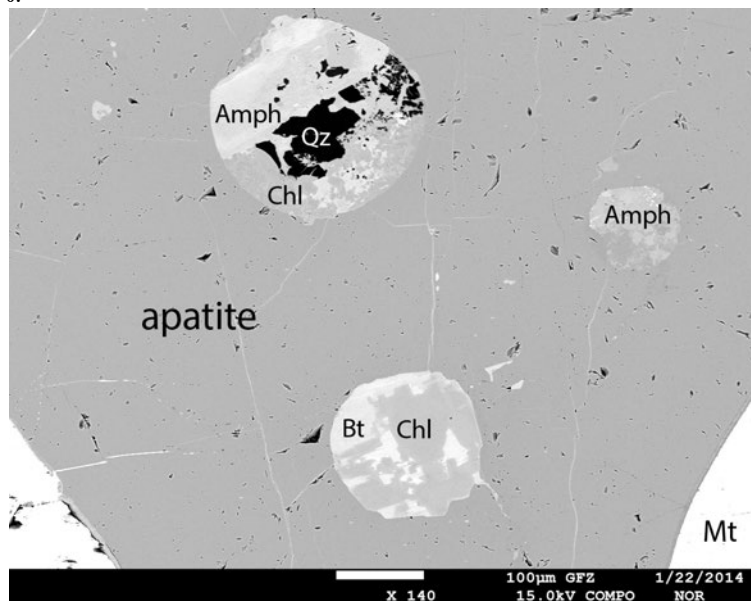
Fig. 2. BSE images of apatite-hosted inclusions from a nelsonite layer in the Upper Zone of the Bushveld Complex, South Africa. Abbreviations for phases: Amph – amphibole; Bt – biotite; Chl – chlorite; Mt – magnetite; Qz – quartz.

References:

Fischer LA, Wang M., Charlier B., Namur O., Roberts RJ., Veksler IV, Cawthorn RG, Holtz F (2016) Immiscible iron-and silica-rich liquids in the Upper Zone of the Bushveld Complex. EPSL, 443: 108-117.

Lester GW, Clark, A.H., Kyser, T.K., & Naslund, H.R. (2013) Experiments on liquid immiscibility in silicate melts with H2O, P, S, F and Cl: implications for natural magmas. Contrib. Mineral. Petrol, 166:, 329-349.

Philpotts AR (1967) Origin of certain iron–titanium oxide and apatite rocks. Econ. Geol., 62: 303–315.

Wang M, Veksler I, Zhang Z, Hou T, Keiding JK (2017) The origin of nelsonite constrained by melting experiment and melt inclusions in apatite: The Damiao anorthosite complex, North China Craton. Gondwana Res., 42: 163-176.

IMPORTANCE OF VARIOUS AL SUBSTITUTION MECHANISM INTO BRIDGMANITE UNDER HIGH PRESSURE

Inoue T.[1,2], Kakizawa S.[2], Noda M.[2], Takakuwa Y.[2]
[1]Hiroshima University, Higashihiroshima, Japan, toinoue@hiroshima-u.ac.jp
[2]Ehime University, Matsuyama, Japan

Bridgmanite (Mg-silicate perovskite) is the most abundant mineral in the lower mantle. The bridgmanite occupies about 70% in the lower mantle (Irifune, 1994), if we assume pyrolite mantle. Al_2O_3 is an important compornet after SiO_2, MgO and FeO. When we consider the pyrolite mantle, the Al_2O_3 content is ~4.3 wt% (Sun, 1982). Because the Al is mainly incorporated into bridgmanite in the lower mantle, the investigation of the Al substitutution mechanism into bridgmanite is very important.

The phase diagram in the system $MgSiO_3$-Al_2O_3 has been investigated so far based on high pressure experiments (Irifune et al., 1996; Kubo and Akaogi, 2000). In the phase diagram, the Al substituion is considered to be Tschermak substitution ($Mg^{2+} + Si^{4+} = 2Al^{3+}$). However the compositions of the synthesized bridgmanites show the deviation from the ideal join of $MgSiO_3$-Al_2O_3. Some researchers insist that oxygen-vacancy substitution ($Si^{4+} = Al^{3+} + 1/2Vo$, here Vo shows oxygen vacancy.) exist for the Al substitutution into bridgmanite (e.g. Kojitani et al. 2007). In addituion, we recently recognized that Al-bearing bridgmanite can contain significant amount of water up to ~0.8 wt% because of the Al-H

coupling substitution ($Si^{4+} = Al^{3+} + H^+$) (Inoue, 2016). Thus, the Al substitution mechanism into bridgmanite is very complicated.

To clarify the preferred Al substitution mechanism into bridgmanite, we conducted the series of high pressure experiments. The targets to be clarified are as follows: 1) Are there any compositional dependence for the preferred substitutions as a function of Al? That is, which substitution is preferred in low Al or high Al content? 2) If hydrogen exists in the lower mantle, hydrous bridgmanite is preferred to be formed? 3) If there are no hydrogen in lower mantle, which substitution is preferred, Tschermak substitution or oxygen-vacancy substitution? 4) Are there any compositional dependence to be preferred Al substitution in the terms of MgO excess or SiO_2 excess condition? 5) What is the reason for the deviation from the ideal join of $MgSiO_3$-Al_2O_3 in the previous works? 6) What kind of Al-bearing bridgmanite should be existed in the lower mantle?

To investigate the above issues, we have conducted high pressure and high temprature experiments at ~28 GPa and ~1600°C using Kawai-type multi-anvil high pressure apapratus (Orange 3000) in GRC, Ehime University. Special care has been done for the sample preparation and capsulation. Especially, to achieve the extremly anhydrous condition in our experiment, the glass rods were used as the starting materials to eliminate the absorbed water on the sample surface. The characterization of the recovered sample was done using SEM-EDS and XRD. Those results will be presented.

References:

Inoue, T. (2016) Hydrous bridgmanite: Water storage capacity in the lower mantle. presented in International Symposium "Advances in High-pressure Research – III: Towards Geodynamic Implications-2016" Novosibirsk, Russia, August 29-30, 2016.

Irifune, T. (1994). Absence of an aluminous phase in the upper part of the Earth's lower mantle. *Nature* 370: 131 - 133.

Irifune, T., Koizumi, T., & Ando, J. I. (1996). An experimental study of the garnet-perovskite transformation in the system $MgSiO_3$- $Mg_3Al_2Si_3O_{12}$. *Physics of the Earth and Planetary Interiors*, 96(2-3): 147-157.

Kojitani, H., Katsura, T., & Akaogi, M. (2007). Aluminum substitution mechanisms in perovskite-type $MgSiO_3$: an investigation by Rietveld analysis. *Physics and Chemistry of Minerals*, 34(4): 257-267.

Kubo, A., & Akaogi, M. (2000). Post-garnet transitions in the system $Mg_4Si_4O_{12}$- $Mg_3Al_2Si_3O_{12}$ up to 28 GPa: phase relations of garnet, ilmenite and perovskite. *Physics of the Earth and Planetary Interiors*, 121(1): 85-102.

Sun, S. S. (1982). Chemical composition and origin of the Earth's primitive mantle. *Geochimica et Cosmochimica Acta*, 46(2): 179-192.

THE RESULTS OF MELT INCLUSION STUDY IN MINERALS OF LEUCITE MELANEPHELINITES OF PLEISTOCENE VOLCANOES (UDOKAN VOLCANIC FIELD)

Isakova A.T.[1], Sekisova V.S.[1,2]

[1]Institute of Geology and Mineralogy, Siberian Branch of the Russian Academy of Sciences, Novosibirsk, Russia, atnikolaeva@igm.nsc.ru

[2]Novosibirsk State University, Novosibirsk, Russia, sekisova@igm.nsc.ru

The Udokan volcanic field is located in the south of Eastern Siberia in the central part of Udokan Ridge and closes a chain of volcanic occurrences of the Baikal Rift System from the north-east side (Stupak, 1983, 1987). The volcanism of the Udokan Ridge occurred in three phases – Miocene-Early Pliocene, Pliocene-Early Quaternary, and Pleistocene-Holocene (Stupak, 1987). The volcanic activity of the first two phases lasted about 17 million years was predominantly represented by fissure eruption, which formed a thick series of sodic lava. The volcanic sequences of these two phases have homodromic character: from hawaite to trachyte and from basanite to trachyte. The end of the second phase was related with the activities of the central volcanoes Turuktak and Inarichi, composed of predominantly mugearite and trachyte. The shortest Pleistocene-Holocene phase (duration is less than 1 million years) was characterized only by eruptions of central type. Most volcanic centers are small in size and confined to three main volcanic lines of Udokan volcanic field: Syni-Vakatskaya, Sakukan-Ingamakitskaya, and Khangura-Issakachinskaya lines. The Syni-Vakatskaya line is located in the axial region of Udokan Ridge and matches the strike line of the Baikal rift structure, whereas the Sakukan-Ingamakitskaya and the Khangura-Issakachinskaya lines are oriented in the northwestern direction transversally to the Syni-Vakatskaya line and enclose the volcanic field from North-East and South-West, respectively (Fig. 1 A). The most studied volcanoes are Ingamakit and Munduzhyak volcanoes of Pleistocene age, located on the extreme northwestern part of Sakukan-Ingamakitskaya line (Fig. 1 B, C, respectively). They are small volcanoes of the central type, their early lavas contain leucite. For this reason, the study of these rocks is of great interest to petrologists. The studied rocks consist of small (100-200 μm) phenocrysts of olivine and clinopyroxene and groundmass composed of clinopyroxene, nepheline, leucite, potassium feldspar, magnetite, ilmenite, rare biotite laths, apatite and analcime grains. Olivine phenocrysts are common in the rock and have prismatic shape. Their composition varies from Fo 91 to Fo 72 and contains 0.13-0.39 wt.% NiO. Clinopyroxene phenocrysts are rare in the rock, have zonal composition varying from diopside to augite and titaniferous fassaite, whereas clinopyroxene grains in groundmass are homogeneous augite and titaniferous fassaite. Moreover TiO_2 content varies from 0.3 to 4.9 wt.%, Al_2O_3 – from 0.7 to 8.2 wt.%, Cr_2O_3 content is up to 0.8 wt.%, MnO – up to 0.25 wt.%, and Na_2O – up to 1.8 wt.%/ The 100Mg/(Mg+Fe) ratio varies from 84 to 62, decreasing from the center to the rim of phenocrysts and to the grains of groundmass.
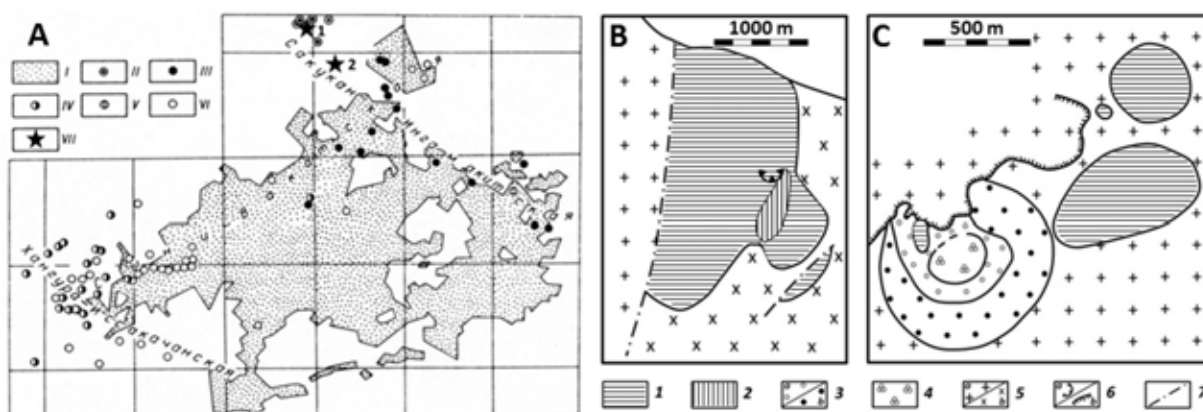
Fig. 1. The scheme of location of Pleistocene volcanoes and extrusions (A) and schematic geological structure of Ingamakit (B) and Munduzhyak (C) volcanoes (after F. M. Stupak, 1983, 1987): A: I – Pre-Pleistocene volcanics; II-VI – Pleistocene volcanics (II – melaleucitite, melanephelinite, III – basanite, IV – hawaite, V – mugearite, VI – unknown in composition); VII – Ingamakit volcano (1) and Munduzhyak volcano (2). B, C: 1 – early-stage lava; 2 – late-stage lava; 3 – pyroclastic material (a – early-stage explosion, b – late-stage explosion); 4 – agglutinate; 5 – basement rock (a – granite; b – granodiorite); 6: a – fragments of lava levee, b – cliff margins, 7 – fractures.

This work is devoted to melt and fluid inclusion study of melanephelinites of Ingamakit and Munduzhyak volcanoes. Previous similar investigation of these rocks conducted by Litasov (1992) includes first data on temperatures of clinopyroxene crystallization (1100-1200 °C), composition of residual glasses in melt inclusions hosted in olivine and clinopyroxene. He suggested that evolution of alkali basaltic magma of Udokan volcanic field occurred with consistent increasing of Si, Al and alkaline contents and decreasing of Mg, Ca, Fe contents. Nevertheless issues such as the chemical composition of daughter phases of melt inclusions and initial melts, as well as volatile content have not been sufficiently studied. This work gives some answer to these issues. In addition, Polyakov with coauthors (1985) received the first data about PT-parameters of formation of alkaline olivine basalts of early phases of Udokan volcanism: P = 3.6-4.5 kbar, T = 1330-1200 °C for olivine and 1290-1190 °C for clinopyroxene.
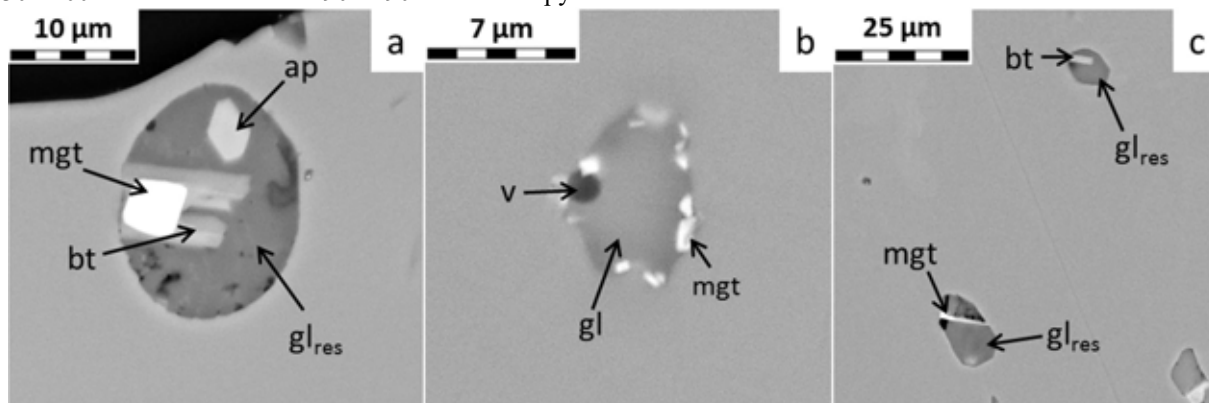
Fig. 2. BSE-image of primary melt inclusions hosted in olivine (a – inclusion before heating experiment, b – inclusion after heating experiment) and clinopyroxene (c – inclusions before heating experiment): ap – apatite, bt – biotite, mgt – magnetite, gl- glass, gl_{res} – residual glass, v – gas bubble.

Melt and fluid inclusions were found in olivine and clinopyroxene phenocrysts. Olivine contains sporadically located primary melt inclusions (Fig. 2 a) with less than 20 µm size. Melt inclusions are completely or partially crystallized, sometimes they contain insignificant amount of residual glass. The daughter phases are represented by clinopyroxene, biotite, nepheline, leucite, apatite, and magnetite (Table 1, ans. 1-9). The fluid phase is predominantly represented by liquid CO_2 and gas CO_2 at room temperature according to optical microscopy and Raman spectroscopy methods. The heating and homogenization experiments were conducted up to 1250 °C microscope heating stage TK-1500 with constant flow of an inert gas as inclusion decrepitated on further heating without reaching homogenization. At this temperature all daughter phases melted except clinopyroxene. After the quenching of inclusions in olivine the tiny crystals of magnetite were precipitated on the periphery of the vacuole and concentrated Fe and Mg (Fig. 2 b). The latter caused the depletion of these elements in the glass of heated inclusion. Clinopyroxene phenocrysts contain a lot of coexisting partially crystallized melt inclusions and carbon-dioxide fluid inclusions. The melt inclusions are often unlaced, irregular "wormy" form, rarely isometric with less than 10 µm sizes. They contain daughter phases of biotite, nepheline, leucite (Table 1, ans. 13-15), magnetite crystallite (Table 1, an. 16), residual glass and fluid phase, represented by CO_2. The homogenization temperature of these inclusions is higher than 1200 °C, which consistent with data of previous investigations (Litasov, 1992, Polyakov, 1985).

The chemical composition of daughter clinopyroxene corresponds to the composition of clinopyroxene grains of groundmass (Table 1, ans. 1, 2). Biotite from olivine-hosted melt inclusions (Table 1, ans. 3, 4) contains more MgO content, less FeO, Al_2O_3, and BaO contents in comparison with biotite from clinopyroxene-hosted melt inclusions (Table 1, an. 13). The compositions of nepheline from melt inclusions in olivine and clinopyroxene also differ (Table 1, an. 5 and 14, respectively); more specifically nepheline in olivine contains less SiO_2, CaO, and Na_2O contents and more FeO and K_2O contents than in clinopyroxene. Leucite is characterized by the same composition in olivine- and clinopyroxene-hosted melt inclusions (Table 1, ans. 6 and 15, respectively). The composition of magnetite in olivine-hosted melt inclusions varies from titanomagnetite to magnetite (Table 1, ans.7, 8), and clinopyroxene includes only magnetite (Table 1, an. 16). The daughter apatite in olivine-hosted melt inclusions contains (wt.%) 2.87 SrO, 0.30 SO_3, 0.25 Cl and 2.99 F (Table 1, an. 9). It should be noted that the association of daughter phases in olivine- and clinopyroxene-hosted melt inclusions corresponds to groundmass mineral association. It probably evidences that crystallization of olivine and clinopyroxene phenocrysts in initial melt began in a closed system and had continued until the moment when rapid ejection to the surface occurred. It leads to the instantaneous crystallization of groundmass minerals and to the loss of the volatiles.

Table 1. Representative chemical composition of daughter and crystal phases and residual glass of melt inclusions hosted in olivine (1-12) and clinopyroxene (13-17).

Oxide	Cpx		Bt		Ne	Lc	Mgt		Ap	Gl res from Ol			Bt	Ne	Lc	Mgt	Gl res from Cpx
	1	2	3	4*	5	6	7*	8*	9*	10	11	12	13*	14	15	16*	17
SiO_2	47.66	38.79	36.35	36.82	44.28	55.13	0.58	0.32		55.00	59.26	60.74	36.63	46.85	55.22	0.90	51.13-61.28
TiO_2	3.70	6.12	11.76	7.61	0.22	0.47	12.31	4.24		bld	0.82	0.48	10.23	bld	0.22	3.47	0.20-0.92
Al_2O_3	5.42	11.07	13.20	14.85	31.33	22.37	1.95	0.36		24.24	12.11	18.78	15.46	31.18	22.50	4.70	19.56-22.71
Cr_2O_3	0.25	bld	0.35	bld			0.91	1.15					bld			bld	
FeO_t	6.20	9.71	9.99	9.84	1.62	0.95	76.19	83.93	0.76	1.62	4.45	0.94	12.59	0.85	0.78	80.50	0.71-2.66
MnO	bld	bld	bld	bld			0.49	0.45		bld	bld	bld				0.65	bld
MgO	13.37	9.58	14.13	12.49			2.44	2.01	0.33	1.29	1.63	bld	9.29		0.30	1.41	0.83-2.62
CaO	22.18	22.30	0.39	bld	0.99	0.14	0.11	0.25	50.81	0.50	bld	bld	0.49	1.30	0.88	0.56	0.39-5.88
Na_2O	1.11	0.63	bld	2.48	14.23	0.61				13.49	8.05	4.50	1.02	16.00	0.44		5.04-11.53
K_2O			8.78	6.94	8.00	19.33				2.64	8.55	10.19	6.37	3.48	18.79	0.35	4.58-9.89
P_2O_5		0.55							38.86	bld	bld	0.27					<0.53
Cl									0.25	0.18	0.37	0.49					0.17-0.60
Total	99.89	98.75	94.95	96.89	100.6	99.00	95.38	93.18	97.17	98.97	96.56	96.40	99.90	99.66	99.13	93.49	94.59-100.9

Note: Ol – olivine, Cpx – clinopyroxene, Bt – biotite, Ne – nepheline, Lc – leucite, Mgt – magnetite, Ap – apatite, Gl_{res} – residual glass in inclusion, bld – below limit detection. Asterisk (*) denotes analyses including (wt.%): 4 an. – 4.88 BaO, 0.98 F; 7 an. – 0.40 V_2O_3; 8 an. – 0.47 V_2O_3; 9 an. – 2.87 SrO, 0.30 SO_3, 2.99 F; 13 an. – 7.82 BaO; 16 an. – 0.77 ZnO, 0.18 V_2O_3.

The chemical compositions of the residual glasses of the melt inclusions in olivine and clinopyroxene irregularly vary from tephriphonolite to phonolite depending on degree of crystallization of inclusion (Table 1, ans. 10-12 and 17, respectively) and are consistent with previous data of Litasov (1992) on the chemical composition of residual glasses.

Table 2. Representative chemical composition of melanephelinite lava (1-3) and glass of heated melt inclusions hosted in olivine (4-13) and clinopyroxene (14, 15).

Oxide	1	2	3	4(3)	5(3)	6	7	8	9	10	11	12(2)	13(2)	14	15
SiO_2	40.39	40.63	40.03	44.81	47.42	49.74	43.90	45.10	49.78	49.50	45.70	47.09	47.26	50.47	48.82
TiO_2	3.07	3.01	2.75	4.99	2.47	2.32	3.07	3.00	2.34	1.93	2.60	3.16	2.42	2.69	1.58
Al_2O_3	11.12	11.16	11.33	16.50	15.17	15.00	16.23	16.12	14.34	17.12	18.99	17.86	18.54	18.93	17.99
Cr_2O_3	0.06	0.05	0.06	bld	bld	bld	bld	bld	bld	0.09	bld	bld	bld	bld	bld
FeO_t	13.53	13.41	14.31	5.54	6.33	6.97	5.38	5.42	6.30	6.97	4.43	4.51	5.17	4.54	6.18
MnO	0.17	0.17	0.18	0.04	0.12	0.13	bld	0.12	0.19	bld	bld	0.05	0.05	bld	bld
MgO	12.19	12.54	13.14	3.25	2.90	3.48	3.86	3.30	5.59	3.22	2.62	3.98	3.97	1.89	2.52
CaO	10.82	10.66	10.45	7.30	7.58	8.28	8.13	9.84	8.16	6.86	5.65	4.89	3.97	2.41	5.08
Na_2O	3.58	3.25	3.20	5.29	4.77	5.84	5.66	4.89	4.88	7.13	6.56	5.92	5.82	4.43	5.49
K_2O	2.57	2.75	2.37	5.42	4.72	4.46	5.63	4.72	3.85	4.05	6.83	5.29	6.05	7.12	6.89
BaO	0.10	0.10	0.11	0.36	0.07	bld	bld	bld	0.23	0.28	0.54	bld	0.18	1.45	bld
P_2O_5	0.94	0.99	0.73	1.21	1.26	1.40	2.57	1.60	1.54	0.96	1.40	0.28	0.45	0.73	0.48
S	bld	bld	bld	0.13	0.17	0.36	0.67	0.22	0.77	0.05	0.20	0.52	0.11	0.13	0.09
Cl	-	-	-	0.15	0.14	0.15	0.14	0.15	0.13	0.14	0.18	0.12	0.14	0.19	0.16
Total	98.52	98.72	98.66	95.00	93.14	98.13	95.24	94.48	98.10	98.30	95.70	93.65	94.10	94.98	95.28

Note: bld – below limit detection. The number of analyses is given in brackets.

As content of inclusions is not completely homogenized over risk of decrepitation during heating experiment and daughter clinopyroxene does not melt, the composition of quenched melt in inclusions (Table 2, ans. 4-15) corresponds not to the composition of the initial melt, but to the composition of the evolved (fractionated) melt. This melt has varying alkaline ultramafic-mafic composition from foidite to phonotephrite, contains less FeO, MgO, CaO contents and more SiO_2, Al_2O_3, alkalis in comparison with the composition of studied melanephelinites (Table 2, ans. 1-3). Moreover the composition of olivine-hosted melt (Table 2, ans. 4-13) is generally similar to that of clinopyroxene-hosted melt (Table 2, ans. 14, 15) corresponding to foidite-tephriphonolite with small differences: olivine-hosted glasses are enriched in Mg, Ca, and Na and depleted in Si, Al, and K. According to the phase composition of inclusions and the chemical composition of the glasses of inclusions the initial melt are enriched in such fluid components as CO_2, fluorine, phosphorus (up to 0.3-2.6 wt% P_2O_5), sulfur (0.05-0.8 wt.%), and chlorine (0.1-0.2 wt.%).

Conclusion: Obtained data are consistent with the results of the previous studies (Litasov, 1992; Polyakov, 1985). Thus, the crystallization of melanephelinite lava began with the olivine phenocryst formation at sufficiently high temperatures (more than 1250 °C) most likely from an alkali ultramafic melt enriched in fluid components (CO_2, P, S, Cl, F). Further crystallization of clinopyroxene phenocrysts (T_{cryst} more than 1200 °C) occurred from the foidite-tephriphonolite melt, which was depleted in FeO, MgO, and CaO and enriched in SiO_2, Al_2O_3, and alkalis during crystallization. Such-like evolution trend is typical for majority of alkaline basaltic systems.

References:

Litasov YuD (1992) Alkali basaltic volcanoes Ingamakit and Munduzhyak (Udokan Plateau, Northern Trans-Baikal): peculiarities of evolution. In: Simonov VA, Kolobkov VYu (eds) Thermobarogeochemistry of mineral formation processes. Issue 2. Problems of magmatism and metamorphism: scientific proceedings. UIGGM, Novosibirsk, pp. 16-29.

Polyakov AI, Turkov VA, Muravyeva NS, Nesmeyanova LI, Ignatenko KI (1985) Physico-chemical conditions of processes of generation and evolution of basalt magmas of the Baykal rift zone. Geochemistry International. 1: 41-57.

Stupak FM (1983) Alkalibasaltic volcanoes in the lower course of the Lurbun River (Udokan ridge, Northern Trans-Baikalia). Geology and geophysics. 8: 79-87.

Stupak FM (1987) Cenozoic volcanism of the Udokan ridge. Nauka. Novosibirsk.

MORPHOLOGY AND COMPOSITION OF ORE-FORMING CHROMIAN SPINELS OF THE LEVOPAYERSKOE–I ORE BODY (POLAR URALS, RUSSIA)

Kadebskaya L.[1], Plechov P.[2], Rudnev A.[3]
[1]Lomonosov Moscow State University, Moscow, Russia, **lyubov.georg@gmail.com**;
[2] Mineralogical Museum of the Russian Academy of Sciences, Moscow, Russia, **pplechov@gmail.com**;
[3]All-Russian Scientific-Research Institute of Mineral Resources named after N. M. Fedorovsky, Moscow, Russia, rud-met@mail.ru.

The Levopayerskoe-I ore body is one of ore occurrences of the Levopayerskoe ore field among dunite-harzburgite rocks of the Voikar hyperbasite massif of the east slope of the Polar Urals (Russia). Levopayerskoe-I ore occurrence (Lat. 66.640 °N, Long. 64.388 ° E) and surrounding rocks were sampled in 2016, Aug. Cr-spinel morphology and composition was a purpose of the study. Analyses were produced with Jeol 773 microprobe (Fersman Mineralogical Museum, Russian Academy of Sciences, Moscow, Russia).
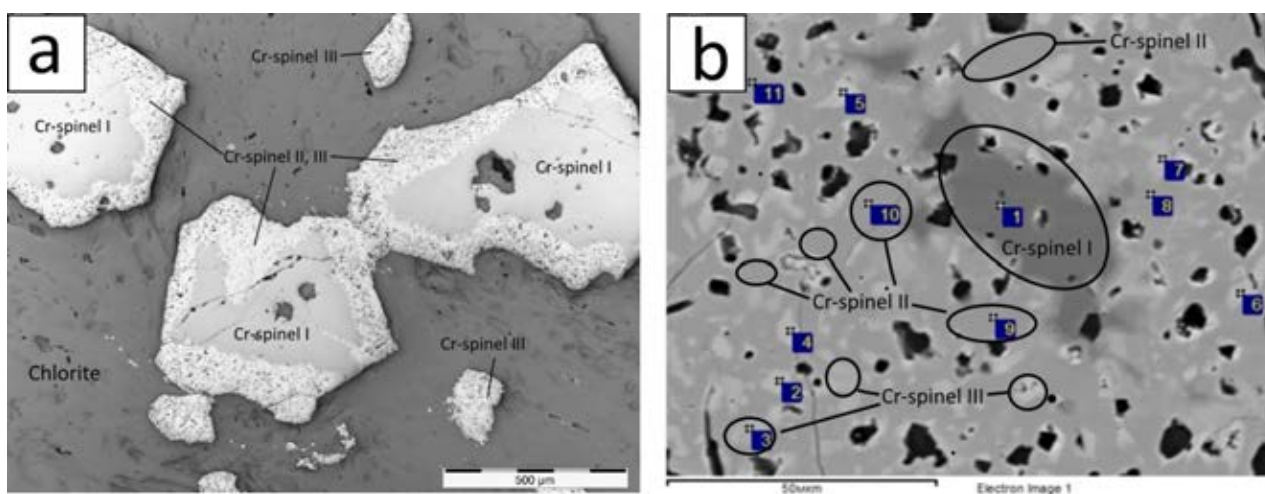
Fig 1. Microphotos of Cr-spinels from ore body: a) grains of Cr-spinel in the chlorite matrix; b) "spongy" edging in outermost zones of Cr-spinel

Ore body chromitites are composed of grains of chromian spinel (the average size 2 - 3 mm) which placed in the chlorite matrix (fig. 1a). Cr-Spinel is rimmed by reactionary "spongy" edging which is presented by two different spinelids

intimately intermixed to each other and with chlorite (fig. 1b). Relics of early Cr-spinels can remain in this "spongy" edging.

The earliest generation of Cr-spinel (Cr-spinel I in fig. 1) is well preserved in central parts of grains. Microprobe analyses of this Cr-spinel show the lowest Cr# ($Cr/(Cr+Al+Fe^{3+})$ = 0.45 - 0.47 among all analyzed spinels. The Cr-spinel of this generation contains up to 30 wt.% Al_2O_3.

The second morphology variety (Cr-spinel II in fig. 1) forms the "spongy" edging in intergrowth with Cr-spinel III and chlorite. Some innermost parts of "spongy" zone are composed by pure Cr-spinel II. This generation contains up to 60% of Cr_2O_3, that's much bigger than in Cr-spinel-I. Another generation of a Cr-spinel (Cr-spinel III in fig. 1) forms small bright spots (in a reflected light) in the "spongy" edging, as well as small grains in the chlorite matrix. This generation is much more ferrous ($FeO + Fe_2O_3$) and has Cr# = 0.47-0.51 (Fig.2).

Cr-Spinel of the surrounding harzburgites contains up to 40 wt. % Al_2O_3 and has Cr# = 0.32 - 0.35. Three generations of a Cr-spinel from an ore body in comparison with compositions of a chromian spinel from the surrounding harzburgite shown in Fig.2.
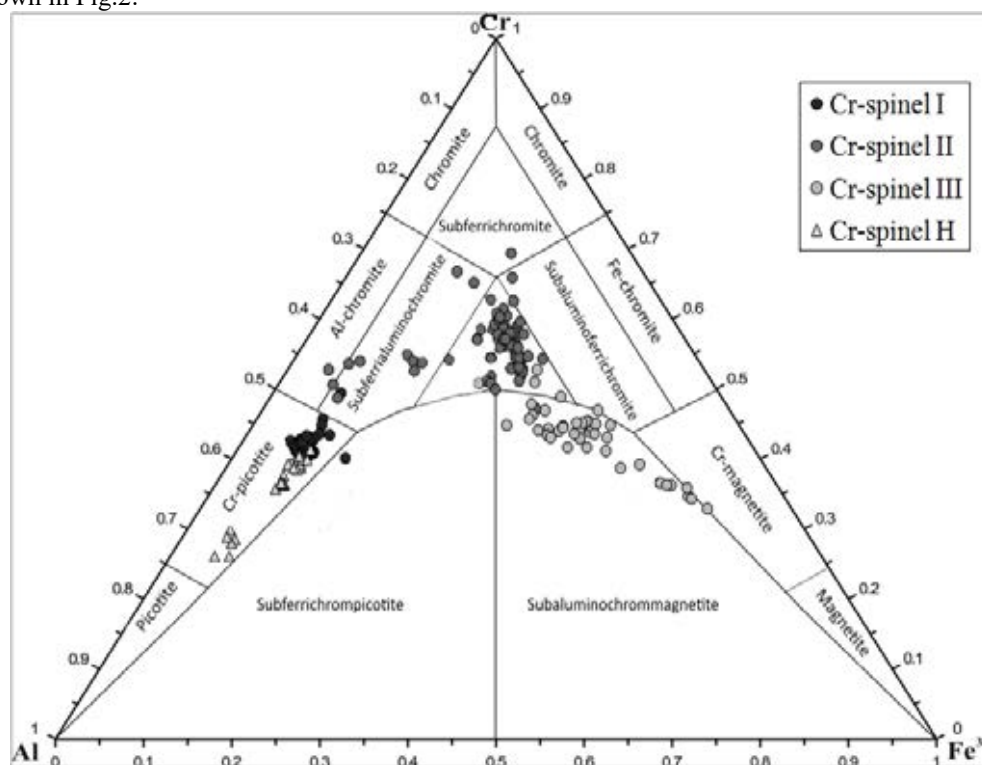
Fig 2. Compositions of three Cr-spinel generations from the Levopayerskoe-I ore body in comparison with Cr-spinel compositions from the host harzburgite depending on a ratio in their composition of trivalent cations (Al, Fe, Cr).

The primary Cr-spinel from podiform ore bodies is often close in compositions with Cr-spinel from a host harzburgite (Arai, 2016). The same relations are observed in our case also. Changes in the composition of Cr-spinel due to superimposed processes manifested in decreasing MgO and Al_2O_3 and in increasing both $FeO + Fe_2O_3$ and #Cr. The similar picture is observed in changing composition of Cr-spinel from stratiform chromitites of the stratified Kampo Formozo's intrusion (Garuti et al., 2007).

Cr-spinels from Levopayerskoe-I ore body were formed in several stages that are reflected in its morphology and chemical composition. The earliest generation of chromian spinel from ore body has the same composition with Cr-spinel from surround harzburgite. Variations of a structure are caused by the superimposed processes of a recrystallization with a presence of a chrome-bearing chlorite.

References

Arai S., Miura M. (2016) Formation and modification of chromitites in the mantle. Lithos: 277-295.

Garuti G., Proenza J. A., Zaccarini F.(2007) Distribution and mineralogy of platinum-group elements in altered chromitites of the Campo Formoso layered intrusion (Bahia State, Brazil): control by magmatic and hydrothermal processes. Mineralogy and Petrology 89: 159-188.

PRESSURE-INDUCED REACTIONS IN ORGANIC COMPOUNDS

Kagi H.[1], Fujimoto C.[1], Takahashi S.[1], Shinozaki A.[2], Nishida T.[3], Mimura K.[3]
[1]The University of Tokyo, Tokyo, Japan, kagi@eqchem.s.u-tokyo.ac.jp
[2]Hokkaido University, Sapporo, Japan
[3]Nagoya University, Nagoya, Japan

Pressure-induced behavior of aromatic compounds has been a subject of intensive research because of their great importance in both fundamental and applied chemistry. At high pressure, organic compounds exhibit various structural phase transformations followed by pressure-induced irreversible chemical reactions.

Pressure-induced oligomerization was reported on aromatic hydrocarbons represented by the simplest benzene with delocalized electrons in the π orbital (e.g., Shinozaki et al., 2013, 016; Yasuzuka et al., 2011). High pressure behavior of aromatic hydrocarbons is an important subject in planetary science. Stability of benzene and formation processes of polycyclic aromatic hydrocarbons (PAHs) in the planetary interior condition affects attentions because benzene and/or PAHs have been found in carbonaceous meteorites, Martian meteorites, and the atmospheres of giant planets and icy satellites.

Organic compounds having –OH group undergo dehydration condensation at high pressure (e.g., Shinozaki et al., 2013). We have recently found that amino acid (L-alanine) polymerize by forming peptide bonds at high pressure and room temperature through pressure-induced dehydration condensation (Fujimoto et al., 2015). Polymerization of amino acid was also observed in an aqueous solution of amino acid in spite of the dehydration condensation. We observed pressure-induced oligomerization of amino acid in its aqueous solution at pressures higher than 5 GPa where ice VII is the stable form of ice. The obtained results suggest that pressure-induced freeze-concentration of amino acid into the grain boundaries of ice enhanced the pressure-induced reaction (Takahashi et al., 2017). The pressure-induced reactions in organic compounds will open new avenue on evolution of organic compounds toward life-related molecules. We will review our recent results in the talk.

References:

Fujimoto C., Shinozaki A., Mimura K., Nishida T., Gotou H., Komatsu K. and Kagi H. (2015) Pressure-induced oligomerization of alanine at 25 °C. *Chemical Communications*, **51**, 13358-13361.

Shinozaki A., Mimura K., Kagi H., Komatsu K., Noguchi N. and Gotou H. (2014) Pressure-induced polymerization of benzene at room temperature as a precursory reaction of amorphization. *Journal of Chemical Physics,* **141**, 084306.

Shinozaki A., Noguchi N. and Kagi H. (2013) In-situ spectroscopic observations of pressure-induced condensation of trimethylsilanol and behavior of dehydrated molecular water. *Chemical Physics Letters*, **574**,66-70.

Shinozaki A., Mimura K., Nishida T., Inoue T., Nakano S. and Kagi H. (2016) Stability and partial oligomerization of naphthalene under high pressure at room temperature. *Chemical Physics Letters*, **662,** 263-267.

Takahashi S., Kagi H., Fujimoto C., Shinozaki A., Gotou H., Nishida T. and Mimura K. (2017) Pressure-induced freeze concentration of alanine aqueous solution as a novel field of chemical reaction. *Chemistry Letters*, **46**, 334-337.

Yasuzuka T., Komatsu K. and Kagi H. (2011) A revisit to high pressure transitions of pyridine: a new phase transition at 5 GPa and formation of a crystalline phase over 20 GPa. *Chemistry Letters* **40,** 733-735.doi:10.1246/cl.2011.733

RARE-EARTH AND RARE-METAL MINERALIZATION IN TRACHYTES OF THE KHULAM COMPLEX (KABARDINO-BALKARIA REPUBLIC, RUSSIA).

Kaigorodova E.N.
Institute of Geology of Ore Deposits, Petrography, Mineralogy and Geochemistry of the Russian Academy of Sciences, Moscow, Russia, katmsu@mail.ru

Jurassic magmatic formations of the area are mainly represented by subvolcanic near surface facies with basalt-rhyolite-trachyte composition. Apparently here was developed the subsurface magma-submitting system, supplied the medium-upper Jurassic volcanoes that have not been preserved at the modern erosional level.

The largest indigenous outcrop of trachytes is Khulamsky sill located to the east direction from the ruins of village El Khulam. It consists of several substratum bodies separated by thin layers of mudstone. Contacts of trachytes with mudstone are tearing. In the contact zone argillites are intensively wrinkled and fragmented, and injected by numerous small apophyses of trachytes. Trachytes in contacts are brecciated. Width of trachytic breccia varies from 2 to 4 m. This is a typical eruptive breccia for subvolcanic bodies. Above eruptive breccias occur the trachytes with clearly visible fluidity containing different size fragments of paleozoic granites. Accumulation of granite xenoliths in a small area may indicate magma-supplying channel position. Sometimes in trachytes outcrop of Khulamsky sill small lenticular bodies of hornfelsed argillites, trapped by magma during intrusion in the sedimentary Jurassic rocks are observed.

Trachytes are presented by massive rocks of pink, light brown with a greenish colours and porphyry structure with lots of pink feldspar phenocrysts. Porphyroblasts are composed mainly by K-Na-feldspar, orthoclase, albite, sometimes completely chloritized and carbonated dark-colored minerals. Number of phenocrysts varies from 2 to 30% of the rock volume. Their size changes from 2 mm to 1 cm. Phenocrysts of K-Na-feldspar are intensively albitized to produce in some cases new growths of albite porphyry. Orthoclase phenocrysts are pelitized; on it sometimes develops chlorite and carbonate.

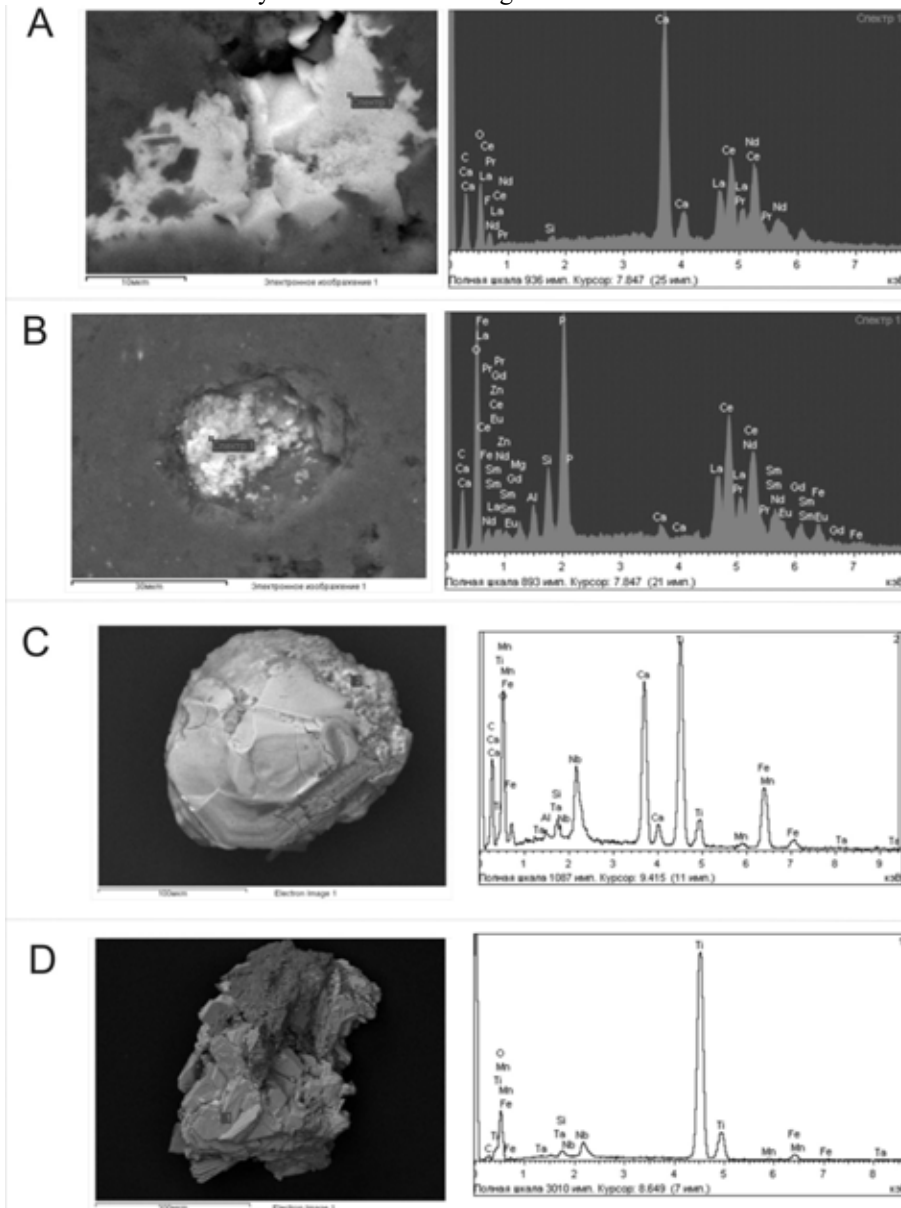**Fig.1**. Carbonatized breccia of trachytes on contact with argillites.

Fig. 2. Rare-earth and rare-metal minerals from the trachytes of the Khulam sill. A - synchyzite (sample RC-7) $CaCe(CO_3)_2F$; B - monazite (sample RC-7) (Ce, La, Nd, Th)PO_4; C - perovskite (sample X-4) $CaTiO_3$; D - pseudobrookite with an Nb content of 5.5% (sample X-5) Fe_2TiO_5.

Ground mass of trachytes is holocrystalline or microcrystalline with trachytic or microlitic structure with fluidal and fluidly-banded texture (Fig. 1). It consists mainly of parallel laths of K-Na-feldspar with subordinate albite and orthoclase. In the ground mass newly growths of quartz, chlorite, carbonate, analcime and flakes of muscovite are observed.

Accessory minerals are zircon and apatite. Ore minerals: pyrite, chalcopyrite, galena, sphalerite, pyrrhotite. The chemical composition of trachytes characterized by significant fluctuations of SiO2 content - 58,10 - 70,99%, probably due to their intensive postmagmatic changes. Most samples have SiO2 values from 63,67 to 68,25%.

Changes of trachytes are basically presented by three types: propylitization, silicification and argillic alteration.

In the zones of carbonatization and chloritization we detected rare-earth and rare-metal mineralization. Rare earth mineralization is represented by monazite, synchisite (Fig. 2 A,B). Rare-metal mineralization is represented by enriched by niobium perovskite and pseudobrukite (Fig. 2 C,D). Two generations of monazite (primary magmatogenic and hydrothermal redeposited) were detected.

The total contents of $\Sigma TR2O3$ attains 0,25% (from 0,03% to 0,25%). The largest contents are associated with altered zones. The contents reaches: Ta - 23 g/t; Nb - 348 g/t; Y = 357 g/t; La - 296 g/t; Ce - 394 g/t; Nd - 215 g/t.

For the trachytes of the Khulam complex an analogy can be drawn with the ores of the Dubbo deposit (Australia).

Conclusions: rare earth and rare metal mineralization in the trachytes of the Khulam complex is associated with processes of propylitization and carbonatization with hydrothermal post-volcanic solutions.

The work was carried by Governmental task of IGEM RAS on the theme "Development of an integrated information system for spatially-temporal modeling of ore objects and ore-forming processes based on GIS technologies".

DETERMINATION OF STABILITY REGION AND SUBSTITUTION MECHANISM OF AL-BEARING SUPERHYDROUS PHASE B

Kakizawa S.[1], Inoue T.[1,2], Nakano H.[1], Sakamoto N.[3], and Yurimoto H.[3]
[1]Ehime University, Matsuyama, Japan, kakizawa@sci.ehime-u.ac.jp
[2]Hiroshima University, Higashihiroshima, Japan
[3]Hokkaido University, Sapporo, Japan

Water is the most abundant volatile component on the Earth. It has significant influences on the chemical and physical properties of mantle minerals (e.g., melting temperature, elastic properties, electrical conductivity, and so on.). Water can exist as the nominally anhydrous minerals (NAMs), high pressure hydrous minerals (e.g., dense magnesium hydrous silicates; DHMSs), and fluid in the deep mantle. Phase D ($MgSi_2(OH)_2$) and Phase H ($MgSi(OH)_2$), which are the DMHSs stable in the lower mantle conditions, can contain a large amount of aluminum. The stability regions expand due to aluminum effect in the previous studies (Ohira et al., 2014, Pamato et al., 2015, and Ohtani et al., 2015). Moreover, Phase D and Phase H have the Al-rich end-members ($Al_2SiO_4(OH)_2$ and $AlOOH$, respectively). In this report, we focused on superhydrous phase B ($Mg_{10}Si_3O_{14}(OH)_4$), which is the important hydrous phase in the mantle transition zone.
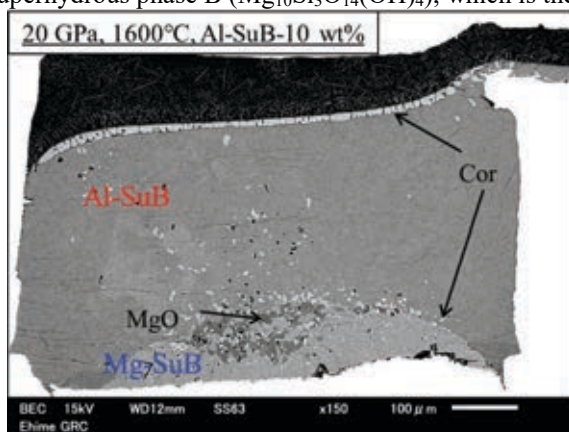
Fig. 1. Back scattered electrion image of recovered sample at 20 GPa and 1600℃. Mg-SuB, Mg-superhydrous phase B; Al-SuB, Al-superhydrous phase B; Cor, corundum.
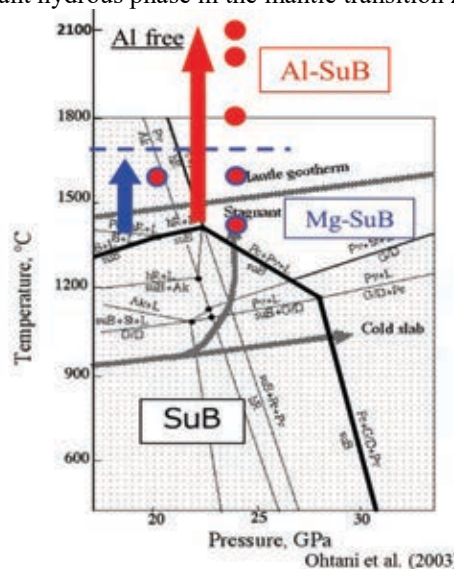
Fig. 2. Stability region of of superhydrous phaseB. Solid black line (SuB, Mg-endmember superhydrous phase B), Blue (Mg-SuB), and Red (Al-SuB)

The high pressure and high temperature experiments were conducted using Kawai-type multi-anvil apparatus (ORANGE-2000) installed at Ehime University, Japan. The experimental conditions were 20-24 GPa, 1600-2100℃. Water content was measured by secondary ion mass spectrometry (SIMS) installed at Hokkaido University. San Carlos Olivine (6-50 ppmwt% water), superhydrous phase B (5.82 wt% water), and Phase A (11.84 wt% water) were used as H standard

material for SIMS. Chemical composition and crystal structure of the recovered samples were determined using SEM-EDS and micro-focused XRD, respectively.

We succeeded to synthesize Al-bearing superhydrous phase B, which contained significant amount of Al_2O_3 (maximum content is 37 wt%) in our all experiments. The two types of Al-bearing superhydrous phase B were coexisted in the same sample capsule (Fig.1). They had different chemical compositions, especially in Al_2O_3 content, but the almost same crystal structure in powder X-ray diffraction level. This result shows that two types of superhydrous phase B exist in different Al_2O_3 content, and the crystal structures should slightly change with increasing Al_2O_3 content. In this study, we named those superhydrous phase Bs as Mg-superhydrous phase B and Al-superhydrous phase B, respectively. Fig.2 shows stability region of Al-bearing hydrous phase B. The stability region of superhydrous phase B expanded to higher temperature by the effect of Al_2O_3 than that of Mg-endmember superhydrous phase B (Ohtani et al., 2003; Inoue et al., 2006). Our synthesized Al-bearing superhydrous phase B was still stable even in ~2100℃, which is much higher than the mantle geotherm.

Fig.3 shows the chemical compositional trend of superhydrous phase B as a function of Al content. There were two tendencies in different Al content. In low Al content, Mg and Si decreased and H increased with increasing Al content. This tendency can be described as the substitution of $2Mg^{2+} + Si^{4+} \leftrightarrows 2Al^{3+} + 2H^+$. The maximum water content was 11.1 wt%. This was 1.9 times water content compared to Mg-endmember superhydrous phase B. On the other hand, Mg increased and Si, H decreased with increasing Al content in high Al content. The water content decreasing corresponded to the temperature increasing of the run products. Therefore, this tendency should show the dehydration of superhydrous phase B, and can be described as the substitution of $Si^{4+} + 16H^+ \leftrightarrows 4Mg^{2+} + 4Al^{3+}$.
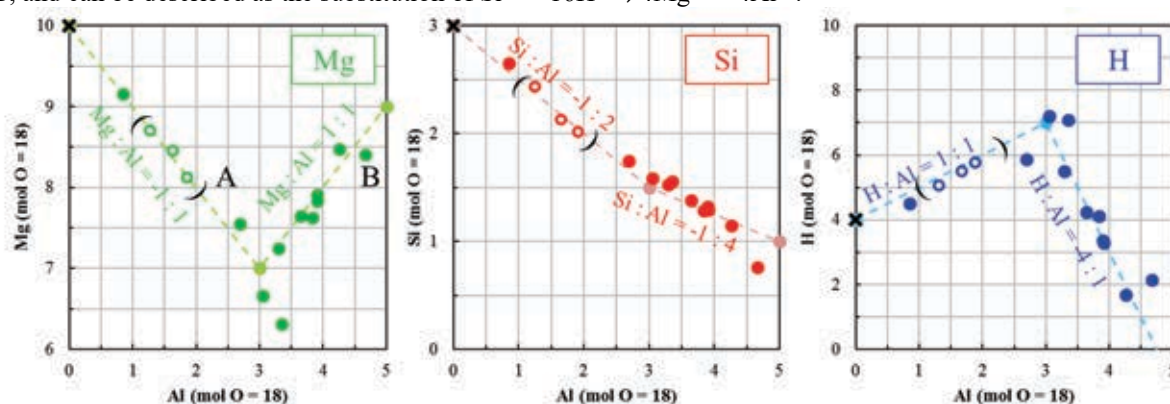
Fig. 3. Compositional trend (Mg, Si, and H) of supurhydrous phaseB as a function of Al content. O=18.

References:

Inoue, T, Ueda, T, Higo, Y, Yamada, A, Irifune, T, Funakoshi, K (2006) High-pressure and high-temperature stability and equation of state of superhydrous phase B, In "Earth's deep water cycle, Geophysical monograph series 168", Ed. by Steven D. Jacobsen and Suzan van der Lee, AGU, pp.147-157

Ohira I, Ohtani E, Sakai T, Miyahara M, Hirao N, Ohishi Y, Nishijima M (2014) Stability of a hydrous δ-phase, AlOOH–MgSiO$_2$(OH)$_2$, and a mechanism for water transport into the base of lower mantle. Earth and Planetary Science Letter 401:12-17. doi: 10.1016/j.epsl.2014.05.059

Ohtani E, Toma M, Kubo T, Kondo T, Kikegawa T (2003). In situ X-ray observation of decomposition of superhydrous phase B athigh pressure and temperature. Geophysical Research Letters. 30:2:1029. doi: 10.1029/2002gl015549.

Ohtani E. (2015) Hydrous minerals and the storage of water in the deep mantle. Chemical Geology 418:6-15. doi: 10.1016\j.chemgeo.2015.05.005.

Pamato MG, Myhill R, Ballaran TB, Frost DJ, Heidelbach F, and Miyajima N (2015) Lower-mantle water reservoir implied by the extreme stability of a hydrous aluminosilicate. Nature Geoscience 8:75-79. doi: 10.1038/ngeo2306

NITRIDES AND CARBONITRIDES FROM THE LOWER MANTLE AND THEIR IMPORTANCE IN THE SEARCH FOR EARTH'S 'LOST' NITROGEN

Kaminsky F.V. [1], *Wirth R.* [2]

[1]KM Diamond Exploration Ltd., Vancouver, Canada, felixvkaminsky@aol.com
[2]GeoForschungsZentrum, Potsam, Germany

Earlier, we reported upon finds of a series of iron carbides with admixtures of up to 7.3-9.1 at.% N (N/(N+C) = 0.19-0.27), included in lower-mantle diamonds, in association with native iron and graphite. It was established that the iron carbides formed within the Earth's core at a pressure interval of 50-130 GPa; these grains having crystallised from an iron-carbon melt, rich in nitrogen (Kaminsky and Wirth 2011). Subsequently, nitrocarbides and carbonitrides, $Fe_2(N,C)$, $Fe_3(N,C)$, $Fe_7(N,C)_3$ and $Fe_9(N,C)_4$, with 12.8-18.42 at.% N and N/(N+C) = 0.37-0.60 were identified in a

lower-mantle microxenolith (Kaminsky et al. 2015). In our recent studies, we have identified as inclusions in diamond other carbonitrides and pure nitrides, which we report herein.

Nitrides and carbonitride as inclusions in lower-mantle diamond from Rio Soriso, Brazil are herein reported. These grains were identified and studied with the use of transmission electron microscopy (TEM), electron diffraction analysis (EDX) and electron energy-loss spectra (EELS). Among nitrides, trigonal Fe_3N and orthorhombic Fe_2N are present. Carbonitride is trigonal $Fe_9(N_{0.8}C_{0.2})_4$. These mineral phases associate with iron carbide, Fe_7C_3, silicon carbide, SiC, Cr-Mn-Fe and Mn-Fe oxides; the latter may be termed Mn-rich xieite.

Two types of iron nitride grains were distinguished among inclusions (Fig. 1). The first type comprise tabular or equidimensional single-phase grains, 1-2.5 ⬜m in size (Fig. 1a). Some of such inclusions are intergrown with smaller (300-400 nm) grains of oxides. The second type is represented by 8-10 ⬜m elongated inclusions, consisting of an aggregate of nitride and/or replacing it polycrystalline graphite (Fig. 1b). Nitride forms irregular, 0.5-1.5-⬜m grains along the periphery of the aggregate and smaller (0.1-0.3 ⬜m), irregularly-shaped, relics within the graphite matrix, demonstrating a typical structure of resorption of the initial nitride grain by graphite. In dark- and bright-field images the relic iron nitride grains show the same crystallographic orientation, confirming that they belong to a former, single large crystal.
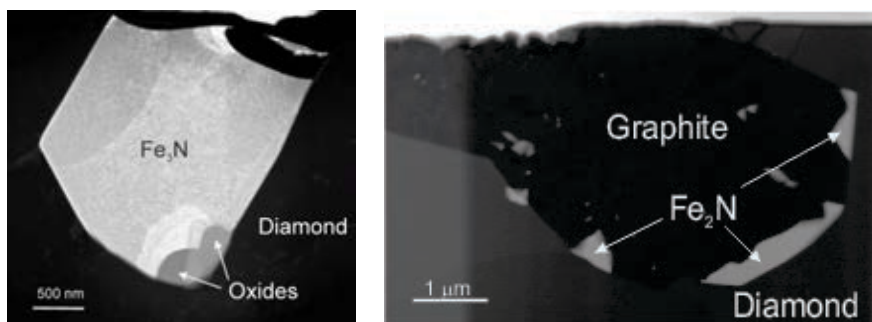
Fig. 1. TEM dark-field images of iron nitrides included in diamond.

Type 1 inclusions were identified as Fe_3N, with a trigonal $P312$ structure; type 2 inclusions were identified as Fe_2N, with an orthorhombic $Pbcn$ structure. The diffuse and strongly smeared-out diffraction spots in the electron diffraction pattern suggest a mosaic structure to the grain with numerous subgrains that are slightly misoriented with respect to each other. The individual subgrains may belong to a single phase or to two different iron nitride phases.

In addition to pure nitrides, in one of the inclusions a carbonitride, $Fe_9(N_{0.8}C_{0.2})_4$, grain, 6×7 µm in size was identified (Fig. 2). It has straight, sharp borders with the host diamond, except for the area in the upper part of the image, where the inclusion is corroded, - possibly by a fluid in a pore, which opened during the course of the focussed ion beam (FIB) sample preparation. The EDX and EEL spectra of carbonitride indicate the presence of three major elements Fe, N and C and an admixture of Si, like in some of the iron nitrides.

Two straight lamellae of 100-500 nm thickness cut the hosting iron carbonitride grain (Fig. 2). They do not contain nitrogen; only iron and carbon are present, with the ratio Fe/C = 2.46, close to the ideal ratio for Fe_7C_3 (2.33). This composition is confirmed by the electron diffraction data, according to which the lamellae are of an orthorhombic iron carbide, Fe_7C_3.
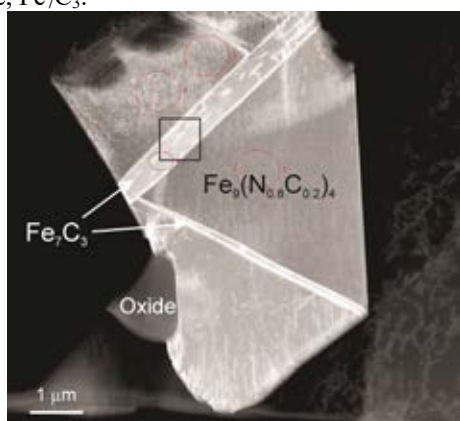
Fig. 2. HAADF image of iron carbonitride, $Fe_9(N_{0.8}C_{0.2})_4$, with lamellae iron carbide, Fe_7C_3, hosted as an inclusion in diamond. In the lower left part of the image an idiomorphic crystal with spinel-type structure is observed intergrown with carbonitride. he outlined square area corresponds to regions for Si and C elemental maps. Circles show areas for which EDX spectral analyses were determined.

The identified finds demonstrate a wide field of natural compositions from pure carbide to pure nitride, with multiple stoichiometries from $M_5(C,N)_3$ to $M_{23}(C,N)_6$ and M/(C,N) from 1.65 to 3.98. We conclude that the studied iron nitrides and carbonitrides were formed in the lowermost, lower mantle as the result of the infiltration of liquid metal, containing light elements, from the outer core into the D" layer, with the formation of the association: native Fe^0 + iron nitrides, carbides and transitional compounds + silicon carbide.

Nitrogen, the seventh most abundant element in the Solar System, remains one of the most enigmatic in studies of Earth's geochemistry. There is a so-called 'missing nitrogen' problem in the Earth's inner parts because, according to existing estimates, nitrogen is at one order of magnitude less than other volatile elements, with the value of bulk

Earth/carbonaceous chondrite ratio equal to 0.11 % (Marty 2012). The calculated atomic ratio for N/Si in the bulk Earth is several orders of magnitude lower than that for the remaining terrestrial planets/or bodies within the asteroid forming zone (Bergin et al. 2015). As a result, nitrogen is considered as a trace element in the major silicate reservoirs, even as "a useless element in mantle geochemistry" (Cartigny and Marty 2013) owing to extensive nitrogen outgassing during the Earth's early history. On the other hand, Li et al. (2013) concluded that the mantle may still contain an amount of nitrogen one to two orders of magnitude larger than the present atmospheric reservoir. Nitrogen is suggested to have siderophile behavior in the core's metal alloy and extremely high solubility, with partitioning of nitrogen $K^{\text{Metal/Silicate}}$ around 10,000 (Miyazaki et al. 2004). Such high value implies a nitrogen mass, in the core, hundreds of times greater than that in the atmosphere; an estimate for the total proportion of nitrogen in the core by Miyazaki et al. (2004) is $\sim 1 \times 10^{24}$ g. This suggestion is supported by high concentrations of nitrogen in iron meteorites and provides a basis to consider the Earth's core as a major reservoir to nitrogen, containing perhaps 97 % of its total planetary inventory (McDonough 2014). The most recent calculations conclude that the fraction of nitrogen within the Earth's core may be between 10 % and 90 %, depending upon the oxygen fugacity values in force during metal-silicate equilibration, and whether the core is a significant, but not dominant reservoir of terrestrial nitrogen (Dalou et al. 2016).

Accepting a conventional concentration of nitrogen in the core at 5,000 ppm (Adler and Williams 2005) and the partition coefficient between metal core and mantle material at 40 (McDonough 2014), and considering the total core mass as 1.972×10^{27} g and mantle mass as 4.043×10^{27} g (Yoder 1995), the total mass of nitrogen in the core could be $9,660 \times 10^{21}$ g and in the bulk mantle 505×10^{21} g, comprising accordingly 94.97 % and 4.97 % of the total nitrogen in the Earth. In this case, the total nitrogen concentration in bulk Earth is 17.03 ppm, which fully corresponds (with an error of $\pm$ 2 %) to the concentration of nitrogen as determined in chondrite meteorites.

References:

Adler, J.F. and Williams, Q. (2005) A high-pressure X-ray diffraction study of iron nitrides: Implications for Earth's core // Journal of Geophysical Research 110, B01203.

Bergin, E.A., Blake, G.A., Ciesla, F., Hirschmann, M.M., Li, J. (2015) Tracing the ingredients for a habitable earth from interstellar space through planet formation // Proceedings of the National Academy of Sciences of the U.S.A.112, 8965–8970.

Cartigny, P., Marty, B. (2013) Nitrogen isotopes and mantle geodynamics: The emergence of life and the atmosphere–crust–mantle connection // Elements 9, 359-366.

Kaminsky, F.V. and Wirth, R. (2011) Iron carbide inclusions in lower-mantle diamond from Juina, Brazil // Canadian Mineralogist 49(2), 555-572.

Kaminsky, F.V., Wirth, R., Schreiber, A. (2015) A microinclusion of lower-mantle rock and some other lower-mantle inclusions in diamond // Canadian Mineralogist 53(1), 83-104.

Li, Y., Wiedenbeck, M., Shcheka, S., Keppler, H. (2013) Nitrogen solubility in upper mantle minerals // Earth and Planetary Science Letters 377, 311-323.

Marty, B. (2012) The origins and concentrations of water, carbon, nitrogen and noble gases on Earth // Earth and Planetary Science Letters 313–314, 56–66.

McDonough, W.F. (2014) Compositional Model for the Earth's Core. In: Treatise on Geochemistry, 2nd edition. Vol. 3 (Ed. R.W. Carlson), p. 559-576. Elsevier.

Miyazaki, A., Hiyagon, H., Sugiura, N., Hirose, K., Takahasi, E. (2004) Solubilities of nitrogen and noble gases in silicate melts under various oxygen fugacities: Implications for the origin and degassing history of nitrogen and noble gases in the Earth // Geochimica et Cosmochimica Acta 68, 387–401.

Yoder, C.F. (1995) Astrometric and geodetic properties of the Earth and the solar system. In: T.J. Ahrens (ed.) Global Earth Physics: A Handbook of Physical Constants, Vol. AGU Reference Shelf, pp. 1–31. Washington, DC: American Geophysical Union.

SPATIAL ZONING OF KIMBERLITES AND RELATED ROCKS OF THE ARKHANGELSK DIAMOND PROVINCE (ARKHANGELSK, RUSSIA) AS THE REFLECTION OF THE MAGMOGENERATING ZONE EVOLUTION

Kargin A.V.[1], Nosova A.A.[1], Sazonova L.V.[1,2], Yutkina E.V.[1], Golubeva Yu.Yu.[3], Lebedeva N.M.[1,2], Dokuchaev A.Y[1], Kondrashov I.A.[1]

[1]Institute of Geology of Ore Deposits, Petrography, Mineralogy and Geochemistry of the Russian Academy of Sciences, Moscow, Russia, kargin@igem.ru
[2]Lomonosov Moscow State University, Moscow, Russia
[3]Central research institute of geological prospecting for base and presious metals, Moscow, Russia, jugolubeva@gmail.com

Kimberlites are generally located within large provinces of the alkaline-ultramafic magmatism and associated with orangeites, ultramafic lamprophyres, alkaline picrites, melilitites, carbonatites, etc. Large kimberlite areas have often the zonal allocation (sharing) of objects with different geochemical characteristics. For example, one of this areas is the Arkhangelsk Diamond Province (ADP).

Existing models of the kimberlites and related alkaline-ultramafic rocks formation allow identifying the main factors, which determine their location and reflect heterogeneity and structure of the subcontinental lithospheric mantle (SCLM):

1. SCLM thickness, which determines the depth of the melts generation and the stability of various metasomatic phases in it (K and/or Na).

2. SCLM permeability, which controls the ascent and evolution of alkaline-ultramafic melts, including the lithospheric assimilation, mantle metasomatism, megacrysts fractionation, separation of carbonate melts/fluids, etc.

3. SCLM heterogeneity that is expressed in the presence of eclogites lenses and metasomatic vein paragenesis such as MARID (mica-amphibole-rutile-ilmenite-diopside), PIC (phlogopite-ilmenite-clinopyroxene), etc., which could participate in the mantle source of kimberlites and related rocks.

Arkhangelsk Diamond Province contains two series of kimberlites and related ultramafic-alkaline rocks those are distinct in mineral composition and geochemical characteristics (Arkhangelsk Diamondiferous Province, 1999; Kononova et al., 2011 and references herein; unpublished data):

Fe-Ti-series – is group of ilmenite-bearing (ilmenite megacrysts, phenocrysts and mantle xenoliths with ilmenite metasomatism) kimberlites and related ultramafic-alkaline rocks (the Kepino pipe cluster, the Grib pipe, the Ermakovskaya-7 pipe and sills of the Mela River) with high TiO_2 concentrations (>1 wt.%). These pipes are located in central and eastern parts of ADP. Their isotopic characteristics are similar to the Group 1 kimberlites of the South Africa and reflect an asthenospheric origin of their mantle source (Sablukov and Sablukova 2008; Kononova et al., 2011). Additionally, the Grib kimberlite contain a large number of Mg-Si phases (olivine, serpentine). *Fe-Ti*-kimberlites in the northern part of ADP (the Ermakovskaya-7 pipe and sills of the Mela River) are enrich in carbonate, phlogopite and REE. *Fe-Ti*-kimberlites in the eastern part of ADP are characterized by an increase in the Fe and Ti concentrations (the Kepino pipe cluster).

Mg-Al-series – is group of ilmenite-poor ultramafic-alkaline rocks (kimberlites and orangeites of the Zolotitsky pipe cluster, olivine melilitites and alkaline picrites of the Chidviya, Izhma, Suksoma and Nenoksa pipe clusters). This series has lower TiO_2 (<1 wt %) and higher Al, Si and Na concentrations in compare with *Fe-Ti*-kimberlites. These pipes are located in the western and marginal parts of ADP. Isotopic-geochemical compositions of these rocks suggest the contribution of the ancient lithospheric mantle in their source.

Spatial zoning of the ADP ultramafic-alkaline rocks. The study both mantle xenoliths and the wall-rocks isotopic composition (Sablukov et al., 2000; 2009; Sablukov and Sablukova 2004; 2008) showed that *Mg-Al-* and *Fe-Ti*-kimberlites within ADP differ in the metasomatism degree of the lithospheric mantle by asthenospheric melts. The central part of the province has a high degree of the source rocks metasomatism, whereas in the marginal parts the degree of the metasomatism decreases and the lithosphere component prevails in the source rocks composition.

Kimberlites and related ultramafic-alkaline rocks of ADP are localized in the Paleoproterozoic collisional zone (Samsonov et al., 2012). A lithospheric mantle stage is distinguished between the rocks of the two series (Sablukov et al., 2000), which implies a decrease in the SCLM thickness in the transition from *Fe-Ti* to *Mg-Al*-series (from 180-210 to 150 km, respectively).

The objects and purposes of the study. The results of studying the compositions of kimberlites and related rocks of ADP (XRF, ICP-MS), as well as mantle xenoliths and minerals of the megacrysts (EMPA, SIMS methods) from the Grib kimberlite were summarized (Sazonova et al., 2015; Kargin et al., 2016a, 2016b; Larionova et al., 2016; Nosova et al., 2017; Lebedeva et al., this issue). This made it possible to estimate the primary compositions corresponding to the formation of *Fe-Ti*-kimberlites, using the example of the Grib kimberlite. Also, taking into account the known data about the zonal structure of ADP and the composition of SCLM, it was possible to trace the evolution of these components in interaction with the lithosphere, which determined the observed variations in the geochemical composition of the ADP alkaline-ultramafic rocks.

The ADP magmatism age. The ages of the kimberlites crystallization can be defined as 376 ± 3 Ma for the Grib pipe, 380 ± 2 Ma for the Karpinskiy-1 pipe, 375 ± 2 Ma for the Karpinskiy-2 pipe, and 377 ± 0.4 Ma for the Ermakovskaya-7 pipe (Larionova et al., 2016).

Not only the emplacement of the Grib kimberlite and other ADP objects marked the Late Paleozoic tectonothermal activity on the northeastern part of the East European Craton (EEC), but also the formation of the Kola alkaline province. According to the last geochronological summary (Arzamastsev and Wu, 2014), this province was generated within an interval of around 30 Ma, starting from the alkaline-ultramafic magmatism at 383 ± 7 Ma in the Khibiny and Lovozero calderas to the carbonatite formation at 379 ± 7 Ma (Kovdor complex, Afrikanda, etc.). In this case, the formation of large alkaline provinces and closely spaced kimberlite occurrences may be considered as a display of a single tectonothermal event. This makes it possible to allocate a single large alkaline ultramafic Cola-Arkhangelsk magmatic zone in the northeastern part of EEC (Kargin et al., 2016a; Yutkina et al., this issue).

The mantle metasomatism in the Grib kimberlite formation. The minerals study within mantle-derived coarse and sheared peridotite xenoliths, metasomatic clinopyroxene-phlogopite xenoliths and megacrysts (olivine, garnet, clinopyroxene, phlogopite) from the Grib kimberlite (Sazonova et al., 2015; Kargin et al., 2016a, 2016b; Nosova et al., 2017; Lebedeva et al., this issue) has shown that the kimberlitic melts interacted with the SCLM with intensive metasomatism of the latter. The geochemical features of garnets and clinopyroxenes from mantle peridotite xenoliths allow to reconstruct the following sequence of metasomatic events related to the Grib kimberlite formation:

1. Ascent of high-temperature asthenospheric or mantle plume material led to a partial melting of a carbonated peridotite and the formation of REE-enriched proto-kimberlite melt containing significant amounts of carbonate, Fe-Ti and K-H$_2$O phases. That protokimberlite melt started to interact with the surrounding mantle rocks during its evolution and ascent, and caused metasomatic modification of both coarse and sheared peridotites in the basement of SCLM.

2. Further proto-kimberlite melt evolution during the ascent and the interaction with the mantle (e.g. mantle-rock assimilation and/or fractionation) led to changes in the kimberlites composition from REE-enriched carbonate-depleted to carbonate-riched ultramafic silicate magmas with low concentrations of REE.

3. During the ascent and percolation of the proto-kimberlite melt through the SCLM, intensive mantle metasomatism occurs with the transformation of mantle garnet peridotites to clinopyroxene-phlogopite metasomatic rocks (Lebedeva et al., this issue), as well as the fractionation of megacrysts minerals. The main volume of metasomatism occurred when kimberlite melts had moved from the basement of the lithosphere at depths corresponding to P <3 GPa.

Was probably, that successive pulses of ascending kimberlite melts progressively metasomatised the conduit along which later kimberlite pulses ascended, producing progressively decreasing interaction with the surrounding mantle rocks (Giuliani et al., 2016). In this case, subsequent portions of the primary kimberlite melt could rise to the surface in its original form without experiencing intensive interaction with the lithospheric mantle.

Evolution of the ADP magmogenerating zone. The evolution of the Grib kimberlite melts can be considered as a basic model for the formation of *Fe-Ti*- and *Mg-Al*-kimberlites. In this case, we can suggest the following sequence of the magmogenerating zone evolution:

Stage 1. Ascent of the primary kimberlitic melt, which was enriched Fe-Ti, carbonate, K and H$_2$O, led to metasomatism of the lithosphere basement to the lithosphere basement (at depths corresponding P = 6-7 GPa) with the formation of clinopyroxene-phlogopite rocks and fractionation of the Fe-Ti phase (ilmenite) at depths corresponding with P = 4-5 GPa. At this stage, the formation of transport zones (conductors) for the raising of kimberlites (conducting channels in the lithospheric mantle) and the formation of kimberlites, which carry a large number of mantle and crustal xenoliths and megacrysts (like the Grib kimberlite), occurred.

Stage 2. The receipt of new portions of early kimberlite melts and their ascent through already formed channels. At that stage, kimberlites and related rocks of the Kepino pipe cluster, the Mela sills and the Ermakovskaya-7 pipe were formed. These rocks are enriched with both carbonate and Fe-Ti and K-H$_2$O components. The isotope-geochemical characteristics of these rocks are close to the primary melt parameters, because the melt ascent occurred without active interaction with the lithospheric mantle.

Stage 3. Formation of the *Mg-Al*-kimberlites and alkaline-ultramafic rocks of the Zolotitsky field could be connected with a decrease in the lithosphere thickness under kimberlites and related *Fe-Ti*- and *Mg-Al*-rocks from 180-210 km to 150 km, respectively (Sablukov et al., 2000). New portions of the protokimberlite melt (at the depths of the corresponding 4-5 GPa) contributed to the partial melting of the lithosphere containing the clinopyroxene-phlogopite metasomatic veins formed in Stage 1. As a result, kimberlites and orangeites of the Zolotitsky field were formed.

In the south-south-western part of ADP the rocks of the Chidvia-Izhmozersky and Nenoksky fields were formed. Their mineralogical and petrogeochemical characteristics shows the predominance of sodium metasomatism in the lithosphere. This metasomatic character probably indicates a decrease in the thickness of SCLM in the direction from the ADP center to margins of the province.

References:

Afanasiev VP, Ashchepkov IV, Verzhak VV, O'Brien H, Palessky SV (2013) PT conditions and trace element variations of picroilmenites and pyropes from placers and kimberlites in the Arkhangelsk region, NW Russia. J. Asian Earth Sci. 70–71:45–63. doi:10.1016/j.jseaes.2013.03.002

Arkhangelsk Diamondiferous Province (1999) Bogatikov OA, Ed., Moscow: MGU. 524 p.

Arzamastsev AA, Wu F-Y (2014) U-Pb geochronology and Sr-Nd isotopic systematics of minerals from the ultrabasic-alkaline massifs of the Kola province. Petrology 22:462–479. doi: 10.1134/S0869591114050026

Giuliani A, Phillips D, Kamenetsky VS, Goemann K (2016) Constraints on kimberlite ascent mechanisms revealed by phlogopite compositions in kimberlites and mantle xenoliths. Lithos 240–243:189–201. doi:10.1016/j.lithos.2015.11.013

Kargin AV, Sazonova LV, Nosova AA et al. (2016a) Sheared peridotite xenolith from the V. Grib kimberlite pipe, Arkhangelsk Diamond Province, Russia: Texture, composition, and origin. Geosci. Front. doi:10.1016/j.gsf.2016.03.001 (in press).

Kargin AV, Sazonova LV, Nosova AA, Tretyachenko VV (2016b) Composition of garnet and clinopyroxene in peridotite xenoliths from the Grib kimberlite pipe, Arkhangelsk diamond province, Russia: Evidence for mantle metasomatism associated with kimberlite melts. Lithos 262:442–455. doi:10.1016/j.lithos.2016.07.015

Kononova VA, Bogatikov OA, Kondrashov IA, 2011. Kimberlites and lamproites: Criteria for similarity and differences. Petrology 19:34–54. doi:10.1134/S0869591111010024

Larionova YO, Sazonova LV, Lebedeva NM, Nosova AA, Tretyachenko VV, Kargin AV (2016) Kimberlite Age in the Arkhangelsk Province, Russia: Isotopic Geochronologic Rb-Sr and 40Ar/39Ar and Mineralogical Data on Phlogopite. Petrology 24:562–593. doi:10.1134/S0869591116040020

Lebedeva NM, Kargin AV, Sazonova LV, Nosova AA, (2017) Clinopyroxene-phlogopite xenoliths from the Grib kimberlite (Arkhangelsk province, Russia): isotopic characteristics and composition of Cpx and Phl. This issue.

Nosova AA, Dubinina EO, Sazonova LV, Kargin AV, Lebedeva NM, Khvostikov VA, Burmii ZP, Kondrashov IA, Tret'yachenko VV (2017) Geochemistry and oxygen isotopic composition of olivine in kimberlites from the Arkhangelsk province: Contribution of mantle metasomatism. Petrology 25:150–180. doi:10.1134/S0869591117010064

Sablukov S, Sablukova LI (2004) 3-D mapping of mantle substrate in the Zimny Bereg area, Russia, in: 8th International Kimberlite Conference. FLA-0059: 1-5.

Sablukov SM, Sablukova LI (2008) Asthenospheric effect on the mantle substrate and diversity of kimberlite rocks in Zimni Bereg (Arkhangelsk province), in: 9th International Kimberlite Conference. Frankfurt, p. 9IKC-A-00162.

Sablukov SM, Sablukova LI, Griffin WL (2009) Distribution of trace elements in deep-situated minerals from kimberlite as indication of plume processes in the North of Russian Platform (In Russian), in: Deep-Situated Magmatizm, Its Source and Plumes. Institute of Geography SB RAS, Miass, pp. 135–170.

Sablukov SM, Sablukova LI, Shavyrina MV (2000) Mantle xenoliths from the Zimnii bereg kimberlite deposits of rounded diamonds, Arkhangelsk diamondiferous province. Petrology 8, pp. 1466–494.

Samsonov AV, Tretyachenko VV, Nosova AA, Larionova YO, Lepekhina E, Larionov AN, Ipatieva IS (2012) Sutures in the Early Precambrian Crust as a Factor Responsible for Localization of Diamondiferous Kimberlites in the Northern East European Platform, in: 10th International Kimberlite Conference. Bangalore, p. 10IKC35. doi:10.1134/S1028334X09020111

Sazonova LV, Nosova AA, Kargin AV et al. (2015) Olivine from the Pionerskaya and V. Grib kimberlite pipes, Arkhangelsk diamond province, Russia: Types, composition, and origin. Petrology 23:227–258. doi:10.1134/S0869591115030054

Yutkina EV, Nosova AA, Sazonova LV, Laptsevich AG, Kuzmenkova OF, Volkova GD, Sysoev IV (2017) Sources and geochemical zoning of the Devonian magmatism in the Pripyat-Dnieper-Donets rift zone. This issue.

ISOTOPIC CONSTRAINTS ON THE SOURCES AND TIMING OF NOBLE METAL MINERALIZATION IN CRATON-SCALE PALEO-PLACERS: ROLE OF PRECAMBRIAN MAGMATISM AND PLATE TECTONICS

Kepezhinskas N.P.[1], Kamenov G.[1], Kepezhinskas P.K.[2], Widom E.[3], Foster D.[1], Kuentz D.[3], Hennigh Q.[4], Katella A.S.[5]

[1]University of the State of Florida, Gainesville, USA
[2]PNK GeoScience, Tampa, USA
[3]Miami University, Oxford, USA
[4]Novo Resources Corp, Vancouver, Canada
[5]Vostok Mining Corporation, Khabarovsk, Russian Federation

Precambrian cratonic terranes host spectacular giant ore deposits such as Witwatersrand (40% of world's gold resource), the 550 km-long Great Dyke of Zimbabwe and the Talnakh ultramafic-mafic intrusions in Siberia (world-class Cu-Ni-Co-PGE deposits), Bayan-Obo REE-Nb-Fe deposit (45% of world's REE production) in Inner Mongolia, China, as well as many others. Among these giant Precambrian ore systems ancient paleo-placers, represented by the behemoth Witwatersrand auriferous basin, occupy a truly special place as they carry an impressive inventory of metals such as gold, silver, platinum group elements, molybdenum, copper, uranium, rare earths and even diamonds. Mineralized sedimentary basins, to various extents similar to Witwatersrand, have been identified within most Precambrian cratons rendering their origin and conditions of metal accumulation among the most fundamental problems of modern geology. Genesis of these ore systems is subject of a hot debate (Robb and Meyer, 1995; Hayward et al., 2005; Mathur et al., 2013; Phillips and Powell, 2015; Heinrich, 2015) with three models – detrital, hydrothermal and combined reworked detrital – currently being supported by most of available data. In this paper we present data for two such craton-scale mineralized systems, the Archean Hamersley Basin in the Pilbara Craton of western Australia and the Proterozoic Nemui conglomerates from the SE Siberian Craton, which we compare with the classic Witwatersrand mineralization in an attempt to constrain possible noble metal sources and evaluate potential role of Precambrian magmatism and plate tectonic processes.

Auriferous conglomerates of the 2.77-2.63 Ga-old Fortesque Group carry reef-type gold mineralization associated with typical "buck-shot" pyrite and gold grades of 1 to 10 g/t over widths of several meters. The total drilling-supported resource stands at 6.4 million tonnes with a grade of 2.7 g/t Au, resulting in 560,000 ounces of Au. The Fortesque group metasediments are broadly comparable to auriferous conglomerates from the Witwatersrand Basin. Based on the lithology and mineralogy of the Fortesque Group sediments, and the ubiquitous presence of older greenstones (komatiites, basalts) and granites among the heterolithic conglomerate clasts, the main sources of metals in the Hamersley Basin are inferred to be mafic-ultramafic volcanics and associated granites from a Mesoarchean granite-greenstone Pilbara terrain.

Pb isotope ratios in gold and sulfide from the Fortesque Group conglomerates determine an imprecise isochron of 2875 Ma, consistent with available geological and geochronological data. These ages correlate with 2.8-3.0 Ga ages of multiple magmatic arc complexes in the East Pilbara terrain which, as supported by clast lithology, are likely sources of metals in Hammersley basin. Sulfides from the Fortesque Group display the lowest Pb isotope ratios and are, therefore, most probably of Archean detrital origin (Fig. 1). Gold, on the other hand, has the most radiogenic Pb isotope signatures (Fig. 1), suggesting that it was deposited during a later (metasomatic?) event that introduced high U/Pb ratios to noble

metal mineralization in the Hammersley basin. Re-Os isotope analyses of gold and pyrite separates are underway to help determine the age and source of the gold. Preliminary data on one gold sample indicates that it has a relatively low Os abundance (0.375 ppb) compared to gold from Witwatersrand, for which Os concentrations in gold separates are ~10 – 10,000-fold higher, ranging from ~4 to >4,000 ppb Os (Kirk et al., 2001; 2002). The Os concentration of the gold in the present study is instead at the high end of the range reported for the younger Moeda deposit, which ranges from only ~0.01 to >0.1 ppb (Kirk et al., 2002). The relatively low Os concentration in the gold may be indicative of a crustal origin, sourced from rocks relatively low in PGEs compared to the mantle or komatiites. The measured $^{187}Os/^{188}Os$ ratio of 4.00 ± 0.02 is furthermore highly radiogenic compared to gold of Witwatersrand (0.108 – 0.892), also consistent with – but not definitive of – a crustal origin for the Os. However, unlike the Witwatersrand case for which the highly unradiogenic $^{187}Os/^{188}Os$ ratio of 0.108 directly provides a model mantle extraction age (~3 Ga), interpretation of the radiogenic $^{187}Os/^{188}Os$ measured in our gold separate will require determination of a gold-pyrite Re-Os isochron to evaluate the age and initial $^{187}Os/^{188}Os$ signature – and thus the source of the Os and Au.
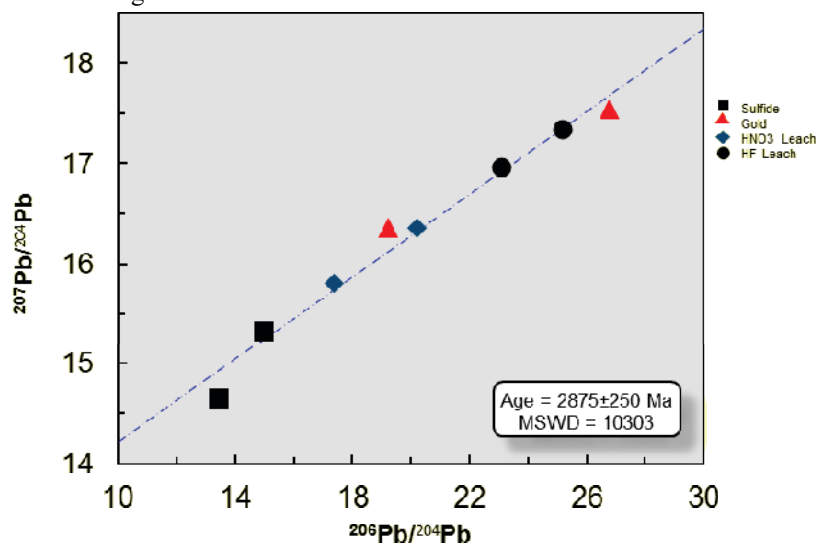
Fig. 1. Pb isotope variations in gold and pyrite from the Fortesque Group conglomerate (Hamersley Basin, Pilbara craton) define an imprecise isochron at 2875 Ma.

Metalliferous Nemui conglomerates fill a large (300 by 100 km) pericratonic basin comparable in size to both Witwatersrand and Hamersley basins. Some petrographic features observed in Nemui sediments, such as presence of matrix biotite and laminated pyrite, also suggest close similarities with auriferous conglomerates from the Kaapvaal and Pilbara cratons. U-Pb zircon ages from the Nemui conglomerates determine an isochron age of 1831 Ma with potential re-setting around 169 Ma (Fig. 2). While the Paleo-proterozoic Nemui ages suggest derivation of gold and other metals from Batomga greenstones and granites along the SE edge of the Siberian craton (Vovna et al., 2014; Guryanov et al., 2016), Jurassic ages suggest large-scale re-mobilization of noble metals within the Nemui basin due to the thermal influence of the giant Uda-Murgal-Stanovoy subduction zone/magmatic arc (Goryachev and Pirajno, 2014).
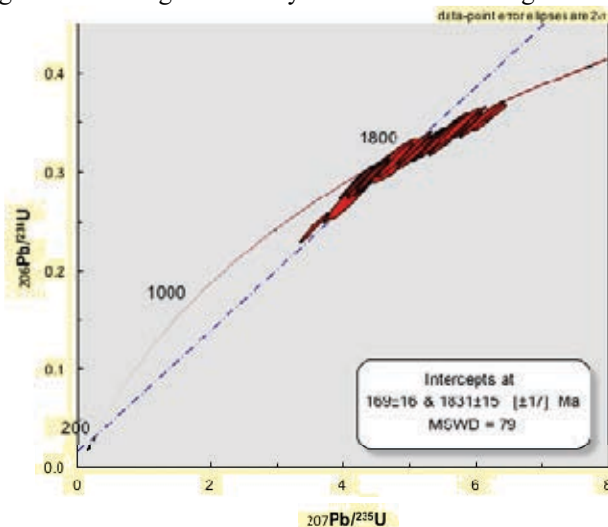
Fig. 2. Distribution of zircon U-Pb ages from the Nemui metalliferous conglomerates (SE Siberian Craton) defining a primary depositional age at 1831 Ma and re-activation of Nemui basin associated with Uda-Murgal-Stanovoy subduction system at 169 Ma

Granite-greenstone terrains are the main sources of metals in Precambrian craton-scale paleo-placers. Komatiites and basalts contribute PGEs and some gold, while TTGs are responsible for Au, Ag, Mo, REE and U budgets. Copper is somewhat enigmatic but is most probably sourced within granite-greenstone lithologies. Archean auriferous basins such as Witwatersrand and Hamersley are linked to erosion of a collage of oceanic plateaus and magmatic arcs accreted against cratonic nuclei during initiation of a modern-style Wilson cycle in the Mesoarchean. Proterozoic mineralized sedimentary systems such as Jacobina and Nemui are associated with an increasing rate of post-Archean subduction, which culminated in the Neoproterozoic with the establishment of modern plate tectonic processes.

Gold mobilization in the crust-mantle system is closely linked to Precambrian subduction episodes, enabled especially by their intensity and duration. Three major gold-forming subduction episodes are recognized: sporadic Paleoarchean to Mesoarchean (3.5-3.0 Ga) subduction, intermittent Paleoproterozoic to Early Mesoproterozoic (2.5-1.5 Ga) subduction, and an avalanche subduction pulse in the Neoproterozoic (younger than 1 Ga). Evidence of the earliest subduction episodes in the Hadean and Eoarchean are so far very rare, and no metal mineralization can be yet attributed to these very nascent stages of plate tectonic development.

Most, if not all, giant Precambrian paleo-placer deposits were accumulated within pull-apart basins formed at rifted cratonic margins. Metal distribution appears to be structurally controlled by strike-slip faulting. Gold and other metals are accumulated in two principal stages: detrital (along with diamonds derived from older kimberlites) coupled with coeval, large-scale felsic volcanism, followed by later hydrothermal overprinting. Most of the combined metal resource in such Precambrian paleo-placers as Witwatersrand, Hammersley, Birimian-Tarkwaian goldfields, KMA, Jacobina and Nemui was most probably accumulated during the detrital stage, through extensive erosion of preceding granite-greenstone sources.

References:

Goryachev NA, Pirajno F (2014) Gold deposits and gold metallogeny of Far East Russia. Ore Geol Rev 59: 123-152

Guryanov VA, Didenko AN, Peskov AYu, Roganov GV, Dymovich V.A. (2016) Precambrian granitoids of the Batomga inlier of the southeastern Siberian Platform basement: age and geodynamic formation settings. Rus J Pac Geol 10: 168-188

Hayward CL, Reimold WU, Gibson RL, Robb LJ (2005) Gold mineralization within the Witwatersrand Basin, South Africa: evidence for a modified placer origin, and the role of the Vredefort impact event. Geol Soc London Spec Publ 248: 31-58

Heinrich CA (2015) Witwatersrand gold deposits formed by volcanic rain, anoxic rivers and Archaean life. Nature Geosci 8: 206-209

Kirk J, Ruiz J, Chesley J. Tilley S., Walshe, J. (2001) A detrital model for the origin of gold and sulfides in the Witwatersrand basin based on Re-Os isotopes. Geochim Cosmochim Acta 65: 2149-2159.

Kirk J, Ruiz J, Chesley J, Walshe J., England GA (2002) A major Archean gold- and crust-forming event in the Kaapvaal craton, south Africa. Science 297: 1856-1858

Mathur R, Ganert C, Ruiz J, Linton P (2013) Evidence for mixing of Re-Os isotopes at < 2.7 Ga and support of a remobilized placer model in Witwatersrand sulfides and native gold. Lithos 164-167: 65-73

Phillips GN, Powell R (2015) Hydrothermal alteration in the Witwatersrand goldfields. Ore Geol Rev 65: 245-273

Robb LJ and Meyer FM (1995) The Witwatersrand Basin, South Africa: geological framework and mineralization processes. Ore Geol Rev 10: 67-94

Vovna GM, Mishkin MA, Lennikov AM. Oktyabrskii RA, Polin VF. Badredinov ZG, Yasnygina TA (2014) Geochemistry and metamorphic parameters of rocks in the Batomga granite-greenstone terrane, Aldan Shield. Geochem International. 51: 968-980

ADAKITES, HIGH-NB BASALTS AND GIANT METAL DEPOSITS IN MAGMATIC ARCS

Kepezhinskas P.K.[1], Kepezhinskas N.P.[2]
[1]PNK GeoScience, Tampa, USA, pavel_k7@yahoo.com
[2]University of Florida, Gainesville, USA

Slab melting and associated mantle-wedge hybridization by felsic melts derived from metabasalt are widely recognized as common petrologic processes operating in modern and ancient magmatic arcs (Kepezhinskas et al., 1996; Martin, 1999; Yogodzinski et al., 2001; Proteau et al., 2001; Defant and Kepezhinskas, 2001; Widom et al., 2003). Typically melting of garnet amphibolite (metabasalt) in the downgoing slab to produce adakite is confined to young and, therefore, hot subduction zones associated with subduction of either young (< 30 Ma) oceanic crust or a spreading r/aseismic ridge. Later, other convergence-related tectonic settings have been recognized as plausible enviornments to trigger slab melting and adakite production. These "extended" adakite tectonic environments now include (Defant and Kepezhinskas, 2001; Yogodzinski et al., 2001); initial stages of subduction (subduction initiation – Phillipines), slower subduction (Bakening volcano, Kamchatka), flat subduction (Andes), oblique converegence (Japan), dissection of an "old" subduction system by a major fracture zone/transform fault (Grenada, Lesser Antilles), slab tear and warm-up of an old slab by mantle flow around the edge of a torn subducting plate (West Aleutians – Central Kamchatka). Petrological and geochemical features of adakitic magmatism are summarized in Table 1.

In many magmatic arcs, adakites are temporally and spatially associated with high-Nb basalts (Kepezhinskas et al., 1996; Defant and Kepezhinskas, 2001; Hastie et al., 2011; Kepezhinskas et al., 2017). Typical high-Nb basalts are olivine-clinopyroxene-plagioclase-phyric lavas that exhibit some OIB-like geochemical traits such as lack of negative Nb and Ta anomalies and generally alkaline character (they plot into trachybasalt field on TAS diagram).

However, their MORB-like Sr-Nd-Pb isotope signatures (Fig.1) preclude involvement of OIB mantle in their petrogenesis and suggest that high-Nb basalt magmas originate via melting of a previously depleted sub-arc mantle wedge

metasomatized by adakite melt. Under this scenario (Kepezhinskas et al.,1996; Defant and Kepezhinskas, 2001), both mantle wedge and metasomatizing slab melt share MORB-like isotope ratios but slab melt-mantle interaction results in crystallization of HFSE-rich phases (rutile, various spinels) in the hybrid mantle source which serves as a reservoir for Nb and Ta. Later-stage melting of such slab melt-hybridized source generates high-Nb basalt magmas that carry a unique combination of HFSE enrichments (reflecting petrogenetic processes) and MORB-like isotopic signatures (reflecting source characteristics). High-Nb basalts from Utila Island offer a direct evidence for adakite-induced mantle wedge metasomatism beneath the Northern Honduras recorded by presence of Na- and Al-rich siliceous glasses with high Sr contents (SiO_2=55.08-57.94 wt.%, Na_2O=4.97-5.72 wt.%, Sr=2700-3400 ppm).

Table 1. Main Petrologic and Geochemical Characteristics of Adakite

Adakite Features	Possible Interpretations
Abundant high- to low-pressure amphibole (megacrysts to phenocrysts)	Water in the source region/hydrous multi-stage fractionation
High SiO_2 content	Melting of basaltic source (garnet amphibolite or eclogite)
High Al_2O_3 and Na_2O content	High pressure partial melting of eclogite (Gr) or amphibolite (Pl)
High Sr and absence of negative Eu anomaly	Melting or lack of plagioclase in the residue
Low Yb and Y, high La/Yb and Sr/Y ratios	Garnet in the residue
High Zr/Sm	Amphibole fractionation
Low K/La, Rb/La, Ba/La, low $^{87}Sr/^{86}Sr$, low $^{206}Pb/^{204}Pb$, high $^{143}Nd/^{144}Nd$	MORB-like basaltic source
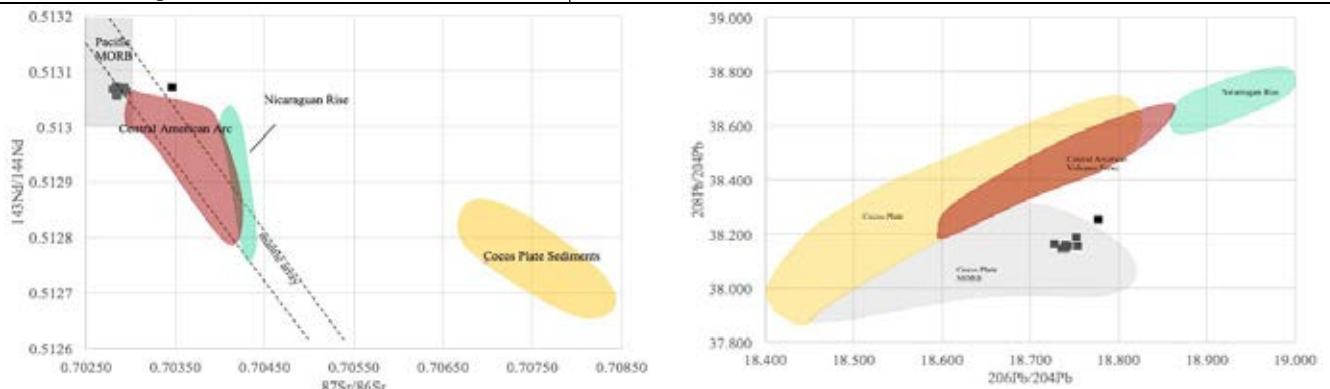
Fig. 1. Sr-Nd-Pb isotopic systematics of alkaline high-Nb basalts from Utila Island, Honduras, Central American arc – a classic high-Nb basalt locality in unusual back-arc setting.

Many authors documented clear spatial and temporal association with adakites and high-Nb basalts with base and precious metal mineralization in subduction zones (Mungall, 2002). In fact, some of the largest Cu (Au, Mo,Ag)—porphyry and epithermal deposits in magmatic arcs are ultimately associated with adakite and/or high-Nb basalt (Table 2).
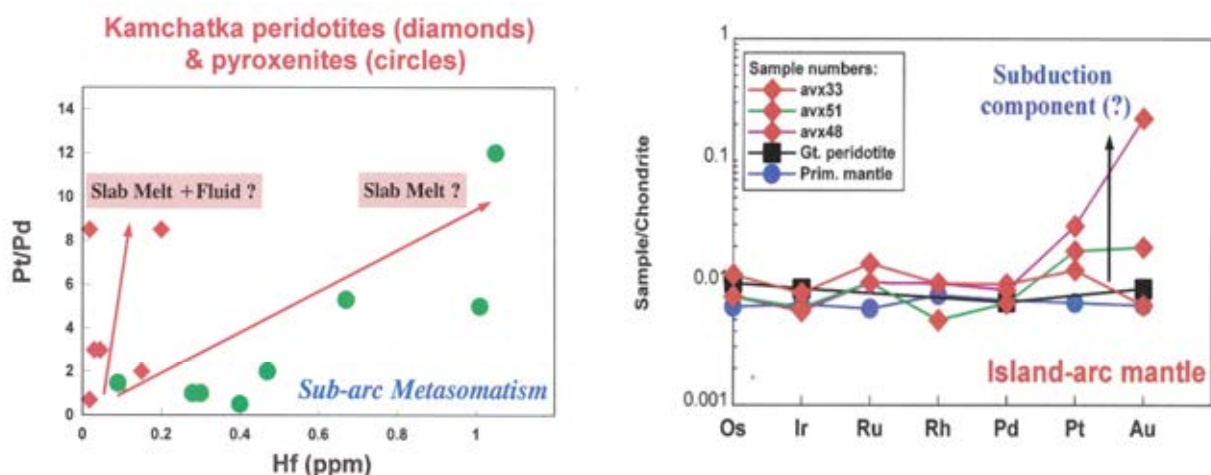
Fig. 2. Distribution and behavior of Platinum Group Elements in mantle wedge xenoliths from Kamchatka volcanic arc (Kepezhinskas et al., 2002). Platinum and gold enrichments reflected in elemental ratos are also confirmed by radiogenic Os isotope compositions of Kamchatka xenoliths consistent with large-scale metasomatism of sub-arc mantle wedge (Widom et al., 2003).

This spatial and temporal association (as illustrated in Table 2) is consistent with behavior of noble metals (Au and PGE) during sub-arc mantle metasomatism by hydrous slab melts (Defant and Kepezhinskas, 2001; Kepezhinskas et al., 2002). Data from slab melt-metasomatized mantle wedge xenoliths from Kamchatka arc clearly links levels of Au and Pt in mantle samples with degree of slab melt hybridization indicated, for example, by variations of Hf in Kamchatka

peridotite xenoliths (Fig. 2). Other HFSE elements such as Nb and Ta follow the same enrichment trend suggesting that the metasomatizing agent beneath Kamchatka as slab melt (adakite) not fluid which is characterized by extremely low solubility of all HFSE elements. This is also supported by formation of metasomatic Fe-Ti oxides and amphiboles (HFSE reservoira) as well as secondary sulfide (Au and PGE reservoir) in Kamchatka peridotite xenoliths.

Table 2. Giant ore deposits in magmatic arcs associated with adakites and high-Nb basalts

Deposit (Location)	Metal Resource	Age	Host Magmatic Rocks (Regional Tectonic Setting)
Mt. Kare (PNG)	42.5 Mt at 1.54 g/t Au	6 Ma	High-Nb basalts
Ladolam (Lihir Island, PNG)	29.7 Mt at > 1 g/t Au; geologic reserve of 43 Moz Au	1.5-0.18 Ma	High-Nb basalts intruded by K-adakites
Emperor (Fiji)	14.7 Mt at 8.1 g/t Au	3.8-4.8 Ma	High-Nb basalts intruded by K-adakites
Porgera (PNG)	51 Mt at 7 g/t Au	6 Ma	High-Nb basalts
Ok Tedi (PNG)	854 Mt at 0.64% Cu and 0.78 g/t Au	2.4-6.9 Ma	K-adakites intruded by late-stage, post-mineralization HNBs
Batu-Hijau (Sumbawa, Indonesia)	914 Mt at 0.53% Cu and 0.4 g/t Au	3.67-3.76 Ma	Adakites
Grasberg	700 Mt at 1.4% Cu and 1.8 g/t Au	2.7-3.3 Ma	Adakites, K-adakites
Santo Tomas II (Luzon, Philippines)	187 Mt at 0.24% Cu and 0.49 g/t Au	1.4-2.1 Ma	Adakites
Yanacocha (Peru)	> 70 Moz Au at 0.5 to 1.6 g/t Au	9.3-8.2 Ma	Adakites
El-Teniente (Chile)	20.731 Gt at 0.62% Cu, 0.019% Mo, 0.52 g/t Ag and 0.005 g/t Au	8.2-4.82 Ma	Adakites intruded by late-stage, post-mineralization HNBs

Adakites and high-Nb basalts are characterized by elevated Au and Cu contents although this is hardly a defining characteristic in their evident association with epithermal gold and porphyry copper mineralization in Pacific oceanic and continental arcs (Oyarzun et al., 2001). Gold and, to a certain extent, Pt are highly soluble in aqueous fluids especially in presence of chlorine and fluorine (Li and Audetat, 2013; Van den Bleeken and Koga, 2015). Adakites are hydrous melts (> 4 wt. H_2O) as illustrated by ubiquitous presence of amphibole and, as such, are excellent agents for gold mobilization during slab-mantle interactions (Mungall, 2002). Moreover, hydrous adakites are also highly oxidized magmas with oxidation state of > FMQ +1.3-2. It was proposed on this basis that early crystallization of magnetite from adakite melt will facilitate partitioning of gold and copper into ore-forming supercritical fluids (Sun et al., 2004). High sulfur (in excess of 1000 ppm) and chlorine contents will also assist gold and platinum incorporation into large-scale mineralization in modern volcanic arcs (Van den Bleeken and Koga, 2015). In addition, alkaline character of high-Nb basalts (they are essentially trachybasalts) and associated alkaline-chloride (possibly carbonated) aqueous fluids promote delivery of large volumes of noble metals into intra-crustal magma chambers. Thus, the entire magmatic plumbing system associated with "adakitic" arcs serves as a giant conduit that channels Cu-Au-Pt-enriched fluids into the evolving sub-arc crust. Local conditions in these crustal reservoirs (such as fluctuations in fluid pressure and temperature) will cause deposition of base and noble metals in epithermal and porphyry environments.

References:

Defant MJ, Kepezhinskas P (2001) Evidence suggests slab melting in arc magmas. EOS Trans Amer Geophys Union 82: 65-69

Hastie AR, Mitchell SF, Kerr AC, Minifie MJ, Millar IL (2011) Geochemistry of rare high-Nb basalt lavas: are they derived from a mantle wedge metasomatized by slab melts? Geochim Cosmochim Acta. 75: 5049-5072

Kepezhinskas PK, Defant MJ, Drummond MS (1996) Progressive enrichment of island arc mantle by melt-peridotite interaction inferred from Kamchatka xenoliths Geochim Cosmochim Acta 60: 1217-1229

Kepezhinskas P, Defant MJ, Widom E (2002) Abundance and distribution of PGE and Au in the island-arc mantle: implications for sub-arc metasomatism. Lithos. 60: 113-128

Li Y, Audetat A (2013) Gold solubility and partitioning between sulfide liquid, monosulfide solid solution and hydrous mantle melts: implications for the formation of Au-rich magmas and crust-mantle differentiation. Geochim Cosmochim Acta 118: 247-262

Martin H (1999) Adakitic magmas: modern analogues of Archaean granitoids. Lithos 46: 411-429

Mungall JE (2002) Roasting the mantle: slab melting and the genesis of major Au and Au-rich Cu deposits. Geology 30: 915-918

Oyarzun R, Marquez A, Lillo J, Lopez I, Rivera S (2001) Giant versus small porphyry copper deposits of Cenozoic age in northern Chile: adakitic versus normal calc-alkaline magmatism. Mineral Deposita 36: 794-798

Proteau G, Scaillet B, Pichavant M, Maury R (2001) Evidence for mantle metasomatism by hydrous silicic melts derived from subducted oceanic slab. Nature 410: 197-200

Sun W, Arculus RJ, Kamenetsky VS, Binns RA (2004) Release of gold-bearing fluids in convergent margin magmas prompted by magnetite crystallization. Nature 431: 975-978

Van den Bleeken G, Koga KT (2015) Experimentally determined distribution of fluorine and chlorine upon hydrous slab melting and implications for F-Cl cycling through subduction zones. Geochim Cosmochim Acta. 171: 353-373

Yogodzinski GM, Lees, JM, Churikiva TG, Dorendorf F, Woerner G, Volynets ON (2001) Geochemical evidence for the melting of subducting oceanic lithosphere at plate edges. Nature 409: 500-504

Widom E, Kepezhinskas PK, Defant MJ (2003) The nature of metasomatism in the sub-arc mantle wedge: evidence from Re-Os isotopes in Kamchatka peridotite xenoliths. Chem Geol 196: 283-306.

PETROGRAPHIC EVIDENCE OF MAGMA MIXING IN KYRDEM GRANITOIDS, NORTHEAST INDIA, MEGHALAYA

Kh Mohon Singh

Imphal College, Imphal, India; khuraijammohon@yahoo.co.in

The evidence of magma mixing in Kyrdem Granitoids (KG) is gathered from the field relations and petrographic studies in the field. Field and petrographic evidences strongly suggest that the microgranular enclaves (ME) represent mafic to hybrid coeval magma globules, which are mingled and undercooled into a partly crystalline, relatively cooler felsic host KG. Some of the ME contain K-feldspar megacrysts and smaller felsic-mafic xenocrysts, which appear more-or-less identical to that observed in felsic host KG except their crystal boundaries. Particularly the K-feldspar megacrysts in ME seem aligned in the direction of ME elongation and correlate well to those of felsic host KG, which must have attained in the semi-solidified conditions of ME and felsic melt. It is therefore suggested that both ME magma globules and partly crystalline felsic melt co-mingled in plutonic setting. The xenocrysts bearing ME in KG should represent hybrid product of felsic-mafic magmas. Ocellar quartz grains rimmed by fine mafic minerals and presence of mafic (biotite) and felsic (K-feldspar and plagioclase) xenocrysts in ME are indication of mechanical mixing forming the hybrid ME magma zone at deeper level. Abundant acicular apatites are ubiquitous in some ME, which can be formed when undercooling (quenching) of ME (hybrid) magma occurred against relatively cooler felsic host KG. Elongated ME and alignment of its constituting minerals in the direction of felsic KG magma flowage strongly suggest stretching of ME globules due to its partial molten state in felsic magma. It is more probable that enclave magma derived by melting of mantle or lower crustal rocks intruded into crustal derived felsic (KG) melt, and mixed to form the ME (hybrid) melt which later dispersed into relatively cooler felsic KG. Thus unlike ideal situation of a closed-system differentiation, magma mixing turns into an open system and the products are likely to be more diversified.

RIPHEAN MAGMATISM PRECEDING THE DISCLOSURE OF URAL PALEOOCEAN AND THE ORE GENESIS OF BASHKIR MEGANTICLINORIUM AS A REFLECTION OF RIFTING PROCESS GEODYNAMICS

Kholodnov V.V., Fershtater G.B., Shagalov E.S., Shardakova G.Yu., Kiseleva D.V.

Institute of Geology and Geochemistry, Ural Branch of the Russian Academy of Sciences, Ekaterinburg, Russia, holodnov@igg.uran.ru

The contemporary eastern edge of the East European Platform (EEP), being at the same time the western paleocontinental slope of modern Urals, is characterised by the repeated manifestation of epiplatform rifting processes ranging from the Lower to Middle Riphean, and reaching its highest rifting activity during the Middle Riphean. Vein, intrusive and other magmatic rocks of Middle-Riphean, aged 1395-1385 Ma, form a typical large igneous province (LIP) as understood by R. Ernst (Ernst, 2014), which formation is explained by the plume influence. Rocks of this stage have some common geochemical features, not contradicting their plume nature. The subsequent disclosure of the Middle Riphean grabens of Kuvash-Mashak rift repeats almost all the stages of continental crust destruction, preceding the formation of "sub-oceanic" structures, probably with almost complete rupture of the lithosphere continuity (metavolcanics of Nazyam rift). The composition of volcanic rocks and dyke swarms of Bashkir meganticlinorium (BMA) in this period, as well as the most typical intracontinental rift systems of the world, is characterised by the directed evolution of rock chemistry - from earlier, more alkaline and sub-alkaline varieties to the rocks substantially depleted by incoherent lithophile rare elements and potassium. The directed alteration of ore formation from the mantle titanomagnetitic and rare-metallic to barite-polymetallic deposits of sedimentary exhalative type (SedEx-type) (Maslov et al., 2001) is connected with this evolution.

Such evolution is especially pronounced in the rocks of the northernmost Kuvash graben. Here, in the east, late tholeitic volcanics occur (Nazyam metavolcanic strata), having the lowest content of potassium and associated incompatible rare elements. Nazyam amphibolites are compositionally close to the oceanic basalts of N-MORB type. The occurrence of such rocks is apparently determined by the fact that in the north of Kuvash-Mashak rift structure (in the eastern part of the Kuvash graben), the stretching of the continental crust was the most intense. This fact has defined the deep rift basin formation (Nazyam rift) with the graben floor depth not less than 20 km, and possibly deeper, as evidenced from the previously published petrological data (Fershtater et al., 2005; Kholodnov et al., 2006). Earlier (Karsten et al., 1997), based on the analysis of geochemical data on volcanics of Mashak suite, it was concluded that volcanism in BMA in the Middle Riphaean was not initially of a continental rifting nature, but corresponded to a highly thinned crust of suboceanic type.

In general, the entire range of the Middle Riphean magmatite compositions of BMA reflects a general evolution trend - from rocks having the geochemical parameters of E-MORB and OIB- type enriched mantle (trachybasalts of Ai suite, basalts of Mashak suite, trachybasalts of Sibirka, gabbronorites of Medvedevsky massif, etc.) to the rocks close to N-MORB - type (Nazyam amphibolites) (Fig. 1). It allowed an analogy to be drawn with the geodynamic settings, directly preceding and accompanying the disclosure of rift structures, such as the East African Rift, the Red Sea and the Gulf of Aden. However, the duration of existence of the Red Sea "oceanic" structure on the territory of BMA (Nazyam Rift) was not very long. As evidenced by the K-Ar dating of amphiboles from the most metamorphosed Nazyam volcanics, this structure had apparently closed in the age range of 1250-1150 million years.
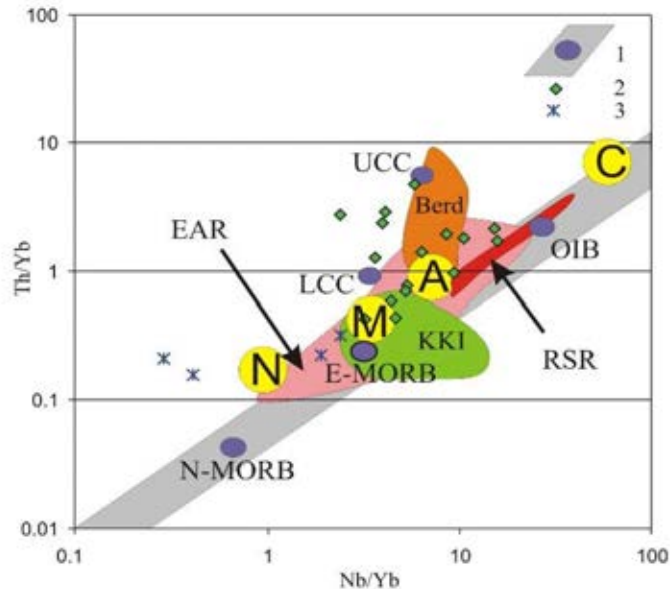
Fig. 1. Nb/Yb - Th/Yb correlation in igneous rocks of Bashkir meganticlinorium. 1 - Mantle sequence and points of mantle (N-MORB, E-MORB, OIB) and crustal (UCC and LCC - upper and lower continental crust) source average compositions; fields: RSR - Red Sea Rift; EAR - East African Rift, according to (http://georoc.mpch-mainz.gwdg.de/georoc/Start.asp); 2 - Dyke complexes; A - Ai suite; M - Mashak suite; C - Sibirka trachybasalts; N - mean value, and 3 - points of analysis of amphibolites from Nazyam mountains; KKI - gabbro-norite from massifs of Kusinsk-Kopan intrusion; Berd - gabbro from Berdyaush massif.

Perhaps this was due to the manifestation of one of the early stages of the Grenville tectogenesis, which traces are identified in some other structural material complexes of the western slope of the Urals (Krupenin, 2004; Petrov, 2016).

The evolution of petrochemical and geochemical characteristics of the Middle Riphean rocks of BMA towards MORB correlates with the evolution of isotope-geochemical data thus reflecting the increase over time of the degree of lithospheric mantle depletion. Mature pre-Riphean continental crust of BMA in grabens is converted into the crust of "suboceanic" type during the Lower and Middle Riphean.

The primary neodymium isotope ratios vary from negative values, indicative of mature magmatic rocks of the continental crust, to positive (+4 .. + 5 and higher), characterising the participation of igneous rocks (Nazyam metavolcanics) in the petrogenesis of mantle, which was already highly depleted during the process of rifting. Based on the analysing the data on the magmatic evolution of Ural's western slope in the Lower and Middle Riphaean, involving the data on neodymium and strontium isotope ratios of all subsequent steps of formation the Urals epioceanic orogen (1400-250 Ma), a conclusion can be drawn that, after passing the pre-rifting stage, Ural paleoocean could have started its active disclosure in the second half of the Middle Riphean. This was preceded by the formation of relatively small sized (such as within the boundaries of BMA) rift structures of the Red Sea type. Later, apparently, beginning since the age range of 1300-1200 Ma, similar primary "rifting-spreading" structures have been disclosed resulting in the formation of a large Ural Riphean-Vendian ocean to the east of the EEP. Long, relatively amagmatic period (1250-700 Ma), which is reflected in Fig. 2, apparently, characterises the long disclosure of this paleoocean to the east of EEP.

The above isotopic and age data on igneous rocks in the age interval of 1400-250 million years demonstrated that a large Wilson megacycle with duration of more than 1.0 billion years can be allocated in the Urals. This megacycle includes both the early stages of EEP epiplatform rifting in the age range of 1750-1300 Ma, and the subsequent stages of the most active disclosure of the Ural ocean (1300-700 million years), and its closure in the range of 700-250 Ma, accompanied by the new continental crust formation of the Ural epioceanic orogen.

The above observations are generally in a good agreement with the independent data on the history of the continental margin formation of the Ural paleoocean within the Kvarkush-Kamennogorsk meganticlinorium (in one of the marginal structures of the EEP), recently obtained by G.A. Petrov (Petrov, 2016; etc.).

Fragments of riftogenic basite-granite magmatism are also fixed in the further southern parts of the Central Ural uplift, adjoining the Main Uralian Fault (MUF) zone (Ufaley block, Urtalau zone). In the central part of the Ufaley block, granite-gneisses and associated amphibolites (as a part of Egustin and Slyudyanogorsk suites) are geochemically close to the riftogenic formations of the Middle Riphean BMA (Kholodnov et al., 2006; Shardakova et al., 2005; Shardakova, 2015). This fact is in agreement with the occurrence of magnetite-hematite-ilmenite deposits and ore manifestations in the eastern part of the Ufaley block, such as Antsiferovskoe, Maukskoye, Zakharovskoe, Teplogorskoe and Kurtinskoe, which represent metamorphosed analogs of titanomagnetite and ilmenite ores that are referred to Kusa type in the Southern Urals. The presence of such Fe-Ti mineralisation, compositionally similar to the Middle Riphean BMA deposits, in the metamorphosed basalts of the Ufaley block, is an independent argument in favour of the spatial, age and genetic relation of the described above structural-formational megazones of the western slope of the Southern Urals (BMA,

Ufaley, and, probably, some others). It is noteworthy, that within the boundaries of the Ufaley block adjacent to the BMA, the age of 579-533 Ma (Rb-Sr, Ar-Ar) and a ratio of $^{87}Sr /^{86}Sr = 0.703389$ was determined for the gneiss-granites of the Nikolsky massif. It implies that the fraction of the depleted mantle substance in the substrate was significant at this stage (Shardakova 2015).
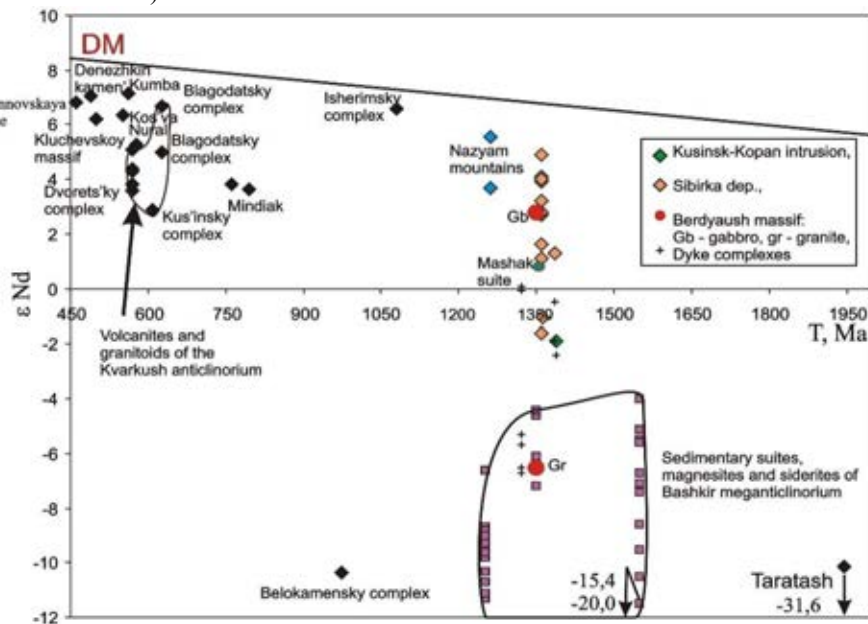
Fig. 2. The T-εNd diagram in the range of 2000-450 Ma for igneous, ore-metasomatic and metamorphic complexes of the Middle and Southern Urals.

Apparently, the eastern boundary of the Middle Riphean rifting manifestations in the marginal part of the EEP could be further withdrawn to the East. The fragments of the microcontinental Riphean riftogenic structures also might be found among the asynchronous island arc-oceanic terranes of the eastern slope of the Urals, that later were connected to the EEP outskirts. The fragments of oceanic and island arc Late Riphean-Vendian rocks occur, for example, in the Maksyutov eclogite-glaucophane complex, their presence is presumed in Sysert-Ilmenogorsky massif as well (Krasnobaev et al., 1998; Puchkov 2010). Vendian Lushnik suprasubduction volcanogenic-sedimentary complex dated 590 Ma (zircon in rhyolite tuffs) is isolated in the Kazakh part of the Southern Urals (Ebetin zone). The formation of the Vendian volcanic rocks of the Lushnikov suite in the suprasubduction setting on the active continental margin (Ryazantsev, 2016; Samygin et al., 2010), as well as finding the timanids on the EEP polar margin, also supposes the presence of the ocean to the east of the EEP in the Late Proterozoic and Vendian.

The ideas about the initial disclosure time of the Ural Ocean and formation of one of its continental margins (the eastern periphery of the EEP), based on new factual data, are consistent with a number of concepts (Zonenshayn et al., 1990; Samygin et al., 2010; Scarrow et al., 2001; etc.), which also substantiate the existence of the ocean basin to the east of the EEP during the Riphean, Vendian, Early and Middle Paleozoic.

References:

Ernst RE (2014) Large Igneous provinces. Cambridge University Press

Karsten LA, Ivanov KS, Maslov AV et al. (1997) The nature of the Mashak volcanogenic-sedimentary association of the Bashkir anticlinorium: new geochemical data. The Riphean of Northern Eurasia. Geology. General problems of stratigraphy. Ekaterinburg: UB RAS, pp 155-165

http://georoc.mpch-mainz.gwdg.de/georoc/Start.asp

Kholodnov V. V, Fershtater GB, Borodina NS, Shardakova GYu, Pribavkin SV, Shagalov ES, Bocharnikova TD (2006) Granitoid magmatism of the Ural and the East European Platform juncture zone (Southern Urals). Lithosphere. 3:3-27

Krasnobaev AA, Davydov VA, Cherednichenko NV (1998) Zircon geochronology of the Ilmenogorsk suite. Ezhegodnik-1997

Krupenin MT (2004) Mineragenic and geodynamic significance of the Middle Riphean time on the western slope of the Southern Urals. DAN 399: 4:503-505

Maslov AV, Krupenin MT, Gareyev EZ, Anfimov LV (2001) Riphean of the western slope of the Southern Urals (standard sections, sediment- and lithogenesis, minerageny, geological monuments of the nature). T.1 IGG UB RAS, Ekaterinburg

Petrov GA (2016) Geology of the pre-Palaeozoic complexes of the middle part of the Ural mobile belt. Autoref ... doctor geol.-min. Sciences. Ekaterinburg

Puchkov VN (2010) Geology of the Urals and the Cis-Urals (relevantl issues of stratigraphy, tectonics, geodynamics and metallogeny). Dauria, Ufa

Ryazantsev AV (2016) Vendian suprasubduction magmatism in the south of the Uraltau zone (Southern Urals). In: Geology, minerals and problems of geoecology of Bashkortostan, the Urals and adjacent territories: Materials and reports

/ 11th Interregional Scientific and Practical Conference, dedicated to the 65th anniversary of the Institute of Geology, Ufa Science Center, Russian Academy of Sciences, Ufa, May 17-19, 2016. DesignPress, Ufa, pp 21-23

Samygin SG, Belova AA, Ryazantsev AV, Fedotova AA (2010) Fragments of the Vendian Convergent Margin in the Southern Urals. DAN. 432:5: 644-649

Scarrow JH, Pease V, Fleutelot C, Dushin V (2001) The late Neoproterozoic Enganepe ophiolite, Polar Urals, Russia: an extension of the Cadomian arc. Precambrian Research. 110: 255-275

Shardakova GYu (2015) New data on the Rb-Sr age of granites of the Nikolsky Massif (Ufaley block). Lithosphere. 4: 90-93

Shardakova GYu, Shagalov ES, Ronkin YuL., Lepikhina OP, Popova OYu (2005) Rb-Sr age and geochemistry of intrusive granitoids of the Ufaley zone (S. Ural). DAN. 405: 6:799-803

Fershtater GB, Kholodnov VV, Pribavkin SV, Borodina NS, Bocharnikova TD (2005) Riftogenic magmatism and ore mineralization of the Southern Urals. Geology of ore deposits. 47:421-443

Zonenshayn LP, Kuzmin MI, Natapov LM (1990) Tectonics of lithospheric plates of the USSR territory. Book. 1. Nedra, Moscow.

COPPER MINERALIZATION IN TSOGTTSETSII STUDY AREA

Kim In Joon
Korea Institute of Geoscience and Mineral Resources, Daejeon, Korea

Tsogttsetsii area, an intrusive complex associated with Cu porphyry mineralization, is located in the South Gobi, Mongolia. The largest porphyry-type deposits are the Devonian porphyry-Cu-Au deposits of Oyu Tolgoi, Tsagaan Suvarga, Kharmagtai, Shuteen in South Mongolia. Porphyry deposits formed in an island or a continental arc environment and are associated with calc-alkaline porphyry stocks, intruded volcanic and granitoid rocks in island arc or orogenic series in continental arcs. We performed the cross gechemical and extended exploration survey in Tsogttsetsii area. Cu mineralization in Tsogttsetsii area is porphyry Cu type related with alkali granite intruded in Late Carboniferous to Early Permian.

To comparative of the correlation porphyry copper deposits (after Enkhjargal et al., 2014) in Tsogttsetsii study area, The granitic rocks divided in to three groups by T.A.S diagram : Groups (I)-syenite, syeno-diorite, diorite, (II)-granodiorite, granite, (III)-granite; (I)-gabbro, gabbrodiorite, diorite, (II)-granodiorite, granite, (III)-granite, and belongs to metaluminous, I-type, continental and island arc type granites, metaluminous, I-type granites rather than S-type granites and continental and island arc type granites by A/CNK-A/NK diagram, and also to high-potassic calc-alkaline to shoshonite series, medium potassic calc-alkaline and high-potassic calc alkaline by SiO_2/K_2O diagram.

In the concentrated occurring to malachite appears extensively prophylitic alteration zone having a chlorite and epidote. As results of the survey, Cu contents of potable XRF and of chemical composition foe altered rocks ranges 1.08 to 18.3% in the 30 points and 1.08 to 32.9% in the 13 points, respectively.

Ore minerals identified in XRD analysis and polarizing microscope that samples of copper oxides were composed mainly of malachite, azurite, permingeatite and cuprite and the other minerals are pyrite, chalcopyrite, pyrargyrite, dickite, calcite, chlorite and epidote (Fig. 4). Mineralization can be considered occurring to selectively some granite of the surrounding aplite and faults in the only lower part coming up the hydrothermal solution of the remaining residual magma after the aplite intrusion. In conclusion, our study area formed in the continental and island arc type granites related magmatism. This is in accordance with the tectonic development characteristics of porphyry copper type deposits in Southern Mongolia.

References

Davaasuren, O.E., Lee, B.H., Kim, I.J.,· Ryoo, C.R., Heo, C.H. (2016) Characteristics of the Copper Mineralization in Tsogttsetsii Area, Mongolia, Journal of the Mineralogical Society of Korea, v.29, p.23-34.

Goldenberg, V.I. and Sanjaadorj, D. (1978) Geological mapping scale 1:200,000 on territory of Omnogovi, Dundgovi and Dornogovi aimaks. Ulaanbaatar, Ministry of Geology of Mongolia, open file Report No. 2724 (in Russian).

Jamiyandorj, O. and Zoljargal, A. (2010) Geological map of Mongolia, Ikh luusiin uul sheet K-48-V (1 : 200,000 scale). Mineral Resources Authority of Mongolia (in Mongolian).

Korea Institute of Geoscience and Mineral Resources (KIGAM) (2015) Exploration and Potential Evaluation of Overseas/North Korea/Arctic circle Mineral Resources. Ministry of Science, ICT & Future Planning, GP2015-033-2015(1) (in Korean).

Lee, B.H., Park, G.S., Kim, I.J., Lee, G., Heo, C.H., and Koh, S.-M. (2012) Characteristics of Fe-Mn Mineralization in Ugii Nuur and Tamir Gol, Mongolia. Journal of the Mineralogical Society of Korea, 25, 313-322 (in Korean with English abstract).

Lee, B.H., Park, G.S., Kim, I.J., and Heo, C.H. (2015) Resource Estimation of Ugii Nuur Fe-Mn Occurrence Area, Mongolia. Journal of the Mineralogical Society of Korea, 28, 1-7 (in Korean with English abstract).

Yoo, B.C. and Koh, S.-M. (2011) Rare Earth Elements Resources and Mushgai Khudag Deposit in Mongolia. Journal of the Mineralogical Society of Korea, v.24, p.55-62. (in Korean with English abstract).

CONDITIONS OF EPITHERMAL VEIN AND MASSIVE SULFIDE OREBODY FORMATION AT BOR (SERBIA)

Klimentyeva D.N., Heinrich C.A., Von Quadt A.

ETH Zurich, Zurich, Switzerland, dina.klimentyeva@erdw.ethz.ch

The origin of massive sulfide deposits containing a high sulfidation Cu±As±Au assemblage and their link to the porphyry copper systems has been debated for more than 50 years, with the role of seawater, submarine vs subaerial deposition and stratovolcanoes vs collapsed calderas being the central questions (e.g. Sillitoe, 1983; Stix, 2003). Sites of massive enargite- or covellite-bearing sulfide bodies include within zones of advanced argillic alteration, vuggy silica caps and the boundary between propylitic to argillic alteration zones. The Bor deposit is the largest example of an ore system where both porphyry copper mineralization (Borska Reka deep underground) and high-sulfidation orebodies are present as both veins and massive sulfide ore-bodies in the open pit and shallow underground mines.
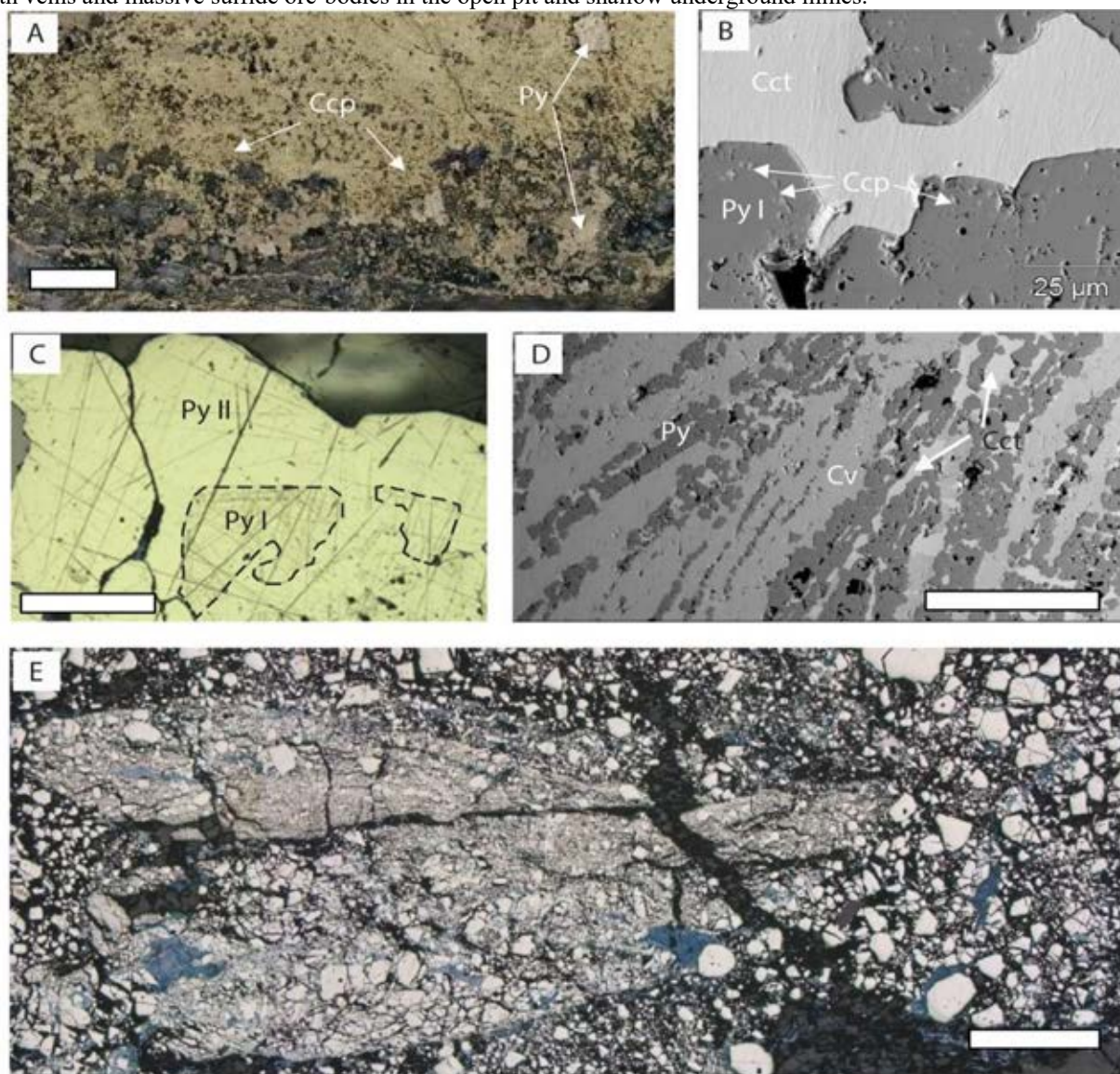
Fig. 1. Ore textures at Bor: A) Pyrite + chalcopyrite equilibrium texture, lower part of T massive sulfide orebody. Hand sample, scale bar = 1 cm. B) Cu-poor core of pyrite followed by chalcopyrite inclusions at the core edge, overgrown by a rim of Cu-rich pyrite. BSE image, sample B-77 from upper levels of Tilva Ros massive sulfide orebody, C) Two generations of pyrite, Cu-poor core and Cu-rich rim, high sulfidation epithermal vein from Borska Reka in plane polarized light. D) Chacocite and covellite blades overgrown by late generation, Cu-rich pyrite. BSE image, sample B-77 from upper levels of Tilva Ros massive sulfide orebody. E) Brecciated pyrite, high sulfidation epithermal vein from Borska Reka in plane polarized light. All scale bars except in (A) and (B) are 500 μm. Abbreviations: ccp – chalcopyrite, cct – chalcocite, cv – covellite, py – pyrite

The Bor metallogenic zone is hosted within the Timok magmatic complex, which is located in the Serbian part of the Apuseni-Banat-Timok-Srednogorie belt. It contains sixteen ore fields comprising porphyry copper, high- and low-

sulfidation epithermal deposits, with total resources estimated at 20 Mt Cu and 1000 t Au (Jelenković et al., 2016). Volcanic activity that formed the Timok magmatic complex occurred during the Turonian age of the Late Cretaceous epoch.

The ore-bodies at Bor are hosted entirely by early stage Timok andesites, including lavas and pyroclastic rocks. Diorite porphyry dykes 50-150 m wide were documented at deeper levels of Borska Reka (Janković et al., 1980). Shallower, small-scale porphyry dykes are present in the central part of Borska Reka. The Bor conglomerates are outcropping to the East of Bor deposit and at deep levels of Borska Reka; they contain clasts of andesite with advanced argillic alteration. However, no ore fragments have been found in conglomerates, hence it is suggested that the orebodies were not eroded at the time of the conglomerates' formation (Jelenković, 2002). Resources estimate for the Bor metallogenic zone amounts to 20 million tons of Cu and 1000 tons of Au (Jelenković et al., 2016)

Mineralization at Bor is contained in veins and in 30 to 50 m isometric massive sulfide ore-bodies (Tilva Ros, T, T1 and T2). Earliest, sinuous A-type veins are cross-cut by B-type quartz-pyrite($\pm$chalcopyrite) veins and pyrite paint veins, which are in turn cross-cut by D-type pyrite-quartz veins and late alunite veins.

Massive sulfide ore from the T orebody contains at least two generations of pyrite: first as replacement of amphibole and biotite phenocrysts, second as rims around the phenocrysts and pervasive replacement of the matrix. Variable degree of the preservation of initial textures is observed, depending on local heterogeneity of the andesite and possibly compaction/welding degree of the volcanic rock within the same unit.

Alteration in the closest proximity of the massive sulfide ore bodies is advanced argillic, grading into sericitic and propylitic style alterations, with chlorite present as a distal phase. Massive sulfide veins with mineral assemblage similar to massive sulfide orebodies cross-cut early A-type sinuous quartz and B-type quartz-pyrite veins related to Borska Reka.

Based on ore textures, we establish the following sequence of mineral assemblages for the high-sulfidation epithermal veins and massive sulfide orebodies:

1. Early pyrite, sometimes with chalcopyrite ($\pm$ bornite) inclusions, that later gets brecciated and resorbed. Chalcopyrite and pyrite co-exist in equilibrium in the lower levels of T orebody (fig. 1. A, E).
2. Chalcocite is not in equilibrium with earlier generations of pyrite, but overgrows early pyrite and is present as inclusions in later stage pyrite (fig. 1, B).
3. Covellite overgrowing earlier brecciated pyrite and displaying equilibrium textures. Rim of Cu-rich pyrite overgrowing early, Cu-poor pyrite (fig. 1, C).
4. Latest stage - covellite and fine-grained pyrite overgrowing covellite blades (fig. 1, D).

References:

Janković, S., Terzic, M., Aleksic, D., Karamata, S., Spasov, T., Jovanovic, M., & Antonijevic, I. (1980). Metallogenic features of copper deposits in the volcano-intrusive complexes of the Bor District, Yugoslavia. European Copper Deposits. SGA Spec. Publ, 1, 42-49.

Janković, S., Jelenković, R., & Koželj, D. (2002). The Bor copper and gold deposit. QWERTY, Bor, 298.

Jelenković, R., Milovanović, D., Koželj, D., & Banješević, M. (2016). The Mineral Resources of the Bor Metallogenic Zone: A Review. Geologia Croatica, 69(1), 143-155.

Sillitoe, R. H. (1983). Enargite-bearing massive sulfide deposits high in porphyry copper systems. Economic Geology, 78(2), 348-352.

Stix, J., Kennedy, B., Hannington, M., Gibson, H., Fiske, R., Mueller, W., & Franklin, J. (2003). Caldera-forming processes and the origin of submarine volcanogenic massive sulfide deposits. Geology, 31(4), 375-378.

GEODYNAMIC REGIME OF THE CARBONATITES (ABSOLUTE PALEOTECTONIC RECONSTRUCTIONS)

Kogarko L.[1], Veselovskiy R.[2,3]
[1]Vernadsky Institute of Geochemistry and Analytical Chemistry of the Russian Academy of Sciences, Moscow, Russia;
[2]Lomonosov Moscow State University, Moscow, Russia;
[3]Institute of the Earth Physics of the Russian Academy of Sciences, Moscow, Russia

Carbonatites is several percent prevalence alkali formations, however, they have a very high potential for strategic metals, such as, for example, niobium and rare earths. Currently, the entire international market of niobium and rare earth carbonatite deposits controlled by large - Baiyun Obo (China), Araxa (Brazil) and many others. etc. The analysis of existing databases. (Kogarko et al, 1995, Woolley and Kjarsgaard, 2008;. Frolov et al, 2003) shows that the vast majority of carbonatite is located on the continent and is confined to ancient cratons. A small number of carbonatites developed on oceanic islands - Canaries, islands of Cape Verde, the island of Kerguelen (Woolley and Kjarsgaard, 2008).

Geodynamic conditions of formation of carbonatites are still being actively discussed. Some researchers consider carbonatites in close connection with the rise of large volumes of deep mantle material from the core, lower mantle (Ernst, 2010). Indeed, the observed association of carbonatites with large igneous provinces (LIPs), the genesis of which, according to most researchers (Ernst, 2014 references therein), to determine the activity of mantle plumes. Our data showed that some of the world's largest carbonatite of the world, located in the North of Siberia (Maimecha-Kotuiskaya province Gulinskii array) formed synchronously with the Siberian superplume- with the age 250 MA (Kogarko, Zartman,

2008) and are confined to the marginal zone Siberian Permo-Triassic traps. Carbonatites also well represented in the major alkaline provinces: East African Rift Zone, Cretaceous-Parana Etendeka, Cretaceous-Paleogene Deccan and others. Nevertheless, it should be noted that not all large magmatic events associated with carbonatite and alkaline magmatism.

Studies isotope geochemistry carbonatites (Kramm, 1993; Bell, 2001) have shown that the sources of these species contains components FOZO, EM1, HIMU, DMM (Nelson et al, 1988; Kogarko and Zartman, 2008; Ruchklov et al., 2015) are typical of the mantle source of basalts of oceanic islands (OIB). Geochemistry of noble gas isotopes of carbonatites also confirms their relationship with the deep mantle reservoirs (Tolstikhin et al., 2002). Found carbonates as inclusions in diamonds of a lower (Kaminsky et al., 2015) may also serve as proof of the possibility of generating carbonatite melts on the border of the lower mantle-core, probably in D" layer (Kaminsky et al., 2015).

However, the experimental study of equilibria with CO_2 at high temperatures and pressures corresponding to the thermodynamic conditions of deep zones of the lower mantle, are ambiguous. Mathematical modeling of reactions involving carbon (Kaminsky et al., 2015) and experimental studies (Dasgupta and Hirschman, 2006) do not confirm the likelihood of the formation of the equilibrium carbonate melts at great depths, mainly as a result of a very low oxidation potential of oxygen deep zones of the lower mantle. At the same time, quantitative modeling of partial melting of rising from the deep zones of the mantle protolith in conditions with elevated CO_2 potential (Collerson et al., 2010), as well as experimental work on phase equilibria of carbonates in the conditions corresponding to the transition zone of the lower mantle-core (Dalou et al., 2009; Walter et al, 2008), clearly showed the possibility of the formation of carbonatite melts at depths corresponding to the core-mantle boundary.

One problem with the adoption of the model due carbonatites with deep mantle plumes is the development in the lithospheric mantle metasomatized and carbonated zone. A large number of publications shows that these phenomena are developed in the continental lithosphere (Ionov, 1998, Kogarko et al., 2007), and in the ocean (Kogarko et al., 1995). On the basis of these data it has been hypothesized occurrence of carbonatite melts as a result of the partial melting of carbonated mantle lithosphere.

In our view, the rise of deep mantle protolith (plume) causes partial melting as a result of adiabatic decompression at depths of about 200-300 km. This process is accompanied by the release of large amounts of volatile components, mainly CO_2, H_2O, and melts, characterized by very small degrees of melting protolith, which are the main agents of carbonate metasomatism lithospheric mantle.

The main objective of the present article is to identify regularities of manifestations Phanerozoic magmatic carbonatite in relation to the largest global areas of low seismic velocities in the lower mantle (LLSVP, Large Low Shear-wave Velocity Provinces) which are considered as gigantic mantle plumes.

Objects and Methods

It is well known that the lowest mantle contains large density heterogeneities, which represent considerable thickened areas of the D'' transitional layer (up to 500-600 km in height). In Russian literature, these density anomalies usually called "hot fields" (Zonenshain and Kuzmin, 1997), but now the most used term is the Large Low Shear-wave Velocity Provinces (LLSVPs). Many scientists believe that these structures play an important role in the global geodynamics and can be responsible for episodes of the true polar wander (TPW), assembly and breakup of the supercontinents, working of geodynamo and so on. Moreover, Kuzmin et al. (2011) showed that the evolution of the Siberian within-plate magmatism at the Paleozoic-Mesozoic boundary could be correlated with the processes in the LLSVP.

According to the modern point of view (Torsvik et al., 2010, 2014, and many others), there are three LLSVPs in the lowest mantle. Two of them are the most famous and the largest: the first one is located under Africa and named after John Tuzo Wilson "Tuzo", the second LLSVP is placed under western part of the Pacific Ocean and named "Jason" after Jason Morgan. These two LLSVPs have 8-10 thousand kilometers in diameter each and are located in the equatorial plane, almost symmetrically to the mass center of the Earth. The third LLSVP is much smaller than "Tuzo" and "Jason" and its projection falls in the European part of Russia; this LLSVP named "Perm" after Russian city Perm. Attenuation of S-waves in LLSVPs explains by increased temperature of their matter relative to the surrounding mantle (Torsvik et al., 2010).

It was shown (Torsvik et al., 2010), that there is a spatial correlation between the modern and reconstructed locations of the Large Igneous Provinces (LIPs) and kimberlites and a projection of the contour of 1% S-waves attenuation, called Plume Generation Zone (PGZ). It is important, that this contour corresponds to the highest temperature gradient between LLSVP and the mantle. Recently, using by assumption about long-term stability of the LLSVPs relative to the mantle, the absolute plate kinematic model for the whole Phanerozoic time was suggested (Domeier and Torsvik, 2014). According to this model, in total about 80% LIPs and kimberlites are located above PGZ.

In this study, we used the data about 180 Phanerozoic carbonatite magmatism manifestations from the world. We also used the absolute plate kinematic model (Domeier and Torsvik, 2014), GPlates 1.4 software (Williams et al., 2012) and EarthByte model of the finite rotations (Muller et al., 2008) to reconstruct their initial position in the past with a resolution at 10 million years. Paleogeographic reconstructions were made with using the Euler poles, calculated for main continental lithospheric plates for the 140-540 Ma time interval and corrected for TPW (Domeier and Torsvik, 2014; Torsvik et al., 2014).

Discussion

Using by our own carbonatite database and Phanerozoic absolute plate kinematic model (Domeier and Torsvik, 2014), positions of the carbonatite magmatism manifestations for the last 500 Myr were reconstructed in coordination

with LLSVPs' projections onto the Earth's surface (Fig. 1). Analysis of these reconstructions allows us to conclude, that 118 (66%) of all Phanerozoic carbonatites are projecting to the central or peripheral areas of the African LLSVP ("Tuzo"): it can be viewed as an evidence for their mantle plume origin. On the contrary, significant part (17%) of the Phanerozoic carbonatites (for instance, from China and Kola Peninsula) were located above the zones of increased S-waves speed (Fig. 1) at the time of their origination. An absence of the carbonatites, originated above the Pacific LLSVP ("Jason"), is a striking illustration of the importance of the thick and old continental lithosphere for birth of the carbonatite melts. It also confirms the permanent presence of the oceanic lithosphere in this area (at least during the last 500 Myr), where the carbonatite manifestations are quite rare.
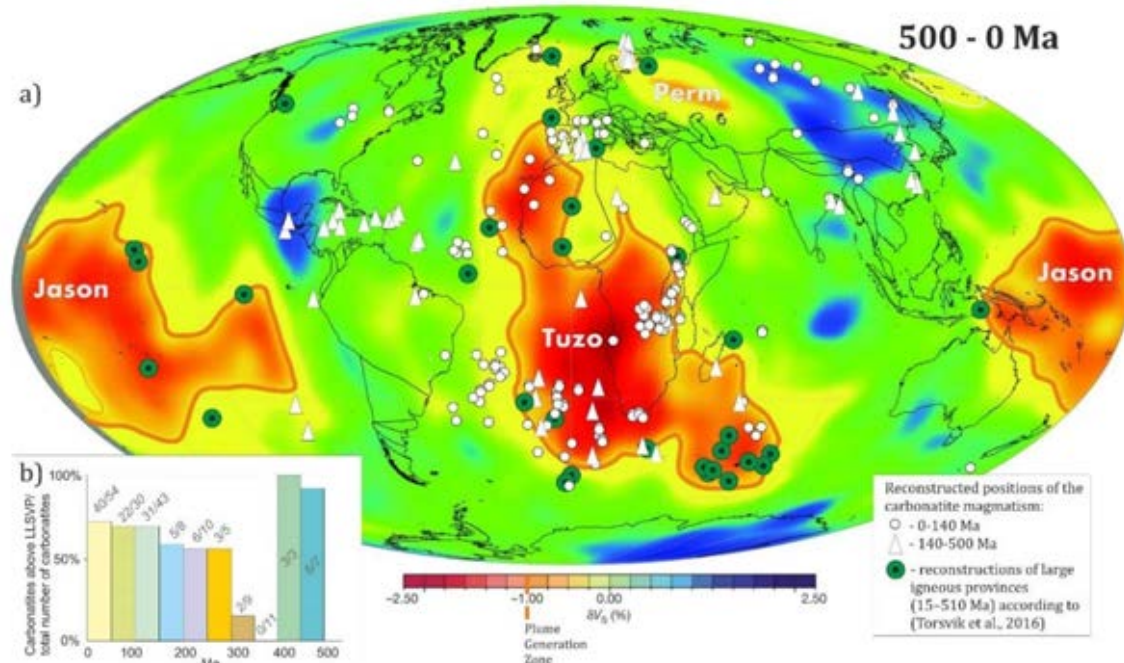
Kogarko and Veselovskiy, Fig. 1

Comparison of the reconstructions on Fig. 1, presented in this work, and Fig. 1 from the paper (Torsvik et al., 2010) let us to conclude, that the reconstructed positions of the carbonatites, LIPs and kimberlites, which are related to the African LLSVP, coincide. This can be resulted from a genetic similarity of these magmatic formations, but it should be noted that kimberlites, as distinct from carbonatites, did not appear above increased S-waves anomalies in the lowermost mantle. The same is true and for LIPs, which formed above LLSVP only. This feature can be connected with special physical and/or chemical (geodynamic?) conditions of the carbonate magmas creation as opposed to the kimberlites, alkaline and tholeiite continental basalts. It is important, that significant number of the "anomalous" carbonatites (for example, Devonian carbonatites in Fennoscandia), according to the paleotectonic reconstructions were formed in the central parts of the supercontinents or supercratons, where we can expect the additional sources of heat from radioactive decay or endogenous heat flow screening, which is necessary for creation of the carbonate magmas.

Unfortunately, our conclusions are not so reliable for the Paleozoic time, because they are based on limited number of carbonatites with the ages between 250-500 Myr (35 objects) comparable with Cenozoic and Mesozoic ones (145 objects).

Conclusions

Place of the carbonatite magmatism manifestations in the system of global absolute paleotectonic reconstructions confidently show their link with plume generation zones in the lowest mantle. This conclusion can be considered as an argument for the deep mantle source of carbonate magmas. At the same time, about 30% of carbonatites were formed far from LLSVPs, that makes possible to assume their shallow (lithospheric) origin.

References:

Becker T.W., Boschi L. A comparison of tomographic and geodynamic mantle models // Geochem. Geophys. Geosyst. 3, 1003, doi:10.1029/2001GC000168 (2002).

Bell K. Carbonatites: relationships to mantle-plume activity. In. Ernst RE, Buchan KL (edit) Mantle plumes: their identification through time // Geological Society of America, Special Paper. 2001. 352. 267–290.

Collersona K.D., Williamsb Q., Ewarta A.E., Murphyc D.T. Origin of HIMU and EM-1 domains sampled by ocean island basalts, kimberlites and carbonatites: The role of CO2-fluxed lower mantle melting in thermochemical upwellings 2010 // Physics of the Earth and Planetary Interiors 2010. 181. 112–131.

Dalou C., Koga K.T., Hammouda T., Poitrasson F. Trace element partitioning between carbonatitic melts and mantle transition zone minerals: Implications for the source of carbonatites // Geochim Cosmochim Acta 2009. 73(1). 239-255.

Dasgupta R. and Hirschmann M.M. Melting in the Earth's deep upper mantle caused by carbon dioxide // Nature. 2006. 440. 659–662.

Domeier M., Torsvik T.H. Plate tectonics in the late Paleozoic // Geoscience Frontiers. 2014. 5. 303-350.

Ernst R.E. & Bell K. Large igneous provinces (LIPs) and carbonatites // Miner Petrol. 2010. 98. 55–76.

Ernst R.E. Large Igneous Provinces. Cambridge University Press. 2014. 666 p.

Frolov A.A., Tolstov A.V., Belov S.V., Carbonatite Deposits of Russia. NIA-Priroda, Moscow 2003. (494 pp, in Russian).

in Peridotite Xenoliths from Alkali Basalts JOURNAL OF PETROLOGY 1998 11-12,1931-1941

Ionov D. Trace Element Composition of Mantlederived Carbonates and Coexisting Phases

Kaminsky F.V., Ryabchikov I.D., Wirth R. A primary natrocarbonatitic association in the Deep Earth. Mineralogy and Petrology. 2015. DOI 10.1007/s00710-00015-00368-00714.

Kaminsky, F.V., Ryabchikov, I.D., McCammon, C.A., Longo, M., Abakumov, A.M., Turner, S., Heidari, H., 2015. Oxidation potential in the Earth's lower mantle as recorded by ferropericlase inclusions in diamond // Earth Planet. Sci. Lett. 417. 49-56.

Kogarko L.N., Henderson C.M.B., Pacheco H. Primary Ca-rich carbonatite magma and carbonate-silicate-sulphide liquid immiscibility in the upper mantle // Contrib. Mineral. Petrol. 1995. V. 121. P. 267-274.

Kogarko L.N., Kononova V.A., Orlova P., Woolley A.R., Alkaline Rocks and Carbonatites of the World. Part Two: Former USSR. March, Chapman & Hall, 1995, 224pp

Kogarko L.N., Kurat G., Ntaflos T., Henrymeyerite in metasomatised upper mantle of Eastern Antarctica, Can. Mineralogist 45, 2007, 497-501

Kramm U. Mantle components of carbonatites from the Kola Alkaline Province, Russia and Finland: A Nd - Sr study // Eur. J. Mineral. 1993. 5. 985-989.

Kuzmin M. I., Yarmolyuk V. V., Kravchinsky V. A. Phanerozoic Within-Plate Magmatism of North Asia: Absolute Paleogeographic Reconstructions of the African Large Low-Shear-Velocity Province // Geotectonics, 2011, Vol. 45, No. 6, pp. 415–438.

Müller R.D., Sdrolias M., Gaina C. and Roest W.R. Age, spreading rates and spreading asymmetry of the world's ocean crust, Geochemistry, Geophysics, Geosystems, 2008. 9, Q04006, doi:10.1029/2007GC001743.

Nelson D.R., Chivas A.R., Chappell B.W., and McCulloch M.T. Geochemical and isotopic systematics in carbonatites and implications for the evolution of ocean-island sources // Geochimica et Cosmochimica Acta. 1988. 52. 1–17.

Rukhlov A., Bel K.l., and Amelin Y. Symposium on critical and strategic materials // British Columbia Geological Survey Paper. 2015. pp. 39-64.

Tolstikhin I.N., Kamensky I.L., Marty B., Nivin V.A., Vetrin V.R., Balaganskaya E.G., Ikorsky S.V., Gannibal M.A., Weiss D., Verhulst A., Demaiffe D. Rare gas isotopes and parent trace elements in ultrabasic-alkaline-carbonatite complexes. Kola Peninsula: identification of lower mantle plume component // Geochim Cosmochim Acta. 2002. 66. 881–901.

Torsvik T.H., Burke K., Steinberger B., Webb, S.J., Ashwal L.D. (2010): Diamonds sampled by plumes from the core-mantle boundary. - Nature, 466, 7304, 352-355, 10.1038/nature09216.

Torsvik T.H., Van der Voo R., Doubrovine P., Burke K., Steinberger B., Ashwald L.D., Trønnes R.G., Webb S.J., Bull A.L. Deep mantle structure as a reference frame for movements in and on the Earth // Proceedings of the National Academy of Sciences of the United States. 2014. V.111. N.24. P.8735-8740.

Torsvik T.H., Steinberger B., Ashwal L.D., Doubrovine P.V., Trønnes R.G. Earth evolution and dynamics – a tribute to Kevin Burke // Can. J. Earth Sci. 53: 1–15 (2016) dx.doi.org/10.1139/cjes-2015-0228.

Walter M. J., Bulanova G. P., Armstrong L. S., Keshav S., Blundy J. D., Gudfinnson G., Lord O. T., Lennie A. R., Clark S. M., Smith C. B. and Gobbo L. Primary carbonatite melt from deeply subducted oceanic crust. Nature. 2008. 454. 622–625.

Williams S., Müller R.D., Landgrebe T.C.W., Whittaker J.M. An open-source software environment for visualizing and refining plate tectonic reconstructions using high resolution geological and geophysical data sets // In: GSA Today. 2012. 22. No. 4/5. DOI: 10.1130/GSATG139A.1.

Woolley A.R., and Kjarsgaard B.A., Carbonatite occurrences of the world: map and database // Geological Survey of Canada, Open File 5796, 1 CD-ROM plus 1 map. 2008.

Zonenshain L.P., Kuzmin M.I. Paleogeodynamics. The Plate Tectonic Evolution of the Earth. AGU. Washington, D.C., 1997. P.220.

EVIDENCE FOR MANTLE HYDRATION BY PHLOGOPITE METASOMATISM BENEATH ARKHANGELSK DIAMONDIFEROUS PROVINCE

Kolesnichenko M.V.[1,2], Zedgenizov D.A.[1,2], Shchukina E.V.[1,2], Litasov K.D.[1,2]

[1]Institute of Geology and Mineralogy, Siberian Branch of the Russian Academy of Sciences, Novosibirsk, Russia, m.kolesnichenko@igm.nsc.ru

[2]Novosibirsk State University, Novosibirsk, Russia

Olivine is major mineral of peridotites and may be an important host of hydrogen in the Earth's upper mantle, and the OH abundance in this mineral defines many important physical properties of the planet's interior [Bell et al., 2003]. It

is widely known that mantle olivine samples could contain different amounts of water from minimal to the maximal water storage capacity [Schmädicke et al., 2013]. Peridotite xenoliths from V. Grib kimberlite pipe (Arkhangelsk diamondiferous province, Russia) have been studied in order to identify metasomatic alteration and water enrichment.

The incorporation of hydrogen in olivine of mantle xenoliths from V. Grib kimberlite pipe was investigated by infrared spectroscopy. IR spectra were collected in the OH stretching region on oriented single crystals using a conventional IR source at ambient conditions. The preparation of samples for IR included several stages. First, we selected most transparent fragments of minerals with no optically or macroscopically visible inclusions or cracks. Then, we determined the orientation of minerals by observing interference figures using a petrographic microscope. Finally, each fragment was fixed on a glass slide with Crystalbond thermoplastics and then double-side polished using abrasive clothes. Olivine grains were analyzed twice in two perpendicular orientations with the polarizer parallel to the optical indicatrix. Absorption bands due to O-H vibrations in olivines of V. Grib peridotite xenoliths are located between 3700 and 3100 cm^{-1}.

a   *b*
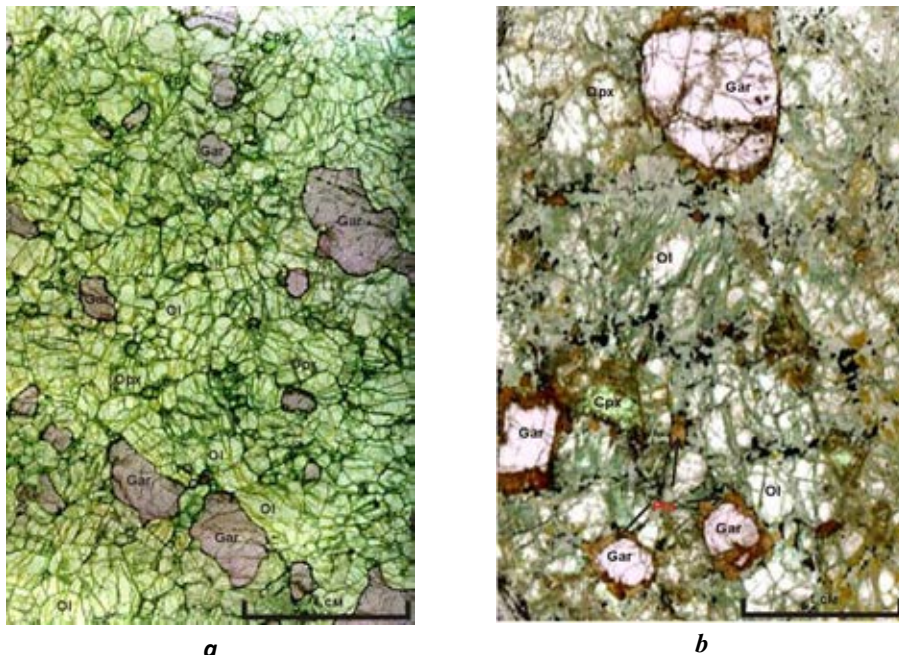
Fig. 1. Photographs of peridotites. a, garnet lherzolite; b, phlogopite-garnet lherzolite.
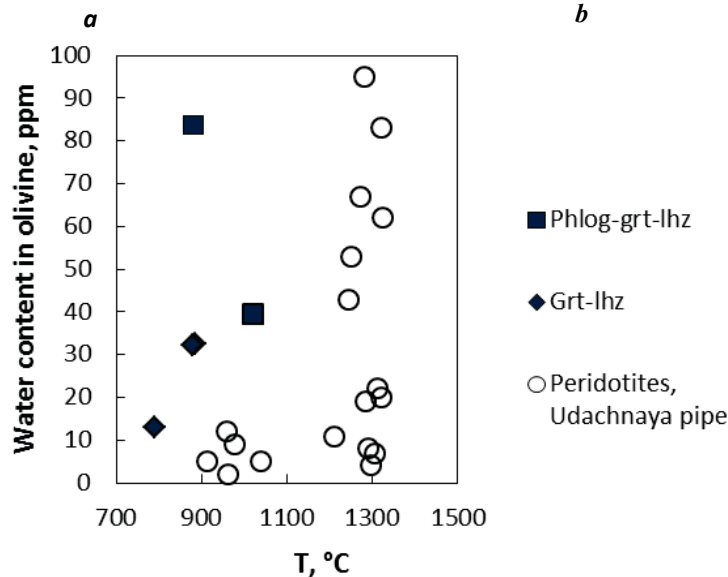
Fig. 2. Olivine water content vs. temperature calculated using [Brey & Koehler, 1990].

The samples are divided into two groups: garnet lherzolites and phlogopite-garnet lherzolites (Fig.1). The peridotites of both groups are of two structural varieties: protogranular and transitional from protogranular to porphyroclastic. Olivines from garnet lherzolites are characterized by higher Mg# 92.2-92.6 compared with olivines from phlogopite-bearing xenoliths (Mg# 90.9-91.5). Water content in olivines decreases with increasing magnesium number Mg#. The calculated equilibration temperatures [Brey & Koehler, 1990] for studied lherzolites vary from 790 to 1020 °C (Fig.2). This correlation were not previously observed in olivines from peridotites of Udachnaya kimberlites (Yakutia, Russia), where high- and low-temperature trends differ by water content [Kolesnichenko et al., 2017]. The higher water content is found in olivines from low-temperature phlogopite-garnet lherzolites from V.Grib pipe, 39-84 ppm. Higher amounts of water in phlogopite-garnet lherzolite may indicate an enrichment caused by phlogopite metasomatism.

References:

Bell, D.R., Rossman, G.R., Maldener, J., Endisch, D., Rauch, F. (2003). A quantitative determination of the absolute amount and calibration of the IR spectrum. J. Geophys. Res., 108: B2, 2105

Brey, G.P., Koehler, T. (1990) Geothermobarometry in four-phase lherzolites II. New thermobarometers, and practical assessment of existing thermobarometers. J. Petrol., 31, 1353-1378.

Kolesnichenko M.V., Zedgenizov D.A., Litasov K.D., Safonova I.Yu., Ragozin A.L. (2017) Heterogeneous distribution of water in the mantle beneath the central Siberian Craton: Implications from the Udachnaya Kimberlite Pipe. Gondwana Res. http://dx.doi.org/10.1016/j.gr.2016.09.011.

Schmädicke, E., Jürgen, G., Witt-Eickschen, G., Brätz, H. (2013). Hydroxyl incorporation and mineral composition. Am. Min., 98: 1870-1880.

LI-F GRANITES ASSOCIATED WITH A-TYPE GRANITES, SOUTH KARELIA: SOME GEOCHEMICAL FEATURES, PHYSICAL-CHEMICAL CONDITIONS OF FORMATION

Konyshev A.A.[1,2]

[1]Vernadsky Institute of Geochemistry and Analytical Chemistry of the Russian Academy of Sciences, Moscow, Russia;
[2]Institute of Experimental Mineralogy, Chernogolovka, Russia, icelopa@gmail.com

The study of the physico-chemical formation conditions of Li-F rare-metal granites is necessary to understand their transition from the magmatic to the postmagmatic stage of mineral formation, the processes leading to the formation of deposits specialized in Sn, W, Mo, Ta, Nb, Li, Be.

The studied rocks are located in Pitkaranta ore field, in the northwestern area of the Salmi pluton. The body of the pluton is submerged in this place under the metasedimentary Proterozoic layers. Li-F granites exposed on the surface are satellites of the Uuksu stock of Li-F granites, the stock itself is not available for direct observation.

The Salmi pluton located at the junction of the Karelian craton and the paleoproterozoic crust belongs to the anorthosite-rapakivigranite association. Salmi pluton contains a wide variety of rocks from gabbros and anorthosites to biotite leucogranites and topaz-bearing Li-F granites. According to the data on the age of rocks obtained by isotopic methods it was established that they had intruded sequentially in a short period of time, 1547-1530 million years ago (Neymark et al., 1994, Amelin et al., 1997). Considered Li-F granites are the latest intrusive phases. A low oxygen fugacity was detected for the early intrusive phases of the Salmi pluton with presence of fayalite and ilmenite. The latest granite intrusions were formed at high oxygen fugacity.

The temperatures of homogenization of melt inclusions in topaz-bearing granites of the Uuksu stock (the sample of core from a depth of 265 m,) (Poutiainen and Scherbakova, 1998) show the following: at a minimum pressure of 200 MPa the temperature of solidus is 640-680 and liquidus 770-830 °C. At the earliest stages of crystallization magma was not saturated with water (3 wt.%), but the final melt was water-saturated.

As a result of the fieldwork the stone material of the Li-F granites (satellites of the Uuksu stock), topaz-bearing leucogranites (near the Hopunvaara), as well as earlier intrusive granite phases and metasedimentary rocks of the frame was collected. The composition of the samples was studied by XRF (IGEM RAS) and ICP-MS (IMGRE, standard decomposition and decomposition with preliminary fusion with Li metaborate). Compositions of micas were investigated by RSMA (IEM RAS) and LA-ICP-MS (IGEM RAS) methods. Outcrop of Li-F granite is located on the crossing of the railway track by a road near the village UUKSU (Sal4). Granite solidus of Sal4 was determined by melting of the sample powder on the "High pressure device" and a "gasbomb" (IEM RAS), by the methodic of Weidner (Weidner and Martin, 1987).

The investigated body of Li-F granites has a layered texture and heterogeneous structure - mostly fine-grained, but also coarse-grained - pegmatoid, minerals contain "gel-like" inclusions. According to other authors, "colloids" also took part in the formation of the pegmatites and Li-F granites (Peretyazhko, 2010).

The regular increase of the gross amount of Ta occurs with the increase in the degree of crystalline differentiation of granites at the closing to the final stage (Fig. 1), reaching 39 ppm in the Sal4 and 70 ppm in the Sal12.

In the granite rocks considered in this work, the M-type tetrad effect is observed (Irber, 1999) (Fig.2 a,b). The tetrad effect - is a violation of the smooth distribution of REE, which leads to its separation in to the form of a "zigzag" curve into four parts (tetrads): La-Nd, Sm-Gd, Gd-Ho and Er-Lu (Fidelis, Siekierski, 1966). This effect is associated with the complexation in an aqueous environment involving an incompletely filled electron f-shell. The appearance of the tetrad effect is positively correlated with the removal of Eu, accumulation of Ta, the decrease of the Zr/Hf value (Sal4 - 5,6), and is probably due to the increase of the amount of F and water in the magma, and the decrease of the solidus temperature.

Ovoid amphibole-biotite and biotite, as well as equigranular biotite granites are characterized by the predominance of light lanthanides over heavy ones, significant values of the tetrad effect are not observed.

The distinctive feature of Leucogranites is the predominance of heavy normalized lanthanides over light ones, LREE / HREE ≤1, while the normalized Er-Lu are at the level of concentrations in the earliest granite phases. The increase of the concentration of heavy lanthanides in the magma of leucogranites may be connected with their introduction by

means of an F-containing fluid (Balashov, 1976, Wood, 1990). This can be realized by boiling magma from a deeper source or by separating the fluid from the melt after crystallization of less evolutionarily advanced granites with a higher solidus temperature.
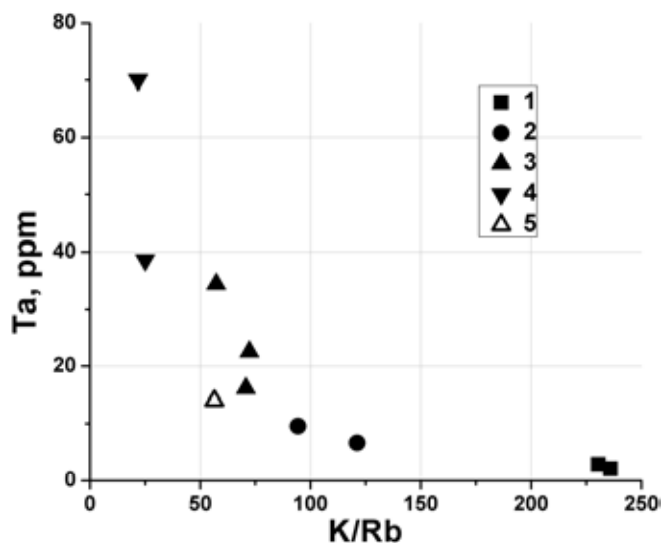
Fig. 1. Ta concentration in the rocks of Salmi pluton in dependence with K/Rb ratio, reflecting the evolutionary grade of granitic rocks (Alexandrov, 1980).
1 - Early phases, piterlites and ovoid biotite granite: Sal1, Sal2
2 – Equigranular biotite granite: Sal10, Sal19
3 – Leucogranite: Sal15, Sal16, Sal17
4 – Li-F granite: Sal4, Sal12
5 - Li-F granite: 403-13 (Larin, 2011)

The host metasedimentary Proterozoic rocks (Sal9 and Sal13), near the contact with (Sal4 and Sal14), have a sharply distinct REE spectrum: the absence of an Eu negative anomaly, a significant total tetrad effect is not observed. This can be interpreted as the accumulation of heavy REEs in granites during the magmatic stage.

Li-F granites keep, as well as in the earlier granite phases, the predominance of light lanthanide contents over heavy lanthanides. In contrast to earlier phases, the leucogranites – like addition of HREE in Li-F granites is observed. The distinctive feature of Li-F granites is the depletion of all rare-earth elements in comparison with earlier phases. In Fig. 2-A the REE spectra from literature sources are also shown. Sample 403-13 is almost identical to the Sal4 sample, while Sal12 is even more lean in all of the REEs, which is similar to the pattern observed in the rapaki- granite stock of Euraioki (a sample of topaz-containing rhyolites 97/IH/67 (Haapala, 1997)). The stock of Euraoki is a satellite of the rapikivigranite batholite Laitila (southwestern Finland), formed, like the Salmi pluton, during the uprise of rapakivigranitic intrusive magmatism on the East European platform.
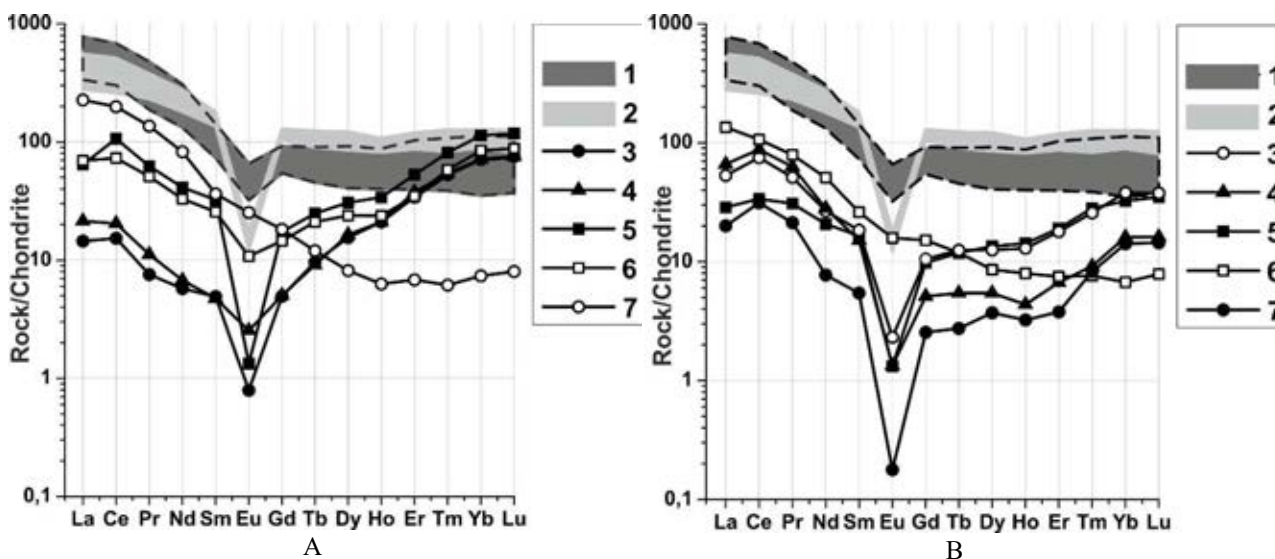
Fig. 2. Spectra of REE of Salmi Pluton granitic rocks normalized to chondrite (Andres and Grevese, 1989).
1 – Early phases, piterlites and ovoid biotite granite: Sal1, Sal2; 2 – Equigranular biotite granite: Sal10, Sal19
A – Hopunvaara. Leucogranite: 3 – Sal15, 4 – Sal16, 5 – Sal17; 6 – aplite vein, Sal14; 7 - biotite gneiss Sal13 (host-rock for Sal14).
B – Uuksu: Li-F granites: 3 – Sal4, 4 – Sal12, 5 – 403-13 (Larin, 2011), 7- 97/IH/67 (Haapala, 1997); 6 – biotite gneiss Sal9 (host-rock for Sal4).

As a result of experiments on the melting of Li-F granite powder (Sal4) it was established that the temperature of the water-saturated solidus at 200 MPa is 570 ºC, and 640 ºC in "dry" condition (in OH-containing minerals contains about 0.6% by weight of water).

The mica from selected samples of granites belong to siderophyllite - Li-siderophyllite - zinnwaldite sequence (from piterlite to Li-F granites). It was defined by geological observation, mica was formed at the final stages of crystallization. Mica compositions calculations were carried out by using program "PetroExplorer". Using geofluorimeters for mica (Aksyuk, 2002), the author's determination of solidus temperature of 570-640°C for Li-F granites (Sal4), published data for temperatures of piterlite formation and equigranular biotite granites 830°C (Larin, 2011), the following concentrations of M HF (M - mol/dm^3) in the fluid were obtained: piterlites 0.02 M, biotite equigranular granites 0.047 M, Li-F granites 0.24-0.34 M. But as the temperature of mica formation was not determined, the values obtained for the concentration of fluorine in fluid should be considered preliminary.

Conclusions:

The concentration of fluorine in the magmatic fluid from the piterites to the Li-F granites increased by 1.7 orders of magnitude with the maximum estimate, but was lower than for the Ta-Nb deposits in the Eastern Transbaikalia - 0.43 M HF at Orlovka and 0.73 and Etyka Ta-Nb deposites (Aksuyk, 2009). From the solidus of Li-F granites of the Uuksu stock to the final formation of its apophyses, the temperature had to drop by at least 70 °C, to 570 °C.

References:

Aksyuk A.M. (2002) Experimentally-validated geofluorimeters and fluorine regime in granite fluids. Petrology. v. 10, № 6. pp. 628-642

Aksyuk A.M. (2009) Fluorine regime in deep hydrothermal fluids and near-surface waters (experimental studies), abstract of the thesis for the degree of Doctor of Geological and Mineralogical Sciences, GEOKHI RAS (in russian)

Aleksandrov I.V. (1980) Geochemistry of dispersed and ore elements in granitoids. Nauka, Moscow, 198 pages (in russian)

Amelin Yu.V., Larin A.M., Tucker R.D. (1997) Chronology of multiphase emplacement of the Salmi rapakivi granite-anorthosite complex, Baltic Shield: implications for magmatic evolution. Contrib Mineral Petrol v127: pp. 353-368

Andres E., Grevese N. (1989) Abundances of the elements: meteoritic and solar. Geochimica et Cosmochimica acta, v 53 pp. 197-214

Balashov Yu.A. (1976) Geochemistry of rare-earth elements. Nauka, Moscow, 267 pages (in russian)

Irber W. (1999)The lanthanide tetrad effect and its correlation with K / Rb, Eu / Eu *, Sr / Eu, Y / Ho, and Zr / Hf of evolving peraluminous granite suites. Geochimica et Comochimica Acta. v.63, No.3 / 4, pp. 489-508

Haapala I. (1997) Magmatic and Postmagmatic Processes in Tin-mineralized Granites: Topaz-bearing Leucogranite in the Eurajoki Rapakivi Granite Stock, Finland. Journal of petrology, v. 38, №12, pp.1645-1659

Fidelis I., Siekierski S. (1966) The regularities in stability constants of some rare earth complexes. Journal of Inorganic and Nuclear Chemistry, №28, pp.185-188

Larin A.M. (2011) Rapakivi Granits and associative rocks. Nauka, St. Petersburg, 402 pages (in russian)

Neymark L.A., Amelin Yu.V., Larin A.M. (1994) Pb-Nd-Sr isotopic and geochemical constrains on the basis of 1.54-1.56 Ga Salmi Rapakivi Granite-Anorthosite Batolith (Karelia, Russia). Mineralogy and petrology, v.50, pp.173-193

Peretyazhko I.S. (2010) Processes of formation of miarolic granitic pegmatites. Abstract of the thesis for the degree of Doctor of Geological and Mineralogical Sciences, Irkutsk (in russian)

Pontiainen M, Scherbakova T. F. (1998) Fluid and melt inclusion evidence for the origin of idiom orphic quarz crystal in topas-bearing granites from the Salmi batholith, Karelia, Russia. Lithos. v.44, pp.141-151

Weidner, J. R., Martin R.F. (1987) Phase equilibria of a fluorine-rich leucogranite from the St. Austell pluton, Cornwall // Geochimica et Cosmochimica Acta, v.51, pp.1591-1597

Wood S.A. (1990) The aqueous geochemistry of the rare-earth elements and yttrium, 2. Theoretical predictions of speciation in hydrothermal solutions to 350°C at saturation water vapor pressure. Geol. v. 88, pp.99-125.

NATIVE IRON FROM BASITES AND ITS GEOCHEMISTRY

Kopylova A.G.

Diamond and Precious Metal Geology Institute of Siberian Branch Russian Academy of Sciences, Yakutsk, Russia, Kopylova@diamond.ysn.ru

Large occurrences of native iron are known from basites in Disco Island (Greenland), Europe (Germany), and the Djaltul, Khungtukun, Khininda and Maimecha intrusions in the northern Siberian platform, Krasnoyarsk Territory (Bird, Weathers, 1977, Oleinikov et al., 1985, Ulff-Moller, 1977) . Native iron occurs as nodular segregations of tabular and rounded form, commonly 20-50 cm across, rarely forming large blocks. The weight of the iron nodules varies from hundreds of grams to a few hundred kilograms. In the Khungtukun intrusion, iron nuggets weighing 60, 150 and 250 kilograms have been found. One of the rock exposures revealed a native iron block with its protruding portion weighing as much as10 tons. Native iron segregations occur in bedrocks and placers, sometimes having a large areal extent.

In accordance with structure, several morphological types of the metallic phase can be distinguished. The sideronitic type is formed by large iron drops making up 30-40% of the rock volume. The spongy-textured type is represented by a single metallwork consisting of small iron drops which constitute more than 60-80% of the rock volume. The massive type results from intimate connection of minute iron drops which amount to 80-90%. In the case of complete coalescence of individual iron drops we have nuggets, but they are rare in occurrence.

Table. Chemical composition of native iron (wt. %, ppm; in the basites Au, PGE - ppb)

№ проб	Ni%	Co%	Au	Ag	Pt	Pd	Rh	Os	Ir	Ru	Ge	Cu%
					Native iron with the massive texture of nodule							
6-29Д	2,90	0,57	3,23	0,56	3,85	17,0	1,17	0,0095	0,016	0,37	200	0,99
10Б-8а	3,21	0,74	5,25	0,36	3,68	5,25	2,56	0,14	0,18	1,36	660	0,71
10Б-4а	4,35	0,95	6,25	0,22	7,78	14,6	3,43	0,096	0,14	1,92	450	0,40
34Д-1	3,43	0,77	4,60	0,35	7,8	22,2	2,48	0,21	0,19	3,72	390	0,46
35Б-15	4,32	1,28	6,85	0,56	4,4	20,3	4,80	0,33	0,30	3,99	450	0,63
					Native iron with the sideronitic texture of nodule							
81-14	2,13	0,68	2,38	0,34	3,43	1,09	0,97	0,055	0,094	0,31	240	
10Б-5а	3,34	0,84	3,94	0,21	4,12	18,5	1,09	0,0072	0,008	0,02	240	0.40
10Б-19	3,01	0,72	3,55	0,65	1,61	1,9	0,48	0,0061	0,0046	0,13	250	0,82
10А-21	3,53	0,96	3,23	0,19	2,42	5,15	1,47	0,031	0,026	0,20	270	1,02
11А-27	2,50	0,63	1,69	0,35	4,00	8,70	0,30	0,031	0,04	0,33	180	0,12
34-15с	2,4	0,48	1,86	0,20	0,71	13,1	0,34	0,029		0,34	88	0,59
					Native iron with the spongy texture of nodule							
35-9н	0,96	0,22	0,33	0,36	1,09	0,89	0,98	0,007			100	0,42
48-3а	0,10	0,02	0,01	0,03	0,15	0,16	0,03	0,0018	0,0022	0,012	5,7	0,17
48-4а	0,91	0,09	0,32	0,13	0,37	0,96	0,17	0,024	0,013	0,094	28	0,34
49-17	0,99	0,20	0,54	0,52	0,71	4,2	0,40	0,045	0,039	0,42	32	0,54
42-37	0,11	0,06	0,24	0,60	0,40	0,25	0,01	0,0030	0,0031	0,037	9,1	0,41
45-8а	0,06	0,02	0,15	0,19	0,09	0,13	0,01	0,26			13	0,19
Basites	219	50	3,7	0,19	14	16	2	1,9	2,8	13	1,4	210
					Iron meteorites							
Elʼga	8,18	0,49	2,22	1,5	28,8	3,7	1,5	5,81	4,39	11,9	72	
Tobychan	7,70	0,58	1,45	0,36	56,7	2,5	1,2	8,92	6,72	14,6	75	
Dolguchan	6,52	0,46	0,45	0,11	18,3	1,2	5,2	28,6	24,8	26,5		

№ проб	As	Sb	W	Ga	Th	U	La	Sm	Eu	Tb	Yb	Lu
					Native iron with the massive texture of nodule							
6-29Д	148	8,62	0,004	5,18	11,6	4,65	0,65	0,26	0,35	13,1	0,79	0,13
10Б-8а	642	25,3	0,007	2,1	9,9	4,13	2,90	0,095	0,68	6,18	0,91	0,28
10Б-4а	770	34,3	0,009	5,18	4,21	2,40	3,40	1,69	0,35		0,31	0,29
34Д-1	607	20,2	0,016	5,3	16,5	7,10	2,13	0,14	18,1	10,9	2,58	0,038
35Б-15	1539	17,9	0,01	8,15	31,9		5,40	0,19	0,26			0,2
					Native iron with the sideronitic texture of nodule							
81-14	405	18,0	0,012	2,67	8,44	1,9	3,1	0,2			1,21	0,14
10Б-5а	793	40,7	0,018	6,9	17,1	6,1	0,68	0,35	0,8		0,71	
10Б-19	608	46,6	0,008	6,05	25,5	3,5	3,59	0,56	1,92		1,02	0,12
10А-21	851	57,8	0,01	5,37	23,2	1,5	6,23	1,54	0,67		0,61	0,049
11А-27	382	27,1	0,032	5,79	9,78	8,8	0,77	0,76	0,75		0,79	0,11
					Native iron with the spongy texture of nodule							
48-3а	119	5,84	0,006	3,39		3,54	1,01	0,17		1,96		0,056
48-4а	207	16,3	0,004	3,46	3,22	2,0	0,5	0,17	1,38	0,79	1,78	0,28
49-17	50,6	3,26	0,002	1,02	1,73	2	0,15	0,033			2,04	0,019
42-37	43	6,07	0,002	3,39	1,93	0,7	0,7	0,076		2,73	0,5	0,052
Basites	18,9	3,25	0,32	5,79	0,87	1,1	6,45	2,96	1,39	0,22	3,24	0,28
					Iron meteorites							
Elʼga	21,0	1,08	0,005	0,82		2,2	20,4	0,79			1,27	0,79
Tobychan	12,2	0,47	0,003	3,61		5,0	1,57	0,18			0,16	1,11
Dolguchan	7,75	1,17	0,034	0,45		1,9	8,8				1,84	

The dominant mineral in the nodules is native iron. Nickel is the principal admixture element. Iron nodules from the Djaltul and Khungtukun massifs have average Ni contents of 2% and 1%, respectively. In the Djaltul intrusion we discovered iron grains with as much as 5-7% Ni. This value corresponds quite exactly to that in a meteorite mineral kamacite. In association with kamacite, two more high-Ni phases, known earlier only in meteorites, have been found.

These are taenite γ – (Ni, Fe) with Ni content of 26-32% and tetrataenite (Fe, Ni) containing up to 45-50% Ni. In the Khininda and Maimecha bodies, the native iron phase is represented by ferrite with Ni content no higher than tenths of a fraction of percent.

The nodules may contain subordinate amounts of cohenite and troilite. On the periphery, a rim of accessory sulfide mineralization (chalcopyrite, cobalt pentlandite, cubanite, bornite, chalcosine, and mackinawite) is present. In association with native iron there are also found exotic for terrestrial conditions meteorite minerals such as schreibersite (Fe_3P) and armalcolite (Mg, Fe) Ti_2. Iron is able to concentrate many elements that can form solutions in liquid and solid metal. Subsequent exsolution produces a number of intermetallides – tetrataenite and Co_2Fe, Ni_3Sn, and Ni_3Sn_2 phases identified in the native iron nodules. Cu is poorly soluble in iron, and therefore it forms an independent phase – nickel copper, containing 0.9-2.5% Ni. It is present in the nodules as an auxiliary mineral, forming spherules in the Fe-phase or it occurs in association with troilite or cohenite.

The aim of this work is to study, based on considerable analytical material (> 85samples), distribution of rare elements in native iron from basites. The table shows representative analyses of samples. Geochemical analysis of native iron showed the presence of gold and platinum-group elements in concentrations hundreds and even thousands of times higher than in the enclosing silicate rocks. These values are close to those found in iron meteorites. Average contents of noble metals in native iron from different intrusions differ greatly. Rather high concentrations are observed in the Ni-bearing native metal mineralization of the Djaltul and Khungtukun massifs as compared with Ni-depleted iron of the Khininda and Maimecha massifs. The amounts of rare elements in different types of the Fe-phase range widely. Maximum values of noble elements are found in massive nuggets (ppm):7.4 Au, 12.9 Pt, 22.2 Pd, 4.8 Rh, 4.00 Ru, 0.33 Os and 0.30 Ir. They also have the highest contents of nickel. There is a relationship between the size of iron drops in the nodules with sideronitic and spongy textures and the concentration of rare elements in them: The larger the size of the drops the higher the Ni contents and the total amount of microelements. Minimum values of Ni and microelements are specific for the spongy-textured nodules. Strong correlation is only established between Ni and Au. Pt, Pd, Rh and Ru also show a trend towards accumulation in the Ni-rich Fe-phase. No relationship is found between the Ni content and the amounts of Ag, Cu and Os in the nodules. Silver shows more or less even distribution in native iron from different massifs. In some samples it is not found at all. Its concentration in the host basites and in the Fe-phase is within the same range of 0.1-1.5ppm. This suggests the lack of high Ag accumulations in the metallic phase of the basic rocks. Silver is quite insoluble in iron, and most likely forms small emulsion segregations, as does copper.

Comparison between the Au, Ag and PGE contents in the metallic phase of terrestrial basites and in iron meteorites showed that their Au ranges and the average Au contents are quite the same. Their Pd and Rh concentrations are similar too. However, in contrast to meteorites in which the Pt/Pd ratio always exceeds one, the prevalence of Pd over Pt is evident for the terrestrial metallic phase. The Os and Ir amounts in terrestrial iron are two orders of magnitude smaller than in meteorites, while the Ag content is much higher. At the present stage of investigation we could not find Au- and PGE-concentrating elements in the Fe-phase from basites. Noble metals are likely present in the iron nodules as isomorphic impurity. It is worth noting that though iron meteorites contain high values of Au and PGE, own minerals of these elements have not been described from them. A unique association of noble metal phases has been found in the Djaltul massif in the zone of contact between the gabbro-dolerites and the cutting dike of graphite- and ferrite-bearing microdolerites (Ryabov, Lapkovsky, 2010). Among them are Pt-breithauptite (11.37% Pt) and minerals and alloys with Pd content varying from 6.12 to 53.2%.

Along with the noble metals, the metallic liquid intensely concentrates Ge, As, and Sb with distinct siderophile properties. There is a direct correlation between these elements and the amount of nickel. High concentrations of radioactive elements such as Th (up to 32 ppm) and U (up to 9 ppm) are established in the native iron, with their amounts in the rock not exceeding 1-2 ppm. Tungsten and gallium, possessing siderophile properties, are constantly present in the Fe-phase of basites in quantities no more than in the silicate rocks. Part of the native iron was analyzed for a wide range of elements. Some of the samples of Ni-bearing iron showed large amounts (ppm) of Ba (up to 5600), Rb (up to 760), Zr (up to 840) and Ta (25), the elements that are uncharacteristic of basic rocks. REE were established practically in all samples, in contents no higher than in the host rock. The presence of these lithophile elements in native iron is likely due to liquid inclusions represented by two phases: a high-Si-alkali phase and a phase rich in TiO_2, P_2O_5 and FeO.

So, what is the origin of this unique native metal mineralization? Researchers who studied native iron from Disco Is. proposed the mantle origin of telluric iron (Bird, Weathers, 1977). This opinion is shared by some Russian investigators who believe that ascending convective flows (plumes) extracted the core's late condensates from the mantle parts at the border with the core (Shkodzinsky, Kopylova, 2002). Siberian scientists hold to the idea that origin of native iron in basites of ancient platforms was due to the processes of interaction of a basaltic melt with a reducing transmagmatic fluid largely of hydrogen-methane composition, which caused the extraction of metals from the melt and reduction (Oleinikov et al., 1985, Ryabov, Lapkovsky, 2010). The fluid played also a substantial part as a supplier of many metals, among them noble ones, which accumulated in native iron segregations. Studies of the gaseous phase of native iron (Djaltul intrusion) show that it consists of a mixture of gases with dominating hydrogen (>75%) and subordinate amounts of CH_4, Na_2+CO and CO_2.

References:

Bird J.M., Weathers M.S. Native iron occurrences of Disko Island, Greenland // Jour. Geol. 1977. Vol. 85. P. 359-371.

Oleinikov, B.V., Okrugin, A.V., Tomshin, M.D. et al., Native metal formation in platform basites. Yakutsk, 1985, 188 p. (in Russian).

Ryabov V.V., Lapkovsky A.A. Unique polymineral association of Co-Ni and noble metal phases in gabbro-dolerite of the Dzhaltul trap intrusion (Siberian Platform) // Doklady Earth Sciences. 2010. T. 434. № 2. C. 1325-1329.

Shkodzinsky, V.S. and Kopylova, A.G., Siderophile elements in native iron and its genesis // Domestic Geology, 2002, No. 4, p. 36-39 (in Russian).

Ulff-Moller F. Native iron bearing intrusions of the Hammers Dal complex, North-West Disko // The Geological Survey of Greenland Report. 1977. Vol. 81. P. 15-33

ROCK-FORMING MINERALS OF TIKSHEOZERSKY MASSIF (NORTH KARELIA, RUSSIA)

Kovalskaya T.N., Kotelnikov A.R., Varlamov D.A.

Institute of Experimental Mineralogy, Chernogolovka, Russia, Tatiana76@iem.ac.ru

The studying of the Tiksheozersky massif was starting at 2005 (but field investigations 2010-2015 years new data arrived.

Tiksheozersky massif is located in North Karelia, Russia. It is referred to the Karelian-Kola Alkaline Province, but it is located to the south of the main complex of carbonatite massifs. Carbonatites of the Caledonian-Hercynian period (Kovdor Massif, etc.), the Tikshoozero Massif belongs to the earliest Proterozoic subplatform complex on the territory of the Fennoscandian Shield. The literature data indicate estimates of the age of the massif in the interval 1.8-1.9 billion years, which sharply differs from the other alkaline-carbonatite complexes of the Karelian-Kola province, whose age is estimated as the Middle Paleozoic.

An earlier study, as well as an analysis of literature data, showed that olivinites in the Tikshozero massif are extremely rare. During field investigations, we discovered a fairly large body of olivinites 3 km southwest of Sierpovidnoe Lake. Below the section, ditch networks were discovered earlier in the study of the massif - samples of pyroxenites, ore zone, gabbro and pyroxenites with alkaline pyroxenes were selected after the clearing. During the field seasons 2010 - 2015 years the main types of rocks of the Tiksheozero massif were studied in detail: olivinites, pyroxenites of varying degrees of variation (from essentially unchanged to sodalite, prenite, cancrinite, strongly altered with calcite and other secondary minerals, alkaline rocks with aegirine-type pyroxenes and nepheline. Minerals are studied at Tescan VEGA-II XMU electron scanning microscope with an INCA Energy 450 energy dispersive spectrometer and an Oxford INCA Wave 700 wave dispersion spectrometer, approximately 500 analyses were performed.

Olivinites of the Tiksheozersky massif are large-crystalline rocks composed of large crystals of olivine (up to 70%), clinopyroxene diopside-hedenbergite series (up to 20%), orthopyroxene (5%). Of accessory minerals in olivinites were found pyrrhotite and pentlandite. Some olivinites are serpentinized (fig. 1). In the serpentine zones carbonate is also found. The compositions of clinopyroxenes are shown in Table 1.
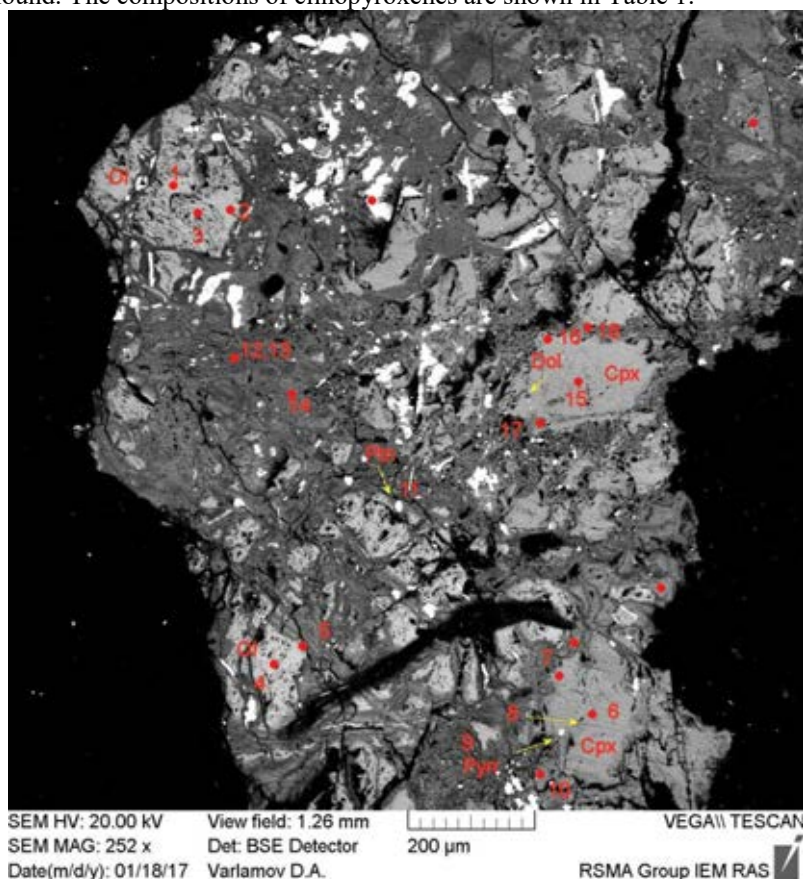
Fig. 1. Serpentinized olivinite from Tikshozersky massif.
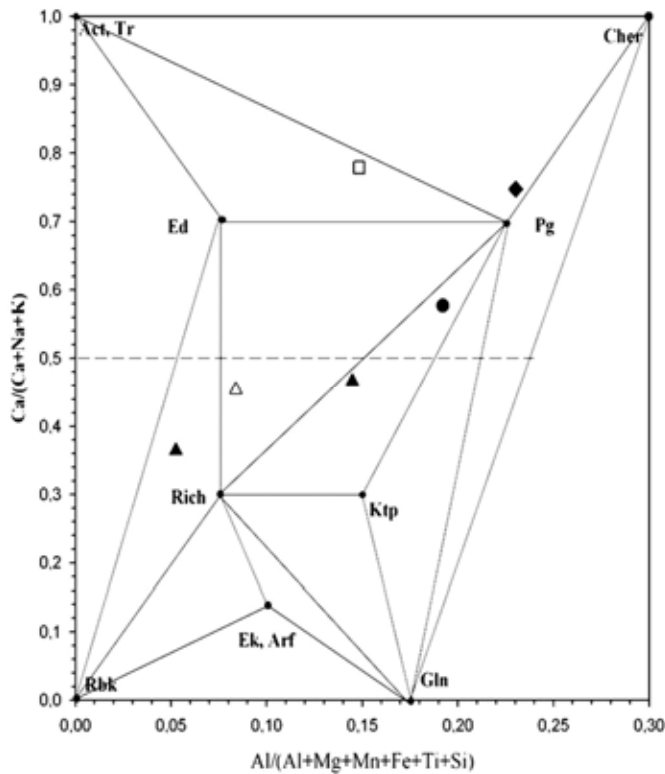
Fig. 2. The compositions of different amphiboles in the rocks of Tiksheozersky massif.

We also studied accessory minerals. So ilmenite, magnetite and chromite were found mainly in the basic and ultrabasic rocks of the massif, sphene of composition $Ca_{0.99}Al_{0.02}Ti_{0.98}SiO_5$, the orthite of composition $Ca_{1.84}La_{0.09}Ce_{0.2}Pr_{0.02}Nd_{0.09}Fe_{0.86}Al_{2.12}Ti_{0.01}Si_{3.25}O_{13}H$, F-apatite and pyrochlore - in alkaline rocks and partly in carbonatites. These minerals - concentrators of light rare earth elements, are typical for such complexes. Magnetite was also found in carbonatites.

In rocks of the massif different amphiboles are developed - in olivinites, pyroxenites and gabbros, amphiboles of the pargasite group are present, and in the iiolite-urtites and syenites, the groups of richterite-cataphorite are present. Compositions of amphiboles of rocks of the massif are shown in fig. 2. The determination of orthopyroxenes in olivinites makes possible the use of a two-pyroxene geothermometer Lindsley (Lindsley, 1983), an olivine-orthpyroxene geothermometer for a more accurate determination of mineralogenesis conditions. Previous studies (Kovalskaya et al., 2006,2007, Ustinov et al., 2006) made it possible to determine by thermometry the conditions for the formation of certain pyroxenites, sodalite-containing associations. Thus, the formation temperatures of pyroxenites of the massif using Cpx-Amf, Bi-Amf and Px-Bi geothermometers (Perchuk, Ryabchikov, 1976) are estimated in the range 710-980oC. New data will allow in the near future to make the calculation for formation temperature of olivinites parageneses.

Table 1. The compositions (in wt.%) of clinopyroxenes of the Tiksheozersky massif.

	T158-66	T7	T176-140-1	T176-140-2	t158-210	t158-213	T23-1	T23-2	Tiksh-47-1	Tiksh-47-2	T49-03
SiO_2	48.09	54.67	52.96	56.03	53.65	48.00	52.69	55.31	55.70	52.09	52.68
TiO_2	1.95	0.42		1.98		2.13	0.38			0.42	0.61
Al_2O_3	4.99	2.13	0.20		0.11	6.04	1.59	3.07	2.09	0.81	2.29
FeO	9.68	14.48	7.84	10.06	7.97	7.22	6.40	8.82	8.67	8.07	3.97
MnO	0.16	0.12	0.11		0.16		0.03			0.10	0.12
MgO	10.98	15.56	13.22	17.80	14.16	12.34	15.04	18.56	18.89	14.68	18.66
CaO	22.36	12.61	25.40	14.13	22.93	23.67	24.10	13.79	13.72	23.83	21.03
Na_2O	1.55		0.23		1.02	0.60	0.08	0.46	0.94		
K_2O	0.26										
Cr_2O_3							0.03				0.59
Summ	100.00	100.00	99.99	100.00	100.00	100.00	100.0	100.0	100.00	100.00	99.94

References:

Kovalskaya T.N., Kotelnikov A.R., Kovalsky A.M.Features of mineralogenesis of the Tiksheozero Massif (North Karelia) (In Russian) //The materials of International symposium of alkaline Magmatism of the earth and its mineralization. Kiev, 2007.hh. 99-102.

Kovalsky A.M., Kotelnikov A.R., Koval'skaya T.N. Experimental modeling of mineralogens of the Tiksheozero massif (In Russian) // Proceedings of the All-Russian Conference "Geochemistry, Petrology, Mineralogy and Genesis of Alkaline Rocks" September 18-23, 2006, Miass. Pp. 99-102.

D.H. Lindsley, D. J. Andersen A two-pyroxene thermometer // Journal of Geophysical Research Volume 88, Issue S02, 1983 Pages A887–A906 .

Metallogeny of magmatic complexes of intraplate geodynamic environments (in Russian), Moscow, GEOS, 2001, 640 p.

Perchuk L.L., Ryabchikov I.D. Phase matching in mineral systems(In Russian). M .: Nedra, 1976. 287 p.

Ustinov V.I., Grinenko V.A., Kotelnikov A.R. Suk N.I., Kovalska T.N., Smirnova E.P. Thermometry of sodalite-bearing associations of rocks of Lovozero and Tiksheozero alkaline massif (In Russian) // Proceedings of the All-Russian Conference "Geochemistry, petrology, mineralogy and genesis of alkaline rocks" September 18-23, 2006, 2006. Miass. Pp. 267-271.

RARE-EARTH CARBONATITES OF THE VUORI-YARVI (KOLA REGION): FIRST RESULTS OF THE STUDY

Kozlov E.N.[1,2], Fomina E.N.[1], Mytsa D.D.[3], Kirkin V.V.[2]

[1]Geological Institute, Kola Scientific Center of the Russian Academy of Sciences, Apatity, Russia, kozlov_e.n@mail.ru
[2]Apatity Branch of MSTU, Apatity, Russia
[3]Institute of Earth Sciences SPbSU, St.-Petersburg, Russia

The study of late magnesio- and ferrocarbonatites draws attention due to their high economic potential as a source of such strategic metals, as rare earth (REE) and high field strength elements (HFSE), as well as Ba, P, Fe and other valuable components (Jones et al., 2013). This is exactly the type of rocks, which the Tomtor and Bayan-Obo REE-Nb deposits-supergiants are associated with. At the same time, many researchers noted that in the formation of the carbonatites under consideration, late fluids were of major importance (Le Bas, 1999 and many others). Due to the metasomatic alteration, initiated by these fluids, late carbonatites underwent a multistage mineral rearrangement (Ngwenya, 1994; Broom-Fendley et al., 2016). As a result of this impact, rocks acquire a unique petrographic appearance, which is caused by the presence of various superimposed parageneses of minerals. The purpose of this study was to unravel the sequence and relationships of superimposed processes, as well as their reflection at the mineralogical level through a number of original research approaches. The latter are based on the extensive use of a variety of statistical methods, the integrated application of which has made it possible to compare geochemical and mineralogical data.

The object of this study is the rare-earth carbonatites of the Vuori-yarvi alkaline-ultrabasic carbonatite complex (Kola region). This massif is one out of more than 20 alkaline-ultrabasic carbonatite complexes of the Devonian Kola Alkaline Province (Downes et al., 2005). The composite geological structure of the complex under investigation is related to its multiphase nature. During its formation the Vuori-yarvi massif consistently introduced geochemically contrasting magmas, which crystallization products were as follows (in the sequence of formation): olivinites, pyroxenites, foidolites, nepheline syenites and at the final stage – carbonatites. The latter are widely distributed in the southeastern part of the massif and form rod-like and stockwork bodies near the Tukhta- and Neske-vara uplands. Most of them are calciocarbonatites with ore specialization for apatite, magnetite, niobium and tantalum (Afanasyev, 2011). Our attention was drawn to the specific carbonatites of the eastern flank of the massif, which outcrops were observed on the slope of the Petyayan-vara Mountain. Here the rocks, enclosing carbonatites, are ijolites and pyroxenites, and considerable amount of the latter have been metasomatically converted into coarse- and gigantic-grained phlogopite micas. In the early 1960s, during the exploration of micas, which were industrially interesting at that time, the carbonatites were discovered in the Petyayan-vara. However, despite the fact that more than 50 years have passed since the discovery of these carbonatites, they have not been studied so far.

According to our data, the Petyayan-vara carbonatites are (a) predominantly - magnesiocarbonatites with a significant fraction of silicocarbonatites, and (b) more than half of them are rich in rare earths, so that ΣREE_2O_3 vary from >1 wt.% to 13 wt.%. These carbonatites form long veins and lenses up several hundred meters in length, with a width reaching first tens of meters, and they are spatially connected with phlogopite micas. The described bodies in terms of orientation and morphology are similar to those of calcicarbonatite-sovites from the nearest environment of the Petyayan-vara area. Aluminosilicate rocks near carbonatites are permeated with veins and veinlets with a thickness up to first decimeters, composed mainly of ancylite–(Ce). The variety of rare-earth carbonates in them is either confined to leached cavities, or has a spotted distribution in the bulk of the rock. Pyroxenites near the bodies of carbonatites are intensely carbonized by cleavage cracks, while the very carbonatites near the contacts contain xenoliths of pyroxenites.

Mineralogical studies have shown that the content of rock-forming and minor minerals in the Petyayan-vara carbonatites is reached by dolomite (Fe, Mn), calcite, strontianite, ancylite– (Ce), hydroxyl-bastnaesite–(Ce), baryte, quartz, microcline, phlogopite, fluorapatite, and goethite. At the same time, such complex microstructure relationships of these phases and the structural-constitutional taxicity of rocks make it difficult to assess the mineral content in the samples and, as a consequence, do not allow us to trace the relationship of mineral composition with geochemistry. This has necessitated the use of alternative approaches.

To identify links in the behavior of chemical components, the cluster and factor analyses were used. Since the distributions of many components turned out to be lognormal, cluster analysis by the K-average method was performed on

the basis of the Spearman pair correlation matrix. With a significance level of $p=0.05$, the critical value of the correlation coefficient for a sampling of 43 samples was 0.30. For clustering, the insignificant coefficients were replaced by 0, the coefficients above the critical value were replaced by 1, and for those coefficients, which were lower than –0.30, we assigned a value of –1. The obtained results indicate the presence of two groups of elements, in the behavior of which there is a clear antagonism. A more detailed separation of these groups was achieved with the help of factor analysis in the modification of the principal component analysis (PCA), the results of which showed the presence of 4 subgroups of elements: (1a) "magnesian–barium" – Mg, Mn, Ca, Ba, S; (1b) "strontium–rare-earth" – Sr, La-Tb, Th; (2a) "aluminosilicate" – Si, Ti, Al, K, Na, Li, Rb, Cs, Nb, Ta, Fe, Ni, Co, V, Cr, Zn, Cu, Pb, Mo, Sc; (2b) "phosphate" – P, U, Y, Dy-Lu, Zr, Hf.

The primary comparison of geochemistry and mineralogy was carried out according to an original technique, which was also based on the factor analysis. Like a "mirror" reflecting the mineral composition, the absolute intensity values were used for the X-ray diffractograms of the whole rock samples. The measuring range of the angle 2θ was from $3°$ to $70°$ in steps of 0.02 °. When conducting factor analysis in the PCA modification, calculations were performed by means of the Pearson pair correlation matrix between the intensities, measured at each value of 2θ. As the additional parameters, the contents of petrogenic and rare elements were introduced. Since the volume of information, concentrated in "geochemical variables", was about 1% of the total volume of primary data, these variables did not have any noticeable effect on the structure of the identified factors. At the same time, this method made it possible to relate initially "mineralogical" factors to geochemistry. Thus, we introduced geochemical data to the mineralogical "soil".

The obtained results appeared to be impressive. Our calculations revealed several tens of factors, for 14 of which the meaningful relations with the distribution of the investigated components were established. Interpretation of all 14 factors turned out to be quite simple, since the growth of the factorial loadings in the investigated range of 2θ coincided with the position of the majority of X-ray reflections on the diffractograms of "pure" minerals, taken from specialized databases (ICDD PDF-2, AMCSD, RRUFF, etc.) (Fig. 1). Thus, in addition to the 11 factors that correspond to the previously listed minerals, the factors of albite, aegirine and ankerite were revealed. Subsequently, these phases were purposefully found in the samples, the values of corresponding factors in which were the highest. Considering the close position of X-ray reflections of ankerite and dolomite, this indicates a rather high sensitivity of the proposed method. The analysis of factorial loadings for chemical components revealed both "trivial" connections and non-obvious ones. Thus, significant factorial loadings of barium and sulfur on the barite factor ($Ba_{0.92}S_{0.93}$), magnesium and manganese on dolomite ($Mg_{0.49}Mn_{0.46}$), calcium on calcite ($Ca_{0.73}$) and others are regular.

At the same time, considering the values of factorial loadings, it can be stated that in the studied samples the bulk of strontium and rare earths is contained in the ancylite, and not in strontianite and hydroxyl-bastnaesite ($Sr_{0.71}REE_{0.88}$ against $Sr_{0.63}REE_{0.16}$ and $Sr_{-0.01}REE_{0.19}$, respectively). By analogy it is found that the main concentrator of Si in the sample is not quartz but microcline, and the distribution of Na is equally influenced by albite and aegirine etc. It is also found that Ti, Nb and Ta are primarily associated with microcline and mica, while Zr and Hf - with apatite and aegirine. In this way, during the formation of Petyayan-vara carbonatites, there were involved processes, facilitating the effective separation of geochemically similar elements (LREE and HREE, Ti-Nb-Ta and Zr-Hf).
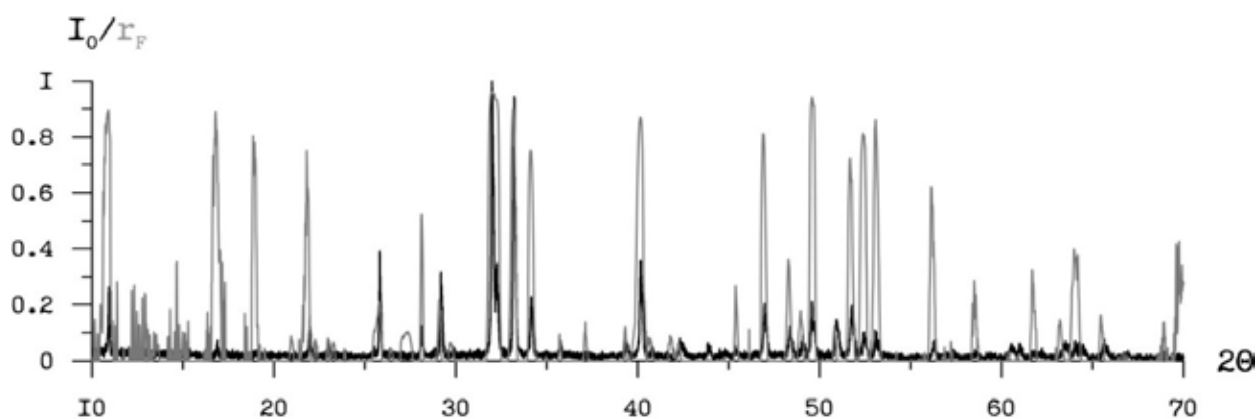
Fig. 1. Comparison of the X-ray diffractogram of fluorapatite from the RRUFF database (Downs, 2006) (analysis R050529, black line; I_O – relative intensities, the largest peak value is taken as 1) with the factorial loadings values (r_F) for the detected apatite factor (gray line, negative factorial loadings are excluded with a view to simplifying) for values of 2θ ranging from $10°$ to $70°$.

The importance of the drawn conclusions is emphasized by another finding - a visual analysis of the Pearson pair correlation curves (r) between the absolute values of the intensity for angles 2θ and the content of each component (Fig. 2). This know-how allows us to consider all the links between geochemistry and mineralogy of the complex. The observed pattern is fully consistent with the results of the analysis of "mineralogical" factors. For example, near the X-ray reflections of apatite from the planes (211), (112) and (300), the maximum value of r for P is 0.97, for U – 0.87, for Y – 0.90, for Dy-Lu – 0.85 ... 0.90, for Zr – 0.86, for Hf – 0.71 (the bundle of lines 1 in Fig. 2b). For comparison, the corresponding loadings on the "mineralogical" apatite factor are: $P_{0.92}$, $U_{0.82}$, $Y_{0.87}$, Dy-$Lu_{0.81-0.87}$, $Zr_{0.82}$, $Hf_{0.67}$. It should be recalled, that these

elements were united into a single group of "phosphate" elements already at the initial stage of the study. At the same time, a thorough analysis of the curves of correlation coefficients meanings provided more detailed separating of other previously identified geochemical groups and establishing the links at the level of mineral associations.
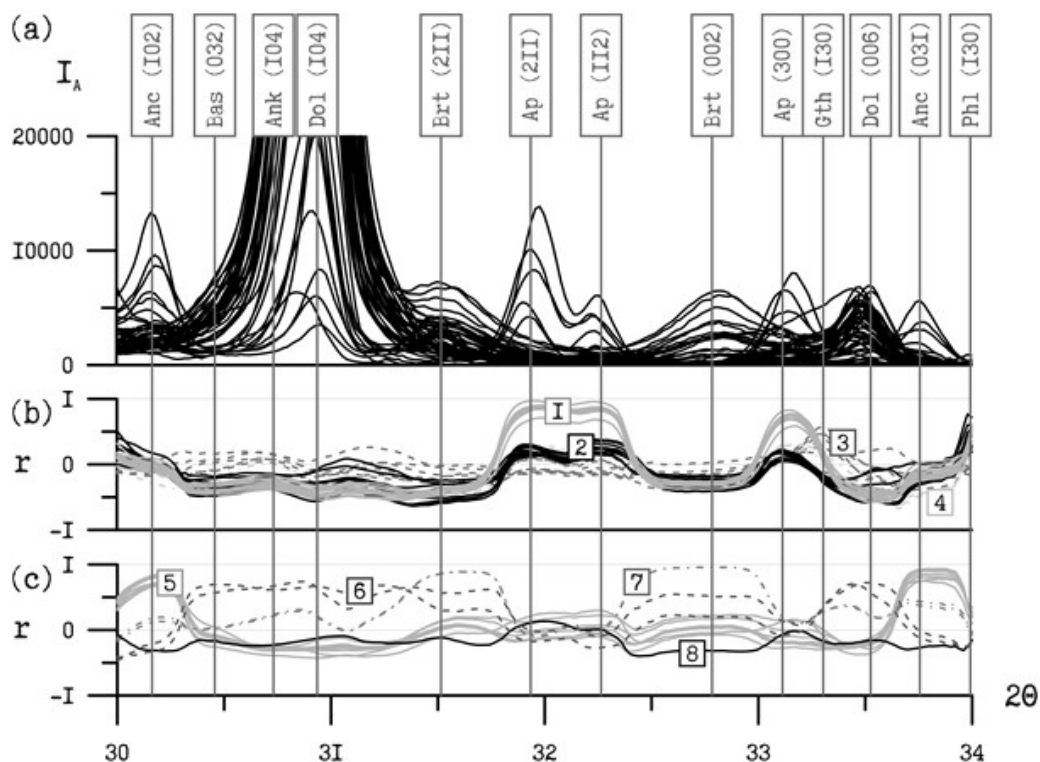
Fig. 2. An example of comparing (a) the X-ray diffraction patterns of the Petyayan-vara carbonatite samples and (b-c) curves of the Pearson pair correlation (*r*) between the content of each component and the absolute intensity values (I_A) for the angles 2θ (data taken from the range of 2θ = 30°... 34°) for the same sampling. Vertical lines are the position of X-ray reflections from the planes of minerals [abbreviations of minerals and (hkl) of the appropriate reflections - in the upper part of the figure]. Bundles of the correlation curves:1 – P, U, Y, Dy-Lu, Zr, Hf; 2 – Si, Al, Ti, Nb, Ta, K, Na, Li, Rb, Cs; 3 – Ni, Co, Cr, Zn, Cu, Pb, Mo; 4 – Fe, V, Sc; 5 – Sr, La-Tb; 6 – Mg, Mn; 7 – Ba, S; 8 – Ca.

Summarizing results, which are a peculiar mineralogical-geochemical model of the rare-earth carbonatites of Petyayan-vara, we can state the following:

1) Ca takes a special place (line 8 on Fig. 2c), and the only mineral, which peaks calcium has a direct correlation with, is calcite. Ca has neither any connection or negative correlation with peaks of other minerals;

2) Dolomite, the concentrator of Mg and Mn (the bundle of lines 6 in Fig. 2c), and barite, the main concentrator Ba and S (the bundle of lines 7 in Fig. 2c), are closely related to each other. At the same time, ancylite (Sr, LREE, a bundle of lines 5 on Fig. 2c) apparently took up the place of dolomite in the rocks, which, however, did not affect on the content of barite. Possibly, the distribution of these elements is the result of several processes;

3) Microcline and phlogopite crystallized on dolomite. It complies (at least for microcline) with petrographic observations. This process was caused by Si, Al, Ti, Nb, Ta, K, Na, Li, Rb, Cs added to the rocks (the bundle of lines 2 in Fig. 2b). Apparently, microclinization and apatitization were connected with apatitization, associated with the addition of P, U, Y, Dy-Lu, Zr, Hf (bundle of lines 1 on Fig. 2b), and formation of a goethite, concentrating Fe, Ni, Co, V , Cr, Zn, Cu, Pb, Mo, Sc (bundles of lines 3 and 4 on Fig. 2b). This may indicate the inheritance of the chemical particularity of sulphides and magnetite by the goethite, which replaces them.

The proposed methodological innovations can be recommended for studying a variety of geological objects (including exploratory researching of poorly studied complexes) and solving a wide range of mineralogical-geochemical problems (rapid determination of mineral composition of rocks; directed search for samples that contain minerals of interest, for example – minerals-geochronometers; determination of minerals-concentrators of components; identification of mineral associations, etc.).

Further investigations of the Petyayan-vara carbonatites are to provide a meticulous study of the microstructural relationships of the mineral associations. The latter were examined to confirm and refine the revealed dependencies and substantiate the sequence of processes, as well as an analysis of isotope-geochemical data, that can carry genetic information (C, O, Sm-Nd and Rb-Sr isotopic systematics).

References:

Afanasyev BV (2011) Mineral resources of alkaline-ultrabasic massifs of the Kola Peninsula [Mineral'nyye resursy shcholochno-ul'traosnovnykh massivov Kol'skogo poluostrova (in Russian)]. St.-Petersburg, "Roza vetrov". 224 p.

Broom-Fendley S, Styles MT, Appleton JD, Gunn G, Wall F (2016) Evidence for dissolution-reprecipitation of apatite and preferential LREE mobility in carbonatite-derived late-stage hydrothermal processes. Am Min. 101:596–611.doi: 10.2138/am-2016-5502CCBY

Downes H, Balaganskaya E, Beard A, Liferovich R, Demaiffe D (2005) Petrogenetic processes in the ultramafic, alkaline and carbonatitic magmatism in the Kola Alkaline Province: a review. Lithos. 85:48–75. doi: 10.1016/j.lithos.2005.03.020

Downs RT (2006) The RRUFF Project: an integrated study of the chemistry, crystallography, Raman and infrared spectroscopy of minerals. In: Program and Abstracts of the 19th General Meeting of the International Mineralogical Association in Kobe, Japan. P. 117.

Jones AP, Genge M, Carmody L (2013) Carbonate Melts and Carbonatites. RiMG. 75:289–322. doi: 10.2138/rmg.2013.75.10

Le Bas MJ (1999) Ferrocarbonatites: geochemistry and magma–fluid state. Geol Soc India Mem. 43:785–802.

Ngwenya BT (1994) Hydrothermal rare earth mineralisation in carbonatites of the Tundulu complex, Malawi: processes at the fluid/rock interface. Geochim Cosmochim Acta. 58:2061–2072. doi: 10.1016/0016-7037(94)90285-2.

SYSTEMATISATION OF GARNET GROUP MINERALS ON CHEMICAL COMPOSITION USING THE RHA-METHOD

Krasnova N.I., Petrov T.G., Ruban V.P.

Saint-Petersburg State University, Saint-Petersburg, Russia, nataly_krasnova@rambler.ru, tomas_petrov@rambler.ru, varenka1987@mail.ru

Use by the geologists worldwide of any databanks and catalogues both for minerals, and for rocks is complicated with presence of language distinctions, imperfection of the nomenclature, and first of all, absence of connection with essential properties of object. At the same time clear all common "language" exists – it is language of chemical elements and their compounds. On the basis of this chemical language, and also of the information theory and thermodynamics more than 35 years ago (Petrov, 1971) the information language – the method RHA – was worked out. It is intended for the uniform description, ordering, automatic grouping of the data on chemical compounds of anyone geological (and others) objects. Unlike other ways of composition data processing, the RHA method describes analyses as the whole – integrally, therefore the characteristics which reflect simultaneously all major elements of the composition are used. The description of any analytical data in RHA system consists of three components: R – rank formula; H (En) – information entropy, which was defined by Shannon as a measure of complexity: $En = -\sum p_i * \log p_i$; now An – anentropy, which was defined by T. Petrov as a measure of purity of composition: $An = -\sum \log p_i$. 1. – Rank formula – R is a sequence of symbols of chemical elements on decreasing atomic %. R is identical to result of ordering of chemical elements on decrease of the sums of all their coefficients in crystal-chemical formula, without taking into account the valence of elements or their site position. The symbol "=" between two elements shows that $p_i/p_{i+1} \pm 1,15$, which corresponds to the difference between the neighbouring components not more than 15 relative percents. Using the R, En, and An, which can serve as a "object's composition passport", all objects can be classified. For linear ordering of RHA-data R is accepted for a "word" in which symbols of components play a part of "letters". These "words" are ordered by a dictionary principle, (as in dictionaries) according to "alphabet". For the "alphabet" the sequence of chemical elements in Periodic Table is accepted. As a result a simple (monosematic), hierarchically and dictionary ordered classification of any composition set is created. The full table is available in Internet by address: The table 1 shows the RHA data for theoretical composition of most of all known garnets. We had not included some rare species without SiO4 groups. This table 1 shows that mostly the mineral species (such as katolite, majorite, yamatoite, calderite etc.) have different crystallochemical and empirical formulas, what is caused by difficulties of analysis of elements with different valence (Fe, Mn, Ti etc.), or some water (OH) content. Using the RHA system, we have no problems with hetrovalent elements, because the rank formula reflects the bulk content of them, in addition we exclude the analyses with bad sums. The last IMA report about "Nomenclature of the garnet supergroup" (Grew et al., 2013) recommended many good corrections to the names of garnet species, e.g.: the names with suffixes have been replaced by root names – elbrusite-(Zr) to elbrusite etc. It is pity, that these corrections not always are taken in consideration by mindat.org and webmineral systems, both of them are sometimes behind of these renovations made by IMA.

Table 1. Rank formulas of garnet group minerals and their crystallochemical formulas (Internet resources).

*webmineral.com - mostly, empirical
**mindat.org
*** IMA

Rank formula						Name	Crystallochemical formula
H= O Ca Al						katoite ***	$Ca_3Al_2(OH)_{12}$
O H Ca Al Si						katoite *	$Ca_3Al_2(SiO_4)_{1.5}(OH)_6$
O H Ca Al Si						hibschiie **	$Ca_3Al_2(SiO_4)_{3-x}(OH)_4$
O H Ca Al= Si						hibschite*	$Ca_3Al_2(SiO_4)_2(OH)_4$
O H Ca Si Al						katoite **	$Ca_3Al_2(SiO_4)_{3-x}(OH)_{4x}$
O H Ca Si= Mn						henritermierite **	$Ca_3Mn^{3+}_2(SiO_4)_2(OH)_4$
O H Ca Si Mn Al						henritermierite **empirical	$Ca_3Mn^{3+}_2Al_{0.5}(SiO_4)_2(OH)_4$
O Mg= Si						majorite **	$Mg_3(MgSi)(SiO_4)_3$
O Mg= Si Al						pyrope* & **	$Mg_3Al_2(SiO_4)_3$
O Mg= Si Cr						knorringite* & **	$Mg_3Cr_2(SiO_4)_3$
O Al= Ca Sb= Sn						bitikleite-(SnAl)**	$Ca_3(SbZr)_2(Fe^{3+}O_4)_3$
O Si Mg Fe Al						majorite ** empirical	$Mg_3(Fe_{1.2}Al_{0.6}Si_{0.2})(SiO_4)_3$
O Si Mg= Y Ca						menzerite-(Y)**	$(Y^{3+}_2Ca)Mg_2(SiO_4)_3$
O Si= Ca Al						grossular* & **	$Ca_3Al_2(SiO_4)_3$
O Si= Ca Ti= Fe						morimotoite* & **	$Ca_3TiFe^{2+}(SiO_4)_3$
O Si= Ca V						goldmanite* & **	$Ca_3V^{3+}_2(SiO_4)_3$
O Si= Ca Cr						uvarovite* & **	$Ca_3Cr^{3+}_2(SiO_4)_3$
O Si= Ca Fe						andradite* & **	$Ca_3Fe^{3+}_2(SiO_4)_3$
O Si= Ca Sc						eringaite **	$Ca_3Sc^{3+}_2(SiO_4)_3$
O Si= Mn Al						spessartine* & **	$Mn^{2+}_3Al_2(SiO_4)_3$
O Si= Mn V						yamatoite **	$Mn^{2+}_3V^{3+}_2(SiO_4)_3$
O Si Mn V Ca Al						yamatoite*	$(Mn^{2+},Ca)_3(V^{3+},Al)_2(SiO_4)_3$
O Si= Mn Fe						calderite **	$Mn^{2+}_3Fe^{3+}_2(SiO_4)_3$
O Si Mn Fe Ca Al						calderite*	$(Mn^{2+},Ca)_3Fe^{3+},Al)_2(SiO_4)_3$
O Si= Fe Al						almandine* & **	$Fe^{2+}_3Al_2(SiO_4)_3$
O Ca Al Cl Si						wadalite **	$Ca_6Al_5Si_2O_{16}Cl_3$
O Ca Al Cl Si Mg Fe						wadalite* empirical	$Ca_6Al_{3.3}Fe^{3+}_{0.3}Mg_{0.6}Si_{2.7}O_{16}Cl_{2.9}$
O Ca Al= Zr Si						kimzeyite **	$Ca_3Zr_2(Al_2Si)_3O_{12}$
O Ca Al= Sn Si						irinarassite **	$Ca_3Sn_2(Al_2Si)_3O_{13}$
O Ca Al Sn Ti Si Sb						irinarassite ** empirical	$Ca_3(Sn_{1.02}Zr_{0.41}Ti_{0.26}Sb_{0.24}Fe^{2+}_{0.08}U_{0.02})(Al_{1.4}Fe_{0.8}Si_{0.5}Ti_{0.4})_3O_{12}$
O Ca Si Ti Fe Al						schorlomite*	$Ca_3(Ti,Fe^{3+})_2[(Si,Fe^{3+},Fe^{2+})O_4]_3$
O Ca Si Zr Al Ti Fe						kimzeyite*	$Ca_3(Zr,Ti)_2(Si,Al,Fe^{3+})_3O_{12}$
O Ca Si Sc Fe Ti Al						eringaite ** empirical	$Ca_3(Sc_{0.82}Ti_{0.44}Fe^{3+}_{0.24}Zr_{0.21}Cr_{0.08})(Si_{2.48}Al_{0.39}Fe_{0.13})O_{12}$
O Ca Ti= Fe Si						schorlomite **	$Ca_3Ti_2(Fe^{3+}_2Si)_3O_{12}$
O Ca Fe= Zr Si						kerimasite **	$Ca_3Zr_2(Fe^{3+}_2Si)_3O_{12}$
O Ca= Fe Zr= Sb						bitikleite-(ZrFe)**	$Ca_3(SbZr)_2(Fe^{3+}O_4)_3$
O Ca= Fe Zr= U						elbrusite-(Zr)**	$Ca_3(U^{6+}Zr)_2(Fe^{3+}Fe^{2+}_4)O_{12}$
O Ca Zr Fe Si= Al Ti						kerimasite ** empirical	$Ca_3(Zr_{1.72}Nb_{0.14}Ti_{0.08})(Fe^{3+}_{1.23}Si_{0.86}Al_{0.82}Ti_{0.09})_3O_{12}$
O Mn Si						blythite **	$Mn^{2+}_3Mn^{3+}_2(SiO_4)_3$
O Mn Si Cr						Grt UM1984-37***	$Mn^{2+}_3(Cr^{3+}Mn^{3+})_2(SiO_4)_3$

The end-members in minerals of the garnet supergroup mostly correspond to the minals, real analogues of which are unknown in nature. We cannot find in any rocks the garnets similar to ideal formula of pyrope, of knorringite, almandine, uvarovite, andradite etc., firstly because the real minerals due to addition of some isomorphic elements have more complicated composition and long R. The system RHA reflects the real composition of all objects, in the same way, as we receive the analysis by the electron microprobe method (the last should be ordered according to decreasing of component's content. We do not need to use lot of triangles to distinguish the mineral species, on which unfortunately the different analyses not always can be simple shown and named. In our case, the diagnostic of mineral by its analysis is very simple, which we had done for garnets without names from some publications (see table 2, e.g. in bold type: the garners from reference 1515 –Sobolev, 1964).

In this table 2 one can see the two analyses (marked Italic – 6-1160-t17…from Deer et al., 1962 with name "pyrope" and next 43-1162, named "almandine". The similar En and An point to the possibility, that these analyses are

identical, what was easily proofed by examining of the original analyses (see table 3) and the recalculation them to minals and crystallochemical formulas show that they both correspond to pyrope but not almandine.
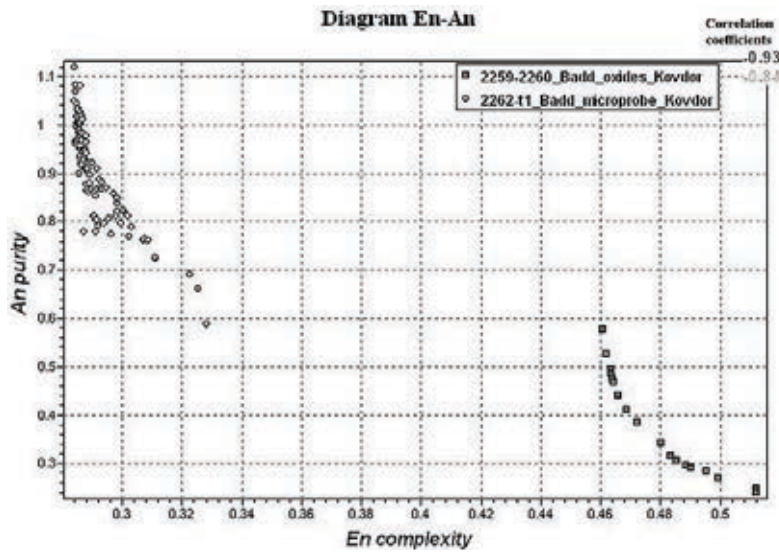
Fig. 1. Comparison of results of baddeleyite chemical analyses, received by means of a microprobe and a method of wet chemistry (in oxide form) on diagram En-An (complexity-purity). It is obviously that the analyses of baddeleyites in oxide form are more complex and less pure because of influence of different inclusions.

Table 2. Fragment of the table "RHA_Grt-7 ranks" composed from published 418 analyses of garnet group minerals
Full table is available at site Research Gate, by author Krasnova N.I.

		Rank formula					En	An	Description: No in BD_garnet name_No sample (color)_location	Wrong diagnostic & a new name
3	4	5	6	7	8	10	14	15	16	17
O	Si	Al	Mg	Fe	Ca	H	1.520	0.773	44-1162-V3,No1,p57-60_almandine_Vasugupaleyem,Madras,India	1-pyrope
O	Si	Al	Mg	Fe	Ca	H	1.520	0.800	6-1160-t17_pyrope_eclogite gabbro_Sittampundi,Madras,India-G3	
O	Si	Al	Mg	Fe	Ca	H	1.520	0.800	43-1162-V3,No1,p57-60_almandine_Sittampundi,Madras,India	2-pyrope
O	Si	Al=	Mg=	Fe	Ca=	H	1.511	0.859	21-1162-V3,No1,p36-37_pyrope_Val Kadera,Italy-G4	
O	Si	Al=	Mg	Fe	Ca	H	1.492	0.906	17-1162-V3,No1,p36-37_pyrope_Rodgaugen,Sondmor-G4	
O	Si	Al	Mg	Fe	Ca	H	1.492	0.959	18-1162-V3,No1,p36-37_pyrope_Vadugupaleyem,Madras,India-G4	
O	Si	Al	Mg	Fe	Ca	K	1.471	1.031	22-1162-V3,No1,p36-37_pyrope_pipe Obnazhennaya,Russia-G4D	
O	Si	Al	Mg	Fe	Ca	Ti	1.494	1.130	19-1162-V3,No1,p36-37_pyrope_pipe NIIGA-1,Russia-G3	
O	Si	Al=	Mg	Fe	Ca	Cr	1.487	0.873	15-1162-V3,No1,p36-37_pyrope_pipe Mir,Russia-G9	
O	Si	Al	Mg=	Fe	Ca	Mn	1.504	1.011	7-1160-t17_pyrope_gabbro_Gor-Mountain,St.New York,USA-G3	
O	Si	Al	Mg	Fe	Ca	Mn	1.504	1.011	4-1160-t17_pyrope_eclogite Zo_Zilberbach,Fichtel Mt.,Germany-G3	
O	Si	Al	Mg	Fe	Ca	Mn	1.501	1.031	5-1160-t17_pyrope_eclogite Ky_Zilberbach,Fichtel Mt.,Germany-G3	
O	Si	Al	Mg	Fe	Ca	Mn	1.490	1.117	23-1162-V3,No1,p36-37_pyrope_pipe Chomur,Russia-G4	
O	Si	Al	Mg	Fe	Ca	Mn	1.492	1.031	20-1162-V3,No1,p36-37_pyrope_pipe Marshrutnaya,Russia-G4	
O	Si	Al	Ca=	Mn	Fe	Ti	1.501	1.137	25-1162-V3,No1,p50-51_spessartine_Victoria,Nevada,USA	
O	Si	Al	Mn	Ca	Mg	Fe	1.487	0.813	300-1515-tl_Grt_shist_E.Shikoku,Japan	spessartine
O	Si	Al	Mn	Ca	Fe	Mg	1.513	0.846	26-1162-V3,No1,p50-51_spessartine_Kaneushi,Japan	
O	Si	Al=	Mn	Ca	Fe	Mg	1.504	0.806	7-1160-t18_spessartine_crystal shists_Welly-Ford,California,USA	
O	Si	Al=	Mn	Fe	H	Mg	1.490	0.952	18-1162-V3,No1,p50-51_spessartine_Sama,Ireland	
O	Si	Al	Mn	Fe	Mg	Ca	1.499	0.892	19-1162-V3,No1,p50-51_spessartine_NewHampshire,USA	
O	Si	Al=	Mn	Fe	Mg	Ca	1.455	1.137	17-1162-V3,No1,p50-51_spessartine_Marshikov,Czechoslovakia	
O	Si	Al=	Mn	Fe	Mg	Ca	1.453	1.243	14-1162-V3,No1,p50-51_spessartine_Kolmozero,Kola pen.,Russia	
O	Si	Al	Mn	Fe	Ca	H	1.561	0.635	296-1515-tl_Grt_shist_Kotu mine,E.Shikoku,Japan	spessartine
O	Si	Al	Mn	Fe	Ca	H	1.492	0.892	21-1162-V3,No1,p50-51_spessartine_Alakurtti, Russia	
O	Si	Al	Mn	Fe	Ca	Mg	1.481	0.972	20-1162-V3,No1,p50-51_spessartine_Gola,Poland	
O	Si	Al=	Mn	Fe	Ca	Mg	1.455	1.130	23-1162-V3,No1,p50-51_spessartine_Blumov mine,Ural,Russia	
O	Si	Al=	Mn	Fe	Ca	Mg	1.455	1.686	6-1160-t18_spessartine_peg._Delaver,Pennsylvania,USA	
O	Si	Al=	Mn	Fe	Ca	K	1.453	0.985	13-1162-V3,No1,p50-51_spessartine_Emerald mines,Ural,Russia	
O	Si	Al=	Mn	Fe	Ca	Ti	1.455	1.785	1-2274-tl_spessartine_Leiper's quarry,Avondale,Pennsylvania,USA	
O	Si	Al	Fe	Mg	H	Na	1.504	0.826	36-1162-V3,No1,p57-60_almandine_bugitov complex,Ukraine	
O	Si	Al=	Fe	Mg	Ca	H	1.451	1.296	25-1162-V3,No1,p57-60_almandine_charnokite_S.Madras,India	
O	Si	Al=	Fe	Mg	Ca	Ti	1.451	1.104	27-1162-V3,No1,p57-60_almandine_Wieselburg,Austria	
O	Si	Al	Fe	Mg	Ca	Mn	1.515	0.747	207-1515-tl_Grt_marbor_Dol,Ol,Di_N.Zaval'e,Ukraine	almandine
O	Si	Al	Fe=	Mg	Ca	Mn	1.511	0.959	42-1162-V3,No1,p57-60_almandine_S.Haris,External Hebrides	
O	Si	Al	Fe	Mg	Ca	Mn	1.506	0.925	39-1162-V3,No1,p57-60_almandine_Ghana	
O	Si	Al	Fe	Mg	Ca	Mn	1.497	1.038	40-1162-V3,No1,p57-60_almandine_pipe Mir,Yakutia,Russia	
O	Si	Al=	Fe	Mg	Ca	Mn	1.481	1.058	24-1162-V3,No1,p36-37_pyrope_pipe Kao,Lesoto-G4	3-almandine
O	Si	Al	Fe	Mg	Ca	Mn	1.478	0.972	12-1160-t14_almandine_Ky-Grt-Ged_Oriphyno,St.Idaho,USA	
O	Si	Al	Fe	Mg	Ca	Mn	1.476	0.998	25-1162-V3,No1,p36-37_pyrope_W.Belomorie,Karelia,Russia-G4	4-almandine
O	Si	Al=	Fe	Mg	Ca	Mn	1.464	0.985	18-1162-V3,No1,p57-60_almandine_Adirondack,St. New York,USA	
O	Si	Al	Fe	Mg	Ca	Mn	1.435	1.104	31-1162-V3,No1,p57-60_almandine_Anabar massif,Russia	
O	Si	Al=	Fe	Mg	Ca	Mn	1.435	1.316	26-1162-V3,No1,p57-60_almandine_Lyadova,Forednestr reg.,Ukraine	

Table 3. Comparing of chemical analyses

Description	SiO$_2$	TiO$_2$	Al$_2$O$_3$	Fe$_2$O$_3$	FeO	MnO	MgO	CaO	H$_2$O	Total
44-1162-p57-60_almandine_India	41.5	0.08	22.4	0.95	14.6	0.29	14.8	5.36	0.36	100.27
6-1160-t17_pyrope_eclogite_India	40.7	0.08	22.3	1.31	16.5	0.33	12	6.77	0.23	100.26
43-1162-p57-60_almandine_India	40.7	0.08	22.3	1.31	16.5	0.33	12	6.77	0.23	100.26
21-1162-p36-37_pyrope_Italy	39	0.12	19.9	5.03	19.1	0.17	14	2.17	0.33	99.69

By examination of full table we established, that most of all doubtful analyses, brought to light using the ***RHA***-method, were wrong specified. Work on a method is provided with program PETROS-2 or PETROS-3 worked out by S.V. Moshkin (Petrov, Moshkin, 2015). Chemical *R*-classifications (*CRchem*) of mineral groups composition are included into uniform linear hierarchical periodic classification of chemical composition of any objects, general for all national languages. A variety of application of a method is reflected more than in 70 publications, most of which are available at web site Research Gate by authors names: Petrov T.G. and Krasnova N.

We tried to use some traditional statistic methods in order to distinguish the garnets, but at factor and caster diagrams, the points, corresponding to different mineral species, can be plotted together (see fig. 2).
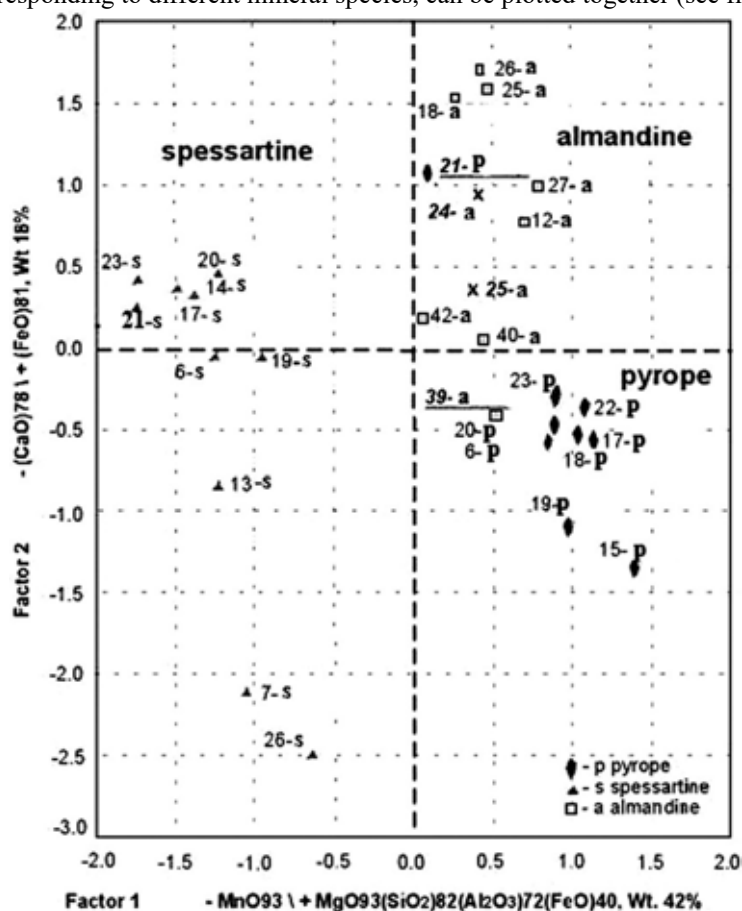
Fig. 2. Diagram of two factors for chemical analyses of some pyropes, almandines and spessartines.

Two points of analyses (are underlined): one 21-p (21-1162-V3,No1,p36-37_pyrope) was plotted in the field of almandine, and the second – 39a (39-1162-V3,No1,p57-60_almandine) is situated in the field of pyrope. This shows that the statistical methods give us no possibility to distinguish the mineral species unequivocal, while the RHA method easily shows the composition of mineral, reveals the similar analyses, and gives the possibility not only find the mistakes of diagnostic, but give the more suitable names for unnamed minerals.

References

Grew E.S., Locock A.J., Mills S.J., Galuskina I.O. Galuskin E.V. & Halenius U. (2013) IMA report. Nomenclature of the garnet supergroup. // Am. Miner. V. 98. Pp. 785-811.

Petrov T.G. 1971 The justification of variant of general classification for geochemical systems. // Vestnik of Leningrad State University. No 18. 30-38. (In Russian).

Petrov T.G., Moshkin S.V. (2015). Method RHAT and its implementation in the software package PETROS-3 // News of science and educations. No 2 (26). Pp. 70-80.

Sobolev N.V. (1964) Paragenetic types of garnets. Moscow. Nauka Press. 217 p. (In Russian).

COMPOSITION OF A CARBONATIC MELT IN EQUILIBRIUM WITH PERIDOTITE AT 5.5–6.3 GPA AND 1350°C

Kruk A.N.[1,2], _Sokol A.G._[1,2], _Palyanov Yu.A._[1,2]

[1]Institute of Geology and Mineralogy, Siberian Branch of the Russian Academy of Sciences, Novosibirsk, Russia
[2]Novosibirsk State University, Novosibirsk, Russia, krukan@igm.nsc.ru

Mantle carbonatitic melts are considered as important metasomatic agents in the subcratonic lithosphere (Wallace and Green, 1989; Becker and Le Roex, 2006). Carbonatite metasomatism has been inferred to be related to kimberlite generation (Becker and le Roex, 2006; Kogarko, 2006, Sokol et al, 2016), and low-SiO_2 carbonate melt is even suggested to be parental to most group I kimberlites (Kamenetsky et al., 2014). Judging from kimberlite chemistry, metasomatic agents may have been derived from either carbonate-bearing rocks subducted to mantle depths (Becker and le Roex, 2006; Coe et al., 2008) or from oxidized domains in rising plumes (Becker and le Roex, 2006).

Percolation of such melts to the roots of the subcratonic lithosphere results in metasomatic alteration of peridotites (Wallace and Green, 1989). According to Brey et al. (2009), the carbonatitic melt crystallizes under the subcontinental thermal regime (most likely, partially) and forms magnesite rich domains/veins, which may be potential sources of kimberlite magmas. An important fact on the composition of protokimberlitic melts is provided by inclusions in fibrous diamonds crystallized immediately before their removal by magma to the surface. The captured material of inclusions are represented by an ultrapotassic, high density, mostly carbonate melts/fluids (Kopylova et al. 2010).

There are numerous experimental studies of the composition of carbonatitic melt equilibrated with mantle peridotite, but only some of them consider the mechanisms of generation of melts with a high concentration of alkalis (Wallace and Green, 1989; Brey et al., 2011). According to the model Foley (1992), an alkaline melt is generated during heating of metasomatized areas of the lithosphere by the mechanism of hybridization: (1) dissolution of minerals of host rocks in a melt of the material of the metasomatic agent, when the liquidus temperature of vein material is lower than the temperature of the host rock solidus; (2) mixing of melts formed upon incomplete melting of vein material and partial melting of host rock, when the temperature of the vein material liquidus is higher than the temperature of the host rock solidus.

Our study was aimed at investigation of the composition of the melt produced in long experiments (150 h) as a result of interaction of lherzolite and harzburgite with carbonatites of various compositions at 5.5–6.3 GPa and 1350°C (typical of the base of the subcratonic lithosphere) and on estimation of the mechanism of hybridization during the formation of ultra-alkaline carbonatitic melts in metasomatized peridotites.

Table 1. Compositions of starting lherzolite (LC), harzburgite (HC), carbonatites (GS, B6, and B10), and bulk compositions of sandwiches

Sample	SiO_2	TiO_2	Al_2O_3	Cr_2O_3	FeO	MnO	NiO	MgO	CaO	Na_2O	K_2O	Total*
LC	45.9	0.18	4.07	0.47	7.55	0.11	0.35	37.8	3.2	0.33	-	100.00
HC	46.3	0.01	2.68	1.08	7.00	0.11	0.18	41.8	0.9	0.02	-	100.00
GS	0.6	0.02	0.73	-	3.97	-	-	4.8	15.7	0.18	31.3	57.26
B10	16.0	0.19	0.30	0.11	18.31	0.34	0.08	22.2	8.3	0.47	5.8	72.12
B6	8.0	0.27	0.46	-	7.42	0.23	0.05	23.3	13.3	0.8	10.04	63.84
LC-B10	35.0	0.18	2.71	0.34	11.41	0.19	0.25	32.1	5.0	0.38	2.09	89.78
LC-B6	32.2	0.21	2.76	0.30	7.49	0.15	0.24	32.5	6.8	0.5	3.61	86.80
LC-GS	29.5	0.12	2.86	0.30	6.25	0.07	0.22	25.9	7.7	0.28	11.27	84.43
HC-B10	33.54	0.07	1.71	0.69	10.80	0.19	0.14	33.08	3.51	0.18	2.09	85.99
HC-B6	30.66	0.10	1.77	0.65	6.88	0.15	0.13	33.47	5.29	0.30	3.62	83.01
HC-GS	27.99	0.01	1.87	0.65	5.63	0.06	0.11	26.80	6.16	0.08	11.27	80.64

* Without account for CO_2

The composition of the melt formed in carbonated pelite at 8 GPa, and 1100°C (GS) (Grassi and Schmidt, 2011) was used for modeling the carbonatitic melt, which may be potentially generated in the subduction zones. Asthenospheric carbonatite was simulated using the composition of the melt formed in potassium rich carbonated harzburgite at 6 and 10 GPa and 1400°C (B6 and B10, respectively) Brey et al., 2011. Compositions HZ86, hereafter referred to as LC (Hart and Zindler, 1986) and HC, of Brey et al. (2011) (but without the addition of K_2CO_3) were used to model garnet lherzolite and garnet harzburgite. The compositions of the starting samples are given in Table 1. The samples were assembled layer-by-layer (the sandwich method): peridotite–carbonatite (36%)–peridotite and then loaded into graphite containers. Four to six containers were placed in a one cell assembly.

Experiments were performed using a BARS multi anvil apparatus at 5.5 and 6.3 GPa and 1350°C. The formation of equilibrium associations in the samples was provided by the long duration of runs (150 h). The accuracy in pressure and temperature control was ±0.1 GPa and ±20°C, respectively (Palyanov et al., 2010).

The temperature pattern within the low-gradient zone of the high-pressure cell was estimated by simulation using the software of Hernlund et al. (2006). The virtual cell included a graphite container with samples (forsterite + NaCl) shifted off the heater axis in the low-gradient zone, with the temperatures at the center of the container set at 1350 °C. The obtained temperature gradient in experimental samples was close to 10°C/mm.

After experiments, the samples were dried, mounted in epoxy, and then prepared to the study on a scanning microscope (Tescan MYRA 3 LMU) and microprobes (Cameca Camebax micro and Jeol JXA8100) using the standard methodologies. The limits of impurity detection were 0.01–0.02 wt %. The phase and chemical compositions of experimental samples are given in Tables 2 and 3. The phase concentrations in the samples were calculated on the basis of the microprobe data by the method of mass balance.
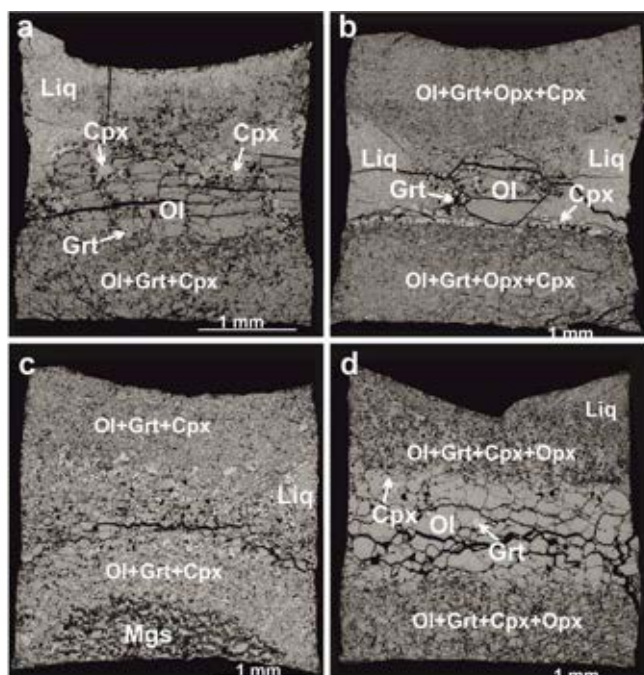
Fig. 1. Scanning electron micrographs of the representative samples after experiments at different temperatures. a: #1673, LC–GS, 1350 °C (bottom); b: #1673, HC–GS, 1350 °C (top) c: #1673, HC-B6, 1350 °C (top); and d: #1673, LC-B10, 1350 °C (bottom). Phase abbreviations: Ol=Olivine; Opx=Orthopyroxene; Cpx=Clinopyroxene; Grt=Garnet; Mgs=Magnesite; and Liq =Melt.

Comparison of the results of computer modeling with experimental data shows that the textures of the samples were controlled by: (1) layered charge; (2) carbonatite composition; and (3) position of peridotite–carbonatite "sandwiches" in the low gradient zone (Fig. 1). In all cases, melt migrated through the sample to the high temperature zone; the melt phase in the bottom "sandwiches" migrated to the top of the capsule (Fig. 1 a) while that from the top "sandwiches" moved to the sides (Fig. 1 b, c). After the runs, the samples with the layered (peridotite–carbonatite–peridotite) starting material consist of three zones. The first zone of the quenched melt occupies 20–37 vol %. The second zone with comparable sizes contains large (up to 500 μm), often euhedral newly formed crystals of olivine, clinopyroxene, and garnet. This zone occurs in the central part of the sample at the place of the carbonatite layer in the starting sandwich. Crystals have various orientations within this zone in most of the samples. In particular, sample LC-GS (Fig. 1 a) is characterized by a system of subparallel grains, most likely crystallized in the regime of geometric selection. The third zone of the peridotite matrix occupies up to 50% of the sample volume and is composed of anhedral olivine, clinopyroxene, orthopyroxene, and euhedral garnet with a grain size of ≤150 μm. Sometimes, the size of clinopyroxene grains reaches 350 μm (Fig. 1 d). Phases in the samples are unzoned and have identical compositions. Mg# in olivines and orthopyroxenes changes regularly from 84–87, in the most iron rich systems (LC-B10 and HC-B10), to 86–91 in other systems. The concentrations of CaO and Al_2O_3 in ortopiroxene obtained at 6.3 GPa are 1.3 and 0.6 wt.%, respectively. With decreasing pressure to 5.5 GPa, the concentration of Al_2O_3 in orthopyroxene increases up to 0.9 wt % and the concentration of CaO decreases to 1.1 wt %. Most of the garnets that crystallized in the sandwich samples with B6 and B10 carbonatite have Ti/Cr ratio from 0.1 to 1.0, typical of garnet in sheared lherzolite and metasomatized Cr-pyrope lherzolite. Some garnets (B10) have low Mg# (62–66) due to high bulk FeO in the system. Garnets with low Ti/Cr ratio and high Mg# (77–82) formed in peridotite matrices upon interaction with GS carbonatite and have compositions intermediate between garnet from depleted high-Cr peridotite and those from metasomatized Cr-pyrope lherzolites or sheared varieties. According to the concentrations of CaO and Cr_2O_3, garnets from the four-phase Ol + Grt + Opx + Cpx and three-phase Ol + Grt + Cpx associations are related to the area of the lherzolitic and wehrlitic parageneses, respectively (Sobolev et al.,1969). Ca# of clinopyroxenes increases from 0.36 to 0.41 with increasing bulk concentration of Ca in the system. The concentration of Na_2O ranges from 0.5 to 0.9 wt %; Al_2O_3 ranges within 1.05–1.3 wt %. Magnesite crystallized in sandwich-type samples with B10 having slightly higher FeO (8.3–9.5 wt.%) than magnesite in other carbonatite samples (5.0–7.3 wt.%). The concentration of CaO ranges from 2.2 to 3.4 wt.%.

The melt equilibrated with the four phase (Ol + Grt + Cpx + Opx) or three phase (Ol + Grt + Cpx) associations (Table 2) contained from 3.5 to 7 wt % SiO_2. In contrast to the initial carbonatite B6 and B10 (Ca# = 29 and 20), melts formed during interaction of peridotite with them have much lower concentrations of MgO and slightly lower concentrations of SiO_2 and K_2O. The melt synthesized in runs with carbonatite GS differs from the starting carbonatite by a slightly higher concentration of SiO_2 and lower concentration of K_2O. MgO/CaO ratio in such melt increases significantly (from 0.3 to 1). As a result, Ca# of melts ranges slightly (from 40 to 44) at 6.3 GPa and slightly increases up

to 47 at 5.5 GPa and, therefore, almost does not depend on the composition of the starting carbonatite (Tables 1, 3). This allows us to conclude that the composition of the carbonatitic melt is buffered by the peridotitic matrix. Moreover, Ca# of melts obtained during the interaction of peridotite with carbonatites of various compositions is generally consistent with Ca# of melts obtained in the peridotite–CO_2 system (Dasgupta and Hirschmann, 2007). The concentration of K_2O in melts in equilibrium with peridotite ranges from 7.6 to 26.6 wt %, and, due to the absence of other potassium hosted phases (≤0.5 wt % K_2O in clinopyroxene), is controlled by the composition of the starting carbonatite.

The data obtained show that the composition of melts formed as a result of the interaction of deep metasomatic agents (carbonatitic melts) of various origin with peridotite of the subcratonic lithosphere is controlled by a number of factors. The concentrations of CaO and MgO in them are buffered by silicate phases of peridotite, whereas the concentrations of alkalis (mostly K) and FeO depend on the composition of the starting carbonatite. Melts in equilibrium with the lherzolitic or wehrlitic phase associations are essentially carbonatitic at 5.5–6.3 GPa and 1350°C. They are characterized by low concentrations of SiO_2 (<7 wt %) and Ca# from 0.40 to 0.47.

Table 2. Phase composition of the samples (wt %)

Run no.	Sample	P,GPa	Ol	Grt	Opx	Cpx	Mst	Melt
1097-1	LC-B6	5.5	44	9	10	5	-	32
1673-1	LC-B6	6,3	55	12	1	12	-	20
1673-2	LC-B10	6,3	44	10	9	6	-	31
1673-3	LC-GS	6,3	34.5	12	-	16.5	-	63
1673-5	HC-B6	6.3	42.5	8.5	10	6	8	25
1097-3	HC-B10	5.5	43	8	22	-	5	22
1097-2	HC-GS	5.5	35	8	7	10	-	40
1673-4	HC-GS	6.3	43	9	<1	10	-	38
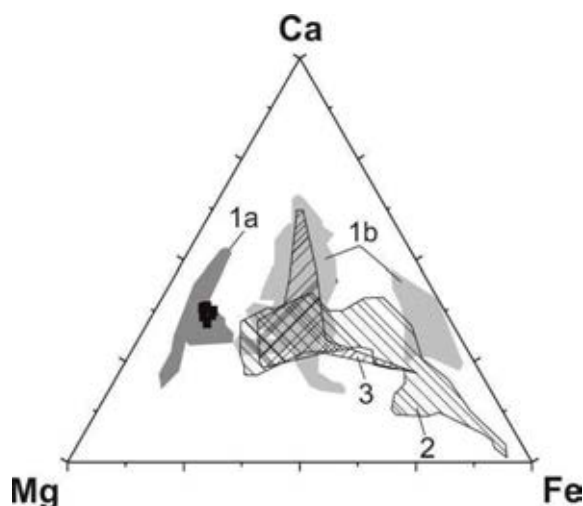
Fig. 2. Carbonatite melts equilibrated with peridotite (bold rectangles) and fluid inclusions in fibrous diamonds in Mg–Fe–Ca mol% ternary diagram. Fields 1a and 1b are after (Klein-Ben David et al., 2009); 2 is after (Zedgenizov et al., 2009); and 3 is after (Kopylova et al., 2010).

The most K-rich melt obtained in the experiment with GS carbonatite generally simulates the composition of K-rich inclusions in fibrous diamonds. The compositions of carbonatitic melts in equilibrium with peridotites plot in the narrow area on the Mg–Ca–Fe diagram (Fig. 2). Note, their composition is consistent with that of the high-magnesium series of carbonatitic inclusions in Yakutian fibrous diamonds only (Kopylova et al., 2010). This allows us to conclude that only some fibrous diamonds could crystallize from the carbonatitic melt in equilibrium with peridotite. The wide compositional variations of other carbonatitic inclusions could result from equilibrium with non-peridotitic matrix. The obtained data allows us to conclude that the formation of kimberlite like melts relatively enriched in SiO_2 (>15 wt %), the relationships of which with carbonatite are assumed on the basis of geochemical reconstructions (Becker and le Roex, 2006), requires additional source of heat of the mantle plumes and most likely H_2O fluid.

References:

Becker, M., le Roex, A.P.(2006) Geochemistry of South African on- and off-craton, group I and group II kimberlites: petrogenesis and source region evolution. Journal of Petrology 47, 673–703.

Brey, G.P., Bulatov, V.K., Girnis, A.V. (2009) Influence of water and fluorine on melting of carbonated peridotite at 6 and 10 GPa. Lithos 112, 249–259.

Brey, G.P., Bulatov, V.K., Girnis, A.V. (2011) Melting of K-rich carbonated peridotite at 6–10 GPa and the stability of K-phases in the upper mantle. Chemical Geology 281, 333–342.

Coe, N., Le Roex, A., Gurney, J., Pearson, D.G., Nowell, G. (2008) Petrogenesis of Swartruggens and Star Group II kimberlite dyke swarms, South Africa: constraints from whole rock geochemistry. Contributions to Mineralogy and Petrology 156, 627–652.

Dasgupta, R., Hirschmann, M.M. (2007) A modified iterative sandwich method for determination of near-solidus partial melt compositions. II. Application to determination of near-solidusmelt compositions of carbonated peridotite. Contributions to Mineralogy and Petrology 154, 647–661.

Hart, S.R., Zindler, A. (1986) In search of a bulk-earth composition. Chemical Geology 57, 247–267.

Hernlund, J., Leinenweber, K., Locke, D., Tyburczy, J. (2006) A numerical model for steady-state temperature distributions in solid-medium high-pressure cell assemblies. American Mineralogist 91, 295–305.

Kamenetsky, V.S., Golovin, A.V., Maas, R., Giuliani, A., Kamenetsky, M.B., Weiss, Y. (2014) Towards a new model for kimberlite petrogenesis: evidence from unaltered kimberlites and mantle minerals. Earth-Science Reviews 139, 145–167.

Klein-Ben David, O., Logvinova, A.M., Schrauder, M., Spetius, Z.V., Weiss, Y., Hauri, E.H., Kaminsky, F.V., Sobolev, N.V., Navon, O. (2009) High-Mg carbonatitic microinclusions in some Yakutian diamonds — a new type of diamond-forming fluid. Lithos 112 (Suppl. 2), 648–659.

Kogarko, L.N. (2006) Alkaline magmatism and enriched mantle reservoirs: Mechanisms, time, and depth of formation. Geochemistry International 44, 3-10.

Kopylova, M., Navon, O., Dubrovinsky, L., Khachatryan, G. (2010) Carbonatitic mineralogy of natural diamond-forming fluids. Earth and Planetary Science Letters 291, 126–137.

Palyanov, Y.N., Borzdov, Y.M., Khokhryakov, A.F., Kupriyanov, I.N., Sokol, A.G. (2010) Effect of nitrogen impurity on diamond crystal growth processes. Crystal Growth & Design 10, 3169–3175.

Sokol A.G., Kruk A.N., Chebotarev D.A., Palyanov Yu.N. (2016) Carbonatite melt–peridotite interaction at 5.5–7.0 GPa: Implications for metasomatism in lithospheric mantle. Lithos, , v. 248-251, p. 66-79

Wallace, M.E., Green, D.H. (1988) An experimental determination of primary carbonatite magma composition. Nature 335, 343–346.

Zedgenizov, D.A., Ragozin, A.L., Shatsky, V.S., Araujo, D., Griffin, W.L., Kagi, H. (2009) Mg and Fe-rich carbonate-silicate high-density fluids in cuboid diamonds from the Internationalnaya kimberlite pipe (Yakutia). Lithos 112 (Suppl. 2), 638–647.

METALLIFEROUS SEDIMENTS OF THE HYDROTHERMAL FIELD POBEDA-1, MID-ATLANTIC RIDGE: KEY TO THE GEOCHEMICAL AND TEMPORAL EVOLUTION OF THE VENTING SYSTEM

Kuksa K.A., Tabuns E.V., Bich A.S., Petrov A.Yu., Maksimov F.E.

Saint-Petersburg State University, Saint Petersburg, Russia, katerina.kuksa@spbu.ru

Metalliferous sediments are associated with seafloor hydrothermal vent systems widely developed at mid-ocean ridges. They record modern and/or ancient hydrothermal activity and can be extremely informative in understanding of geochemical evolution of the system, sources of metals and processes of ore accumulation. As the last heavily depends on the time span of the vent system circulation it becomes crucial to reconstruct the duration and periodicity of hydrothermal activity. Apart from sulfide dating, important chronological information can be obtained from examination of sediment cores. Unlike sulfides they maintain continuous records of the hydrothermal events and thus can play a crucial role in understanding of the duration and time span of the ore-forming processes. Despite the fact, that they also encounter some obstacles due to the changes in sedimentation rate, interruption of sedimentation process, disturbance of the accumulated sediments and some others it still remains quite informative.

In order to reconstruct geochemical and temporal evolution of hydrothermal system within recently discovered Pobeda ore field (Bel'tenev et al., 2015) we have performed geochemical and geochronological study of sulfide ores and a core of metalliferous sediments. The field Pobeda-1 is located at 17°09′ N, a depth of 1950-2400 m at the eastern slope of the rift valley and consists of four sulfide ore bodies (fig. 1) composed of several ~10 m high edifices and ore talus. Together with metalliferous sediments it covers an area of about 750 m^2 (Bel'tenev et al., 2016). Core 75k (64 cm deep) was recovered by TV grabs from the depth of 2208 m below water surface in close proximity to sulfide ore body II.
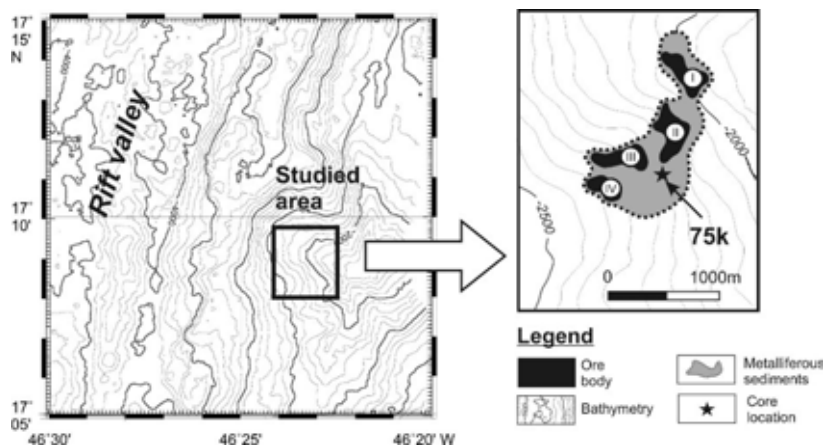
Fig. 1. Schematic map of Pobeda-1 hydrothermal field with the positions of the studied core (modified after Bel'tenev et al., 2016).

Sediments are mainly foraminiferal oozes with small amounts of sand material and organic detritus (bivalvia and pteropod shells). On-board observation revealed gradual contacts between different lithological units within the core except for one at a level 46 cmbsf between the metalliferous and overlying sediments (Bel'tenev et al., 2016).

The core was put to detailed geochemical investigation through each 1 cm. Sixty-two samples were analyzed for S, Mn, Fe, Cu, Zn, Pb, As, V, Cr, Co, Ni, Si, Ti, Al, Mg, Ca, K, P, Sr, and Ba concentrations by XRF spectrometry. Chemical composition of 12 sulfide ore samples from hydrothermal field Pobeda-1 was also determined by the same method and set of elements in the same Keppen-Laboratory of the St. Petersburg State University. Seven ^{14}C data were also performed in the Laboratory for the different parts of the sediment core.
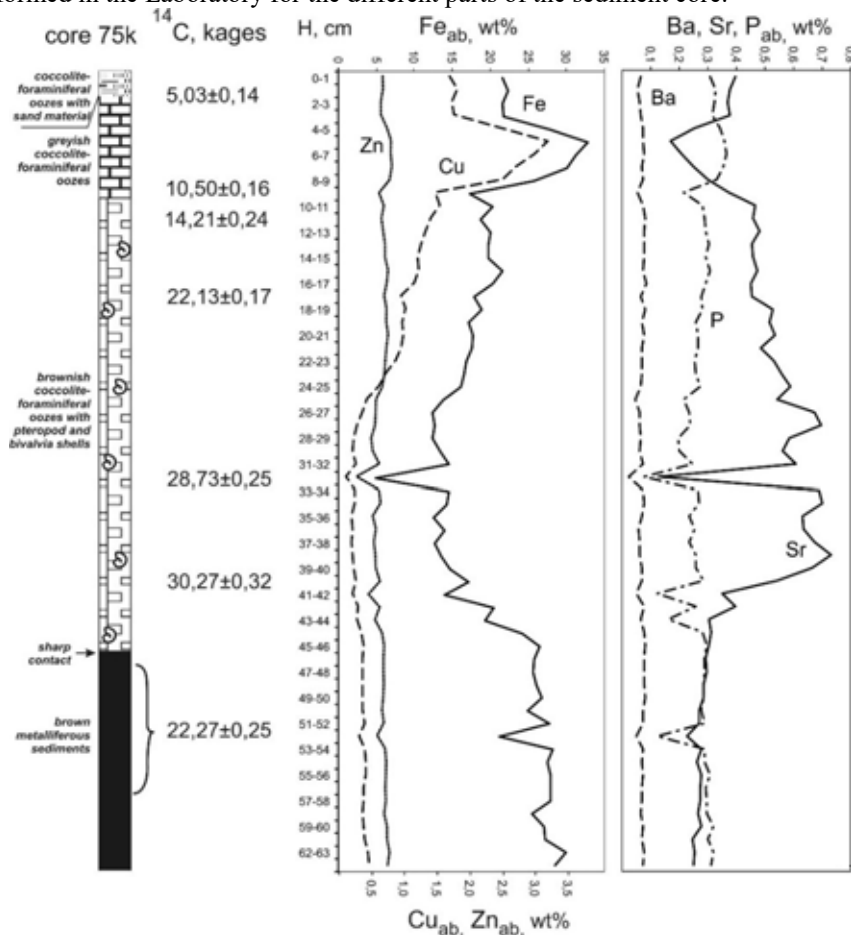
Fig. 2. Lithological composition of core 75k, its ^{14}C ages and down core distribution of elements.

Geochemical composition of studied core is typical for metalliferous sediments – they are strongly enriched in Fe, Mn, and other transition elements relative to normal pelagic sediments. Besides $CaCO_3$ which content varies from 34 to 71 wt%, the main constituents are Fe (3-18 %) and Si (0,6-7,0 %). Among minor elements are Cu (0,2-1,7 %), Al (0,2-1,8%), Mg (0,1-1,8%), K (0,1-0,5 %) and also P, Sr, Mn, Zn and V (up to 0,2%). Sulfides are composed of massive pyrite-marcasite ores with pyrrhotite relicts, pyrite-chalcopyrite and pyrite-sphalerite assemblages, ore breccias and stockwork. The bulk chemical and trace-element analysis indicate that the high Cu and Zn, concentrations (up to 18 and 2% respectively), and elevated Ba, Sr, As, Co, Ni are typical for chalcopyrite and sphalerite-bearing samples whereas pyrite-marcasite ores are moderately enriched in Fe, Mn, Pb and V.

Vertical distribution pattern of some elements in the core shows levels of pronounced enrichment of Fe, Mn, Cu, Zn, V, Cr and Pb which maxima occur at 4-9, 12-17 and 46-63 cmbsf (fig. 2). The edge of last maximum corresponds to the sharp interlayer contact observed between coccolite-foraminiferal oozes and metalliferous deposits. Others such as Sr, Ba, Al, Ti, K, As and Si tend to follow distinct patterns, sometimes opposite to that of ore elements.

A strong positive correlation was revealed between Fe and Co, Zn, Pb, V, As, P and Ba. On the other hand, P correlates negatively with Sr and Ba. The source for the first group of elements might be hydrothermal precipitates as it was established earlier for Pacific sediments (see for example Dymond, 1981; Gurvich, 2006). Other elements exhibited bimodal distribution in the sediments or no linear relations at all. Figure 3 demonstrates a typical example of such bimodal element distribution: with Fe/Cu ratio 81 (1) and with Fe/Cu ratio 8 (2). Projection of the first correlation line will inevitably end up at an area of pyrite-chalcopyrite (Cu-type) ores while the second trend will end up close to pyrite-marcasite ores (Fe-type). It allows us to suggest that different parts of the core sediments present mixtures of three end-member phases – enriched in Cu and Fe (A), enriched in Fe (B) and depleted in both elements (C). Phase C is probably a carbonate matter, whereas phases A and B correspond more likely to hydrothermal fluid precipitates which composition evolved through the studied time interval (about 40 ky) from Fe- and Pb- to Cu- and Zn-enriched.

International Conference on Magmatism of the Earth and Related Strategic Metal Deposits

Figure 2 presents preliminary ^{14}C ages of core sediments which were calculated without accounting of isotope exchange effects. It is well known that marine carbonate rocks are prone to isotope exchange with the dissolved hydrocarbonates of near-bottom ocean water which affects its primary isotopic composition. So, these ages should not be accounted as definite. Nevertheless, we can assume that ages of the sediments vary from 5 ky at the top to 30.3 ky at a layer 40-42 cm. It is interesting enough that underlying metalliferous deposits demonstrates younger ^{14}C age of 22.3+/- 0.25 ky. This might be caused by sediment perturbations (like downslope displacement). According to ^{14}C data the average rate of sedimentation for the core 75k was about 1.6 cm/ky. It varies with the depth from 0.9 cm/ky for the upper 2-18 cm to 2.8 cm/ky for the lower 18-40 cm. However, it is in a good agreement with the rate of sedimentation for metalliferous deposits at other Mid-Atlantic Ridge hydrothermal fields: Logatchev-1 (1.35 cm/ky), Krasnov (1.30-0.94 cm/ky) and Ashadze-2 (2.6-0.48 cm/ky) obtained by ^{230}Th chronometry (Kuznetsov, Maksimov, 2012).
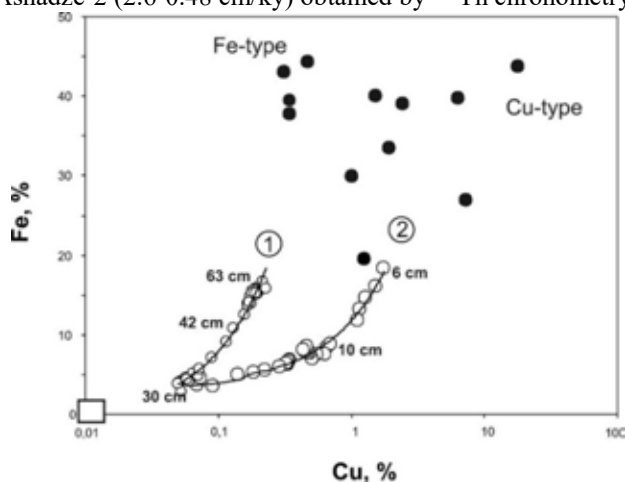
Fig. 3. Linear relationship between Cu and Fe in the sediments (open circles) and sulfide ores (filled circles). Open square shows theoretical position for phase C (see text for further explanations). Cu-type correspond to pyrite-chalcopyrite ores, Fe-type for pyrite-marcasite ores. Numbers in circles indicate two different correlation trends.

Taking into account the position of ore elements maxima and ^{14}C ages of sediments we can calculate the time span of hydrothermal activity which led to the formation of metalliferous layers. It fits in interval of 6.4-9.6 ka which is similar to estimation of ~10 ka given by E.G. Gurvich (Gurvich, 2006).

Authors would like to thank Dr G.A. Cherkashov for the initiation of this study and improvement of the abstract and also Dr E.A. Popova and V. E. Bel'tenev for their help with materials.

References:

Bel'tenev V., Narkevsky E.V., Dobretsova I.G., Gablina I.F., Galkin S.V., Molodtsova T.N., Layba A.A. (2015) Resul'taty 37 reisa NIS "Professor Logatchev", SAH [The results of 37 cruise of RV Professor Logatchev, MAR // Materials of the XXI International Conference on Marine Geology, M., p. 126-128 (in Russian).

Bel'tenev V. et al. (2016) Poiskoviye raboty na ploschady Rossiyskogo razvedochnogo rayona v Atlanticheskom okeane s ocenkoy prognoznykh resursov GPS P_1 i P_3 v blokah 31-45 [Geological surveys at Russian Exploration Area MAR with the estimation of the potential resources of P_1 and P_3 in blocks 31-45 // Fond PMGE, Lomonosov (in Russian).

Cherkashev G., Kuznetsov, V., Kuksa K., Tabuns E., Maksimov F., Bel'tenev V. (2016) Sulfide geochronology along the Northern Equatorial Mid-Atlantic Ridge // Ore Geology Reviews, in press (doi: 10.1016/j.oregeorev.2016.10.015).

Dymond J. (1981) Geochemistry of Nazca plate surface sediments: An evaluation of hydrothermal, biogenic, detrital, and hydrogenous sources // Geol. Soc. Amer. Mem., V. 154, p. 133-174.

Gurvich E.G. (2006) Metalliferous sediments of the orld Ocean. Fundamental theory of deep-sea hydrothermal sedimentation. Springer-Verlag, 423 p.

Kuznetsov, V.Yu., Maksimov F.E. (2012) Geochronometrical methods of the quaternary deposits in paleogeography and marine geology. SPb: Nauka. 191 p. (in Russian).

THE ROLE OF CARBONATE-FLUORIDE MELT IMMISCIBILITY IN SHALLOW REE DEPOSIT EVOLUTION: NEW EVIDENCE FROM THE LUGIIN GOL HIGH GRADE REE DEPOSIT, MONGOLIA

Kynicky J.[1,2], Smith M.P[3], Song W.[1,2], Chakhmouradian A.R.[4], Xu Ch.[5], Fryzova R.[1], Kopriva A.[2], Brtnicky M.[2]

[1]Mendel University in Brno, Brno, Czech Republic
[2]Brno University of Technology, Brno, Czech Republic
[3]University of Brighton, Brighton, United Kingdom
[4]University of Manitoba, Winnipeg, Canada
[5]Peking University, Beijing, China

The Lugiin Gol deposit, Mongolia, is hosted by a range of carbonatite dikes mineralized in rare-earth elements (REE). Both these dikes, and composite nepheline syenite-fluorite-calcite veinlets, are host to a previously unreported macroscale texture involving pseudo-graphic intergrowths of fluorite and calcite. The inclusions within calcite occur as either pure fluorite, with associated REE minerals within the surrounding calcite, or as mixed calcite-fluorite inclusions,

with associated Zr minerals. Consideration of the nature of the texture, and the proportions of fluorite and calcite present (~29and 71mole %, respectively), indicates that these textures formed through either cotectic crystallization of the immiscible separation of carbonate and fluoride melts. Pure fluorite inclusions are depleted in REE relative to the calcite. A model is proposed, in which a carbonate-fluoride melt phase enriched in Zr and the REE, separated from a phonolitic melt, and then either unmixed or underwent cotectic crystallization to generate an REE-rich carbonate melt and an REE-poor fluoride phase. The separation of the fluoride phase (either solid or melt) may have contributed to the enrichment of the carbonate melt in REE, and ultimately its saturation with REE minerals. Previous data have suggested that dry carbonate melts separated from silicate melts are relatively depleted in the REE, and thus melt immiscibility cannot result in the formation of REE-enriched carbonatites. The observations presented here provide a mechanism by which this could occur, as under either model the textures imply initial separation of a mixed carbonate-fluoride melt from silicate magma. Multistage silicate-carbonate-fluoride melt immiscibility may be a previously unrecognized, but important process in the generation of REE-mineralized carbonatites.

NEW INSIGHTS INTO ORIGIN OF PLATINUM DEPOSITS IN LAYERED INTRUSIONS FROM THE UNDERCUTTING MERENSKY REEF OF THE BUSHVELD COMPLEX

Latypov R.M.[1], Chistyakova S.Yu.[1], Barnes S.J.[2], Hunt E.J.[1]
[1]University of the Witwatersrand, Johannesburg, South Africa, rais.latypov@wits.ac.za
[2]CSIRO Mineral Resources, Perth, Australia

Models proposed to explain Merensky-type reefs in layered intrusions fall into two major groups: (a) orthomagmatic ones, which consider platinum-group element (PGE) mineralization as an integral part of magma crystallization processes in the chamber; and (b) hydromagmatic ones, which attribute PGE mineralization to volatile-rich fluids exsolved from cooling cumulate piles (e.g. Mungall & Naldrett, 2008; Cawthorn, 2011; Godel, 2015). Most recent studies on stratiform PGE Reefs appear to favour an orthomagmatic approach and interpret them as the result of accumulation of highly PGE-enriched immiscible sulphide liquids on the temporary floor of the host magma chamber. Here we specifically focus on the orthomagmatic models, which can be subdivided into two major categories invoking either (1) gravity-induced settling of crystals from the overlying magma onto the chamber floor, with subsequent sorting of minerals during late-stage slumping of the cumulate pile or (2) *in situ* crystallization of all minerals, including chromite and sulphides, directly on the chamber floor, accompanied by re-deposition of the minerals in association with convection in the magma chamber. The resolution of this dilemma has an important implication for our understanding of processes of crystallization and differentiation of magma as well as formation of economically viable magmatic mineral deposits.

A unique feature pertinent to this issue is the undercutting Merensky Reef (MR) of the Bushveld Complex, South Africa, which is commonly associated with potholes, roughly circular depressions in which footwall rocks are removed by magmatic erosion (Fig. 1). The undercutting MR forms sill-like apophyses of medium- to coarse-grained harzburgite and orthopyroxenite enriched in sulphide and chromite, which extend laterally from pothole margins into.
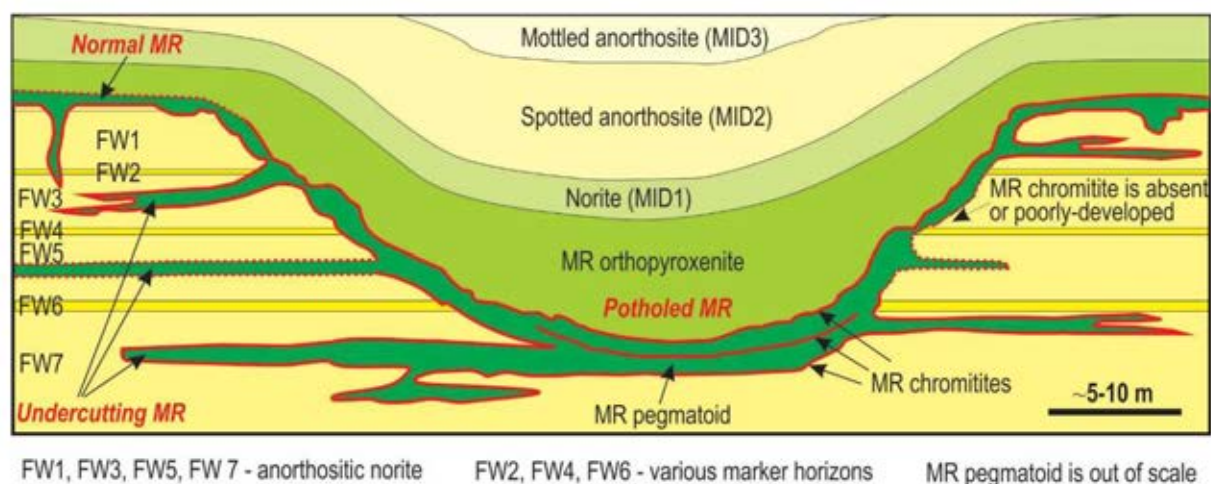
Fig. 1. A sketch of a typical MR pothole at the Impala Platinum Mine, Western Bushveld (modified from Golenya, 2007) illustrating the transgressive relationship of the normal and potholed MR to its footwall. Note that the potholed MR along the edge of the pothole is accompanied by undercutting MR bodies that are sill-like sulphide- and chromite-mineralized protrusions extending laterally from pothole margins into footwall rocks. Morphology of undercutting MR is depicted based on our personal observations from the Pilanesberg Platinum Mine and those of Ballhaus (1988) from the Rustenburg Platinum Mine. FW – footwalls; MID – middling.

They vary in thickness from 5 cm to 1-2 m and can be traced away from pothole margins for distances from a few centimeters to dozens of meters (in one case up to 300 m). Locally there may be several (six or more) apophyses of

undercutting MR that are vertically stacked within the footwall cumulates in the vicinity of a single pothole. The most telling field, textural and geochemical features of the undercutting MR are as follows: (a) there is no evidence of deformation of igneous layering or rotation of xenoliths associated with these reefs; (b) thin reaction-type selvages of almost pure anorthosite after host leuconorite or mottled anorthosite are commonly developed along both margins of undercutting MR; (c) undercutting MR are mineralogically zoned; thin seams of massive chromitite are commonly developed along both margins and pass inwards into rocks with decreasing amounts of disseminated chromite (Fig. 2); sulphides can be most abundant at the base, along both margins or in the centre of the apophyses; (d) undercutting MR are also compositionally zoned, with rocks displaying either an increase or decrease in whole-rock MgO content from the margins inwards; (e) undercutting MR are highly enriched in PGE, which are mostly controlled by sulphides and chromite, with the grade and tenor being comparable to those of the normal MR.
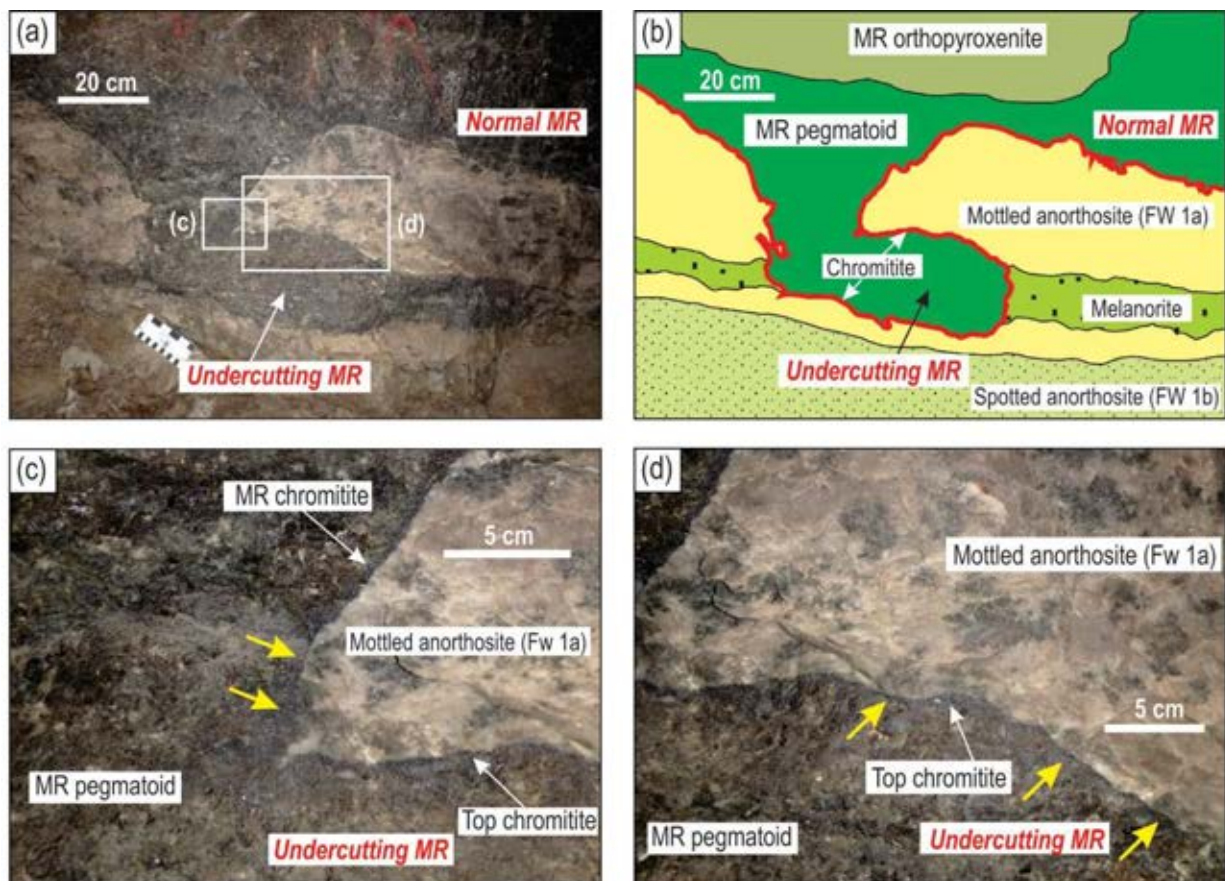
Fig. 2. Photo (a) and sketch (b) of undercutting MR that is rimmed by chromitite seams. Note the lack of deformation of layering in footwall rocks by undercutting MR. Close-up photos showing details of undercutting MR (c-d) rimmed by chromitite seams. Note that the chromitite seams appear to cut across single pyroxene oikocrysts in host mottled anorthosites (yellow arrows). 22mE 9B RSE, Shaft 3 of the Karee mine, Lonmin Platinum, Western Bushveld Complex.

A key inference is that the development of the undercutting MR within footwall rocks, in some cases many metres below a temporary chamber floor, completely eliminates their origin by gravitational settling from the overlying magma. *In situ* crystallization appears to be the only possible mechanism through which these zoned reefs could be produced. The undercutting MR is interpreted to develop along particularly amenable horizons at pothole margins through thermal/chemical erosion of the footwall rocks by superheated magma, followed by *in situ* crystallization within the resulting cavities. This indicates that scavenging of PGE by sulphides and chromite must have been taken place essentially *in situ*; that is, directly on magma–cumulate interfaces and that this process must have been remarkably efficient to concentrate PGE to an economically viable extent (10-60 ppm in grade). This process appears to have been just as efficient in the undercutting environment as in normal "open" MR, based on the observed similarity in the PGE tenors of the sulphides in both settings. This appears to only be possible if convective magma flow has acted as a conveyor that delivered a large amount of fresh, PGE-undepleted magma towards the crystal-liquid interface. Formation of PGE-rich cumulates in such sill-like bodies is possible because the rate of mass transfer by convection (km/year to km/day) is typically several orders of magnitude higher than the rate of crystallization (0.5-1.0 cm/year). This means that magma in the apophyses could exchange with the main body of magma in the chamber rapidly, compared to the rate of crystallization in the undercutting bodies. It follows that *in situ* crystallization was the dominant mechanism for the formation of not

only undercutting MR, but also of the more common normal and potholed MR, which occur along flat and inclined portions of the chamber floor, respectively. The same inference may be valid for platinum deposits in other layered intrusions that do not display convincing field evidence for *in situ* crystallization due to a lack of potholes and their associated sill-like protrusions into footwall rocks.

To conclude, the new field, textural and geochemical observations on undercutting MR reinforce our idea (Latypov et al., 2015; 2017) that the formation of PGE deposits in layered intrusions does not require long-range gravitational settling of chromite and sulphide droplets from overlying magma, as implied in most current models. The gravity settling mechanism does not appear to be crucial for the origin of either PGE deposits or the host layered intrusions. The highly mineralized undercutting MR bodies in the Bushveld Complex are remarkable evidence for the attainment of high PGE concentrations in stratiform PGE deposits of layered intrusions through *in situ* crystallization directly on crystal-liquid interfaces.

References:

Ballhaus, C. (1988). Potholes of the Merensky reef at Brakspruit shaft, R.P.M. - primary disturbances in the magmatic stratigraphy // Economic Geology 83, 1140-1158.

Cawthorn, R.G. (2011). Geological interpretations from the PGE distribution in the Bushveld Merensky and UG2 chromitite reefs // Journal of the South African Institute of Mining and Metallurgy 111, 67-79.

Godel, B. (2015). Platinum-group element deposits in layered intrusions: recent advances in the understanding of the ore forming processes. In: Charlier B., Namur, O., Latypov R., Tegner, C. (eds). Layered Intrusions // Springer p.379-432. (1st Edition ed.). Weteringschans: Springer International Publishing. New York City: Springer.

Golenya, F. (compiler). (2007). No. 17 Shaft Project . Geology & valuation sub-team report // Bull. Geol. Dept. Impala Platinum Ltd (unpubl.), 502, Addendum 1, Vol. 1, 81 pp.

Latypov, R. M., O'Driscoll, B. & Lavrenchuk, A. (2013). Towards a model for in situ origin of PGE reefs in layered intrusions: insights from chromitite seams of the Rum Eastern Intrusion, Scotland // Contributions to Mineralogy and Petrology 166, 309-327.

Latypov, R.M., Chistyakova, S.Yu, Page, A. & Hornsey, R. (2015). Field evidence for the in situ crystallization of the Merensky Reef // Journal of Petrology 56, 2341–2372.

Latypov, R.M., Chistyakova, S.Yu., Barnes, S.J. & Hunt, M. (2017). Origin of platinum deposits in layered intrusions by in situ crystallization: evidence from undercutting Merensky Reef of the Bushveld Complex // Journal of Petrology (accepted manuscript).

Mungall, J.E. & Naldrett, A.J. (2008). Ore deposits of the platinum-group elements // Elements 4, 253-258.

TOWARDS A NOVEL HYPOTHESIS FOR ORIGIN OF MASSIVE CHROMITITES IN THE BUSHVELD IGNEOUS COMPLEX

Latypov R.M., Chistyakova S.Yu., Mukherjee R.

University of the Witwatersrand, Johannesburg, South Africa, rais.latypov@wits.ac.za

The origin of stratiform layers of massive chromitite (60-90 vol.% chromite) is a long-standing puzzle in petrology mafic-ultramafic sills and layered intrusions (e.g. Alapieti et al., 1989; Marques & Ferreira Filho, 2003; Naldrett *et al.*, 2012, Maier *et al.* 2013, Mungall, 2014; Cawthorn, 2015). The origin of chromitites in the Bushveld Complex has been attributed to two principal mechanisms: (1) gravity-controlled settling of chromite onto the chamber floor from magma that was saturated in chromite, either initially or due to some internal process; or (2) gravity- and size-controlled separation of chromite from co-existing olivine and orthopyroxene within crystal-rich slurries, either formed directly within the chamber or brought into the chamber from some deep staging reservoirs. Here we present field observations from potholes, roughly circular structures in which footwall rocks were removed by magmatic erosion, that rules out both approaches. A key observation is that UG1/UG2 chromitites drape the irregular margins of potholes, even where they are vertical or overhanging (Fig. 1). These relationships eliminate both early settling of chromite from the overlying magma and late mechanical segregation of chromite within cumulates as viable hypotheses. In addition, thick chromitites commonly consist of several texturally and compositionally distinct sublayers that are locally separated by thin partings of silicate rocks. The absence of thick sequences of intervening silicate rocks from which chromite may have been separated to form these sublayers refutes an origin from crystal slurries. Transgression of chromitite-orthopyroxenite units by hanging wall rocks excludes the origin of chromitites from crystal slurries that intrude as late-stage sills into pre-existing cumulates. The field relationships appear to be compatible only with the emplacement of superheated, dense magma along the temporary base of the chamber that led to intense melting and dissolution of the pre-existing floor cumulates, followed by the *in situ* crystallization of chromite directly on the irregular chamber floor.
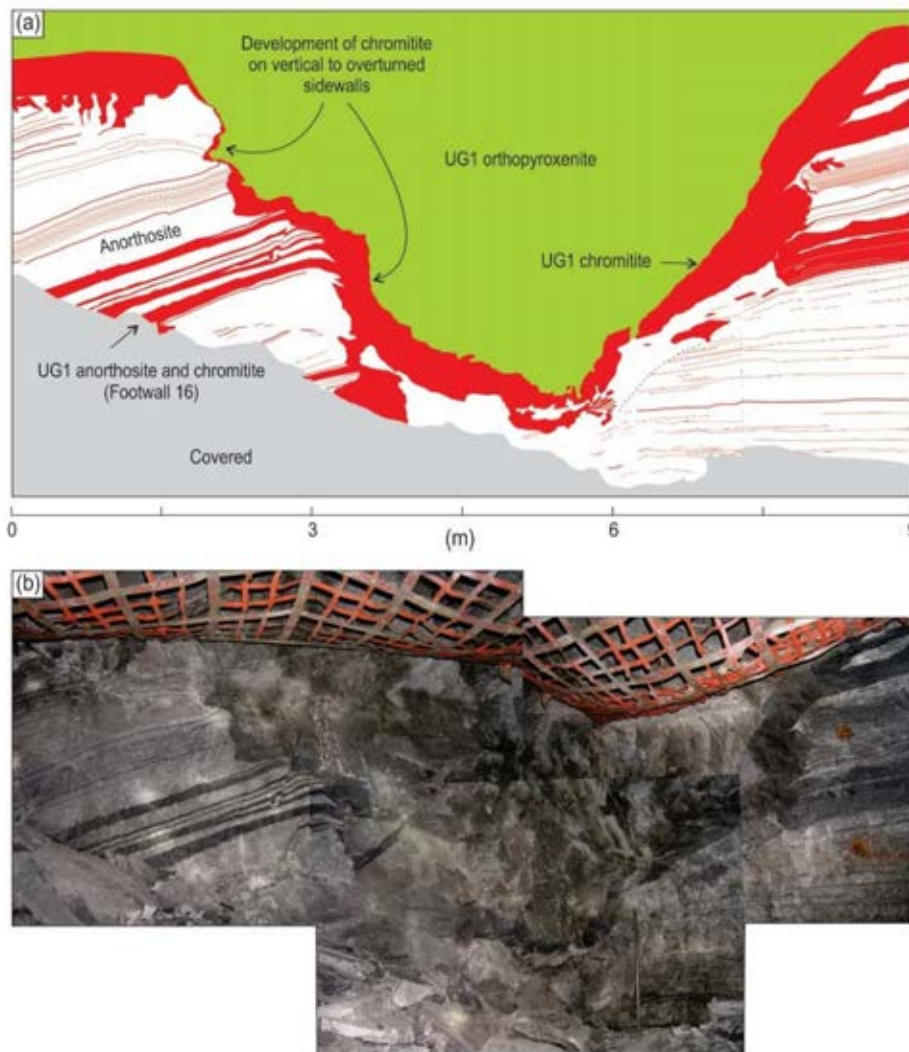
Fig. 1. Sketch (a) and photograph (b) of an oblique cross-section showing UG1 chromitite draping over steeply-inclined to overhanging walls of a pothole. Note crosscutting relationships of the UG1 chromitite with interlayered anorthosite and chromitite in the footwall rocks and disrupted layering on the right side of a pothole. Level 15, Shaft 10 of the Impala Platinum Mine, Western Bushveld.

Based on the above premises, we advance a novel hypothesis for origin of UG1/UG2 chromitites in the Bushveld Complex that involves the following sequence of events: (1) new dense and superheated magmas replenished the chamber with little to no mixing with the stratified melt in the chamber; (2) the magma spread out laterally along the floor of the chamber and caused intense thermochemical erosion of the floor cumulates, resulting in an igneous unconformity; on cooling, most of these magmas crystallized orthopyroxenite cumulates; (3) some batches of magma were, however, chromite-saturated and, after cooling, crystallized chromite directly on the chamber floor, draping all irregularities produced by the previous erosion; (4) chromite and sulphide droplets that grew directly at the crystal-liquid interface extracted PGE from a large volume of fresh magma delivered to the base of the chamber by vigorous flow/convection in the basal layer. (5) Formation of chromitite occurred through prolonged replenishment of the chamber by chromite-saturated magmas, which caused multiple cycles of thermochemical erosion of pre-existing cumulates followed by *in situ* crystallization of chromite on the chamber floor; this resulted in the formation of thick layers of PGE-rich chromitite that consist of several sublayers with distinct textural and compositional characteristics. (6) The formation of chromitites was commonly terminated by the emplacement of pulses of new magma that were not saturated in chromite and therefore resulted in local thermal/chemical erosion of chromitites with subsequent deposition of hanging wall orthopyroxenite. Thus, chromitites are both underlain and overlain by cumulate rocks produced from magmas that replenished the chamber. These rocks developed from magmas that were similar in composition and therefore lack cryptic variations in mineral composition above and below the chromitite layers.

It should be noted that the field relationships of UG1/UG2 chromitites with their footwall and hanging wall rocks are very similar to those of the Merensky Reef (Latypov *et al.,* 2015; 2017). This provides support for the opinion (e.g. Irvine & Sharpe, 1986) that the chromitite of the Merensky Reef can essentially be regarded as the UG4 chromitite. This also suggests that there are no substantial differences in the origin of the UG1/UG2 and Merensky Reef chromitites, i.e. they are essentially products of the same process – which we interpret to be basal replenishment of the chamber by chromite-saturated magmas. This scenario appears to be conceptually the simplest and physically most plausible explanation for origin of thick chromitites in the Bushveld Complex and we infer that these processes can be extrapolated to chromitites in other mafic-ultramafic layered intrusions.

References:

Alapieti, T.T., Kujanpää, J., Lantinen, J.J. & Papunen, H. (1989). The Kemi stratiform chromitite deposit, Northern Finland // Economic Geology 84, 1057-1077.

Cawthorn, R.G. (2015). Bushveld Complex. In: Charlier B., Namur, O., Latypov R., Tegner, C. (eds) // Layered Intrusions, p. 517-587. Springer International Publishing. New York City: Springer.

Irvine, T.N. & Sharpe, M.R. (1986). Magma mixing and the origin of stratiform oxide ore zones in the Bushveld and Stillwater Complexes. In: Gallagher, M. J., Ixer, R. A., Neary, C. R. & Pritchard, H. M. (eds) // Metallogeny of Basic and Ultrabasic Rocks. Instit. Mining Metallurgy, London, 183-198.

Latypov, R.M., Chistyakova, S.Yu, Page, A. & Hornsey, R. (2015). Field evidence for the in situ crystallization of the Merensky Reef // Journal of Petrology 56, 2341–2372.

Latypov, R.M., Chistyakova, S.Yu., Barnes, S.J. & Hunt, M. (2017). Origin of platinum deposits in layered intrusions by in situ crystallization: evidence from undercutting Merensky Reef of the Bushveld Complex // Journal of Petrology (accepted manuscript).

Maier, W.D., Barnes, S.J. & Groves, D.I. (2013). The Bushveld Complex, South Africa: formation of platinum–palladium, chrome- and vanadium-rich layers via hydrodynamic sorting of a mobilized cumulate slurry in a large, relatively slowly cooling, subsiding magma chamber // Mineralium Deposita 48, 1-56.

Marques, J.C. & Ferreira Filho, C.F. (2003). The chromite deposits of the Ipueira-Medrado Sill, Bahia, Brazil' // Economic Geology 98, 87–108.

Mungall, J.E. (2014). Geochemistry of Magmatic ore deposits. In: Holland, H. D. & Turekian, K. K. (eds) // Treatise on Geochemistry. Volume 13, Pergamon, Oxford, pp. 195-218.

Naldrett, A., Kinnaird, J., Wilson, A., Yudovskaya, M. & Chunnett, G. (2012). The origin of chromitites and related PGE mineralization in the Bushveld Complex: new mineralogical and petrological constraints // Mineralium Deposita 47, 209-232.

CPX-PHL XENOLITHS FROM THE V. GRIB KIMBERLITE (ARKHANGELSK DIAMOND PROVINCE, RUSSIA): ISOTOPIC CHARACTERISTICS AND GEOCHEMICAL COMPOSITION OF CPX AND PHL

Lebedeva N.M.[1,2], Kargin A.V.[1], Sazonova L.V.[1,2], Nosova A.A.[1], Kostitsyn Yu.A.[3]

[1]Institute of Geology of Ore Deposits, Petrography, Mineralogy and Geochemistry of the Russian Academy of Sciences, Moscow, Russia, namil@mail.ru
[2]Lomonosov Moscow State University, Moscow, Russia
[3]Vernadsky Institute of Geochemistry and Analytical Chemistry of the Russian Academy of Sciences, Moscow, Russia

Kimberlites are ultrabasic igneous rocks consisting of (1) juvenile magmatic material; (2) crustal and mantle-derived xenoliths and xenocrysts; and (3) set of megacrysts, such as Grt, Cpx, Phl, Ol, and Ilm.

Xenoliths of clinopyroxene-phlogopite rocks (from garnet-phlogopite peridotite to clinopyroxene-olivine-phlogopite wehrlite) are direct indicators of progressive modal metasomatism that has been widely studied in xenoliths from kimberlites (e.g. van Achterbergh et al., 2001). Probably, this metasomatism takes place due to the progressively substitution of the harzburgitic mineral assemblage (garnet, olivine, and orthopyroxene) by Cpx and Phl (O'Reilly and Griffin, 2013). At present, the origin and composition of metasomatic fluids or melts are still being discussed. Melts genetically related to kimberlite of Group II (volatile-rich alkaline mafic silicate melt,(van Achterbergh et al., 2001), H_2O-containing K-rich carbonatic melt, and melt/fluid) are usually considered as agents contributed to the formation of mantle metasomatic clinopyroxene–phlogopite association (Gregoire et al., 2003).
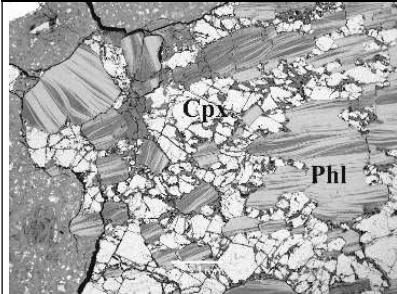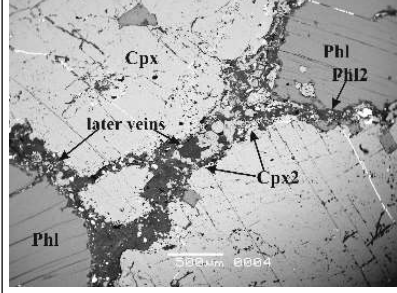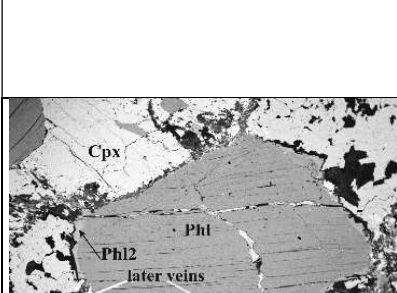
Another formation mechanism of Cpx-Phl rocks is supposed for minerals megacrystic association (Moore and Belousova, 2005). Those rocks are formed due to fractional crystallization of protokimberlite melt. They like pegmatitic veins in thermal aureole surrounding the kimberlite magma in the mantle.

We studied the major (EMPA) and trace (SIMS) elements composition and isotopic-geochemical characteristics (Rb-Sr and Sm-Nd, TIMS) of Cpx and Phl from xenoliths.

The V. Grib kimberlite pipe (376±3 Ma, Larionova et al., 2016) is located in the central part of Arkhangelsk diamond province (ADP) in the Paleoproterozoic collisional suture zone under Archean lithosphere roots. According to the geochemical and Sr-Nd isotopic composition, the Grib kimberlite is classified as Group I kimberlite (Kononova et al., 2007). The V. Grib kimberlite pipe is unique in ADP; because it contains diamonds in industrial concentrations and has an abundance of xenoliths of mantle peridotite, eclogite, metasomatic mantle rocks, and megacrysts of garnet, clinopyroxene, phlogopite, olivine and ilmenite (Sazonova et al., 2015 and references herein).

Three Cpx-Phl xenoliths were withdrawn from the Grib kimberlite (drillcore 1/1000). The samples were kindly provided by the Territorial Fund of the Geological Information of the Northwestern Federal District, Arkhangelsk, Russia. Their petrographic description is given in Table 1.

Table 1. Petrographic characteristics of the Cpx–Phl xenoliths from the V. Grib kimberlite (SEM, backscattered electron image)

	S.14GR-1-296-1. The xenolith is about 1 cm in size with rounded shape and granoblastic with elements of lepidoblastic (parallel align of Phl grains) microstructures. The xenolith consist of intergrowths of Cpx and Phl grains (50x50 vol. %). Phl laths are variety of size – from 1 to 5 mm and are strongly altered. Cpx occur as angular-irregular grains, from 0.5 up to 3 mm in size. The majority of Cpx grains are fractured.
	S.14GR-1-715-4. The xenolith has rounded shape with 4x6 cm in size. The rock consists of Cpx (60%) and Phl (40%) and has medium- to coarse-grained granoblastic texture. Phl occurs as short-flaky grains, 1-4 mm in size. Cpx occur as angular-irregular crystals, 1-5 mm in size. Some clinopyroxenes contain small (up to 100-200 μm) rounded inclusions of olivine grains that have similar composition (Fo_{92}) with olivine from mantle peridotite xenoliths from the Grib kimberlite (Sazonova et al., 2015). The xenolith is cross - cut by thin veinlets (up to 0.2-0.3 mm) of carbonate + phlogopite + Cr-spinel ± secondary undefined Mg-Fe-Si phase that probably altered kimberlite melt or originated from a residual H_2O-silicate fluid. Along the contact with veinlets and at the edges of grains, Cpx and Phl change their composition and become lighter by backscattered electron image. The rock also contains Mg-ilmenite, rutile, and magnetite.
	S.14GR-1-799-4. The xenolith is 2x3 cm in size with irregular and angular shape and granoblastic with texture. The xenolith consist of intergrowths of Cpx (60 vol. %) and Phl (40 vol.%). Phl laths are different in size – from 0.*n* to 3 mm; their elongation coefficient is about 2.0. Cpx forms angular isometric grains of 2-4 mm in size. The rock contains numerous fine veinlets that are compositionally similar to ones form sample 14GR-1-715-4. At the contact with these veinlets, Cpx and Phl change their composition; newly formed Cpx2 and Phl2 occur.

Clinopyroxenes are represented by Cr-diopside with Cr_2O_3 contents from 0.85 to 2.49 wt.%. Cpx from the Cpx-Phl xenoliths show typical "peridotitic" major element compositions, with high Mg#, Cr# and Ca# values and enrichment in Al_2O_3, Na_2O but they depleted in TiO_2 in compare with other "classical" Fe-Ti-megacryst suites worldwide. Clinopyroxenes show REE patterns with strongly fractionated MREE and HREE. At the same time, there are negative anomalies of Zr-Hf and Ti. Low contents of Nb, Zr, Hf, and Ti suggest that grains clinopyroxenes were formed due to fractionation of ilmenite that is present in the Grib kimberlite as megacrysts and intergrowths with clinopyroxenes grains (Golubkova et al., 2013; Sablukov et al., 2000). The late clinopyroxene (Cpx2) appear along veinlets filled by the kimberlite-associated material. Cpx2 has sharp boundaries in BSE and an increase TiO_2 contents and Ca# values with decreasing in Na_2O contents.

Phlogopite. Phl correspond to the low-Cr and low-Ti Phl from garnet peridotite xenoliths and macrocryst cores from V. Grib kimberlite (Larionova et al., 2016). The marginal zones of Phl (Phl2) are enriched by Cr and Ti with high Al_2O_3 contents. Phlogopites correspond to Phl from marginal zones of Phl grains, which are in matrix of garnet peridotite xenoliths, and to small Phl flakes around garnet porphyroblasts of garnet peridotite xenolith from V. Grib kimberlite (Larionova et al., 2016).

As the carbonate mineral with the high content of Sr was found in fissures of Cpx, that the samples for the isotopic analysis had to be pretreated with acetic acid.

Table 2. Sr and Nd isotope composition of clinopyroxene and phlogopite from Cpx-Phl xenoliths

Sample (mineral)	Rb, ppm	Sr, ppm	$^{87}Rb/^{86}Sr$*	$^{87}Sr/^{86}Sr$ ±2σ	Sm, ppm	Nd, ppm	$^{147}Sm/^{144}Nd$	$^{143}Nd/^{144}Nd$±2σ
14Gr1-296-1 (Cpx)	4	295	0.0432	0.705088±6				
14Gr1-715-4 (Cpx)	1	747	0.00580	0.707906±4	2	9.6	0.13032	0.512530±17
14Gr1-799-4 (Cpx)	6	507	0.0351	0.706151±16	3	17.6	0.11403	0.512430±9
14Gr1-296-1 (Carb)	0.3	17	0.0521	0.708433±38				
14Gr1-715-4 (Carb)	1	35	0.0875	0.709927±17				
14Gr1-715-4 (Phl)	553	200	8.02	0.751727±8	0.14	0.98	0.08716	0.512421±40
14Gr1-799-4 (Phl)	422	82	14.92	0.786426±8	0.12	0.79	0.09278	0.512444±13
The error of the determined $^{87}Rb/^{86}Sr$ ratio was assumed to be 1%.								

These carbonate-containing extracts were analyzed. To estimate the effect of the carbonate contribution to the Sr concentration in the Cpx, sample 14Gr1-715-4 was also analyzed without the preliminary handling with acetic acid. In this case, the Sr content reached 1410 ppm, i.e., it is almost two times higher than in the purified sample (747 ppm) and higher than the Sr content obtained by SIMS method (av. 450 ppm). The initial isotopic ratios were calculated using the age (376±3 Ma) of the V. Grib kimberlite pipe (Larionova et al., 2016).
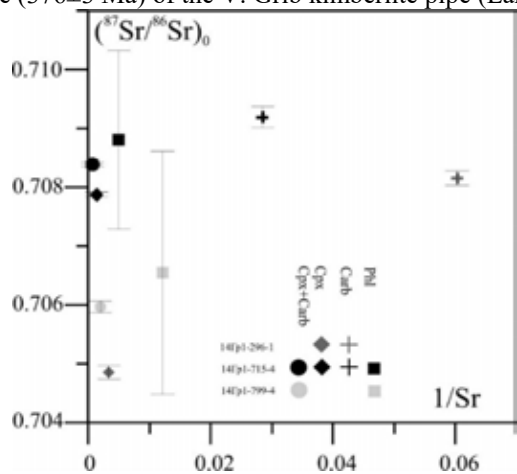
Fig. 1 $^{87}Sr/^{86}Sr$ vs reverse Sr concentrations.
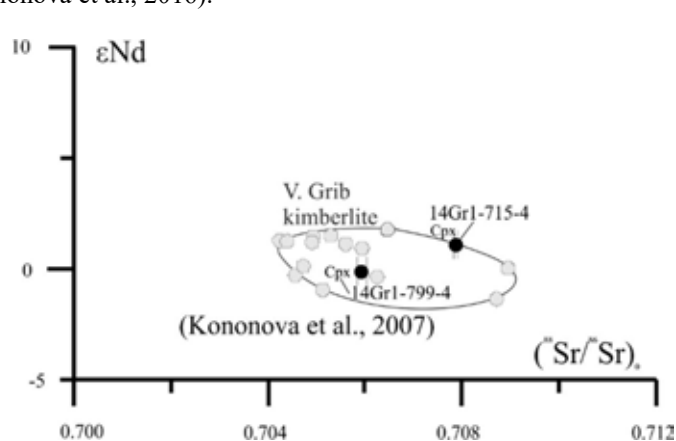
Fig.2 Initial ($^{87}Sr/^{86}Sr$) versus eNd(t) values of Cpx, t=376. Compared with V. Griba kimberlite data (Kononova et al., 2007)

There is no evidence of simple two-component mixing between Cpx and Carb. Unpurified Cpx data points do not lie along a straight line on a "mixing" diagram (Fig.1). High Sr initial isotopic ratios in Cpx probably have no link to carbonate material, because (1) initial Sr isotopic composition of Cpx in several xenoliths significantly varied and (2) these initial Sr isotopic ratios of Cpx and Carb do not produce a single mixing line. Probably, primary melt had heterogeneous Sr isotopic composition. A two-point isochron for the Cpx and Phl samples yields an age of 380 Ma.

$\varepsilon_{Nd(376)}$ values for Cpx mineral fraction were –0.1 and 1.1. The isotopic ratios of Sr and Nd in Cpx were close to corresponding values in the V. Grib kimberlite (Fig. 2).

Petrographic and geochemical compositions of Cpx and Phl from Cpx-Phl xenoliths indicate their genetic relationship with clinopyroxenes of garnet peridotites xenoliths associated with processes of mantle metasomatism during the formation of kimberlite melts (Kargin et al., 2016a, 2016b, Larionova et al., 2016). The existence of an olivine relict in clinopyroxene grain from the Cpx-Phl xenolith (S.14GR1-715-4), which compositionally (Fo$_{92}$) is similar to olivine within garnet peridotite xenoliths from the Grib kimberlite (Sazonova et al., 2015) is an evidence for metasomatic origin of Cpx-Phl xenoliths. The enrichment of Cpx in LREE and a relative depletion in Nb, Ta, Zr, Hf, and Ti suggest that Ilm was in the equilibrium with high-alkaline ultramafic kimberlitic melt (Gregoire et al., 2003). The isotopic Sr and Nd characteristics of the Cpx and Phl are close to those of rocks from the V. Grib kimberlite; also, this confirms the hypothesis about their geochemical equilibrium with the kimberlite melt during its evolution.

References:

Golubkova, A.B., Nosova, A.A., Larionova, Y.O., 2013. Mg-ilmenite megacrysts from the Arkhangelsk kimberlites, Russia: Genesis and interaction with kimberlite melt and postkimberlite fluid. Geochemistry Int. 51, 353–381. doi:10.1134/S0016702913030038

Gregoire, M., Bell, D.R., Le Roex, A.P., 2003. Garnet Lherzolites from the Kaapvaal Craton (South Africa): Trace Element Evidence for a Metasomatic History. J. Petrol. 44, 629–657. doi:10.1093/petrology/44.4.629

Kargin, A.V., Sazonova, L.V., Nosova, A.A., Pervov, V.A., Minevrina, E.V., Khvostikov, V.A., Burmii, Z.P., 2016a. Sheared peridotite xenolith from the V. Grib kimberlite pipe, Arkhangelsk Diamond Province, Russia: Texture, composition, and origin. Geosci. Front. doi:10.1016/j.gsf.2016.03.001

Kargin, A.V., Sazonova, L.V., Nosova, A.A., Tretyachenko, V.V., 2016b. Composition of garnet and clinopyroxene in peridotite xenoliths from the Grib kimberlite pipe, Arkhangelsk diamond province, Russia: Evidence for mantle metasomatism associated with kimberlite melts. Lithos 262, 442–455. doi:10.1016/j.lithos.2016.07.015

Kononova, V.A., Golubeva, Y.Y., Bogatikov, O.A., Kargin, A.V., 2007. Diamond resource potential of kimberlites from the Zimny Bereg field, Arkhangel'sk oblast. Geol. Ore Depos. 49, 421–441. doi:10.1134/S1075701507060013

Larionova, Y.O., Sazonova, L.V., Lebedeva, N.M., Nosova, A.A., Tretyachenko, V.V., Travin, A.V., Kargin, A.V., Yudin, D.S., 2016. The age of kimberlites fromthe Arkhangelsk province: Rb–Sr, 40Ar/39Ar isotope data for phlogopite. Petrology 24. http://dx.doi.org/10.7868/S0869590316040026.

Moore, A., Belousova, E., 2005. Crystallization of Cr-poor and Cr-rich megacryst suites from the host kimberlite magma: Implications for mantle structure and the generation of kimberlite magmas. Contrib. to Mineral. Petrol. 149, 462–481. doi:10.1007/s00410-005-0663-x

O'Reilly, S.Y., Griffin, W.L., 2013. Mantle Metasomatism, in: Harlov, D.E., Håkon, A. (Eds.), Metasomatism and

the Chemical Transformation of Rock SE - 8. Springer Berlin Heidelberg, pp. 471–533. doi:10.1007/978-3-642-28394-9_12

Sablukov, S.M., Sablukova, L.I., Shavyrina, M.V., 2000. Mantle xenoliths from the Zimnii bereg kimberlite deposits of rounded diamonds, Arkhangelsk diamondiferous province. Petrology 8, 466–494.

Sazonova, L.V., Nosova, A.A., Kargin, A.V., Borisovskiy, S.E., Tretyachenko, V. V., Abazova, Z.M., Griban', Y.G., 2015. Olivine from the Pionerskaya and V. Grib kimberlite pipes, Arkhangelsk diamond province, Russia: Types, composition, and origin. Petrology 23, 227–258. doi:10.1134/S0869591115030054

van Achterbergh, E., Griffin, W.L., Stiefenhofer, J., 2001. Metasomatism in mantle xenoliths from the Letlhakane kimberlites: estimation of element fluxes. Contrib. to Mineral. Petrol. 141, 397–414. doi:10.1007/s004100000236

LAYERED DUNITE-TROCTOLITE-GABBRO SERIES OF THE GANKUVAYAM OPHIOLITE (KUYUL TERRANE, KORYAK HIGHLAND, RUSSIA): CRUSTAL PLUTONIC SEQUENCE OF AN ANCIENT BACK-ARC SPREADING CENTER

Ledneva G.V.[1], Bazylev B.A.[2], Kuzmin D.V.[3,4], Kononkova N.N.[2]
[1]Geological Institute RAS, Moscow, Russia, gledneva@gmail.com
[2]Vernadsky Institute of Geochemistry and Analytical Chemistry of the Russian Academy of Sciences, Moscow, Russia, bazylev@geokhi.ru, nnzond@geokhi.ru
[3]Institute of Geology and Mineralogy, Siberian Branch of the Russian Academy of Sciences, Novosibirsk, Russia, kuzmin@igm.nsc.ru
[4]Novosibirsk State University, Novosibirsk, Russia

Investigations of dredged back-arc plutonic rocks, which are important for understanding of conditions and modification processes of mantle-derived magma on their way to a surface, are rather limited (Shcheka et al., 1995; Laz'ko, Gladkov, 1991; Sanfilippo et al., 2013). However they can be reconstructed via studies crustal plutonic rocks (commonly represented by dunite-troctolite-gabbro and dunite-wehrlite-pyroxenite-gabbronorite sequences) of suprasubduction ophiolites assumed to be originated in a back-arc spreading environment (see summary by Dilek, Furnes, 2011). One of such objects is the late Jurassic Gankuvayam ophiolite (the Kuyul terrane, Koryak Highland) whose suprasubduction origin is well proved by compositions of basaltic lavas, basic to felsic dikes (Grigor'ev et al., 1995), plagiogranite (Luchitskaya, 1996) and residual spinel peridotites (Khanchuk, Panchenko, 1994; Sokolov et al., 1996, 2003). In this study we focus on layered dunite-troctolite-gabbro series of this ophiolite that wasn't previously studied in details.

The Kuyul terrane (Khanchuk et al., 1990) belongs to the Koryak-Kamchatka fold system, which is made of far-travelled terranes accreted to the Asian continental margin in the middle Miocene and Oligocene (Sokolov et al., 2001). The Kuyul terrane includes several tectonic nappes composed of serpentine mélanges and basic-ultrabasic rocks. The Gankuvayam ophiolite is one of the largest nappes. It represents the pile of several tectonically disturbed slices composed of residual spinel peridotites with podiform dunites and pyroxenite dikes, plutonic sequences of dunite-wehrlite-pyroxenite, dunite-troctolite-gabbro and plagiogranite, sheeted dikes and lavas with pelagic sediments (Khanchuk et al., 1990). It resembles the Penrose ophiolite sequence (Anonymous, 1972) and a lithosphere of fast spreading oceanic centers (Dick et al., 2006).

The layered dunite-troctolite-gabbro series is made of mainly clinopyroxene-plagioclase dunite, troctolite, olivine gabbro-norite and gabbro, olivine-free gabbro-norite and gabbro, hornblende gabbro, and minor wehrlite. Petrographic studies indicate that dunite and troctolite are mainly composed of euhedral olivine and Cr-spinel while anhedral clinopyroxene and plagioclase fill interstices between them. Troctolite also contains minor hornblende developed at olivine-plagioclase grain boundaries. Wehrlite is constituted by euhedral clinopyroxene and anhedral olivine. Olivine gabbro-norite and olivine gabbro are made of anhedral olivine, ortho- and clinopyroxene, plagioclase, subordinate hornblende, accessory sulfide and Cr-spinel (only in some samples). Orthopyroxene is subordinate relative to clinopyroxene; hornblende is normally confined to olivine-plagioclase and clinopyroxene-plagioclase grain boundaries. Gabbro is composed of clinopyroxene, hornblende whose amount varies from a few to 45 %, plagioclase, Ti-magnetite, ilmenite and accessory sulfides. Hornblende rims clinopyroxene and forms individual grains. Hornblende gabbro is free of clinopyroxene. By modal composition plutonic sequence is similar to those of fast spreading centers (Dick et al., 2006).

Metamorphic transformations are expressed in a partial replacement of primary minerals, e.g. olivine by mesh-textured serpentine, Cr-spinel by Cr-magnetite, plagioclase by hydrogrossular and prehnite aggregates rimmed by chlorite at contacts with olivine in dunite and troctolite and mainly by prehnite in gabbroic rocks, clinopyroxene and hornblende by actinolite-tremolite and chlorite. Linear microfractures in dunite and troctolite are filled with magnetite, serpentine and presumably brucite. The metamorphic transformations observed are typical of ultrabasic and basic plutonic rocks of oceanic spreading centers (Frost, Beard, 2007; Beard et al., 2009; Kodolányi et al., 2012).

Olivine shows narrow variations of Mg# in dunite and troctolite (88-91, where Mg#=100Mg/(Mg+Fe) hereinafter in all minerals except spinel) and wide interval of Mg# (77-91) in olivine gabbroic rocks partly overlapping with that in dunite and troctolite. Mg# olivine negatively correlates with NiO contents which drop from 0.27-0.32 wt. % in dunites and troctolites to 0.13-0.24 wt. % in gabbroic rocks. In wehrlite Mg# olivine is 87-89 and NiO contents are 0.13-0.15 wt. %. In comparison to mid-ocean spreading centers (PetDB, compilations by Dick et al., 2002), olivine of the rocks

investigated are higher in NiO at given Mg# olivine but they show similar Mn/Fe, Ni/(Mg/Fe) and Ca/Fe ratios close to those of mantle peridotite values.

Clinopyroxene has Mg# ranging in the interval of 90-92 in dunite and troctolite, 82-92 in olivine gabbroic rocks, 73-88 in gabbro and hornblende gabbro. Clinopyroxene Cr_2O_3 contents are negatively correlates with Mg# clinopyroxene, and they drop from 1.2 wt. % in dunite to 0.1 wt. % in hornblende gabbro. Clinopyroxene is low to moderately low in TiO_2 (0.1-0.7 wt. %), Al_2O_3 (1.7-3.8 wt. %) and Na_2O (0.2-0.45 wt. %) that are poorly correlated with Mg# clinopyroxene. By sodium contents clinopyroxene of the least Mg# gabbro and hornblende gabbro is comparable with gabbroic rocks of the East Pacific Rise fast-spreading center (PetDB data). Orthopyroxene of olivine gabbro-norite and gabbro has Mg# of 83-87 and is in equilibrium with coexisting clinopyroxene with Mg# of 85-89. Orthopyroxene is low in TiO_2 (0.1-0.2 wt. %) and Al_2O_3 (1.4-2.0 wt. %), moderate in Cr_2O_3 (0.1-0.45 wt. %) and free of sodium.

Primary hornblende is mainly tschemakitic and magnesio-hornblende although pargasitic and edenitic hornblende, edenite and silicic edenite also occur in olivine and olivine-free varieties, respectively. Hornblende is moderately high in Al_2O_3 (11-13 wt. %) whose variations don't depend on Mg# Hbl. TiO_2 concentrations increase from 0.2 to 2.6 wt. % as Mg# Hbl drops; K_2O contents are as low as 0.01-0.16 wt. %.

Plagioclase is homogeneous, and its composition varies from bytownite-anorthite (xAn 85-91) in olivine gabbroic rocks to labradorite-bytownite (xAn 51-89) in gabbro and hornblende gabbro. Values of xAn are negatively correlated with Mg# of olivine, clinopyroxene and hornblende. At given Mg# of silicate xAn in gabbroic rocks investigated is higher than those in gabbroic rocks of oceanic spreading centers.

Cr-spinel of dunite, troctolite, olivine gabbro and gabbro-norite exhibits a narrow Cr# (100*Cr/(Cr+Al)) range of 52-44. One of the samples of olivine gabbro contains Cr-spinel with Cr# of 50 coexisting with olivine with Mg# of 91; these compositions fall into the field of the olivine-spinel mantle array (Arai, 1994). This indicates that a melt primary for olivine gabbro was equilibrated with mantle peridotites remained after a moderate degree of partial melting. Other compositions of the coexisted spinel and olivine locate out of this field; their Cr#Spl slightly decreases as Mg#Ol decreases, which produces a trend typical of low and moderately low pressure cumulates. Wehrlite composing thin discontinuous layers in layered rocks contains spinel with Cr# of 32-40 coexisting with olivine with mg# of 87-89. Spinel is low in TiO_2 contents (0.3-0.9 wt. %) which are generally lower in comparison to those of spinel from gabbroic rocks of oceanic spreading centers. Concentrations of NiO (0.1-0.2 wt. %), V_2O_3 (0.1-0.4 wt. %) and ZnO (0.1-0.5 wt. %) in studied spinel are consistent with their cumulative nature.

Equilibrium temperatures are estimated at about 640-770°C (Ballhaus et al., 1991) for olivine-Cr-spinel pair, 880-970°C (Brey, Köhler, 1990) and at 910-1000°C (Wells, 1977) for two-pyroxenes, and 660-1040°C (Ridolfi et al., 2009) for hornblende. Pressure of rock crystallization is assessed at about 2.2 (±0.5) kbar (Al-in-Hbl; Ridolfi et al., 2009). Oxygen fugacity corresponds to QFM+1.8 to QFM+3.0 (Ballhaus et al., 1991).
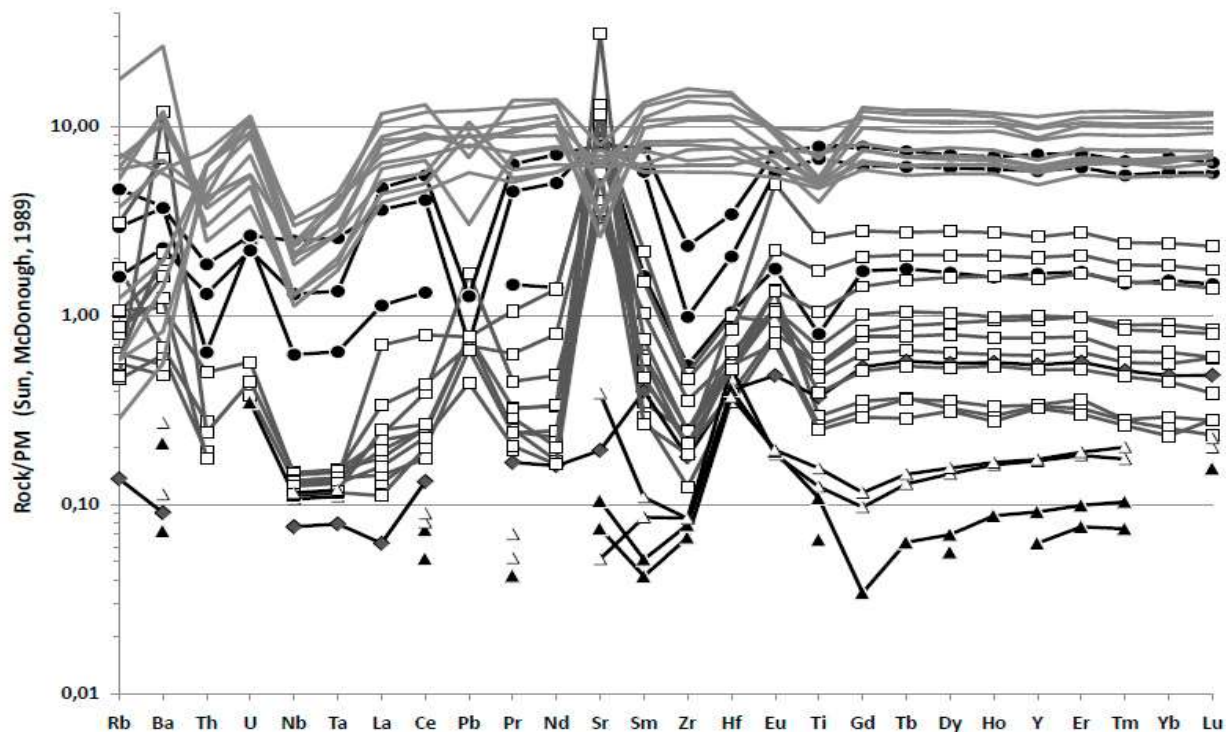
Fig. 1. Multi-element spectra of the Gankuvayam ophiolite rocks: filled and open triangles are dunite and troctolite, respectively, filled diamond is wehrlite, open squares are gabbroic rocks except hornblende varieties, filled circles are hornblende gabbro; spectra without symbols are dikes and lavas basaltic to dacitic in composition.

The bulk compositions of the plutonic rocks investigated cover the range typical of plutonic rocks of oceanic and back-arc spreading centers although in the comparison to the latter dunite and troctolite are more widespread in the

International Conference on Magmatism of the Earth and Related Strategic Metal Deposits

Gankuvayam ophiolite. Hornblende gabbro being the most evolved plutonic rocks of the Gankuvayam ophiolite of the Kuyul terrane closely resemble basic dikes and lavas of the ophiolite studied. All plutonic rocks have similar spectra of primitive mantle normalized trace elements although their absolute contents differ by two orders of magnitude. The multi-element spectra exhibit depletion in light REE relative to heavy ones, positive anomalies of Sr-Eu and negative anomalies of Zr-Hf and Rb-Ba that are complementary to those in andesite and dacite dikes. Gabbroic rocks also show negative anomalies of Nb-Ta (Fig.1). The spectra of hornblende gabbro mimic those of basalt and basaltic andesite dikes and lavas that are typical of island-arc tholeiites derived from depleted mantle sources modified by subduction-related fluids.

Thus compositional variations of minerals and bulk rocks of layered dunite-troctolite-gabbro series of the Gankuvayam ophiolite of the Kuyul terrane suggest their formation beneath back-arc presumably fast spreading center. Drawing an analogy with oceanic spreading centers modification of mantle-derived island-arc tholeiitic magma resulted in layered dunite-troctolite gabbro sequences can be assigned to (a) fractional crystallization; (b) repeated magma replenishment and (c) reaction porous flow between melt and cumulus mesh.

References:

Anonymous (1972) Penrose field conference on ophiolites. Geotimes 17: 24-25.

Arai S (1994) Characterization of spinel peridotites by olivine-spinel compositional relationships: review and interpretation. Chem Geol 113(3-4): 191-204. Doi: 10.1016/0009-2541(94)90066-3

Ballhaus C, Berry RF, Green DH (1991) High pressure experimental calibration of the olivine-orthopyroxene-spinel oxygen geobarometer: implications for the oxidation state of the upper mantle. Contrib Mineral Petrol 107(1): 27-40. Doi: 10.1007/BF00311183

Beard JB, Frost BR, Fryer P, McCaig A, Searle R, Ildefonse B, Zinin P, Sharma SK (2009) Onset and progression of serpentinization and magnetite formation in olivine-rich troctolite from IODP Hole U1309D. J Petrol 50(3): 387-403. Doi: 10.1093/petrology/egp004

Brey GP, Köhler T (1990) Geothermometry in four-phase lherzolites: II. New thermobarometers, and practical assessment of existing thermobarometers. J Petrol 31: 1353–1378. Doi: 10.1093/petrology/31.6.1353

Dick HJB, Natland JY, Ildefonse B (2006) Past and future impact of Deep Drilling in the oceanic crust and mantle. Oceanography 19(4): 72-80. Doi: 10.5670/oceanog.2006.06

Dick HJB, Ozawa K, Meyer PS, Niu Y, Robinson PT, Constantin M, Hebert R, Maeda J, Natland JH, Hirth JG, Mackie SM (2002) Primary silicate mineral chemistry of a 1.5-km section of very slow spreading lower ocean crust: ODP Hole 735b, Southwest Indian Ridge. Proceedings of the Ocean Drilling Program, Scientific Results. Natland JH, Dick HJB, Miller DJ, Von Herzen RP (eds.) 176: 1-61. Doi: 10.2973/odp.proc.sr.176.001.2002

Dilek Y, Furnes H (2011) Ophiolite genesis and global tectonics: Geochemical and tectonic fingerprinting of ancient oceanic lithosphere. Geol Soc Am Bull 123: 387-411. Doi: 10.1130/B30446.1

Frost BR, Beard JS (2007) On silica activity and serpentinization. J Petrol 48(7): 1351-1368. Doi: 10.1093/petrology/egm021

Grigor'ev VN, Sokolov SD, Krylov KA, Golozubov VV, Pral'nikova IE (1995) Geodynamic typification of the Triassic–Jurassic volcanic–siliceous complexes of the Kuyul terrane (Koryak highland). Geotektonika -(3): 59–69.

Khanchuk A I, Grigor'ev VN, Golozubov VV, Govorov GI, Krylov KA, Kurnosov VB, Panchenko IV, Pral'nikova IE, Chudaev OV (1990) In Kuyul Ophiolite Terrane. DVO AN SSSR, Vladivostok, 93p.

Khanchuk AI, Panchenko IV (1994) Mineral assemblages of Gankuvayam ophioltic section in the Kuyul ophiolitic terrane of the Russia Far East. Ofioliti 19(2a): 257-268.

Kodolányi J, Pettke T, Spandler C, Kamber B, Gméling K (2012) Geochemistry of ocean floor and fore-arc serpentinites: Constrains on the ultramafic input to subduction zones. J Petrol 53(2): 235-270. Doi: 10.1093/petrology/egr058

Laz'ko YeYe, Gladkov NG (1991) Ultramafic and gabbroic rocks of the IPOD basin (Yap fracture zone, Philippine Sea). Int Geol Rev 33(7): 704-725. Doi: 10.1080/00206819109465721

Luchitskaya MV (1996) Plagiogranites of the Kuyul ophiolite massif, Northeasten Russia. Ofioliti 21: 131-138.

Ridolfi F, Runzelli A, Puerini M (2009) Stability and chemical equilibrium of amphibole in calc-alkaline magmas: an overview, new thermobarometric formulations and application to subduction-related volcanoes. Contrib Mineral Petrol 160: 45-66. Doi: 10.1007/s00410-009-0465-7

Sanfilippo A, Dick HJ, Ohara Y (2013) Melt-rock reaction in the mantle: Mantle troctolites from the Parece Vela ancient back-arc spreading center. J Petrol 54: 861-885. Doi: 10.1093/petrology/egs089

Shcheka SA, Vysotsky SV, S'edin VT, Tararin IA (1995) Igneous rocks of the main geological structures of the Phillipine Sea floor. In Geology and geophysics of the Philippine Sea. Tokuyama H et al. (eds). Terra Scientific Publishing company, pp. 251-278.

Sokolov SD (2001) Accretionary tectonics: terms, problems, and prospects. In Problems of Global Geodynamics. Proceedings of Theoretical Seminar of OGGGGN RAN 2000–2001. Volume 2. Rundkvist DV (ed). RAN, Moscow, pp. 32-56.

Sokolov SD, Luchitskaya MV, Silantyev SA, Morozov OL, Ganelin AV, Bazylev BA, Osipenko AB, Palandzyan SA, Kravchenko-Berezhnoy IR (2003) Ophiolites in accretionary complexes along the Early Cretaceous margin of NE Russia; age, composition, and geodynamic diversity. In Ophiolites in Earth history. Dilek Y, Robinson PT (eds.). Geological Society, London, Special Publication. 218: 619-664. Doi: 10.1144/GSL.SP.2003.218.01.31

Sokolov SD, Peive AA, Krylov KA, Grigor'ev VN, Batanova VG, Golozubov VV, Luchitskaya MV, Aleksyutin MV (1996) Ordered structure in serpentinite mélange. Geotectonics 30(1): 53–63.

Wells PRA (1977) Pyroxene thermometry in simple and complex systems. Contrib Miner Petrol 62:129–139. Doi: 10.1007/BF00372872

A PRELIMINARY SURVEY ON THE ORE DEPOSITS IN THE OYON MINERALIZED DISTRICT, CENTRAL PERU

Lee Jaeho

Korea Institute of Geoscience and Mineral Resources, Daejeon, Korea

In this paper I provide fundamental data on the geological characteristics and the occurrence mode of ore bodies, Korea Institute of Geoscience and Mineral Resources(*KIGAM*) and Instituto Geologico Minero y Metalurgico(*INGEMMET*) of Peru carried out joint exploration.

Patterns of sedimentation, magmatism, and tectonism in the Mesozoic and Tertiary history of central Peru are dominated by long-lived belts of Andean trend developed within a continental basement of Paleozoic to Precambrian age.

The major intrusive body of the Cordillera Blanca batholith was emplaced into folded shelf sediments between 12 to 9 Ma and a chain of high-level stocks extends southward from the batholith. Gravity modeling suggests that these intrusions extend upward from a deeper mass of granite and igneous rock samples from Churin and Raura have given ages of 13 and 10 Ma. This chain of stocks is closely associated with the polymetallic belt in northern Peru where mineralization closely followed intrusion. At Raura, for example, mineralization is bracketed between 10 and 7.8 Ma. These deposits, therefore, fit into the grouping of middle to upper Miocene metasomatic lodes with copper, lead, zinc, and silver, recognized as one of the three principal metallogenetic epochs in Peru.

The surveyed mines are located in a polymetallic vein, replacement, and skarn mineral district in the central Andes of Peru. Iscaycruz, which includes underground and open pit mines that produce zinc and lead concentrates, was the largest mineral deposit of an important group of base metal deposits in the Andes of central Peru. The deposits are sub-vertical seams of polymetallic ores(Zn, Cu, and Pb). These seams are hosted by Jurassic and Cretaceous sedimentary rock formation. The intrusion of igneous rocks in these formations originated metallic deposits of metasomatic and skarn types. The Raura mine is composed of polymetallic deposit of veins and replacement orebodies. The main sedimentary unit in the area is Cretaceous Machay Limestone. The Raura depression contains several orebodies each with different mineralization: predominantly Pb-Zn bearing Catuvo orebody; Ag-rich galena-bearing Lake Ninacocha orebody; Cu-Ag bearing Esperanza and Restauradora orebody. Huaron is a hydrothermal polymetallic deposit of silver, lead, zinc, and copper mineralization hosted within structures likely related to the intrusion of monzonite dikes, principally located within the Huaron anticline. Mineralization is encountered in veins parallel to the main fault systems, in replacement bodies known as "mantos" associated with the calcareous sections of the conglomerates and other favourable stratigraphic horizons, and as dissemination in the monzonitic intrusions at vein intersections.

References:

Mukasa, S. B., and Tilton, G. R., 1983, Temporal relations and Pb systematics in plutonic rocks of the western and coastal cordilleras, Peru: Am. Geophys. Union Trans., v. 64, p. 321.

Bussell, M. A., and Wilson, C. D. V., 1985, A gravity traverse across the Coastal batholith of Peru: Geol. Soc. London Jour., v. 142, p. 633-641.

Cobbing, E. J., Pitcher, W. S., Wilson, J. J., Baldock, J., Taylor, W. P., McCourt, W. J., and Snelling, N.J., 1981, The geology of the Western Cordillera of northern Peru: Inst. Geol. Sci., London Overseas Mem., no. 5, 143 p.

Noble,D .C., 1980, Potassium-argon determinations on rocks from Raura and Uchucchacua: Lima, Peru, Cia de Minas Buenaventura S.A., unpub. rept., 2 p.

Petersen, G., and Vidal, C., 1983, Tres epocas metalogeneticas evidenciadas en el Cenozoico del Peru: Geol. Soc. Peru Bol., v. 71, p. 107-112.

PETROGENESIS AND SIGNIFICANCE OF THE JEBEL DUMBIER ALKALINE-CARBONATITE COMPLEX FROM NORTH MARGIN OF NUBA MOUNTAINS, SUDAN

Lianxun W.[1], Changqian M.A.[1], Mushaal M.A.S.[2], Mohammed A.I.M.[1,2]

[1]China University of Geosciences, Wuhan, China
[2]University of Kordofan, El Obeid, Sudan

Scientific study of the geology and mineral resources in Sudan is rather limited. Jebel Dumbier is the first identified carbonatite-bearing alkaline complex in Sudan by El Sharkawi & El Raba'a in 1973. It is located in Northern Kordofan Province on the northeastern margin of the Nuba Mountains. The complex exposed as small elliptical hills with northeast-southwest trending. The outcrops is around 8 km2. Jebel Dumier complex is composed of dominant orthoclasite and ditroite (Fig. 1) and subdominant carbonatite and fluorite dykes in the northeast part of the complex. The dykes are

controlled by a NNE strike-slip fault system which has been reactivated in 1966 and 2007 triggering around 5.1 magnitude earthquakes. The fluorite dykes are mined and have similar isotopic features to associated syenitic rocks and carbonatites. Therefore the genetic relationships of the fluorite, carbonatite and distinct syenitic rocks are of great interests and attracted much attention (Harris et al., 1983; Ouf, 2007; Galil, 2008).

Geology and petrography of the complex

The ditroite is in grey color, medium-grained and commonly occurrs as lentoids or inclusions in the orthoclasite. It consists of perthite (50-70%), augite-aegirine (10-30%), nepheline (partially altered to cancrinite, 6-20%), sodalite-group minerals (8-20%), and minor annite-phlogopite (< 5%) and richterite (< 5%). Common accessories are interstitial fluorite, euhedral titanite, apatite and zircon. Orthoclasite is the dominant rock type, with outcrops of more than 80% of the exposed complex. The rocks are pink, coarse-grained, and composed of orthoclase (60-80%), kalsilite (15-35%) and few interstitial biotite (< 5%) and calcium carbonate (< 5%). Fluorite, apatite and zircon are common accessory phases and occasionally occur as large crystals of size 500×200 μm (zircon). On the west margins of complex, ditroites commonly contain abundant country rock (gneiss) xenoliths. Hybridisation textures (e.g., clinopyroxene with reverse zonation; Fig. 2), attributable to interaction between ditroite magma and xenolith, present on the contact between the xenoliths and the host. Carbonatites are sovites containing more than 80% calcite. They occur as dykes and elliptical patches of carbonatitic breccia. The NNE trending fluorite dykes are dominated by fluorite but also carry quartz, carbonate and clinopyroxene.
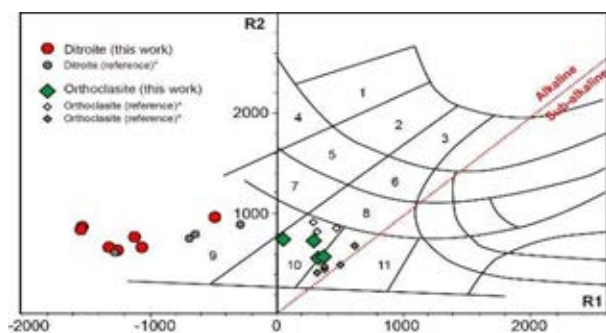
Fig. 1. Chemical classification of the Jebel Dumbier alkaline rocks after de la Roche's (1986). R1=4Si-11(Na+K)-2(Fe+Ti), R2=6Ca+2Mg+Al. 1. melteigite; 2.theralite; 3. alkali gabbro; 4. ijolite; 5. essexitic gabbro; 6. syenogabbro; 7. essexite; 8. nepheline syenodiorite; 9. nepheline syenite; 10. nepheline-bearing syenite; 11. syenite
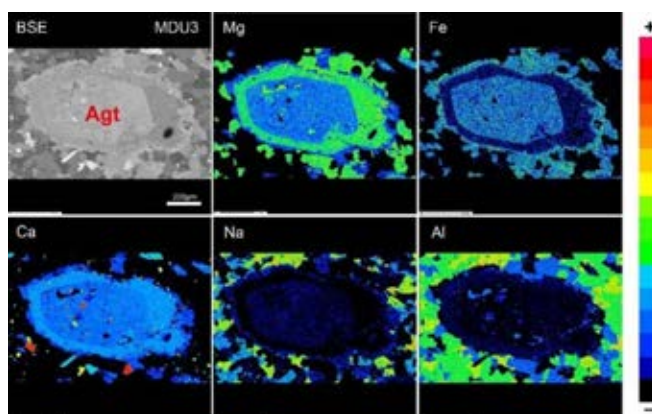
Fig. 2. Backscattered electron image of zoned clinopyroxene grain in the ditroite of Jebel Dumbier complex.

Dating and geochemical features of the complex

LA-ICPMS zircon dating results reveal that both orthoclasite and ditroite emplaced at around 600 Ma and indistinguishable within error. Geochemical data show that orthoclasites are ultrapotassic rocks with K2O contents up to 15 wt% and K2O/Na2O ratios of 6-48, whereas ditoites are sodic-potassic rocks (K2O/Na2O = 0.6-0.9). Relative to orthoclasites, ditroites display higher FeOtotal and MgO contents and lower Al2O3 contents. They are more depleted in LILEs (Rb, Sr, Ba) and enriched in HFSEs (Nb, Ta, Zr, Hf, Th, U) and REEs. Note that ditroites are enriched in volatile elements (F, Cl, Br, S) and have surprisingly high Nb/Ta ratios (mean of 32). Isotopic data imply that the ditoite, orthoclasite, fluorite dyke and carbonatite dykes from Jebel Dumbier originated from a common source of depleted mantle affinities, with identical low initial 87Sr/86Sr ratios (0.702-0.704) and highεNd (t) values (1.7-2.0).

Petrogenesis and tectonic implications

We propose that the ditroites, orthoclasites, carbonatites and fluorites are products of variable degrees of fractional crystallization of mantle-derived magmas. Crustal contamination might be also involved as evidenced by the gneissic xenoliths. The enrichment of CO2, F, Cl and Br in rocks suggest the source rocks are initially volatile-rich. The Jebel Dumbier alkaline -carbonatite complex correlates with the vast coeval A-type granites in many parts of the Arabian-Nubian Shield, representing the post-orogenic alkaline magmatisms during the end evolution of Pan-African orogen (650-550 Ma).

References:

El Sharkawi, M.A., El Raba'a, S.M. 1973. First record of carbonatite in Sudan. In: Hailu, T. (ed.), Second Conference of African Geology, *Addis Abba: Geol. Soc. Africa*, 129-135.

Harris, N.B.W., Mohammed, A.E.R.O., Shaddad, M.Z. 1983. Geochemistry and petrogenesis of a nepheline syenite-carbonatite complex from the Sudan. *Geological Magazine*, 120(2), 115-127.

Ouf, M.A.I. 2007. The Geotectonic setting of Jebel El Dumbier Area and vicinity, North Kordofan State, Sudan. *Master thesis, Al Neelain University*. pp. 1-163.

Galil, M.Y.A. 2008. Geology and mineralization related to anorogenic igneous complexes of Northern Nuba Mountains and Northern Kordofan, Sudan. *Master thesis, Al Neelain University*. pp. 1-245.

FEATURES OF NI-RICH SULFIDE MELT INCLUSIONS IN YAKUTIAN DIAMONDS

Logvinova A.M.[1,2], Wirth R.[3], Skomorokhova A.V.[1,2], Sobolev N.V.[1,2]

[1]Institute of Geology and Mineralogy, Siberian Branch of the Russian Academy of Sciences, Novosibirsk, Russia, logv@igm.nsc.ru
[2]Novosibirsk State University, Novosibirsk, Russia
[3]Helmholtz Centre Potsdam, GFZ German Research Centre for Geosciences, Potsdam, Germany

Sulfide inclusions are the most abundant inclusions in diamonds. They provide important information about the distribution of chalcophile elements in the mantle and are intensively studied over many years (Sharp, 1966; Efimova et al,1983; Bulanova et al, 1996; Pearson et al, 1998; Taylor et al., 2009). A large number of sulfides in diamonds and in several cases intergrowths with undoubtedly diamond syngenetic minerals (olivine, enstatite, clinopyroxene, pyrope) testify that sulfides are also syngenetic or protogenetic. Sulfide inclusions in diamonds are pyrrhotite, pentlandite, chalcopyrite, pyrite, troilite and monosulfide solid solution (Mss), at that similar to the other diamond inclusions they belong to two types of paragenesis: eclogite (0-12% Ni) and peridotite (22-36% Ni) (Bulanova et al, 1996). Sometimes sulfide and phlogopite intergrowths occur in the diamond matrix. All these facts are evidence that sulfide phases occur in the mother substance during diamond nucleation and growth. The typical sulfide inclusions were encapsulated as a monosulfide solid solution (Mss) in the Fe-Ni-S system with a minor amount of Cu, Co as well. The observed mineralogy of mantle sulfides, however, likely represents low temperature (<300°C) re-equilibration of high-temperature sulfide melt (Taylor et al, 2009). A question about diamond crystallization from sulfide melt is still under discussion though currently researchers tend to believe that diamond crystallization from the sulfide melt is impossible without the transitional metals like Fe and Ni (Shushkanova et al, 2008) in its composition. Experimental studies have shown that this type of crystallization is possible only at the temperature above 1600°C and pressure over 6 GPa, that is rather high parameters for natural conditions (Usselman, 1975; Litvin et al., 2005; Palyanov et al., 2006). The study of submicroinclusions in diamond captured at the initial stage of crystallization is of paramount importance in studies of chemical and phase composition of diamond forming medium. Sulfide melt inclusions have been first described in the work (Klein-BenDavid et al., 2003). Logvinova and co-authors (2008) have been the first to identify sulfide phases in the composition of polymineral melt/fluid microinclusions in diamond.

This work demonstrates original data on nanosize sulfide inclusions located in the nucleus of different types of diamonds from the kimberlite pipes (Komsomolskaya, Udachnaya, Yubileinaya and Internatsionalnaya) and alluvial deposits of Yakutia.

Using FIB/TEM method (Wirth, 2004) we investigated nanometer-sized inclusions in diamonds from peridotitic and eclogitic xenoliths and sulfide-graphite and sulfide-olivine intergrowths; sulfide-silicate-sphen-aragonite, sulfide-apatite and sulfide–phlogopite-dolomite–ilmenite-magnetite–apatite–fluid multiphase inclusions in the diamonds from the available diamond monofractions. These inclusions are also divided into two above-mentioned parageneses. The marked difference in Ni concentrations in sulfides between peridotite- and eclogite-hosted diamonds has been used as a paragenetic indicator.

Sulfide melt inclusions of eclogite paragenesis were identified in diamonds from the Yubileinaya and Internatsionalnaya kimberlite pipes by paragenesis with omphacite. All of them are homogenous in their chemistry (Fe/Ni ratio is constant) and accompanied of fluid bubbles. The main phase is pyrrhotite. In diamonds from eclogite xenolith, copper sulphide (bornite or cubanite) is also determined.

Of greatest interest are the inclusions of sulfides of the peridotite paragenesis, which were found in individual diamonds from the Komsomolskaya, Yubileinaya pipes, and diamondiferous peridotite xenolith from the Udachnaya kimberlite pipe. All of identified sulfide melt inclusions are characterized by a high-Ni composition. The Ni content exceeds 48 wt. %. Nanosized sulfides in four diamonds from Udachnaya peridotite xenoliths are characterized by enriched nickel compositions (millerite). And inclusions of millerite have a cover of pure nickel or nickel oxide (undefined). They are associated with silicates, carbonates, halides and fluid. The nitrogen content measurements showed that the diamonds, containing high-Ni sulfides, practically do not contain nitrogen, or in small amounts (over 100 ppm). This is also seen for diamond containing aragonite-sulfide association of inclusion. While the Ni content in sulfide phase of sulfide-olivine intergrowths in the central part of diamonds is much lower, 17-21 wt.%.

Based on the data obtained, among the nanoscale sulfide inclusions localized in the central part of the diamond matrix, in contrast to the inclusions placed throughout the volume of the crystal, three types of compositions can be distinguished: high-Ni (> 48 wt.%, including millerite), Ni-rich (> 17 wt.%) and pure Ni (< 6 wt.%). Thus, the compositions of primary sulfide melts correspond to the compositions of polyphase inclusions in diamonds of peridotite and eclogite parageneses. The constant Ni/(Ni+Fe), the wide S/(S+Ni+Fe) range, the presence of varying amounts of alka;is and Mg and the association with carbonatitic melts suggest that the sulfide-bearing inclusions contain sulfide melt. The high-Ni sulfide assemblages of inclusions with carbonatite and fluid phases, water-bearing silicates, makes it possible to assume that they are formed during cooling stage of the homogeneous deepest carbonate-silicate-sulfide melt.

References:

Bulanova GP, Griffin WL, Ryan CG, Shestakova OY, Barnes SJ (1996) Trace elements in sulfide inclusions from Yakutian diamonds. Contributions to Mineralogy and Petrology 124:111-125. doi: 10.1007/s004100050179

Efimova ES, Sobolev NV, Pospelova LN (1983) Sulphide inclusions in diamonds and peculiarities of their paragenesis (in Russian). Zapiski Vsesoyuznogo Mineralogicheskogo Obshchestva 92:300-309.

Klein-BenDavid O, Logvinova AM, Izraeli ES, Sobolev NV, Navon O.(2003) Sulfide melt inclusions in Yubileinayan (Yakutia) diamonds. 8th International. Kimberlite Conference, Extended Abstract, FLA 0111.

Litvin YA, Shushkanova AV, Zharikov VA (2005) Immiscibility of sulfide-silicate melts in the mantle: Role in the syngenesis of diamond and inclusions (based on experiments at 7.0 GPa) // Doklady earth Sciences 403 (5) :719-722. WOS:000231093000016

Logvinova AM, Wirth R, Fedorova EN, Sobolev NV (2008) Nanometer-sized mineral and fluid inclusions in cloudy Siberian diamonds: new insights on diamond formation. Eur. J. Mineral (Special issue on Diamonds) 20 : 317-331. doi: 10.1127/0935-1221/2008/0020-1815

Palyanov YN, Borzdov YM, Khokhryakov AF, Kupriyanov LN, Sobolev NV (2006) Sulfides melts – graphite interaction at HPHT conditions: implications for diamond genesis.Earth Planet. Sci. Lett. 250:269-280. doi: 10.1016/j.epsl.2006.06.049

Pearson DG, Shirey SB, Harris JW, Carlson RW (1998) Sulphide inclusions in diamonds from the Koffiefontein kimberlite, S Africa: constraints on diamond ages and mantle Re-Os systematic. Earth and Planetary Sci. Letters 160:311-326. DOI: 10.1016/S0012-821X(98)00092-2

Sharp WE (1966) Pyrrhotite, a common inclusion in South African diamonds. Nature .211 (5047):402-403.

Shushkanova AA, Litvin YA (2008) Diamond nucleation and growth in sulfide-carbon melts: an experimental study at 6.0 – 7.1 GPa. Eur. J. Miner.20 :349-355. doi:10.1127/09351221/2008/0020-1819

Taylor LA, Liu Ya.(2009) Sulfides inclusions in diamonds: not monosulfide solid solutions // Russian Geology and Geophysics 50:1201–1211. doi: 10.1016/j.rgg.2009.11.018

Usselman TM (1975) Experimental approach to state of core. Part 1. Liquidus relations of Fe-rich portion of Fe-Ni-S system from 30 to 100 kbars. Amer. J. Sci. 275: 278-290. WOS:A1975V838500004

Wirth R (2004) Focused Ion Beam (FIB): a novel technology for advanced application of micro- and nanoanalysis in geosciences and applied mineralogy. Eur. J. Mineral.16 : 863-876 doi: 10.1127/0935-1221/2004/0016-0863

BASEMENT OF THE SIBERIAN TRAPS SECTION IN THE MAYMECHA VALLEY: PETROGRAPHY OF THE PRAVOBOYARSKY BASALTIC TUFF LAVAS FILLED WITH DETRITAL QUARTZ

Makhatadze G.V.[1,2], Plechov P.Yu.[1,3]
[1]Lomonosov Moscow State University, Moscow, Russia
[2]Vernadsky Institute of Geochemistry and Analytical Chemistry of the Russian Academy of Sciences, Moscow, Russia,
makhatadzeg36@gmail.com
[3]Mineralogical Museum of the Russian Academy of Sciences, Moscow, Russia

Permo-Triassic Siberian Large Igneous Province (SLIP) is the largest igneous province known on the Earth. It is composed mostly of pyroclastic materials (Fedorenko et Czamanske, 1997) and the most volume of its rocks formed within exceptionally short period of time (~1 Ma) in which the Permo-Triassic Great Extinction took place (Kamo et al., 2003). It is naturally to expect connection between these two events. In the Norhtern-Eastern part of SLIP there is Maymecha-Kotuy alkaline province, composed mostly of alkaline-ultrabasic volcanites and carbonatites as well as tholeiitic basalts and dolerites. Moreover, there is unique meimechitic rocks located there (Fedorenko et Czamanske, 1997). These petrological peculiarities that are requiring special geodynamic conditions for its origin provokes great interest.

The section of the Maymecha-Kotuy Traps is one of the most complete in the whole SLIP. It covers directly sedimentary rocks of Siberian Craton. Near the lower contact they are represented by Permian terrigenous carboniferous deposits (Vasil'ev et Zolotukhin, 1975). The section is (from lower parts to upper): Pravoboyarsky Formation (in the Maymecha Valley) and its facial analogue Arydjangsky Formation (in the Kotuy Valley), then Kogotoksky Group and Del'kansky and Maymechinsky Formations. The upper two formations are represented only in the Maimecha Valley (Pavlov et al., 2015). Arydjangsky and Del'kansky Formations are composed of alkaline-ultrabasic volcanic rocks (including melilite-bearing ones). Maymechinsky Formation is composed of meimechites. Kogotoksky Group consists of basaltoids. Pravoboyarksy Formation is made of tuffites (Fedorenko et Czamanske, 1997).

Pravoboyarksy Formation is of variable thickness, while the most part is about 150 meters. In the northern-eastern part where it is replaced by Arydjangsky Formation the thickness is least. The most thick parts of Formation are about 320 meters. The lower contact is erosional (Fedorenko et Czamanske, 1997). The age is determined upon spore-pollen and phyto- and zooplanktonic (phyllopods) complexes as Late Permian – Early Triassic (Shikhorina, 1970 after Fedorenko et Czamanske, 1997). Moreover, it is correlated with the volcanic formations of Norilsk region (Fedorenko et Czamanske, 1997; Kamo et al., 2003) and Arydjangsky Formation, which age is measured isotopically (251.7 Ma after Kamo et al., 2003).

The Formation consists mainly of pyroclastic rocks with rare layers of terrigenous deposits (Vasil'ev et Zolotukhin, 1975). It is located in the basement of the whole Traps section and despite its significance for modelling of Maymecha-Kotuy province origin there is no detailed petrographic description. The most abundant rocks are described as basalts and basaltic tuffs (Fedorenko et Czamanske, 1997) with no more details. In addition, among these rocks are distributed unrecognized bodies (flows or later sills) made of aphyric fine-grained amphibole-bearing biotite-orthopyroxene-

clinopyroxene-plagioclase trachybasalts and glassy clinopyroxene-olivine limburgites (Fedorenko et Czamanske, 1997). Thereby there is an issue of Pravoboyarsky Formation's general petrographic description.

Methods

Samples were collected in the August, 2016 in the Maymecha bottom land where the middle part of Pravoboyarsky Formation is exposed and at the top of the Kuranakh-Kaya where the lowest parts of the Formation lay directly on the Permian terrigenous rocks (according to the State Geological Map of Russia in the scale of 1:200 000, sheet R-47-XVII,XVIII). In the laboratory polarized light microscopy (Olympus BX-53) and electron microscopy (JSM-6480LV) with electron-probe microanalysis (X-Max-N50 energy-dispersion spectrometer and INCA-21b software) were used. The voltage was 20 kV, with current 10 nA. Polished thin sections were coated with graphite.

Results

Volcanic rocks from the top of the Kuranakh-kaya represent the lowest part of the Pravoboyarsky Formation. Visually they are black, vitreous and massive. Microscopically rocks are heterogeneous, gray with dark yellowish patches of different size (from hundreds microns to many millimeters, first millimeters are the most common), massive tuff lava.

Grains are represented by different types. Lithoclasts (1) are rare. They are made of ophitic dolerites. Among the grains vitreous (2) are the most abundant. They contain sometimes pores and plagioclase crystals and usually are smooth shaped. The glass is devitrified but often is optically isotropic. Quartz grains (3) are widely spread among the rock. Usually they are rounded. Their surfaces often are covered with chlorites and other secondary minerals. Reaction structures are sometimes seen at the contact with the ground mass (fig. 2b). At the figure 1 two of these grain types could be seen.
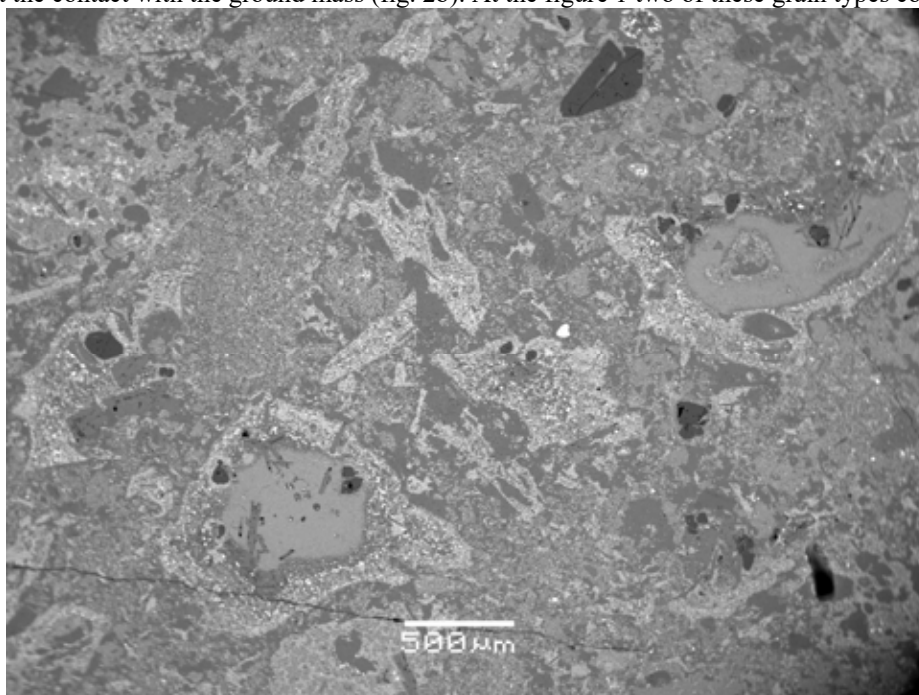
Fig 1. BSE-image of the tuff lava from the lowest part of the Pravoboyarksy Formation; general view: glassy clasts and detrital quartz are in the plagioclase-augitic ground mass; Qtz – for quartz, gg – for devitrified glassy grains with pores and plagioclase, gm – for plagioclase-augitic ground mass.
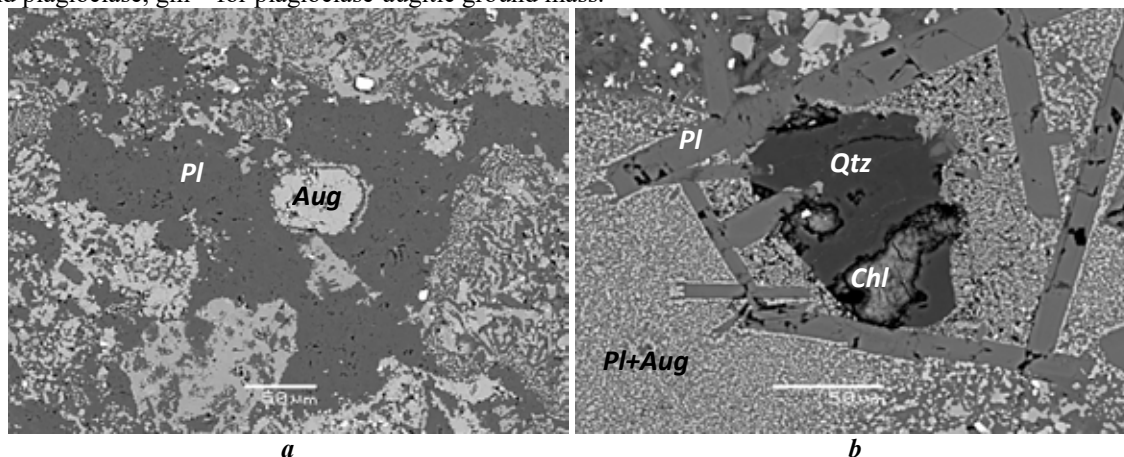
Fig 2. BSE-image of the tuff lava from the lowest part of the Pravoboyarsky Formation; a) the closure view of the plagioclase-augitic ground mass; b) the closure view of the quartz grain with reaction structures among vitreous clasts, ground mass and plagioclase crystals; Pl – for plagioclase, Aug – for augite, Qtz – for quartz, Chl – for chlorite

International Conference on Magmatism of the Earth and Related Strategic Metal Deposits

Ground mass is presented by devitrified glassy material similar to that of vitreous clasts (fig. 2a). Devitrification appears in formation of plagioclase-pyroxenic aggregate of different sizes of individual crystals. Sometimes it contains plagioclase crystals. These crystals are often common with those of vitreous grains and intersect grains borders (fig. 2b).

The most common rocks the Pravoboyarsky Formation from its middle part represent as tuffs. They consist of devitrified vitreous clasts, pieces of dolerites and basalts and quartz and feldspars detrital grains. The quantity of quartz in the rocks varies from 0 to 20 vol. %.

Pyroxenes in doleritic and basaltic patches from rocks are presented by Augite or much rarely Diopside. Feldspar composition (fig. 3b) varies from bytownites and labradorites in the lowermost rocks to alkaline in the middle part. Alkaline feldspar belongs to two distinct groups: Na-rich and K-rich ones. Both these groups are altered while plagioclases from the lower part of the suit are fresh and sometimes preserves an igneous zoning. Vitrous patches and ground mass has been also analyzed and its composition is usually basaltic, sometimes slightly more silica rich (fig. 3a). **Discussion**

There are several issues on the petrology of the Pravoboyarsky Formation.

Firstly, the origin of quartz must be discussed. The facts that its grains are rounded, altered with no concordance to condition of their surroundings and sometimes have reaction structures with them – are strongly imply detrital origin of quartz. Considering that there are terrigenous deposits beneath the Formation we assume that the quartz in volcanic rocks is also terrigenous. Presence of two distinct types of alkaline feldspars supports this assumption since there are both igneous and sedimentary types of feldspar. Na-rich feldspars could be product of basic igneous plagioclases alteration while K-rich feldspars could come terrigenously or also be a product of alteration.
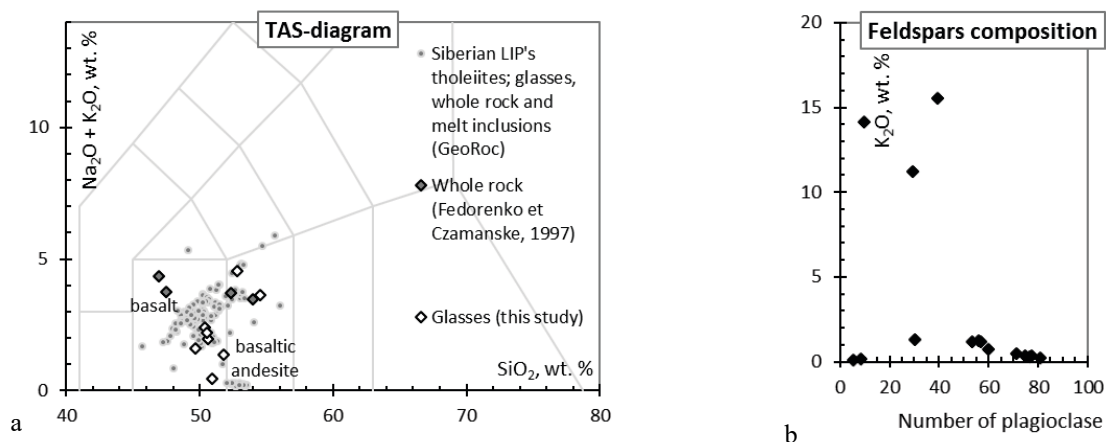
Fig. 3. a) Total alkali-silica diagram (Le Bas et al., 1986) for microprobe-analyzed vitreous grains from Pravoboyarsky Formation, its whole rock-analysis (Fedornko et Czamanske, 1997) in comparison with SLIP's tholeiites (data from GeoRoc); b) composition of microprobe-analyzed feldspars from Pravoboyarsky Volcanites; number of plagioclase is calculated as $Ca/(Ca+Na)\cdot100$ in atomic units.

Secondly, there are textural evidences of presence of liquid lavas on the surface and igneous origin of basic plagioclases. Glassy ground mass containing a lot of glassy smooth-shaped (not sharp) grains resulting in fiamme-like textures are most likely to have formed during explosive eruption or eruptions with a lot of hot lava drops piled with each other or probably in lava flow. Moreover, while melt was cooling the elongated plagioclase crystals grew up forming sometimes ophitic-like framework intersecting grains and ground masse's boundary.

Thirdly, whole rock composition of lava material is to be examined. There are ultrabasic and alkaline-ultrabasic rocks widely spread among the region. There were some evidences also for intermediate of even acid composition according to explosive style of eruptions and the presence of huge amount of quartz. Nevertheless, since (1) the quartz is terrigenous, (2) the only igneous mineral (crystallized from magma) is basic plagioclase and (3) the glassy material is basaltic or basaltic andesitic we can conclude the tholeiitic basaltic to basaltic andesitic composition of magmas erupted there and then similar to those of another continental flood-basalts.

Conclusion

As a summarize we can say that petrographical study of the Pravoboyarsky Formation was conducted and the main rocks of its basement could be described as tholeiitic basaltic to basaltic andesitic plagioclase tuff lavas with terrigenous quartz.

References:

Fedorenko V., Czamanske G. (1997) Results of New Field and Geochemical Studies of the Volcanic and Intrusive Rocks of the Maymecha-Kotuy Area, Siberian Flood-Basalt Province, Russia. Int Geol R 39:479-531

Kamo S.L., Czamanske G.K., Amelin Y., Fedorenko V.A., Davis D.W., Trofimov V.R. (2003) Rapid eruption of Siberian flood-volcanic rocks and evidence for coincidence with the Permian-Triassic boundary and mass extinction at 251 Ma. Earth Plan Sc L 214:75-91

Le Bas M.J., Le Maitre R.W., Streckeisen A., Zanettin B. (1986) A Chemical Classification of Volcanic Rocks Based on the Total Alkali-Silica Diagram. J Pet 27 (3):745-750

Pavlov V., Fluteau F., Veselovskiy R., Fetisova A., Latyshev A., Elkins-Tanton L.T., Sobolev A.V., Krivolutskaya N.A. (2015) Chapterr 5: Volcanic pulses in the Siberian Traps as inferred from Permo-Triassec geomagnetic secular variations. In: Schmidt A., Fristad K.E., Elkins-Tanton L.T. (eds) Volcanism and Global Environmental change. Cambridge University Press, pp 63-78

Sarbas B., Nohl U., Busch U., Kalbskopf B., Youssa C. (2017) Geochemical Rock Database (GeoRoc). Max Planck Institute for Chemistry Mainz, Germany, http://georoc.mpch-mainz.gwdg.de/georoc/Start.asp.

Vasil'ev Yu.R., Zolotukhin V.V. Pinus G.V. (ed) (1975) Petrology of ultrabasites of the North of the Siberian Platform and some issues on its origin. Op. of IGG SB AS USSR 166, Nauka, Novosibirsk (in Russian)

CACO3 AND MGCO3 INTERACTION WITH METALLIC IRON: IMPLICATION FOR THE STABILITY OF CARBONATES IN THE DEEP MANTLE

Martirosyan N.S.[1,2], *Shatskiy A.*[1,2], *Litasov K.D.*[1,2], *Chanyshev A.D.*[1,2]

[1]Institute of Geology and Mineralogy, Siberian Branch of the Russian Academy of Sciences, Novosibirsk, Russia
[2]Novosibirsk State University, Novosibirsk, Russia, martirosyanns@gmail.com

Subduction of oceanic slabs is the major source of CO_2 in the mantle (Dasgupta and Hirschmann, 2010). CO_2 in the form of carbonates transported by oceanic crust causes formation of mantle heterogeneity, as it affects mantle oxidation state, trigger partial melting, alter major and trace element composition and rheological properties of the mantle rocks (P okhilenko et al., 2015). Thus, stability of carbonates during subduction is an important issue for the global geodynamic processes, diamond formation and the carbon cycle.

Beneath island arcs carbonates are subjected to negligible decomposition and melting, and significant amount of them appear to be transported to deeper levels (Kerrick and Connolly, 2001a; Kerrick and Connolly, 2001b). Experimental and theoretical studies confirm carbonate stability under the *P-T* conditions of the upper and lower mantle (Katsura and Ito, 1990; Isshiki et al., 2003; Ono et al., 2005; Ono et al., 2007; Boulard et al., 2011; Boulard et al., 2012). However the deep Earth's interior can be too reduced to favor stable carbonates (Frost et al., 2004).

In contrast to the subducted slabs, large parts of the ambient mantle is highly reduced. Studies of natural peridotite xenoliths show that mantle $f(O_2)$ continuously decreases with increasing pressure (Woodland and Koch, 2003). Thermodynamic calculations and experiments (Frost et al., 2004; Rohrbach et al., 2007) suggest that it becomes metal saturated at 250 km depth and in all mantle regions below as a result of Fe^{2+} disproportionation in perovskite and garnet. The large contrast in the redox conditions causes a redox interactions between carbonate-bearing subducted slab and Fe^0-saturated surrounding mantle (Frost and McCammon, 2008; Stagno and Frost, 2010).

The details of carbonate reduction are still poorly constrained. The complexity of this system impedes particular reconstruction of redox reaction, so composite systems should be studied. One of the principal redox exchange reactions at the slab-mantle interface during subduction is carbonate–Fe^0 interaction. Using uniaxial press multianvil apparatus, we have studied interaction of $MgCO_3$ and $CaCO_3$ with Fe^0 at 650–1400 °C and 4–16 GPa. To determine water influence on the reaction, additional experiments were conducted in the hydromagnesite–Fe^0.

For water free systems following redox reactions have been established:

$$3CaCO_3 \text{ (aragonite)} + 13Fe^0 = 3CaFe_2O_3 \text{ (Ca-wüstite)} + Fe_7C_3 \tag{1}$$
$$MgCO_3 \text{ (magnesite)} + 5Fe^0 = MgO \text{ (wüstite)} + 2FeO \text{ (wüstite)} + Fe_3C \tag{2}.$$
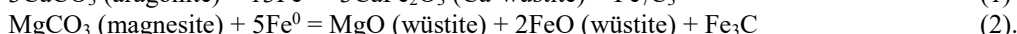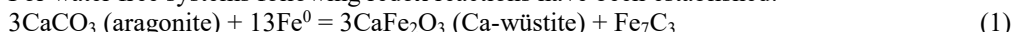
The mechanism of hydromagnesite–Fe^0 interaction is more complicated and includes 3 stages. On the basis of experiments, we propose the following scheme for the redox interaction:

$$Fe^0 + H_2O \text{ (F)} = FeO \text{ (wüstite)} + H_2 \text{ (F)} \tag{3}$$
$$MgCO_3 \text{ (magnesite)} + 2 H_2 \text{ (F)} = 2 H_2O \text{ (F)} + MgO \text{ (wüstite)} + C \text{ (Gr or F)} \tag{4}$$
$$15 Fe^0 + 4CO_2 \text{ (F or magnesite)} = Fe_7C_3 + C(Gr) + 8 FeO(\text{wüstite}) \tag{5}$$
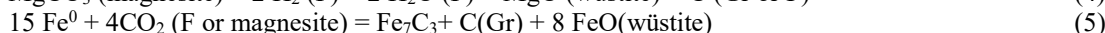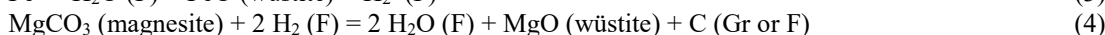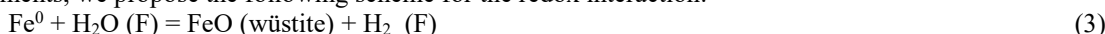
(3) the reaction of metallic iron with water liberated as a result of hydromagnesite decomposition; (4) hydrogen transported in the aqueous fluid reacts with the carbonate $MgCO_3$ to form a layer of Mg-wüstite and graphite; (5) formation of carbide due to counter transport of components through the aqueous fluid: carbon from the side of carbonate, iron and hydrogen from the side of metallic iron.

Despite the difference between water-free and water saturated systems, diffusion of components was suggested to be the major rate – limiting process with the reaction rate constant (k) being log-linear in 1/T (Fig 1, 2). Temperature dependence of k for Ca-carbonate – iron interaction were fit to Arrhenius equations, which can be written as: be k [m^2/s] = $2.8 \times 10^{-5} \exp(-211/RT)$ at 4-6 GPa and k [m^2/s] = $2.1 \times 10^{-11} \exp(-56/RT)$ at 16 GPa. Reaction rate constant for magnesite – iron reaction is higher than that for the $CaCO_3$-Fe^0, and can be presented by following equations: k [m^2/s] = $3.55 \times 10^{-5 \times} \exp(-(194)/RT)$ at 6.5 GPa.

In the water-bearing system, reactions were governed by solubility of components in the water fluids, and were controlled by the hydrogen fugacity. Water acts as a transporting agent for the reactants. Calculations of kinetic parameters clearly detected, that the rate of product formation in the hydromagnesite–Fe^0 system increases by two orders of

magnitude in comparison with the MgCO$_3$–Fe^0. Temperature dependence of k can be written as: k [m^2/s] $=4.8^x10^{-7x}$exp(-107/RT) at 4-6 GPa and k [m^2/s] $=3^x10^{-2x}$exp(-259)/RT) at 16 GPa.

The experimental results allow to calculate the length scale over which the reaction kinetics between carbonates and metallic iron is likely effective. Using relatively simple relationship between the characteristic distance of diffusion as a function of k and duration of the process, we estimated the length scale of the reaction for time scales 4-16 Myr, which corresponds to subduction rates of 2-8 cm/year from 250 km (metal-saturation boundary) to 470 km for different slab P-T-profiles. Assuming that carbonates are in a direct contact with iron and there is no water in the system, the maximum degree of carbonate reduction can be evaluated using the results of our study and the data on CO$_2$ distribution in altered oceanic basalts. The estimates suggest that up to 0.5, 12, and 20 vol. % of carbonates can be reduced in water free system during subduction down to the mantle transition zone at the conditions of cold, medium and hot geotherms, respectively. The calculations for water-containing system, from the other hand, give 12, 50 and 100 vol. %.

The sluggish kinetics of the MgCO$_3$-Fe^0 and CaCO$_3$-Fe^0 reactions established in our study suggests that carbonates could survive during subduction from metal saturation boundary near 250 km depth down to the transition zone. At the same time, in the water-containing systems carbonates would be significantly consumed, with total reduction to carbide or diamond in the case of hot geotherm.
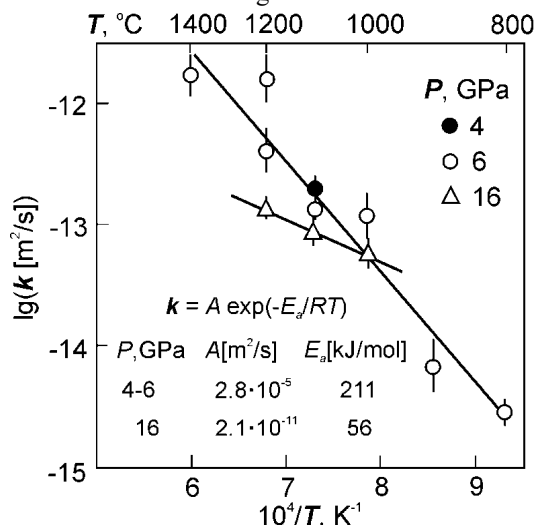
Fig. 1. Logarithm of the reaction rate constant ($k = \Delta x^2/2t$) versus reciprocal temperature 3 CaCO$_3$ (aragonite) + 13 Fe^0 (metal) = Fe$_7$C$_3$ (carbide) + 3 CaFe$_2$O$_3$ (Ca-wüstite). Two solid lines are linear regressions from data at 4-6 GPa and 16 GPa. The error bars show the uncertainties.
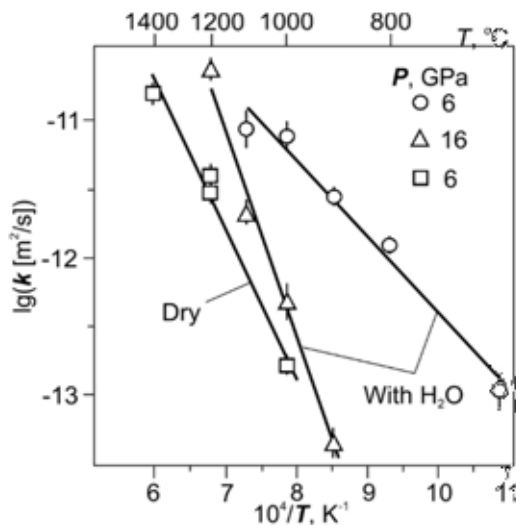
Fig. 2. Logarithm of the reaction rate constant ($k = \Delta x^2/2t$) versus reciprocal temperature for MgCO$_3$+Fe^0 interaction in H$_2$O- bearing system in comparison with k calculated for the reaction in "dry" conditions based on data from. Solid lines are linear regressions from data at 6 GPa and 16 GPa. The error bars show the uncertainties.

References:

Boulard, E., Gloter, A., Corgne, A., Antonangeli, D., Auzende, A.L., Perrillat, J.P., Guyot, F., Fiquet, G., 2011. New host for carbon in the deep Earth. Proceedings of the National Academy of Sciences of the United States of America, 108: 5184-5187.

Boulard, E., Menguy, N., Auzende, A.L., Benzerara, K., Bureau, H., Antonangeli, D., Corgne, A., Morard, G., Siebert, J., Perrillat, J.P., Guyot, F., Fiquet, G., 2012. Experimental investigation of the stability of Fe-rich carbonates in the lower mantle. Journal of Geophysical Research-Solid Earth, 117: B02208.

Dasgupta, R., Hirschmann, M.M., 2010. The deep carbon cycle and melting in Earth's interior. Earth and Planetary Science Letters, 298: 1-13.

Frost, D.J., Liebske, C., Langenhorst, F., McCammon, C.A., Tronnes, R.G., Rubie, D.C., 2004. Experimental evidence for the existence of iron-rich metal in the Earth's lower mantle. Nature, 428: 409-412.

Frost, D.J., McCammon, C.A., 2008. The redox state of Earth's mantle. Annual Review of Earth and Planetary Sciences, 36: 389-420.

Isshiki, M., Irifune, T., Hirose, K., Ono, S., Ohishi, Y., Watanuki, T., Nishibori, E., Takata, M., Sakata, M., 2003. Stability of magnesite and its high-pressure form in the lowermost mantle. Nature, 427: 60-63.

Katsura, T., Ito, E., 1990. Melting and subsolidus phase relations in the MgSiO3-MgCO3 system at high pressures-Implications to evolution of the earth's atmosphere. Earth and Planetary Science Letters, 99: 110-117.

Kerrick, D., Connolly, J., 2001a. Metamorphic devolatilization of subducted oceanic metabasalts: implications for seismicity, arc magmatism and volatile recycling. Earth and Planetary Science Letters, 189: 19-29.

Kerrick, D.M., Connolly, J.A.D., 2001b. Metamorphic devolatilization of subducted marine sediments and the transport of volatiles into the Earth's mantle. Nature, 411: 293-296.

Ono, S., Kikegawa, T., Ohishi, Y., 2007. High-pressure transition of CaCO3. American Mineralogist, 92: 1246-1249.

Ono, S., Kikegawa, T., Ohishi, Y., Tsuchiya, J., 2005. Post-aragonite phase transformation in CaCO3 at 40 GPa. American Mineralogist, 90: 667-671.

Pokhilenko, N., Agashev, A., Litasov, K., Pokhilenko, L., 2015. Carbonatite metasomatism of peridotite lithospheric mantle: implications for diamond formation and carbonatite-kimberlite magmatism. Russian Geology and Geophysics, 56: 280-295.

Rohrbach, A., Ballhaus, C., Golla-Schindler, U., Ulmer, P., Kamenetsky, V.S., Kuzmin, D.V., 2007. Metal saturation in the upper mantle. Nature, 449: 456-458.

Stagno, V., Frost, D.J., 2010. Carbon speciation in the asthenosphere: Experimental measurements of the redox conditions at which carbonate-bearing melts coexist with graphite or diamond in peridotite assemblages. Earth and Planetary Science Letters, 300: 72-84.

Woodland, A.B., Koch, M., 2003. Variation in oxygen fugacity with depth in the upper mantle beneath the Kaapvaal craton, Southern Africa. Earth and Planetary Science Letters, 214: 295-310.

TRACE ELEMENTS IN CHIMNEYS AS INDICATORS OF HOST ROCK COMPOSITION AND MATURITY OF SEAWATER/ROCK HYDROTHERMAL INTERACTION VERSUS MAGMATIC-HYDROTHERMAL CONTRIBUTION TO VMS DEPOSITS

Maslennikov V.V.[1], Tretyakov G.A.[1], Melekestseva I.Yu.[1], Maslennikova S.P.[1], Lein A.Yu.[2], Large R.R.[3], Danyushevsky L.V.[3], Ishiyama D.D.[4], Tseluyko A.S.[1], Revan K.M.[5]

[1]Institute of Mineralogy, Ural Branch of the Russian Academy of Sciences, Miass, Russia, mas@mineralogy.ru
[2]P.P. Shirshov Institute of Oceanology of Russian Academy of Sciences, Moscow, Russia
[3]CODES, University of Tasmania, Hobart, Australia
[4]Akita University, Akita, Japan
[5]General Directorate of Mineral Research and Exploration (MTA), Ankara, Turkey

The very well preserved chimneys have been found in many Ordovician-Devonian (Urals and Rudny Altai), Cretaceous (Pontides) and Miocene (Hokuroko) VMS deposits. Most chimneys are broadly similar to modern black, gray, white and clear smokers by mineral and trace element zonation. The results of the quantitative laser ablation inductively coupled plasma mass spectrometry (LA-ICP-MS) show that concentration and zonality of most trace metals in sulfides of different chimneys is mostly a function of physico-chemical parameters. Trace elements, which may be enriched in the same mineral phases under variable temperature, redox conditions or mixing, can be used as a tool to identify the physico-chemical conditions typical of each zone of the chimneys.

The study has shown systematic trace element distribution patterns across the chimneys. The coarse-grained layers of chalcopyrite in the central conduits are relatively rich in Se and Sn, but are depleted in other elements. Chalcopyrite at the margins of such layers is enriched in Bi, Co, Au, Ag, Pb, Mo, Te, and As, which reside in microinclusions of tellurides and/or sulfoarsenides. Sphalerite in the conduits and the outer chimney wall contains has elevated Sb, As, Pb, Co, Mn, U, and V contents. Antimony, As, and Pb reside in microinclusions of a galena–fahlore assemblage, whereas Co and Mn likely substitute for Zn^{2+} in the sphalerite structure. The highest contents of most trace elements are found in colloform pyrite of the outer wall of the chimneys and likely result from rapid precipitation under high-temperature conditions. In colloform pyrite of the outer walls of most chimneys, the trace element contents decrease in the following order: Tl> Ag> Ni> Mn> Co> As> Mo> Pb> Ba> V> Te> Sb> U> Au> Se> Sn> Bi, which is governed by strong temperature gradient. In contrast, pyrite of the high- to medium-temperature central conduits exhibits high Se, Sn, Bi, Te, and Au contents. In the zone between the inner conduit and outer wall, the colloform pyrite is recrystallized to euhedral pyrite, which becomes depleted in all trace elements except Co, As and Se. The mineralogical and trace element variations between chimneys are likely due to increasing fO_2 and decreasing temperature caused by mixing of hydrothermal fluids with cold oxygenated seawater. Average values of Se (a "high-temperature' element) decrease from black to white smoker chimneys. The medium-temperature association (Te, Bi, Co, Mo, Au) is typical of grey smoker chimneys. The white smoker chimneys are characterized by low contents of most elements except for Ag, Tl, Te, Sb and As, probably due to dilution of the vent fluid by seawater, which penetrates to the deeper parts of the hydrothermal system. Uranium and V are concentrated in the outer wall of most chimneys due to their extraction from seawater associated with more reduced fluids of black and grey smokers (e.g., Maslennikov et al., 2009; Revan et al., 2013). However, similar mineral chimney types of the deposits hosted into different rocks s are distinct in trace element concentrations.

The chimney-bearing Urals deposits can be ranged by host rock composition and associated ore types and subtypes: ultramafic (Atlantic type: Dergamysh) → mafic (Cyprus type: Buribay) → bimodal mafic (Urals type, U1, U2, and U3 subtypes: Yubileynoe (U1) → Sultanovskoye (U1) → Yaman-Kasy (U2) → Molodezhnoe (U3) → Uzelga-4 (U3)) → bimodal felsic (Kuroko or Baymak type: Oktyabrskoe → Valentorskoe → Tash-Tau → Uzelga-1 → Talgan → Alexandrinskoe) sequences. In the Urals, only Saf'yanovka deposit may be considered a proxy of the Altai type (pelitic-felsic) hosted by intercalated felsic and black shale complex. Numerous felsic-hosted chimney-bearing VMS deposits are known in Rudny Altai (Nikolaevskoe, Artem'evskoe, Zarechenskoe, Korbalikhinskoe). Most chimney-bearing deposits of Pontides (Kutlular, Chaely, Lakhanos, Kisilkaya, Killik) and Hokuroko (Ezury, Mitsumine, Kosaka-Uchinotay, Kosaka-Motoyama, Ainai, Hanawa) areas are related to Kuroko (or Pontides) type of bimodal felsic sequences. The wide range of host rocks allows comparison of trace element contents of genetically homonymous sulfides of the same chimney types.

Except for Altai type of VMS deposits, trace element assemblages in chalcopyrite reflect the host rock composition: ultramafic (high Se, Sn, Co, Ni, Ag and Au contents) → mafic (high Co, Se, and Mo and low Bi, Au and Pb contents) → bimodal mafic (high Te, Au, Ag, Bi, Pb, and Co, moderate Se, and variable As and Sb contents) →

bimodal felsic (high As, Sb, Mo, and Pb, moderate Bi, and low Co, Te and Se contents). In sphalerite of the same range, the contents of Bi, Pb, Ag, Au and Sb increase versus Fe, Se and Co. The variations in trace elements in colloform pyrite coincide with these changes. In the same range, colloform pyrite is characterized by decrease in Co, Se, and Sn contents with increasing Au, Ag, Tl, Pb, Bi, Sb, and As contents. Tellurium is concentrated in the intermediate part of the range. In Altai type of the deposits, the highest Sn, Co, Ni, and Se contents are detected in sphalerite and chalcopyrite (Maslennikov et al., 2016).

However, there are several exceptions in these trends. In modern oceans, the chimneys associated with basalts of fast- and slow-spreading mid-oceanic ridges (MORs), hot spots and back-arc basins are strongly distinct. The mineralogy and trace elements of chimneys, which were formed under same geological setting, can also be variable. This is explained by differences in maturity of seawater/rock hydrothermal interaction, which can be modeled in the Selector program at 350 °C and 25 MPa. The maximum extraction of major ore-forming elements of massive sulfide deposits from basalts occurs under reducing conditions: $2.9 \cdot 10^{-3}$ m Fe at ξ (–lg$_{rock/seawater}$) = 2.1; $3.3 \cdot 10^{-4}$ m Zn at ξ = 0.625; and $5.02 \cdot 10^{-5}$ m Cu at ξ = 1.4. Major transport complexes of these elements in hydrothermal fluids are $FeCl_2^0 > FeCl^+ > Fe^{2+}$, $ZnCl^+ > ZnCl_2^0 > ZnCl_3^-$, $CuCl_3^{2-} > CuCl_2^-$. According to the widely accepted recycling model, the mafic rocks (gabbros, basalts) are most likely sources of metals for hydrothermal sulfide systems. The results of physico-chemical modeling suggest strong difference in the immature and mature stage of basalt alteration. At initial stage of seawater/rocks interaction, olivine, pyroxene, and, probably, hornblende are the main subjects to be decayed.

At immature stage, Fe, Cu, Se, and Co are leached from basalt. At mature stage, which is accompanied by decay of feldspar, the amount of leached Te, Bi, Au, Ag, As, Sb, Pb, Ba, and Tl increased significantly. Related fluid enriched in latter trace elements could be involved in melting of the altered rocks with formation of fluid-saturated metal-rich felsic magma. It can be an additional source of heavy metals and semimetals during recrystallization. The plagiogranite intrusions and their xenoliths in lava flow versus dolerite and relic gabbro xenoliths are considered to be indicators of mature hydrothermal system in some barite-rich Urals VMS deposits (Uzelga, Aleksandrinskoe).

According to modeling, the Au and Ag minerals are not predicted to precipitate from hydrothermal fluids under reasonable seawater/rock ratio over a wide temperature range. This suggests that an additional contribution to the hydrothermal system is required in order to achieve saturation in precious metals. At example of the Semenov-2 hydrothermal field (Mid-Atlantic Ridge, MAR), magmatic input can be suggested by the occurrence of plagiogranites and tonalities, which could be a potential source of Au-rich magmatic fluids, and by mineralogical and geochemical similarities with magma-related, low- to intermediate-sulfidation epithermal systems, namely high Au and Ag grades, high (Cu + Zn + Pb)/Au and Au/Ag ratios, and presence of Ag, Bi, and Te minerals (Melekestseva et al., 2017). The likely crucial role of silicic melts in producing high Au and Ag grades suggests that exploration for precious metal-rich, volcanic-hosted massive sulfide deposits should be primarily directed to sites in which evolved igneous rocks occur on seafloor. Both in modern and ancient mafic-hosted deposits, zones characterized by abundant deposition of silica could be good clues to the presence of significant gold.

Additional magmatic contribution to high-sulfidation style of some bimodal mafic and felsic-hosted black smokers of the Urals, Pontides, Altai and Kuroko VMS deposits, as well as modern vent sites of the low-spreading MORs, hot spots and island arcs, could be suggested. In contrary, in the fast-spreading centres (e.g., EPR), the magmatic-hydrothermal systems become immature due to refreshing basalts in the reaction zones. Some features of magmatic-hydrothermal contribution of SO_2 can be found in the bimodal felsic-hosted Kuroko-type of VMS deposits, where advanced argillic alteration of footwall rocks is common. Potential criteria for extraction of metals (Sn, Mo, W) directly from magmatic-hydrothermal sources are provided by chimneys of the Aleksandrinka deposit (Urals). However, the enrichment in Sn, Mo or W themselves is probably insufficient evidence for magmatic-hydrothermal contribution. In felsic-hosted deposits of Altai-type, the high W and Sn contents of chimneys are consistent with abundantf black-shales in the footwall volcano-sedimentary sequences (e.g., Nikolaevskoe and Saf'yanovka deposits). The high Sb contents of chimneys of ultramafic-hosted Deramysh deposit could be explained by magmatic-hydrothermal contribution or simply higher maturity of seawater/rocks hydrothermal system in comparison to some serpentinite-hosted vent sites of MAR. The Bi concentrations could be related to magmatic contribution, maturity of seawater/rocks hydrothermal systems or sedimentary source, as well as sediment-covered MORs. Our results are broadly consistent with general conclusion of Huston et al. (2011) that criteria to advocate or exclude of magmatic-hydrothermal contribution to VMS deposits are equivocal. Thus, the trace element study of chimney sulfides can be one of the fruitful methods to find the value of different processes, which form VMS deposits.

References:

Huston D.L., Relvas J.M.R.S., Gemmel J.B., Drieberg S. (2011) The role of granites in volcanic-hosted massive sulfide ore-forming systems and assessment of magmatic contributions. Miner Deposita 46:473–507.

Melekestseva I.Yu., Maslennikov V.V., Tretyakov G.A., Nimis P., Beltenev V.E., Rozhdenstveskaya I.I., Maslennikove S.P., Belogiub E.V., Danyushevsky L., Large R., Yuminov A.M., Sadykov S.A. (2017) Gold- and silver-rich massive sulfides from the Semenov-2 hydrothermal field, 13°31.13′ N, Mid-Atlantic Ridge: A case of magmatic contribution? Econ Geol 112 (in press).

Maslennikov V.V., Maslennikova S.P., Large R.R., Danyushevsky L.V. (2009) Study of trace element zonation in vent chimneys from the Silurian Yaman-Kasy VMS (the Southern Urals, Russia) using laser ablation inductively coupled plasma mass spectrometry (LA-ICP MS). Econ Geol 104:1111–1141.

Maslennikov V.V., Maslennikova S.P., Large R.R., Danyushevsky L.V., Herrington R.J., Ayupova N.R., Zaykov V.V., Lein A.Yu., Tseluyko A.S., Melekestseva I. Yu., Tessalina S.G. *(*2017) Chimneys in Paleozoic massive sulfide mounds of the Urals VMS deposits: Mineral and trace element comparison with modern black, grey, white and clear smokers. Ore Geol Rev doi.org/10.1016/j.oregeorev.2016.09.012.

Revan M.K., Genc Y., Maslennikov V.V., Maslennikova S.P., Large R.R., Danyushevskiy L.V. (2014) Mineralogy and trace-element geochemistry of sulfide minerals in hydrothermal chimneys from Upper-Cretaceous VMS deposits of the eastern Pontide orogenic belt (NE Turkey). Ore Geol Rev 62:129–149.

TECTONIC EVOLUTION AND METALLOGENY OF WEST ASIA

Mei W., Ma C.Q.
China University of Geosciences, Wuhan, China, meiwei09@cug.edu.cn

West Asia is located in the western section of the eastern Tethyan tectonic domain, belonging to Africa-Arab collision zone. The research scope mainly includes Turkey, Iran and parts of Pakistan. Although Pakistan is not located in West Asia geographically, Iran and parts of Pakistan are located in a continuous metallogenic domain with a similar metallogenic features (such as porphyry copper deposit et al.) (Hou and Zhang, 2015). Consequently, this paper adds parts of Pakistan into our research. The research area consists of a group of diverse Tethyan blocks, including the Istanbul, Sakarya, Anatolide - Taurides, Central Iran and Sanandaj-Sirjan (Fig. 1), which were separated from Gondwana, drifted northwards and accreted to the Eurasian continent by opening and closing of two successive Tethyan Oceanic basins (Paleo-Tethyan and Neo-Tethyan), and subsequent continental collision.
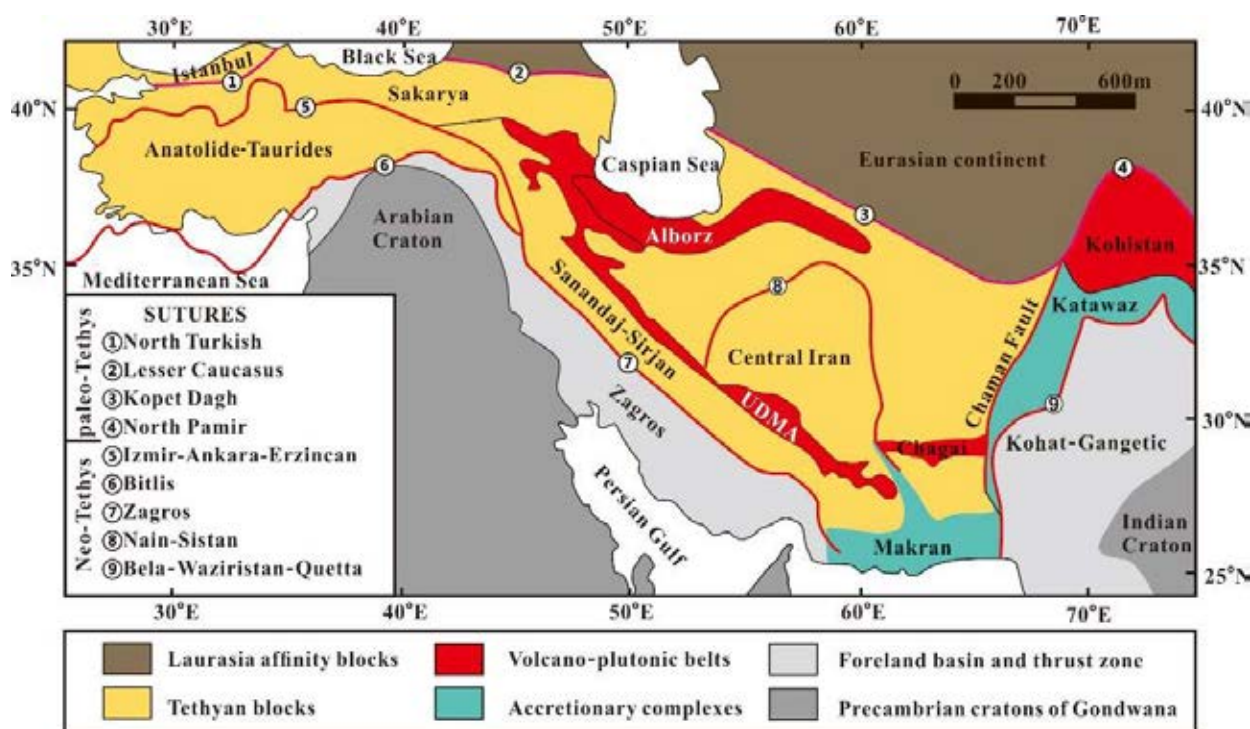
Fig. 1. Tectonic framework in West Asia (modified after Moix et al., 2008; Mouthereau et al., 2012; Hou and Zhang, 2015).

The tectonic evolution of West Asia includes four stages. (1) D_3-T_3, evolution of Paleo-Tethyan ocean; (2) J, formation of Neo-Tethyan ocean basin; (3) K-E_2, subduction and closure of Neo-Tethyan ocean; (4) E_2-N_1, continental collision, which can be divided into three processes: Eocene to Oligocene syn-collisional continental convergence, early-middle Miocene late-collisional tectonic transform, and late Miocene post-collisional crustal extension. The last three stages are the main mineralization stages and each forms distinct types of ore deposits in specific settings. This paper identifies six mineralization, including Porphyry Cu-Mo-Au, sediment-hosted Pb-Zn (-Ag) (MVT type and SEDEX type), magmatic chromite, VMS Cu-Pb-Zn, epithermal Au-polymetallic and skarn Fe-polymetallic deposits (Fig. 2).
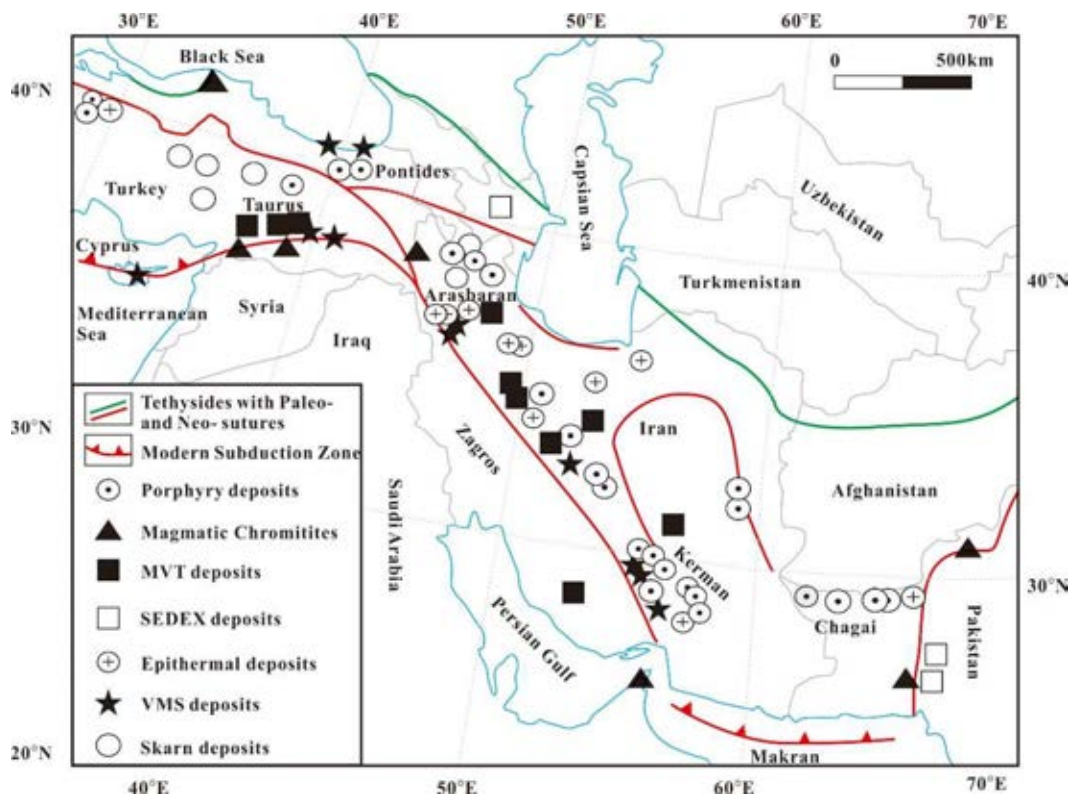
Fig. 2. Spatial distribution of some major deposits types in West Asia (modified after Leach et al., 2005; Hou and Zhang, 2015).

Metallogenesis within West Asia occurred throughout almost entire history of the tectonic evolution of the western section of the eastern Tethyan domain from Jurassic accretion to Cenozoic collision, and the domain hosts a wide variety of mineral deposits (Fig. 3).
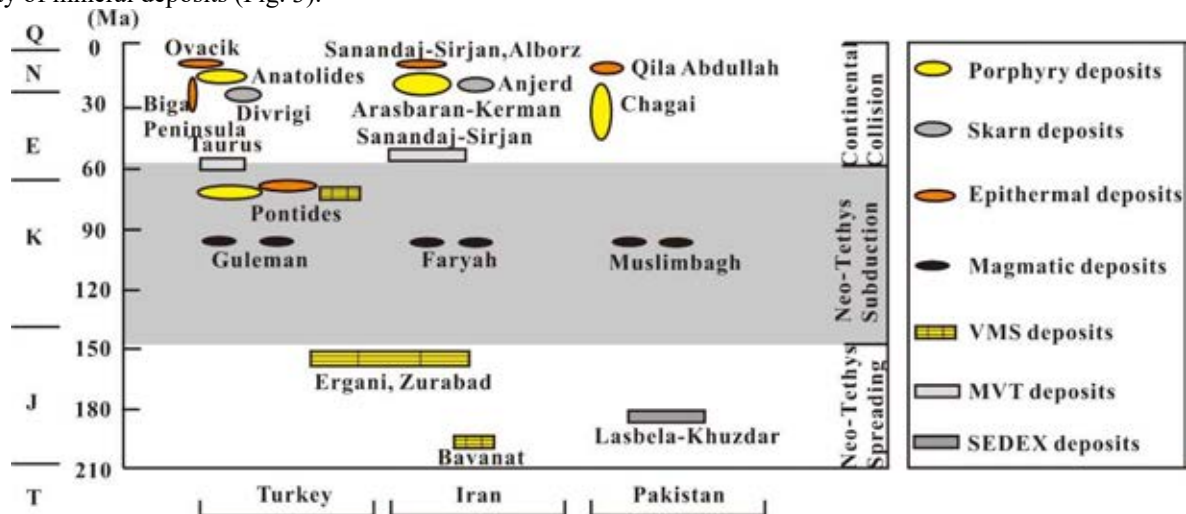
Fig. 3. Major tectonic and mineralization events in West Asia (modified after Hou and Zhang, 2015)

The spreading of Neo-Tethyan ocean basin in this area is associated with the formation of Lasbela-Khuzdar SEDEX Pb-Zn deposits of Pakistan(Sillitoe, 1978), and Cyprus-type volcanogenic massive sulfide (VMS) Cu-Pb-Zn deposits of Turkey and Iran (Franklin et al., 2005) and Besshi-type volcanogenic massive sulfide (VMS) Cu-Pb-Zn deposits of Iran (Mousivand et al., 2012). The subduction and closure of Neo-Tethyan ocean basin in this area is related with the formation of Pontides porphyry copper metallogenic belt (Moix et al., 2008), HS epithermal Cu-Au-Ag deposits (Yigit, 2006; Yigit, 2009), Kuroko-type volcanogenic massive sulfide (VMS) Cu-Pb-Zn deposits (Yigit, 2009), and a continuous magmatic chromite deposits along the sutures (Yigit, 2009; Yaghubpur and Hassannejad, 2006; Arif and Jan, 2006). Whereas continental collision in this domain produced numerous economically significant metallogenic belt. Such as, MVT-type, Anatolides, Arasbaran-Kerman and Chagai porphyry copper belt, epithermal deposit, skarn Fe-polymetallic deposit, etc (Hanilçi and Öztürk, 2011; Rajabi et al., 2012; Aghazadeh et al., 2015; Somarin and Moayyed, 2002; Yigit, 2006).

References:

Aghazadeh M, Hou Z, Badrzadeh Z, Zhou L. Temporal–Spatial Distribution and Tectonic Setting of Porphyry Copper Deposits in Iran: Constraints from Zircon U–Pb and Molybdenite Re–Os Geochronology. Ore Geology Reviews, 2015, 70: 385-406.

Arif M, Jan M Q. Petrotectonic significance of the chemistry of chromite in the ultramafic–mafic complexes of Pakistan. Journal of Asian Earth Sciences, 2006, 27(5): 628-646.

Franklin J M, Gibson H L, Jonasson I R, Galley A G. Volcanogenic massive sulfide deposits. Economic Geology 100th anniversary volume, 2005, 98: 523-560.

Hanilçi N, Öztürk H. Geochemical/isotopic evolution of Pb–Zn deposits in the Central and Eastern Taurides, Turkey. International Geology Review, 2011, 53(13): 1478-1507.

Hou Z, Zhang H. Geodynamics and metallogeny of the eastern Tethyan metallogenic domain. Ore Geology Reviews, 2015, 70: 346-384.

Leach D, Marsh E, Bradley D, Gardoll S, Huston D. The distribution of SEDEX Pb-Zn deposits through Earth history. Springer Berlin Heidelberg, 2005.

Moix P, Beccaletto L, Kozur H W, Hochard C, Rosselet F, Stampfli G M. A new classification of the Turkish terranes and sutures and its implication for the paleotectonic history of the region. Tectonophysics, 2008, 451(1): 7-39.

Mousivand F, Rastad E, Meffre S, Peter J M, Mohajjel M, Zaw K, Emami M H. Age and tectonic setting of the Bavanat Cu–Zn–Ag Besshi-type volcanogenic massive sulfide deposit, southern Iran. Mineralium Deposita, 2012, 47(8): 911-931.

Mouthereau F, Lacombe O, Vergés J. Building the Zagros collisional orogen: timing, strain distribution and the dynamics of Arabia/Eurasia plate convergence. Tectonophysics, 2012, 532: 27-60.

Rajabi A, Rastad E, Canet C. Metallogeny of Cretaceous carbonate-hosted Zn–Pb deposits of Iran: geotectonic setting and data integration for future mineral exploration. International Geology Review, 2012, 54(14): 1649-1672.

Sillitoe R H. Metaliogenic evolution of a collisional mountain belt in Pakistan: A preliminary analysis. Journal of the Geological Society, 1978, 135(4): 377-387.

Somarin A K, Moayyed M. Granite- and Gabbrodiorite-Associated Skarn Deposits of NW Iran. Ore Geology Reviews, 2002, 20(3): 127-138.

Yaghubpur A, Hassannejad A A. The Spatial Distribution of Some Chromite Deposits in Iran, Using Fry Analysis. Journal of Sciences, 2006, 17: 147-152.

Yigit O. Gold in Turkey—a missing link in Tethyan metallogeny. Ore Geology Reviews, 2006, 28(2): 147-179.

Yigit O. Mineral Deposits of Turkey in Relation to Tethyan Metallogeny: Implications for Future Mineral Exploration. Economic Geology, 2009, 104(1): 19-51.

A COMBINED SEM, QEMSCAN AND LA-ICP-MS STUDY OF ORE AND ALTERATION MINERALS FROM A NEW INTRUSION-RELATED GOLD SYSTEM IN THE TRUN REGION , W BULGARIA

Metodiev S.[1], Kouzmanov K.[2], Peytcheva I.[1], Dimitrova D.[1], Stefanova E.[1]
[1]Geological institute, Bulgarian Academy of Science, Sofia, Bulgaria, chefi_met@yahoo.com
[2]University of Geneva, Geneva, France, kalin.kouzmanov@unige.ch

Mineral and geochemical signatures are crucial for characterization of ore deposits and their definition as specific genetic type. Besides the conventional methods for mineral identification techniques such as QEMSCAN® and LA-ICP-MS can be jointly used for quantitative mineralogical and elemental distribution analyses. In this contribution, we report results from a combined use of both techniques to study the Au-Ag-W deposits in the Tran region of western Bulgaria. The study is focused on the Nadezhda, Logo and Ruy deposits that form a cluster in the Carboniferous Ruy pluton and its Lower Paleozoic low-metamorphic basement. The main features of the deposits define them as an Intrusion-Related Gold System (IRGS). These are: i) association with the reduced Ruy pluton; ii) structural control on the intrusion and mineralization; iii) Au - Bi correlation; iv) approximately coeval magmatism and mineralization (330-333 Ma); v) low sulfide content; vi) presence of CO_2 in the hydrothermal fluids. Although age dating of magmatism and hydrothermal molybdenite and rutile point to Variscan age of the system, a Late Alpine (Eocene) magmatic and hydrothermal activity overprinted the region making the discrimination of hydrothermal processes complicated. In order to establish geochemical criteria for the distinction of the two hydrothermal events electron microprobe, SEM and LA-ICP-MS analyses on hydrothermal white micas and pyrite from mineralized (pluton and metamorphics) and barren (Eocene subvolcanic dykes) samples have been performed.

Our results reveal gold is present mainly as native gold or electrum, varying in size (from 10 μm to macroscopic). In the intrusion-hosted deposits (Nadezhda and Ruy) it is associated with quartz, white micas, and pyrite - attached or in fractures. In the metamorphic-hosted ores gold is presented mainly in fractures, attached or "locked" in pyrite crystals. Only 6 vol% of the gold is presented as submicroscopic. These features are important for future gold extraction using environmental-friendly technologies. Pyrite in the Eocene dykes is trace, small in size and often irregular in shape. Positive gold grades in the dykes are uncommon and the element is participating only as nano-inclusions in pyrite. Specific feature here is the high As content that correlates positively with Au, while in the Paleozoic rocks pyrites are low in As.

The hydrothermal white mica is a common alteration mineral in the deposits. QEMSCAN analyses provide quantitative data on the distribution of it in both hosts - the pluton and the Eocene dykes. In the intrusive the main K-

bearing mineral is K-feldspar reaching up to 40 vol%. White mica is concurrent alteration mineral with 10 and 20 vol%. Quartz is another major mineral varying between 19 and 75 vol%. In the Eocene dykes K-feldspar is almost absent, whereas white mica ranges from 27 to 29%, and quartz – from 57 to 61%. Significant compositional differences of hydrothermal white micas (e.g., F and Ba content) have been identified between the Variscan and the Eocene events.

This first combined application of QEMSCAN with LA-ICP-MS analyses of ore samples from an IRGS in Bulgaria reveals the potential of these techniques in solving scientific and industry-oriented problems.

THE CAPE VERDE ARCHIPELAGO PRIMARY MELTS: PETROLOGICAL SYSTEMATICS

Migdisova N.A., Kogarko L.N.
Vernadsky Institute of Geochemistry and Analytical Chemistry of RAS, Moscow
kogarko@geokhi.ru, migdisova@geokhi.ru

The representative collection of samples was obtained during the complex geological expeditions of the Geological Institute of the Academy of Sciences of the USSR and the 9th cruise of Akademician Boris Petrov (GEOKHI RAS) on the islands of the Cape Verde during the three field seasons (1982-1986) within the framework of the national project "Lithos" and the "World Ocean" program.

The collection of primary magmas from the islands of Sal, Santiago, San Vicente, Boavista, Fogu, Mayu and San Nicolau consists of 39 samples. X-ray fluorescent, microprobe, and ICP studies were conducted in the Geokhy RAS.

In the work contemporary GeoRock and PetDB databases were used. The dataset on the Cape Verde rocks from the databases was compiled of 1100 individual analyzes. Thorough work according to the databases and this study individual analysis was performed to select the primary magmas samples that are suitable for comparison. Sampling frame consists only of volcanic rocks with available chemical analyzes for all major and rare (including rare-earth) elements.
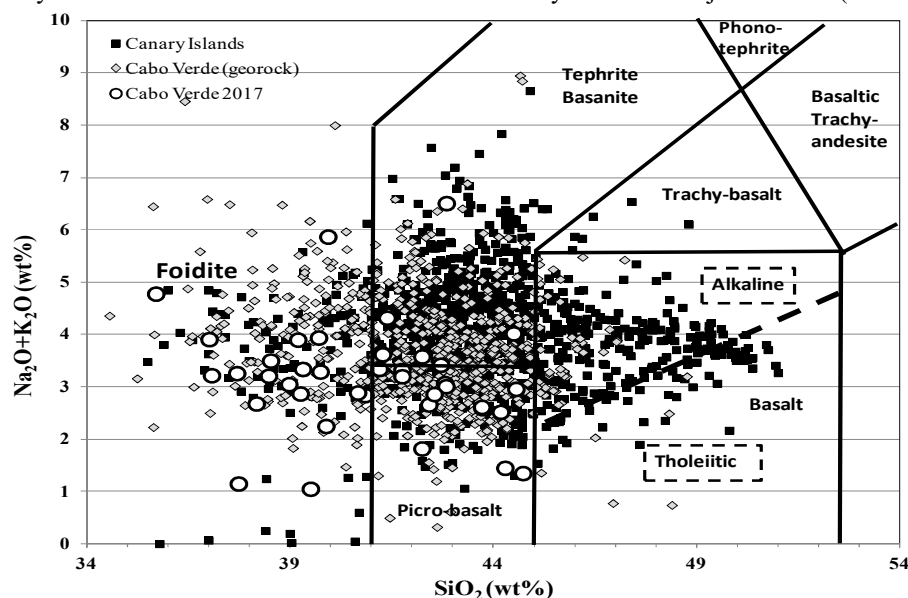
Fig. 1. Typification of primary lavas of the Cape Verde Islands.

In our study, we have focused on primitive high-magnesian magmas produced by partial melting of the mantle, which have not undergone profound differentiation and have not been affected by secondary processes.

Primary melts are characterized by high magnesian numbers, significant nickel content, and they are in equilibrium with mantle olivine (Green, Ringwood, 1967). Systematization of the data revealed the range for high-magnesia rock compositions of the Cape-Verde and Canary Islands within Mg # from 44 to 78 interval (roughly corresponding to a MgO content in the range of 6.8 to 24% by weight). Melts with increased magnesia (more than 24 wt.% MgO) were not used in this work, due to their likely origin of heterogeneous olivine-melt systems resulting in olivine cumulates, imprinting the fact that the melts of increased alkalinity have the very wide olivine crystallization field, as it was demonstrated in the experimental works of Green & Ringwood (Green, Ringwood , 1967).

The systematic of primary melts of the Cape Verde Islands was carried out using TAS diagram. For the petrochemical classification, compositions from the primary magma sample were plotted on the diagram with the sum of alkali-silica (Fig. 1), first proposed by Le Bas and Streckeisen (LeBas, Streckeisen 1991).

The compositions of alkaline magmas of the Cape Verde Islands fall into four fields: foidites, picrobasalts - picrites, tephrites - basanites and basalts (Fig. 1). Basaltic field, in turn, we subdivide into two zones - the field of subalkaline basalts and basalts of normal alkalinity (tholeiite). This division was proposed by McDonald (McDonald, 1974), the section line is known as the McDonald-Katsura line. Thus, the primary melts of the Cape Verde form five petrochemical types:

1. Foidites (27%) are low-silica (below 41 wt% SiO$_2$) rocks, usually with a high content of alkalis and normative nepheline (up to 15%). Among this group there are rocks with normative larnite and modal melelite. For most volcanics the content of alkali is higher than 4%. The group is characterized by the elevated MgO content and the presence of feldspathoids.

2. Picrobasalts (ankaramites) (28%) - along with a high content of MgO are characterized by low values of normative nepheline (about 5%).

3. Bazanite-tephrites (39%) - the most representative group; differs from the previous two in terms of the level of content of alkalis - about 6-8%. Along with a high content of MgO high concentrations of normative nepheline are characteristic. Modal nepheline or other feldspathoids are often present. In this group the contents of alkalis and magnesium oxide vary greatly with a relatively narrow range of SiO_2 contents (41-45% by weight).

4. Alkaline basalts (5%) contain normative nepheline. The group is characterized by a fairly weak dispersion in respect of petrogenic elements.

5. Basalts of normal alkalinity - tholeiites (1%). These rocks have tholeiitic composition, they are quartz-normative or with exceptionally low content of normative nepheline. However, these rocks cannot be attributed to the typical tholeiites (MORB) of the ocean floor according to Hofmann (Hofmann, 2003), because their geochemical and isotopic characteristics are similar to alkaline basalts. It can be concluded that basanitic-tephritic magma types prevail among the rocks of the Cape Verde Islands, amounting to 39%. The subsequent Cape Verde rocks types are foidite and picrite, 27% and 28%, respectively. Basalts constitute the very small group (total 6%), in which alkaline basalts have a significantly higher prevalence (5% versus 1% of tholeiites). Thus, the alkaline magmatism of the Cape Verde Islands is mainly constituted by basanits, while the foidite and picritic rock types play a second role, being represented in equal parts. The basalts obviously have a subordinate character (Fig. 1).

The distribution of magmatic rock types in the Atlantic Ocean islands (OIB) is an interesting and contemporary issue. Earlier was shown (Kogarko et al., 2002) that the primary high alkaline associations of the foidite and basanitic types compose more than 40% of the total number of primary magmas in the OIB, the most common rocks are tholeiites, amounting to 47%. Then follow the basanites (23%) and alkaline basalts (18%), foidites and picrits have the lowest prevalence (8% and 4%, respectively).
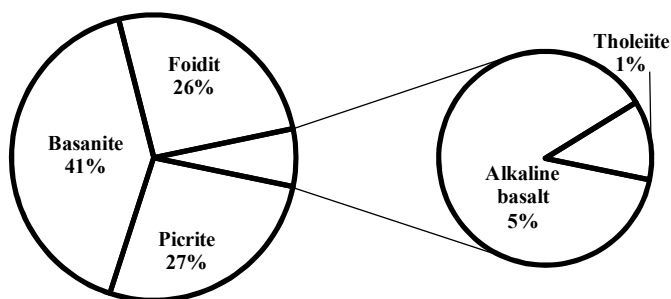
Fig.2 Percentage of different types of melts of the Cape Verde Islands

In general the Cape Verde magmatism is more alkaline in compare to the other Atlantic OIB. It can be concluded that the Cape Verde alkaline magmatism has a large depth origin combined with the high pressures of volatile components in the primary melts. Such conditions are typical for the alkaline magmatism parental to the carbonatite manifestations, which are rare on the Islands of the Atlantic.

References:
Green DH, Ringwood AE (1967) The genesis of basaltic magmas. Contrib. Mineral. Petrol 15:103-190.
Hofmann AW (2003) Sampling mantle heterogeneity through oceanic basalts: isotopes and trace elements. Treatise on Geochemistry. 2:61–101.
Le Bas MJ & Streckeisen AL (1991) The IUGS systematics of igneous rocks. J. Geol. Soc. London. 148: 825-833.
MacDonald R (1974) Nomenclature and petrochemistry of the peralkaline oversaturated extrusive rocks. Bulletin Volcanologique. 38:498-516.
Classification of igneous rocks and the glossary of terms. Recommendations of the subcommission on the taxonomy of igneous rocks of the International Union of Geological Sciences. (1997) Nedra, Moscow, 248 p.
Kogarko LN, Asavin AM, Ryakhovsky VI (2002) Typification of primary melts and petrochemical zoning of intraplate alkaline magmatism of the Atlantic // Reports of the Academy of Sciences. 385(1):1-4.

QUANTITATIVE MICROANALYSIS WITH ELECTRON PROBE SXFIVE

Moret M.P.[1], Fedik I.[2], Robbes A.S.[1], Henderson C[1], Zamyatin D.A.[3], Shilobreeva S. N.[4], Senin V. G.[4]
[1]CAMECA, Gennevilliers, Paris, France
[2]AMETEK, Moscow, Russia
[3] Zavaritsky Institute of Geology and Geochemistry, UB RAS, Yekaterinburg, Russia
[4]Vernadsky Institute of Geochemistry and Analytical Chemistry of Russian Academy of Sciences, Moscow, Russia

CAMECA, leader in scientific instruments, has been manufacturing Electron Microprobe (EPMA) since 1958 with the MS85, and has been followed by the MS46, Camebax, SX50, SX100 and fifth-generation SXFive instruments (Fig. 1). Furthermore, in recent years, the technique has not only maintained its relevance, but has expanded into new areas where detection limits and spatial resolution have been brought to new extremes with the development of the Schottky emitter and its implementation as electron source in the field of electron. No longer exclusively a research laboratory technique, EPMA instruments may now be found running as fully-automated tools in the manufacturing environment.
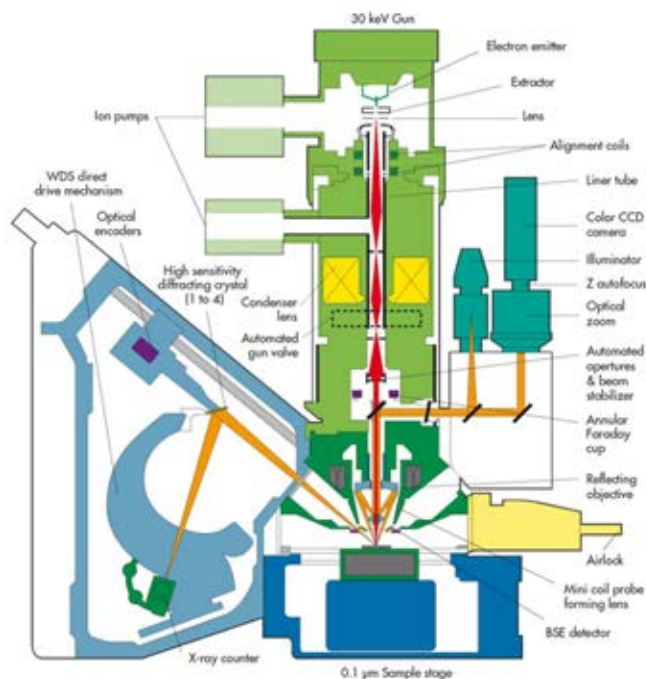
Fig.1 Synoptic of the SXFive CAMECA Electron MicroProbe.

Technical implementation of the method

The basics of the EPMA will be reviewed. The different types of detectors used to analyze samples and perform quantitative analysis such as wavelength dispersive spectrometers (WDS) or Energy dispersive spectrometers (EDS) will be compared (Fig. 2). Spectral resolution of WDS spectrometer is 20eV at the line Mn Ka whereas EDS spectrometer has resolution of 129eV.
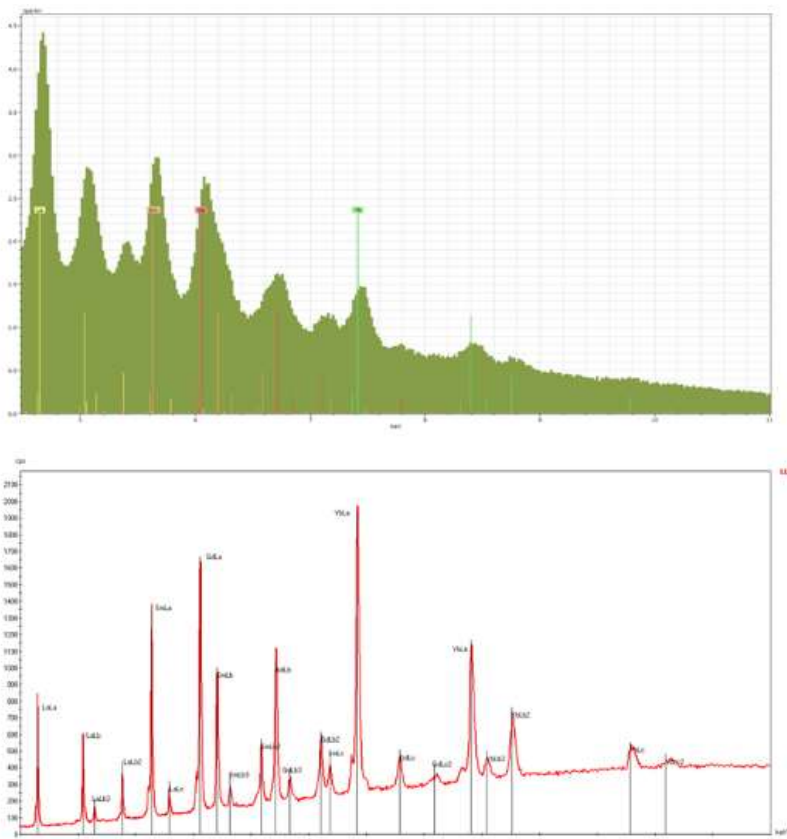
Fig. 2 A Wavelength Dispersive Spectrum of rare earth elements (REE) showing the need of energy resolution to measure high peak density sample. The sample is a Glass containing 0.5 wt% of all REE.

In electron microprobe column, different Tungsten, LaB6 and field-emission sources can be used with different technical features. With the development of the Schottky emitter and its implementation as electron source in Electron Microprobe, small features are commonly analyzed down to sub-micrometer scale; tungsten source allows to analyze grains sized several micron. The challenges and usage optimization of such sources will be reviewed. The use of low-energy X-ray lines for quantitative analysis presenting new analytical challenges will also be reviewed briefly. Design of

the column allows to achieve high stability of current of +/- 0.5% in an hour (Field emission source and W). Thanks to its precision, its reproducibility and its stability, Electron Microprobe is a well suited technique for accurately analyzing nearly all chemical elements at concentration levels down to few 10's ppm with a spatial resolution of about 1 μm, which is relevant to microstructures in a wide variety of materials and mineral specimens.

Applications of the technique

Typical EPMA SXFive outputs and results will be shown from various domains such as geology, metallurgy and materials science. Quantification of various elements in different matrics will be shown: light elements in metals or minerals, gechronology, ceramics interface, as well as thin layer analysis. CAMECA is also manufacturing shielded EPMA to be used in hot cells for radioactive samples, examples will be shown on measurements of fuel cells and metallurgical samples. In particular, experience of use EPMA CAMECA SX100 in Zavaritsky Institute of Geology and Geochemistry UB of RAS (Analytical Center "Geoanalitik", Yekaterinburg) for solution of nontrivial tasks in Earth Science will be presented.

Chemical composition of meteorites

The stony-iron meteorite has been investigated with SXFive instrument. The specimen has been observed at 15keV – 40nA enabling to get information about the minerals organization.

Trace elements in quartz and corundum

Concentration of trace elements define color characteristics of minerals. Measurement of trace elements Ti, Al in quartz, V, Cr, Ga in corundum with low detection limits (down to 10 ppm) will be shown.

Chemical dating of U-Th-minerals

Chemical U-Th-total Pb dating of concentrator minerals for U, Th (monozite, zircon, uraninite, etc.) is the complicated but vital task which can be solved with EPMA. This task is complicated by determination of the element composition under conditions of many interfering characteristic lines (up to 10 and more).
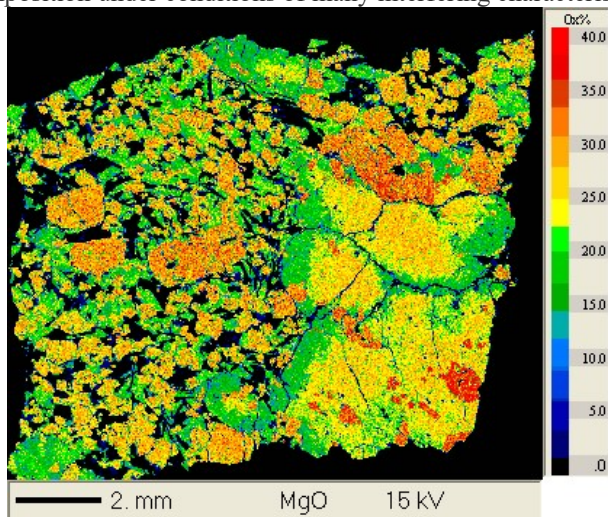
Fig. 3. Typical output of the SXFive: Elemental Mapping. Here the Mg distribution in a 2 mm wide area has been measured in a moon meteorite.

Carbon

Carbon is one of the main gas-forming elements which widely participates in redox reactions proceeding in Earth's interior. It is found in samples from Earth shells in various chemical forms, such as molecular forms (CO_2, CO, etc.), in the form of CO_3 radical in carbonates and other minerals, free phases (graphite, diamond), carbides and in atomic state.

Basic difficulty in studying of the solid samples containing carbon is the limited amount of the studied substance (50-100 mg) with its complex phase and chemical composition and small phase sizes (several micrometers). Concentration of carbon in these phases is around 10^{-3} to 10^{-4} wt.%. Therefore many local methods appear to be unsuitable for carbon content determination due to insufficient lateral resolution, sensitivity, and other factors. Therefore the problem of determination of low carbon contents is essential in geochemical researches with the direct use of the electron probe microanalysis.

A complex method called "autoradiography-electron probe microanalysis" has been used for carbon content determination in natural and experimental samples. Principle of the method comprises EPMA imaging of radioautograms acquired by contacting a radioisotope containing sample with nuclear-track emulsion (Fig. 4). Activation of samples is performed either by introduction of a radioisotope (Senin, et al., 1991; Senin, et al., 1994) or with use of activation methods (Shilobreeva, et al. 1994). Given that the content of radioisotopes in the sample is proportional to amount of silver on the radioautogram, EPMA is used to detect silver. The intensity of characteristic X-ray Ag Lα line serves as an analytical signal. Detection limit for carbon in silicate samples using this method is as low as 10^{-5} wt.%.

A non-destructive approach using the ^{12}C (d,n)^{13}N nuclear reaction as well as electron microprobe analysis was also undertaken to demonstrate the distribution of carbon in natural glass from alkali basalts of the Shavaryn Tsaram eruptive center, in Mongolia. The occurrence of calcium carbonate phases in glass originating from deep in the mantle is reported. The carbon content of the natural basaltic glass matrix in which the carbonate phases were found was 0.16 wt.%.

a)   b)
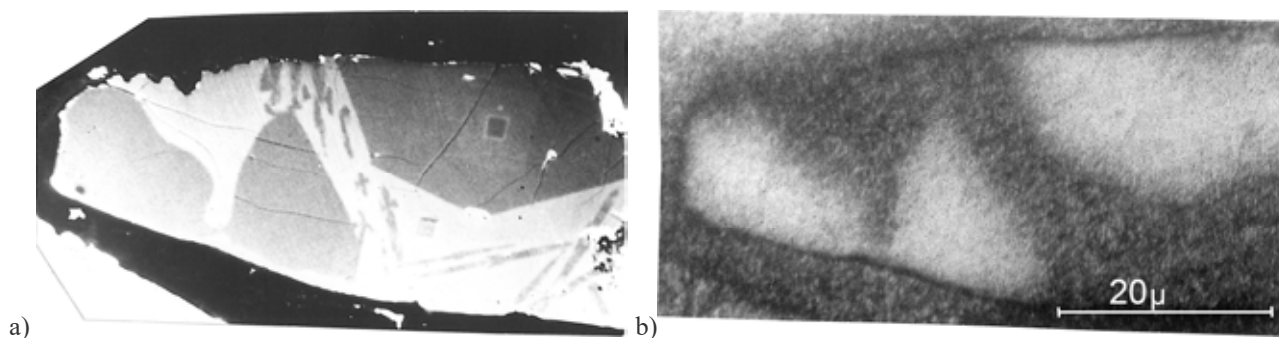
Fig.4 Electron image of the sample surface containing carbon in glassy phases and forsterite crystal (a). Surface of the same sample covered with nuclear-track emulsion which has been developed (b)

References:

Senin V.G., Shilobreeva S.N. (1994) Industrial laboratory, N8, P17-21

Senin V.G., Shilobreeva S.N., Kadik A.A., Pavlova L.F. (1991) Nukleonika, vol1-12, p.45-58

Shilobreeva S.N.; Minaev V.M.; Senin V.G. (1994) JOURNAL OF TRACE AND MICROPROBE TECHNIQUES, V 17, N 4, P 433-443

VIRUNGA LEUCITE BASANITES: MANTLE METASOMATISM OR CRUSTAL CONTAMINATION?

Muravyeva N.S.[1], Belytsky B.V.[2], Senin V.G.[1], Ivanov A.V.[3]

[1]Vernadsky Institute of Geochemistry and Analytical Chemistry of the Russian Academy of Sciences, Moscow, Russia,
natash@geokhi.ru, nmur@mail.ru
[2]Federal State Budgetary Enterprise 'A. P. Karpinsky Russian Geological Research Institute', Saint-Petersburg, Russia
[3]Institute of the Earth`s Crust of the Siberian Branch of the Russian Academy of Sciences, Irkutsk, Russia

The Western Branch of the East African Rift is a region with classic occurrences of ultra-potassic magmatism (Bailey, 1974; Eby et al., 2003; Foley et al., 1987; Rosenthal et al., 2009). The trace element geochemistry of these ultrapotassic rocks indicates derivation from an enriched mantle source (e.g. Eby et al., 2003).

Volcanism in the Western Rift is limited to four main regions in addition to isolated small areas where volcanic intrusions are present; from north to south these are Toro-Ankole, Virunga, South Kivu and Rungwe. In general, the volcanics form spatially isolated rock units that occur in conjunction with the rift grabens. Western Rift volcanism in the Virunga Province approximately 12 million years ago and is still active today.

The regional scale geodynamic setting is discussed in more detail by Ebinger and Furman (2002). Nyiragongo and nearby Nyamuragira mark the western edge of the Virunga volcanic field, with Virunga volcanoes erupting extremely fluid, low-silica, high-alkaline lavas. Several fault systems meet at Nyiragongo: the main N–S fault which was active in the 1977 and 2002 eruptions, a NW–SE trending system linking Nyiragongo to Nyamuragira, a NE–SW trending fault system including the Rushayo chain of scoria cones (formed in 1948), and possibly a further fault approximately parallel butwest of the Rushayo chain.

We focused on an investigation of leucite basanites and kamafugites from Virunga provinces in the northern part of the Western Branch of the East African Rift. The objects of this study were the volcanic rocks from volcanoes Visoke and Mahavura. Samples of the ugandite and its probable differentiates (melaleucitite and leucitite) from Visoke volcano in the Virunga are included in this study.

Visoke is a 3711-m-high extinct stratovolcano, which contains a 450-m-wide summit crater lake. The age of Visoke volcanism is unknown, but whole rock K–Ar ages for the nearby Karisimbi volcano range from 30,000 to 120,000 years (De Mulder, 1985; Rogers et al., 1992, 1998). Visoke together with Nyiragongo and Nyamuragira is the only volcano that has been active historically in the area.

Mahavura is an extinct volcano in the Virunga Mountains on the border between Rwanda and Uganda. At 4,127 metres Muhabura is the third highest of the eight major mountains of the mountain range, which is a part of the Albertine Rift, the western branch of the East African Rift. The goals of the present work are to elucidate the mantle source composition on the basis of Nd - Sr - Pb whole-rock systematic and to evaluate the magma crystallization conditions on the basis of determining the phenocrysts composition.

The leucite basanites are a specific group of rock that is transitional between basalts and kamafugites, leucitites, nephelenites, i.e. without-feldspar rocks. They are not so widely distributed in the World, but are found a lot in the Western Branch of the East African Rift. Leucite basanites by chemical composition are similar to basalts (45 – 48 % SiO_2) and

by normative composition they contain > 10% olivine. Phenocrysts contain olivine, clinopyroxene, plagioclase, ore minerals. Leucite presents either as phenocryst or as microlith in groundmass.

The chemical (major and trace elements) and isotope composition of leucite basanites was determined. It revealed that all lava are not primitive (Mg# - from 0.50 up to 0.59), enriched by large ion trace elements (Fig.1, 2).
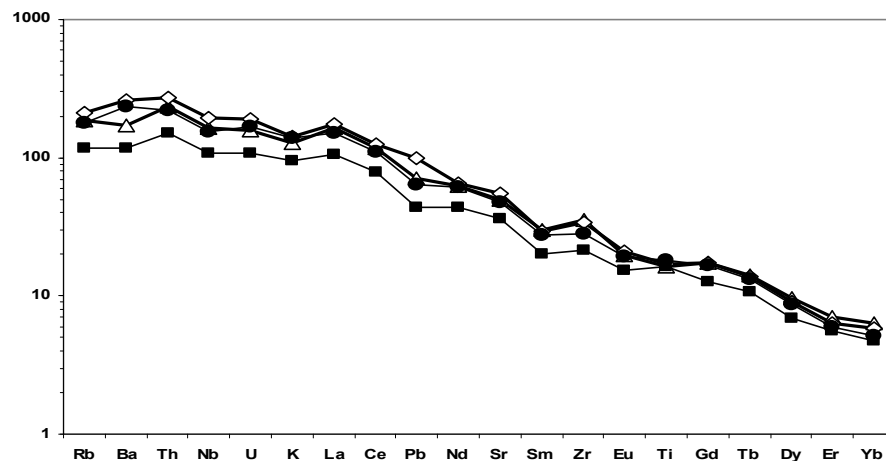
Fig.1. Mantle-normalized (Sun & McDonough, 1995) abundance patterns for selected lavas from the eastern Virunga province, showing the generally smooth and convex-upwards profiles of the leucite basanite lavas from Muhavura and Visoke.
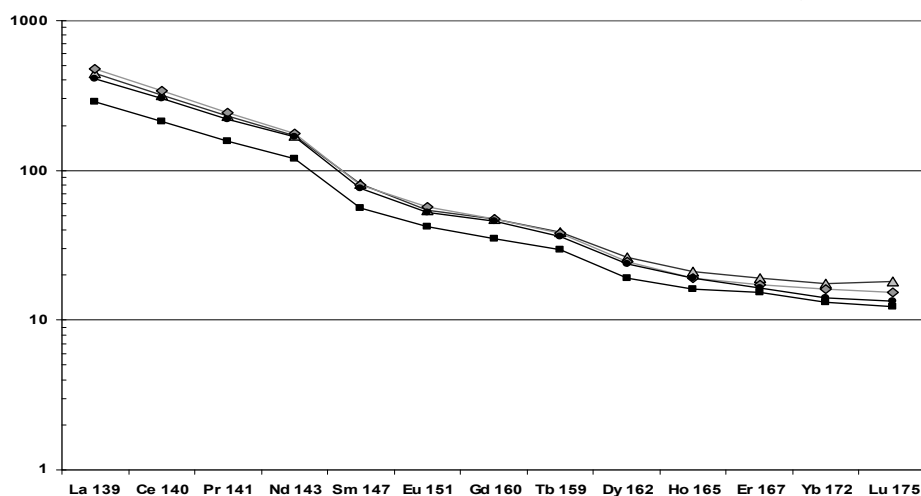
Fig. 2. Chondrite-normalized abundance patterns for leucite basanite lavas from Visoke and Mahavura volcanoes of the eastern Virunga province.

The isotope composition of Sr, Nd, and Pb leucite basanites from the Visoke and Mahavura volcanoes of the Virunga province revealed that these rocks differ from the previously studied Toro-Ankole kamafugites not only in chemical, mineral but isotope composition - they are enriched with radiogenic strontium and can not be regarded as primary-mantle rocks (Fig.3).
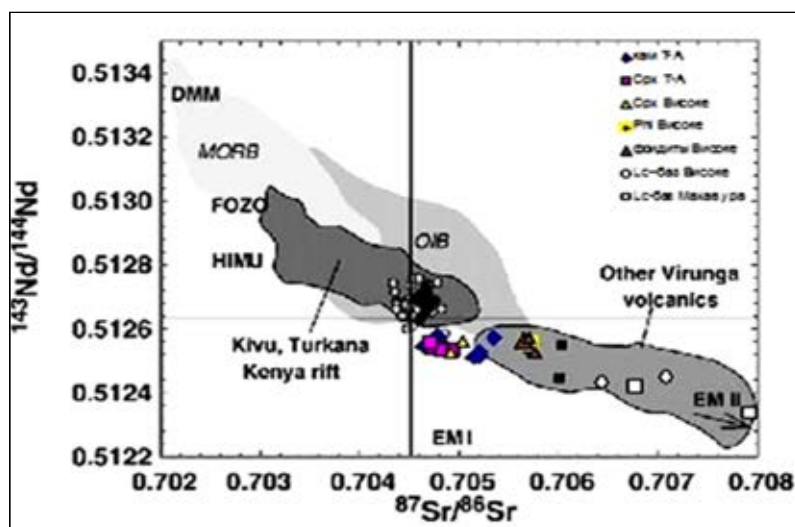
Fig. 3. The plot of correspondence $^{143}Nd/^{144}Nd$–$^{87}Sr/^{86}Sr$ where the isotopic compositions of ultrapotassic rocks East African Rift are shown. The compositions of alkaline effusive rocks from other volcanic fields of the East African rift, basalts of Mid-oceanic ridges (MORB), ocean Islands (OIB) and different model mantle sources (DMM, EM I, EM II, HIMU) are shown also.

The composition of phenocryst minerals of leucite basanites varies in some range: the olivine composition is Fo_{55} – Fo_{90} with NiO content 0.01 - 0.4 % wt.; clinopyroxenes have Mg# - from 0.65 up to 0.86 with Cr_2O_3 content 0.02 – 1.5% wt. The most of plagioclases are labrador (50 – 70% An). The ore minerals occurred are titanomagnetite and

ilmenite. The evaluation of T-fO$_2$ phenocryst crystallization based on titanomagnetite and ilmenite composition by method Sauerzarpf et al. (Sauerzarpf et al, 2008) show that it taked placed under buffer QFM.

Xenocrysts of quartz (Fig. 4) and rutile (Fig. 5) in the lava were found in Visoke leucite basanite. The presence of quartz and rutile together with phenocrysts of olivine Fo$_{88}$ indicates to the contamination of this melt by crustal material. In another sample of Visoke leucite basanite nonequilibrium megacrysts of high-magnesian olivine (Fo$_{90}$) were found, indicating to mixing of leucite-basanite magma with a portion of a more primitive melt.

One more noticeable result of our study is identification within single Visoke volcano two melts formed from different mantle sources. According to isotopic data (Muravyeva et al., 2014) Visoke ugandite and its possible derivatives (melaleucitite and nepheline leucitite) are generated from mantle source while leucite basanites enriched with radiogenic strontium and cannot be regarded as primary-mantle rocks.
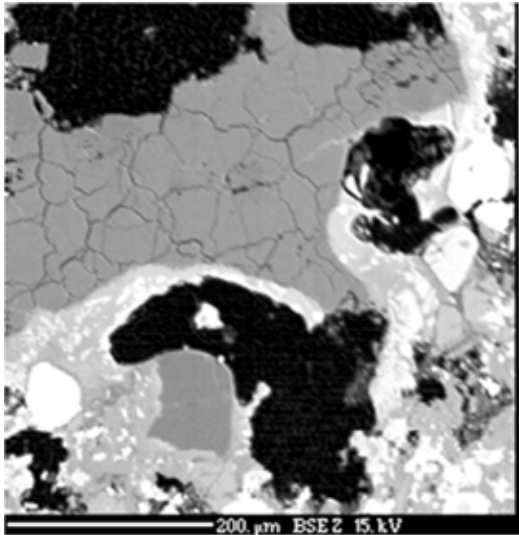
Fig. 4. The quartz xenolith with the reaction rim minerals in leucite basanite of Visoke Volcano from Eastern Virunga.
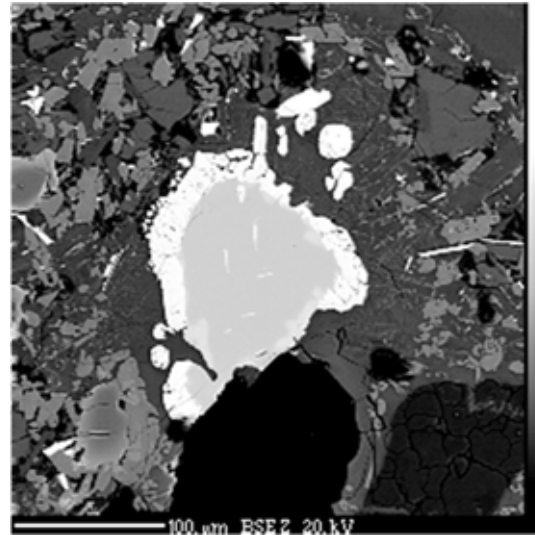
Fig. 5. The rutile xenocryst surrounded by the reaction rim of ilmenite in leucite basanite of Visoke Volcano from Eastern Virunga. Very thin parallel ilmenite neadles are visible within rutile xenocryst too.

Some features of mineral composition of Visoke leucite basanites (xenocrysts of quartz and rutile) obviously indicate melt contamination by crustal material despite on whole rock isotope composition lies on trend beenig explained by processes of mantle metasomatism.

References:

Bailey, D.K., 1974. Continental rifting and alkaline magmatism. In: Sorensen, H. (Ed.), The alkaline rock. John. Wiley and Sons, London – New York – Sidney – Toronto, pp. 148–159.

De Mulder, M., 1985. The Karisimbi Volcano, (Virunga). Musee Royale de l'Afrique Centrale, Tervuren, Belgique Annales, Serie in Octavo Sciences Geologique. p. 90.

Ebinger, C., Furman, T., 2002. Geogynamical setting of the Virunga volcanic province. Acta Vulcanologica 14 (15), 9–16.

Eby, G.N., Lloyd, F.E.,Woolley, A.R., Stoppa, F.,Weaver, S.D., 2003. Geochemistry and mantle source(s) for carbonatitic and potassic lavas, Western Branch of the East-African Rift System, SW Uganda.Geolines 15,23–27.

Foley, S.F., Venturelli, G., Green, D.H., Toscani, L., 1987. The ultrapotassic rocks: characteristics, classification, and constraints for petrogenetic models. Earth Science Review 24, 81–134.

Rogers, N.W., De Mulder, M., Hawkesworth, C.J., 1992. An enriched mantle source for potassic basanites: evidence from Karisimbi volcano, Virunga volcanic province. Rwanda Contribution to Mineralogy and Petrology 111, 543–556.

Rogers, N.W., James, D., Kelley, S.P., De Mulder, M., 1998. The generation of potassic lavas from the Eastern Virunga Province, Rwanda. Journal of Petrology 39, 1223–1247.

Rosenthal, A., Foley, S.F., Pearson, D.G., Nowell, G.M., Tappe, S., 2009. Petrogenesis of strongly alkaline primitive volcanic rocks at the propagating tip of the Western Branch of the East African Rift. Earth and Planetary Science Letters 284, 236–248.

Sauerzarpf, U., Lattard, D., Burchard M., Englemann R., 2008. The titanomagnetite-ilmenite equilibrium: new experimental data and thermooxybarometric application to the crystallization of basic to intermediate rocks. Journal of Petrology 49, 1161-1185.

PYROCHLORE U-PB-SHRIMP-DATING OF THE ILMENY-VISHNEVOGORSKY ALKALINE-CARBONATITE COMPLEX, URALS, RUSSIA

Nedosekova I.L[1], Belyatsky B.V.[2], Lepekhina E.N.[2], Antonov A.V.[2], Plyatsok L.V.[3], Sergeev S.[2]

[1]Institute of Geology and Geochemistry, Ural Branch of the Russian Academy of Sciences, Ekaterinburg, Russia, vladi49@yandex.ru
[2]Federal State Budgetary Enterprise 'A. P. Karpinsky Russian Geological Research Institute', Saint-Petersburg, Russia
[3]University Jean Moulin Lyon 3, Lyon, France

The dating of ore-deposit mineralization and ore-forming processes remains a challenge despite the successful development of analytical methods of isotope geochronology within the last years. The best mineral-geochronometer, as is well known, is zircon, but the nature of zircon, if it is present in ores, is not always definitely clear (sometimes it has allochthonous origin). Pyrochlore as an acceptor of sufficiently high U and Th can be a geochronological alternative to zircon and used to date the processes of rare-metal ore formation. The application of pyrochlore as a geochronometer has some limitations, for example, its crystalline lattice is often highly metamict (Lumpkin, Ewing, 1995), the variety of secondary mineral transformations and inconsistency of the U-Th-Pb system (Pöml et al., 2007) etc. However, local isotopic analysis (SIMS or laser ablation) of the individual phases and domains of mineral grains allows to selects uitable for dating areas of pyrochlore crystals (Wetzel et al., 2010).

Another problem for U-Pb pyrochlore dating – the share of common lead in pyrochlore could be up to tens of percent. Since there are divalent cations, including calcium and lead in the crystallographic position "A" of the pyrochlore crystal structure the all pyrochlore group minerals have a relatively high proportion of common lead (Pb_c) compared to radiogenic and, correspondingly, low isotope ratios of $^{206}Pb/^{204}Pb$. While among the most widespread dated minerals – zircon, baddeleyite, monazite, apatite, it is easier to find standards with a minimum content of common lead, for the pyrochlore it is not the case. At the same time, with accurate and precise measurement of the Pb isotopic composition, as well as true correction for the composition of common Pb (non-radiogenic), the resulting reproducibility of the obtained geochronological data can be ± 2% and ensures a satisfactory coincidence of SIMS age estimations with data of other isotope-geochronological methods (isotopic dilution and TIMS, laser ablation and ICP-MS).

Pyrochlore is the main ore mineral in the Ilmeny-Vishnevogorsky alkaline-carbonatite complex and it is present in different kind of rocks – in miaskites and syenites, especially in pegmatoid varieties, in miaskite-pegmatites, syenite-pegmatites and alkaline metasomatites (albitites, fenites, micaceous rocks etc). In the most significant quantities, pyrochlore is present in the Vishnevogorsk miaskite massif in both the early and late stages of carbonatite-formation (sövite I and sövite II, respectively). Pyrochlore-ore contents found in calcite-dolomite carbonatites (sövite III) and accompanying alkaline rare-metal metasomatites of the Buldym and Spirikha ultrabasite massifs (Levin et al., 1997; Zoloev et al., 2004; Nedosekova, 2007; Nedosekova et al., 2009; Nedosekova, Pribavkin, 2015).

More than 10 deposits and ore occurrences of pyrochlore are associated with carbonatites witnin the Ilmeny-Vishnevogorsky complex. The Vishnevogorsk ore-deposit, the first niobium deposit in Russia, which is exploited to produce industrial niobium raw materials, is associated with pyrochlore-containing carbonatites of the Vishnevogorsk miaskite massif. Within the Central alkaline zone the Potanino niobium deposit, Svetloozerskoe, Baidashevskoye, Ishkulskoe, and Uvildinskoe ore occurrences, which are also associated with carbonatites, have been explored. The Buldym, Khaldikhinsky, Spirikhinsky ultrabasite massifs, which are surrounded the miaskite intrusions, the same Nb-REE deposits associated with carbonatites and alkaline metasomatites are also established (Levin et al., 1997; Zoloev et al., 2004; Nedosekova, 2007).

We have studied the U-Th-Pb isotope system of previously chemically characterized samples (Nedosekova, Pribavkin, 2015) from the Potanino ore-deposit: from the early carbonatites (K-37-95, sövite I) and late carbonatites (K-43-62, sövite II); from the Vishnevogorsk deposit – from the late carbonatites (sample 331, sövite II) and the Buldym deposit – from dolomite-calcite carbonatites (sample 3296) and phlogopitic metasomatites (sample K2-18).

The dating of Nb-rare metal ore-deposit within the Ilmeny-Vishnevogorsky alkaline complex of the Urals (IVAC) was performed by the local U-Pb isotope analysis using SIMS SHRIMP-II, mainly, and LA-ICP-MS (high U-Th variaties) of individual pyrochlore crystals. The IVAC pyrochlore collection study, U-Th-Pb isotope ratio and element content measurements and the standard calibration were made at the Center for Isotope Research of VSEGEI (St. Petersburg). Since the crystallochemistry of pyrochlore differs significantly from zircon at the first stage, the optimal regime and the sequence of ion current recording with allowance for possible isobaric overlap have been experimentally chosen, and apropriate scheme of the measurement protocol and U-Pb age calculation have been developed. The pyrochlore local dating was preceded by a detail chemical composition study of the crystals at the micro level.

Pyrochlore-331 represented by octahedral crystals and light brown, yellow- and reddish-brown grains from the sample of the Vishnevogorsky massif sövite II was used as internal laboratory standard. It was accurately studied by various isotope methods – isotope dilution and TIMS, laser ablationand ICP-MS, SIMS SHRIMP-II. This pyrochlore is characterized by a relative space geochemical homogeneity and according to (Atencio et al., 2010) is classified as Sr-REE-containing (1.5-4.5 wt% SrO and 1-2.5 wt% LREE) oxycalciopyrochlore. Our systematic U-Pb dating of a large number of pyrochlore-331 grains within 2 years by two local methods (SHRIMP-II and LA-ICP-MS) has resulted in less than 0.5-1.0 m.y. differences and the U content varies within ± 30%. The correction of the measured Pb isotope composition of the internal pyrochlore standard for the isotope composition of the nonradiogenic component was carried out according to the Pb composition of syngenetic calcite (the Pb acceptor mineral with a high Pb/U ratio) and also according to the corresponding parameters of the Earth Pb evolutionary curve (Stacey, Kramers, 1975) at 230 Ma:

$^{207}Pb/^{206}Pb = 0.851$, $^{208}Pb/^{206}Pb = 2.082$ and $^{206}Pb/^{204}Pb = 18.35$. The measured $^{206}Pb/^{238}U$ ratios of "unknown" pyrochlore and internal pyrochlore standard normalized to a value of 0.0363, which corresponds to an age of 230 Ma established by independent methods for this standard (pyrochlore-331). The estimation of ^{238}U concentration in the analyzed pyrochlore grains was made with respect to the averaged U content (~ 1500 ppm) of the pyrochlore-331 (which is U-inhomogeneous).

The U-Pb isotope system of the studied pyrochlores from samples 3296 and 43-62 is practically undisturbed and the age within the error limits is concordant. The relatively low error of single measurements of isotope ratios in terms of age leads to an error of concordant estimates at a level of 5-6 m. yrs. The results of pyrochlore U-Th-Pb isotope analysis are presented in table 1.

Table 1. Chemical and isotope (U-Th-Pb isotope) characteristics of pyrochlores from Nb-deposits of the Ilmeny-Vishnevogorsky complex (Urals)

Sample	Host rocks	Pyrochlore chemical type [Atencio, 2010]	Main composition of pyrochlore (wt.%)	Pyrochlore U-Th-Pb system	U-Pb age Ma
Central alkaline zone, Potanino deposit					
K-37-95	sövite I	U-(Ta)- containing oxycalciopyrochlore	Na_2O – 4.6 CaO – 9.1 Nb_2O_5 – 42.5 (Pb+Th+U) – 20	[U]: 130000-240000 Th/U: 0.3-0.9	378.3±4.9 n = 28
K-43-62	sövite II	Ta-containing fluorocalciopyrochlore	Na_2O – 8.4 CaO – 14.6 Nb_2O_5 – 60.7 (Pb+Th+U) – 2	[U]: 300-2800 Th/U: 8.6-92.0 $^{206}Pb_c$: 25-68 %	216 ± 5.0 n = 15
Vishnevogorsk miaskite massif, Vishnevogorsk deposit					
331	sövite II	Sr-containing oxycalciopyrochlore	Na_2O – 8.5 CaO – 13.1 Nb_2O_5 – 65.1 (Pb+Th+U) – 1	[U]: 620-4700 Th/U: 0.7-5.2 $^{206}Pb_c$: 9-39 %	230 ± 1.5 n = 40
Buldym ultrabasite massif, Buldym deposit					
K2-18	phlogopitic metasomatites	high-U oxycalciopyrochlore	Na_2O – 6.0 CaO – 12.2 Nb_2O_5 – 45.0 (Pb+Th+U) – 21	[U]: 110000-190000 Th/U: 0.3-0.4	332.1±9.1 n = 15
3296	sövite III	oxycalciopyrochlore	Na_2O – 8.5 CaO – 13.1 Nb_2O_5 – 65.1 (Pb+Th+U) – 1	[U]: 640-1030 Th/U: 6.5-11.3 $^{206}Pb_c$: 44-56 %	236 ± 6.0 n = 15

Note. The U-Pb dating of pyrochlore was carried out using by SIMS SHRIMP-II and LA-ICP-MS (high U-Th varieties) of individual pyrochlore crystals. [U] – the uranium content (in ppm) calculated with respect to the uranium concentration (1500 ppm) of the laboratory standard pyrochlore-331, $^{206}Pb_c$ – relative proportion of unradiogenic lead, n – a number of individual analyses of pyrochlore grains

The early pyrochlore generation from the early carbonatites (sövites I) of the Potanino deposit (sample K-37-95, U-(Ta)-oxycalciopyrochlore) and from the phlogopite metasomatites of the Buldym deposit (sample K2-18, U-oxycalciopyrochlore) are characterized by a partially disturbed U-Pb system and have an age of 378.3 ± 4.9 and 332.1 ± 9.1 Ma, respectively. The observed break-up of the closed isotope system of these pyrochlores reflects not only the increased degree of metamictization of the mineral crystalline structure due to the high U and Th content, but also the influence of late processes associated with the post-collisional ore-metasomatic stage of the complex evolution at 220-250 m.y. ago.

The pyrochlore from the dolomite-calcite carbonatites of the Buldym deposit (sample 3296, oxycalciopyrochlore) has an age of 235 ± 6 Ma comparable with the age of pyrochlore 331 from the late carbonatites (sövites II) of the Vishnevogorsk deposit (230 ± 1.5 Ma), which was dated earlier and was used as an intralaboratory standard. The youngest among the studied pyrochlores are the pyrochlores from the late carbonatites (sövite II) of the Potanino ore-deposit (K-43-62, Ta-containing fluorocalciopyrochlore) with the age 216 ± 5 Ma.

Thus, the U-Pb system of the studied pyrochlore samples indicates a multi-stage formation of the Nb-mineralization within the Ilmeny-Vishnevogorsky complex. The earliest stage of ore formation (380 Ma) is fixed by isotope U-Pb systems of U-(Ta)-pyrochlores from Potanino ore-deposit and, possibly, is associated with initial crystallization of alkaline-carbonatite magmatic system (Krasnobaev et al., 2010; 2014; Nedosekova et al, 2010; 2014; Ivanov et al, 2010; Nedosekova, Belyatsky, 2012). The next stages of the ore formation are widely manifested in Buldym (235 ± 6 Ma) and in Vishnevogorsk (230 ± 1.5 Ma) ore-deposits. The pyrochlores from the Potanino-deposit late carbonatites are dated by the age 217.2 ± 1.9 Ma and are supposedly related to the remobilization of alkaline-carbonatite and rare-metal substances at the metamorphogenic stage of the IVAC transformation. It is very probable that the ore mineralization (pyrochlore formation from the HFSE-enriched fluid) completed the metamorphic rock transformations,

which are also recorded by late newly formed zircons from miaskites and carbonatites at 250 Ma (Kramm et al, 1993; Krasnobaev et al., 2010; Nedosekova et al., 2014).

Source of financial support (Projects № 17–05–00154 and № 15-11-5-17).

References:

Atencio D, Andrade MB, Christy AG (2010) The pyrochlore supergroup of minerals: nomenclature. Canad Mineral 48:673-698

Ivanov KS, Erokhin YV, Pogromskaya OE, Valizer PM (2010) Genesis of carbonatites of fold belts (exemplified by the Urals) Dokl Earth Sci 435 № 1:1423-1426

Kramm U, Chernyshev IV, Grauert S. (1993) Zircon typology and U-Pb systematics: a Case Study of zircons from nefeline syenite of the Il'meny Mountains, Ural. Petrology 1 № 5:474-485

Krasnobaev AA, Rusin AI, Busharina SV, Valizer PM (2010) Zirconology of calcite carbonatite of the Vishnevogorsk massif, Southern Urals. Dokl Earth Scie 431 № 1:390-393

Krasnobaev AA, Valizer PM, Nemov AB, Busharina SV, Anfilogov VN (2014) Zirconology of pegmatites of the Ilmeny Mountains. Dokl Earth Scie 457 № 2: 960-964

Levin VY, Ronenson BM, Samkov VS, Levina IA, Sergeev NS, Kiselev AP (1997) Shchelochno-karbonatitovyye kompleksy Urala [Alkaline-carbonatite complexes of the Urals]. Ekaterinburg Uralgeolkom (in Russian)

Lumpkin GR, Ewing RC (1995) Geochemical alteration of pyrochlore group minerals: pyrochlore subgroup. Am Miner 80:7320-743

Nedosekova IL (2007) New data on carbonatites of the Ilmensky-Vishnevogorsky alkaline complex, the Southern Urals, Russia. Geol Ore Deposits 49 № 2: 29-146

Nedosekova IL, Belousova EA, Belyatsky BV (2014) U-Pb vozrast i Lu-Hf izotopnyye sistemy tsirkonov Ilmeno-Vishnevogorskogo shchelochno-karbonatitovgo kompleksa, Yuzhnyy Ural [U-Pb age and Lu-Hf isotope systems of zircons of the Ilmeno-Vishnevogorsky alkaline-carbonatite complex, Southern Urals] // Lithosphere 5:19-32 (in Russian).

Nedosekova IL, Belousova EA, Sharygin VV (2010) Sources of matter for the Ilmeno-Vishnevogorsky alkaline complex: evidence from Lu-Hf isotopic data for zircon. Dokl Earth Scie. 435 № 1:1487-1491

Nedosekova IL, Belyatsky BV (2012) Age and substance sources of the Ilmeno-Vishnevogorsky alkaline (Southern Urals) complex: Rb-Sr, Sm-Nd, U-Pb, and Lu-Hf isotopic data. Dokl Earth Scie 446 № 1:1071-1076

Nedosekova IL, Pribavkin SV (2015) Rudnaya niobiyevaya mineralizatsiya redkometalnykh mestorozhdeniy i rudoproyavleniy Ilmeno-Vishnevogorskogo shchelochno-karbonatitovogo kompleksa (Yuzhnyy Ural) [Ore-bearing niobium mineralization of rare-metal deposits and ore occurrences of the Ilmeno-Vishnevogorsk alkaline-carbonatite complex (Southern Urals). Yearbook-2014 Ekaterinburg IGG UB RAS 162:175-183 (in Russian)

Nedosekova IL, Vladykin NV, Pribavkin SV, Bayanova TB (2009) Ilmeno-Vishnevogorskii miaskite-carbonatite complex: origin, ore content, sources of matter (Ural, Russia). Geol Ore Deposits 51 № 2:157-181

Pöml P, Menneken M, Stephan T (2007) Mechanism of hydrothermal alteration of natural self-irradiated and synthetic crystalline titanate-based pyrochlore. Geochim Cosmochim Acta 71:3311-3322

Stacey JS, Kramers JD (1975) Approximation of terrestrial lead isotope evolution by a two-stage model. Earth Planet Sci Letters 26:207–221

Wetzel F, Schmitt AK, Kronz A, Worner G (2010) In situ ^{238}U-^{230}Th disequilibrium dating of pyrochlore at sub-millennial precision. Amer Mineralogist 95:1353–1356

Zoloyev KK, Levin VY, Mormil SI, Shardakova GY (2004) Minerageniya i mestorozhdeniya redkikh metallov. molibdena. volframa Urala [Minerageny and deposits of rare metals, molybdenum, tungsten in the Urals] Ekaterinburg (in Russian)

FEATURES OF MINERAL COMPOSITION OF APATITE-MAGNETITE ROCKS, MUSHUGAI-KHUDUK COMPLEX (MONGOLIA)

Nikolenko A.M.[1], *Doroshkevich A.G.*[1,2]

[1]Institute of Geology and Mineralogy, Siberian Branch of the Russian Academy of Sciences, Novosibirsk, Russia,
nikolenkoam@igm.nsc.ru
[2]Geological Institute, Siberian Branch of the Russian Academy of Sciences, Ulan-Ude, Russia

Mushugai-Khuduk is an alkaline complex of volcanic, plutonic and pyroclastic rocks, varying in composition from melanefelinites to trachyriodacites in the volcanic facies and from shonkinites to quartz syenites in the plutonic facies (Samoilov and Kovalenko, 1983; Vladykin, 2013). Also carbonatites, magnetite-apatite, apatite and fluorite rocks occur in the structure of this massif. The age of the rocks of the massif is determined by the K-Ar method and is 150-120 Ma (Samoilov and Kovalenko, 1983). The host rocks are represented by Paleozoic limestones and basic volcanics.

The present work includes the results of a detailed investigation of the composition of minerals in the apatite and apatite-magnetite rocks of the complex, and also the products of hydrothermal alteration of these rocks.

Apatite and apatite-magnetite rocks exposed in the eastern part of the Mushugai-Khuduk complex (Apatite Hill) were chosen for investigation.

The rocks are exposed in two stocks 30 * 70 m and 10 * 30 m in size. Monomineral giant-grained magnetite rocks are in the central part of the stocks, the rocks gradually change to magnetite-apatite (apatite appears in the interstices),

then apatite - phlogopite and apatite rocks. Apatite and phlogopite form grains up to 10-20 cm in size. Contacts with the host rocks are not exposed. Near the contact, apatite becomes fine-grained and shows trachytoid texture.

A zone of hydrothermally altered apatite and apatite-magnetite rocks is in the southern part of the stock. The rocks get a mealy appearance of whitish and greenish shades. The main minerals of the hydrothermal association are phosphosiderite, monazite-(Ce), goethite, hematite, celestite, quartz, fluellite, fluorite, barite, gypsum, pyrite.

Below we consider the characteristic features of the composition of minerals from apatite and apatite-magnetite rocks.

Magnetite contains TiO_2 from 0.4 to 4 wt.%, MnO up to 2.9 wt.%, Al_2O_3 up to 2.5 wt.%. Magnetite contains ilmenite lamellae oriented in the [111] direction of magnetite crystals. An essential feature of the composition of ilmenite is the presence of MnO (0.4-4 wt.%), V_2O_3 (up to 0.8 wt.%), and Al_2O_3 (up to 1.5 wt.%). Rarely, rutile (anatase?) replaces ilmenite; the mineral contains Nb_2O_3 (up to 1 wt.%), Al_2O_3 (up to 1.7 wt%). Sometimes magnetite is hematitized along the edge of the grains and along the cracks. Zinc admixture (ZnO up to 1 wt.%) was detected in hematite.

Magnetite is almost completely replaced by goethite in the areas of the most intensive hydrothermal processing. Goethite contains P_2O_5 (up to 4 wt.%), SiO_2 (up to 3 wt.%) and CaO (up to 1 wt. %).

Phlogopite has higher amounts of TiO_2 (up to 3.3 wt.%) and F (up to 5.1%). The feature of the mineral is the presence of Na_2O (up to 0.86 wt.%). The average composition of phlogopite corresponds to the formula: $(K_{1.69}Na_{0.17})$ $(Mg_{4.42}Fe_{1.104}Ti_{0.316}Mn_{0.028})$ $(Si_{5.92}Al_{2.03})$ $O_{20}(F_{1.945}OH_{2.055})$.

Apatite refers to fluorapatite (F from 3.3 to 4.1 wt.%). A special feature of the mineral is the presence in the composition of SiO_2 (up to 2.2 wt.%), SO_3 (up to 1.9 wt.%), SrO (up to 1.7 wt.%), Na_2O (up to 0.6 wt.%). The content of REE in apatite varies from 2.0 to 4.8 wt.%. The average ratios Ce/La, Ce/Nd and La/Nd are 2.3, 2.7 and 1.3, respectively. The mineral in the BSE has an internal spot-zonal structure with variations in the composition of admixture components, where the dark zones contain, for example, a lower amount of SO_3 (0.9 wt% vs 1.9 wt%) and Ce_2O_3 (1.3 wt% % vs. 2.1 wt.%). According to G.S. Ripp et al. (2005), such variations are associated with the recrystallization of apatite and its refining with a decrease in REE and silica, and an increase in phosphorus and calcium.

Due to hydrothermal alterations, higher REE and silica content is reported for apatite in comparison with the mineral from unaltered rocks. The content of SiO_2 is increased up to 6.9 wt.%, the ∑LREE reaches 15 wt.%. The average ratios are Ce/La = 1.7, Ce/Nd = 3.6, La/Nd = 2.2 (fig. 1a).
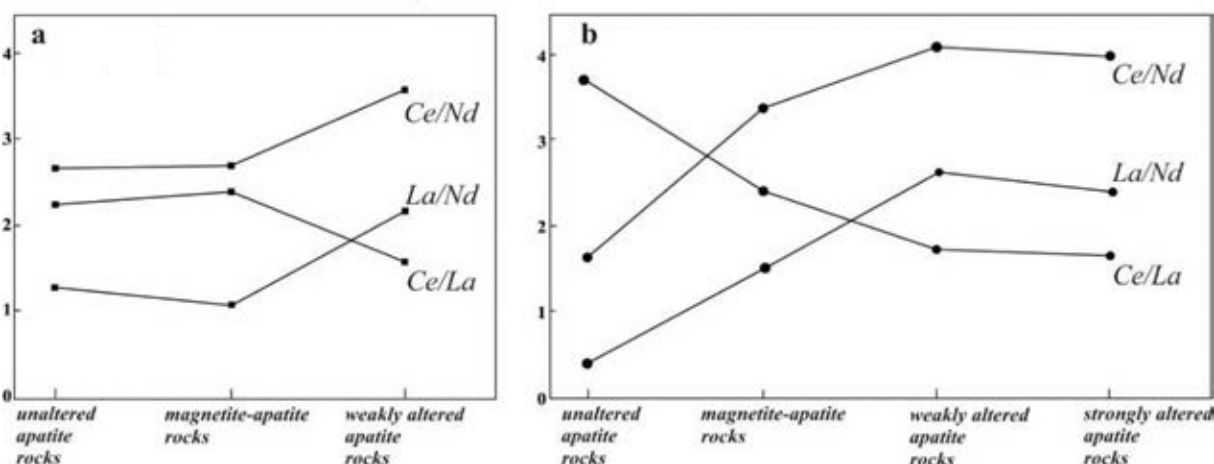
Fig. 1. The average Ce/La, Ce/Nd and La/Nd ratios for apatite (a) and monazite (b).

In the areas of hydrothermal reworking, monazite-Ce and phosphosiderite replace apatite, forming partial or complete pseudomorphs (fig. 2a).

The Raman spectrum of *phosphosiderite* contains typical peaks at 285, 480, and 985 cm^{-1}. Mineral consists of SO_3 up to 0.8 wt.%, SiO_2 up to 3.5 wt.%, Al_2O_3 up to 6,4 wt.%.

Monazite-Ce in weakly altered rocks forms rare inclusions (monazite I). In the areas of intensive hydrothermal reworking, the mineral forms a net of the finest microveinlets (monazite II) along the cracks and in the rims of apatite grains (fig. 2b).

Monazite Ce I is characterized by a lower amount of SrO (2.1 wt.%) compared to monazite-Ce II (SrO 3.6-8 wt.%). In monazite-Ce I, the average ratios Ce/La, Ce/Nd and La/Nd are 1.7, 3.6 and 2.2, respectively. In monazite-Ce II, the ratios Ce/La, Ce/Nd and La/Nd slightly differ 1.6, 3.9 and 2.4, respectively (see fig. 1b).

As regards the composition of other minerals of hydrothermal genesis, baryte and fluellite are present only in magnetite-apatite rocks; for barite, the presence of SrO up to 2 wt.% is typical. Celestine is an accessory mineral in apatite rocks, a specific feature of the composition of celestine is the presence of BaO up to 5 wt.%.

The data obtained by us indicate that initially the melt was enriched in sulfate-ion; this is confirmed by its high concentrations in fluorapatite, monazite Ce. Experimental data (Katsura and Nagashima, 1974, Luhr et al, 1984) verify the dependence of the level of sulfate sulfur concentration in rocks and minerals on the amount of SO_3 in the melts. Natural examples include SO_3-enriched phosphates from the rocks of the carbonatite complexes of Western Transbaikalia (Doroshkevich et al., 2003), carbonatites of Kandaguba and Vuoriyarvi (Bulakh et al., 2000).

For the Mushugai-Khuduk complex, as well as for the carbonatites of Western Transbaikalia, the presence of celestite, anhydrite, barite is typical. These minerals are found in the daughter phases in silicate-salt and salt melt inclusions in the minerals from the rocks of the above-listed complexes (Andreeva et al., 1994, 1998; Doroshkevich et al., 2004). The significant role of the sulfate-ion is also traced at the hydrothermal stage with the formation of sulfates (gypsum, barite), sulfides (pyrite) and monazite II enriched in SO_3.
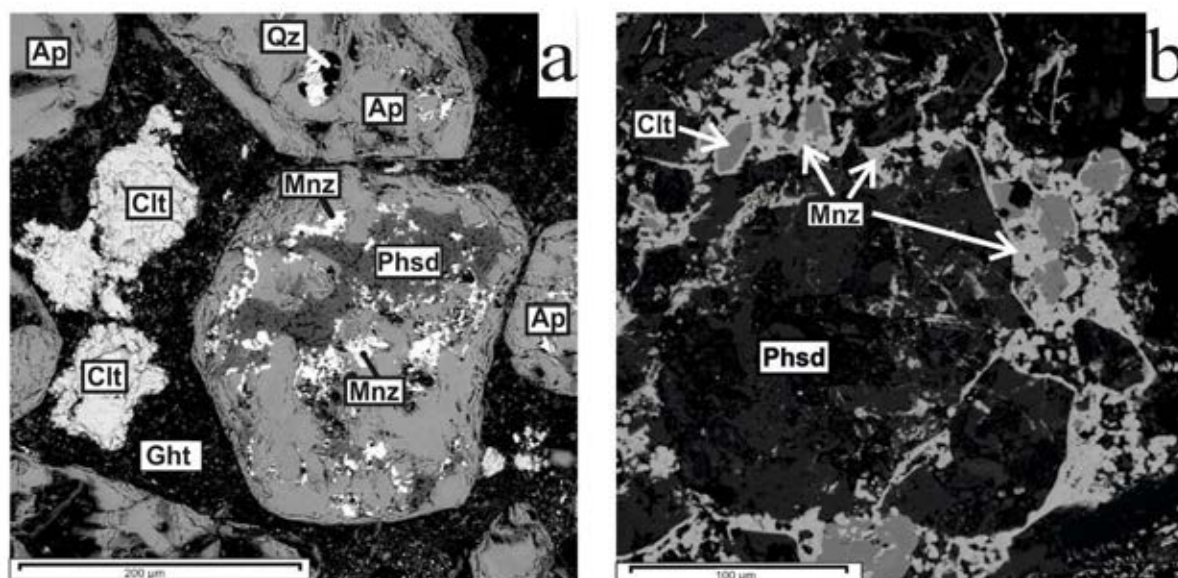
Fig. 2. BSE images showing: a - the replacement of apatite (Ap) by phosphosiderite (Phsd) and monazite (Mnz); b – monazite II forms a net of microveinlets in the rim of apatite. Clt – Celestine, Ght – goethite, Qz – quartz.

In the alkaline high-temperature hydrothermal environment, sulfur is practically the only and very powerful oxidant for fluid-transported cations.

The high chemical activity of sulfur in the hydrothermal solution, in our opinion, led to the fact that apatite began to resolve with the release of phosphate and fluorine ions. The latter upon interaction with water could bind calcium to form fluorite. Magnetite in the high oxidation state is converted to hematite, part of which, upon interaction with the aggressive sulfate ion, formed an unstable soluble salt, which then formed phosphosiderite with phosphate ion. Possibly, a part of iron was included into the hydrothermal solution.

Possible reactions of the hydrothermal reworking of apatite-magnetite rocks:

1. $Ca_5(PO_4)_3F + 5SO_4^{2-} + 5nH_2O \rightarrow 3PO_4^{3-} + 5CaSO_4 \cdot nH_2O \downarrow + F^-$
2. $Fe_2O_3 + 3H_2SO_4 = Fe_2(SO4)_3 + 3H_2O$
3. $Fe_2(SO4)_3 + 2PO_4^{3-} + 2H_2O \rightarrow 2FePO_4 \cdot H_2O \downarrow + 3SO_4^{2-}$

The alteration of apatite was also accompanied by formation of monazite-Ce. Experimental studies (Harlov et al., 2002b; Harlov and Förster, 2003) show that monazite inclusions are usually formed as a result of the internal redistribution of REE in apatite under the influence of hydrothermal solutions. These data are also supported by natural examples (Li and Zhou, 2015, Prokopyev et al., 2017).

It should be noted that for the Mushugai-Khuduk complex the values of the Ce/Nd ratio increased from unaltered to altered apatite and from early monazite-Ce I to later monazite-Ce II. Similar changes in the Ce/Nd ratio are typical for hydrothermal process (Fleischer, 1978), including carbonatitic occurrences (Zaitsev et al., 1998; Doroshkevich et al., 2008) which is explained by an increase of "carbothermal" fluid in the hydrothermal system.

References:

Andreeva I., Naumov V., Kovalenko V., Listratova E., & Kononkova N. (1994). Magmatic Celestine in melt inclusions in apatites of alkaline igneous complex Mushugai-Khuduk (Southern Mongolia). Doklady Akademii Nauk. 337 (4), 499-502

Andreeva, I. A., Naumov, V. B., Kovalenko, V. I., & Kononkova, N. N. (1998). Fluoride–Sulfate and Chloride–Sulfate Salt Melts of the Carbonatite-Bearing Complex Mushugai-Khuduk, Southern Mongolia. Petrology, 6(3), 307-315.

Bulakh, A. G., Nesterov, A. R., Zaitsev, A. N., Pilipiuk, A. N., Wall, F., & Kirillov, A. S. (2000). Sulfur-containing monazite-(Ce) from late-stage mineral assemblages at the Kandaguba and Vuoriyarvi carbonatite complexes, Kola peninsula, Russia. Neues Jahrbuch Fur Mineralogie Monatshefte, (5), 217-233.

Doroshkevich, A. G., Kobylkina, O. V., & Ripp, G. S. (2003). Role of sulfates in the formation of carbonatites in the Western Transbaikal Region. Doklady earth sciences. Vol. 388, pp. 131-134.

Doroshkevich, A. G., & Ripp, G. S. (2004). Estimation of the conditions of formation of REE-carbonatites in Western Transbaikalia.Russ Geol Geophys, 45(4), 492-500.

Doroshkevich, A. G., Ripp, G. S., Viladkar, S. G., & Vladykin, N. V. (2008). The Arshan REE carbonatites, southwestern Transbaikalia, Russia: mineralogy, paragenesis and evolution. Can Mineral, 46(4), 807-823.

Fleischer, M. (1978). Relative proportions of the lanthanides in minerals of the bastnaesite group. Can Mineral, 16, 361-363.

Harlov DE, Andersson UB, Förster H-J, Nyström JO, Dulski P, Broman C (2002b) Apatite-monazite relations in the Kiirunavaara magnetite-apatite ore, northern Sweden Chem Geol 191:47–72

Harlov DE, Förster H-J (2003) Fluid-induced nucleation of REE-phosphate minerals in apatite: nature and experiment. Part II. Fluorapatite. Am Mineral 88:1209–1229

Katsura, T., & Nagashima, S. (1974). Solubility of sulfur in some magmas at 1 atmosphere. Geochim. Cosmochim. Acta, 38(4), 517-531.

Li, H., Zhou, M.F., 2015. Multiple stages of hydrothermal REE remobilization recorded in fluorapatite in the Paleoproterozoic Yinachang Fe–Cu–(REE) deposit, Southwest China. Geochim. Cosmochim. Acta 166, 53–73

Luhr, J. F., Carmichael, I. S., & Varekamp, J. C. (1984). The 1982 eruptions of El Chichón Volcano, Chiapas, Mexico: mineralogy and petrology of the anhydritebearing pumices. Journal of Volcanology and Geothermal Research, 23(1-2), 69-108.

Prokopyev I.R, Doroshkevich A.G., Ponomarchuk A.V.,Sergeev S.A. (2017) Mineralogy, age and genesis of apatite-dolomite ores at the Seligdar apatite deposit (Central Aldan, Russia), Ore Geology Reviews, 81 (1), 296-308

Ripp, G. S.; Karmanov, N. S.; Kanakin, S. V.; Doroshkevich, A. G.; Andreev, G. V. (2005): Cerium britholite from the Mushugai ore deposit (Mongolia). Zapiski Rossiiskogo Mineralogicheskogo Obshchestva 134, 90-103. (in Russian)

Samoilov V.S. and Kovalenko V.I. (1983), "Complexes of Alkaline Rocks and Carbonatites in South Mongolia," Nauka, Vol. 35, p. 196 (in Russian).

Vladykin N.V. (2013) Petrology and composition of rare-metal alkaline rocks in the South Gobi Desert (Mongolia)// Russ Geol Geophys, 54 (4), 545-568.

Zaitsev, A. N., Wall, F., & Bas, M. J. L. (1998). REE-Sr-Ba minerals from the Khibina carbonatites, Kola Peninsula, Russia: their mineralogy, paragenesis and evolution. Mineralogical Magazine, 62(2), 225-250.

SULFIDE-BEARING ASSEMBLAGES IN MANTLE-DERIVED GARNETS FROM CHOMPOLO LAMPROPHYRES (CENTRAL ALDAN)

Nikolenko E.I., Lobov K.V., Sharygin I.S., Rezvukhin D.I.

Institute of Geology and Mineralogy, Siberian Branch of the Russian Academy of Sciences, Novosibirsk, Russia, nevgeny@igm.nsc.ru

Sulfide inclusions in minerals of mantle origin are widely used by scientists as a source of information about deep processes in the earth's mantle. Sulfides in diamonds from kimberlites are the most studied varieties because they carry direct information on the diamond-forming medium and age of diamonds (e.g. Pearson, 1999; Shirey, Richardson, 2011). However, the prevalence of kimberlites in the central and north-eastern parts of the North Asian craton imposes restrictions on the study of mantle processes in the south of the craton. Lamproites and especially lamprophyres receive much less attention, although they also contain xenocrysts of mantle minerals. Thereby garnet xenocrysts with mineral inclusions from lamprophyres of the Central Aldan are an important source of information on the subcontinental lithospheric mantle.

The Chompolo field is located in the southern part of the North Asian craton within the Amga tectonic melange zone, separating the West Aldan granite-greenstone terrane from the Central Aldan granulite-gneiss superterrane. About 450 grains of garnets containing mineral inclusions from two lamprophyre bodies of the Chompolo field were investigated. Inclusions of sulfides were found in 13 garnets from the Aldanskaya dike and in 3 garnets from the Ogonek diatreme. Minerals within exposed inclusions were identified by Raman spectroscopy and electron probe microanalysis (by both EDS and WDS spectrometry). Minerals within unexposed inclusions were identified by Raman spectroscopy only. The problem of determining the bulk composition of sulfides is well known (Taylor, Liu, 2009) and it is obvious that the studied polished sections of sulfide inclusions may not reflect their total phase composition. Instrumental investigations were carried out in Analytical Center for multi-elemental and isotope research SB RAS (Sobolev Institute of Geology and Mineralogy, Novosibirsk).

The composition of garnets containing inclusions of sulfides, namely high content of Cr_2O_3 and Mg#, indicate on their mantle origin. Cr_2O_3 content in garnets varies from 2.0 to 5.8 wt% at Mg# = 74.6-81.0 and Ca# = [100Ca / (Ca + Mg + Fe + Mn)] = 10.9-15.3. TiO_2 concentration does not exceed 0.24 wt%. Almost all points (with the exception of s2) are located in a dense group within the lherzolite trend on the CaO-Cr_2O_3 diagram (Fig. 1a).

Inclusions are represented either only by sulfides or have a more complex phase composition and contain silicate (forsterite, diopside, enstatite, phlogopite, amphiboles), carbonate (magnesite, dolomite), oxide minerals (chrome spinel, ilmenite, rutile, crichtonite group mineral) as well as apatite and graphite (Fig. 1b, Fig. 2). Inclusions of sulfides have a rounded shape (s113, s163, s207), an irregular shape (s115, s213), and a crystalline morphology (s38, s1, s296, n6). Size of the inclusions is usually in the range of 20-200 μm; however, small inclusions of about 5 μm are also present. Inclusions are surrounded by disc-shaped stress halos and radial cracks along which the sulfide substance is sprayed. In polyphase inclusions the relationship of sulfides with other phases is shown in Fig. 2 (b, c, d). Sulfide inclusions are inhomogenous and consist of pentlandite (Pn), chalcopyrite (Cp), bornite solid solution (BnSS), unnamed mineral with empirical formula $CuFe_2S_4$, monosulfide solid solutions (Mss1, Mss2), and occasionally heazlewoodite (Hz) (Fig. 1-3).

Sample	Inclusion assemblages
s1	**Pn, Cp, CuFe₂S₄**
s2	**Pn, Bn$_{SS}$, Hz, Mss1, Mss2**, Cr-Sp, Dy, Tc
s9	**Pn, Cp, CuFe₂S₄** Phl, Rt
s38	**Pn, Cp, CuFe₂S₄**
s113	**Cp, Mss1**, Dol, Phl
s115	**Cp, Mss2**, Cr- Sp, Dy, Chl
s163	**Pn, Bn$_{SS}$, Cp,**
s213	**Cp, Mss1**, Dol, Cr-Sp
s291	**Pn, Cp, Mss2**, Mgs, Cr-Sp, Phl, Fo, Mkt, Ctn
s296	**Cp, Mss1, Mss2**
s317	**Bn$_{SS}$**, Mgs, Cr-Sp, Phl, Rt, Ids
sx2	**Cp, Bn$_{SS}$,Mss1** Ts, Rt
1n11	*Cp, Mgs, Gr, Fo, Dy, Ts, Rt, Ilm, Ap, Ids*
s207	*Cp, Fo, Dy, Rt*
n6	*Cp, Dy*
n7	*Cp, Fo, Rt*
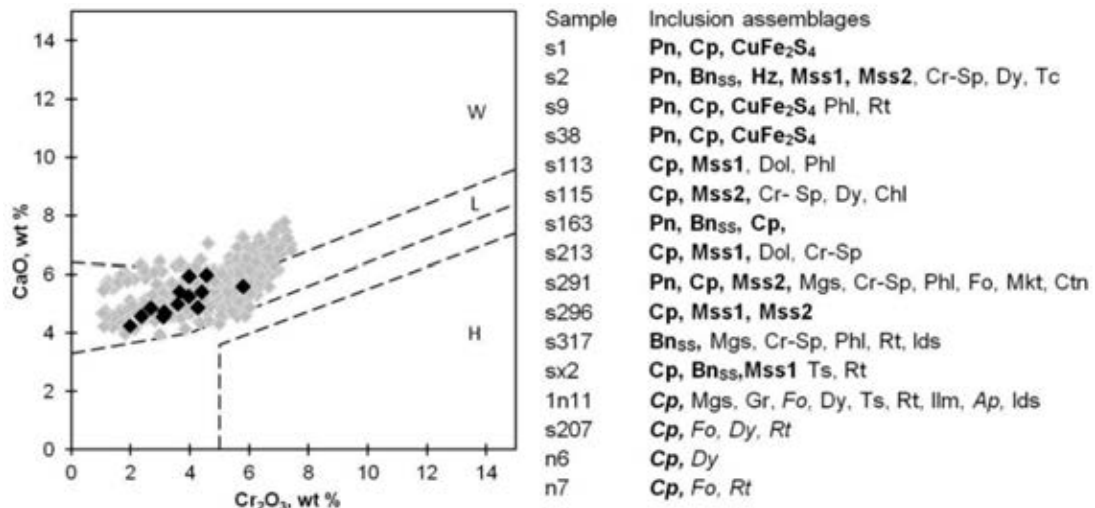
Fig. 1. (a): Composition of the studied pyrope garnets with sulfide inclusions (black rhombs) from Aldanskaya dike and Ogonek pipe on the Cr_2O_3-CaO discriminant diagram (Sobolev et al., 1973). Composition of all peridotitic garnets from Ogonek and Aldanskaya lamprophyre bodies is shown by grey rhombs (author's data). Letters stand for parageneses: H – harzburgitic–dunitic; L – lherzolitic; W – wehrlitic. (b): Inclusion assemblages in pyropes, *italic* indicates minerals identified in unexposed inclusions only by Raman spectroscopy.
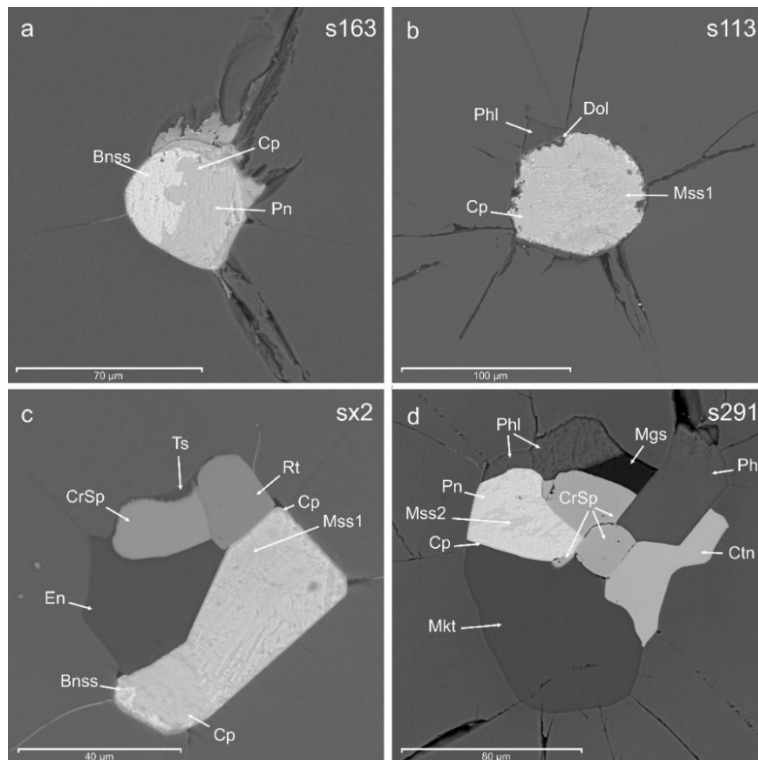
Fig. 2. BSE images of isolated sulfide (a) and polyphase (b, c, d) inclusions in pyropes from Chompolo lamprophyres, Central Aldan. BnSS – bornite solid solution; Cp – chalcopyrite; CrSp –chromium spinel; Ctn – crichtonite group mineral; Dol – dolomite; En – enstatite; Mgs – magnesite; Mkt – magnesio katophorite; Mss – monosulfide solid solution; Pn – pentlandite; Phl – phlogopite; Rt – rutile; Ts – tschermakite.

Pentlandite ($[FeNi]_9S_8$) is the most abundant phase in the investigated inclusions. It fills the main volume of inclusion, as far as it can be judged from the observed polished slice. Chemical composition of pentlandite is characterized by the predominance of Ni over Fe (Ni / (Ni + Fe) = 0.56-0.70), with maximum Ni content up to 46 wt%. The content of Cu and Co impurities varies in the ranges 0.36-1.63 and 0.56-0.82 wt%, respectively.
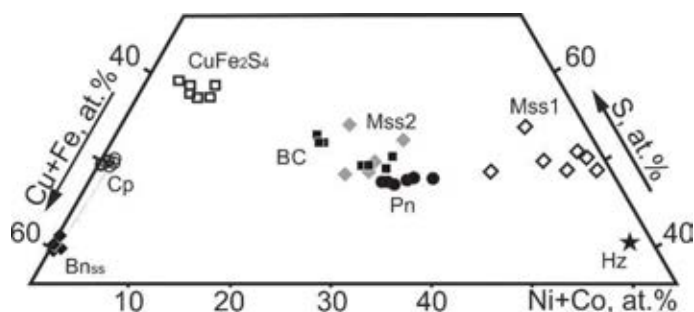
Fig. 3: Composition of studied sulfides on the (Fe + Cu)–(Ni + Co)–S diagram; BC – bulk composition of sulfide inclusions.

Chalcopyrite ($CuFeS_2$) is localized in the outer part of inclusion or forms rims around it and fills the associated radial cracks. Chalcopyrite composition is close to stoichiometric and only Fe content slightly exceeds that of Cu, which is expressed in the ratio (Fe + Ni) / Cu = 1.01-1.09. Ni concentration in chalcopyrite is from 0.38 to 1.43 wt%. Unexposed inclusions of chalcopyrite in garnets 1n11, n6, n7, s207 have been identified only by Raman spectroscopy; therefore their total phase composition is unknown.

Bornite solid solution ($Cu_{5\pm x}Fe_{1\pm x}S_{4\pm y}$) has been found together with pentlandite, chalcopyrite, heazlewoodite and monosulfide solid solution (Mss1). In sample s317 it comprises the whole inclusion. Bornite solid solution is characterized by the (Fe + Ni)/Cu ratio in the range 0.22-0.26 at Fe = 10.6-13.1 wt% and Cu = 57.7-61.8 wt%.

Heazlewoodite (Ni_3S_2) is found only in sample s2 together with pentlandite, bornite solid solution and Mss1. Its composition is characterized by an admixture of Fe and Cu in equal quantity of 1.4 wt%.

In samples s1, s9 and s38 Fe-Cu-sulfide with the calculated formula $(Cu, Ni)_{1.10-0.93}(Fe, Co)_{1.90-2.07}S_4$ has been found in association with pentlandite and chalcopyrite. It is characterized by the predominance of Fe over Cu with the content of these components in the ranges 33.1-34.9 and 12.0-16.0 wt%, respectively. The Fe-Cu-sulfide is also high in Ni (2.4-8.3 wt%) and Co (1.4-2.2 wt%). Me/S ratio varies in the range 0.69-0.75, and S content is 42.0-44.2 wt%. A sulfide with the empirical formula $CuFe_2S_4$ was previously described in Fe-Ni ores of Lovnoozero deposit, Kola Peninsula (Orsoev et al., 2016).

Monosulfide solid solution $(FeNi)_{1\pm x}S$ (Mss1) is determined as one of the phases in the inhomogeneous sulfide inclusions and is characterized by a high content of Ni (55.6-61.9 wt%), high Ni/(Ni + Fe) = 0.92-0.97 and Me/S ratio in the range 0.96-1.06. The content of Fe and Co impurities is 2.0-2.80 and 0.37-0.65 wt%, correspondingly. The Cu content in Mss1 reaches 3.4 wt%. Inclusions also revealed Mss2, which is characterized by a different ratio of Ni/(Ni + Fe) = 0.54-0.60 with Ni content 31.1-35.9 wt% and S content 33.4-36.3 wt%. The impurity of Co (up to 1.9 wt%) is observed in varieties of Mss relatively rich in Fe and substantially lower in Cu and Ni, which may be absent. Monosulfide solid solution with composition close to Mss1 was found in olivines from Smoky Butte lamproites (Sharygin at al., 2003).

All assemblages are likely to be the low-temperature re-equilibrated products of initial high- temperature monosulphide solid solutions. The assumed initial composition of sulfide inclusions and its further evolution should be considered in the quaternary Fe-Ni-Cu-S system. It should be noted, however, that Fe-Ni-Cu-S system remains understudied, and thus the pressure factor probably influencing the mutual position of the stability fields of sulfide phases is not taken into account. The bulk composition of the inclusions (s1, s2, s9, s291, s38) corresponds to the general formulae $(Fe, Ni)_{1\pm x}S$ with variations of Ni and Fe within 26.2-37.7 wt% and 23.5-32.1 wt%, respectively, and contains Cu impurity up to 7.4 wt% in relatively Ni-rich varieties. Phase composition of the investigated inclusions shows that products of the solid solution breakdown are characterized by a significant amount of Cu and Ni-rich minerals and there are no Fe-rich sulfides, including pyrrhotite, that are characteristic of inclusions in mantle minerals and diamonds (Efimova et al., 1983, Barashkov et al., 1997). Given that the association lacks high-temperature Fe-rich Mss, the appearance of the continuous solid solution field $(FeNi)_{1\pm x}S$ in the phase diagram Fe-Ni-S (Kullerud, 1969) at a temperature below 990 °C (at 1 atm) allows us to estimate the maximum temperature at which the initial monosulfide melt could have been captured. A multistage decomposition of inclusion contents and separation of solid solution based on bornite SS, Mss1, Mss2, and also pentlandite and chalcopyrite occurred as a result of a temperature decrease. The formation of pentlandite in a four-component system is possible as a result of a peritectoid reaction between Mss and HzSS at ~ 580°C (at 1 atm) (Peregoedova et al., 1995). The coexistence of pentlandite, Mss, Chalcopyrite SS and Bnss is possible below this temperature (Hill, 1984). Phase $CuFe_2S_4$ in association with pentlandite and chalcopyrite can also result from a solid-phase decomposition reaction of the initial solid solution.This conclusion is based on the Me/S ratios in the coexisting phases and calculated bulk composition of the inclusion.

The estimation of ambient PT conditions for sulfide-bearing assemblages in the mantle was carried out by the combination of mineral thermobarometers. For garnets s115, s2, s207, 1n11 a single clinopyroxene thermobarometer by Nimis and Taylor (2000) was used. For olivine and garnet coexistence in s291 temperature and pressure were estimated by combination of O'Neill and Wood (1979) Fe^{2+}-Mg exchange thermometer, later corrected by O'Neill (1980), and garnet barometer by Grutter (2006). Pressure and temperature estimations obtained from Cpx inclusions in listed above garnets are 2.88-3.55 GPa and 690-790 °C. For s291 the combination of garnet-olivine Fe^{2+}-Mg exchange thermometer and garnet barometer yielded slightly different value for pressure (2.6 GPa) and close temperature values (~670 °C). Thus, estimates of temperature for the described mineral association in inclusions determined by mineral thermobarometers and estimates of temperature for captured initial Mss show similar values.

References:

Barashkov YP, Griffin WL, Tal'nikova SB (1997) Trace Elements in Sulfide Inclusions in Olivine from the Udachnaya Kimberlite Pipe, Yakutia. Geochemistry International 35: 676-680.

Efimova ES, Sobolev NV, Pospelova LN (1983) Sulphide inclusions in diamonds and characteristics of their paragenesis. Zap. VMO 3: 300-310.

Hill RET. (1984) Sulfide deposits in mafic and ultramafic rocks: Institute of Mining and Metallurgy Special Publication.

Nimis P, Taylor WR (2000) Single clinopyroxene thermobarometry for garnet peridotites. Part I. Calibration and testing of a Cr-in-Cpx barometer and an enstatite-in-Cpx thermometer. Contrib. Mineral. Petrol. 139: 541-554.

O'Neill HSC, Wood B. (1979) An experimental study of Fe-Mg partitioning between garnet and olivine and its calibration as a geothermometer. Contrib. Mineral. Petrol. 1979, 70: 59-70.

O'Neill HSC (1980) An experimental study of Fe-Mg partitioning between garnet and olivine and its calibration as a geothermometer: corrections. Contrib. Mineral. Petrol. 72: 337-337.

Grutter H, Latti D, Menzies A (2006) Cr-saturation arrays in concentrate garnet compositions from kimberlite and their use in mantle barometry. J. Petrol. 47: 801-820.

Orsoev DA, Kanakin SV, Pakhomovsky YA, et al. (2016) Mineral $CuFe_2S_4$ from sulfide Copper-Nickel ores of the Lovnoozero deposit, Kola Peninsula. Geology of Ore Deposits 58: 579-585.

Pearson DG, Shirey SB, Bulanova GP, Carlson RW, Milledge HJ (1999) Re-Os isotope measurements of single sulfide inclusions in a Siberian diamond and its nitrogen aggregation systematics. Geochimica Et Cosmochimica Acta 63: 703-711.

Peregoedova AV, Fedorova, ZN, Sinyakova EF (1995) Physicochemical conditions of the pentlandite formation in Cu-bearing sulfide paragenesis (according to experimental data). Russian Geology and Geophysics 36: 91-98.

Sharygin VV, Pospelova LN., Smirnov SZ, Vladykin NV (2003) Ni-rich sulfide inclusions in early lamproite minerals. Russian Geology and Geophysics 44: 855-866.

Shirey S. B., Richardson S. H. (2011) Start of the Wilson cycle at 3 Ga shown by diamonds from subcontinental mantle. Science 6041: 434-436.

Sobolev N, Lavrent'ev YG, Pokhilenko N, Usova L (1973) Chrome-rich garnets from the kimberlites of Yakutia and their parageneses. Contrib. Mineral. Petrol 40: 39-52.

Sobolev NV, Kaminsky FV, Griffin WL, et al. (1997) Mineral inclusions in diamonds from the Sputnik kimberlite pipe, Yakutia. Lithos 39: 135-157.

Taylor LA, Liu Y (2009) Sulfide inclusions in diamonds: not monosulfide solid solution. Russian Geology and Geophysics 50: 1201-1211.

OCELLI IN THE EARLY TRIASSIC CHADOBETS ULTRAMAFIC LAMPROPHYRE (SW SIBERIAN CRATON): EVIDENCE OF LATE STAGE EVOLUTION OF THE LAMPROPHYRE FLUID – MELT SYSTEM

Nosova A.A.[1], Sazonova L.V.[2]

[1]Institute of Geology of Ore Deposits, Petrography, Mineralogy and Geochemistry of the Russian Academy of Sciences, Moscow, Russia, nosova@igem.ru
[2]Lomonosov Moscow State University, Moscow, Russia

Behavior of volatiles in silicate melts during ascent and exsolution is complex and as yet poorly understood. Most of igneous rock lack direct evidence for the presence of magmatic fluid (except for microinclusions in minerals) due to its exsolution from parental magma and rapid escape. The rapid ascent of volatile-rich lamprophyre magmas from the lower crustal or upper mantle depth results in the decompression and, correspondingly, fluid oversaturation and exsolution. Quench cooling of lamprophyre (which typically occurs as small bodies) prevents escape of a fluid from the system and preserves specific textures named ocelli, which are a characteristic feature of the lamprophyre rocks. The ocelli are small sub-rounded mainly leucocratic segregations of carbonate and/or felsic silicate. embedded in a groundmass.. They have been interpreted as amygdales or vesicles filled with late-stage minerals or as products of silicate–carbonate or silicate–silicate liquid immiscibility (Azbej et al., 2006 and reference therein). In some lamprophyres, ocelli have been interpreted as conserved pockets of solidified exsolved immiscible late (residual) magmatic fluid (liquid or gas) (Mauger, 1988; Andronikov, Foley, 2001).

The goal of this study is to constrain the origin of the various types of ocelli observed in the ultramafic lamprophyres from the Chadobets Uplift, South-Western Siberian craton, based on petrographic and electron microprobe data. We also attempted to decipher the late stage evolution of the lamprophyre fluid – melt system, including changes of volatile composition and signs of fluid immiscibility.

Geological position and petrographic description. The Chadobets lamprophyre occurrence is located at the western margin of the Siberian craton in the Chadobets Uplift within the Irkineeva-Chadobets Trough, filled by Mezo-Neoproterozoic and Paleozoic sediments. Early Triassic alkalic–ultramafic sills, dykes and pipes intrude sediments and gabbro–dolerite sills of the Siberian Traps. The Chadobets alkalic-ultramafic complex consists of kimberlite, carbonatite, alnoite and diverse lamprophyres, including aillikite and damtjernite (Lapin, 2001).

Aillikite and damtjernite contain variable amounts of phenocrysts of primary carbonate, abundant olivine, phlogopite, and sometimes clinopyroxene. Aillikite groundmass consists of primary carbonate, fine laths of phlogopite, abundant perovskite, rare amphibole, clinopyroxene, fine grains of apatite, spinel, Ti-magnetite, rutile. Damtjernite groundmass, in addition to these minerals, contains potassium feldspar and nepheline. Globular varieties contain globules also known as ocelli, which occur as rounded, elliptical, dumbbell structures (0.15 – 4 mm size) and differ from host groundmass in mineral composition and texture.

The ocelli description. Ocelli are more abundant in damtjernyte (up to 15 vol.%) than in aillikite and usually have small to medium size (1 to 2 mm). They are filled with carbonate and/or felsic silicate minerals and have elliptical to polyhedral shape. Some ocelli are merged (coalescent) (Fig. 1f). Ocelli are devoid of early magmatic minerals, such as olivine or clinopyroxene, and, in contrast, contain minerals that are absent in groundmass.

Based on shape, mineralogy, and relation with surrounded groundmass, we distinguish three types of ocelli: silicate-dominant (SDO), carbonate-dominant (CDO), and transitional (TO).

The SDO have subrounded and polyhedral shape with irregular outlines due to invasion of groundmass minerals (mainly long prismatic or needle-shaped nepheline, as well individual crystal of clinopyroxene and phlogopite) inwards (Fig. 1b). The SDO are unzoned. The ocelli consist of Na silicates enriched in Cl, F, S, H_2O such as natrolite, sodalite or scapolite (50-80 vol % of ocelli), as wel as rare quartz, and minor calcite. (Figs. 1a-1b). Natrolite appears as laths, tabular crystals or needle-shaped radial aggregates (Figs. 1a, 1b). Sodalite and scapolite form massive aggregates of tabular anhedral crystals (fig. 1c). Quarts is interstitial to the Na-silicates (Fig. 1a). Carbonate in the SDO shows weak spotted zoning. Sometimes the SDO contain Ti-magnetite and apatite.
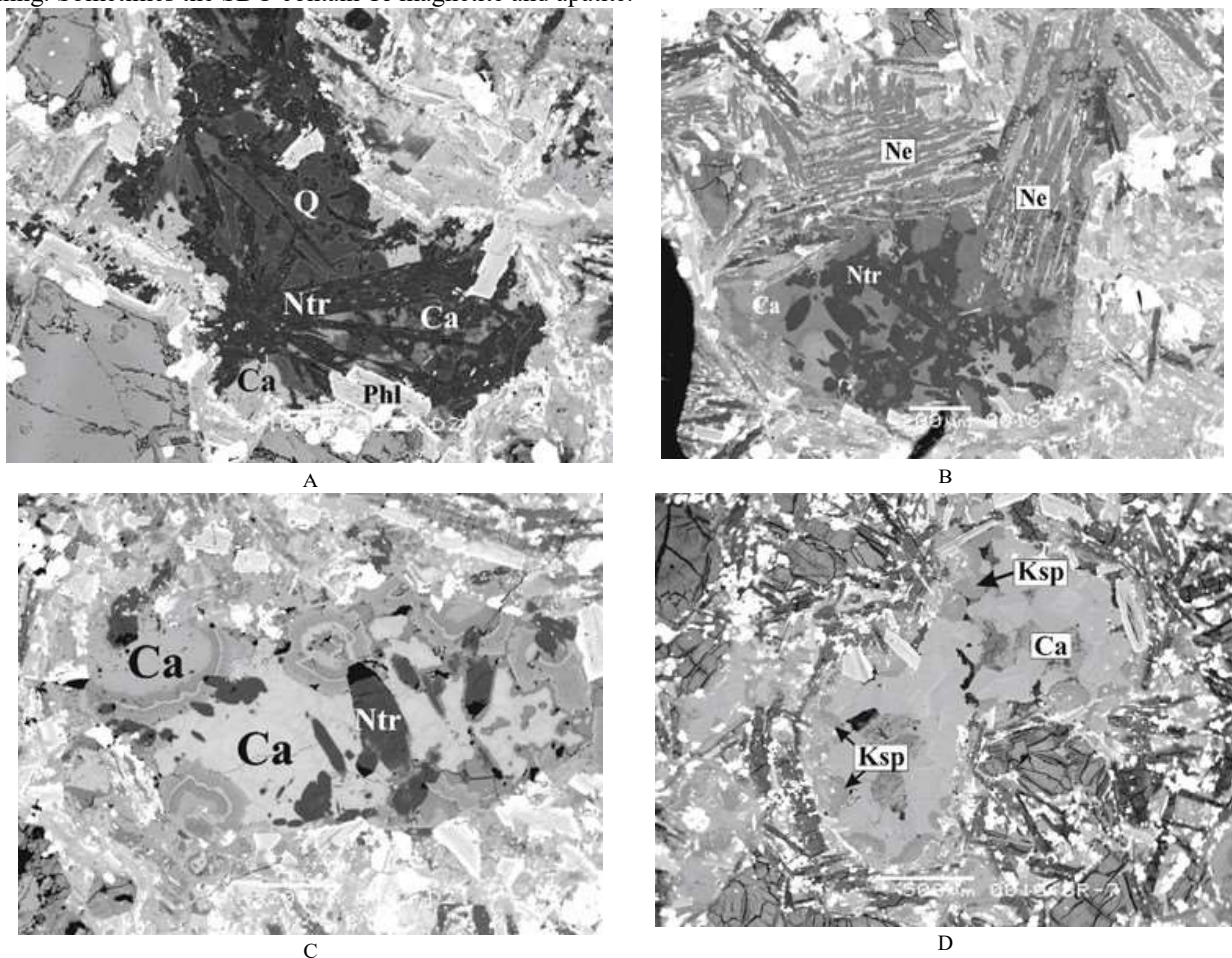
Fig. 1. Ocelli in the Chadobets aillikites and damtjernites: a) the silicate-dominant ocelli (SDO) filled with Na-silicate minerals (natrolite), minor quartz and calcite; b) invasion of long prismatic or needle-shaped groundmass nepheline into silicate-dominant ocelli; c) the transitional ocelli (TO) consisting of natrolite and carbonate d) two slightly deformable and coalescing carbonate-dominant ocelli (CDO). BSE images.

The second-type ocelli (CDO) have rounded elliptical morphology with smooth outlines (Fig.1d). They consist mainly of carbonate with minor amounts of potassium feldspar (Ksp), albite, apatite, and phlogopite. Carbonate amounts to 80-90 vol.% of the ocelli. Kfs occurs as spherulitic aggregates on the ocelli walls and as a spherulite or spherulite clusters in their centers. Carbonate occurs as single crystal grains with mosaic subgrain texture and exhibits calcite-dolomite zoned structure (Figs. 1e, 1f). Silica glass transformed to a cryptocrystalline aggregate is frequently present in the central part of the ocelli. Some ocelli reveal clear concentric zoning: carbonate occupies the central part of the ocelli, while their margins consist of Kfs, apatite, phlogopite, and Ti-magnetite . CDO are usually connected by thin (1-2 mm)

carbonate with minor silicate (Kfs) veinlets. The network of the veinlets indicates that the host rock was mechanically rigid, but not completely crystallized.

Ocelli ascribed to the TO type have intermediate composition between SDO and CDO. They consist of Na-silicate mineral (natrolite, scapolite) and carbonate (Fig. 1c).

Origin of ocelli. We suppose that textural and mineralogical features of the ocelli and their host rock can be interpreted as follows: i) the SDO are droplets of a Na-Cl-F-S-Al-Si-CO_2-H_2O dense fluid with significant amount of melt component; ii) the CDO are bubbles of K-P-CO_2 fluid liberated from almost solidifed magma; iii) the TO are droplets or bubbles of a transitional Na-silicate--carbonate fluid.

Thus we can suggest that rapid decompression during ascent of volatile-rich aillikite and especially damtjernite magma led to fluid oversaturation and exsolution. Differences between the SDO and the CDO morphology (polyhedral for the SDO versus elliptical for the CDO) and style of interaction with host groundmass (active chemical reworking for the SDO and slight mechanical deformations for the CDO) indicate earlier formation of the SDO relative to the CDO.

Fluid – melt system evolution. Transition from the SDO through the TO to the CDO exhibits a subsequent multi-stage fluid – melt system evolution during late stage lamprophyre crystallization and rapid cooling. In general, our observations are roughly consistent with the qualitative model by R.L.Mauger (1988). However, recent researches in silicate-carbonate melt-fluid system (Sierralta et al., 2002; Webster et al., 2014 and others) should be taken into account to adapt our data to this model.

According to (Mauger, 1988), the rapid ascent of the volatile (hydrous and carbonate) - rich silica-undersaturated alkaline lamprophyre melt from the lower crustal or upper mantle depth results in the oversaturation in hydrous fluid-phase and carbonate-melt components. Pressure decrease leads to decreasing water and carbonate solubility in a silicate melt and volatile exsolution (Morizet et al., 2014; Botcharnikov et al., 2005; Webster et al., 2014 and others). The mineral composition of the SDO (sodalite, scapolite, natrolite) indicates that the SDO fluid was CO_2-bearing H_2O-rich dense fluid with high Na, Cl, S amounts and significant fraction of melt components such as Al and Si. Separation of H_2O-rich fluid of the SDO from melt can reduce bulk CO2 (molecular CO_2 and $CO3^{2-}$) diffusivity because H_2O has an accelerating effect on the diffusivity of bulk CO_2 in silicate melt (Sierralta et al., 2002). This effect can result in the slower exsolution of CO_2-rich fluid and formation of the CDO.

The experimental data on fluid - phonolitic-trachytic melts at pressure 2MPa (Webster et al., 2014) demonstrate that increasing Cl in the fluid can reduce the CO_2 concentration in coexisting melts and increase its content in the fluid. The loss of CO_2 from the lamprophyre melt facilitates solubility of fluid in the melt (Mauger, 1988) and may lead to the SDO redisolution. Increasing of fluid solubility in the melt and decreasing of melt component solubility in the fluid phase results in the TO and the CDO appearance.

Alternatively, simultaneous appearance of the TO (natrolite or scapolite-bearing) and the CDO which both characterized by similar elliptical shape and passive relations with host rock can be produced by immiscibility in the H_2O-CO_2-NaCl fluids system. Experimental studies indicate the presence of a miscibility gap between low-density CO_2-H_2O rich vapor and NaCl-H_2O-rich brine even for low-salinity CO_2-H_2O fluids at a wide range of P and T. (Manning et al., 2013 and reference therein). The experimental results (Newton, Manning, 2002) for the H_2O-$CaCO_3$-NaCl system at 10 kbar and 1000-800°C corresponding to the late stages of alkalic magmatism suggest that a mantle-derived supercritical fluid, which was initially saturated in $CaCO_3$ and relatively depleted in NaCl, would precipitate calcite and produce more and less CO_2-rich fluids and more saline NaCl-rich fluid. Interaction of NaCl with feldspar components of melt or crystallized groundmass can produce the scapolite observed in the TO.

Based on experimental models of carbonate-silicate melt-fluid system, the interpretation of the ocelli origin in the Chadobets lamprophyre is not fully adequate and indicates complexity of natural melt-fluid system.

Comparison of chemistry and formation sequence of the ocelli in the Chadobets lamprophyre with recently studied primary melt and secondary fluid inclusions in olivine rims at the Bultfontein kimberlite (Guiliani et al., 2016) demonstrates similarity in fluid composition and dynamics during late stage of those rocks emplacement. Primary inclusions in olivine rims trapped alkali-Si-bearing Ca-Mg-rich carbonate melts, which represent either a fractionation product of the kimberlite magma or a fluid that exsolved after crystallization of olivine and some other minerals. Secondary fluid inclusions in olivine rims are Na ± K- C-O-H-Cl in composition, which represent residual fluids during groundmass crystallization (Guiliani et al., 2016). The alkali-silicate Ca-Mg-rich carbonate melts/fluids of primary inclusions can be compared with the SDO, and residual Na ± K-rich C-O-H-Cl fluids of secondary inclusions can be correlated with the TO and the CDO. Nevertheless, there are some differences between the Chadobets lamprophyres and Bultfontein kimberlite. The earlier fluid exsolved before complete groundmass crystallization in the Chadobets lamprophyre (CDO fluid) was more hydrated, silicate rich and carbonate depleted than fluid from primary inclusions in olivine rims at the Bultfontein kimberlite. It is highly probable that the residual fluid in the Chadobets lamprophyre was immiscibly split into two fluids: Na-Cl-carbonate TO and the K-carbonate CDO.

The SDO and CDO are enriched in different alkali metals: Na preferably distributed into the former whereas K preferably distributed into the latter. Experimental study (Moor et al., 2013) demonstrated that K-rich silicate melts could accommodate more CO_2 in their structure than Na-rich melts. Accordingly, the lower CO_2 solubility in Na-rich silicate melt (the SDO) will provide increase of a carbonate component in a residual K-rich melt. The K-bearing CDO composition reflects both CO_2 and K accumulation in the residual melt.

Conclusions. The Chadobets lamprophyres (aillikites and damtjernites) contain elliptical to polyhedral shaped ocelli filled with carbonate and/or felsic silicate minerals. Based on morphology, mineralogy and relation with host

groundmass, we distinguish three types of ocelli: (1) silicate-dominant (SDO), containing natrolite and sodalite, (2) carbonate-dominant (CDO) containing minor potassium feldspar, and (3) transitional (TO), containing carbonate, scapolite and sodalite. We suppose that the SDO are droplets of a Na-Cl-F-S-Al-Si-CO_2-H_2O dense fluid with significant amount of melt-phase component, the CDO are bubbles of K-P-CO_2 fluid liberated from almost crystallized magma and the TO are droplets or bubbles of transitional dense Na-silicate to carbonate fluid. The SDO represent the earlier hydrated, silicate rich and carbonate depleted fluid exsolved before complete crystallization of the groundmass. Subsequent residual fluid was immiscibly split into two fluids represented by the Na-Cl-carbonate TO and the K-carbonate CDO. Study of the ocelli origin in the Chadobets lamprophyre indicates demonstrates a complex behavior of the melt-fluid system at the late stages of alkalic magmatism.

References:

Azbej T, Szabo C, Bodnar RJ, Dobosi G. (2006) Genesis of carbonate aggregates in lamprophyres from the northeastern Transdanubian Central Range, Hungary: Magmatic or hydrothermal origin? Mineralogy and Petrology 88: 479–497. doi:10.1007/s00710-006-0123-y.

Mauger RL. (1988): Ocelli:Transient Disequilibrium Features in Lower Carboniferous Minette near Concord, North Carolina. Canadian Mineralogist 26:117-131.

Andronikov AV, Foley SF (2001) Trace element and Nd-Sr isotopic composition of ultramafic lamprophyres from the East Antarctic Beaver Lake area. Chemical Geology 175: 291-305. doi:10.1016/S0009-2541(00)00296-5

Lapin AV. (2001) Kimberlites of the Chadobets Uplift in relation with problem of formation–metallogenic analysis of platform alkaline ultrabasic magmatic rocks. Otechestvennaya Geol. 4: 30–35 (in Russian).

Botcharnikov R, Freise M, Holtz F, Behrens H (2005) Solubility of C–O–H mixtures in natural melts: new experimental data and application range of recent models. Annals of Geophysics. 48:633-646

Sierrata M, Nowak M, Keppler H (2002) The influence of bulk composition on the diffusivity of carbon dioxide in Na aluminosilicate melts. American Mineralogist 87:1710–1716.

de Moor JM, Fischer TP, King PL, Botcharnikov RE, Hervig RL, Hilton DR, Barry PH, Mangasini F, Ramirez C (2013) Volatile-rich silicate melts from Oldoinyo Lengai volcano (Tanzania): Implications for carbonatite genesis and eruptive behavior, Earth and Planetary Science Letters 361:379–390. doi:10.1016/j.epsl.2012.11.006

Morizet Y, Paris M, Gaillard F, Scaillet B (2014) Carbon dioxide in silica-undersaturated melt Part II: Effect of CO2 on quenched glass structure Geochimica et Cosmochimica Acta 144:202–216. doi: 10.1016/j.gca.2014.08.034

Manning CE, Shock EL, Sverjensky DA. (2013)The Chemistry of Carbon in Aqueous Fluids at Crustal and Upper-Mantle Conditions: Experimental and Theoretical Constraints. Reviews in Mineralogy & Geochemistry 75:109-148.

Newton RC, Manning CE (2002) Experimental determination of calcite solubility in H_2O-NaCl solutions at deep crust/upper mantle pressures and temperatures: Implications for metasomatic processes in shear zones. American Mineralogist 87:1401–1409

Webster JD, Goldoff B, Sintoni MF, Shimizu N, de Vivo (2014) C-O-H-Cl-S-F Volatile Solubilities, Partitioning, and Mixing in Phonolitic-Trachytic Melts and Aqueous-Carbonic Vapor Saline Liquid at 200 MPa. Journal of Petrology 55:2217-2248. doi:10.1093/petrology/egu055

Giuliani A, Soltys A, Phillips D, Kamenetsky VS, Maas R, Goemann K, Woodhead JD, Drysdale RN, Griffin WL (2016) The final stages of kimberlite petrogenesis: Petrography, mineral chemistry, melt inclusions and Sr-C-O isotope geochemistry of the Bultfontein kimberlite (Kimberley, South Africa), Chem. Geol. doi: 10.1016/j.chemgeo.2016.10.011.

UNDERSTANDING THE ORIGIN OF CARBONADO, AN ENIGMATIC POLYCRYSTALLINE DIAMOND, THROUGH ANALYSIS OF PRIMARY NANO-INCLUSIONS

Ohfuji H.[1], Asano N.[1], Kagi H.[2]

[1]Geodynamics Research Center, Ehime University, Matsuyama, Japan, ohfuji@sci.ehime-u.ac.jp
[2]The University of Tokyo, Tokyo, Japan

Carbonado is a type of polycrystalline diamond, which shows a grayish to black color and a massive and irregular morphology with a porous internal texture. It is distinct from ordinary mantle-derived diamonds in the following respects: extremely low carbon isotope composition (-25~-30 ‰), absence of mantle-derived primary inclusions, high concentration of radiogenic noble gases, etc (Kagi et al., 1994; Heaney et al., 2005; Kagi et al., 2007). Therefore, the origin of carbonado has long been controversial. A recent study (Ishibashi et al., 2010) found several lines of evidence that H_2O-rich fluid is present within constituent diamond grains of carbonado, suggesting its formation in close association with C-H-O fluid in the Earth's mantle. However, the detail of the formation process and condition of carbonado is still unclear.

Here, we found, for the first time, primary mineral inclusions (majoritic garnets, phengite, rutile, apatite, etc.) in nano-sized negative crystals within diamond grains by detailed FE-SEM and TEM observations. Those precipitates usually occur as an assemblage of a few to several mineral phases that are mostly in euhedral forms in the negative crystals. They are most likely quenched products from silicic fluid that were trapped during the crystal growth of diamonds that comprise carbonado. The presence of these mineral phases in negative crystals suggests that the formation of carbonado occurred in fluid-saturated environments to which crustal materials (e.g. basalt) are supplied potentially by the subduction of oceanic plates or extensive collision of continental plates to form a thick mantle keel.

References:

Heaney PJ, Vicenzi EP, De S (2005) Strange diamonds: the mysterious origins of carbonado and framesite. Elements 1:85-89.

Ishibashi H, Kagi H, Sakurai H, Ohfuji H, Sumino H (2012) Hydrous fluid as the growth media of natural polycrystalline diamond, carbonado: Implication from IR spectra and microtextural observations. American Mineralogist 97:1366-1372.

Kagi H, Takahashi K, Hidaka H, Masuda A (1994) Chemical properties of Central African carbonado and its genetic implications. Geochimica et Cosmochimica Acta 58:2629-2638.

Kagi H, Sato S, Akagi T, Kanda H (2007) Generation history of carbonado inferred from photoluminescence spectra, cathodoluminescence imaging, and carbon-isotopic composition. American Mineralogist 92:217-224.

PHYSICAL PROPERTIES OF IRON-LIGHT ELEMENT ALLOYS AND COMPOSITION OF THE EARTH'S CORE

Ohtani E.

Tohoku University, Sendai, Japan

The Earth's core is believed to contain certain amount of light elements based on seismological observations and mineral physics data. The major potential candidates of the light elements of the core are considered to be S, Si, O, and H. Recent studies on the Fe-Si-O system revealed that Si and O have mutual avoidable nature in metallic liquid (Takafuji et al., 2005; Sakai et al., 2006), and precipitation of silicates such as SiO_2 or $FeSiO_3$ occurred during cooling of the liquid core (e.g., Hirose et al., 2015). Therefore, the composition of the inner core crystallizng from metallic liquid core should be ether Fe-O-S or Fe-Si-S alloy, i.e., coexistence of Si and O are prohibited to occur in the solid inner core crystallizing from a metallic outer core.

Our sound velocity measurements of hcp-Fe at high pressure and temperature revealed that both sound velocity (Vp) and density of pure hcp-Fe are greater than those of the PREM inner core indicating that the major light elements in the inner core must reduce both sound velocity and densty of hcp-Fe (Sakamaki et al., 2016). Our sound velocity measurements of iron-light element compounds revealed that S, Si and H can meet with this requrements, wheras the sound veocity of FeO is very high compared to the PREM inner core. Thus, O is not likely to be the major light element of the inner core (Tanaka et al., 2016). The most plausible candidates of the light elements in the core are likely to be S, Si, H without O. Based on our measurements of the sound velocity of iron (Ohtani et al., 2013; Sakamaki et al., 2016), iron-silicon alloy (Sakairi et al., 2017), Fe_3S (Kamada et al., 2014), and FeH (Shibazaki et al., 2012) and the solid-liquid partitioning in the Fe-Si-S system at high pressure and temperature, we constrained the composition of the inner and outer cores. The present experiments on the solid-liquid partitioning of S and Si revealed that the major element of the inner core is Si whereas that in the outer core is S. H also can reduce both sound veocity and density of hcp-Fe, and can account for a light element of the PREM inner core.

The present results on sound velocity measurements and solid-liquid partitioning of iron alloy indicate that an iron alloy with about 5 wt.% of Si and 0.1 wt. % of S can explain the physical properties of the PREM inner core, whereas the PREM outer core contains both S and Si (about 7 wt.% S and 3 wt% Si) without O if we assume that the inner core contains a negregible amount of H. The amounts of S and Si in the inner and outer cores estimated above would be the upper bounds and they could be lower if some amounts of hydrogen exist in the core.

References:

Hirose, K. et al. (2015). AGU 2015 fall meeting, abstract, DI41B-03, San Francisco, Dec 14-18. (1) Kamada. S. et al. (2014). Am. Mineral. **99**, 98-101, 342.

Ohtani et al. (2013). Geophys. Res. Lett., 40, 5089–5094. L06313.

Takafuji et al. (2005). Geophys. Res. Lett. 32,

Sakai, T. et al. (2006). Geophys. Res. Lett., 33, L15317.

Sakairi , T. et al. (2017) Am. Mineral., in review,Sakamaki et al. (2016), Sci. Adv., 2: e1500802.

Shibazaki, Y. et al. (2012). Earth Planet. Sci. Lett., 313–314, 79–85.

Tanaka, R. et al. (2016) AGU fall meeting, abstract, San Fransisco, Dec 14-18.

PLATINUM MINERALIZATION OF IOVSKY MASSIF, NORTHERN URALS

Palamarchuk R.S.[1], Stepanov S.Yu.[1], Khanin D.A.[2,3]

[1]Saint-Petersburg Mining University, Saint-Petersburg, Russia, palamarchuk22@yandex.ru, Stepanov-1@yandex.ru
[2]Institute of Volcanology and Seismology, Far Eastern Division RAS, Petropavlovsk-Kamchatsky, Russia
[3]Lomonosov Moscow State University, Moscow, Russia, mamontenok49@yandex.ru

Iovsky dunite massif is a part of «Ural Platinum-bearing Belt», which is located in the north of Sverdlovsk region, 20 kilometers to the west of Karpinsk. This massif has been studied enough in terms of petrographic composition and geological-structural position (Yefimov, 1984; Ivanov, 1997). However, the data on platinum primary mineralization,

except episodic analyses (Lazarenkov et al., 1992; Garuti et al., 2002) are missed. Therefore, the originality of this work is in the novelty of the obtained data.

The purpose of the work is to characterize the minerals of the platinum group (further PGM) from chromitites of Iovsky massif. To achieve the objectives were described the chromitites' segregations of dunite. Morphological features and chemical composition of the PGMs have also been studied. The results were compared to data on chromit-platinum mineralization from Yudincky (Northern Urals), Nizhnetagilsky, Svetloborsky, Veresovoborsky and Kamenushensky massifs (Middle Urals).

The samples investigated during field works in 2016 were selected. Six large-volume probes (50 kg each) of massive and vein-disseminated chromitites weighting were taken. The probes were crushed into fractions of less than 1 mm and enriched with the centrifugal concentrator «KR-400». PGMs grains were extracted from the resulting concentrate by the "blow-off" method. Morphological features of the units were studied using Scanning electron microscopes JSM-6390LV (Zavaritsky Institute of Geology and Geochemistry UB RAS, authors) and CamScan MX2500 (Russian geological research institute, analyst A.V. Antonov) which were equipped by energy-dispersion spectrometers. The chemical composition of chromite is also this microscopes studied. The chemical composition of the PGM was determined using X-ray spectral microanalyzer Camebax SX50 (Department of Mineralogy, Geological Faculty, Lomonosov Moscow State University, Analyst D.A. Khanin) with wavelength-dispersion detectors.

Iovsky massif is a part of the Konzhakovsky clinopyroxenite-dunite massif, which, like other massifs of Ural Platinum-bearing Belt, is located in Tagilo-Magnitogorsk megazone, near the Main Ural Fault. It consists of rocks of two associations - ultramafic (series of rocks from dunite to clinopyroxenite) and gabbroid (amphibole and olivin gabbro). The rocks are poorly serpentenized, in contrast to the rocks of the clinopyroxenite-dunite massifs from the middle Urals (Ivanov, 1997).

The Iovsky dunite massif is located in the north-eastern part of the Konzhakovsky massif. In general, it is composed of fine-grained dunites (average grain size <0.1 mm), in the central parts passing into small-grained (average grain size from 0.1 mm to 0.5 mm). O.K. Ivanov noted the findings of dunite-pegmatites and miarole cavity with chromian diopside. Thus, the peculiarities of the structure of the Iovsky massif in general are analogous to the features of the structure of the Nizhnetagilsky massif.

In the central part of the Iovsky massif there is a zone with increased content of chromite. The chromitites form a system of steeply dipping (up to vertical) parallel veins, lenses and nests, often of complex shapes with a thickness of up to 0,3 m. The chromites of Iovsky massif are characterized by an isometric shape with an average grain size of 1-1.5 mm. Sometimes especially in vein-disseminated chromitites, the individuals of chromit are characterized by idiomorphic shape with an octahedron habit. According to the diagram of N.V. Pavlov (Pavlov, 1979), the composition of chromite of Iovsky massif is located in the field of subferrichromite. In comparison with the chromites of Nizhnetagilsky, Svetloborsky, Veresovoborsky and Kamenushensky massifs, as well as Yudinsky massif (fig. 1), the Iovsky' chromites are characterized by elevated Cr_2O_3 contents. Despite this, the compositions of the investigated chromite fit the trend (fields 2-6-10 in fig. 1), typical of Uralian-Alaskan-type complexes (Lazarenkov et al., 1992).
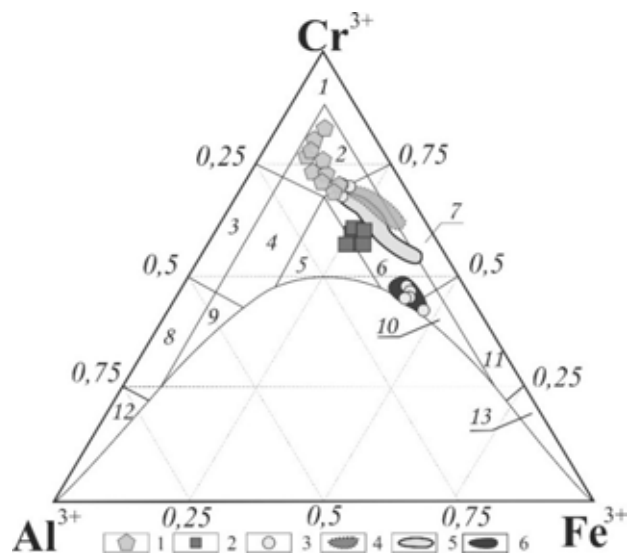
Fig. 1. The position of figurative points of the cromite's compositions on the N.V. Pavlov's diagram. Data on massifs of the Middle Urals are taken from literature sources (Tolstykh et al., 2011; Malich et al., 2015). Field's designation: 1 – chromite; 2 – subferrichromite; 3 – alumochromite; 4 – subferrialumochromite; 5 – ferrialumochromite; 6 – subalumoferrichromite; 7 – ferrichromite; 8 – chrompicotite; 9 – subferripicotite; 10 – subalumochrommagnetit; 11 – chromite; 12 – picotite; 13 – magnetite. Figure legend: 1 – Iovsky and 2 – Yudinsky massifs; 3 – Svetloborsky massif; 4–6 – fields of PGM compositions: 4 – Veresovoborsky, 5 – Kamenushensky and 6 – Nizhnetagilsky clinopyroxenite-dunite massifs.

Most of the PGM from the chromitites of the Iovsky massif are individuals and aggregates of Pt-Fe minerals with average dimensions of 0.4 mm. They have mainly isometric (fig. 2.a) or elongated (fig. 2.b) shapes. Idiomorphic individuals of the hexahedron habit are widely distributed (fig. 2.c, 2.d). They form up to 20% of the volume of all grains. The faces of the cube are covered by a combination hatching relatively rare. Such hatching is formed by alternating of a hexahedron and a tetrahexahedron (fig. 2d). Most of the crystals have hatching, which we diagnosed as inductional. This hatching indicates the combined growth of Pt-Fe minerals with chromites (fig. 2.a, 2.e).

Single inclusions of the Ir-rich osmium possess a pinacoidal habit, forming hexagonal plates with sizes of about 300 microns (fig. 2.f). Osmium crystals of similar morphology are widely spread in the Pt-Fe minerals of Svetloborsky, Kamenushensky and Veresovoborsky massifs (Tolstykh et al., 2011; Malich et al., 2015).
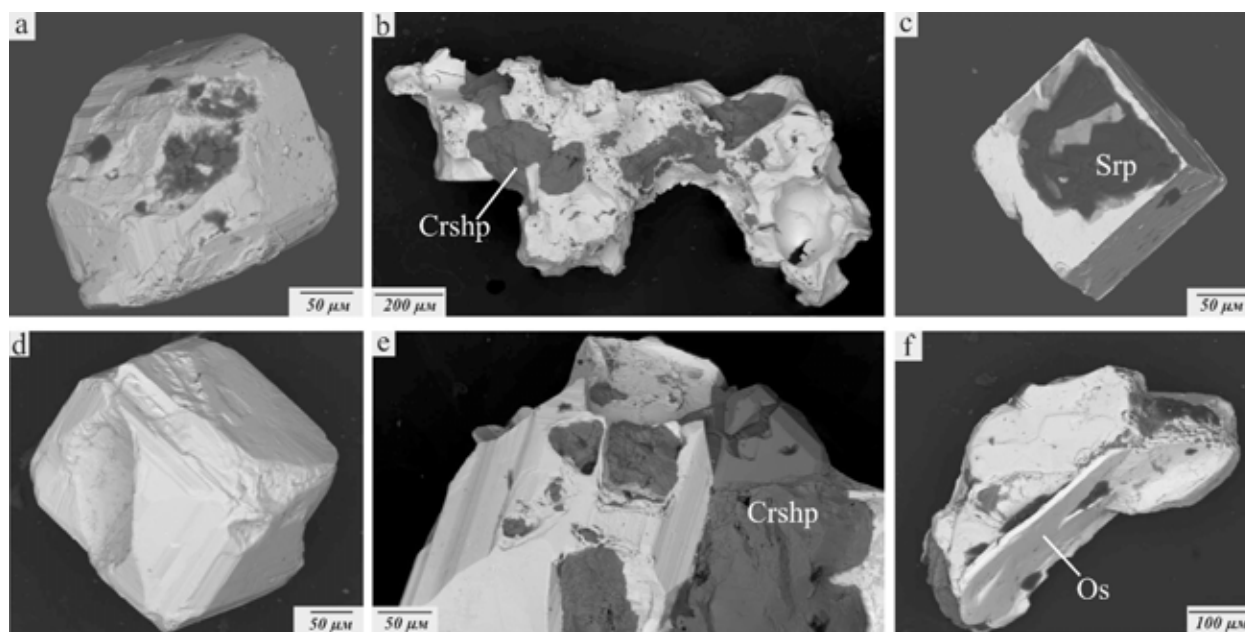
Fig. 2. The grains of Pt-Fe minerals (gray) from the massive chromitites of Iovsky massife. SEM-photos in reflected electrons. Crshp - chromite, Srp - serpentine.

Among the Pt-Fe solid solutions of Iovsky massif, there are minerals with the composition of isoferroplatinum (Pt_3Fe) and ferroplatinum (Pt_2Fe). The occurrence of both minerals is approximately similar. The secondary Pt-Fe minerals replace the isoferro- and ferroplatinum. The composition consists mostly of the 3 minerals: tetraferroplatinum (PtFe), tulameenite ($PtFe_{0,5}Cu_{0,5}$), and Ni-rich tetraferroplatinum ($PtFe_{0,65}Ni_{0,25}Cu_{0,1}$) – a mineral of the intermediate composition of the isomorphic series of tetraferroplatinum-ferronickelplatinum with a permanent admixture of Cu. Tetraferroplatinum and Ni-rich tetraferroplatinum develop on a mineral with an isoferroplatinum composition, sometimes replacing it completely. Tulameenite replaces the Pt-Fe solid solution in stoichiometry corresponding to the ferroplatinum.
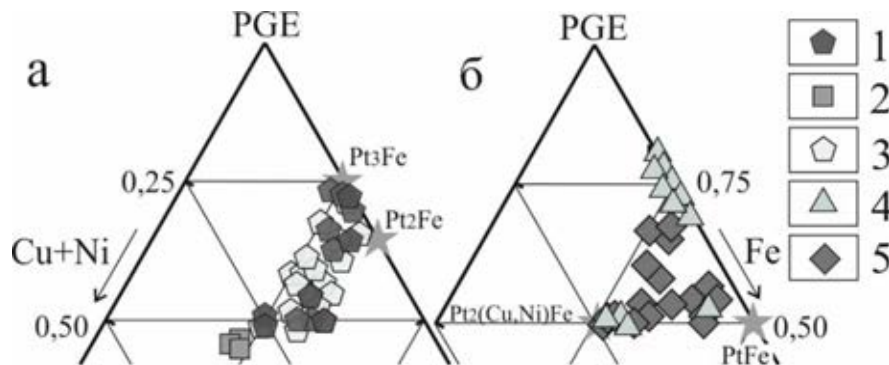
Fig. 3. Composition of Pt-Fe minerals. Iovsky massif: 1 - new data; 2 - data (Garutti et al., 2002). 3 - Yudinsky dunite massif (Garutti et al., 2002). 4 - Svetloborsky and 5 - Nizhnetagilsky massifs (Tolstykh et al., 2011; Malich et al., 2015).

A number of authors is associated the formation of secondary Cu and Ni-rich Pt-Fe minerals with the serpentinization of the rocks of the Nizhnetagilsky massif (Pushkarev et al., 2007). However, the weak serpentinization of rocks and, at the same time, the widespread of development of secondary platinum minerals on the Iovsky massif allows us to assume the interconnection of these processes.

Among the latest secondary minerals replacing primary Pt-Fe minerals, single findings of irarsite with the chemical formula $Ir_{0,93}Rh_{0,20}As_{1,10}S_{1,00}$ (calculated for 1 atom of S) are recorded. The found grain of irarsite (0.1 mm in diameter) has complex outlines and probably completely replaces the primary Pt-Fe mineral. Analogous findings of irarsite were noted for PGM samples from placer of the Nizhnetagilsky massif (Begizov et al., 1976), as well as for a number of placer from the Middle and Southern Urals, connected with dunite-gazburgit massifs of the ophiolite complexes (Zaikov et al., 2016).

Detailed research on the mineralogy of the platinum of Yudinsky massif is presented in G. Garutti's work (Garutti et al., 2002). In a comparative analysis of associations of PGMs from the chromitites of Yudinsky and Iovsky massifs many common features have been described. Among them is the widespread distribution of Pt-Fe minerals with the stoichiometry of both isoferroplatinum and ferroplatinum. A large number of secondary PGMs are also noted. Among the PGMs of the Yudinsky massif there are single findings of osmium, erlichmanite, cupeerite, Rh-Ir-Pt thiospinels,

possibly prassoite. All the listed minerals, excluding osmium, have not been found among the PGMs of Iovsky massif by the moment. However, the similarity of the associations of Pt-Fe minerals of Yudinsky and Iovsky massifs allows to expect the findings of the listed minerals in the chromitite of the latter.

The platinum mineralization of Iovsky massif is characterized by the presence of the two parageneses – the early parageneses, with an approximately equal amount of minerals with the stoichiometry of Pt_3Fe and Pt_2Fe, and the late one, with a wide development of Cu-, Ni-rich minerals of the isomorphic series of tetraferroplatinum-tulameenite-ferronickelplatinum. A similar distribution of PGM is also observed on Yudinsky massif. In addition, because of the development of secondary Ni-rich minerals, the platinum mineralization of Iovsky massif, compared with the clinopyroxenite-dunite massifs of the Middle Urals, is mostly similar to the association of the PGM of Nizhnetagilsky massif.

Most characteristics, such as the predominance of Pt-Fe minerals and their relationship with chromites, the platinum mineralization of Iovsky massif, confirm the belonging of Iovsky massif and, accordingly Konzhakovsky massif to the massifs of the dunite-clinopyroxenite-gabbro formation (Uralian-Alaskan-type complexes).

References:

Begizov V.D., Zavjalov E.N., Hvostova B.P. The minerals of series erlichmanite-laurit and hollingvortit-irarsit from Ural's alluvial // Notes of the VMS. Spb.: Mining university, 1976. V.2, P. 213-218. [Mineraly ryada erlikmanit-laurit i khollingvortit-irarsit iz uralskikh rossypey // Zapiski VMO. Spb.: Gornyy institut]

Efimov A.A. Habbro-hyperbasite complexes of the Urals and the ofiolit's problem. M.: Scientist, 1984. 232 p. [Gabbro-giperbazitovyye kompleksy Urala i problema ofiolitov // M.: Nauka]

Zaikov V.V., Melekestseva I.Yu., Kotlyarov V.A., Zaykova E.V., Krainev Yu.D. The outgrowths of PGE minerals in the Miass' placer zone (South Ural) and their indigenous sources // Mineralogy, 2016. № 4, P. 31-47.[Srostki mineralov EPG v Miasskoy rossypnoy zone (Yuzhnyy Ural) i ikh korennyye istochniki // Mineralogiya]

Ivanov O.K. Zoned ultramafic complexes of Ural (Mineralogy, petrology, genesis). Ekaterinburg: Publishing house Uralsky University, 1997. 488 p.

Lazarenkov V.G., Malich K.N., Sahjanov L.O. Platinum mineralization of zonal ultrabasic and komatiits massifs. L.: Bowels, 1992. 217 p. [Platinometalnaya mineralizatsiya zonalnykh ultraosnovnykh i komatiitovykh massivov L.: Nedra]

Malich K.N., Stepanov S.Yu., Badanina I.Yu., Khiller V.V. Platinoids' mineral associations of the Svetloborsky, Veresovoborsky and Nizhnetagilsky clinopyroxenite-dunite massifs of Middle Ural // Newsletter of Urals branch of the RMS. Ekaterinburg: IG&G UrB RAS, 2015. № 12, P. 65-84. [Mineralnyye assotsiatsii platinoidov Svetloborskogo. Veresovoborskogo i Nizhnetagilskogo klinopiroksenit-dunitovogo massiva Srednego Urala // Vestnik Uralskogo otdeleniya RMO. Ekaterinburg: IGG UrO RAN]

Pavlov N.V., Grigorieva I.I., Grishina N.V. Formation and genetic types of chromite's deposits of geosynclinal regions // Conditions of formation of magmatic ore deposits. M .: Science, 1979. P. 65-79. [Obrazovaniye i geneticheskiye tipy khromitovykh mestorozhdeniy geosinklinalnykh oblastey // Usloviya obrazovaniya magmaticheskikh rudnykh mestorozhdeniy. M.: Nauka.]

Pushkarev E.V., Anikina E.V., Garuti G., Zakkarini F. Hrom-platinum mineralization of Nizhnetagilsky type on Urals: structural-material characteristic and problem of genesis // Lithosphere, 2007. № 3, P. 28-65. [Khrom-platinovoye orudeneniye Nizhnetagilskogo tipa na Urale: strukturno-veshchestvennaya kharakteristika i problema genezisa // Litosfera]

Tolstykh N.D., Telegin Yu.M., Kozlov A.P. Platinum mineralization of the Svetloborsky and Kamenushensky massifs (Urals Platinum Belt) // Russian Geology and Geophysics, 2011. V. 52, № 6, P. 775-793.

Garuti G., Pushkarev E., Zaccarini F.Composition and paragenesis of Pt alloys from chromitites of the Uralian-Alaskan type Kytlym and Uktus complexes, northern and central Urals, Russia // The Canadian Mineralogist, 2002. Vol. 40, P. 357-376.

TIME SCALES OF ORE DEPOSITS: CONSTRAINTS FROM U-PB ZIRCON DATING, THERMOCHRONOLOGY AND SR ISOTOPE GEOCHEMISTRY OF THE PORPHYRY-CU-(MO-AU) SYSTEM IN ELATSITE, BULGARIA

Peytcheva I.[1,2], Loretz M.[2], Von Quadt A.[2], Georgiev S.[1], Kounov A.[3], Gerdjikov I.[4], Guillong M.[2]

[1]Geological institute, Bulgarian Academy of Science, Sofia, Bulgaria, peytcheva@erdw.ethz.ch
[2]Institute of Geochemistry and Petrology, Zurich, Switzerland, quadt@erdw.ethz.ch
[3]Basel University, Basel, Switzerland, a.kounov@unibas.ch
[4]Sofia University, Sofia, Bulgaria, ian.gerdjikov@gmail.com

The formation of ore deposits results from a chain of process, related to the interaction of lithosphere and crust, regional and local tectonics, magmatism and geochemistry, which eventually lead to fluid focusing and metal precipitation (Heinrich, C., unpublished lectures at ETH-Zurich). One important variable in these processes is the time. Apparently, the time influences not only the geochemistry but also the fertility of magma and magmatic-hydrothermal system (e.g. Rohrlach and Loucks, 2005; Chiaradia, 2009; Richards, 2011; Carrichi et al., 2014). Therefore, it is important to choose the most reliable methods which will allow not only to date the ore-formation but also to distinguish the age of precipitation from that of the consequent overprinting processes. Here we present new high-precision low-blank CA-ID-TIMS (Chemical Abrasion-Isotope Dilution-Thermal Ionization Mass Spectrometry) and LA-ICP-MS U-Pb zircon ages from the

porphyry-Cu-(Mo-Au) deposit Elatsite in Bulgaria (Fig. 2, Von Quadt et al., this volume). They are compiled with low-temperature FT (fission track) and (U-Th)/He thermochronology analysis and finally compared to previously published age data from other methods in aim to better constrain the time of the economic mineralization and the role of post-magmatic processes for the deposit preservation. Sr-isotope geochemistry is used as a proxy of magmatic and fluid-rock interaction that may change the primary characteristics of minerals and rock, and hence their age (calculated from Rb/Sr isotope system).

Geology of Elatsite porphyry system

The Elatsite porphyry-Cu-(Mo-Au) deposit is situated in the northernmost parts of the Panagyurishte ore district in the Central Sredna Gora of Bulgaria, which belongs to the Late Cretaceous magmatic and metallogenic Apuseni-Banat-Timok-Srednogorie Belt (ABTSB; Gallhofer et al., 2016 and references therein) of the Carpathian-Balkan orogen. The latter formed due to northward oceanic crust subduction and collision of continental blocks with the European continental margin during the convergence between the African and European plates (e.g., Schmid et al., 2008). ABTSB is characterized by broadly calc-alkaline magmatism and hosts a number of important Cu-Au-(Mo) ore deposits, e.g., Majdanpek and Bor in Serbia, as well as Elatsite, Chelopech, Medet, Assarel (Fig. 2 in Von Quadt et al., this volume) and smaller porphyry and epithermal deposits in Bulgaria (e.g. Popov et al., 2012; Gallhofer et al., 2016).

The formation of Elatsite deposit is related to the multiple Late Cretaceous intrusion of porphyritic dykes. They are hosted in the granodiorites of the Carboniferous Vezhen pluton and the Lower Paleozoic low-grade metamorphic rocks (phyllites, diabases, chlorite and actinolite schists) of the Berkovitsa Group, which are transformed to hornfelses in the contact zones to the pluton. Mineralization in Elatsite comprises several successive stages characterized by the following associations (e.g. Georgiev, 2008; Stefanova et al., 2014): early magnetite-quartz, followed by magnetite-bornite-chalcopyrite, pyrite-chalcopyrite, quartz-molybdenite, and late quartz-pyrite, quartz-galena-sphalerite, and quartz-carbonate-zeolite. Potassic alteration accompanies the quartz-magnetite and magnetite-bornite-chalcopyrite mineralization stages, whereas both potassic and propylitic have been described for the pyrite-chalcopyrite stage. The quartz-pyrite assemblage is observed mostly in veins with well-preserved sericitic alteration halos.

Time relations of dykes, veins, and mineralization are summarized by von Quadt et al. (2002) and Stefanova et al. (2014). Conventional U-Pb zircon dating of the porphyritic dykes revealed a short duration of ore-related magmatism between 92.1 ± 0.3 Ma (pre- or syn-ore quartz-monzodioritic dyke) and 91.84 ± 0.31 to 91.42 ± 0.15 Ma (syn- to post-ore granodiorite-porphyries; von Quadt et al., 2002). Additionally to the overall magmatic succession Stefanova et al. (2014) describe the magmatic to hydrothermal transition in Elatsite and pay special attention to the aplites; the latter are interpreted as volumetrically minor residual melts that evolved directly from granodiorite porphyries at the level of deposit formation.

Sampling strategy and analytical techniques

For the present study we resampled or re-dated the monzodiorite- and granodiorite porphyries (Fig. 1 in Von Quadt et al., 2002) in aim to refine their age using low-blank CA-ID-TIMS techniques. LA-ICP-MS analyses were applied either on annealed (ML samples), or on annealed and leached zircons (AvQ006), using the equipment at IGP, ETH Zurich (Resonetics Resolution 155 laser ablation system coupled to a Thermo Element XR sector-field ICP-MS) and GI-BAS, Sofia (a New Wave excimer laser UP-193FX attached to a Perkin-Elmer ELAN DRC-e ICP-MS). We compiled these data with high-precision CA-ID-TIMS dating of the aplitic veins and Sr-isotope studies of micro-drill whole-rock and mineral samples of the aplites and hosting rocks (Fig. 3 in Loretz, 2016). Details of the applied analytical technique are given in Von Quadt et al. (2002), Buret et al., (2016) and Peytcheva et al. (2015). The sample for zircon and apatite thermochronology was taken from the Carboniferous Vezhen granodiorite outside the mine, approximate 300 m east of the open pit. Applied analytical techniques of FT and (U-Th)/He analysis are described in Kounov et al. (in review).

Results

U-Pb-zircon LA-ICP-MS data for all studied samples reveal a spread of single zircon ages over 5-8 Ma, mainly between 93 and 88 Ma. Due to the larger uncertainties of individual measurements the sample data overlap yielding a Concordia age of 92.06 ± 0.38 (uncertainties are internal 95% conf.) for the monzodiorite porphyry (ML1300), 91.21 ± 0.33 and 90.94 ± 0.43 Ma for the granodiorite-porphyries (ML1120 and ML1060), and 90.33 ± 0.65 Ma for the aplitic veins (ML1080). The mean age of the CA-treated zircons of sample AvQ006 ("late-post-ore granodiorite porphyry", not plotted on Fig. 1) is defined at 91.34 ± 0.68 Ma (internal 2 sigma uncertainties) which is slightly higher than the mean value but still overlapping with all dated granodiorite porphyries within their uncertainties. Inheritance from the host rocks (Variscan and Cadomian) is abundant in the earliest monzodiorite porphyry and intermediate to minor in the later intrusions.

The CA-ID-TIMS dating results are shown on Fig. 1 together with the LA-ICP-MS $^{206}Pb/^{238}U$ ages. As argued in previous publications the CA-techniques related to low age uncertainties ($\leq 0.1\%$ to $\leq 0.02\%$) allow a better distinction of magma pulses by the youngest zircons in the analyzed population (Von Quadt et al., 2011; Buret et al., 2016). The age of the monzodiorite porphyry is now better constrained to 92.329 ± 0.021 Ma, which is slightly older than the granodiorite porphyries and the aplites giving ages of 92.079 ± 0.026 Ma and 92.050 ± 0.019 Ma, respectively.

FT and (U-Th)/He dating on zircons are in good agreement and yield ages of 81.8 ± 8.2 Ma (2 SE) and 81.2 ± 4.6 Ma, respectively. As these chronological systems close at ~250°C and ~180°C, respectively we interpret these ages as either reflecting protracted high thermal flow for a period of 5 to 10 Ma after the main magmatic and ore-formation stage, or as results of a renewed increasing of the heat flow at ~81 Ma related to a new distinct magmatic-hydrothermal event. (U-Th)/He apatite age is defined at 39.3 ± 3.0 Ma (2 SE) and corresponds to a cooling of the host rock to temperature bellow 75°C.
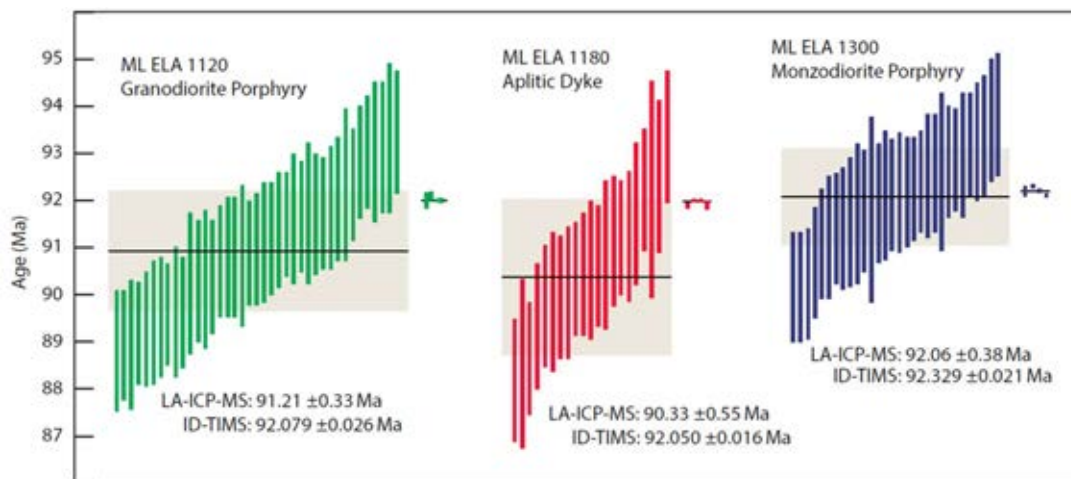
Fig. 1. LA-ICP-MS and CA-ID-TIMS U-Pb zircon data for ore-related porphyry dykes in Elatsite.

Initial strontium ratios $^{87}Sr/^{86}Sr$ of Late Cretaceous granodiorite-porphyry vary in a range 0.7031-0.7039 (matrix and plagioclase in granodiorite-porphyry dyke), between 0.7086-0.7104 in the Carboniferous Vezhen granites and reaches 0.7239 in the Cambrian hornfelses. The $(^{87}Sr/^{86}Sr)_i$ ratio in the crosscutting aplites changes from 0.7058 in the contact to the Late Cretaceous granodiorite-porphyry and Carboniferous granitoids to 0.7112 in contact with the hornfelses.

Discussion and conclusions

The application of the high-precision CA-ID-TIMS U-Pb zircon method helped refining the age of porphyry and aplitic dykes that bracket the time of porphyry Cu-(Mo-Au) deposit formation in Elatsite. From our new age data the main mineralization is confined by the individually dated igneous events between 92.329 ± 0.021 Ma and 92.050 ± 0.019 Ma, thus the entire time span for ore-forming magmatism and high-temperature hydrothermal activity extended over a maximum duration of 0.31 Ma, instead of the 1.1 Ma constrained by the conventional ID-TIMS U-Pb zircon dating (Von Quadt et al., 2002). This data come closer to ore-formation period reported from numeric modelling of porphyry systems between ~100 and 5000 yrs (Cathles et al., 1997; Weiss et al., 2012). In the case of multiple intrusions the magmatic-hydrothermal system might be recharged, reheated and revived but precise dating of young porphyry systems (with lower absolute uncertainties) argue again for a life-span of 6000 yrs (one magmatic impulse) to <29000 yrs of the whole dyke succession (e.g. Bajo de la Alumbrera, Argentina; Buret et al., 2016).
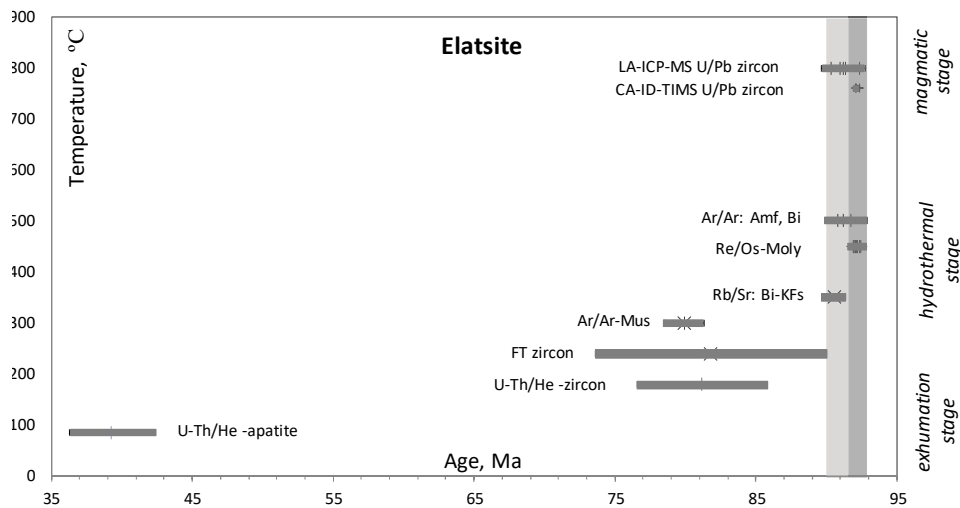
Fig. 2. Compilation of age data for the Elatsite porphyry-Cu deposit (data from this study and Handler et al., 2004; Lips et al., 2004; Zimmerman et al., 2008). Vertical bars correspond to estimated life-span of magmatic-hydrothermal system; dark grey bar is based on CA-ID-TIMS U/Pb zircon and Re/Os molybdenite dating.

There is a disagreement about life-spans of porphyry deposits, especially when using wide range of isotope systems (see summary of Chiaradia et al., 2013) covering also wide range of mineral closure temperatures. The three minerals and isotope methods that generate results with the highest precision and accuracy for dating a magmatic-related hydrothermal system are U/Pb on zircon, Re/Os on molybdenite and $^{40}Ar/^{39}Ar$ on potassium-rich minerals. Deposit formation period of up to 1.0-2.0 Ma is assumed for the giant El Teniente porphyry-copper system (summary of Chiaradia et al., 2013) and supported by multiple intrusions (field relationships and ID-TIMS U/Pb zircon dating) and molybdenite precipitation (Re/Os dating). The protracted cooling history of the system is constrained by $^{40}Ar/^{39}Ar$ dating of alteration minerals. Unfortunately, some potassium rich minerals as white mica may crystallize not only from circulating fluids during the cooling of the main magmatic-hydrothermal system but also during later overprinting processes. In Elatsite a thermal anomaly at ~81 Ma is suggested by the FT and (U-Th)/He dating of zircons (Fig. 2), similar to published Ar/Ar sericite age of 79.9 ± 1.4 Ma (Lips et al., 2004). These ages differ substantially from the Re/Os molybdenite ages (92.4 ± 0.3 to 91.88 ± 0.5 Ma; Zimmerman et al., 2008), from Ar/Ar (Lips et al., 2004; Handler et al., 2004) and Rb/Sr (Von Quadt et al., 2002) ages of minerals with higher blocking temperature than sericite such as amphiboles, and the biotite and K-

feldspar from the potassic alteration assemblage (91.7 ± 1.4 Ma to 90.55 ± 0.8 Ma). Therefore we can conclude that most probably the main magmatic-hydrothermal activities ceased at ~90-91 Ma, whereas ascription of ages ~80 Ma to distinct magmatic and/or hydrothermal event needs further detailed studies. Working hypotheses include reheating from deeper plutons along major faults and/or focused thermal and fluid flow in regions with high rock permeability.

Strontium isotope system in the magmatic-hydrothermal system of Elatsite is altered due to magmatic and fluid-rock interaction. Our data revealed this system as one of the most susceptible to thermal- and fluid-caused diffusion and resetting. Reliable dating by Rb/Sr method will be possible only by accurate separation of mineral associations and unaltered rocks.

The majority of the world-class porphyry-Cu deposits are Cenozoic. The preservation of the Late Cretaceous Elatsite deposit might be explained by the Paleocene-Eocene compression in the Balkan belt (Balkanska et al., 2012) that lead to the tectonic burial and consequent preservation of the deposits. In Late Eocene-Oligocene time (U-Th/He apatite ages of 39.3 ± 3.0 Ma) the region was cooled down to temperatures below 75°C and afterward exhumed to the surface uncovering the 3-4 km deep porphyry system.

References:

Buret, Y., von Quadt, A., Heinrich, C., Selby, D., Wälle, M., Peytcheva, I. (2016) From a long-lived upper-crustal magma chamber to rapid porphyry copper emplacement: Reading the geochemistry of zircon crystals at Bajo de la Alumbrera (NW Argentina). Earth and Planetary Science Letters, 450:120–131.

Carrichi, L., Simpson, G., Schaltegger, U. (2014) Zircons reveal magma fluxes in the Earth's crust. Nature 511:457-461.

Cathles, L. (1997) Thermal aspects of ore formation. In: Barnes, H. (ed) Geochemistry of hydrothermal ore deposits (3rd edition). John Wiley, New York, pp.125-190.

Chiaradia, M., Schaltegger, U., Spikings, R. Wotzlaw, J.-F., Ovtcharova, M. (2013) How Accurately Can We Date the Duration of Magmatic-Hydrothermal Events in Porphyry Systems? Economic Geology 108/4:565–584.

Gallhofer, D., von Quadt, A., Peytcheva, I., Schmid, S., Heinrich, C.A. (2015) Tectonic, magmatic, and metallogenic evolution of the Late Cretaceous arc in the Carpathian-Balkan orogen. Tectonics 34, doi:10.1002/ 2015TC003834.

Georgiev, G. (2008) A genetic model of the Elatsite porphyry copper deposit, Bulgaria. Geochemistry, mineralogy and petrology 46:143-160.

Balkanska, E., Gerdjikov, I., Vangelov, D., Kounov, A. (2012) Thick-skinned compression in Central Balkanides coeval with extension in the uppermost part of the orogen core. Proc. of International conference "Geological schools of Bulgaria. The school of Prof. Zhivko Ivanov", pp. 13–16,

Handler, R., Velichkova, S., Neubauer, F., Ivanov, Z. (2004) $^{40}Ar/^{39}Ar$ age constraints on the timing of the formation of Cu–Au deposits in the Panagyurishte region, Bulgaria. Schweiz. Mineral. Petrograph. Mitt. 84/1:119–132.

Kounov, A., Gerdjikov, I., Vangelov, D., Balkanska, E., Lazarova, A., Georgiev, S., Stockli, D. (2017) First thermochronological constraints on the Cenozoic extension along the Balkan Fold-Thrust Belt (Central Stara Planina Mountain, Bulgaria). International Journal of Earth Sciences, in review.

Lips, A., Herington, R., Stein, H, Kozelj, D., Popov, K., Wijbrans, J. (2004) Refined timing of porphyry copper formation in the Serbian and Bulgarian portions of the Cretaceous Carpatho-Balkan Belt. Econ. Geology 99:601-609.

Loretz, M. (2016) In-situ Sr Measurements and Zircon Analysis of Aplitic Dykes in Cu-Mo-Au Porphyry Deposit Elatsite, Bulgaria. MSc Thesis, ETH Zurich, 44 pp.

Richards, J. P. (2011) High Sr/Y arc magmas and porphyry Cu ± Mo ± Au deposits: Just add water. Economic Geology, 106/7:1075–1081.

Peytcheva, I., von Quadt, A., Georgiev, S., Stoykov, S. (2015) Improved U/Pb dating of CA-treated zircons from northern parts of Central Srednogorie for accurate geological interpretation. "GEOSCIENCES 2015", Proceedings of BGS conference, S., BGS, 73-74.

Rohrlach, B. D., Loucks R. R. (2005) Multi-Million-Year Cyclic Ramp-Up of Volatiles in a Lower Crustal Magma Reservoir Trapped Below the Tampakan Copper-Gold Deposit by Mio-Pliocene Crustal Compression in the Southern Philippines. PGC, Adelaide, Australia., 270 pp.

Schmid, S. M., Bernoulli, D., Fügenschuh, B., Matenco, L., Schefer, S., Schuster, R., Tischler, M., Ustaszewski, K. (2008) The Alpine-Carpathian-Dinaridic orogenic system: Correlation and evolution of tectonic units. Swiss J. Geosci. 101/1:139–183.

Stefanova, E., Driesner, T., Zajacz, Z., Heinrich, C., Petrov, P., Vasilev, Z. (2014) Melt and Fluid Inclusions in Hydrothermal Veins: The Magmatic to Hydrothermal Evolution of the Elatsite Porphyry Cu-Au Deposit, Bulgaria. Economic Geology 109:1359–1381.

Von Quadt, A., Peytcheva, I., Kamenov, B., Fanger, L., Heinrich, C.A., Frank, M. (2002) The Elatsite porphyry copper deposit in the Panagyurishte ore district, Srednogorie zone, Bulgaria: U-Pb zircon geochronology and isotope-geochemical investigations of magmatism and ore genesis. In: Blundell, D.J., Neubauer, F., von Quadt, A. (eds) The Timing and Location of Major Ore Deposits in an Evolving Orogen. Geol. Soc., London, Spec. Public. 204:119-135.

Von Quadt, A., Erni, M., Martinek, K., Moll, M., Peytcheva, I., Heinrich, C. (2011) Zircon crystallization and the life times of magmatic-hydrothermal ore systems. Geology 39/8:731–734.

Weis, P., Driesner, T., Heinrich, C.A. (2012) Porphyry-Copper Ore Shells Form At Stable Pressure Temperature Fronts Within Dynamic Fluid Plumes. Science 338:1613-1616.

Zimmerman, A., Stein, H., Hannah, J., Kozelj, D., Bogdanov, K., Berza, T. (2008) Tectonic configuration of the Apuseni-Banat-Timok-Srednogorie belt, Balkans-South Carpathians, constrained by high precision Re-Os molybdenite ages. Mineralium Deposita 43:1-21.

TRACE ELEMENT GEOCHEMISTRY OF SCHEELITE FROM THE ZHALTYRKOL POPHYRY CU OCCURRENCE, SOUTH URALS, KAZAKHSTAN

Plotinskaya O.Y.[1], Baksheev I.A.[2], Minervina E.A.[1], Grabezhev A.I.[3], Yapaskurt V.O.[2]

[1]Institute of Geology of Ore Deposits, Petrography, Mineralogy and Geochemistry of the Russian Academy of Sciences, Moscow, Russia, plotin@igem.ru
[2]Lomonosov Moscow State University, Moscow, Russia
[3]Institute of Geology and Geochemistry, Ural Branch of the Russian Academy of Sciences, Yekaterinburg, Russia

Porphyry copper deposits supply most of World's Cu, Mo, and Re resources as well as significant amount of Au, and, to lesser degree, Ag, Pd, Te, Se, Bi, Zn, and Pb (Sillitoe, 2010); most of the aforementioned elements are considered as strategic metals (EU Commission 2014). This determines the importance of study magma and fluid sources, and PTx conditions of porphyry Cu deposits formation. In this paper, we report in-situ LA-ICP-MS data for hydrothermal scheelite from the Zhaltyrkol poprhyry Cu occurrence, compare it to the ICP-MS data for country rocks, and discuss the possible fluid sources, physicochemical conditions, and possible mechanisms of the ore-forming process.

The Zhaltyrkol poprhyry Cu occurrence is located in the South Urals, near the Western boarder of the Valeryanovka Early Carboniferous volcanic terrane (Grabezhev and Belgorodskii, 1992; Plotinskaya et al., 2017 and references therein), ca. 100 km south of the well-known Benkala porphyry Cu deposit (Fig.1a). The country rocks are the Fammenian to Lower Tournasian tuffaceous sediments, which are intruded by the Buget-Zhaktyrkol tonalite-granodiorite pluton (Fig.1b). The latter was dated as 336±3Ma (Grabezhev et al., in press) and thus, is linked to the activity of an Andean-type margin of the Kazakh continent (Samygin and Burtman, 2009).
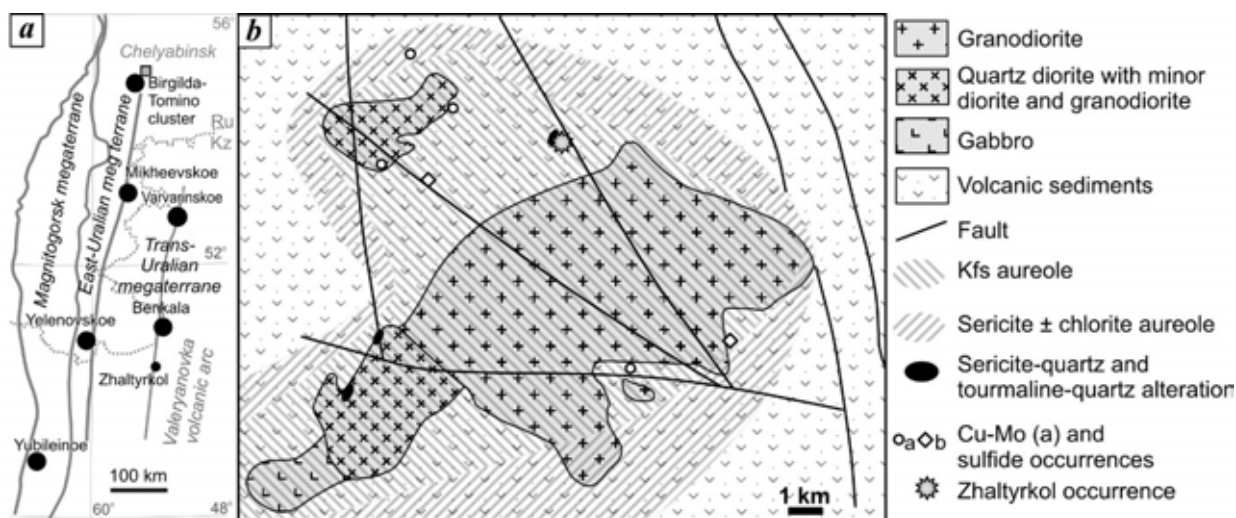
Fig. 1. Position of the Zhaltyrkol occurrence and major porphyry Cu deposits in the South Urals (a) and map of the Buget-Zhaltyrkol ore field (b) simplified after (Grabezhev and Belgorodskii, 1992).

The Zhaltyrkol occurrence comprises a series of NNE trending steeply dipping veinlet-dissemination zones 20 to 70 m wide and over 1 km long with K-feldspar and sericite alteration (Grabezhev and Belgorodskii, 1992). The following sequential ore-bearing mineral assemblages are revealed: (1) quartz + hematite + wolframite + scheelite; (2) tourmaline (the oxy-dravite—povondraite series) + magnetite; (3) pyrrhotite + pyrite + molybdenite + chalcopyrite + sphalerite + bornite; (4) the superimposed low-grade metamorphic assemblage is composed of siderite, calcite, chamosite.

Scheelite belongs to the early mineral assemblage and is overgrown by magnetite and chalcopyrite (Fig.2a). UF and SEM study revealed two generations of scheelite: scheelite-1 forms pseudooctahedral crystals up to 1 mm in size (Fig.2b-e); sometimes scheelite-1 contains inclusions of earlier wolframite (Fig. 2 d, f). Scheelite 2 overgrows and replaces scheelite 1 as fine-grained aggregates (Fig.2b-d).

The chemical composition of scheelite was determined on a JEOL JSM-6480LV electron microscope equipped with an Inca Energy-350 EDS and Inca Wave-500 WDS at the Laboratory of Analytical Techniques of High Spatial Resolution, Department of Petrology, Moscow State University Moscow State University. Trace element examination of scheelite was performed using the New Wave 213UP laser coupled with the Thermo X Series2 quadrupole ICP-MS at the Institute of Geology of Ore Deposits, Petrography, Mineralogy, and Geochemistry (IGEM RAS, Moscow), operated at a laser

frequency of 10 Hz, 16-17mJ input power, acquisition time 30 s, and 60μm diameter spot size. Standard reference materials NIST SRM 614 and 612 were used for external calibration.

EMPA data evidence scheelite-1 enriched in MoO_3 ranging from 0.64 to 0.86 wt.%, mean 0.74 wt.% for n=7, while in sheelite-2 MoO_3 content is much lower (0.08 to 0.20 wt.%, mean 0.14 wt.% for n=2).

According to LA-ICP-MS data (Table 1), Mo in scheelite-1 varies from 4 808 to 7 256 ppm (mean 5 998 ppm, n=8), which is in a good agreement with EMPA data, whereas in scheelite-2 it makes up 3692 ppm (n=1), most likely due to admixture of sheelite-1.
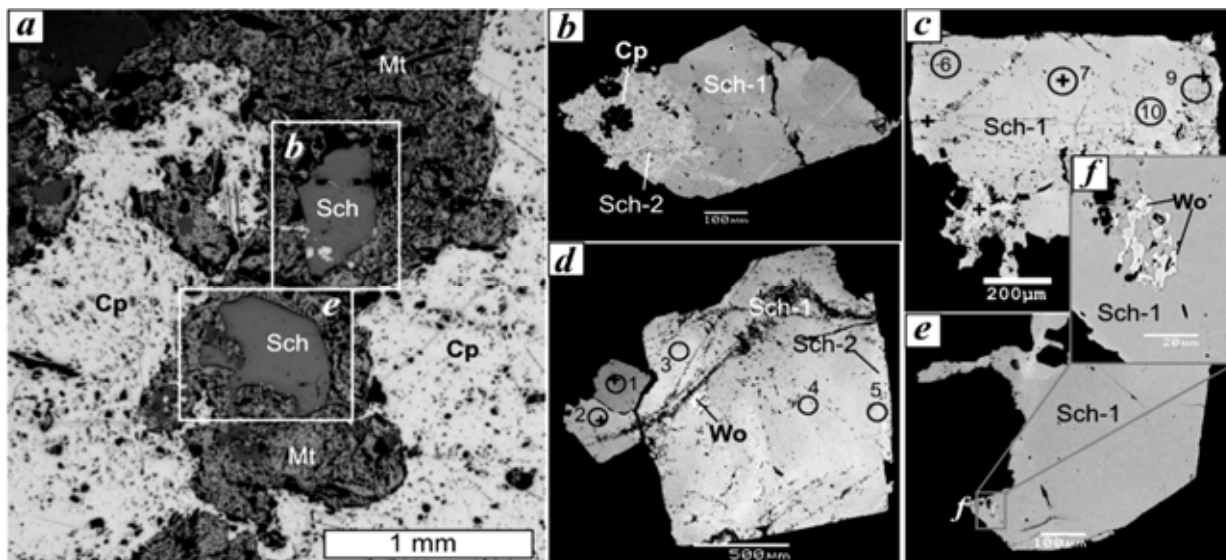
Fig. 2. Mineral assemblages of scheelite (a) and BSE images (b–f) of its grains analyzed with EDS (crosses) and LA-ICP-MS (circles, numbers of circles correspond to the table 1). (a) Scheelite (Sch) overgrown by magnetite (Mt) and chalcopyrite (Cp), reflected light; (b,c,d) relationships between scheelite 1 and 2, (d,e,f) wolframite inclusions in scheelite 1.

Table 1. Trace elements composition of scheelite, LA-ICP-MS data

	Na	Mn	Fe	Cu	Sr	Y	Mo	La	Ce	Pr	Nd	Sm	Eu	Gd	Tb	Dy	Ho	Er	Tm	Yb	Lu	U
SD %	3.9	6.2	39.2	3.2	5.5	5.7	7.5	5.1	5.5	4.9	3.7	7.5	4.8	6.1	4.6	7.4	5.1	2.4	3.9	3.9	2.8	4.2
AE%	3	8	15	3	1	2	6	1	3	3	7	5	1	3	1	5	1	4	6	4	7	1
Scheelite 1																						
1	371	4	30	1.14	284	627	7256	98	225	49	321	112	32	145	21	120	26	64	6.88	33.7	4.7	0.99
2	304	3	40	1.47	254	880	6541	99	235	56	375	143	42	207	30	168	38	98	9.89	44.7	6.8	1.07
3	470	6	38	0.16	279	755	6428	93	221	53	353	133	39	194	27	154	33	81	7.91	37.5	5.3	0.38
4	166	2	25	1.43	240	603	6226	75	187	43	304	109	34	161	22	127	27	66	6.24	31.4	4.0	0.25
6	2233	11	72	2.47	242	343	5582	49	121	28	189	70	20	93	12	73	15	38	3.92	15.1	2.3	0.00
7	2000	9	55	1.39	253	536	5557	72	168	37	247	85	28	123	18	109	23	59	6.01	29.0	4.3	0.35
9	2324	13	60	1.23	229	321	4808	41	100	24	164	59	20	84	12	70	15	36	3.49	17.6	2.3	0.00
10	1978	9	62	1.06	243	498	5584	50	122	29	206	83	26	123	17	102	21	53	5.55	24.7	3.4	0.24
Scheelite 2																						
5	152	1	23	0.49	207	443	3692	54	148	36	245	92	25	125	18	100	20	48	5	20	3	0.09

Note. SD- standard deviation, AE- analytical error.

The Mn and Na contents in scheelite 1 (4-13 and 371-2324 ppm, respectively) is higher than those in scheelite 2 (1 and 152 ppm, respectively). The Sr content is similar in the both generations (229-284 ppm in scheelite-1 and 207 ppm in scheelite-2). There is a significant negative correlation between Na and ΣREE (R = –0.9, Fig. 3a) and significant positive one between Mo and total REE (R = +0.82, Fig. 3b). Both 1 and 2 scheelite generations display similar chondrite-normalized REE distribution patterns (Fig. 3b): remarkably enriched in MREE to LREE (La_N/Sm_N= 0.39–0.56, mean 0.47) and MREE to HREE (Gd_N/Yb_N= 3.50–5.09, mean 4.07) and slightly enriched in LREE to MREE (La_N/Yb_N = 1.46–2.33, mean 1.80). All spectra are characterized by small negative Ce and Eu anomalies (Ce/Ce^* = 0.77–0.83 and Eu/Eu^* = 0.71–0.85).

The high Mo content in the both scheelite generations of the Zhaltyrkol occurrence is compared to that in scheelite from skarn deposits (Sciuba et al., 2016), whereas scheelite from greisen and orogenic gold deposits has much lower Mo concentrations. In addition, high Mo content was found in scheelite from the Yubileinoe porphyry Au deposit (Plotinskaya et al., 2016). High Mo content in scheelite suggests oxidizing conditions (Song et al., 2014 and references therein), which

is in a good agreement with the presence of hematite in assemblage with scheelite-1. Scheelite-2, being depleted in Mo, could precipitate at less oxidizing conditions.

The Na content in scheelite from the Mt. Carbine greisen-type is as low as 50 ppm (Krneta, 2011) while in the Yubileinoe scheelite it is below detection limits by LA-ICP-MS (Plotinskaya et al., 2016). Scheelite from the Kalgoorlie-Norseman orogenic gold deposits contains up to a few hundred ppm of Na (Ghaderi et al., 1999). The authors of the cited papers conclude that scheelite from reported deposits crystallized from fluids with low (Mt. Carbine and Yubileinoe) and high (Kalgoorlie-Norseman) Na activity. Taking into account extremely high content of Na in the Zhaltyrkol scheelite, we conclude that this mineral was deposited from fluid with high Na activity. In addition, scheelite from above greisens and orogenic gold is characterized by a positive correlation between Na and total REE that corresponds the following isomorphic substitution $2Ca^{2+} \rightarrow REE^{3+} + Na^+$. Negative correlation between Na and total REE in the Zhaltyrkol scheelite requires additional examination.
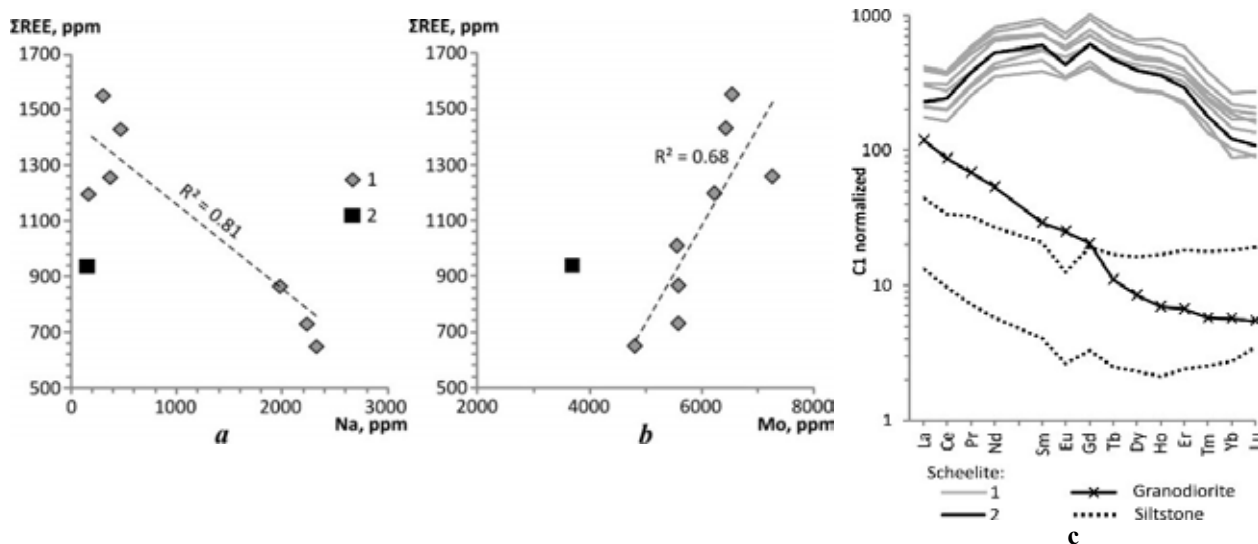
Fig. 3. REE vs. Na (a), REE vs. Mo (b) and C1 normalized (Sun, McDonough, 1989) REE spectra of scheelite and countr rocks(c)

The Zhaltyrkol granodiorite is strongly enriched in LREE and depleted in HREE (La_N/Yb_N= 20.92) without Eu anomaly. Altered tuffaceous siltstone displays flat REE distribution pattern with weak enrichement in LREE (La_N/Yb_N= 2.46–4.83) and weak negative Eu anomaly (Eu/Eu* = 0.63-0.72). As seen from Fig. 3c, REE distribution patterns in scheelite are drastically different from those in igneous and altered volcanic sedimentary rock. Therefore, the scheelite composition was strongly fluid-controlled. However, the inheritance of the negative Eu anomaly from the host tuffaceous siltstone cannot be ruled out.

Thus, scheelite from the Zhaltyrkol occurrence was formed from fluid with high Na activity under oxidizing conditions. The chemical composition of scheelite was controlled by fluid rather than by igneous rocks.

References:

EU Commission 2014 Critical Raw Materials for the EU. Report of the Ad-Hoc Working Group on Defining Critical Raw Materials (Brussels: EU Commission).

Ghaderi M., Palin J.M., Campbell I.H., Sylvester P.J. (1999) Rare Earth Element Systematics in Scheelite from Hydrotherma Gold Deposits in the Kalgoorlie-Norseman Region, Western Australia. Econ Geol 94: 423-438.

Grabezhev A.I., Belgorodskii E.A. Ore-Bearing Granitoids and Metasomatites of Copper Porphyry Deposits. Nauka, Yekaterinburg, 1992. (in Russian).

Krneta S. (2011) Mineral paragenesis and alteration of the Mt. Carbine tungsten deposit from north Queensland. Late stage evolution of S-type granite. Honours thesis, Adelaide University

Plotinskaya O.Y., Baksheev I.A., Minervina E.A. (2016) REE distribution in scheelite from the Yubileinoe Au-porphyry deposit (S. Urals): LA-ICP-MS data. In: Proc. of intern. conf. to the 300th anniversary of the Fersman Mineralogical Museum. Moscow, pp 138-139. (In Russian).

Plotinskaya O.Y., Grabezhev A.I., Tessalina S., Seltmann R., Groznova E.O., Abramov S.S. (2017) Porphyry deposits of the Urals: geological framework and metallogeny. Ore Geol Rev 85. doi: 10.1016/j.oregeorev.2016.07.002

Samygin S.G., Burtman V.S. (2009) Tectonics of the Ural Paleozoides in comparison with the Tien Shan. Geotectonics 43: 133-151.

Sciuba M., Beaudoin G., Hout F. (2016) Texture, cathodoluminescence, and trace elements compositionof scheelite, indicator of orogenic gold deposits
https://consorem.uqac.ca/presentation_pub/forum_techno_2016/presentations_forumt_016/13H50_SCIUBA_DIVEX_2 016.pdf (accessed 13.02.2017).

Sillitoe R.H. (2010) Porphyry copper systems. Econ. Geol 105: 3−41.

Song G., Qin K., Li G., Evans N.J., Chen L. (2014) Scheelite elemental and isotopic signatures: implications for the genesis of skarn-type W-Mo deposits in the Chizhou area, Anhui Province, Eastern China. Am. Mineral 99: 303-317.

Sun S.S., McDonough W.F. (1989) Chemical and isotopic systematics of oceanic basalts: implications for mantle compositions and processes. Magmatism in the Ocean Basins. 42: 313-345.

SPINELIDE FROM THE XENOLITHS OF MEGACRYSTALLINE PERIDOTITES OF UDACHNAYA KIMBERLITE PIPE (YAKUTIA)

Pokhilenko L.N.

Institute of Geology and Mineralogy, Siberian Branch of the Russian Academy of Sciences, Novosibirsk, Russia, lu@igm.nsc.ru

Megacrystalline harzburgite-dunites (MHD) – a very rare group of the most depleted peridotites encountered in individual kimberlite pipes. The rocks are composed of nearly pure olivine (90% and more) - one, rarely 2-3 megacrystals. Less than 10% of rocks make up a Cr-pyrope garnet ± enstatite ± chromite. Chemical composition of the minerals is identical to that of mineral inclusions in diamonds (Pokhilenko et al., 2014). MHD from its formation and to brining to the surface by kimberlite repeatedly subjected to metasomatic effects. Studying of variations of a chemical composition of different generations of spinelide from MHD, their relationships with other minerals of the rock gave the chance to track the difficult transformations taking place to rocks since their formation and before carrying out on a surface by kimberlite.

MHD exposed to deep oxidized alumina and potassium-rich fluids. One result of this influence was the growth rims around garnet: the rim between garnet and surrounded olivine (rim1); continuous or interrupted phlogopite bands situated around the rim1 sometimes together with enlarged rim1 minerals of the same name (rim2); phlogopite-spinel-magnetite rim located between the garnet and adjacent kimerlite (rim3). Spinelide from the rims of garnet is the reaction product of the host garnet, so the content of chromium and other components in it is largely determined by the number of components in the rock forming pyrope.
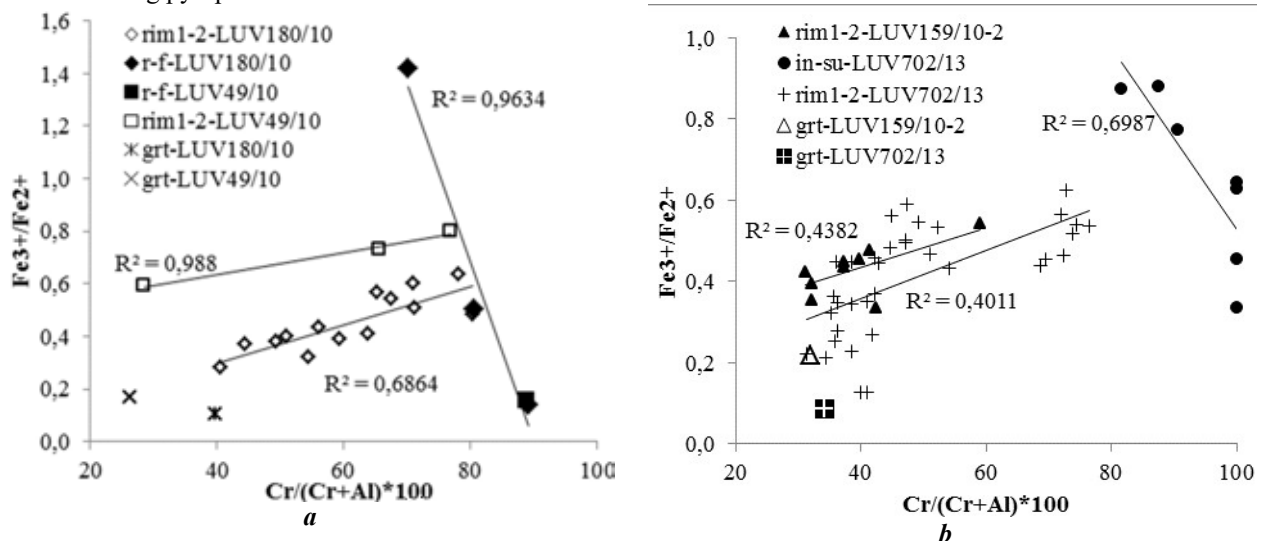
Fig. 1. Diagram Cr#-Fe3+/Fe2+ for different kinds of spinelides of megacrystalline peridotites from Udachnaya pipe: a – Chromite&Garnet-bearing megacrystalline peridotites, b - Garnet-bearing megacrystalline peridotites. R-f – rock forming chromite, rim 1-2 – spinelide from the rims around garnet, grt – garnet, in su – spinelide-inclusion in sulphide, R2 - correlation coefficient.

Cr# and Fe^{3+}/Fe^{2+} are indicators of the depth and redox mantle conditions. According to Fig. 1a, falling of the chrome content at sharp increase of a role Fe^{3+} in rock forming chromite from the grain center to the rim testifies to increase in potential of oxygen during its growth up to formation of a fringing from magnetite (see also Table 1, 8C-RR). Conversion to minals shows the decrease in the amount of chromite ($Fe^{2+}Cr_2O_4$) and the growing role of ferrite ($MgFe^{3+}_2O_4$) (fig. 2a). Chrome-spinel from the rims around garnet, on the contrary, shows a positive correlation (fig. 1), i.e., increasing Fe^{3+}/Fe^2 with increasing chromium component. The highest values of chrome from the rims are observed in the central parts of shpinelides from rim2. Then there is a decrease of the component to minimum value in spinel from rim1 (however not less than chrome content in pyrope-host). As can be seen from the Fig. 2 (c, e, f), the predominant minal of center of chrome-spinel from rim2 is chromite $Fe^{2+}Cr_2O_4$, while spinel from rim1 composed mainly by Al-spinel $MgAl_2O_4$.

Table 1. Representative compositions of rock forming spinelides of megacrystalline peridotites from Udachnaya pipe. 1 – LUV2/09, 2 – LUV26/10-1, 3 – LUV137/01-1, 4 – LUV164/09, 5 – LUV43/01, 6 – LUV521/11, 7 – LUV588/11, 8 – LUV180/10: C –center, R – rim, CR – between C and R, RR – edge of a rim, Cr#=Cr/(Cr+Al)*100.

Sample	1	2	3	4	5	6	7	8C	8CR	8R	8RR
TiO_2	0.25	0.32	0.38	0.11	0.36	0.30	0.11	0.92	4.46	13.4	3.55
Al_2O_3	5.06	13.30	5.09	8.02	4.13	10.28	4.89	5.21	8.03	6.94	0
Cr_2O_3	65.1	47.4	61.0	63.2	64.2	59.5	65.3	63.7	49.5	24.4	1.0
FeO	18.1	26.8	22.8	15.4	17.2	18.3	18.0	19.8	26.7	42.2	93.1
MnO	0.27	0.28	0.24	0.24	0.28	0.24	0.28	0	0	0	1.33
MgO	11.5	11.5	10.7	13.0	11.9	11.4	11.4	10.4	11.1	13.1	1.0
Total	100	99.6	100	99.9	98.1	100	100	100	99.7	100	100
Ti	0.006	0.008	0.009	0.003	0.009	0.007	0.003	0.023	0.110	0.319	0.095
Al	0.198	0.503	0.200	0.308	0.165	0.395	0.192	0.206	0.310	0.259	0.000
Cr	1.712	1.202	1.611	1.629	1.723	1.536	1.723	1.690	1.281	0.610	0.029
Fe tot	0.503	0.720	0.637	0.419	0.489	0.499	0.502	0.556	0.730	1.115	2.762
Mn	0.008	0.007	0.007	0.006	0.008	0.007	0.008	0.000	0.000	0.000	0.040
Mg	0.568	0.552	0.530	0.631	0.601	0.552	0.568	0.518	0.542	0.618	0.051
Total	2.996	2.992	2.994	2.996	2.995	2.996	2.996	2.994	2.972	2.920	2.976
Fe^{2+}	0.423	0.436	0.461	0.360	0.390	0.441	0.422	0.487	0.485	0.461	0.933
Fe^{3+}	0.080	0.284	0.175	0.059	0.099	0.058	0.080	0.069	0.245	0.653	1.829
Fe^{3+}/Fe^{2+}	0.190	0.651	0.380	0.164	0.253	0.131	0.191	0.141	0.505	1.418	1.961
Cr#	89.6	70.5	89.0	84.1	91.3	79.5	90.0	89.1	80.5	70.2	

Spinelide of microcracks is apparently rock forming chromite of the later generation, as can be evidenced by the high chromium content in the center of the grain (Table 2, fig. 2d) and small grain sizes. Small chromite inclusions in olivine were weakened area through which the crack passed in the period preceding the capture of the rock by kimberlite melt. Probably during the growth of this spinelide the rock has been exposed to some deep mantle fluids, as titanium (ilmenite minal) was found in its composition. Strongly oxidized edge part of the grain was formed under the influence of kimberlite melt; it shows enriching with ferrite component (fig. 2d). The difference in the composition of spinelide inclusions from the central and marginal zones of sulfide appears to reduce the chromite minal with an increase of ilmenite minal (fig. 2b). Being well conserved in the center of primary sulfide, spinelide has not undergone a deep impact of metasomatic fluids: it represented almost pure chromite. Fluids affecting chromite later generation of microcracks, yielding in titanium, have left their mark on the composition of the spinelide inclusions from the edge zones of sulphide (fig. 2d).
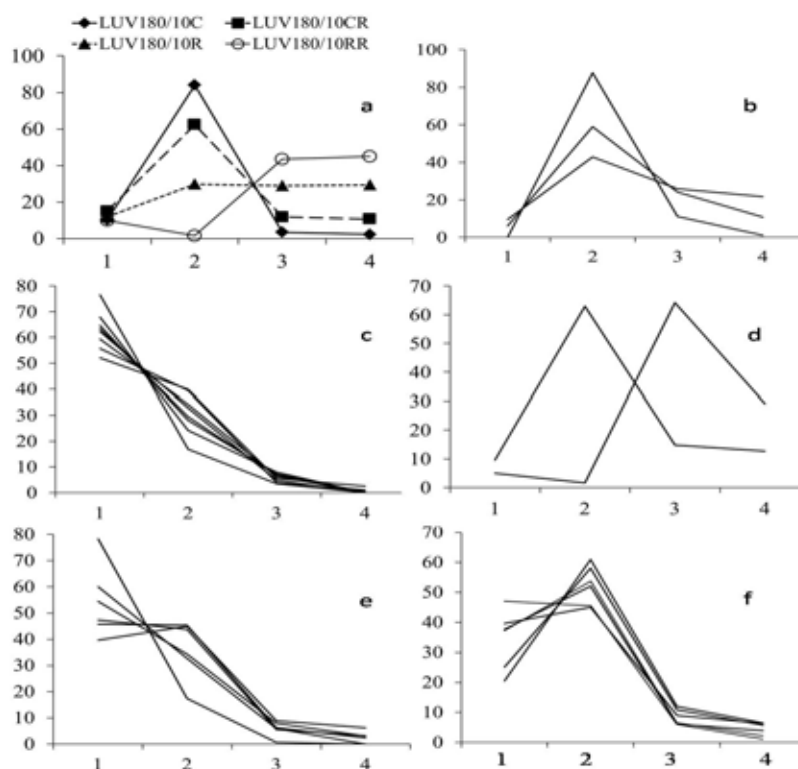
Fig. 2. Minals of different kinds of spinelides of megacrystalline peridotites from Udachnaya pipe: a – rock forming chromite from LUV180/10, b - spinelide-inclusions in sulphide from LUV702/13, c - spinelides from rim1, d – zonal spinelide from the microcrack, e - the edge parts of spinelides from rim2, f - the central parts of spinelides from rim2. 1 – spinel $MgAl_2O_4$, 2 – chromite $Fe^{2+}Cr_2O_4$, 3 - ferrite $MgFe^{3+}_2O_4$, 4 – ilmenite $FeTiO_3$. C – center, R – rim, CR – between C&R, RR – edge of a rim.

High chrome of the central parts of some spinelides from rim2 and chromite inclusions in sulfide indicate a high activity of Cr in metasomatic fluid on one of the stages of megacrystalline rocks transformation.The compositional variations in spinelides of the rims around garnet, their small sizes, zonality and nonequilibrium suggest the abrupt change in the PT and redox conditions which took place immediately before the explosion and rocks rise to the surface.

Table 2. Representative compositions of the spinelides of megacrystalline peridotites from Udachnaya pipe. Su – sulphide, C –center, R – rim, , RR –edge of a rim, r-f – rock forming spinelide, rim 1-2 – spinelide from the rims around garnet, inc-in-grt – spinelide-inclusion in garnet, Cr#=Cr/(Cr+Al)*100.

Sample	LUV702/13					LUV49/10			LUV71/10
Location	CHR in su		microcrack in olivine			r-f	rim1	rim2	inc-in-grt
			C	R	RR				
TiO_2	0.44	9.05	5.46	12.72	3.58	0.08	0.00	1.05	2.51
Al_2O_3	0	5.15	5.08	2.78	0	5.64	37.77	26.34	14.55
Cr_2O_3	64.08	34.04	50.67	1.3	0	65.78	26.92	38.84	46.56
FeO	23.52	41.7	27.18	72.45	91.15	16.46	14.52	17.90	22.36
MnO		1.42		1.69	0.6	0.212	0.58	0.57	0.235
MgO	10.48	7.78	11.42	8.65	4.27	12.21	18.23	15.13	12.86
Total	98.52	99.14	99.81	99.59	99.60	100.38	98.02	99.81	99.06
Ti	0.011	0.229	0.135	0.315	0.093	0.002	0.005	0.025	0.060
Al	0.000	0.204	0.198	0.108	0.000	0.219	1.260	0.899	0.544
Cr	1.760	0.906	1.322	0.034	0.000	1.716	0.605	0.935	1.168
Fe tot	0.683	1.173	0.750	1.994	2.645	0.454	0.345	0.454	0.593
Mn	0.000	0.040	0.000	0.047	0.018	0.006	0.014	0.014	0.006
Mg	0.542	0.390	0.561	0.424	0.221	0.600	0.770	0.666	0.608
Total	2.997	2.943	2.966	2.921	2.977	2.997	2.998	2.996	2.980
Fe^{2+}	0.460	0.626	0.472	0.607	0.784	0.392	0.217	0.325	0.396
Fe^{3+}	0.223	0.547	0.278	1.386	1.860	0.062	0.127	0.129	0.197
Fe^{3+}/Fe^{2+}	0.485	0.873	0.588	2.284	2.371	0.158	0.593	0.381	0.498
Cr#	100.0	81.6	87.0	23.9		88.7	32.4	51.0	68.2

Kimberlite effects on MHD manifested in the crystallization of a number of kimberlite minerals in the microcracks and intergranular space, formation of magnetite rims on chrome spinels in microcracks, as well as in the rim3 formation as a result of reaction of kimberlite melt with adjacent garnet or, what is the most likely, transformation of the rim1-2 by kimberlite magma.

References:

Pokhilenko L. N., Mal'kovets V. G., Kuz'min D. V., and Pokhilenko N. P. (2014). New Data on the Mineralogy of Megacrystalline Pyrope Peridotite from the Udachnaya Kimberlite Pipe, Siberian Craton, Yakutian Diamondiferous Province. Doklady Earth Science 454 (2):179-184.

KIMBERLITES AND CARBONATITES OF THE SNAP LAKE DYKE SYSTEM, SLAVE CRATON, CANADA: UNIQUE TYPE OF PRIMARY ASSOCIATION OF ULTRA-DEEP ORIGIN

Pokhilenko N.P., Agashev A.M., Pokhilenko L.N., Vavilov M.A.

[1]Institute of Geology and Mineralogy, Siberian Branch of the Russian Academy of Sciences, Novosibirsk, Russia, chief@igm.nsc.ru

Highly diamondiferous kimberlite dyke system located in the Snap Lake (SL) area, South Slave Craton, NWT, Canada, was discovered in 1997. Initial studies of the unique kimberlite-carbonatite association of the SL dyke system provided a number of important results suggested abnormally thick lithosphere beneath the SL area (Pokhilenko et al., 2000, 2004), and unusual character of the SL kimberlite-carbonatite rocks mantle sources (Agashev et al., 2008). These results together with unusual geometry of the kimberlite bodies suggest that the SL dyke system represent a new type of large primary diamond deposit. The SL kimberlite dyke system occupies an area of approximately 4 x 5.5 km, and main part of which is located beneath the Snap Lake. This system is presented by several gently (8-25°) dipping dykes composed mostly by massive kimberlite of hypabyssal type. The main NW dyke gently (9-13°) dips to E-NE and its upper part was found beneath the thin cover of glacial deposits on small peninsula situated in the eastern corner of Snap Lake. NW dyke averages nearly 3 meters in thickness with individual drill intersections up to 16 metres. The SL dyke system mainly comprises massive hypabissal kimberlite; kimberlite breccias and carbonatites are minor components. The emplacement age of this dyke system has been estimated near 530 Ma (Agashev et al., 2008). Over 80% of studied sections of SL dyke system is composed by massive kimberlite of macrocrystic texture (macrocrystic hypabissal kimberlite, Mitchell, 1986), and much less by kimberlites of aphyric texture with very low amount of xenogenic material, carbonate enriched

kimberlites and their breccias and carbonatites. This association looks different from cases of similar type described before (Dawson, 1966). Macrocrysts of massive kimberlite are presented by serpentine and carbonate pseudomorphs after olivine (2-30 mm, mostly 3-15 mm in size) in variable amounts: from 3-5 up to 40 vol.%. The groundmass minerals are presented by serpentine, phlogopite (often significantly replaced by chlorite), carbonates and opaque minerals. Phlogopite is important component of the groundmass and its amount varies from 1-2 up to 20-25 vol.% of groundmass; so significant part of the SL kimberlites belongs to the mica enriched varieties. There are significant variations of other mineral contents in the studied kimberlites groundmass. Thus, amount of opaque minerals presented mainly by spinelides of variable composition can reach sometimes 15-20 vol.% of groundmass, although in some samples they are minor components of the rock groundmass (<0.1 vol.%). Rounded xenoliths of low crust and upper mantle rocks are very rare. Carbonate-rich kimberlites and carbonatites despite of their limited distribution in the studied dyke system are characterized by wide variations of their mineral composition and variable textural-structural peculiarities. Practically complete absence of porphyric grains is the common feature of carbonate-rich kimberlites and carbonatites. Kimberlite with fresh <u>olivine</u> was drilled in the northern part of the SL dyke system at depth over 1.5 km where one thin intersection contains unaltered olivine microphenocrysts less than 0.1mm in size, and some of them are zoned as follows: Mg# (normal): 92.2 to 90.1 (Fig. 1); Mg# (reversed): 87.5 to 91.4; Cr2O3: <0.01 to 0.16 wt.%; MnO: 0.10 to 0.23 wt.%; NiO (normal): 0.36 to 0.07 wt.% and (reversed): 0.19 to 0.35 wt.%; CaO (normal): 0.02 to 0.10 wt.%, (reversed) 0.05 to 0.02 wt.% and (complex): 0.04-0.02-0.05 wt.%), and these features are comparable to ones observed for olivine from polymict breccia xenoliths (Pokhilenko, 2009). In relatively fresh hypabissal kimberlite, 78 analyses of olivine macrocrysts demonstrated a range in Mg# between 87.5 and 93.4 with a mean of 91.2 (Fig. 1). NiO conent ranges from 0.18 to 0.42 wt.% with a mean of 0.35 wt.%.
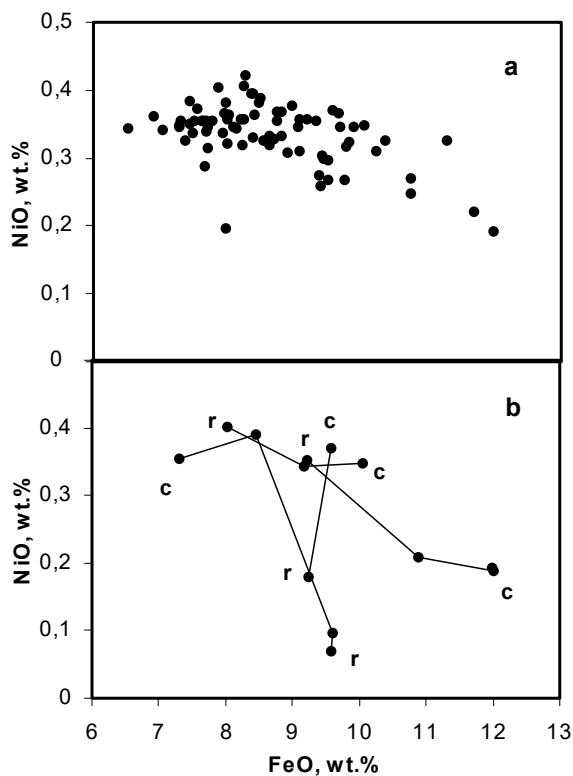
Fig. 1: Plots NiO vs FeO for olivines of SKL kimberlite (a) and for zoned olivine microphenocrysts of the SKL kimberlite groundmass (b).
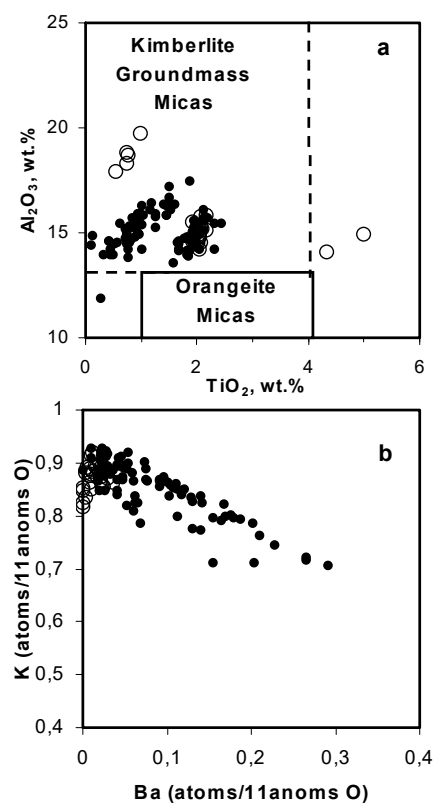
Fig. 2: Plots Al2O3 vs TiO2 (a) and K vs Ba (atomic) (b) for SKL fresh kimberlite groundmass.

<u>Carbonates</u> in the groundmass of fresh kimberlite are mostly dolomite in which FeO content (1.0 to 6.9 wt.%) is negatively correlated with SrO content (0.07-0.94 wt.%), and calcite (Table 2) that contain admixed SrO (to 5.7 wt.%) and BaO (to 1.6 wt.%). Some carbonate grains are Ca-Sr carbonates with an SrO content of up to 23.8 wt.% (Table 2). Rare barite (with minor FeO) grains also occur in the groundmass (Table 1, sample 5). <u>Phlogopites</u> of the SL kimberlite groundmass are characterized by variations in F content (<0.10 to 1.46 wt.%); TiO2 content (0.32 to 4.99 wt.%, but mainly between 0.8 and 2.0 wt.%); Cr2O3 content (0.01 to 2.85 wt.%), and extremely wide – in BaO content (0.1 to 9.3 wt.%). A wide variation of Al2O3 content (11.8 to 19.6 wt.%) is sown the Al2O3 vs TiO2 plot (Fig. 2a), where is visible a presence of at least three separate clusters inside the kimberlite groundmass micas field (field position after R.H.Mitchell, 1995). Of special interest is absence of the fresh kimberlite groundmass micas (open circles) in central group of flogopites with moderate Al2O3 content and relatively low TiO2 (Fig. 2a). These phlogopites are characterized by minimal Ba and maximal K contents as well if compare with compositions of groundmass phlogopites of the main part of SL kimberlites (Fig. 2b). <u>Opaque minerals</u> of the SL kimberlite groundmass are presented mainly spinelides of

two groups: Cr-spinels with less than 30 mol.% magnetite + ulvospinel, and Al-Cr-Mg-Ti magnetites of relatively uniform composition. Rutile and sulphides round out the opaque suite of minerals in kimberlite groundmass.

<u>Indicator mineral</u> abundance in this kimberlite is low. Indicator minerals comprise: a) garnets: content is ~150-200g/t; ~ 96% of them are Cr-pyropes with extremely wide range of Cr_2O_3 content (0.1 – 17.0 wt.%), but relatively low proportion of G10 garnets (Pokhilenko et al., 2000), and ~ 4% - E-type garnets; b) chromites: content ~ 100-150 g/t, and high proportion of high-Cr (>62 wt.% Cr_2O_3) and low-Ti (<0.7 wt.% TiO_2) varieties (25-27%). Cr-diopside grains are very rare. No grains of Mg-ilmenite were found within the heavy mineral fraction from large (~500 kg) initial samples.
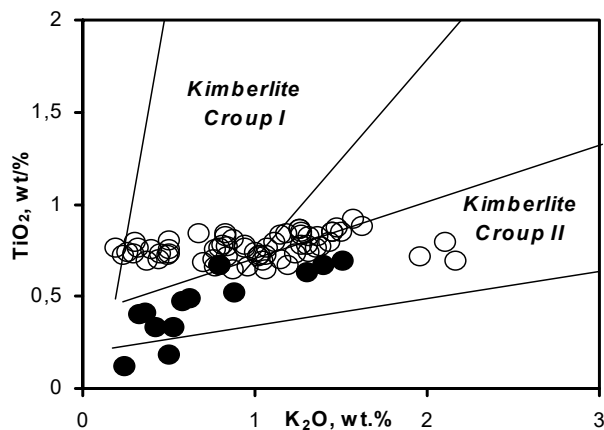
Fig. 3: Plot TiO_2 vs K_2O for SL kimberlite composition (solid dots – carbonatites and carbonate enriched kimberlites).

The SL kimberlites show arrange of geochemical characteristics that differentiate them from both Group 1 and Group 2 kimberlites (Agashev et al., 2008). These kimberlites show REE distribution and isotopic characteristics similar to Group 1 ones. However, abundances of the most incompatible elements (Pb, Rb, La, Ce) are intermediate between Group 1 and 2 kimberlites and Ba and Th abundances more closely resemble of Group 2 kimberlites. Relatively to SKL kimberlites, trace element abundances of carbonatites associated with these kimberlites are depleted in Cs, Rb, K, Ta, Ti and enriched in U, Sr, P, Zr, and Hf, as well as in MREEs and HREEs. Trace element portioning between kimberlite and carbonatite of SL dyke system contrast with experimental portioning data within immiscible carbonate and silicate liquids where the latter shows preferential portioning of HREE, Y and Zr into silicate liquid, whereas Rb, K, and Ba are preferentially enriched in the carbonate-rich liquid. The most likely mantle source for the SL kimberlite-carbonatite association is slightly carbonated (0.5-0.6 vol.% of carbonate) depleted Cr-pyrope lherzolite. Partial melting (0.5-2.5 %) of these rocks at pressures over 70 kbar can produce the range of kimberlite-carbonatite melts observed in this association. The Nb/Ta ratio in SL carbonatites ranges from slightly superchondritic (Nb/Ta = 22 at SiO_2 = 17 wt.%) to highly superchondritic (Nb/Ta = 81 at SiO_2 = 3.7 wt.%). By contrast, this ratio in SL kimberlites scatters around the chondritic value of 18. This suggests that the initial partial melt of the carbonated lherzolite source was carbonatic and possessed superchondritic Nb/Ta and Zr/Hf ratios. Some of petrological and petrochemical characteristics described above are also of intermediate between ones for kimberlites of Group 1 and 2. For example, combined variations of K_2O and TiO_2 contents are close to ones for kimberlites of Group 2 (Fig. 3), and mica enriched texture of groundmass of significant part of the SL kimberlites are also similar to ones for kimberlites of Group 2, but: a) SL kimberlite groundmass mica composition is different from "orangeite" micas (Mitchell, 1995)and close to ones for Group 1 kimberlite (Fig. 2); b) many other petrochemical and petrographic features of SL kimberlites are close for kimberlites of Group 1. These results demonstrate some of the unique characteristics of the SL kimberlite- carbonatite association and allow us to propose its origin combined to initial stages of partial melting of slightly carbonated depleted Cr-pyrope lherzolite at P-T conditions of ultra-deep lithosphere close to way described by (Dalton, Presnall, 1998).

Table 1. Representative analyses of SKL kimberlites (1-5, 7) and carbonatite (6).

Sample	1	2	3	4	5	6	7
SiO_2	35.6	34.8	33.4	26.8	23.6	13.5	20.3
TiO_2	0.76	0.88	0.69	0.52	0.33	0.67	0.18
Al_2O_3	3.14	3.60	3.43	2.06	1.60	3.19	1.84
Fe_2O_3	8.64	8.95	8.05	6.09	6.30	9.58	5.48
MnO	0.15	0.16	0.16	0.17	0.22	0.25	0.16
MgO	34.7	30.8	32.1	25.2	20.3	21.1	21.2
CaO	1.80	3.87	6.05	12.4	20.6	16.5	20.7
Na_2O	0.01	0.01	0.01	0.01	0.01	0.01	0.01
K_2O	1.07	1.62	2.16	0.88	0.42	0.79	0.50
P_2O_5	0.33	0.80	0.56	0.20	1.49	0.36	6.74
LOI	13.7	14.5	13.4	25.7	24.9	34.9	21.9
Total	99.9	100.0	100.1	100.0	99.8	100.8	99.0

Table 2. Representative analyses of carbonates from the SKL kimberlite groundmass.

Sample	1	2	3	4	5
FeO	1.60	6.15	0.63	0.59	0.17
MnO	0.58	0.29	0.50	0.21	0.01
MgO	21.2	19.6	0.32	1.62	0.03
CaO	28.6	30.5	55.7	28.3	0.01
BaO	0.01	0.01	0.01	5.51	62.0
SrO	0.94	0.18	0.91	23.8	0.03
Total	52.9	56.7	58.1	60.0	62.2

International Conference on Magmatism of the Earth and Related Strategic Metal Deposits

References:

Agashev A., Pokhilenko N., Takazawa E., McDonald J., Vavilov M., Watanabe, T., Sobolev N. (2008) Primary melting sequence of a deep (> 250 km) lithospheric mantle as recorded in the geochemistry of kimberlite–carbonatite assemblages, Snap Lake dyke system, Canada. Chemical Geology 255: 317-328.

Dalton J.A., Presnall D.C. (1998) Carbonatitic melts along the solidus of model lherzolite in the system CaO-MgO-Al2O3-SiO2-CO2 from 3 to 7 GPa. Contributions to Mineralogy and Petrology 131: 123-135.

Dawson J.B., (1966) The kimberlite–carbonatite relationship. In: Naidu, P.R.J. (ed) Papers and Proceedings of the 4th General Meetings, Intl. Mineral. Assoc., IMA Volume. Mineralogical Society of India, pp. 1–4.

Mitchell R.H. (1986) Kimberlites: Mineralogy, Geochemistry, and Petrology. Plenum Press, New York.

Mitchell R.H. (1995) Kimberlites, Orangeites, and Related Rocks. Plenum Press, New York and London.

Pokhilenko N.P., Sobolev N.V., Tcherny S.D., Mityukhin S.I., and Yanygin Yu.T. (2000) Pyropes and chromites from kimberlites of Nakyn Field (Yakutia) and Snap Lake area (Slave Province, Canada): evidence of anomalous lithosphere structure. Doklady Akademii Nauk, 372 (3): 356-360 (in Russian).

Pokhilenko N., SobolevN., Reutsky V., Hall A., Taylor L., (2004) Crystalline inclusions and C isotope ratios in diamonds from the Snap Lake/King Lake kimberlite dyke system: evidence of ultradeep and enriched lithospheric mantle. Lithos 77: 57-67.

Pokhilenko N. (2009) Polymict breccia xenoliths: Evidence for the complex character of kimberlite formation. Lithos 112: 934-941.

Plume complexes of the Urals and their metallogenic potential

Puchkov V.N.

Institution of Russian Academy of Sciences Institute of geology of the Ufimian scientific centre, Ufa, Russia

The question of the role of plumes in metallogeny of the Urals was raised only recently (Puchkov, 2010, 2016a) and still needs a discussion, because the very idea of an importance of plume processes in the Urals is still in the process of confirmation (Puchkov, 2016b).

There are eight magmatic complexes in the Urals that may be regarded (or suspected) as plume manifestations (Figs.1, 2).

1. *Navysh episode.* In the Southern Urals near the base of the Lower Riphean (Uppermost Paleoproterozoic), covering the crystalline Taratash complex there are volcanic deposits of the Navysh Subformation, represented mostly by trachybasalts. The age of the unit was determined as 1752±11 Ma. (All the dates in the paper are obtained from zircons, U−Pb SHRIMP method if not indicated otherwise). It is shown that volcanic rocks of the age range of 1750−1780 Ma are developed in some other places of Baltica, and also in the Northern Africa, Siberia, Laurentia, parts of the Nuna supercontinent of that time.

2. *Mashak episode.* Higher up the section of the Riphean, at the Middle Riphean (Mid−Mesoproterozoic) base, rhyolites of the Mashak Formation were dated by SHRIMP and CA-IDTIMS U−Pb methods in three isotopic laboratories as 1380−1385 Ma. The same ages have also basalts, rapakivi granites, layered gabbro (Kusa−Kopan ntrusion), carbonatites (Sibirka) and dolerite dykes and sills that widely developed in the Southern Urals and are encountered in boreholes of East European platform; magmatic rocks of the same age are traced to Greenland, Laurentia and Siberian cratons and represent the beginning of the Nuna supercontinent break-up.

3. *Igonino episode.* In the Tirlyan syncline in the east of the Bashkirian meganticlinorium (BMA) there is a volcanic Igonino Formation. The study of zircons from this formation gave two pulses: 707.0±2.3 Ma and 732.1±1.7 Ma Comparable ages have nearby granite massifs Barangulovo and Mazara, layered gabbro-ultramafic Sarana intrusion in the Middle Urals, and also Misaelga ferrogabbrodiabase-picrite differentiated intrusions in the Taratash uplift (726 ± 13 Ma, Rb-Sr method). In the 1-Kipchak borehole, on the East European platform, lava flows are dated as 730 Ma (Rb−Sr method). All these magmatic rocks may belong to a hypothetical LIP, developed on a fragment of breaking-up Rodinia supercontinent (Kalahari+Laurentia+North China+Amasonia+Western Australia+Baltica). 4. *Kiryabinka episode* is represented by Kiryabinka layered peridotite-pyroxenite-gabbro intrusion, situated at the North-Eastern margin of the

BMA (680±3.4 Ma). The even-aged magmatic rocks are found toward South from this point in the Bashkirian meganticlinorium (Krivaya Luka) and toward North, in the Middle Urals − Schegrovitsk trachybasalt, Zhuravlik wehrlite-gabbro-granodiorite and Troitsk granitoid formations (Petrov, 2006). In the East European platform, comparable ages belong to basites of the Onega graben. 5. *Kidryas episode* is represented by subalkaline volcanics connected with a rift process that started at ca. 490 Ma, and led to oceanic spreading and formation of the Paleouralian ocean. This accompanied the formation of the Baltica passive margin that can be attributed to a plume-connected volcanic type. 6. *Ushat episode* was marked by an eruption of trachytes in the Bashkirian meganticlinorium, and was dated between 435 and 455 Ma. It can be correlated with the early, principal stage of development of the Vishnevogorsk plume-related carbonatite complex. 7. *Devonian magmatic series* consists probably of several episodes, and the Frasnian is the strongest one. The Middle-Upper Devonian dolerite and basalt complex is traced along the western slope of the Urals to Pay−Khoy and Novaya Zemlya (Puchkov et al., 2016). The rocks match excellently with the Middle-Upper Devonian volcano-intrusive

complexes of the East European platform, including flood basalts, dolerite dykes, alkaline and carbonatite intrusions and kimberlites, and belong to the marginal part of the LIP called Kola−Dnieper.
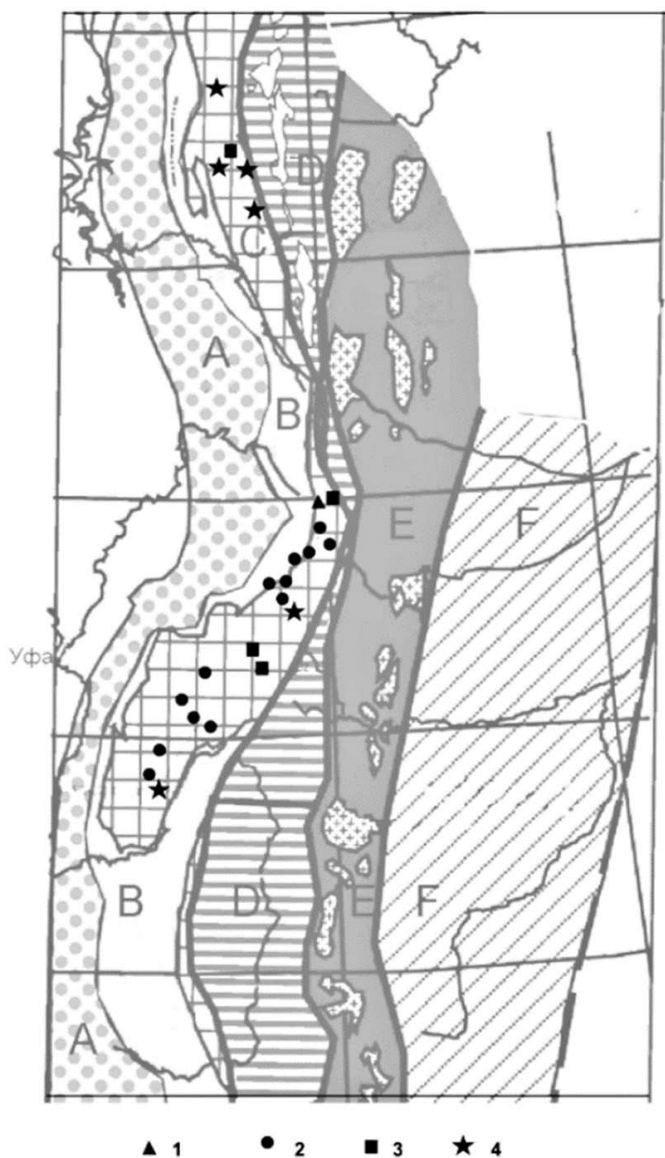
Fig. 1. Riphean (Meso− and Neoproterozoic magmatic complexes probably of plume nature in the Central Uralian zone of the Southern and Middle Urals. In grey colour is shown a scheme of tectonic zonation of the Urals (after fig.11 in Puchkov, 2010): A− Preuralian foredeep, B – West Uralian folded zone, C− Central Uralian zone, D− Tagil-Magnitogorsk zone, E− East Uralian zone, F−Transuralian zone. The symbols under the scheme: 1−volcanics of the Navysh event of the Lower Riphean, ~1750 Ma, 2− Magmatic complexes of the Middle Riphean, 1380−1385Ma (Mashak event); 3 – magmatic complexes of the Igonino event (Terminal Riphean), 710−740 Ma, 4 – magmatic complexes of the Kiryabinka event, 670−680 Ma (Terminal Riphean).
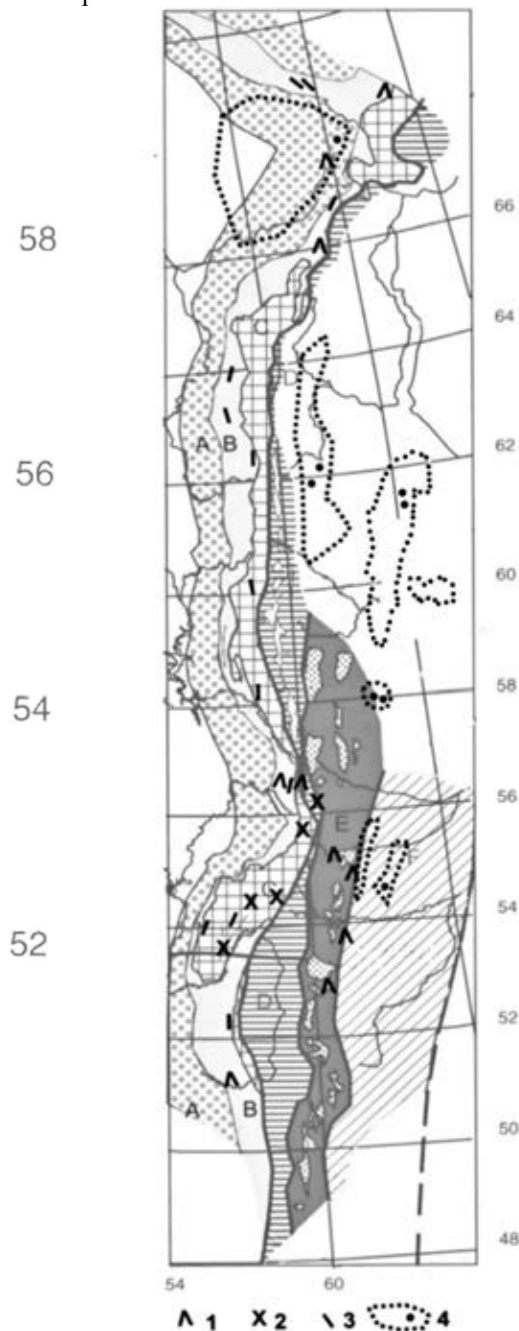
Fig. 2. Paleozoic and Traissic magmatic complexes probably of plume nature in the Urals and Pai−Khoy. A scheme of tectonic zonation of the Urals is shown in grey (after Puchkov, 2010, see Fig.1). Symbols under the scheme: 1. Kidryas complex: Early and Middle Ordovician volcanics of rift type, corresponding to passive continental margin of a volcanic type; 2 – Ushat complex: Ordovician−Silurian volcanics and carbonatites; 3− Devonian dykes and volcanics; 4 – areas of development of flood basalts and sampling points of isotope- and pollen-dated volcanics in them.

8. *Uralo−Siberian LIP and superplume* are represented by Lower Triassic flood basalts, dolerite and rhyolite dikes traced from the easternmost parts of the Southern and Middle Urals to the western margin of the Polar Urals. It became evident that they belong to the Uralo-Siberian LIP, developed above the African" superswell (Reichow et al., 2009).

The history of geodynamic development of the Urals can be subdivided into several major stages, each characterized by a specific style of processes and their own structural patterns. The magmatic, metamorphic and sedimentary processes and complexes of each stage (and substage) typically overlie and overprint the previous ones. The major stages are as follows (Puchkov, 2010): a) The Archean to Paleoproterozoic (Pre-Timanide) crystalline basement of the East European platform under the western part of the Southern and Middle Urals; b) The Meso- to Neoproterozoic complexes of the Timanides, with their external part developed mainly as a deep and wide sedimentary basin as a result of several successive mantleplume/rifting events prior to final late Precambrian collision and orogeny (developed at its best in the BMA , and their internal part, which inherited oceanic, microcontinental, subductional and accretionary complexes of a complete Wilson Cycle; c) The Cambrian to Early Jurassic Uralides, primarily products of the Paleouralian Ocean, which was opened as a result of the Late Cambrian to Ordovician epicontinental plume−accompanied rifting and subsequent oceanic spreading and closed through subduction in the Late Ordovician to Early Carboniferous, followed by collisions in the Late Paleozoic and Early Jurassic, of another complete Wilson Cycle; the area was again subjected to several paroxisms of plume activity; d) Jurassic to Miocene platform complex, formed when the orogen was finally eroded to a hilly country and then to a peneplain, with related deep weathering; e) Late Cenozoic neo-orogenic complex, formed when new orogenic deformations started and new mountains rose along some tectonic lines of the Uralides.

The metamorphic complexes of the Archean to Paleoproterozoic crystalline basement (a) are exposed in the rather small Taratash and probably in some other small massifs. In seismic sections, it is traceable to the east until the middle of the Urals to a depth of ca 30 km. The basement consists of para- and orthometamorphic rocks, regionally metamorphosed to granulite and amphibolite facies, and more locally, in shear zones, displaying a retrograde, low-grade metamorphism. According to isotopic data (Krasnobaev et al., 2011; Ronkin et al., 2012), the oldest U–Pb age of zircons from granulites is 3504 ± 210 Ma, and the youngest isotopic age of greenschist metamorphism is 299 ± 43 Ma. The youngest age
for the amphibolite metamorphism and granite formation is close to 1800 Ma. The block is too small to infer a participation of plumes in it, though Archean LIPs, described in many better exposed areas of the world (e.g. Ernst, 2014), suggest plume activity with formation of thick basalt-komatiite series. Both types of the rocks, though highly metamorphosed, are present in the Taratash block.

The Timanides (b) were formed during the Timanian orogeny (600–550 Ma) in place of the Pechora oceanic basin and a continental margin of Baltica craton (Puchkov, 2010). They strike parallel to the Uralides in the South and Middle Urals, but acquire a northwest strike in the Sub-Polar and Polar Urals and continue into the crystalline basement of the Timan–Pechora basin. Puchkov (2010a) proposed two parts in the Timanides: the Externides, belonging to the pericratonic part of Baltica continent and affected by several plume events, and the Internides, formed in place of the Pechora Ocean, its microcontinents and island arcs. The Externides of Timanides are exposed in the South and Middle Urals. The Meso− and Neoproterozoic sedimentary formations in the South Urals (BMA) reveal the most complete sequences, up to 15 km thick. They form a deep and vast sedimentary basin, catagenetically transformed, owing to a deep submersion and a heat supply from several magmatic series, which belong to short epochs of intrusive and volcanic activity.

The stratified Riphean (Meso- and Neoproterozoic) mafic–ultramafic complexes host titanomagnetite (with vanadium) deposits (Kusa–Kopan group of intrusions in the South Urals and Yubrishka in the North Urals); high-alumina chromites with PGE (Sarana group of deposits in the Middle Urals) with hot expulsion of waters, squeezed out of the sediments, along with an iterative rifting events. These processes could be responsible for formation of a series of stratiform, epigenetic, hydrothermal–sedimentary low–middle-temperature deposits. The richest of them are Satka (magnesite), Bakal (siderite) ore clusters, Suran (sellaite–fluorite) and smaller deposits of the same type in the Lower and Middle Riphean (Mesoproterozoic) carbonate sediments. There is also a series of smaller barite, barite–polymetallic and polymetallic deposits and occurrences, probably of SEDEX type with a later hydrothermal overprint in the Upper Riphean (e.g., Kuzha, Verkhnyaya Arsha and others) (Maslov et al., 2001). In the BMA, there are also well known gold–sulphide–quartz lode deposits of the Verkhneavzyansk group, hosted in the Riphean schists. Along the western and northern periphery of the Beloretsk dome in the South Urals, Mesoproterozoic black shales were reported to contain gold, gold–palladium and palladium–gold–REE mineralization. This prospective zone can be traced for a great distance along the western slope of the South and Middle Urals and is attributed tentatively to the same type as the Sukhoi Log deposit, which is treated by many researchers as metamorphogenic–hydrothermal. More or less confidently, to this type is attributed the Ashka deposit in this zone In the mineralized zones of Bashkortostan, black shales were influenced by high-temperature (up to 500 °C) fluid (Kovalev et al., 2013). Gold and platinum also form noticeable concentrations in hematite-enriched matrix of basal conglomerates of the Mashak Formation of the BMA at the Shatak range (Kovalev et al., 2013).

Mineralization in the BMA was studied recently with application of new precise methods of isotopic dating and characterization of mineralizing fluids. In particular, a new model of formation of magnesite deposits was suggested, as a result of interaction of primarily hot, cooling (440 to 85 °C) brines, probably of evaporite nature, with porous brecciated dolomites soon after their deposition (Krupenin et al., 2013). Formation of Bakal siderites, according to isotopic and mineralogical data, was also connected with the action of ~250 °C fluids (Maslov et al., 2001). The U–Pb (baddeleyite) age of the Main Bakal dyke was constrained as 1385.3 ± 1.4 Ma (Ernst et al., 2006). It was noted (Maslov et al., 2001) that the thermal influence of the dyke initiated an intense brucite replacement of the hosting magnesite, which leaves only a small time window between the origin of the Lower Riphean Bakal Formation and the dyke intrusion, contemporaneous

with the Mashak volcanism. The siderites of Bakal were formed much later, at the Middle to Late Riphean transition (1010 ± 100 Ma Pb–Pb isochron from the least altered siderites; and 1090 Ma according to Th–Pb method) (Maslov et al., 2001). The ages of the latest overprinting hydrothermal processes, including barite and polymetallic mineralization, correspond to the Latest Riphean (Arshinian): 615 ± 6 Ma (Rb–Sr), 632 ± 12 and 610 ± 6 Ma (K–Ar) (Maslov et al., 2001).

Because of this, and in contrast to the above-described Middle Riphean deposits, the barite-polymetallic occurrences are hosted in the Lower and Middle Riphean, as well as in the Upper Riphean sequences. In the Suran low-temperature (230–50 °C) hydrothermal deposit, several types of fluorite were recognized. The purest optical fluorite is the latest and is dated as 1219 ± 120 Ma (Sm–Nd isochron) (Maslov et al., 2001), which suggests a link to the Mashak magmatism.

In fact, this territory was part of the Riphean platform. The most important metallogenic factor here could be a widely distributed thermal–magmatic   Mashak episode at ca 1380 Ma, corresponding to a mantle plume event of a subglobal scale. This magmatism activated mineral formation in the deep sedimentary basin of the Externides. Layered mafic intrusion of the Kusa–Kopan complex, as well as the Berdyaush rapakivi pluton, have the same age as Mashak. Recently, the Sibirka carbonatite, situated not far to the east of the Berdyaush pluton, was dated as 1350–1360 Ma, and therefore this carbonatite may also belong to the same plume episode.

Among the Neoproterozoic mafic complexes that may be attributed to mantle plumes (Igonino and Kiryabinka episodes), one can mention layered pyroxenite-gabbro intrusions. One of them, the Sarana intrusion, hosting the chromite deposit of the same name, is dated as ca 745 Ma, which is close to the Igonino event of BMA. Another layered intrusion, hosting Kiryabinka 680 ± 3.4 Ma sulphide copper mineralization, has its age equivalents in the Middle Urals. These Neoproterozoic magmatic formations may also represent fragments of concealed LIPs. Therefore, most metallogenic processes in the Externides of Timanides can be associated with mantle plumes.

Development of the Uralides (c) corresponds to classic Wilson Cycle and comprises epicontinental rifting in the latest Cambrian to Early Ordovician, formation of the Paleouralian Ocean with its continental passive margins and eastward-dipping subduction zones in the Late Ordovician to Late Devonian, arc–continent collision in the Late Devonian, formation of the Nevada-type subduction zone in the Early Carboniferous, continental collisions in the Late Moscovian to Permian, Triassic mantle plume/rifting episode and, finally, new collision in the Early Jurassic.

After the Timanian orogeny in the Vendian (Ediacaran) and a short−lived platform stage, when a peneplain was formed, a stage of epicontinental rifting started, which smoothly evolved into an oceanic
spreading in the Middle Ordovician, with simultaneous formation of passive continental margins, of which only one margin can be recognized in the modern Urals.

Mineralization of the Ordovician is represented, among others, by barite-polymetallic stratiform deposits (Saurey), hosted by Ordovician riftogenic volcanic rocks — probably associated with mantle plume activity (Kidryas episode) , accompanying a passive margin of a volcanic type. In the western slope of the Middle Urals the stratiform polymetallic and copper-polymetallic ores are present in the Ufaley uplift.

In the sedimentary successions of the passive continental margin, rift formations are followed by purely sedimentary formations, demonstrating a transition from shelf to continental slope. Late Ordovician to Early Silurian subalkaline magmatism and carbonatitic metasomatism in the Middle Urals have led to formation of rare metal (Ta, Nb) deposits of the Ilmeny–Vishnevye Gory ultramafic–alkaline (miaskite)–carbonatite complex. The substrate of the complex is represented by Paleoproterozoic (ca. 1800 Ma) Selyankino gneisses. According to Nedosekova (2012 and references therein), dating of zircons from miaskites corresponds to the early stages of crystallization of miaskite–carbonatite complex at 446–420 Ma (Late Ordovician to Early Silurian); the younger clusters of zircons correspond to later tectonic stages of the region development during Middle-Late Devonian, Lower Carboniferous and Permian–Triassic stages and belong to the superimposed metamorphic processes. These processes led to anatexis, pegmatite formation of several types, metasomatism and mineralization, and in particular, the formation of famous precious stones of the Ilmeny State Reserve.

I suggested that the initially magmatic Ordovician/Silurian Ilmeny–Vishnevye Gory complex is the trace of a mantle plume, affecting the continental margin (like in the Montreal area), tied up to the opening of a new ocean (Puchkov, 2010). Trachybasalts of the same age occur immediately to the west, in the Bashkirian meganticlinorium (Ushat plume event). In the western slope of the Middle Urals this magmatic stage was manifested as syenite-porphyries of the Verkhneserebryanski complex (age − 447 ± 8 Ma, (Petrov, 2006). Similar processes probably took place in the Polar and Sub-Polar Urals, in particular, in the Turupya syenite-hosting zone of mineralization in the Ordovician deposits. Along with K–Ar Late Paleozoic ages, in the north of the Urals were obtained the Late Ordovician to Early Silurian Rb–Sr and U–Pb ages (420–460 Ma, like in the Vishnevye Gory) for granites, hosting rare metal mineralization: Kharbey, Tai-Keu and also Man'-Khambo) (Udoratina and Larionov, 2005).

Another mantle plume event can be reconstructed for the Devonian magmatism on the western slope of the Urals (see above). It was reported (Goldin et al., 1972) that larger sills associated with the Devonian Uralian dyke swarm are differentiated. In some rare cases, the length of sills reaches 5–10 km, and they are up to 100–250m thick. For instance, large differentiated bodies were mapped in the north (Sub-Polar Urals and Pay-Khoy). In typical cases these differentiated bodies include picrite, biotite-bearing olivine gabbro, olivine-free gabbro-dolerite, essexite-diabase, quartz dolerite and monzonite. They contain magmatic titanomagnetite (e.g., Tima-is Range) and pyrrhotite–pentlandite–chalcopyrite lens-like bodies (in Pai-Khoy) at the bottom parts of the intrusions (Yushkin et al., 2007).

A "shadow" longitudinal zone was suggested under the northern part of the South Urals, where alkaline and subalkaline magmatic formations are concentrated (carbonatites of the Ilmeny–Vishnevye Gory complex, as well as Sibirka deposit, Berdyaush and other plutons) (Levin et al., 1997). Perhaps, the lithosphere under this zone was metasomatically affected and had an ability of producing alkaline complexes. In development of this idea, I propose an existence of another, much more extensive zone ("corridor") of such type, with the Khibiny alkaline complex having their continuation in the Archangelsk kimberlite fields, and further on, to the east, to the kimberlites and carbonatites of the Timan and probably to concealed kimberlites of the easternmost part of the platform close to the North Urals.

In the Triassic period, collisional processes have stopped, and the mode of tectonic activity has changed. It was characterized by an intense flood basalt volcanism, connected with the widest Early Triassic Siberian superplume event. In this connection, a possibility of discovering the Norilsk-type deposits and kimberlites in the Uralian part of this superplume may be promoted.

References:

Ernst RE. (2014). Large Igneous Provinces. Cambridge University Press, 633 p.

Ernst, R.E., Pease, V., Puchkov, V.N., Kozlov, V.I., Sergeeva, N.D., Hamilton, M. (2006). Geochemical characterization of Precambrian magmatic suites of the southeastern margin of the East European Craton, Southern Urals, Russia. Geological Digest No 5. Geological Institute, Ufimian Scientific Centre, Russian Academy of Sciences, DesignPoligraph Service, Ufa, 119–161.

Goldin, B.A., Kalinin, E.P., Puchkov, V.N. (1999). Magmatic Formations of theWestern Slope of the North of the Urals and Their Minerageny, Syktyvkar , 213 pp. (in Russian).

Kovalev, S.G., Vysotskiy, I.V., Puchkov,V.N., Maslov,A.V., Gareev,E.Z. (2013). Geochemical Specialization of Structural-Material Complexes of the Bashkirian Mega-anticlinorium. Dizain Press, Ufa, 268 pp. (in Russian).

Krasnobaev, A.A.,Kozlov, V.I., Puchkov,V.N., Busharina, S.V., Berezhnaya, N.G., Nekhorosheva,A.G. (2011). Zirconology of iron quartzites of Taratash Complex (Southern Urals). Dokl. Earth Sci. 437 (2), 527–532.

Krupenin, M.T., Garaeva, A.A., Kliukin, Y.I., Baltybaev, S.K., Kuznetsov, A.B. (2013). Fluid regime of the magnesite metasomatism in Satka deposits of the South-Uralian province (thermocryometry of fluid inclusions). Lithosphere, 2, 120–134 (in Russian).

Levin, V.Y., Ronenson, B.M., Samkov, V.S., Levina, I.A. (1997). Alkaline–Carbonatite Complexes of the Urals. Uralgeolcom, Ekaterinburg, 274 pp. (in Russian).

Maslov, A.V., Krupenin,M.T., Gareev, T.Z., Anfimov, L.V. (2001). The Riphean of theWestern Slope of the South Urals (Classical Sections, Sedimento- and Lithogenesis,Minerageny, Geological Monuments). V.1. UB RAS, Ekaterinburg, 351 pp. (in Russian).

Nedosekova, I.L. (2012). The age and sources of matter of the Ilmeny–Vishnevye Gory alkaline complex (Urals, Russia): geochemical and isotope Rb–Sr, Sm–Nd, U–Pb, Lu–Hf data. Lithosphere 5, 77–95 (in Russian).

Petrov, G.A. (2006). Geology and Mineralogy of the Main Uralian Fault Zone in the Middle Urals. Uralian State Mining University, Ekaterinburg ,195 pp.(in Russian)

Puchkov V.N. (2010). Geology of the Urals and Cis-Urals (actual problems of stratigraphy,tectonics, geodynamics and metallogeny). – Ufa: Design Poligraph Service, 280 p. (In Russian).

Puchkov V.N (2016 a). General features relating to the occurrence of mineral deposits in the Urals: What, where, when and why, Ore Geol. Review, doi:10.1016/j.oregeorev.2016.01.005 (publ. online).

Puchkov V. (2016b). Magmatic complexes of the Urals as suspect parts of Large Igneous Provinces. IOP Conf. Series: Earth and Environmental Science **44**. 022003 doi:10.1088/1755-1315/44/2/022003

Puchkov V.N, Ernst R.E, Hamilton M.A, Söderlund and Sergeeva N. (2016) A Devonian > 2000- km long dolerite swarm belt and associated basalts along the Urals-Novozemelian fold-belt: part of an East-European (Baltica) LIP tracing the Tuzo Superswell. GFF J., 138 (1), 6−16.

Reichow MK, Saunders AD, Pringle MS et al. (2009). The timing and extent of the eruption of the Siberian Traps large igneous province: Implications for the End-Permian environmental crisis. Earth and Planetary Sci. Letters, 277, 1–2: 9–20.

Ronkin, Y.L., Sindern, S., Lepikhina, O.P. (2012). Isotopic geology of the most ancient formations of the Southern Urals. Lithosphere, 5, 50–76 (in Russian).

Udoratina, O.V., Larionov, A.N. (2005). The age of granitoids of Tai-Keu massif (Polar Urals): U–Pb data. Structure, Geodynamics andMineragenic Processes in Lithosphere. Materials of the 11th International Conference. Geoprint, Syktyvkar, 346–349 (in Russian).

Yushkin, N.P., Kunts, A.F., Taranina, T.I. (2002). Barites of the Urals-Pay-Khoy Province. Uralian Branch of Russian Academy of Sciences, Ekaterinburg, 337 pp. (in Russian).

THE HIGH H2 CONTENT OF THE GAZ COMPONENT OF KARNASURT LOVOZERO LAYERED COMPLEX ROCKS

Puha V.V.[1], Asavin A.M.[2], Nivin V.A.[1], Chesalova E.I.[3], Litvinov A.V.[4]

[1]Geological Institute, Kola Scientific Center of the Russian Academy of Sciences, Apatity, Russia
[2]Vernadsky Institute of Geochemistry and Analytical Chemistry of the Russian Academy of Sciences, Moscow (aalex06@inbox.ru)
[3]Vernadsky State Geological Museum of Russian Academy of Sciences, Moscow, Russia
[4]National Research Nuclear University MEPhI, Moscow, Russia

Hydrogen is one of the most interesting gases found in rocks. The emission of free hydrogen from ultrabasic rocks, associated with serpentine processes, is the most prominent process. However, more recently attention was paid to high hydrogen content in alkaline rocks [Nivin, 2016]. Unfortunately, hydrogen is one of the most volatile gases, and therefore, when estimating of gas emission is made by traditional methods, there is the possibility that we measure some residual flux

Fig. 1. Appearance of WSN equipment. A- in the box the transmitting unit and the battery; B - The author of the article downloads the current datas from the hub to the laptop; C- Hydrogen sensor with the protective case removed. A sensor chip and a connector for cable are visible.

We developed a specialized equipment based on MDM hydrogen sensors [Nikolaev et al. 2007] and WSN telecommunication technology for long-time monitoring of hydrogen content in the atmosphere. Unlike existing methods, the developed equipment allows to carry out measurements directly in the zone of blasting operations with high discreteness in time. A part of the data obtained (about 500 measurements) is presented in Fig. 2. This is the result of the autonomous work of the WSN monitoring network.
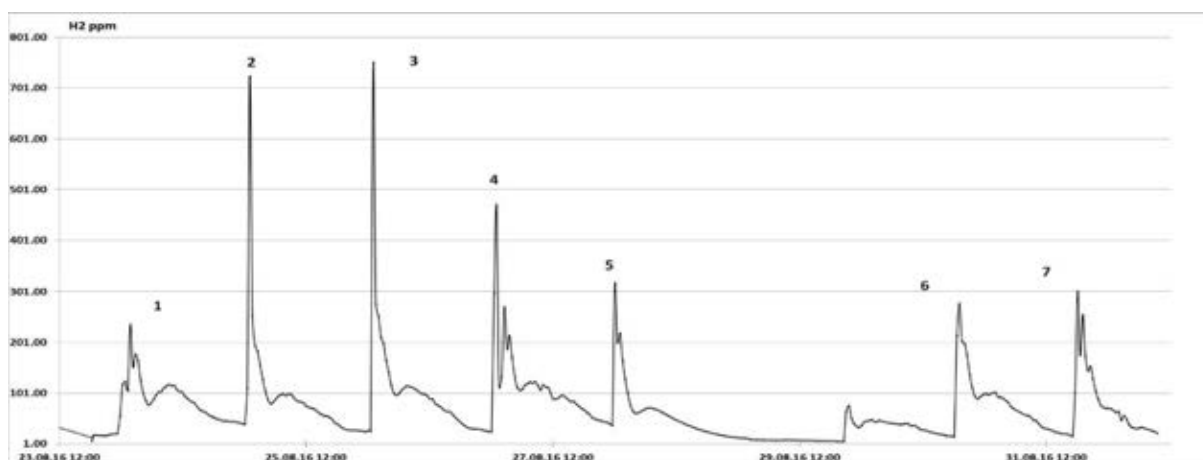
Fig. 2. Time series of H2 content in underground atmosphere of explosive zone of Karnasurt mine.

The network node together with the power battery allow working autonomously approximately 2 to 3 weeks. After the discharge of power supplies, the batteries were replaced and the information collected on the hub are downloaded.

Unfortunately, low temperatures in the tunnel and high measurement frequency led to a rapid discharge of autonomous power supplies. According to the plan, the autonomy of the network should have been about 1 month. However, it really happened about once a week to check the charge of batteries.

Thus, the working scheme of the network is as follows: The sensor is in the zone closest to the explosion zone; it is connected by cable to the network node; the node is equipped with sensor radio control equipment; the system of data collection and transfer of information to a neighboring node and further to the central hub was established

In the segment of the network, which we used at the mine, there were 3-5 nodes. It was done in order to duplicate the measurement in the vicinity of the explosion and to maximally secure the data collection hub. The tests were carried out in two drifts (Fig. 3). They are quite different of a level of water saturation condition. The maximal water flow was in the network segment of upper track number 13. This created the most unfavorable conditions for radio communication. It was the working network segment, where was the explosion station.

Figure 2 shows typical graphical form of hydrogen content associated with explosions Blasting operations are usually performed once a day almost at the same time. There were no explosion operations on 29 august, and there are no peaks on the graph on this day. Reduction of hydrogen content occurs quickly, because of good ventilation system. At the same time, an unexpected fact, which was established by our measurements, is the significant difference between background and peak hydrogen content. Even in our time-limited monitoring, this difference reaches 800, and usually the change is 12-40 times. These data indicate the possibility of dangerous hydrogen contents in the atmosphere immediately after the explosion, and the occurrence of seriously explosive and dangerous situation.
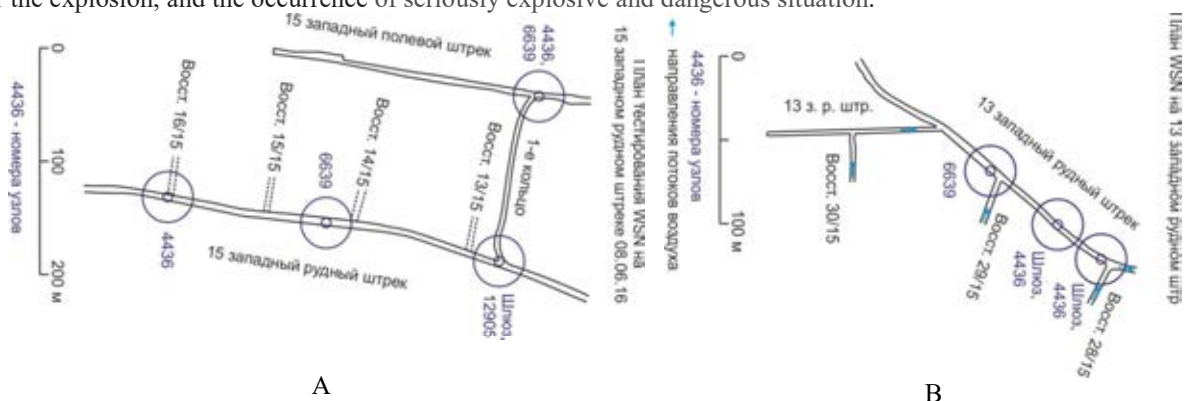
Fig. 3. Location of WSN network nodes in two driveways 15 (A) and 13 (B). Circles on schema show node location. The explosion zone is located in the rising tunnel 30/15. The closest node to the explosion is 6639.

Very interesting fact that resulting maximum vary in depend of the day of explosion. What is the reason? Is that of peculiarities of the rocks portion of or periodical cosmic events? These questions remain unanswered and for their solution research and further long-term monitoring are required.

The second important observation, which no one has previously described, is that the peaks has the quite unusual form, which apparently reflects the dynamics of lithosphere hydrogen emission as a result of explosion (Fig. 4). The general form is double-humped curve. Between the peaks, there is a small interval, where the concentration sharply decreases - the "quick minimum". At the second maximum, which is about half of the first, the concentration increases sharply, and then falls again, but at a slower rate - the "second peak". During half hour after the explosion, the concentration drops to minimum - the "main minimum", and then gradually decreases to a background (almost zero value) after a small increase.
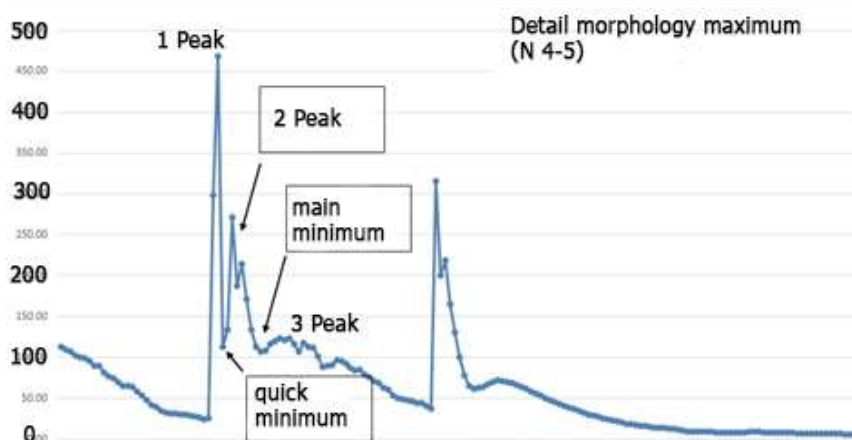
Fig. 4. Typical graphical form of hydrogen content maximum associated with explosions

The quick minimum not always can be observed. Main minimum observed on each anomaly of H_2 concentration. The reason of such multi-pick anomaly can be as result of different source of H_2 into the breaking rocks or multiplex source from different sites mining explosive zones. The last idea can explained identical form for 3-pick. But cannot

explain "quick-minimum" and cumulative difference between anomaly's. If the speed of gas wave equal air speed in tunnel the critical distance for multiplexing H_2 flow from different sources must be about 500m. If real distance between different mining explosive zone more 500m sensor will show unique peak of concentration on the time series graphic. For these preliminary considerations, we still keep to the first point of view that the causes of the complex shape of the anomaly lie in the genetic difference of gas sources from fractured rocks.

In any case we can calculate we can graphically calculate volume of H_2 corresponding each of the peaks on the anomaly and analyses they relationship (Tabl.1).

Table 1. Calculation of the volume of H_2 released from the rocks after the explosion (input calculation parameters: 11.9m2 gallery section, 0.7m / s flow rate, sampling interval 10sec).

№ maximum on Fig1.	Square maximum on the Fig1 graphic (c.u.)			Duration sec.			Volume H_2 m^3		
	1 peak	2 peak	3 peak	1 peak	2 peak	3 peak	1 peak	2 peak	3 peak
1	10840	10790	67500	10840	10790	67500	11	11.6	42.6
2	17980		70140	17980		70140	23		35.3
3	18040		66540	18040		66540	34		38.3
4	5390	14380	64860	5390	14380	64860	12.4	20	46
5	3530	12580	70190	3530	12580	70190	6.4	13.4	24.5
6	16130		66650	16130		66650	22		33
7	5330	53980		5330	53980		7.4	33.11	

Interpretation of the revealed pattern of gas flow distribution requires further research, but even now some assumptions can be made. It is obvious that the first peak corresponds to the most mobile gas component. This gas located in the liberated cracks and large pores of the blasted rock mass. This most mobile part is immediately thrown into the mine space and gives a sharp 1-peak maximum release.

However, later, with a little discontinuity in time, an additional source of hydrogen appears. What could it be? This is unlikely to be an occluded gas in the rock minerals, since its outflow will be slower due to the gradual opening of small pores or gradual seepage of gases from them. We assume that it is also a free crack gas, but it locate around the overburden area. The blocks of the mountain mass that were previously closed by the block are opened, pressure is released and half-open cracks give a new peak - the "second peak" that we fix.

The 3-peak, gradually slowly falling to the background value. Such due to the slow emission of gases from inclusion. A more gradual decrease in concentration indicates a slow outflow of gases, which can be explained by the gradual decrepitation of inclusions from the minerals. Although the outflow is more smooth, but the total volume is also quite large. We calculate this volume as areas under the curve after the "main minimum".
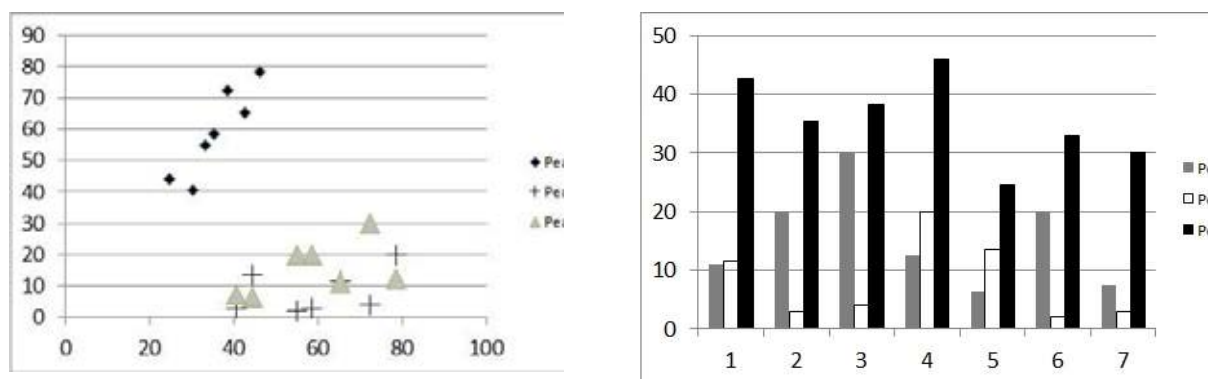
Fig. 5. Relationship between total gas volume and volumes H_2 in different peaks.

It can be seen from Table 1, we failed to make a correct separation of the peaks for all the anomalies. Often the "fast-minimum" is not allocated. And then 1- and 2-peaks are summed. In general, the 2-peak is usually much smaller than the first, although for example in the fifth anomaly the ratio is reversed. Sometimes there is a situation when the "main minimum" is not manifested. In that case, we unite 2 and 3 peaks. However, if we try to carry out an interpretation on our limited material, then we can construct the histograms Fig. 5. On this graphic we try to see on the relation between total volume of anomaly H_2 and parts of H_2 connected with different peaks. We can see that total volume correlate with H_2 3-peak, but there is no any correlation with quick gas from 1-2 peaks. The share of fast gas in the total volume is approximately 30-50%. It is interesting estimates because it turns out that very large quantities of gas were not previously taken into account in calculations or were randomly included as abnormal deviations. The advent of high-resolution monitoring tools can reveal new aspect of the behavior of high volatile gases.

References:

Nivin, V. A. (2016). Free hydrogen-hydrocarbon gases from the Lovozero loparite deposit (Kola Peninsula, NW Russia). *Applied Geochemistry*, *74*, 44-55.

Nikolaev, I.N., Litvinov, A.V., Emelin, E.V., (2007). Applicability of MDS-sensors as detector elements of gas analyzers. *Datchiki & Systemi* (*Sensors & Systems*) 5, 66-73 (in Russian).

Ankaramite – the primary melt for the Ural-Alaskan-type intrusions and the source of platinum-group minerals

Pushkarev E.[1], Kamenetsky V.[2], Gottman I.[1]

[1]Institute of Geology and Geochemistry, Ural Branch of the Russian Academy of Sciences, Yekaterinburg, Russia, pushkarev@igg.uran.ru
[2]University of Tasmania, Hobart, Australia

The Ural-Alaskan-type mafic-ultramafic complexes all over the world contain a great amount of high-Ca and high-Mg rocks, such as clinopyroxenites, olivine clinopyroxenites, Cpx-phyric melanogabbros. The proportion of clinopyroxenites in the Ural Platinum Belt is about 30-40%, gabbro – 50-60% and dunite is only 5-10%. The Duke Island complex in the S-E Alaska belt contains 60% of clinopyroxenites (Himmelberg, Loney, 1995; Irvine, 1974). The reconstruction of parental melt compositions should take into account that total volumes of clinopyroxenites significantly exceed those of dunites, implying unusually high, for mantle-derived melts, abundances of CaO, and by inference $CaO/Al_2O_3 >1$. The only example of such high-Ca melt is represented by ankaramites (Barsdell, Berry, 1990; Medard et al, 2006; Schmidt et al, 2004) that have been considered as a parental magma for the dunite-clinopyroxenite complexes in the south-east Alaska (Irvine, 1973). Additional support to the idea of the ankaramite being a parental magma to the Ural-Alaskan mafic-ultramafic complexes is provided by the magmatic-plutonic association in the Urals (Kamenetsky et al., 2015; Krause et al, 2007; Pushkarev et al., 2014). The differentiation trends of both ankaramites and dunite-clinopyroxenite-gabbro intrusions are controlled by the same olivine-Cr-spinel- clinopyroxene cotectic fractionation and similar mineral compositions.

In the Urals ankaramites were first noted in the tectonic melange of the Main Uralian Fault (Spadea et al, 2002). We demonstrate that Cpx-phyric volcanics of ankaramite affinity are widespread in the Irendyk and other Paleozoic island-arc formations in the Southern and Central Urals (Pushkarev et al., 2014). These volcanics contain phenocrysts of Cr-diopside and high-Cr spinel that are compositionally identical to those in island-arc ankaramites in Pacific region and in ultramafites of the Ural-Alaskan complexes. The most primitive ankaramite was found as dykes and lavas in serpentine melange 30 km to north-west from the town of Uchaly. The dykes cut serpentinites and contain their small xenoliths. The ankaramite is accompanied by trachyandesite lava with pahoehoe surfaces. Dykes of trachyandesite sometimes intersect ankaramites.

The Uralian ankaramite contains 20-30% of clinopyroxene, olivine and (or) orthopyroxene and chromite phenocrysts in the fined grained chilled groundmass. Clinopyroxene phenocrysts are the most abundant and form crystals from 3-5mm up to 4 cm. It varies in colour and composition from apple-green Cr-diopside (Mg# = 0.92–0.93, Al_2O_3 = 0.5–0.7%) to dark green augite (Mg# = 0.80–0.75, Al_2O_3 = 2.5–3.0%). Octahedral grains of Cr-spinel (Mg# = 0.59 – 0.6, Cr_2O_3 = 60-64%, Cr/(Cr+Al) = 0.89 – 0.91) are present as microphenocrysts, up to 2-3 mm in size and as small inclusions in Cr-diopside. The Cr-spinel contains rare inclusions of olivine (Fo_{90}) and Cr-diopside (Mg# = 0.92-0.93) and abundant melt inclusions, comprised of clinopyroxene, orthopyroxene, amphibole and felsic glass. Other phenocrysts represented by euhedral grains are totally replaced by chlorite. They are tentatively identified as olivine, although orthopyroxene cannot be excluded. The groundmass is dominated (up to 40-50%) by zoned clinopyroxene crystals (5-50 µm). The representative compositions of minerals are in the Table 1.

Table 1. Representative composition of minerals from ankaramite.

Sample	Pe1466							
Mineral	Clinopyroxene				Chromite		Olivine	
SiO_2	55.26	53.97	52.49	51.18	0	0	40.12	41.17
TiO_2	0.03	0.06	0.11	0.27	0.15	0.16	0	0
Al_2O_3	0.42	0.79	1.61	3.14	4.25	4.92	0	0
Cr_2O_3	0.55	0.35	0.12	0.08	63.82	62.31	1.38	0
FeOtot	2.72	5.05	7.7	10.1	19.40	20.11	0.38	8.86
MnO	0.06	0.19	0.31	0.33	0.15	0.08	7.96	0
MgO	19.04	17.62	15.88	14.16	11.15	11.10	49.91	49.97
CaO	22.26	21.76	20.98	20.64	0	0	0.26	0
Na_2O	0.11	0.14	0.13	0.2	0	0	0	0
K_2O	0	0.01	0	0.01	0	0	0	0
Total	100.46	99.93	99.32	100.10	98.92	98.67	100.00	100.00
Mg/(Mg+Fe)	0.93	0.86	0.79	0.72	0.56	0.56	0.92	0.91

The bulk composition of ankaramites is characterised by high Mg# (0.80) and CaO (16-17%) and moderate enrichment in light rare-earth elements La_N/Yb_N=3-4, whereas the contents of Al_2O_3, TiO_2 and alkali elements are very low (Table 2). The groundmass and homogenised melt inclusions are compositionally similar to the bulk rocks, thus re-enforcing the affinity to ankaramite melts (Table 2).

Table 2. Representative bulk composition of ankaramites, groundmass (GM) and homogenized melt inclusion (MI).

Sample	Pe1465	Pe1466	Pe1467	Pe1492	Pe1566	Pe1466 GM		MI
SiO_2	46.08	45.43	46.14	43.89	46.32	47.90	47.83	46.50
TiO_2	0.16	0.17	0.18	0.15	0.13	0.00	0.00	0.16
Al_2O_3	6.02	6.60	7.01	6.24	6.36	10.69	10.05	7.12
Fe_2O_3	5.41	4.74	3.98	5.95	3.89	n.d.	n.d.	n.d.
FeO	3.50	4.20	5.00	2.80	4.20	9.38	9.85	13.75
MnO	0.19	0.20	0.24	0.29	0.20	0.00	0.00	0.28
MgO	18.44	17.70	16.60	17.68	15.05	16.26	17.44	18.88
CaO	16.50	16.79	17.08	20.01	21.12	15.77	14.82	10.49
Na_2O	0.10	0.10	0.11	0.07	0.18	0.00	0.00	0.84
K_2O	0.04	0.01	0.01	0.00	0.02	0.00	0.00	0.34
P_2O_5	0.12	0.11	0.13	0.12	0.06	0.00	0.00	0.08
LOI	3.40	3.70	3.50	3.10	2.50	n.d.	n.d.	n.d.
Total	99.94	99.75	99.97	100.30	100.04	100.00	100.00	100.00
Mg/(Fe+Mg)	0.80	0.79	0.78	0.80	0.78	0.76	0.76	0.71
CaO/Al_2O_3	2.74	2.54	2.44	3.21	3.32	1.48	1.48	1.47

The Cr-spinel microphenocrysts contain the platinum-group minerals (PGM), typically 1-3 µm in size, represented by Fe-Pt alloys (Fig. 1a) entrapped with clinopyroxene, ankaramite glass and sulphides of Os, Ru, Rh, Cu, Ni (Kamenetsky et al., 2015). The composition of PGM corresponds to those in dunites and chromitite of the Ural-Alaskan-type complexes and may explain the enrichment by platinum in the PGE geochemical budget of ankaramite (Fig. 1b). We infer that the ankaramite magma, capable of generating large volumes of olivine-clinopyroxene cumulates and Pt-Fe alloys could be the primary melt for the Ural-Alaskan-type mafic-ultramafic complexes.
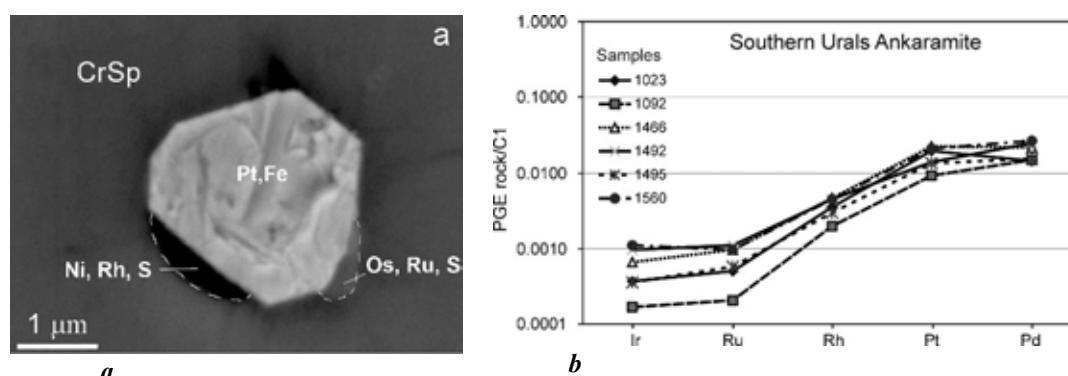
Fig. 1. a) Magmatic inclusion of PtFe alloy and PGE sulfides in chromite phenocryst from the Uralian ankaramite. b) Chondrite normalized PGE concentrations in the Uralian ankaramites

References:

Barsdell M., Berry, R. F. (1990) Origin and evolution of primitive island-arc ankaramites from Western Epi, Vanuatu. Journal of Petrology. 31: 747–777.

Della-Pasqua F. N., Varne R. (1997) Primitive ankaramitic magmas in volcanic arcs: a melt-inclusion approach. The Canadian Mineralogist. 35: 29l-312.

Himmelberg G.R., Loney R.A. (1995) Characteristics and petrogenesis of alaskan-type ultramafic-mafic intrusions, Southeastern Alaska. Reston: United States Geological Survey (USGS), Professional Paper. 47.

Irvine T.N. (1973) Bridget Cove volcanics, Juneau are, Alaska: possible parental magma of Alaskan-type ultramafic complexes. Carnegie Institute Year-Book-72. 1973: 478-491.

Irvine T.N. (1974) Petrology of the Duke Island ultramafic complex Southeastern Alaska. The Geological Society of America. Memoir 138, Ontario. 176.

Kamenetsky V.S., Park J-W., Mungall J.E., Pushkarev E.V., Ivanov A.I., Kamenetsky M.B., Yaxley G.M. (2015) Crystallization of platinum-group minerals from silicate melts: Evidence from Cr-spinel–hosted inclusions in volcanic rocks. Geology. 43. 10: 903–906.

Krause J., Brugmann G.E., Pushkarev E.V. (2007) Accessory and Rock Forming Minerals monitoring the Evolution of Zoned Mafic-Ultramafic Complexes in the Central Ural Mountains. Lithos. 95: 19-42.

Medard E., Schmidt M.W., Schiano P., Ottolini L. (2007) Melting of amphibole-bearing wehrlites: an experimental study on the origin of ultra-calcic nepheline-normative melts. Journal of Petrology. 47. 3: 481–504.

Pushkarev E.V., Kamenetsky V., Gottman I. & Yaxley G. (2014) The PGM-bearing volcanic ankaramite (Urals, Russia): bridging ankaramite parental magmas and the Ural-Alaskan-type intrusions. 12-th International Platinum Symposium.Yekaterinburg: IGG UB RAS, pp 204-205.

Schmidt M. W., Green D.H., Hibberson W.O. (2004) Ultra-calcic Magmas Generated from Ca-depleted Mantle: an Experimental Study on the Origin of Ankaramites. Journal of Petrology. 45. 3: 531-554.

Spadea P., Antonio M.D., Kosarev A., Gorozhanina Y., Brown D. (2002) Arc-Continent collision in the Southern Urals: petrogenetic aspects of the forearc-arc complexes. // Mountain building in the Uralides: Pangea to the Present. Geophysical monograph 132. pp 101-134.

ZIRCONIUM AND NIOBIUM ENRICHMENT IN THE KOVDOR CARBONATITE-PHOSCORITE COMPLEX

Rass I.T., Petrenko D.B.

Institute of Geology of Ore Deposits, Petrography, Mineralogy and Geochemistry of the Russian Academy of Sciences, Moscow, Russia, rass@igem.ru

Carbonatites, rocks of vast ore potential, are genetically related to complexes of alkaline–ultramafic rocks produced by mantle magmas. Crustal differentiation of magmas derived from the mantle at low degrees of melting is known to result in ore deposits, including giant ones, of Nb, Zr, REE, Sr, and other elements (Kogarko, 1977, 2015; Kogarko et al., 1988). Since the distribution coefficients of trace elements are very small, $K_{Nb, Zr, La, Ce}$ *Ol*/silicate melt < 0.0001 (Green, 1994), fractional crystallization of magmas in closed systems at little varying bulk distribution coefficients of trace elements should result, according to Rayleigh crystallization model of parental magmas, in the progressive enrichment of these elements in successive derivatives of the magmas.

It was thought until lately that the uniquely high concentrations of Nb, Zr, and REE of carbonatites in alkaline-ultramafic complexes are produced by liquid immiscibility between carbonate and silicate magmas at a high enough degree of differentiation of the primary alkaline ultramafic melts. However, recent experiments aimed at evaluating the distribution coefficients of elements between immiscible silicate magma and magmas of other composition (Veksler et al., 2012) have proved that these elements are preferably concentrated in the silicate liquid compared to the carbonate one and also that these elements can be concentrated in fluoride and phosphate (but not carbonate) melts as compared to the silicate ones. Experimental data on the distribution of REE in the course of partial melting in the peridotite-carbonate-phosphate system have discovered immiscibility between the silicate and phosphate-bearing carbonatite melts at high pressures (20-30 kbar) and temperatures 950-1000ºC (Ryabchikov et al., 1989, 1993) and concentration of REE and Ti(?) in the latter.

Carbonatites in alkaline–ultramafic complexes are sometimes accompanied by phoscorites. which are plutonic ultramafic rocks, comprising magnetite, apatite, one of silicate minerals (forsterite, phlogopite or tetraferriphlogopite) and often carbonate – calcite or dolomite (Krasnova et al., 2004₁). Key accessories are baddeleyite et pyrochlore. The Kovdor massif is a typical (and one of the most thoroughly studied) ring complexes of alkaline-ultramafic rocks, carbonatites, and phoscorites; it hosts a unique magnetite-apatite-rare-metal deposit. We have analyzed seven phoscorite and six carbonatite samples by XRF and ICP-MS (analysts A.I. Yakushev and E.V.Kovalchuk, respectively). These rocks crystallized during successive evolutionary stages of the Kovdor phoscorite-carbonatite complex that were distinguished in (Krasnova et al., 2004₂). Complex Ti, Nb, and Zr oxides and minerals of the perovskite, pyrochlore, and ilmenite groups are the principal trace-element concentrators (Chakhmouradian, 2006), and the contents of these elements in the phoscorites are higher than in the carbonatites (Fig.1). The highest Sr concentrations were found in the calcite carbonatite. The Zr and Nb concentrations in the phoscorites are notably higher than in the coeval carbonatites. The REE concentrations in the rocks of both types are comparable (Rass, Kovalchuk, 2015). The plots of logarithmic concentrations of pairs of incompatible elements (for example, of Zr and Y) in these rocks show two different evolutionary trends, none of which follows the trends in silicate alkaline-ultramafic rocks (Fig.2).

According to the hypothesis of local equilibrium (Korzhinskii, 1973), thermodynamic equilibrium is reached at any point of a system at any given moment of time in the course of an irreversible process if the rate of this process (such as fractional crystallization, solution filtration, or diffusion of a component) is lower then the rate of establishing equilibrium between the outermost portion of the solid phase and the liquid (either melt or solution). The sequence of equilibria established between the outermost part of the solid phases and liquid is "recorded" in the zoning of the minerals. This zoning provides information on the evolution of the physicochemical conditions under which the mineral crystals grew. Data on the zoning of equilibrium minerals and the principle of phase coexistence [Perchuk and Ryabchikov, 1976] provide insight into relations between the zoning of minerals, physicochemical parameters of the mineral-forming processes (P, T, fO_2, pCO_2 αSiO_2), and their kinetic characteristics in magmatic and metasomatic rocks.
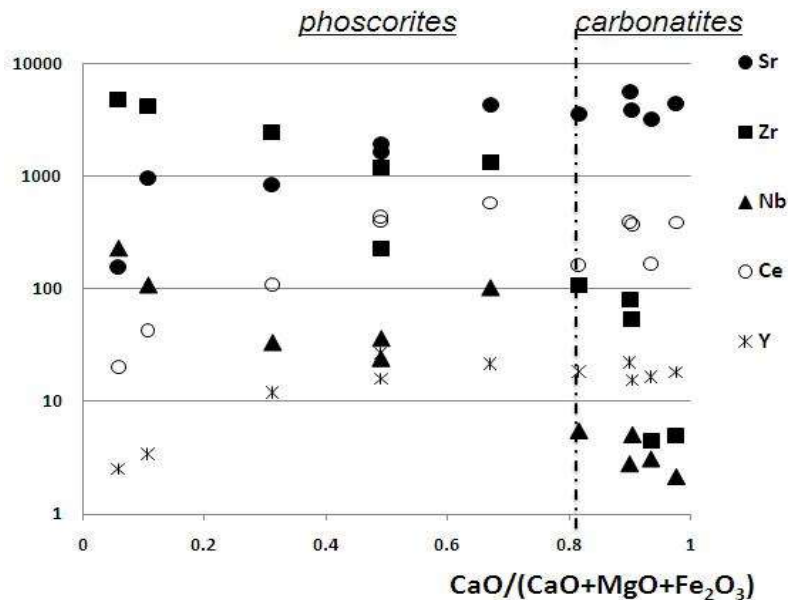
Fig. 1. Trace element concentrations (ppm) in phoscorites ($CaO/(CaO+MgO+Fe_2O_3) < 0.8$) and carbonatites ($CaO/(CaO+MgO+Fe_2O_3) > 0.8$).

We have analyzed coexisting minerals in 10 successive phoscorites and 8 relative carbonatites by ICP-MS (analyst E.V. Kovalchuk). Differences in the compositions and zoning of equilibrium rock-forming magnetite, apatite, calcite, and dolomite (and, where possible, also accessory ilmenite, baddeleyite, and pyrochlore) were examined by using microprobe analyses of these minerals. The very high contents of the magnesioferrite component, up to 7.8 wt.% MgO, are fixed in magnetites from phoscorites whereas MgO concentrations in magnetites from carbonatites are < 5.3 wt.%. The TiO_2 concentration decreases from the cores to their margins of magnetite grains in carbonatites (Fig.3a). The Al_2O_3 concentrations are at a maximum (>2 wt %) in magnetite from some phoscorites and decrease from the cores to margins of the crystals.
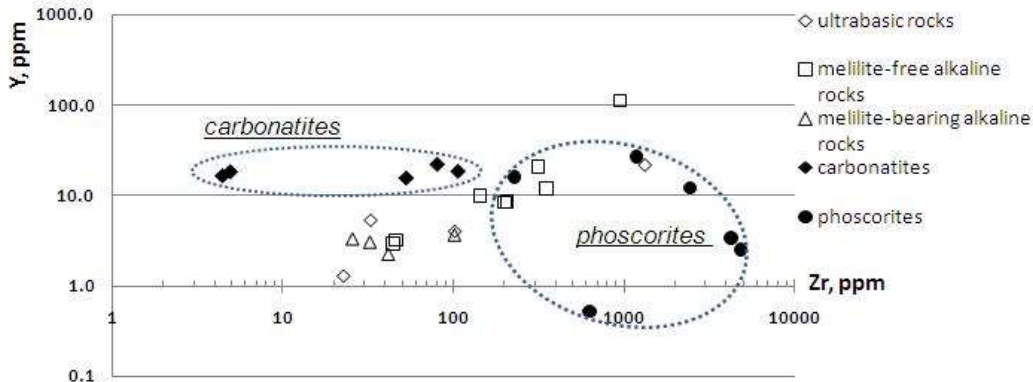
Fig. 2. The plots of logarithmic concentrations of pairs of incompatible Zr and Y (ppm) in phoscorites and carbonatites.

The ilmenite-magnetite [Spencer and Lindsley, 1981] crystallization temperature is 647°C at log fO_2 = -18 for the older phoscorite and 474°C for the younger one. Some of the analyzed ilmenite grains were rejected from the set used to determine the parameters because of their anomalously high concentrations of MgO (up to 25%) or MnO (13.6%). Phoscorites started to be formed at the Lyulekop deposit in the Palaborwa Complex, South Africa, at temperatures of 630–750°C (magnetite–ilmenite and dolomite–calcite thermometry) (Sharygin et al., 2011).

The apatite of the both phoscorites and carbonatites is F-apatite, and its F concentrations vary from 1.09 to 2.60 wt % in the phoscorites and from 1.35 to 2.20 wt % in the carbonatites (Fig. 3b). Practically all apatite grains are zoned in F, with their F concentrations increasing from cores to margins. The SrO concentrations of apatite in carbonatites and phoscorites are practically equal and slightly increase only from older to younger rock varieties within the range of 0.20-0.70 wt %. The Ce_2O_3 concentration of apatite in the phoscorites and carbonatites are also closely similar and mildly increase from older to younger rock varieties.

Compared to the coexisting apatite, the calcite is poorer in REE and richer in Sr. The apatite/calcite distribution coefficients of SrO and Ce_2O_3 seem to be equal in the older phoscorites and carbonatites. The magnetite/calcite distribution coefficients of MnO and MgO are also equal in the older phoscorites and carbonatites.
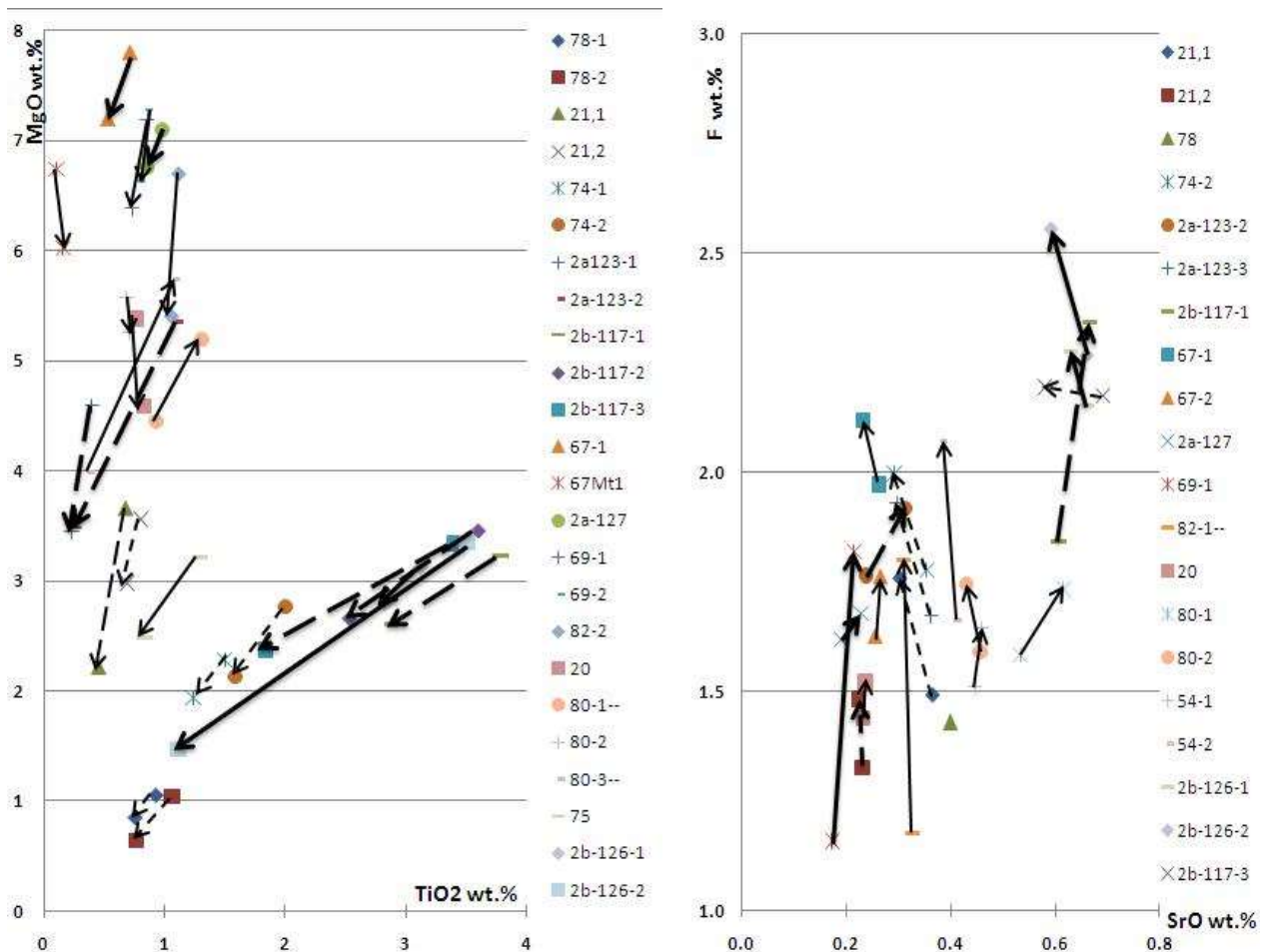
Fig. 3. Core-to-rim zoning of coexisting magnetite (a), and apatite (b) in phoscorites (solid arrows) and carbonatites (dashed arrows). 3a - Heavy lines with arrowheads show magnetite zoning in the reference older and younger rock varieties with, respectively, higher and lower MgO concentrations. 3b - Heavy lines with arrowheads correspond to F and SrO concentrations in apatite grains from the same reference older and younger rock varieties with lower or higher concentrations, respectively.

Geology of the Kovdor magnetite-apatite-rare metal deposit (Rimskaya-Korsakova, Krasnova, 2002; Krasnova et al., 2004[2]), data on pyrochlore zoning in the Sokli phoscorite-carbonatite complex, Finland (Lee et al., 2006), and our petrochemical data suggest liquid immiscibility between the phosphate-magnetite and carbonatite liquids at lower temperatures, likely slightly above the solidus temperature of carbonatite magma. A seeming immiscibility between phosphate and carbonatite liquids was first detected in melt inclusions (Andreeva, Kovalenko, 2003) within the likely temperature range of $500 < T < 900$ºC. Experimental data on the maximum Zr solubility in fluorite complexes (Migdisov et al., 2011) provide support for the hypothesis of possible liquid immiscibility between phosphate and carbonate melts, and our data on zoning of equilibrium magnetite, apatite and calcite in the Kovdor phoscorites and carbonatites are also consistent with this hypothesis.

Refrences:

Andreeva I.A., Kovalenko V.I. (2003) Magma compositions and genesis of the rocks of the Mushugai-Khuduk carbonatite-bearing alkaline complex (southern Mongolia): evidence from melt inclusions. Per. Mineral 72, special issue:

Chakhmouradian A.R. (2006) High-field-strength elements in carbonatitic rocks: Geochemistry, crystal chemistry and significance for constraining the sources of carbonatites. Chem geol 235: 138-160.

Green T.H. (1994) Experimental studies of trace-element partitioning applicable to igneous petrogenesis – Sedona 16 years later. Chem geol 117: 1-36.

Kogarko L.N. (1977) Genesis of agpaitic magmas. Nauka, Moscow (*in Russian).*

Kogarko L.N. (2015) Geochemical models of superlarge deposits of strategical metals in alkaline rocks Eastern Fennoscandia). In: Kogarko L.N. (ed) Alkaline magmatism of the earth and related strategic metal deposits. GEOKHI RAS, Moscow, pp 58-60.

Kogarko L.N., Lazutkina L.N., Krigman L.D. (1988) Conditions of Zr concentrating in magmatic processes. Nauka, Moscow (*in Russian).*

Korzhinskii D.S. (1973) Theoretical fundamentals of analysis of mineral assemblages. Nauka, Moscow (*in Russian).*

Krasnova N.I., Petrov T.G., Balaganskaya E.G., Garcia D., Moutte J., Zaitsev A.N., Wall F. (2004[1]) Introguction to

phoscorites: occurrence, composition, nomenclature and petrogenesis. In: Zaitsev A.N., Wall F. (eds) Phoscorites and carbonatites from mantle to mine: the key example of the Kola alkaline province. Min. Soc. of Great Britain & Ireland, London, pp 45-74.

Krasnova N.I., Balaganskaya E.G., Garcia D.(2004$_2$) Kovdor – classic phoscorites and carbonatites. In: Zaitsev A.N., Wall F. (eds) Phoscorites and carbonatites from mantle to mine: the key example of the Kola alkaline province. Min. Soc. of Great Britain & Ireland, London, pp 99-132.

Lee M.J., Lee J.I., Garcia D., Moutte J., Williams C.T., Wall F., Kim Y. (2006) Pyrochlore chemistry from the Sokli phoscorite-carbonatite complex, Finland: implications for the genesis of phoscorite and carbonatite association. Geochem. J. 40: 1-13.

Migdisov A.A., Williams-Jones A.E., van Hinsberg V., Salvi S. (2011) An experimental study of the solubility of baddeleyite (ZrO_2) in fluoride-bearing solutions at elevated temperature. Geoch. Cosmoch Acta. 75: 7426-7434.

Perchuk L.L., Ryabchikov I.D. (1976) Phase equilibria in mineral systems. Nedra, Moscow (*in Russian*).

Rass I.T., Kovalchuk E.V. (2015) Phoscorite-Carbonatite relations in the Kovdor complex. In: Kogarko L.N. (ed) Alkaline magmatism of the earth and related strategic metal deposits. GEOKHI RAS, Moscow, pp 92-93.

Rimskaya-Korsakova O.M., Krasnova N.I. (2002) Geology and mineral deposits of the Kovdor Massif, SPgU, St.-Petersburg (*in Russian).*

Ryabchikov I.D., Baker M, Wyllie P.J. (1989) Phosphate-bearing carbonatite melts in equilibrium with mantle lherzolite at 30 kbar. Geokhimiya 5: 725-729.

Ryabchikov I.D., Orlova G.P., Senin V.G., Trubkin N.V. (1993) Partitioning of rare earth elements between phosphate-rich carbonatite melts and mantle peridotites. Mineral Petrol 49: 1-12.

Sharygin V.V., Zhitova L.M., Nigmatulina E.N. Fairchildite K2Ca(CO3)2 IN in phoscorites from Phalaborwa, south Africa: the first occurrence in alkaline carbonatite complexes. Geol Geophys **52: 261-275.**

Spencer K.J., Lindsley D.H. (1981) A solution model for coexisting iron-titanium oxides. Amer Mineral 66:1189-1201.

Veksler I.V., Dorfman A.M., Dulski P, Kamenetsky V.S., Danyushevsky L.V. Jeffries T., Dingwell D.B. (2012) Partitioning of elements between silicate melt and immiscible fluoride, chloride, carbonate, phosphate and sulfate melts, with implications to the origin of natrocarbonatite. Geoch Cosmoch Acta 79: 20-40.

Magmatic and Metallogenic Evolution of the Chagai-Raskoh Arc, Balochistan, Pakistan

Rehanul Haq Siddiqui

Balochistan University of Information Technology, Engineering and Management Sciences, Quetta, Pakistan, rehanhs1@gmail.com

The Chagai-Raskoh magmatic arc occurs in the western part of Pakistan (Figure 1). In the regional geotectonic scenario this arc belongs to an ancient Tethyan convergence zone, which was initiated probably during Early Cretaceous, due to an intra-oceanic convergence in Ceno Tethys. In this Magmatic arc several episodes of magmatism occurred during the Late Cretaceous to Quaternary. The Late Cretaceous and Paleocene volcanism is dominated by basaltic-andesites with minor basalts and andesites with their volcaniclastic counterparts, whereas Eocene onwards volcanism is generally dominated by andesites with minor dacites and their volcaniclastic equivalents. The mafic mineralogy (augite-biotite), anorthite contents (An_{68-15}) and phenocrysts to groundmass ratios (20 : 80 - 45 : 55) in the volcanics rocks generally show progressive evolution towards younger volcanics.

Petrochemical studies show that the Late Cretaceous lava to Paleocene lavas of the Chagai-Rskoh arc belong to the tholeiite series, whereas Eocene and younger lava flows belong to the calc-alkaline series. Substantial amounts of Miocene shoshonites are also found towards west-central part of the Chagai arc. The Cr versus Y and Zr versus Zr/Y studies show that Late Cretaceous and Paleocene lava flows are fractionated from 15 to 30 % partially melted depleted mantle source, whereas Eocene and younger lava flows are fractionated from 10 to 15 % partially melted enriched mantle source. The trace element ratios including Ti/V, Zr/Y, Ce/Yb, La/Yb, Ta/Yb and Th/Yb of Chagai-Raskoh arc terrane generally show progressive increase towards younger volcanics, whereas Ti/Zr and Zr/Nb ratios exhibit similar decrease. These ratios in Late Cretaceous to Eocene lava flows are consistent with oceanic island arcs, whereas in Oligocene and younger lava flows these ratios are more consistent with continental margin type arcs. The Zr versus Zr/Y and Ta/Yb versus Th/Yb studies also reveal that Late Cretaceous to Paleocene volcanics exhibit oceanic island arc character, the Eocene volcanics exhibit transitional character, representing overlapping chemistry of both oceanic and continental margin arcs, while Oligocene onwards all the volcanics show typical continental margin (Andean) type arc affinities. The LILE/HFSE, LREE/HREE, $^{88}Sr/^{86}Sr$ ratios and ΣREE generally show progressive overlapping increase towards younger volcanics. The LILE/HFSE, LREE/HREE ratios and ΣREE are much higher in Oligocene and Miocene volcanics are much higher than their Quaternary counterparts. This suggests that during Oligocene-Miocene period, comparatively more LILE and LREE enriched fluids from the subducting slab were added to the sub-arc mantle source. It is further suggested that high rate of addition of these fluids may be related with the rapid and shallow subduction of Arabian oceanic plate below the Zagros-Makran convergence zone that might have been developed due to the opening and rapid spreading of the Red Sea during that period. The studies farther suggested that arc magmatism in Kohistan-Ladakh, Kandhar, Chagai-Raskoh, Zagros arc, Semail, Bela, Muslim Bagh and Waziristan back-arc terrenes were probably started in a single segmented convergence zone, which developed in the Ceno Tethys during the Early Cretaceous (Figure 2, Siddiqui et al., 2012).
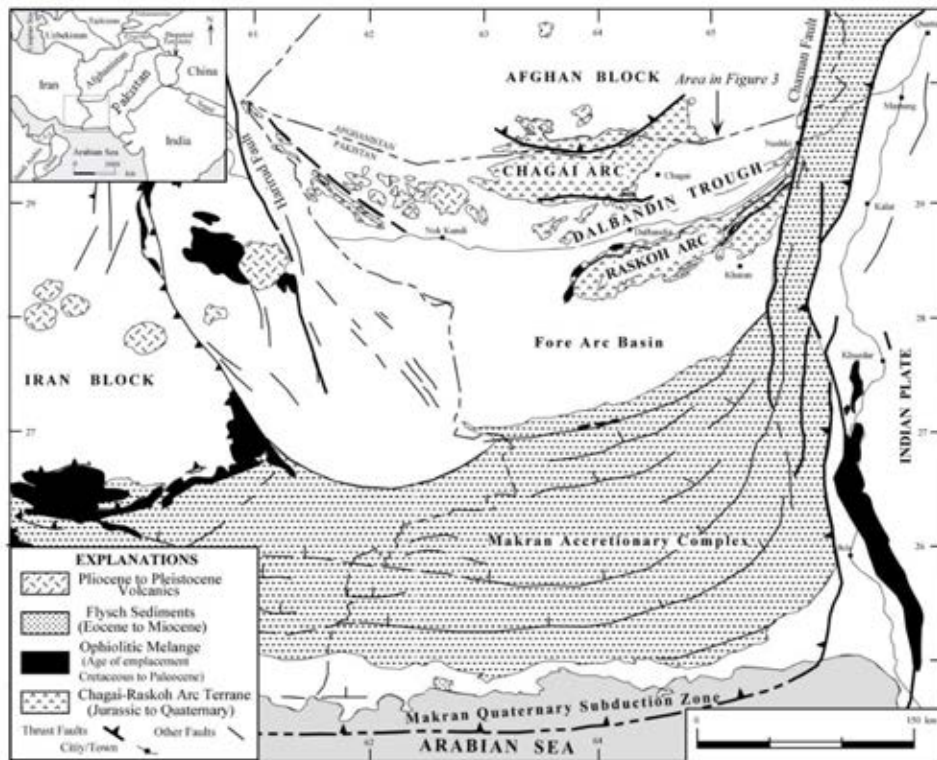
Fig. 1. Geological map of Chagai-Raskoh arc terrane, Balochistan, Pakistan (modifies and reproduced after Bakr and Jackson, 1964; Siddiqui et al., 2009, 2012).

The Chagai-Raskoh arc is one of the metallogenically most important mountain belts of Pakistan, as many important metal deposits including porphyry (Mo-Au-Ag), manto and vein type copper, stratiform and skarn type iron, volcanogenic gold and sulphur, kuroko type lead-zinc- silver-copper are associated with the magmatic rocks. The volcaonogenic iron and manganese ore deposits are associated with Late Cretaceous lava flows. The Kuruko type sulphide deposit is also found in the Late Cretaceous dacite porphyry stock intruded into the Late Cretaceous volcanics. The Skarn type iron ore is associated with the Eocene pyroxene-diorite. Large to giant porphyry Cu-Mo-Au deposits are generally associated with the Oligocene-Miocene tonalite, quarts-diorite and granodiorite porphyry stocks. The gold, sulfur and travertine deposits are assoc iated with the Quaternary volcanics of the Chagai arc.
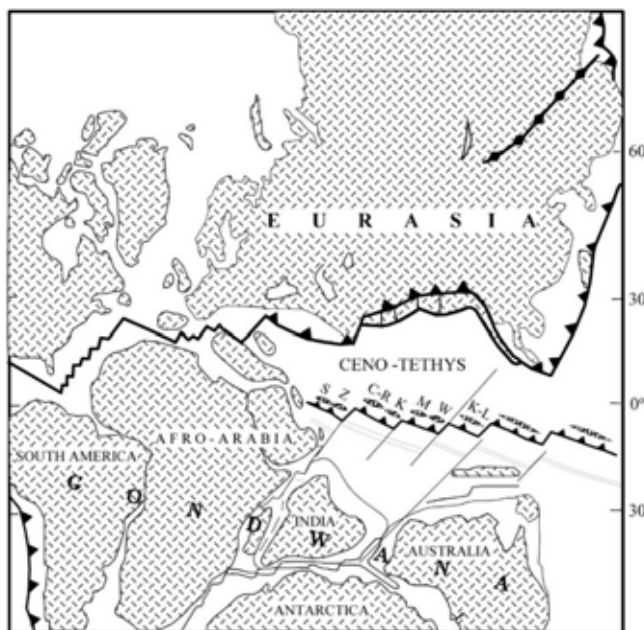
Fig. 2. Paleogeographic reconstruction of Ceno-Tethys and surrounding continents during 150-130 Ma (modified after Kazmin, 1991; Siddiqui et al., 2012). The S, Z, C-R, K, M, W and K-L represent Semail, Zagros, Chagai-Raskoh, Kandhar, Muslim Bagh, Waziristan and Kohistan-Ladakh arcs respectively.

References
Bakr, M. A. and Jackson, R. O., 1964. Geological Map of Pakistan. Geolological. Survey of Pakistan, Quetta.

Kazmin, V. G., 1991. Collision and rifting in the Tethyan Ocean: geodynamic implications. Tectonophysics 196, 371-384.

Siddiqui, R. H., Naka, T., Haque, M., 2009. Ceno-Tethyan Jurassic Radiolarian Fauna from the Ras Koh Arc. Balochistan, Pakistan Acta Geoscientica Sinica 30, 70-78.

Siddiqui, R. H., Jan, M. Q. and Khan, M. A., 2012. Petrogenesis of Late Cretaceous Lava Flows from a Ceno-Tethyan Island Arc: The Raskoh Arc, Balochistan, Pakistan. Journal of Asian Earth Science, 59, 24-28.

High pressure and high temperature carbon isotope fractionation in Fe–C system and its geochemical consequence

Reutsky V.N.

Institute of Geology and Mineralogy, Siberian Branch of the Russian Academy of Sciences, Novosibirsk, Russia, reutsky@igm.nsc.ru

Carbon forms very few mineral phases in the Earth's mantle at depths exceeding 200 km. The major phases are native carbon (graphite or diamond) and metal (mainly Fe) carbides (Stagno, Frost, 2010). It is widely accepted now that there is a possibility of metal saturation of the mantle below 150 km (Rohrbach et al, 2007; Frost, McCammon, 2008, Dasgupta, Hirschmann, 2010). Therefore, the presence of carbon in association with iron would allow for the formation of iron carbides. Not much is known about relationship of carbon isotope compositions between named phases. Empirical studies of carbon in meteorites show that cohenite ($(Fe,Ni,Co)_3C$) is depleted in ^{13}C relative to graphite from the same meteorite in a range from 0 to 15‰ (Deines, Wickman, 1973; 1975; Newton, Sugiura, 2000). Carbides are also found as inclusions in diamonds (Kaminsky, Wirth, 2011, Smith et al., 2016). Mikhail et al. (2014) have reported 7‰ depletion in ^{13}C of iron carbide inclusions compared to host diamond from the Jagersfontein mine, South Africa.

Looking to the Fe–C phase diagram (Fig. 1) one can see not much possibility for co-crystallization of iron carbides and graphite/diamond from a Fe–C melt within geochemically feasible PTx conditions (Lord et al, 2009). It is possible only within restricted area of peritectic reaction where the $L+Fe_3C+Dm/Gr$ association is stable. Early experimental investigation of carbon isotope fractionation in the solid part of the Fe-C phase diagram within the $Gr(Dm)+Fe_3C$ and $Gr(Dm)+Fe_7C_3$ fields failed to determine the value of isotope fractionation for diamond-carbide pairs because the metastable Fe–Gr eutectic melting, which is approximately 100° lower than the actual Fe-Fe$_3$C eutectic (Strong, Chrenko, 1971). This metastable melting provides carbon re-crystallization via Fe-C melt rather than solid state synthesis of equilibrium diamond and carbide (Reutsky, Borzdov, 2013). On the other hand, extremely slow carbon isotope diffusion in diamond prevents re-equilibration of isotope compositions at solid state conditions.
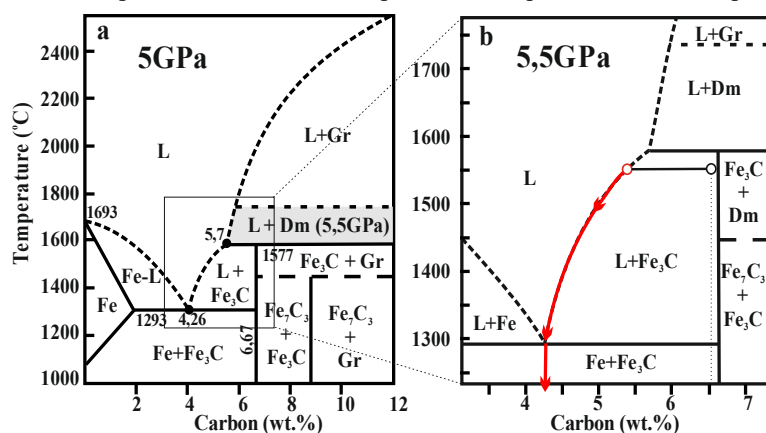
Fig. 1. (*a*) Iron rich part of the Fe-C diagram at 5 GPa (Lord et al., 2009) modified to show the L+Dm field at 5.5 GPa (Strong, Chrenko, 1971). L – field of Fe-C melt; Gr – graphite; Dm – diamond; Fe – iron; Fe$_3$C and Fe$_7$C$_3$ – corresponding carbides. (*b*) Particular region of experiments. Open circles – initial compositions of the mixture and first portion of melt Expected change of melt composition is shown with arrows.

In our earlier experiments (Reutsky et al., 2015) we had crystallizing Fe-C melt at 6.3GPa and 1600°C with slow cooling down to 1400°C during 3 hrs. Different initial proportion of iron metal (grade 99,998) and graphite ($\delta^{13}C_{VPDB}$=-23.0‰) provides crystallization of carbide with or without diamond. After experiments about 20% of Fe-C melt was quenched forming fine iron-carbide aggregate. This allows examination δ ^{13}C of Fe-C melt from which crystallization took place along with cohenite and diamond crystals.

In carbon-rich compositions diamond crystals were grown first from Fe-C melt at 1600°C within L+Dm stability field. These diamonds had higher $\delta^{13}C$ values (–20.3 to –22.2‰) than the carbon isotope composition of the starting mixture testifies early crystallization of diamond from Fe-C melt with expected isotope fractionation coefficient (Reutsky et al., 2008). Iron carbide starts to grow later at about 1570°C due to peritectic reaction $L+Dm \rightarrow L+Fe_3C$. The carbon isotope composition of Fe$_3$C in these experiments changes from -26.2 up to -24.8‰ along direction of growth.

In carbon-poor compositions the L+Dm field was not crossed and no diamond was found. Fe$_3$C aggregates show measurable isotope trends in directions of growth testifies isotope fractionation during cohenite crystallization. However, in this case the trend of δ ^{13}C in Fe$_3$C aggregate have opposite direction and starts from -24.8 going down to -26.8‰. Direct measurements of δ ^{13}C of iron carbide and quenched Fe-C melt nearby phase's boundary reveal 2.0±0.5‰ enrichment of crystalline phase by ^{13}C isotope in both carbon-rich and carbon-poor experiments.

In terms of carbon isotopes, the peritectic reaction looks like $L_1+Dm \rightarrow L_2+Fe_3C$ and L_1 differs from L_2 in carbon isotope ratio by adding heavy isotope from reacting diamond. Bearing in mind twice as much isotope fractionation at

diamond growth in comparison with cohenite, both of the trends represent isotope depletion in accordance with Rayleigh's equations (Reutsky et al., 2015).

Next series of experiments for HPHT crystallization of carbon-poor Fe-C melt using a range of $\delta^{13}C_{VPDB}$ of initial graphite from -52 up to +39 ‰ show the same relationship of crystalline Fe_3C and quenched Fe-C melt. In these series we were applying different cooling rates. The scale of cohenite enrichment in heavy carbon isotope relative to the melt varies from 9.3 to 0.6‰ and correlates with crystallization rate. Experiments with different initial $\delta^{13}C$ but the same cooling rates give equal scale of carbon isotope fractionation, meaning dominated role of kinetics. SIMS technique reveals pronounced down-trends of $\delta^{13}C$ values in direction of growth of the crystalline iron carbide regardless of actual $^{13}C/^{12}C$ value.

Difference of carbon isotope composition between diamond and residual melt in our experiments is within 6–7‰ which fits well results of Mikhail et al. (2014) for diamond-carbide inclusion relationship. This similarity can suggest crystallization of sample, investigated by S.Mikhail with co-workers, near the peritectic region of Fe-C diagram.

Documented differences of $\delta^{13}C$ values between carbide and quenched melt near the crystallization interface along with gradual depletion of Fe_3C by heavy carbon isotope indicate selective ^{13}C capture by crystallizing cohenite. Isotope profiles within crystalline Fe_3C aggregate also indicate that carbon isotope diffusion does not provide compositional relaxation of isotope heterogeneity under the experimental conditions near the melting point. These observations provide basis for consideration of Fe-C crystallization as one of mechanisms for generation of carbon isotope heterogeneity in the mantle. Crystallization of Fe-C melt in the Earth's mantle is suggested being responsible for genesis of extra-large diamonds (Smith et al., 2016). If correct, significant amount of iron carbide crystallized from this melt also can present in the mantle. If the melt was able to migrate while crystallize, the last portions of carbide can be significantly depleted in heavy carbon isotope in comparison with initial isotope ratio. This mechanism can be applicable for early Earth differentiation when metal (mainly iron) melts had oozed through the forming silicate mantle. Because carbon is virtually insoluble in minerals (Shcheka et al., 2006), at metal-silicate interface it goes to metal. Thus, significant part of primordial carbon should have gone into the Earth's core dissolved in metal melts (Dasgupta, 2013, Chi et al., 2014). Some fraction of this carbon has remained in the silicate mantle in the form of accessory phases, including graphite and diamond. Both minerals are heavier in carbon isotope composition compared to Fe-C melt and its crystallization provides depletion of the melt by ^{13}C isotope. Partial crystallization of the metal-carbon melts to carbide leads to further depletion of residual liquid in ^{13}C isotope even at high temperature and high pressure. Accounting potential amount of the melt and carbide, the core-forming metal melts can be extremely isotopically light in comparison with initial carbon isotope ratio. Carbon reservoirs differing in isotope composition could be generated by iron carbide and diamond crystallization during the primary differentiation of the Earth, even if it was initially well-homogenized. The carbon isotope ratio in these reservoirs should significantly lowering with depth. The existence of such reservoirs is widely discussed on the basis of carbon isotope compositions of mantle xenoliths and diamonds (Cartigny, 2010; Deines, 2002; Stachel et al, 2009).
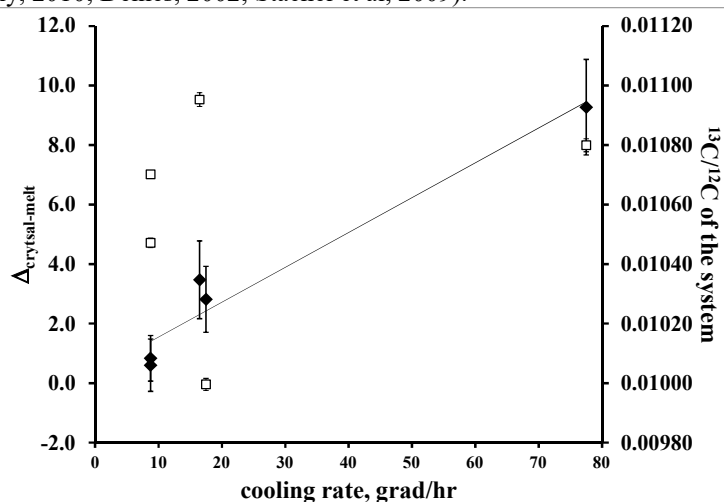
Fig. 2. Kinetic dependence of carbon isotope fractionation at Fe_3C crystallization from Fe-C melt. Black diamonds – $\delta^{13}C_{carbide}$- $\delta^{13}C_{melt}$ values, Open squares – initial $\delta^{13}C$ compositions of particular experiments.

Particular form of carbon depends on the metal/C ratio and metal composition of certain region of the mantle. At depth greater than 250-300 km a Fe-Ni-C melt phase assumed to be present (Rohrbach et al., 2014). The presence of nickel lowers the eutectic temperature of the Fe-C system and blocks the formation of carbides. Therefore, such a composition restricts the occurrence of carbides in the mantle. However, metasomatized crustal slabs low in nickel could be good example for potential source of iron carbides in association with diamond and melts (Rohrbach et al., 2014). On the other hand, nickel, as well as sulfur and silicon, lowers the solubility of carbon in metal melt (Dasgupta et al., 2013, Chi et al., 2014). Increasing pressure with depth decreases carbon solubility in Fe-Ni-C alloy as well (Narygina et al., 2011). At equal metal/C ratio, increasing Ni-content and depth provides an increase in carbon saturation and a lowering of the carbon amount needed for diamond nucleation. In case of sulfur-rich melt the temperature over 1600°C is required for diamond nucleation (Palyanov et al., 2006). Silicon carbide also can occur at

great depth, where carbon is depleted in heavy isotope. It can explain systematically low δ ^{13}C of SiC found in kimberlites (Shiryaev et al., 2008, Trumbull et al., 2009).

Considering the carbon abundance and metal/C ratio, Dasgupta and Hirschmann (2010) have shown that the assemblage of (Fe, Ni) carbide+Fe-Ni metal can be stable from ca. 50 to 500 ppm C at Fe^0 contents up to 1wt. %, which corresponds to OIB source mantle. In contrast, the MORB source mantle, with 10-30 ppm C and the same Fe^0 content, must hold all of the carbon as light alloying elements in metals. Our data on carbon isotope fractionation provides evidence that iron carbide and carbon-bearing metal must be isotopically distinct carbon reservoirs.

References:

Stagno V, Frost DJ (2010) Carbon speciation in the asthenosphere: Experimental measurements of the redox conditions at which carbonate-bearing melts coexist with graphite or diamond in peridotite assemblages. Earth Planet Sci Lett 300: 72–84.

Rohrbach A, Ballhaus C, Golla–Schindler U, Ulmer P, Kamenetsky VS, Kuzmin DV (2007) Metal saturation in the upper mantle. Nature 449: 456–458.

Frost DJ, McCammon CA (2008) The redox state of Earth's mantle. Annu Rev Earth Planet Sci 36: 389–420.

Dasgupta R, Hirschmann MM (2010) The deep carbon cycle and melting in Earth's interior. Earth Planet Sci Lett 298: 1–13.

Deines P, Wickman FE (1973) The isotopic composition of graphitic carbon from iron meteorites and some remarks on the troilitic sulfur of iron. Geochim Cosmochim Acta 37: 1295–1319.

Deines P, Wickman FE (1975) A contribution to the stable carbon isotope geochemistry of iron meteorites. Geochim Cosmochim Acta 39: 547–557.

Newton J, Sugiura N (2000) Carbon isotope measurements in iron meteorites. Meteorit Planet Sci 35: A118.

Kaminsky FV, Wirth R (2011) Iron carbide inclusions in lower-mantle diamond from Juina, Brazil. Canad Min 49: 555-572.

Smith EM, Shirey SB, Nestola F, Bullock ES, Wang J, Richardson SH, Wang W (2016) Large gem diamonds from metallic liquid in Earth's deep mantle. Science 354(6318): 1403-1405.

Mikhail S, Guillermier C, Franchi IA, Beard AD, Crispin K, Verchovsky AB, Jones AP, Milledge HJ (2014) Empirical evidence for the fractionation of carbon isotopes between diamond and iron carbide from the Earth's mantle. Geochem Geophys Geosystems 15(4): 855-866.

Lord OT, Walter MJ, Dasgupta R, Walker D, Clark SM (2009) Melting in the Fe–C system to 70 GPa. Earth Planet Sci Lett 284: 157–167.

Strong HM, Chrenko RM (1971) Properties of Laboratory-Made Diamond. J Phys Chem 76: 1838-1843.

Reutsky VN, Borzdov YuM (2013) A comment on "Experimental determination of carbon isotope fractionation between iron carbide melt and carbon: 12C-enriched carbon in the Earth's core?" by M. Satish-Kumar, H. So, T. Yoshino, M. Kato, Y. Hiroi [Earth Planet. Sci. Lett. 310 (2011) 340–348]. Earth Planet Sci Lett 368: 219–221.

Reutsky VN, Borzdov YM, Palyanov YN (2015). Carbon isotope fractionation during high pressure and high temperature crystallization of Fe–C melt. Chem Geol 406: 18-24.

Reutsky VN, Borzdov YM, Palyanov YN (2008) Carbon isotope fractionation associated with HPHT crystallization of diamond. Diam Relat Mater 17: 1986-1989.

Shcheka SS, Wiedenbeck M, Frost DJ, Keppler H (2006) Carbon solubility in mantle minerals. Earth Planet Sci Lett 245: 730–742.

Dasgupta R (2013) Ingassing, storage, and outgassing of terrestrial carbon through geologic time. Rev Min Geochem 75: 183–229.

Chi H, Dasgupta R, Duncan MS, Shimizu N (2014) Partitioning of carbon between Fe-rich alloy melt and silicate melt in a magma ocean – Implications for the abundance and origin of volatiles in Earth, Mars, and the Moon. Geochim Cosmochim Acta 139: 447–471.

Cartigny P (2010) Mantle-related carbonados? Geochemical insights from diamonds from the Dachine komatiite (French Guiana). Earth Planet Sci Lett 296: 329–339.

Deines P (2002) The carbon isotope geochemistry of mantle xenoliths. Earth-Sci Rev 58: 247–278.

Stachel T, Harris JW, Muehlenbachs K (2009) Sources of carbon in inclusion bearing diamonds. Lithos 112: 625.

Rohrbach A, Ghosh S, Schmidt MW, Wijbrans CH, Klemme S (2014) The stability of Fe–Ni carbides in the Earth's mantle: Evidence for a low Fe–Ni–C melt fraction in the deep mantle. Earth Planet Sci Lett 388: 211–221.

Narygina O, Dubrovinsky LS, Miyajima N, McCammon CA, Kantor IYu, Mezouar M, Prakapenka VB, Dubrovinskaia NA, Dmitriev V (2011) Phase relations in Fe–Ni–C system at high pressures and temperatures. Phys Chem Minerals 38: 203–214.

Palyanov YuN, Borzdov YuM, Khokhryakov AF, Kupriyanov IN, Sobolev NV (2006) Sulfide melts–graphite interaction at HPHT conditions: Implications for diamond genesis. Earth Planet Sci Lett 250: 269–280.

Shiryaev AA, Wiedenbeck M, Reutsky V, Polyakov VB, Mel'nik NN, Lebedev AA, Yakimova R (2008) Isotopic heterogeneity in synthetic and natural silicon carbide. J Phys Chem Solids 69(10): 2492-2498.

Trumbull RB, Yang JS, Robinson PT, Di Pierro S, Vennemann T, Wiedenbeck M (2009) The carbon isotope composition of natural SiC (moissanite) from the Earth's mantle: New discoveries from ophiolites. Lithos 113(3): 612-620.

OXIDE MINERAL INCLUSIONS IN CR-PYROPES FROM THE ALDANSKAYA LAMPROPHYRE DYKE, YAKUTIA

Rezvukhin D.I., Nikolenko E.I., Sharygin I.S., Malkovets V.G.

Institute of Geology and Mineralogy, Siberian Branch of the Russian Academy of Sciences, Novosibirsk, Russia,
m.rezvukhin@igm.nsc.ru

Kimberlite and lamproite/lamprophyre magmas sample a wide variety of xenoliths and xenocrysts from the subcontinental lithospheric mantle (SCLM). Cr-rich pyrope, along with chromite and picroilmenite, is common kimberlite indicator mineral. Xenocrysts of Cr-pyrope from kimberlites and other deep-seated magmatic rocks have been widely used by geochemists in recent decades in order to obtain information about composition and structure of the SCLM. Oxide inclusions within pyropes are of particular interest. Mineralogical studies have shown that pyrope may contain uncommon Ti-rich oxides, such as rutile, picroilmenite, armalcolite, srilankite, carmichaelite, crichtonite group minerals, and other varieties (Varlamov et al., 1996; Wang et al., 1999; Vrana, 2008; Alifirova et al., 2012; Ziberna et al., 2013; Rezvukhin et al., 2016a, 2016b; Malkovets et al., 2016). These inclusions are commonly enriched in rare and incompatible elements and represent composition, which is not typical to depleted peridotites of the lithospheric mantle. Metasomatic origin of Cr-pyrope in the SCLM of ancient cratons is widely discussed in literature on the basis of both mineralogical and geochemical criteria (Hoal et al., 1994; Griffin et al., 1999; Stachel et al., 2004; Malkovets et al., 2007, 2012; Agashev et al., 2013; O'Reilly, Griffin, 2013). Further detailed studies will shed light on the features of pyrope genesis in deep areas of the earth's upper mantle. Here we report the result of investigation of twenty six chrome-rich pyropes with oxide mineral inclusions derived from the eluvium of the Aldanskaya lamprophyre dyke, Aldan province of alkaline magmatism, southeast of the Siberian craton.

Size of studied pyrope grains ranges from 2 to 4 mm. Crystals were implanted in epoxy mounts and polished to bring individual inclusions to the surface. All studied inclusions are primary and are not associated with cracks. Pyrope garnets are predominantly of lherzolitic paragenesis with Cr_2O_3 content from 2.1 to 6.5 wt%. Four Ti- and/or Cr-rich phases have been investigated as inclusions in pyropes: rutile, picroilmenite, chromite and crichtonite group minerals. Inclusions of Ti-oxides are commonly needle- or blade-like, with round or polygonal cross-sections. Laths and tablets are less abundant. Chromite is presented as isometric inclusions, either octahedral or round. Both elongated blades and isometric inclusions are commonly black and opaque, although thin needles of rutile are more brownish. Sometimes needle-like inclusions are strictly oriented in the host pyrope along the certain crystallographic directions. Diameter of studied needle-like inclusions ranges from 5 to 50 μm and size of isometric chromite inclusions is up to 300 μm. In studied samples oxide inclusions are in association with silicates (namely olivine, ortho- and clinopyroxene). Oxides may form intergrowths and composite inclusions with each other or with silicates; rutile commonly forms intergrowths with Mg-ilmenite.
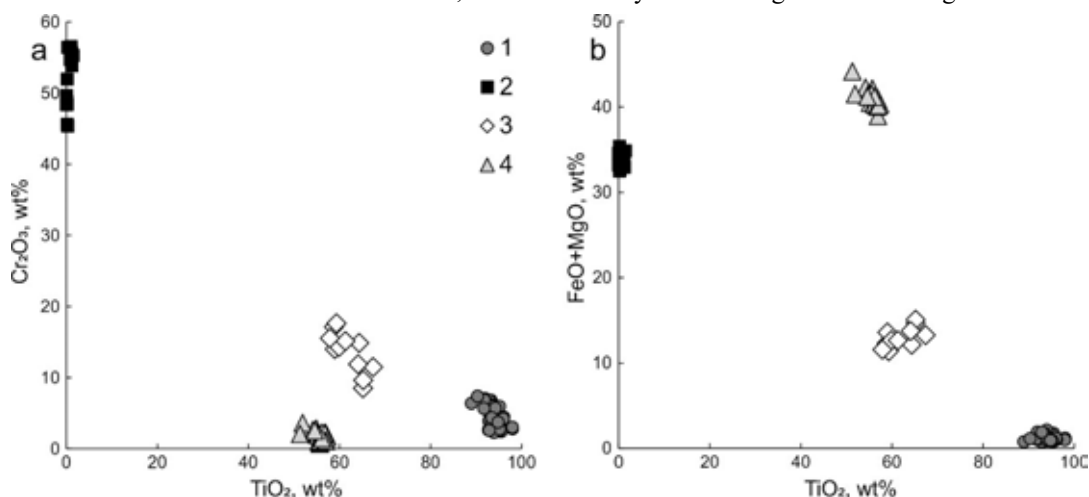
Fig. 1. Composition of oxide mineral inclusions in Cr-pyropes from the Aldanskaya dyke on TiO_2-Cr_2O_3 (a) and TiO_2-FeO_{total}+MgO (b) plots. 1 – rutile; 2 – chromite; 3 – crichtonite group minerals; 4 – picroilmenite.

Chemical composition of studied inclusions in terms of main constituent components is shown on Fig. 1 (a, b). Composition of inclusions is uniform in a single pyrope host, but varies among different pyrope crystals; however, the scatter is not broad and compositional fields for each mineral are clearly constrained. Similar to host pyrope, inclusions are commonly Cr-rich. There is a positive correlation between Cr content in Ti-oxide inclusions and host garnet. Similar

correlations have been recorded previously between Ti-oxide inclusions and host garnets from the Internatsionalnaya pipe (Rezvukhin et al., 2016a, 2016b), as well as in the same mineral association from the ultrabasic diatreme of the Garnet Ridge cluster, Arizona, USA (Wang et al., 1999). Chromite inclusions contain 45.4-58.7 wt% Cr_2O_3. It is interesting to note the significant decrease of Cr_2O_3 content up to 1.5 wt% in host pyrope in thin domains just around the large chromite inclusions. Cr is also the most abundant substituting component in members of the high-Ti association (rutile, picroilmenite, crichtonite group minerals). Cr_2O_3 content in rutile ranges from 2.3 to 7.4 wt%, in picroilmenite from 0.7 to 3.6 wt%. In chromite inclusions MgO varies from 8.2 to 10.4 wt%, FeO from 22.4 to 26.6 wt%, Al_2O_3 from 8.2 to 20.2 wt%. Chromite also contains up to 1.5 wt% TiO_2. In rutile inclusions TiO_2 content ranges from 89.0 to 98.0 wt%. Except elevated amounts of Cr, rutile contains 0.8-3.3 wt% FeO and up to 0.6 wt% ZrO_2. Mg-ilmenite contains 51.3-57.4 wt% TiO_2, 8.3-13.6 wt% MgO, 25.7-35.5 wt% FeO.

Crichtonite group minerals are rare oxides (titanates) with general formula $ABC_{18}T_2O_{38}$. Crichtonite group minerals are of particular interest due to enrichment in wide variety of incompatible elements, which occupy all four structural positions. Main constituent elements, which fill mostly C and T sites, are in typical range for crichtonite group minerals stable in the lithospheric mantle. TiO_2 is 54.2-67.4 wt%, Cr_2O_3 is 6.9-19.8 wt%, FeO is 7.7-11.6 wt%, and MgO is 1.6-4.1 wt%. Within the group the minerals are distinguished on the basis of dominant cations in A, B, C and T sites. The most important is A site, where large cation of incompatible element is stored. In studied grains 7 cations (Ba, Sr, Na, K, Ca, La, Ce) in A site are presented in different proportions. The dominant cations (at%) are Ca and Ba. B site is occupied by Zr (1.5-5.9 wt% ZrO_2) and Fe. Thus studied crichtonite group minerals are similar to either loveringite (Ca-dominant member of the group) or LIMA series (**li**ndsleyite-**ma**thiasite, Ba and K members of the group, respectively), widely reported from the kimberlites of South Africa (Haggerty et al., 1983; Haggerty, 1991; Konzett et al., 2013). On Fig. 2 the occupancy of A site in different crichtonite group minerals is shown. LIMA series is Ba or K rich, while hitherto reported inclusions in pyropes contain more Ca, Na, LREE or Sr, and the little overlap between fields is presented. Crichtonite group minerals in pyropes from the Aldanskaya dyke somewhat differ in terms of A site occupancy from grains investigated in pyropes from other localities. Compositional points fall in both fields and comprise intermediate trend between LIMA series and Ca/Na/LREE/Sr-rich minerals in pyropes from other localities. However, lindsleyite and mathiasite in kimberlites from the Kaapvaal craton are commonly Al-poor (<1 wt% of Al_2O_3), while inclusions in pyropes are Al-rich (>1 wt% Al_2O_3), including studied grains in pyropes from the Aldanskaya dyke, which contain 1-2 wt% Al_2O_3.

Table 1. EMP analyses of crichtonite group minerals in pyropes from the Aldanskaya dyke

Grain	ALD-1	ALD-2	ALD-3	ALD-4	ALD-5	ALD-6	ALD-7	ALD-8	ALD-9	ALD-10	ALD-11
SiO_2	0.08	0.06	0.10	0.14	0.23	0.10	0.13	0.13	0.16	0.07	0.02
TiO_2	58.80	58.98	59.32	65.19	64.34	67.40	59.90	61.30	65.21	57.90	64.10
Al_2O_3	1.57	1.42	1.58	1.28	1.43	1.09	1.28	1.47	1.39	1.48	1.02
MgO	2.96	3.11	3.31	3.68	3.59	3.92	3.20	3.46	4.07	3.25	3.80
Cr_2O_3	17.12	13.99	17.63	8.49	14.87	11.47	14.30	15.13	9.62	15.53	11.87
FeO^*	9.32	10.48	8.07	10.99	8.56	9.36	9.47	9.18	11.00	8.32	9.95
BaO	0.88	3.06	1.18	0.32	0.19	0.32	0.64	1.08	0.78	5.07	1.00
SrO	0.50	0.32	0.23	0.51	0.34	0.39	0.60	0.56	0.58	0.25	0.57
Na_2O	0.20	0.09	0.21	0.31	0.55	0.61	0.18	0.22	0.26	0.04	0.55
K_2O	0.64	0.57	0.65	0.69	0.50	0.54	0.87	0.65	0.63	0.30	0.46
CaO	1.51	0.85	1.47	1.51	1.66	1.59	1.37	1.56	1.67	0.69	1.39
La_2O_3	0.01	0.04	0.05	0.11	n.d.	0.08	0.01	n.d.	0.04	n.d.	n.d.
Ce_2O_3	0.67	1.34	0.65	0.67	0.33	0.40	0.51	0.66	0.68	1.91	0.50
ZrO_2	4.02	4.65	3.89	4.52	2.27	1.76	5.21	3.37	1.64	4.93	3.00
NiO	0.04	0.03	0.04	0.06	0.02	0.07	0.05	0.06	0.07	0.04	0.07
V_2O_3	0.65	0.91	0.55	0.88	0.60	0.53	0.81	0.70	0.60	0.76	0.47
MnO	0.12	0.10	0.11	0.17	0.16	0.17	0.13	0.14	0.17	0.09	0.13
Nb_2O_5	n.d.	n.d.	n.d.	n.d.	n.d.	n.d.	n.d.	n.d.	n.d.	n.d.	n.d.
HfO_2	0.06	0.19	0.23	0.18	0.06	n.d.	0.13	0.12	0.07	0.14	0.12
Total	99.14	100.18	99.26	99.69	99.71	99.80	98.78	99.80	98.64	100.78	99.00

n.d. – not determined, *total Fe as FeO.

The genesis of studied inclusions is debatable. Oxide needles in garnet may result from exsolution processes, or they could be syngenetic or even protogenetic in relation to the host pyrope. It is assumed that Ti-oxides tend to form oriented elongated inclusions in pyrope matrix even if their formation is related to fluid/melt phase. The diameter of studied grains is relatively big; we suggest that formation of large oxide inclusions (especially inclusions of crichtonite group minerals) via exsolution is highly unlikely and they are probably syngenetic with the host pyrope. Nevertheless, Ti-rich mineral association enriched in incompatible elements (Fe, Ti, Ba, Zr and others) in pyropes indicates that these pyropes in the lithospheric mantle underneath the Aldanskaya dyke have metasomatic origin. Incompatible elements were introduced by metasomatic fluid/melt phase, while high chromium content in both pyropes and inclusions was inherited from Cr-rich peridotite protolith, where Cr is concentrated mainly in chromite and subcalcic harzburgitic or dunitic garnet.
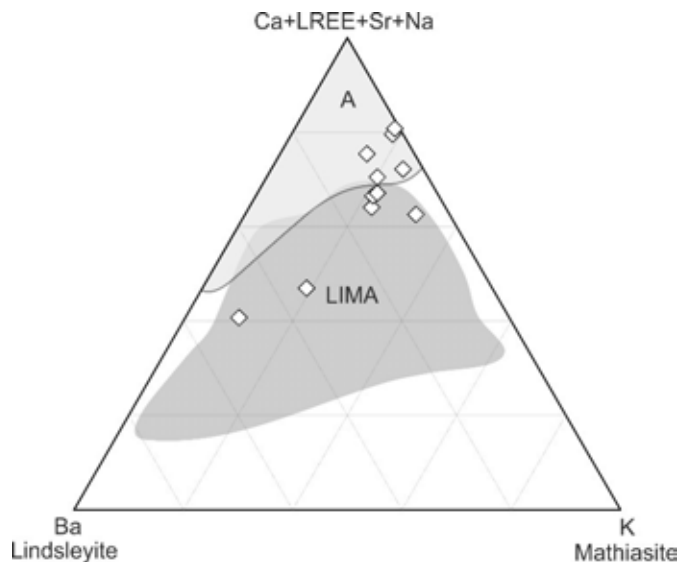
Fig. 2. Composition of inclusions of crichtonite group minerals in Cr-pyropes from the Aldanskaya dyke on the ternary diagram Ba – K – Ca+LREE+Sr+Na (A-site occupancy, at%). Outlined fields: (A) – inclusions in Cr-pyropes from other localities (Wang et al., 1999; Vrana, 2008; Rezvukhin et al., 2016a); (LIMA) – minerals of lindsleyite-mathiasite series from South African kimberlites (Haggerty et al., 1983; Haggerty, 1991; Konzett et al., 2013).

Described above mineral association represent conventional set of high-Ti and/or Cr oxides, which is typical for Cr-pyropes from several localities described in literature (Varlamov et al., 1996; Wang et al., 1999; Vrana, 2008; Rezvukhin et al., 2016a, 2016b). However, variations in composition of oxide inclusions in studied pyropes and in other pyropes reported elsewhere indicate on a different composition of metasomatic agent. If compositional features of inclusions reflect the peculiarities of metasomatic phase, then by studying both pyropes and inclusions it is possible to reconstruct geochemical features of parental fluids/melts. Rutile and crichtonite group minerals are important storage sites of incompatible elements in the SCLM. Rutile in metasomatised mantle associations, and as inclusions in pyropes, is often enriched in HFSE, particularly in Nb_2O_5 (Jones et al., 1982; Tollo, Haggerty, 1987; Schulze, 1990; Wang et al., 1999; Konzett et al., 2013; Rezvukhin et al., 2016b). However, neither rutile nor crichtonite group minerals in pyropes from the Aldanskaya dyke contain significant Nb or Ta. Crichtonite group minerals in pyropes from the Aldanskaya dyke represent more Ba- and K-rich compositions in comparison with inclusions of these minerals in other pyropes, and several grains almost coincide with LIMA by composition. However, LIMA series from South Africa is lower in Al, and may contain up to 1.5 wt% Nb_2O_5 (Konzett et al., 2013). What is especially notable is that minerals of LIMA series commonly occur in *garnet-free* phlogopite–K-richterite peridotites (Erlank et al., 1987).

We note finally that pyropes from the Aldanskaya dyke and other lamprophyres of the Chompolo field contain complex association of inclusions: oxides, silicates, sulfides, and composite assemblages consisting of above-mentioned minerals + carbonates and hydrous phases. Thereby metasomatism in the SCLM underneath the Aldan shield is manifold in its occurrences and may be multistage. Further geochemical investigations are required to clarify its exact nature.

References:

Agashev AM, Ionov DA, Pokhilenko NP, Golovin AV, Cherepanova Y, Sharygin IS (2013) Metasomatism in lithospheric mantle roots: Constraints from whole-rock and mineral chemical composition of deformed peridotite xenoliths from kimberlite pipe Udachnaya. Lithos 160-161: 201-215.

Alifirova TA, Pokhilenko LN, Ovchinnikov YI, Donnelly CL, Riches AJV, Taylor LA (2012) Petrologic origin of exsolution textures in mantle minerals: evidence in pyroxenitic xenoliths from Yakutia kimberlites. International Geology Review 54(9): 1071-1092.

Erlank A, Waters F, Hawkesworth C, Haggerty S, Allsopp H, Rickard R, Menzies M (1987) Evidence for mantle metasomatism in peridotite nodules from the Kimberley pipes, South Africa. In: Mantle metasomatism, pp. 221-311.

Griffin WL, Shee SR, Ryan CG, Win TT, Wyatt BA (1999) Harzburgite to lherzolite and back again: metasomatic processes in ultramafic xenoliths from the Wesselton kimberlite, Kimberley, South Africa. Contributions to Mineralogy and Petrology 134: 232-250.

Haggerty SE (1991) Oxide mineralogy of the upper mantle. In: Lindsley DH (ed) Oxide Minerals: Petrologic and Magnetic Significance, Vol. 25, pp. 355-416.

Haggerty SE, Smyth JR, Erlank AJ, Rickard RS, Danchin RV (1983) Lindsleyite (Ba) and mathiasite (K): two new chromium-titanates in the crichtonite series from the upper mantle. American Mineralogist 68: 494-505.

Hoal K, Hoal B, Erlank A, Shimizu N (1994) Metasomatism of the mantle lithosphere recorded by rare earth elements in garnets. Earth and Planetary Science Letters 126: 303-313.

Jones AP, Smith JV, Dawson JB (1982) Mantle metasomatism in 14 veined peridotites from Bultfontein mine, South Africa. The Journal of Geology 90(4): 435-453.

Konzett J, Wirth R, Hauzenberger C, Whitehouse M (2013) Two episodes of fluid migration in the Kaapvaal Craton lithospheric mantle associated with Cretaceous kimberlite activity: evidence from a harzburgite containing a unique assemblage of metasomatic zirconium-phases. Lithos 182-183:165-184.

Malkovets VG, Griffin WL, O'Reilly SY, Wood BJ (2007) Diamond, subcalcic garnet, and mantle metasomatism: Kimberlite sampling patterns define the link. Geology 35(4): 339-342.

Malkovets VG, Griffin WL, Pearson NJ, Rezvukhin DI, O'Reilly SY, Pokhilenko NP, Garanin VK, Spetsius ZV, Litasov KD (2012) Late metasomatic addition of garnet to the SCLM: Os-isotope evidence. 10th International Kimberlite Conference, Long Abstract №10IKC-173.

Malkovets VG, Rezvukhin DI, Belousova EA, Griffin WL, Sharygin IS, Tretiakova IG, Gibsher AA, O'Reilly SY, Kuzmin DV, Litasov KD (2016). Cr-rich rutile: A powerful tool for diamond exploration. Lithos 265:304-311.

O'Reilly SY, Griffin WL (2013) Mantle metasomatism. In: Metasomatism and the chemical transformation of rock, Springer, pp. 471-533.

Rezvukhin DI, Malkovets VG, Sharygin IS, Kuzmin DV, Gibsher AA, Litasov KD, Pokhilenko NP, Sobolev NV (2016) Inclusions of crichtonite group minerals in pyropes from the Internatsionalnaya kimberlite pipe, Yakutia. Doklady Earth Sciences 466(2): 206-209.

Rezvukhin DI, Malkovets VG, Sharygin IS, Kuzmin DV, Litasov KD, Gibsher AA, Pokhilenko NP, Sobolev NV (2016) Inclusions of Cr-and Cr–Nb-Rutile in pyropes from the Internatsionalnaya kimberlite pipe, Yakutia. Doklady Earth Sciences 466(2): 173-176.

Schulze DJ (1990). Silicate-bearing rutile-dominated nodules from South African kimberlites: Metasomatized cumulates. American Mineralogist 75: 97-104.

Stachel T, Aulbach S, Brey GP, Harris JW, Leost I, Tappert R, Viljoen KF (2004) The trace element composition of silicate inclusions in diamonds: a review. Lithos 77(1): 1-19.

Tollo RP, Haggerty SE (1987) Nb-Cr-rutile in the Orapa kimberlite pipe, Botswana. Canadian Mineralogist 25: 251-264.

Varlamov DA, Garanin VK, Kostrovitskiy SI (1996) Exotic high-titanium minerals as inclusions in garnets from lower crustal and mantle xenoliths. Trans Russ Acad Sci Earth Sci 345: 352-355.

Vrana S (2008) Mineral inclusions in pyrope from garnet peridotites, Kolín area, central Czech Republic. Journal of Geosciences 53: 17-30.

Wang L, Essene EJ, Zhang Y (1999) Mineral inclusions in pyrope crystals from Garnet Ridge, Arizona, USA: implications for processes in the upper mantle. Contributions to Mineralogy and Petrology 135: 164-178.

Ziberna L, Nimis P, Zanetti A, Marzoli A, Sobolev NV (2013) Metasomatic processes in the central Siberian cratonic mantle: Evidence from garnet xenocrysts from the Zagadochnaya kimberlite. Journal of Petrology 54(11): 2379-2409.

U-Pb SHRIMP-II Dating of titanite and pyrochlore in Lovozero and Khibiny alkaline rocks and ORES

Rodionov N.V.[1], Lepekhina E.V.[1], Antonov A.V.[1], Belyatsky B.V.[1], _Arzamastsev A.A._[2,3] Sergeev S.A.[1]

[1]Federal State Budgetary Enterprise 'A. P. Karpinsky Russian Geological Research Institute', Saint-Petersburg, Russia, bbelyatsky@mail.ru

[2]Saint-Petersburg State University, Saint-Petersburg, Russia, arzamas@ipgg.ru

[3]Institute of Precambrian Geology and Geochronology of the Russian Academy of Sciences, Saint-Petersburg, Russia

Abundant age-data obtained during recent decades for alkaline polyphase Khibiny and Lovozero massifs using mineral fractions and U-Pb, Rb-Sr, Sm-Nd and Ar-Ar isotope systems, and whole-rock Rb-Sr, Sm-Nd and Pb-Pb isochrones, allow to limit the activity time of the ore-magmatic system for a period of 383-362 Ma for Khibiny and Lovozero massifs (Kramm, Kogarko, 1994; Arzamastsev and others, 2013; Arzamastsev, Wu, 2014; Zartman, Kogarko, 2014). At the same time, the closing temperatures of the used isotope systems (Kylander-Clark et al., 2008) differ significantly (by more than 300-400°C, e.g. between U-Pb system of perovskite or zircon and Rb-Sr and Ar-Ar systems of phlogopite). It remains unclear whether the resulting time interval (about 10-20 my.) is related to the actual duration of magmatic activity, the consequent intrusion of melts of alkaline-ultrabasic series, alkaline syenites, carbonatites and the formation of apatite-rare metal ores, or reflects variations in the closure temperature of specific isotope systems. In order to answer this question we have dated a number of samples of alkaline rocks and apatite-nepheline ores from these massifs using a single approach - a local isotopic analysis of titanite U-Pb system by SHRIMP-II. Titanite fractions from the main varieties of rocks of the two largest alkaline intrusions of the Kola Peninsula represent agpaitic syenites of the both massifs, foidolites, and rocks adjacent to the deposits of apatite-nepheline, titanite-apatite, eudialyte and loparite ores.

**Titanite U-Pb SHRIMP-II analysis.** Hand-picked titanite grains were implanted into the epoxy resin along with the OLT1 standard titanite grains. The surface of the resin was ground and polished about half the thickness of the grains, and then a gold coating was applied. Optical images of the investigated grains in reflected and transmitted light, as well as images in back-scattered electrons (BSE) were used for selection suitable sites for isotope dating. Titanite cathodoluminescent images were not applied due to absence of any CL of titanite crystal structure. Measurements of the titanite U/Pb ratios were performed on a high-resolution secondary ion microprobe SHRIMP-II at the Isotope Research Center (VSEGEI, St-Petersburg) in a similar approach to those described in (Kennedy et al., 2010).

The results of a titanite U-Pb local analysis were plotted on a diagram with a concordia in the Tera-Wasserburg coordinates as measured, i.e. uncorrected for common Pb content, $^{207}Pb/^{206}Pb$ and $^{238}U/^{206}Pb$ ratios. A linear trend was calculated on the basis of the correlation of the whole set of analytical data. The lower intersection of this trend line with the concordia was determined as an $^{238}U/^{206}Pb$ age of the titanite. An additional method of age calculation included constructing an "anchored" mixing line, i.e. the line passed through a fixed point with a priori certain coordinates. Usually,

the value $^{207}Pb/^{206}Pb$ of the point of intersection of the mixing line with the ordinate axis is determined according to the Stacey-Kramers model of the evolution of the Earth's Pb isotope composition for the titanite age calculated by the previous method. In our case this value of the $^{207}Pb/^{206}Pb$ ratio is equal to 0.86 and corresponds to the composition of common Pb 360-370 m.y. ago. The coincidence of the ages calculated by these methods is a necessary confirmation of the truth of the obtained estimation of the age of the dated titanite. In addition, the use of "anchored" mixing lines makes it possible to significantly reduce the error value in the age determined, especially if the variations in the values of the measured isotope ratios are limited to a narrow interval.

The age of silicate rocks and apatite-nepheline ores of the Khibiny massif.
The ages of titanite from melteigite-ijolite layered complex, kalsilite-bearing nepheline-syenite (rischorrite) and the central foyaite intrusion (Fig.1), vary in a narrow range of 367-382 Ma with the error-value of ± 7-11 m.y., suggesting the synchronous evolution of the U-Pb system of the studied samples. In order to test this assumption, we calculated the U-Pb age for the whole set of 121 analyses from 5 samples of rocks, based only on the analytical scatter of the data. A linear stretching of the data-points along the trend from the lower intersection with the concordia-line to the upper one obtained a fairly accurate estimation of 379.6 ± 5.8 Ma (MSWD =1.06) (Fig.2a). The presence in this set of two analyses with a U less than 1 ppm makes it possible to determine the position of the upper intersection of the calculated trend with a smaller overall error of 375.9 ± 3.5 Ma with a higher MSWD (1.1). However, calculating the weighted average $^{206}Pb/^{238}U$ age adjusted for the common Pb content obtain the value of 374.1 ± 3.7 Ma (MSWD = 1.04, probability of 0.36). This date is taken as the most accurate age estimation of titanite crystallization time of the Khibiny alkaline agpaitic syenites.
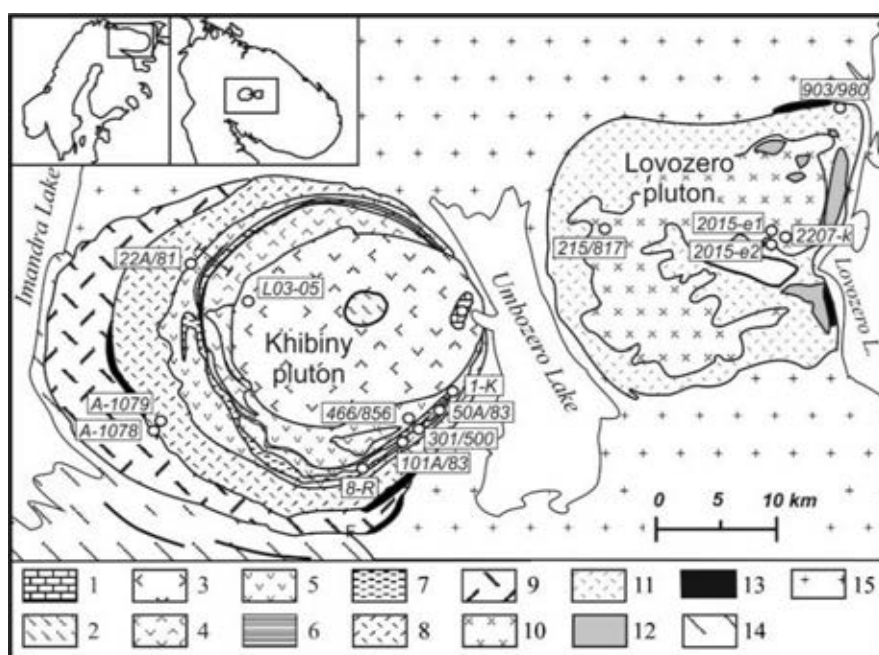
Fig. 1. Schematic geological map of the Khibiny and Lovozero massifs with the location of the samples studied. 1 - carbonatite, 2 - pulaskite, 3 and 4 - foyaite, 5 - kalsilite-bearing nepheline syenite (rischorrite), 6 - apatite-nepheline rock, 7 - foidolite, 8-9 - nepheline syenite (khibinite), 10 – eudialyte-lujavrite, 11 - differentiated lujavrite-foyaite-urtite complex, 12 - subalkaline volcanics, 13 - alkaline-ultrabasic rocks, 14 and 15 - rocks of Precambrian basement.
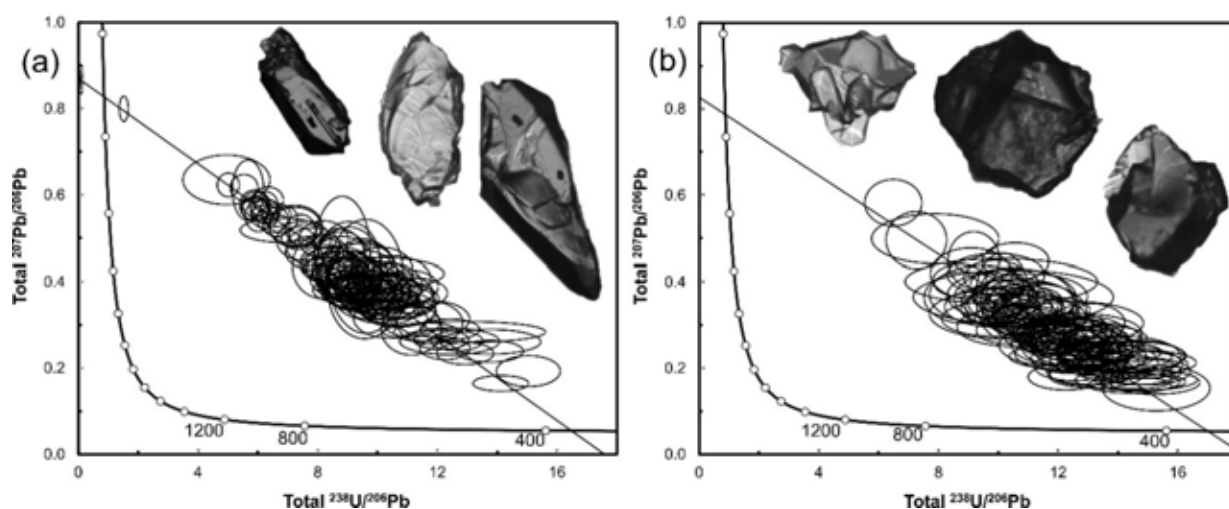
Fig. 2. U-Pb concordia Tera-Wasserburg diagrams without correction for common Pb for the studied titanite of the Khibiny alkaline massif: (a) titanite from a polyphase ijolite-urtite complex: T = 379.6 ± 5.8 Ma, MSWD = 1.06, n = 121; and (b) titanite from varieties of apatite-nepheline ore: T = 368 ± 10, MSWD = 1.8, n = 120.
The size of the data-point error ellipses corresponds to the 2σ. Typical grains of the studied titanite samples, 200-400 μm in size, in transmitted light are also shown.

Calculation and construction of mixing lines for U-Pb titanite data of each of the samples representing varieties of apatite-nepheline ores of the Khibiny massif show that the age of these titanites varies in the range from 365 to 376 Ma. Despite the relatively large error of the measured $^{238}U/^{206}Pb$ ratios, which is determined by the low U, all the analytical data (120 analyses) form a compact cluster that is approximated by the isochron crossing the concordia line at a point with an age of 368 ± 10 Ma with MSWD 1.8 (Fig. 2b). The calculation of the weighted average age according to the $^{206}Pb/^{238}U$ ratio with correction of the measured Pb isotope composition for the common Pb using ^{207}Pb yields the same estimation within the error, but significantly smaller scatter 371 ± 4.2 Ma (95% confidence interval, MSWD = 1.7, n = 120). It should be noted that the use of the method of calculation of the mixing line with the unradiogenic Pb component having the isotopic ratio $^{207}Pb/^{206}Pb$ equal to 0.86 provides actually identical age estimation: 374.6 ± 4.2 Ma at MSWD equal to 1.8. Comparison of the weighted average age estimations for titanite from silicate rocks and phosphate ores of the Khibiny massif gives 374.1 ± 3.7 Ma and 371 ± 4.2 Ma, respectively, thus providing evidence for the their synchronous origin.

The age of lujavrites and titanite mineralization of the Lovozero massif. The analysed dark-brown large fragments of grains and titanite crystals from the lujavrite of the differentiated rocks within the Alluaiv area have an elevated U content up to 12 ppm and Th up to 40 ppm, a very constant Th/U ratio (2.2-3.2) and a significantly larger common Pb compared to the Khibiny massif titanite. The entire set of 52 analyses form a compact group of data-points in the U-Pb diagram at a considerable distance from the concordia (Fig. 3), which determines significant uncertainties in line-propagation and age interpretation. Using the observed analytical scatter of U-Pb ratios, it was possible to calculate and construct a linear trend corresponding to an age of 383 ± 13 Ma and MSWD equal to 1.1, whereas a mixing line under the assumption of a mixing unradiogenic component with $^{207}Pb/^{206}Pb$ equal to 0.86 defines a significantly younger age - 359.8 ± 3.6 Ma and elevated MSWD - 1.3. Calculation of the weighted average $^{206}Pb/^{238}U$ age due to correction of the isotope composition from the measured ^{207}Pb for 47 analyses (5 analyses with the maximum individual errors were excluded from the calculation) allows to obtain an age estimation at 380.9 ± 4.5 Ma (1.2%, 2σ) with the best statistical parameters - MSWD 1.1 and probability 0.24. This age is accepted as the best estimation for the time of the U-Pb isotope system formation and titanite crystallization during lujavrite intrusion within Lovozero massif.
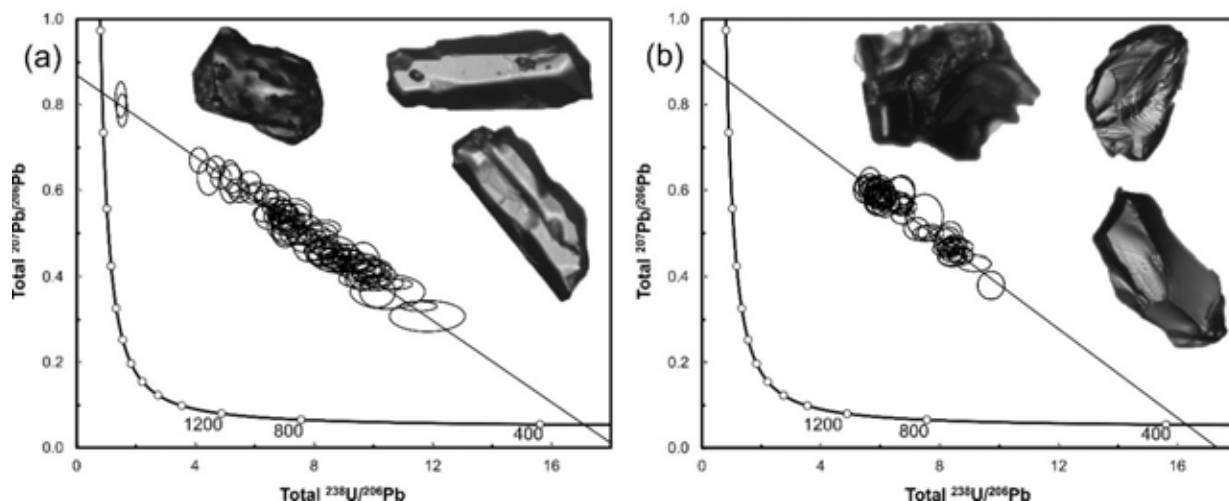
Fig. 3. U-Pb concordia diagrams without correction for common Pb for the studied titanite of the Lovozero alkaline massif: (a) titanite from the lujavrite of the differentiated complex: T = 383 ± 13 Ma, MSWD = 1.1, n = 52; (b) titanite from apatite-titanite ore-bearing ijolite: T = 366.1 ± 8.7 Ma, MSWD = 1.6, n = 88. The size of the error-ellipses corresponds to the 2σ. Typical grains of studied titanite 250-350 μm are also shown in transmitted light.

The other studied samples come from alkaline syenite which forms a deep core of the Lovozero massif (drill-hole 980, depth > 1180 m). This rock contains both accessory zircon and pyrochlore (Fig.1). The obtained age estimation of zircon (374 ± 23 Ma) (Arzamastsev et al., 2007) coincides with the age of the differentiated lujavrite-foyaite-urtite complex of the Lovozero massif and the intrusion of agpaitic nepheline-syenites of the Khibiny massif (381 Ma and 374 Ma, respectively, according U-Pb titanite data). The calculated U-Pb age of pyrochlore formation and host syenite is 381 ± 5.5 Ma indicates the synchronous crystallization of the alkaline syenite and the differentiated complex of the Lovozero massif.

A set of 88 U-Pb titanite measurements of three samples 2015-e1, 2015-e2 and 2207-K from the apatite-titanite ore-bearing ijolites of the Suluay area located at the contact of the eudialyte-lujavrites and lujavrite-foyaite-urtites (Fig.1) makes it possible to calculate the total mixing lines and to produce assessment of the U-Pb ages. The data-points of three titanite samples (Fig. 3) form a single linear trend, which allows to calculate the $^{238}U/^{206}Pb$ age at the intersection with the concordia with good statistical parameters - MSWD at 1.6 (including only analytical data scatter), and the error of ± 8.7 m.y. (2.4%, 2σ). Comparison of the results of age calculation performed in different ways: 366.1 ± 8.7 Ma and 361.5 ± 3.4 Ma (at $^{207}Pb/^{206}Pb$ = 0.86 for common Pb, MSWD = 1.6, probability 0.13), allows with a high degree of probability to consider the weighted average $^{206}Pb/^{238}U$ age 361.4 ± 3.2 Ma (0.9%, 2σ, MSWD - 1.2, probability 0.13) as a best estimation of the crystallization time of titanite of mineralized ijolites in the Suluay area. The close geochemical U-Pb

isotope signatures of the studied titanites from Suluay and those from lujavrite-foyaite-urtite complex indicate their possible close origin. However, time interval of 20 m.y., significantly exceeding the analytical error of age-determination gives evidence for a long-term activity of the magmatic source of the Lovozero massif and its hydrothermal-metasomatic processes. Additional argument for this conclusion is the obtained age determinations of zircon from ilmenite-microcline-albite veins in the contact zone of the Lovozero, which give age of 359 ± 5 Ma (Arzamastsev et al., 2007).

Thus, the obtained U-Pb titanite ages for magmatic rocks and ores from Lovozero and Khibiny massifs coincide well with age estimations of these massifs earlier obtained by different geochronological methods (Kramm et al., 1993; Kramm, Kogarko, 1994; Arzamastsev et al., 2007; Kogarko et al., 2010; Zartman, Kogarko, 2014; Arzamastsev, Wu, 2014). The whole set of obtained age estimations of the intrusions allow to suggest the earlier formation of the Lovozero massif.

References:

Arzamastsev AA, Arzamastseva LV, Travin AV, Belyatsky BV, Shamatrina AM, Antonov AV, Larionov AN, Rodionov NV, Sergeev SA. (2007) Duration of Formation of Magmatic System of Polyphase Paleozoic Alkaline Complexes of the Central Kola: U–Pb, Rb–Sr, Ar–Ar Data. Doklady Earth Sciences. 413A(3): 432–436.

Arzamastsev AA, Arzamastseva LV, Zhirova AM, Glaznev VN. (2013) Model of Formation of the Khibiny–Lovozero Ore-Bearing Volcanic–Plutonic Complex. Geology of Ore Deposits. 55(5): 341–356.

Arzamastsev AA Wu Fu-Yan (2014) U–Pb Geochronology and Sr–Nd Isotopic Systematics of Minerals from the Ultrabasic Alkaline Massifs of the Kola Province. *Petrology* 22 (5): 462-479. DOI: 10.1134/S0869591114050026.

Kogarko LN, Zartman RE. (2007) A Pb isotope investigation of the Guli massif, Maymecha-Kotuy alkaline-ultramafic complex, Siberian flood basalt province, Polar Siberia. *Mineral Petrol* 89: 113-132. DOI 10.1007/s00710-006-0139-3.

Kogarko LN, Lahaye Y, Brey GP. (2010) Plume-related mantle source of super-large rare metal deposits from the Lovozero and Khibina massifs on the Kola Peninsula, Eastern part of Baltic Shield: Sr, Nd and Hf isotope systematics Miner Petrol 98:197–208. DOI 10.1007/s00710-009-0066-1

Kramm U, Kogarko LN, Kononova VA, Vartiainen H. (1993) The Kola Alkaline Province of the CIS and Finland: Precise Rb-Sr ages define 380-360 age range for all magmatism. *Lithos.* 30: 33-44.

Kramm U, Kogarko LN (1994) Nd and Sr isotope signatures of the Khibina and Lovozero agpaitic centres, Kola Alkaline Province, Russia. *Lithos* 32: 225-242.

Kylander-Clark ARC, Hacker BR, Mattinson JM. (2008) Slow exhumation of UHP terranes: titanite and rutile ages of the Western Gneiss Region, Norway. Earth Planetary Sci. Letters. 272: 531–540.

Zartman RE, Kogarko LN. (2014) A Pb isotope investigation of the Lovozero agpaitic nepheline syenite, Kola Peninsula, Russia. Doklady Earth Sciences. 4(1-1): 25–28.

PHYSICAL CHEMICAL CONDITIONS CHARACTERIZING MANTLE SOURCES OF KIMBERLITES AND ALKALINE-ULTRAMAFIC MAGMAS

Ryabchikov I.D.

Institute of Geology of Ore Deposits, Petrography, Mineralogy and Geochemistry of the Russian Academy of Sciences, Moscow, Russia

Redox potential is an important factor governing trends of magmatic evolution and formation of some valuable minerals including diamond. I shall focus on redox potential of primary magmas formed during the partial melting of mantle material.

Primary magmas for alkaline and carbonatitic series are represented by ultramafic alkaline melts for example meimechites from the Siberian trap province.

To access redox potential of meimechites and other hi-Mg magmas under near liquidus conditions I proposed new version of geooxometer based on spinel melt equilibrium: $2Fe_3O_4$ (spinel) $=6FeO$ (melt) $+ O_2$ which I used with simultaneous estimates of temperature by a new version of olivine+melt geothermometer, which takes into account presence of ferric iron in the melt.

The usefulness of this method follows from the fact that in hi-Mg magmas Cr-spinel together with olivine belongs to early crystallizing minerals, whereas other geooxometers e.g. Ilm+TiMt characterize later stages of magmatic crystallization. Melt inclusions often provide compositions of coexisting spinels and melts.

The meimechites and other magmas related to deep mantle sources are characterized by relatively oxidizing conditions (by comparison with MORB's). This seemingly contradicts to the observed decrease of relative oxygen fugacity with depth estimated for the lithospheric mantle rocks and to expected presence of metallic Fe-Ni alloy in lower mantle and in transition zone. The existence of this alloy follows from experimentally established disproportionation of ferrous iron into ferric and metallic iron.

Relatively oxidizing conditions in certain domains of deep mantle follows from the investigation of mineral inclusions in sublithospheric diamonds. For this I estimated position of the stability fields of carbon-bearing crystalline compounds coexisting with rock-forming minerals of the pyrolitic lower mantle. This diagram demonstrates that the field of diamond stability is separated from that of Fe-rich metallic alloy by the field of co-existence of iron carbides with

prevailing silicates and oxides. It implies that the formation of diamond in lower mantle requires more oxidizing conditions by comparison with the predominant part of this geosphere.

The absence of metallic phase is also corroborated by the Ni contents in minerals of lower mantle paragenesis. Ni is a sensitive monitor of the presence of metallic alloys in mineral assemblage: in the absence of alloy Ni in ferropericlase is close to 1%, whereas at c.a. 1% of metallic phase this value is significantly lower.

If we compare these results with Ni concentrations in mineral inclusions in sublithospheric diamonds, it can be seen that with the exclusion of the data for Brasilian diamonds, which contain an unusually high proportion of Fe-rich ferropericlase and magnesiowuestite, the majority of analyzed grains fall in the range of 1 ± 0.2 % Ni. It confirms the absence of metallic alloy from diamond-forming domains in lower mantle.

Oxidizing conditions in some zones of lower mantle are supported by measurements of valence state of Fe in ferropericlase from lower mantle. f_{O2}-values were estimated from measured $Fe^{3+}/\Sigma Fe$ ratios in ferropericlases included in diamonds from lower mantle (Kaminsky et al., 2015a), based upon experimental data by (Otsuka et al., 2013). Estimated values confirm relatively oxidizing conditions in the zones of diamond formation. Some fall into field of carbonates.

There may be several factors controlling this redox differentiation including subduction of oxidized crustal material, loss of metallic phase produced by FeO disproportionation etc. Perhaps the leading role belongs to effect of increasing temperature on redox reactions.

Using available experimental data I calculated equilibrium constant of the reaction

$3FeO$ (FP) = Fe_2O_3 (Brt) + Fe^0(met)
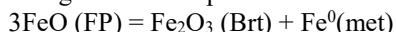
and used very simplified model for FeO and Fe_2O_3 activities for pyrolite bulk composition (Brt is bridgmanite (Tschauner et al., 2014), Mg-rich metasilicate with perovskite structure).

Below 1750°C phase assemblage of pyrolitic composition includes metallic phase. At this stage f_{O2} is controlled by FP+Met. Above 1750°C metallic phase disappears and f_{O2} is controlled by FP+Brt, leading to significant increase of normalized f_{O2} with further heating.

Such temperature dependence of f_{O2} is similar to phase relations in Fe-O system even at low pressures. With increasing temperature the extent of FeO disproportionation drastically decreases, and f_{O2} normalized to IW buffer rises with further heating. If temperature increases by several hundreds of degrees the carbonate stability field may be reached.

It is possible that in hot mantle plumes relatively oxidizing conditions exist which lead to the formation of diamond, whereas in the prevailing part of lower mantle with temperature close to AMA carbon is mainly present in the form of carbides.

An important role for the formation of diamonds may be played by melts formed during the ascent of mantle plumes. Under relatively oxidizing conditions near-solidus melts must be represented by carbonate liquids (Wyllie and Ryabchikov, 2000), or considering similar contents of carbon and phosphorus in the primitive mantle these melts should have carbonate+phosphate composition (Ryabchikov and Hamilton, 1993).

Products of solidification of such melts were recently described as inclusions in diamonds by (Kaminsky et al., 2015b). Such inclusions are composed of dolomite, magnesite, sodium-bearing phosphate $Na_4Mg_3(PO_4)_2(P_2O_7)$. Similar melts quenched into carbonate-phosphate (silica-free) glass were observed in the products of experiments with silicate – carbonate – phosphate compositions (Ryabchikov and Hamilton, 1993). Migration of such melts in lower mantle into the colder and less oxidized domains may result in the formation of diamond due to the reduction of carbonates.

CONCLUSIONS.

The formation of diamond in lower mantle requires more oxidizing conditions by comparison with the prevailing part of this geosphere, because in the presence of metallic alloy carbon would be present as iron carbide.

These relatively oxidizing conditions are consistent with similarly oxidizing parameters characteristic of primary magmas of alkaline and carbonatitic series, e.g. meimechites.

An important reason of elevated oxygen fugacities in some domains of lower mantle may be the effect of temperature on redox equilibria: with increasing temperature the extent of disproportionation of FeO may decrease and relative oxygen fugacity may grow faster than for reference IW buffer.

The link between sublithospheric diamond formation and high temperatures of certain mantle domains confirms that the formation of diamonds in deep geospheres and genesis of kimberlite magmas are related to mantle plumes.

References:

Kaminsky, F.V., Ryabchikov, I.D., McCammon, C.A., Longo, M., Abakumov, A.M., Turner, S., Heidari, H., 2015a. Oxidation potential in the Earth's lower mantle as recorded by ferropericlase inclusions in diamond. Earth Planet. Sci. Lett. 417, 49-56.

Kaminsky, F.V., Ryabchikov, I.D., Wirth, R., 2015b. A primary natrocarbonatitic association in the Deep Earth. Mineralogy and Petrology, DOI 10.1007/s00710-00015-00368-00714.

Otsuka, K., Longo, M., McCammon, C., Karato, S., 2013. Ferric iron content of ferropericlase as a function of composition, oxygen fugacity, temperature and pressure: Implications for redox conditions during diamond formation in the lower mantle. Earth Planet. Sci. Lett. 365, 7-16.

Ryabchikov, I.D., Hamilton, D.L., 1993. Interaction of carbonate-phosphate melts with mantle peridotites at 20-35 kbar. S. Afr. J. Geol. 96, 143-148.

Tschauner, O., Ma, C., Beckett, J.R., Prescher, C., Prakapenka, V.B., Rossman, G.R., 2014. Discovery of bridgmanite, the most abundant mineral in Earth, in a shocked meteorite Science 346, 1100-1102.

Wyllie, P.J., Ryabchikov, I.D., 2000. Volatile components, magmas, and critical fluids in upwelling mantle. Journal of Petrology 41, 1195-1206.

MINERAL ORE FORMATION IN ARGILLIZATED ROCKS OF PAUZHETKA HYDROTHERMAL SYSTEM OF SOUTH KAMCHATKA

Rychagov S.N.[1], *Sergeeva A.V.*[1], *Chernov M.S.*[2]

[1]Institute of Volcanology and Seismology, Far Eastern Division RAS, Petropavlovsk-Kamchatskii, Russia, rychsn@kscnet.ru
[2]Lomonosov Moscow State University, Moscow, Russia

Argillizated rocks are widely developed in the volcanic regions. The study of formation conditions for such rocks and study of argillization processes' impact on origin of mineral deposits was addressed in research papers of many leading scientists of the world: D.S. Korzhinsky, S.I. Naboko, V.L. Rusinov, V.A. Eroshev-Shak, J. Hemley, W. Jones, A. Reyes et al. The authoring team focused on a special role of hydrothermal clays in the Quaternary and modern volcanism regions: they form extended strata in the upper layers of thermal anomalies (thermal fields) and act as a water-confining stratum and a thermal insulator within the structure of hydrothermal systems; a compex geochemical barrier is confined to the stratum of hydrothermal clays (Rychagov et al., 2009). It is demonstrated that these rocks represent a long-lived (throughout Holocene or longer) highly dynamic mineralogical-geochemical system that functions at macro-, micro, and nano-levels (Rychagov et al., 2010). In addition, the basis of clays stratum is especially interesting because mineral ore associations, never previously diagnosed in the research practice, are formed there (Rychagov et al., 2015). The objective of this work is to define composition, structure and conditions of mineral associations' origin in the zones that we studied in East-Pauzhetka thermal field (th/f).

East-Pauzhetka th/f is situated on the slope of the Kambalny volcanic ridge that is characterized as a resurgent tectonic magmatic high in the Pauzhetka caldera of the Quaternary age (The long-lived…, 1980). The thermal field is among the large zones where hydrothermae discharge within the structure of Pauzhetka system (Fig.1) but it has not been adequately studied due to a remote location of producing sections of the geothermal deposit. Th/f is confined to a ring tectonic magmatic high 400-500 m in plan size (Structure of geothermal..., 1993). The central section is distinguished by steaming soils heated up to 105°C; steam-gas jets and boiling water-mud pots. The waters that are discharged on the surface are acid sulphate and low-acid hydrocarbonate-sulphate with wide cation composition and a general mineralization of $\geq$ 0.8-1.0 g/l. The steam condensate has a similar chemical composition.
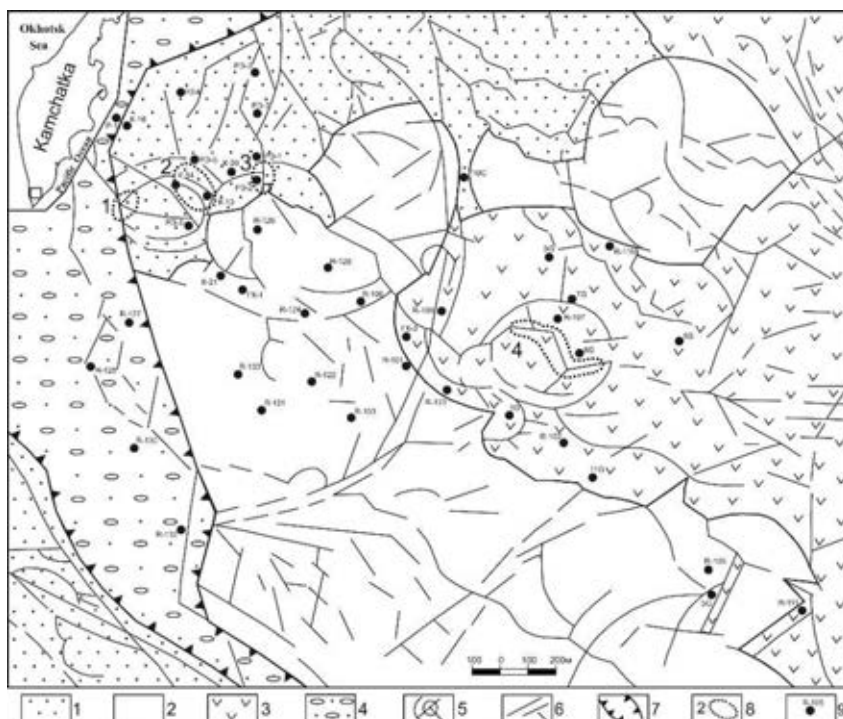
Fig. 1. An approximate geological map of Pauzhetka hydrothermal system.
1 – tuffites and tuffs of the Upper-Pauzhetka sub-suite of the Upper Neogene-Lower-Quaternary age; 2 – lava-extrusive complex of acid rocks of the Middle Quaternary age; 3 – andesites and andesibasalt of the Middle Quaternary age; 4 – alluvial boulder-cobble deposits; 5 – ring tectonic faults; 6 – linear tectonic faults; 7 – Pauzhetka trough of the Upper Quaternary age; 8 – thermal fields: 1 – South-Pauzhetka, 2 – Upper-Pauzhetka, 3 – Lower-Pauzhetka, 4 – East-Pauzhetka; 9 – drill holes.

The thickness of clays was established through prospecting pits (up to a depth of 4.0 m) and core drilling (up to 8.9 m). The stratum is characterized by zonal structure. The following layers with clear boundaries are distinguished (up – down): 1) clays of sulphuric-acid leaching composed of kaolinite and the minerals of alunite group (natroalunite, minamiit, ammoniojarosite, ammonioalunite, alunite, jarosite) contain iron oxides, pyrite, α-quartz, native sulphur; clays of dense and medium dense consistence; 2) clays composed of well-crystallized kaolinite, α-quartz, opal, feldspars, pyrite and marcasite (in subordinate quantity); these clays sharply differ in terms of consistence from overlying and underlying

ones: from stiff-high-plastic to very soft clay; 3) "blue clays" (saturated with pyrite and other sulphides) composed of kaolinite and smectite in comparable amounts as well as pyrite, α-quartz and opal: firm breccia-like clays due to solid fragments presented by silicified material; composed of smectite, pyrite, quartz, opal and others; the layer is transition to the firm basis of the stratum – fractured argillizated lavas of andesites. In general, it was found that the whole stratum of hydrothermal clays was formed *in situ* owing to hydrothermal-metasomatic changes of andesite lavas of the Kambalny volcanic ridge.

The layer of "blue clays" has a flat-dipping zone concordant with the general structure of the stratum and including mineral ore associations. The zone is missing in the clay stratum cross-cut of the Central (hot) area. At the boundary of the Central area, the zone consists of two layers (veins) with clear boundaries: the lower one is presented by siliceous-carbonate-sulphide deposits, the upper one is presented by phosphate-alumosilicate-sulphide ones. Both layers contain a large amount (up to 1-2 volume %) of regular round or flattened particles (globules) often forming aggregates by composition similar to the ground mass of the stratum from which they were singled out (Rychagov et al., 2015). The zone structure changes at a distance of 15-30 m from the area boundary: there, it has a single vein, thickness increases (from 0.4 to ≤ 0.6 m), chemical and mineral compositions become significantly more complicated. The vein globules are often flattened and form concretions-aggregates up to 25 mm in size. The aggregates are dense and massive. Their composition includes the following: carbonates, clay minerals, pyrite, quartz (and other silica minerals), iron oxides (mgnetite and titanomagnetite) and titanium (ilmenite), amphiboles, pyrite (up to 25 volume %). Based on data of infra-red spectroscopy, the main minerals, apart from pyrite, are magnesian calcite and smectite.

Microstructure of globules is varied (Fig. 2). The matrix is composed of pyrite (aggregates of crystals often have the ideal regular cubic shape, Fig. 2a), carbonates (banded microstructures, Fig. 2b) and smectite that forms cellular and globular shapes. Well-crystallized elongated phosphate crystals (most often apatite) in association with smectite and carbonates (Fig. 2c) are distinguished. A high content of other phosphates and pyrite micro crystals in the mass of alumosilicates is distinctive (Fig. 2d). A microglobular structure (Fig. 2e) and microbanding (Fig. 2f) of the surface of pyrite crystals due to formation of other mineral phases are revealed.
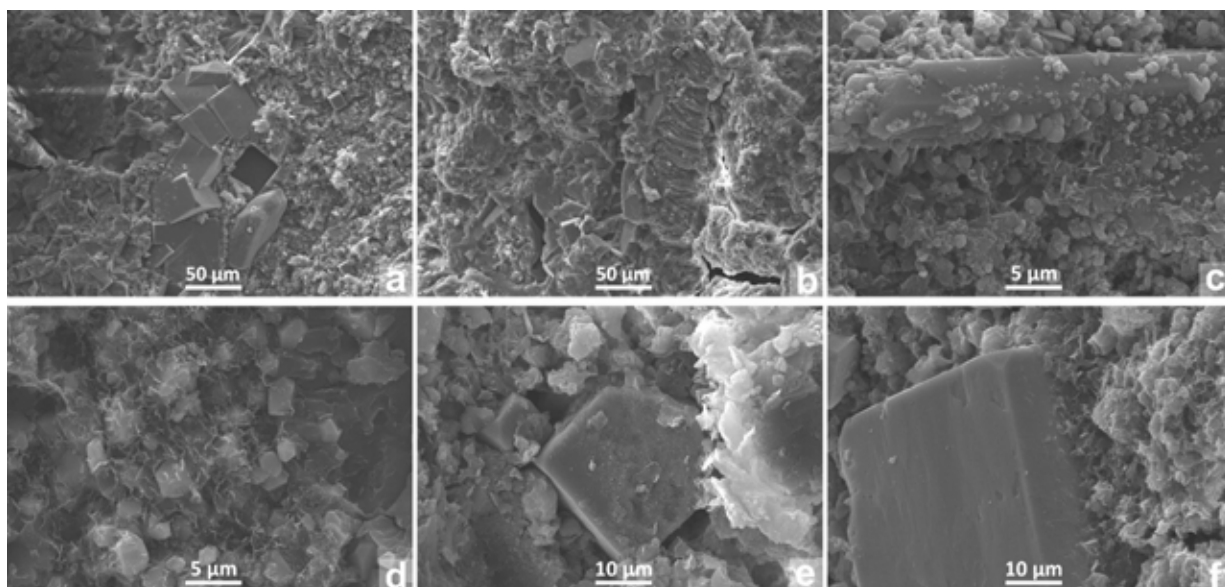
Fig. 2. Structure of globules based on data of scanning electronic microscope (SEM LEO 1450VP, Geological faculty of M.V. Lomonosov State Moscow University).

The studies by means of VEGA 3 scanning electronic microscope equipped with energy-dispersion spectrometer (EDS) X-MAX 80 with AZtec firmware (Institute of Volcanology and Seismology of FED RAS, Petropavlovsk-Kamchatsky, operator T.M. Filosofova) identified even larger variety of structures and composition of the globules (Fig.3). Many particles have a breccia-like structure of the ground mass (Fig. 3a): the cement is presented by carbonates and alumosilicates, whereas "chips" are presented by smectite, quartz, opal, iron and titanium oxides, phosphates and others. The most typical is a relatively homogeneous structure of globules, which is governed by dominance of carbonates in the ground mass. The carbonates include crystals of other minerals or pores lined with smectite, phosphates, oxides and others (Fig. 3b). A system of micro fissures in crystals and in the main matrix is pronounced. A zonal sequence caused by the mineral phases of titanium is also characteristic; the zone sequence of the ground mass is governed by distribution of phosphates (hydrous phosphates Al, Fe, Ca, Na and others) (Fig. 3d); the zone sequence in carbonates is governed by an elevated content of Mn (до 12-15 %) in separate microbands (Fig. 3e). Phosphates form micro-nanoglobular structures (Fig. 3f). Rare earh mineralisation in the form of miniscule (up to 5 μm) crystals that are concentrated around pores and micro fissures (Fig. 3g) is detected. Large crystals (up to 1.5 – 2.0 mm) of edenite amphibole (Fig. 3h) are identified. Edenite was also diagnosed based on X-ray powder diffraction and electron-probe microanalysis performed in the resource centres of St. Petersburg State University (operator E.S. Zhitova).

In general, the mineral composition of ore zone depositions include calcite, magnesian calcite, manganocalcite (the content of Mn reaches 12-15 wt. %), smectite, kaolinite (in subordinate quantity among alumosilicates), quartz and opal, epidote, K-feldspar, amphibole (edenite), apatite, sphalerite, chalcopyrite, ilmenite, rutile, titanite, magnetite and titatomagnetite, zircon, hydrous phosphates (the most probable are phosphates Al, Na, Ca, Fe, Mn: variscite, metavariscite, the minerals of wicksite group). Based on data of ICP MS (quadrupole mass-spectrometer Agilent 7500ce, Geochemistry institute SB RAS, Irkutsk, research associate G.P. Sandimirova), higher contents (up to 1 order) of rare alkaline (Li, Rb, Cs) and base alkaline elements (Na, Mg, K, Ca), As, Ba, rare earth and other metals (La, Ce, Nd, Eu, W, Tl, Th) in the composition of both the globules and ground mass of the zone are detected.
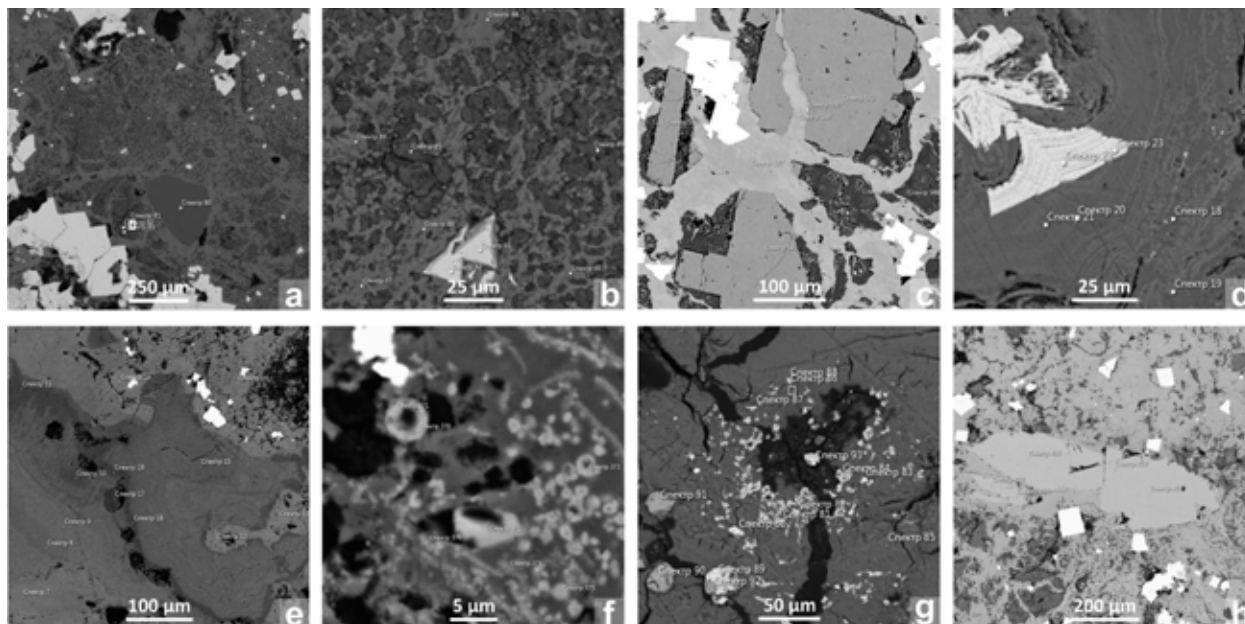
Fig. 3. The microstructure of globules was identified based on data of microprobe studies performed in Institute of Volcanology and Seismology of FED RAS.

On the basis of complex geological-geochemical and mineralogical studies, the following model of ore zone formation in the stratum of geothermal clays is suggested. In the hypergenesis zones of modern Pauzhetka hydrothermal system, bed rocks (andesite lavas) are altered into clays under the impact of acid sulphate and hydrocarbonate-sulphate waters. Long evolution of the field (probably, throughout the Holocene) resulted in the formation of a layer of ductile clays with the properties of the upper water-confining layer and heat-insulating layer. This served as an additional factor for formation of decompacted, penetrable for hydrothermae, zones in the basis of the clay stratum (as a rule, the basis of the stratum is confined to the foot or top of lava flows having a higher primary fracturing and brecciatedness of rocks). Introduction of a high temperature alkaline chloride-hydrocarbonate solution into the decompacted area caused its intense boiling, cooling and supersaturation with respect to silica minerals, carbonates, sulphides and formed the corresponding mineral association. Then, this solution mixed with near-surface sulphate waters, became supersaturated to other phases (phosphates, first of all) and phosphate-alumosilicate-sulphide association was formed. As a result, the ore vein with a distinct zone sequence formed. Apparently, the change of structure and complication of the ore vein composition along the strike from the thermal field's Central (hot) area to its boundaries and formation of the single zone can be attributed to a lateral spread of hydrothermae (Structure..., 1993) and further influence of an ascending alkaline hydrothermal fluid on the stratum of hydrothermal clays. The most probable source of phosphorous, alkaline elements, barium, arsenic, REE element and other rare elements are magmatic magma chambers of the Kambalny volcanic ridge.

References:

Long-lived center of endogenic activity in South Kamchatka (1980) Moscow: Nauka, 172 p.

Rychagov SN, Davletbayev RG, Kovina OV (2009) Hydrothermal clays and pyrite of geothermal fields: significance of modern endogenic processes (South Kamchatka) in geochemistry // Vulcanologiya i seismologiya. No 2, pp 39-55.

Rychagov SN, Sergeyeva AV, Chernov MS, Filosofova TM (2015) Varied composition globules in the stratum of hydrothermal clays of East-Puazhetka thermal field (South Kamchatka): on the question of phosphorous sources and transport of metals // Volcanism and associated processes. Petropavlovsk-Kamchatskii: Institute of Volcanology and Seismology of FED RAS, pp 271-276.

Rychagov SN, Sokolov VN, Chernov MS (2010) Hydrothermal clays as highly dynamic colloid-dispersive mineral-geochemical system // Reports of AS. Vol 435, pp 806-809.

Structure of geothermal system (1993). Moscow: Nauka, 298 p.

MODAL METASOMATISM OF MANTLE PERIDOTITES: NATURAL EXAMPLES EXPERIMENTAL CONSTRAINTS AND PHASE EQUILIBRIA MODELING

Safonov O.G., Butvina V.G.

Institute of Experimental Mineralogy, Chernogolovka, Russia, oleg@iem.ac.ru

Transformation of mantle rocks via external fluids and melts resulting in crystallization of newly formed phases atypical of common peridotites and eclogites, such as amphiboles, phlogopite, apatite, carbonates, sulfides, titanite, ilmenite, etc is collectively named as modal mantle metasomatism regardless of the provenance and composition of the fluids and melts (e.g. Harte, 1983; O'Reilly, Griffin, 2013). This process actively involves so-called perfectly mobile components, whose activities are controlling reactions, but remaining thereby unchanged themselves. The activities of H_2O and/or CO_2 are commonly thought to be the most important driving forces of mantle metasomatism (O'Reilly, Griffin, 2013 and references therein). At the same time, other components can also undoubtedly manifest characteristics of perfectly mobile components in this process. These are, for instance, K and Na, which are actively involved in processes of modal mantle metasomatism. The present study reviews mineral reactions that can be used as monitors of K and Na activities in fluid that transformed upper mantle peridotites.

The most common mineral indicator of modal mantle metasomatism is phlogopite (O'Reilly, Griffin, 2013). This mineral ubiquitously forms in peridotites until the original garnet (or spinel)-bearing harzburgites or lherzolites is completely transformed into phlogopite wehrlites in progress of the metasomatic process via following general reactions
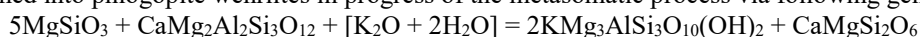
$$5MgSiO_3 + CaMg_2Al_2Si_3O_{12} + [K_2O + 2H_2O] = 2KMg_3AlSi_3O_{10}(OH)_2 + CaMgSi_2O_6$$
(orthopyroxene + garnet + [K_2O + H_2O] in fluid = phlogopite + clinopyroxene)
$$7/2MgSiO_3 + 1/2Mg_2AlO_4 + [1/2K_2O + H_2O] = 1/2Mg_2SiO_4 + 2KMg_3AlSi_3O_{10}(OH)_2$$
(orthopyroxene + spinel + [K_2O + H_2O] in fluid = olivine + phlogopite)
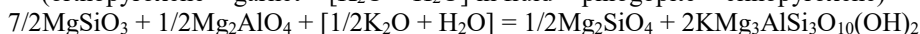
leading to recrystallization of the primary clinopyroxene and olivine or crystallization of new populations of these minerals. In contrast to the primary clinopyroxene, the metasomatic clinopyroxene is often poor in Na_2O and Al_2O_3 suggesting a loss of the jadeite and Ca-Tschermack components. The association clinopyroxene + phlogopite can be formed in xenoliths via the reaction of pargasite amphibole with orthopyroxene
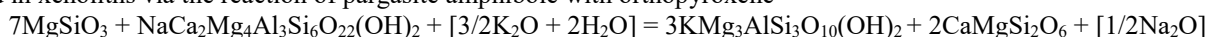
$$7MgSiO_3 + NaCa_2Mg_4Al_3Si_6O_{22}(OH)_2 + [3/2K_2O + 2H_2O] = 3KMg_3AlSi_3O_{10}(OH)_2 + 2CaMgSi_2O_6 + [1/2Na_2O]$$
(orthopyroxene + pargasite + [K_2O + H_2O] in fluid = phlogopite + clinopyroxene + [Na_2O] in fluid)

indicating that phlogopite–amphibole equilibria in peridotite are controlled by the ratio of the K and Na activities in the fluid. At high sodium activity, pargasite amphibole becomes an indicator of alkali activity. However, beyond the pressure stability of pargasite (i.e. above ~3 GPa) or at low water activity, amphibole gives place to jadeite-bearing clinopyroxene, for example (for spinel-facies peridotites)
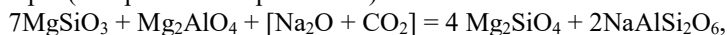
$$7MgSiO_3 + Mg_2AlO_4 + [Na_2O + CO_2] = 4 Mg_2SiO_4 + 2NaAlSi_2O_6,$$
(orthopyroxene + spinel + [Na_2O] in fluid = olivine + jadeite-bearing clinopyroxene)

Maximum intensity of metasomatism in peridotites leads to the crystallization of K-bearing richteritic amphibole when both alkali activities increase:
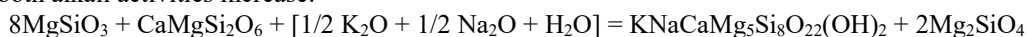
$$8MgSiO_3 + CaMgSi_2O_6 + [1/2 K_2O + 1/2 Na_2O + H_2O] = KNaCaMg_5Si_8O_{22}(OH)_2 + 2Mg_2SiO_4$$
(orthopyroxene + clinopyroxene + [K_2O + H_2O] in fluid = K-richterite + olivine)

This mineral crystallizes in garnet-free peridotite varieties oversaturated with alkalis, i.e. bulk-rock (K_2O + Na_2O) > Al_2O_3.

At low water activity and pressures below 2 GPa, the increase of both alkali activity can result in formation of alkali feldspars, e.g.
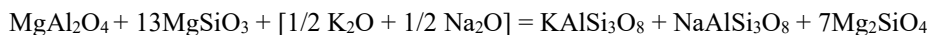
$$MgAl_2O_4 + 13MgSiO_3 + [1/2 K_2O + 1/2 Na_2O] = KAlSi_3O_8 + NaAlSi_3O_8 + 7Mg_2SiO_4$$
(spinel + orthopyroxene + [K_2O + H_2O] in fluid = alkali feldspar + olivine)

Above reactions controlled by K and/or Na activities in metasomatized upper mantle peridotites share common features. The first is that a reactant mineral in all of these reactions is orthopyroxene, which is unstable in the presence of alkaline fluids, regardless of their composition, and is found in metasomatized peridotites only as a relict phase. Transformations controlled by K and Na activities started in peridotite with the decomposition of Al-rich minerals (garnet, spinel, pargasite). These reactions may be initiated already at relatively low K and Na activities, and the progress of these reactions would depend on the proportions of garnet (spinel)/orthopyroxene in the precursor rocks, being controlled by both bulk composition and pressure.

Some of these relations and tendencies are modeled in sparse experiments on peridotite interaction with K- and Na-salt-bearing fluids and hydrous melts: H_2O–K_2CO_3-(Na_2CO_3) (Thibault, Edgar, 1990; McNeil, Edgar, 1987; Sokol et al., 2015), H_2O–KCl and H_2O–CO_2-NaCl (Safonov, Butvina, 2013, 2016). Experimental data confirm that, in the presence of K and/or Na-bearing fluid, regardless of its anionic composition (carbonate, chloride, or aqueous silicate), orthopyroxene is unstable with Al_2O_3-rich minerals. Up to high concentrations of K-salts in the aqueous solutions, the only K-bearing phase is phlogopite, whose content systematically increased relative to those of orthopyroxene, olivine, and clinopyroxene with increasing salt concentration in the solutions. The lower the H_2O activity in fluid in equilibrium with peridotite, the higher K_2O activity at which phlogopite becomes stable. The main reaction controlling the origin of pargasite amphibole reflects the instability of pyroxenes in the presence of spinel or garnet and aqueous Na-bearing fluid. Increase of alkali activity and decrease of water activity displaces composition of amphibole toward richeterite end-member. However, peridotite interaction with either alkalic fluids does not produce K-richteritic amphibole, which can

likely be formed only at certain ratios of K_2O, Na_2O, and H_2O activities, none of which has still been constrained in the available experiments. Outside the amphibole stability field, Na-rich pyroxene is the main indicator of Na activity in the fluid.

Experimental data on reactions of peridotite assemblages with fluid containing variable concentrations of dissolved alkali salts show that the products of these reactions involving chloride and carbonate fluid components are generally similar. This conclusion enabled us to qualitatively compare these reactions and corresponding mineral associations by simulating phase relations by means of $\log(a_{H_2O})$–$\log(a_{K_2O})$ and $\log(a_{H_2O})$–$\log(a_{Na_2O})$ diagrams using the Gibbs free energy minimization approach (PERPLE_X software; Connolly, 2005). Calculations for the average composition of primitive garnet lherzolite at the parameters near the continental geotherm show negative slopes of phlogopitization reactions in terms of $\log(a_{H_2O})$ and $\log(a_{K_2O})$, i.e. high H_2O activity is favorable for peridotite transformation at lower K_2O activity. Within a narrow $\log(a_{K_2O})$ range at constant $\log(a_{H_2O})$, all associations of metasomatized garnet peridotite are stable, from unaltered lherzolite (orthopyroxene + olivine + garnet + clinopyroxene) through phlogopite-bearing garnet-free peridotite (orthopyroxene + olivine + clinopyroxene + phlogopite) to phlogopite wehrlite (olivine + phlogopite + clinopyroxene) in accordance with the above reactions. At near-zero $\log(a_{H_2O})$ values (i.e. $a_{H_2O} \sim 1$), Na–Ca amphibole remains stable up to very high $\log(a_{K_2O})$, suggesting that the stability of amphibole with phlogopite requires simultaneously high activities of both K_2O and H_2O. Beyond the pressure stability of amphibole, lherzolite can be transformed into phlogopite-bearing wehrlite at any water activity. Increase of a_{K_2O} in clinopyroxene-free garnet harzburgite results in formation of clinopyroxene and phlogopite, as it is modeled for a harzburgite nodules from the Letlhakane kimberlite pipe in Botswana (van Achterbergh et al., 2001). High a_{Na_2O} and a_{K_2O} at low a_{H_2O} are favorable for the origin of the alkali feldspar-bearing associations without phlogopite and amphibole in peridotites, as modelled for peridotite xenoliths from the Khamar Daban alkali basalts (Ionov et al., 1995). Modeling of phase relations in terms of $\log(a_{K_2O})$ and $X_{CO2} = CO_2/(CO_2 + H_2O)$ in a fluid for the average composition of primitive garnet lherzolite reproduced various metasomatic upper-mantle assemblages. They vary from carbonate-bearing phlogopite wehrlites, which are specific for the sources of ultrapotassic magmas (e.g. Foley, 1992), to carbonate-bearing phlogopite orthopyroxenites and websterites, which are present as xenoliths in magmas erupted in "hot" subduction zones (for example in Cascades; Ertan, Leeman, 1996).

Thus, the proposed methods allow to adequately reproduce some natural assemblages, to estimate variations of potassium and sodium activities during the upper mantle metasomatism, to predict successions of mineral assemblages, and to compare metasomatic processes in rocks of various bulk composition and various fluid compositions (carbonic, aqueous).

References:

Connolly J. A. D. (2005) Computation of phase equilibria by linear programming: a tool for geodynamic modeling and its application to subduction zone decarbonation. Earth Planet. Sci. Lett. 236: 524–54.

Ertan I.E., Leeman W.P. (1996) Metasomatism of Cascades subarc mantle: evidence from rare phlogopite orthopyroxenite xenolith. Geology 24: 451-454.

Foley S. (1992) Petrological characterization of the source components of potassic magmas: geochemical and experimental constraints. Lithos 28: 187-204.

Harte B. (1983) Mantle peridotites and processes—the kimberlite sample. In: Hawkesworth, C. J. and Norry M. J. (eds) Continental Basalts and Mantle Xenoliths. Cheshire, Shiva, pp. 46-91.

Ionov D. A., O'Reilly S. Y., Ashchepkov I. V. (1995) Feldspar–bearing lherzolite xenoliths in alkali basalts from Hamar–Daban, southern Baikal region, Russia. Contrib. Mineral. Petrol. 122: 174–190.

McNeil A. M., Edgar A. D. (1987) Sodium–rich metasomatism in the upper mantle: Implications of experiments on the pyrolite–Na_2O–rich fluid system at 950°C, 20 kbar. Geochim Cosmochim Acta 51: 2285–229.

O'Reilly S.Y., Griffin W.L. (2013) Mantle metasomatism. In Harlov D.E. and Austerheim H. (eds) Metasomatism and the chemical transformation of rock, Berlin Heidelberg, Springer, pp. 471-533.

Safonov O. G., Butvina V. G. (2013) Interaction of model peridotite with H_2O–KCl fluid: experiment at 1.9 GPa and its implications for upper mantle metasomatism. Petrology 21: 599–615.

Safonov O. G., Butvina V. G. (2016) Indicator reactions of K and Na activities in the upper mantle: natural mineral assemblages, experimental data, and thermodynamic modeling. Geochem. Int. 54: 858-872.

Sokol A. G., Kruk A. N., Chebotarev D. A., Pal'yanov Yu. N., Sobolev N. V. (2015) Conditions of phlogopite formation upon interaction of carbonate melts with peridotite of the subcratonic lithosphere. Dokl. Earth Sci. 462: 638–642.

Thibault Y., Edgar A. D. (1990) Patent mantle–metasomatism: inferences based on experimental studies. Proc. Ind. Acad. Sci.–Earth and Planetary Sci. 99: 21–37.

van Achterbergh E., Griffin W. L., Stiefenhofer J. (2001) Metasomatism in mantle xenoliths from the Letlhakane kimberlites: estimation of element fluxes. Contrib. Mineral. Petrol. 141: 397–414.

RARE-METAL MINERALIZATION IN SPHERULITIC PERLITES OF YAGODNINSKY ZEOLITIC DEPOSIT (SOUTH KAMCHATKA)

Sandimirova E.I., Rychagov S.N., Phylosofova T.M.

Institute of Volcanology and Seismology, Far East Branch, Russian Academy of Sciences,
Petropavlovsk-Kamchatskii, Russia, sand@kscnet.ru

For the first time ever, minerals containing rare, rare-earth and radioactive elements were identified in spherulitic perlites of extrusive-subvolcanic complex consisting of mainly acid composition enclosing rocks of Yagodninsky deposit of high quality zeolitic resources (South Kamchatka). It was established that the minerals of perrierite, pyrochlore, euxenite, monazite and xenotime group were the main concentrators of these elements. Monazite and xenotime whose formation is associated with potassic metasomatism processes occur most widely in spherulitic perlites.

Yagodninsky deposit of zeolitic resources, perlites and active mineral additives (full name (Nasedkin et al., 1988)) is situated in Banno-Karymshinsky geothermal (ore) district of South Kamchatka. The district is characterised by contrasted magmatism, wide development of alkaline pyroclastic rocks and formation of large multi-phase intrusive and extrusive-subvolcanic complexes (Rychagov et al., 2015). The deposit is confined to the extrusive-subvolcanic complex at elevation 1081 (Nasedkin, 1983). The enclosing rocks are rhyolitic and dacitic litho-vitroclastic tuffs, various composition perlites, rhyolitic lavas and extrusions, near-vent tuffs and tuffites (Boykova, 2015). Of special interest (owing to varied composition, structure and texture) are spherulitic perlites that form extrusions, short lava streams and separate blocks drawn to contacts of subvolcanic intrusions with tuffs and rhyolites.

Mineralogical studies of spherulitic perlites specified a chemical composition of rock-forming minerals as well as a group of accessory minerals containing rare, rare-earth and radioactive elements. The studies were conducted by means of VEGA 3 scanning electronic microscope equipped with energy-dispersion spectrometer (EDS) X-MAX 80 with AZtec firmware (Institute of Volcanology and Seismology of FED RAS, Petropavlovsk-Kamchatskii, research associates V.M. Chubarov end T.M. Phylosofova). The studies were conducted on 3 x 4 cm polished sections which were subjected to carbon coating. Base, rare, rare-earth and radioactive elements were detected by comparison with reference materials whose composition had been checked for homogeneity and content of elements.

Table. 1 Content of rare-earth minerals from spherulitic perlites of Yagodninsky zeolitic deposit based on data of energy-dispersion spectrometer (% wt.)

Oxides	Pyrochlore		Euxenite		Perrierite		Monazite		Xenotime	
	1	2	3	4	5	6	7	8	9	10
Al_2O_3					2.12	2.80	8.50	8.66		
SiO_2	2.15				19.80	20.45	26.82	25.01	9.35	4.81
P_2O_5							17.36	15.95	14.12	13.15
Na_2O	0.47	0.49								
K_2O							2.33	2.16	1.35	0.69
CaO	11.98	11.51			4.37	4.66	3.14	2.45	0.59	0.83
V_2O_5									1.69	1.11
TiO_2	21.97	22.67	32.12	26.95	14.53	15.09				
MnO	1.95	2.23								
FeO	2.81	2.71	1.02	0.99	8.79	9.09	0.98	1.87		
As_2O_5							6.01	5.64	18.03	19.71
Y_2O_3	2.39	1.81	14.66	17.40	2.30	1.49	3.96	3.24	35.96	38.59
ZrO_2					0.90	1.57				
Nb_2O_5	18.38	20.08	15.54	24.33						
Ta_2O_5	7.14	3.31	3.14	4.31						
La_2O_3					8.58	7.97	8.62	8.10		
Ce_2O_3	2.20	2.17			19.81	19.58	15.12	16.69		2.13
Pr_2O_3		0.63			2.50	3.00		1.79		
Nd_2O_3	1.15	1.75			7.48	7.85	4.79	6.96	1.32	2.63
Sm_2O_3					1.63	1.65				
Dy_2O_3		0.67	2.11	2.82					3.07	3.03
Er_2O_3			2.17	1.76					2.09	2.84
Yb_2O_3			2.54	2.99		0.57			4.63	3.86
$\sum REE$			2.17		1.77	0.70			1.38	2.07
ThO_2	1.42				0.37	0.73	0.94	1.56		
UO_2	23.97	24.39	19.83	10.04						
$\sum$	97.98	94.42	95.30	91.59	94.94	97.20	98.57	100.08	93.58	95.45

Note. $\sum REE - (Pm, Eu, Gd, Lu)_2O_3$.

The texture of perlites in studied samples is massive, brecciated, finely banded, fluidic; the structure is spherulitic, porphyritic or microfelsitic. The perlites contain a small amount of inclusions − 2−3 % of rock volume. The inclusions are presented with barium-containing potassium-sodium feldspar, acid plagioclase, biotite, titanomagnetite (up to 5.1 % wt TiO_2) and ilmenite. Apart form inclusion, they have spherulites of feldspathic composition and feather-like quartzo-feldspathic aggregates. In terms of alkalis content, perlites are referred to the moderate alkaline type (6-8 wt% of Na_2O + K_2O). In unaltered glasses, Na_2O (4.6-5.7 wt%) dominates over K_2O (1.2-3.3 % wt.).

Two types of hydrothermal-metasomatic alteration are typical for spherulitic perlites: zeolitization and K-feldspathization. Zeolitization of glass starts along concentrically-zonal perlite fissures without displacement with formation of a metacolloidal matter. The quantitative analysis of such zones demonstrates that their aluminium content is approximately the same as in theorignial glass. At the same time, silicon content significantly decreases, sodium content drops almost to zero, K_2O increases by approx. 1 % wt., CaO increases by 3.5 wt%. Sum deficit in assays is 13-24 % wt., which is, most probably, due to presence of water.

K-feldspathization develops along transverse rock fissures, along contacts of porphyritic minerals and spherulites with glass, and along intermittent bands in fluidized perlites. The sections of K-feldspathized glass, as compared to alkaline feldspar of inclusions, do not have sodium and barium, aluminium content slightly decreases, silicon content increases, potassium content increases (up to . % wt. of K_2O). Sum deficit in assays is on the average 4-5 % wt. Along with K-feldspar, secondary quartz and hydromica are formed.

The minerals of perrierite, pyrochlore, euxenite, monazite and xenotime group are the main concentrators of these elements. Minerals-concentrators are complex multicomponent solid solutions which makes it difficult to classify them definitively. The typical chemical constituents of the minerals are shown in the table. Rare earth metals are also observed as trace elements in zircon (Hf), apatite (Y, Nd, Yb), fluorite (Yb, Lu), haematite (Ce), rutile (Zr, Nd) and sphen (Y, Nb, Ta, Nd).

Uranium-containing titanate - tantalate-niobates. This group of minerals is characteristic for alkaline syenites, alkaline granites, pegmatitic granits etc. (Geochemistry…, 1964; Rikhvanov et al., 1989 et al.). Pyrochlore and euxenite were detected in spherulitic perlites in the form of irregularly-shaped inclusions in ilmenite (Fig. 1, b). Ilmenite is associated with oligoclase, barium-containing potassium-sodium feldspar, biotite, titanomagnetite (up to 5.1 % wt TiO_2), zircon, apatite and sphene. In inclusions, pyrochlore and euxenite form concretions with distinct smooth-line boundaries. In euxenite, zonality is observed which is caused by fluctuation of base elements – Ti, Y, Nb and U.
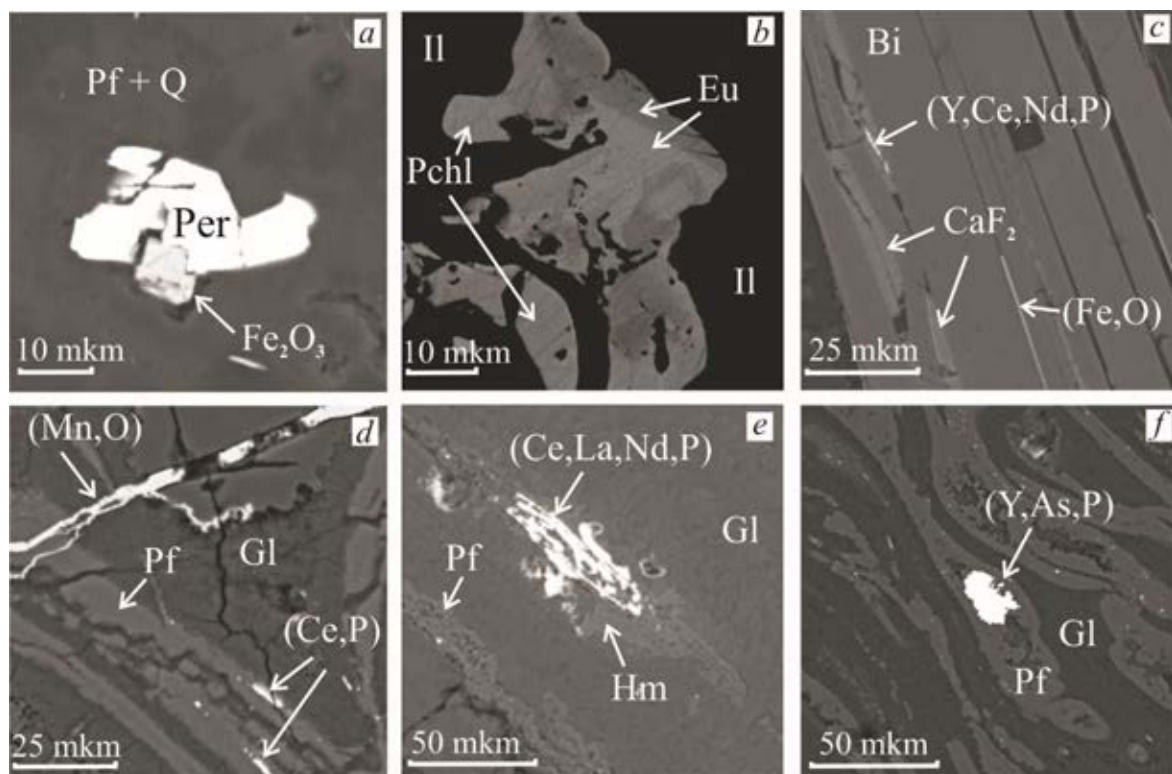
Fig. 1. Rare-metal minerals in spherulitic perlites of Yagodninsky zeolitic deposit:
a – Perrierite (Per) in concretion with haematite in the aggregate of quartz-feldspathic (Q + Pf) composition; b – pyrochlore (Pchl) in concretion with zonal euxenite (Eu) in ilmenite (Il); c – fluorite with cerous phosphate along cleavage planes in biotite (Bi); d – cerous phosphate in K-feldspathized (Pf) glass along perlite fissures; e – cerous phosphate along the fissure in glass (Gl) in association with hydromica (Hm); f – xenotime with arsenic in schliers of K-feldspathized glass of fluidized perlite.

Titaniumsilicate perrierite occurs rarely. It is known that this mineral was found in granite pegmatites, alkaline metasomatites, quartz-feldspathic veins, apatite ores and in other rocks as well as in volcanic sediments of different origin (Bonshtedt-Kupletskaya, 1972; Andreyev, Ripp, 1995). Perrierite in spherulitic perlites is confined to quartz-feldspathic areas of decrystallization of glass (Fig.1, *a*). It forms rhomboid crystals or irregularly-shaped grains up to 30 μm in size; sometimes it forms concretions with haematite. The main components present in the mineral are as follows: SiO_2 (20–21%), TiO_2 (14,5–18,4 %), Ce_2O_3 (19,6–21,6 %), FeO (7,1–9,5 %), La_2O_3 (8-9,7 %), Nd_2O_3 (5,9-7,9 %).

Phosphates of rare earths are widely spread. They are confined to zones of K-feldspathized glass where they are observed as concentrations of numerous fine grains less than 3 μm in size, as linearly extended uniform masses; spongy, needle-like or nodular formations the size of which does not exceed 50 μm ((Fig. 1, *c-f*). Phosphates are also deposited along fissures in the crystals of potassic feldspar and in albite, together with fluorite they develop along cleavage planes in biotite and form concretions with rutile. Two groups of phosphates are distinguished – ceric and yttrium ones. By composition, they are closer to monazite and xenotime. Water is often present in phosphates, which is evidenced by the sum deficit in assays. Xenotime contains a significant amount of As and, most probably, have the form of a solid solution with minerals of the chernovite series. Elevated content of arsenic in the rhyolites of the deposit may be associated with this mineral.

Conclusion

A large group of accessory minerals containing rare, rare-earth and radioactive elements was found in the spherulitic perlites of extrusive-subvolcanic complex enclosing Yagodninsky zeolitic deposit. It is known that confinedness of elements to one or another group of minerals depends on the acidity-alkalinity of environment and on ion activity of sodium and potassium. Probably, an important role of sodium in crystallization of the acid melt promoted the formation of uranium-containing titanate-tantalate-niobates, whereas at the stage of hydrothermal-metasomatic transformation of rocks, when the role of potassium incoming with deep-level metal-bearing hydrothermae increased (Serezhnikov, Zimin, 1976; Rychagov et al., 2015), titanosilicates and cerous phosphates as well as yttrium phosphates were deposited. Thus, rare-metal mineralization in the rocks of the extrusive-subvolcanic complex of Yagodninsky zeolitic deposit says in favour of the fact that both the original melt and the ascending hydrothermal fluid flow are enriched with rare earth and other elements.

References:

Andreev GV, Ripp GS (1995) Perrierite from apatite ores of South Mangolia // ZRMO. No 1, pp 83-84

Boykova IA (2015) Petrographic and petrochemical characteristic of the productive stratum of zeolitic tuffs of Yagodninsky deposit (Kamchatka) // Proceedings of XII petrographic meeting "Petrography of Magmatic and Metamorphic rocks." Petrozavodsk: Karelsky Scientific Center RAS, pp 525-528.

Bonshtedt-Kupletskaya EM (1972) Perrierite group. Minerals. Vol. III. Issue I. Moscow: Nauka, 1972, pp 776-792.

Geochemistry, mineralogy and genetic types of rare elements (1964) Vol. III. Moscow: Nauka, 830 p

Nasedkin VV (1983) Acid volcanism and water-containing volcanic glasses of the USSR's North-East. Moscow: Nauka, 103 p.

Nasedkin VV, Solov'yeva TN, Nistratova IE et al. (1988) Comparative characteristic of mineralogical composition of the zeolitic rocks of Yagodnaya mountain and the products of modern mineral formation of the Bannaya river valley, Kamchatka peninsula / Modern hydrothermae and mineral formation. Moscow: Nauka, pp 70-86.

Rikhvanov LP, Potseluyev AA, Sarnayev SI et al. (1989) Geochemistry of rare, rare-earth and radioactive elements in rock- and ore-forming processes. Novosibirsk: Nauka, Siberian Division, pp 130-148

Rychagov SN, Boykova IA, Sandimirova EI (2015) Yagodninsky-Bannaya hydrothermal-magmatic system (Kamchatka): control of zeolitic, ore and geothermal deposits // Proceedings of XII petrographic meeting "Petrography of Magmatic and Metamorphic rocks." Petrozavodsk: Karelsky Scientific Center RAS, pp 534-539.

Serezhnikov AI, Zimin VM (1976) Geological structure of Paratunka geothermal district, influence of separate geological factors on modern geothermal activity / Geothermal systems and thermal fields of Kamchatka. Vladivostok, pp 115-142.

A ROLE OF DEFORMATION-INDUCED PROCESSES IN THE OPHIOLITE ULTRAMAFIC ROCK AND CHROMITITE ORIGIN. AN EVIDENCE FROM KRAKA OPHIOLITE, THE SOUTHERN URALS

Saveliev D.E.[1], Blinov I.A.[2], Sergeev S.N.[3]
[1]Institute of Geology of the Ufimian Centre of RAS, Ufa, Russia
[2]Institute of Mineralogy, Urals Branch of RAS, Miass, Russia
[3]Institute for Metals Superplasticity Problems RAS, Ufa, Russia

The Kraka ophiolite is located in the northern part of Zilairskaya megazone (megasynclinorium) of the Southern Urals western slope. Geological and structural features of these ultramafic rocks as well as relationships with surrounding rocks were considered in previous works (Kazantseva, Kamaletdinov, 1969; Senchenko, 1976). The internal structure of

the massif and bulk-rock chemistry of different petrological units were described in (Savelieva, 1987; Denisova, 1990; Saveliev et al., 2008). Here is presented the very brief geological summary about mantle sections framework.

The Kraka ophiolite contains four bodies: Severny (Northern), Uzyansky, Yuzhny (Southern) and Sredny (Middle). The first three of them are comprised of peridotites with subordinate dunites. It was found that considerable amount of lherzolites present in the Severny Kraka in contrast with the dunite bodies, which were almost not found there. In the Uzyansky and Yuzhny Kraka, a banded dunite-harzburgite unit is widespread. Dunite bodies present not more than 10% of its volume. The most complicated composition is characteristic for the Sredny Kraka. Its central and eastern parts consist of spinel peridotites (lherzolites and diopside-containing harzburgites). Rarely these rocks include small dunite and spinel-plagioclase-lherzolite veins. Toward the south-west, the spinel peridotite shows a gradational transition to dunite-harzburgite unit, where dunite dominates. Further, to the west, the dunite-harzburgite unit gives way to the crustal section (wehrlite, clinopyroxenite, gabbro).
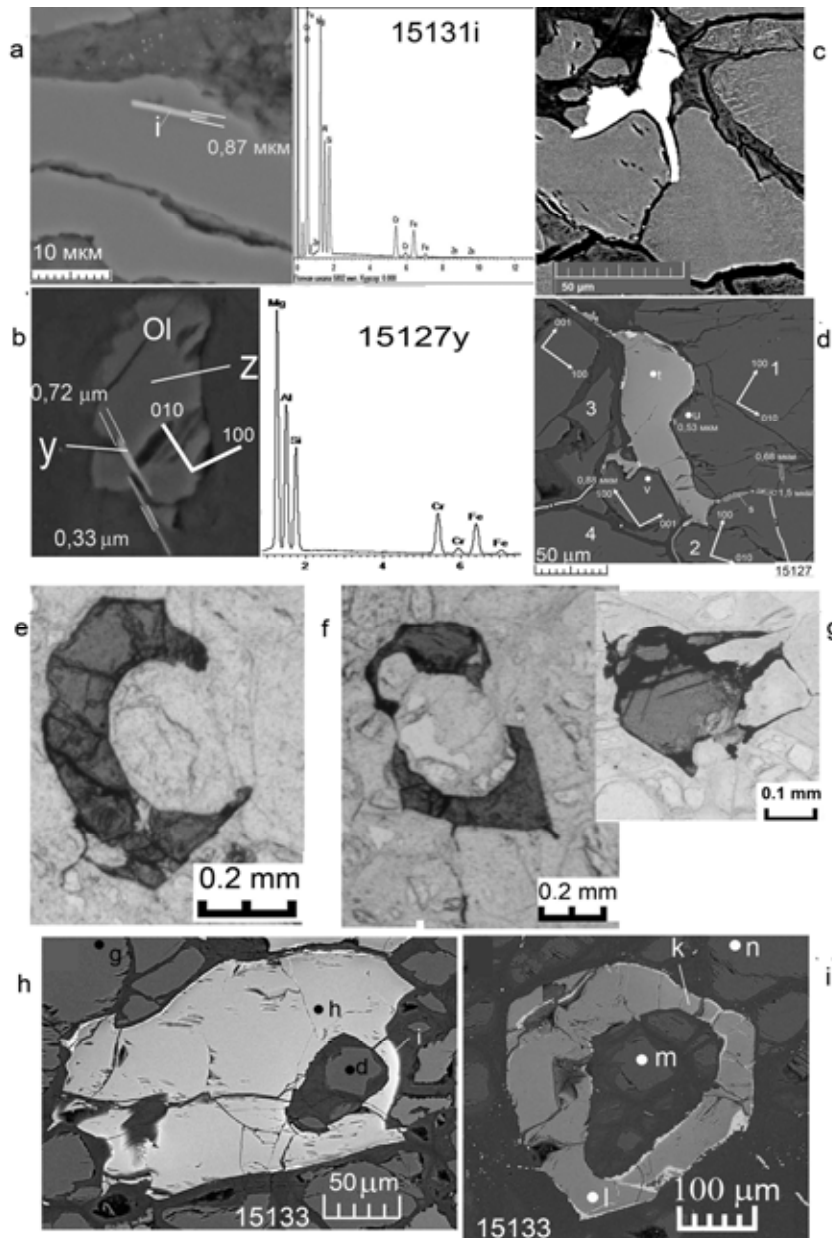
Fig.1. Different stages of chromium spinel formation in the plastic deformed olivine a-b – needle-like exsolutions of chrome spinels in olivine grain volume along [010]; c-d – precipitation and coalescence of spinel grains along olivine grain boundaries; e – g - coalescence and enclosing of olivine matrix by new-forming spinels; the beginning of spheroidization of spinel crystals; h – i – eugedral spinel crystals occupying equal olivine grains. Image (h) shows a deformation thinning of spinel wall and chemical inhomogeneous of its

All the four Kraka blocks have chrome ore occurrences; however, they are more abundant in the southwestern part of Sredny Kraka (Saksey-Klyuchevskaya area) and in the western part of Yuzhny Kraka (Apshakskaya and Bashartovskaya areas). The Kraka deposits were described in detail (Saveliev, 2012; Saveliev et al., 2008), so here we consider the particular characteristics such as chrome spinel chemistry. Usually, the chrome ore is hosted by dunite. In some cases, it is represented by large bodies close to the Moho boundary, but, some time, the occurrences are presented by the relatively small dunite lenses and tabular bodies (envelopes) within a mantle peridotite section. According to morphological classification of (Cassard et al., 1981), almost all occurrences are concordant, and disseminated ores predominate. The ophiolite chromitite mineralization is usually connected with dunite. Therefore, investigation of tiny dunite veinlets in the peridotite may give an important information about the ore formation initial stage. We studied some dunite streams in detail.

The outcrop CK-103-2LB is situated at a distance of 2 m from the Deposit #33 chromitite orebody, located in the east of massif. Dunite veinlets which are several mm to 5 cm in thickness are found to be branching from the main dunite body and crossing a peridotite matrix having up to 30% of pyroxene grains. One of these veinlets was studied in detail by chemical and structural methods. As it was investigated by means of X-ray tomography, there is an inhomogeneous distribution of chrome spinel grains even in a small dunite sample. They are segregated into thinnest streams elongated parallel each other. The chrome spinel grains occupy about 3% of dunite sample volume. This is more than 2–3 time higher compared with an average concentration in the peridotite.

Olivine grains from both peridotite and dunite show a developed dislocation fabric that typical for mantle tectonites. By means of oxided decoration, we observed single dislocations, their walls, glide bands, cross-slip sites and blocks with different dislocations density. We have investigated some of thin sections from dunite veinlet on the universal stage (Fedorov stage) and found that olivine grains have a strong crystallographic preferential orientation (CPO) indicating the rock origin at high-T plastic flow condition. It was revealed that olivine was deformed by slip system {0kl}[100] (Saveliev and Blinov 2015).
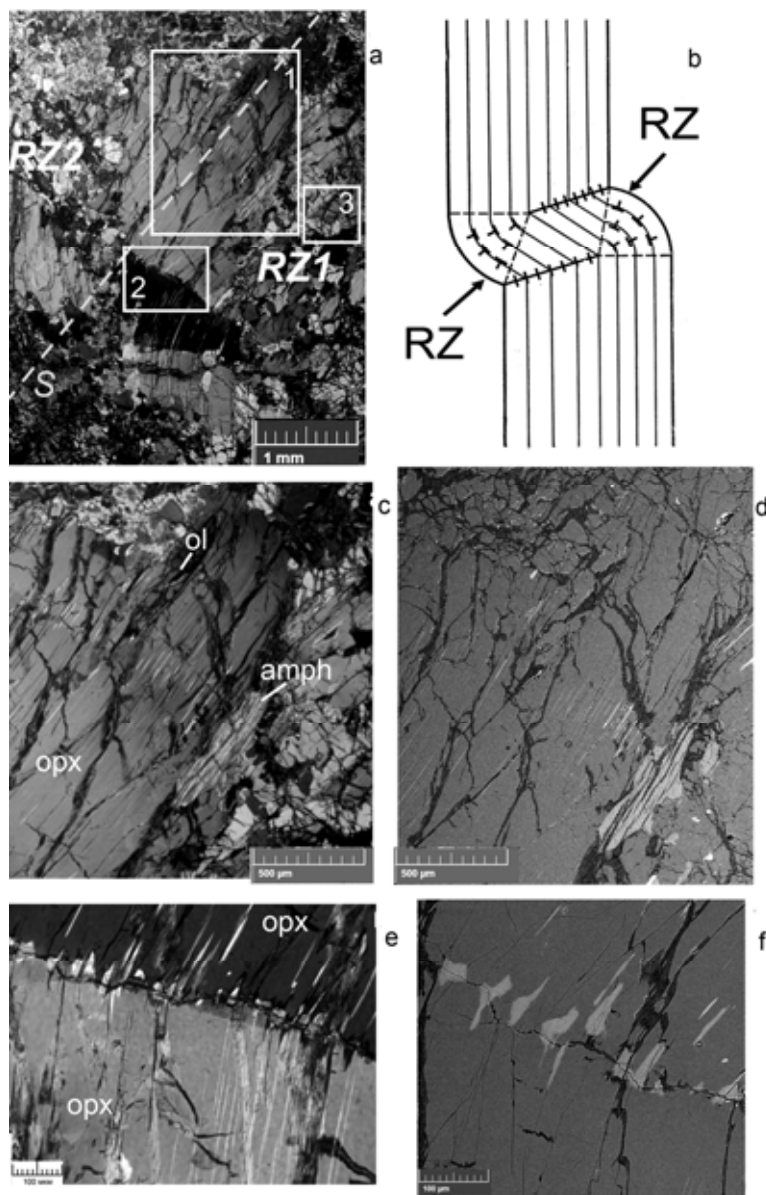
Fig.2. The large plastic-deformed orthopyroxene crystal, structural and chemical changing of it a – general view of opx porphyroclast, recrystallization zone (RZ) and trace of foliation plane (S), b – theoretical outline of kink-band; c-d – an edge part of opx grain adjacent to RZ; there are pargasite lamellae within enstatite and one lager amph precipitation on the external border of opx; e – f – pargasite flame-like bodies along a tilt subgrain boundary of enstatite; c, e – photomicrograph in cross-polarized light, d, f – BSE-images.

Numerous new-formed spinel grains were observed in the polycrystalline olivine of the same sample (fig. 1). They vary in morphology and sizes. The thinnest acicular precipitates (only 0.3–0.5 μm in thick and up to 10 μm in length) are aligned in olivine grains along [010] axis (fig. 1). The similar orientation of spinel needles was noted by (Franz and Wirth 2000) who have stuied ultramafic rock xenoliths from Papua New Guinea basalt. Bigger long irregular chrome spinel precipitates usually occur along grain and subgrain boundaries, occasionally within grains themselves along [100] axis. Often there are needle-like spinels ranging 50 to 200 μm as branches from larger crystals (fig.1). Transitions from fine irregular precipitates of chrome spinels to bigger euhedral crystals are observed.

The main trigger of impurity segregation and coalescence in the olivine grain could be a plastic deformation that is accompanied by a mantle upwelling in the decompression zones. The rise on the less dense levels of lithosphere is accompanied by a decrease of the olivine cell capacity for impurities, in particular, the chromium and aluminum. On the other hand, they were an obstacle for movement of dislocations in the olivine grains which promoted their blocking and polygonization. The exsolutions of the harder phase such as spinel formed much of strain near to themselves due to a decrease of the solid flow speed. As a result of these processes a redistribution of two mineral phases in space was made. A spheroidization is a final stage of exsolutions arranging to the eugedral chrome spinel crystals which are typical for the ophiolitic dunite. This process is shown in a tendency to take their crystallographic habitus. A driving force of spheroidization is the grain boundary free energy minimization, as this was understood in metals many years ago. Since peridotites was undergone a very high rate of plastic deformation during mantle upwelling, it can be suggested that mechanisms of solid redistribution of the mineral particles were responsible for both mantle rocks and ores formation.

Besides, it was found that other deformation-induced process were taking place in peridotite wall rock. It is diffusional decomposition of enstatite I to enstatite II+pargasite+olivine+ Cr-spinel in a recrystallization zone. There is not clear evidence of interaction of the peridotite and any melt from external sources. Fig.2 shows a large kinked enstatite crystal which contains 1) numerous lamellae of Na-Cr-rich pargasite parallel to (100) of host and 2) frame-like bodies of the same mineral from kink-boundary into zone of recrystallization. In addition, the enstatite porphyroclast contains a few of olivine crystals elongated along (100) of host.

The recrystallization zones contain numerous fine-grained equal-size neoblasts of enstatite II and olivine Fa_{10} with tiny Cr-spinel precipitations along their grain boundaries. Ibid, some angedral (vermicular) segregations were found, similar in chemistry to pargasite described above (fig. 3). The vermicular segregations are extended parallel to a sample foliation. In the immediate vicinity, numerous tiny chromite grains and olivine neoblasts are found.
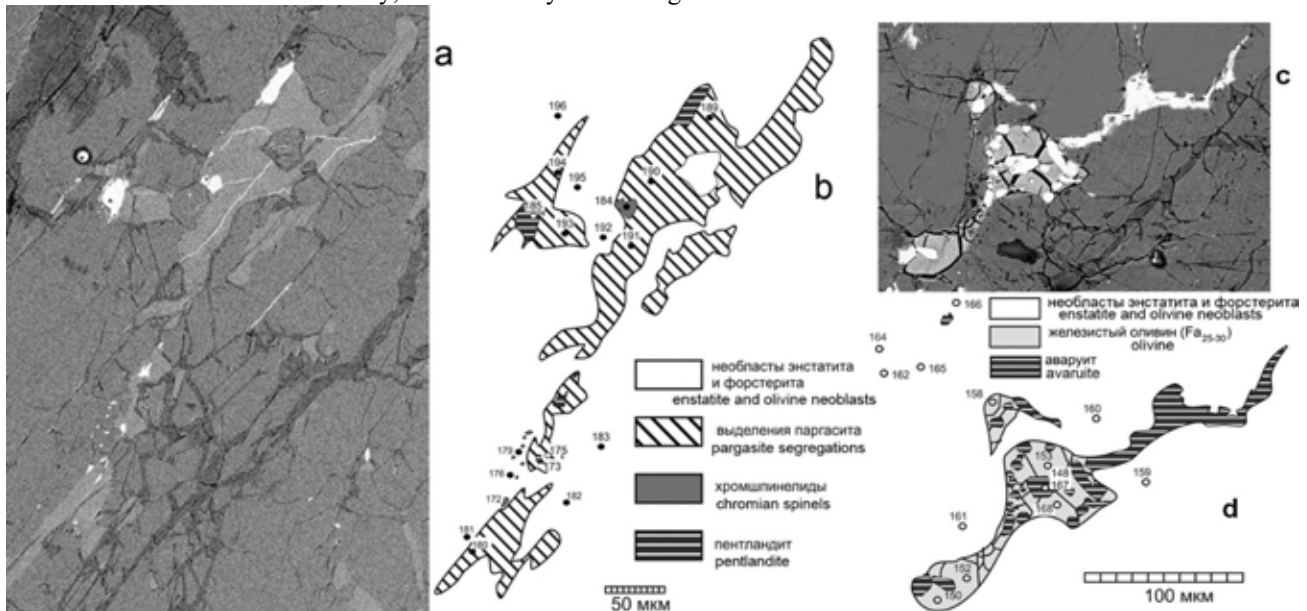
Fig.3. Shliren-like bodies of amphibole and olivine-avaruite in the recrystallization zone
a-b – amphibole large angedral body in RZ according with a few of tiny spinel and pentlandite grains, c-d – iron-enriched angedral body (Fo_{25-30} and awaruite), a – c – BSE-images.

Using these facts, we infer that pargasite crystallizations in the enstatite are due to deformation of the host-mineral. The first kind of precipitation along (100) of enstatite host-grain can be regarded as an amphibole-type stacking fault as described by [Skrotzki, 1994]. The second kind is expressed more extensively. It is located on tilted boundary of disoriented enstatite subgrains, at the bend-line. It is very important: pargasite formation begins only from kink-band of enstatite. This can be explained as a result of deformation-induced diffusional dissolution of enstatite with follows melting of newly-formed amphibole. A frictional melting is one of the possible mechanisms, that is caused by a release of energy in the form of heat from deformed minerals at a sliding interface [Spray, 1988; 1992].

This process is sensitive to rheological properties of deformed minerals. In particular, enstatite is a strong phase but olivine is a weak phase. The latter is deformed easily changing its crystal morphology according to a main stress direction. In contrast, a single active glide system (100)[001] can be taken in enstatite crystal so this mineral accumulates a deformation energy as defects of crystalline structure are increased. This energy is spent for bending and increasing of crystal temperature (internal energy) that activates diffusional processes in grain. For example, amphibole-type defects may be formed (Skrotsky, 1994) and melted because they have a lower point of melting than the host enstatite.

Besides described amphibole segregation, the recrystallization zone (RZ) contains less abundant Fe-rich segregations, also vermicular in form. They consist of Fe-rich olivine (Fa_{25-30}) and avaruite grains. It is possible that they were formed as a fast-frozen intergranular liquid (fig. 3). We have performed a simple calculation that shown a possibility of basalt melt generation (61 % wt) after a crystallization of forsterite (30% wt), enstatite II (5% wt) and Cr-spinel (4% wt) as a residual (tabl. 1).

Table 1. Mass balance for a deformation-induced mobilization of partial melt from enstatite (wt %)

	parental melt			restite			basalt
percentage	*0,8*	*0,2*	*1*	*0,05*	*0,3*	*0,04*	*0,61*
phase	"pargasite"	Fe-rich olivine	mix	enstatite II	olivine	spinel	rest of melt
n	25	5	**calculated**	54	43	27	**calculated**
SiO_2	47.35	44.42	**46.77**	57.02	41.71	0.00	51.40
TiO_2	0.28	0.01	**0.23**	0.02	0.02	0.02	0.36
Al_2O_3	12.90	0.03	**10.33**	1.36	0.00	34.34	14.55
FeO	2.04	22.35	**6.10**	4.39	6.46	13.90	5.55
MnO	0.02	0.17	**0.05**	0.06	0.06	0.21	0.04
MgO	20.84	32.42	**23.15**	36.20	51.25	15.13	8.78
CaO	11.31	0.10	**9.07**	0.41	0.01	0.00	14.81
Na_2O	2.84	0.07	**2.29**	0.02	0.01	0.00	3.73
K_2O	0.09	0.03	**0.08**	0.02	0.02	0.00	0.12
Cr_2O_3	2.19	0.07	**1.77**	0.38	0.05	35.71	0.49
NiO	0.17	0.31	**0.20**	0.09	0.38	0.11	0.12
sum*	100	100	**100**	100	100	100	100

*Analyzes performed on the SEM Vega 3 Tescan with EDA, average compositions normalized to 100%; n – number of analyzes

Tabl. 2 shows results of a chemical balance calculation for an olivine neoblasts formation during a deformation-induced diffusional dissolution of enstatite according to a reaction En I= Amph + Ol+En II. It is shown that this process could take place without an influence of external source of matter. Olivine formation during enstatite recrystallization could be more intensive if a very small amount of hydrous fluid is presented [Carter, 1976], an appearance of which is proved by presence of amphibole. Silica content should be increased in residual enstatite II in comparison with the former enstatite I. Impurities (CaO, Al_2O_3, Cr_2O_3 etc) could be extracted by amphibole melt or crystallized as residual Cr-spinel tiny grains which are clearly visible in RZ. In fact, the enstatite II neoblasts are depleted by all impurities (fig.4) and contain MgO, SiO_2 and a small amount of FeO only (tabl. 2).

Table 2. Mass balance for a deformation-induced diffusional dissolution of enstatite (wt %)

percentage	*0,75*	*0,2*	*0,05*	*1*	*1*
phase	enstatite II (residual)	"pargasite"	olivine	enstatite I	enstatite I (natural)
n	54	25	43	calculated	5
SiO_2	57.02	47.35	41.71	54.32	55.32
TiO_2	0.02	0.28	0.02	0.07	0.03
Al_2O_3	1.36	12.90	0.00	3.60	3.41
FeO	4.39	2.04	6.46	4.02	5.72
MgO	36.20	20.84	51.25	33.88	33.97
CaO	0.41	11.31	0.01	2.57	0.65
Na_2O	0.02	2.84	0.01	0.58	0.30
Cr_2O_3	0.38	2.19	0.05	0.72	0.45
sum*	100	100	100	100	100

*Analyzes performed on the SEM Vega 3 Tescan with EDA, average compositions normalized to 100%; n – number of analyzes

Thus, as reported above, one of possible mechanisms to extract chromium from silicate phases is cooperative action of solid-state flow and partial melting of rock forming silicates. We have shown some facts which allow to make visible this deformation-induced process in terms of petrography and mineralogy in the natural ultramafic rocks.

Conclusion

We believe that all marked attributes of the Kraka dunite and chromitite may be well explained only by a rheomorphic model that suggests cooperative changes of both ultramafic rocks structure and chemistry during their solid flow. The main trigger of impurity segregation and coalescence in the olivine grain could be a plastic deformation that is accompanied by a mantle upwelling in the decompression zones. The rise on the less dense levels of lithosphere is accompanied by a decrease of the olivine cell capacity for impurities, in particular, the chromium and aluminum. On the other hand, they were an obstacle for movement of dislocations in the olivine grains which promoted their blocking and polygonization. The exsolutions of the harder phase such as spinel formed much of strain near to themselves due to a decrease of the solid flow speed. As a result of these processes a redistribution of two mineral phases in space was made.

A spheroidization is a final stage of exsolutions arranging to the eughedral chrome spinel crystals which are typical for the ophiolitic dunite. This process is shown in a tendency to take their crystallographic habitus. A driving force of spheroidization is the grain boundary free energy minimization, as this was understood in metals many years ago (e.g. Novikov, 1986).
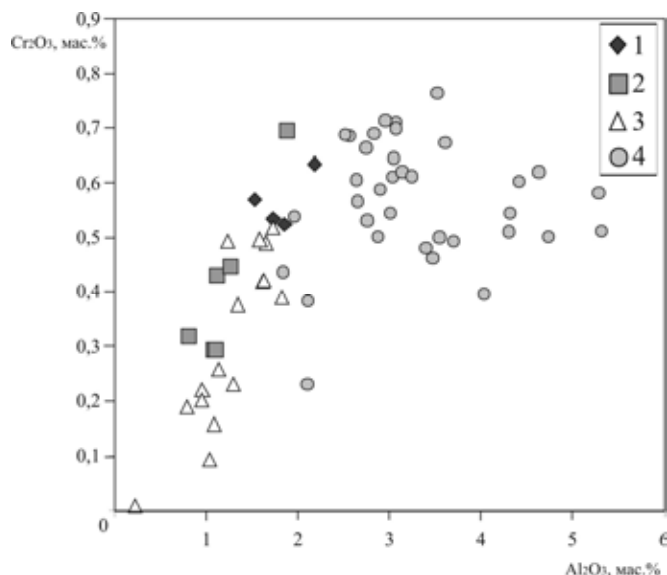
Fig.4. A changing of orthopyroxene chemistry during a recrystalization 1 – places of opx large grain without pargasite lamellae, 2 – the same, next to pargasite precipitations, 3 – enstatite neoblasts in RZ, 4 – opx large grains from Kraka peridotites after [Savelieva, 1987; Saveliev et al., 2008].

A thermodynamic base of mineral phases redistribution in the mantle solid flow was given by [Saveliev and Fedoseev, 2011; 2014; Fedoseev, 2016]. It is suggested that a localization of plastic flow into the weakest layers should occur during decompression accompanying ascending of the mantle. Since olivine is the softest mineral of the mantle as shown in [Carter, 1976; Saveliev, Fedoseev, 2011], a solid flow should be faster in dunite than that in peridotite. Therefore, the mineral phase redistribution in dunite is more efficient too. Chromite could be brought into dunite in two ways.

First, as mentioned above, it could be the deformation-induced impurities segregation from olivine grains. Second, it could be a deformation-induced break down of pyroxene grains because those are more brittle than olivine. Therefore, during flow they could be reduced and dissolved. Under stress the chrome spinel grains composition could be changed from high-Al to high-Cr. For all these above-mentioned processes the critical zone is the narrow contact between dunite and peridotite where only we can see numerous new-formed chrome spinel exsolutions.

References:

Carter N.L. (1976) Steady state flow of rocks. Rev. Geophys. and Space Phys. 14:301-360.

Cassard D., Nicolas A., Rabinowitch M., Moutte J., Leblanc M., Prinzhoffer A. (1981) Structural Classification of Chromite Pods in Southern New Caledonia. Economic Geology. 76:805-831.

Denisova E.A. (1990) Stroyeniye i deformatsionnyye struktury ofiolitovykh massivov s lertsolitovym tipom razreza [Framework of Yugnyy Kraka ultrabasical massif (the Southern Urals)]. Izvestiya AN USSR, Geologiya, 1:45-63 (in Russian)

Fedoseev V.B. (2016) Stratification of two-phase monodisperse system in a laminar planar flow. Journal of Experimental and Theoretical Physics, 149(4):1-11.

Franz L., Wirth R. (2000) Spinel inclusions in olivine of peridotite xenoliths from TUBAF seamount (Bismarck Archipelago/Papua New Guinea): evidence for the thermal and tectonic evolution of the oceanic lithosphere. Contrib Mineral Petrol. 140:283-295.

Kazantseva T.T., Kamaletdinov M.A. (1969) Ob allokhtonnom zaleganii giperbazitovykh massivov zapadnogo sklona Yuzhnogo Urala [About an allochtonous position of ultrabasical massifs of western slope of the Southern Urals]. Doklady AN USSR, 189:1077-1080 (in Russian)

Novikov I.I. (1986) Teoriya termicheskoy obrabotki metallov [Theory of thermal processing of metals]. Moscow, Metallurgiya, p. 480 (in Russian)

Saveliev D.E , Fedoseev V.B. (2014) Plasticheskoye techeniye i reomorficheskaya differentsiatsiya veshchestva v mantiynykh ul'tramafitakh [Plastic flow and rheomorphic differentiation of the mantle ultramaflc rocks]. Vestnik Permskogo universiteta. Geologiya, 4(25):22-41 (in Russian) doi: 10.17072/psu.geol.25.22

Saveliev D.E. (2012) Khromitonosnost giperbazitovykh massivov Yuzhnogo Urala [Chromite-bearing of ultrabasitical massifs of the Southern Urals]. Dissertation. University of Perm, p.410 (in Russian)

Saveliev D.E., Blinov I.A. (2015) Sindeformatsionnyye vydeleniya khromshpinelidov v plasticheski deformirovannykh agregatakh olivina (ofioly Kraka, Yuzhnyy Ural) [Syndeformation chrome spinel exsolutions in the plastic deformed olivine aggregates (Kraka ophiolite, the Southern Urals)]. Vestnik Permskogo Universiteta. Geologiya, 4(29):45-69 (in Russian). doi: 10.17072/psu.geol.29.44

Saveliev D.E., Fedoseev V.B. (2011) Segregatsionnyy mekhanizm formirovaniya tel khromititov v ultrabazitakh skladchatykh poyasov [Segregation mechanism of chromitite body formation in the ultrabasic rocks of fold belts]. Rudy i metally, 5:35-42 (in Russian)

Saveliev D.E., Snachev V.I., Savelieva E.N., Bazhin E.A. (2008) Geologiya, petrogeokhimiya i khromitonosnost' gabbro-giperbazitovykh massivov Yuzhnogo Urala [Geology, petrogeochemistry, and chromite content of gabbro - hyperbasic massifs of the South Urals]. DizaynPoligrafServis. Ufa, p. 320 (in Russian)

Savelieva G.N. (1987) Gabbro-ultrabazitovyye kompleksy ofiolitov Urala i ikh analogi v sovremennoy okeanicheskoy kore [Gabbro-ultrabasitical complexes of the Urals ophiolites and their analogues in the present-day oceanic crust]. Nauka. Moscow, p. 230 (in Russian)

Senchenko G.S. (1976) Skladchatyye Struktury Yuzhnogo Urala [The folding structures of the Southern Urals]. Nauka. Moscow, p. 172 (in Russian)

Skrotzki W. (1994) Defect structure and deformation mechanisms in naturally deformed augite and enstatite. Tectonophysics. 229:43-68.

Spray J. G. (1992) A physical basis for the frictional melting of some rock-forming minerals. Tectonophysics. 204:205-221.

Spray J.G. (1988) Generation and crystallization of an amphibolite shear melt: an investigation using radial friction welding apparatus. Contrib. Mineral. Petrol. 99:464-475.

Hydrothermal Fluid Evolution at the Batu Hijau Cu-Au porphyry Deposit, Indonesia

Schirra M., Zwyer T., Driesner T., Heinrich C.A.
Eidgenössische Technische Hochschule, Zürich, Switzerland

The giant Cu-Au porphyry deposit Batu Hijau is located in the southwestern part of Sumbawa Island, Indonesia. It is associated with multiple generations of low-K tonalite porphyry intrusions emplaced at shallow depths ($\leq$ 2km) into volcano-sedimentary sequences around 3.7 Ma ago (Meldrum et al., 1994; Garwin, 2000). Volatile components expelled from the intrusions during emplacement and subsequent crystallization initiated a hydrothermal system fed by fluids from an inferred larger magma chamber below, which produced intense alteration and stockwork vein formation. Based on cross cutting relationships a time sequence of vein formation, correlating with the evolution of the hydrothermal fluid, can be established (Gustafson & Hunt, 1975). Copper-iron sulfides typically occur within different generations of quartz veins formed during early alteration or less frequently as later sulfide veinlets associated with transitional alteration (Mitchell et al., 1998; Clode et al., 1999). Principal ore minerals are chalcopyrite and bornite together with minute blebs of native gold (Arif & Baker, 2004). Fluid inclusions (FIs) entrapped within different vein generations record the chemical and physical evolution of the hydrothermal fluid and can provide information about sulfide precipitation conditions. Based on FIs, Garwin (2000) described vein formation temperatures decreasing from 700°C to <400°C. However, later studies focused on FIs reported constant temperatures around 300°C and pressures around 50 bar, supposedly independent of vein types and contained sulfides (Imai & Ohno, 2005; Imai & Nagai, 2009).

During the last decade, cathodoluminescence (CL) imaging has become increasingly popular in FI studies focused on porphyry copper deposits (e.g. Rusk & Reed, 2002, 2006; Landtwing et al., 2010; Rottier et al., 2016). In several cases quartz textures obtained by CL-imaging showed that ore minerals were introduced by reopening of previously formed quartz veins (e.g. Redmond et al., 2004; Landtwing et al., 2010; Frelinger et al., 2015). Since quartz veins host most of the FIs, the timing of quartz relative to sulfide precipitation is essential for determining accurate temperature and pressure conditions of ore formation.

The aim of the present work is to refine the present model of ore formation at the Batu Hijau porphyry Cu-Au deposits regarding its fluid history. FIs entrapped in different vein types will be investigated using conventional petrography, CL imaging and microthermometry in order to constrain the physical conditions of vein formation as well as ore precipitation, extending the work of Zwyer (2010).

Mineralization, Alteration and Veining

Mineralization at Batu Hijau is related to the emplacement of multiple porphyry tonalite stocks (Meldrum et al., 1994; Mitchell et al., 1998; Garwin, 2000). Three generations can be distinguished: 1) old tonalite (OT), 2) intermediate tonalite (IT), and 3) young tonalite (YT; Mitchell et al., 1998; Proffett, 1998). The small-volume OT and dominant IT are intensely mineralized but difficult to distinguish, while the YT intrusion is only weakly mineralised. The shell-shaped ore body is situated at depths between 150 and 900 m below the pre-mining surface. Highest ore grades with ppm Au/wt.% Cu ratio >1 by weight are in the upper central part of the ore shell, while the deeper periphery is generally of lower grade with Au/Cu ratio <1. At greater depths, a sharp drop in ore grades in combination with high vein densities delineates the barren core.

Excluding the barren core, ore grades at Batu Hijau correlate with vein density (Mitchell et al., 1998), which indicates their importance for mineralization. Based on geometry, mineralogy, associated alteration, and mutual time relationships veins can be classified into five different types: A-, AB-, B-, C-, and D-veins in chronological order (Mitchell et al., 1998; Clode et al., 1999; Imai & Ohno, 2005; Zwyer, 2010).

A-type veinlets represent the earliest hydrothermal products. They are typically thin, discontinuous, quartz-dominated veins with irregular wall contacts (Fig. 1A). Besides quartz, magnetite is a common mineral that occurs in the early formed veins (Am-veinlets, Fig. 1B).

AB-veins are the most abundant vein type in Batu Hijau. They represent a transition from earlier A-veinlets to later B-veins as evidenced by cross cutting relationships. In contrast to A-type veinlets, they are thicker (up to 8 cm), show more regular wall contacts, and straighter propagation. However, compared with later B-veins, they are still undulated. In the mineralized region, bornite and chalcopyrite appear as either disseminated grains or massive accumulations within the quartz veins (Fig. 1B). In the deeper parts, AB-veins are barren and occasionally contain magnetite, often along wall rock contacts.

B-veins are the latest quartz-dominated vein-type and characterized by their straight and planar wall rock contacts and prismatic quartz textures. The defining feature of B-veins is the presence of a centerline with euhedral quartz and a final fill of chalcopyrite and minor bornite, as well as traces of chlorite. In the lower parts of Batu Hijau, B-veins additionally contain anhydrite and minor molybdenite (Fig. 1A).

C-veins are fundamentally different compared to the previously described vein-types. They can be described as thin cracks partially filled by sulfide minerals and associated with mm-thin alteration halos marked by complete transformation of earlier mineral assemblages to chlorite and sericite (Fig. 1B and C). Sulfides described as disseminated grains hosted by the porphyry rocks often appear to be aligned along such thin cracks that are barely visible. Earlier quartz veins seem to contain higher quantities of ore minerals close to intersections with C-veins. Furthermore, sulfide centerlines of B-veins show explicit similarities with C-veins.

Phase	Area %
Unassigned	0.24
Epoxy	5.10
Quartz	31.80
Sericite	23.78
Albite	8.20
Chlorite	19.30
Chalcopyrite	8.97
Bornite	1.96
Rutile	0.22
Calcite	0.40
Magnetite	0.02
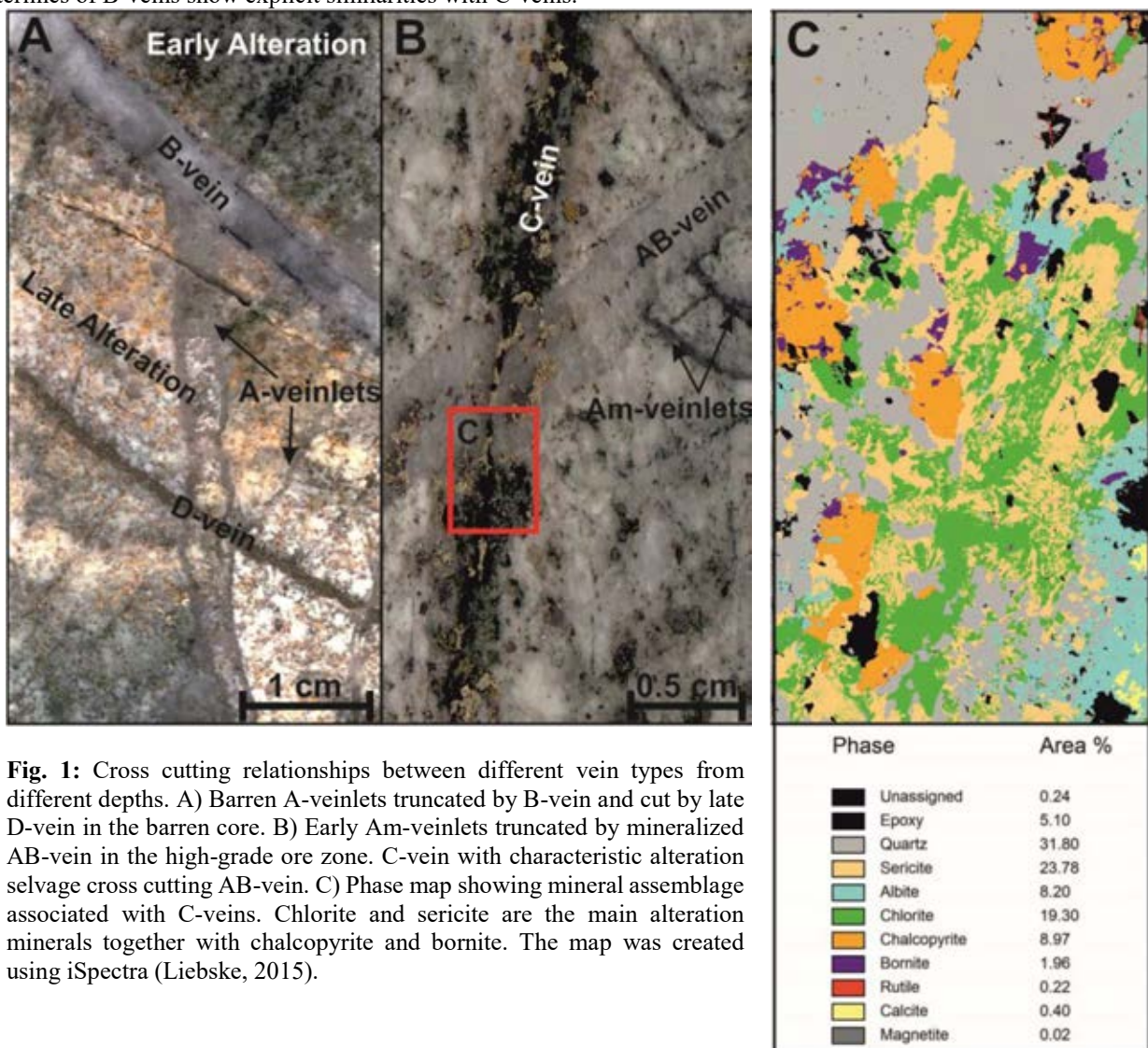
Fig. 1: Cross cutting relationships between different vein types from different depths. A) Barren A-veinlets truncated by B-vein and cut by late D-vein in the barren core. B) Early Am-veinlets truncated by mineralized AB-vein in the high-grade ore zone. C-vein with characteristic alteration selvage cross cutting AB-vein. C) Phase map showing mineral assemblage associated with C-veins. Chlorite and sericite are the main alteration minerals together with chalcopyrite and bornite. The map was created using iSpectra (Liebske, 2015).

D-veins represent the latest vein generation at Batu Hijau and consist entirely of pyrite with minor quartz grains (Fig. 1A). Feldspar-destructive alteration is associated with this late veining event, which seems to postdate the main mineralization stage.

Hydrothermal Vein Quartz Textures and Sulfide Precipitation

CL-imaging of hydrothermal vein quartz revealed the occurrence of temporally superimposed quartz generations, representing a complex fluid history involving precipitation, dissolution, and recrystallization. In mineralized AB- and B-veins, at least three generations of quartz formation can be distinguished (Fig. 2). The first generation (Q1) is characterized by white to slightly grey shades and represents the largest portion of all quartz present. Locally, euhedral growth zones document crystal growth into open space. Dissolution fronts in Q1 followed by reprecipitation of medium grey quartz define the onset of Q2. Both generations are closely related to each other and summarized as Q1-2. Interestingly, sulfide

grains are never completely enclosed in grains of the first two generations. In contrast, the last generation, marked by dark luminescent quartz filling cracks and interstitial spaces, seems to be genetically related to sulfide precipitation. All sulfide grains observed so far are embedded within this late quartz generation. Apparently, the late quartz generation follows the cross cutting C-veins, indicating their importance for ore formation. Irregular edges of Q3 and truncation of earlier growth zones are signs of dissolution processes (Frelinger at al., 2015) associated with the emergence of C-veins in Batu Hijau.

Fluid Inclusion Petrography and Microthermometry

In the stockwork vein-system of Batu Hijau FIs are abundant and range in size from less than 5 to 50 μm in diameter. Four different types of FIs can be distinguished based on phase proportions at room temperature: intermediate density (ID), aqueous (A), vapor-rich (V), and brine (B) inclusions. ID inclusions consist of two phases, vapor and liquid, in approximately equal proportions (Fig. 3A). In a few cases an opaque solid phase might be present. They are dominant in the deeper quartz veins but quantitatively decrease towards the mineralized part. The high-grade ore zone is marked by the predominance of V and B inclusions. B inclusions are characterized by one or multiple daughter minerals and a low vapor to liquid ratio (10-20 Vol.% vapor, Fig. 3B). In contrast, V inclusions show high vapor to liquid ratios, more than 70 Vol.% vapor, and no solid phase is present (Fig. 3C). Both inclusion types occur together in the same quartz grains belonging to Q1-2. Trails of coexisting B and V inclusions (boiling trails) are no rarity. ID, V, and B inclusions always show negative crystal or rounded shapes. Aqueous (type A) inclusions are irregular, flat, and in some cases elongated. Like ID and V inclusions, they consist of two phases but with a low vapor to liquid ratio of less than 20 Vol.% vapor (Fig. 3D). In general, A inclusions are rather uncommon, occurring in most cases along the intersections of C-veins with earlier quartz veins. The Q3 generations contains predominantly tiny (< 1 μm) A inclusions. In order to get meaningful results, fluid inclusion assemblages (FIAs, as defined by Goldstein & Reynolds, 1994) were identified and used for microthermometry. Homogenization temperatures (TH) and salinities (in wt.% NaCleq.) of FIAs correlate with depth, vein type, and ore grades. ID inclusions homogenize to the liquid phase at around 370°C with salinities between 3 to 7 wt.% NaCleq.. The homogenization temperatures and salinities of B inclusions increases from depth (320°C, 35 wt.% NaCleq) towards the high-grade zone (380°C, 45 wt.% NaCleq). Due to the high portion of vapor, Th and salinities of V inclusions could not be precisely measured. However, rather high TH of more than 500°C and low salinities in the range of 1 to 5 wt.% NaCleq can be presumed. A inclusions along C-veins show low TH and salinities of around 250°C and 1 to 3 wt.% NaCleq.
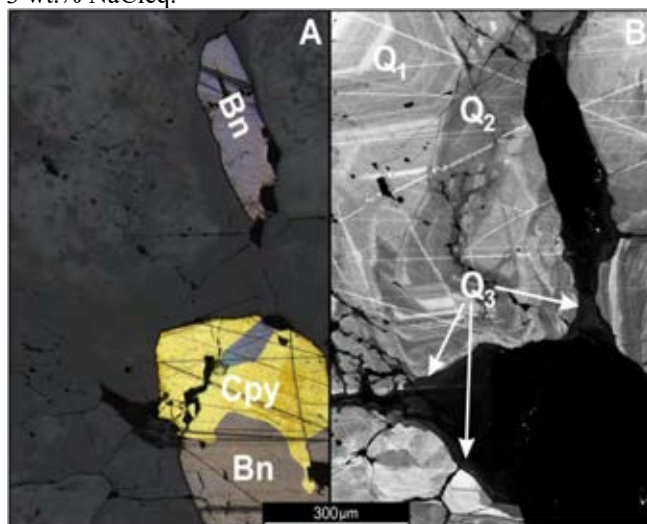
Fig. 2: Bornite (Bn) and chalcopyrite (Cpy) along the centerline of a B-vein from the high-grade ore zone. A) Reflected light image B) CL-image showing the different quartz generations.
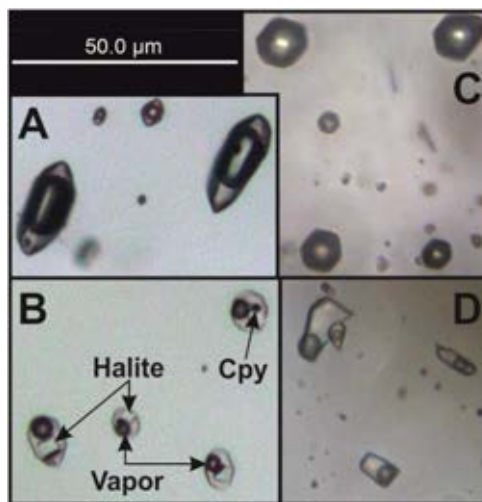
Fig. 3: FI-types occuring in hydrothermal quartz veins at Batu Hijau. A) ID inclusions from the barren core. B) B containing halite and chalcopyrite (cpy) daughter crystals and C) V inclusions from the high-grade ore zone. D) A inclusions close to C-vein.

Implications for metallogenesis at Batu Hijau

The evolution of the hydrothermal fluid in time and space led to the formation of different vein-types associated with distinct alteration stages and eventually sulfide precipitation under favorable conditions. The early fluid history is preserved in quartz veins at greater depths in form of ID FIAs showing initial minimum entrapment temperatures of around 370°C. However, depending on pressure conditions, the original temperature of the fluid could be significantly higher, possibly in the range proposed by Garwin (2000). Separation into a low-density low-salinity vapor and a high-density high-salinity brine phase resulted from ascent to shallower depths and an associated drop in pressure. Although these fluid types are dominant in the high-grade ore zone, the two-phase fluid was probably preceding ore formation as revealed by CL-imaging. Sulfides precipitated either together with or shortly after the formation of Q3. The presence of A FIs in combination with the general absence of V and B inclusions in Q3 indicates that ore formation took place during a period of cooling from around 400°C to 250°C, whereby overlapping salinities permit the possibility of direct cooling of the magmatic vapour or a single-phase intermediate-density fluid to a denser aqueous fluid. Alternatively, a

contribution of brine dilution by meteoric fluids may be a localising factor for the high-grade ore shell (Fekete et al., 2016). In summary, Batu Hijau is another porphyry copper ± gold deposit besides Butte (Rusk), Bingham Canyon (Landtwing et al., 2005), Elatsite, (Stefanova et al., 2014) and probably also Far South East (Hedenquist et al., 1998), where ore metal precipitation dominantly postdates the formation of the quartz stockwork veins and is more closely associated with quartz re-dissolution and incipient feldspar-destructive alteration.

References:

Arif J. & Baker T. (2004) Gold paragenesis and chemistry at Batu Hijau, Indonesia: implications for gold-rich porphyry copper deposits. Miner. Deposita 39:523-535.

Clode C. Proffett J.M., Mitchell P., Munajat I. (1999) Relationships of intrusion, wall-rock alteration and mineralisation in the Batu Hijau copper-gold porphyry deposit. PACRIM'99 Proceedings: Bali Indonesia, pp 10-13.

Fekete S., Weis P., Driesner T., Bouvier A.-S., Baumgartner L., Heinrich C.A. (2016) Contrasting hydrological processes of meteoric water incursion during magmatic–hydrothermal ore deposition: An oxygen isotope study by ion microprobe. Earth Planet Sc. Lett. 451:263-271.

Frelinger S.N., Ledvina M.D., Kyle J.R., Zhao D. (2015) Scanning electron microscopy cathodoluminescence of quartz: Principles, techniques and applications in ore geology. Ore Geol. Rev. 65:840-852.

Hedenquist J.W., Arribas A., Reynolds J.T. (1998) Evolution of an intrusion-centered hydrothermal system: Far Southeast-Lepanto porphyry and epithermal Cu-Au deposits, Philippines, Econ. Geol. 93:373-404.

Imai A. & Ohno S. (2005) Primary ore mineral assemblage and fluid inclusion study of the Batu Hijau porphyry Cu-Au deposit, Sumbawa, Indonesia. Resour. Geol. 55.3:239-248.

Imai A. & Nagai Y. (2009) Fluid inclusion study and opaque mineral assemblage at the deep and shallow part of the Batu Hijau porphyry copper-gold deposit, Sumbawa, Indonesia. Resour. Geol. 59:231-243.

Garwin, S. L. (2000) The setting, geometry and timing of intrusion-related hydrothermal systems in the vicinity of theBatu Hijau porphyry copper-gold deposit, Sumbawa, Indonesia. Dissertation, University of Western Australia.

Goldstein R.H. & Reynolds T.J. (1994) Systematics of fluid inclusions in diagenetic minerals. Society for sedimentary geology short course 31:199.

Gustafson L.B. & Hunt J.P. (1975) The porphyry copper deposit at El Salvador, Chile. Econ. Geol. 70:857-912.

Landtwing M.R., Pettke T., Halter W.E., Heinrich C.A., Redmond P.B., Einaudi M.T., Kunze K. (2005) Copper deposition during quartz dissolution by cooling magmatic-hydrothermal fluids: The Bingham porphyry. Earth Planet Sc. Lett. 235:229-243.

Liebske C. (2015) iSpectra: An open source toolbox for the analysis of spectral images recorded on scanning electron microscopes. Microsc. Microanal. 21:1006-1016.

Mitchell P.A., Proffett J.M., Dilles J.H. Geological review of the Batu Hijau porphyry copper-gold deposit, Sumbawa Island, Indonesia.

Meldrum S.J., Aquino R.S., Gonzales R.I., Burke R.J., Suyadi A., Irianto B., Clarke D.S. (1994) The Batu Hijau porphyry copper-gold deposit, Sumbawa Island, Indonesia. J. Geochem. Explor. 50:203-220.

Redmond P.B., Einaudi M.T., Inan E.E., Landtwing M.R., Heinrich C.A. (2004) Copper deposition by fluid cooling in intrusion-centered systems: New insights from the Bingham porphyry ore deposit, Utah. Geology 32:217-220.

Rottier B. Kouzmanov K., Bouvier A., Baumgartner L.P., Wälle M., Rezeau H., Bendezú R., Fontboté L. (2016) Heterogeneous melt and hypersaline liquid inclusions in shallow porphyry type mineralization as markers of the magmatic-hydrothermal transition (Cerro de Pasco district, Peru). Chem. Geol. 447:93-116.

Rusk B.G. & Reed M. (2002) Scanning electron microscope–cathodoluminescence analysis of quartz reveals complex growth histories in veins from the Butte porphyry copper deposit, Montana. Geology30:727-730.

Rusk B.G., Reed M.H., Dilles J.H., Kent A.J. (2006) Intensity of quartz cathodoluminescence and trace-element content in quartz from the porphyry copper deposit at Butte, Montana. American Mineralogist 91:1300-1312.

Stefanova E., Driesner T., Zajacz Z., Heinrich C.A., Petrov P., Vasilev Z. (2014) Melt and fluid inclusions in hydrothermal veins: the magmatic to hydrothermal evolution of the Elatsite porphyry Cu-Au deposit, Bulgaria. Econ. Geol. 109:1359-1381.

Zwyer (2010) Temporal and spatial evolution of hydrothermal, ore-related fluids in the Batu Hijau porphyry copper-gold deposit, Sumbawa (Indonesia). Unpublished Master Thesis, ETH Zürich.

GARNET MEGACRYSTS FROM THE GRIB KIMBERLITE PIPE (ARKHANGELSK DIAMOND PROVINCE, RUSSIA): EVIDENCE OF LATE MODAL METASOMATISM

Selyutina N.E.[1], Sazonova L.V.[1,2], Nosova A.A.[2],Kargin A.V.[2]

[1]Lomonosov Moscow State University, Moscow, Russia, nata-me98@mail.ru

[2]Institute of Geology of Ore Deposits, Petrography, Mineralogy and Geochemistry of the Russian Academy of Sciences, Moscow, Russia, sazonovalv52@mail.ru

The Grib kimberlite pipe is located in the central part of the Arkhangelsk diamond province (ADP, Chernoozerskiy kimberlite field) in the northern area of East European Craton (Larionova et al, 2016). Kimberlites often contain xenoliths of mantle peridotites, eclogites, metasomatic mantle rocks, and megacrysts of garnet, clinopyroxene, phlogopite, olivine and ilmenite (Sazonova et al., 2015; Kargin et al., 2016a).

One of the distinguishing features of the Grib pipe (from other objects of alkaline-ultramafic magmatism in ADP) is that on the one hand there is signs of lithospheric mantle clinopyroxene-phlogopite metasomatism, on the other hand there is no any evidence of mantle amphibolization(Sablukov and Sablukova, 2004). At the same time, in some xenoliths of mantle rocks (primarily eclogites) and garnet megacrysts amphibole is observed in association with other minerals as one of the modal metasomatic phases.

This work presents the results of the modal metasomatism study in two megacrysts of Grt (samples 754, 796) from the Grib pipe kimberlites. Because of this metasomatic activity, amphibole was formed together with phlogopite, clinopyroxene and Cr-spinel.

Garnet megacrysts have a rounded-angular isometric shape with sizes 1,5x1,3 cm and 1,3x1,2 cm. They are strongly fissured. As inclusions, there are numerous small grains of picroilmenite.

Megacrysts can be formed by fractional crystallization from a primary kimberlite melt or its derivatives, induced by silicate-carbonate liquid immiscibility or melt crystallization and hybridization of lithospheric material (e.g. Moore and Belousova, 2005; Kamenetsky et al., 2014 and references herein). Another mechanism for the formation of megacrysts can be the interactional reaction of a kimberlite melt or fluid with mantle peridotites.

Investigation methods. Minerals were analyzed at the Laboratory of Analytical techniques of High Spatial Resolution at the Department of Petrology, Geological Faculty of the Moscow State University, on a JEOL JSN-6480LV scanning electron microscope (SEM) equipped with an INCA-Energy-350 EDS analyzer. The accelerating voltage was 15 kV, the current was 15 ± 0.1 nA, and the analytical spot was 4 μm in diameter. The images were taken in back-scattered electrons. All elements were analyzed accurate to no worse than ±10% at concentrations of 1–5 wt %, ±5% at concentrations of 5–10 wt %, and ±2% at concentrations of >10 wt %. The detection limits were, depending on the analyzed elements, from 0.1 to 0.3 wt %.

Compositional features of garnet megacrysts and Mg-ilmenite. The analysis of megacrysts' chemical compositions showed that Grt refers to the almandine-pyrope series with a pyrope component content of 70-72%. The composition is quite homogeneous. Mg# ((Mg/(Mg+Fe)) of both samples are 0.80-0.81. Megacrysts relate to a low-Cr association with contents (wt %) (in samples 754 и 796, respectively): Cr_2O_3 – 2.67-3.42 and 2.52-3.34; TiO_2 – 0.86-1.13 and 0.76-0.91; CaO – 4.48-4.84 and 3.38-3.71; MgO –12.92-17.62 and 11.85-13.95. Mg-ilmenite is included in Grt megacrysts. The oxides contents vary in it (wt %) (in samples 754 и 796, respectively): Al_2O_3 – 0.64-2.46 and 0.43-1.29; Cr_2O_3 – 2.51-4.15 and 1.6-4.88; FeO – 26.73-29.76 and 21.91-28.83. Mg-ilmenite compositions coincide with the compositional field of Mg-Ilm megacrysts from the Grib pipe kimberlites (Golubkova et al., 2013), that proves the simultaneous generation of garnet megacrysts and Mg-ilmenites.

Features of the later transformations in Grt-megacrysts. Megacrysts are split by large amounts of winding veins, which can reach about tens of microns in width. These veins often include isometric bulges to hundreds of microns in diameter (Fig.1). The veins and their bulges are filled with the same phases, but these sequences, composition and way of their transformation can be observed only in bulges as the phases in veins are too small and form a thin mixture. It is able to track the following phases in bulges (from the contact with Grt to the central part of a bulge):

$$Grt \rightarrow Amf + CrSpl\ (\pm Cpx) \rightarrow Phl \rightarrow Carb + \text{"glass"}\ (1)$$
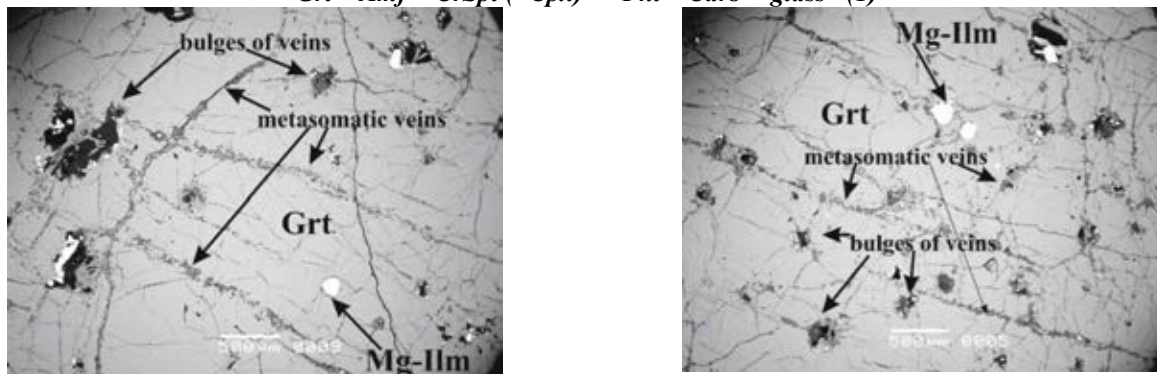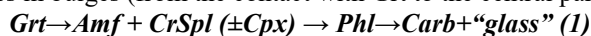
Fig. 1. Fragments of garnet megacrysts with numerous thin metasomatic veins and their bulges.

"Glass" is represented by cryptocrystalline Mg-Si water-containing phases with a small amount of calcite. This "glass" can be interpreted as result of melt/fluid cristallization. Probably, initially it was a kimberlite melt or a fluid that got into a Grt through thin cracks and weakened zones.

Cr-Spl compositions are homogeneous for both samples. Spl often have a zonal textrure: for samples 754 and 796, respectively: Mg# of central and edge zones are 0,60-0,61 and 0,71-0,75, Cr# (Cr/(Cr+Al)) of central and edge zones are 0,38-0,53 and 0,12-0,29.

Amf was formed on the contact zone of the "glass" and Grt. Amf replaced the latter. The phlogopite often overgrows on the amphibole (Fig.2, 3a). There are single garnet relicts in Amf. The amphibole composition corresponds to a pargasite group with Mg# 0,83-0,94 and 0,85-0,91 for samples 796 and 754, respectively. Amf have a "spotty" metasomatic zoning (Fig. 3a). Content of oxides vary (in wt %), for samples 754 и 796, respectively: Na_2O – 2,0-2,7 and 1,53-3,58; Al_2O_3 – 13,9-17,0 and 13,6-17,1; K_2O 1,08-1,87 and 0,50-2,29; CaO 10,51-11,66 and 7,91-12,18; Cr_2O_3 – 0,41-1,24 and 0,30-2,10; TiO_2 – 1,40-2,04 and 1,04-4,10. In Amf Na content is decreased with increasing K in the

direction from Grt to the "glass" or phlogopite. Neither regular changes in Mg# nor the content of other elements in the direction from garnet to "glass" was detected. However, the contents of various elements in Amf depend on its Mg# . (Fig. 4).
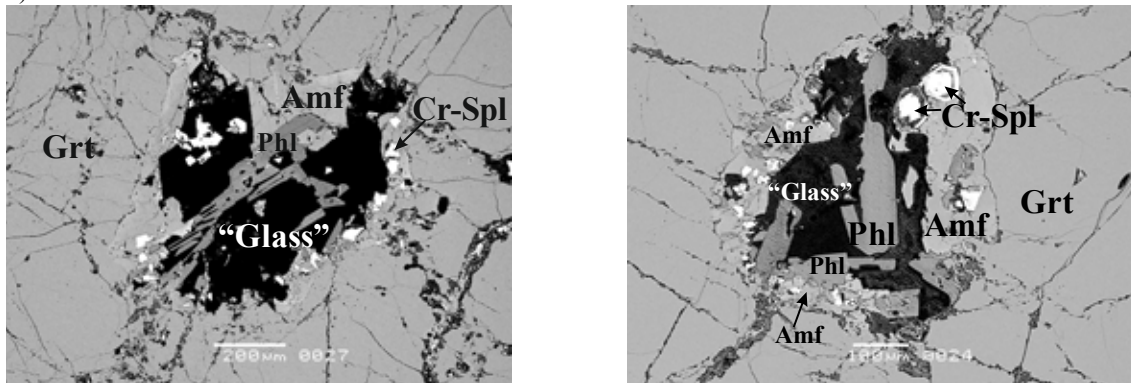
Fig. 2. Isometric bulges in garnet megacrysts which are filled with different phases.
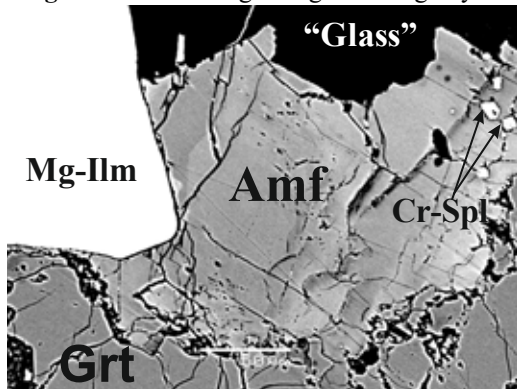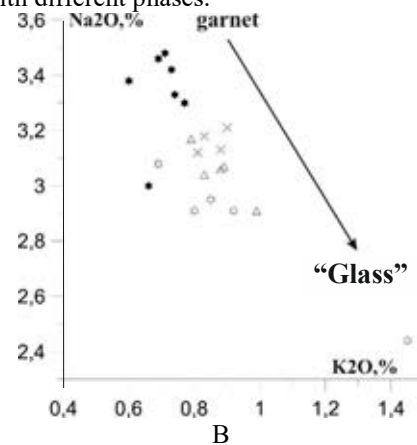
Fig.3. (a) Amphibole with inclusions of Cr-Spl from bulge veins located in garnet. It is clearly seen that it has a non-homogeneous-spotted zonal structure. (b). Ratio of K_2O and Na_2O in amphibole grains in the direction from Grt to kimberlite. Different icons show different grains.
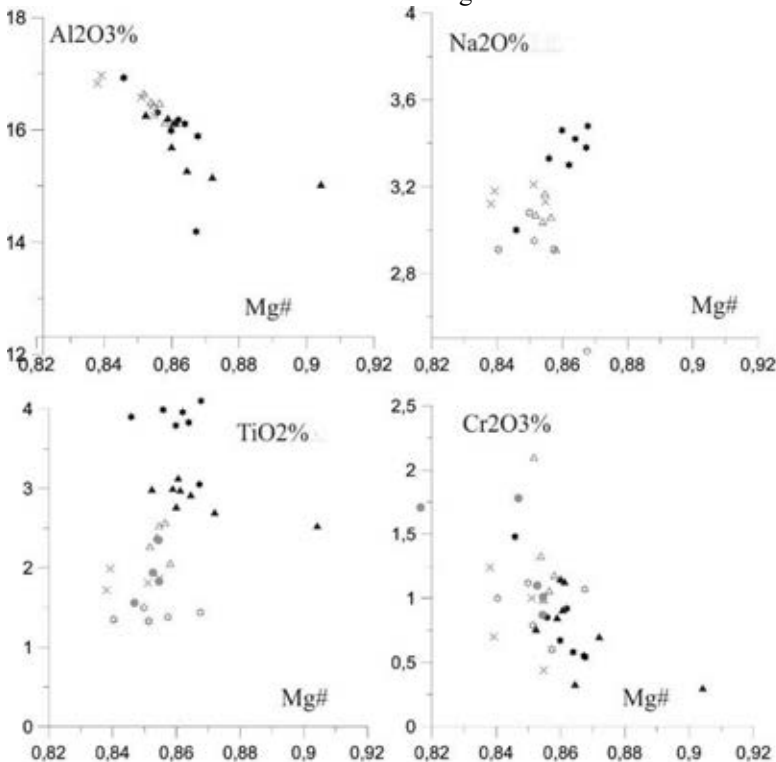
Fig.4. Distribution of various elements as a function of Mg # in amphibole grains. Different icons show different grains.

Phl usually overgrows on the amphibole or forms independent grains in a "glass" (Fig. 2). Mg# Phl are 0.879 - 0.882. The Phl composition is close to phlogopites from the Grib pipe kimberlites (Larionova et al., 2016). Contents of oxides (in wt %) are following (for samples 754 and 796, respectively): Na_2O – 0.4-1.38 and 0.26-2.07; Al_2O_3 – 16.65-

18.76 and 15.56-19.10; Cr_2O_3 – 0.24-1.41 and 0.81-2.15; TiO_2 – 1.87-2.95 and 1.70-3.21. It should be noted that the chemical variability of Phl is defined by a decrease in the Na_2O, Cr_2O_3 and Al_2O_3 concentrations with increasing TiO_2 in the direction from Grt to the "glass" (Fig. 5).

The metasomatic nature of Amf and Phl. Non-homogeneity amphibole composition, the K increase in the direction from Grt to the "glass", garnet relics in amphibole grains, and concealed zonality of Phl described above are signs of metasomatic change of the garnet due to the influence of a kimberlite melt/fluid that was saturated Mg, K, Ti and some other components. Probably, the Grt transformation occurred according to the following scheme:

$$Grt + kimberlite\ melt / fluid \rightarrow Amf\ (Crx) + Cr\text{-}Spl + Phl\ (2).$$
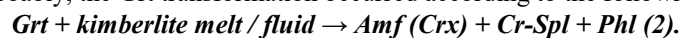
The P-T parameters of the garnet megacrysts genesis and modal metasomatism. The average formation parameters of the megacrysts association are estimated: P about 50 kbar and T about 1100 °C (Golubkova et al., 2013). It is known that amphibole stability field in peridotite lithospheric mantle has a pressure rupture between ~30 and 60 kbar, Ca-amphiboles (pargasite, kersutite) are stable in metasomatized peridotites at depths corresponding to P< 30 kbar. At depths corresponding P> 60 kbar K-amphibole (richterite) is stable. It was formed due to phlogopite (Konzett et al., 1997).

Thus, the absence of amphibole in the Grib pipe mantle xenoliths (which experienced modal metasomatism with the formation of a Cpx-Phl association) may indicate the depths of their formation corresponding to P> 30 and < 60 kbar, that agrees with our estimates of their formation (Kargin et al., 2016a). However, in the late stages of kimberlites existence the low-pressure metasomatism took place.
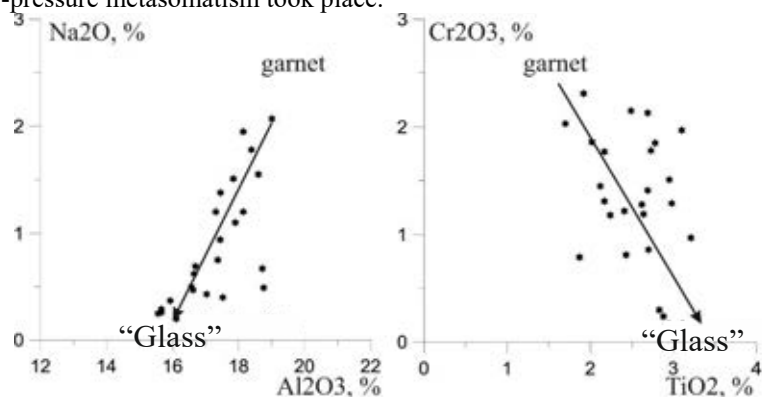
Fig. 5. Change in phlogopite compositions from the garnet to the "glass".

Conclusion: Garnet megacrysts from the Grib kimberlite pipe, formed at the early stages of the evolution of kimberlite melt (Kargin et al., 2016b), contain veined mineralization, which indicates that in the late stages of the kimberlite melt evolution (at depths corresponding to P <30 kbar) there was Na-K-rich and low-carbonate, essentially silicate and H2O-rich fluid.

References:
Golubkova, A.B., Nosova, A.A., Larionova, Y.O. (2013) Mg-ilmenite megacrysts from the Arkhangelsk kimberlites, Russia: Genesis and interaction with kimberlite melt and postkimberlite fluid. Geochemistry Int. 51, 353–381. doi:10.1134/S0016702913030038

Kamenetsky, V. S., Belousova, E. A., Giuliani, A., Kamenetsky, M.B., Goemann, K., Griffin, W. L. (2014) Chemical abrasion of zircon and ilmenite megacrysts in the Monastery kimberlite: Implications for the composition of kimberlite melts. Chemical Geology 383: 76–85

Kargin, A.V., Sazonova, L.V., Nosova, A.A., Pervov, V.A., Minevrina, E.V., Khvostikov, V.A., Burmii, Z.P. (2016a) Sheared peridotite xenolith from the V. Grib kimberlite pipe, Arkhangelsk Diamond Province, Russia: Texture, composition, and origin. Geosci. Front. doi:10.1016/j.gsf.2016.03.001

Kargin, A.V., Sazonova, L.V., Nosova, A.A., Tretyachenko, V.V. (2016b) Composition of garnet and clinopyroxene in peridotite xenoliths from the Grib kimberlite pipe, Arkhangelsk diamond province, Russia: Evidence for mantle metasomatism associated with kimberlite melts. Lithos 262: 442–455. doi:10.1016/j.lithos.2016.07.015

Larionova Yu. O., Sazonova L. V., Lebedeva N. M., Nosova A. A., Tretyachenko V. V., Travin A. V., Kargin A. V., and Yudin D. S. (2016) Kimberlite Age in the Arkhangelsk Province (Russia): Isotopic Geochronologic Rb--Sr and $^{40}Ar/^{39}Ar$ and Mineralogical Data on Phlogopite. Petrology 24: 562–593. doi: 10.1134/S0869591116040020

Moore A., Belousova E. (2005) Crystallization of Cr-poor and Cr-rich megacryst suites from the host kimberlite magma: implications for mantle structure and the generation of kimberlite magmasContrib Mineral Petrol 149: 462. doi:10.1007/s00410-005-0663-x

Sablukov S., Sablukova L.(2004) 3-D mapping of mantle substrate in the Zimny Bereg area, Russia. In: 8th International Kimberlite Conference. p. FLA_0059: 1-5.

Sazonova, L.V., Nosova, A.A., Kargin, A.V., Borisovskiy, S.E., Tretyachenko, V. V., Abazova, Z.M., Griban', Y.G. (2015) Olivine from the Pionerskaya and V. Grib kimberlite pipes, Arkhangelsk diamond province, Russia: Types, composition, and origin. Petrology 23: 227–258. doi:10.1134/S0869591115030054

Variations of U–Pb zircon ages of granitoids from the copper porphyry deposits of the Urals, Russia

Shardakova G.Yu., Grabezhev A.I., , Ronkin Yu.L., Azovskova O.B.

Institute of Geology and Geochemistry, Ural Branch of the Russian Academy of Sciences, Ekaterinburg, Russia,
shardakova@igg.uran.ru

The eastern slope of the Urals and the western Trans-Urals are the new large industrial copper porphyry province of Russia. Porphyry mineralization is confined to small massifs of quartz diorites, localized exclusively within the submeridional volcanogenic zones of the island-arc type, which are separated by sialic zones (Figure). In the Southern Urals, the Mikheevsk Cu ± (Au, Mo) deposit is being mined and the Tomino-Kalinovsk Cu ± (Au, Mo) ore field is preparing to exploration. Their balance reserves are 1.4-1.8 million tons of Cu with an average Cu content of 0.4-0.6 wt. % (Grabezhev, 2012; Ploninskaya et al, 2014, etc.). A number of deposits of a smaller scale are being developed. These are the Gumeshky Cu-(Au) deposit with skarn and vein-disseminated mineralization, Yubileynoe Au-Cu-porphyry and Varvarinsk Cu(±Au) deposits, as well as a number of smaller objects. In recent years, authors have obtained many U-Pb datings of zircons from the ore-bearing quartz diorite of the Urals (Grabezhev, 2014; Grabezhev, Ronkin, 2011; Grabezhev et al, 2014; Grabezhev et al, 2016, etc).
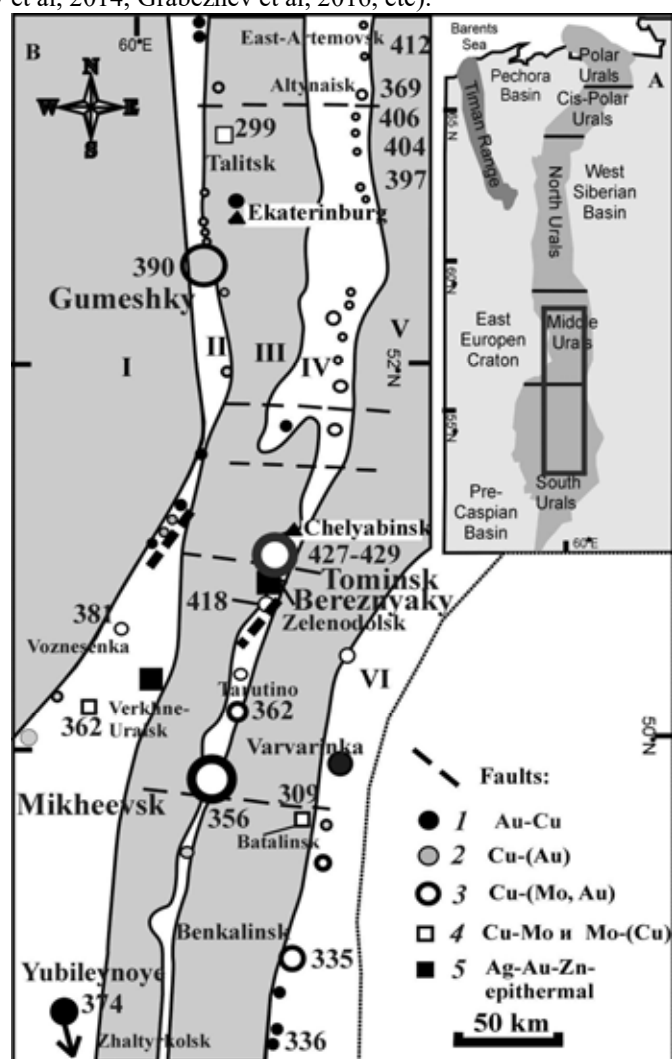
Fig. 1. The scheme of localization of copper porphyry deposits in the Middle and Southern Urals (A) and their position inside the Uralian structures (B). I–VI – main structures of the Urals. Sialic megazones (grey color): I – Central Uralian, V – East-Uralian and III – Trans-Uralian. Volcanogenic (isl arcs)megazones (white color): II – Tagil-Magnitogorsk-Zapadnomugodzharsk, IV – East-Uralian and VI – Valerianovsk. 1–5 – ore composition. Big circles mean large deposits (now proceeding), small circles are small deposits and occurrences. There are ages of zircons from ore-bearing granites of select deposits.

The ore-magmatic systems of the Urals differ from most other copper porphyry regions of the world where ore-bearing granitoids usually have a calc-alkaline or subalkaline composition (monzonite model) and they were formed predominantly during the Mesozoic and Cenozoic time (Cooke et al, 2005; Sillitoe, 2010; Vry et al, 2010 etc). In the Urals, Cu- (Au) -, Au-Cu- and Cu- (Au, Mo) porphyry deposits of all three volcanogenic zones (Tagil-Magnitogorsk, East Uralian and Valerianovsk) correspond, with single exceptions, to a diorite model of copper porphyry systems (island-arc type). A feature of the majority of Uralian objects is their plagiogranitoid composition (quartz-diorites predominate) and incompleteness of granitoid series. Granitoids are hydrothermally altered in varying degrees (albitized, sericized, chloritized and carbonatized). A detailed petrographic characteristic of granitoids is given by us earlier (Grabezhev, Belgorodsky, 1992; Grabezhev et al, 2014 etc). The contents of K_2O, Rb, REE in granitoids are very low and somewhat increase in the east direction from Tagil-Magnitogorsk to the East Uralian and further to Valerianovsk zones. In quartz diorites and tonalites of the Southern Urals, these concentrations are: K_2O (wt%) - 0.8-1.4, 1.1-1.6 and 1.6-2.0; Rb (ppm):

4-17, 16-25 and 21-42; ΣREE (ppm) - 23-48, 32-47, 45-58. The REE-patterns of all granitoids are very close. Their characteristic feature is a weak or absent europium anomaly. Two-feldspar granitoids of the diorite-granodiorite composition of several deposits (Yubileynoe, Verkhneuralsk, Artemovsk-Altynaisk, Batalinsk) contain up to 2.5-3.6 wt. % K_2O and more Rb, REE than in the typical plagiogranitoids.

Isotope U-Pb ages of zircons from ore-bearing granitoids of different zones are shown in Fig. and in the Table. They vary in a wide range. For the Middle and Southern Uralian parts of the region, the ages range from 427-429 to 309 Ma (S_2-C_{1-2}), the interval is about 119 million years. Such long life of ore-bearing magmatic systens is not typical for most large porphyry provinces in the world (usually duration is 15-25 million years (Hedrnquist et al, 1998 et al)).

Significant intervals of age variation were obtained for porphyry deposits and within individual volcanic zones of the Urals. In more western Tagil-Magnitogorsk-Zapadnmugodzharsk zone, the ages range from 380-390 (D_{1-2}) Ma (early island arc stage) to 362 (D_3^2-C_1^1) Ma (late island arc stage, Verkhneuralsk occurrence). In the most ore-bearing East-Uralian zone there is a wide dispersion of the ages. The most ancient South Uralial objects are the Tomino-Bereznyaky ore deposit (429-427 Ma) and the Zelenodolsk deposit (418 Ma). Within the S-D_1 Alapaevsk-Sukholozhsk zone, the ages vary from 411 ± 3 to 397 ± 4 Ma, with quartz-diorite magmatism replaced by diorite-tonalite-granodiorite. The Mikheevsk field, which is the largest in the Urals, is also near the eastern boundary of the Eastern Uralian volcanogenic zone and has a D_3^2-C_1^1 (362 ± 4 Ma) age.

Table. U–Pb and Rb–Sr ages of ore-bearing granitoids from Cu-porphyry deposits of the Urals

Deposit/massif, rock	Ore mineralization	Age, Ma
Tagil-Magnitogorsk-Zapadnomugodzharsk volcanogenic megazone		
Verkhneuralsk, hornblende-biotite monzogranire	Cu–Mo	362±9*
Yubileynoe, hornblende-biotite adamellite-porphyre	Au–Cu	374±3
Voznesenka, fine-medium grained hornblende quartz diorite sericitized	Cu–(Mo, Au)	381±5
Gumeshky, fine-medium grained hornblende quartz diorite propilitized	Cu–(Au)	390.0±2.8
Гумешевское, мелко–среднезернистые кварцевые диориты пропилитизированные	Cu–(Au)	393±18*
East Uralian volcanogenic zone		
Tomino-Bereznyaky ore field: Tominsk, quartz diorite sericitized	Cu±(Mo, Au)	429±4 428±3***
Bereznyaky, quartz diorite sericitized, subvolcanic	Ag–Au–Cu	427±6***
Zelenodolsk, diorite porphyrite sericitized	Cu–(Mo, Au)	418.3±1.3**
Yaluninogorsk, quartz diorite sericitized	Cu–(Au)	411.5±1.6**
Altynay, grained hornblende quartz diorite	Cu±(Mo,Au)	405.9±3.8 405.7±2.5
Artemovsk, porphyric granite	Cu±(Mo, Au)	404.2±2.4
Shata location, rhyodacite subvolcanic porphyre	Cu	397.2±3.8
Vostochno-Artyomovsk, grained hornblende quartz diorite	Cu	369±18*
Тарутинское, quartz diorite porphyrite sericitized	Cu–Mo–(Au)	362±4
Mikheevsk, quartz diorite porphyrite sericitized	Cu±(Mo, Au)	356±6
Valerianovsk island arc zone		
Benkalinsk, quartz diorite porphyrite sericitized	Cu±(Mo, Au)	334.7±2.9**
Zhaltyrkolsk, biotite granodiorite	Cu±(Au)	336.4±2.9**
Trans-Uralian sialic zone		
Batalinsk, biotite granodiorite	Cu–Mo	309.1±0.7

* Rb–Sr age of granitoids. ** La ICP-MS U–Pb age of zircons from granitoids. *** U–Pb SHRIMP–IIe/mc Pb age of zircons from granitoids. Other values are U–Pb SHRIMP–II age of zircons from granitoids.

In general, quartz diorite-porphyries of the largest industrial ore fields were introduced twice in the Urals. They have S (429-418 Ma) and D_3^2-C_1^1 (362 ± 4 Ma) age. Between them, small manifestations of copper formed in the Tagilo-Magnitogorsk-Zapadnomugodzharsk zone and in the Lower Carboniferous in the Valeryanovsk zone. The interval of isotope ages after the Silurian diorite-porphyry ore-bearing massifs is 390-335 Ma (ems-vise).

So, an important result of this work: in the Southern Urals, in the lateral section from west to east (at a distance of about 160 km), the rejuvenation of isotope ages from D_{1-2} (390 and 380 Ma) in the Tagil-Magnitogorsk zone to D_3^2-C_1^1 362, 356 Ma) in the eastern part of the East Uralian volcanogenic zone and C_{1-2} (336 and 335 Ma) in the Valerianovsk zone. In the indicated direction, ore specificity also changes: Cu- (Au) - and Au-Cu-porphyry deposits are replaced by Cu- (Au, Mo) -porphic deposits. A significant decrease in the age of diorite-porphyry from west to east is accompanied by a relatively small increase in their silicic acidity and in the contents of K, Rb, and REE. This probably corresponds to an increase in the degree of emanation-crystallization differentiation of diorites in this direction. This is also indicated by the increasing of Mo content in ores.

In addition to the lateral change in the ages of quartz diorite-porphyry, vertical changes in the age of ore-bearing granitoids occur within individual volcanogenic zones in the Southern Urals. It is most clearly expressed within the

Devonian Magnitogorsk island arc: 390, 381, 374 and 362 Ma (Grabezhev, 2014). In this series, the composition of ore-bearing granitoids varies from quartz-diorite to granodiorite-tonalite (Yubileynoe deposit) and shoshonite (Verkhneuralsk ore occurrence). A significant increase in the contents of K, Si, Rb and REE is observed in granitoids.

Our isotope data (Grabezhev, 2009) allow making a conclusion about the source of ore-bearing melts. For all deposits, the $(^{87}Sr/^{86}Sr)_t$ ratios in ore-bearing granitoids and carbonates from veins correspond to mantle marks with a small admixture of crustal material (0.7039-0.7051 and 0.7043-0.7046, respectively). The same is confirmed by the values $(\varepsilon Nd)_t$ of granitoids +(4.1-6.6). The maximum admixture of crustal material, $(^{87}Sr/^{86}Sr)_t = (0.7049-0.7051)$ is characteristic of the diorites of the largest deposits (Mikheevsk and Tominsk).

The incompleteness of ore-bearing complexes and isotope-geochemical data indicate that the island type of diorites is the result of selective melting from the lower crustal metabasalts or mantle wedge material. Such melting could occur repeatedly as the source of melting shifted from west to east of the Urals from the Silurian to the Lower Carboniferous.

References:

Grabezhev A.I. (2009) Sr-Nd-C-O-H-S isotope-geochemical description of SouthUrals porphyry-copper fluid-magmatic systems: probable sources of matter. Litosfera: 66–89. (in Russian).

Grabezhev A.I. (2012) Rhenium-bearing Uralian porphyry-copper systems:geological position, isotope-petrogeochemical and spatial-timing lateral zoning. Litosfera 4: 190–207. (in Russian).

Grabezhev A.I. (2014) The Yubileinoe porphyry Cu-Au deposit (South Urals, Russia): Shrimp-II U-Pb zircon age and geochemical properties of ore-bearing granitoids. Doklady Earth Sciences 454 (1): 72-75.

Grabezhev A.I., Belgorodskij E.A. (1992) Productive granitoids and metasomatic rocks of porphyry-copper deposits. Ekaterinburg, 199 p. (in Russian).

Grabezhev A.I., Ronkin Yu.L. (2011) U-Pb age of zircons from ore-bearing granitoids of the South Urals porphyry-copper deposits. Litosfera 3: 104–116. (in Russian).

Grabezhev A.I., Ronkin Yu.L., Puchkov V.N., Korovko A.V., Gerdes A., Azovskova O.B., Pribavkin S.V. (2014) Alapaevsk–Sukhoi Log porpyry copper zone (Middle Urals): U–Pb age of produktive magmatism. Doklady Earth Sciences 459 (2):1479-1482.

Grabezhev A. I, Ronkin Ju.L., Puchkov V.N., G.Ju.Shardakova, O.B.Azovskova, A. Gerdes. (2016) Silurian U–PB zircon age (LA–ICP–MS) of granite of Zelenodol Cu–porphyric deposit Southern Urals. Doklady Earth Sciences 466 (3): 68–71.

Puchkov V.N. Ocherk mineragenii Urala (2006) Problems of geology and ore genesis. Syktyvkvar: Geoprint: 195–222. (in Russian).

Puchkov, V.N., 2010. Geology of the Urals and Cis-Urals (Actual Problems Of Stratigraphy, Geodynamics and Metallogeny. Ufa, Dauriya: 411 (in Russian)

Cooke D.R., Hollings P., Walshe J. (2005) Giant porphyry deposits: Characteristic, distribution and tectonic control. Econ. Geol. 100 (5): 801–818.

Hedenquist J.W., Arribas A., Reynolds T.J. (1998) Evolution of an intrusion–centered hydrothermal system: far Southeast–Lepanto porphyry and epithermal Cu–Au deposits, Philippines. Econ. Geol. 93 (4): 373–405.

Plotinskaya O.Yu., Grabezhev A.I., Groznova E.O., Seltmann R, Lehmann B. (2014) The late Paleozoik porphyry–epithermal spectrum of the Birgilda−Tomino ore cluster in the South Urals, Russia. Journal of Asian Earth Sciences 79: 910–931.

Plotinskaya O Yu., Grabezhev A. I., Tessalina S., Seltmann R., Groznova E. O., Abramov S. S. (2016) Porphyry deposits of the Urals: geological framework and metallogeny. Ore Geol. Rev. (in press).

Sillitoe R.H. (2010) Porphyry copper systems. Econ. Geol. 105 (1): 3–42.

Vry V. H., Wilkinson J.J., Seguel J., Millan J. (2010) Multistage intrusion, brecciation and veining at EI Teniente, Chile. Evolution a Nested system. Econ. Geol. 105 (1):119–153.

Geochemistry of the Mid-Paleoproterozoic Elet'ozero titaniferous syenite-gabbro intrusive complex, Northern Karelia, Russia

Sharkov E.V.[1], *Chistyakov A.V.*[1], *Bogina M.M.*[1], *Shchiptsov V.V.*[2], *Frolov P.V.*[2]

[1]Institute of Geology of Ore Deposits, Petrography, Mineralogy and Geochemistry of the Russian Academy of Sciences, Moscow, Russia
[2]Institute of Geology Karelian Research Center Russian Academy of Science, Petrozavodsk, Russia

The Elet'ozero complex in Northern Karelia is the oldest (2086±30 Ma) and one of the largest (about 100 km^2) syenite-gabbro intrusions in the world. It belongs to the Mid-Paleoproterozoic Jatulian-Ludicovian large igneous province in the eastern Fennoscandian Shield, which is composed of alkali Fe-Ti basalts and tholeiitic basalts with variable Ti-contents (Sharkov, Bogina, 2006). The tholeiitic basalts are predominant rocks, whereas alkaline volcanics were found only in the Kuetsjarvi Group, Pechenga structure (Kola Peninsusula) and are not found in Karelia yet.

The Elet'ozero layered syenite-gabbro complex was formed in two intrusive phases, where mafic-ultramafic rocks of its first phase predominates (Bogachev et al., 1963; Kukharenko et al, 1969; Schpiptsov, 2007; Sharkov et al., 2015). Marginal group of the massif is mainly made up of thin-grained ferrogabbros (with contaminated gabbronorite in contact), while prevailing inner portion (Layered Series) is represented by alternation of ferroclinopyroxenite, ferroperidotites,

ferrogabbros (olivine gabbro, gabbro, gabbro-anorthosite, as well as orthoclase gabbro, phlogopite gabbro, etc), and their ore-bearing varieties. All rocks of the Layered Series are variably enriched in Fe-Ti-oxides (magnetite, titanomagnetite and ilmenite), amounting up to 30-70 vol.% and more in ore varieties, averaging 10 vol.%. The most evolved apatite-bearing rocks are developed in the central part of the intrusion (Nyatovara section) and the highest temperature rocks were found in the eastern part of the intrusion near the Marginal group (Surivara section). The structure of the massif is difficult to decipher due to intricate, frequently cross-cutting relations between rocks, which is related to the replenishment (multiple injecta) of fresh magma in a solidified intrusive chamber. The core of the massif (about 10% of the area) consists of alkaline rocks (syenites and Ne-bearing syenites) of the second phase, which cross-cut ferrogabbros.

All rocks of the Elet'ozero complex are characterized by the elevated alkalinity. In binary diagrams they define common trends (Fig. 1). Cr and Ni have trace concentration in the rocks. Mafites and ultramafies of almost coeval titaniferous Gremyakha-Vyrmes syenite-gabbro complex in the Kola Peninsula are close in composition to the rocks of the Elet'ozero complex. However, its rocks as compared to the Elet'ozero complex are enriched in CaO, Al_2O_3 and TiO_2, and have wide variations of MgO, Fe_2O_3T and P_2O_5. Alkaline syenites form independent compact fields where K_2O and Na_2O widely vary relative to Al_2O_3, CaO and Fe_2O_3T (Fig. 1). Their fields lie on the continuation of ferrogabbros trends, but transitional rock varieties are absent.
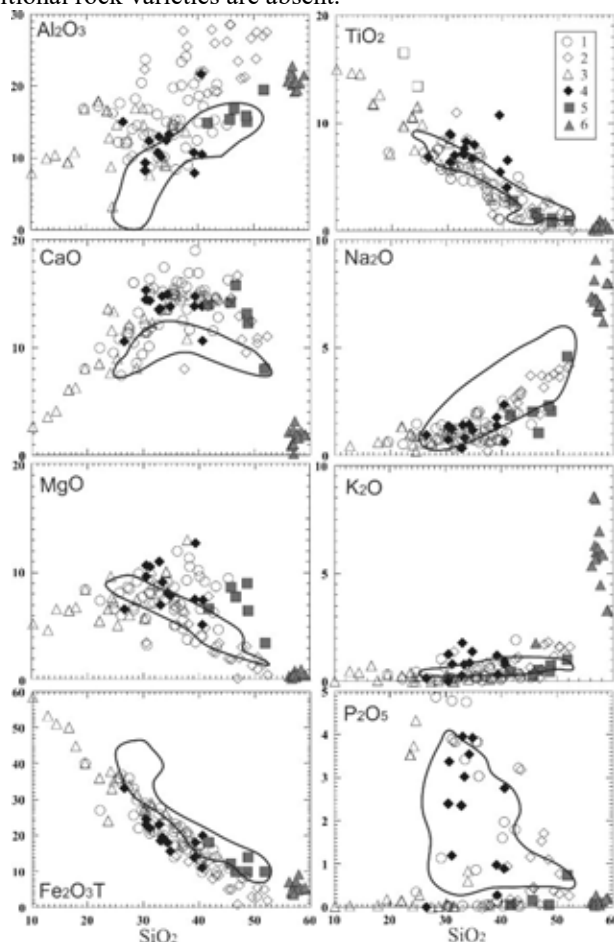
Fig. 1. Variations of the Elet'ozero complex rocks's composition.

1 – Ol ferrogabbro and ferrogabbro (Fe-Ti oxides <10 vol.%); 2 – gabbro-anorthosites; 3 – ore ferrogabbro (Fe-Ti oxides >20 об.%); 4 – Bt-Ol ferroclinopyroxenites and ferrogabbros (Bt >15%); 5 – marginal contaminated gabbronorites; 6 – alkali syenites. Outlined fields are gabbro-peridotite rocks of the Gremyakha-Vyrmes complex (after Arzamastsev et al., 2006).

The rocks of both intrusive phases of the Elet'ozero Complex have similar strongly fractionated REE patterns $((Ce/Yb)_n=6.8-28.3; (Gd/Yb)_n=2.1-8.1)$, but differ in the trace element diagrams (Fig. 2). The rocks of the first phase are enriched in Ba, Sr, and Ti relative to syenites, showing the positive anomalies in the spidergrams. Both the phases are enriched in Nb and Ta. Rocks of the Surivara section practically do not contain apatite and, accordingly, have no P at relatively high V content; they are characterized by low Sr, Zr, Ba, Y, Nb and REE contents at relatively low fractionation of LREE and HREE $((Ce/Yb)_n=6.8-10.3; (La/Sm)_n=1.1-2.0; (Gd/Yb)_n=2.1-4.4)$. Positive correlation of MgO and CaO with La assume that the main REE carrier was *Cpx*.

In contrast to Surivara, the rocks of Nyatovara section are enriched in P (apatite presence), LILE (Ba, Sr), HFSE (Y, Th, U, Nb), and REE at steeper fractionation of LREE and HREE $((Ce/Yb)_n = 11.2-28.3; (Gd/Yb)_n=5.42-8.08))$. This indicates that the central part of the complex is made up of late derivatives that accumulated incompatible elements. Main REE carrier in these rocks was apatite which underlined by positive correlation of La and P_2O_5.

The gabbros in the both sections show small positive Eu-anomaly (Eu* – up to 1.7 in ferrogabbros and to 5.2 – in gabbro-anorthosites), which is likely, controlled by *Pl* content in rocks.

Positive Nb-anomaly (Nb* from 1.2 to 5.6 in ore-bearing varieties) is found in the Surivara ferrogabbros, whereas the Nyatovara rocks have essentially lower anomaly (Nb* – 0.5), except for ore-bearing rocks – up to 1.65 (samples E20/1 and E22/4) (Fig. 2).

Gabbronorite from the direct contact with the country Archean granite-gneisses (sample. E38), in spite of distinct evidence of contamination (εNd_{2080} = -4.26 at Ndi 0.509725 as against +2.99 and +3.09 at Ndi - 0.510095 and 0.51001 in ferrogabbros of the Layered series and syenites accordingly, our unpublished data), is geochemically close to ferogabbros from the inner part of the complex (Fig. 2). In terms of total REE (185.55 g/t) content, the garbbronorite is close to the Nyatovara rocks, but resemble the Surivara gabbros in terms of LREE enrichment relative to HREE (($Ce/Yb)_n$=9.9; $(La/Sm)_n$=2.4 and $(Gd/Yb)_n$=2.9). Negative Eu anomaly (Eu*=0.7) and lowered Ti and Ba contents at high U and Th are, probably, results of contamination also.

Syenites, like ferrogabbros, have positive Nb-anomaly (Nb/Nb* from 1.3 to 2.8) due to the presence of pyrochlore and magnetite in syenites, however, show the negative Eu anomaly (Eu*=0.6), which is not typical of ferrogabbros. Syenites are characterized by high LREE fractionation relative to HREE $(Ce/Yb)_n$ = 11.3-16.5), which is close to the Nyatovara rocks. However, unlike them, syenites has lower level of HREE $((Gd/Yb)_n$ = 2.8-3.2), at low P and Sr contents, but higher concentrations of Ta and Nb (due to presence of pyrochlore). Thus, syenites, as the Nyatovara rocks, are evolved rocks, have similar REE abundance, but differ in the the contents of such incompatible elements as P and Ba. These facts suggest that syenites were formed independently of the rocks of the first phase and were derived from a different source.
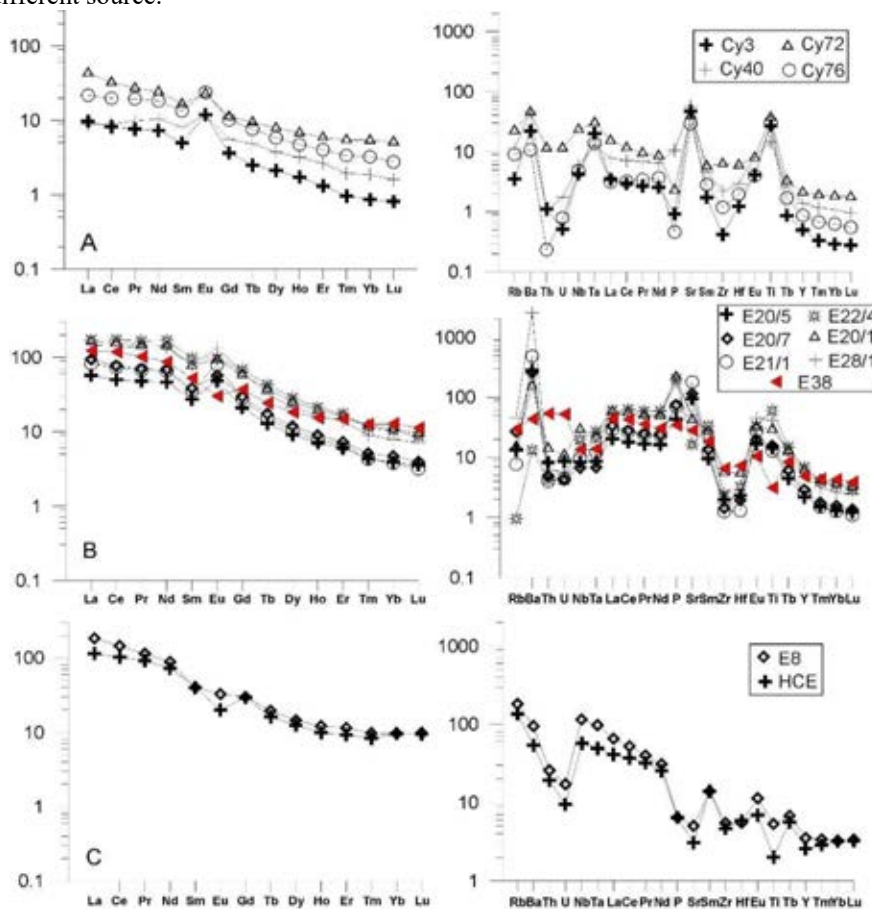
Fig. 2. Geochemical features of the Elet'ozero complex rocks; Cr and Ni contents are greatly low then in primitive mantle (after McDonough, Sun, 1995). Left column - composition of rocks normalized to chondrite C1 and right column - normalized to primitive mantle (after McDonough, Sun, 1995). A - samples from Surivara, B - from Nyatovara with gabbronorite from endocontact (sample E38), and C - alkali syenites of the second phase.

Thus, all rocks of the bimodal Elet'ozero intrusive complex are: (1) enriched in Fe, Ti, and alkalis; (2) form common geochemical trends for most components; (3) characterized by close patterns of rare components, enrichment in LILE, and depletion in Cr, Ni, and Co; (4) have highly fractionated REE patterns, both for LREE and HREE; (5) syenites occur on the continuation of ferrogabbros geochemical trends, however followed the owing evolution trend and were not derived by crystallization differentiation of the first phase.

Problem of the parental melts of the Elet'ozero complex.

It was shown above that gabbros in contact with country rocks are strongly contaminated by crustal material and cannot be taken as a chilled zone *sensu stricto* for further genetic consideration. It is also hardly possible to calculate the average composition of the intrusion, and correspondingly to calculate the primary composition of magma due to active replenishment of magmas in a solidified intrusive chamber. Only geochemical and experimental data may provide insight in the nature of parental magmas.

Enrichment of the Elet'ozero's mafic rocks in Fe-Ti oxides, appearance of essexites, *Bt*- and *Ort*-ferrogabbros as a result of crystallization differentiation, frequent presence of normative Ne in mafic rocks, as well as geochemical signatures (high Nb, Ta, and incompatible elements content) evidence that the rocks of the first phase were derived from the OIB type mid-alkaline Fe-Ti basalts.

Based on study of REE composition of clinopyroxene and *Cpx*/melt partition coefficients experimentally obtained for mid-alkaline basalts at high *PT* parameters (Hart, Dunn, 1993; Hauri et al., 1994), we calculated trace element content

in equilibrium melts. REE patterns and spiadergrams of model melts in shape, anomalies, and degree of fractionation are similar to those of mid-alkaline Fe-Ti basalts of the Paleoproterozoic (2.2-2.06 Ga) Kuetsjarvi Group (Fig. 3). Slightly higher concentration of rare elements in hypothetical melts is probably, related to their evolved composition, which is in a good agreement with moderate magnesium number of *Cpx* (mg# 80) and *Ol* (mg# 70). Thus, the rocks of the first phase were likely derived from typical for LIPs mid-alkaline Fe-Ti basalts, the origin of which is usually thought to be related to the mantle plume activity.

Origin of alkali and Ne syenites of the Elet'ozero second phase is a special problem. In spite of the fact that their geochemical features are close to the ferrogabbros of the first phase, they have independent origin. We assume that generation of alkali trachytes (parental melts of syenites) was related to the processes in mantle plume head where two magma generation zones exist practically simultaneously (Sharkov, Bogatikov, 2017). The major zone of adiabatic melting produce basaltic melts, whereas the second zone (incongruent melting) occurred in the upper cooled margin of the plume head due to fluids, which percolated from underlying zone of adiabatic melting and produce trachyte melt. In other words, basaltic and trachyte melts derived from the same protoliths, but by the different ways.
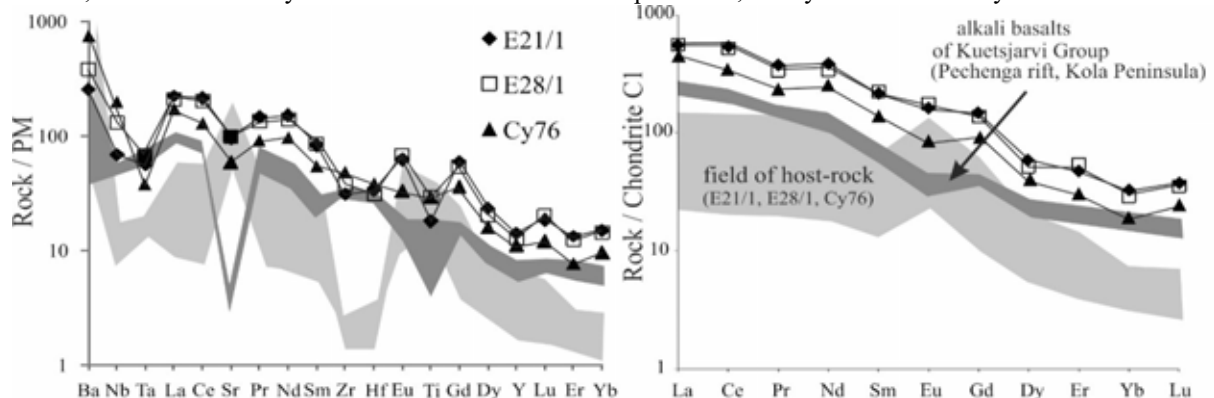
Fig. 3. Trace-element and REE patterns for melts in equilibrium with clinopyroxenes of the Elet'ozero complex as compared to their host rocks.

So, the first phase of the Elet'ozero complex was derived from mid-alkaline Fe-Ti basalts. Syenites of the second phase are close to alkali trachyte in composition and were likely, derived from such melts. Thus, the studied complex is an intrusive analogue of the bimodal basalt-trachyte association, which is common of LIPs. This intrusion could serve as transitional chamber of mid-alkaline Fe-Ti basaltic system of the Jatulian-Ludicovian LIP, where processes of melt accumulation, their crystallization differentiation, mixing, and crustal contamination occurred.

References:

Arzamastsev AA, Bea F, Arzamastseva LV, Montero P (2006) Petrology 14: 361-389.

Bogachev AI, Zak SI, Safronova GP, Inina KA (1963) Geology and Petrology of the Elet'ozero Gabbroid Massif of Karelia, Moscow: AN USSR (in Russian).

Hart SR, Dunn T (1993) Experimental Cpx/melt partitioning of 24 trace elements. Contrib. Mineral. Petrol. 113: 1-8.

Hauri EH, Wagner TP, Grove TL (1994) Experimental and natural partitioning of Th, U, Pb, and other trace elements between garnet, clinopyroxene, and basaltic melts. Chem. Geol. 117: 149-166.

Kukharenko AA, Orlova MP, Bagdasarov EA (1969) Alkaline Gabbroids of Karelia. Elet'ozero Massif - Petrology, Mineralogy, and Geochemistry, Leningrad: Izd-vo LGU (in Russian).

Shchiptsov VV (2013) Industrial minerals of the Tikshozero-Eletozero alkaline ultramafic-carbonatitic and alkaline gabbroic complexes in Karelia, Russia. In *12 SGA Biennial Meeting Mineral Deposits Research for a High Tech World,* Uppsala 4: 1781-1783.

Sharkov EV, Belyatsky BV, Bogina MM et al. (2015) Genesis and Age of Zircon from Alkali and Mafic Rocks of the Elet'ozero Complex, North Karelia. Petrology 23(3): 259-280.

Sharkov EV, Bogatikov OA (2017) A Likely Reason for the Appearance of the Daly Gap in Magmatic Series of Large Igneous Provinces. Doklady Earth Sci. 472(2): 231-236.

Ore-bearing breccias as a manifestation of magmatogenic-fluidogenic-ore systems of the Earth

Sharpenok L.N., Kukharenko E.A., Kostin A.E., Stepanov S.Yu.

Federal State Budgetary Enterprise 'A. P. Karpinsky Russian Geological Research Institute', Moscow, Russia, Lyudmila_Sharpenok@vsegei.ru

The concept of regular genetic relationship of ore deposits of a certain type with particular magmatic formations is not always confirmed, as is known. Geological practice evidences that in most cases ore mineralization is not a derivative of specific igneous rocks, but is a result of magmatogenic-fluidogenic-ore systems. In most instances, not magmatic rocks are ore-bearing but fluid flows, which are to some extent associated with parent magmas at different stages of evolution of these systems.

Accordingly, the relationship between magmatic complexes and mineralization is primarily paragenetic, rather than genetic. Attenuation of magmatic activity leads to the separation of the fluid from the crystallizing magma. In this case, the fluid, moving under certain geodynamic conditions to higher crust levels, undergoes changes in thermodynamic parameters and the chemical composition, extracting different components, including ore ones, from various rocks it migrates through. In addition, on higher crust levels the fluid is enriched with groundwater, and the magmatogenic system as a whole acquires the water-fluid character.

A reliable indication and evidence of high fluid saturation of ore-forming systems is the presence of explosive breccias in significant part of various mineral deposits. Many Russian researchers drew attention to this fact (P. F. Ivankin, Z. M. Nurbaev, V. S. Kuzebny, P. V. Inshin, G. I. Tugovik, etc.). Nevertheless, these ore-generating and ore-hosing formations are still underestimated. Hence, it follows that it is necessary to systematize explosive, mainly cryptoexplosive breccias and to work out their diagnostic features and principles of studying as the most important elements of magmatogenic-fluidogenic-ore systems in order to justify their forecasting and discovery.

Endogenic breccias, if one excludes tectonogenic ones from consideration, are a result of strains (compressional, explosive, and decompressional) in a "flowable" medium, which is a liquid, liquid-gas, gas, and sometimes solid-liquid-gas substance. This substance, depending on the fluid content, is subdivided into the ***magma proper, the fluidized magma and the fluid proper***.

Magma proper is mainly silicate melted medium containing fluid in a distinctly subordinate amount that little contributes to breccia formation.

Fluidized magma is a silicate-fluid melted medium in which the amount of the fluid phase is closely comparable with the amount of silicate component (F.A. Letnikov, 1992). Such a fluid melt obtains to a great degree features of the fluid proper and differs from normal silicate melts in a number of physicochemical properties. Among them, the most typical and important property for the formation of breccias is the ability of such flowable medium to cool down below the crystallization temperature of the coexisting melt, silicate matrix, that ensures its extreme explosivity.

Fluid proper is an essentially gaseous or liquid-gaseous flowable substance, which is mainly formed by volatile components (H_2O, CO_2, CO, N_2, H_2, CH_4 and other hydrocarbons, as well as halogenic and sulfurous components) with an admixture of petrogenic, ore and other elements, sometimes solid particles, including protomagmatic segregations. This flowable medium of a particular composition is transferred to the subsurface rocks mass of the upper crust (Letnikov, 1999) and, under certain conditions, it is characterized by extreme explosivity.

Different types of breccias due to each type of "flowable medium" under certain geodynamical conditions are formed (Fig. 1).
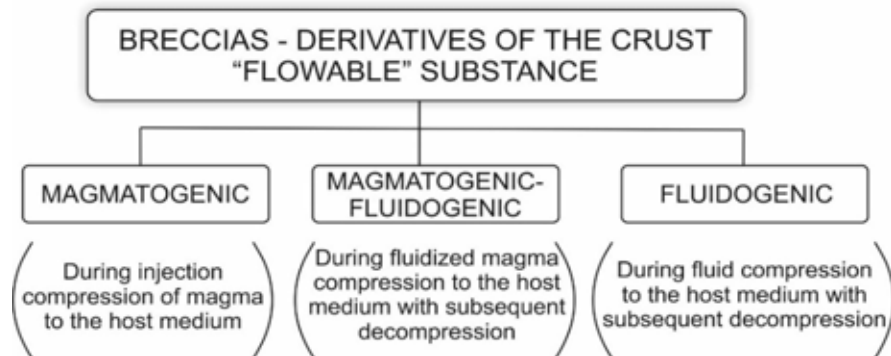
Fig. 1. Types of breccia rocks – derivatives of the "flowable" substance of the Earth's crust

Magmatogenic breccias are in most instances near-contact facies zones of plutonic, hypabyssal, subvolcanic bodies, rarely intraintrusive formations. These breccias are generally similar in composition to igneous rock, but contain fragments of enclosing rock, less often rock of earlier phases of intrusives. Commonly, the formation of these breccias is not accompanied by syngenetic mineralization.

Magmatogenic-fluidogenic cryptoexplosive breccias are formed as a result of fluidized magma exposure on host substance. Fluidized magma is mobile, aggressive with high potential explosivity, realized under favorable geodynamic conditions. The shape of the clasts is a diagnostic property of breccias: along with sharp-edged clasts, rounded fragments often can be found. As a result, "pebble" or "boulder dykes" (according to American terminology) appear. Evidences of processes leading to the formation of breccias are typical: *compressional* (kinkband structures, dynamic twinning of grains, planar elements in quartz, granulation) (Fig. 2); *decompressional* (micro-explosive fragmentation of grains); *crystallization* (formation of cement minerals, orbicules, regeneration of mineral grains, etc.); *replacement* (silicification, sericitation, carbonatization, serpentinization), etc. These processes can be manifested both in mineral grains and in lithoclasts. *Substantial composition* of such breccias corresponds to a mineral association of magmatic and fluid origin that combines grains formed as a result of magmatic crystallization (of mafic, intermediate, felsic or other compositions) with mineral derivatives of the fluid component – quartz-micaceous, siliceous-carbonate, argillizite, illite-smectite, serpentinite and others with an admixture of ore components, as well as hematite, chlorite-siderite, etc.

The most important property of magmatogenic-fluidogenic breccias is their *enrichment with ore components*, syngenetic to the breccia formation that leads under favorable conditions to the formation of ore deposits, including large ones. E.g., the Kalgutinskoe rare metal deposit (Gorny Altai) that is conjugated with acid magma, the Korshunovskoe

iron ore deposit (Angara-Ilim region) with basic magma, the Karasugskoe complex rare-earth deposit (Central Tuva) with the carbonatite fluid melt.

Kalgutinskaya breccia structure, Gorny Altai. Explosive magmogenic-fluidogenic breccias are an inherent part of the ore sites of the rare metal deposit where they associate (Dashkevich et al., 1991; Annikova, 2001; Potseluev, 2008; Gusev et al., 2010) both with granitoids of the Kalgutin Massif (Group I breccias) and with smaller bodies and dykes of granite-porphyry, rhyolite-porphyry, ongonite and elvan (Group II breccias). Breccia formations and conjugate rare metal ores are syngenetic; they are derivatives of a single evolving magmatogenous-fluidogenic system.

Ore mineralization associated with the Group I breccias consists of three morphological types: ore-bearing breccia, vein-disseminated breccia ores and vein formations. The bulk of the ore matter is concentrated in the quartz-mica breccia cement and along the periphery of the debris; ore minerals are molybdenite, pyrite, chalcopyrite and insignificant amount of wolframite. Veinlet-disseminated ores are typical of peripheral zones of breccia bodies; vein type consists of a series of wolframite-quartz veins crosscutting mineralized breccias.
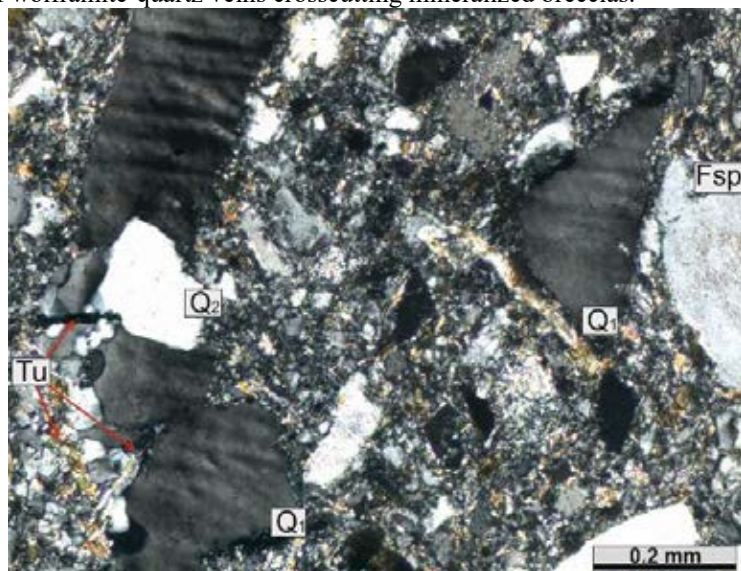
Fig. 2. Kinkband structure in quartz in magmatogenic-fluidogenic breccia; Kalgutinskoye deposit. A micrograph of a thin section; cross-polarised light. Q1 - protomagmatic quartz, Q2-newly formed, Tu - tourmaline, Fsp - potassium-sodium feldspar.
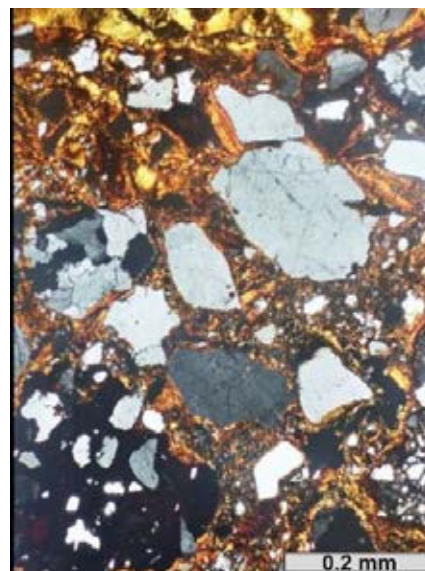
Fig. 3. Tuff-like fluidogenic breccia with ferrous-illite-smectite cement; Efimovskoye deposit. A micrograph of a thin section; cross- polarised light.

Group II breccias mineralization consists of rare metal high-Li-Cs ores on apatite-bearing ongonite (kalgutite) and elvan. Main minerals of commercial importance are wolframite, molybdenite, beryl, bismuthine and bismuth minerals, chalcopyrite. In the ore, along with widespread oxides, sulfides and sulfosalts, there are native elements: gold, bismuth, copper, carbon (graphite and its amorphous varieties).

Fluidogenic cryptoexplosive breccia rocks are mainly resulted from compressional, explosive and decompressional phenomena. Fluids can contain some silicate phase, but in a quantity clearly subordinated to the fluid phase, and therefore have no significant effect on fluidogenic processes.

Fluidogenic breccias have a number of features caused by the specificity of fluid flows: origination of fluids at various depths, their extreme mobility and aggressiveness, the ability to transfer protomagmatic mineral grains and fragments of magmatic melts in suspension. At the same time, along the way towards the upper levels, they are saturated with clastic material and chemical components of wall rock, and, in places of their explosions and unloading, with components and fragments of host rocks and with meteoric waters. They are not directly connected with igneous rock, but the presence of protomagmatic minerals or relict magmatic inclusions in them allows in many cases judging to some extent the source of fluids. The combination of the listed components of various geneses in the composition of fluidogenic breccias predetermines their structural heterogeneity and mineral disequilibrium, which are not characteristic of endogenic rocks of other types (Makhlaev, Golubeva, 1999; Lukyanova, Zhukov, Kirillov et al., 2000; Sharpenok, Lukyanova, 2003; Sharpenok, Golubeva, Lukyanova et al., 2008; Sharpenok, Kukharenko, Kostin, 2015).

Substantial characteristic of fluido-explosive breccias (FEB), containing both angular and rounded fragments, is very specific. Discovering protomagmatic and newly formed minerals, establishing deformation features in mineral grains (including planar elements and grain twinning) and in lithoclasts, determining composition and structure of the cementing mass, studying gas-and-liquid inclusions, etc. play an important role in their diagnostics. So, detailed petrographic studies of these rocks and their components including studies at large magnifications and in reflected electrons become of primary importance. *Breccia cement* is fluidogenic: argillizite, quartz-micaceous, carbonate-siliceous, illite-smectite and other cement, usually with an admixture of ore components, mainly sulphides, as well as ore one: iron oxide (hematite, goethite), sulfide, etc. (Fig. 3).

FEB ore potnetial. Summarizing the aforementioned features of fluido-explosive breccia rocks, it should be noted that they generally show an additive character due to the structural heterogeneity and mineral disequilibrium of the rocks.

However, their most important feature is the *exceptional enrichment with ore components* – gold, rare metals, rare earth elements, copper, iron, uranium, lead, zinc, mercury, nickel, platinum, diamonds, etc. (Shcheglov, 1994; Tugovik, 1974; 1984; Korobeinikov, 2009, Petrov, Shatov, Sharpenok et al., 2012, etc.). This specific FEB nature is due to the fact that among "flowable" substances of endogenic origin, fluids are the most promising concentrators of ore components at all stages of system development. Accordingly, the ore mineralization, in many cases complex, is as a rule, associated with fluidogenic-breccia structures to form mineral deposits, up to giant ones. Examples of such structures are as follows.

Olympic Dam breccia structure in Australia, with which the iron-gold-copper-uranium deposit is associated (Reynolds, 1991). The structure is formed by a series of impulse-phases of ore-bearing breccias with indistinct phase and facies transitions. Individual northwest-oriented zones or large bodies are distinguished depending on the amount of hematite in cement; cement content increases in breccia rocks from the periphery to the center of the structure. A coarse-concentric zoning is manifested in the structure somewhat complicated by the intermittency of breccia varieties.

Major part of ore reserves of the copper-uranium-gold-silver type deposit is associated with phases of heterolith and hematite breccias; gold ore type deposits are related to the hematite-quartz breccia phases. In general, the ores of the deposit are characterized by high contents of ore elements: up to 8% Cu, up to 0.1% U, up to 0.52 g/t Au, up to 15.6 g/t Ag, up to 1% Σ REE, with Ce prevalence up to 0.5%.

Koksay breccia structure, Kazakhstan, is a molybdenum-copper-porphyry deposit. The ore deposit is almost completely located in the breccia pipe and repeats its shape. In most instances, main molybdenum-copper ore mineralization (main ore minerals are pyrite, magnetite, chalcopyrite, bornite, molybdenite) is recorded both in fragments and in the binding mass of breccias of two impulses having different age. However, there are breccias within the deposit, in which such mineralization is recorded only in fragments, including fragments of the previous breccia, and later molybdenum-polymetallic mineralization is established in the cement. All this indicates a polyimpulse character of fluidogenic breccia formation (Nurbaev et al., 1977).

Khingan breccia structure, the Far East, is a tin deposit, characterized by multi-stage formation. First-stage breccias (cassiterite-chlorite-quartz with an admixture of sulphide) form funnel-shaped bodies, which mainly occur in upper parts of sections. Second-stage breccias of cassiterite-sulphide-chlorite-fluorite type mainly occur in chimney-shaped bodies sharply tapering with depth and wedging out; spatially, breccias of this type occur on intermediate and deep horizons of the deposit. Ore bodies are characterized by zonal structure: central part of the bodies consists of a breccia with large clasts; towards the periphery, it is the stockwork zone with a dense network of branching veinlets. The tin ore of the deposit is cassiterite. Its distribution is random and depends on the nature of the breccia rocks. Areas of elevated cassiterite concentration correspond to zones of maximum breccia formation.

Delmachik breccia structure, the Eastern Transbaikalia, is a gold ore deposit. In this deposit, breccia bodies and conjugate ore lodes mainly occur in the zone of manifestation of a multi-stage NW dyke complex. Breccia bodies host ore-bearing breccias of "quartz-tourmaline" and "polymetallic" stages. All mineral associations of the second stage contain microscopic gold in varying amounts, but its concentrator is parageneses with arsenopyrite and chalcopyrite.

Diamondiferous breccia structure – Efimovskoye deposit, the Perm Territory. The deposit consists of (Diamondiferous ..., 2011) at least three phases–generations of breccia rocks, differing in petrologic composition, structural and textural features and diamond potential. During the first phase, coarse detrital tuff-like breccias with rounded quartz grains were formed; during the second stage, breccias with moderate amount of fragments cemented with a sometimes ferrous smectite-hydromicaceous fluidogenic mineral association hosting diamonds appeared; the third phase is characterized by the formation of dense argillizite rocks with a small amount of detrital material.

Vorontsovskaya breccia structure, the Northern Urals is a *gold deposit*, which is an element of the magmatogenic-fluidogenic-ore system associated with the formation of the Auerbachovskiy gabbro-diorite-granodiorite intrusive. Structure corresponds to a complex "stock-like" body of fluido-explosive breccias with subhorizontal apophyses formed in the limestone series. Low-temperature mineral association with pyrite-auripigment-realgar gold-bearing cement is formed with later manifestations of breccias. The leading role of brecciation processes during the formation of the deposit is confirmed by the specific geological structure, the absence of tectonic control over mineralization, the shape of the breccia ore body and mineralogical-petrographic and geochemical characteristics of ore-bearing breccias and ores.

Summarizing the material presented it should be reiterated that the diverse and often exceptionally high syngenetic mineralization is one of the most important features, that are, to a varying extent, characteristic of breccia rocks, both of magmatogenic-fluidogenic and fluidogenic types. This is mainly due to the following features of their genesis.

Mineralization is one of the most important features, to a varying degree, characteristic of brecciated rocks, which are both of the magmatically-fluid-like and fluid-like types.

   – *High mobility and physicochemical aggressiveness of fluidized magmas and fluid flows that form breccias.*
   - *Specific physicochemical parameters of the fluid-enriched system.*
   - *The degree of saturation with useful components of the fluid constituent of the system.*
   - *Closeness of the magmatogenic-ore system that lead to cryptoexplosive character of breccia formation.*
   - *Predominance during breccia formation of minerogenesis conjugated with processes of compressions, explosions and decompressions, which facilitate extraction, fallout of ore components from the fluid.*
   - *Polyphase, polyimpulse formation of breccias facilitating the formation of complex ores.*
   - *Change of gradually weakening processes of breccia formation to hydrothermal-metasomatic mineral formation.*

TAINIOLITE FROM CHUKTUKON CARBONATITE MASSIF, CHADOBETS UPLAND, RUSSIA

Sharygin V.V.[1,2]

[1]Institute of Geology and Mineralogy, Siberian Branch of the Russian Academy of Sciences, Novosibirsk, Russia,
sharygin@igm.nsc.ru
[2]Novosibirsk State University, Novosibirsk, Russia

The Chuktukon massif is one of intrusions within southern Chadobets upland (SW Siberian Platform, Krasnoyarsk territory, Russia) (Lapin & Lisitsyn, 2004). Intrusive rocks of the Chadobets upland are represented by the ultramafic alkaline rocks (melilitite-nephelinites and pyroxene peridotites, picrites, melteigites), carbonatites and kimberlite-like rocks (carbonatite lapilli tuffs ?), which occur as veins, dykes and stocks. Several stock-like carbonatite bodies with the sizes of 1,2x0,7 km are mapped within the Chuktukon massif (Slukin, 1994; Lapin, 1997, 2001; Lapin and Lisitsyn, 2004; Kirichenko et al., 2012; Doroshkevich et al., 2016a).
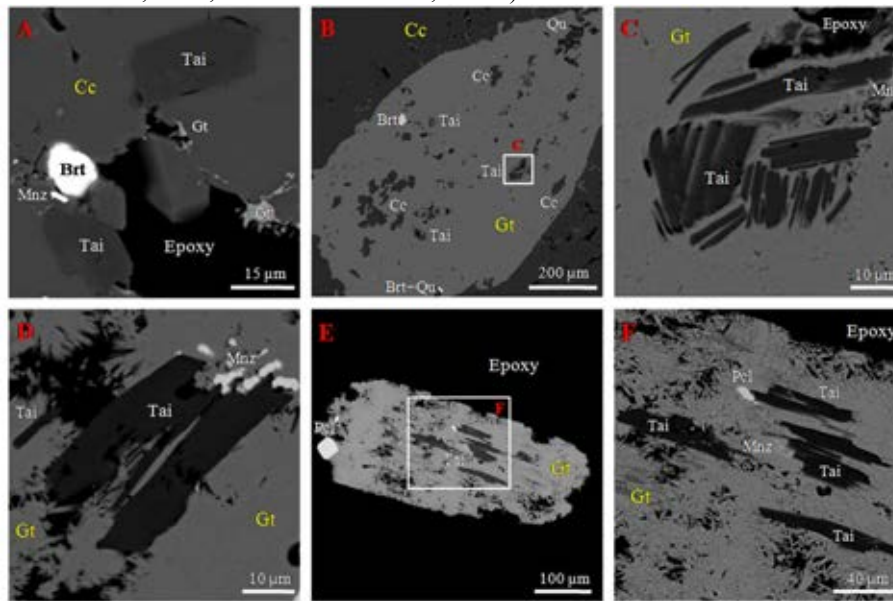
Fig. 1. Tainiolite in the Chuktukon carbonatite (BSE images). A – tainiolite crystals in carbonatite groundmass; B-F - tainiolite crystals in unidentified mineral completely pseudomorphed by goethite.
Symbols: Tai – tainiolite; Cc – calcite; Brt – barite; Gt – goethite; Mnz – monazite-(Ce); Qu – quartz; Pcl – fluorcalciopyrochlore.

Table 1. Chemical composition (EMPA+SIMS, wt.%) of tainiolite from the Chuktukon carbonatite.

	Individual grains in carbonatite groundmass									Ideal
n	*2*	*8*	*4*	*4*	*2*	*3*	*1*	*2*	*6*	
SiO_2	58.58	58.88	58.66	58.87	58.76	58.78	59.14	58.71	59.17	59.35
TiO_2	0.13	0.12	0.12	0.17	0.14	0.16	0.04	0.15	0.10	
Al_2O_3	0.09	0.13	0.15	0.10	0.13	0.16	0.09	0.10	0.04	
FeO	0.99	0.94	0.83	0.78	0.81	1.11	1.06	0.71	0.68	
MnO	0.00	0.01	0.01	0.01	0.01	0.01	0.00	0.01	0.01	
ZnO	0.01	0.02	0.01	0.01	0.01	0.01	0.00	0.04	0.01	
MgO	19.66	19.56	19.73	19.74	19.74	19.47	19.43	19.42	19.70	19.90
Na_2O	0.03	0.14	0.15	0.06	0.11	0.02	0.13	0.05	0.06	
K_2O	11.57	11.54	11.55	11.49	11.52	11.53	11.59	11.62	11.53	11.63
Li_2O	3.50	3.40		3.57		3.52	3.49	3.40	3.44	3.69
Rb_2O	0.07	0.04	0.01	0.15	0.08	0.00	0.01	0.10	0.00	
H_2O	0.22	0.40		0.20		0.25	0.19	0.16	0.10	
F	9.13	8.85	8.90	9.22	9.06	9.31	9.35	9.25	9.13	9.38
Sum	103.98	104.02	100.13	104.36	100.36	104.33	104.52	103.73	103.96	103.95
$O-F_2$	3.84	3.72	3.75	3.88	3.81	3.92	3.94	3.89	3.84	3.95
Sum	100.14	100.29	96.38	100.48	96.54	100.41	100.58	99.83	100.12	100.00

CaO, BaO and SrO are below detection limits (<<0.01 wt.%), Li_2O and H_2O are determined by SIMS. Ideal – ideal composition $KMg_2Li(Si_4O_{10})F_2$.

Tainiolite $KMg_2Li(Si_4O_{10})F_2$ was found in calciocarbonatites from boreholes. These rocks are fine-grained and altered in different grade by metasomatic/hydrothermal process. Li-mica is related to primary mineral assemblage, who also includes calcite (>>50 vol.%), fluorcalciopyrochlore, rippite, fluorapatite, fluorite, Nb-rutile, olekminskite, K-feldspar, Fe-Mn-rich dolomite, pyrite and quartz-1 (Doroshkevich et al., 2016b; Sharygin et al., 2016b). The calcite-

dolomite coexistence assumes crystallization temperature near 837°C for the primary paragenesis. Goethite (goethite + other Fe-rich hydroxides), francolite (collomorphic Sr-rich carbonate-fluorapatite) and psilomelane (romanèchite ± hollandite) aggregates as well as barite, quartz-2, monazite-(Ce), parisite-(Ce), synchysite-(Ce) and Sr-Ba-Pb-rich hydropyrochlores occur interstitially among grains of primary minerals (Chebotarev et al., 2016; Sharygin et al., 2016a-b). Burbankite, strontianite, daqingshanite-(Ce), ferrohagendorfite, barite, unidentified Na-REE-Ba-Sr-Ca-rich and Na-Fe-rich phosphates occasionally appear in secondary inclusions in fluorapatite and calcite (Sharygin et al., 2016a). The above minerals are related to a stage of metasomatic (hydrothermal) alteration of the carbonatites.

In first order tainiolite was studied in carbonatite sample (546-193.5), which is the holotype for a new mineral, rippite $K_2(Nb,Ti)_2(Si_4O_{12})O(O,F)$ (IMA 2016-025; Doroshkevich et al., 2016b; Sharygin et al., 2016b). This sample is the least unaltered carbonatite and the content of goethite, psilomelane and francolite is <<50 vol.%. Tainiolite forms euhedral blades (up to 50 μm) in carbonatite groundmass and individual crystal inclusions in unidentified prismatic mineral completely pseudomorphed by goethite (Fig. 1). In chemical composition it is close to ideal $KMg_2Li(Si_4O_{10})F_2$; the contents of Al_2O_3, FeO, H_2O and other minor oxides are not high (Table 1), the core-to-rim deviations are negligible. The concentrations of Li_2O and H_2O were determined by secondary ion mass-spectroscopy (SIMS). In general, the content of H_2O is very low (0.1-0.4 wt.%). Moreover, the low H_2O is supported by Raman spectra of the analyzed tainiolites due to very illegible bands in the 3500-3600 cm^{-1} region (Fig. 2).
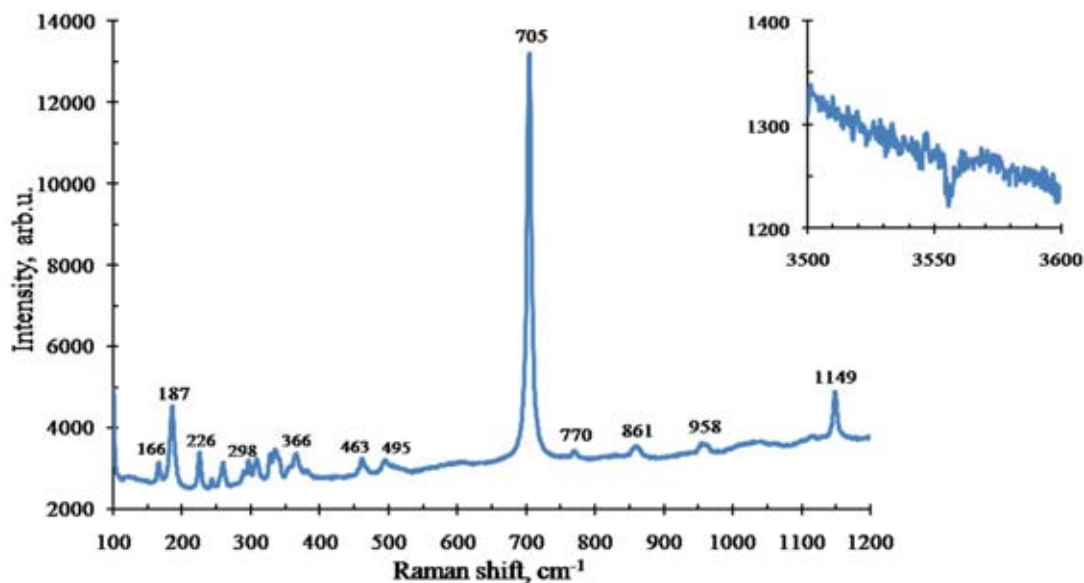
Fig. 2. Raman spectrum for the Chuktukon tainiolite in the 100-1200 and 3500-3600 cm^{-1} ranges.

The occurrence of tainiolite in the Chuktukon massif and other carbonatite complexes worldwide raises again the question of the status of Li as a "carbonatitic element" (e.g., Cooper et al., 1995). However, the findings of tainiolite, which can be considered as a primary magmatic mineral of igneous carbonatites, are not numerous: magnesiocarbonatite of the Bayan Obo complex, China (Le Bas et al., 1992); søvite dyke of the Dicker Willem complex, Namibia (Cooper et al., 1995); magnesiocarbonatite of the Araxá complex, Brazil (Traversa et al., 2001), carbonatite of the Sokli complex, Finland (Al-Ani , Sarapää, 2016) and calciocarbonatite of the Chuktukon massif (this work). In other alkaline ultrabasic or ultrabasic-carbonatite complexes worldwide, Li is mainly concentrated as tainiolite or tainiolite–rich micas in late-magmatic ultraagpaitic veins and in fenites, and on the contact of magmatites and sedimentary/metamorphic carbonate rocks (Erd et al., 1983; Cooper et al., 1995; Pekov et al., 2003; Armbruster et al., 2007; Chakhmouradian et al., 2007; Cooper, Paterson, 2008; Sharygin, Kryvdik, 2014 and references herein).

In general, tainiolite in the Chuktukon carbonatite is minor to accessory mineral, which is crystallized after fluorcalciopyrochlore (see Fig. 1F) and rippite and, possibly, before or together with calcite. The appearance of the first two minerals and K-feldspar in the studied carbonatites seems to be evidenced about the presence of moderate contents of Si, K and F in an initial carbonatite melt. However, the accumulation of Li in this melt is still enigmatic. Possibly, it may be a result of silicate-carbonate liquid immiscibility or other fractionation process within the Chadobets upland alkaline province (Slukin, 1994; Lapin, 1997, 2001; Lapin and Lisitsyn, 2004; Kirichenko et al., 2012; Doroshkevich et al., 2016a).

References:

Al-Ani T., Sarapää O (2016) Abundance of REE bearing minerals in carbonatite and lamprophyre dikes in Kaulus area, Sokli carbonative complex, NE Finland. Geologian Tutkimuskeskus, 7/2016.

Armbruster T, Richards RP, Gnos E, Pettke T, Herwegh M (2007) Unusual fibrous sodian tainiolite on phlogopite from marble xenoliths of Mont Saint-Hilaire, Québec, Canada. Can Mineral 45: 541–549. DOI: 10.2113/gscanmin.45.3.541

Chakhmouradian AR, Halden NM, Mitchell RH, Horváth L (2007) Rb-Cs-rich rasvumite and sector-zoned "loparite-(Ce)" from Mont Saint-Hilaire (Québec, Canada) and their petrologic significance. Eur J Mineral, 19: 533-546. DOI: 10.1127/0935-1221/2007/0019-1739

Chebotarev DA, Doroshkevich AG, Sharygin VV (2016) Niobium mineralization in carbonatites of Chuktukon massif, Chadobets upland (Krasnoyarsk territory, Russia). Abstract volume of 33rd International conference «Alkaline Magmatism of the Earth and related strategic metal deposits», Moscow, Russia, Editor-in-chief L.N. Kogarko, M.: GEOKHI RAS, pp 36-36 (in Russian).

Cooper AF, Paterson LA (2008) Carbonatites from a lamprophyric dyke-swarm, South Westland, New Zealand. Can Mineral, 46: 753-777. DOI: 10.3749/canmin.46.4.753.

Cooper AF, Paterson LA, Reid DL (1995) Lithium in carbonatites - consequence of an enriched mantle source. Mineral Mag, 59: 401-408. DOI: 10.1180/minmag.1995.059.396.03

Doroshkevich AG, Chebotarev DA, Sharygin VV (2016a) Alkaline ultrabasic carbonatitic magmatism of the Chadobets upland. Abstract volume of Moscow International School of Earth Sciences – 2016, Editor-in-chief L.N. Kogarko, M.: GEOKHI RAS, pp 31-32.

Doroshkevich AG, Sharygin VV, Seryotkin YV, Karmanov NS, Belogub EV, Moroz TN, Nigmatulina EN, Eliseev AP, Vedenyapin VN, Kupriyanov IN (2016b) Rippite, IMA 2016-025. CNMNC Newsletter No. 32, August 2016, page 919. Mineral Mag, 80: 915-922.

Erd RC, Czamanske GK, Meyer CE (1983) Taeniolite, an uncommon lithium-mica from Coyote Peak, Humboldt County, California. Mineral Record 14: 39-40.

Kirichenko VT, Zuev VK, Perfilova OYu, Sosnovskaya OV, Smokotina IV, Markovich LA, Borodin VP, Mironyuk EP (2012) The state geological map of the Russian Federation. Scale 1: 1 000 000 (third generation). Angaro-Yeniseisky series. Sheet O-47 – Bratsk. Explanatory note. SPb.: VSEGEI cartographical factory, 470 pages, pp 163-179 (in Russian).

Lapin AV (1997) Structure, formation conditions and ore potential of the main types of REE in the carbonatite weathering crusts. Otechest Geol, 11: 15-22 (in Russian).

Lapin AV (2001) About kimberlites of the Chadobets upland in connection with a problem of the formational-metallogenic analysis of the platform alkaline-ultramafic magmatites. Otechest Geol, 4: 30-35 (in Russian).

Lapin AV, Lisitsyn DV (2004) About mineralogical typomorphism of alkaline ultrabasic magmatites at Chadobets upland. Otechest Geol, 6: 83-92 (in Russian).

Le Bas MJ, Keller J, Tao KJ, Wall F, Williams CT, Zhang PS (1992) Carbonatite dykes at Bayan Obo, Inner Mongolia, China. Mineral Petrol, 46: 195-228. DOI: 10.1007/BF01164647

Pekov IV, Chukanov NV, Ferraris G, Ivaldi G, Pushcharovsky DYu, Zadov AE (2003) Shirokshinite, $K(NaMg_2)Si_4O_{10}F_2$, a new mica with octahedral Na from Khibiny massif, Kola Peninsula: descriptive data and structural disorder. Eur. J. Mineral., 15: 447–454. DOI: 10.1127/0935-1221/2003/0015-0447

Sharygin VV, Doroshkevich AG, Chebotarev DA (2016a) Na-Sr-Ba-REE-carbonates and phosphates in carbonatite minerals of Chuktukon massif, Krasnoyarsk territory. Abstract volume of 17th Russian Conference on Fluid Inclusion Studies, Ulan-Ude, GI SB RAS, pp 180-182 (in Russian).

Sharygin VV, Doroshkevich AG, Seryotkin YV, Karmanov NS., Belogub EV, Moroz TN (2016b) A new K-Nb-cyclosilicate $K_2(Nb,Ti)_2(Si_4O_{12})O(O,F)$ from Chuktukon carbonatite massif, Chadobets upland, Russia. Abstract volume of 2nd European Mineralogical Conference, Rimini, Italy, pp 421-421.

Sharygin VV, Kryvdik SG (2014) New minerals in alkaline metasomatites at Dmitrovka, Azov Sea region, Ukraine. Proceedings of 8th conference dedicated to the memory of academician E.Lazarenko ''Mineralogy: real and future'', Lviv-Carpathians, PH of Lviv National University, pp 167–170 (in Russian).

Slukin AD (1994) Bauxite deposits with unusually high concentrations of REE, Nb, Ti and Th, Chadobets upland, Siberian platform. Inter Geol Rev. 36: 179-193. DOI: dx.doi.org/10.1080/ 00206819409465454

Traversa G, Gomes CB, Brotzu P, Buraglini N, Morbidelli L, Principato MS., Ronca S, Ruberti E (2001) Petrography and mineral chemistry of carbonatites and mica-rich rocks from the Araxá complex (Alto Paranaíba Province, Brazil). Anais Academ Brasil Ciências, 73: 71-98. DOI: 10.1590/S0001-37652001000100008

MULTIPHASE INCLUSIONS IN ZIRCONS FROM CHUKTUKON CARBONATITE MASSIF, CHADOBETS UPLAND, RUSSIA

Sharygin V.V.[1,2], *Doroshkevich A.G.*[1,3]

[1]Institute of Geology and Mineralogy, Siberian Branch of the Russian Academy of Sciences, Novosibirsk, Russia, sharygin@igm.nsc.ru

[2]Novosibirsk State University, Novosibirsk, Russia

[3]Geological Institute, Siberian Branch of the Russian Academy of Sciences, Ulan-Ude, Russia, doroshkevich@igm.nsc.ru

The Chuktukon massif is one of intrusions within southern Chadobets upland (SW Siberian Platform, Krasnoyarsk territory, Russia) (Lapin & Lisitsyn, 2004). Intrusive rocks of the Chadobets upland are represented by the ultramafic alkaline rocks (melilitite-nephelinites and pyroxene peridotites, picrites, melteigites), carbonatites and kimberlite-like rocks (carbonatite lapilli tuffs ?), which occur as veins, dykes and stocks. Several stock-like carbonatite bodies with the sizes of 1.2x0.7 km are mapped within the Chuktukon massif (Slukin, 1994; Lapin, 1997, 2001; Lapin and Lisitsyn, 2004; Kirichenko et al., 2012; Doroshkevich et al., 2016a).

We studied zircon concentrates from one of boreholes (no. 546) within the Chuktukon massif. The samples were donated by A.S. Varganov (company "Krasnoyarskgeosyomka", Krasnoyarsk). The zircons were selected from the following depths of the borehole (in meters): 13 – kaolinite clays (61 grains); 24.6 – ochre kaolinite clays with sand and gravel (4 grains); 44.3 – carbonatite tuffs with lapilli (2 grains); 160.7 – weathered carbonatites (2 grains). The first goal of our studies was to discriminate zircons by their nature (carbonatitic or non-carbonatitic) using zircon-hosted crystal inclusions and the further selection of carbonatite-related grains for U-Pb dating. In general, fresh crystal inclusions are rare in studied zircons. The majority of zircon-hosted inclusions are altered due to weathering and now represented by mixture of secondary minerals (kaolinite, Nb-rich goethite and unidentified Ba-Sr-Ca-REE-rich hydrated aluminophosphate). The chemical variations for the latter mineral are follows (EDS, wt.%): SiO_2 – 0.3-1.0, P_2O_5 – 24.1-27.9, Al_2O_3 – 26.0-29.5, FeO – 0.2-2.4, CaO – 2.7-4.1, BaO – 5.8-8.5, SrO – 2.7-5.5, La_2O_3 – 1.6-2.8, Ce_2O_3 – 1.4-3.0, Nd_2O_3 – 0.9-1.4, F – 0.8-2.0.

Unfortunately, low quantity of zircon grains and paucity of inclusions did not allow confident recognition of two horizons (24.6 and 44.3 m). Fluorapatite and calcite were found in zircons from the 24.6 m depth (ochre kaolinite clays), whereas Ca-Ba-carbonate were identified in zircons from the 44.3 m depth (carbonatite tuffs).

Rare inclusions were observed in the weathered carbonatite from the 160.7 m depth. They seem to be primary in origin and located in the core of the host zircon (Fig. 1). In general they are carbonate in composition and multiphase: calcite + dolomite or alkali-rich carbonates (nyerereite ? + shortite + burbankite).
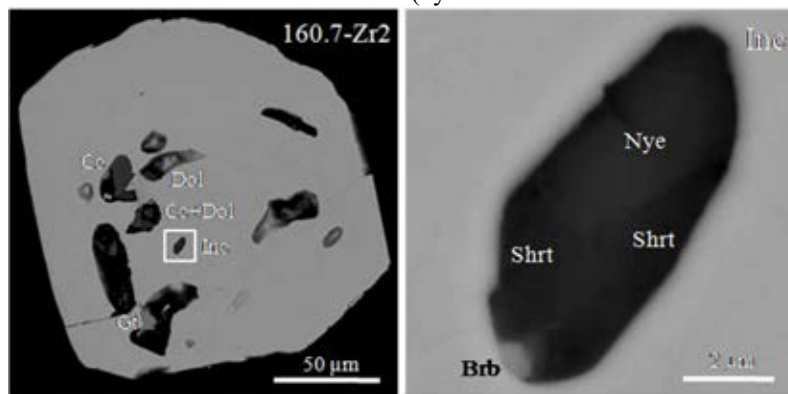
Fig. 1. Primary (?) multiphase inclusions in zircon from carbonatite (depth 160.7 m), BSE images.
Cc – calcite, Dol – dolomite, Gt – goethite, Nye – nyerereite (?), Shrt – shortite, Brb – burbankite; Inc – inclusion.

Abundant single and multiphase inclusions were found in zircons of the upper horizon (the 13 m depth, kaolinite clays, Fig. 2-3). Fluorapatite are dominant phase among single crystal inclusions and commonly decorates the growth zones in host zircons (Fig. 2). The pyrochlore-group minerals (U-, Th-, REE-rich species, from fluorcalciopyroclore to keno-hydropyrochlores), annite and rutile occur rarely as individual inclusions. Some multiphase inclusions are confined to interior of zircon crystals and seem to be primary in origin (Fig. 2). They are silicate-rich in compositions. One of such inclusions consists of albite, K-feldspar, annite, catapleiite, a cancrinite-group mineral and minor calcite, dolomite, a pyrochlore-group mineral, sodalite, columbite-(Fe) and Na-rich zeolite (Fig. 2). All above minerals were determined by EDS, elemental maps and supported by Raman spectra. Another inclusion contains magnesioarfvedsonite (K_2O – 1.5, F – 1.4 wt.%) and thorite (Fig. 2).
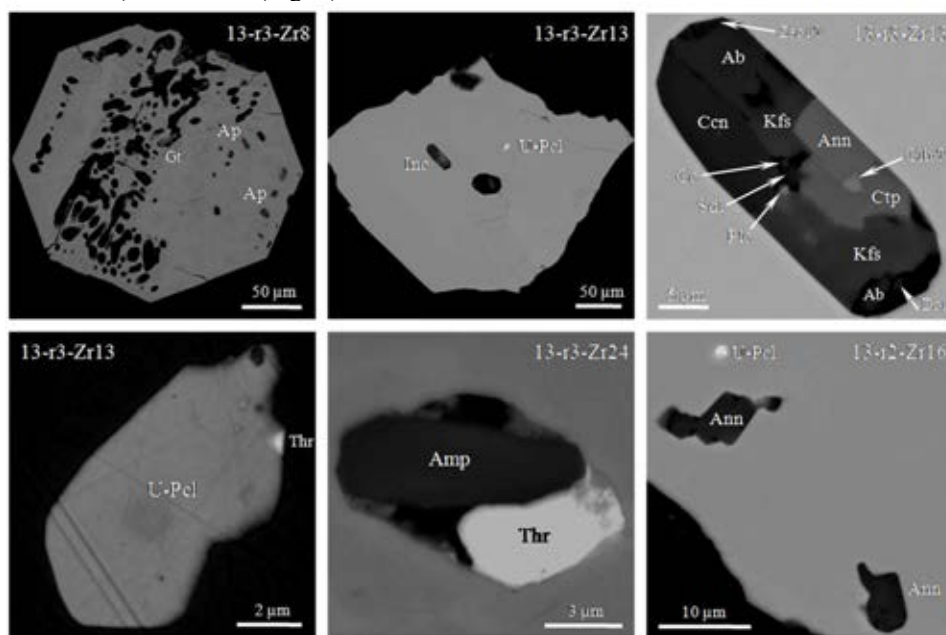
Fig. 2. Primary (?) multiphase inclusions in zircons from kaolinite clays (depth 13.0 m), BSE images.
Gt – goethite, Ap – fluorapatite, Inc – inclusion, U-Pcl – U-rich oxycalciopyrochlore (UO_2 – up to 29 wt.%), Cc – calcite, Ann – annite, Kfs – K-feldspar, Ab – albite, Ccn – a cancrinite-group mineral, Zeol ? – Na-rich zeolite mineral (?), Sdl – sodalite, Pcl – a pyrochlore-group mineral, Ctp – catapleiite, Clb ? – columbite-(Fe) (?), Thr – thorite, Amp – magnesioarfvedsonite.

One of zircon grains from this horizon is riddled with inclusions (Fig. 3A). They are secondary in origin and confined to healed fractures in the host zircon. Most of them are multiphase and sometimes contain gas bubble visible in transmitted light. Such inclusions are strongly variable in mineral composition: from silicate-carbonate to phosphate-carbonate and pure carbonate (Fig. 3B-F). Fluorine-rich phlogopite is dominant silicate within inclusions (EDS, wt.%): SiO_2 – 38.2-40.4, TiO_2 – 0.9-1.2, Al_2O_3 – 9.6-10.6, FeO – 13.6-15.3, MnO – 0.9-1.1, MgO – 15.3-17.5, K_2O – 9.0-9.8; BaO – up to 0.5, F – 2.6-3.7. The deficiency of Al_2O_3 in this mica suggests a tendency towards tetraferriphlogopite or tainiolite composition. Fluorapatite, nyerereite ?, calcite, burbankite-khanneshite and Na-rich hydrated carbonate are common in phosphate-carbonate and pure carbonate inclusions (Fig. 3B-F). Nyerereite phase contains 3.8-6.8 wt.% K_2O.
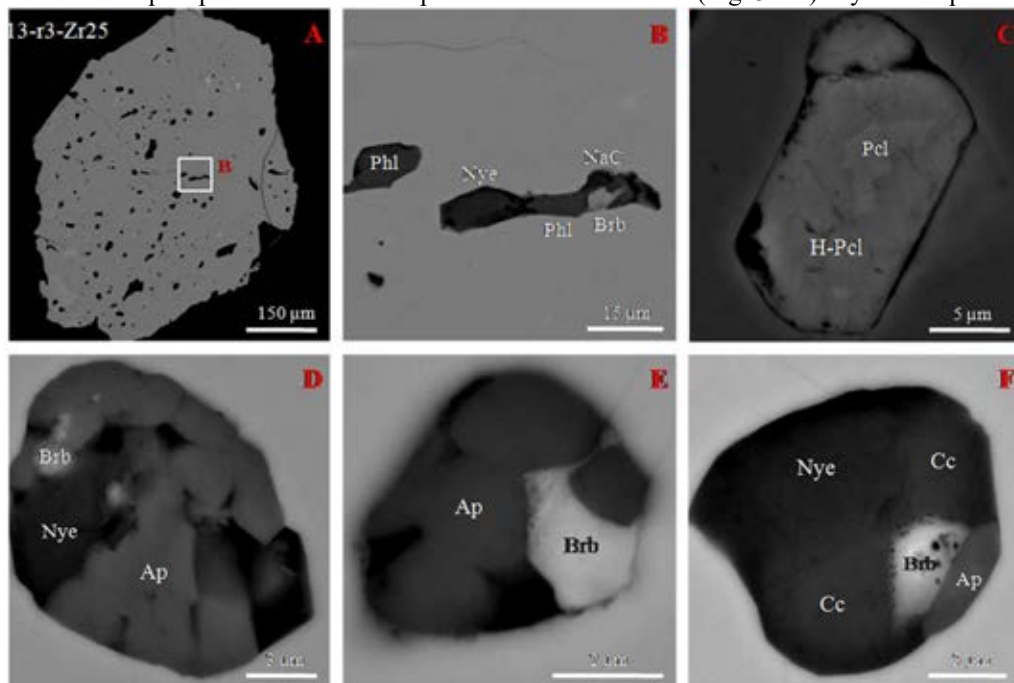
Fig. 3. Secondary multiphase inclusions in zircon from kaolinite clays (depth 13.0 m), BSE images.
Phl – F-rich phlogopite (F – up to 3.6 wt.%), Nye – nyerereite (?), Brb – burbankite-khanneshite, NaC – Na-rich hydrated carbonate, Pcl – fluorcalciopyrochlore, H-Pcl – hydropyrochlore, Ap – fluorapatite, Cc – calcite.

The present study of inclusions in the Chuktukon zircons is evidenced about different sources of this mineral. Zircons from weathered carbonatite strongly show carbonatite affinity, whereas zircons from clays indicate two possible sources: alkaline silicate rocks (probably from nearby Terinovsky massif, northern Chadobets upland) and silicate-carbonate rocks (carbonatite tuffs). It should be noted that nyererite, burbankite-khanneshite and shortite are common phases in carbonate-rich inclusions in zircon. Ba-Sr-REE-Ca-carbonates (burbankite-khanneshite, strontianite, etc.) are accessory phases in carbonatites (Chebotarev et al, 2016; Doroshkevich et al., 2016a, Sharygin et al., 2016a-b) and carbonatite tuffs of the Chuktukon massif, whereas no Na-Ca-carbonates are found yet in these rocks. However, alkali-rich carbonates (nyerereite, shortite, eitelite, bradleyite, northupite, burbankite and others) are omnipresent in multiphase mineral-hosted inclusions from carbonatites, phoscorites and silicate rocks of many intrusive ultramafic alkaline complexes around the world: Guli and Krestovskiy, Polar Siberia, Russia; Gardiner, Greenland; Belaya Zima and Bol'shaya Tagna, Eastern Sayan, Russia; Kovdor, Afrikanda and other complexes, Kola, Russia; Phalaborwa complex, South Africa; Oka, Canada (see review in Chakhmouradian et al., 2016; Sharygin, Doroshkevich, 2017).

In general, the phase composition of multiphase inclusions in zircons (presence of nyerereite and shortite) reflects certain features of the Chuktukon carbonatite massif at the late stage of its evolution, in particular points the possible appearance of Na-rich carbonatite melt.

References:

Chakhmouradian AR, Reguir EP, Zaitsev AN (2016) Calcite and dolomite in intrusive carbonatites. I. Textural variations. Mineral Petrol, 110: 333-360.

Chebotarev DA, Doroshkevich AG, Sharygin VV (2016) Niobium mineralization in carbonatites of Chuktukon massif, Chadobets upland (Krasnoyarsk territory, Russia). Abstract volume of 33rd International conference «Alkaline Magmatism of the Earth and related strategic metal deposits», Moscow, Russia, Editor-in-chief L.N. Kogarko, M.: GEOKHI RAS, pp 36-36 (in Russian).

Doroshkevich AG, Chebotarev DA, Sharygin VV (2016a) Alkaline ultrabasic carbonatitic magmatism of the Chadobets upland. Abstract volume of Moscow International School of Earth Sciences – 2016, Editor-in-chief L.N. Kogarko, M.: GEOKHI RAS, pp 31-32.

Doroshkevich AG, Sharygin VV, Seryotkin YV, Karmanov NS, Belogub EV, Moroz TN, Nigmatulina EN, Eliseev AP, Vedenyapin VN, Kupriyanov IN (2016b) Rippite, IMA 2016-025. CNMNC Newsletter No. 32, August 2016, page 919. Mineral Mag, 80: 915-922.

Kirichenko VT, Zuev VK, Perfilova OYu, Sosnovskaya OV, Smokotina IV, Markovich LA, Borodin VP, Mironyuk

EP (2012) The state geological map of the Russian Federation. Scale 1: 1 000 000 (third generation). Angaro-Yeniseisky series. Sheet O-47 – Bratsk. Explanatory note. SPb.: VSEGEI cartographical factory, 470 pages, pp 163-179 (in Russian).

Lapin AV (1997) Structure, formation conditions and ore potential of the main types of REE in the carbonatite weathering crusts. Otechest Geol, 11: 15-22 (in Russian).

Lapin AV (2001) About kimberlites of the Chadobets upland in connection with a problem of the formational-metallogenic analysis of the platform alkaline-ultramafic magmatites. Otechest Geol, 4: 30-35 (in Russian).

Lapin AV, Lisitsyn DV (2004) About mineralogical typomorphism of alkaline ultrabasic magmatites at Chadobets upland. Otechest Geol, 6: 83-92 (in Russian).

Sharygin VV, Doroshkevich AG (2017) Mineralogy of secondary olivine-hosted inclusions in calcite carbonatites of the Belaya Zima alkaline massif, Eastern Sayan, Russia: Evidence for late-magmatic Na-Ca-rich carbonate composition. Jour Geol Soc India, 89 (submitted).

Sharygin VV, Doroshkevich AG, Chebotarev DA (2016a) Na-Sr-Ba-REE-carbonates and phosphates in carbonatite minerals of Chuktukon massif, Krasnoyarsk territory. Abstract volume of 17th Russian Conference on Fluid Inclusion Studies, Ulan-Ude, GI SB RAS, pp 180-182 (in Russian).

Sharygin VV, Doroshkevich AG, Seryotkin YV, Karmanov NS, Belogub EV, Moroz TN (2016b) A new K-Nb-cyclosilicate $K_2(Nb,Ti)_2(Si_4O_{12})O(O,F)$ from Chuktukon carbonatite massif, Chadobets upland, Russia. Abstract volume of 2nd European Mineralogical Conference, Rimini, Italy, pp 421-421.

Slukin AD (1994) Bauxite deposits with unusually high concentrations of REE, Nb, Ti and Th, Chadobets upland, Siberian platform. Inter Geol Rev. 36: 179-193. DOI: dx.doi.org/10.1080/ 00206819409465454

CLINOPYROXENE–MG-CARBONATE REACTIONS AT 6 GPA: IMPLICATIONS FOR PARTIAL MELTING OF CARBONATED LHERZOLITE

Shatskiy A.F.[1,2], **Podborodnikov I.V.**[1,2], **Arefev A.V.**[1,2], **Litasov K.D.**[1,2]
[1]Institute of Geology and Mineralogy, Siberian Branch of the Russian Academy of Sciences, Novosibirsk, Russia
[2]Novosibirsk State University, Novosibirsk, Russia, shatskyaf@igm.nsc.ru

The reaction between clinopyroxene and Mg-carbonate is supposed to define the solidus of carbonated lherzolite at pressures exceeding 5 GPa. To investigate the effect of alkalis on this reaction, subsolidus and melting phase relations in the systems $CaMgSi_2O_6 + 2MgCO_3$ (Di + 2Mgs), $CaMgSi_2O_6 + NaAlSi_2O_6 + 2MgCO_3$ (Di + Jd + 2Mgs), $CaMgSi_2O_6 + Na_2Mg(CO_3)_2$ (Di + Na2Mg), and $CaMgSi_2O_6 + K_2Mg(CO_3)_2$ (Di + K2Mg) have been examined at 6 GPa. The Di + 2Mgs system begins to melt at 1400 °C via the approximate reaction $CaMgSi_2O_6$ (clinopyroxene) + $2MgCO_3$ (magnesite) = $CaMg(CO_3)_2$ (liquid) + $Mg_2Si_2O_6$ (orthopyroxene) leading to essentially carbonate liquid (L) with composition of $Ca_{0.56}Mg_{0.44}CO_3$ + 3.5 mol% SiO_2. The initial melting in the Di + Jd + 2Mgs system occurs at 1350 °C via the reaction $2CaMgSi_2O_6$ (clinopyroxene) + $2NaAlSi_2O_6$ (clinopyroxene) + $8MgCO_3$ (magnesite) = $Mg_3Al_2Si_3O_{12}$ (garnet) + $5MgSiO_3$ (clinopyroxene) + $2CaMg(CO_3)_2$ (liquid) + Na_2CO_3 (liquid) + $3CO_2$ (liquid and/or fluid) yielding the carbonate liquid with approximate composition of $10Na_2CO_3 \cdot 90Ca_{0.5}Mg_{0.5}CO_3$ + 2 mol% SiO_2. The systems Di + Na2Mg and Di + K2Mg start to melt at 1100 and 1050 °C, respectively, via the reaction $CaMgSi_2O_6$ (clinopyroxene) + $2(Na$ or $K)_2Mg(CO_3)_2$ (solid) = $Mg_2Si_2O_6$ (orthopyroxene) + (Na or $K)_4CaMg(CO_3)_4$ (liquid). The resulting melts have alkali-rich carbonate compositions of $Na_2Ca_{0.4}Mg_{0.6}(CO_3)_2$ + 0.4 mol% SiO_2 and $43K_2CO_3 \cdot 57Ca_{0.4}Mg_{0.6}CO_3$ + 0.6 mol% SiO_2. These melts do not undergo significant changes as temperature rises to 1400 °C retaining their calcium number, high Na_2O, K_2O and low SiO_2. We suggest that the clinopyroxene–Mg-carbonate reaction controlling the solidus of carbonated lherzolite is very sensitive to the carbonate composition and shifts from 1400 °C to 1050 °C at 6 GPa yielding K-rich carbonate melt if subsolidus assemblage contains $K_2Mg(CO_3)_2$ compound. Such a decrease in solidus temperature has been observed previously in the K-rich carbonated lherzolite system. Although a presence of eitelite, $Na_2Mg(CO_3)_2$, has a similar effect, this mineral cannot be considered as a potential host of Na in carbonated lherzolite as far as whole Na added into the system dissolves as jadeite component in clinopyroxene if bulk Al/Na ≥ 1. The presence of jadeite component in clinopyroxene has little impact on the temperature of the solidus reaction decreasing it to 1350 °C at 6 GPa.

Comparison with lherzolite-CO2 systems

The CMAS-CO2 system. In their manuscript, Dalton and Presnall (1998a) reported results on near-solidus phase relations of synthetic lherzolite in the CMAS-CO2 system at pressures ranging from 3 to 7 GPa. Their starting composition can be expressed via mineral fractions (mol%) as 36.7Fo + 31.7En + 8.3Di + 4.9Prp + 18.4Mgs. Six phases (Ol+Opx+CPx+Grt+Mgs+L) were established on the solidus at 1380 °C and 6 GPa (Dalton and Presnall, 1998a). The solidus temperature is consistent with the position of the reaction (1) in our study. The reported compositions of phases yield following mole fractions below [34.6Ol + 47.4Opx + 4.1Cpx + 3.2Grt +10.8Mgs] and above solidus [35.2Ol + 51.0Opx + 2.8Grt + 6.5Mgs +5.5L]. Note that in the starting composition used by Dalton and Presnall (1998a) as well as in the subsolidus assemblage, an amount of Mgs more than twice exceeds the Cpx mole fraction. Therefore, in accordance with the reaction (1) Cpx must be completely consumed above the solidus in Dalton and Presnall (1998b) experiments. Indeed, to achieve mass balance convergence for their results at 1405-1505 °C, we need to exclude Cpx. After that, the following modal abundances of phases can be obtained: [40.6Ol + 38.9Opx + 6.2Grt + 14.4L] at 1405 °C and [41.7Ol + 31.4Opx + 3.1Grt + 23.6L] at 1505 °C.

Similar to the present study, the near-solidus melt at 1380 °C and 6 GPa has essentially dolomitic composition (Ca# = 49 mol%, 4.5 mol% SiO_2, 47.5 mol% CO_2) (Dalton and Presnall, 1998a). However, drastic increase of MgO and

SiO$_2$ in the melt at 1405 °C and 1505 °C (Dalton and Presnall, 1998b) appears to be inconsistent with our results in the Di+2Mgs system. This discrepancy would be attributed to the differences in the compositions of the Di+2Mgs and CMAS-CO$_2$ systems. Alternatively, the discrepancy would be caused by applying the wavelength dispersive microprobe technique to determine a bulk composition of polycrystalline quenched products of melt in Dalton and Presnall (1998b) study. The use of stationary electron beam, which diameter is comparable with quenched melt grain size, leads to significant uncertainty of average melt composition (Dalton and Presnall, 1998b). Besides, a stationary electron beam with an acceleration voltage of 15 kV and a current of 10 nA used in their study could results in carbonate burning. This, as well as possible presence of small residual silicate crystals within liquid pool in relatively short (6 h) experiments, may cause overestimation of SiO$_2$ and MgO concentrations in the melt.

The MixKLB-1-CO$_2$ systems. Dasgupta and Hirschmann (2007) examined near-solidus phase relations in natural peridotite MixKLB-1 with adding 5.8 mol% CO$_2$ (PERC2 composition) at 6.6 GPa. The PERC2 composition expressed via mole fraction of minerals is 60.2Ol + 5.9Opx + 10.5Cpx + 4.9Grt + 18.4Mgs, where all minerals have Fe# = 10.3 mol% and Cpx contains 3.6 mol% jadeite. The subsolidus assemblage established at 1250 and 1300 °C includes Ol, Opx, Cpx, Grt, and Mgs. First melt observed at 1330 °C. At this temperature, Mgs and Cpx fractions decrease below 1 mol%. Similar to our study in the Di+Jd+2Mgs system, Dasgupta and Hirschmann (2007) observed distinct change in Cpx composition across the solidus, namely, drop in concentration of jadeite from 2.1 to 1.4 mol% and increase of enstatite concentration from 19 to 28 mol%. These observations as well as an increase in the Grt fraction at 1360 °C are in a good agreement with the reaction (3) established in our study. Unlike the Di+Jd+2Mgs system, where Mg$_2$Si$_2$O$_6$ liberated above the solidus is completely consumed by the Cpx solid solution, in the PERC2 composition most of Mg$_2$Si$_2$O$_6$ forms Opx according to the reaction (1). In spite of the large difference in jadeite concentration in Cpx and presence of 5.8 mol% FeO, MgO/(MgO+FeO) = 0.9, in the PERC2 composition, the solidus temperatures of these two systems are consistent within experimental uncertainty. Furthermore, the partial melt obtained in the PERC2 system at 1330-1360 °C has essentially carbonate composition (2-3 mol% SiO$_2$, 45-48 mol% CO$_2$, 1.2-1.4 mol% Na$_2$O, Ca# = 40-45) similar to that established in the Di+Jd+2Mgs system at 1350-1400 °C. Thus, the presence of Na as jadeite component in Cpx does not affect significantly the reaction (1), controlling the solidus of magnesite-bearing lherzolite. Based on our results the maximum temperature decrease in the CaO-MgO-Al$_2$O$_3$-SiO$_2$-Na$_2$O-CO$_2$ system with Al/Na ratio ≥ 1 relative to the CMAS-CO$_2$ system would not exceed 50 °C at 6 GPa. Besides, this comparison also implies that the presence of Fe has no apparent effect on further reduction of the solidus temperature.

Brey at al. (2008) also studied the melting phase relations in the system similar to PERC2 (SC1+MgCO$_3$). The SC1+MgCO$_3$ composition expressed via mole fraction of minerals is 54.7Ol + 10.7Opx + 10.9Cpx + 5.7Grt + 18.0Mgs, where all minerals have Fe# = 9.2 mol% and Cpx contains 4.3 mol% jadeite. They observed partial melting over the entire temperature range beginning from 1300 °C at 6 GPa. They succeeded to analyze partial melt quenched at 1350 °C and 6 GPa. The melt has lower Ca# = 34 and surprisingly more silica-rich (9 mol% SiO$_2$) and sodium-depleted (0.4 mol% Na$_2$O) composition compared with that in Dasgupta and Hirschmann (2007) study. The mass balance calculations based on Brey et al. (2008) results show that at 1350 °C Cpx and Mgs disappear, whereas fraction of Grt and Opx increases. The calculated mole fractions of phases in their study are [49.5Ol + 11.2Opx + 12.3Cpx + 15.7Grt + 11.0Mgs + (trace)L] at 1300 °C and [47.8Ol + 20.5Opx + 17.7Grt + 13.9L] at 1350 °C. Thus, Brey et al. (2008) results are consistent with our observations and suggest that partial melting of natural carbonated lherzolite at 6 GPa is controlled by combination of reaction (1) and reaction (3) established in our study.

In their study Dasgupta and Hirschmann (2007) also examined two compositions with lower bulk CO$_2$ contents, PERC (2.9 mol% CO$_2$) and PERC3 (1.2 mol% CO$_2$), keeping proportions of other component identical to the MixKLB-1 peridotite. The principle difference from PERC2 is the lower Mgs mole fraction in subsolidus runs as follows from mass balance calculations: PERC2 [57.4Ol + 6.7Opx + 13.2Cpx + 11.1Grt + 11.6Mgs], PERC [62.8Ol + 7.2Opx + 13.0Cpx + 11.1Grt + 5.9Mgs], and PERC3 [64.3Ol + 7.8Opx + 14.4Cpx + 11.1Grt + 2.4Mgs]. Despite of almost the same compositions of subsolidus minerals, the apparent solidus temperatures decreases with decreasing bulk CO$_2$: 1315±15 °C/5.8 mol% CO$_2$, 1262±13 °C/2.9 mol% CO$_2$, 1205±15 °C/1.2 mol% CO$_2$. The authors attributed these observations to increasing bulk Na$_2$O/CO$_2$ mole ratio from 0.04 to 0.21 and connected the decrease in solidus temperature with increasing "availability" of Na$_2$O in the bulk rock. Our results appear to be inconsistent with the above hypothesis, because bulk Na$_2$O/CO$_2$ ratio of the Di + Jd + 2Mgs system is 0.21, while its solidus temperature matches that of PERC2 with Na$_2$O/CO$_2$ = 0.04. We suggest that a simple change of the reagent ratio (Cpx/Mgs) would not affect the temperature of the reaction (3) and, therefore, cannot increase the "availability" of Na$_2$O, i.e. redistribution of Na$_2$O from Cpx (chief reservoir of Na$_2$O) to carbonate. There should be another reason, which, however, remains unclear owing lack of information on partial melt compositions obtained in the PERC and PERC3 systems.

K-rich carbonated lherzolite. Brey et al. (2011) reported experimental results on melting phase relations in K-rich carbonated lherzolite (LC) at 6-10 GPa. The LC composition expressed via mole fraction of minerals is 54.4Ol + 6.2Opx + 12.9Cpx + 5.3Grt + 8.2Mgs + 13.0K$_2$Mg, where all minerals have Fe# = 9.0 mol% and Cpx contains 3.4 mol% jadeite. They observed partial melt coexisting with Ol, Opx, and Grt over the entire temperature range of 1200-1600 °C at 6 GPa. Considering the Cpx : Mgs : K$_2$Mg proportions in the starting mixture, the established supersolidus assemblage can be explained by a simultaneous operation of the reactions (3) and (5). Our results in the Di + K$_2$Mg system at 6 GPa suggest that K$_2$Mg(CO$_3$)$_2$ is a main host of K below the LC solidus, whereas reaction (5) is a dominant solidus reaction yielding K-rich carbonate melt at 1050 °C. Similar to the Di + K$_2$Mg system, the initial melt in the LC system has K-rich carbonate composition, which does not change significantly with temperature increase from 1200 to 1400 °C (0.5-2.5 SiO$_2$, 19-21

MgO, 3-5 FeO, 2-4 CaO, 0.3-0.5 Na$_2$O, 13-17 K$_2$O, in mol%). Interestingly, the melts from the LC and Di+K$_2$Mg systems at 6 GPa differ only in Ca# (11-18 and 30-40, respectively); both containing low SiO$_2$, despite the fact that the higher temperature (1400 °C) experiments are 300-350 °C above the solidus. Over a similar temperature range (1400-1600 °C), the liquid compositions at 6 GPa changed more dramatically, especially with respect to the silica concentrations (29 mol% SiO$_2$ at 1600 °C in LC and 17 mol% SiO$_2$ at 1500 °C in Di+K$_2$Mg).

References:

Brey, G.P., Bulatov, V.K., Girnis, A.V., and Lahaye, Y. (2008) Experimental melting of carbonated peridotite at 6-10 GPa. Journal of Petrology, 49(4), 797-821.

Brey, G.P., Bulatov, V.K., and Girnis, A.V. (2011) Melting of K-rich carbonated peridotite at 6-10 GPa and the stability of K-phases in the upper mantle. Chemical Geology, 281(3-4), 333-342.

Canil, D., and Scarfe, C.M. (1990) Phase relations in peridotite+CO$_2$ systems to 12 GPa: implications for the origin of kimberlite and carbonate stability in the Earth's upper mantle. Journal of Geophysical Research: Solid Earth, 95(B10), 15805-15816.

Dalton, J.A., and Presnall, D.C. (1998a) Carbonatitic melts along the solidus of model lherzolite in the system CaO-MgO-Al$_2$O$_3$-SiO$_2$-CO$_2$ from 3 to 7 GPa. Contributions to Mineralogy and Petrology, 131(2-3), 123-135.

-. (1998b) The continuum of primary carbonatitic-kimberlitic melt compositions in equilibrium with lherzolite: Data from the system CaO-MgO-Al$_2$O$_3$-SiO$_2$-CO$_2$ at 6 GPa. Journal of Petrology, 39(11-12), 1953-1964.

Dasgupta, R., and Hirschmann, M.M. (2007) Effect of variable carbonate concentration on the solidus of mantle peridotite. American Mineralogist, 92(2-3), 370-379.

PREDICTING DISCOVERY OF NEW RARE-EARTH DEPOSITS oF the Anadol DEPOSIT type IN the azov region

Sheremet Ye.M.[1], Kryvdik S.G.[1], Agarkova N.G.[1], Strekozov S.N.[2]

[1]N. P. Semenenko Institute of Geochemistry, Mineralogy and Ore Formation of the NAS of Ukraine, Kiev, Ukraine
[2]Azov Integrated Exploration Company, State-Run Enterprise Pivdenukrgeologiya, Volnovakha, Ukraine
evgsheremet@yandex.ru

The Anadol orthite (allanite) deposit, which is the new type of rare-earth mineralization, has been discovered in the Azov Geoblock of the Ukrainian Shield (USh). The main ore body is of the vein form called also as orthite dike. A number of smaller veins and zones of similar mineralization are recognized. Near the zone of crush, cataclasis and mylonitization 30 to 400 m thick ore body has been traced by 1,000 m on the strike and to the depth of 400 m (its thickness is of 0.7 to 3.0 m). Pockets, lenses and vein allocations of orthite (allanite) 10–15 cm and more in size contain britholite, cerite parasite and bastnasite . Average $\sum TR_2O_3$ content of 105 samples is 1.5 % varying of 0.2 to 15–20 %. Zones of fenitization are exhibited in exocontacts. According to all indications the deposit is attributed to carbonatite complex.

Approach to predicting discovery of such type of deposits based on the analysis of geological setting and geophysical survey can be of some interest not only for the Azov Region (Ukrainian Shield) but also for other regions of similar geologic structure.

Geological evidence

The Azov Geoblock is best saturated with alkaline rocks and rare-earth occurrences and deposits compared to other geoblocks of the UkranianShield (Kryvdik, Tkachuk, 1990). In particular this is typical for the East Azov Region. Very likely that by density of occurrences of alkaline metasomatites only the Kirovograd Geoblock, for which typical are uraniferos albitites, can be compared to the Azov Geoblock. Unfortunately, express criteria to differentiate these uraniferousalbitites from albite fenites of carbonatite complexes have not been worked out at the moment. Most of naturally fractured metasomatites of the East Azov Region are more likely fenites of carbonatite complex. The example is Khlebodarovka open pit mine where association of such alkaline metasomatites with vein carbonatites has been proved. For that reason discovery of the deposits related to carbonatite complex like the"anadol type" (Anadol, Petrovo-Gnutovo and Chernigovka deposits) is highly promising. Exocontact (areal) alkaline metasomatites, some areas of which become fractured, are typical just for carbonatite complexes. Other complexes of alkaline rocks (foyaites, mariupolites of Oktyabrskoe Massif, agpaitic feldspatoid syenites of Khibiny Massif, Lovozerovo Massif and Ilimaussaq Massif) are usually not accompanied by exocontact aureoles of fenitization (or they are unperceivable). However, all rocks of carbonatite complexes, both carbonatites and silicate rocks (ijolite-melteigites, jacupirangites, nepheline syenites, melilitolite and other) are accompanied by fenite aureoles thickness of which is close to the thickness of the mentioned fenitized rocks or to the diameter of alkaline-ultrabasic intrusions.

In our opinion the most promising area for discovery of rare-earth deposits and ore occurrences in the East Azov Region is Krasnovka ore field with Pavlopol, Pishchevik, Druzhba, Chermalyk and numerous point rare-earth ore occurrences of carbonatite-type.

The ore field by its geologic structure (the nature of host rocks and structural settings and tectonics), morphogenetical types of ore bodies, wallrock alteration, mineral type and level of concentration of commercial elements is close to the ore field of one of the largest in the world rare-earth deposits – the Mountain Pass deposit in the USA. The

main distinction of the Mountain Pass deposit is that within its boundaries, apart from carbonate veins and mineralized zones one stock-like body of carbonatites 210×720 m in size has been discovered. It contains 90 % of rare-earth reserves of the ore field: of 5 to 10 millionton. The classic carbonatite deposits associate with complexes of alkaline rocks of ultrabasic composition of central-type platform intrusions. They are often compared to such world famous deposits as the Mountain Pass in USA and the Bayan-Obo in Chine. Sometimes carbonatites form independent vein fields and irregular large bodies outside of igneous complexes. Very likely, by small erosional truncation such fields form in the top of the massifs. Notably quite often the massifs have not been identified (Fremont County, Mountain Pass in the USA, Karonga in Kenya and other).

Carbonate veins of Krasnoska field are similar to the described above ore bodies of the Kalmius zone. Within the boundaries of Krasnovka field in the course of delineation one can find new carbonatite veins with rare-earth mineralization (with the total content of rare-earths of more than 1 %, 3–4 % on average) which can be of commercial interest. Even if 10 such veins have been explored, the promising ΣTR_2O_3 resources of P_3 category should be assessed of 20 to 40 thousand ton. The main exploration target shall be delineation of relatively large carbonatite body. The most favorable sites to discover such body are the area of Volodarsk and Konka tectonic zones intersection (the zone of about 3.0 km wide and 8.0 m long) and dome selvage.

In the East Azov Region there is one more potential to discover the Azov-type deposits (Sheremet et al., 2012) containing britholite-orthite-zircon and zircon ores which are strongly similar to ores of the Anadol deposit but distinct in their belongings to other complexes.

The outcome of geophysical predicting

Using geoelectric AMTS method subsurface electrical profiles and a number of magnetotelluric profiles were laid out transverse to the strike of the whole Kalmius fault zone based on which depth geoelectric model has been constructed (Sheremet et al., 2010, Sheremet et al., 2011).

It is apparent from the distribution model that there is an isolated field of depth conductors in the Kalmius fault zone, in its south-west part, that coincides with Krasnovka ore field described above. The second field of depth conductors is confined to Gruzsko-Elanchik depth fault zone, and the third field of depth conductors covers the junction zone of the East Azov Region with the Dnieper-Donets depression.

This model was the basis for conducting geoelectrical surveying in the zones of occurrences of alkaline-type metasomatism.

Field geoelectrical survey by audio-magnetotelluriczondingmethod (AMTS) and magnetotelluric sounding method(MTS)was conducted along the lines of manifestation of alkaline-type metasomatism (fenitization zones). Subsurface electrical profiles were constructed along those lines. On the basis of their detailed analysis we came to the following conclusions:

i) All the explored occurrences of metasomatites are characterized by alternation of low- and high-resistivity anomalies up to a depth of 5 km, spreading at times up to a depth of 10 km.

ii) To our opinion, hypothetic nature of low-resistivity anomalies is confinedness of metasomatites under consideration to the upper part of the Kalmius fault zone which is characterized by increased fracturing and maybe water content. Electrical resistance distribution pattern shows that together with disintegrated rocks (presumably granites) in the form of relics there also exist more soft and hard rocks (crystalline shales and granulites, as may be supposed). There is a standpoint that alkaline metasomatites of the East Azov Region have formed owing to carbonatite magma fluids the bodies of which are not covered as yet. Highly permeable sections of deep fault zones, such as the Kalmius fault zone, could be conducting channels for such fluids.

Predicting rare-earth mineralization occurrences based on the construction and analysis of the previously created 3-D geoelectric model (Sheremet et al., 2010, Sheremet et al., 2011) and the results of subsequent field geoelectrical survey made it possible to create a model for predicting rare-earth occurrences of the East Azov Region.

The first promising area (in the Kalmius fault zone) coincides with the deep conductor in the 3-D model and with the area of mineralization occurrences Krasnovka ore zone. This area can be recommended for integrated detailed survey and is promising for delineation of new rare-earth occurrences and deposits of carbonatite Anadol-type.

The second area is Gruzsko-Elanchik fault zone where rare-metal grorudite dikes are spread.

The third area is the junction zone of the East Azov Region with Donbass. It is characterized by manifestations of alkaline-ultrabasic magmatism with the developed fenitization processes in exocontacts of the massifs, with occurrences of postmagmatic carbonatization which are accompanied by injection of rare elements (Nb, Zr, TR) and volatile components (P, F, H_2O and other). Beyond that in the closing stages of alkaline-ultrabasic magmatism rare-metal (with increased concentration of rare-earth elements of cerium group) alkaline dikes (grorudites) have manifested.

Therefore the East Azov Region is still the promising area for discovery of rare-metal and rare-earth deposits of different genetic types, the most probable of which can be associated with carbonatite complex or sub-alkaline syenites of South Kalchik-type to which the Azov deposit of britholite-orthite-zircon and zircon ores is confined.

References:

Kryvdik S. G., Tkachuk V. I. Petrology of Ukrainian Shield alkaline rocks. – Kiev: Naukova Dumka, 1990. –408 p. (inRussian).

Sheremet Ye. M., Melnikov V. S., Strekozov S. N. et al. The Azov rare-earth deposit of the Azov sea region megablock of Ukrainian shield (geology, mineralogy, geochemistry, genesis, ores; integrated exploration criteria, problems of exploitation). – Donetsk: Knowledge (Donetsk Branch), 2012. –374 p.(inRussian)

Sheremet Ye. M., Krydiik S. G., Pigulevsky P. I. et al.SubalkalinePrecambrian Magmatism and Tectono-Geophysical Peculiarities of the East Azov Region of the Ukrainian Shield. –Donetsk: Knowledge (Donetsk Branch), 2010. –289 p. (in Russian).

Sheremet Ye. M., Kulik S. N., Krivdyk S. G. et al. Geologic-Geophysical Criteria of Ore Content and Metallogeny of Subduction Zones of the Ukrainian Shield; Antsiferov, A. V., Ed.; UkrNIMI. –Donetsk: Knowledge (Donetsk Branch), 2011. –285 p. (inRussian).

ONSHORE-OFFSHORE MESOZOIC TO PALEOGENE MAGMATISM OF THE SOUTHERN CRIMEA

Shniukova K.

N. P. Semenenko Institute of Geochemistry, Mineralogy and Ore Formation of the NAS of Ukraine, Kiev, Ukraine,
shniukova@nas.gov.ua

Magmatic formations are known all along the southern Crimean coast (with gaps) beginning from cape Fiolent (Sevastopol region) up to Alushta region. In the adjacent Black Sea area underwater outcrops of igneous rocks have been revealed to the south-west and to the south of cape Fiolent. In general, from west to east there are three main magmatic regions onshore-offshore Southern Crimea: (1) Lomonosov submarine massif (LSM) located in the Black Sea southwestwards from Sevastopol; (2) cape Fiolent (F) with located to the south of it Foros ledge (FL) of the Black Sea continental slope; (3) complex of small intrusions of the Mountainous Crimea (SI) and Ayu-Dag mountain (AD) between Gurzuf and Alushta. The last region is situated within the Tauric zone of the Southern Crimea (Nikishin et al., 2015) where the main Crimean stratigraphic unit, namely Tauric flysch of the Triassic-Early Jurassic, is displayed. It serves as a country rock for small intrusions, being absent in two more western regions. These two regions differ greatly both from SI-AD and between each other. Their igneous rocks have been examined in details by the author (Shniukova, 2016). Petrography of SI and AD was well studied as long ago as last century, while their geochemistry was almost unknown until now. This paper aims to substantiate a various origin of magmatic rocks of the above three regions on the basis of their geochemical features and to present their geodynamic interpretation.

(1) The LSM magmatic complex includes both volcanic and plutonic rocks. Three series have been divided among the LSM volcanic rocks, namely high-magnesian (HM), moderate-magnesian (MM) and shoshonite. First two series belong to normal sequence: basalt – andesibasalt – andesite – dacite – plagiorhyodacite – plagiorhyolite. Their common petrochemical features are high MgO content (being higher for HM) when low TiO_2 and K_2O content; both normal volcanic series are calc-alkaline. HM series has been identified with low-Ca boninite series despite some distinctions: their REE patterns being slightly LREE-enriched unlike more flat MM basics' ones aren't typically boninitic U-shaped and are characterized by negative Eu anomaly due to plagioclase fractionation. MM series as a whole answer to the calc-alkaline island-arc series. The third (shoshonite) volcanic series includes basic-intermediate rocks of subalkaline sequence: absarokite – shoshonite – trachyandesibasalt (banakite) – trachyte. Plutonic rocks embrace full number of rocks: gabbro – diorite – quartz diorite – tonalite – plagiogranite (trondhjemite). Among them three series have been picked out, namely potassic-sodic, sodic and trondhjemite. Last two series were proved to be connected with SSZ ophiolites. Sodic series approximates to the so-named "oceanic plagiogranites"; trondhjemite series most of all corresponds to a "trondhjemite" concept.

As a result of study, an island-arc subduction-related origin has been recognized for the LSM. Boninites, being almost entirely restricted to subduction settings, for a long time were considered to be a variety of calc-alkaline series. Recently a new petrochemical scheme was suggested (Pearce & Robinson, 2010): as boninites represent an anomalous supra-subduction zone (SSZ) magmatism and must stand apart, the boninitic series should be first separated from the rest and then the remaining rocks of normal island-arc BADR series may be divided into calc-alkaline and tholeiitic ones. When using such approach it appears that BADR rocks are very few in the LSM; HM series really belongs to boninite one; MM series locates in the transitional field between BADR and boninite series. Thus, the LSM volcanites may be formed by combination of island arc and subduction initiation or slab edge. The favoured scenario for subduction initiation is a slab roll-back which leads to near-trench magmatism in an extensional environment. It is this scenario that used now to explane the opening of the Black Sea as a back-arc basin. Geochemical peculiarities of the LSM magmatic rocks reflect their complicated origin. In primitive mantle-normalized multi-element diagrams they display well pronounced Nb and Ti troughs like an average typical subduction magma (Kovalenko et al., 2010), Pb and U peaks interpreted as a result of the crustal involvement, while Rb-Ba minimum corresponds rather to MORB than arc magmas. Behavior of elements indicated that the LSM magmatites were formed by both subduction and spreading processes combined with crustal contamination; the latter shows itself most in shoshonites and least in sodic plutonites. Finally, the LSM has been considered to be a fragment of paleoisland arc with a clear petrochemical zonality being expressed in potassium increase and magnesium decrease in the rocks from south-east towards north-west approximately across the island arc's strike which is northeastern, i.e. subparallel to the Mountainous Crimea. Then the eastern part of the LSM (boninites and oceanic plagiogranites) represents the arc front and the western part (shoshonites) – its back. The LSM magmatic rocks originated under the back-arc opening by slab roll-back following subduction initiation, probably near a slab edge. Subduction-related magmatism was displaying more than once during the LSM formation.

(2) Magmatic region in the southernmost part of the Geraclean plateau around cape Fiolent has been divided into three parts, namely western, central and eastern, each of which reflects a certain phase of magmatism. Acid magmatic

rocks play an essential role only in the central part, elsewhere basic rocks being predominant. Eastern part is composed of amygdaloidal non-spilitized basalts; central part around cape Fiolent itself is occupied mainly by a spilite-plagiorhyolite thickness crossed by the diabase dykes. Western part differs greatly from two previous ones, being composed mainly of plutonic and hypabyssal rocks: gabbro-diabases, gabbro-norites interbedded with ultrabasic rocks and specific high-magnesian andesites and plagiorhyolites (the last were drilled in the Geraclean plateau).

Petrochemical features of F volcanics contrasting with those of LSM ones are as follows: bimodal distribution; subalkaline character of basics (rarely calc-alkaline); low MgO while high TiO_2 content in them. Rocks from the eastern F part are distinguished from other by obvious non-subduction origin. A number of peaks and troughs in primitive mantle-normalized multi-element diagrams show maximum similarity with MOR magma for the rocks of the eastern part whereas those of central and western parts have some subduction signs along with MOR ones. Their chondrite-normalized REE patterns are somewhat LREE-depleted without Eu anomaly. Geochemistry testifies to the predominance of extensional geodynamical conditions under the formation of F, at least of F volcanic rocks. As regards the basic-ultrabasic plutonites of the western F part, the author suggests their ophiolitic origin. They may be a fragment of ophiolites which have not been found within the LSM and refer most probably to cumulose parts of ultrabasic volcanics of ophiolitic dyke complex.

Offshore cape Fiolent magmatic products are exposed in Foros ledge. In contrast to the LSM, pyroclastic and volcanogenic-sedimentary rocks resembling an onshore Albian tuff thickness of Balaklava region are widespread here. Volcanic FL rocks are represented mainly by basic rocks: trachybasalts, amygdaloidal basalts, subalkaline magnesian basalts; rarely andesibasalts, latite-like andesites and dacites. They are highly titanous, low magnesian and subalkaline or almost alkaline, rare andesites being calc-alkaline. Low magnesian rocks with the highest K_2O content have no analogues both on- and offshore, whereas subalkaline magnesian basalts and dolerites are analogous to those of F. Moreover, amygdaloidal basalts are identical to the same rocks of the eastern F part, that is best demonstrated by REE patterns. Abrupt sloping REE curve of trachybasalt with LREE enrichment and HREE depletion is characteristic for the within-plate basalts. Primitive mantle-normalized multi-element diagram for trachybasalt also shows similarity with the continental within-plate basic magma, except Pb peak and Nb trough; the latter is due to neighboring K peak. Nb enrichment is often registered for the amygdaloidal basalts of both F and FL as well as for the FL dacites. Alkaline potassic-sodic series to which trachybasalts belong marks the extensional geodynamic conditions probably of passive continental margin setting, while an appearance of calc-alkaline andesitic rocks indicates the transition to compressional regime of an active continental margin. Until that time magmatic products of the FL and the eastern F part had formed a single unit; later on it was broken by strike-slip fault, eastern block having been displaced southwards and submerged.

(3) Magmatic region between Gurzuf and Alushta embraces several mountains (Kastel, Sharha, Uraga, Chamhy-Burun, Aj-Jora, Seraus), which are traditionally united into "complex of small intrusions", and the largest Crimean intrusion Ayu-Dag. Complex of small intrusions consists of hypabyssal bimodal gabbro-plagiogranite series. Some massives such as Sharha and Aj-Jora are composed from exclusively acid porphyritic rocks (tonalite to plagiogranite), other ones such as Uraga, Chamhy-Burun are made up of only basic rocks (gabbro-diabases and diabases). In the third type of massives there are both acidic and basic rocks, being more contrasting in composition like Seraus or less like Kastel. The last includes rare intermediate rocks of andesibasalt and even andesite composition. Certain smaller massives include andesites, too (e.g. Chungur-Kaja). Ayu-Dag and adjoining Partenit are usually reputed apart from SI since intermediate rocks are predominant here: gabbrodiorite – diorite – quartz diorite along with almost volcanic andesibasalt - andesite. All rocks of this region belong to the normal sequence and contrary to the first two regions are predominantly tholeiitic. Since the 1990s an opinion of the island-arc origin for these rocks prevails among domestic geologists. Later it was supported by foreign scientists. On the basis of very poor geochemical information Crimean volcanism was declared to be subduction-related: volcanics were formed in a subduction setting on the overriding plate due to the northward subduction below Crimea from middle Jurassic to Early Cretaceous; subduction zone located far to the south of Crimea; the Black sea opening occured since the Early Cretaceous (Meijers et al., 2010). This opinion contradicts reconstructions of those scientists who prefer a southward Jurassic subduction zone between Crimea and Pontides (Stampfli & Kozur, 2006) or insist on the Cenomanian – Coniacian time of the Black Sea opening (Nikishin et al., 2015). True, last opinion assumes small intrusions to be a component of Bajocian subduction-related volcanic belt preceded Middle Cimmeride orogeny. More extensive geochemical data just for SI-AD region show that it is not so simple.

According to $MgO-TiO_2-SiO_2$ content SI-AD rocks indeed fall into the BADR field for island arcs and back-arc basins. But their chondrite-normalized curves more resemble E-MORB (although have Eu minimum): REE patterns of SI-AD basic rocks are situated higher (with isolated exception) and show more essential LREE-enrichment than those of the LSM. Primitive mantle-normalized multi-element diagrams for basics of SI and especially of AD differ greatly from the typical subduction magma by U trough, Th peak and high Be position, although weak Nb and Ti minima in them are fixed, too. Small intrusions display poor-peak or flat Pb but Ayu-Dag has its trough. As a whole, AD spiders most correspond to MORB while those of SI reflect some subduction influence.

Age of magmatism is still one of the most disputable issue for the Southern Crimea. The LSM rocks were dated by K-Ar method in the 1990s (Shniukova, 2016). K-Ar datings refer mainly to Cretaceous and Paleogene (from 147 to 41 Ma, isolated datings 170 and 26-31 Ma) with two peaks: Early Cretaceous (about 125 Ma) and Late Cretaceous – Early Paleogene (about 65 Ma). Datings are almost absent between Albian and Coniacian, i.e. at the time of most powerful rifting. There is only one reliable U-Pb SHRIMP dating for the zircon from MM andesite (168,5±1,7 Ma). Besides the LSM, K-Ar whole-rock dating for dacite from FL showed 197 Ma, i.e. the beginning of the Jurassic (magmatic rocks of this age are unknown onshore the Crimea), and plagiorhyolite from the central F part yielded 174 Ma. Several K-Ar

datings were carried out for SI and AD in the 1960-80s: Sharha plagiogranite – 185 Ma; that of Seraus – 159 and 163 Ma; that of Kastel – 170 Ma; Uraga gabbro-diabase – 162 Ma; that of Ayu-Dag – 140 and 161 Ma. Single fission-track dating of zircons for Kastel diorite yielded 149 Ma (Solov'ev & Rogov, 2010). Dating by "total lead" method performed for zircons from Seraus diabase in Macquire University (Australia) gave 71 Ma. It should be noted that zircons from certain LSM rocks and those from acid SI rocks have unusual geochemical features.

For the rocks of all three regions an attempt has been made to detect a crustal contamination and somewhat mantle composition geochemically with Th, Yb, Ta, Nb, Zr, Y using their ratio diagrams. Thus, Zr/Y-Nb/Y projection (Condie, 2005) indicate that almost all studied basics are of non-plume sources. Being plotted on Condie's Nb/Th-Zr/Nb diagram, they are located on the different sides from upper crust point: all the LSM, SI, AD rocks and basics from central and western F parts fall into low-Nb boundary of the arc-related basalts with maximum subduction effect while Nb-enriched Foros and eastern-Fiolent basics are drawn towards oceanic basalts. The most useful is a Th-Nb proxy: on the Nb/Yb-Th/Yb diagram (Pearce, 2008) oceanic (non-subduction) basalts lie within a diagonal MORB-OIB array while crustally-contaminated basalts erupted in subduction zones (especially volcanic arc basalts) are displaced above this array, the higher the more magma-crust interaction. All the LSM rocks form a separate array close to volcanic arc one, SI and AD rocks locate a little higher within the same array, central and western F basics plot a little lower, and FL and eastern F volcanics plot even lower, closest to MORB-OIB. On the modified for tectonic setting Ta/Yb-Th/Yb diagram (Gorton & Schandl, 2000) most of the LSM, SI and AD rocks fall into the field of active continental margins whereas other rocks (F, FL) correspond to the within-plate volcanic zones. Certain SI (mostly Kastel) points which get into the field of oceanic arcs belong to the rocks with the highest Th/Ta ratio (i.e. most crustally contaminated) showing some calc-alkaline features. On the contrary, rare Seraus diabases with the lowest Th/Ta ratio show exotic REE distribution, point beyond the non-plume field by Condie and yield too young zircon age.

Summing up all the information obtained during the last 25 years the author proposes the following progression of magmatic and geodynamic events in the Southern Crimea. The magmatism of the south-western Crimean outskirts had been developing as that of the passive continental margin from the Carboniferous up to the beginning of the Jurassic with the short-term transition to an active continental one at the end of the Early Jurassic. This magmatism is manifested now both in the Geraclean plateau and Foros ledge of the continental slope. The latter is a moved south fragment of the Scythian Platform beeing now its southernmost ending. In the Middle Jurassic extensional conditions dominated in Fiolent region while the formation of small intrusions (and later on Ayu-Dag) started further east accompanied by the transition to compressional conditions. Beginning from the Middle Jurassic an island arc originated in the northern part of the present-day Western Black Sea due to a southward directed subduction. The Istanbul Zone of the Pontides acted as an over-riding continental lithosphere. Magmatic products of this stage are represented in the LSM predominantly by volcanic calc-alkaline series. Trondhjemites as a component of the ophiolites are less reliably attributed to this stage. The first island arc had been functioning throughout the Late Jurassic and Early Cretaceous until the Albian. At about the Early - Late Cretaceous boundary the LSM was a highland with the plutonic potassic-sodic magmatism while the South-Western Crimea (now both on- and offshore) was characterized by the intensive pyroclastic activity. A new LSM island arc was established in the Late Cretaceous (beginning from the Coniacian) back to the gently sloping (flat-slab) northward directed Anatolian subduction zone. A continental lithosphere beneath which subduction occured was represented by the Scythian Platform. Slab roll-back and rifting resulted in the opening of the Black Sea as a back-arc basin were accompanied by slab edge melting and/or slab detachment leading to the formation of boninites. The LSM island arc was passing all the way from young to mature one up to the Eocene. "Oceanic plagiogranites" in the arc front is a plutonic member of the ophiolites whose remnants are preserved in the most south-western part of the Fiolent region. Meanwhile to the east, quite different non-subduction intrusions were penetrated in the Late Cretaceous.

So, this study demonstrates a diversity of Mesozoic to Paleogene magmatism of the Southern Crimea. One of three regions has obviously subduction origin (LSM), second region has nothing common with subduction processes (F and FL), and subduction-related origin for the third region (SI and AD) is possible but doubtful.

References:

Condie K.C. (2005) High field strength element ratios in Archean basalts: a window to evolving sources of mantle plumes? Lithos 79: 491-504.

Gorton M., Schandl E. (2000) From continents to island arcs: a geochemical index of tectonic setting for arc-related and within-plate felsic to intermediate volcanic rocks. Canadian Mineral 38: 1065-1073.

Kovalenko V. I., Naumov V. B., Girnis A. V., Dorofeeva V. A., Yarmolyuk V. V. (2010) Average composition of basic magmas and mantle sources of island arcs and active continental margins estimated from the data on melt inclusions and quenched glasses of rocks. Petrology 18: 1-26.

Meijers M.J.M., Vrouwe B., van Hinsbergen D.J.J. et al. (2010) Jurassic arc volcanism on Crimea (Ukraine): implications for the paleo-subduction zone configuration of the Black Sea region. Lithos 119: 412-426.

Nikishin A. M., Wannier M., Alekseev A. S. et al. (2015) Mesozoic to recent geological history of southern Crimea and the Eastern Black Sea region. In: Sosson M., Stephenson R.A. &Adamia S. A. (eds) Tectonic Evolution of the Eastern Black Sea and Caucasus. Geological Society, London, Special Publications, 428.

Pearce J.A. (2008) Geochemical fingerprinting of oceanic basalts with applications to ophiolite classification and the search for Archean oceanic crust. Lithos 100: 14-48.

Pearce J.A., Robinson P.T. (2010) The Troodos ophiolitic complex probably formed in a subduction initiation, slab edge setting. Gondwana Research 18: 60-81.

Shniukova K. (2016) Magmatizm zony sochlenenija Zapadno-Chernomorskoj vpadiny, Gornogo Kryma i Skifskoj plity (Magmatism in the junction zone of the Western Black Sea, Mountainous Crimea and Scythian Platform). Naukova Dumka, Kiev.

Solov'ev A. V., Rogov M. A. (2010) First fission-track dating of zircons from Mesozoic complexes of the Crimea. Stratigraphy and Geological Correlation 18: 298-306.

Stampfli G.M., Kozur H.W. (2006) Europe from the Variscan to the Alpine cycles. In: D.G.Gee & R.A.Stephenson (eds) European Lithosphere Dynamics. Geological Society, London, Memoirs 32: 57-82.

TITANIUM-BEARING PHASES IN THE MgO–SiO2–TiO2±Al2O3 SYSTEM AT 10–24 GPa AND 1600°C): PHASE RELATIONS, STRUCTURAL FEATURES AND SOLID SOLUTIONS

Sirotkina E.A.[1,2,3], *Bobrov A.V.*[1,2,3], *Bindi L.*[4], *Irifune T.*[5]

[1]Vernadsky Institute of Geochemistry and Analytical Chemistry of the Russian Academy of Sciences, Moscow, Russia, ekaterina.a.sirotkina@gmail.com
[2] Lomonosov Moscow State University, Moscow, Russia
[3]Institute of Experimental Mineralogy, Chernogolovka, Russia
[4]Università di Firenze, Firenze, Italy
[5]Ehime University, Matsuyama, Japan

The influence of minor elements on structural peculiarities of high-pressure phases is poorly investigated, although incorporation of even small portions of them may have a certain impact on the PT-parameters of phase transformations. Titanium is one of such elements with the low bulk concentrations in the Earth's mantle (0.2 wt % TiO2); however, Ti-rich lithologies may occur in the mantle as a result of oceanic crust subduction. Thus, the titanium content is ~2 wt% TiO2, in MORB (Wilson, 1989). Accumulation of titanium in the Earth's mantle proceeds through crust-mantle interaction during the subduction of crustal material to different depths of the mantle.

Our experiments were aimed to the study of phase relations, achieve synthesis of Ti-bearing phases (rutile, weberite, geikielite, bridgmanite etc.) and their solid solutions in the MgSiO3–MgTiO3 system and to study of the conditions of formation, structural peculiarities, and compositional changes of Ti-rich phases. At 10–24 GPa and 1600°C, we studied the full range of the starting compositions in the MgSiO3 (En) – MgTiO3 (Gkl) system in increments of 10–20 mol% Gkl and 1–3 GPa, which allowed us to plot the phase PX diagram for the system MgSiO3–MgTiO3 and synthesize titanium-bearing phases with a wide compositional range. The experiments were performed using a 2000-t Kawai-type multi-anvil high-pressure apparatus at the Geodynamics Research Center, Ehime University (Japan). The quenched samples were examined by single-crystal X-ray diffractometer, and the composition of phases was analysed using SEM-EDS.

The main phases obtained in experiments were rutile, wadsleyite, MgSiO3-enstatite, MgTiO3-ilmenite, MgTiSi2O7 with the weberite structure type (*Web*), Mg(Si,Ti)O3 and MgSiO3 with perovskite-type structure. At a pressure of ~13 GPa, an association of *En+Wad+Rt* is replaced by the paragenesis of *Web+Wad+Rt*, for Ti-poor bulk compositions, With increasing Glk content, *Gkl+Wad+Rt* association is formed. It was found, that the solubility of titanium into synthesized phases is different. Our data indicate an immiscibility with an MgTiO3-rich bridgmanite. Thus, in our experiments at 24 GPa we have two different phases with perovskite-type structure such as Mg(Si,Ti)O3-bridgmanite with up to 60 mol% MgTiO3 and MgSiO3-bridgmanite with a relatively modest solubility of MgTiO3-component (~15 mol%). We observed an increase in MgTiO3 solubility with pressure in bridgmanite.

Addition of Al to the starting material allows us to simulate the composition of natural bridgmanites, since lower mantle bridgmanites are characterized by significant Al contents. In addition, this study shows that, in contrast to Al, the high contents of Ti can stabilize bridgmanite-like compounds at considerably lower pressure (18 GPa) in comparison with pure MgSiO3 bridgmanite.

Small crystals of titanium-rich phases, including new Ti-bearing bridgmanite-like phase and MgTiSi2O7 with the weberite structure type were examined by single-crystal X-ray diffractometer, which allowed us to study the influence of Ti on crystallochemical peculiarities of the mantle phases and on the phase transformations.

The Al-Ti-bridgmanite was found to be orthorhombic, space group *Pnma*, with lattice parameters a = 14.767(3), b = 6.958(1), c = 4.812(1) Å, V = 494.4(2) Å3, which represents a 3$\mathbf{a} \times \mathbf{b} \times \mathbf{c}$ superstructure of the typical *Pnma* perovskite structure. The superstructure mainly arises from the ordering of titanium in one of the octahedral positions. Crystal-chemical details of the different polyhedra in the superstructure are discussed in comparison to pure MgSiO3. This is the first documented superstructure of a bridgmanite phase. The study also shows that large amounts of Ti can stabilize bridgmanite-like compounds at considerably lower pressure than lower mantle conditions (Bindi et al., 2017).

MgTiSi2O7 was found to crystallize with the weberite-3T structure type, space group *P*3121, with lattice parameters a = 6.3351(7), c = 16.325(2) Å, V = 567.4(1) Å3. The successful synthesis of this phase demonstrates that titanium can stabilize heretofore unknown Mg-Si-oxides, The major Earth and rocky planet-forming materials, and can provide new constraints on thermobarometry of wadsleyite / Ringwoodite, and garnet-bearing assemblages (Bindi et al., 2017).

References:

Bindi L., Sirotkina E.A., Bobrov A.V., Pushcharovsky D.Yu, Irifune T. (2017) Discovery of MgTiSi2O7: a new high-pressure silicate with the weberite structure synthesized at transition-zone conditions. Phys. Chem. Minerals. V. 44. DOI: 10.1007/s00269-016-0868-8.

Bindi L., Sirotkina E.A., Bobrov A.V., Walter M.J., Pushcharovsky D.Yu, Irifune T. (2017) Bridgmanite-like crystal structure in the novel Ti-rich phase synthesized at transition zone condition. Am. Mineral. V. 102. No. 1. P. 227-230. DOI: 10.2138/am-2017-5937.

Wilson M. Igneous Petrogenesis—A global tectonic approach. Kluwer, Dordrecht. 1989. 466 p.

THREE TYPES OF CLINOPYROXENES FROM AILLIKITE, ILBOKICHESKOE AND CHADOBETS UPLIFTS, SW SIBERIA

Smirnova M.D.[1,2], Sazonova L.V.[1], Nosova A.A.[2], Kargin A.V.[2]

[1]Lomonosov Moscow State University, Moscow, Russia, petitmx@gmail.com, sazonovalv52@mail.ru,
[2]Institute of Geology of Ore Deposits, Petrography, Mineralogy and Geochemistry of the Russian Academy of Sciences, Moscow, Russia, nosova@igem.ru, kargin-igem@mail.ru

Major and trace element data are reported for clinopyroxenes from aillikites of the Chadobets and Ilbokich uplifts (SW Siberia, Russia). The Siberian craton contains more than 1000 intrusions of kimberlite and ultramafic alkaline rocks, which are divided into three Phanerozoic magmatic events: 1) Silurian to Early-Carboniferous (420-345 Ma); 2) Triassic (245-215 Ma); and 3) Late-Jurassic (160-149 Ma). The most of them are located within the northeastern Siberian craton and only a few occurrences of ultramafic lamprophyres (UML) are known within southwestern edge of the platform. These are Triassic UML of Chadobets (Lapin et al., 2007) and Devonian aillikite of Ilbokich (Kargin et al., 2016).

The studied rocks, – aillikites ,are melanocratic with porphyritic or massive, occasionally globular texture and high content of carbonate (up to 50 volume %),. Phenocrysts are represented by olivine (up to 30 v. %) and clinopyroxene (up to 15 v.%), groundmass consists of carbonate (up to 50 v. %), phlogopite (up to 40 v. %), clinopyroxene (up to 20 v. %), amphibole (<5 v.%), perovskite (up to 8 v. %), Ti-Mag (up to 10 v. %), apatite (up to 5 v. %), rutile, ilmenite, and spinel (<5 v. %), and rare high-Ti andradite (up to 1 v.%).

In terms of morphology and chemistry, clinopyroxenes can be divided into 3 groups: (1) xenocrysts - clinopyroxene from xenoliths, (2) phenocrystic clinopyroxenes as; and (3) groundmass clinopyroxene in.

First group clinopyroxenes occur as rare subhedral grains (70x100 mkm) within altered olivine from Ilbokicheskoe aillikites (fig. 1a). The grains are partly altered and show no chemical zoning. These clinopyroxenes are high-Cr diopside (Cr_2O_3 0.7-1.1 wt.%) with Mg# 89 and TiO_2 0.13 wt.%, Al_2O_3 0.6 wt.%, CaO 22.6, MnO 0.1 wt.%, Na_2O 1.1 wt.% contents.

Second group includes clinopyroxene phenocrysts from Chadobets UML. They form sub- and euhedral crystals, 1-3 mm in diameter, with homogeneous cores and heterogeneous rims with spotted zoning. Boundary between rim and core can be clearly distinguished (fig. 1b).
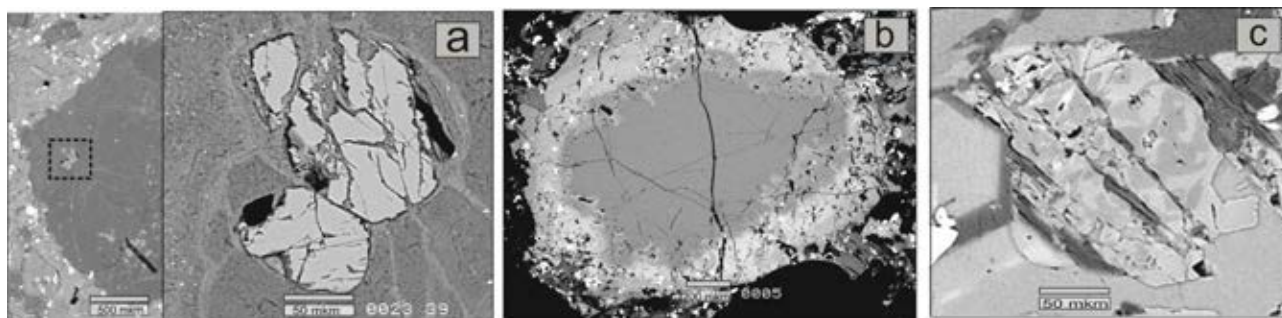
Fig. 1. a – clinopyroxenes from altererd olivine, group 1; b - clinopyroxene of group 2a with rim 2b; d– clinopyroxene of group 3 in ground mass.

Occasionally, rims contain inclusions of phlogopite, magnetite, Ti-magnetite and calcite. The cores and rims are distinguished, respectively, as groups 2a and 2b. The group 2a shows the following variations in composition (20 analyses): Mg# 82-84, TiO_2 1.1 – 1.5 wt.%, Cr_2O_3 0.0 – 0.4 wt %, Al_2O_3 4.7 – 6.5 wt.%, CaO 20.1 - 21.0 wt.%, MnO 0.1 – 0.2 wt. %, Na_2O 1.0 – 1.2 wt.. Group 2b shows following variations (23 analyses): Mg# 80 - 91, TiO_2 1.0 – 5.7 wt.%, Cr_2O_3 0.0 – 0.9 wt %, Al_2O_3 08 – 10.0 wt. %, CaO 22.0 - 24.3 wt.%, MnO 0.0 – 0.3 wt. %, Na_2O 0.3 – 1.0 wt. %.

Third group includes small size (up to 200-300, rare 500 mkm), anhedral grains with patchy zoning (fig.1c) Clinopyroxenes of this group forms intergrowths with groundmass carbonate, and occur as interstitial between other minerals. In a few samples, elongated grains are developed in rims of olivine or fully replace it. This group is represented by diopside, Mg-rich hedenbergite and salite (high-Ca dipside) join. Compositional variations are as follows (132 EMPA

analyses): Mg# 47 – 98 , TiO_2 0 – 4.4 wt. %, Cr_2O_3 0 wt %, Al_2O_3 0 – 6.9 wt.%, CaO 20.2 - 26.1 wt.%, MnO 0 – 0.6 wt. %, Na_2O 0 – 2.1 wt. %.

Comparison of group 1 clinopyroxenes with clinopyroxenes from various deep-seated rocks (fig. 2) shows that group 1 is similar to clinopyroxenes from orangeites, spinel lherzolites and peridotite xenoliths metosomatised by a kimberlitic melt (Nimis et al., 2009). At the same time, the group 1 clinopyroxenes slightly differ from those of spinel lherzolites and orangeites (fig. 2), and are identical to clinopyroxenes from metasomatized spinel lherzolite. This suggests that group 1 clinopyroxenes are xenocrysts. The clinopyroxenes and host altered olivine are xenoliths of metosomatized mantle peridotite.
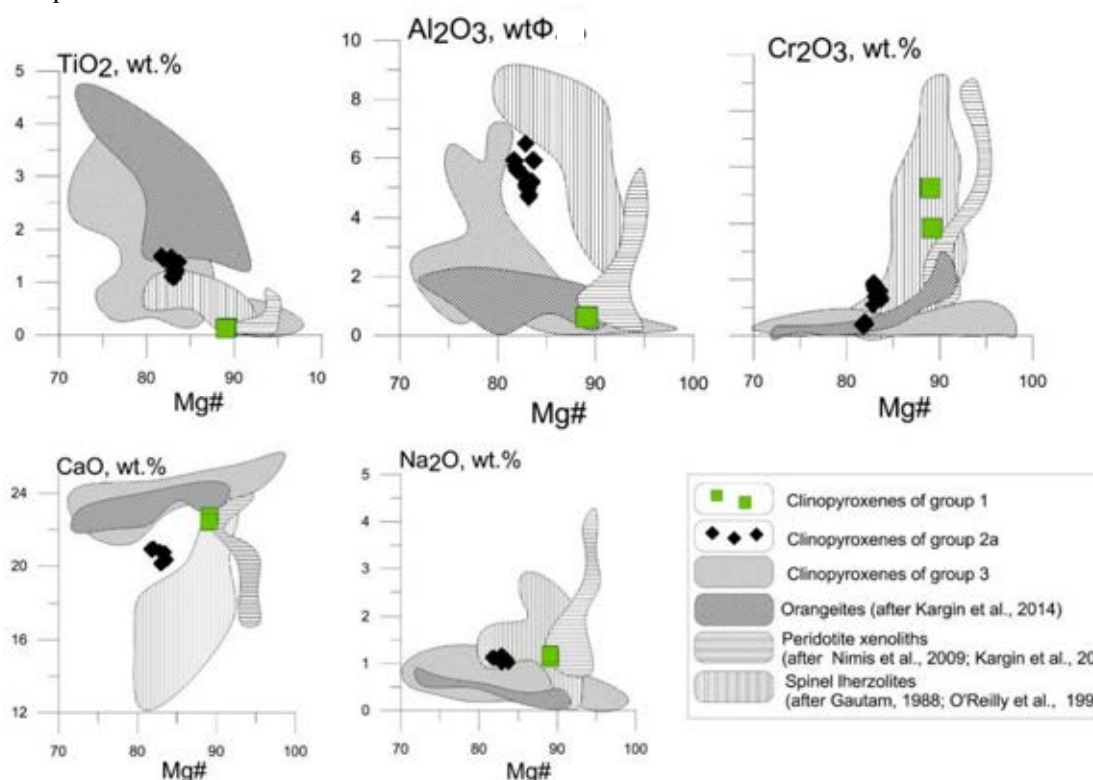
Fig. 2. Chemical composition of clinopyroxenes of group 1, 2 and 3 aas compared to clinopyroxenes from peridotite xenoliths, orangeites and spinel lherzolites.

Trace element patterns for Cpx phenocrysts are similar to those of ultramafic lamprophyres (Tappe et al., 2004 & 2006). Clinopyroxenes of group 2a were studied by secondary ion mass spectrometry. 10 analyses was made in clinopyroxene cores from 2 samples (53-452; 32-87). The REE pattern (fig.3) is characterized by enrichment in LREE, and depletion in HREE. The average REE ratios are $(La/Yb)_n$=53.7; $(Ce/Yb)_n$=42.0; $(Dy/Yb)_n$= 3.0; $(Gd/Er)_n$ = 4.0. HREE depletion in clinopyroxene may be related to equilibrium with garnet. LREE enrichment may be associated with high LREE content in a parental melt.
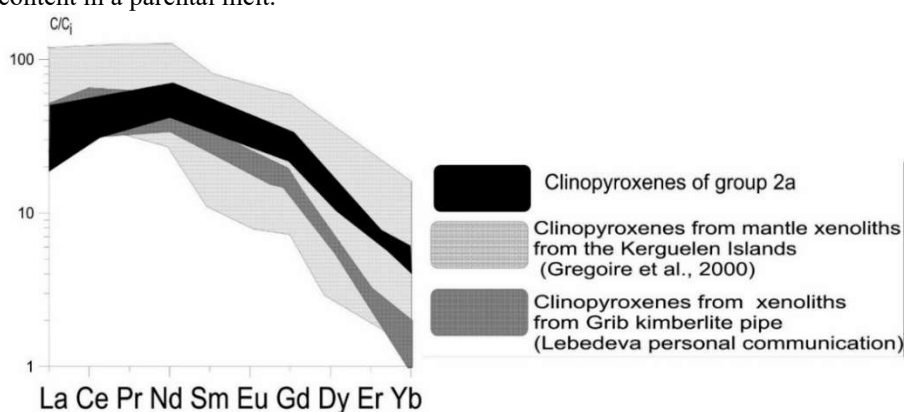
Fig. 3. REE distribution pattern for clinopyroxenes of group 2a, results of SIMS analysis as compared to clinopyroxenes from xenoliths, Grib kimberlite pipe and mantle xenoliths from Kerguelen

The composition of modal melts were calculated using partition coefficients for silica (Hart and Dunn, 1993) and carbonate (Dasgupta et al., 2009) systems in proportion 80/20 (fig. 4). This model may be used because petrographic and chemical compositions of rocks and minerals allow us to assume, that group 2a clinopyroxenes crystallized from carbonate-silica melts. As can be seen in fig. 4, the modal melts are similar to whole rocks compositions, which were analyzed by ICP-MS. But calculated melts resemble more differentiated UML. This indicates that the group 2a clinopyroxenes are phenocrysts. The rims (2b) were formed as group 3 pyroxene subjected to late stage autometasomatism.

It should be noted that groups 2b and 3 are similar in their heterogeneous zoning, mineral inclusions, wide range of compositions, and their trends of changes in the composition, which presumably points to their metasomatic origin, at the late stages of evolution of the system. Meanwhile, the petrological and chemical features of groups 1 and 2a sharply differ from groups 3 and 2d. They have more euhedral morphology, relatively stable composition, lower concentrations of Ca, Mn and higher of Cr.
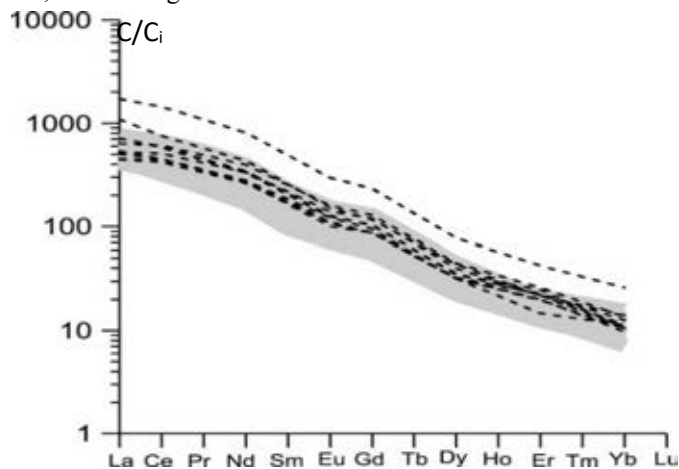
Fig. 4. Compositions of the Chadobets ULM (ICP MS data – grey field) as compared to calculated model melts (dash lines). The calculations were made on the basis of REE concentrations in clinopyroxenes of group 2a.

Thus, we may conclude that clinopyroxenes from Ilbokicheskoe and Chadobets aillikites can be divided into 3 groups on the basis of petrological and mineralogical criteria, and their genesis. The first group of clinopyroxenes are the rarest and represent xenoliths of peridotite, which were metasomatized by interaction with high-volatile magma. The second group are phenocrysts and they were crystallized from parental magmas. Study of REE distribution in clinopyroxene, shows that the parental magma was in equilibrium with garnet and had a carbonate-silica composition. Third, the widest spread group and rims around phenocrysts (2b) formed at late, autometasomatic stage of magma evolution.

References:

Gautam S (1988) Petrogenesis of spinel lherzolite and pyroxenite suite xenoliths from the Koolau shield, Oahu, Hawaii: implications for petrology of the post-eruptive lithosphere beneath Oahu. Contributions to Mineralogy and Petrology 100.1: 61-91.

Grégoire, M., Moine, B. N., O'Reilly, S. Y., Cottin, J. Y., & Giret, A. (2000). Trace element residence and partitioning in mantle xenoliths metasomatized by highly alkaline, silicate-and carbonate-rich melts (Kerguelen Islands, Indian Ocean). Journal of Petrology, 41(4), 477-509.

Hart, S. R., & Dunn, T. (1993). Experimental cpx/melt partitioning of 24 trace elements. Contributions to Mineralogy and Petrology, 113(1), 1-8.

Kargin, A. V., Nosova, A. A., Larionova, Y. O., Kononova, V. A., Borisovsky, S. E., Koval'chuk, E. V., & Griboedova, I. G. (2014). Mesoproterozoic orangeites (kimberlites II) of West Karelia: Mineralogy, geochemistry, and Sr-Nd isotope composition. Petrology, 22(2), 151-183.

Kargin, A. V., Sazonova, L. V., Nosova, A. A., & Tretyachenko, V. V. (2016). Composition of garnet and clinopyroxene in peridotite xenoliths from the Grib kimberlite pipe, Arkhangelsk diamond province, Russia: Evidence for mantle metasomatism associated with kimberlite melts. Lithos, 262, 442-455.

Lapin, A. V., A. V. Tolstov, and A. V. Antonov. "Sr and Nd isotopic compositions of kimberlites and associated rocks of the Siberian craton." Doklady Earth Sciences. Vol. 414. No. 1. Springer Science & Business Media, 2007.

Nimis, P., Zanetti, A., Dencker, I., & Sobolev, N. V. (2009). Major and trace element composition of chromian diopsides from the Zagadochnaya kimberlite (Yakutia, Russia): Metasomatic processes, thermobarometry and diamond potential. Lithos, 112(3), 397-412.

O'Reilly, S. Y., Griffin, W. L., & Ryan, C. G. (1991). Residence of trace elements in metasomatized spinel lherzolite xenoliths: a proton-microprobe study. Contributions to Mineralogy and Petrology, 109(1), 98-113.

Sun, S. S., & McDonough, W. S. (1989). Chemical and isotopic systematics of oceanic basalts: implications for mantle composition and processes. Geological Society, London, Special Publications, 42(1), 313-345

Tappe, S., Jenner, G. A., Foley, S. F., Heaman, L., Besserer, D., Kjarsgaard, B. A., & Ryan, B. (2004). Torngat ultramafic lamprophyres and their relation to the North Atlantic Alkaline Province. Lithos, 76(1), 491-518.

Tappe, S., Foley, S. F., Jenner, G. A., Heaman, L. M., Kjarsgaard, B. A., Romer, R. L., ... & Hoefs, J. (2006). Genesis of ultramafic lamprophyres and carbonatites at Aillik Bay, Labrador: a consequence of incipient lithospheric thinning beneath the North Atlantic craton. Journal of Petrology, 47(7), 1261-1315.

SPECIFIC FEATURES OF EUDIALYTE DECOMPOSITION IN OXALIC ACID

Smirnova T.N.[1], Pekov I.V.[1,2], Varlamov D.A.[3], Kovalskaya T.N.[3], Bychkov A.Y.[2], Bychkova Y.V.[2]

1Vernadsky Institute of Geochemistry and Analytical Chemistry RAS, Moscow, Russia
2Faculty of Geology, Moscow State University, Moscow, Russia
3Institute of Experimental Mineralogy RAS, Chernogolovka, Russia

One of the main aspects of a possible practical use of eudialyte today is extracting of Zr, Hf, REE (especially HREE) and U. Numerous attempts to solve this problem using full decomposition of eudialyte by strong inorganic acids were not successful in technological aspect: silicon converts into solution forming the filterable gel which strongly hampers any processes of isolation and purification of valuable components.

We have studied the processes and products of eudialyte decomposition in dilute oxalic acid, $H_2C_2O_4$, and for comparison – in HCl, at $t < 100°C$. For the experiments, two eudialyte varieties were used: (1) from rischorritic pegmatite, the Oleniy Ruchey apatite deposit (sample OLE-9), Khibiny, and (2) from naujaitic pegmatite, Mt. Alluaiv (sample UMB-2), Lovozero (both Kola peninsula, Russia). The Lovozero eudialyte is enriched with *REE* and Zr and has, according to our data, more defective crystal structure in comparison with the Khibiny sample.

Experiments with 1 and 3% $H_2C_2O_4$ gave similar results for the Khibiny eudialyte: it alters only from the surface to opal-like phase with overgrowing crystals (Fig. 1). Using the EMPA and IR spectroscopy data, we undoubtedly identified these crystals as Ca-Zr oxalates. In experiments with 7% $H_2C_2O_4$ the Khibiny eudialyte completely decomposes with the formation of a gel-like opal phase closely associated with crystalline oxalates of Ca and Zr with admixed *REE*.
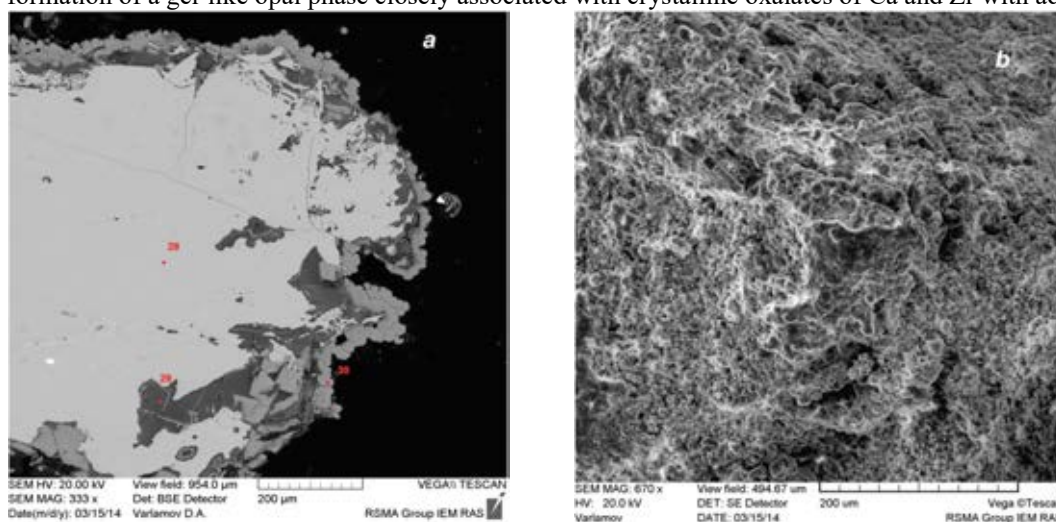
Fig. 1. The Khibiny eudialyte after the experiment with 1% $H_2C_2O_4$. On section (a), an opal-like phase (p.29) and Ca-Zr oxalate crusts (30) overgrowing unaltered eudialyte (28) are observed. On the rough surface (b), Ca-Zr oxalate crystals are abundant. SEM image: (a) BSE, (b) SE.
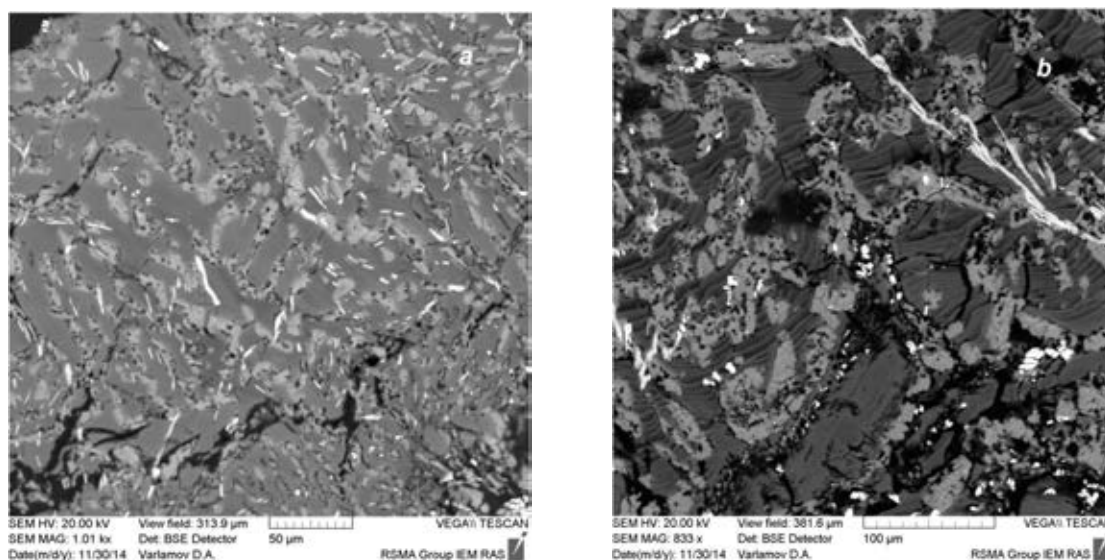
Fig. 2. Surface of the opal-like product formed as a result of full decomposition of eudialyte in 7% (a) and 5% (b) $H_2C_2O_4$ [SEM (BSE) image]. White zones correspond to *REE* oxalates and light gray zones to Ca-Zr-oxalates.

Lovozero eudialyte fully decomposes in 3, 5 and 7% $H_2C_2O_4$. On the surface of the opal phase formed, crystals (up to 40 μm) of both Ca-Zr and *REE* oxalates (Fig. 2) are detected. Two types of *REE* oxalates were formed, one with essentially yttrium cationic composition (enriched also with *HREE*) whereas another is *LREE*–rich.

Thus, in a system with $H_2C_2O_4$ a separation of mobilized from eudialyte *REE* from other cations in the *solid crystalline (oxalate) phase* happens. These oxalates are almost insoluble in water and oxalic acid, and release of *REE* into the solution is minor, unlike a system with HCl. It seems very important for their further extraction because we see a relatively easy way to convert *REE* into the molecular (rather than colloid!) solution using a complexing agent without any reaction with opal, a dried silica gel. It seems also important that a dilute solution of $H_2C_2O_4$ is used: oxalic acid is an agent which, unlike corrosive and volatile mineral acids, may be easily transported and stored in an environmentally safe solid form.

Extraction of Zr (and Hf) into solution in experiments with $H_2C_2O_4$ is reduced as compared to HCl, but still significant. Also note the solubility of eudialyte significantly depends on the perfection of its structure (Ca-Fe-Zr-Si heteropolyhedral framework): the Khibiny sample is considerably more resistant to acid degradation than the Lovozero mineral.

Table. 1 Contents of rare elements and Ti (ppm) in thousandfold diluted solutions after the experiments with HCl and $H_2C_2O_4$ of different concentrations and eudialyte from Khibiny (OLE-9) and Lovozero (UMB-2).

| | HCl | | | | | | $H_2C_2O_4$ | | | | | | |
| | OLE-9 | | | UMB-2 | | | OLE-9 | | | | UMB-2 | | |
	10%	7%	2%	10%	7%	2%	7%	5%	3%	1%	7%	5%	3%
Zr	2486	1671	135	1600	1528	390	306	260	477	122	1100	1739	1311
Hf	36	20	1.2	28	26	5	-	bdl	-	1.8	22	35	28
Ti	93	91	-	79	72	41	-	-	-	-	-	85	57
Ta	bdl	0.1	bdl	bdl	0.3	0.6	-	-	-	0.7	4	5	0.7
Th	0.8	0.8	0.3	0.8	1.1	0.4	bdl	bdl	bdl	bdl	0.2	0.6	0.3
U	1.5	1.6	0.5	0.5	0.7	0.3	0.4	0.3	0.5	0.3	0.2	0.6	0.5
Sr	176	182	56	210	157	94	5	4	4	3	5	5.5	5.5
Ba	44	45	13	2	1.8	2	10	7	6	4	0.8	0.6	0.1
Y	43	44	12	107	86	53	0.4	0.2	bdl	bdl	0.9	1.1	0.9
La	25	26	7	49	5	24	0.7	0.3	bdl	bdl	1	1.8	0.1
Ce	32	31	14	101	87	50	1	0.4	bdl	0.1	0.9	1.2	0.2
Pr	5.5	5.5	1.5	13	18	6	bdl	bdl	bdl	bdl	bdl	0.1	bdl
Nd	22	23	6	58	79	28	0.3	0.15	bdl	bdl	bdl	0.1	bdl
Sm	5	5	1.5	17	24	9	bdl	bdl	bdl	bdl	bdl	bdl	bdl
Eu	2	2	0.5	6	8	2.9	bdl	bdl	bdl	bdl	bdl	bdl	bdl
Gd	6.5	6.5	1.5	18	27	8.5	0.1	bdl	bdl	bdl	bdl	bdl	bdl
Tb	1.2	1.2	0.3	3.8	5	2	bdl	bdl	bdl	bdl	bdl	bdl	bdl
Dy	8	8	2	24	32	12	bdl	bdl	bdl	bdl	bdl	bdl	0.1
Ho	1.8	1.8	0.5	4.6	6.5	2	bdl	bdl	bdl	bdl	bdl	bdl	bdl
Er	5.5	6	1.5	14	20	7	bdl	bdl	bdl	bdl	bdl	0.1	0.1
Tm	0.8	0.9	0.2	2	2.8	1	bdl	bdl	bdl	bdl	bdl	bdl	bdl
Yb	5	5	1.5	12	17	6	bdl	bdl	bdl	bdl	0.2	0.4	0.3
Lu	12	8	0.2	1.7	17	0.8	bdl	bdl	bdl	bdl	bdl	8.5	7

ICP MS data; bdl – below detection limit; dash – not analysed.

MICROINCLUSIONS IN THE EARLY OLIVINE OF ULTRAMAFIC ROCKS OF THE UITKOMST INTRUSION, SOUTH AFRICA

Solovova I.P.[1], Yudovskaya M.[1], Zinovyeva N.[2], Borisovski S.[1], Girnis A.[1]

[1]Institute of Geology of Ore Deposits, Petrography, Mineralogy and Geochemistry of the Russian Academy of Sciences, Moscow, Russia, solovova@igem.ru

[2]Lomonosov Moscow State University, Moscow, Russia

The genesis and composition of parent magmas and the thermodynamic conditions of the formation of layered ultramafic complexes are still debatable (e.g., Wilson, 2012; Yudovskaya et al., 2003). Some estimates of the compositions of parent magmas for the Bushveld Complex in South Africa are given in Table 1. The experimental study of inclusions in minerals is a promising approach to this problem, because it provides direct information on the compositions and parameters of magmas. We studied a satellite intrusion of the Bushveld Complex, in which melt inclusions could be preserved in olivine from primitive rocks, such as dunites and peridotites.

Samples were taken from a borehole in the depth interval from 628.6 to 665 m. The dominant mineral of the ultramafic rocks is olivine of two generations, Ol I and Ol II. The earliest generation (Ol I) is represented by large (up to 3 mm) phenocrysts. The olivine *mg#* is 0.90-0.92, NiO content is up to 0.5 wt%, and CaO is up to 0.15 wt%.

Ol I contains rare melt inclusions (not larger than 40 ▢m) and multiphase inclusions of crystals up to 150 ▢m in size. Naturally crystallized melt inclusions contain euhedral anisotropic daughter phases (Figure, Series I), including olivine and orthopyroxene. These inclusions were classified as primary on the basis of universally accepted criteria (Melnikov et al., 2008), such as the constant proportions of daughter phases, morphology and distribution in olivine.

During heating experiments, gradual resorption of crystalline phases, appearance of melt, and separation of a fluid phase were observed in the inclusions. A similar behavior was observed in the silicate part of combined inclusions (spinel + silicate) (Figure, Series II). In some experiments, the decrepitation of inclusions and loss of matter were observed (Figure, Series II, 1330°C). The complete homogenization of the inclusions was not achieved at a temperature of 1430°C. The contents of components in the melt inclusions (Table 1, columns 1-3) are correlated with MgO (14.5-17.5 wt %). The maximum contents of volatile components are 0.2 wt % H_2O, 0.07 wt % S, 0.2 wt % Cl and 0.07 wt % F. The obtained melt compositions differ from the previous model estimates of the parental Bushveld magmas in lower CaO contents (<3.5 wt %) and much higher alkalis (Table 1).

Table 1. Melt compositions, wt%

	1	2	3	4	5	6	7
SiO2	57.44	55.33	56.37	55.15	54.95	55.24	50.41
TiO2	0.08	0.08	0.26	0.31	0.34	0.38	0.37
Al2O3	12.64	10.21	12.51	10.61	11.25	12.13	10.56
FeO	6.55	8.69	6.32	9.50	9.61	9.2	2.86
MgO	14.38	17.65	15.73	14.63	13.29	12.97	17.89
MnO	0.08	0.11	0.10	0.18	0.18	0.15	0.08
CaO	1.25	3.82	2.57	6.16	6.39	6.84	7.66
Na2O	5.24	3.57	3.65	1.60	1.51	1.75	5.09
K2O	1.24	1.16	1.49	0.79	0.85	0.88	1.81
Total	98.88	100.61	98.99	98.93	98.37	99.54	96.74
mg#	0.80	0.78	0.82	0.73	0.71	0.72	0.92
T,°C exp.	1330	1350	1200	H&S	B	D	Cryst

Note. 1-3 - melt inclusions; 4-6 - model estimates of primary magmas of the Bushveld complex: H&S (Harmer, Sharpe, 1985); B (Barnes et al., 2010); D (Davies et al., 1980); 7 - estimated bulk composition of polyphase crystalline aggregates in olivine. Chemical analyses were obtained in a wavelength-dispersion mode, using a Superprobe JEOL JXA-8230 electron microprobe at the Laboratory of High Spatial Resolution Analytical Techniques, Department of Petrology, Geological Faculty, Moscow State University.
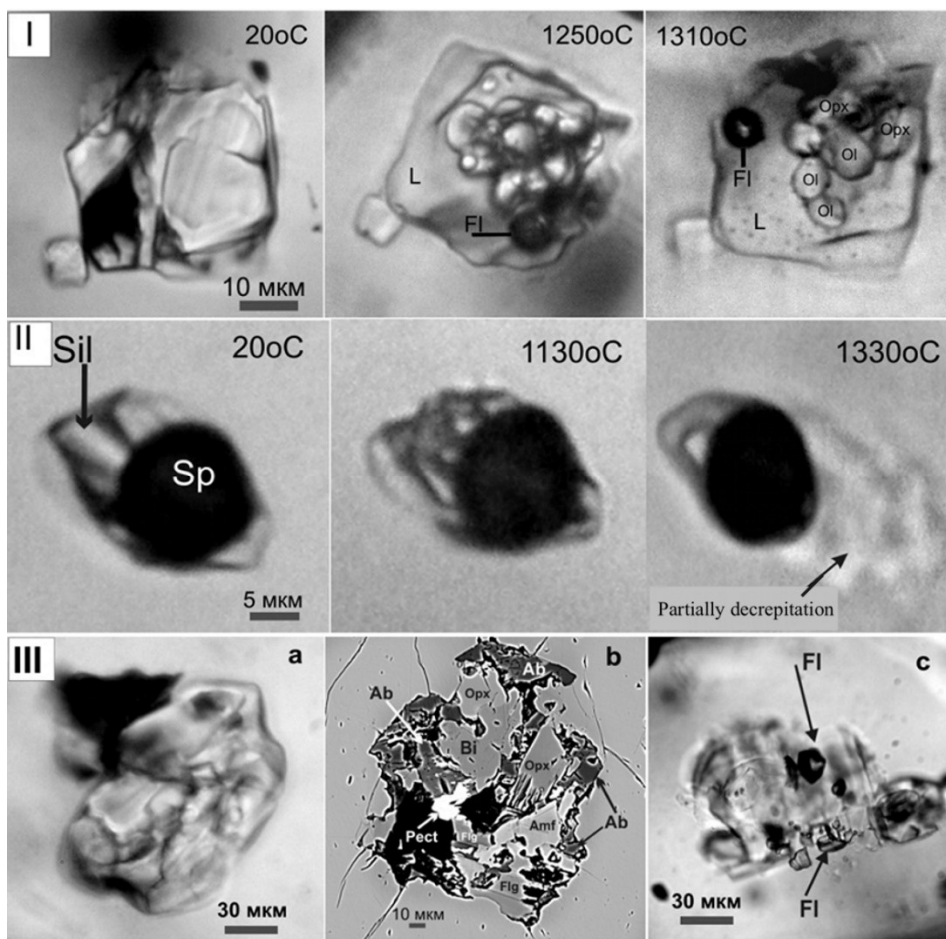
Fig.1 Melt, combined spinel + melt and crystalline inclusions. Series I and II are transmitted-light images showing phase changes in primary melt and combined spinel + silicate inclusions in Ol I. At a temperature of 1310°C, primary melt inclusions contain up to 20 vol % unmelted daughter olivine and orthopyroxene and a fluid phase. Complete melting is not achieved up to 1410°C. Series III shows crystalline aggregate inclusions in Ol I: (a) smoothed outlines of a crystalline aggregate (transmitted light), (b) BSE image of a crystalline aggregate, and (c) partly decrepitated aggregate with fluid within the volume and on the surface of it (transmitted light).

In addition, widespread inclusions of polymineralic aggregates in Ol I were studied in detail. It was supposed that they can be interpreted as crystallized melt inclusions, because their appearance is typical of intrusive rocks. The aggregates are irregular or rounded in shape (Figure, series III). In some cases, they contain a fluid phase and/or are decrepitated. Their mineral assemblage is olivine (*mg#* 0.90, 0.08 wt % CaO, and 0.35 wt % NiO) + orthopyroxene + amphibole + phogopite + pectolite + albite (Table 2) and an opaque phase.

Table 2. Compositions of phases from crystalline aggregates, wt %

	Orthopyroxene	Amphibole	Phlogopite	Bi	Pectolite	Albite
SiO_2	55.09	46.25	40.35	39.72	53.25	66.86
TiO_2	0.12	2.29	0.41	0.28	0.00	-
Al_2O_3	1.68	10.53	14.77	15.40	0.37	20.64
Cr_2O_3	0.00	0.02	0.04	0.22	-	-
FeO	6.72	3.75	3.09	2.76	0.31	0.39
MnO	0.16	0.05	0.05	0.00	0.25	-
MgO	34.59	20.08	25.16	25.50	0.14	0.11
CaO	0.67	11.46	0.02	**2.37**	32.15	0.71
Na_2O	0.02	3.60	1.62	6.35	8.58	11.43
K_2O	-	0.21	8.59	1.15	0.05	0.13
NiO	0.09	0.09	0.21	-	0.04	-
Cl	-	0.02	0.14	-	0.03	-
F	-	0.19	0.42	0.25	0.09	-
SrO	-	-	0.14	-	0.18	-
BaO	-	-	0.12	-	0.07	-
Total	99.04	98.45	94.91	93.94	95.45	100.28
mg#	0.90	0.91	0.94	0.94		

Intergranular melt and a gas bubble appeared in the aggregates at 1100-1150°C. The fluid phase was dissolved in the melt at 1250°C. A high degree of crystallinity (no less than 80 vol %) was observed up to the maximum experimental temperature (1340°C). Based on the experimental observations, it was concluded that the polymineralic inclusions were trapped by growing olivine as mineral aggregates. The mineral assemblage of such inclusions does not correspond to that of the rocks of the complex. According to Hornsey (1999) and Sarkar et al. (2008), the appearance of hydrous minerals, such as phlogopite, amphibole and pectolite, results from magma-xenolith interaction. The presence of intergranular melt and fluid in the aggregates, the high contents of volatiles (up to 3 wt % H_2O and 0.2 wt % F) and alkalis (up to 7 wt % Na_2O+K_2O) (Table 1) up to the crystallization of albite and pectolite, and very high alkalis in primary melt inclusions may indicate fluxing with a hot fluid. This is supported by the presence of subparallel trails of tiny fluid inclusions (≤1 μm) in cumulative olivine.

References
Barnes C.-J., Maier W., Curl E. (2010) Composition of the marginal rocks and sills of the Rustenburg Layered Suite, Bushveld Complex, South Africa: Implications for the formation of the platinum-group element deposits. Econ Geol 105: 1491-1511.

Davies G., Cawthorn R. G., Barton J., Morton M. (1980) Parental magma to the Bushveld Complex. Nature 287: 33-35

Harmer R., Sharpe M. (1985) Field relations and strontium isotope systematics of the marginal rocks of the eastern Bushveld Complex. Econ Geol 80: 813-837.

Melnikov Ph., Prokophyev V., Shatagin N. (2008) Thermobarogeochemistry. Moscow State University

Sarkar A, Ripley E., Li C., Maier W. (2008) Stable isotope, fluid inclusion, and mineral chemistry constraints on contamination and hydrothermal alteration in the Uitkomst Complex, South Africa. Chem Geol 257 :129–138

Wilson A. A (2012) Chill Sequence to the Bushveld Complex: Insight into the First Stage of Emplacement and Implications for the Parental Magmas. J Petr 53 (6): 1123-1168

Yudovskaya M. A., Kinnaird J. A., Sobolev A. V., Kuzmin D. V., McDonald L. Wilson A. H. (2003) Petrogenesis of the Lower Zone Olivine-Rich Cumulates Beneath the Platreef and Their Correlation with Recognized Occurrences in the Bushveld Complex. Econ Geol 108 (8) : 1923-1952

ZIRCON FROM THE POLYPHASE PROTEROZOIC ALKALINE-ULTRABASIC MASSIF GREMYAKHA-VYRMES: U-PB AGE, MORPHOLOGY, GEOCHEMISTRY AND GENESIS

Sorokhtina N.V.[1], _Belyatsky B.V._[2], _Rodionov N.V._[2], _Lepekhina E.N._[2], _Antonov A.V._[2], _Sergeev S.A._[2]

[1]Vernadsky Institute of Geochemistry and Analytical Chemistry of the Russian Academy of Sciences, Moscow, Russia, nat_sor@rambler.ru

[2]Federal State Budgetary Enterprise 'A. P. Karpinsky Russian Geological Research Institute', Saint-Petersburg, Russia

The Gremyakha–Vyrmes massif (GV) is a largest Proterozoic alkaline–ultramafic polyphase pluton located in the northwestern part of the Kola Peninsula and cuts across the Late Archean gneisses of the Kola–Belomorian Complex. The massif consists of three subsequently formed intrusive rock complexes of ultramafic–mafic rocks, foidolites, alkaline granites and granosyenites. The alkaline metasomatites and carbonatites with Zr-Nb mineralization were evidently formed later than foidolites. They are distributed within extended contact area (of 2 to 10 km) bordering the foidolite body, while carbonatites are considered as separate carbonatite veins.

High magmatic activity within the Kola Peninsula has been long lasted from 2.45 Ga to 380 Ma with the largest alkaline province formation (Table 1). The magmatism at about 1.9 Ga was accompanied by alkaline magmatism also. At this time GV massif was formed, the averaged time interval is 1.97-1.87 Ga. Geochronological data confirm the multistage nature and crystallization of main rock types: for ultramafics and mafics - from 1810 to 1973 Ma, for alkaline rocks – from 1870 to 2070 Ma, and for alkaline granites and syenites – from 1800 to 1940 Ma, carbonatites from 1765 ± 390 to 1945 ± 4 Ma (Savatenkov et al., 1999). The last one could be reflected influence of metamorphism manifested within the Kola Peninsula.

Table 1. The stages of alkaline, alkaline-ultramafic and carbonatite magmatism in the Fennoscandian area (Richard Ernst http://www.largeigneousprovinces.org; Mints & Erickson, 2016)

Age (Ma)/massif	LIPs and tectono-magmatic characteristics
~2500-2700 Siilinjärvi	Lapland LIP plume activity, plate tectonics process, long-lived volcanic-sedimentary belts (Pechenga-Imandra-Varzuga) formation, komatiite and early alkaline magmatism, high-t° metamorphism
~1800-2100 Gremyakha–Vyrmes, Elet'ozero, Soustov, Tiksheozero, Laivajoki, Kortejärvi, Kimozero kimberlites	North-Baltic-2 LIP plume activity, dyke magmatism, layered ultramafic–mafic intrusion, intracraton extension, Svecofennian Ocean spreading, rifting, intracontinental collisional orogeny, alkaline magmatism
~1750-1790 Halpanen, Naantali, Panjavaara	orogeny and high-t° metamorphism, initiation of the E.Fennoscandia subduction, carbonatite and dykes emplacement
~600 Fen, Alnö	Baltic Scandinavian LIP dyke magmatism, carbonatite emplacement
~400 Lovozero, Khibiny, Sokli, Seblyavr, Kovdor etc. (>20 massifs)	Western European LIP plume activity, volcanic activity, East European platform global uplift, rifting, dyke magmatism, Kola Alkaline Province formation

The correspondence in the time of the ore-process and alkaline-ultramafic melt intrusion, carbonatites and metasomatism is a key to creation a genetic model for the massif and rare-metal ore formation, and reconstruction of the geochemical evolution of mantle source. To clarify the age of the crystallization of intrusive and post-magmatic phases we studied the U-Pb system of accessory zircon, which is present in varying amounts in all rock types of the GV. Silica-undersaturation and alkalies-oversaturation of parent melts can lead to the absence of the magmatic zircon or to the low-U zircon crystallization, which limits the possibility of its using for accurate dating of rock formation processes. Moreover, the interaction of the fluid phase dissolved in the alkaline melt with the crystallizing rock-forming and accessory minerals increases diffusion of the parent and daughter elements up to the isotope systems opening and re-equilibrated. This is resulted in the considerable time intervals attributed to the evolution of the alkaline-ultramafic phases of the GV.

The U-Pb isotope systematics and the age of accessory zircon from more than 20 samples representing the main rock varieties of the GV was determined by the secondary-ion microprobe SHRIMP-II. The local chemical composition (microprobe, SIMS) and the morphological features of the grains observed by cathodoluminescence (CL) for the genetic identification of zircon were studied also (fig.1). Zircon of all types of magmatic rocks is characterized by primary growth zoning, but zircon from granites and foidolites contain of many inclusions. The distinctive feature of metasomatic zircon is a reaction rim, signatures of desilicification and matrix destruction, partial dissolution and so on. All of these are results of interaction with highly alkaline and low-silica fluid.

Zircon composition changes from U-, Hf-poor, zoned, unaltered stoichiometric grains to U-, Th-, Hf-, HREE-, Fe-, Ca-, Y-rich hydrated zones. Metamict parts of some zircon grain are depleted in Si and Zr, cations' sum is lowered to 80%. The studied zircons are characterized by sharp geochemistry diversity reflected specific composition of the parent magmas. Gabbro zircons differ by mid content of U 150-1000 ppm and in some cases up to 4000 ppm, high Th - from 100 to 600 and in some cases is up to 5000 ppm, and with typical for magmatic zircon Th/U ratio within 0.4-1.4 and share of common Pb <0.3%. Foidolite zircons are low-U 1-3 (rarely up to 40 ppm), high - Th 200-2000 ppm with Th/U ratio

from 200 to 3000 (sometimes ~30-40), and common Pb share is 0.1-3%. Metasomatic zircon from contact zone between carbonatites and albitites is also low-U 4-40 ppm, high Th 10-2000 ppm and Th/U 2-50 with common Pb at 0.1-1.5%. In metasomatic zircons there are a lot of inherited grains from gabbros and foidolites with a corresponding chemistry and morphology, nevertheless the new-formed grains are low to mid U: 2-200 ppm (rarely up to 600 ppm), mid to high Th: 10-1000 ppm, and high Th/U 2-300, and common Pb at: 0.1-5%.
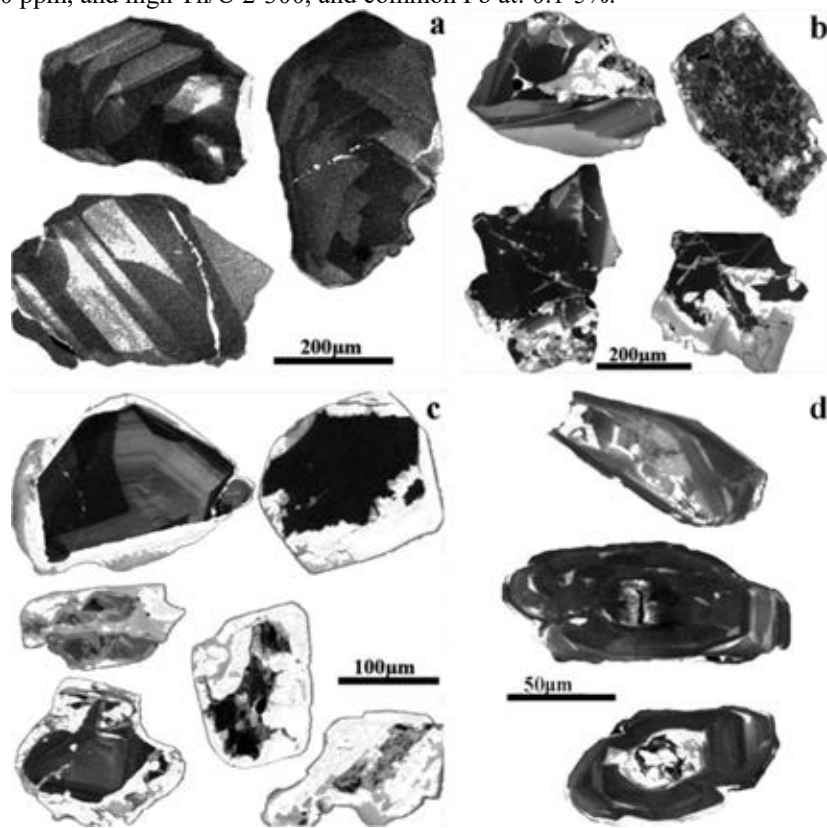
Fig. 1. Cathodoluminescence images of studied zircons from main rock varieties of GV: a – fragments of gabbro zircon grains with growth zoning; b – foidolite zircon with numerous inclusions, corroded faces and irregular zoning; c – fragments of metasomatic zircon grains with abundant inclusions and bright CL rim reflecting zone of interaction with fluid phase, reaction shell and reworked matrix of inherited zircon from transformated rocks; d – granitoid zircon crystals with bipyramid and prism faces and growth zoning.

Nevertheless, for the main intrusive phases we got the U-Pb age estimations, which are determined by concordant zircon data-points from two or more samples of each rock variety. Thus, the weighted average gabbro zircon age (5 samples) is 1981.7 ± 5.9 Ma, and for 4 foidolite samples is 1894 ± 12 Ma (Fig.2). The time of carbonatite intrusion, metasomatite formation and initiation of rare-metal mineralization are not so obvious. The results of zircon U-Pb analysis completely reflect the origin of the metasomatites – we get the time of the protolith formation on which develops certain metasomatites (aegirinites, albitites). We believe that rare-metal albitites and aegirinites, like contact metasomatic rocks, were formed as a result of the interaction of residual fluid-saturated melt, in composition close to carbonatites, with earlier foidolites. The presence of carbonatites among metasomatites suggests that the metasomatism is associated with carbonatite intrusion. Possible carbonatites were the late derivatives of alkaline melt, which was the parent one for foidolites. The carbonatite intrusion in combination with a complex tectonic history caused extensive metasomatism of host ultramafics and alkaline rocks (mainly foidolitic composition) of the central part of the massif. Carbonatites as fluid-saturated systems could be a source and active carrier of U, Th, Zr, Nb and REE, and albitites and aegirinites act as a geochemical barrier within which mineralization formed. The irregular distribution of rare metals in metasomatites and carbonatites proves the multistage ore formation. However, based on coincidence of zircon U-Pb ages of metasomatites of different composition, and close age estimations for pyrochlore and zircon from carbonatite and ore-bearing albitite we suggest this evolution step was no later than 1886±10 Ma (Fig.3). The coincidence of the ages makes it possible to establish the time of carbonatite formation, which is close, but does not coincide with the crystallization time of the foidolites, again confirming the genetic connection of these rocks.

Zircon from main phase of alkaline granites reflects varying degrees of transformation under the influence of post magmatic fluid and characterized by a higher Th (up to 0.5%) and U (up to 0.4%), Th/U>1 (up to 9) and an increased up to 13% of common Pb, which is mainly due to the porous matrix of the grains. Such geochemical characteristics of zircon are resulted in increased errors in the determination of radiogenic Pb and Pb*/U ratios, and to significant shifts of data-points on the diagrams relative to concordia, and to the great uncertainty of discordia-age esimations. Zircon in granite melts with relatively low melting temperatures, trapped from the enclosing rocks during the intrusion or transport of the melts, or contaminated within igneous chamber, often retains not only their typical crystal forms but also isotope-geochemical system undisturbed. And as a result for the samples of the studied alkaline granites, zircons captured from gabbroids are often observed, which differ from the granitic ones according to morphological characteristics and geochemistry, and the age determined by U-Pb systems of such zircons will reflect the crystallization time of the host gabbroids, but do not granitic melt intrusions. This is clearly observed in the contact zones where the xenoliths of the host gabbroids are often found in granites. Grains with the signs of melting and dissolution and absence of crystal faces so

typical for zircons crystallizing from granitoid melts characterize inherited zircon. The calculated U-Pb zircon age of 3 samples from studied 5 completely coincides with the age estimations obtained for gabbros. However, for two samples, granite-aplite and the main intrusive phase granite, zircon is characterized by moderate U (50-500 ppm) and Th (30-120 ppm) and common Pb less than <1 % (^{206}Pb), that allows to determine the concordant age estimations coincided for these samples within the errors 1868.6 ± 7.7 and 1871.1 ± 8.8 Ma, respectively (Fig.2d). Thus the alkaline granites were the latest GV magmatic phases and completed the magmatic development of the massif, which began 100-150 m.y. before the intrusion and crystallization of the gabbo-peridotite phase.
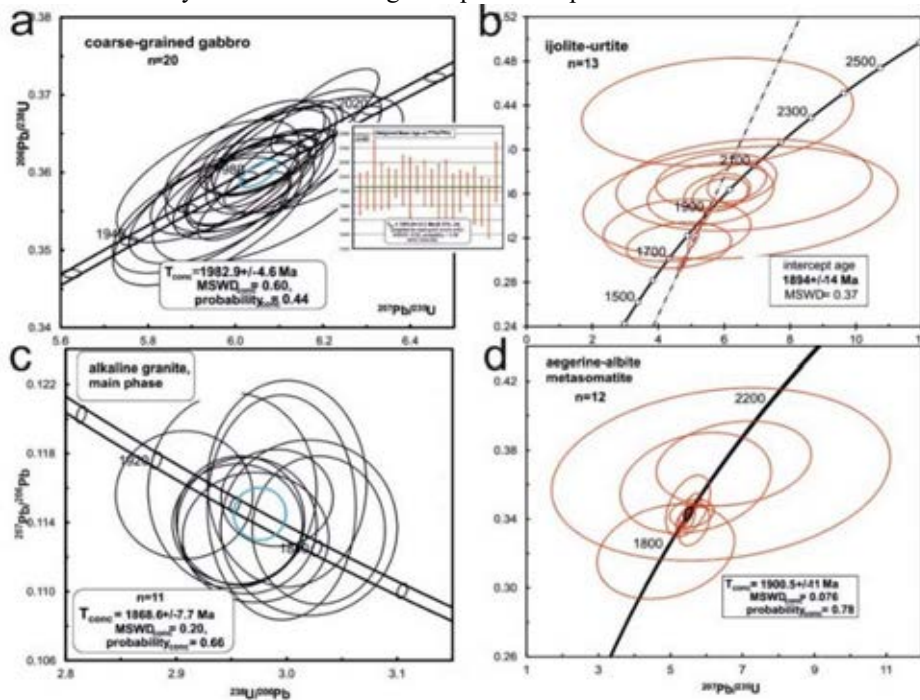
Fig. 2. U-Pb concordia diagrams for zircon from the main rock varieties of the Gremyakha-Vyrmes massif. a – concordant cluster of the data-points for zircon from gabbro, weighted mean age on 5 samples corresponds to 1981.7 ± 5.9 Ma; b – discordia line for 13 data-points of zircon from foidolite, the weighted average age of zircon from 4 samples is: 1894 ± 12 Ma; c – concordant data-points for zircon from main phase of alkaline granite; d – concordant age cluster for zircon from aegirine-albite metasomatite samples.
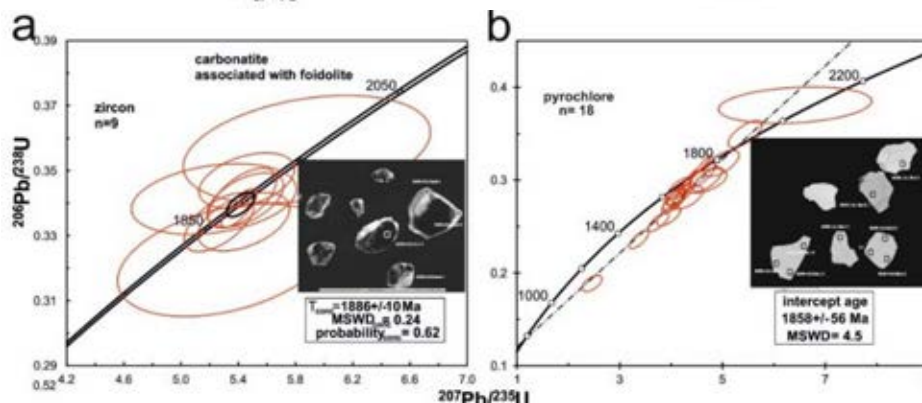
Fig. 3. U-Pb concordia diagrams for zircon (a) and pyrochlore (b) from carbonatite associated with foidolite.

The rare-metal ore mineralization within the massif is recorded by various isotope systems at 1760-1740 Ma, but this reflects rather a stage of secondary enrichment with the recrystallization of ore minerals under the influence of fluid. The development of the all ore-magmatic system within the GV was a long-term process and accompanied by the successive intrusions of gabbroids and foidolites separated in time. However, the mantle sources of their melts had similar isotope-geochemical characteristics, which suggest a genetic relationship of these intrusions - the formation of mantle melts could originate from the evolved mantle source, and spatial merging in a single massif is due to tectonic factors, increased permeability of this lithosphere and long-lived thermal activity of the upper mantle.

References:

Ernst R., http://www.largeigneousprovinces.org

Mints, MV, Erickson, PG (2016) Secular changes in relationships between plate-tectonic and mantle-plume engendered processes during Precambrian time // Geodyn. & Tecton. 7. 2. 173-232.

Savatenkov, VM, Pushkarev, YuD, Sergeev, AV, Sulimov, RB (1999) Carbonatites as indicators of new ore specialization of the Gremyakha–Vyrmes Massif, Russia // Geol. Ore Deposits. 41. 5. 409–413.

GENETIC NATURE OF BLUE SAPPHIRES IN SYENITE PEGMATITES FROM ILMEN MOUNTAINS, SOUTH URALS OF RUSSIA: EVIDENCE FROM EMPA, LA-ICP-MS, AND RAMAN SPECTROSCOPY

Sorokina E.S.[1], Nishanbaev T.P.[2], Nikandrov S.N.[2]

[1]Vernadsky Institute of Geochemistry and Analytical Chemistry of the Russian Academy of Sciences, Moscow, Russia, elensorokina@mail.ru
[2]Ilmen State Nature Reserve, Miass, Russia

Blue sapphire – natural α-modification of Al_2O_3 colored by different concentrations of Ti and Fe – is common found in placer deposits related to interplate basaltic fields. Discovery of mineral *in-situ* within the host rocks is significantly rare.

Blue corundum in syenite pegmatites of llmen Mountais was known since the beginning of 19th century (Barbot-de-Marni 1828, Anosov 1829). In different time, Ilmen corundum has been characterized by Belyankin (1915), Rusakov (1927), Ustinova (1940), Makarochkin and Makarochkina (1955) etc. Meanwhile to date, there are virtually no detailed studies have been done on it from mineralogical and geochemical standpoints. For this work, we characterized geochemistry of blue sapphires and studied their solid and fluid inclusions for better understanding the processes influenced on the formation of corundum mineralization.

At the Ilmen Mountains, located in the South Urals of Russia, blue-colored corundum megacrysts sized up to 6 cm in length are found *in-situ* within syenite pegmatites in mines 298, 299, 311, and 349. Pegmatite veins hosting a mineral belong to the exo-contact area of the main intrusive body of alkaline rocks called Ilmenogorsky massif. The occurrence is situated inside of the Ilmen State Reserve and its commercial exploration is forbidden (Sorokina et al. 2016a, 2016b).

Electron micro-probe analysis (EMPA) showed lower Fe content found in sapphires from mines 298 and 349 (2355-3275 ppmw) and higher content in mines 299 and 311 (5412– 6653 ppmw) (Sorokina et al. 2017). Ga varied from 175 - 368 ppmw and V values 41 – 73 ppmw were detected on the measured samples from all mines. Mg, Ti, and Cr were below EMPA detection limit. Ratio 10000Ga/Al is above 2.7, which is in the range of magmatic sapphires (Peucat et al. 2007). Laser ablation – Inductively coupled plasma – Mass spectrometry (LA-ICP-MS) data are in accordance with those of EMPA. By LA-ICP-MS measurements, Ti reached 180 ppmw in one sample caused likely to the presence of ilmenite, but, for all other measurements, it was < 35 ppmw. Cr was below 9.5 ppmw and Mg was below 8 ppmw. Li, Be, and B were close to the detection limit. The Ga/Mg ratio is >29, Fe/Mg> 420, Cr/Ga<0.075, and Fe/Ti>28 (Sorokina et al. 2016a, 2017) all in the range of magmatic sapphires (Peucat et al. 2007). The measurements obtained on the studied samples by using a statistical model based on the calculation of discriminating factors from the concentration of oxides in corundum by Giuliani et al. (2014) were plotted out on the area with sapphires of plumasitic origin (Sorokina et al. 2017). Using the geochemical diagram Fe_2O_3 - Cr_2O_3 - MgO - V_2O_3 *vs.* Fe_2O_3 + TiO_2 + Ga_2O_3 by Giuliani et al. (2014), the samples were plotted in the area with syenitic sapphire and more in the metasomatic corundum area (Sorokina et al. 2017).

Formation of blue corundum in syenite pegmatites occurred during at least 2 stages. The 1st stage is magmatic, where corundum is crystallized in association with columbite, orthoclase, and ± microcline-perthite. It is related with the reaction following the later waves of emanation of syenitic magma containing much less silica and subsequent destabilization of nepheline by the reaction:

$3(K,Na)AlSiO_4 \rightarrow (m\ NaAlSi_3O_8;\ n\ KAlSi_3O_8) + Al_2O_3$ (Sorokina et al. 2016a, 2017).
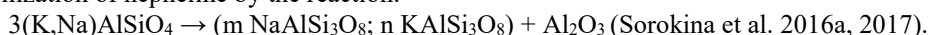
The 2nd stage is metasomatic, where diaspore and muscovite mica were formed by the reaction:

$Al_2O_3 + K(AlSi_3O_8) + H_2O \leftrightarrow KAl(AlSi_3O_{10})(OH)$ (Sorokina et al., 2016a 2017).
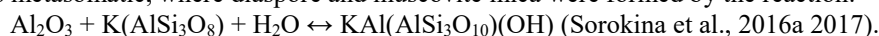
By using of a Raman spectroscopy (RS), solid phases trapped in pseudo-secondary fluid inclusions (FI) have been determined as diaspore (Sorokina et al. 2016a, 2016b). Fermi doublet for the vapor and liquid phases at 1282.9 - 1283.2 and 1387.2 - 1387.6 cm^{-1} both determined as $^{12}CO_2$ with less intense symmetrical "hot bands" at approximately 1264 and 1408 cm^{-1} and a small band at 1370 cm^{-1} due to $^{13}CO_2$ (Sorokina et al. 2016a, 2016b). The CO_2 homogenization temperature occurred in the liquid phase at 30.1° - 30.7°C. By freezing of FI, final melting temperature of solid CO_2 determined at -57.4 to -63.8°C (Sorokina et al. 2016a, 2016b). RS acquired in the 2000–4000 cm^{-1} range did not show H_2O, CH_4, or N_2-related bands. By geothermo-barometric reconstructions, formation of blue sapphires occurred at PT-path from around 730 to 590 ºC and pressure at around 2.9 to 1.9 kbar in metasomatic condition of CO_2-fluid environment (Sorokina et al., 2017).

Syngenetic inclusions within corundum from Ilmen Mountains were identified as ferrocolumbite $Fe^{2+}_{0.80-0.81}Mn_{0.16-0.17}Nb_{1.92}O_6$, zircon $ZrSiO_4$ with 0.8 wt.% of HfO_2, and alkali feldspar group minerals $(K, Na)Si_3O_8$ and are typical for mineral assemblages in corundum syenite pegmatites (Sorokina et al., 2017). Protegenetic monazite-Ce $Ce_{0.42-0.43}La_{0.19-0.20}Nd_{0.12}Th_{0.11-0.12}(P_{0.86-0.87}O_4)$ and muscovite mica $K_{0.62-0.87}Al_{2.98-3.08}Si_{2.99-3.03}O_{10}(OH)_{1.8}F_{0-0.08}$, exsolved micron-sized needles of ilmenite $K_{0.62-0.87}Al_{2.98-3.08}Si_{2.99-3.03}O_{10}(OH)_{1.8}F_{0-0.08}$, and 500 nm grains of uraninite UO_2 with 0.19 *apfu* of Zr were found as well (Sorokina et al., 2017).

Ilmen blue sapphires have many similar mineralogical and geochemical features with those found in secondary placer deposits of interplate basaltic fields in Australia, Cambodia, and Russia's Far East. Further studies are necessary for better understanding the genetic linkages between these deposits and geological processes occurred during their formation.

References:

Anosov PP (1820) About Uralian corundum. Mining Journal 1: 131-140 (in Russian)

Barbot-de-Marni PN (1828) About a new deposit of zircon, tantalite and corundum. Mining Journal 3: 171 - 172 (in Russian)

Belyankin DS (1915) Petrographic map of Ilmen Mountains. Proceedings of Radium expedition of the Academy of Sciences 3: 1 – 58 (in Russian)

Giuliani G, Caumon G, Rakotosamizanany S, Ohnenstetter D, Rakototondrazafy M (2014) Classification chimique des corindons par analyse factorielle discriminante: application à la typologie des gisements de rubis et saphirs. Revue de Gemmologie 188: 14 – 22

Makarochkin BA, Makarochkina MS (1955) Ishkul mines. Unpubl Rpt, Ural branch RAS, Ilmen State reserve, Miass (in Russian)

Peucat JJ, Ruffault P, Fritch E, Bouhnik-Le-Coz M, Simonet C, Lasnier B (2007) Ga/Mg ratio as a new geochemical tool to differentiate magmatic from metamorphic blue sapphires. Lithos 98: 261–274

Rusakov MP (1927) Materials for the description of corundum deposits in Ilmen Mountains. Materials on General and Applied Geology 71: 1 – 68 (in Russian)

Sorokina ES, Karampelas S, Nishanbaev TP, Nikandrov SN, Muyal J (2016a) Blue sapphires in the syenite pegmatites from Ilmen Mountains, South Urals. In: Proceedings of International Geological Congress general meeting, Cape Town. Paper No 4013

Sorokina ES, Koivula JI, Muyal J, Karampelas S (2016b) Multiphase fluid inclusions in blue sapphires from the Ilmen Mountains, Southern Urals. Gems Gemol 52: 209 – 211

Sorokina ES, Karampelas S, Nishanbaev TP, Nikandrov SN, Semiannikov BS (2017) Blue sapphire megacrysts in syenite pegmatites from Ilmen Mountains, South Urals (Russia): Advances in understanding of their genetic nature. Can Mineral (submitted)

Ustinova TI (1940) Mines of north and middle parts of Ilmen reserve. Unpubl Rpt, Ural branch RAS, Ilmen state reserve, Miass (in Russian)

THE PETROCHEMICAL STUDIES ON THE GRANITES OF NARSAPUR, MEDAK DISTRICT, TELANGANA STATE, INDIA

Srinivas M., Ningam N.

Osmania University, Hyderabad, India, vaishnavi111@yahoo.com

Granitic suite of rocks find a widespread distribution in the continental areas particularly the Precambrian shields and quite a few younger orogenic belts. However, whether granitic suite of rocks shouldbe viewed as products of partial melts derived directly from the mantle, or as products of magmatic differentiation of silicate melts and, the relationships among silicate rocks still awaits a convincing explanation.

These rocks representing a facet of acidic magmatism, and bordering the western and eastern sides of the intracratonic Mesoproterozoic Cuddapah basin, a part of Eastern Dharwar Craton representing Precambrian rocks in Peninsular India. The uniqueness of this suite is that it is association with felspathoidal syenites, lamprophyres, syenites on one hand and gabbros on the other hand corresponding to the alkaline and basic magmatism on the eastern side and associated with the kimberlites on the western side of the Cuddapah basin

It is a well known fact that Proterozoic granite magmatism has played a significant role in the evolution, growth and stabilization of the Precambrian continental crust world over. The continental crust evolution in the Indian shield appears to have started around the Mid-Archaean and completed by the Paleo-Proterozoic. Eastern fragments of India, Australia and Antarctica represent discrete crustal blocks that were a part of the Proterozoic assembly of the Gondwana (McWilliams, 1981).The area comprising the eastern margin of the Proterozoic Cuddapah basin, the Precambrian NSB and EGGB terrane in Dharwarcraton of eastern Gondwana witnessed wide spread rift related mafic-alkaline magmatism; anorogenic felsic magmatism and emplacement of 100 sq km slice of NW-SE trending cumulus gabbro-sheeted dyke complex at Kandra (SeshaSai, 2009) during the Paleo-Mesoproterozoic times; and, hence, represent a complex orogen with both juvenile accreted components and exotic microcratons with terrane lifespan of 100 Ma.

The Narsapur area, (78°05'E- 78°00'E and 17°35' N -18° 00'N) in the Medak district of Telangana State , is spread over an area of 160km^2 , is dominated by granitic suite of rocks that are emplaced in a basement complex comprising of amphibolites, and unclassified crystallines.

Petrographically they vary in composition from tonalite and quartz diorite through granodiorite, adamellite and granite to Alkali feldspar granite. On the basis of chemistry these granitic rocks are distinguished as potash-rich granites, calc-alkaline granites and tonalite-quartz granite variants. By far, the potash-rich granites (alkali-feldspar granites) and calc-alkaline granites (granodiorites, quartz-monzodiorites, granites and adamellites) are predominant. Tonalites and

quartz diorites occur as xenoliths as well as local variants that are subjected to local deformation. Alkali-feldspar granite along with the quartz syenite appears to have intruded and truncated all the other granitic units which suggest that they are the last of the granitic emplacements. Dolerite and pegmatite dykes represent the final stages of the emplacement.

The granitic suite of rocks in the Narsapur area, Medak district is emplaced into the older amphibolites, peninsular gneissic complex that is constituted by epidote-hornblende-gneisses and biotite-gneisses of the Archaean age. The granites are marked by a simple mineralogy consisting predominant of felsic minerals like K-feldspar (represented by microcline perthite), plagioclase and quartz (in the order of decreasing abundance). Mafic minerals are amphibole, biotite and garnet. Presence of discrete plagioclase grains in substantial proportions clearly demonstrates subsolvus conditions of crystallisation of parental magma.

There is enough number of clues provided in the petrography and that fractional crystallisation of the early anhydrous liquidus phases like K-feldspar, plagioclase, amphibole and biotite had increased the water a H_2O activity in the evolving magma that led to stabilization of amphibole.

Though the granites of Narsapur area have abundant amphibole and biotite demonstrating that they are crystallised from a melt having significant amounts of water. Ti- bearing mineral phases like sphene appears to have crystallised from a melt with sufficiently high Ca/Al ratio and a relatively oxidized rock is formed from a H_2O- rich melt. Thus several lines of evidences emphasise that the granites of Narsapur have experienced enrichment of water activity.

The Al_2O_3 / ($CaO+Na_2O+K_2O$) ratios of all the units in the three suites of granites exceed 1.0, and hence they are *peraluminous* granites. The granites have an initial calc-alkaline signature with a low iron enrichment trend and they are presumed to have originated from metasomatised K-and LILE-enriched lithospheric mantle in a subduction zone. The syenites of the Narsapur have a low Ti values similar to the subduction related magmas.

From the geochemical characteristics it is surmised that a shoshonitic magma (generated from a subduction) modified subcontinental lithospheric mantle having phlogopite-spinel composition has undergone low degree of partial melting under thickened continental crust and the melt has utilised the deep seated lithospheric weak planes as channels for its emplacement into the mid-crustal levels.

The chondrite normalised REE patterns of the granites of Narsapur are marked by high LREE/HREE ratio and display LREE-enriched and HREE-depleted patterns with a near parallel to subparalell trends hinting at the fractional crystallisation process. The Eu positive anomaly demonstrate the role of feldspar in their genesis and is also attributed to the presence of hornblende, and minor phases like garnet and sphene in the source. In view of the above, it is postulated that the granites of the Narsapur area appear to have evolved by fractional crystallisation aided by the low degree of partial melting of the upper mantle and coupled with the involvement of the assimilation of the lower crustal or upper mantle regions to produce granites during the Archaean period.

PETROGENESIS OF A RECENTLY DISCOVERED KIMBERLITE PIPE ASSOCIATED WITH CARBONATITE AT KHADERPET, WAJRAKARUR FIELD, INDIA

Srinivas M., Phani P.R.C.
Osmania University, Hyderabad, India, madabhooshi111@gmail.com

In recent years, there has been a great impetus in the exploration of kimberlites in India. The cratonic part of Indian subcontinent forms a favourable ground for kimberlite exploration (e.g., Chalapathi Rao et al., 2016). With the advent of liberalised economic policies by the government of India two decades ago, many international companies have invested huge exploration budgets and successfully discovered new outcropping kimberlites. Out of all the kimberlite fields in India, the Wajrakarur kimberlite field (WKF) has witnessed highest number of kimberlite discoveries in the recent past. Petrogenesis of one suchrecently discovered kimberlite pipe occurring at Khaderpetwhere India's first kimberlite occurrence associated with carbonatite has been discovered by the Rio Tinto group (CRAEI, 2004, Smith et al., 2013), has been attempted here using whole rock geochemistry.

The Khaderpet pipe is a chloritised kimberlite-granite breccia hosted by soviticcarbonatite. This kimberlite pipe displays intense metasomatic alteration in the wall rock granitoids resulting in deeply reddened feldspars by the injection of by hematite from metasomatism and appears to be an ultramafic lamprophyre rather than a typical kimberlite or lamproite(Smith et al., 2013). The Khaderpet pipe is an intensely altered kimberlite showing incipient pelletal lapilli indicating diatreme facies(Smith et al., 2013). Smith et al. (2013) have demonstrated difficulties in classifying altered and country rock contaminated intrusives from the WKF and adjacent kimberlite fields into strictly defined rock-types based on petrography and geochemistry. Three to four carapaces like outcrops of kimberlite- granite beccia have been located in the field. The sovite-carbonatite out crop could not be traced out by the authors and hence only chloritised kimberlite-granite breccia with varied proportions of granititc clasts (10-50%) has been sampled and analysed in this study.

In the present study, ten samples of kimberlite exposed in an old well cutting at Khaderpet have been collected and analysed for major, trace and rare earth elements. The samples appear to be silica saturated (SiO_2: 43.8- 61.8 wt.%), $Na_2O > K_2O$ (0.42- 4.57 and 0.82- 3.69 wt.% respectively), CaO (1.087- 13.56 wt.%), MgO (4.4- 14.56 wt.%), P_2O_5 (0.19- 0.51 wt.%), TiO_2 (0.45- 0.91 wt.%). The compatible trace element concentrations are, Sc (6-11 ppm), V (64- 139 ppm), Cr (27- 405 ppm), Co (18-71 ppm) and Ni (62- 1120 ppm). Among the incompatible trace elements, concentrtionsof Large Ion lithofilic elements (LILE) are, Ba (211- 911-xxx ppm), Rb (31.2- 101.1 ppm), Sr (212- 412 ppm) and Ce (93.5- 161 ppm) while the High Field Strength Elements (HFSE) concetrations are, Zr (62- 162 ppm), Nb (9- 63.4 ppm), Hf (1- 3.1 ppm), Th (10.1- 21.8 ppm) and U (2.8- 10.1 ppm). The average REE concentrations are observed

to be lower than those of the WKF, south African and world kimberlites, which might be attributed to the high degree of crustal contamination.

The Clement's (1982) crustal contamination index (C.I.) values for the Khaderpet samples are extremely higher (3.78- 11.13) than the kimberlites of WKF, south Africa and world. It is clearly evident that the samples which have more kimberlitic material and less crustal xenolith clasts have lowest C.I. values. At the same time, samples with less proportion of crustal granitoid clasts possess low SiO_2 content. The Mg# for Khaderpet pipe ranges from 55 to 80, well within the range of WKF and south African kimberlites. The Khaderpet samples show a garnet-lherzolite source composition in the binary plot involving ratios of Zr/Nb versus La/Y (Fig.1, Sobolev and Shimizu, 1993).
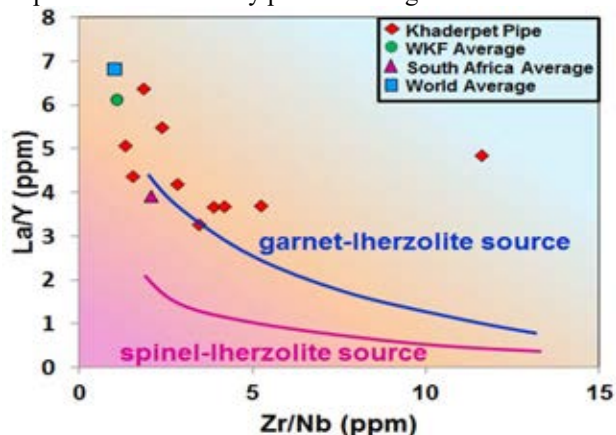
Fig. 1.Descrimination plot between Zr/Nb versus La/Y ratios.Trajectories for source regions are after experimental studies of Sobolev and Shimizu (1993). Reference data: WKF (Srinivas Choudary et al., 2007), south Africa (le Roex et al., 2003) and world average (Muramatsu, 1983).
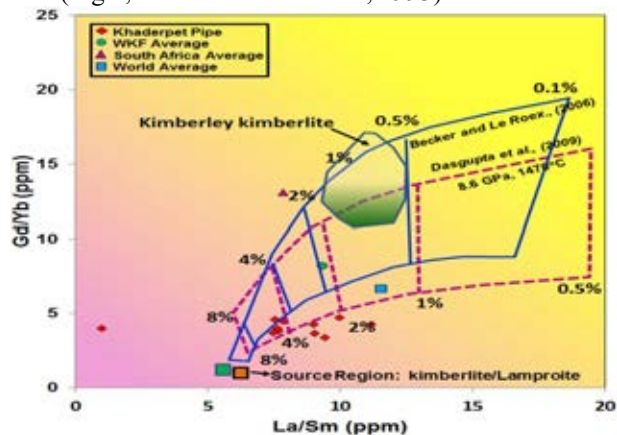
Fig. 2.Binary variation diagram with La/Sm and Gd/Yb ratios for the new pipe in comparison withaverage values of the WKF, south African and world kimberlites. Curves drawn indicate melting trajectories of kimberlites and orangeites source regions with numbers showing degree of melting. Meltingtrajectories: Solid blue- partition coefficients from Becker and le Roex (2006) and Pink dashed- experimentally calculated bulk peridotite/ melt partition coefficients at 8.6 GPa and 1470°C(Dasgupet et al., 2009). Source region and field for Kimberley kimberlites from Becker and leRoex (2006). Adopted from Dongre et al., (2016).Reference data as in Fig.1.
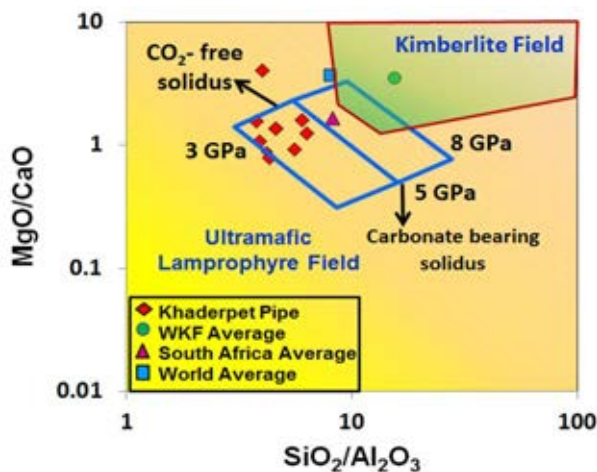
Fig.3. Binary plot between SiO_2/Al_2O_3 and MgO/CaO ratios showing compositions of melts generated in equilibrium with garnet lherzolite in the CMAS-CO_2 system for kimberlites and ultamaficlamprphyres (Rock, 1991). Field for kimberlites from Ilupin and Lutz, 1971). Adopted from Gudfinnson and Presnall (2005).Reference data as in Fig.1.
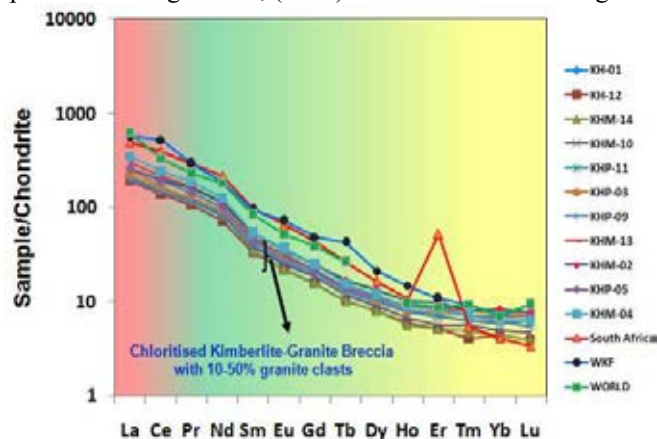
Fig. 4. Chondrite normalized (Sun and McDonough, 1989) plot for Khaderpet samples in comparison with the average values of the WKF, south frica and world kkimberlties.Reference data as in Fig.1.

In the binary plot of La/Sm and Gd/Yb ratios, the Khaderpet kimberlite shows higher degree of partial melting (from 2% to >8%) when copared to average values of Wajrakarur, south African and world kimberlite (Fig.2, Becker and le Roex, 2006). The higher degree of partial melting is attributed due tothe presence of unseparable granitic clasts in the samples. Similar degree of partial melting is alsonoticedwhen plotted with melting trajectories calculated from partition coefficients at 8.6 GPa and 1470°C (Fig.2, Dasgupta et al., 2009).
From the binary plot between SiO_2/Al_2O_3 versus MgO/CaO ratios (Fig.3, Gudfinnson and Presnall, 2005), it can be envisaged that the Khaderpet pipe samples plot in the Ultramafic Lamprophyre field (Fig.3). The chondrite normalized

(Sun and McDonough, 1989) plot (Fig. 4), the Khaderpet samplesdisplay no anomalous concentration of the REEs. The LREE trend of Khaderpet samples similar to the WKF kimberlites indicates similar source region and parent magma composition.

This work forms a part of Ph.D. dissertation of the second author.

References:

Becker M. and Le Roex, A.P. (2006) Geochemistry of South African on-and offcraton Group-I and II kimberlites; petrogenesis and source region evaluation. Journal of Petrology, 47: 673-703.

Chalapathi Rao, N V, Dongre AN, Wu FY, Lehmann B, (2016) A Late Cretaceous (ca. 90 Ma) 8 kimberlite event in southern India: implication for sub-continental lithospheric mantle evolution and 9 diamond exploration Gondwana Research. http://dx.doi.org/10.1016/j.gr.2015.06.006

Clement C R (1982) A comparative geological study of some major kimberlite pipes in northern Cape and Orange Free State. Ph.D. Thesis (2 Volumes), University of Cape Town.

CRAEI, (2004) Final Report of all Exploration for Diamond and Other Mineral Commodities Completed in the Anantapur and Kurnool District of Andhra Pradesh by CRAE(I), during the Term of RP Nos. GOMS No.24- 27s, from January 2001 to February 2004. CRA Exploration (India) Pvt. Limited (Rio Tinto Group) (51 p.). http://www.ibm.nic.in/writereaddata/files/07112014113446APR_14_to_17.pdf

Dasgupta R, Hirschman MM, McDonough W F, Spiegelman M, Withers A C, (2009) Trace element partitioning between garnet lherzolite and carbonatite at 6.6 and 8.6 GPa with applications to the geochemistry of the mantle and of mantle-derived melts. Chemical Geology, 262: 57-77.

Dongre A N, Chalapathi Rao, N V, Vijolen, K S, Lehmann B, (2016) Petrology, genesis and geodynamic implication of the Mesoproterozoic- Late Cretaceous Timmasamudram kimberlite cluster, Wajrakarur fiels, Eastern Dharwar Craton, southern India. Geoscience Frntiers (In Press), 1-13.), http://dx.doi.org/10.1016/j.gsf.2016.05.007.

Gudfinnson G H, and Presnall D C, (2005) Continuous gradations among primary carbonatitic, kimberlitic, melilititic, basaltic, picritic and komatiitic melts in equilibrium with garnet lherzolite at 3–8 GPa. Journal of Petrology, 46:1645–1659.

Ilupin I P and Lutz B G (1971)The chemical composition of kimberlite and questions on the origin of kimberlite magmas. SovetskayaGeologiya 6, 61–73 (in Russian).

leRoex AP, Bell DR and Davis P (2003) Petrogenesis of Group- I kimberlites from Kimberley, South Africa : Evidence from Bulk-rock geochemistry, Journal of Petrology, 44: 2261- 2286. doi:10.1093/petrology/egg077.

Muramatsu Y (1983)Geochemical investigations of kimberlites from the Kimberley area, South Africa. Geochem. Jour..17: 71-86.

Rock NMS (1991) Lamprophyres, B.lackie, Glasgow, U.K.

Shaikh A M, Patel S C, Ravi S, Behera D, Pruseth K L (2016) Mineralogy of the TK1 and TK4 'kimberlites' in the Timmasamudram cluster, Wajrakarur Kimberlite Fiels, India: Implications for lamproite magmatism in a field of kimberlites and ultramafic lamprophyres. Chemical Geology, In Press, 23 p http://dx.doi.org/10.1016/j.chemgeo.2016.10.030

Smith CB, Haggerty S E, Chatterjee B, Beard A, Townend R, 2013. Kimberlite, lamproite, ultramafic lamprophyre, and Carbonatite relationships on the Dharwar Craton, India; an example from the Khaderpet pipe, a diamondiferous ultramafic with associated carbonatiteintrusion. Lithos, 182-183: 102- 113.

Srinivas Choudary V, Rau T K, Bhaskar Rao K S, Sridhar M, Sinha K K, 2007. Timmasamudram kimberlite cluster,Wajrakarur Kimberlite Field, Anantapur district, Andhra Pradesh. J. Geol. Soc. India 69:597- 609.

Sun S-s and McDonough W F (1989): Chemical and Isotopic systematics of oceanic basalts: implications for mantle compositions and processes. In Saunders A.D. and Norry M.J., Magmatism in the Oceanic Basins, Geol.Soc. Spec. Pub. No. 42: 313- 345.

ULTRAMAFIC, ALKALINE AND CARBONATITIC SUITE OF ROCKS FROM PAKKANADU-MULAKKADU, NORTHERN TAMIL NADU, INDIA

Srinivas M., Rajendra Prasad K., Sreenu K.

Osmania University, Hyderabad, India, vaishnavi111@yahoo.com

Alkaline complexes, alkaline-carbonatite complexes, and complexes devoid of syenites, and yet related to alkaline magmatism, with or without a significant component of ultramafic rocks do find a widespread distribution in southern granulite terrain (SGT), India. A close scrutiny of these complexes in the backdrop of regional tectonic set-up, with a holistic approach by integrating geological, geophysical and geochemical data by earlier workers has provided an impetus to classify the aforesaid complexes based on geotectonic environments into three groups (Gopalakrishnan, 1996; Gopalakrishnan and Subramanian 2007; Gopalakrishnan et al 1990, 1991, 2002).

Group I: Dominant alkali granite complexes that are associated with a minor or insignificant component of syenite and /or carbonatite; eg. Chengannur, Peralimala, Ambalvayal etc

Group II: Constituted by nepheline syenite complexes , that are neither associated with carbonatites nor ultramafic rocks; eg. Pikkili, and Sivamalai.

Group III: Represented by syenites that are in association with non-alkaline ultramafics and carbonatites; eg. Pakkanadu, Samalpatti, Sevattur and Elagiri.

The ultramafic alkaline carbonatite body under investigation – the Pakkanadu – Mulakkadu complex, belongs to Group III. The suite of rocks composing Group III is located in northern Tamil Nadu; these intrusions are located within the Dharmapuri (suture) rift zone (DSRZ) that is bounded by two sub-parallel lineaments trending in the NE-SW direction..

The ultramafic- alkaline-carbonatite (UMAC) complex at Pakkanadu-Mulakkadu, is a structurally controlled, unmetamorphosed and undeformed plutonic complex, emplaced into the epidote -hornblende- biotite gneisses of Archaean age, defines the SW extremity of the Dharmapuri Suture Rift Zone in the northern part of Tamilnadu, that is traversed by a set of deep seated faults and fracture systems trending in E-W, NNE-SSW, ENE-WSW and NE-SW directions.

The complex at Pakkanadu – Mulakkadu, happens to be a part of the DSRZ that has a close proximity to the Pandyan Mobile Belt (PMB) of Southern Granulite Terrain that has striking similarities with the Paleoproterozoic Limpopo mobile belt of southern Africa that occurs between the Zimbabwe craton in the north and the Kaapvaal craton in the south. Ramakrishnan (2003) views that Pandyan Mobile belt assume greater significance in the light of reconstruction of the Eastern Gondwana in view of its strong geological linkage with Eastern Antartica, Madagascar and Sri Lanka.

The ultramafic alkaline carbonatite complex of Pakkanadu-Mulakkadu is dominated by syenite, dunite- pyroxenite and carbonatites (in that order), and is invaded by a veins and dykes of albitite and pegmatites of syenitic composition. Clear cut intrusive contact, absence of gradational and lithological variations between the dunite – pyroxenite – syenite - carbonatites imply that the rocks have evolved independently at the present level of erosion.

While the dunites are highly altered, the pyroxenites are fresh and both coarse and fine grained, exhibiting equigranular to inequigranular, hypidiomorphic textures with interlocking and triple junctions grain contacts implying equilibrium crystal growth. Coarse grained clinopyroxene grains exhibit features like exsolution lamellae and Fe-Ti oxides along the cleavage planes suggesting that they underwent slow cooling.

Geochemically the pyroxenites of PK-MK are ultrabasic (SiO_2 = 39.50 -- 40.72 wt%, and ultramafic (MgO= 24.6 – 25.1 wt %), olivine normative in character and carry a reasonably high content of Al_2O_3 (4.36-8.34 wt.%,), $Fe_2O_3^T$ (7.62 -15.30 wt%) and CaO (6.66-1.24%) and lower concentration of MnO, P_2O_5 , TiO_2 , Na_2O and K_2O. The calculated Mg number ranges from 64.53- to 76.70, only to demonstrate their cumulate nature.

The pyroxenites of PK-MK display a distinctive enrichment in the total budget of LILE such as Rb Ba, and Sr, Rb content in general is higher and it hints a biotite controlled fractional crystallization. The overall depleted nature of REE content in pyroxenites of Pakkanadu – Mulakkadu and the depicted concave-up REE pattern suggests differentiation by fractional crystallization and accumulation processes of clinopyroxene. The conspicuous negative trough at Nb-Ta, Zr-Hf and Ti, relative to LREE, Rb, Sr and Ba suggest that the pyroxenite magma was derived from an enriched mantle source.

The syenites in the Pakkanadu- Mulakkadu are medium to very coarse grained, with few pegmatoidal variants that are mainly composed of K feldspar (microcline perthite) that forms the bulk mineral phase (42- 75%) noticed both as independent megacrysts and interstitial material implying that they were the liquidus phase during entire course of crystallisation of syenite magma that underwent slow cooling. The near absence or presence in neglible proportion of plagioclase clearly demonstrates the hypersolvus conditions of crystallisation of magma. The mafic minerals like clinopyroxene, amphibole biotite and garnet appear in varying proportions. Titanite, magnetiteand apatite phases are seen constituting the accessory phases.

The syenites are geochemically distinctive and appear to be oversaturated in terms of SiO_2 and carry high K_2O that is supported by petrography and their low iron enrinchment and initial calc alkaline nature brings them closer to the composition of shoshonitic suite of rocks. The study of syenites of Pakkanadu indicates that they are originated from metasomatised K and LILE enriched lithospheric mantle in a subduction zone. The low Ti values in the syenites also strengthen the argument in favour of the subduction related magmas controlling the genesis of the syenites of PK-MK. Thus, the parental magma of shoshonitic composition generated from subduction modified subcontinental lithospheric mantle, underwent low degree of partial melting is being invoked for the evolution of the syenitic melt that has utilised the deep seated faults as the avenues for its emplacement into the mid- crustal levels.

The chondrite normalised REE patterns of the syenites at PK-MK have a high LREE/HREE ratio and exhibit LREE enriched and HREE depleted patterns, and display a near parallel to subparalell trends hinting at the fractional crystalllisation process as a major process and Eu positive anamoly amply indicating the role of feldspar in their genesis and is attributed to the presence of hornblende, and minor phases like garnet and sphene in the source and suggesting a low degree of partial melting of upper mantle.

The carbonatites of Pakkanadu-Mulakkadu are mostly dominated by carbonates (mostly calcite), mafic minerals like pyroxene, biotite, etc. Apatite is an important accessory mineral, pyrochlore, rare zircon, monazite and sphene are also noticed. The carbonatites are medium to coarse grained and exhibits polysynthetic twinning and deformed to some extent as indicated by the kinked boundaries, and undulatory twinning. The associated phlogopites along with the calcites have serrated margins and display stringered tendency provides an ample proof for the tectonic remobilization involving ductile flow the carbonatites experienced. These rocks are marked by a rather low Ti- concentration, suggesting that the

carbonatitic magmas could have been derived from a phlogopite- and/or pyroxene- rich source as a consequence of the subduction related activity.

The study of the carbonatites of Pakkanadu and Mulakkadu adjoining areas indicates that they are originated from metasomatised K and LILE enriched lithospheric mantle in a subduction zone. The role of subduction components in the source materials is reflected in the form of negative Nb and Ti signatures in the spidergram. Similarly, the high La/Nb and K/Yb ratios are suggestive of the role played by subduction related processes in the source region.

In general, the carbonatites of Pakkanadu display the LREE enriched and HREE depleted patterns, which is expected from a magmas generated at upper mantle supported by low degrees of partial melting. However the carbonatites display concaving up at HREE which is genrally controlled by clinopyroxene, apatite and amphibole at the source regions. The HREE patterns also hint at the presence of hornblende, and minor phases like garnet and sphene in the source.

In view of the above, it is postulated that ultramafic rocks (dunite and pyroxenite) syenites and carbonatites of Pakkanadu - Mulakkadu have evolved independently from the mantle at different periods of time. Low degree of partial melting and assimilation processes account for the generation of (quartz normative) syenites.The unmixing of the parental melts produced ultramafics, syenites and carbonatites via liquid Immiscibility and fractional crystallisation, of melts generated at sub continental lithospheric mantle and modified by subduction related processes.

CRYSTAL-RICH INCLUSIONS IN SPINELS FROM CALCIPHYRES OF TAZHERAN MASSIF (WESTERN BAIKAL REGION, RUSSIA)

Starikova A.E.[1,2], Stepanov K.M.[1,2], Timina T.Yu.[1]
[1]Institute of Geology and Mineralogy, Siberian Branch of the Russian Academy of Sciences, Novosibirsk, Russia
[2]Novosibirsk State University, Novosibirsk, Russia, a_sklr@mail.ru

The Tazheran alkaline massif (470-460 Ma) is located on the western shore of the Baikal Lake, Russia, being a component of the Lower Paleozoic collisional orogen at the margin of the Siberian craton (Donskaya et al., 2017). The massif is syn-collisional and is characterized by complex structure, composed of various magmatic rocks: sills of syenite, nepheline syenite and subalkaline gabbro, rare dykes of plagioclase porphyrite and numerous late veins of granite pegmatite [Fedorovsky et al., 2010]. In addition, abundant bodies of various size and shape, composed of brucite marbles present at the southern part of the massif, and wide field of beerbachites was mapped at the northern part [Sklyarov et al., 2009]. Syenites and beerbachites were the earliest phase (470 Ma), then nepheline syenite and subalkaline gabbro intruded alternatively (455-460 Ma). The last syn-collisional phase was dykes of plagioclase porphyrite (Sklyarov et al., 2013).

Despite the small size (~6 km^2), the Tazheran massif is characterized by the richest mineralogy (including rare minerals). The main "concentrators" of rare minerals (tazheranite, azaproite, zirconolite, aenigmatite-rönite, jerfisherite, kirshteinite, lueshit, etc.) are metasomatic rocks, also abundant at the southern part of the massif (Konev, Samoylov, 1974; Starikova et al., 2014). The most usual metasomatic rocks are magnesian skarns and calciphyres. Mg-skarns form rims (1 cm-0.5m) at the contacts of nepheline syenites and brucite marbles. Calciphyres occur as veins in brucite marbles.

There are no doubts about genesis of Mg-skarns but mechanism of calciphyre formation is still debated. One of the questions is about the nature of host brucite marbles. They form different-shaped or vein-like bodies that injected into nepheline syenites, and gabbroids and contain their "xenoliths" (Sklyarov et al., 2013). There are two possible explanations of such phenomena: viscous-plastic injection of marbles or melt intrusion. Stable isotope data showed values typical for sedimentary carbonates ($\delta^{18}O$ +23.3 - +26.2‰; $\delta^{13}C$ −1.9 - −4.4‰) (Doroshkevich et al., 2016). However, the hypothesis of carbonate melt as a result of sedimentary carbonate melting still exists. Brucite forms idiomorphic grains with onion-skin structure in marbles that interpreted as periclase pseudomorph (Konev, Samoylov, 1974). Periclase marbles supposedly were transformed from embedding dolomites after high-temperature contact metamorphism. Nevertheless, there was no evidence of periclase relicts in marbles from the Tazheran massif.

Basic minerals of exoskarn and calciphyres are forsterite, spinel and calcite. Accessory minerals are magnetite, baddeleyite ZrO_2, tazheranite $Ca_2Zr_5Ti_2O_{16}$, zirconolite $CaZrTi_2O_7$, zirkelite $CaZrTiO_5$, perovskite $CaTiO_3$ and ilmenite $FeTiO_3$ (skarn) or geikielite $MgTiO_3$ (calciphyres) [Starikova, 2007]. The amount of accessories in calciphyres is the same as in exoskarns that can indicate high mobility of such inert elements for skarn processes as Ti, Zr, Nb and Hf. FeO content in basic minerals is the main difference between exoskarn and calciphyres. Spinel and forsterite from exoskarn contains higher concentration of FeO (up to 13 wt.% and up to 8.8 wt.% correspondently) compared to calciphyres (1.5-4 wt.% and 1-1.2 wt.% correspondently).

Calciphyres can be divided into three types due to spinel color: with greenish spinel, with light pink spinel and with saturated purple spinel. Spinel is the earliest high-temperature phase. It occurs as octahedral crystals and sometimes displays fine-grained intergrowths with olivine. The difference in spinel color reflect the difference in FeO and TiO_2 concentrations. Greenish spinel is Ti-free and contains 3-4 wt.% of FeO_{tot}. Rims of some spinel grains show some admixture of TiO_2 (up to 0.5%). Concentration of FeO_{tot} in pink and purple spinels is 1.2-1.8 wt.%. TiO_2 content in pink spinel does not exceed 0.85 wt.%. Its concentration in saturated purple spinel can reach 1.9 wt.%. Numerous oriented inclusions of geikielite were found in purple spinel intensifying its color. It should be noted that average TiO_2 content in spinel from exoskarn is less than 0.2 wt.%.

Round grain of periclase (20 µn) was found as crystal inclusion in purple spinel. It is the first finding of periclase in the Tazheran massif.

Table 1. Mineral phases detected in primary crystal-rich fluid inclusions of spinal from different types of calciphyres

Mineral name	Formula	greenish spinel	pink spinel	purple spinel
Ca-Na-K carbonate (AC)		abundant	abundant	abundant
Unknown (KNMF)	$(K,Na)Mg[CO_3]F$	rare	-	abundant
Parascandolaite (Par)	$KMgF_3$	abundant	-	-
Neighborite (Nbr)	$NaMgF_3$	-	abundant	rare
Northupite (Nor)	$Na_3Mg(CO_3)_2Cl$	-	-	sporadic
Nyerereite (Ny)	$Na_2Ca(CO_3)_2$	-	-	rare
Periclase (Per)	MgO	-	rare	rare
Brucite (Brc)	$Mg(OH,F)_2$	sporadic	-	-
Calcite (Cal)	$Ca[CO_3]$	abundant	abundant	abundant
Dolomite (Dol)	$CaMg[CO_3]_2$	rare	-	sporadic
Fluorapatite (Ap)	$Ca_5[PO_4]_3(F,OH)$	abundant	abundant	abundant

Note: Abbreviations of mineral phases are showed in brackets. All analysis were done by MIRA 3 LMU SEM (TESCAN Ltd.) equipped with an INCA Energy 450 XMax 80 microanalysis system (Oxford Instruments Ltd.)

Primary crystal-rich fluid inclusions were found in spinels from all types of calciphyres. Inclusions have negative relief and small size (2-15 µn, rare up to 20 µn). Composition of inclusionsand phase proportion is quite constant in each type of calciphyres. Detected phases are showed in Table 1. The main phases are calcite and Ca-Na-K carbonates. Heterogenous structure of alkaline carbonates has been detected on the SEM elemental maps. Unfortunately, small size of crystals does not allow to analyze their exact composition by other methods. Fluorapatite, dolomite, periclase and ore minerals (magnetite, geikielite, baddeleyite) found also as individual crystal inclusions in spinels can be interpreted as trapped phases. Despite general alkaline specific, some important features of inclusions should be noted for each type of calciphyres. Having similar alkaline specifics inclusions of each types of spinels differ in their peculiarities.

The most common daughter phases of inclusions in greenish spinel are Ca-Na-K carbonates, K-Mg-fluoride (parascandolaite) and calcite (Fig. 1). The last one can be also trapped phase. Two main Ca-Na-K carbonates was detected due to approximate ratio (K+Na)/Ca: 2/1 (nyerereite-like) and 1/1 (probably, hydroxyl-carbonate). Na/K ratio vary from 0.8/0.2 to 0.7/0.3. Magnetite was the only ore phase detected as inclusion in greenish spinels.
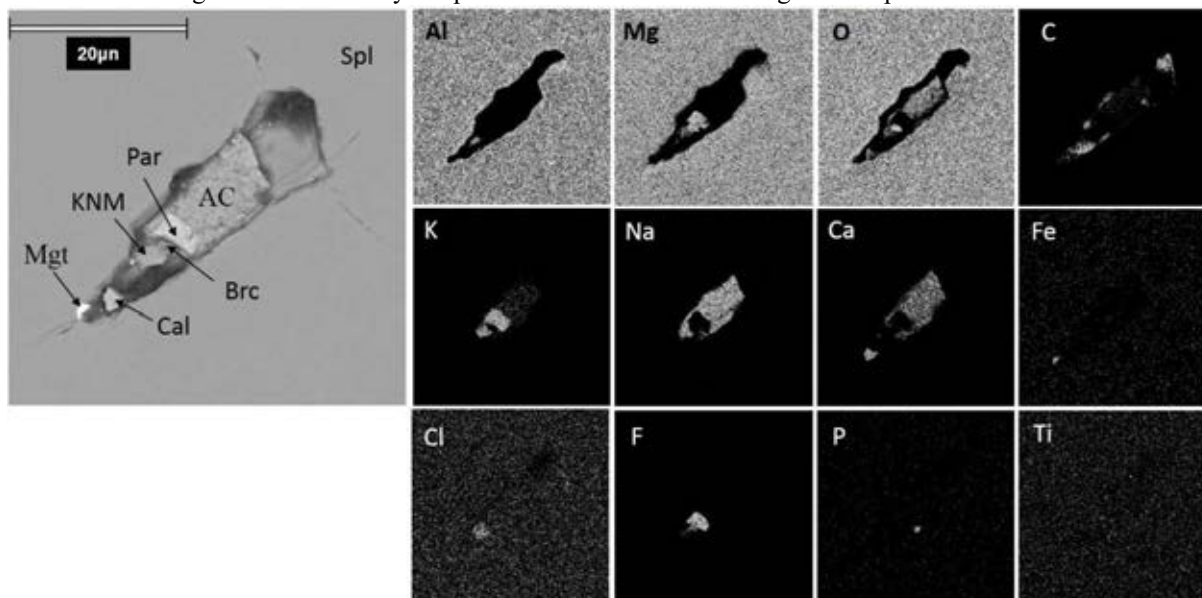
Fig. 1. Crystal-rich fluid inclusion in greenish spinel (BSE image and elemental maps). Mgt – magnetite, Spl – spinel. EDS were made at an accelerating voltage of 10 kV.

Size of inclusions in pink spinels does not exceed 8 µn that made impossible any kind of analysis except SEM elemental mapping. Na-Mg-fluoride (neighborite) is typical for pink spinel inclusions instead of K-Mg-phase in greenish spinel (Fig. 2). Ti-phases (geikielite, perovskite) are abundant as crystal inclusions. Zr-mineral (baddeleyite) was also described as trapped phase.

Inclusions in purple spinels are characterized by less amount of Ca-Na-K carbonates (Fig.3). Approximate formula of the most abundant alkaline phase can be written as $(K,Na)Mg[CO_3]F$. It is unknown among registered approved mineral species. Na\K ratio is usually near 0.7/0.3. The admixture of chlorine (~2 wt.%) was always detected. Na-Cl carbonate

(northupite) was found in some inclusions. The amount of Ti- and Zr-minerals (geikielite, perovskite, baddeleite, tazheranite) is the highest in calciphyres with purple spinel.
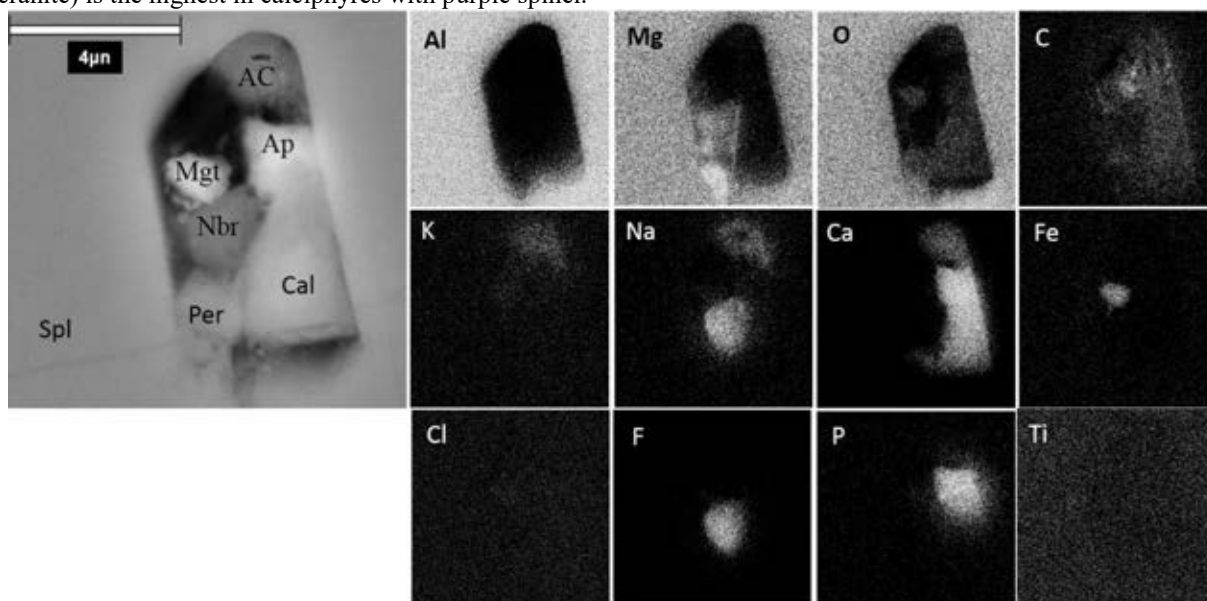
Fig. 2. Crystal-rich fluid inclusion in pink spinel (BSE image and elemental maps). EDS were made at an accelerating voltage of 20 kV.
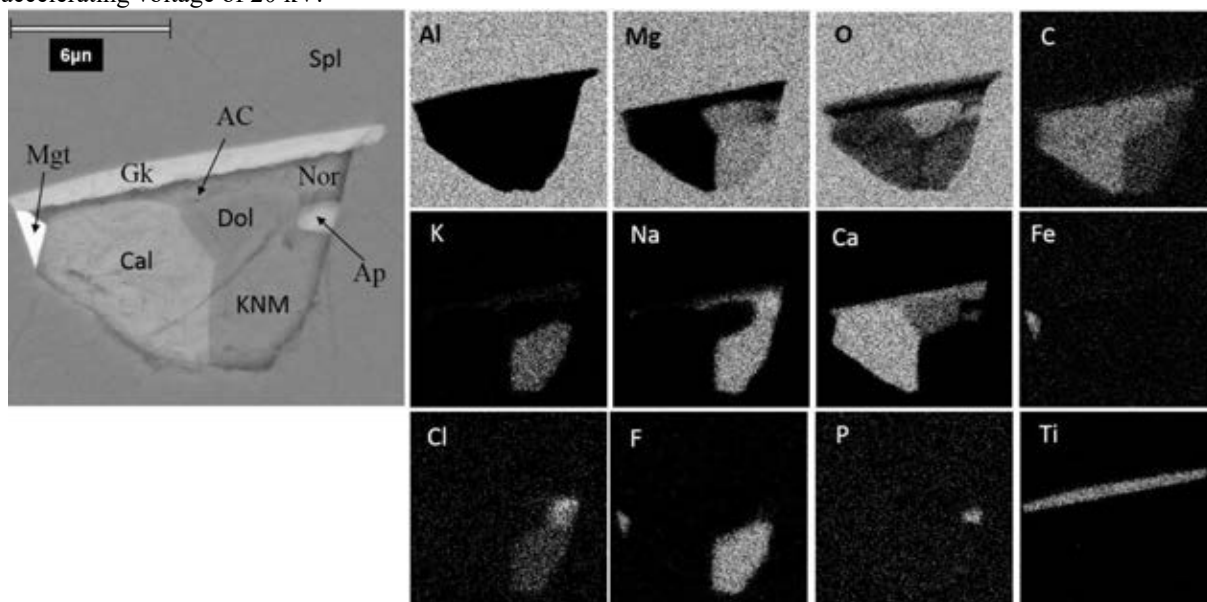
Fig. 3. Crystal-rich fluid inclusion in purple spinel (BSE image and elemental maps). EDS were made at an accelerating voltage of 10 kV.

Presence of Na- and K-phases in inclusions reflects great role of alkaline fluids in calciphyres formation. Calciphyres with pink and purple spinels were formed before periclase was replaced by brucite. Brucite in the greenish spinel can be daughter phase. Variation of inclusion phase composition for three types of spinels can be explained by 1) different fluid sources 2) evolution of one source during metasomatic process.

References:

Donskaya T.V., Gladkochub D.P., Fedorovsky V.S., et al. Pre-collisional (≥0.5 Ga) complexes of the Olkhon terrane (southern Siberia) as an echo of events in the Central Asian Orogenic Belt // Gondwana Research. 2017. Vol. 42. P. 243–263.

Doroshkevich A., Sklyarov E., Starikova A., et al. Stable isotope (C, O, H) characteristics and genesis of the Tazheran brucite marbles and skarns, Olkhon region, Russia // Mineralogy and petrology. 2016. Vol. 115. P. 153-169.

Konev A.A., Samoylov V.S. Contact metamorphism and metasomatism in the areole of the Tazheran alkaline intrusion. 1974. Novosibirsk. Nauka. 246 p.

Sklyarov E.V., Fedorovsky V.S., Kotov A.B., et al. (2009): Carbonatites in collisional settings and pseudo-carbonatites of the Early Paleozoic Ol'khon collisional system // Russ Geol Geophys. 2009. V. 50(12). P. 1091-1106.

Sklyarov E.V., Fedorovsky V.S., Kotov A.B., et al. Carbonate and Silicate–Carbonate Injection Complexes in Collision Systems: the West Baikal Region as an Example // Geotectonics. 2013. V. 47(3). P. 180-197.

Starikova A.E. Ti-Zr accessory mineralization in calciphyres of the Tazheran massif (Western Baikal aria) // Alkaline magmatism, its sources and plumes. Irkutsk, IG SB RAS. 2007. P. 223-236

Starikova A. E., Sklyarov E.V., Kotov et. al. Vein calciphyre and contact Mg skarn from the Tazheran massif (Western Baikal area, Russia): Age and genesis // Doklady Earth Sciences. 2014. Vol. 457 (2). P.1003-1007.

Fedorovsky V.S., Sklyarov E.V., Izokh A.E., et al. Strike-slip tectonics and subalkaline mafic magmatism in the Early Paleozoic collisional system of the western Baikal region // Russ Geol Geophys. 2010. V. 51. P.534– 547.

EVOLUTION OF THE CHROMITE-PLATINUM MINERALIZATION OF ZONAL CLINOPYROXENITE-DUNITE MASSIFS OF THE MIDDLE URAL

Stepanov S.Yu.[1,2] *Palamarchuk R.S.*[1,2] *Kutyrev A.V.*[3]

[1]Saint-Petersburg Mining University, Saint-Petersburg, Russia, Stepanov-1@yandex.ru
[2]Federal State Budgetary Enterprise 'A. P. Karpinsky Russian Geological Research Institute', Saint-Petersburg, Russia
[3]Institute of Volcanology and Seismology, Far Eastern Division RAS, Petropavlovsk-Kamchatsky, Russia

Nizhnetagilsky, Svtoloborsky, Veresovoborsky and Kamenushensky clinopyroxenite-dunite massifs are situated in the Middle Urals in the western part of the Tagil-Magnitogorsk megazone. These massifs belong to the Kachkanar complex, which petrotype is Nizhnetagilsky massif. The central part of the massifs are composed of dunites, which are characterized by different granularity. The coarse-grained dunites and dunite pegmatites are found in the central part of the dunite core of the Nizhny Tagil and Veresovoborsky massifs. Medium-grained dunites rim the bodies of coarse-grained dunites. Fine-grained dunites are located in the marginal part of dunite core in the immediate vicinity of pyroxenite. The clusters of chromite bodies incline to the contacts of dunite bodies differing in grain size. The largest content of platinum group minerals (PGM) is an attribute of chromitites located on contact of coarse-grained and medium-grained dunites, which was previously established for the Nizhnetagilsky massif (Ivanov, 1997; Pushkarev at al., 2007). A similar pattern was revealed for the Vresovsborsky massif as a result of our research.

The chromitites build up vein-interspersed bodies with an average thickness of 0.15 m, traced along a strike by 1.5-2 m. These bodies form ore zones, which thickness can reach 20-25 m, at a strike of 60-80 m. Massive veins of chromites, characterized by transverse contacts, are less common and have a thickness of 0.05-0.15 m. Sometimes, transition from vein-disseminated chromites to massive ones is observed. In general, the character of the structure of chromite bodies allows us to assume their origin due to the crystallization of residual oxide melts in a hard-plastic substance.

The main part of the platinum group minerals is concentrated in the chromitites. It should be noted that in vein-disseminated chromitites, platinum minerals are distributed evenly and do not form large aggregates. Meanwhile, massive chromites are characterized by the presence of large concentrations of PGM with dimensions of few centimeters from the extremely uneven distribution. Among the platinum group minerals in chromitite of the zonal clinopyroxenite-dunite massifs of the Middle Urals Pt-Fe solid solutions in stoichiometry corresponding to the isoferroplatinum Pt_3Fe and ferrous platinum Pt_2Fe are predominate. Numerous inclusions were found in the individuals and aggregates of these minerals.

Os–Ir–(Ru) intermetallides, laurite and erlichmanite, kashinite and bowieite, also thiospinels are found as inclusions in Pt-Fe solid solutions. Hexagonal plates of native osmium predominate over the number of inclusions in the Pt-Fe minerals Veresvoboskrky and Kamenushensky massifs. The predominance of native iridium of inclusions in Pt-Fe minerals is characteristic of Nizhnetagilsky, Svtloborsky and, to a lesser extent, Kamenushensky massifs. Minerals of the laurite- erlichmanite and kashinite- bowieite isomorphous series, and thiospinels are distributed in a very subordinate amount in the Pt-Fe minerals of all the massifs, probably except for Svitborskiy massif. Inclusions of PGE sulphides predominate over the intermetallides in the Pt-Fe minerals of the Svetloborsky massif.

Most individuals of inclusion minerals in the Pt-Fe matrix have their own idiomorphic faceting. Native osmium is found as the hexagonal pinacoidal crystals (fig 1a-c). Sometimes idiomorphic crystals of osmium are found in individuals of chromspinelide (fig 1b). Os, Ru, Ir, and Rh sulfides coalesce with chromospinelide and crystallize before Pt-Fe solid solutions, as evidenced by their idiomorphic faceting. Thus, mineragenesis within chromite-platinum ore systems begins with the crystallization of native osmium. Then crystallize chromspinelide. Laurite, ekrilikmanite, kashinite, boite, cuprodensite and cuproiridsite are formed directly behind the development of chromespinelide.

Crystallization of the bulk of Pt-Fe solid solutions occurs after the formation of minerals-inclusions. In part, they crystallize together with the last growth zones of chromospinelide individuals. The induction surfaces between isoferroplatinum or ferruginous platinum and chromospinelide testify in favor of this (fig 1.d).

It should be noted that most aggregates of Pt-Fe solid solutions, chromespinelides, and osmium plates undergone significant brittle and plastic deformations. This is especially characteristic for the minerals described from the chromitite of the Nizhny Tagil and Veresovoborsky massifs.

After deformations, aggregates and individuals of Pt-Fe minerals undergo substitution with secondary minerals of the tetraferroplatinum group. The most common mineral from the tetraferroplatinum group is tulameenite. This mineral forms a fringe of substitution around the primary iron-platinum alloys (fig 1e), sometimes with the formation of complete pseudomorph. The substitution around consists of numerous parallel oriented elongated individuals (fig 1f), which is clearly seen in polarized reflected light due to anisotropy of the minerals of the tetraferroplatinum group. At the same

time, for chromitites of the Nizhny Tagil massif, it was established that Fe-Pt solid solutions in stoichiometry, corresponding to ferruginous platinum, are replaced by tulameenite, meanwhile Pt-Fe minerals with isoferroplatinum stoichiometry are are substituted by ferronickelplatinum.
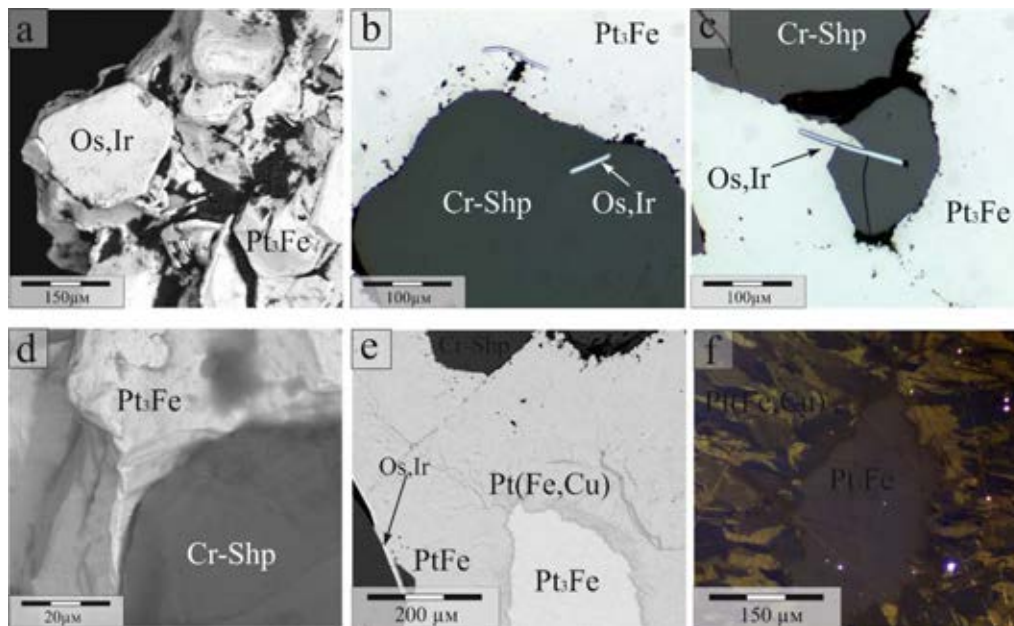
Fig. 1. Morphology and internal structure of platinum group minerals. Legend: Pt3Fe – a mineral in stoichiometry corresponding to isoferroplatinum, Cr-Shp – chromospinelide, Pt(Fe, Cu) – tulameenite, Os,Ir –native osmium, often with an admixture of iridium.

Sulfides, arsenides, sulfoarsenides and sulfostibenides of platinum group elements are among the latest minerals that replace tetraferroplatinum group minerals. So, during our research we found: irarsite, hollingvorite, tolovkite and Pd-Cd-Hg not named minerals. These minerals are characterized by being found in the form of small inclusions of less than 50 microns, mainly in tetraferroplatinum group minerals. In one of the samples from the Veresovoborsky massif, serpentine vein crosses a large clump of platinum group minerals. In the near-contact part, the primary Pt-Fe minerals and the secondary tetraferroplatinum group minerals developed on them are replaced by a complex fine-grained aggregate composed of Os-Ir intermetallics, oxygen containing Pt-Fe solid solutions and a Pd-Cd-Hg mineral with the assumed formula Pd_2CdHg.
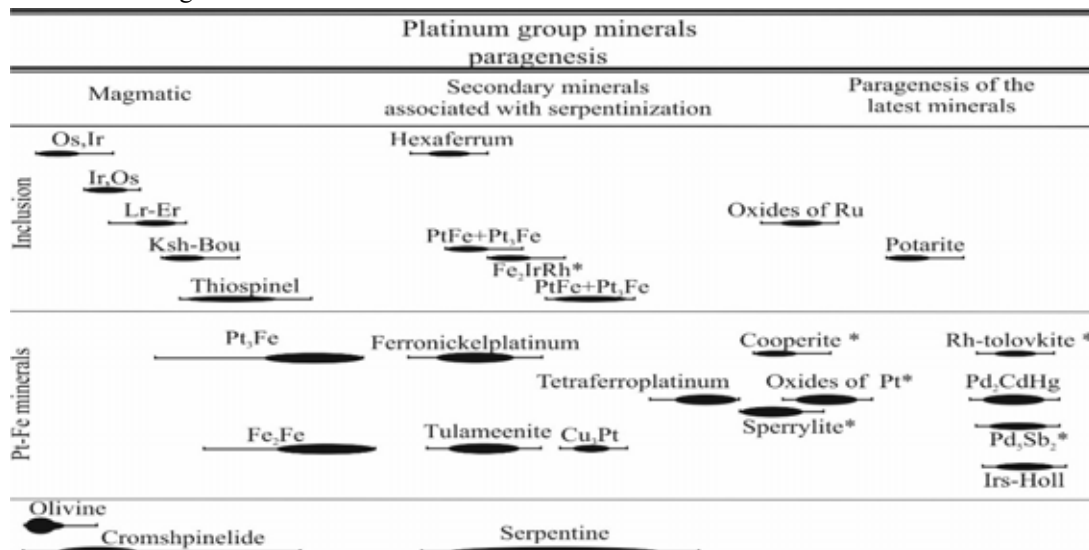
Fig. 2. The order of formation of platinum group minerals in chromitites of clinopyroxenite-dunite massifs (Middle Ural), * – on the basis of the description of minerals in N.D. Tolstykh (Tolstoy et al., 2011). Legend: Os,Ir – iridium osmium, Ir,Os – osmous iridium, Lr – laurite, Er – erlichmanite, Ksh - kashinite, Bou - bowieite, Pt3Fe - Pt-Fe solid solution in composition corresponding to isoferroplatinum, Pt_2Fe – Pt-Fe solid solution in composition corresponding to glandular platinum, PtFe - tetroferroplatinum, Irs - irarsit, Holl - Hollingworthite.

So, in the cumulative evidence of the study platinum group minerals from the clinopyroxenite-dunite massifs of the Middle Urals three parageneses have been established (fig 2). Isoferroplatinum and ferrous platinum with numerous inclusions belong to the first parageneses - magmatic. Tulameenite, ferronickelplatinum and tetraferroplatinum refer to the paragenesis of secondary minerals. Its formation is associated with active serpentinization of dunites. The formation

of the latest paragenesis with the predominance of arsenides, stibnites and sulphides of platinum group elements, as well as mercury-containing minerals, is a result of interaction with hydrothermal fluids generated by late tectonic-magmatic activation processes. This is concluded due to the introduction of very unusual elements for ultrabasic rocks, such as As, Sb, Hg. So dunites of Kamenushensky massif are intruded by silurian granites. Probably, these granites could be a source of not typical elements for mafic and ultramafic rocks.

If we consider the history of geological development of clinopyroxenite-dunite massifs, then the formation of primarily magmatic paragenesis of minerals must be related to the crystallization of dunites. The problem of the formation of dunites of the Uralian Platinum Belt to the present time is debatable. However, recent data on the dating of zircon from dunite (Malitch at al., 2009), as well as laurite and Os-Ir-(Ru) solid solutions (Malitch at al., 2014), confirms the stated A.A. Efimov's (Efimov, 2009) assumption of a tectonic introduction of the formed dunite bodies in the late ripheissian time into the structure of dunite-clinopyroxenite-gabbro complexes. Several authors (Johan, 2002; Okrugin, 2004; Toltykh at al., 2011) believe that the formation of dunites occurred during the differentiation of picrite melts with the segregation of the oxide-ore liquid, mainly of chromite composition. Proceeding from the genetic relationships of minerals in dunites and platinum-containing chromites, this model is, in our opinion, the most relevant to reality. The formation of dunites, taking into account the current data, occurred at the stage of late rifting Riphean within the incipient Ural fold region, in analogy with the clinopyroxenite-dunite massifs of the Aldan Shield, which are spatially related to continental rifts (Efimov, Tavrin 1997). In this case, picrite magmatism, in general, corresponds more to the riftogenic structures than to the suprasubduction volcanic arcs. Structurally-material complexes composing the Uralian Platinum Belt were formed precisely in the condition of island-arc magmatism in the Ordovician period.

One of the important details that makes it possible to understand the ontogeny of platinum mineralization in the chromitites of the clinopyroxenite-dunite massifs of the Middle Urals is the spread of brittle deformations in chromospinelides and native osmium and plastic deformation in Pt-Fe minerals. Probably, these deformations reflect the general character of powerful tectonic transformations of dunites at the stage of involving dunite bodies in the structure of dunite-clinopyroxenite-gabbro complexes. The clinopyroxenite-dunite massifs in the Early Paleozoic were found in the subduction zone. The rocks of the massifs underwent interaction with hydrothermal fluids, mainly by aqueous solutions, which caused powerful serpentinization (Ivanov, 2011). It is possible to assume that the tectonic transformations of dunites were combined with their metasomatic alteration. It is the large-scale powerful metasomatic transformation of dunites with the development of serpentinized dunites that led to the formation of minerals of secondary paragenesis replacing the primary magmatic Pt-Fe minerals and inclusions therein.

References:

Efimov A.A. (2009) Platinonosnyj poyas Urala: sovremennoe sostoyanie predstavlenij o geologii, prirode i istorii formirovaniya unikal'nogo rossijskogo ob'ekta [Uralian Platinum Belt: the current state of ideas about the geology, nature and history of the formation of a unique Russian object]. Ultrabasite-basite complexes of folded regions and associated deposits. Ekaterinburg. 1: 176-179

Efimov A.A., Tavrin I.F. (1978) Common origin of platinum-dearing dunites of the Urals and Aldan shield. Doklady of the Academy of Sciences of the USSR. 243 (4): 75-79

Ivanov K.S. (2011). Genesis of chromium-platinum ore mineralization of the Uralian (Nizhnii Tagil) type. Doklady Earth Sciences, 441 (1): 1489-1491.

Ivanov O.K. (1997) Koncentricheski-zonal'nye piroksenit-dunitovye massivy Urala. [Concentrically-zoned pyroxenite-dunite massifs of the Urals: Minerology, petrology, genesis]. USU, Yekaterinburg, 488 p.

Johan Z. (2002) Alaskan-type complexes and their platinum-group element mineralization. The geology, geochemistry and mineral beneficiation of platinum-group elements (Cabri l.J. ed.). Special volume 54. Canadian Institute of mining, metallurgy and petroleum.: 669-719.

Malitch K.N., Badanina I.Yu., Belousova E.A., Hiller V.V. (2014) Himicheskij sostav i osmievo-izotopnaya sistematika blagorodnometal'nogo orudeneniya zonal'nogo Nizhnetagil'skogo massiva (Sverdlovskaya oblast', Rossiya)[Chemical composition and osmium-isotopic taxonomy of noble metal mineralization of the zone Nizhnetagilsky massif (Sverdlovsk Region, Russia)]. Writings of the Zavaritsky Institute of Geology and Geochemistry, UrB RAS. 161. Ekaterinburg: IGG UrB RAS: 316-321.

Malitch K.N., Efimov A.A., Ronkin Yu.L., (2009) Archean U-Pb isotope age of zircon from dunite of the Nizhny Tagil massif (the Uralian Platinum Bely). Doklady Earth Sciences, 427 (5): 851-855.

Okrugin A.V. (2004) Kristallizacionno-likvacionnaya model' formirovaniya platinoidno-hromitovyh rud v mafit-ul'tramafitovyh kompleksah [Crystallization-liquation model of the formation of platinum-group elements chromitites ores in mafic-ultramafic complexes]. Pacific geology. 23 (2): 63-75

Puskarev E.V., Anikina E.V., Garuti G., Zaccarini F. (2007). Hrom-platinovoe orudenenie nizhnetagil'skogo tipa na Urale: Strukturno-veshchestvennaya harakteristika i problema genezisa [Cromium-platinum deposits of Nihny-Tagil type in the Urals: Structural-substantial characteristic and problem of genesis]. Lithosphere, 3, p. 28-65

Stepanov S.Yu. Malitch K.N. (2016) O prirode tulaminita i ferronikel'platiny iz hromititov klinopiroksenit-dunitovyh massivov Srednego Urala [About the nature of tulaminite and ferronicelplatinum from chromitites of clinopyroxenite-dunite massifs of the Middle Ural]. Metallogenees of ancient and modern oceans. 22: 228-232

Tolstykh N.D. Telegin Yu.M., Kozlov A.P. (2011) Platinum mineralization of the Svetloborsky and Kamenushinsky massifs (Urals Platinum Belt). Russian Geology and Geophysics, 52 (6): 603-619

TIMESCALES AND GEOCHEMICAL EVOLUTION OF THE MIDDLE TRIASSIC SHOSHONITIC MAGMATISM IN THE SOUTHERN ALPS (NORTHERN ITALY)

Storck J.-C.[1], Brack P.[1], Wotzlaw J.-F.[1] & Ulmer P.[1]

[1] Institute of Geochemistry and Petrology, ETH Zürich, 8092 Zürich, Switzerland, julian.storck@erdw.ethz.ch

The middle Triassic magmatism in the Southern Alps and particularly in the Dolomites and Lombardian Alps comprises widespread and irregularly distributed volcaniclastic deposits intercalated with pelagic sediments and platform carbonates, basaltic lava flows and plutonic complexes. Previous work mainly based on field observations and geochronology studies concluded that the Middle Triassic magmatism initiated with silicic products (Brack & Rieber, 1993). Related thin ash layers, crystal-rich tuffs and bentonites can be observed in stratigraphic sequences throughout the Southern Alps. More mafic products occur further up-section in the form of shallow intrusions and basaltic lava flows. In the central and western Dolomites stratigraphically unconstrained shoshonitic intrusive and effusive bodies including those at Monzoni and Predazzo were emplaced during the late stages of explosive volcanic activity.

In this study we applied high-precision CA-ID-TIMS U-Pb dating of single zircon crystals together with trace element geochemistry and Hf isotopes on zircons obtained by LA-(MC)-ICP-MS in order to unravel the evolution and the interplay between the acidic volcaniclastic deposits and the mafic to intermediate sub-volcanic/intrusive magmatism. We present a detailed stratigraphic framework and a comprehensive zircon petrochronology data set that constrain the timing as well as the chemical and isotopic evolution of this magmatic province. High-precision zircon U-Pb geochronology provides absolute tie-points for felsic ash layers that also bracket and thus constrain the timing of effusion of basaltic lava flows. These data furthermore place precise constraints on the emplacement history of stratigraphically unconstrained intrusive bodies and their genetic links to effusive and explosive volcanic products.

References:

Brack P. & Rieber H. (1993) Towards a better definition of the Anisian/Ladinian boundary: New biostratigraphic data and correlations of boundary sections from the Southern Alps. Eclogae geol. Helv., 86/2, 415-527.

PREPARATION AND MEASUREMENTS OF A ROCK STANDRAD FOR HELIUM ISOTOPES FROM THE KOLA COMPLEX, KOVDOR (RUSSIA)

Storck J.-C.[1], Hopp J.[2], Trieloff M.[2]

[1] Institute of Geochemistry and Petrology, Zürich, Switzerland, julian.storck@erdw.ethz.ch
[2] University of Heidelberg, Heidelberg, Germany

In noble gas mass spectrometry the content of unknown samples is always calibrated against standard gases of known composition. For intermediate to heavy noble gases such as Neon, Argon, Krypton and Xenon clean air can be applied as a standard. Since helium occurs only in traces in natural air either a synthetic or natural gas with elevated helium concentrations and $^3He/^4He$-ratio is necessary for calibration purposes. Elevated standard $^3He/^4He$ ratios are of advantage during measurements of mantle material that are generally enriched in ^3He, minimizing systematic offsets due to the highly discrepant isotope ratios (for example, typical MOR-basalts have an eight times higher $^3He/^4He$-ratio than air, some ocean island basalts even show a ca. 35 times higher value). The disadvantage of synthetic gas ist that a small volume extracted from the gas cylinder can possibly lead to isotope fractionation during the transfer process to the gas line. In order to eliminate these factors geochemists are in search of a homogeneous standard material resembling those that are typically analyzed in earth sciences. Igor Tolstikhin provided a pyroxene separate from a carbonatite of Kovdor (Kola Peninsula, Russia) whose $^3He/^4He$ composition was already determined at the Kola Scientific Centre, Apatity in Russia. The intention was to get an easily accessible and homogeneous natural rock standard for Helium isotopes for interlaboratory calibration.
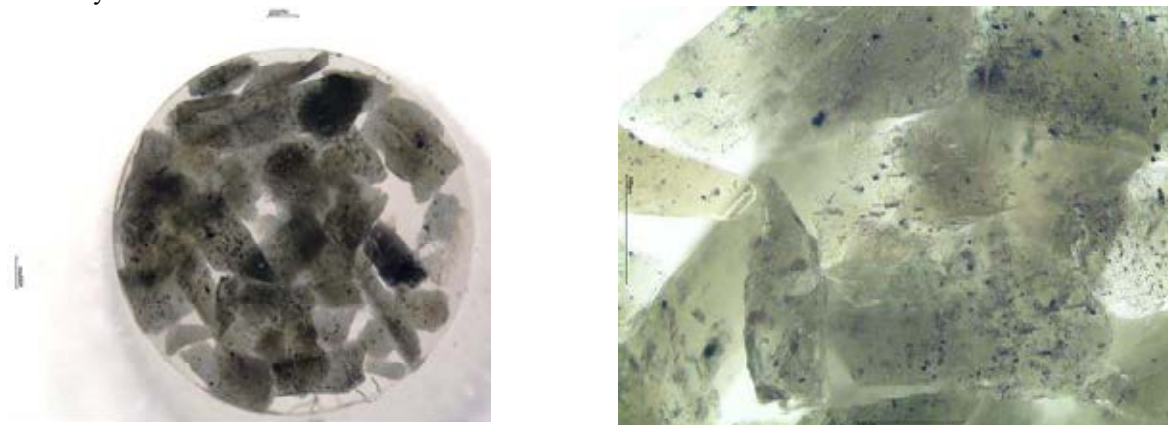
Fig. 1. Selected separate of only slightly altered pyroxenes (green) with opaque inclusions (Fe oxides). Grain sizes are in the range of 500 to 2000 μm.

We report the results of a noble gas study (with focus on He isotopic composition) utilizing stepwise heating and crushing experiments. At closer inspection we recognized that the respective pyroxene sample contained significant amounts of impurities (altered pyroxene and mineral impurities). In a first step we therefore characterized the samples by optical selection criteria using optical microscopy, and only relatively pure pyroxene phases were selected for further noble gas analyses (Fig. 1). In addition, a representative set of pyroxene and mineral impurities were investigated by scanning electron microscopy (SEM) and x-ray powder diffraction (XRD) analyses. Major purpose of these analyses was to identify alteration phases or mineral impurities within the pyroxene separate which could be possible carriers of radiogenic ^{4}He*. We checked the scale of potential homogeneity by measuring different weights of aliquots (ca. 10 – 20 – 40 – 80 mg).

Furthermore, we also analysed the suite of rejected mineral grains in order to quantify the potential degree of contamination and thus, success of our purification procedure. Our stepwise heating provided evidence that the mineral phases contain significant amounts of mantle helium, but also in-situ produced ^{4}He. The results were compared to measurements of the working group by Igor Tolstikhin. Evidently, the initial untreated pyroxene separate containing altered pyroxene and impurities showed higher 4He/3He-ratios indicative of in situ radiogenic contributions of ^{4}He* compared to the prepared "purer" pyroxene-separate. On the scales the analysed pyroxene appears homogeneous in both He isotopic composition and concentration, but existing variations are still too large for implementation as a standard material sensu strictu which would require reproducibility in the order of few permil. However, this initial assessment showed, that a careful preparation of an unaltered pyroxene separate void of impurities may well result in a suited standard material for He analysis.

MAGMATISM, METALLOGENY AND GEODYNAMICS OF THE EAST MAGNITOGORSK ISLAND ARC (SOUTH URALS)

Surin T.N.

Federal State Budgetary Enterprise 'A. P. Karpinsky Russian Geological Research Institute', Saint-Petersburg, Russia

The East Magnitogorsk island arc is the Eastern branch of the Magnitogorsk paleovolcanic belt, which is a complex system of "double island arc – interarc basin" (Gusev et al., 2000; Surin, 1993, 1995). This arc had been very active for a long time, from the end of Eifelian through the late Visean, i.e. more than 50 million years (Surin, Moseychuk, 1995). That is the reason for the exceptional diversity of endogenous ore formations, which had been formed during its evolution. This evolution is most clearly represented in the Northern part of the arc.

According to the modern views, there are four tectono-stratigraphic zones in the Northern part of East-Magnitogorsk arc. From east to west, these zones are Gumbeyskaya, Uchalino-Alexandrinskaya, Magnitogorskaya and Kizil'skaya (Fig. 1). In the first three of them all key ore deposits, mineralization shows and points, governing the metallogeny of the area, are concentrated.

Gumbeyskaya zone is generally composed of porphyritic Middle-Devonian (Eifelian to late Givetian, inclusive) volcanites of basic and, less often, intermediate composition. They belong to calc-alkaline island arc series. At the late stages of zone development, with attenuating volcanism, there were emerging separate volcanic edifices of andesites and andesidacites, which the formation of shallow volcanogenic sulfide-gold-silver stringer-disseminated ores with adularia, chalcedony, hydromicas and quartz in the wall metasomatite rocks are associated with (Kurosanskoye ore field, North and South Kurasan deposits). The ratio of Au/Ag in the ores equals to around 2:5, considering the relatively small size of the ore bodies. On the modern surface they could be traced by the fields of hematite-siliceous sediments with sulfides and high concentrations of manganese and noble metals. Previously mentioned deposits have been described as massive sulfide and copper-porphyritic by different scientists. Meanwhile, their geological and structural position, metasomatic rocks and ores composition features, described above, in our opinion, allow to consider them the typical examples of the "gold-silver formation of island arcs", which is ubiquitous in many island-arc structures of the Western framing of Pacific Ocean. It is important to note that such deposits, despite the small size, always form a "chain" of clusters within volcanic belts. That indicates high prospects of Gumbeyskaya zone for gold-silver mineralization. The small bodies of collisional granitoids belonging to Gumbeyskiy complex (Middle Carboniferous) are containing non-commercial rare metals mineralization (W, Mo, Bi, Sn, etc.).

In Uchalino-Alexandrinskaya zone several magmatic and terrigenous complexes are allocated, each of them bearing its own metallogenic features. Lateral-time series of the Devonian volcanic complexes, reconstructed in this zone, includes (from early to late): contrastic basalt-rhyolite (early Givetian), a continuous basalt-andesite-dacite-rhyolite (late Givetian - early Frasnian), basalt-andesibasalts (late Frasnian) and trachybasalt-trachyandesite-trachydacite (early Famennian). This series coincides with the petrogeochemical island-arc successive series: tholeiite and palingenetic calc-alkaline - calc-alkaline - calc-alkaline – shoshonite; it reflects a constructive step in island arc formation, i.e. its evolution from "young" to "advanced" and "mature" stages of evolution. In the series, the formation depth of primary magmas increases, resulting in a gradual increase of K, Ti, amount of alkalis, P, lithofiles and REE in magmatites. These changes have been interpreted as an increase of tangential compression during the development of magmatism and are correlated with the increase in thickness and sialition of the crust. The interaction between magmas and the crust reached its peak at the early stage of the arc development, which is associated with the peak warming of crust during the transition from tension to compression.
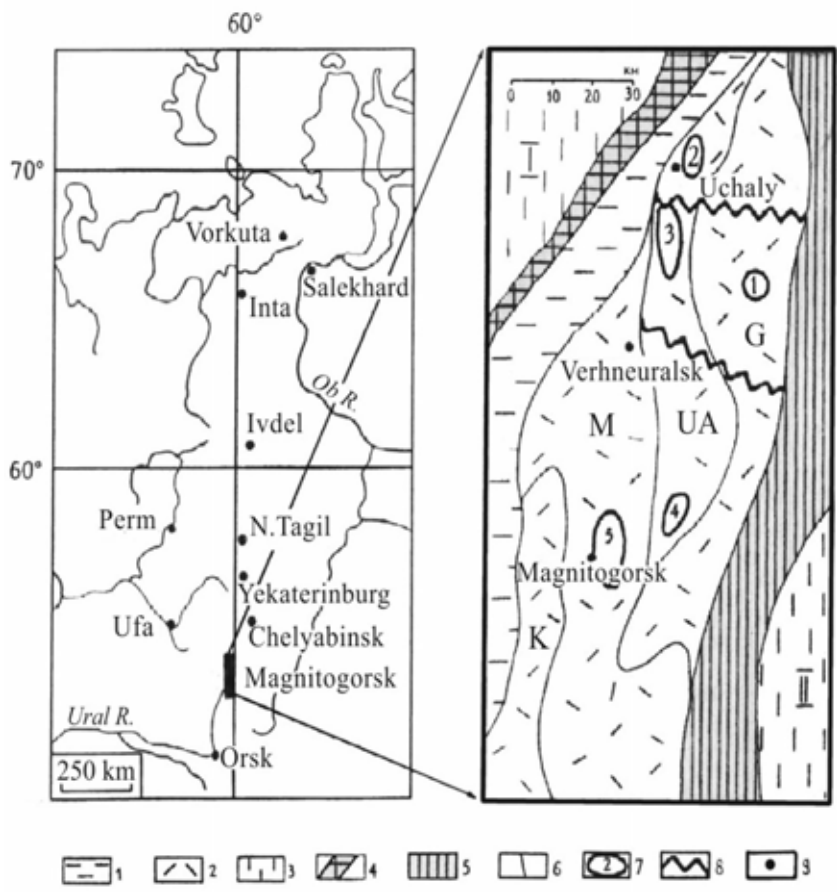
Fig.1. The location and tectono-stratigraphic zoning of the Northern part of East-Magnitogorsk paleo-island arc. 1 – The formations of West-Magnitogorsk paleo-island arc and interarc basin; 2 – tectono-stratigraphic areas of East-Magnitogorsk paleo-island arc (G – Gumbeyskaya, UA – Uchalino-Alexandrinskaya, M – Magnitogorskaya, K – Kizil'skaya); 3 - First order adjacent structures: Central Ural (I) and East Ural (II) rises; 4-5 – major suture zones: Main Uralian (4) and Uysko-Katsbakhskaya (5); 6 – the borders between zones; 7 – major ore fields: 1 - Kurosanskoye (gold ores), 2-4 – copper-zinc-massive sulfide (2-Uchalinskoye, 3-Uzelginkoye, 4-Alexandrinskoye), 5-Magnitogorskoye (iron ores); 8 – cross-dislocation zones; 9 – large cities.

Volcanism of early Givetian basalt-rhyolite (Karamyltashskiy) contrast complex accounts for the formation of the largest copper-zinc-massive sulfide deposits of Uzelginskoje and Uchalinskoye ore fields, where 10 industrial ore objects are located. All of them are described in detail in the literature. The highest peak of sulfide mineralization is confined to the upper part of the contrast complex section and is directly linked with the temporary maximum of acid volcanism in the end of early Givetian. The complex is polygenic and there are the two main series in its composition: tholeiite and palingenetic calc-alkaline. Tholeiite series is equivalent to tholeiite series of early development stages of island arcs. The axis of basalt ridges reflect ancient magma-outflow faults of the tension phase. Differentiation of magmas occurred under the conditions of low oxygen fugacity and increased total and fluid pressure (the deployment of "anorthosite trends"), which indicates the transition from tension to compression. Palingenic magma melting proceeded with an elevated geothermal gradient. Lateral compression contributed to the separation of magmas from the substrate and to the formation of intermediate magmatic focuses, which was the underlying cause of hydrothermal massive sulfide-bearing systems emergence. Squeezing of domes at a late stage of formation development occurred due to compression increase.

Late Givetian low-potassic volcanites of the continuous basalt-andesite-dacite-rhyolite (Ulutau) complex are ore-bearing for massive sulfide ore shows with increased concentrations of base metals (Yujno-Molodejnoye, Rjavtsy, Kamennaya Gora, ore bodies of the upper floor of Zapadno-Ozernoye deposit and Barsuchye mineralization show, etc.). The prominent evolution of massive sulfide ores composition over space and time is ovserved. For instance, copper-massive sulfide shows are localized exclusively in Karamyltashskiy complex, whereas they are absent in Ulutau complex. Copper-zinc-massive sulfide deposits and shows are primarily localized among the rocks of the upper part of the Karamyltashskiy complex geological section, individual ore bodies are also present in Ulutau complex sediments. Zinc-massive sulfide shows are numerously detected in Karamyltashskiy (upper part of the section) and Ulutau complexes. Sulfur-massive sulfide shows form a background, from which the ore fields stand out. Massive sulfide-base metals shows with high contents of gold and silver are the youngest formations, which often show a distinct spatial linkage with tectonic faults. Probably the formation of Aleksandrinskoye ore field massive sulfide ores characterized by low sulfur contents and high content of all primary and accompanying mineral components is also associated with the formation of volcanites of continuous complex. Intrusive comagmatic rocks of Ulutau complex are associated with slight copper- molybdenum mineralization.

In early Frasnian siliceous shales of Mukasovsky complex there are spotted infiltration and volcanogenic - sedimentary shows of manganese (mounts Ostraya, Spytkova, Krasny Kamen'). They are often confined to siliceous rocks shattering zones.

In weakly differentiated calc-alkaline volcanites of late Frasnian Novovoroninsky complex copper-zeolite shows (Cherny Bugor) have been spotted. With gabbroids of Pogorelsky complex, comagmatic to them, the shows of cumulative-segregational bornite-titanomagnetite ores with high vanadium content (Pogorel'skoe, Volkovskoye type) are

associated. As it was recently established, they are characterized by significant concentrations of gold, silver and palladium, which is of practical interest for geological exploration and requires the evaluation of their ore elements resources.

Intrusive rocks of early Famennian volcano-intrusive Verhneural'sky complex, which is a typical island-arc shoshonite series, account for copper-molybdenum-porphyritic ore shows and non-industrial contact- metasomatic iron shows. Verkhneuralsk copper-molybdenum-porphyritic show have been studied in detail in the recent years. Unlike other similar Uralian shows, it bears a high concentration of molybdenum and has a low Cu/Mo ratio in ores, amounting to 10-20. The main prospects of the show are associated with molybdenum mineralization, which is mainly focused in its deep levels. In the Western part of Uchalino-Alexandrinskaya zone, amid flyschoids of late Framennian Samarinskaya strata (which is overlapping Famennian volcanites with conformity), the show of copper sandstones is present. The alternation of gray-colored, red-colored and calcareous sandstones is observed in the section. Mineralisation is represented by fine-grained impregnation of pyrite, sometimes with chalcopyrite and bornite. Sulphide clusters form the thin layers, bedding with conformity with syngenetic micro folding and plication; sulfides are also present in small clasts and gritstones as impregnated structures. Tournaisian calc-alkaline granitoids of Kasselskiy complex bear non-industrial skarn-magnetite and gold (gold-sulfide-quartz vein, Krasny Partisan shows, Popovskaya vein) mineralization.

Within the limits of Magnitogorsk zone the following deposits and shows are explored: one large deposit (Magnitogorsk), one medium sized (Maly Kuibas) and a number of small deposits and shows of magnetite ores, accompanied by pyroxene-garnet skarns. Moderate titanium-magnetite high-grade ore bodies have been detected at M. Kuibas. All of these deposits are in detail described in the literature. In Magnitogorsk zone the following time series of late Devonian and early Carboniferous volcanogenic complexes is reconstructed: basalt-basaltic andesite (late Frasnian) - trachybasalt-trachybasaltic andesite (late Frasnian - early Famennian) - trachybasalt-trachyandesite-trachydacite (Famennian-Tournaisian) - bimodal trachybasalt-rhyodacite (Tournaisian - Visean), and trachybasalt-trachybasaltic andesite-trachydacite-rhyolite (Tournaisian - early Visean). Petro-geochemical series, corresponding to the above-mentioned complexes, is: calc-alkaline – shoshonite – high-titanium shoshonite ("rifting") – potassium-sodium subalkaline and palingenic calc-alkaline – potassium-sodium subalkaline. This series reflects the destructive stage of island arc structure forming, i.e. the formation of narrow graben-shaped tension structure in its rear part at the end of the early Famennian and its further development in Tournaisian-Visean. It is reflected in a sharp increase in Ti, Na, Fe and decline in K, P, lithophile elements and rare-earth elements in magnetite composition, which is interpreted as a result of reduction in the melting depth for primary magmas against the background of the Earth's crust thinning. The ore formation is associated with the generation of hypabyssal intrusions of the Magnitogorsk series, comagmatic to Visean subalkaline volcanites. Magnetite ores, skarns and metasomatites, concomitant to them, occur among late Devonian and early Carboniferous formations of different facies and ages. The bulk of ores are concentrated in the basement of early Visean volcanic edifices. The formation of ore-bearing volcanic-intrusive complex occurred at local sites in high compression conditions. It is reflected by disposition of thrusts and reverse faults in volcanic edifices basement and emphasized by positive landforms of its paleotopography. Local high compression environments caused the formation of large hypabyssal magmatic focuses, which accounted for energy and fluid activity of the hydrothermal system. Titanomagnetite ores are localized in stock-like gabbroid bodies of differentiated Magnitogorsk series, yet they are also developed within local uplifts. Volcanites of subalkaline potassium-sodium series, which are close by age and composition, had been formed in adjacent structures in the conditions of tension, and are traced by fissure outflow of lavas and small extrusions. Under the conditions of low-explosion volcanism type and absence of large hypabyssal magmatic focuses it was not accompanied by ore formation.

Kizil'skaya zone comprises backarc basin, consisting of organogenic-detrital limestones of Kizil suite. It had been continuously forming from the beginning of the late Visean until the beginning of Bashkirian. Kizil suite is overlain by carbonate-terrigenous deposits of Urtazymskaya suite, Bashkirskiy and Moskovsky stages. In the upper part of the section, these deposits are covered by Yangelsk suite terrigenous sediments, deposited in late Carboniferous- Permian time. In Urtazymskaya suite, the large deposit of gypsum and anhydrite (Agapovskoye) has been discovered. It belongs to chemogenic-infliltrational type and had been formed in passive continental margin conditions.

To sum up, based on this overview, the following conclusions can be made. In the East-Magnitogorsk island arc the following metallogenic time series is specified: Cu - Cu,Zn - Cu,Zn,Pb(Au,Ag) - Cu,Ti,Fe(V) - Cu,Mo - Fe. This series generally reflects metallogenic evolution, typical for "ocean-continent" transition zones. Moreover, there is a strong correlation between the ores and ore-bearing magmatites composition, the migration of island arc magmatism centers from East to West is clearly demonstrated. Lateral Devonian-early Carboniferous metallogenic series is close to the time series. It also generally matches with lateral metallogenic zoning of island arcs, in which the migration of magmatic centers from the front to the rear part is revealed. Consequently, the Eastern part of the arc is the front one and the Western is the rear one. This is not consistent with the opinion about progressive Eastwards dipping of subduction paleozone during Magnitogorsk-Mugodzhar island arc system formation, almost universally accepted among Ural geologists. Apparently, the system was developing as a double island arc with the vergence change in subduction zone. The subduction zone polarity turnover is an important moment in the history of Magnitogorsk zone (Surin, 1993, 1995; Moseychuk, Surin, 2001). Similar occasions are known in nature, they are described in the literature for New Hebrides, Solomon, Luzon island arcs and South Fiji marginal sea. Geodynamics is a leading factor in forming the deposits of ore formations in Magnitogorsk megazone. It is crucial for obtaining suitable conditions for launching of ore formation mechanisms. Massive sulfide mineral deposits of copper-zinc-massive sulfide formation (Ural type) had formed in

complex geodynamic conditions during the transition from tension to compression at the early stage of island arc formation. To some extent, they mark the beginning of a long constructive phase of island arc development. Magnetite ore deposits of skarn-magnetite formation were generating during the destructive stage of "mature" island arc development in the local conditions of compression against the background of general tension. Such a difficult combination could probably be explained by the beginning of the collision between island arc and the continent. In each of the aforementioned examples, the magmatic focuses that had occurred during the «geodynamic pauses» at the transitions from tension to compression produced large ore bodies.

References:

Gusev G.S., Gushchin A.V., Zaykov V.V., Maslennikov V.V., Mezhelovsky N.V., Perevozchikov B.V., Surin T.N., Filatov E.I., Shirai E.P. Geology and Metallogeny of Island Arcs // Geodinamics and Metallogeny: Theory and Implications for Applied Geology. M.: MNR RF, I-RCGC (GEOKART), 2000. P. 213-295.

Moseychuk V.M., Surin T.N. Collision tectonics and depth structure of Southern Ural // 7th Zonenshain International Conference on Plate Tectonics. M.: Science World, 2001. P. 409-412.

Surin T.N. Geodinamics and paleovolcanic activity of the Magnitogorsk paleovolcanic belt (South Ural) // L.P.Zonenshain conference on plate tectonics. M: IO RAN-GEOMAR, 1993. P. 141.

Surin T.N. Geodinamics of the Magnitogorsk-Mugodjar paleoisland-arc system development (the South Urals) // 5th Zonenshain conference on plate tectonics. M: IO RAN - GEOMAR, 1995. P. 93-94.

Surin T.N., Moseychuk V.V. Geodinamika razvitiya Magnitigorskogo paleovulkanicheskogo poyasa (Geodinamic development of Magnitogorskiy palaeovolcanic belt) // Vestnik of SPbSU. Ser. 7. 1995. Vol. 4 (№ 28). P. 11-18. (In Russian).

MASSIVE SULFIDE BEARING ORE-MAGMATIC SYSTEM (URALIAN TYPE)
Surin T.N.

Federal State Budgetary Enterprise 'A. P. Karpinsky Russian Geological Research Institute', Saint-Petersburg, Russia

Volcanogenic massive sulfide-bearing magmatic system is a set of formation processes of ore-bearing magmas, volcanites and massive sulfide ores and metasomatites associated with them. The result of spatially combined interrelated processes of magmatism, sedimentation, metasomatism and ore formation is the emergence of a lithotectonic unit, that includes ore-bearing magmatic rocks, wall metasomatic rocks, ore-bearing sediments and ores (Surin, 1999).

The author have created a model of evolution and development of the system on the example of Uchalino-Alexandrinskaya zone, the largest massive sulfide-bearing structure of the Southern Ural. This volcanogenic structure is located in the northern part of East-Magnitogorsk paleo-island arc (see the article in this collection). It is elongated submeridionally, extending for almost 150 km. Within its limits, 12 deposits and several hundred shows of massive sulfide ores are known. Most of deposits in the zone are the classical examples of weakly deformed ore objects of the Ural type, which allows us to consider them as a standard for reconstruction of the massive sulfide-bearing ore-magmatic system of the Urals type.

The main paleovolcanic structures of Uchalino-Alexandrinskaya zone had formed in Givetian stage, which can be divided into early and late Givetian sub-stages.

Two dominant types of volcanism of the Early Givetian sub-stage are fissure and central-type. During the sub-stage, the ore-bearing "contrast" basalt-rhyolite formation was generated. After the end of the phase of active fissure volcanism, complex composite volcanoes started to emerge. In the course of shield volcanoes development, pyroclastic cones, peripheral and apical calderas had formed within their domes. In post-caldera stages, basalt edifices were upbuilded with dome volcanoes and extrusive domes of acid composition. The volcanism occurred in subaqueous environment and was accompanied by fumarolic activity. In total, about a dozen of large shield volcanoes and stratovolcanoes are known at Uchalino-Alexandrinskaya zone, along with about thirty dome volcanoes and acid extrusive domes. To some of them, massive sulfide deposits are confined. The chains of basalt volcanoes form uneven-aged ridges, pronounced in the paleotopography. Case study of the basalt ridges of Uchalinsky and Verhneuralsky ore-bearing districts, illustrates that the younger Mejozernaya basaltic ridge partly overlaps the slope of the older Uchalinskaya. This indicates that the so-called "levels" of massive sulfide ores localization are limited in space.

During late Givetian sub-stage, volcanism was continuing almost permanently. In this period the continuous basalt-andesite-dacite-rhyolite formation had formed. At this time, residual focuses of acidic magmas of the contrast formation were still functioning, as well as ring volcanic edifices that have formed areal volcanism fields with extrusive domes and dome volcanoes.

Massive sulfide ore formation occurred at the early stage of island arc formation with the following sequence of geodynamic environments changes: 1) In the interarc basin with weak tension under the conditions of diffuse spreading (Uchalinsky ore-bearing district); 2) The tension shifts to compression and marginal part of the interarc basin is accreting into the island arc (Verkhneuralsky ore region) 3) Intense lateral compression in the narrow rift trough in the rear part of the arc that occurred due to fault blocks movement in separate volcanic edifices (Alexandrinsky ore region) (Surin, 1993a; , 1993b, 1995, 1997a, 1997b, 1999; Tesalina et. al., 1998). Thus, as the result of massive sulfide-bearing ore-magmatic system functioning, the lateral-age series of massive sulfide deposits have been formed, which provides an opportunity to identify the traits of its evolution. In the aforementioned series, not only petro-geochemical features, but also the ore-

bearing magmas generation method is discretely changed: 1) High-iron differentiates of tholeiitic melts (according to "Fenner trend"); 2) Palingenic smeltings of the metamorphosed mafic substrate in the lower part of the crust; 3). Medium-acid calc-alkaline differentiates of basalt melts (according to "Bowen trend") (Surin, 1993a, 1995,1997b; Tesalina et. al., 1998). In the series, the geochemical characteristics of the ores naturally change. Firstly, Cu / Zn ratio and Pb, Se, Te, In, Cd, Ba, Au, Ag contents increase; these changes are geochemical indicators of the longitudinal-lateral zonation of the paleo-island arc structure, i.e. its gradual offset from the seismofocal plane as it moves from north to south; and secondly, the sulfur content decreases and its average isotopic composition in ores changes in the following way: mantle - crustal - mantle (Surin, 1993b, 1995; Tesalina et. al., 1998). Accordingly, the mineral composition of ores becomes much more complicated with a gradual decrease in the size of separate ore bodies. Paleovolcanic conditions for the ores localization also vary in the series: 1) Syn-volcanic depressions in the roof of acid domes on the periphery of basaltic shield volcanoes (Uchalinsky region); 2) Deep curve shaped caldera depressions filled with thick strata of acid volcanites and located on the slope of a huge multi-vent basalt shield volcano (Verkhneuralsky region) 3) Thin interbeds on the slope of a small accumulative multiphase volcanic edifice (Alexandrinsky region) (Surin, 1993b, 1999; Tesalina et. al., 1998). In the author's opinion, the formation depth of massive ores gradually decreases in the series, which correlates with the increase of base metals concentration in them (Tesalina et. al., 1998). The reduction of ore formation depth is also reflected in lithological composition of sedimentary rocks.
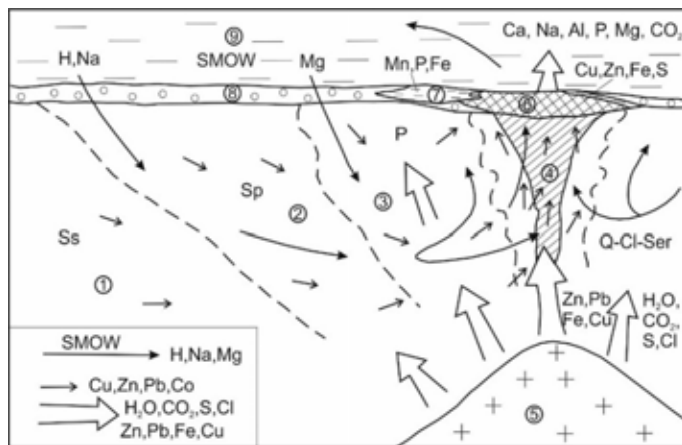
Fig. 1. The convective-postmagmatic model of massive sulfide ore formation
Numbers in the circles: 1-4 – Metasomatic zones: 1 – weakly modified rocks zone (saussurite – Ss), 2 – zone of calcium subtraction (spilitization – Sp), 3 – propylite zone (P), 4 - quartz-chlorite-sericite metasomatite zone (Q-Cl-Ser). 5 – near-surface acid magma focus. 6 – massive sulfide ores, 7 – manganese-iron sediments. 8 – volcanogenic sedimentary and tuffogenic sedimentary rocks. 9 – sea water (SMOW). Dashed lines indicate the conventional borders of metasomatic zones. Diagonal hatching marks out the ore channel. Long thin arrows reflect the sea water circulation, shot thin arrows – the migration of chalcophile elements, wide arrows – the movement of postmagmatic ore-forming solutions, emitted during magmatic focus degassing.

The maximum of massive sulfide mineralization is confined to palingenic acidic rocks, localized in the upper part of the section of "contrast" basalt-rhyolite formation. The abrupt enriching of palingenic acid rocks with normative albite, in contrast with normative anorthite and orthoclase indicates that they are the volcanic analogues of trondhjemites. The composition of palingenic rocks is generally equal to the experimentally established values at P (H2O) = 5 kbar. Besides, very high values of the ratio between normative albite and normative orthoclase, combined with the presence of normative corundum, suggests the equilibrium of melts with hornblende. Since amphibole is not a constant liquidus phase during the melts crystallization, it can be concluded that it played the role of restite during their crystallization. Fractional melting of amphibolite, as the possible mechanism of trondhjemite melts generation, is generally accepted. It should be noted that even the beginning of acidic magmas melting at a pressure of 5 kbar under the conditions of the amphibolite facies upper stage requires a rather high geothermal gradient, which can be reached in the roots of the island arc due to the heat supply with basaltic magma. The shift from tension to compression at the end of the early stage of the island arc formation also contributes to the increase of heat flow and separation of magmas from the substrate in the depths of around 20 km. The fact that the magmas are enriched with refractory and volatile components can be explained by their high melting temperatures (1000°C and higher), which is confirmed by thermometric study of inclusions from quartz phenocrysts. At such temperatures, under the 5 kbar pressure, amphibole stability limit and the temperature boundary between amphibolite and granulite facies of metamorphism are overcome. That leads to considerable substrate dehydration and to the reactionary relationship between the melt and the amphibole. Thereby, the most probable mechanism for palingenic acidic melts generation is the fractional melting of mafic heterogeneous amphibole-containing substrate in the lower part of the island arc base. As they were rising to the surface, they experienced degassing together with the release of significant amount of H_2O, CO_2, sulfur and chlorine. Thus, the advancing front of volatile components is created. This results in the propylitization of basalts on the surface. The differentiation of magmas occurred in the near-surface focuses at the low depths (1-8 km).

It should be noted that all the geological evidences indicate that generation of palingenic rocks of "contrast" formation occurred under the conditions of permanent decrease in the permeability of the crust. The most reliable interpretation of this presumes a change from tension conditions, in which the lower part of the section had been formed, to lateral compression conditions, under which the formation of the upper parts of the section took place. Thereby, the formation of near-surface focuses of acidic magmas, and, as the direct result, massive sulfide deposits, marks the

geodynamic "stop" during this shift. Squeezing of the acid domes marks the final phase of generation of the formation in the compression conditions.The analysis of the main factors of the deposits formation and synthesis of the available data led us to the conclusion that in the case we are considering, a combined convective-postmagmatic model for massive sulfide ores formation is implemented (Fig. 1). Its essence is that in the ore formation process, two linked mechanisms act simultaneously: a convective near-surface cell of sea water recirculation and the active peripheric magmatic focus, which is located in the center of the cell, actively producing hydrothermal solutions. In the author's opinion, the proposed model takes into account the genetic relationship between massive sulfide ore formation and acid magmatism of the basalt-rhyolite (bimodal) formation, with four types of this relationship: spatial, temporal, energy and material (Surin, 1993b, 1995). Spatial connection represents the confinement of massive sulfide deposits to the centers of acidic volcanism. Besides, the scale and composition of mineralization demonstrate a strong correlation with the size of volcanic edifices and the composition of ore-bearing acid rocks. The temporal connection is expressed in massive sulfide ores localization in the form of layer bodies at certain ore-controlling sublevels among the tephroid-sedimentary rocks, which record interruptions between separate acid volcanism rhythmites. The revealed temporal evolution of mineralization scale and composition is a consequence of the self-regulation of ore-magmatic systems that "adapt" to local changes of geodynamic situation (Surin, 1999). The pulsation activity of acid magma focuses also determines the structure of ore channels, composed of quartz-sericite metasomatites. Moreover, the composition of the latter also reveals a close relationship with the composition of the ores. As the percentage of copper decreases and the content of lead rises in the chemical composition of metasomatites, the increasing proportion of alumina, magnesium, calcium, potassium and carbon dioxide is observed, while the concentration of silicic raw materials, Fe_{sum} and sulfur is falling (Surin, 1993b; Tesalina et. al., 1998). The energy relationship is attributable to the occurrence of near-surface acid magma focuses as the main condition of the existence of the convective-postmagmatic hydrothermal system. Mineralization scale reduction over time is a consequence of the energy activity decreasing, i.e. gradual "decay" of hydrothermal system. The material connection is expressed in the fact that the near-surface acid magma focuses were the sources of ore-forming solutions. These solutions contained large volumes of hydrogen sulphide and carbon dioxide. It was their influx into the upper horizons of the crust that triggered the formation and long-term functioning of the hydrothermal system. In addition, hot postmagmatic fluids significantly increased convection (Surin, 1993b). The composition of ore-bearing solutions was changing significantly over time towards reducing the concentration of vadose ("sea") waters and increasing the content of carbon dioxide and the alkaline components. More reductive conditions are the consequence of lower sulfur content in the ore-bearing solution. That is represented in polymetallic composition of the youngest ore formation (close to the "Kuroko" type) (Tesalina et. al., 1998). It is evident that the acid magma focuses had also played the role of sources of metals (predominantly zinc and lead), which is confirmed by the calculations of the substance budget of the paleo-hydrothermal system and experimental data on the behavior of ore elements during the acid magmas crystallization (Surin, 1993b, 1999). Synchronous implementation of convective and hydrothermal-postmagmatic ore-forming mechanisms apparently is the reason for the unique geochemical enrichment of massive sulfide deposits of the Ural type, i.e. simultaneous enrichment with iron, sulfur, copper and zinc, comparing to massive sulfide-bearing objects of other types. Depending on local geological settings, the contribution of the main ore formation mechanisms to the final result may vary at different sites. That explains the special features of individual deposits, including the differences in the ore composition.

To sum up, the obtained data set makes it possible to substantially specify the existing views on the formation, self-regulation, and temporal evolution of the massive sulfide-bearing ore-magmatic system of the Ural type (Surin, 1997a, 1999).

References:

Surin T.N. Petrologiya i geokhimiya vulkanitov rannezhivetskoy bazal't-riolitovoy kolchedanonosnoy formatsii (Yuzhnyy Ural). (Petrology and geochemistry of volcanites of early Givetian basalt-rhyolite massive sulfide-bearing formation (South Urals)). Ufa: UfNC RAN, 1993a. 45 p. (In Russian).

Surin T.N. Metasomatoz i kolchedannoye rudoobrazovaniye (Verkhneural'skiy rudnyy rayon). (Metasomatism and massive sulfide ore formation (Verkhneuralsky ore region)). Ekaterinburg: Nauka, 1993b. 104 p. (In Russian).

Surin T.N. Geodinamika, petrogenezis kontrastnoy formatsii Yuzhnogo Urala i kolchedannoye rudoobrazovaniye. (Geodynamics, petrogenesis of the Southern Urals contrast formation and massive sulfide ore formation). // Aktual'nyye problemy magmaticheskoy geologii, petrologii i rudoobrazovaniya. Ekaterinburg: Uralgeolkom, 1995. P. 137-146 (In Russian).

Surin T.N. Kolchedanonosnaya rudno-magmaticheskaya sistema ural'skogo tipa: opredeleniye, geodinamicheskiye usloviya formirovaniya i evolyutsiya (Uchalino-Aleksandrinskaya zona, Vostochno-Magnitogorskaya paleoostrovnaya duga, Yuzhnyy Ural). (Massive sulfide-bearing ore-magmatic system of the Ural type: definition, geodynamic conditions of formation and evolution (Uchalino-Alexandrinskaya zone, East-Magnitogorsk palaeo-island arc, Southern Ural)) // Paleogeograficheskiye i geodinamicheskiye usloviya obrazovaniya vulkanogenno-osadochnykh mestorozhdeniy. Miass: IMin UrO RAN, 1997a. P. 178-179 (In Russian).

Surin T.N. Petrologo-mineralogicheskiye issledovaniya magmatitov Vostochno-Magnitogorskogo poyasa (Yuzhnyy Ural). (Petrological and mineralogical studies of magmatites of the East-Magnitogorsk belt (Southern Urals). Miass: Geotur, 1997b. 310 p. (In Russian).

Tesalina S.G., Maslennikov V.V., Surin T.N. Aleksandrinskoye medno-tsinkovo-kolchedannoye mestorozhdeniye (Vostochno-Magnitogorskaya paleoostrovnaya duga, Ural). (Alexandrinskoye copper-zinc-massive sulfide deposit (East-Magnitogorsk palaeo-island arc, the Urals)). Miass: IMin UrO RAN, 1998. 228 p. (In Russian).

Surin T.N. Model' razvitiya kolchedanonosnoy rudno-magmaticheskoy sistemy ural'skogo tipa (Uchalino-Aleksandrinskaya zona, Vostochno-Magnitogorskaya paleoostrovnaya duga, Yuzhnyy Ural)/ (The model of the development of massive sulfide-bearing ore-magmatic system of the Ural type (Uchalino-Alexandrinskaya zone, East-Magnitogorsk palaeo-island arc, Southern Urals) // Modeli vulkanogenno-osadochnykh rudoobrazuyushchikh sistem. SPb, 1999. (MAGRM, MPR RF, RAN, RAYEN, VSEGEI, VNIIOkeangeologiya, GSF "Mineral") Pp. 134-136 (In Russian).

MINERALOGICAL CHARACTERISTIC OF MICRO-INCLUSIONS IN OLIVINE IN PALLASITE
Takayama Y., Ohfuji H.

Ehime University, Matsuyama, Japan, takayama@sci.ehime-u.ac.jp

Pallasite is a type of meteorite that consists of a mixture of olivine and Fe-Ni alloy. Its mineral composition and characteristic texture have attracted the attention of many meteoriticists and mineralogists. So far, various models have been proposed to explain its origin, and among them the most popular models are 1) formation by magmatic differentiation of silicate-metal melt at the CMB condition (Boesenberg et al., 2012), and 2) formation by mechanical mixing of different asteroids through extensive impact(s) (Yang et al., 2010). However, the origin and the formation mechanism of pallasite has still been unclear. Here, we performed detailed micro-texture observation of pallasite using SEM and TEM and found droplet-shaped micro-inclusions composed of such as Fe-Ni alloy, FeS, oxides and silicates in olivine crystals. Since such micro-inclusions might have recorded a thermal history of the pallasite during or after its formation, investigating the formation process would provide useful information on the origin of pallasite.

The sample studied was Seymchan (MG pallasite) discovered from the Yasachinaya river in Russia. The microstructure and the chemical composition of olivine and its inclusions were investigated using a field-emission-type scanning electron microscope (FE-SEM) equipped with an energy dispersive X-ray spectrometer (EDS). We also prepared thin foil sections from some inclusions using a focused ion beam (FIB) system and analyzed the structure and chemical composition of the constituent mineral phases by transmission electron microscopy (TEM).

SEM-EDS analysis showed that the micro-inclusions in olivine are composed mainly of troilite (FeS) and Fe-Ni phases (kamasite and taenite) with small amounts of stanfieldite ($Ca_4(Mg, Fe^{2+})(PO_4)_6$), chromite (($Mg, Fe^{2+})Cr_2O_3$) and tridymite ($SiO_2$) as minor phases. Those inclusions are most likely melt inclusions which formed through the infilled of the melt along cracks in olivine followed by thermal healing to form the droplet-shapes, since most of them are arranged linearly in the host olivine. The fact that they consist of multiple phases separated by sharp boundaries suggests that they crystallized at a slow cooling rate rather than upon quenching. Chemical quantification analysis revealed that the Fe-Ni phases in the inclusions have larger variation in Ni content than those in the matrix of the pallasite, while minor phases are almost uniform in composition among many inclusions. This means that the micro-inclusions in olivine in Seymchan pallasite were all produced simultaneously from a single source melt, which may have been formed as a result of partial melting of the Fe-Ni alloy in the pallasite matrix, or provided by a completely different event after pallasite formation. In either case, the presence of tridymite implies that the formation of the micro-inclusions likely occurred through a low pressure event after pallasite formation.

References:

Giulio F.D. Solferino, Gregor J. Golabek, Francis Nimmo, Max W. Schmidt (2015) Fast grain growth of olivine in liquid Fe-S and the formation of pallasites with rounded olivine grains. Geochemica et Cosmochimica Acta 162:259-275

Jijin Yang, Joseph I. Goldstein, Edward R.D. Scott (2010) Main-group pallasites: Thermal history, relationship to IIIAB irons, and origin. Geochemica et Cosmochimica Acta 74:4471-4492

Joseph S. Boesenberg, Jeremy S. Delaney, Roger H. Hewins (2012) A petrogical and chemical reexamination of Main Group pallasite formation. Geochemica et Cosmochimica Acta 89:134-158

PHASE ASSOCIATIONS AND PARTITIONING OF MINOR ELEMENTS UPON PARTIAL MELTING OF MODEL PYROLITE UNDER THE CONDITIONS OF THE TRANSITION ZONE AND LOWER MANTLE OF THE EARTH
Tamarova A.P.[1], Bobrov A.V.[1], Sirotkina E.A.[1], Bindi L.[2,3], Irifune T.[4]

[1]Lomonosov Moscow State University, Moscow, Russia
[2]Università di Firenze, Firenze, Italy [3]Istituto di Geoscienze e Georisorse, Firenze, Italy,
[4]Matsuyama University, Matsuyama, Japan, dragon.of.rainbow@yandex.ru

Partitioning of trace and rare-earth elements between mantle minerals and melts at high pressures and temperatures is of key importance for all geochemical models involving melting of the Earth's mantle. According to existing models (Harte, 2010), ringwoodite-ahrensite (Mg_2SiO_4–Fe_2SiO_4 with spinel structure) solid solution and majoritic garnet [$(Ca,Mg,Fe)_3Al_2Si_3O_{12}$–$(Mg,Fe)_4Si_4O_{12}$)] (Akaogi, 2007) are the major rock-forming minerals in the deep transition zone (Ringwood, 1991). Bridgmanite ($MgSiO_3$ with perovskite-type structure), calcium perovskite ($CaSiO_3$ with perovskite-type structure), and ferropericlase (($Mg,Fe)O$ with NaCl-type structure) are the major rock-forming mineral phases in the lower mantle of the Earth. As is evident from previous experimental studies, trace and rare-earth elements in the lower mantle preferably distribute to calcium perovskite in relation to bridgmanite and ferropericlase (Corgne et al., 2003). Calcium perovskite is often enriched in LREE, wheras bridgmanite is depleted with them (Kaminsky, 2012). Most of

minor elements are incompatible in bridgmanite; only Si, Mg, Sc, Zr, Lu and Hf are consistently compatible. Partition coefficients of REEs in bridgmanite increase from La (D_{La} = 0.01) to Lu (D_{Lu} up to ~1.5) (Liebske et al., 2005).

Experiments at 21-24 GPa and 1200-2200°C were performed using a 2000 ton split-sphere press installed at the Ehime University (Matsuyama, Japan). Starting compositions were represented by the simplified composition of pyrolite (Ringwood, 1966). Agents of partial melting included (1) H_2O in the composition of brucite $Mg(OH)_2$ (2 wt % H_2O), (2) mixture of carbonates (10 and 15 wt % of carbonate mixture). The carbonate composition was multicomponent: $CaCO_3$, $MgCO_3$, $FeCO_3$, Na_2CO_3 (25 wt% of each), and corresponded to the carbonatite end-member of the carbonate–silicate matter of primary inclusions in natural diamonds (Schrauder, Navon, 1994). In each starting composition, a trace-element mixture was added in a weight ratio of 1/99. This mixture included La, Ce, Pr, Nd, Sm, Eu, Gd, Tb, Dy, Ho, Er, Tm, Yb, Lu, Y, Hf, Zr, Nb, Sc, Ta, Pb, Zn oxides, RbCl and Sr-, Ba-, and Li-carbonates and was prepared and homogenized by prolonged grinding in the presence of ethanol.

Several parageneses were registered in experimental samples. In the carbonate-silicate system, the evidence for partial melting was observed at ≥1700°C. In the hydrous system, partial melting occurred at ≥1900°C. the following parageneses are typical of the carbonate-silicate system: fPer+L; L+fPer+Brd+CaPrv; fPer+Brd+ CaPrv+Carb. The samples produced in the hydrous system consisted of L+fPer+Brd+CaPrv; fPer+Brd+CaPrv. Our experiments substantiated the mechanisms isomorphism in the bridgmanite structure: $Mg^{2+}_A + Si^{4+}_B = Al^{3+}_A + Al^{3+}_B$ and $2Si^{4+}_B + O^{2-}_O = 2Al^{3+}_B + V_O$ (Akaogi, 2007) with prevalence of the second scheme. Chromium and aluminum content decrease with increasing magnesium content in bridgmanite.

We have found that in the hydrous system sodium preferably incorporates in ferropericlase, due to calcium perovskite. In addition, sodium content in ferropericlase increases with temperature. Aluminum content increases with increasing calcium content in calcium perovskite. Chromium content decreases with increasing magnesium content in ferropericlase. It is shown that bridgmanite and ferropericlase are depleted in LREE. Partition coefficients (CaPrv/L) of REEs in calcium perovskite decrease with temperature. The results obtained indicate that under the conditions of the Earth's lower mantle, trace and rare-earth elements may be accumulated not only in the $CaSiO_3$ perovskite (Ringwood et al., 1988), but in ferropericlase and bridgmanite as well.

References:

Akaogi M (2007) Phase transitions of minerals in the transition zone and upper part of the lower mantle. Advances in High-Pressure Mineralogy: Geological Society of America Special Paper 421:1–13.

Andrault D (2007) Properties of lower-mantle Al(Mg,Fe)SiO$_3$ perovskite. Ohtani, E., ed., Advances in High-Pressure Mineralogy: Geological Society of America Special Paper 421:15–36

Corgne A, Alan NL, Wood BJ (2003) Atomistic simulations of trace element incorporation into the large site of MgSiO$_3$ and CaSiO$_3$ perovskites. Phys Earth Planet Inter 139:113–127

Dobson DP, Jacobsen SD (2004) The flux growth of magnesium silicate perovskite single crystals. Am Mineral 89:807–811

Harte B (2010) Diamond formation in the deep mantle: the record of mineral inclusions and their distribution in relation to mantle dehydration zones. Miner Mag 74:189–215

Kaminsky FV (2012) Mineralogy of the lower mantle: A review of 'super-deep' mineral inclusions in diamond. Earth-Sci Rev 110, p. 127–147

Liebske C, Corgne A, Frost DJ, Rubie DC, Wood BJ (2005) Compositional effects on element partitioning between Mg-silicate perovskite and silicate melts. Contrib Mineral Petrol 149:113-128

Ringwood AE, Irifune T (1988) Nature of the 650-km seismic discontinuity: implications for mantle dynamics and differentiation. Nature 331:131–136

Schrauder M, Navon O (1994) Hydrous and carbonatitic mantle fluids in fibrous diamonds from Jwaneng, Botswana. Geochim Cosmochim Acta 58:761–771.

MOHO AND MAGMATIC UNDERPLATING IN CONTINENTAL LITHOSPHERE

Thybo H.[1,2], *Artemieva I.M.*[3]
[1]University of Oslo, Norway, thybo@geo.uio.no
[2]Istanbul Technical University, Istanbul, Turkey; h.thybo@gmail.com
[3]University of Copenhagen, Copenhagen, Denmark, irina@ign.ku.dk, iartemieva@gmail.com

Underplating was originally proposed as the process of magma ponding at the base of the crust and was inferred from petrologic considerations. This process not only may add high density material to the deep crust, but also may contribute low density material to the upper parts of the crust by magma fractionation during cooling and solidification in the lower crust. Separation of the low density material from the high-density residue may be a main process of formation of continental crust with its characteristic low average density, also during the early evolution of the Earth.

Despite the assumed importance of underplating processes and associated fractionation, the available geophysical images of underplated material remain relatively sparse and confined to specific tectonic environments. Direct ponding of magma at the Moho is only observed in very few locations, probably because magma usually interacts with the surrounding crustal rocks which leads to smearing of geophysical signals from the underplated material.

In terms of processes, there is no direct discriminator between the traditional concept of underplated material and lower crustal magmatic intrusions in the form of batholiths and sill-like features, and in the current review we consider both these phenomena as underplating. In this broad sense, underplating is observed in a variety of tectonic settings, including island arcs, wide extensional continental areas, rift zones, continental margins and palaeo-suture zones in Precambrian crust. We review the structural styles of magma underplating as observed by seismic imaging and discuss these first order observations in relation to the Moho.

References:

Thybo H., Artemieva I.M. (2013). Moho and magmatic underplating in continental lithosphere. Tectonophysics 609, 605–619, http://dx.doi.org/10.1016/j.tecto.2013.05.032

RARE METAL-RARE EARTH MINERALIZATION OF THE NORTHERN TIMAN (MALYJ KAMESHEK MASSIF)

Udoratina O.V.[1], Varlamov D.A.[2], Andreichev V.L.[1]

[1]Komi Science Center Institute of Geology, Ural Branch of the Russian Academy of Sciences, Syktyvkar, Russia, udoratina@geo.komisc.ru,
[2]Institute of Experimental Mineralogy, Chernogolovka, Russia, dima@iem.ac.ru

The alkaline magmatism revealed quite widely in Timan and Kanin Peninsula in the Late Precambrian. Monzonites are exposed in the northwestern part of the Kanin Peninsula (120x40m). In Northern Timan alkaline and nepheline syenites form massifs of the Bolshoy Rumyanichny, Krayny and Malyj Kameshek Capes. Here in the mouth of the Rumyanichnaya River a small exposure (150x120 m) of olivine-kersutite gabbro can be observed. In Middle Timan in the southeastern part of the Chetlassky Kamen a dyke series of alkaline picrites is observed; and in the South Sub-Timan, the syenites have been exposed by boreholes 1- and 4-Izkosgora at depth of 830 m.

The rare metal – rare earth mineralization is associated with the rocks of the Malyj Kameshek syenite massif located in the central part of the Rumyanichnaya fault zone. The massif has an isometric shape with the area of about 2 km^2. Within the massif the syenites form two dike-like bodies about 100 m thick each, oriented northwestward and cutting the metamorphic shales of Upper Riphean Barmin series and metabasites. The contact with the shales, observed in the northeastern part of the massif, is clear, intrusive. In the exocontact zone with the syenites the shales are slightly hornfelsed. In the endocontact zone the syenites are represented by fine-grained, non-nepheline varieties. The primary intrusive contact between the basic and alkaline rocks is obscured by the processes of syenitization of metabasites and later processes of dislocation metamorphism and has the form of a gradual transition.

The intrusive syenites are represented by massive light gray or pink medium- and coarse-grained rocks containing nepheline in the most cases. The central part of the massif is composed of intensely syenithized metabasites transformed into apobasite syenites. These rocks have a more melanocratic appearance and are more fine-grained than the syenites. Depending on the degree of syenitization their color varies from dark gray to pink. The apobasitic syenites in the contact zone with the intrusive syenites are cut by thin (0.1-0.2 m) veins of syenite-aplites.

All magmatic formations of the Malyj Kameshek massif are cut by zones of mylonitization of the northwestern and sublatitudinal strikes. The sublatitudinal gneissic structure, observed in all varieties of syenites, is expressed by the orientation of finely flaked aggregates of biotite coinciding with the direction of the zones of intensive cleavage and mylonitization. The apobasitic syenites and syenitized metabasites of the central part of the massif, located within the sublatitudinal zone of intense dislocation metamorphism, suffered processes of silicification, carbonatization, muscovitization.

In the same part of the massif the main part of thin isometric albitite bodies is concentrated, which occur among the gneissic apobasite syenites and are confined to the intersections of cleavage and mylonitization zones. Separate bodies of albitites are observed in the north-eastern and north-western parts of the massif. The albitites are represented by massive fine-grained, mainly albite, red-pink and yellowish-white metasomatites on blastomylonites of apobasite syenites. The rocks have been drilled by a series of samples 172(1-4) and 174(1-4) in the central part of the massif and in the northwest part by samples 149(1-4).

Albitites are represented by massive, fine-grained rocks of red and beige color; the rock's color is conditioned by spreading fine-dispersed hematite and iron hydroxides on it. The basic matrix is represented by the association quartz + alkaline feldspar + albite, the microstructure is mainly lamellar. The microscopy reveals cataclase and mylonitization structures (Fig. 1). The rock composition: albite, alkaline feldspar (orthoclase), quartz; micas (biotite, muscovite) is rarely observed; the main accessory minerals are zircon, apatite, barite; secondary – ferrous chlorite. Rare metal - rare earth ore minerals are located in the intergranular space. Minerals were studied by microprobe analysis in epoxy-based thin sections (IEM RAS, Chernogolovka).

Our investigations found that the main bulk of the rocks is composed by albite with subordinate quartz and Kfs. All other mineral associations are located in the intercataclase space. We determined the presence of barium phases everywhere (Ba-containing Kfs and high-Ba rims in it, as well as a large amount of barite). Dark-color minerals are represented by micas: biotite and muscovite (possibly part of them with lithium). We found a wide development of various carbonate phases (calcite, dolomite, Fe-dolomite, manganese varieties). Fluorite is developed. Rare earth minerals are represented by phosphates (monazite, xenotime) and fluorine-rich carbonates (bastnesite, parisite, synchyzite and their high-potassium analogues). Rare metal minerals are represented by the smallest grains of pyrochlore and fergusonite,

significantly Nb- and W-enriched rutiles. Titanium minerals are also represented by ilmenite and high-Mn ilmenite.
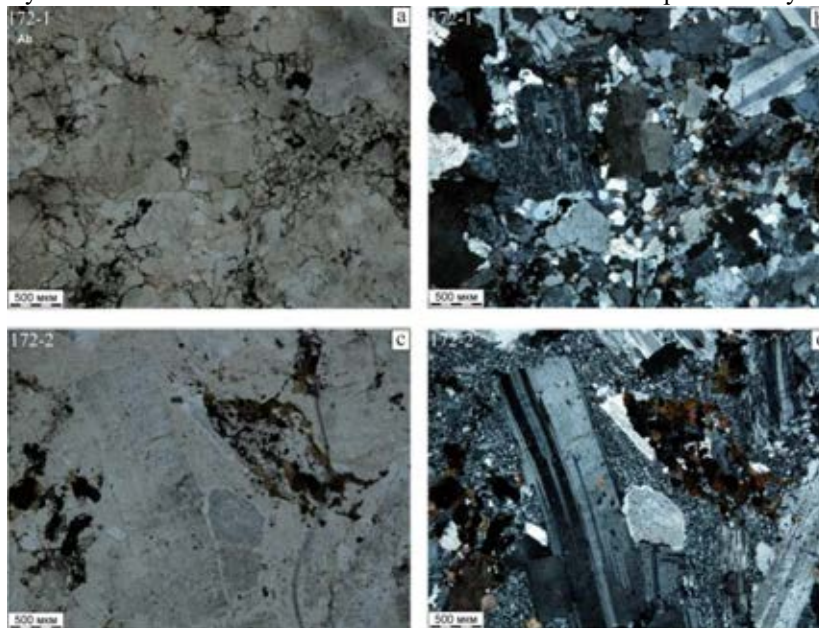
Fig. 1. Microstructures of ore-bearing albitites. Quartz-feldspar-albite aggregate with newly formed carbonates (a-b), large albite crystals in a mylonitized quartz-feldspar-albite matrix (c-d). a, c – without the analyzer.

Albite composes the matrix of the rocks, the chemical composition of the albite is without impurities. Potassium feldspar, in contrary, has an unusual chemical composition, barium enrichment is observed. Barium-potassium feldspar (barium orthoclase) forms spotted accumulations in the rocks associating them with carbonates and fluorite (Fig. 2, Fig. 3 a-c), the content of BaO in the main grains is 0-7 wt%, the content in the rims increases to 5-13 wt%.
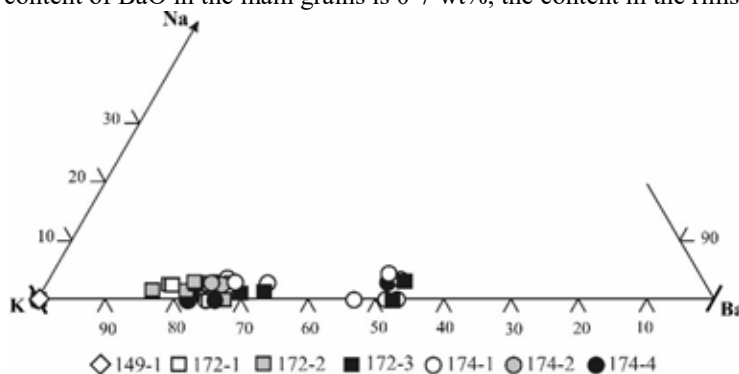
Fig. 2. K and Ba ratio in the orthoclase.

A group of carbonates is represented by calcite and dolomite (including Fe- and Mn-containing varieties), as well as fluorine-rich REE carbonates – bastnesite, synchisite and parizite (Fig. 3 d-e). Carbonates are noted in the intergranular space, aggregates 50-150 mkm in association with rutile, xenotime and thorium phases. The content of CaO in synchysite (wt.%) varies from 12 to 20, SrO 0-1.2, Y_2O_3 0-2, LREE oxides 20-42, MREE 6-24, HREE 0-0.7, thorium (ThO_2) 0-12. High-thorium synchisite-like phases is distinguished, in which the content of thorium (ThO_2) is from 14 to 34 wt%, CaO 10-20, SrO 0-1.2, Y_2O_3 0.2-1.4, the amount of rare earths drops noticeably LREE 10-27, MREE 3-5, HREE is absent. The content of CaO in parisite (wt.%) varies from 8 to 11, SrO 0-1, Y_2O_3 0-2.3, LREE 42-58, MREE 5-21, HREE 0-0.3, thorium is always present ThO_2 0-3. The quantity of rare earths in bastnesite (oxide wt.%) is LREE 52-64, MREE 6-10, HREE 0, SrO 0-0.3, Y_2O_3 0-0.8, thorium is also present – ThO_2 0-1.5. Distribution LREE$_{(La-Pr)}$−MREE$_{(Nd-Dy)}$−HREE$_{(Ho-Lu)}$ and Ca-Sr-Th in fluorine-rich REE carbonates is shown in Fig. 4-5.

Zircon-thorite phases. Zircon is observed as both separate, almost non-thorium phases (small idiomorphic, occasionally zonal crystals and rounded shell individuals), and high-thorium varieties in the joints with thorite and its derivatives, often with xenotime border (Fig. 3f). Fergusonite and pyrochlore were observed in single small aggregates.

Despite a high content of minerals of light rare earths (carbonates), there is a lot of xenotime in the rocks.

Xenotime forms individual grains and crystals, up to 50-70 mkm, developed everywhere, the content of Y_2O_3 is 26-43 wt%. Dy and Gd high enrichment is observed in the rims (up to 9 wt.% of Dy_2O_3 and 14 wt.% Gd_2O_3). The observed Y, Ce, Ca, Nb, Ta, Ti microphases are estimated by eschinite-euxenite.

Rutiles and ilmenites form aggregates in association with carbonates (Fig. 3 g-h), niobium content in Nb-rutile reaches 15 wt% of Nb_2O_5, tungsten in W-rutile up to 5 wt% of WO_3, manganese content in Mn-ilmenite reaches 25 wt% MnO.
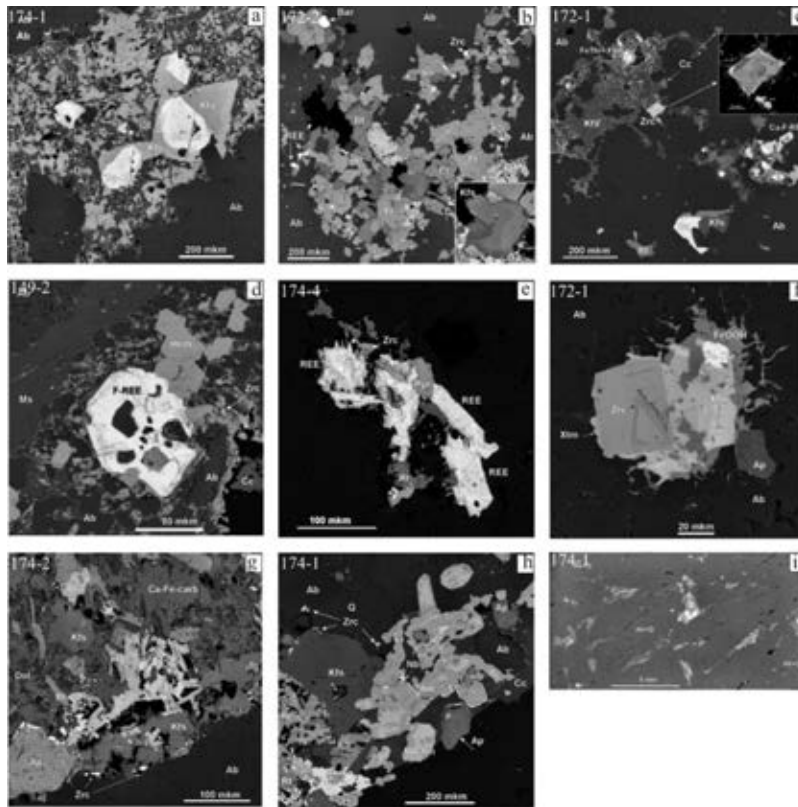
Fig. 3. Ore accessory minerals. Distribution in rocks grains of high-barium Kfs (a-c), aggregates of fluorine-rich REE carbonates (d-e), zircon and xenotime joint in albite matrix (f), Nb-rutile and apatite in carbonate-feldspar aggregate (g), Mn-rich ilmenite (h), the distribution of ore minerals in the intercataclase space in the albitites (i).
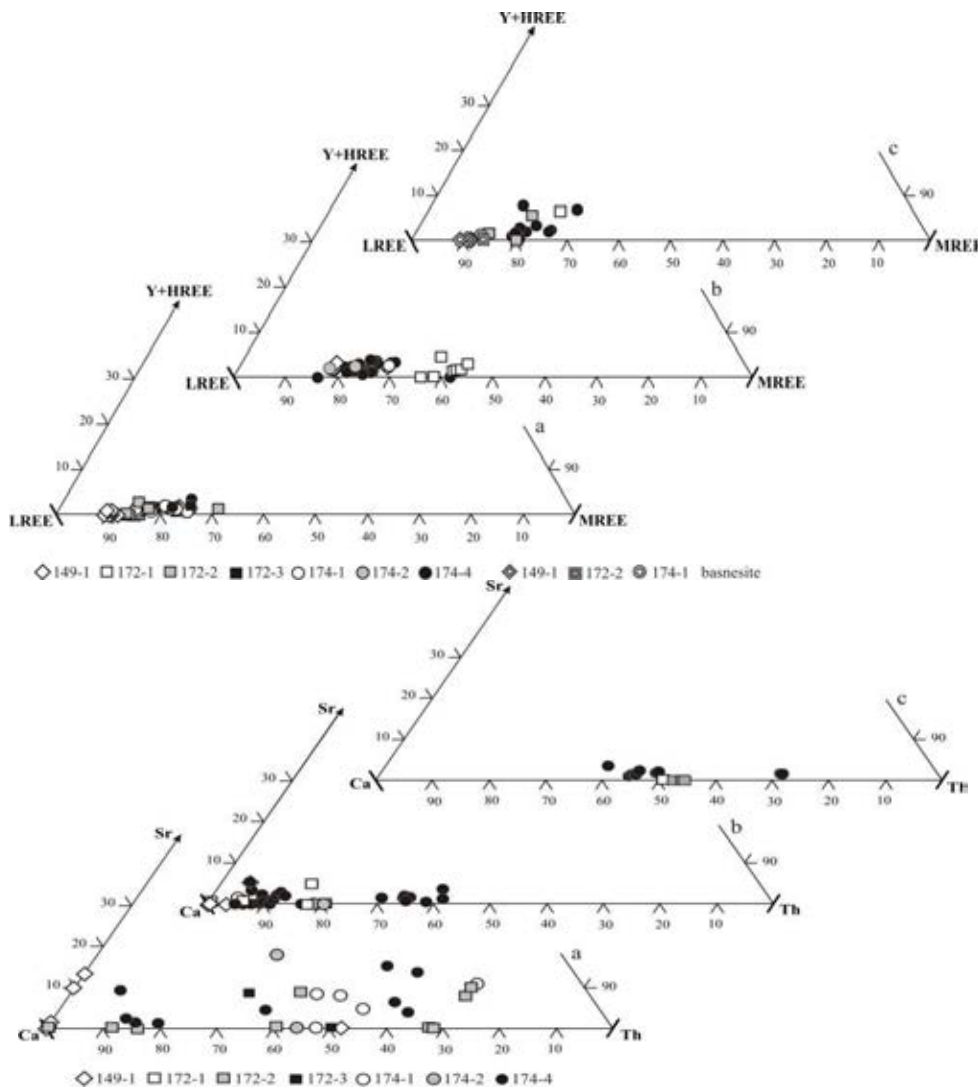
Fig. 4. Ratio of $LREE_{(La-Pr)}$–$MREE_{(Nd-Dy)}$–$HREE_{(Ho-Lu)}$ in fluorine-rich rare earth carbonates. A – parisite, b – synchisite, c – Th-synchitisite and bastnesite.

Fig. 5. Ratio of Ca-Sr-Th in fluorine-rare earth carbonates (for a-c see fig. 4).

Thus, in albitites the main ore mineralization is shown in the form of grains (fluorine)carbonates of REE in the intergranular spaces (Fig. 3i). In association with carbonates – high-barium feldspar, xenotime (including HREE-enriched), a wide range of titanium minerals (rutile, Nb- and W-rutile, ilmenite, Mn-ilmenite), zircons (low- and high-thorium) and thorites, as well as undiagnosed mixed phases (Zr-Th -Si+Y-P), phases with niobium and uranium, in single structures monazite, pyrochlore, fergusonite were found. The rocks show an unusually high content of thorium, there is a large number of undiagnosed thorium phases (REE carbonates, phosphorus and ferro-thorites, etc.). Rare sulfides are represented by micrograins of pyrite, galenite, molybdenite. The role of barium mineralization in the form of high-barium feldspars and abundant barite is high. The albitites are saturated with hematite and iron hydroxides. The main REE minerals are fluorine-rich REE carbonates (TR wt.%): bastnesite (61-72), synchisite (34-58), Th-synchitisite (13-33), parisite (53-72).

MINERALS OF THE PYROCHLORE SUPERGROUP FROM METASOMATIC ASSOCIATIONS OF MINERALS OF CHALCOPHILE ELEMENTS IN THE PELAGONIAN MASSIF, MACEDONIA

Varlamov D.A.[1,2], Ermolaeva V.N.[1,3], Jančev S.[4], Chukanov N.V.[2]

[1]Institute of Experimental Mineralogy, Chernogolovka, Russia
[2]Institute of Problem of Chemical Physics of the Russian Academy of Science, Chernogolovka, Russia
[3]Vernadsky Institute of Geochemistry and Analytical Chemistry of the Russian Academy of Sciences, Moscow, Russia, cvera@mail.ru
[4]Faculty of Technology and Metallurgy, Saints Cyril and Methodius University, Skopje, Macedonia

Metamorphic rocks, which form exocontact aureoles around metha-rhyolitic bodies among early Paleozoic metamorphic complex near Nežilovo village in Pelagonian massif (Macedonia), are characterize by anomalous high concentrations of chalcophile elements, first of all As, Sb, Zn, Pb, Cu (Jančev, Chukanov, 2008; Chukanov et al., 2015; Jančev et al., 2016). Unlike the majority of endogenous associations of minerals of these elements, Nežilovo metasomatites practically don't contain sulfides and sulfosalts. Arsenic concentrates here mainly in tilasite, which in some areas is the main mineral of the rock, as well as in accessory apatite-group minerals. Zinc enters into rock-forming silicates (pyroxenes, amphiboles, micas, talc), which contain several % of ZnO, and in spinel-group minerals (mainly gahnite and franklinite), with are important accessories and in some cases rock-forming minerals. Different secondary and accessories minerals of metasomatites (including rinmanite, various members of epidote, pyrochlore, högbomite and hollandite supergroups, plumboferrite and crichtonite groups) are the main concentrators of Pb and Sb. These parageneses show unusual conditions of mineral formation are characterized by a wide diversity. Postmagmatic fluids, connected with meta-rhyolites are considered as a possible source of some specific chalcophile and rare elements (Pb, Zn, Sb, As, Cu, Ba, *REE* etc.) in the contact-metasomatic rocks (Jančev, Bermanec, 1998).

In this work we study isomorphism and compositional variations of pyrochlore-supergroup minerals (PSM) from metasomatites of the ore body No. 9 located in dolomitic marbles, as well as their relationships with associated minerals as indicators of local geochemical situations. Metasomatic bodies and dolomitic marbles are crossed by tilasite-baryte veinlets with variable quantities of silicates, quartz, calcite and dolomite, in which PSM play the main role among accessories. These minerals have a varying composition and complex zoning. Other secondary and accessory minerals of this association are K-feldspar, albite, Zn-containing minerals (clinopyroxene, magnesioriebekite, ferribarroysite, phlogopite, talk, members of the högbomite supergroup), braunite, hematite, zircon, Zn spinels, almeidaite, Pb-containing members of the epidote supergroup, minerals of the rutil-tripuhyite series, As-bearing fluorapatite, gasparite-(La).
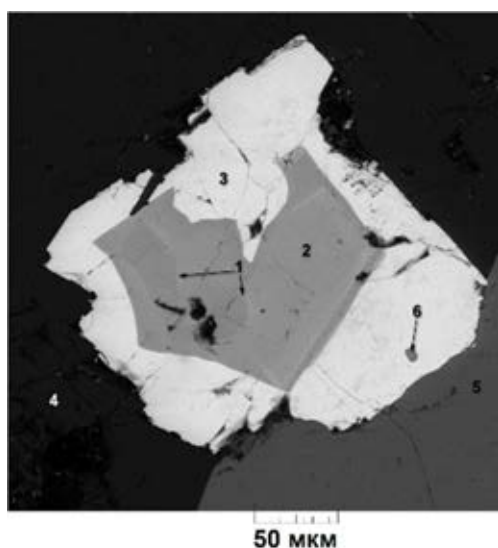
Fig. 1. Zoned crystal of PSM: hydroxycalcioroméite (1), fluorcalcioroméite (2), hydroxyplumboroméite (3). Associated minerals are: albite (4), tilasite (5), zircon (6). Sample 9999B. BSE image.

50 МКМ

Electron microprobe analyses were carried out using a Tescan VEGA-II XMU electronic microscope (EDS mode, 20 kV, 400 pA). Data reduction was carried out by means of a modified INCA Energy 450 software package. Typical compositions of PSM and associated accessory minerals from the studied association, are given in Table 1.

Table 1. Chemical composition of PSM and associated minerals (ore occurrence No. 9).

	Hydroxycalcio-roméite	Fluorcalcio-roméite	Hydroxy-plumbo-roméite	Hydroxy-plumbo-betafite	Mineral of the rutil-tripuhyite series	Almeidaite	Gasparite-(La)	As-contai-ning fluor-apatite	Piemon-tite
	Wt.%								
Na_2O	2.72	5.47	bdl	0.58	bdl	bdl	bdl	bdl	bdl
CaO	16.50	15.88	5.85	5.19	bdl	bdl	bdl	54.71	18.67
PbO	6.19	bdl	48.35	46.52	bdl	11.88	bdl	bdl	5.94
CuO	bdl	bdl	bdl	bdl	bdl	bdl	bdl	bdl	0.73
Mn_2O_3	0.60	bdl	0.80	bdl	1.49	7.47	bdl	bdl	10.54
Fe_2O_3	bdl	0.57	bdl	0.86	22.24	18.24	bdl	bdl	7.02
ZnO	0.15	bdl	bdl	bdl	bdl	7.67	bdl	bdl	1.30
La_2O_3	bdl	bdl	bdl	0.75	bdl	bdl	35.11	bdl	0.81
Ce_2O_3	bdl	bdl	1.45	3.19	bdl	bdl	3.89	bdl	1.45
Pr_2O_3	bdl	bdl	bdl	0.18	bdl	bdl	4.59	bdl	0.51
Nd_2O_3	bdl	bdl	bdl	bdl	bdl	bdl	12.45	bdl	0.52
Sm_2O_3	bdl	bdl	bdl	bdl	bdl	bdl	1.02	bdl	0.29
Eu_2O_3	bdl	bdl	bdl	bdl	bdl	bdl	bdl	bdl	1.16
Y_2O_3	bdl	bdl	0.39	0.33	bdl	bdl	bdl	bdl	bdl
Al_2O_3	bdl	bdl	bdl	bdl	bdl	bdl	bdl	bdl	16.57
TiO_2	5.67	bdl	12.61	14.71	29.18	52.63	bdl	bdl	н.п.о.
SiO_2	bdl	bdl	bdl	bdl	bdl	bdl	bdl	bdl	33.85
UO_2	1.21	bdl	0.48	bdl	bdl	bdl	bdl	bdl	bdl
As_2O_5	0.71	bdl	bdl	1.21	bdl	bdl	38.89	7.82	bdl
Sb_2O_5	63.42	76.37	30.01	27.72	48.01	2.78	bdl	bdl	bdl
P_2O_5	bdl	bdl	bdl	bdl	bdl	bdl	3.19	37.32	bdl
F	1.13	4.21	bdl	bdl	bdl	bdl	bdl	3.42	bdl
$-O=F_2$	−0.48	−1.77	–	–	–	–	–	−1.44	–
Сумма	97.82	100.73	99.94	101.24	100.92	100.67	99.14	101.23	99.36
	Formula coefficients								
Na	0.37	0.73	–	0.10	–	–	–	–	–
Ca	1.23	1.18	0.63	0.51	–	–	–	4.99	1.86
Pb	0.12	–	1.23	1.08	–	1.02	–	–	0.14
Cu	–	–	–	–	–	–	–	–	0.05
Mn	0.03	–	0.06	–	0.04	1.81	–	–	0.70
Fe	–	0.03	–	0.06	0.58	4.37	–	–	0.46
Zn	0.01	–	–	–	–	1.81	–	–	0.08
La	–	–	–	0.02	–	–	0.56	–	0.03
Ce	–	–	0.05	0.10	–	–	0.06	–	0.05
Pr	–	–	–	0.01	–	–	0.07	–	0.02
Nd	–	–	–	–	–	–	0.19	–	0.02
Sm	–	–	–	–	–	–	0.02	–	0.01
Eu	–	–	–	–	–	–	–	–	0.04
Y	–	–	0.02	0.01	–	–	–	–	–
Al	–	–	–	–	–	–	–	–	1.72
Ti	0.30	–	0.89	0.95	0.76	12.62	–	–	–
Si	–	–	–	–	–	–	–	–	2.98
U	0.02	–	0.01	–	–	–	–	–	–
As	0.03	–	–	0.06	–	0.04	0.88	0.34	–
Sb	1.64	1.96	0.01	0.89	0.62	0.33	–	–	–
P	–	–	–	–	–	–	0.12	2.66	–
F	0.25	0.92	–	–	–	–	–	0.91	–

In most cases individuals of PSM are idiomorphic in contacts with calcite and dolomite, but xenomorphic in contacts with tilasite. Typically, crystals of PSM are characterized by concentric-zone structure and wide variations of the chemical composition. As a rule, the boundaries between neighboring zones are sharp. In some cases simple zoning is observed: the grain consists of two concentric zones, with internal zone enriched in Sb and Ca, and external zone enriched in Pb and Ti; see Fig. 1). In some cases PSM individuals show thin concentric zoning (Figs. 2, 4, 5). Formula coefficients for the main components in different zones vary from 0.34 to 1.44 for Ca, from 0 to 1.39 for Pb, from 0.29 to 1.05 for Ti, and from 0.77 to 1.68 for Sb. In some cases individuals of PSM completely consist of hydroxyplumboroméite (Fig. 3). They occur in late carbonate veinlets and, probably, are the latest generation of PSM. Earlier generations of PSM typically show different kinds of thin zoning (inner zone of the grain in Fig. 2, grains on Figs. 4, 5).
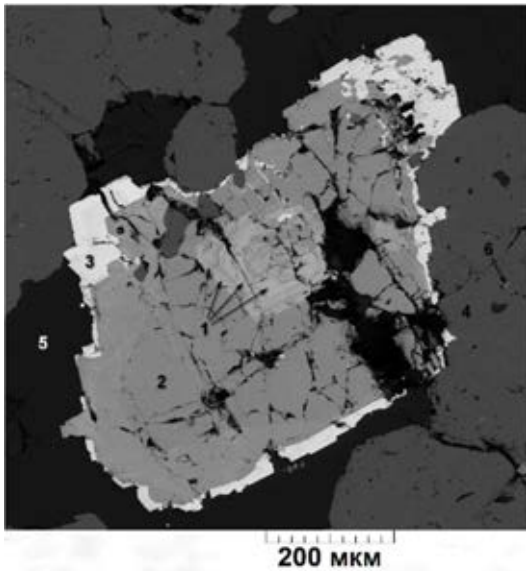
Fig. 2. Zoned crystal of PSM: hydroxycalcioroméite (1), fluorcalcioroméite (2), hydroxyplumboroméite (3). Associated minerals are: tilasite (4), dolomite (5), zircon (6). Sample 9999B. BSE image.

Fig. 3. Hydroxyplumboroméite (1) associated with epidote (2), mineral of the rutil-tripuhyite series (3), calcite (4), quartz (5) and tilasite (6). Sample 9999B. BSE image.
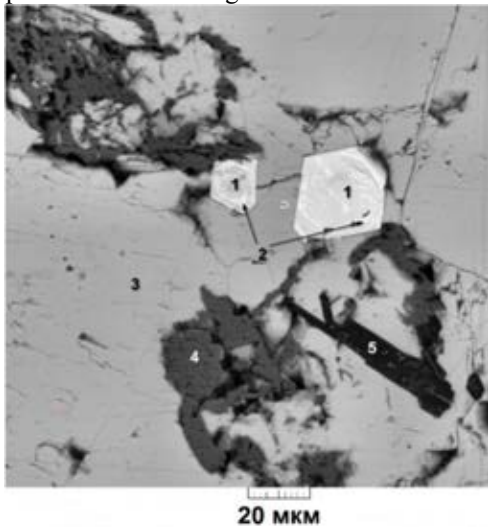
Fig. 4. Hydroxyplumbobetafite (1), hydroxyplumboroméite (2) in barite (3), in association with gahnite (4) and magnesio-riebeckite (5). Sample Alm-31. BSE image.
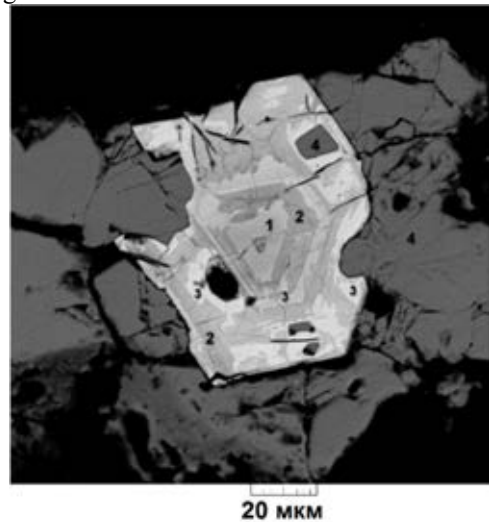
Fig. 5. Hydroxycalcioroméite (1), hydroxyplumbobetafite (2), hydroxyplumboroméite (3) in barite (4). Sample Alm-31. BSE image.

` In most cases inner parts of grains are enriched in Ca and Sb (Fig. 6 shows positive correlation between Ca and Sb, r = 0.943), and outer parts – in Pb and Ti. High negative correlation between Pb and Ca (r = –0.920) (Fig. 7) and between Sb and Ti (r = –0.967) (Fig. 8), obviously, have crystallochemical nature; at the same time, distinct positive correlation between Ca and Sb have geochemical nature: active adding of Sb and Ca occurred synchronously. PSM from sample Alm-31 fall into two compositional areas: plumbobetafite and Pb-bearing calcioroméite (Figs. 6-8). Hydroxy- and fluorcalcioroméite (inner parts of grains) are overgrown with Pb-dominant PSM (outer parts of grains). Some intermediate zones are enriched in Ti up to prevalence of Ti over Sb. Balance of charges in this case is realized according to the scheme Ca + Sb^{5+} + O ↔ Pb + Ti + (OH,F). Thus, the earliest generation of PSM is hydroxycalcioroméite, which is overgrown with fluorcalcioroméite. In the late stages crystallize hydroxyplumbobetafite and hydroxyplumboroméite.

The crystal in Fig. 2 shows compositional evolution of PSM during the geochemical history of the ore body No. 9 most completely. From morphology of minerals in the ore body No. 9 and their spacial relationships one can see that the earliest association includes silicates (clinopyroxene, Zn-bearing amphiboles and phlogopite, albite, K-feldspar), and hematite. Then crystallized Zn spinels (franklinite, gahnite), minerals of the epidote and pyrochlore supergroups, and, finally, carbonates, As-bearing fluorapatite, late generation of baryte, and tilasite. Crystallization of PSM took place throughout all time of the metasomatites formation. Thus, complex zoning of PSM can be considered as an indicator of geochemical evolution of the mineral-forming fluid, during which activities of Pb, Sb, Ti, F and H$_2$O changed in a complex way, with numerous stages of supply of chalcophile elements.

Fig. 6. Correlation between contents of Ca and Sb in PSM (*apfu*).
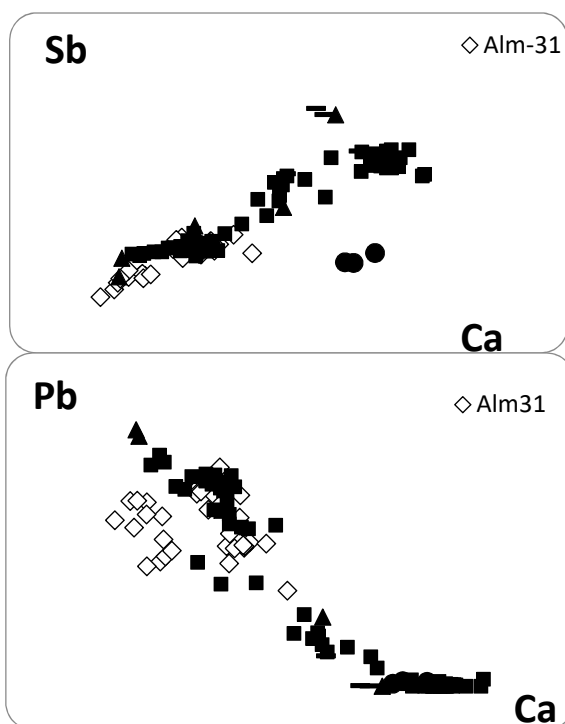
Fig.7. Correlation between contents of Ca and Pb in PSM (apfu).

Fig. 8. Correlation between contents of Ti and Sb in PSM (apfu).

References:

Jancev S., Chukanov N.V. Short review of some rare minerals from a "mixed series" in the pre-Cambrian complex near Nezilovo village, Macedonia // Working Papers of the 1st Macedonian Geological Congress, Ohrid, Macedonia, October 2008. Ohrid: 2008. P. 291–299.

Chukanov N.V., Jančev S., Pekov I.V. The association of oxygen-bearing minerals of chalcophile elements in the orogenetic zone related to the "mixed series" complex near Nežilovo, Republic of Macedonia // Macedonian Journal of Chemistry and Chemical Engineering. 2015. Vol. 34. No. 1. P. 115–124.

Jančev S., Chukanov N.V., Ermolaeva V.N. Association of oxide minerals - concentrators of chalcophile elements (Pb, Zn, Sb) from the "Mixed series" near Nežilovo village, Macedonia // Materials of the Third Congress of Geologists of Republic of Macedonia, Struga, 30 September – 2 October, 2016. Vol. 2. Struga: Macedonian Geological Society, 2016. 416 pp. P. 401–404.

Jančev S., Bermanec V. Solid solution between epidote and hancockite from Nežilovo, Macedonia // Geologia Croatica. 1998. Vol. 51. No.1. P. 23-26.

Ermolaeva V.N., Chukanov N.V., Jančev S., Van K.V. Endogenic oxide parageneses with chalcophile elements in the orogenic zone related to the "Mixed Series" of the Pelagonian massif, Republic of Macedonia. New data on minerals. 2016. (in Russian) (in press).

UNUSUAL MONAZITES AND CE SEGREGATION PROCESS DURING ALKALINE METASOMATOSIS OF ACID SUBSTRATES (KOSYU ORE FIELD, MIDDLE TIMAN)

Varlamov D.A.[1], Udoratina O.V.[2], Burakov N.N.[3]
[1]Institute of Experimental Mineralogy, Chernogolovka, Russia, dima@iem.ac.ru
[2]Komi Science Center Institute of Geology, Ural Branch of the Russian Academy of Sciences, Syktyvkar, Russia, udoratina@geo.komisc.ru
[3]Syktyvkar State University named after Pitirim Sorokin, Syktyvkar, Russia

The ultrabasic, fenite and carbonatite rocks of Chetlassky dike complex are developed in the southern part of Chetlassky Kamen in Middle Timan. The host rocks are terrigenous and terrigenous-carbonate formations of chetlasskaya (R_2) and bystrinskaya (R_3) series. Various alkaline metasomatites (fenites, phlogopite-rich rocks, feldspar metasomatites), carbonatites and hydrothermal vein structures with abundant accessory rare metal – REE mineralization are closely related to the rocks of the complex (Ivensen, 1964, Kostyukhin, Stepanenko, 1987, Nedosekova et al., 2011, 2013). The bodies of the alkaline metasomatites and carbonatites are localized in the same tectonic zones with NE strike as the dike of ultrabasites, but unlike the ultrabasites they occur in separate areas. Enclosing sedimentary metamorphic rocks (sandstones, siltstones, shales and phyllites) form fenites, which are composed of aegirine, alkaline amphibole,

microcline and albite; they are often carbonatized. The phlogopite-rich rocks and feldspar metasomatites are developed on the ultrabasites. At that the shape of their bodies is often completely controlled by the morphology of the ultrabasite bodies. The phlogopite-rich rocks and the largest bodies of carbonatites are widespread in the Kosyu fault zone in the area of the massif ("puff-up" of picrite dike) of the Kosyu River, where formation of carbonatites and associated contact processes of metasomatism are especially intense. Here the stockwork zones of goethite-feldspar rocks are noted, which are closely related to the process of carbonatite formation and, probably, present a hydrothermal stage of carbonatites. The latest quartz-goethite-hematite veins with NE strike intersect all the rocks of the massif.

Geological, petrographic and petrochemical studies of recent years on carbonatites and alkaline picrites are given in the works (Nedosekova et al., 2013), mineralogy data in the works (Kovalchuk et al., 2013, Nedosekova et al., 2017), modern (petro-geochemical, mineralogical and isotope-geochemical) data on alkaline metasomatites are practically absent.

Alkaline metasomatites (fenites), developed along sandstones of visingskaya suite of chetlasskaya series, were taken in the riverheads of Kosyu river. The rock forming and rare metal – REE accessory minerals from them were studied. The material for research was obtained during a field trip in 2016. In weakly and strongly fenitized initially badly sorted sandstones and aleurolites (series of thin sections 340-1, -2, 3, etc.) we found both relict and newly formed minerals. Relics of quartz, plagioclase and Kfs are partially preserved, newly formed albite and Kfs (often – barium-containing) form basal cement alongside with chlorite and sericite. We observe the development of hematite and iron hydroxides. In the process of research, a fairly large number of ore and accessory mineral inclusions have been identified, for the diagnosis of which microprobe study is currently conducted in IEM RAS (Chernogolovka).

Among the newly formed rock-forming minerals were established aegirine, alkaline amphibole, Fe-rich chlorite, fluorine-rich phlogopite and their Al-absent «analogue» $KMg_2Si_5O_{10}F_2$. Among the accessories zircon; different Al-, Ba-, REE phosphates; carbonates: burbankite $(Na,Ca)_3(Sr,Ba,Ce)_3(CO_3)_5$, norsethite $BaMg(CO_3)_2$, unknown Ba-Mn carbonates, different F-rich REE-carbonates; extensive range of thorium minerals, Nb-rich rutile, own Ce-minerals with Mn, Fe, Ba, Pb.

In this paper, some types of monazites from these rocks, quite original in composition and possible genesis, as well as probable processes leading to their formation are considered. Of greatest interest is the formation of cerium-deficient monazites (Fig.1, a-c; Table 1, an.1,3) in which the cerium content falls sharply to 5-6 wt% Ce_2O_3 when cerium is replaced by mainly neodymium and, to a lesser extent, lanthanum in comparison with earlier idiomorphic high-cerium thorium-containing monazites of generation **I**. In contrast, neogenic Ce-deficient monazites **II** , as a rule, have xenomorphic nature, often fill emptiness or are characterized by a needle-like appearance, often located along the grain of rock-forming minerals. An interesting feature is the high concentration of lead (up to 4% PbO) with almost complete absence of radiogenic elements Th and U. It can be explained either by the non-radiogenic origin of similar lead (that demands padding researches as contradicts the majority of postulates in this area), or peculiar metasomatic processes in the formation of these monozites with removal of thorium and concentration of lead (possibly in form Pb^{4+}). Also several micrograins of REE fluorocarbonate with the significant decrease in contents of cerium of rather other REE are revealed.

Together (often practically nearby) still finally not diagnosed own phases of cerium with manganese and iron are formed (table 2; fig. 1 c-d). They are characterized by the absence of other REE, the quite considerable contents of P, Ba and Pb (less often Zn). The impurities Al and Si are probably caused by microinclusions. These phases are localized in aggregates like a containers of iron oxides and hydroxides, Fe- analogues of braunite and high-ferrous (alumo)silicates.
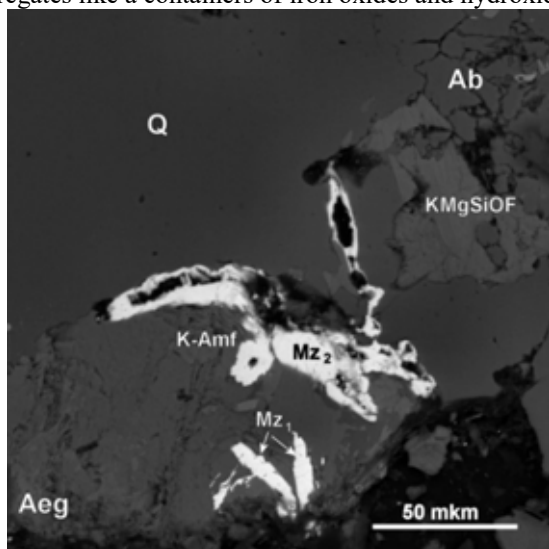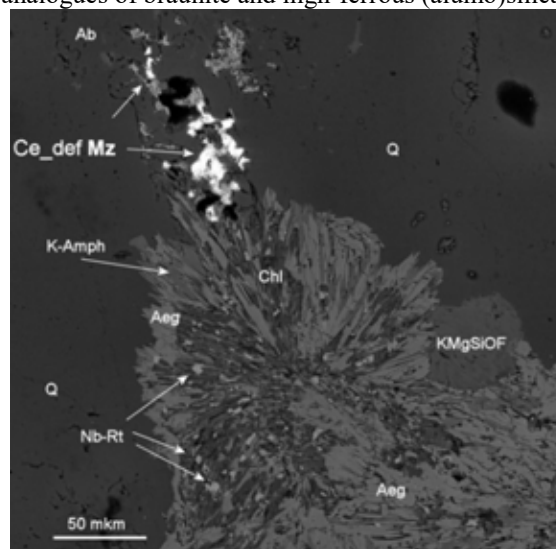
a   b
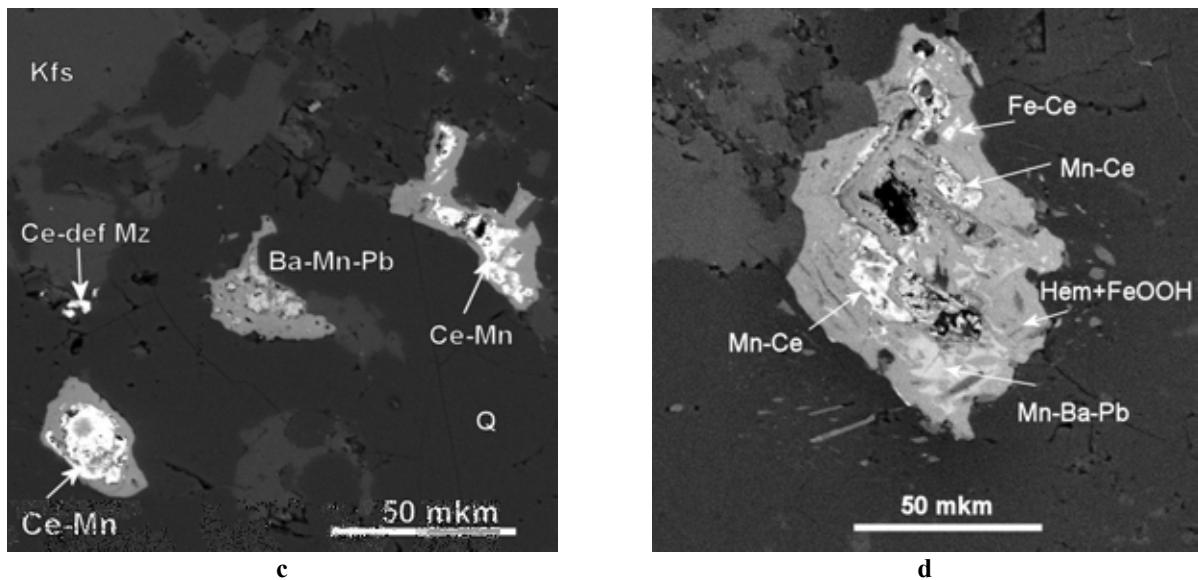
Fig. 1. Microphotographs of monazites and high-Ce phases: (a) monazites of two generations: I –idiomorphic high-cerium Th-bearing Mz1; II –xenomorphic Ce-deficient Th-absent high-Pb Mz2; b) -xenomorphic Ce-deficient at boundary of Aeg+K-Amf+Rt+Chl "sun-like" aggregate; c) Mn-Ce cores in container of iron oxides and hydroxides: (d) Mn-Ce and Fe-Ce phases in aggregate of iron oxides and hydroxides.

Table 1. Chemical composition (wt. %) of different monazites

	sample	P_2O_5	CaO	La_2O_3	Ce_2O_3	Pr_2O_3	Nd_2O_3	Sm_2O_3	Gd_2O_3	PbO	ThO_2	Total
1	340/3-14	29.92	2.31	18.31	5.89	6.03	29.29	4.01	1.01	1.24	0.82	99.65
2	340/3-15	33.39	*0.15*	11.20	29.72	3.59	14.50	2.01	1.00	*0.49*	3.42	99.80
3	340/3-19	29.54	2.20	20.45	6.15	6.46	25.53	3.11	*0.50*	2.79	n.d.	98.16
4	340/2-1	28.36	0.42	12.09	25.95	2.59	12.30	3.94	3.30	0.61	9.27	100.62
5	340/2-2	31.45	n.d.	14.53	33.79	3.68	11.61	1.54	1.25	n.d.	*0.31*	100.24

Remark: Composition of monazites is simplified. I generation (2,4), II generation: Ce-deficient low-Th with high content of Pb (1,3); newly formed Ce-rich Th-absent (5). *Italic* – means lower than 2σ measured.

Table 2. Mn and Fe cerium phases in fenitized quartzite-sandstones (wt.%)

sample	Al_2O_3	SiO_2	P_2O_5	CaO	Mn_2O_3	Fe_2O_3	ZnO	BaO	CeO_2	PbO	Total
340/3-21	4.26	2.08	4.59	0.30	13.38	6.28	n.d.	1.22	55.39	1.18	88.68
340/3-22	3.94	3.00	3.83	0.59	16.12	12.53	0.48	2.27	35.21	1.49	79.46
340/3-26	2.58	4.95	3.98	0.51	2.58	28.24	*0.19*	n.d.	35.43	0.70	79.16
340/3-32	2.98	1.73	4.20	0.34	22.97	4.68	0.24	2.76	44.93	2.18	87.01
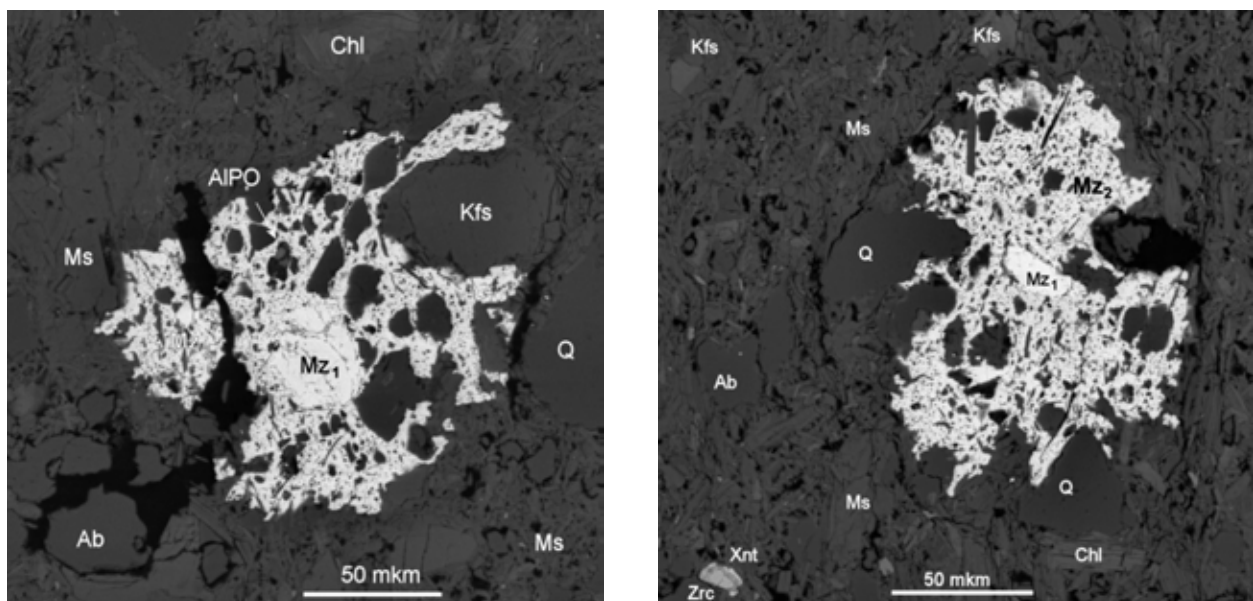
Fig. 2. Microphotographs of two generations of monazite: I – Mz_1 round or idiomorphic with high Th content (up to 11% ThO_2) cores; II – Mz_2 amoeboid-like Th-absent Ce-rich shells.

The similar combination of Ce-deficient REE minerals and actually cerium phases, in our opinion, is associated with the oxidation of cerium from Ce^{3+} to Ce^{4+} at some stage of the process of fenitization, that at once sharply changes its chemical properties in comparison with group of rare earth elements. Some part of cerium remains trivalent (small amount of cerium in neogenic monazites and the F-rich REE carbonates), however, a majority as Ce^{4+} is fixed in own Ce phases of Mn-Ce and Fe-Ce composition. Possibly, this process is bound or is simultaneous with formation of the oxidized ferrous phases – an aegirine, oxides and hydroxides of iron, however, so far early to speak about its correct geological binding.

Also, in the part of the samples, the formation of interesting two-stage monazites was revealed (Fig. 2, analyzes 4-5 in Table 1) having high-thorium (up to 11% ThO_2) idiomorphic or rounded cores (Mz_1), overgrowing amoeboid-like Th-absent Ce-rich aggregates of the second generation (Mz_2). The latter have a porous structure, often contain microinclusions of phosphates (apatites, phosphates Al, Ba, Fe), sometimes enclosed in quartz "containers". Most likely, their formation is associated with the formation of regenerative aggregates of newly formed monazite growing on primary monazites after their partial dissolution. Thorium in this process is mobilized by a fluid with the subsequent fixing in other phases, as evidenced by the appearance of high-thorium F-rich REE carbonates and thorium own phases (xenomorphic thorites, phosphothorites, hydroxothorites, etc.).

Thus, in fenitized sandstones, the genetically bound to the action of igneous rocks of the Chetlasskii complex on terrigenous rocks of chetlasskaya suite, the processes leading to the oxidation of cerium to the tetravalent state are established and are manifested in the removal of cerium from conventional REE minerals and the formation of characteristic Mn-Ce and Fe-Ce phases. It leads to formation of the unusual low-cerium monazites differing in also high contents of lead (up to 3-4% of PbO) in the absence of radiogenic elements that contradicts postulates on radiogenic character of lead in monazites.

Also, aggregates of monazites formed by chemically different generations have been identified, which indicates quite differently directed metasomatic reactions in the process of fenitization of acid (quartzite sandstone) substrates.

References:
Ivensen Yu. P. Magmatism of Timan and Kanin Peninsula // Leningrad: Nauka, 1964. 126 p. (in Russian)

Kostyukhin M.N., Stepanenko V.I. Baikalian magmatism of Kanin-Timan region. // Leningrad: Nauka, 1987. 232 p. (in Russian).

Kovalchuk N.S., Shumilova T.G., Stepanenko V.I., Rare metal mineralization in carbonatites of Kosyu massif (Middle Timan). // ZRMO, No. 3, 2013. pp. 109-132. (in Russian).

Nedosekova I.L., Udoratina O.V., Vladykin N.V., Pribavkin S.V., Gulyaeva T.Ya. Petrochemistry and geochemistry of dike ultrabasites and carbonatites of the Chetlas complex (Middle Timan) // Yearbook 2010, IGG UB RAS, No. 158, 2011, p. 122-130. (in Russian).

Nedosekova I.L., Vladykin N.V., Udoratina O.V., Ronkin Yu. L. Carbonatites of the Chetlas complex (Middle Timan): geochemical and isotopic data. // Yearbook 2012, IGG UB RAS, No. 160, 2013, p. 150-158. (in Russian).

Nedosekova I.L., Zamyatin D.V., Udoratina O.V. Ore specialization of the carbonatite complexes of the Urals and Timan // Lithosphere, 2017, No. 2. (in Russian).

NEOPROTEROZOIC CARBONATITE-BEARING COMPLEX OF THE YENISEI RIDGE: ORIGIN OF MAGMATISM IN THE SOUTH-WESTERN ACTIVE CONTINENTAL MARGIN OF THE SIBERIAN CRATON

Vernikovskaya A.E.[1,2], Romanova I.V.[1,2], Matushkin N.Yu.[1,2]
[1]Trofimuk Institute of Petroleum Geology and Geophysics Sibirian Branch of the Russian Academy of Sciences, Novosibirsk, Russia, VernikovskayaAE@ipgg.sbras.ru
[2]Novosibirsk State University, Novosibirsk, Russia

Alkaline igneous rocks vary from ultramafic to acidic and include carbonatites, which are composed of >50% carbonate minerals, and fenites – exocontact alkaline metasomatites formed at the margins of alkaline and alkaline-ultramafic plutons (Kogarko et al., 1995). Although alkaline complexes are known to be formed in different tectonic settings, excluding mid-oceanic ridges, carbonatite magmatism is commonly associated with mantle plumes (Bell, Simonetti, 1996). Nevertheless, petrological modeling, numerical calculations and experimental data suggest that carbonatite melts could occur in subduction-related settings (Gerya, Meilick, 2011; Tumiati et al., 2013; Poli, 2016). Formation of carbonatites in a subduction setting has been recently demonstrated for the Pliocene-Quaternary magmatic complex in the Tyrrhenian Sea (Pereccerillo, Frezzotti, 2015) and the alkaline ultramafic-mafic carbonatite-bearing Khanka massif from the Early Cretaceous transform margin of the Sino-Korean craton (Khanchuk, 2001).

Formation and age of carbonatites, located along the Tatarka-Ishimba suture zone in the Yenisei Ridge orogen, remains highly debated since Zabrodin and Malyshev (1975). The orogen was formed during collision of the Central Angara terrane with the present-day south-western margin of the Siberian craton in the Neoproterozoic, as suggested by the 760–750 Ma U/Pb zircon ages from syncollisional granitoids within the Tatarka-Ishimba suture zone (Vernikovsky et al., 2003). This zone also contains igneous rocks formed in a late Neoproterozoic active continental margin setting, including nepheline syenites, gabbroids, trachybasalts and A-type granitoids emplaced within the age range of 711–629 Ma (Vernikovsky et al., 2008; Romanova et al., 2012; Vernikovskaya et al., 2013). Recent studies suggest carbonatite

formation during 725–629 Ma. The oldest age of 725.9±6.3 Ma was obtained by ^{40}Ar/^{39}Ar method for magnesio-arfvedsonite (Vrublevskii et al., 2011) and is close to the 711±3 Ma U/Pb age for zircons from a nepheline syenite within the Tatarka-Ishimba zone (Vernikovsky et al., 2008). Younger ^{40}Ar/^{39}Ar ages for phlogopite from carbonatites (647–629 Ma; Vrublevskii et al., 2011; Vernikovskaya et al., 2013) are in good agreement with the emplacement ages of the nearby A-type granites (646–629 Ma, U/Pb zircon ages; Vernikovsky et a., 2003; Vernikovskaya et al., 2013) and with new data for biotite from the nepheline syenite (637±6 Ma). Subalkaline and alkaline rocks from the Tatarka-Ishimba suture zone are characterized by *Niobium geochemical specialization* due to consistently elevated Nb contents in many minerals, such as pyrochlore, columbite, eudialyte, sphene, astrophyllite, amphibole and biotite. Additionally, igneous rocks including carbonatites from this zone have similar mantle Sm-Nd and Rb-Sr isotope characteristics (Sazonov et al., 2007; Fedorova, 2011; Vrublevskii et al., 2012). The Nd-Sr isotope compositions for nepheline syenites and subalkaline rocks fall between EM and DMM (Romanova et al., 2012). Based on these geochronological and geochemical results, carbonatites from the Tatarka-Ishimba suture zone are suggested to be part of the Neoproterozoic Tatarka active continental margin complex, formed during 100 m.y. timeframe from 725 Ma to 630 Ma.

References:

Bell K, Simonetti A (1996) Carbonatite magmatism and plume activity: implications from the Nd, Pb and Sr isotope systematics of Oldoinyo Lengai. J Petrology 137:1321-1339.

Fedorova AV, Tishin PA, Sazonov AM (2011) Petrochemical particularities and variation factors of the composition of rocks from the Sredne-Tatarsky uplift (Transangarian massif). Tomsk State University J 342:214-221.

Gerya T, Meilick FI (2011) Geodynamic regimes of subduction under an active margin: Effects of rheological weakening by fluids and melts. J Metamorphic Geology 29:7-31.

Khanchuk AI (2001) Pre-Neogene tectonics of the Sea-of-Japan region: A view from the Russian side. Earth Sci (Chikyu Kagaku) 55:275-291.

Kogarko LN, Kononova VA, Orlova MP, Woolley AR (1995) Alkaline rocks and carbonatites of the World. Part 2: Former USSR. Chapman and Hall, London.

Peccerillo A, Frezzotti ML (2015) Magmatism, mantle evolution and geodynamics at the converging plate margins of Italy. J Geol Soc London 172:407-427.

Poli S (2016) Melting carbonated epidote eclogites: carbonatites from subducting slabs. Earth and Planetary Sci 3.

Romanova IV, Vernikovskaya AE, Vernikovsky VA, Matushkin NYu, Larionov AN (2012) Neoproterozoic alkaline magmatism and associated igneous rocks in the western framing of the Siberian craton: petrography, geochemistry, geochronology. Geologiya i Geofizika (Russian Geology and Geophysics) 53:1117-1137.

Sazonov AM, Fedorova AV, Zvyagina EA, Leont'ev SI, Vrublevskii VV, Gertner IF, Gavrilenko VV (2007) The Transangara alkaline pluton, Yenisei Range: Rb-Sr and Sm-Nd isotope ages and sources of feldspathoid magmas in Late Precambrian. Dokl Earth Sci 413:469-473.

Tumiati S, Fumagalli P, Tiraboschi C, Poli S (2013) An experimental study on COH-bearing peridotite up to 3.2 GPa and implications for crust-mantle recycling. J Petrology 54:453-479.

Vernikovskaya AE, Datsenko VM, Vernikovsky VA, Matushkin NYu, Laevsky YuM, Romanova IV, Travin AV, Voronin KV, Lepekhina EN (2013) Magmatism evolution and carbonatite-granite association in the Neoproterozoic active continental margin of the Siberian craton: thermochronological reconstructions. Dokl Earth Sci 448:555-562.

Vernikovsky VA, Vernikovskaya AE, Kotov AB, Sal'nikova EB, Kovach VP (2003) Neoproterozoic accretionary and collisional events on the western margin of the Siberian Craton: new geological and geochronological evidence from the Yenisey Ridge. Tectonophysics 375:147-168.

Vernikovsky VA, Vernikovskaya AE, Sal'nikova EB, Berezhnaya NG, Larionov AN, Kotov AB, Kovach VP, Vernikovskaya IV, Matushkin NYu, Yasenev AM (2008) Late Riphean alkaline magmatism in the western framework of the Siberian craton: a result of continental rifting or accretionary events? Dokl Earth Sci 419:226-230.

Vrublevskii VV, Reverdatto VV, Izokh AE, Gertner IF, Yudin DS, Tishin PA (2011) Neoproterozoic Carbonatite Magmatism of the Yenisei Ridge, Central Siberia: ^{40}Ar/^{39}Ar Geochronology of the Penchenga Rock Complex. Dokl Earth Sci 437:443-448.

Vrublevskii VV, Sazonov AM, Gertner IF, Tishin PA, Kolmakov YuV (2012) Geochronology and magmatic sources of alkaline rocks and carbonatites of the southern Transangaria, Yenisei Ridge. Bulletin of the Tomsk Polytechnic University 320(1):63-70.

Zabrodin VYu, Malyshev AA (1975) New complex of alkali-mafic rocks and carbonatites in Yenisei Ridge. Dokl Akad Nauk SSSR 223:1223-1226.

MAGMATISM OF THE NEW SIBERIAN ISLANDS, DE LONG ARCHIPELAGO AND MENDELEEV RISE – IMPLICATIONS FOR PALEOTECTONIC RECONSTRUCTIONS FOR THE ARCTIC

Vernikovsky V.A.[1,2]*, Metelkin D.V.*[1,2]*, Matushkin N.Yu.*[1,2]*, Vernikovskaya A.E.*[1,2]*, Zhdanova A.I.*[1,2]*, Travin A.V.*[1,3]

[1]Novosibirsk State University, Novosibirsk, Russia, VernikovskyVA@ipgg.sbras.ru
[2]Trofimuk Institute of Petroleum Geology and Geophysics Sibirian Branch of the Russian Academy of Sciences, Novosibirsk, Russia
[3]Institute of Geology and Mineralogy, Siberian Branch of the Russian Academy of Sciences, Novosibirsk, Russia

The geology of the Arctic Ocean's Eurasian margin is of high interest from both a research and practical standpoint (Dobretsov et al., 2013; Laverov et al., 2013; Vernikovsky et al., 2013a). Research on arctic objects is difficult first due to their limited accessibility, since the key targets for research are located on the islands of the arctic continental shelf or are located below sea level. The New Siberian Islands and De Long archipelago are such key structures for understanding the geology and evolution of the Arctic region, because they are located tectonically between several folded regions of Eurasia: Taimyr–Severnaya Zemlya, Verkhoyan–Kolyma and Chukotka (Vernikovsky et al., 2013b). Moreover, from the side of the Arctic Ocean there are several submerged structures adjacent to the archipelago and consisting of continental crust – the Lomonosov Ridge, the Mendeleev Rise and the Makarov Basin. Thus, the complexes cropping out and available on the New Siberian Islands are perspective for determining the type of interaction between structures of the Arctic Ocean floor and the continental shelf.

A number of pieces of geochronological evidence support the late Precambrian and Paleozoic ages of the volcanogenic-sedimentary and intrusive rocks that overly the Precambrian basements of the New Siberian Islands and De Long archipelago (Henrietta, Zhokhov and Jeannette islands) (Korago et al., 2014; Matushkin et al., 2016). For the first time, an early Paleozoic age, more specifically Ordovician (471-467 Ma), was obtained by Ar/Ar dating for dolerites and basalts of the submerged Mendeleev Rise (Vernikovsky et al., 2014). Calculated paleomagnetic poles for Cambrian-Ordovician-Silurian rocks from the De Long and Anjou archipelagos form a common apparent polar wander path. Recently published paleotectonic reconstructions for the Arctic structures indicate the emplacement of the Jeannette Island mafic dike complex approximately 550-540 Ma, when the New Siberian terrane was drifting towards the Siberian paleocontinent (Metelkin et al., 2016). Paleomagnetic data indicate that the New Siberian Islands terrane could not be part of Laurentia, Baltica, or Kara, but together with the Omulevka, Prikolyma and probably Omolon terranes was involved in the tectonic evolution of the Kolyma-Omolon superterrane near the Siberian craton. The determined early Paleozoic age of igneous rocks of the Mendeleev Rise and seismic data obtained during the Russian expedition "Arctica 2012", let us suppose that this continental block of the Earth's crust has a Precambrian basement similar to the basement identified for the New Siberian Islands including the De Long archipelago.

References:

Dobretsov NL, Vernikovsky VA, Karyakin YuV et al. (2013), Russ. Geol. Geoph 54:874–887.
Korago EA, Vernikovsky VA, Sobolev NN et al. (2014) Doklady Earth Sciences 457(3):315-322.
Laverov NP, Lobkovsky L.I., Kononov M.V., et al. (2013), Geotectonics 47 (1):1–30
Matushkin NYu, Metelkin DV, Vernikovsky VA et al. (2016). Dokl. Earth Sci., 467: 219–223.
Metelkin DV, Vernikovsky VA, Tolmacheva TYu et al. (2016) Gondwana Research 37: 308–323.
Vernikovsky VA, Dobretsov NL, Metelkin DV et al. (2013a). Russ. Geol. Geophys. 54 (8): 838–858.
Vernikovsky VA, Metelkin DV, Tolmacheva TYu et al. (2013b). Dokl. Earth Sci. 451 (4): 791–797.
Vernikovsky VA, Morozov AF, Petrov OV et al. (2014) Dokl. Earth Sci. 454 (2): 97-102.

TIMING OF MAGMATISM AND MINERALIZATION IN SOUTH EASTERN EUROPE (WESTERN BRANCH OF THE TETHYAN BELT)

Von Quadt A.[1]*, Gallhofer D.*[1,2]*, Georgiev S.*[3]*, Peytcheva I.*[1,3]

[1]Institute of Geochemistry and Petrology, Zurich, Switzerland, quadt@erdw.ethz.ch
[2]Institute of Mineral Resources Engineering, Aachen, Germany
[3]Geological institute, Bulgarian Academy of Science, Sofia, Bulgaria, peytcheva@erdw.ethz.ch

Magmatic arcs form above active subduction zones at convergent plate boundaries, where a continental or oceanic plate margin overrides a subducting oceanic plate. Along a subduction zone, continental and oceanic arcs generally form distinct segments (*Kay et al.*, 1982; *Hildreth and Moorbath*, 1988). In continental-margin arcs, the style of tectonic deformation may differ amongst segments along the arc, and may also vary perpendicular to the arc in response to differences in pre-existing geology, convergence rate and direction, or heterogeneities within the subducting plate. The composition of subduction-related mantle magmas varies as a result of heterogeneous source enrichment, and may be modified by mineral fractionation and crustal assimilation processes, which occur primarily in the lower crust and on further ascent through the mature continental crust (*Hildreth and Moorbath*, 1988; *Annen et al.*, 2006). Conversely, igneous geology and geochemistry can be used to identify magma sources and evolution processes and thus serve as geochemical evidence to interpret the large-scale plate-tectonic setting of complex arcs.
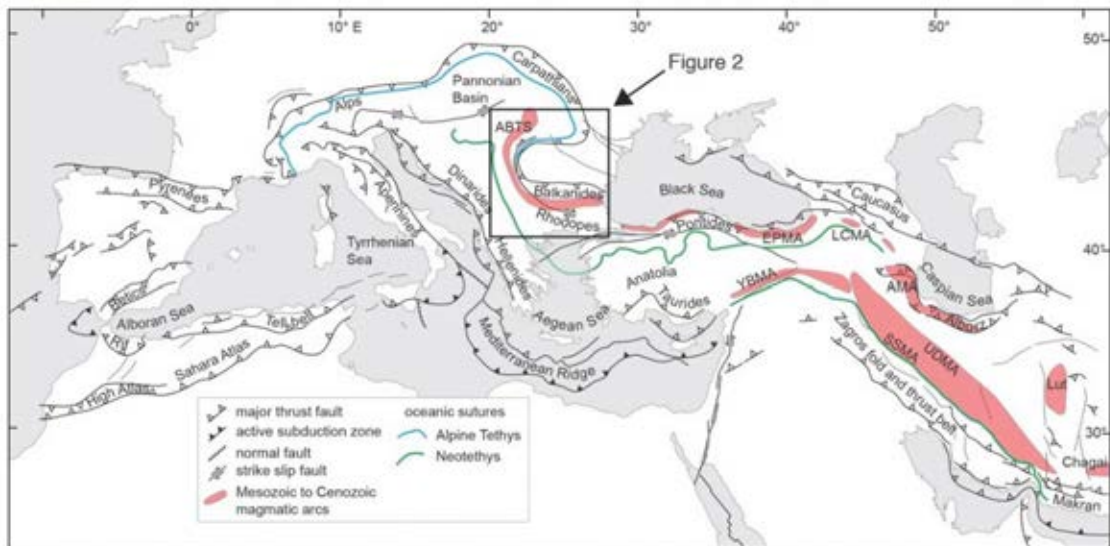
Fig. 1. Tectonic sketch map of western Eurasia (modified from *Morelli and Barrier*, 2004). Major Late-Tertiary to active thrust belts, active subduction zones and recent arc volcanoes are shown in black; older oceanic suture zones and location of Mesozoic to Oligocene magmatic arcs are highlighted by colours. ABTS: Apuseni-Banat-Timok-Srednogorie belt, AMA Alborz magmatic arc, CA Carpathian magmatic arcs, EPMA Eastern Pontide magmatic arc, KB Kerman belt, LCMA Lesser Caucasus magmatic arc, SSMA Sanandaj-Sirjan magmatic arc, UDMA Urumieh-Dokhtar magmatic arc, YBMA Yüksekova-Baskil magmatic arc.
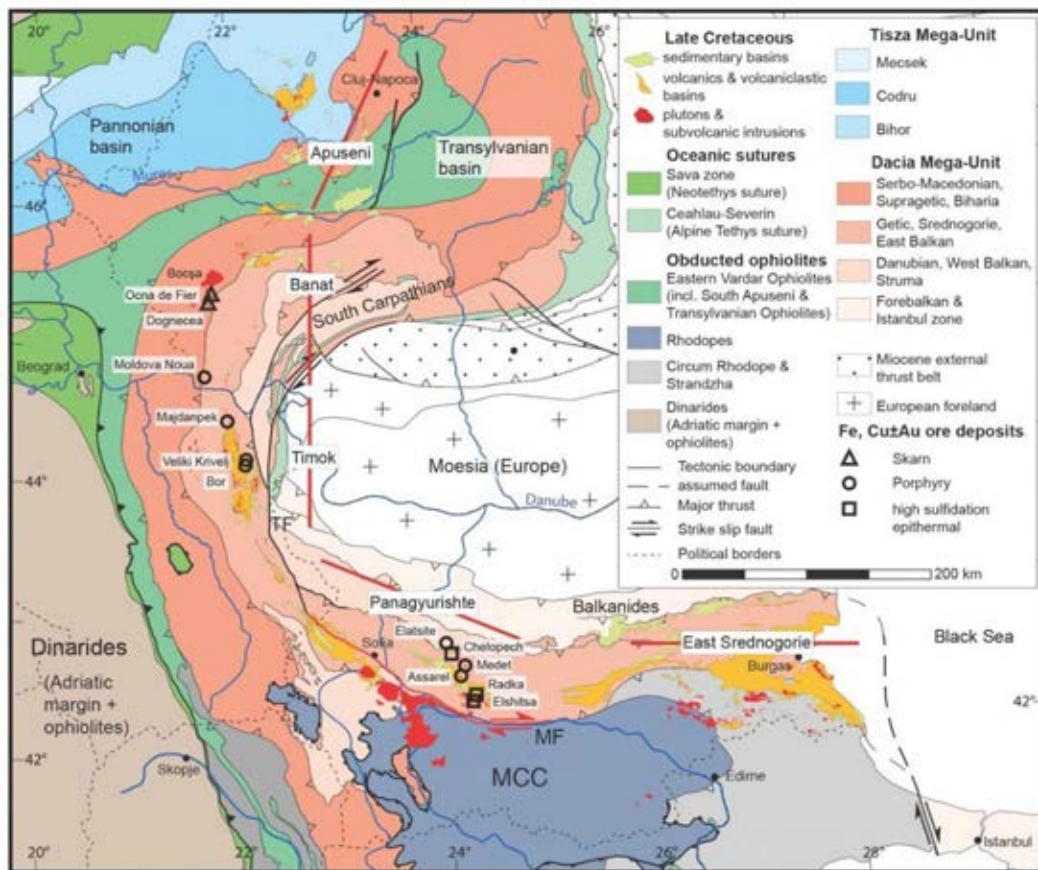
Fig. 2. Geological map of the Carpathian-Balkan orogen, modified from Schmid et al. (2008), showing major tectonic units and the occurrences of Late Cretaceous igneous rocks and sedimentary basins grouped into five segments of ABTS belt. These are, from NW to SE: the Apuseni, Banat, Timok, Panagyurishte and Eastern Srednogorie segments. Red bars are reference lines approximating the present-day orientation of the arc front in each of the five segments, based on geochronological data derived in this and previous studies. MF = Maritsa fault system and TF = Timok fault are major transverse structures used to separate the segments; MCC = Metamorphic ore Complex.

Subduction-related magmatic arcs are frequently endowed with magmatic-hydrothermal porphyry Cu±Au±Mo and epithermal Au±Ag±Cu deposits, which can themselves be taken as tectonic indicators. These deposits usually occur in discrete belts and do not extend along the entire length of magmatic arcs. Barren and mineralised segments are thought to be due to large-scale variations in tectonic stress of the lithosphere, and well-endowed segments empirically correlate with flat slab subduction, subduction of oceanic ridges or subduction reversals (e.g. Cooke et al., 2005; Rohrlach and Loucks, 2005). Major porphyry deposits develop preferentially in arc segments that were subjected to a compressional stress state during ore deposit formation (e.g. Richards, 2003). Horizontal compression can trap magmas in a lower crustal magma chamber, where high-pressure magmatic differentiation and cyclic replenishment lead to enrichment in volatiles and metal content. Compression also helps establishing upper-crustal magma chambers, thus preventing volcanic eruption and unfocused loss of volatiles, but favouring focussed fluid release through intensely veined porphyry stocks (Rohrlach and Loucks, 2005; Richards, 2012).

The Eurasian continental margin includes the world's second-longest magmatic arc system (*Jankovic*, 1997), besides the Circum-Pacific region. Unlike the Circum-Pacific, which is dominated by long-lasting subduction of oceanic plates below continents, the magmatic arcs of Eurasia are embedded in the Alpine-Himalayan intra-continental orogenic system (Fig. 1). Arc magmatism was driven by subduction of the Neotethys ocean in Mesozoic to Tertiary times, but terminated at the time of collision and was subsequently heavily overprinted by major collision-related deformations (e.g. *Schmid et al.*, 2008]. This collisional overprinting makes the reconstruction and interpretation of arc magmatism and the associated geotectonic setting more difficult (*Sosson et al.*, 2010). The Late Cretaceous Apuseni-Banat-Timok-Srednogorie (ABTS) belt in south-eastern Europe is the western-most arc in the Alpine-Himalayan orogenic system related to the subduction of Neotethys (*Berza et al.*, 1998; *Popov et al.*, 2002). This magmatic arc extended over 1000 km length, from the Apuseni Mountains of Romania to the Black Sea (Fig. 1, 2), and was deformed after emplacement on a lithospheric scale (*Neubauer*, 2002). Five segments that show distinct magmatic and mineralisation trends can be distinguished along this arc (Fig. 2). The timing and evolution of the magmatism and its associated ore deposits are well studied in the central and eastern segments (*von Quadt et al.*, 2005; *Georgiev et al.*, 2012; *Kolb et al.*, 2013; Gallhofer et al., 2015, 2016).

The *Apuseni-Banat-Timok-Srednogorie* (ABTS) belt is one of the world's oldest mining areas and played a major role in the history of European civilizations until the present day. Today, it is Europe's premier Cu-Au (-Pb-Zn-Ag) province, especially for gold-rich deposits associated with calc-alkaline magmatism. The ABTS magmatic arc in the Carpathian-Balkan orogen formed on the European margin during closure of the Neotethys Ocean. Trace element and isotopic signatures of the magmas indicate a subduction-enriched source and variable contamination by continental crust. Extensive U-Pb zircon dating combined with reliable published data suggest magmatic activity at a continental margin for 25 Ma (~92–67 Ma) related to oblique subduction and slab steepening. Ore mineralization is related to porphyry systems (Majdanpek, Bor, Veliki-Krivelj (Serbia), Elatsite, Assarel (Bulgaria)) and includes world-class porphyry Cu-Au-Mo deposits, proximal and distal intermediate and high-sulphidation epithermal (Chelopech (Bulgaria), as well as sediment-hosted and carbonate-replacement deposits that are formed during an economically important window of 6-8 Ma (92-86 Ma or 86-78 Ma in the different segments). Predating tectonics and stratigraphy played particularly important role for the location and grade of mineralization.

The magmatic evolution of the ABTS belt in Late Cretaceous times can be subdivided into the following stages:

1) *Active continental margin at ~110 Ma:* The north-dipping subduction of the Neotethys ocean along the Sava trench must have started some time before the onset of arc magmatic activity, most likely during the Albian. The formation of strike-slip and pull-apart basins in the Panagyurishte segment indicates that the dextral Maritsa fault system has already been active at that time. Towards the end of this stage the mantle source was geochemically enriched by subduction fluids, to generate the characteristic subduction-like signature of arc magmas.

2) *Initiation of magmatic activity, steepening of the subduction zone and ore deposit formation (~92 to 75 Ma):* The earliest upper-crustal magmatism is recorded by intrusive rocks from the northern Panagyurishte segment and indirectly by co-magmatic sediments preserved in the Eastern Srednogorie segment (~92 Ma). The onset of magmatic activity systematically became younger towards the west (~89 to 72 Ma) in the other segments of ABTS belt. The ascent of magmas to the upper crust might have been facilitated by the steepening of the subduction zone and was partly focussed by pull-apart structures, e.g., along the Panagyurishte lineament associated with strike-slip faulting along the Maritsa shear zone. At the same time, magmatic activity shifted continuously to the south in all the arc segments except for the Apuseni segment, as is evidenced by progressively younger magmatic ages towards south. Economic porphyry Cu and epithermal Cu±Au deposits coincide with early stages of magmatism in the Panagyurishte and Timok segments.

3) *End of active subduction and arc magmatism by continental collision (~72 to 67 Ma):* Arc magmatism within or near to the intra-arc basins ceased at ~72 Ma in all the segments, but younger plutons occur further south within the Rhodopes and Strandzha unit (Figure 2) south of the Panagyurishte and Eastern Srednogorie segments (69-67 Ma). These latest plutons probably reflect the termination of active subduction of the Sava branch of Neotethys ocean and likely mark the collision between Adria and Europe at the end of Maastrichtian (~66 Ma; *Schmid et al.*, 2008). Younger plutons intruded the Rhodopes only after a significant gap of some 10 Ma (~55 Ma; *Soldatos et al.*, 2008; *Jahn-Awe et al.*, 2010; *Marchev et al.*, 2013).

After the ceasing of subduction, the magmatism shifted to south in the *Serbo-Macedonian-Rhodope* belt (Fig. 2). There, it is directly connected to post-collisional episodes of back-arc extension related to slab break-off and asthenospheric upwelling and delamination (60-40 Ma) and the formation of metamorphic core complexes (MCC) - the

North Rhodope MCC (38-25 Ma) and South Rhodope MCC (after 23-22 Ma). The magmatism preserves largely subduction-related features as sourced in the subcontinental mantle lithosphere and lower crust that were enriched during previous subduction. Several isolated time windows of ore forming processes are obtained (U/Pb zircon data, Ar-Ar, K-Ar data): 43-39 Ma (Au-Ag to Au-W deposits in the western Rhodopes); 38-32 Ma (Pb-Zn/ -Ag-Au) vein and carbonate replacement deposits, Bosnia (e.g. Trepca) through Serbia - Macedonia - Greece and southern Bulgaria; 32-24 Ma and 23-18 Ma (porphyry Cu-Au-(Mo) connected with the extensional magmatism following the MCC formation and finally at 12 - 1.8 Ma several epithermal and Carlin-type Au deposits; e.g. Alchar deposit (Macedonia).

In the Miocene, a main segment of ore-formation is the '*gold quadrilateral' of the Apuseni Mountains* (also known as the Transylvanian gold province). It includes a cluster of large, low-sulfidation epithermal Au-Te vein deposits including Sacarimb and Rosia Montana, which is probably Europe's largest gold resource. The epithermal veins are spatially and temporally associated with small to medium-sized porphyry-style Cu (-Au) deposits in calc-alkaline intrusive centers of Miocene age. Magma generation and the emplacement of numerous intrusive stocks are probably related to extensional accommodation of major strike-slip motions, associated with the north-eastward incursion of the Adriatic-Pannonian micro-continent.

References:

Annen, C., Blundy, J.D., Sparks, R.S.J. (2006). The genesis of intermediate and silicic magmas in deep crustal hot zones. J. Petrol. 47:505-539.

Berza, T., Constantinescu, E., Vlad, S.N. (1998) Upper Cretaceous Magmatic Series and Associated Mineralisation in the Carpathian – Balkan Orogen. Resource Geology 48:291-306.

Cooke, D. R., Hollings, P. and Walsh, J.L. (2005). Giant porphyry deposits: Characteristics, distribution, and tectonic controls. Econ. Geol., 100/5: 801–818, doi:10.2113/100.5.801.

Gallhofer, D., von Quadt, A., Peytcheva, I., Schmid, S.M., Heinrich, C.A. (2015) Tectonic, magmatic and metallogenic evolution of the Late Cretaceous Arc in the Carpathian-Balkan orogeny. Tectonics, pp. 1813-1836, DOI: 10.1002/2015TC003834.

Gallhofer, D., von Quadt, A., Schmid, St., Guillong, M., Peytcheva, I. and Seghedi, I. (2016). Magmatic and tectonic history of Jurassic ophiolites and associated granitoids from the South Apuseni Mountains (Romania), Swiss Journal of Geosciences, DOI 10.1007/s00015-016-0231-6.

Georgiev, S., von Quadt, A., Heinrich, C.A., Peytcheva, I., Marchev, P. (2012) Time evolution of a rifted continental arc: Integrated ID-TIMS and LA-ICPMS study of magmatic zircons from the Eastern Srednogorie, Bulgaria. Lithos 154:53-67.

Hildreth, W., Moorbath, S. (1988) Crustal contributions to arc magmatism in the Andes of Central Chile. Contrib. Mineral. Petrol. 98:455-489.

Jahn-Awe, S., Froitzheim, N., Nagel, T.J., Frei, D., Georgiev, N., Pleuger, J. (2010) Structural and geochronological evidence for Paleogene thrusting in the western Rhodopes, SW Bulgaria: Elements for a new tectonic model of the Rhodope Metamorphic Province. Tectonics 29.

Jankovic, S. (1997) The Carpatho-Balkanides and adjacent area: a sector of the Tethyan Eurasian metallogenic belt. Mineral Deposita 32:426-433.

Kay, S.M., Kay, R.W., Citron, G.P. (1982). Tectonic controls on tholeiitic and calc-alkaline magmatism in the Aleutian Arc. Journal of Geophysical Research: Solid Earth 87, 4051-4072.

Kolb, M., Von Quadt, A., Peytcheva, I., Heinrich, C.A., Fowler, S.J., Cvetkovic, V. (2013) Adakite-like and Normal Arc Magmas: Distinct Fractionation Paths in the East Serbian Segment of the Balkan-Carpathian Arc. J. Petrol. 54: 421-451.

Marchev, P., Georgiev, S., Raicheva, R., Peytcheva, I., von Quadt, A., Ovtcharova, M., Bonev, N. (2013) Adakitic magmatism in post-collisional setting: An example from the Early–Middle Eocene Magmatic Belt in Southern Bulgaria and Northern Greece. Lithos 180–181:159-180.

Morelli, A., Barrier, E. (2004) Geodynamic map of the Mediterranean, sheet 2, in: World, C.f.t.G.M.o.t. (Ed.), Paris.

Neubauer, F. (2002) Contrasting Late Cretaceous with Neogene ore provinces in the Alpine-Balkan-Carpathian-Dinaride collision belt. In: Blundell, D., Neubauer, F., von Quadt, A. (Eds.) Timing and Location of Major Ore Deposits in an Evolving Orogen, Geol. Soc. London, Spec. Public. 204, pp. 81-102.

Popov, P.B., Tudor, Grubic, A., Ioane, D. (2002) Late Cretaceous Apuseni-Banat-Timok-Srednogorie (ABTS) Magmatic and Metallogenic belt in the Carpathian-Balkan orogen. Geol Balcanica 32, 145-163.

Richards, J.P. (2003) Tectono-magmatic precursors for porphyry Cu-(Mo-Au) deposit formation. Econ. Geol. Bull. Soc. Econ. Geol. 98:1515-1533.

Richards, J.P., Spell, T., Rameh, E., Razique, A., Fletcher, T. (2012). High Sr/Y Magmas Reflect Arc Maturity, High Magmatic Water Content, and Porphyry Cu +/- Mo +/- Au Potential: Examples from the Tethyan Arcs of Central and Eastern Iran and Western Pakistan. Econ. Geol. 107:295-332.

Rohrlach, B.D., Loucks, R.R. (2005). Multi-million-year cyclic ramp-up of volatiles in a lower crustal magma reservoir trapped below the Tampakan copper-gold deposit by Mio-Pliocene crustal compression in the southern Philippines. PGC Publishing, Adelaide.

Schmid, S., Bernoulli, D., Fügenschuh, B., Matenco, L., Schefer, S., Schuster, R., Tischler, M., Ustaszewski, K. (2008) The Alpine-Carpathian-Dinaridic orogenic system: correlation and evolution of tectonic units. Swiss Journal of Geosciences 101:139-183.

Sillitoe, R. H. (1997) Characteristics and controls of the largest porphyry copper-gold and epithermal gold deposits in the Circum-Pacific region. Aust. J. Earth Sci. 44/3:373–388.

Soldatos, T., Koroneos, A., Kamenov, B., Peytcheva, I., von Quadt, A., Christofides, G., Zheng, X., Sang, H. (2008) New U-Pb and Ar-Ar mineral ages for the Barutin-Buynovo-Elatia-Skaloti-Paranesti batholoth (Bulgaria and Greece): Refinement of its debatable age. Geochemistry, Mineralogy and Petrology 46:85-102.

Solomon, M. (1990) Subduction, arc reversal, and the origin of porphyry copper-gold deposits in island arcs, Geology, 18/7:630–633.

Sosson, M., et al. (2010) Subductions, obduction and collision in the Lesser Caucasus (Armenia, Azerbaijan, Georgia), new insights. Geol. Soc. London Spec. Publ., 340/1:329–352, doi:10.1144/sp340.14.

Von Quadt, A., Moritz, R., Peytcheva, I., Heinrich, C.A. (2005). Geochronology and geodynamics of Late Cretaceous magmatism and Cu-Au mineralization in the Panagyurishte region of the Apuseni-Banat-Timok-Srednogorie belt, Bulgaria. Ore Geology Reviews 27:95-126.

FEATURES OF CHEMICAL AND PHASE COMPOSITIONS OF MINERALS OF MANTLE XENOLITHS FROM PIPES OF MIR AND OBNAZHENNAYA (YAKUTIAN KIMBERLITE PROVINCE)

Vorobei S.S., Bovkun A.V., Garanin V.K.

Lomonosov Moscow State University, Moscow, Russia, Patesonchic77@mail.ru

Xenoliths of deep rocks found in kimberlites are a unique source of information on the composition, structure and evolution of the mantle lithosphere of continents and flowing in it processes.

The studied structural-textural features, mineral composition and chemistry of rock-forming and accessory minerals, six samples of xenoliths and websterite peridotite-pyroxenite paragenesis of high-diamondiferous pipes in the Mir and not diamondiferous pipes Obnazhennaya (Yakutian kimberlite province).

In the garnet websterites (Samples O-281, M-74, M-91) granat varies widely in content pyrope component (from 55 to 71 mol. %) and contains 20 to 28 mol.% almandine component. In the sample O-281 granate is surrounded by a strong kelyphitic rims zonal structure. Garnet from garnet-spinel lherzolites (samples Ob.-125 and Ob-212 from pipe Obnazhennaya) are characterized by lower contents of almandine component (up to 16 mol.%) and higher pyrope (73 mol %); contains needle inclusions of rutile.

Clinopyroxene and orthopyroxene, forming xenoliths from the pipe Obnazhennaya contain multitude inclusions. Clinopyroxene from garnet websterites and garnet-spinel lherzolites are represented by diopside (71 to 78 mol. % $CaMgSi_2O_6$) with an admixture of jadeitic component (10-16 mol. % $NaAlSi_2O_6$). It contains lamellae of orthopyroxene, rarely needle inclusions of spinel. The clinopyroxene of these rocks corresponds to the composition of enstatite (33 to 36 wt. % MgO) and contains inclusions of clinopyroxene, chrome- spinel and granate.

Chrome spinel from garnet-spinel lherzolites pipe Obnazhennaya contains up to 40 wt. % Cr_2O_3, 34 wt. % Al_2O_3 and 17 wt. % MgO. Needle inclusions of chrome spinel in clinopyroxene are characterized by higher contents of Al_2O_3 (50 wt. %) and lower Cr_2O_3 (17 wt. %).

In ilmenite clinopyroxenite (sampel of M-84) from pipe Mir of the primary grains of clinopyroxene (about 51 mol. % $CaMgSi_2O_6$) on the periphery and of the veins replaced by fine-grained aggregate of secondary clinopyroxene, which differ from the primary higher content of calcium and magnesium (up to 86 mol. % $CaMgSi_2O_6$) and lower contents of sodium and aluminum. Ilmenite forms a separate elongated grains and contain from 48 to 56 wt. % TiO_2 and up to 42 wt. % FeO.

In the studied xenoliths from the kimberlite pipe Obnazhennaya there is a more intense alteration of the primary minerals with the formation of metasomatic amphibole and secondary serpentine and carbonate xenoliths than in the pipe Mir.

In one of the samples of garnet-spinel lherzolite from kimberlite pipe Obnazhennaya (Sample-125) as inclusions in magnesian alumochrome discovered K-Al-Ti-Cr-containing phase, the formation of which is associated with metasomatic changes of rocks in the mantle conditions.. According to crystal-chemical calculations, the phase can be, supposedly, yimengite. Its composition is characterized by high Al_2O_3 content (20.8 wt. %), what distinguishes from the minerals series yimengite-hawthorneite (1,3-4 wt.% Al_2O_3) from the xenoliths of deep rocks kimberlites, Venezuela (Nixon, Condliffe, 1989) and South Africa (Haggerty, Grey, et al., 1989).

References:

Haggerty S.E.,Grey I.E, Madsen I.C., Criddle A.J., Stanley C.J. and Erlank A.J. Hawthorneite, $Ba[Ti_3Cr_4Fe_4Mg]O_{19}$: A new metasomatic magnetoplumbite-type mineral from upper mantle. American Mineralogist, Vol. 74, pages 668-675, 1989.

Nixon P.H. and Condliffe E. Yimengite of K-Ti metasomatic origin in kimberlitic rocks from Venezuela, Mineralogical Magazine, June 1989, Vol. 53, pp. 305-309.

GEOCHEMICAL, ISOTOPIC AND PETROLOGIC SIGNATURES AND THE INTRACRATONIC GEODYNAMIC NATURE OF THE CALC-ALKALINE VOLCANIC ASSOCIATION (NEOARCHEAN KOLMOZERO-VORON'YA GREENSTONE BELT, FENNOSCANDIAN SHIELD)

Vrevsky A.B.

Institute of Precambrian Geology and Geochronology of the Russian Academy of Sciences, Saint-Petersburg, Russia,
a.b.vrevsky@ipgg.ru

The petrology and geodynamic nature of calc-alkaline igneous complexes are one of the most acute problems of the genesis of a juvenile continental crust at the early stages of the Earth's evolution. Commonly, the basalt-andesite-dacite (BAD) associations of the Archean greenstone belts (GB) is considered to be a single indicator of subduction-accretion convergent geodynamic settings in which the continental crust of Archean granite-greenstone provinces was formed. Such volcanic complexes, including those of the Fennoscandian Shield, are suggested to indicate plate tectonic geodynamic scenarios because some of their isotopic-geochemical characteristics are similar to those of Phanerozoic adakitic and boninitic volcanic series (Martinet al., 2006; Puchtel et al., 1999; Svetov et al., 2004).

Geological background
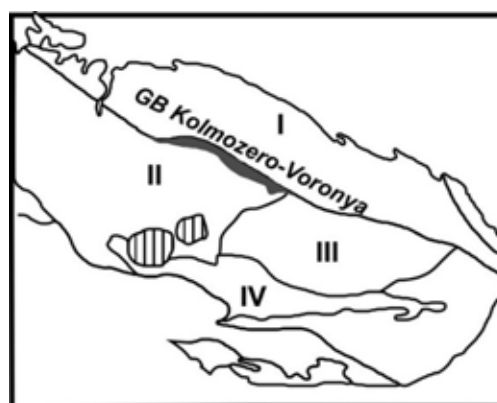
Fig.1. Scheme of the main tectonic terranes of the Kola-Norwegian Province, Fennoscandian Shield: (I) Murmansk terrane, (II) Central Kola terrane, (III) Keivy terrane, (IV) Palaeoproterozoic Imandra–Varzuga structure.

The Polmos-Porosozero structure is the best-preserved part the >300 km long Uraguba-Kolmozero-Voronya Neoarchean greenstone belt which is located in the zone between the Murmansk and Central Kola domains of the Fennoscandian Shield (Fig.1). The volcanic-sedimentary complex of the structure consists of three units (Vrevskii et al., 2003). The lower terrigenous unit is mainly formed by garnet-biotite and biotite schists (metagreywackes). The lower part of the overlying volcanogenic unit is represented by metamorphosed pillow and massive tholeiitic-basalts and komatiitic lava with pyroclastic interbeds. Komatiite and tholeiite volcanics grade into a unit formed of interbeded basalts, andesite-basalts, andesites and dacites with textural signs of lava and tuffs without stratigraphic and tectonic unconformities. The basalt-andesite-dacite (BAD) unit also contains thin interlayers of greywackes, calcareous dolomite, BIF and carbonaceous schists. BAD association is uncomformably overlained by the upper terrigenous unite, which consists of high aluminous gneisses and schists with the lenses of polymictic conglomerates at the base of the section.

Table 1. Average composition of the BAD association from the Polmos-Porosozero structure.

Components	1	2	3	Components	1	2	3
n	7	7	4	n	7	7	4
SiO_2	58,07	57,37	50,58	Ti	2481	3973	2061
TiO_2	0,43	0,69	0,31	Ti/Zr	53,7	25	76
Al_2O_3	14.46	15.01	14.2	Zr/Y	6.5	3.7	2.4
FeO*	8.06	9.25	11.63	Sr/Y	15.9	6.6	9.1
MnO	0.16	0.13	0.22	La	13.51	2.47	1.57
MgO	5.64	4.61	8.41	Ce	29.03	7.33	3.84
CaO	7.63	7.08	8.93	Pr	3.67	1.16	0.61
Na_2O	2.41	3.67	2.04	Nd	14.21	6.04	3.11
K_2O	1.14	0.27	0.26	Sm	2.87	2.14	1.05
P_2O_5	0.15	0.13	0.13	Eu	0.87	0.82	0.4
K_2O/Na_2O	0.58	0.07	0.15	Gd	2.8	2.58	1.32
Ba	26.0	35.1	19.9	Tb	0.43	0.48	0.26
Sr	243.7	132.4	103	Dy	2.45	3.06	1.71
Y	15.3	20.1	11.3	Ho	0.49	0.67	0.4
Zr	99.29	74.04	27.1	Er	1.41	1.89	1.11
Nb	7.62	4.69	1.53	Tm	0.2	0.28	0.18
Hf	2.61	2.14	0.66	Yb	1.26	1.78	1.07
V	139.3	214.4	214.8	Lu	0.2	0.27	0.18
Cr	247	118	296	(Nb/La)n	0.9	2.56	1.1
Co	56.0	44.9	51.3	(Gd/Yb)n	1.81	1.21	1.12
Ni	171.8	63.8	133.3	(Ce/Sm)n	2.43	0.81	0.86

Note:(1) Andesites I; (2) andesites II; (3) basalts

The composition of BAD association generally corresponds to a normal alkalinity of calc-alkaline series. However, based on the variations in the major, trace and REE elements composition of intermediate volcanics, two geochemical groups, namely *andesite-I* and *andesite-II*, were identified. *Andesite-I* consists dominantly of andesite-basalt (SiO_2=55.3-56.6%), poor in TiO_2 (<0.5), have a normal Mg content ($mg^\#$=0.26-0.40). This type of volcanics belongs to a sodic calc-alkaline series and shows a strongly fractionated normalized LREE pattern $(Ce/Sm)_N$=2.38-2.82 and a weakly fractionated HREE pattern $(Gd/Yb)_N$=1.62-2.35(Fig. 1, tabl. 1). A second geochemical group (*andesite-II*) of andesitic and andesitic-dacitic volcanics (SiO_2=56.4-59.7%) is characterized by higher Mg (mg#=0.41-0.46), Ti, V and Ba concentrations and lower Sr, Cr, Co, Ni, Ti contents, as well as lower Ti/Zr and Zr/Y ratios. It shows a more potassic composition of alkalines. The normalized REE patterns of this group volcanics exhibit LREE depletion $(Ce/Sm)_N$=0.62–0.88) and slight HREE fractionation $(Gd/Yb)_N$=1.01–1.58)(Fig. 2, table 1), which is atypical of andesites. Unlike Archean and Phanerozoic adakitic associations, both types of andesites have a lower concentration of "indicator" elements such as Ba, Sr and Y and a lack of negative Nb anomaly $(Nb/La)_N$ =0.9–2.6) on spidergrams.
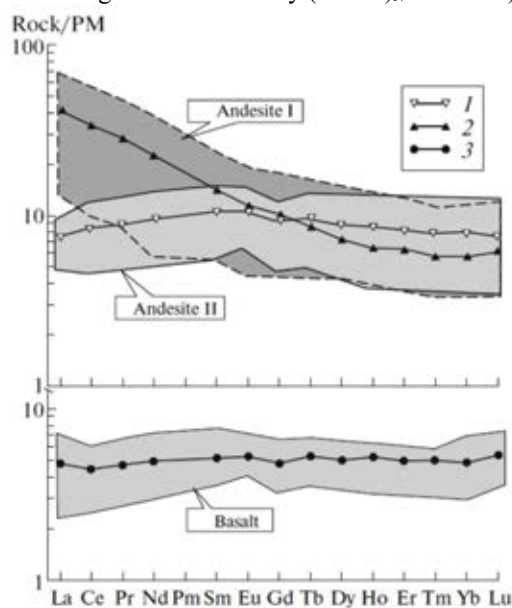
Fig. 2. Primitive mantle–normalized REE distribution patterns in rocks of the BAD association from the Polmos–Porosozero structure. (1–3) average compositions: (1) andesites II, (2) andesites I, (3) basalts.

U-Pb zircon age data (SHRIMP II) and Sm-Nd isotopic systematic

The zircon population from andesites-I were analyzed for U–Pb isotope systematics (U-Pb SHRIMP II) and discordant upper intercept age of 2778.4±5.4 Ma (MSWD=0.75) was obtained.

BAD association shows a significant variation in the initial $^{143}Nd/^{144}Nd$ ratios (Table 2). Andesite-I typically has εNdT_{2780} values varying from +0.8 to +3.7 and the Sm-Nd model age (TDM) from 3050 to 3235 Ma. Andesite-II shows isotopic and geochemical signatures (εNdT_{2780}-1.0 to -6.5), which dramatically differ from andesite-I. Andesite-II is suggested to be formed either from an "enriched" mantle (EMI-type) source or by the significant contamination of the primary melts by the continental crust.

Table 2. Sm–Nd isotope data of the BAD association from the Polmos–Porosozero structure

Sample	Rock type	Sm, ppm	Nd, ppm	$^{147}Sm/^{144}Nd$	$^{143}Nd/^{144}Nd$	$\varepsilon Nd_{T=2780}$
63-a	Basalt	0.81	2.36	0.2121	0.513027	+3,5
155	Basalt	1.44	4.32	0.2018	0.512826	+1,8
161	Basalt	0.98	2.87	0.2069	0.512907	+1,5
137	Andesite II	1.39	4.15	0.2024	0.512416	-6,5
521	Andesite II	2.53	6.77	0.2263	0.513149	-1,0
523	Andesite II	3.03	8.41	0.2175	0.512958	-1,5
537-1	Andesite I	4.65	25.84	0.1118	0.511087	+3,7
529	Andesite I	1.17	3.49	0.2024	0.512832	+2,9
257-a	Dacite I	2.16	10.97	0.1167	0.511200	+0,8
240	Andesite I	2.91	13.37	0.1314	0.511454	+1,1

Petrologic interpretation and discussion

In order to determine protolith of the andesite-II, geochemical modeling based on the trace element and isotopic characteristics and available experimental data (Petermann et al., 2003; Annen et al., 2006;Condie, 2001) was performed. The 3.59+0.42/–0.25 Ga model ages suggest that protolith of andesite-II primary melts had a prolonged evolutionary history of isotopic composition. The best fit solution for protolith is ancient (>3.5 Ga) basic eclogite with $^{147}Sm/^{144}Nd$=0.15, which nature can be interpreted as mafic melts underplated the lower crust. This possible lower crustal candidates was close in their Sm-Nd isotopic composition to the Paleoarchean amphibolites from the Voldozero

terrain of the Fennoscandia Shield (Vrevskii et al., 2010) or the 4.28 Ga Nuvvuagittuq mafic complex of the Superior Province (O'Neil, Carlson, 2008).

Conclusions

The obtained data for the BAD association from the Neoarchean Polmos–Porosozero greenstone structure and the previously defined nature of the komatiite–tholeiite association (Vrevskii et al., 2003;Vrevskii, 2016) can be interpreted in the context of geodynamic of plume–lithosphere interaction, not related to subduction processes. This mechanism of the juvenile crust formation agrees reasonably well with the concept (Condie, 2001) of a long-lived Archean mantle plume (>200 Ma) and is therefore sufficient for explaining the andesite-I data as being derived from melting of the peridotite mantle in a plume head enriched in the fluid components. Therefore, the primary basaltic melts are being the melting products of the hottest axial zone of the plume.

References:

Annen C, Blundy JD, Sparks RSJ (2006) The Genesis of intermediate and silicic magmas in deep crustal hot zones. Journal of Petrology. 47:505–539.

Condie KC (2001) Mantle plumes and their record in the Earth History. Cambridge. 306p.

Martin H, Smith RH, Rapp R, Moyend J-F, Champione D (2005). An overview of adakite, tonalite-trondhjemite-granodiorite (TTG) and sanukitoid: relationships and some implications for crustal evolution Lithos 79:1-24.

O'Neil J, Carlson RW, Francis D, Stevenson RK (2008) Neodymium-142 evidence for Hadean mafic crust Science 321:1828–1839.

Petermann M, Hirschmann MM (2003) Anhydrous partial melting experiments on MORB-like eclogite: phase relations, phase compositions and mineral+melt partitioning of major elements at 2–3 Gpa., Journal of Petrology 44: 2173–2201.

Puchtel IS, Hofmann AW, Amelin YuV, Garbe-Schonberg CD, Samsonov AV, Shchipansky AA (1999) Combined mantle plume-island arc model for the formation of the 2.9 Ga Sumozero-Kenozero greenstone belt SE Baltic Shield: isotope and trace element constraints Geochimica et Cosmochimica Acta 63:3579−3595.

Svetov SA, Huhma H, Svetova AI, Nazarova TN (2004) The oldest adakites of the Fennoscandian Shield. Doklady Earth Sciences. 397: 878−882.

Vrevskii AB, Matrenichev VA, Ruzh'eva MS (2003) Petrology of komatiites from the Baltic Shield and isotope geochemical evolution of their mantle sources Petrology (11):532-561.

Vrevskii AB (2016) Age and Sources of the Anorthosites of the Neoarchean Kolmozero-Voron'ya Greenstone Belt (Fennoscandian Shield) Petrology (24): 527–542.

Vrevsky AB, Lobach-Zhuchenko SB, Chekulaev VP, Kovalenko AV, Arestova NA. (2010) Geological, petrologic, isotopic, and geochemical constraints of geodynamic models simulating formation of the Archean tonalite-trondhjemite-granodiorite associations in ancient cratons Geotectonics (44):305-320.

ON ALTERED CARBONATITES FROM CATANDA, ANGOLA

Wolkowicz K.[1], _Jackowicz E._[1], _Wolkowicz S._[1]

[1]Polish Geological Institute-National Research Institute, Warsaw, Poland, krystyna.wolkowicz@pgi.gov.pl

Geological setting

Catanda carbonatites belong to the lithological unit located at the intersection of four fault systems of Lucapa transcontinental rift structure extent of NE-SW. The structure and the carbonatite complexes were dated to Cretaceous period. Our recent geochronological determination based on pyrochlore indicates much younger age of this intrusion (Paleogene). Carbonatites cover an area of approximately 80 km^2 and occur on the Precambrian basement consisting mainly of granite and acid metamorphic rocks; their overburden consists of eluvial-alluvial sediments. In the present morphology of the carbonatite complex one can distinguish hills surrounding the circular depression, within which there are relics of volcanic vents.

Catanda carbonatite complex is dominated in the volume by pyroclastic rocks, represented by the pyroclastic fall, flow and surge deposits. Carbonatite lavas - calcio- and silicocarbonatites, alternating with pyroclastic deposits, are formed in the most part by welding or agglutination of spatter, which particles are distinguish by positive relief on the surface of layers (Campeny, et al. 2012, 2014).

Object of investigation

The objects of this study were altered silicocarbonatites (12,5 -21,8% SiO$_2$), occurring in the Ngonge and Viallala hills. The phenocrysts and xenocrysts components are pyroxenes (augite, diopside), amphiboles (hornblende, kaersutite), phlogopite, biotite, olivine, apatite, calcite, magnetite and titaniferous magnetite, plagioclase, K-feldspars and rarely quartz. Phenocrysts of mafic minerals, apatite, as well as numerous compounds of groundmass (spinel, perovskite, pyrochlore, zirconolite) exhibit compositional zoning and corroded edges. From the core to the mantle, augites display the increase in En and decrease in Fs content (with Wo52-54), olivines the increase in Fe content, perovskite in Fe, Nb and LREE.

Products of alterations

Silicocarbonatite lavas are altered in the different ways. Some of them underwent above all secondary carbonatization - the numerous veinlets cutting lavas are filled with calcite, which also forms irregular, often discontinuous and not complete rims around phenocrysts. On the mafic minerals there are mixed calcitic-chloritic rims or calcitic rims surrounding thin rims of earlier generation consist of chlorite or smectite.

Another common alterations of lavas resulted in replacing of feldspars (sometimes calcite) by calcium-aluminium-silica hydrated (CASH) minerals (locally with admixture of carbonates) and developing layered rims, containing monticellite and calcium silicates around mafic minerals, plagioclases, potassium feldspars and calcite. These calcium silicates and CASH are recognized, on the base of WDS analysis. The chemical composition suggests, that CASH minerals are probably represented by tobermorite group, though their structural formulae are not correct due to the admixture of others ingredients in pseudomorphs, rims and fissure cracks, where they occur. Among the calcium silicates, cuspidine is predominate, but locally the minerals of Ca-humite group (perhaps kumtyubeite) occur and rarely wollastonite, only as infilling the veinlets in altered phenocrysts. Monticellite from the rims of different phenocrysts have similar composition.

Alteration rims

The rims have different thickness, from thin (several tens of mikrometres) on pyroxenes, amphiboles and phlogopite to relatively wide (up to ~400 mikrometres) on feldspars. Their contact with phenocrysts (or pseudomorph) is sharp, but their opposite margins are locally not clear, because of the presence of very thin, irregular overgrowths, sometimes looking like coronas. They enter into the groundmass, which also contains minerals forming the rims.

The rims of olivine consist mainly of monticellite; pyroxenes and amphiboles have partly discontinuous rims of monticellite and cuspidine, overgrown with inclusions, mainly of Ti-magnetite and apatite. In the rims surrounding feldspars, the inner band is formed of cuspidine or minerals of Ca-humite group (locally with inclusions of Ba-mica), the outer band contains mainly monticellite (locally overgrown with minerals from the inner band). In some rims, particularly around feldspars, one can observe, that monticellite was growing from outer to inner margins of the rims, on the contrary to thin corona.

In less altered lavas, the rims don't contain monticellite. The relics of pseudomorph of tobermorite, probably after feldspars, with the rims consist of cuspidine and remnants of this pseudomorphs.

Conclusions

- Two facies of altered silicocarbonatite lavas have been distinguished; they are characterized by assemblages of the following secondary minerals: 1. chlorites and smectites - calcite; 2. CASH minerals, calcium silicates and monticellite.

- The mentioned minerals form rims on phenocrysts and xenocrysts; monticellite and cuspidine form also thin haloes overgrowing rims. They also occur in the groundmass and with the exception of monticellite, infill the fissures crack. It indicates the genesis of this mineralization after emplacement of lavas.

- Chlorites, smectites, calcite and CASH minerals are the products of postvolcanic activity, but cuspidine, minerals of Ca-humite group and monticellite represent high-temperature assemblage, typical to skarn.

- Features of some phenocrysts relics and their rims suggest the influence of pyrometamorphism on their formation. This process could be caused by coal combustion (Ciesielczuk et. al., 2015) or by another factors, related with the fire activity.

References:

Campeny M., Alfonso P., Melgarejo J.C., Mangas J., Bambi A., Manuel J. (2012) Carbon and oxygen isotopes of the carbonatitic lavas from Catanda, Kwanza Sul, Angola: genetic implications. European Mineralogical Conference Vol. 1, EMC 2012-438.

Campeny M., Mangas J., Melgarejo J.C., Bambi A., Alfonso P., Gernon T., Manuel J. - 2014. The Catanda extrusive carbonatites (Kwanza Sul, Angola): an example of explosive carbonatitic volcanism. Bull. Volcanol. 76: 818-832.

Ciesielczuk J., Kruszewski L. Majka J. (2015) Comparative mineralogical study of thermally-altered coal-dump waste, natural rocks and the products of laboratory heating experiments. Int. Jour. of Coal Geology 139: 114-141.

GEOCHRONOLOGY OF CATANDA CARBONATITIC INTRUSION AND SURROUNDING GRANITES (ANGOLA) – PRELIMINARY STUDIES

Wołkowicz S., Krzemińska E., Wołkowicz K., Jackowicz E., Czupryt Z.J.

Polish Geological Institute-National Research Institute, Warsaw, Poland, stanislaw.wolkowicz@pgi.gov.pl

Catanda carbonatite massif (Cuanza Sul Province), as well as carbonatites from other occurrences in Angola belongs to the Parana-Angola-Namibia magmatic province. The carbonates of this province are most often found in the form of intrusive bodies in central parts of alkaline complexes, rarely appear as extrusive or effusive volcanic products. The igneous and volcanic phenomena were related to the tectonic activity in deep crustal propagating faults cutting the South American and African platforms far landward. Catanda carbonatite massif is still poorly and fragmentarily recognized compared to other carbonatite structures of the Lucapa structure, although it represents very attractive research material coming from rare occurring extrusive carbonatites. Catanda massif (Fig. 1) covers an area of about 80 km^2 and have penetrated Precambrian basement built of granites, migmatite-granite gneisses, quartz schists and diabases and is directly overlain by eluvial-aluvial sediments originating from their weathering (Pinheiro, 2008).
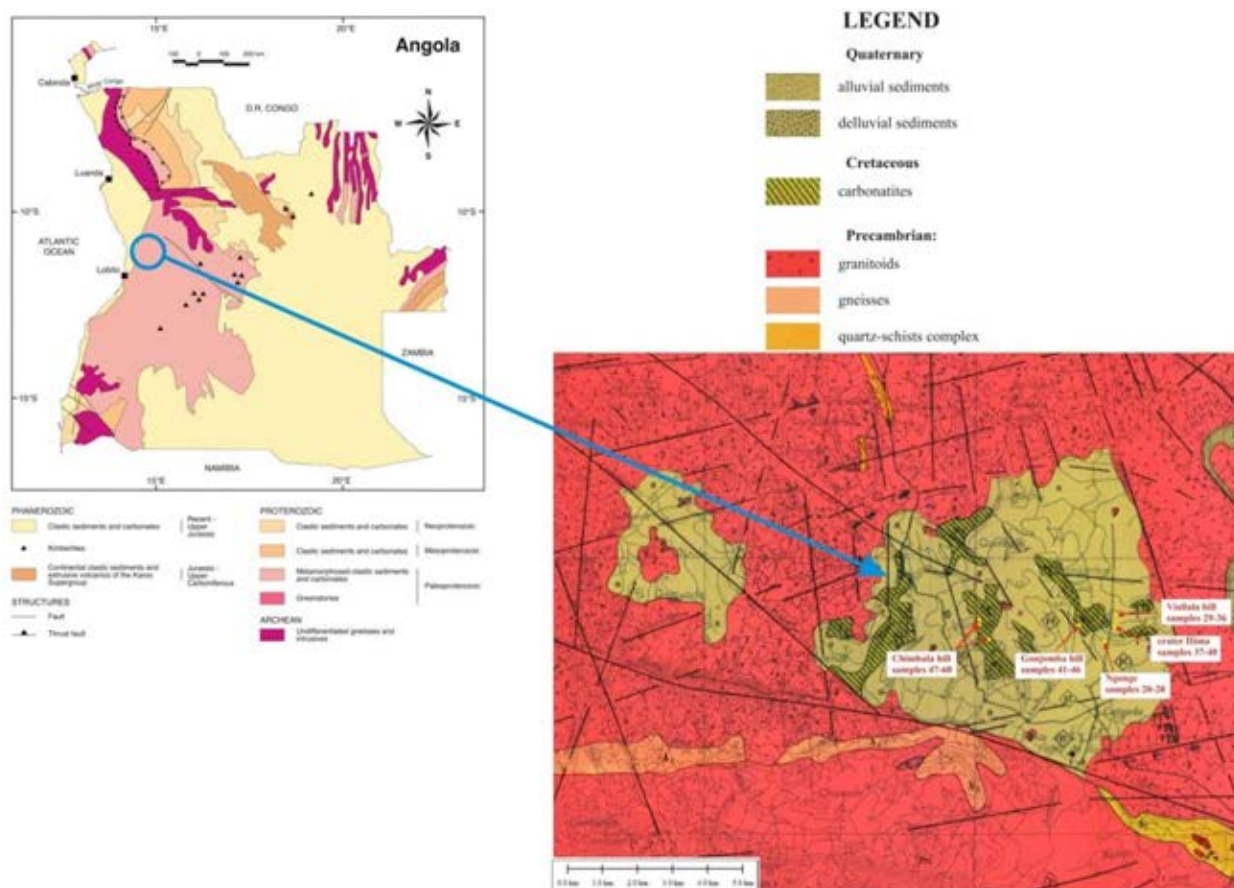
Fig. 1. Geological map of Catanda carbonatitic massif (after Silva, 1973b) with marked sampling points.

Previous studies have shown that carbonatite complexes from Catanda are dominated by pyroclastic rocks, Previous studies have shown that Catanda carbonatite complexes are volume-dominated by pyroclastic rocks, reaching thickness up to 100 m.

These rocks are generally classified as carbonatite tuffs (Silva, 1973a), representing several cycles gradation stratigraphic cycles. In the lower part of the cycles there are agglomerates composed with igneous and metamorphic rocks (granitogneisses, amphibolites, carbonatites and other alkaline rocks), and in the upper ones are carbonatitic lapilli-ash tuffs. Carbonatitic lava forms streams up to several meters thickness, interbedding pyroclastic rocks (Campeny et al., 2012). According to Silva (1973a) these lava are composed of phenocryst of pyroxenes, amphibolites, olivine, biotite, apatite and opaque minerals and microcrystalline, sometimes carbonatic groundmass with apatite, magnetite, pyrochlore and baddeleite. Numerous bubbles are filled with calcite, sometimes barite and kaolinite. As a result of subsequent studies of Catanda carbonatite complexes, lavas were divided into carbonatites and natrocarbonatites (Bambi et al., 2008a), or calciocarbonatites and silicocarbonatites (Campeny et al., 2012). Natrocarbonatites are called lavas, whose phenocrysts are pseudomorphs after nyerereite, and the microcrystalline, calcitic groundmass contains accessory pyrochlore, baddeleite and spinels (Bambi et al., 2008b).

The division into calciocarbonatites and silicocarbonatites was based on the results of the study of the main elements, which was confirmed by the mineral composition of these lavas. Calciocarbonatites are composed of calcite and apatite phenocrysts and calcite groundmass, while silicocarbonatites are aphyric, and their groundmass contains calcium silicates, apatite, ulvospinel, perovskite, pyrochlore and periclase (Campeny et al., 2012). The content of ^{13}C and ^{18}O isotopes in calcite of carbonatites are not typical for mantle magma and indicate the significant influence of the continental crust on the formation of their composition (op.cit.). Perhaps this is due to the long-term hydrothermal activity, as described by Silva (Silva, 1973a) in four craters of hot springs containing calcium or sodium carbonates.

Analytical methods

Age isotopic investigations were realized on monomineral concentrates separated from hand samples 51D and 43 (tuffs an altered lava flow) using conventional procedure (e.g. heavy liquids, magnetic separation and hand peacking). U-Pb measurements have been done on zircons and pyrochlore single grains. In bot of cases Temora2 zircon standard was used as a basic reference material with ratio ^{206}Pb/^{238}U= 0.06683 ^{206}Pb*/^{238}U age of 416.78±0.33 by TIMS (Black et al., 2004).

The similar analytical procedure was applied for U-Pb datings of pyrochlore from Nsungwe Formation (Roberts et a al. 2010).

The zircon and pyrochlore mounts were imaged on Nikon EclipseLV100NPol optical microscope in transmitted and reflected light mode using NIS Elements BR software and on scanning electron microscopy using CL and BSE

detector of HITACHI SU3500 to check homogeneity and internal features of grains and to select a proper place for analyses.

The software of SQUID2.50.11.01.03 and attached Isoplot/Ex v.3.0 Macro of Ludwig (2003) were used for data processing and visual form of results are presented on Tera-Waserburg (^{207*}Pb/^{206*}Pb versus ^{238}U/^{206*}Pb) oraz Wetherilla (^{206*}Pb/ ^{238}U versus ^{235}U/^{207}Pb) concordia diagrams.

In case detrital zircons and high number data it was necessary to use a probability plots and histograms, which are a basic form of data presentation and comparison of age groups and number of populations, that reflect probable source rocks and areas.

Results and conclusions

The age of carbonatite ash and lava flow from Catanda is a matter of longstanding debate. Zircons separated from volcanic ash layers are commonly inferred to date the time of a volcanic eruption. Thus it was one of the basic aim of presented study.

However, this assumption is often problematic due to inheritance or incorporation of slightly older zircons that were derived from older rocks and entrained in the eruption column. Moreover carbonatite may contain a lesser amount of accessory zircon phase. Only two samples (43 and 51D) provided some amounts grains, that allow to perform U-Pb age study. The zircons reveal variability from euhedral to subhedral with shapes ranging from elongate prismatic to squat equidimentional forms, suggesting on the beginning a significant contribution of non-volcanic material. All extracted grains e.g. 74 zircons from sample 51D and 44 zircon from sample 43 were checked and a total of 118 grains were analysed. *Zircon* age populations are similar in both samples and yielded ^{207}Pb/^{206}Pb age in range from 3274 $\pm$ 83 Ma to 1896$\pm$ 26 Ma.

The resultant age data plot a cluster on or around concordia, defining a dominating Paleoproterozoic age of epiclastic material. The similarity of U-Pb zircon record both samples is shown on isotopic radio data set visualized on Tera –Wasserburg concordia diagram and on relative probability plot (Fig. 2), where the compilation of Pb-Pb concordant ages from samples (51D and 43) reveal single modal distribution peaked at 2016 Ma. Moreover, for each sample the most coherent group of grains within error is the same, defining crystallization age of dominated source rocks at 2037±9.9 Ma and at 2031.2±10 Ma respectively. These result perfectly corresponds with age of the local Palaeoproterozoic granitic magmatism documented recently (McCourt et al., 2013) in the Lubango Zone (Lubango with upper intercept age of 2038± 28 Ma) that forms part of southern Angola crustal terrane (Angolan Shield), linked to an active continental margin of that age.

Oxygen isotope ratios of detrital zircon have been used to evaluate the degree of addition of crustal material, because grains that crystallise from mantle derived magmas tend to record a rather narrow range of δ ^{18}O values falling lose to 5.3±0.3‰. Assimilation of crustal components is usually expressed by elevated oxygen isotope composition. The δ ^{18}O values of examined zircons range from 3.95±0.23‰ to 7.36±0.18‰ with mean δ ^{18}O $_{VSMOW}$ values of 6.32±0.15‰ (Wołkowicz et al. 2016).

Carbonatite-specific mineral remain a pyrochlore. Presence of compositionally zoned and euhedral and visually fresh grains of pyrochlore as an accessory phase in carbonatite ash and lava allowed to test the geochronological potential of pyrochlore. Because of expected high abundances of U and Th, the EMP chemical analysis have been performed before the isotopic study. BSE-textures include mostly homogeneous cores and distinct composition of thin rims (Fig. 3 A). Nb, Ti, Ca, and Na generally show only small variations within individual crystals (e.g., ,12.5–16.6 wt% CaO) with amount of niobium up to 68 wt% Nb$_2$O$_5$. In contrast, U and Th concentrations are highly variable and range over 0.2–2.0 wt% and 0.6–6.4 wt%, respectively. The amount of Pb was typically below detection limit of WDS. In general terms pyrochlores extracted from samples 43 and 51D follow regional chemical trends of alteration (Bambi et al., 2012, Torro et al. 2012). The grains contain up to 3 wt.% SrO and variable amount of F (Fig. 3B). Some grains of pyrochlore have clearly secondary genesis having F-, Ca-and Na- rich compositions, but some crystals are not strongly altered and reveal composition close to those from the typical primary pyrochlores.
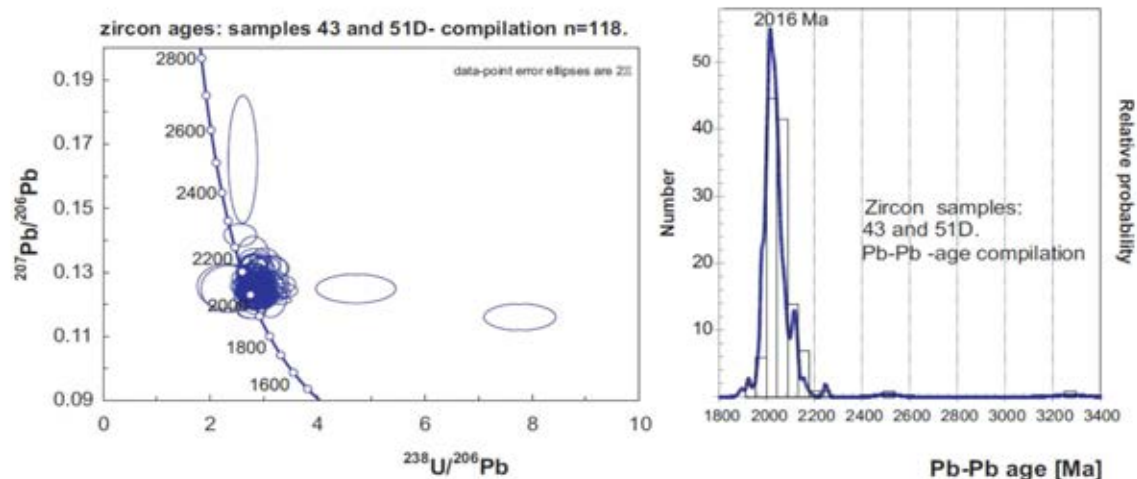
Fig 2. Catanda epiclastic zircon U-Pb age results compiled on Concordia diagram and on relatively probability plot.

U-Pb-Th analyses of pyrochlore grains from Catanda tuff are complicated because the lead concentration is typically low, with variable but relatively high amounts of common-Pb contamination. In consequence preliminary results have relatively large uncertainties and discordances. First data set confirmed that composition of grains is extremely variable (Fig. 3C) with few young results $^{206}Pb/^{238}U$ below 5 Ma.

Calculated isochron for cogenetic samples yielded age of about 26.6 ±6.7 Ma (MSWD= 0.25) with low initial $^{207}Pb/^{204}Pb$, needs more refinements by additional measurements. Such imprecise result, however may tentatively suggest a slightly younger time of effusive activity in Catanda, that correlates with age of carbonatite tuff from the Nsungwe Formation of 24.93±0.49 Ma, known from south western Tanzania defined also on pyrochlore grains (Roberts at al. 2010).
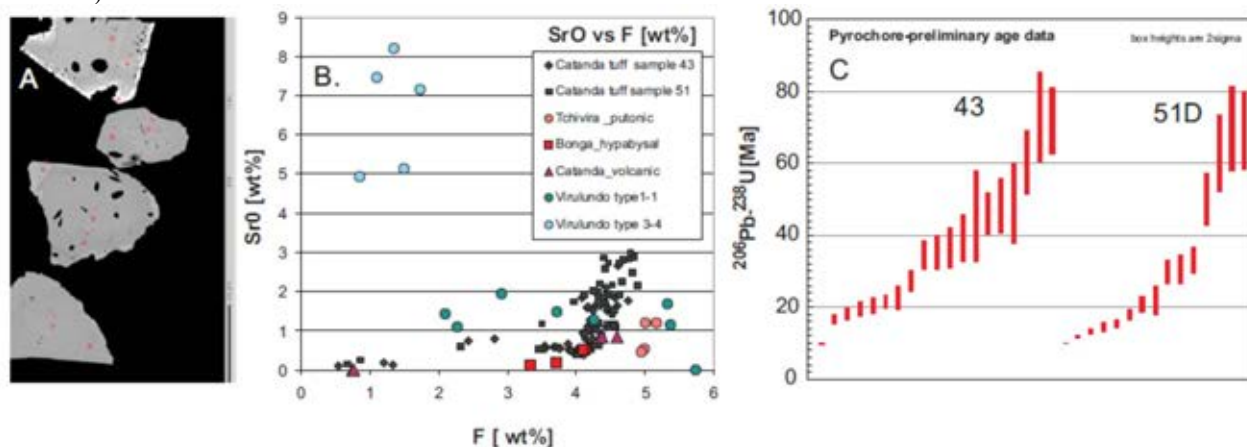
Fig. 3. Chemical and Isotope composition of pyrochlore grains from Catanda tuffs. BSE image and WDS composition on SrO vs F diagram with data for comparison taken from Bambi et al. 2012 and Torro et al. 2012 and preliminary U-Pb age constrain.

References:

Bambi A., Costanzo A., Melgarejo J., Gonçalves A., Alfonso P., Neto A., Manuel J. (2008a) Evolution of Pyrochlore in Carbonatites: the Angola Case. Macla 9: 43-44.

Bambi A. J. M., Costanzo A., Manuel J., Alfonso P., Olimpio A., Melgarejo J. C. (2008b) Natrocarbonatite flows and pyroclastic deposits in the early Cretaceous Catanda carbonatite volcanoes. Publications of the 33rd International Geological Congress, Oslo, Norway.

Bambi, A., Costanzo A., Goncalves A.O., Melgarejo J.C. (2012) Tracing the chemical evolution of primary pyrochlore from plutonic to volcanic carbonatites: the role of fluorine. Mineralogical Magazine, 76(2): 377-392.

Black, L. P., Kamo, S. L., Allen Ch.M., Aleinikoff J.N., Davis D.W., Korsch R.J., Foudoulis, C. (2003) TEMORA 1: a new zircon standard for U-Pb geochronology. Chem. Geol., v. 200: 155-170.

Campeny M., Alfonso P., Melgarejo J.C., Mangas J., Bambi A., Manuel J. (2012) Carbon and oxygen isotopes of the carbonatitic lavas from Catanda, Kwanza Sul, Angola: genetic implications. European Mineralogical Conference Vol. 1, EMC 2012-438.

McCourt S., Armstrong R.A., Jelsma H., Mapeo R.B.M. (2013) New U-Pb SHRIMP ages from the Lubango region, SW Angola: insightsinto the Palaeoproterozoic evolution of the Angolan Ahield, southern Congo Craton, Africa. Journal of the Geological Society v.170; 353-363.

Pinheiro O. Q., 2008 - Análise espacial integrada da informação de arquivo do carbonatito de Catanda. Caso das crateras kimberlíticas. Dissertação para obtenção do título académico de Mestre; Universidade Agostinho Neto, Faculdade de Cienias, Departamento de Geologia. Luanda, Angola.

Roberts E.M., O'Connor P.M., Stevens N.J., Gottfried M.D., Jinnah Z.A., Ngasala S., Choh A.m., Armstrong R.A. (2010) Sedimentology and depositional environments of the Red Sandstone Group,

Rukwa Rift Basin, southwestern Tanzania: New insight into Cretaceous and Paleogene terrestrial ecosystems and tectonics in sub-equatorial Africa. J of African Earth Sciences 57:179 -212.

Silva M.V.S., 1973a. Estrutura Vucanico-Carbonatitica da Catanda (Angola). Boletim dos Servicos de Geologia e Minas, 24.

Silva M.V.S., 1973b. Carta Geologica de Angola. Folha N 207 Gungo. Scale 1:100 000.

Torró L., Villanova C., Castillo M., Campeny M., Gonçalves A., Melgarejo J. 2012 Niobium and rare earth minerals from the Virulundo carbonatite, Namibe, Angola. Min. Mag. 76, 2: 393-409.

Wołkowicz S. et al. 2016. The oxygen isotope study of zircon grains from Catanda extrusive carbonatite (Angola). http://www.americangeosciences.org/sites/default/files/igc/4663.pdf

SEISMIC CRUSTAL STRUCTURE OF THE NORTH CHINA CRATON AND SURROUNDING AREA: SYNTHESIS AND ANALYSIS

Xia B.[1,2], _Thybo H._[3,4], Artemieva I.M.[2], Zheng J.P.[1]
[1]China University of Geosciences, Wuhan, China, bixi@ign.ku.dk
[2]University of Copenhagen, Copenhagen, Denmark, irina@ign.ku.dk.
[3]University of Oslo, Norway, thybo@geo.uio.no
[4]Istanbul Technical University, Istanbul, Turkey, h.thybo@gmail.com

We present a new digital model (NCcrust) for the seismic crustal structure of the Neoarchean North China Craton (NCC) and the surrounding Paleozoic-Mesozoic orogenic belts. All available seismic profiles (50 in total), complemented by receiver function interpretations of crustal thickness, are used to constrain a four layer (sedimentary cover, upper, middle and lower crust) thickness and velocity of the crustal model NCcrust. The model, defined on a 15' × 15' grid, includes the Moho depth, the internal structure of the crust specified for 4 crustal layers sedimentary cover, upper, middle and lower crust, and the Pn velocity in the upper mantle. We document a general trend in the westwards increase in the thickness of the crustal layers and the depth to the Moho. The crust is thin (30-32 km) to the east of the 120° E meridian, much thinner than the global average for the cratonic crust. The average Moho depth in the Western part of the NCC is 38-44 km. The Moho depth of the Sulu-Dabie-Qinling-Qilian orogenic belt ranges from 31 km to 51 km, with a general westwards increase in the crustal thickness. The sedimentary cover is 2-5 km thick in most of the region and typical thicknesses of the upper, middle, and lower crust are 16-24 km, 6-24 km, and 0-6 km, respectively.

There is no systematic regional pattern in the average crustal Vp velocities and the Pn velocity. The average P-wave velocity in the crystalline crust ranges from 6.28 km/s in the northeastern and the central-southern parts of the craton to 6.42 km/s in the western part with the thicker crust (the northern Ordos Basin). The velocity in the uppermost mantle is very heterogeneous with Pn values ranging from 7.8 km/s (along the Tanlu Fault) to 8.3 km/s (the Ordos Basin) and with no clear link to surface geology.

We examine correlations between the Moho depth and topography for 7 tectonic provinces in the North China Craton and speculate on mechanisms of isostatic compensation. We observe strong linear correlations between the topography and the Moho depth in the Trans-North China Orogen, the Yanshan and the Jiao-Liao orogenic belts of the Eastern NCC, and in the Ordos Basin of the Western NCC, which indicate that an Airy-type compensation plays an important role in regional isostasy. In contrast, no correlation exists between the Moho depth and the topography in the Khondalite and Yinshan orogens of the Western Block and the North China Plain of the Eastern Block, suggesting that there regional isostatic compensation is achieved either through mantle heterogeneity, or through lateral density variations in the crust, or through a combination of both.

References:
Xia B., H. Thybo, I. M. Artemieva and J. P. Zheng (2017). Seismic crustal structure of the North China Craton and surrounding area: synthesis and analysis. J. Geophys. Res., in press, DOI: 10.1002/2016JB013848.

A NEW HIGH PRESSURE CELL FOR ACCURATE DIELECTRIC MEASUREMENTS

Yamane R., Komatsu K, Kagi H.
Geochemical Research Center, Graduate School of Science, The University of Tokyo, Tokyo, Japan, yamane@eqchem.s.u-tokyo.ac.jp

High pressure is an effective parameter to tune physical properties of materials, whereas the evaluation of sample state under pressure is not always straightforward due to its limited accessible space. Dielectric measurements, which give us unique information in electro-chemistry such as electrical conductivity, orientation of polarized molecules, relaxation time etc., are also not the exception; its availability under high pressure, particularly for initially liquid sample and at pressure above 3 GPa, has been limited up to date1–3.
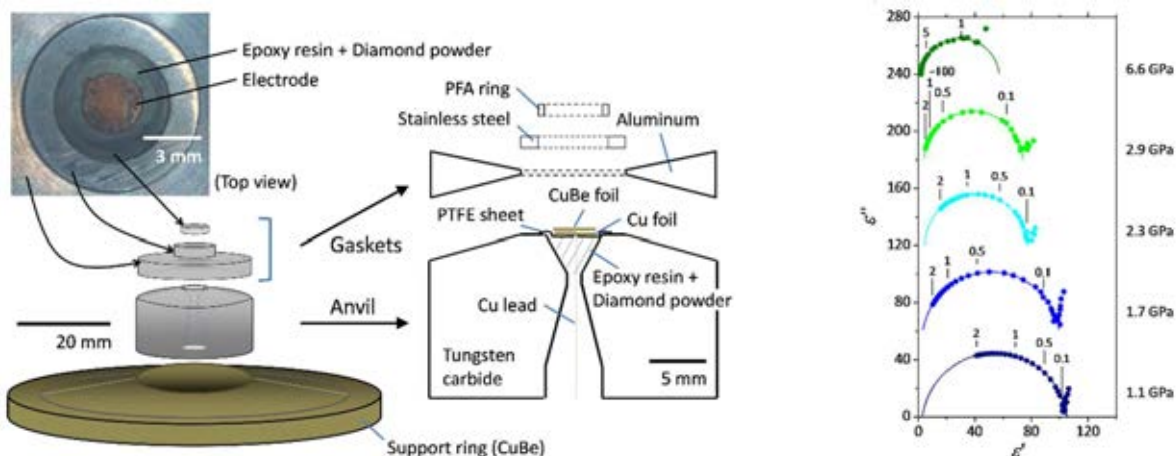
Fig. 1a. Schematic drawings of the developed Bridgman anvil cell and its picture from top, where PTFE and PFA are abbreviations of polytetrafluoroethlene and perfluoroalkoxy alkanes, respectively. Sample, with a volume of ~20 mm^3, is inserted in a PFA ring and loaded with the two anvils from up and down by using a Paris-Edinburgh press (type-V4).

Fig.1b. Representative complex-plane plots of feasibility test for dielectric properties of H$_2$O at high pressures. Numbers on the plots taken at 1.1, 1.7, 2.3 and 2.9 GPa denote the frequencies in MHz and those at 6.6 GPa denote the frequencies in kHz.

We developed a new high pressure cell which allows us to perform accurate dielectric measurements for initially liquid sample and at pressure above 3 GPa4. As shown in Figure 1a, the developed cell is based on Bridgman type opposed anvil cells with electrodes immersed into holes in the anvils in order to make the electrode area constant under compression. As a feasibility experiment, dielectric measurements for H2O was conducted up to 6.6 GPa. Representative complex-plane plots obtained by the developed cell are shown in Figure 1b in the pressure range where ice VI and ice VII are thermodynamically stable. The geometric vacuum capacitance of the cell is about 10-13 F and the developed cell can be applied to any liquid samples which have low dielectric constant.

References:

E. Whalley, J. Chem. Phys. **45**, 3976 (1966).

G.P. Johari and E. Whalley, Faraday Symp. Chem. Soc **6**, 23 (1972).

T. Okada, T. Iitaka, T. Yagi, and K. Aoki, Sci. Rep. **4**, 5778 (2014).

R. Yamane, K. Komatsu, and H. Kagi, Rev. Sci. Instrum. **88**, 046104 (2017)

SOURCES AND GEOCHEMICAL ZONING OF THE DEVONIAN MAGMATISM IN THE PRIPYAT-DNIEPER-DONETS RIFT ZONE

Yutkina E.V.[1], Nosova A.A.[1], Sazonova L.V.[1,2], Laptsevich A.G.[3], Kuzmenkova O.F.[3], Volkova G.D.[2], Sysoev I.V.[4]

[1]Institute of Geology of Ore Deposits, Petrography, Mineralogy and Geochemistry of the Russian Academy of Sciences, Moscow, Russia, eyutkina@gmail.com
[2]Lomonosov Moscow State University, Moscow, Russia
[3]State Enterprise "SPC on Geology", Minsk, Belarus
[4]MGPI-RSGPU, Moscow, Russia

Various magmatic processes accompanied the Late Paleozoic activation of already existing Mesoproterozoic (The White Sea rift system, Timan, Dnieper-Donets, Middle-Russian aulacogens and Vyatka-Kazhimsk paleorift) and newly formed (Pripyat graben) rift structures of the East European platform (EEP). This magmatism had different character and intensity. In the northern EEP, this period was marked by the formation of the Kola alkaline province within the Kola-Arkhangelsk magmatic zone between 360-390 Ma (Arzamastsev, Wu 2014). Kimberlites (380-385 Ma, Larionova et al., 2016), melilitites, basalts are known in the Arkhangelsk diamondiferous province in the southeastern part of the area, and kimberlites are located on the Tersk Shore in the northwestern part of the Kola-Arkhangelsk zone (377 ± 0.4 Ma, Larionova et al., 2016). The largest Devonian magmatic area in the southern part of the EEP is the Pripyat-Dnieper-Donets rift zone (PDDR), which includes the Pripyat and Dnieper-Donets (DDR) rifts, the Northern Pripyat shoulder (including the Zhlobin saddle), the Eastern Azov, the of Donbass—Azov crystalline massif (ACM) junction zone, and the Voronezh crystalline massif (VCM). The PDDR is comparable to the Kola-Arkhangelsk zone on the magmatism time and the rocks spectrum. Alkaline ultrabasic rocks up to kimberlites dominate the magmatic rocks of the Pripyat trough, Northern Pripyat shoulder, and Eastern Azov, whereas tholeiitic basalts are prevalent rocks in the VCM. S

Several controversial hypotheses have been proposed to explain the intraplate magmatism of EEP. Among them are the relationship with the structural and tectonic features of the Precambrian basement of the ancient cratons, plume-subduction interaction and its effect on the formation of rocks sources and their spatial-temporal development. It is noteworthy that the Late Paleozoic (mainly Devonian) PDDR magmatism is the example of the manifestation of intraplate magmatism within a large continental plate simultaneously large-scale subduction and collision events in ocean basin margins (closure of the Rake and opening of the Paleo-Tethys, collision between the Hun and Armorican terranes), they were connected with the Pangaea supercontinent formation. This fact makes it possible to estimate the effect of lithosphere heterogeneity on the character and dynamics of magmatism by consideration of the similar structure of the Precambrian basement of PDDR segments (Shchipansky, Bogdanova, 1996). Also it is important the problem of the kimberlite formation because the East Azov region of PDDR comprises kimberlite field. At present, it is hotly debatable whether the genesis of kimberlites is related to plume or plate tectonics. For example, the formation of Vendian kimberlites of the Superior Craton is thought to be associated with plate motions caused by the accretion or disintegration of a supercontinent, rather than with plume activity (Tappe et al., 2016). However, plume hypotheses are currently more accepted concerning to the intraplate EEP magmatism (Kusznir et al, 1996; Wilson and Lyashkevich, 1996; Torsvik et al, 2010). At the same time, some researchers suggest that the Devonian rifts of the EEP could be formed in a back-arc setting (Sorokhtin, Sorokhtin, 2006; Lyngsie et al, 2007; Sheremet et al., 2014). Others believe that the intraplate magmatism of EEP was caused by large-scale shears in the lithosphere in response to the relative plate motion and rotation of the platform (Chalot-Prat et al, 2007). Lithospheric mantle metasomatized by asthenospheric melts is proposed as a melt source in this model. A similar genesis was proposed for Ethiopian rift volcanics (Ayalew et al, 2016). The authors

suggest that the initial stages of Ethiopian rift formation were accompanied by metasomatism of the lithosphere during asthenosphere upwelling and decompression melting. Thus, the classic "plume" model for the PDDR magmatism needs to be revised in terms of plate tectonics.
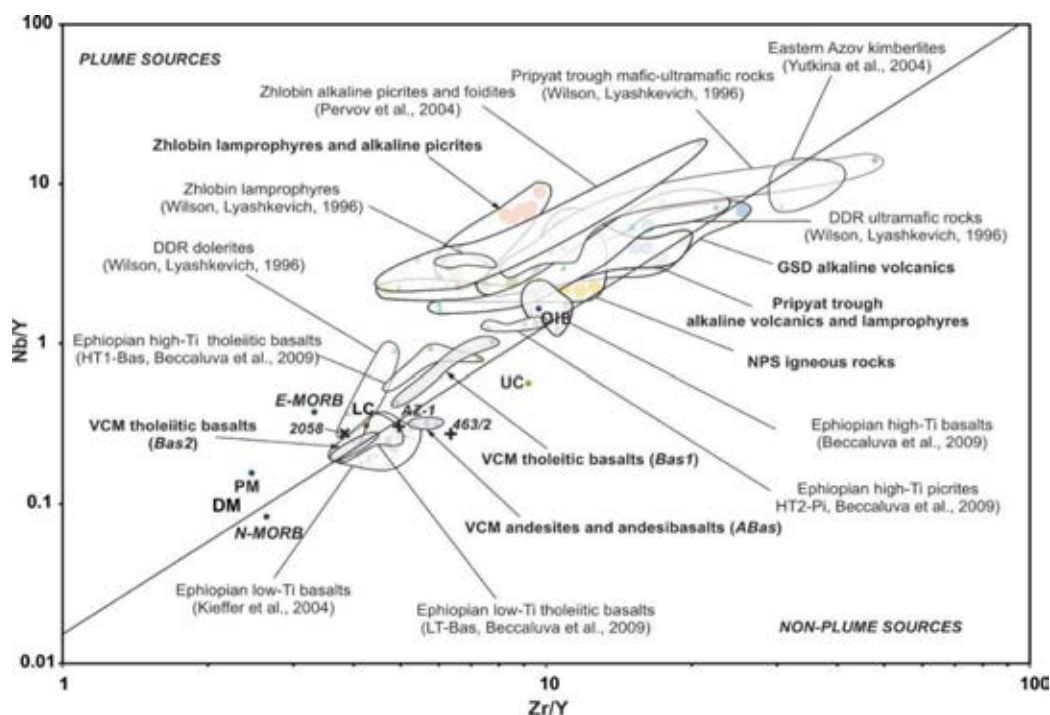
Fig. 1. PDDR Devonian igneous rocks (published and author data) are compared with the the Ethiopian basalts (published data).

Sources of Devonian igneous rocks of PDDR. The petrological and geochemical study showed that the igneous rocks of PDDR were derived from different magmatic sources. In particular, geochemical and isotopic characteristics of VCM basalts reveal a clear sign of crustal contribution in their source. At the same time, the contribution of the Early Precambrian upper crustal material of the VCM to initial melt and melting of the garnet-containing metabasites are excluded (Yutkina et al., 2017). Thus, the metasomatized spinel-bearing peridotites from the upper lithospheric mantle can be taken as possible sources for VCM basalts. This is confirmed by the negative Rb and K anomalies in the PM-normalized patterns, low Rb/Sr and high Ba/Sr ratios (Rosenthal et al, 2009, Ayalew et al, 2016.). At the same time variations of negative K anomalies point to the influence of crustal contamination. High concentrations of Y and concave profile of HREE distribution likely indicate the presence of amphibole in the source (Qian, Hermann, 2013; Tiepolo et al, 2011). High Zn/Cu and low Fe/Zn ratios are assigned to the influence of a pyroxenite source. Thus, the VCR volcanics were probably derived by melting of a network of hornblendite/amphibole-pyroxenite veins in the peridotite protolith or the amphibolized cumulate in the underplating zone. This "layer cake" of amphibole-pyroxenites and peridotites was described as a source for island-arc lithosphere (Tiepolo et al, 2011; Sorbadere et al, 2013), postorogenic sub-alkaline and alkaline basalts above previously existing subduction zones (Dai et al., 2014), and for rift zones. This model, in particular, was applied for low-Ti Ethiopian rift basalts (Ayalew et al., 2016), which are most similar to the VCM volcanics. Isotope and geochemical characteristics suggest that the Devonian magmatic rocks from southeastern segment PDDR (the Eastern Azov and the Donbass—PCM junction area) were derived from at least three types of sources. The first, amphibole-bearing source produced essentially sodium high-Mg rocks. The high-K and high-Ti melts with high HFSE abundance were generated by melting of phlogopite-bearing veins. Depleted asthenosphere is proposed as a source for Azov dolerite dikes, which are similar in composition to DDR dolerites. The possible sources for rocks from the northwestern part of PDDR (Zhlobin saddle, Pripyat trough) were discussed (previously in (Pervov et al., 2004)). It has been shown that these volcanics have rather heterogeneous isotopic and geochemical characteristics, which suggests lithosphere heterogeneity and, hence, several types of sources. The low-Ti alkaline picrites with low Nd isotopic ratios and low Nb, Rb were generated from EM1-type ancient enriched lithospheric mantle. Magmas with high Nd isotopic ratios and high TiO_2, Nb, and Rb have a plume nature. At the same time, the cited authors believe that these magmas can be obtained from crustally contaminated early asthenospheric melts. Petrological, mineralogical and geochemical (unpublished) data obtained by us for a wide range of the PDDR magmatic rocks also suggest the subduction input in the genesis of melts from the northwestern part of the rift zone (negative anomaly of Nb relative La). The rocks from some magmatic manifestations show signs of lithospheric metasomatic reworking and lower crustal contamination. The latter is confirmed by the presence of amphibole-bearing xenoliths (previously in (Marckwick et al., 2001)), as well as high positive correlation of HREE with Zr and Hf (0.8-0.82).

Geochemical zoning of the PDDR magmatism. A definite geochemical zoning in the distribution of rocks and their sources was identified on the basis of complex petrological study of Devonian intraplate magmatic rocks of PDDR in combination with literature data. Mantle sources were determined using the diagram Nb/Y vs Zr/Y by Condie, 2001 (Fig. 1). The field of the tholeiitic VCM basalt compositions coincides with the field of Ethiopian low-Ti tholeiitic basalts

(LT-Bas). The VCM tholeiites (*Bas2* field) are close to DDR dolerites, which supposedly were derived from the most depleted mantle source. At the same time, some of VCM basalts (*ABas* field) are similar to the dolerite dyke from Eastern Azov (samples Az-1, 463/2). On the other hand, the VCM basalts with signs of crustal contamination (*Bas1* field) define a trend towards more enriched source (increase of Nb/Y and Zr/Y ratios). The composition fields of rocks from the western PDDR segment (Pripyat trough, Northern Pripyat shoulder and Gomel structural dam) and Eastern Azov kimberlites lie on the continuation of this trend in the field of most enriched mantle sources with maximum values of Nb/Y and Zr/Y ratios. It should be noted that the Ethiopian geochemically enriched high-Ti basalts and picrites were formed from high-Ti metasomatized mantle melts from the central part of the plume (Beccalluva et al., 2009). These rocks usually occur within the Ethiopian rift axis, which demonstrates the following zoning: rocks in the central parts were obtained from most enriched mantle melts, whereas its margins were abundant in the rocks of tholeiitic series. An opposite lateral geochemical zoning is observed for the PDDR - from depleted mantle in the axial zone of the DDR to more enriched mantle in the marginal parts and so-called rift "shoulders" (the Eastern Azov, VCM).

It should be noted that the composition fields of almost all PDDR magmatites (Fig. 1) are confined to the discrimination line between plume and non-plume sources. This suggests that the genesis of the discussed rocks was controlled by many factors, the main of which were plume-subduction interaction and crustal contamination. In general, a wide spectrum of PDDR Devonian igneous rocks indicates that different mantle sources were involved in the melt generation. The lower lithosphere source was involved in the formation of the Eastern Azov kimberlites and the Zhlobin saddle lamprophyres. Asthenospheric sources simultaneously produced DDR dolerites. Thus, the deepest-seated magmas are confined to PDDR zones developed in the crustal terranes no younger than 2.1-2.0 Ga.

Samp. 2058 is the DDR dolerite by (Wilson, Lyashkevich, 1996), samples Az-1 and 463/2 are Eastern Azov dolerites (author data). Compositions for DM, PM, N-MORB, E-MORB and OIB are from (Sun, McDonough, 1989), upper (UC) and lower (LC) crust by (Rudnick, Gao, 2003). GSD – Gomel structural dam, VCM – Voronezh crystalline massif, NPS – Northern Pripyat shoulder.

References:

Arzamastsev A.A., Wu F.Y. (2014) U-Pb geochronology and Sr-Nd isotopic systematics of minerals from the ultrabasic-alkaline massifs of the Kola province. Petrology 22(5):462-479.

Ayalew D., Jung S., Romer R.L., Kersten F., Pfänder J.A., Garbe-Schönberg D. (2016) Petrogenesis and origin of modern Ethiopian rift basalts: Constraints from isotope and trace element geochemistry. Lithos 258-259:1-14. doi:10.1016/j.lithos.2016.04.001

Beccaluva L., Bianchini G., Natali C., Siena F. (2009) Continental flood basalts and mantle plumes: a case study of the Northern Ethiopian Plateau. J. Petrol 50(7): 1377-1403.

Chalot-Prat F., Tikhomirov P., Saintot A. (2007) Late Devonian and Triassic basalts from the southern continental margin of the East European Platform, tracers of single heterogeneous lithospheric mantle source. J. Earth System Sci.6: 469-495. doi:10.1007/s12040-007-0045-z

Condie K.C. (2001) Mantle plumes and their record in Earth history. Cambridge: Cambridge University Press

Dai, L.-Q., Zhao, Z.-F., Zheng, Y.-F. (2014) Geochemical insights into the role of metasomatic hornblendite in generating alkali basalts. Geochem. Geophys. Geosystems 15: 3762–3779.

Kieffer, B., Arndt, N., Lapierre, H. et al. (2004) Flood and shield basalts from Ethiopia: magmas from the African Superswell. J. Petrol. 45: 793–834. doi:10.1093/petrology/egg112

Kusznir N.J., Kovkhuto A., Stephenson R.A. (1996) Syn-rift evolution of the Pripyat Trough: constraints from structural and stratigraphic modeling. Tectonophysics 268(1-4): 221-236.

Larionova Yu. O., Sazonova L. V., Lebedeva N. M. et al. (2016) Kimberlite age in the Arkhangelsk Province, Russia: Isotopic geochronologic Rb-Sr and Ar-40/Ar-39 and mineralogical data on phlogopite // Petrology 24(6): 562-593.

Lyngsie, S.B., Thybo, H., Lang, R. (2007) Rifting and lower crustal reflectivity: A case study of the intracratonic Dniepr-Donets rift zone, Ukraine. J. Geophys. Res. Solid Earth 112: 1–27. doi:10.1029/2006JB004795

Marckwick A.J.W., Downes H., Veretennikov N. (2001) The lower crust of SE Belarus: petrological, geophysical and geochemical constraints from xenoliths. Tectonophysics 339: 215-237.

Pervov V.A., Nikitin E.A., Levsky L.K. (2004) Ultramafic alkaline volcanic rocks of the Zhlobin field (Belarus): Sources and evolution of magmas. Petrology 12(4): 312-329.

Qian Q., Hermann J. (2013) Partial melting of lower crust at 10-15 kbar: Constraints on adakite and TTG formation. Contrib. Min. Petrol. 165(6): 1195-1224. doi:10.1007/s00410-013-0854-9

Rosenthal A., Foley S.F., Pearson D.G. et al. (2009) Petrogenesis of strongly alkaline primitive volcanic rocks at the propagating tip of the western branch of the East African Rift. Earth Planet. Sci. Let. 284: 236-248. doi: 10.1016/j.epsl.2009.04.036

Rudnick R.L., Gao S. (2003) Composition of the Continental Crust. Treatise on Geochemistry 3: 1-64. doi: 10.1016/B978-0-08-095975-7.00301-6

Rutherford M.J., Hill P.M. (1993) Magma ascent rates from amphibole breakdown: an experimental study applied to the 1980–1986 Mount St. Helens eruptions. J. Geophys. Res. 80: 19667-19685. doi:10.1029/93JB01613

Shchipansky A.A., Bogdanova S.V. (1996) The Sarmatian crustal segment: Precambrian correlation between the Voronezh Massif and the Ukrainian Shield across the Dniepr-Donets Aulacogen. Tectonophysics 268(1-4): 109-125. doi:10.1016/S0040-1951(96)00227-2

Sheremet E.M., Kozar' N.A., Strekozov S.N. and others. (2014) The search for diamonds in the Azov block of the Ukrainian Shield. Donetsk: "Noulidzh" (Donetsk Dep.)

Sorbadere, F., Schiano, P., Métrich, N. (2013) Constraints on the origin of nephelinenormative primitive magmas in island arcs. J. Petrol. 54(2): 215-233. doi:10.1093/petrology/egs063

Sorokhtin O.G., Sorokhtin N.O. (2006) Subduction mechanism of diamond formation. Geology and mineral resources of the oceans. 1: 5-36.

Sun S. S., McDonough W.F. (1989) Chemical and isotopic systematics of oceanic basalts: implications for mantle composition and processes. Magmatism in the Oceanic Basins. Geological society special publication. 42: 313-345. doi:10.1144/GSL.SP.1989.042.01.19

Tiepolo M, Tribuzio R, Langone A. (2011) High-Mg andesite petrogenesis by amphibole crystallization and ultramafic crust assimilation: evidence from Adamello Hornblendites (Central Alps, Italy). J. Petrol. 52(5): 1011-1045. doi:10.1093/petrology/egr016

Torsvik T.H., Steinbergerd B., Gurnise M., Gainab G. (2010) Plate tectonic and net lithosphere rotation over the past 150 My. Earth Planet. Sci. Lett. 291(1-4): 106-112. doi:10.1016/j.epsl.2009.12.055

Wilson M., Lyashkevich Z.M. (1996) Magmatism and the geodynamics of rifting of the Pripyat-Dnieper-Donets rift, East European Platform. Tectonophysics. 268(1-4): 65-81. doi:10.1016/S0040-1951(96)00234-X

Yutkina E.V., Kononova V.A., Kozar N.A., Knyaz'kov A.P. (2003) Sr-Nd isotopic and geochemical compositions of kimberlites from the Eastern Azov Region, their age, and nature of the lithospheric source. Doklady Earth Sciences.. 391(5): 751-754.

Yutkina E.V., Kononova V.A., Bogatikov O.A. et al. (2004) Kimberlites of Eastern Priazov'e (Ukraine) and geochemical characteristics of their sources. Petrology. 12(2): 134-148.

Yutkina E.V., Nosova A.A., Sazonova L.V. et al. (2017) Devonian volcanic rocks of the Voronezh crystalline massif, East European Platform: the evolution of melts and features of crustal contamination. Petrology. 25(3): 241-271. doi:10.1134/S0869591117020060

MORPHOLOGICAL AND GEOCHEMICAL STUDIES OF HEAVY MINERALS IN THE SIWALIK SANDSTONE OF KARAK ANTICLINE, KHYBER PAKHTUNKHWA PAKISTAN

Zaheenullah[1], Muhammad Tahir Shah[2], Nimatullah Khattak[2], Hafizullah Abba Ahmed[1]
[1]China University of Geosciences, Wuhan, China
[2]University of Peshawar, Peshawar, Pakistan

The study area is located in the southern Kohat plateau comprising largely of Karak anticline and its adjoining areas, covering the southern part of district Karak. It is dominantly composed of Siwalik sandstone and fluvial sediments (i.e., gravel, cobbles, sand and silt) deposited by Paloe-Indus River (Ahmad, 2003). This area has been investigated for the first time to study the petrographic characteristic, heavy minerals concentrations, gold grains, geochemical analysis and the provenance of the present lithologies encountered in the region. The samples are collected from the Siwalik sandstone (molasse deposits) present in the core of Karak anticline and its adjoining areas (Figure 1).

Detailed petrographic studies of the representative sandstone samples from Chinji (Lower Siwalik), Nagri, Dhok Pathan (Middle Siwalik) and Soan (Upper Siwalik) formations contains abundant lithics with subordinate amount of quartz and feldspar. Lithic fragments are ranging from 20 to 60%, quartz ranging from 20 to 50% and feldspar ranging from 7 to 35%. Micas (biotite and muscovite) average abundance is 3%. The heavy minerals observed in thin section study are ilmenite, epidote, amphibole, garnet, rutile and zoisite and iron ore minerals (magnetite and hematite etc). The Chinji Formation is dominantly feldspathic litharenite, Nagri and Dhok Pathan formations are feldspathic litharenite and lithic arkose while the Soan Formation is generally litharenite.

The heavy minerals (Plate. A, B) observed in the Siwalik sandstone are zircon, garnet, amphibole, tourmaline, apatite, rutile and epidote. The Dhok Pathan and Soan formations generally have high concentration of zircon, garnet and amphibole concentration, while Chinji and Nagri formations have relatively low concentration of these phases. The other heavy minerals such as tourmaline, apatite, rutile and epidote have very low concentration as compared to zircon, garnet, and amphibole in these formations. The gold grains studied visually in the pan-concentrate of Siwalik sandstone are very fine-grained (color = < 0.3 mm) and are mainly thin flattened and platy nature of gold grains (Duk-Rodkin et al., 2001, Nakagawa et al., 2005 and Garzanti et al., 2015). The gold morphology suggests that it has been transported several hundreds of kilometers from their primary source (Plate. C, D). For the occurrences of placer gold, silver and base metals, this area has been explored through geochemical studies. The samples collected from rocks and stream sediments were crushed to sand size and then treated with shaking table to separate concentrate, middling and tail. The concentrates obtained through shaking table were further investigated for gold, silver and base metals concentrations. The total recovery of gold in the sandstone of the Siwalik Group is 1.077g/t. But the maximum amount of gold (3.08g/t) was recovered in the Soan Formation. Maximum recovery (= 84%) of gold was noticed in the pan-concentrates as compared to middlings and tails. Total silver recovered in the study area is 22.80g/t with the maximum recovery (31.20g/t) of silver in the Nagri Formation. The concentration of Cu is ranging from 1.1-225 ppm, Pb from 0.9-35 ppm, Zn from 2.6-194

ppm, Mn from 57.2-666 ppm, Cr from 0.8-416 ppm, Ni from 3-555 ppm, Co from 5.5-110.4 ppm and Cd from 0.8-19.9 ppm.
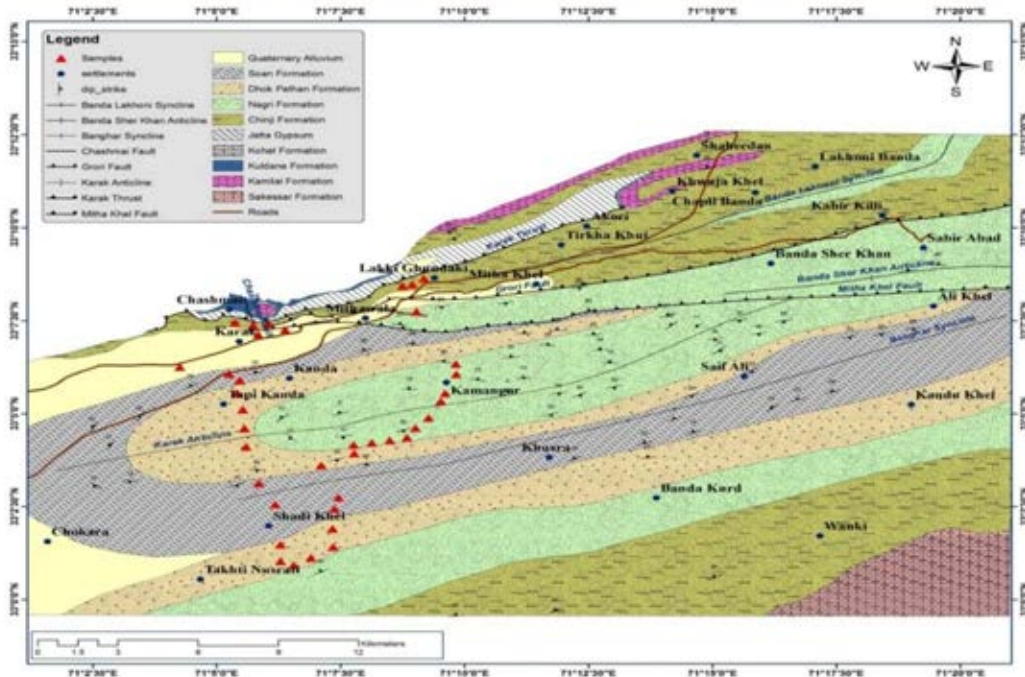
Fig. 1. Geological map of Karak anticline and its adjoining areas (after Ali, 2010) showing samples location.
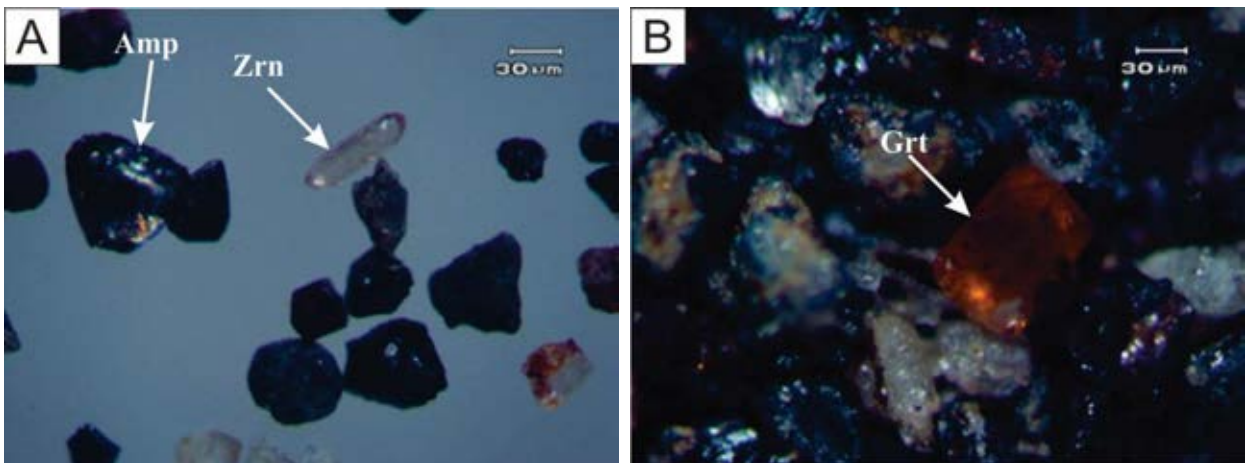
Plate: A photomicrograph showing Zrn (zircon) and Amp (amphibole), **B** photomicrograph is showing Grt (garnet) in Pan-concentrate.
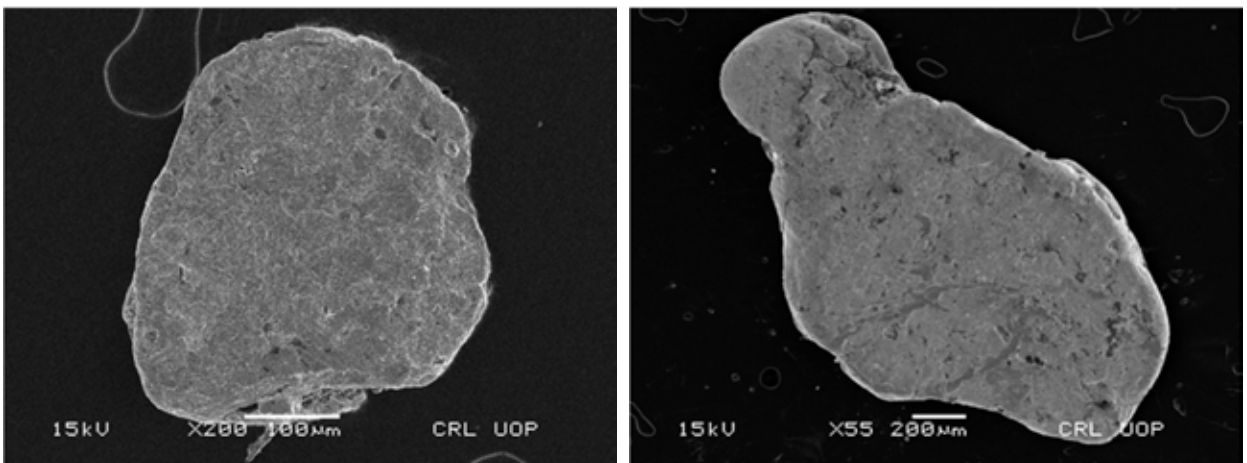
Plates. C, D: Scanning Electron microscope (SEM) photograph showing morphology of the Gold colors.

The sandstone of the Chinji Formation (Lower Siwalik) has major contributions from the underlying Sakesar limestone of the Eocene age and the reworking from marine source rocks. While the sandstone of Nagri and Dhok Pathan formation (Middle Siwalik) contains igneous and metamorphic rock fragments along with medium-high grade metamorphic minerals. The greater input of materials in the Soan Formation (Upper Siwalik) is contributed from the Chinji Formation (Lower Siwalik) and Nagri and Dhok Pathan formations (Middle Siwalik). In conclusion, the Siwalik sandstone has major contributions of sediments through Paleo-Indus River from the Himalayan tectonic units, Trans-Himalaya and Karakoram and Kohistan-Ladakh arc (Abid et al., 1983; Abbasi and Khan, 1990; Ullah, 2009).

References:
Abid, I.A., Abbasi, I.A., Khan, M.A., Shah, M.T., 1983. Petrology and geochemistry of the Siwalik sandstone and its relationship to the Himalayan Orogeny. Geological Bulletin University of Peshawar, 16, pp 65-83.

Abbasi, I. A., Khan, M. A., 1990. Heavy mineral analysis of the molasse sediments, Trans Indus Ranges, Kohat, Pakistan. Geological Bulletin University of Peshawar, 23, pp 215-229.

Ahmad, S., 2003. A comparative study of the structural styles in the Kohat Plateau, NW Himalayas, N.W.F.P, Pakistan. Unpublished Ph.D thesis, University of Peshawar.

Ali, A., 2010. Structural analysis of the Trans Indus Ranges: Implication for the hydrocarbon potential of the NW Himalayas, Pakistan. Unpublished Ph.D thesis, University of Peshawar.

Duk-Rodkin, A., Barendregt, R.W., White, J.M., Singhroy, V.H., 2001. Geologic evolution of the Yukon River: implications for placer gold. Quaternary International 82, pp 5–31.

Garzanti, E., Resentini, A., Ando, S., Vezzoli, G., Pereira, A., Vermeesch, P., 2015. Physical controls on sand composition and relative durability of detrital minerals during ultra-long distance littoral and aeolian transport (Namibia and southern Angola). Sedimentology 62, pp 971–996.

Nakagawa, M., Santosh, M., Nambiar, C.G., Matsubara, C., 2005. Morphology and chemistry of placer gold from Attappadi Valley, Southern India. Gondwana Research 8, pp 213–222.

Ullah, K., 2009. Lithofaceis, petrography and geochemistry of neogene mollase sequence of Himalayan foreland Basin, southwestern Kohat, Pakistan. Unpublished Ph.D thesis, University of Peshawar, pp 251-293.

RARE EARTH ELEMENTS IN COMPLEX NB AND ZR OXIDES FROM THE KOVDOR PHOSCORITES AND CARBONATITES, KOLA, RUSSIA

Zaitsev A.N.[1,2], Chakhmouradian A.R.[3]
[1]Saint-Petersburg State University, Saint-Petersburg, Russia, a.zaitsev@spbu.ru
[2]Natural History Museum, London, UK
[3]University of Manitoba, Winnipeg, Canada, Anton.Chakhmouradian@umanitoba.ca

The Devonian Kola Alkaline province (northern Russia and Finland) contains twenty two plutonic complexes consisting of various ultrabasic and alkaline rocks (Bulakh et al., 2004). Some of these complexes also contain carbonatites and, less commonly, phoscorites. The latter are silicate-phosphate-oxide-rich rocks genetically related to carbonatites. The Kola complexes have been studied in much detail owing to their economic importance, particularly at Khibiny (apatite deposits), Lovozero (loparite) and Kovdor (baddeleyite, apatite, magnetite and vermiculite) (Petrov, 2004).

Kovdor is a complex pluton consisting of olivinites, clinopyroxenites, melilitic rocks, ijolites and urtites. Phoscorites and carbonatites occur in the south-western part of the complex and are the latest crystallised magmatic rocks (Krasnova et al., 2004).

Phoscorites at Kovdor are mineralogically diverse rocks that contain variable proportions of apatite, magnetite, forsterite, phlogopite, tetraferriphlogopite, calcite and dolomite. Several varieties of these rocks can be distinguished on the basis of their relative age of emplacement and mineralogy. Carbonatites are calcitic rocks (with subordinate apatite, magnetite, forsterite, phlogopite or tetraferriphlogopite), with dolomite-bearing or predominantly dolomitic varieties being less common.

Both phoscorites and carbonatites contain a variety of accessory minerals, including simple and complex (multiple) oxides of Zr and/or Nb. The former is represented by baddeleyite, and the latter by pyrochlore-group minerals, perovskite-group minerals, zirconolite and calzirtite.

Pyrochlore-group minerals (pyrochlore, uranpyrochlore and rarely bariopyrochlore) are the most common accessory minerals at Kovdor and occur in calcite- and dolomite-bearing varieties of phoscorites and in all carbonatite types. These minerals contain only light REE (LREE = La ... Sm) at detectable levels; their $LREE_2O_3$ content ranges between 0.5 and 9.0 wt.%, with typical values between 0.5 and 3.0 wt.%.

Perovskite-group minerals (lueshite and isolueshite) are rare in the Kovdor carbonatites. Both minerals contain 1.8-4.0 wt.% $LREE_2O_3$.

Zirconolite is common in phoscorites and carbonatites containing tetraferriphlogopite, and rare in calcite-bearing phoscorites and calcite carbonatites with phlogopite. This minerals contains variable REE concentrations, from nil (in carbonatites with phlogopite) to 17.8 wt.% REE_2O_3 (in calcite phoscorites with phlogopite). Zirconolite from tetraferriphlogopite-bearing rocks contains between 1.3 and 3.7 (rarely up to 6.3) wt.% REE_2O_3. In addition to light REE, it contains heavy lanthanides (Gd, Dy and Er) at levels detectable by electron microprobe.

Calzirtite is a rare constituent of calcite carbonatites and contains little REE (< 0.1 wt.%).

Mass-balance calculations show that complex Nb and Zr oxides concentrate a significant proportion of the REE budget in the Kovdor phoscorites and carbonatites. Our estimates indicate that 4-17 % of this budget is accounted for by pyrochlores and up to 7 % by zirconolite. Like loparite (a Na-REE-dominant perovskite-group mineral) from Lovozero, these complex oxides are a potential source of REE (as well as byproduct Nb and Ta) in multi-commodity phoscorite-carbonatite deposits (e.g., Vuoriyarvi in Kola, or Aley in Canada) with pyrochlore and zirconolite mineralisation.

This work was supported by the St. Petersburg State University, Russia (grant 3.38.224.2015, including "Geomodel" and "X-ray Diffraction" Resource Centers) and the Natural Sciences and Engineering Research Council of Canada.

References:

A.G. Bulakh, V.V. Ivanikov and M.P. Orlova. Overview of carbonatite-phoscorite complexes of the Kola Alkaline Province in the context of a Scandinavian North Atlantic Alkaline Province // In Phoscorites and Carbonatites from Mantle to Mine: the Key Example of the Kola Alkaline Province, Edited by F. Wall and A.N. Zaitsev. Mineralogical Society Series, 10. Mineralogical Society, London, 2004, pp. 1-43.

S.V. Petrov. Economic deposits associated with the alkaline and ultrabasic complexes of the Kola Peninsula // In Phoscorites and Carbonatites from Mantle to Mine: the Key Example of the Kola Alkaline Province, Edited by F. Wall and A.N. Zaitsev. Mineralogical Society Series, 10. Mineralogical Society, London, 2004, pp. 469-490.

N.I. Krasnova, E.G. Balaganskaya and D. Garcia. Kovdor – classic phoscorites and carbonatites // In Phoscorites and Carbonatites from Mantle to Mine: the Key Example of the Kola Alkaline Province, Edited by F. Wall and A.N. Zaitsev. Mineralogical Society Series, 10. Mineralogical Society, London, 2004, 99-132.

KONTAY INTRUSION (POLAR SIBERIA) PETROLOGY, GEOCHEMISTRY, AGE AND GEOTECTONIC SIGNIFICANCE

Zaitsev V.A.[1] Elizarov D.V.[2] Senin V.G.[1] Bayanova T.B.[2]
GEOKHI RAS, Moscow, Russia, va-zaitsev@invbox.ru
GI CSC RAS, Apatity, Russia

The Kontay intrusion is located in the north-west border of Maimecha-Kotuy alkaline province in the junction of Yenisei-Khatanga trough, Anabar anticline and Tungus syncline flanks. The intrusion is hidden beneath Jurassic-Cretaceous sediments and is exposed in the only borehole. Magnetic and gravity data evident that intrusion has form of laccolite with estimated diameter $\sim$7.5 km and thickness $\sim$ 2.5 km (Kushnir, 2005). Initially (Lopatin and Kalashnik, 2004) lower part of intrusion was described as "gabbro-anortozite and anortositic gabbro" and higher part – as "leucocratic granophyric anortosites". We (Zaitsev et al., 2018) use the subdivision in three units based on the lithological criteria: Lower zone (below 1100 m) - layered sequence of leucocratic and melanocratic of biotite- and ortopyroxene-bearing gabbro, with minor alkaline feldspar, Middle zone (1100-700m) - biotite- and K-feldspar bearing gabbro and monzonotes, interstitial space often contain micrographical structures. Biotite corroded clinopyroxene and form interstitial crystals and Upper zone (700-214 m) – porthyric-like quartz-monzonites and granosyenites with phenocrysts of plagioclase, magnetite, clinopyroxene and biotite.

Kontay intrusion rocks form single trend on the petrochemical diagrams (fig. 1). K-sub-alkaline fields. They are slightly less alkaline then country trachybasalt-trachyandesit-trachydacites and much more alkaline then intrusions of Norilsk district and much less alkaline then alkaline-ultramafic intrusions of Maymecha-Kotuy province.

Volcanic rocks of Norilsk and Maymecha-Kotuy area was subdivided for 4 geochemical types, mainly by the Ti-content, Th/U, Gd/Yb and Sm/Yb ratio: Low-Ti-1 (predominated), Low-Ti-2 (well –developed in Norilsk region), Moderate-Ti (developed only in the lower part of volcanic formation in Norilsk region), High-Ti (rare in Norilsk region, but widely spread in Mailecha-Kotuy area) (Fedorenko et al., 2000). Kontay intrusion rocks belong to Moderate-Ti group.

Cumulus minerals composition changed systematically upward.

Ortopyroxene is quite rare, in some cases it partly or completely replaced by secondary minerals. The main minor oxides are 1.5-1.9% CaO, 0.26-0.4 % TiO_2, 0.5-0.6% Al_2O_3 и 0.5-0.9% MnO, Mg# 70-73%. Calcium content in orthopyroxene correspond to the 1000-1100° C (Fig.2). Two populations of diopside-hedenbergite clinopyroxene occur. The first one present only in the lower part of intrusion. It contain 1-1.2% TiO2 2-2.5% Al_2O_3, Mg# 72-75. This pyroxene was formed from the of High-Ti geochemical type melt. The second one present in all three units, Mg# decrease upward from 69-74 to 61-64, concentration of Al_2O_3 upward increase from 0.9-1.36 to 1.3, TiO_2 increase from 0.4 to 0.6. Calcium content in the clinopyroxene systematically decrease upward and correspond to temperatures up to 800°C in the low zone and up to 970°C in the upper zone (Fig 2). REE spectra of clinopyroxene are very similar in form, but High-Ti clinopyroxenes are significantly richer in REE.

Biotite Mg# increase from 0.60-0.62 up to 0.76-0.78, TiO_2 content decrease from 5 -6.2% to 1.9-2.4%, and MnO content increase from 0.1 to 0.3-0.4%. Temperature estimation from the Ti in biotite geothermometer (Henry et al., 2005) are close to the 500-600°C for biotite from the Upper and Middle zones and to the 700 C for biotite form the Lower and Middle zones.

Plagioclase in the lowest part of intrusion contains An_{60}-An_{45} cores and An_{32}-An_{26} rims, in the middle zone – cores An_{36-42} $Ab_{54-61}Or_3$ and $An_{25-30}Ab_{67-70}Or_{3-5}$ rims and in the upper zone - $An_{42-44}Ab_{53-56}Or_{2-3}$.

Progressive evolution of whole-rock composition, and similarity of composition of cumulus phases evident that Kontay intrusion is an example of strongly differentiated intrusion, formed in subvolcanic conditions form the subalkaline moderate-Ti melt.
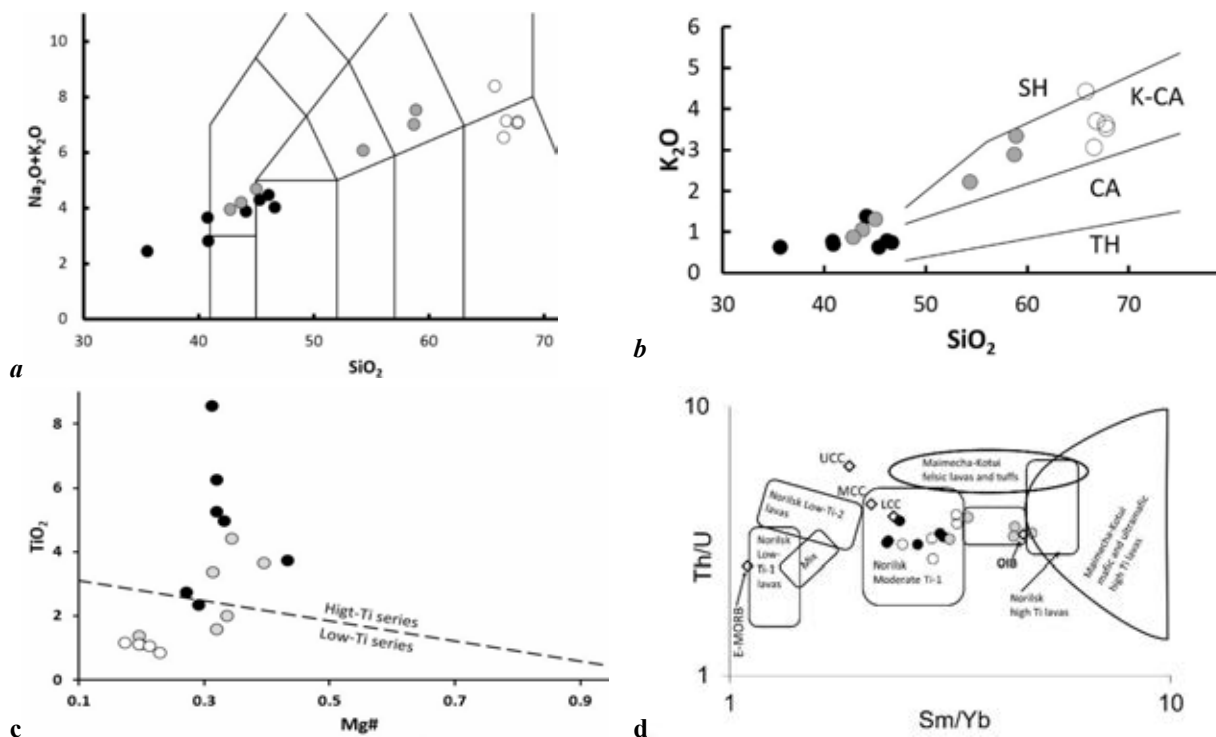
Fig. 1. Whole-rock composition of Kontay intrusion samples on the petrochemical diagrams. Black circles – low, grey circles-middle and open circles- upper zone of intrusion. a) TAS-diagram (lines from Le Bas et al., 1986), b) K2O-SiO2 diagram (lines from Peccerillo and Taylor, 1976,), c) TiO2- Mg# diagram for discrimination of High-Ti and+ Low-Ti continental plume magmas (line from Ivanov and Balyshev, 2005), c) Th/U vs Sm/Nd systematic with simplified fields of Norilsk and Maymecha-Kotuy magmas from (Fedorenko et al., 2000). Reference points for average E-MORB and OIB by (Sun, McDonough 1989), low continental Crust (LCC), middle continental Crust (MCC), upper continental Crust (UCC) – by (Rudnick, Gao 2003).
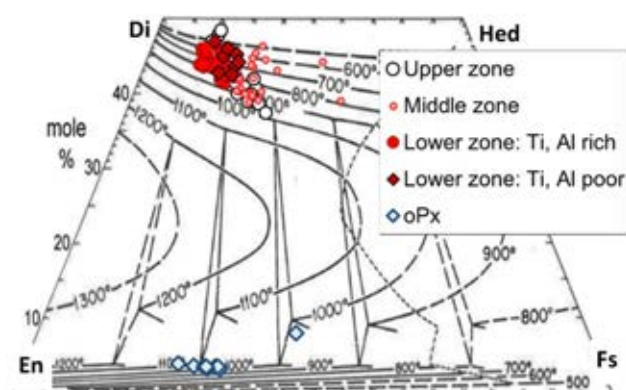
Fig.2 Pyroxenes of Kontay intrusion composition on the Linsley diagram (Linsley, 1983),
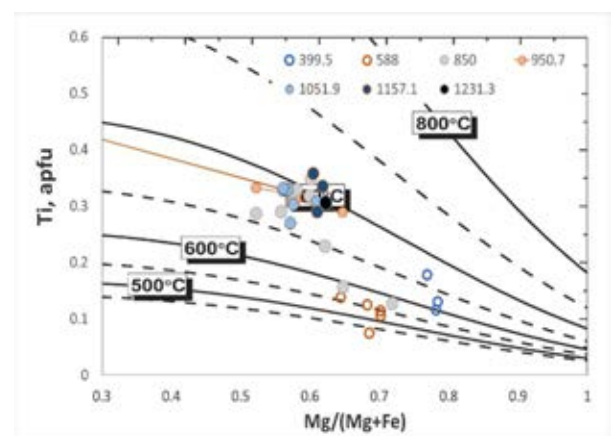
Fig. 3 Biotite composition on the Ti-in biotite thermometry diagram by (Henry et al., 2005). Numbers on legend reflect the sample depth from the hole mouth, in meters.

Post-magmatic processes result in overprinting of primary minerals composition as well as in formation of typical low-grade metamorphic mineral assemblages: amphibole (edenite-feroedenite), biotite, 500-600°C, albite, K-feldspar, hydrobiotite, chlorite, prenite, F,Al-bearing titanite, heulandite-Ca and quartz, fixing, 200- 400˚C, 140-200°C processes.

In $^{87}Sr/^{86}Sr$ vs $^{87}Rb/^{86}Sr$ coordinates (fig.4) Kontay intrusion rocks form trend, corresponding the age of 483±66 Ma and Initial $^{87}Sr/^{86}Sr$ ratio 0.70451±0.00031. Only 1180Px (pyroxene fraction, rich in secondary minerals, mainly

biotite) fall outside this trend. The line passing through 1180Px point and the point of whole-rock composition correspond to age 139 Ma. Similar age of low-grade metamorphism determined from radiometric dating of apophyllite by Spiridonov with co-authors (2000): 232-198 Ma for the prograde zeolitic stage and 164-122 for retrograde zeolitic stage.
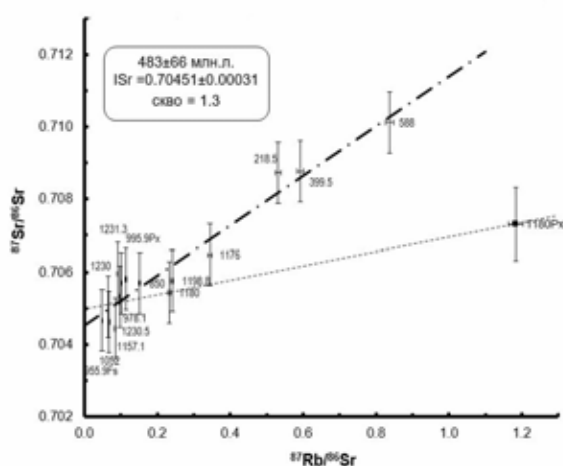
Fig.4 Isochronal diagram for Kontay intrusion rocks and mineral fractions.
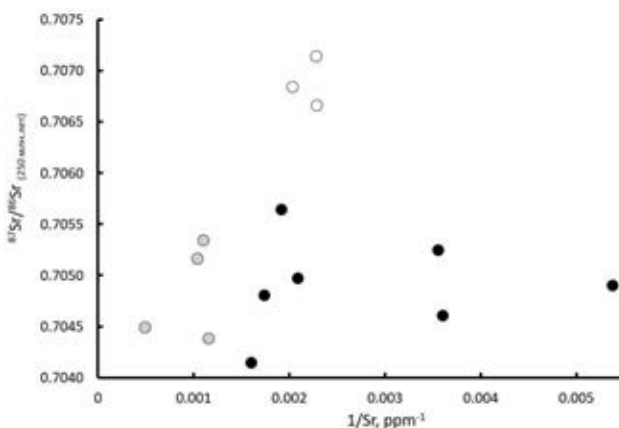
Fig. 5 Strontium mixing test diagram.

Two interpretation of the trend in $^{87}Sr/^{86}Sr$ vs $^{87}Rb/^{86}Sr$ coordinates are ppossible:

1) Data array reflect mixing of two magma sources during the intrusion formation around the Permo-Triassic boundary. But plotting the results on the 87Sr/86Sr(250) vs 1/Sr (fig. 5) diagram do not fit hypothesis of binary mixing at 250 Ma. No geochemical evidence of this mixing was found during the intrusion study.

2) Trend is correspond to the real age of intrusion, formed from the single source in the Early Paleozoic time. However, no one Early Paleozoic magmatic rocks known around at hundreds kilometers from the Kontay intrusion to be candidates to join the magmatic province are.

However, we cannot exclude existing of such Early Paleozoic magmatic province to the north and west from intrusion, below the Permo-Triassic volcanic section of the Yenisei-Khatanga trough and Tungus syncline.

Early Paleozoic detrital zircon grains are usual in late Paleozoic and early Cretaceous strata of Taimyr (Zhang et al., 2013) and in Carboniferous strata of frontal zone of the Verkhoyansk Foldand Thrust Belt (Ershova et al., 2013). They presence was considered a "fingerprint" for Baltica (Zhang et al., 2013), Central Asian Foldbelt, southwestern and southern framework of the Siberian Platform or igneous complexes of Severnaya Zemlya Archipelago (Ershova et al., 2013) input to sediments of Southern Siberia. These hypotheses assume material transfer on distance more than 500 or evel 1000 km. New data allow assuming an existence of Early Paleozoic intraplate magmatic province that can be alternative source of zircons.

References:

Ershova, V.B., Khudoley, A.K. & Prokopiev, A.V. (2013) Reconstruction of provenances and carboniferous tectonic events in the North-East Siberian Craton framework according to U-Pb dating of detrital zircons. *Geotectonics* **47 (2)** 32-41.

Fedorenko V., Czamanske G., Zen'ko T., Budahn J., Siems D. (2000) Field and Geochemical Studies of the Melilite-Bearing Arydzhangsky Suite, and an Overall Perspective on the Siberian Alkaline-Ultramafic Flood-Volcanic Rocks. *Int Geol Rev* **42** 769-804.

Henry, D. J., Guidotti, C. V. and Thomson, J. A. (2005) The Ti-saturation surface for low-to-medium pressure metapelitic biotite: Implications for Geothermometry and Ti-substitution Mechanisms. *Am Mineral*, **90**, 316-328.

Ivanov A.V., Balyshev S.V. (2005) Mass flux across the lower-upper mantle boundary: vigorous, absent, or limited? In: Plates, plumes and paradigms (eds) Foulger G R et al (Princeton: Geological Society of America Special Paper), **388** 327–346.

Kushnir D.G. (2005) Geological structure of transitional zone between Enisey-Khatangski forebelt and Siberian platform between rivers Kheta and Kotuy by geophysical data. Dissertation PhD, Ekatirenburg, 154pp.

Le Bas, M. J., Le Maitre, R. W., Steckeisen, A. & Zanettin, B. (1986). A chemical classification of volcanic rocks based on the total alkali-silica diagram. *J Petrol* **27**, 745-750.

Lindsley DH (1983) Pyroxene thermometry. Am Mineral 68:477–493

Lopatin G.G. and Kalashnik N.N. (2004) The new source of platinum-group metals in Maymecha-Kotuy province. In: Mineral recourses of Taimyr autonomy district and they perspectives. Materials of science-practical conference 25-28 October 2004, Sankt-Pererburg

Peccerillo R., Taylor S.R. (1976) Geochemistry of Eocene calc-alkaline volcanic rocks from the Kastamonu area, Northern Turkey. *Contrib Mineral Petrol*, 58:63-81.

Spiridonov, E.M., Ladygin, V.M., Simonov, O.N., Kulagov, E.A., Sereda, E.V. & Stepanov, V.K. (2000): Metavolcanic rocks of the prehnitepumpelliite and zeolite facies of the trap assemblage, Norilsk region, Siberian Platform. Moscow State University Press, Moscow (in Russ.).

Zaitsev V. A., Elizarov D.V., Bychkova Ya.V., Senin V.G., Bayanova T.B. (2018) The first data about geochemistry and age of Kontay intrusion, Polar Siberia *Geochemistry international, in press.*

Zhang X., Omma J., Pease V., and Scott R. (2013) Provenance of Late Paleozoic-Mesozoic sandstones, Taimyr Peninsula, the Arctic. *Geosciences* **3**, 502–527.

SR-RICH EUDIALYTE GROUP MINERAL (CL-DEFICIENT ANALOGUES OF TASEQITE) FROM ODIKHINCHA MASSIF, POLAR SIBERIA, RUSSIA

Zaitsev V.A.[1], Aksenov S.V.[1,2], Rastsvetaeva R.K.[2], Chukanov N.V.[3]

[1]Vernadsky Institute of Geochemistry and Analytical Chemistry of the Russian Academy of Sciences, Moscow, Russia, va_zaitsev@inbox.ru

[2] FSRC 'Crystallography and Photonics' RAS, Moscow, Russia, aks.crys@gmail.com

[3] Institute of Problems of Chemical Physics RAS, Chernogolovka, Russia

Odikhincha is the second-large alkaline-ultramafic-massif of the Maymecha-Kotuysky province. The massif has a concentric structure, forms by compositionally contrast consistently created intrusions of olivinite, the melilite rocks, jakupirangite-melteigite and ijolite. Rare dykes of the calcite carbonatites and agpaitic nepheline-syenite-pegmatites cut them (Egorov, 1991).

We investigated nepheline-syenite pegmatite, opened with a trench in the southern part of the massif on the left coast of temporary inflow of Ebe-Yuryakh stream. Outcrope of calcite carbonatite with apatite, phlogopite and titanium-bearing garnet exist in a few meters from this trench, but the contact between two rocks was not observed therefore their age ratios are not clear. Pegmatite shows contrast zones with different mineral assemblages: 1) lujavrite-like fine-grained nepheline-feldspar-aegerine with poykilite crystals of lamprophyllite and xenomorphic lovchorrite-like mineral 2) coarse-crystalline zone, with grey K-Na of feldspar, light yellow nepheline, separate lamprophyllite plates and the flattened crystals of a brown Sr-rich eudialyte group mineral (up to 1.5x1.5x0.5 cm).

This mineral was studied by EMPA, IR spectroscopy and single crystal diffraction.

Core-rim microprobe travers of crystals display a primary crystal zoning: from the center to edge Mn content increase while Fe and Sr content decrease. Secondary alteration result on reduction of Na, Fe, REE and content and incensement of Nb, Mn and Ba concentrations. EMPA analyses of eudialyte group mineral are provided in the table 1. Empirical formula is ($Z = 3$): $Na_{12.3-12.4}K_{0.5}Ca_{6-6.4}\ Sr_{1.5-1.7}Fe_{1.9-2.4}Mn_{0.5-0.7}Nb_{0.5-0.6}Ti_{0.2-0.5}Zr_{2.5-2.7}Si_{25.3-25.5}O_{73}(O,H_2O,Cl)_5$ Water content of 0.90 mass.%. was determined by the Alimarin method, that correspond to 3.17 hydrogen atoms per unit.

Table.1 Chemical composition of Sr-rich eudialyte group minerals

	Sr-rich eudialyte group mineral form Odikhincha massif				Ilímaussaq taseqite (Petersen et al., 2004)	Pilansberg «transitional kentbrooksite-taseqite» (Mitchell, Liferovich, 2006)		Khibina «tasequite» (Azarova, 2005)		Fe,Sr-analogue of kentbrooksite (Ekimenkova et al., 2000)*
	Central part	Transitional part	Edge part	Alerted zone						
SrO	5.59	5.31	4.91	5.35	13.98	7.31	7.19	3.95	5.03	4.95
CaO	10.68	10.41	11.26	11.19	8.19	10.88	10.88	12.00	12.41	8.51
Na₂O	12	12.1	12.09	10.97	7.71	7.51	7.30	11.23	11.49	12.90
K₂O	0.66	0.71	0.66	0.63	0.23	0.85	0.86	0.61	0.37	0.34
BaO	0.1	0.08	0.04	0.35		-	-	0.52	0.01	
MgO	0.04	0.05	0.05	0.1				0.10	0.01	
MnO	1.06	1.03	1.64	1.78	3.02	6.39	4.99	1.65	1.82	3.19
FeO	5.35	5.01	4.22	4.09	3.92	1.49	2.38	4.29	5.16	4.51
Ce₂O₃	0	0.29	0.29	0.09	0.08	-	0.47	0.20	0.3	1.56
La₂O₃	0.16	0.34	0.28	0		-	0.25	0.28	0	
Nd₂O₃	0.04	0	0.11	0.08		-	-	-	-	
Y₂O₃	0.05	0	0	0	0.28	-	-	-	-	
Al₂O₃	0.01	0.01	0.02	0.03				0.03	0.07	
SiO₂	48.13	48.14	48.15	47.37	41.64	46.11	46.12	46.64	48.21	47.61
ZrO₂	9.98	10.6	9.63	10.46	9.89	12.41	12.75	11.09		11.96
HfO₂	0.17	0.25	0	0.25	0.32	-	0.39			0.26
TiO₂	0.78	0.55	1.19	0.57		-	-	0.31	0.43	0.47
Nb₂O₅	2.67	2.22	2.58	2.87	4.38	4.19	4.20	3.18	3.77	2.78
Cl	0.8	0.78	0.85	0.59	1.91	1.17	1.21	0.41	0.01	0.96
SO₃	0.17	0.16	0.17	0.14						
Total	98.47	98.05	98.14	96.92	95.55	98.35	98.76	96.49	100.32	100.00*

*Re-calculated from empirical formula to the 100 wt%

IR spectrum of «taseqite» from Odikhincha massif is are quite similar to the other eudialyte group minerals with kenbruksite-structure. This spectrum shows several bands due to H-O; stretching modes (3326 and 3502 cm^{-1}) and bending mode (1643 cm^{-1}) and very weak bands (1415, 1451 and 1505 cm^{-1}) corresponding to the carbonate groups. The band appearing at 527 cm–1 can be attributed to the presence of the $FeØ5$ and $MnØ5$ polyhedrons [1], intensity of band at 542 cm^{-1} (corresponding to square coordinated divalent iron) is low that evident that Fe^{2+} content is insignificant.

The trigonal unit-cell parameters are: $a = 14.2700(6)$, $c = 30.057(1)$ Å; $V = 5300.6(1)$ Å^3; space group $R3m$. The structure is refined to $R = 0.047$ using $1697F > 4\sigma(F)$ and the cation composition of key positions summarized in table 2 (Rastsvetaeva et al., 2017). Table 2 demonstrate that cation occupancies in the key positions are close to the holotype Ilímaussaq taseqite, with some exclusions. The simplified formula of eudialyte-group mineral from Odikhincha is slightly different from Ilimaussak taseqite formula, calculated from structure refinement (2) and chemical date (3).

$$Na_{12}Sr_2Ca_6Fe^{2+}_3Zr_3NbSi_{25}O_{72}(OH,O)_4Cl(H_2O)_{0.2}. \qquad (1)$$
$$Na_{12}Sr_3Ca_6Fe_3Zr_3NbSi_{25}O_{73}(O,OH,H_2O)_3Cl_2 \qquad (2)$$
$$Na_9Sr_5Ca_5Fe_2Mn_2Zr_3NbSi_{25}O_{73}(O,OH,H_2O)_3Cl_2 \qquad (3)$$
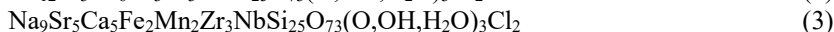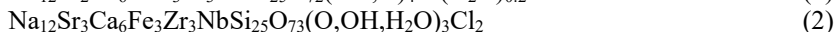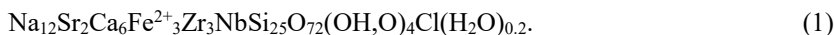
Holotype taseqite contain 2.47 Sr in N4- polyhedrons, 1.1 atoms Sr in Na-dominant N3- polyhedrons, and 0.3 atoms Sr in Ca- octahedral. Interesting that summa of these numbers is 3.87, significantly lower than chemical estimated Sr contaent (4.84 apfu). The last number may evident that Sr is dominant both in N3 and N4 polyhedras) while «taseqite» from Odikhincha, similar with «Fe,Sr-analogue of kentbrooksite» from Lovozero contain Sr only in N4- polyhedrons. In this case, holotype mineral from Ilímaussaq is the only real taseqite.

There are two chlorine-dominant position in holotype taseqite, but only one in eudialyte-group mineral from Odikhincha, and other Sr-rich eudialyte group minerals.

These features are related: N4 position coordinated by X1 position, where Cl prevalent in the all studied minerals, N3- position coordinated by X2 positions, in case of holotype taseqite where X2 positions are Cl dominated, N3 is rich in Sr but in other cases, where X2 do not contain Cl, N3 is Sr-free. This regularity illustrated by Fig 1, showing good correlation between Sr and Cl content in taseqite-like minerals.

Sr-rich eudialyte group minerals usually form as hydrothermal minerals of agpaitic massifs. Type material taseqite is associated with albite, aegirine, analcime, ancylite-(La), calcite, dolomite, catapleiite, fluorapatite, pectolite, and other minerals that occur in a cavity in a late-stage hydrothermal albitite vein in the Ilímaussaq alkaline complex (Peterson et al., 2004). In the Pilansberg massif lujavrites the most Sr–Nb-rich compositions found for the hydrothermal generation of eudialyte-III together with barytolamprophyllite as late hydrothermal phases in terms of NbM(3) and Sr N(4) are transitional to taseqite (Mitchell, Liferovich, 2006).«Taseqite» in Khibina massif is belived to be a result of low-temperature replacing phase after eudialyte and associate with lovoseroite-like mineral, titanite, lamprophyllite, Sr-rich apatite, pectolite, fersmanite, Ca-pyrochlore and loparite (Azarova, 2005). In Lovozero massif «taseqite» (described as Fe,Sr-Analogue of kentbrooksite) was discovered in pegmatite in Alluave mountain.

Table 2. Site occupancies in the key positions of taseqite and taseqite –like minerals.

Position	«Taseqite», Odikhincha	Taseqite, Ilímaussaq (Petersen et al., 2004)	«Fe,Sr-analogue of kentbrooksite», Lovizero (Ekimenkova et al., 2000)
M1	5.85Ca+0.15REE	4.98Ca+0.58Mn+0.3Sr+0.14Y	4.85Ca+0.85Mn+0.30REE
M2a	[2.43Fe]^V	[1.25Fe^{2+}+0.92Mn]^V	[0.87Fe^{2+}]^{IV}
M2b	[0.45Mn]^V	[0.68Fe^{2+}]^V	[1.11Fe^{2+}+0.67Mn+0.19 Ti +0.1Zr+0.04Hf]^V
M3a	0.64Nb	0.97Nb	0.7Nb+0.3Si
M3b	0.33Si		
M4a	0.67Si	0.3Nb	1Si
M4b	0.27Ti	0.45Si	
N3	2.5Na+0.5K	1.9Na+1.1Sr	3Na
N4	1.71Sr+1.29Na	2.47Sr+0.53Na	1.8Sr+0.96Na+0.24K
X1	0.74Cl	0.91Cl	
X2	0.18H$_2$O	0.83 Cl	

Note: The superscripted roman numerals indicate coordination number.
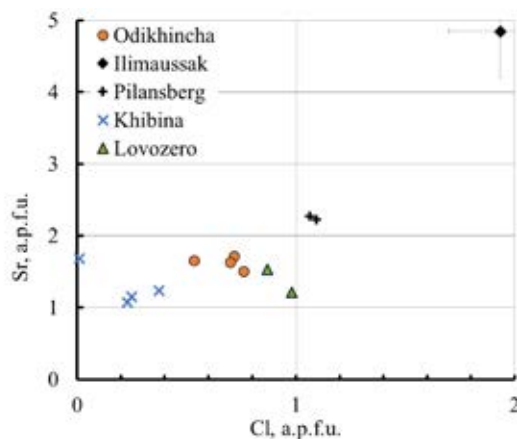
Fig 1. Cl and Sr content in taseqite-like milerals.

Odikhincha massif is the first case of taseqite discovery in early-pegmatite association. As the pegmatite is placed in the neighbourhood of the calciocarbonatite so it can be compared to 'hybrid' calcium-rich agpaitic pegmatites of the Kovdor massif located in calcite carbonatite. The presence of this calcium-rich mineral species of eudialite group (feklichevite, golyshevite and mogovidite) with calcium dominated N4 position is a reflection of the 'hybrid' nature of the pegmatites, i.e., via contamination from the calcite carbonatite that hosts the pegmatite. (Pekov et al., 2001, Chukanov et al., 2005). Geochemical specificity of the Odikhincha pegmatite is high- strontium character of rare-metal

mineralization, including taseqite, high-strontium lovchorrite and lamprophyllite. The simple explanation is high-strontium composition of Odikhincha carbonatites, containing 1.2 - 3% SrO wall rock [15], much more than averige calciocarbonate (0.86%) (Wooley, Kempe, 1989), while calciocarbonatites of Kovdor massif are relatively depleted in strontium (average 0.14-0.37 % SrO) (Afanasev et al., 2011).

References:

Afanasev, B.V. (2011) Mineral resources of the alkaline-ultramafic massifs of the Kola Peninsula. Roza Vetrov, St. Petersburg. 224 pp. (in Russian).

Azarova Yu.V. (2005) Minerals of the Eudialyte group and their alteration products as a geochemical indicator of postmagmatic processes during the formation of the Lujavrite-Malignite complex in the Khibiny massif Geochemistry International. vol. 43 (7): 715-720

Bagdasarov Yu.A. (2001) Metelogeny of carbonatite complexes of Russia. In: Metallogeny of magmatic complexes in intraplate geodynamic settings. Moscow, GEOS, pp.218-506

Chukanov, N.V., Moiseyev, M.M., Rastsvetayeva, R.K., Rozenberg, K.A., and Zadov, A.E., (2005) Golyshevite (Na,Ca)10Ca9(Fe3+,Fe2+)2Zr3NbSi25O72(CO3)(OH)3·H2O, and mogovidite, Na9(Ca,Na)6Ca6(Fe3+,Fe2+)2Zr3[]Si25O72(CO3)(OH,H2O)4, new eudialyte-group minerals from calcium-rich agpaitic pegmatites of the Kovdor massif, Kola Peninsula. Zapiski Rossiyskogo Mineralogicheskogo Obshchestva 134(6)

Egorov L.S. (1991) Ijolite-carbonatite plutonism (the Maimecha-Kotui Complex of Polar Siberia as an example). Leningrad: Nedra Press, 260 pp. (in Russian).

Ekimenkova I. A., Rastsvetaeva R. K., Khomyakov A.P. (2000) Refinement of the Crystal Structure of a Fe,Sr-Analogue of Kentbrooksite. Crystallography Reports, 45 (6): 930--933

Pekov I V, Ekimenkova I A, Chukanov N V, Rastsvetaeva R K, Kononkova N N, Pekova N A, Zadov A E (2001) Feklichevite Na11Ca9(Fe3+,Fe2+)2Zr3Nb[Si25O73](OH,H2O,Cl,O)5, a new mineral of the eudialyte group from Kovdor Massif, Kola peninsula, Zapiski Vserossijskogo Mineralogicheskogo Obshchestva, 130(3): 55-65 47 (in Russian, with English abstract)

Petersen O.V., Johnsen O., Gault R.A., Niedermayr G., Grice J.D. (2004) Taseqite, a new member of the eudialyte group from the Ilímaussaq alkaline complex, South Greenland. Neues Jahrb. Mineral. Monatsh. 2004(2) 83–96.

Rastsvetaeva R.K. Chukanov N.V., Zaytsev V.A. Aksenov C.M., Viktorova K.A. (2017) Crystal structure of the Cl-deficite analogue of taseqite from the Odihincha massif. Crystallography Reports, 62 (6) (in press.)

Woolley A.R., Kempe D.R.C. Carbonatites: nomenclature, average chemical compositions, and element distribution. In: Carbonatites: Genesis and Evolution (K. Bell, Ed.). Unwin Hyman. London. 1989. Pp. 1-14.

EXPERIMENTAL STUDIES OF PHASE FORMATION IN THE OLIVINE – MAGNESITE – SULFUR AND OLIVINE – MAGNESITE – PYRITE SYSTEMS AT HIGH P, T – PARAMETERS

Zdrokov E.V.[1,2], *Bataleva Yu.V.*[1,2], *Palyanov Yu.N.*[1,2], *Borzdov Yu.M.*[1,2]

[1]Institute of Geology and Mineralogy, Siberian Branch of the Russian Academy of Sciences, Novosibirsk, Russia
[2]Novosibirsk State University, Novosibirsk, Russia, zdrokov@igm.nsc.ru

Carbon and sulfur, as well as hydrogen and oxygen, are thought to be the most abundant volatile components in mantle magmatic processes. S and C, being elements with variable valence, have a strong influence on the redox evolution of mantle rocks, melts, and fluids and participate in the processes of mantle metasomatism. It is known that the key role in geochemical cycles of carbon and sulfur belongs to subduction, which provides transportation of various forms of these elements to the deep zones of the Earth and creates the conditions for their interaction with rocks of the silicate mantle. Carbonates are major carbon–bearing minerals in the subducted material; anhydrite and pyrite are the most abundant S–bearing minerals of slab. When subducted, carbonates, sulfates, and sulfides are sources of melts and fluids enriched in C and S, which are potential metasomatic agents. In a number of researches (Evans, 2012) devoted to the estimation of quantity of carbonates and sulfur-containing phases introduced into the mantle in subduction zones, it was found that the annual input flux of a carbonate substance to the mantle is $\sim 4.6 \pm 4.0 \times 10^{12}$ moles, and the addition of sulfur, as well as sulfides and sulfates is $\sim 2.5 \pm 1.5 \times 10^{12}$ moles. The removal of carbon and sulfur in volcanic arcs is 3 to 5 times lower than the above values. The huge difference between the introduction and removal of carbonate and sulfur–containing phases suggests that significant amounts of carbonates, sulfides and sulfates are immersed deep into the mantle, where their interaction with mantle minerals becomes possible. It is now known that subduction of crustal carbonate material can be realized to depths of ≥ 600 km (Shirey et al., 2013), with carbonates being thermodynamically stable even at P, T – parameters of the lower mantle (Oganov et al., 2013). As evidence of the possibility of the presence of carbonates in mantle rocks are the findings of diamonds with carbonate inclusions.

Data on the composition of inclusions in minerals of mantle xenoliths and the results of experimental studies have shown that in the upper mantle, depending on the pressure, temperature and oxygen fugacity, the sulfur can exist in form of sulfides or sulfide melts (Lorand, Gregoire, 2006; Shirey et al., 2013), sulfates (Leung, 1990), C – O – H – S fluids (Giuliani et al., 2013) or to present in dissolved form in silicate melts (Zajacz et al., 2013). In recent years, sulfur behavior has been actively studied in the processes of mantle metasomatism, and the relationship of these processes with the formation of sulfide minerals in eclogites and peridotites of the upper mantle (Alard et al., 2011). Some researchers suggest that sulfides can be formed due to the interaction of S – bearing fluids or melts with mantle silicates, such as

olivine (Lorand, Gregoire, 2006; Eggler, Lorand, 1993; Fleet, MacRae, 1987; Papike et al., 1995; Lehner et al., 2013). As the main reactions of sulfidation the following are assumed:

• $Mg_2SiO_4 + \frac{1}{2}S_2 + C \rightarrow MgSiO_3 + MgS + CO$ (Fleet, MacRae, 1987);
• $Fe_2SiO_4 + S_2 \rightarrow 2FeS + O_2 + SiO_2$ (Papike et al., 1995);
• $2Fe_2SiO_4 + S_2 \rightarrow 2FeS + Fe_2Si_2O_6 + O_2$ (Eggler, Lorand, 1993).

At present, experimental studies on the modeling of the behavior of sulfur- and carbon-bearing phases in subduction processes become urgent, and studies on the interaction of carbonates and sulfur phases (a simplified model of subducted crystal material) with silicate phases at mantle pressures and temperatures are still very rare. The most common silicate phase of the upper mantle is olivine, and the most probable subducted carbonates are the minerals of the magnesite ($MgCO_3$) – calcite ($CaCO_3$) series, therefore, two systems were chosen for experimental studies of silicate – carbonate – sulfur and silicate – carbonate – sulfide interaction: $(Mg,Fe,Ni)_2SiO_4 – (Mg,Ca)CO_3 – S$ and $(Mg,Fe,Ni)_2SiO_4 – (Mg,Ca)CO_3 – FeS_2$.

Two series of experiments (6 in each), at a pressure of 6.3 GPa and a temperature interval of 1050 – 1550 °C (the temperature step of the experiments was of 100 °C) were carried out to simulate the processes of olivine – magnesite – sulfur and olivine – magnesite – pyrite interactions, The duration of the experiments was from 40 to 60 hours. All experiments were carried out on a multi-anvil apparatus of a "split – sphere" type (BARS) (Palyanov et al., 2010).

Experimental studies of interaction in the $(Mg,Fe,Ni)_2SiO_4 – (Mg,Ca)CO_3 – S$ system revealed that in the temperature range 1050 – 1350 °C an association of olivine, ferromagnesite, orthopyroxene and pyrite, coexisting with the sulfur melt / fluid is formed (Fig. 1 a). It was found, that recrystallization of olivine and magnesite was realized, as well as extraction of Fe and Ni from olivine into the melt, with a result of pyrite crystallization in the sulfur melt / fluid (Fig. 1 b). The main reaction in the olivine – magnesite – sulfur system in the temperature range of 1050 – 1350 °C is $(Mg,Fe,Ni)_2SiO_4 + (Mg,Ca)CO_3 + S \rightarrow (Mg,Fe,Ni)_2SiO_4 + (Mg,Fe)_2Si_2O_6 + (Mg,Ca,Fe)CO_3 + (Fe,Ni)S_2 + [S + FeS_2]_{melt}$.
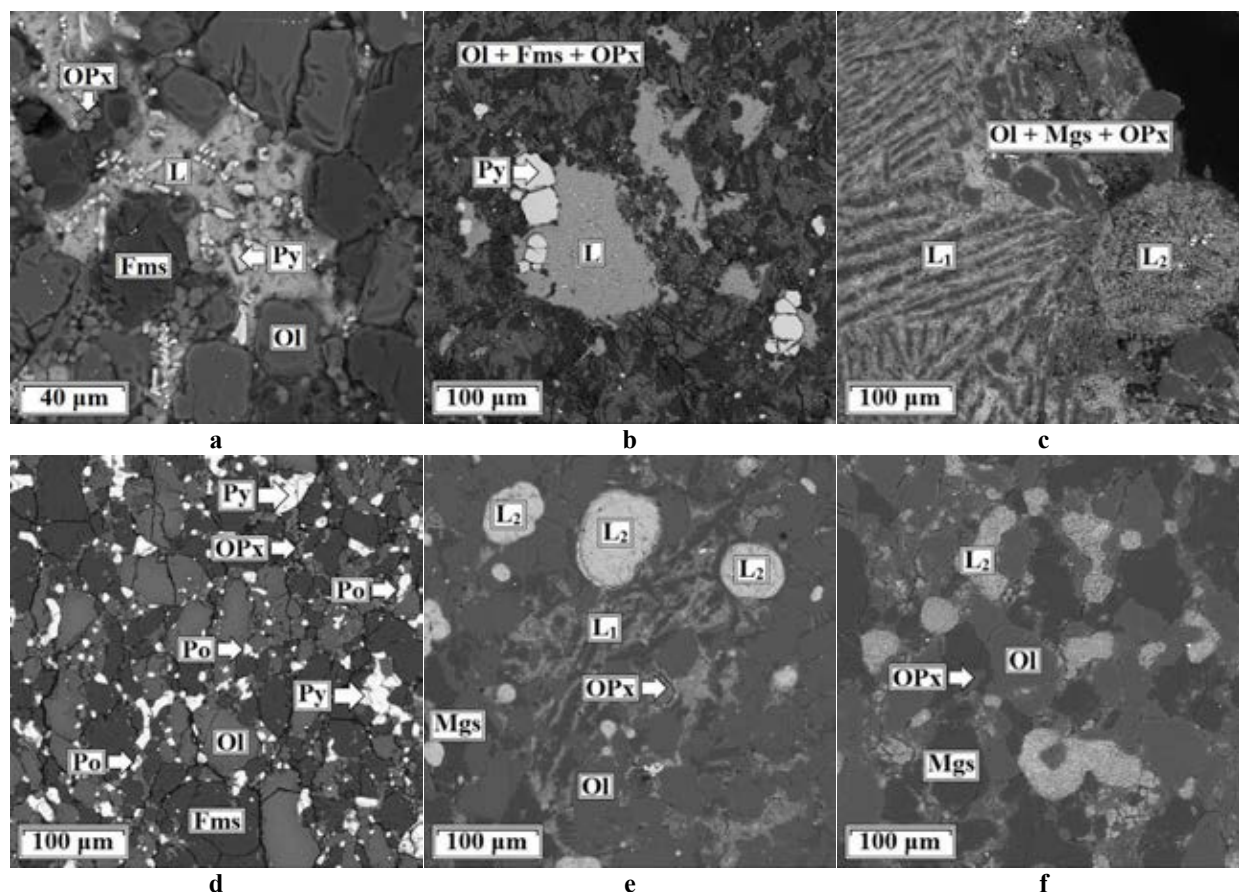
Fig. 1. SEM micrographs: **a** – structure of quenched sulfur melt (1350 °C); **b** – pyrite in quenched melt pool, located in a pyroxene – ferromagmesite – olivine aggregate (1250 °C); **c** – sulfur-sulfide and carbonate-sulfur quenched melts (1550 °C); **d** – olivine, orthopyroxene, ferromagnesite, pyrite and pyrrhotite assemblage (1250 °C); **e, f** – quenched sulfur-sulfide and carbonate-sulfur melts in the pyroxene – magnesite – olivine aggregate (1550 °C and 1450 °C, respectively); Fms – ferromagnesite; L – quenched sulfur melt; L_1 – carbonate-sulfur melt; L_2 – sulfur-sulfide melt; Mgs – magnesite; Ol – olivine; OPx – orthopyroxene; Po – pyrrhotite; Py – pyrite.

At higher temperatures (1450 – 1550 °C), the sulfides and carbonates present as two immiscible melts – carbonate with dissolved sulfur and sulfur-sulfide ones (Fig. 1 c). The resulting carbonate melt contains about 5 % by weight of S and does not contain iron. Fe and Ni, initially presented in the olivine, completely converted into a composition of a

sulfur-sulfide melt (Table 1). Thus, in the olivine – magnesite – sulfur system at temperatures of 1450 and 1550 °C, the basic reaction is assumed to be as follows: $(Mg,Fe,Ni)_2SiO_4 + (Mg,Ca)CO_3 + S \rightarrow (Mg,Fe,Ni)_2SiO_4 + (Mg,Fe)CO_3 + (Mg,Fe)_2Si_2O_6 + [(Mg,Ca)CO_3 + S]_{melt} + [(Fe,Ni)S_2 + S]_{melt}$. In other words, during the study it was found that the interaction of olivine with magnesite and sulfur in the high-temperature range (1450 – 1550 °C) leads to the formation of an association of iron-free (~ 1 wt% FeO) olivine, orthopyroxene and magnesite, coexisting with two immiscible melts, mainly carbonate and sulfide.

Table 1. Compositions of silicate and carbonate phases of the olivine – magnesite – sulfur system.

T, °C	t, h	Phase	N_A	Composition, weight %							
				SiO_2	FeO	NiO	MgO	CaO	CO_2	SO_2	Σ
1050	60	Mgs	4	–	$0,73_{(0,1)}$	–	$49,7_{(0,1)}$	$1,48_{(0,5)}$	$48,09_{(0,5)}$	–	$100_{(0)}$
		Ol	5	$42,14_{(0,6)}$	$7,69_{(1,1)}$	$0,37_{(0,1)}$	$49,38_{(1,0)}$	–	–	–	$99,58_{(0,6)}$
		Opx	2	$58,8_{(0,9)}$	$5,98_{(1,0)}$		$35,17_{(2,0)}$	–	–	–	$99,95_{(0,2)}$
1150	40	Mgs	3	–	$0,83_{(0,2)}$	–	$48,39_{(0,2)}$	$1,19_{(0,4)}$	$49,59_{(0,5)}$	–	$100_{(0)}$
		Ol	4	$41,06_{(0,6)}$	$7,74_{(1,0)}$	$0,39_{(0,1)}$	$50,68_{(1,0)}$	–	–	–	$99,87_{(0,5)}$
		Opx	2	$59,64_{(0,7)}$	$0,62_{(1,1)}$		$39,24_{(2,0)}$	–	–	–	$99,5_{(0,3)}$
1250	40	Mgs	5	–	$0,78_{(0,1)}$	–	$48,52_{(0,1)}$	$1,4_{(0,3)}$	$49,3_{(0,5)}$	–	$100_{(0)}$
		Ol	5	$40,99_{(0,6)}$	$7,79_{(1,0)}$	$0,41_{(0,1)}$	$50,27_{(1,0)}$	–	–	–	$99,46_{(0,5)}$
		Opx	3	$58,2_{(0,8)}$	$3,59_{(1,0)}$		$37,88_{(2,0)}$	–	–	–	$99,67_{(0,2)}$
1350	40	Mgs	4	–	$1,19_{(0,1)}$	–	$47,92_{(0,1)}$	$1,44_{(0,4)}$	$49,45_{(0,5)}$	–	$100_{(0)}$
		Ol	4	$41,2_{(0,6)}$	$8,28_{(0,9)}$	$0,41_{(0,1)}$	$49,97_{(1,0)}$	–	–	–	$99,86_{(0,5)}$
		Opx	4	$59,57_{(0,8)}$	$1,82_{(1,1)}$		$38,54_{(2,0)}$	–	–	–	$99,93_{(0,2)}$
1450	40	Mgs	3	–	$0,89_{(0,1)}$	–	$46,48_{(0,1)}$	$1,79_{(0,4)}$	$50,84_{(0,5)}$	–	$100_{(0)}$
		Ol	5	$42,25_{(0,6)}$	$3,31_{(0,4)}$	$0,22_{(0,5)}$	$54,01_{(0,9)}$	–	–	–	$99,76_{(0,5)}$
		Opx	3	$60,06_{(0,7)}$	$2,00_{(1,1)}$	–	$37,85_{(2,0)}$	–	–	–	$99,91_{(0,2)}$
		L_1	6	$4,52_{(0,8)}$	$0,47_{(0,3)}$	–	$22,16_{(1,0)}$	$10,67_{(0,4)}$	$59,97_{(0,5)}$	$2,21_{(0,6)}$	$100_{(0)}$
1550	40	Mgs	4	–	$1,04_{(0,1)}$	–	$46,69_{(0,2)}$	$2,13_{(0,5)}$	$50,14_{(0,3)}$		$100_{(0)}$
		Ol	4	$42,16_{(0,5)}$	$2,98_{(0,4)}$	$0,17_{(0,6)}$	$54,19_{(0,9)}$	–	–	–	$99,5_{(0,5)}$
		Opx	3	$59,83_{(0,8)}$	$2,41_{(1,0)}$		$37,69_{(2,0)}$	–	–	–	$99,93_{(0,2)}$
		L_1	5	$5,19_{(0,8)}$	$0,41_{(0,2)}$	–	$23,44_{(1,0)}$	$9,33_{(0,3)}$	$58,24_{(0,3)}$	$3,39_{(0,6)}$	$100_{(0)}$

Mgs – magnesite; Ol – olivine; OPx – orthopyroxene; L_1 –carbonate-sulfur melt.

The results of an experimental study aimed at modeling the interaction of the subducted material with mantle silicates in the $(Mg,Fe,Ni)_2SiO_4 – (Mg,Ca)CO_3 – FeS_2$ system were separated into relatively low–temperature (1050 – 1250 °C) and relatively high-temperature (1350 – 1550 °C) intervals. In the course of the interaction of olivine – magnesite – pyrite in the relatively low-temperature interval, an association of olivine, ferromagnesite, orthopyroxene, pyrite and pyrrhotite is formed (Fig. 1 d). It has been established that the main processes occurring in the system at given temperatures are the recrystallization of olivine and magnesite, partial extraction of Fe and Ni from olivine into pyrite, and the formation of pyrrhotite. The reaction $(Mg,Fe,Ni)_2SiO_4 + (Mg,Ca)CO_3 + FeS_2 \rightarrow (Mg,Fe,Ni)_2SiO_4 + (Mg,Fe)_2Si_2O_6 + (Mg,Ca,Fe)CO_3 + (Fe,Ni)S_2 + (Fe,Ni)_{1-x}S$ is proposed as the principal reaction at the temperatures of 1050 – 1250 °C.

In the relatively high-temperature range of experiments in the olivine – magnesite – pyrite system an association of forsterite, enstatite, magnesite, and also the formation of two immiscible melts – carbonate with dissolved sulfur (enriched in Ca) and sulfur-sulfide $((Fe, Ni)_{1-x}S)$ (Fig. 1 e, f) took place. It has been established that at these temperatures the extraction of Fe and Ni from olivine into the sulfide melt occurs almost completely, as a result of which the resulting silicates are characterized by very low concentrations of FeO (~ 1 wt%, relative to the initial ~ 7 wt%) and the absence of an NiO impurity. Thus, the reaction $(Mg,Fe,Ni)_2SiO_4 + (Mg, Ca)CO_3 + FeS_2 \rightarrow Mg_2SiO_4 + Mg_2Si_2O_6 + MgCO_3 + [(Ca,Mg,Fe)CO_3 + S]_{melt} + [(Fe,Ni)_{1-x}S + S]_{melt}$ can be considered as the main reaction between olivine, magnesite and pyrite in the temperature range of 1350 – 1550 °C.

The olivine – carbonate – sulfur and olivine – carbonate – sulfide interactions studied may be considered as the basis for modeling of metasomatic processes accompanied by the formation of mantle sulfides upon subduction of the crustal material into the silicate mantle. It is established that the interaction of subducted carbonates and S with mantle silicates at high P, T – parameters results in generation of potential metasomatic agents: S-rich reduced melts / fluids and carbonate melts. It has been shown experimentally that S-bearing reduced melts / fluids may provide almost complete alteration of olivine, magnesite, and dolomite, which is accompanied by extraction of metals from the solid–phase silicate or carbonate matrix and stimulate the formation of sulfides.

References:

Alard O. et al. Volatile-rich metasomatism in Montferrier xenoliths (Southern France): Implications for the abundances of chalcophile and highly siderophile elements in the subcontinental mantle // J Petrol, 2011, V. 52. (10). 2009-2045 pp.

Eggler D.H., Lorand J.P. Mantle sulfide geobarometry // Geochim Cosmochim Acta, 1993, V. 57. 2213-2222 pp.

Evans, K.A., The redox budget of subduction zones // Earth-Science Reviews, 2012, V.113. 11-32 pp.

Fleet M.E., MacRae N.D. Sulfidation of Mg-rich olivine and the stability of niningerite in enstatite chondrites // Geochim Cosmochim Acta, 1987. V. 51. 1511-1521 pp.

Giuliani A. et al. Mantle oddities: A sulphate fluid preserved in a MARID xenolith from the Bultfontein kimberlite (Kimberley, South Africa) // Earth Planet Sci Lett, 2013, V. 376. 74-86 pp.

Lehner S.W., Petaev M.I., Zolotov M.Y., Buseck P.R. Formation of niningerite by silicate sulfidation in EH3 enstatite chondrites // Geochim Cosmochim Acta, 2013, V. 101. 34-56 pp.

Leung I.S. Silicon carbide cluster entrapped in a diamond from Fuxian, China // Am Mineral, 1990, V. 65. 1110-1119 pp.

Lorand J.P., Grégoire M. Petrogenesis of base metal sulphide assemblages of some peridotites from the Kaapvaal craton (South Africa) // Contrib Mineral Petrol, 2006, V. 151. 521-538 pp.

Oganov A.R., Hemley R.J., Hazen R.M., Jones A.P. Structure, bonding and mineralogy of carbon at extreme conditions // Rev Mineral Geochem, 2013, V. 75. 47-77 pp.

Palyanov Y.N., Borzdov Y.M., Khokhryakov A.F., Kupriyanov I.N., Sokol A.G. Effect of nitrogen impurity on diamond crystal growth processes // Cryst. Growth Des, 2010, V.10, 3169—3175 pp.

Papike J.J., Spilde M.N., Fowler G.W., Layne G.D., Shearer C.K. The Lodran primitive achondrite: Petrogenetic insights from electron and ion microprobe analysis of olivine and orthopyroxene //Geochim Cosmochim Acta, 1995, V. 59. 3061-3070 pp.

Shirey S.B., Cartigny P., Frost D.J., Keshav S., Nestola F., Nimis P., Pearson D.G., Sobolev N.V., Walter M.J. Diamonds and the Geology of Mantle Carbon // Reviews in Mineralogy & Geochemistry, 2013, V. 75. 355-421 pp.

Zajacz Z., Candela PA., Piccoli P.M., Sanchez - Valle C., Waelle M. Solubility and partitioning behavior of Au, Cu, Ag and reduced S in magmas //Geochim Cosmochim Acta, 2013, V. 112. 288-304 pp.

TRACE ELEMENT CHEMISTRY OF PERIDOTITIC GARNETS IN SIBERIAN DIAMONDS

Zedgenizov D.A.[1,2], Ragozin A.L.[1,2], Logvinova A.M.[1,2], Yurimoto H.[3], Sakamoto N.[3], Kuroda M.[3]

[1]Institute of Geology and Mineralogy, Siberian Branch of the Russian Academy of Sciences, Novosibirsk, Russia
[2]Novosibirsk State University, Novosibirsk, Russia
[3]Hokkaido University, Sapporo, Japan

Natural diamonds are well known as valuable source of information about the composition and thermodynamic conditions of the Earth's mantle. Both the geochemistry and mineralogy of diamonds and of their inclusions provides constraints on the conditions and processes of diamond formation. Previous studies of inclusions in diamonds have demonstrated that formation of diamonds in subcontinental lithospheric mantle occurs predominantly in peridotite (P-type) and eclogite (E-type) assemblages (Sobolev, 1977; Meyer, 1987). Peridotitic diamonds are dominantly of a harzburgitic affinity (77%), with lherzolitic diamonds (23%) forming an additional, subordinate population (Stachel, Harris, 2008). Harzburgitic garnets occurring as inclusions in diamonds are subcalcic pyropes and have variable Cr contents which may be as high as 20 wt.% Cr_2O_3. The occurrence of low-Ca peridotitic garnets in heavy mineral concentrates is a widely used exploration tool for diamondiferous kimberlites (Grütter et al., 2004).

The Siberian platform is an important region of occurrence of many economic diamondiferous kimberlite pipes. However comprehensive geochemical information for garnet inclusions in diamond from individual localities of this region is limited. The purpose of this study is therefore to provide a mew comprehensive set of geochemical data (involving REE, Y and Zr) for peridotitic garnets in diamonds from several Siberian kimberlite pipes, with a view on the nature of the metasomatic processes operating up to the time of diamond crystallization within the base of lithosphere. A subset of inclusions, selected on the basis of the microprobe analyses was selected for trace element analysis. Major elements of garnet inclusions were determined using a JEOL JXA 8100 electron microprobe at the V.S. Sobolev Institute of Geology and Mineralogy (Novosibirsk, Russia). The procedure for analysis by X-ray electron probe microanalysis was similar to that described in (Lavrent'ev et al., 2015). The REE compositions of garnets were determined with the Cameca IMS-6f instrument at Hokkaido University (Sapporo, Japan). The full protocol (precision, accuracy and reference materials) is described in details in (Wang, Yurimoto, 1993).

The extensive data base of garnets included in Siberian diamonds consists of about 650 Cr-rich pyropes (Sobolev et al., 2004). These garnets contain CaO up to 20.5 wt.% but generally less than 8 wt.% and Cr_2O_3 up to 21 wt.%. In this study peridotitic garnets were represented by Ca-undersaturated (harzburgitic – H) as well as Ca-saturated compositions (lherzolitic – L and rare wherlitic W) (Fig. 1). The content of CaO of garnets in studied diamonds reach 7.7 wt.% and Cr_2O_3 15 wt.%. All garnets have Mg# (Mg/(Mg+Fe)) between 0.82 and 0.89 with the average near 0.85.

Chondrite normalised rare-earth elements patterns (REE_N) (following the terminology of Banas et al., 2009) for harzburgitic garnets in Siberian diamonds are highly variable and include humped (light REE_N enriched), normal (light REE_N depleted) and sinuous (enriched in Sm_N over Dy_N, and $LREE_N$ enriched) varieties. The mildly subcalcic garnets have less light REE_N and more heavy REE_N. Lherzolitic garnets are characterized by normal and sinuous REE_N patterns. Some rare lherzolitic garnets show light REE_N depleted and flat heavy REE_N patterns.

The studies of garnet inclusions demonstrate that peridotitic diamonds from Siberian platform have been crystallised predominantly in highly depleted subcratonic lithosphere. Garnets that crystallise in such highly depleted lithosphere will inherit the geochemical signature of the host, i.e. will be magnesian, rich in Cr, low in Ca, will have low concentrations of

trace elements, and will have a positive slope for chondrite-normalised rare earth element abundances from light to heavy rare earth elements (Stachel, Harris, 2008). However, the majority of peridotitic garnets in diamonds are characterised by sinusoidal chondrite normalised REE patterns with high Nd contents. The light REE enriched nature of these garnets is consistent with a degree of metasomatic re-enrichment of the harzburgite substrate prior to, or during, the diamond crystallisation event (Stachel et al., 2004). The infiltration of fluids and melts may change the chemistry of depleted subcratonic lithosphere through the re-introduction of e.g. Ca, Fe, Ti, Y, Zr and the REE. It was suggested that comparatively low-temperature, fluid-dominated metasomatism results in sinuous REE patterns, and high Nd and Sr, but not high Y, Zr and Ti in garnet, while high-temperature, melt-dominated metasomatism result in normal REE patterns, and high Y, Zr and Ti in garnet (Griffin et al., 1999). The conversion of highly depleted, Ca and Fe poor harzburgite to more calcic harzburgite, and Ca-saturated lherzolite during the diamond crystallisation process, is presumed to be due to transition from fluid to melt dominated metasomatism (Stachel, Harris, 2008).
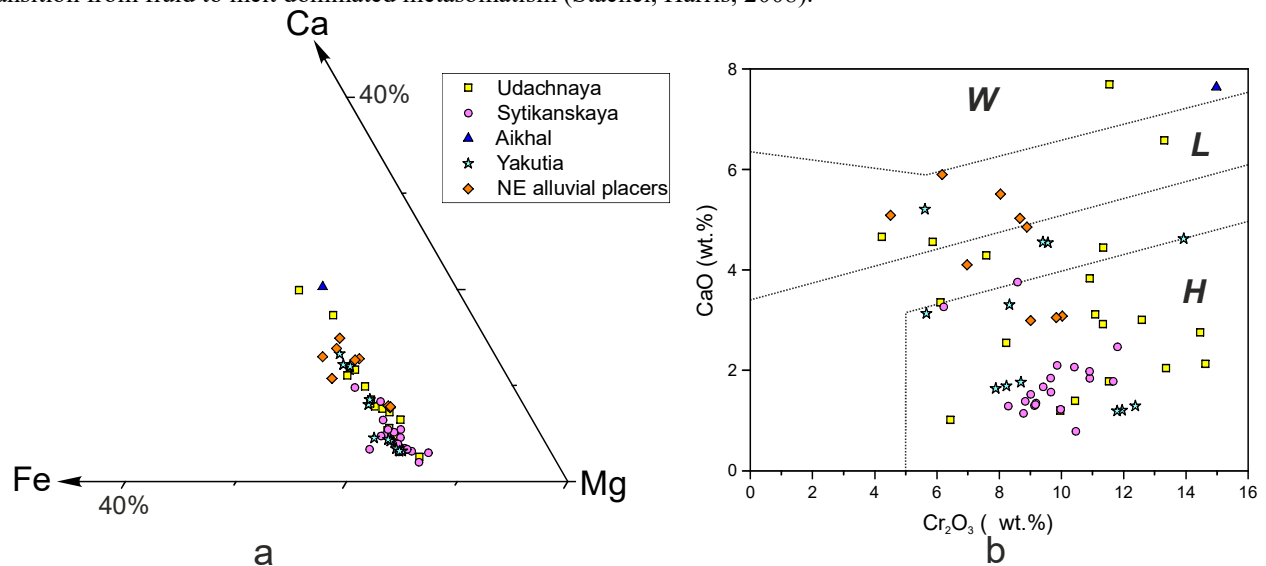
Fig. 1. The compositional features of peridotitic garnets occurring as inclusions in Siberian diamonds.

From this framework it is clear that the peridotitic garnets occurring as inclusions in Siberian diamonds represent different metasomatic specification of their crystallisation process in the deep lithospheric mantle (Fig. 2). The majority of inclusions in diamonds represent almost pristine, highly depleted lithosphere which has been affected by a comparatively very mild form of metasomatism prior to, or during diamond crystallisation. In contrast, the mantle which clearly experienced substantial metasomatic remodification is suggested only for minor populations of inclusions in diamond examined in the present study. The presence of comparatively fertile mantle may be proposed only for lherzolitic garnet. It is clear that the metasomatism of the mantle accompanying diamond crystallisation at Siberian platform, may be effective at introducing LREE, and some Zr into the depleted substrate in some cases, and effective at transporting much Ca, Ti and Y in other cases.
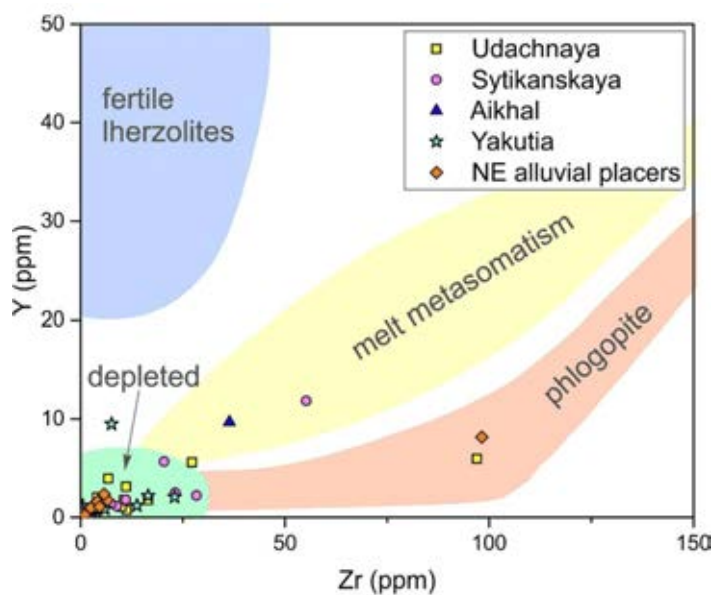
Fig. 2. Y and Zr contents of peridotitic garnets occurring as inclusions in Siberian diamonds. Fields after Griffin et al. (1999).

References:

Banas A., Stachel T., Phillips D., Shimizu N., Viljoen K.S., Harris J.W. Ancient metasomatism recorded by ultra-depleted garnet inclusions in diamonds from DeBeers Pool, South Africa. Lithos. 2009. 112S. 736-746.

Griffin W.L., Shee S.R., Ryan C.G., Win T.T., Wyatt B.A. Harzburgite to lherzolite and back again: metasomatic processes in ultramafic xenoliths from the Wesselton kimberlite, Kimberley, South Africa // Contrib. Mineral. Petrol. 1999. 134. 232-250.

Grütter H.S., Gurney J.J.,Menzies A.H.,Winter F. An updated classification scheme for mantle-derived garnet, for use by diamond explorers // Lithos. 2004. 77. 841-857.

Lavrent'ev Y.G., Korolyuk V.N., Usova L.V., Nigmatulina E.N. Electron probe microanalysis of rock-forming minerals with a JXA-8100 electron probe microanalyzer // Russ. Geol. Geophys. 2015. 56. 1428-1436.

Meyer H.O.A. Inclusions in diamond. In: Nixon, P.H. (Ed.), Mantle Xenoliths. Wiley, London, 1987. 501-522.

Sobolev N.V. Deep-seated inclusions in kimberlites and the problem of the composition of the upper mantle (translated from the Russian edition, 1974) AGU, Washington. 1977. (279 pp.).

Sobolev N.V., Logvinova A.M., Zedgenizov D.A., Seryotkin Y.V., Yefimova E.S., Floss C., Taylor L.A., Mineral inclusions in microdiamonds and macrodiamonds from kimberlites of Yakutia: a comparative study // Lithos 2004. 77. 225-242.

Stachel T., Aulbach S., Brey G.P., Harris J.W., Leost I., Tappert R., Viljoen K.S. The trace element composition of silicate inclusions in diamonds: a review // Lithos. 2004. 77. 1-19.

Stachel T., Harris J.W. The origin of cratonic diamonds - constraints from mineral inclusions // Ore Geol. Rev. 2008. 34, 5-32.

Wang W.Y., Yurimoto H. Analysis of rare earth elements in garnet by SIMS // Ann. Rep. Inst. Geosci. Univ. Tsukuba. 1993. 19. 87-91.

INVENTORY INFORMATION ANALYSIS OF MINERAL ORGANIZATION OF THE KHALDZAN BUREGTEG MASSIF (WESTERN MONGOLIA)

Zenina K.S.
Tomsk State University, Tomsk, Russia

The Khaldzan Buregteg massif in Western Mongolia stands out against the known agpaite granite massifs with the largest number of mineral species and their varieties, which determine its composition and ore specialization. The studies of the previous researchers answered many questions of the pluton genesis, its structure and material constitution. The exceptional abundance of minerals was identified; however, the number of mineralogical studies remains evidently insufficient. This is confirmed by the constant findings of rare and even new mineral species in it (Kartashov et al., 1993a, 1993b, 2002).

The Khaldzan Buregteg alkaline granite massif is located within the Mongolian Altai, on the left bank of the Khovd-Gol River, 40 km away from its estuary (Khar us Nuur). The alkaline-granite massif includes 7 intrusion phases including 2 rare-metal ones with the Zr, Nb, Y and REE mineralization according to V. I. Kovalenko et al. (1985; 2004; 2009). The following groups of magmatic rocks (from the early phases to later ones) are identified: (1) nordmarkites and dolerites synchronous with them; (2) alkaline granites and dolerites synchronous with them; (3) ekerites, small-grained alkaline granites and pegmatites; (4) pantellerites; (5) rare-metal alkaline granites; (6) dyke potassium alkaline basites and conventionally leucocratic syenites; and (7) miarolitic rare-metal alkaline granites. The latter sequence is typical for the Southern outcrop of the Khaldzan-Buregteg massif. The northern outcrop is composed mainly of the 1st-phase nordmarkites; no alkaline granites of the later phases were detected in it (Kartashov, 1993a,b).

The inventory-information analysis within the frames of the this topomineralogical study means the formation of the complete mineralogical inventory including all mineral species and varieties, and the calculation of inventory indicators of the mineral organization. The inventory was compiled on the basis of processing the references and studying the stone material. According to the compiled inventory of the minerals of the Khaldzan-Buregteg massif, it contains 133 mineral species composing the intrusive rocks, their pegmatites and metasomatites. There are about 10 compounds of mineral analogs and varieties. The inventory-information analysis showed that the increase of the number of mineral species occurs from the early phases to later ones. The mineral composition in early alkaline granites and nordmarkites is determined by twelve mineral species. The number of mineral species reaches 40 in rare-metal granites of intrusion phases V and VII. The maximum number of mineral species was identified in metasomatites (65) and pegmatites (83) (Zenina, Konovalenko, 2016).

The analysis of the mineral species distribution by classes of the standard crystal-chemical classification showed that the composition of the Khaldzan-Buregteg massif is determined by the minerals from all known types of non-organic natural compounds. Out of 26 classes of chemical compounds determined in nature, the mineral inventory of the massif is represented by 16 classes. It contains a low amount of simple substances and haloid compounds. Oxygen compounds form most of the mineral species. The latter mostly include silicates followed by oxides and hydroxides, and the other oxygen compounds mainly represented by carbonates have the minor share. The main silicates are nesosilicates (about 50%), followed by single-chain and double-chain inosilicates and phyllosilicates (14% each), and the other structures make less than 10%.

The following generalized crystal-chemical evolution series of the massif has been identified: OS (oxygen salts) > ChC (chalcogen compounds) > SS (simple substances) > haloid compounds (HC). Meanwhile, some crystal-chemical differences are observed in the granite-pegmatite-metasomatite series. In particular, metasomatites contain more chalcogen compounds. The composition of granites is represented almost in full by oxygen compounds, silicates primarily. The crystal-chemical series of some granite phases and their derivatives have the following view: OS > HC (intrusions of phases from I to IV, VII); OS > SS > ChC > HC (intrusion phase V, VI); OS > ChC > HS > SS (pegmatites and metasomatites of the massif).

The mineral and structural organization of the massif is described by the following crystal-symmetric series: Monoclinal (Mon) > Rhombic (Rhomb) > Tetragonal (Tetra) > Cubic (Cub) > Trigonal (Trig) > Hexagonal (Hexa) > Triclinic (Tric). The crystal-symmetric organization of individual massif phases is characterized by the following symmetric-rank formulas, in which the lower index corresponds to the frequency of occurrence (in %): $Mon_{33.30} - Trig_{25.00} - Tric_{25.00} - Tetra_{8.33} - Cub_{8.33}$ (intrusion phase I), $Mon_{66.67} - Trig_{8.34} - Cub_{8.34} - Tric_{8.34}$ (intrusion phases II, III, IV, VI), $Mon_{33.34} - Cub_{16.66} - Trig_{18.18} - Rhomb_{9.09} - Tetra_{9.09} - Hex_{6.05} - Tric_{3.02}$ (intrusion phase V), $Mon_{33.34} - Cub_{21.22} - Rhomb_{16.66} - Trig_{14.28} - Tetra_{9.52} - Hex_{4.76} - Tric_{4.76}$ (intrusion phase VII), $Mon_{41.46} - Tetra_{15.85} - Cub_{12.20} - Rhomb_{10.98} - Trig_{7.32} - Hex_{7.32} - Tric_{4.88}$ (massif pegmatites), $Mon_{43.75} - Tetra_{15.62} - Cub_{10.94} - Hex_{9.37} - Trig_{9.37} - Rhomb_{7.81} - Tric_{3.12}$ (massif metasomatites). The sequence of mineral distribution by syngonies on the basis of the first series members in general corresponds to the distribution recorded by I. I. Shafranovsky for alkaline complexes (Shafranovsky, 1974) and differs abruptly from the current statistic sequence of syngonies (Mon–Rhomb–Trig–Tric–Cub–Hex–Tetra) provided by A. P. Khomyakov (2010). The main crystal-symmetric feature of the mineral inventory of the Khaldzan-Buregteg massif is the high share of the mineral species of the tetragonal syngony and the abrupt deficit of the representatives of the triclinic syngony.

The analysis of the minerals distribution in the complex by symmetry types showed the abrupt predominance of the representatives of planaxial symmetry types. In terms of the number of phases they are followed by the minerals with central symmetry, and the minimum share of minerals has planar symmetry.

The comparative analysis of the distribution of species-forming elements in the minerals shows that the maximum number of mineral species (28) was formed by three species-forming elements, followed in the decreasing order by the mineral species comprising five elements (25), four elements (18), two elements (16), six elements (15) and then seven and eight elements (9). There are 6 single-element mineral species. 133 mineral species determining the massif inventory are composed of 40 species-forming elements (in the decreasing order): O, Si, H, Ca, Fe, Na, Al, Ti, Ce, Y, C, F, Nb, Pb, S, Zn, Mg, As, Zr, Be, K, Mn, Cu, Nd, P, Th, Mo, Ta, U, La, Li, Sn, Ba, Cl, Sr, Au, Sn, V, Sb, and W.

Mineral clarks were calculated for the main elements and the elements determining the ore specialization of the massif. The mineral clark (MC) of a particular chemical element was calculated as the ratio of the number of minerals of a given element to the total number of minerals (Krivovichev, Charykova, 2015). The comparison of the mineral clarks of species-forming chemical elements in the Khaldzan-Buregteg complex was made by matching the calculated clarks with the clarks of the considered elements for the currently known mineral species. For this purpose the mineral clarks of the species-forming elements were calculated for the minerals approved as of May 2016, amounting to 5144 mineral species. The comparative analysis of the mineral clarks of species-forming elements for the massif minerals and the general list of the known mineral species in nature allowed assessing the role of this or other element in the mineral formation. The comparison of the mineral clarks of the species-forming elements allowed dividing them into two groups: excessive (Fe, Ca, Na, O, Si, Ti, Zn, Nb, Ta, Zr, Be, Ce, La, Nd, Y) with the highest role in the mineral organization of the massif in relation to their value in the formation of the total number of mineral species in nature, and deficit (H, F P, Mn, Mg, K, As) of slightly lower value than for the formation of the existing natural mineral variety. In general, the Khaldzan-Buregteg massif in terms of the mineral clerks of profile elements exceeds the mineral clerks of the mineral species known today significantly. This reflects the anomalous nature of this unit in relation to rare earths, primarily light ones, niobium, zircon and beryllium.

The comprehensive study of the mineralogy of the Khaldzan-Buregteg alkaline-granite complex allowed detecting the minerals being new for the unit (cassiterite, torianite, La-allanite, Nd-allanite, stibnite) not noted in its composition before. Moreover, the mineral corresponding to the crystal-chemical formula $(Ca_{1.02}(Nd_{0.54}Ce_{0.24}La_{0.12})_{0.90}Mn_{0.07})_{1.99}(Fe^{3+}_{1.25}Al_{0.85}Fe^{2+}_{0.85}Mn^{2+}_{0.05})_{3.00}Si_{3.00}O_{12}(OH)$, which according to the existing inventory of the minerals of the epidote group can be referred to the new mineral species, ferrialanite-(Nd), was discovered.

The variability of the crystal-chemical and crystal-symmetric indicators from one complex phase to another one reflects the heterogeneity and accentuates the individual features of the mineral formation of granite phases, their pegmatites and metasomatites. The main identified differences are preconditioned by the whole range of reasons, including the alkalinity of the mineral-formation medium, the F and O activity, the asynchronicity of formation of pegmatites in the course of evolution, various conditions of localization of the pegmatite and metasomatic bodies that defined a different scale of impact of the hosting rock chemistry on residual melts-solutions, and a different degree of the exogenous transformation of minerals.

References:

Kartashov PM, Troneva NV, Mokhov AV, Kovalenko VI, Tsareva GM (1993a) On the faulty zinc-bearing senaite from the rare-metal-bearing alkaline granites of the Haldzan-Buragtag massif (Mongolian Altai). Doklady Akademii Nauk 332: 755-758. In Rus.

Kartashov PM, Voloshin AV, Pakhomovskii YA, Kovalenko VI (1993b) Plumbopirochlore from Western Mongolia. Doklady Akademii Nauk 332: 1137-1140. In Rus.

Kartashov PM, Ferraris G, Ivaldi G, Sokolova E, McCammon CA (2002) Ferriallanite-(Ce), CaCeFe^{3+}AlFe^{2+}(SiO$_4$)(Si$_2$O7)O(OH), a new member of the epidote group: Description, X-ray and Mossbauer study. Canadian Mineralogist 40: 1641-1648.

Kovalenko VI, Goregliad AV, Tsareva GM (1985) Khaldzan-Buregteg massif as a new manifestation of rare-metal alkaline granitoids of MPR. Doklady Akademii Nauk 280: 954-959. In Rus.

Kovalenko VI, Yarmolyuk VV, Kovach VP, Sal'nikova EB, Kozlovskii AM, Kotov AB, Khanchuk AI (2004) Multiple magma sources for the peralkaline granitoids and related rocks of the Khaldzan Buregte group of massifs, western Mongolia: Isotopic (neodymium, strontium, and oxygen) and geochemical data. Petrology 12: 497-518.

Kovalenko VI, Kozlovsky AM, Yarmolyuk VV (2009) Trace element ratios as indicators of source mixing and magma differentiation of alkali granitoids and basites of the Haldzan-Buregtey massif and the Haldzan-Buregtey rare-metal deposit, western Mongolia Petrology. 17: 158-177. doi: 10.1134/S0869591109020040

Khomyakov AP (2010) Recent mineral discoveries and their contribution to the knowledge of the evolutionary laws of asymmetry of the mineral world. In: XI Russian Congress of mineralogical society "Modern Mineralogy: from theory to practice", St. Petersburg, Russia, pp 129-131

Shafranovsky II (1974) Essays on mineralogical crystallography. Publishing House Nedra, Leningrad

Zenina KS, Konovalenko SI (2016) Mineralogical features of alkaline granite pegmatites in the Khaldzan-Buregteg massif (Western Mongolia). Proceedings of the Russian Mineralogical Society 145: 63–80. In Rus.

EPOCHS OF INTRUSION-RELATED GOLD MINERALIZATION IN THE NORTHERN TIBETAN

Zhou S.[1], Qiu R.Z.[2], Li S.R[1], Zhu Q.R[1], Lin D.[1], Zhao L.K.[1]
[1]China University of Geosciences, Beijing, China
[2]China Geological Survey, Beijing, China
[3]Tibetan Bureau of Land and Resources, Lhasa, Tibet, China

Tibet area is located at the eastern end of the Alps-Himalaya metallogenic belt, which is one of the world's giant metallogenic belts, and its unique geological environment and evolution history have enriched in mineral resources, of which gold ore is the main mining mineral. The main tectonic components of Qinghai-Tibetan Plateau from north to south are the Songpan-Ganzi accretionary mélange, the east Qiangtang, the west Qiangtang, Lhasa Terranes and Himalayan. Those terranes were separated by Jinsha Suture Zone, Longmu Tso-Shuanghu Suture Zone(LSSZ), Bangong-Nujiang Suture Zone(BNSZ), and Indus-Yarlung Zangbo Suture Zone(Zhu et al.,2012;Qiu et al.,2007). Located in the northern Tibet hinterland, Bangong-Nujiang Suture Zone(BNSZ) is considered to be the demise of the Tethys main belt, is also an important metallogenic belt. In China Bangong-Nujiang tectonics suture extends over 2400 km, and begins from Bangong lake in the west, complemented by Gerze, Dongqao, Dengqen to east, then it turns to Jiayu bridge and Shanglinca, baxoi countynin the south and connects with the Lancang river belt after the Zayu ,Zuogong county, and joins with myitkyina ultramafites in northern myanmar Mandalay area, with southern extension into the Andaman Sea and western to Kashmir India. According to the geographical distribution of the rock band, it is divided into Gaize Bangong Lake-Gerze (West), Dongqiao-Amdo(middle) and Dengqen-Nujiang segments. The gold resources in the band are abundant and widely distributed, the ancient gold mining pits are often found, folk gold mining has never stopped. However, it has been the most underdeveloped area in geological survey and research in our country due to its extremely high altitude (with an average altitude of more than 4500 m), bad weather and inconvenient transportation. In this paper, on the basis of field geological features survey on the Dacha gold mine and Shena copper-gold mine in the western portion of the suture and the Shesuo copper-gold deposit and the Xiawunongba gold placer mine in the middle portion of the suture (Figure 1), we chose several magma samples related to mineralization to carry out the K-Ar isotopic dating, in order to provide the basis for the study of the evolution of the Tethys and the time of mineralization.

1. Dacha gold mine and Shena copper-gold mine

The mine district is located in Gerze region of Tibet, and can be divided into the Sewa continental margin depression area in the collage overlap cover unit of Qiangtang-Sanjiang complex plates in north, Bange- Qindora degradation arc within Gangdese Nyainqentanglha plate in south, and Mugagangri block within the Bangong-Nujiang Suture Zone in the middle part of the area, according to the original formation, deformation and metamorphism of the area, that is, with an "one belt and two zones " pattern in structure (Zhou X., 1989). The structure of this area is dominated by faults, which is characterized by a series of north-trending thrust ones with extending along east-west and almost parallel each other. The faults are distributed intermittently and controlled the distribution of strata and magmatic rocks. The existing data show that the metallogenices of the rock gold deposits in this area are altered rock and quartz vein while that of placer gold deposits are mainly alluvial, eluvial type and outwash type etc.

Dacha gold mine is located in the southeast of the district, at the junction of Nyima and Gerze county and near Cuoqin County to south, with area of about 270 km^2. The east of the area is high while the west is low, with an average elevation of 4800 m, which belongs to the low mountain-hills landform of plateau.

The gold deposits are controlled by two north-south trending faults within the Bangong-Nujiang Suture Zone, where the northern boundary is Bangongcuo-Cantor - Kangtuo-Zigetangcuo, the South sector of the Rutog - Gerze - Nyima fault. The exposed strata in Dachae rock gold deposit belong to Mugagangri subregion of south Qiangtang, here

are the main Jurassic Mugagangri group and that the Quaternary deposits also widely distributed. In the northeast and southeast regions of the deposit, the upper Cretaceous Jingzhushan Format and the lower Cretaceous formation Langshan Format ion are exposed. The magmatic activity at Dachae deposit did not form large-scale magmatite, but its form is more diverse, with intermediate to acidic volcanic rocks, that constitutes the interlayer of Mugagangri group, and subvolcanic rocks and apophysis, dykes and dikes emplaced in Jurassic strata. The main types of rocks are quartz trachyandensite, dacite-porphyrite, quartz diorite-porphyrite, granodiorite and monzonitic granite. The main body of the area is the deep sea facies volcanic rock - flysch sedimentary rock series formed during the extensional rifting stage, which is experienced multiple tectonic movements, and rocks are subjected to regional low temperature dynamic metamorphism. The ore bodies, mineralized bodies, carbonaceous-bearing sericite slate- andesite basalt, intermediate-acid intrusive rocks and fracture structures in the belt consist a spatial pattern of the "four in one".
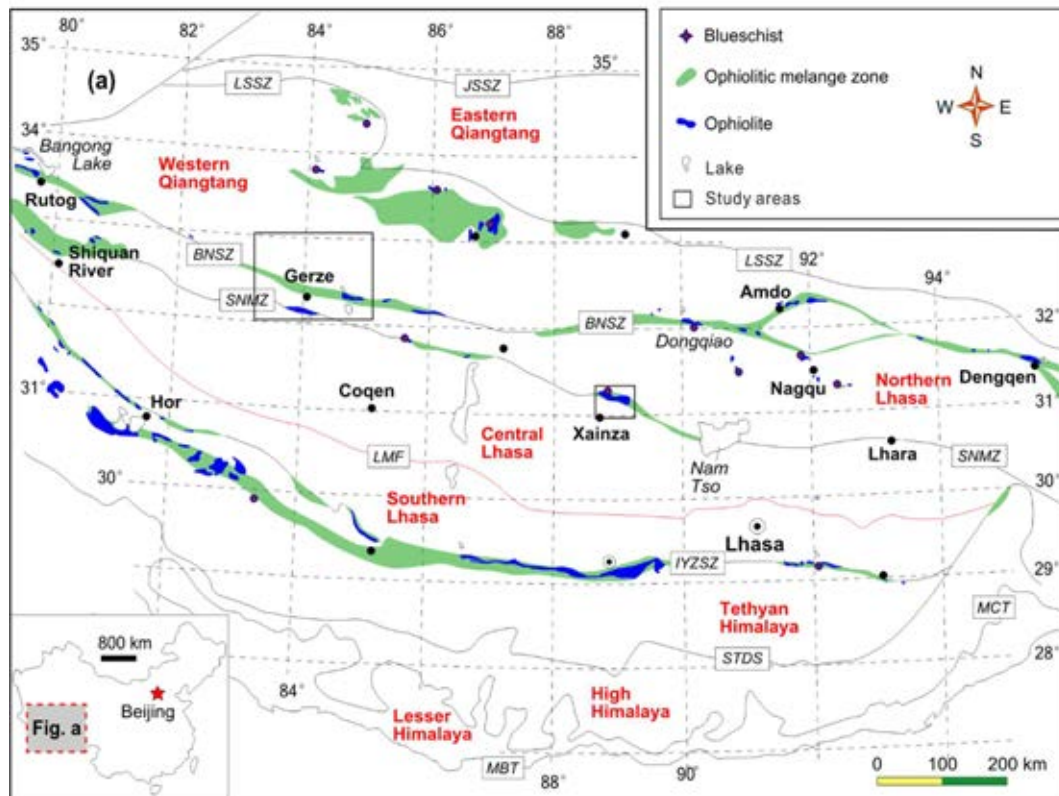
Fig. 1. Tectonic framework of the Tibetan Plateau. JSSZ = Jinsha Suture Zone; LSSZ = Longmu Tso-Shuanghu Suture Zone; BNSZ = Bangong-Nujiang Suture Zone; SNMZ =Shiquan River-Nam Tso Mélange Zone; LMF = Luobadui-Milashan Fault; IYZSZ = Indus-Yarlung Zangbo Suture Zone.

There are three gold deposits have been found in the area, that are Wusula, Luoburiem and Quwengaridongla from west to east (Fig. 2) and nine gold ore bodies with industrial value. The length of ore body is in the range of 300 ~ 400 m, and the width of the ore body is mostly in the range of 2 ~ 4 m, and the depth of the ore body is greater than 50 ~10 m that of (Table 1). The gold deposits are mainly hosted in epimetamorphic clastic rock formation of the second and third Mugagangri Group, within the inner and outer contact of intermediate-acid intrusive rocks. The shapes of ore bodies are mainly vein and lens, and ore deposits are characterized by poor sulfide ores; The mineralization types are primarily altered sericite slate and altered diorite porphyrite, and in quartz vein type is complementary . The wall rocks are mostly sericite slate and altered diorite porphyrite. Wall rock alteration are mainly to beresitization, carbonatization and silicification, chloritization, kaolinite as the auxiliary. The center of mineralization is silicification and pyritization, followed by outward sericite alteration, carbonatization, chlorite and kaolinite. The source rocks of altered rock type ores are mainly diorite porphyrite and sericite slate

Table 1 The geometric features and grade of gold ore in ajor rock gold mining area of Dacha gold district

Segment of ore body	No. of ore body	Scales (m)			Occurrence	Grade (10⁻⁶)
		Length	Thickness	Inferring depth		
Wusula	I	394	3.54	98	south orientated at surface,north orienteated in deep,with dip angle>75 °	4.08
	II	396	2.09	99	south-east orientated at surface,north-west orienteated in deep,with 75 °~82 ° dip angle	3.11
	III	600	1.78	150	NEE-orientated,,branch compound	4.76
	X	340	2.5	85	branch to the West and connect with the second orebody	4.2
Luoburiem	I	80	2.83		330 °∠59 °	10.95
	II	298	3.9		126 °~183 °∠46 °~65 °	1.84~5.51
	III-IV	345	2.35		147 °~160 °∠40 °~78 °	6.48
	VI	260	1.45		165 °~172 °∠41 °~56 °	2.34
	IX	140	1.62		165 °~176 °∠31 °~56 °	2.06
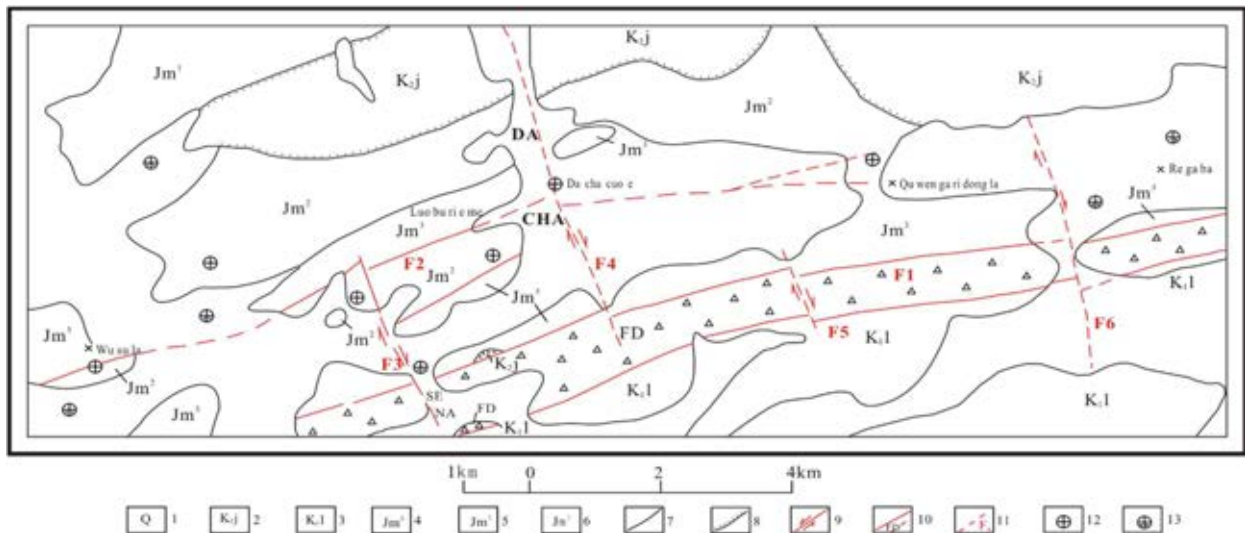
Fig. 2. Geology and mineral resources in Dacha mine.

1-Quaternary; 2- Jingzhushan Formation; 3- Langshan Formation; 4-Third segment of Mugagangri Groups; 5-Second segment of Mugagangri Groups; 6-first segment of Mugagangri Groups; 7-Geological boundary; 8-Angular unconformity;9-Stike-slip fault; 10- Fracture Zone; 11-Supposed Fault; 12-Rock gold spots; 13-Placer gold spots.

The metallogenic stages of this area can be divided into early stage of quartz vein formation, middle stage of sulfide and late stage of carbonate according to the relationship of the mutual intersection of hydrothermal veins. We carry on K-Ar isotopic age determination on rocks at Luoburiem mine, including hornblende and plagioclase phenocryst and feldspar in matrix of unaltered dioritic porphyrite, mica in sericitization dioritic porphyrite, and plagioclase phenocryst in disseminated pyrite mineralization granodiorite porphyrite respectively, which present the three stages of diagenesis and mineralization.

The Cena gold copper orefield is located in the Duolong ore concentration area, about 120 km northwest of Gaize county, with $4839 \sim 5540$ m of an altitude and $200 \sim 700$ m of the relative elevation, which belongs to the medium-high mountain landform of plateau. Duolong ore concentration area is the most remarkable prospecting finding at Bangong-Nujiang Suture Zone in recent years with a series of copper and gold orefields, including the Saijiao, Duobuza (superlarge), Bolon (superlarge)), Rongna, Cena, the east Cena, Gaeqin, south Tiegelong (superlarge), Nandun and the Depunamugang (Figure 3). After exploration it has been controlled by more than 1200×10^4 t of copper resources and more than 400 t of gold resources (Li Xingkui et al., 2015). The area is located in the south margin of the Qiangtang plate at the northern Bangong-Nujiang Suture Zone, stratigraphy, structure, magmatite are nearly east-west distribution, affected by the Bangong-Nujiang subduction.
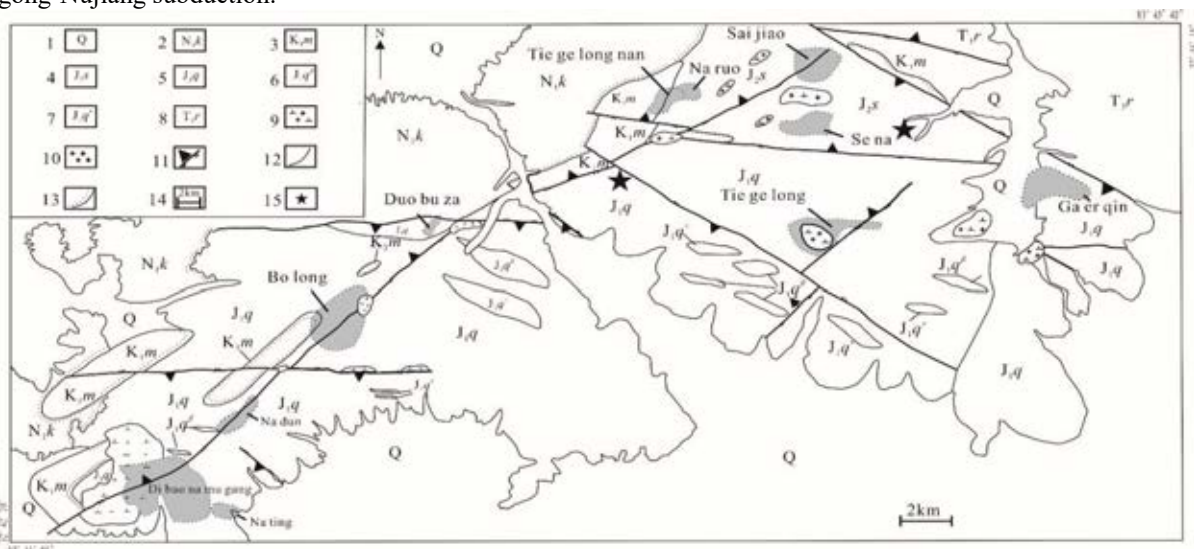
Fig 3. Regional geological map of the Duolong ore concentration area (after Su et al.，2013).

1- Quaternary eluvial and slope wash material；2- the Miocene Kangtuo Formation；3- the Cretaceous Meiriqiecuo Formation；4- Middle Jurassic Sewa Formation；5- Lower Jurassic Quce Formation；6-Lower Jurassic basalt；7-- Gabbro pf Lower Jurassic Quce Formation；8-Upper Triassic Riganpeicuo Formation；9- Granodiorite porphyry；10- Granitic porphyry；11-thrust faults；12-geological boundary；13-unconformity geological boundary；14- Location of samples

Duolong ore concentration area mainly outcropped carbonate rocks in Triassic Riganpeicuo group, epimetamorphismm argillaceous sandstone in lower Jurassic Quse formation (J_1q) interbedded with mafic volcanic rocks and siliceous, which diagenetic age is from 141 to 143Ma（Li J.X.et al.,2013）. The interbedding of siltstone and mudstone with small amounts of basalt, chert in the middle Jurassic Sewa (J_2s), Purple andesite and dacite in Meiriqiecuo Formation of lower Cretaceous(K_1m), unconformity with underlying Sewa Formation (J_{1-2} s), and the zircon SHRIMP age of dacite is 111.1±1.4 Ma (Li G.M et al., 2011), And the purple sand conglomerate in the Miocene Kangtuo formation (N_1k) in Neogene, which contacted unconformityly with underlying the Meiriqiecuo Formation of lower Cretaceous (Jiang S.Q., 2015); There are Quaternary (Q) residual slope sediments and unconsolidated gravel deposits as well as. We surveyed a crater which is about 0.5 km^2 in area between the Rongna and Erping trenches,and collected a rhyollite(Fig.3).

The wall rocks of the Cena rock gold and copper ore section are gray to dark gray medium-thick layered meta-(feldspar) quartz sandstone in Lower Jurassic Quse formation (J_1q);The formation of rocks is about 315 º strike and northeast dip direction with 60º～70º dip angle. There are several dacite porphyrite, diorite and granodiorite porphyrite large and small at the mining area, occurring in a shape of stocks for the larger ones with 0.2 - 0.8 km^2 of exposed area, while in dikes for smaller ones. Ore bodies are distributed in the NWW faults about 295º strike and NNE-orientated with 60º～75º dip angle. The primary metal minerals of the ore in the deposit are pyrite, chalcopyrite and natural gold, and the gangue minerals are quartz, calcite, iron calcite, sericite, chlorite and epidote. The surperfical metal minerals are mainly limonite, malachite, chessylite. Natural gold presented in the shapes of granular, irregular micro vein and dendrite, occurs inward of pyrite, chalcopyrite, quartz and carbonate minerals, internal cracks or boundaries of grains. The main texture of the ore are euhedral-subhedral granular texture for pyrite, anhedral granular texture for chalcopyrite, lepidoblastic texture for sericite, irregular metasomatic texture foe carbonate mineral separators, poikilitic texture and intersertal texture for natural gold, and the like. The structure of ores is mainly breccia structure, sparse and dense disseminated structure, massive structure, banded structure and honeycomb structure.

A diorite porphyrite was exposed in No. TC24 trench of Sena orefied, exposing a length of about 50 m, and rocks have sericite-quartz alteration and beresitization in varying degrees. Diorite porphyrite is circular distribution around Tiege mountain in the shape of dikes and viens. The area of the stock is about 0.1 km2, and the vein is generally about 100 m in length by 20 m in width. They intruded in Yanshiping group and dacite porphyry, and formed a little later than dacite porphyrite; A porphyritioid biotite granite has been found in the trenche, whose occurrence is unclear and not widely distributed.A granite and a diorite are collected in the area for K-Ar dating.

3.Shesuo and Xiawunongba deposit

The Shesuo and Xiawunongba deposit is located in Xainza County, Nagqu, which is in the hinterland of Qinghai Tibet Plateau and belong to the Gangdese Nyainqentanglha plate between the Bangong-Nujiang Suture Zone and the Yarlung Zangbo Suture Zone. Abundant gold deposits (points) are distributed in the area, such as the Bongnazhengbu,Nalong ditch,Tangta, Amdo, Maerqu,and Duocangba (Wei W.S.,2001),and gold mining has a long history. However, the study level of this area is relatively low since the deposit location is more remote, traffic inconvenience and high altitude (4500-5000 m), the scale of the mines are not too big to arouse people's attention. The ophiolite at Bangor-Xainza area can be divided into three subzones from north to south,and distributed almost 200 km in width from north to south(Chen G.R.2004). Shesuo copper polymetallic deposit is located in the Longganggangri-Bangor magmatic arc at north side of the third ophiolite belt(Hu Zhenglong et al., 2004), while Xiawunongba deposit is located in the Geji-Xainza backarc basin at the south side of it. The Shesuo copper polymetallic deposit is one of the few skarn type copper deposits mining now in Gangdise mountain.

The deposit of copper ore (mineralization) are mainly occurred in skarn of granodiorite and Langshan formation carbonate strata contact zone, marble interlayer fracture zone and lens of bedding diopside hornfels, appearing often in irregular veined-bedded-lenticular output, the scale of the deposit is medium with high grade (Liu Y., 2011). We collect a granite and a quartz diorite from Shesuo copper deposit. The Xiawunongba placer gold deposit belongs to medium scale, and mainly developed in Upper Jurassic-Lower Cretaceous Zenong group and Jega formation of volcanic rock in a rift zone and complex terrigenous clastic sedimentary, companying with the ophiolite residue tectonic resetting and covered partly of the epicontinental volcano built of Linzizong group,and overlapped by a Neogene deep basin.The tectonic deformation in this area is characterized by strong folds, thrust and fault block nappe and fault block nappe, and the S type granite rocks in the Himalayan period are relatively developed. At present, the placer gold deposit has been mined, and we have sampled the diorite in the periphery of the deposit.

The results of isotopic dating

The content of K in the determination of K-Ar isotope age was determined by atomic absorption spectrometry (AAS) at the national geological test center(SHIAAS9442), RSD＜3%; The Ar isotope ratio was determined by isotope dilution method using the static vacuum mass spectrometer (MM5400), The quality of the test was determined by using standard samples of biotite (ZBH-25, chinese standard sample, standard age of 133.2 Ma, K content of 7.6%). K-Ar age calculated parameters were calculated by Steiger's ^{40}K abundance constant and decay constant. The error of weighing error, $^{40}Ar/^{38}Ar$, $^{38}Ar/^{36}Ar$ and potassium content were taken into account in the age error, and the error range was 1. Results of K-Ar isotopic age of 13 rocks and mineral separators are shown in table 2.

Our results show that the formation time of hornblende and plagioclase of phenocrysts from unalterated diorite porphyrite of the Dacha gold mine at the west part of the Bangong-Nujiang Suture Zone (18-12a) are 104.88 ± 2.39Ma and 103.17 ± 1.53Ma, consistent each other in the error range, reflecting the formation time of phenocrysts of diorite porphyrite; The K-feldspar age results in the matrix is 98.86 ± 1.47Ma, 6.02Ma later than the phenocrysts, which reflects

the difference of the closure temperature of diorite porphyrite in phenocrysts and matrix formed in different times and different stages of mineral potassium argon system. By chromium beresitization diorite (18 - 10) in chrome sericite K-Ar was 97.51 ± 1.41Ma, reflecting the sample alteration age, the age and the more obvious the mica diorite (18 - 12b) potassium feldspar in similar age (96.54± 1.39 Ma). The determination results of disseminated pyrite mineralization granodiorite porphyrite in plagioclase Shi Banjing was 93.86 ± 2.11Ma. Disseminated pyritization represent the metallogenic media reduction, transition point from alkaline to physical and chemical conditions of acid from oxidation (equivalent to beresitization), and ore-forming material migration from transition to precipitation, is the beginning stage of mineralization. This age can also be seen in this area from Cr beresitization to beresitization, after about 3.65 Ma. This section sets the color area of longkuang porphyritic biotite granite rock K-Ar isotopic age of 123.3 ±1.8 Ma; beresitization flash K-Ar isotopic ages of whole rocks tonalitic porphyrite age determination, income value of 119.25 ±1.73 Ma; the metallogenic epoch may be about 20 Ma earlier than the Bangong Lake Nu River Department of, Rong the gully rhyolites of the K-Ar whole rock age was 105.5 ± 1.6 Ma, age long porphyrite is roughly the same as the Southern Ocean at this time may indicate that flash, Teti has been closed, the geodynamic environment unified control of the Bangong Lake West of the north and south sides of Nu River tectonic suture zone magmatism.

Table2 results of age determination by K-Ar

No. Sample	Location of sample	Type of rocks	mineral separator	K(%)	$^{40}Ar^*(*10^{-10})$mol/g	$^{40}K(*10^{-7})$mol/g	$^{40}Ar_{放}/^{40}Ar_{总}$(%)	Age (Ma)
Duolong ore concentration area at the west segment of Bangong-Nujiang tectonics suture zone								
12-15	TC-24 trench at Cena	diorite	whole rock	2.10	4.500	0.6268	82.09	119.52±1.73
12-18	TC-24 trench at Cena	biotite granite	whole rock	2.11	4.671	0.6298	92.87	123.3±1.8
14−1	west Rongna trench	rhyolite	whole rock	3.87	7.294	1.155	93.4	105.5±1.6
Dacha gold mine at the west segment of Bangong-Nujiang tectonics suture zone								
18-10b	juncture between N0.64 trench at first body of Luoburiem and the big mining pit of west third body	Cr-sericitization diorite porphyrite(medium)	mica	6.50	11.290	1.940	95.02	97.51±1.41
18−12a	N0.64 trench at first body of Luoburiem	diorite porphyrite	potassium feldspar	5.27	9.287	1.573	81.28	98.86±1.47
18-12a	N0. 64 trench at first body of Luoburiem	diorite porphyrite	hornblende	0.54	1.011	0.1612	64.23	104.88±2.39
18-12a	N0. 64 trench at first body of Luoburiem	diorite porphyrite with more mica	plagioclase	1.77	3.259	0.5283	69.83	103.17±1.53
18−12b	N0.64 trench at first body of Luoburiem	diorite porphyrite(with light pink felspar)	potassium feldspar	9.39	16.150	2.803	88.19	96.54±1.39
18−13	fouth body of Luoburiem	disseminated pyritization granodiorite porphyrite	plagioclase	0.72	1.203	0.2149	55.04	93.86±2.11
Sesuo copper metallogenic mine at the middle segment of Bangong-Nujiang tectonics suture zone								
20−1	Sesuo	medium granite	potassium feldspar	7.54	10.80	2.250	86.42	80.73±1.17
20−3	Sesuo	quartz diorite	potassium feldspar	9.74	15.06	2.907	84.33	87.01±1.29
Xiawunongba placer gold deposit at the middle segment of Bangong-Nujiang tectonics suture zone								
21−1	Xiawunongba	coarse diorite	plagioclase	0.96	1.657	0.2865	56.08	96.87±2.12
21−12c	Xiawunongba	diorite	plagioclase	0.45	0.8826	0.1343	39.26	109.69±2.86

Shesuo copper polymetallic deposit of granite and quartz diorite feldspar K-Ar ages were 80.73 ±1.17 Ma and 87.01 ± 1.29 Ma Ma, on behalf of the potash feldspar K-Ar isotope system closed since age; K-Ar age of granodiorite plagioclase under sand gold deposit is Nongba Wu 96.87 ± 2.12 and 109.69 ±2.86 Ma. Time and magmatism of Bangong Lake Nu River tectonic suture belt roughly at the same time, reflects the end of Early Cretaceous magmatic activities in the Tibet area two areas are widely distributed.

References:

Qiu Ruizhao, Zhou Su, Deng Jinfu, Xiao Qinghui, Wu Zongxu, Cai Zhiyong. 2007. The Ophiolite Forming Tectonic-setting in Western Qinghai-Tibetan, China—Evidences from Geology, Petrology and Geochemistry. Journal of Asia Earth Sciences，29（2-3）：215～228

Xiao R, Li S R, Fu L J , et al.2002 .Isotope geochemistry of Dacha gold deposits in Tibet [J] .Geoscience , 16(2): 165～ 169 (in Chinese with English abstract).

Zhou X and Cao Y G ..1989 .Tibetan plate tectonics_formation map (1:1500000) [M] .Beijing: Geol.Pub .House. 1-32 (Chinese with English abstract).

LATE ARCHEAN RARE-ELEMENT PEGMATITES FROM KEIVY-KOLMOZERO ZONE, KOLA PENINSULA, AND DATING (ID-TIMS, EMP) OF PEGMATITIC ZIRCON, MICROLITE, MONAZITE AND THORITE

Zozulya D.R., Kudryashov N.M., Lyalina L.M., Stepenshchikov D.G.

Geological Institute, Kola Scientific Center of the Russian Academy of Sciences, Apatity, Russia, zozulya@geoksc.apatity.ru

Rare-element granitic pegmatites are recognized as important source of some strategic metals (REE, Nb, Ta, Be). The granitic melts contain high concentrations of volatiles, which play a crucial role in accumulation/recrystallization of strategic metals at both late-magmatic and metamorphic/metasomatic overprinting stages.

Keivy-Kolmozero zone, NE Baltic shield, is composed mainly from basic-intermediate-acid metavolcanic suites of 2.83-2.87 Ga age and metamorphosed at amphibolitic facies during 1.8-1.7 Ga. Younger igneous events are represented by voluminous intrusions of 2.73 Ga plagio-microcline granites and small stocks of ca. 2.7 Ga tourmaline granites (in Kolmozero subzone), and intrusions of 2.65 Ga alkali A-type granites (in Keivy subzone).

Four pegmatite fields with total amount of more than 100 bodies are confined to Kolmozero subzone. The pegmatites intrude amphibolites and rarely associated gabbro-anorthosite and are of 50-700m long and of 10-35m thickness. Quartz-albite-microcline pegmatite bodies are extremely enriched in rare element minerals: spodumene (up to

20-50 vol %), pollucite, tantalite, microlite, lepidolite, beryl. The Kolmozero pegmatites are of complex type, spodumene subtype with Li, Cs, Be, Ta, Sn geochemical signature and belong to LCT family according to classification of Cerny and Ercit (2005). They crystallized at relatively high pressure (3-4 kbar) with peralumunious S-type granite as the source magma. We assume that the 2.7 Ga Kolmozero tourmaline granite is most possible source granite. Pegmatitic microlite and granitic tourmaline were dated by U-Pb ID-TIMS method and give the ages of late metamorphic/metasomatic event: 2450 Ma and 2520 Ma, respectively (Fig. 1). The ages correspond to initial magmatic events during Paleoprotherosic rifting of NE Baltic Shield (Pechenga-Varzuga belt).
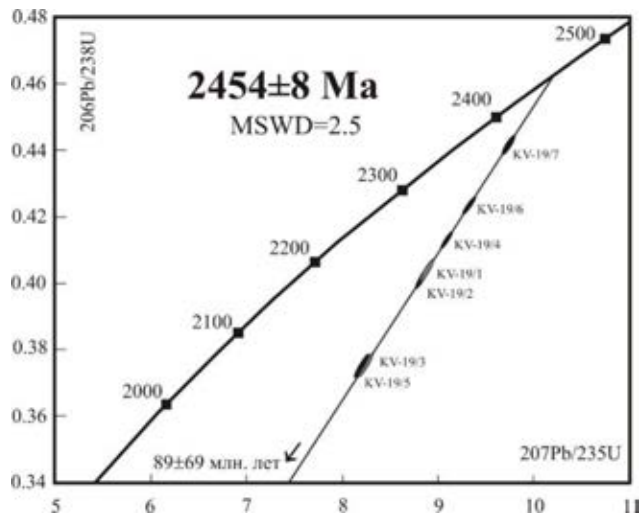
Fig. 1. Diagram with concordia for microlite from rare-metal pegmatites of the Kolmozero (Kudryashov et al., 2015).
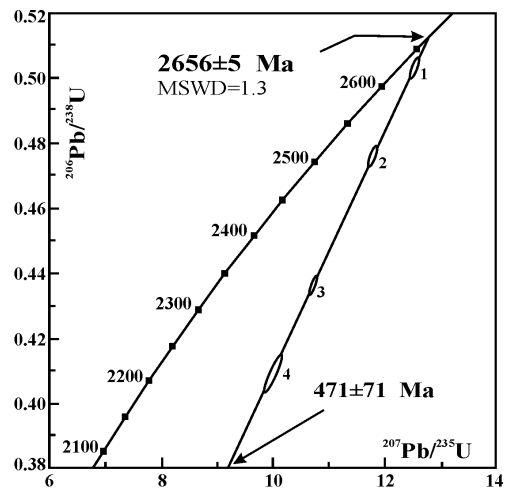
Fig. 2. Diagram with concordia for pegmatitic zircon from White Tundra alkali granite (Lyalina et al., 2012).

Several tens pegmatite bodies from Keivy subzone are confined to inner and outer apical parts of alkali granite intrusions. They are of few tens meters long and of several meters thickness, sometimes are "schlieren" and of oval and irregular shape (so-called "quartzolites"). Keivy pegmatites are subdivided on quartz-microcline, quartz-feldspar-astrophylite and quartz-magnetite-aegirine-arfvedsonite (quartzolite) mineral species. Most abundant rare-element minerals are zircon, fergusonite-(Y), gadolinite-(Y), chevkinite-(Ce), britholite-(Y), yttrialite-(Y), aeshinite-(Y), thorite. Keivy pegmatites are of gadolinite type with Y, HREE, Zr, Ti, Nb>Ta, F signature indicating on its NYF nature. Undoubtly alkali A-type granites are the source of Keivy pegmatites, that is confirmed by the same age of pegmatitic zircon – 2656 Ma (Fig. 2). Keivy pegmatites formed at moderate pressure (1.5-3.7 kbar). The U-Th-total PB EMP ages determined for the monazite-(Ce) from quartzolite range from 1740 Ma to 1600 Ma, with an average of 1670 Ma (Fig. 3).
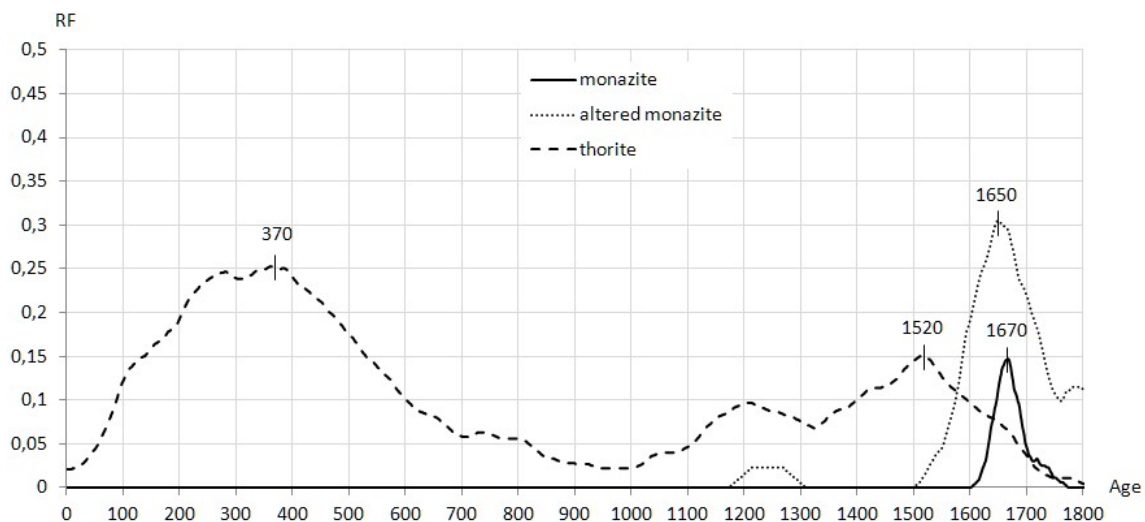
Fig. 3. Relative frequency *vs.* chemical dates for monazite and thorite from rare-metal rich quartzolite and metasomatite, respectively, related to West Keivy alkali granite

It is clearly much younger than the age of formation of the Keivy alkali granite (2650 Ma). It is, however, more similar to the age of the regressive stage of the Svecofennian metamorphic event which affected the Baltic shield at 1.9–1.7 Ga. Otherwise, intracratonic rift evolution with mantle upwelling and emplacement of rapakivi granite at 1.66–1.56 Ga occurred in the south Baltic shield, pointing to possible fluid-thermal activation of the shield during that time. It appears possible that the monazite has recorded the resetting of its age during that event. The EMP dating of thorite from metasomatic rare-metal rich rocks related to alkali granite magmatism give several age peaks, one of them is at ca. 1520

Ma and caused by the same metamorphic/metasomatic event as for monazite (see above), and second one - at ca. 370 Ma, corresponding to well-known Paleozoic alkaline magmatic event in the region.

Unique pegmatite body of amazonite-quartz-albite composition (Ploskaya Mnt) intrudes the Keivy metavolcanic complex. It is of several hundred meters long and several tens meters thickness. The rare-element mineralization is represented by plunbomicrolite, betafite, columbite, plumbopyrochlore, keyviite, keyviite-(Y), yttrofluorite, xenotime, monazite-(Ce), gadolinite-(Y), hingganite, hingganite-(Yb), tengerite, genthelvite, polylithionite, kainosite, cassiterite and has the Y, Yb, Nb, Ta, F, P, Li, Be, Sn (Pb, W, Mo) geochemical signature, indicating on mixed NYF-LCT family. U-Pb ages ranging from 1673 to 1695 Ma are obtained for xenotime, zircon and monazite from pegmatite (Bayanova 2004). No granite of the same age is known in the zone and genesis of pegmatite via metamorphic remobilization of rare metals from alkali granite and hosted gneissic rock is suggested.

Thus, rare-metal minerals from Late Archean pegmatites of Keivy-Kolmozero zone are sensitive indicators of metamorphic/metasomatic events and may record the late resetting of their initial ages (f.e. at 1.65-1.5 Ga and 0.37 Ga).

References:

Bayanova T.B. (2004) The age of reference geological complexes of the Kola region and duration of magmatic processes. Nauka, St Petersburg (in Russian).

Cerny P., Ercit T.S. (2005) The classification of granitic pegmatites revisited. Can Min 43: 2005-2026.

Kudryashov N. M., Lyalina L. M., and Apanasevich E. A. (2015) Age of rare-metal pegmatites from the Vasin-Myl'k deposit (Kola Region): Evidence from U–Pb geochronology of microlite. Dokl Earth Sci 461: 321–325.

Lyalina L.M., Zozulya D.R., Bayanova T.B., Selivanova E.A., Savchenko Ye.E. (2012) Genetic peculiarities of zircon from pegmatites of Neoarchean alkali granites of the Kola region. Zapiski RMO 5: 35-51 (in Russian).

Content